DRYING '80

Volume 2:

Proceedings of the Second International Symposium

Edited by

Arun S. Mujumdar

McGill University, Montreal

HEMISPHERE PUBLISHING CORPORATION
Washington New York London

DISTRIBUTION OUTSIDE THE UNITED STATES
McGRAW-HILL INTERNATIONAL BOOK COMPANY
Auckland Bogotá Guatemala Hamburg
Johannesburg Lisbon London Madrid
Mexico Montreal New Delhi Panama
Paris San Juan São Paulo Singapore
Sydney Tokyo Toronto

DRYING '80 (Volume 2): Proceedings of the Second International Symposium

Copyright © 1980 by Hemisphere Publishing Corporation. All rights reserved. Printed in the United States of America. No part of this publication may be reproduced, stored in a retrieval system, or transmitted, in any form or by any means, electronic, mechanical, photocopying, recording, or otherwise, without the prior written permission of the publisher.

1 2 3 4 5 6 7 8 9 0 BCBC 8 9 8 7 6 5 4 3 2 1 0

Library of Congress Cataloging in Publication Data

International Symposium on Drying, 2d, McGill University, 1980.
Proceedings of the second international symposium.

(Drying '80; v. 2)
Includes bibliographical references and indexes.
1. Drying—Congresses. I. Mujumdar, A. S.
II. Series.
TP363.D79 vol. 2 660.2'8426s [660.2'8426] 80-15493
ISBN 0-89116-188-0 (set)
ISBN 0-89116-201-1 (vol. 2)

CONTENTS

PREFACE ix

SECTION I DRYING THEORY AND FUNDAMENTALS

An Analysis of the Irreversible Thermodynamics Model for Coupled Heat and Moisture Transfer in Unsaturated Porous Media
R.J. Parikh, University of Nebraska, Lincoln, Nebraska, U.S.A., and
J.A. Havens, University of Arkansas, Fayetteville, Arkansas, U.S.A. 1

An Approximate Method for Determination of the Sublimation Limit in Simple Geometrical Porous Bodies
S. Lin and Y.Y. Lin, Concordia University, Montreal, Quebec, Canada;
C.L. Wang, University of Regina, Regina, Sask., Canada 6

Mechanics and Thermodynamics of Drying: A Summary
M.J. Lampinen, Valmet Oy Pansio Works, Turku, Finland 11

Kinetics of Mass Transfer in a Capillary with Account for Movable Adsorbed Layers
O.G. Martynenko, V.V. Levdansky, and N.V. Pavlyukevich, Heat and Mass Transfer Institute, Minsk, U.S.S.R. 17

A Theoretical Model for Solar-Dehumidification Drying of Wood
W.A. Helmer and S.W. Wang, Dept. of Thermal & Env. Eng., South. Ill. Univ., Carbondale, Illinois, U.S.A.; H.N. Rosen and P.Y.S. Chen, North Cent. For. Exp. Stn., USDA For. Serv., Carbondale, Illinois, U.S.A. 21

Modelling and Calculation of the Drying Process of Capillary Porous Materials
S. Szentgyörgyi, K. Molnar and M. Orvos, Technical University, Budapest, Hungary 29

Phenomenological Coefficients for Heat and Mass Transfer Equations in Wet Porous Media
M.A. Roques, Institut National Polytechnique de Lorraine, Nancy, France and
A.R.H. Cornish, Imperial College of Science and Technology, London, England 36

Studies on the Drying Kinetics
R.Z. Tudose and Gh. Cristian, Polytechnic Institute, Jassy, Romania 43

The Thermokinetics of the Moisture Transport in Solids During Drying
J. Valcharova and J. Valchar, National Research Institute for Machine Design, Prague, Czechoslovakia 53

Characterising Moisture Bond in Materials with Respect to Drying Using the State Function Diagram
B. Cermak, National Research Institute for Machine Design, Czechoslovakia 61

Interdependence Between Heat and Mass Transfer in Drying
P.S. Kuts and I.F. Pikus, Luikov Heat and Mass Transfer Institute, BSSR Academy of Sciences, Minsk, USSR 65

Non-Steady-State Surface Evaporation from Porous Bodies with Non-Uniform Pore Distribution
S. Endrenyi, Refrigerating Works, Budapest-Jaszbereny, Hungary 80

SECTION II SIMULATION STUDIES

A Numerical Model of Heat and Mass Transport in Wood During Drying
G.A. Spolek and O.A. Plumb, Washington State University, Pullman, Washington 84

A Mathematical Model for the Drying of Latex Films
N. Pramojaney and J.W. Vanderhoff, Emulsion Polymers Institute, Lehigh University, Bethlehem, Pennsylvania, U.S.A. ; G.W. Poehlein, School of Chemical Engineering, Georgia Institute of Technology, Atlanta, Georgia, U.S.A. ... 93

Search Methods Through Simulation for Parameter Optimization of Drying Process
R. Bertin and Z. Srour, G.R.A.I. Université de Bordeaux I, Talence - France 101

Toward Automatic Control by Microprocessor for Convective Dryer Systems
C. Cazaubon, R. Bertin and M. Blazquez, GRAI, Université de Bordeaux I, Talence - France 107

The Mathematical Model of Final Temperature Behaviour for Textile Materials in a Drying Chamber
J. Spirnek, Research and Development Centre of Automation and Instruments of Precision, Lodz, Poland 112

A Method of Determination of an Optimum Temperature Distribution along a Drying Chamber
I. Dziubinski, Technical University, Lodz, Poland and J. Spirnek, Research and Development Centre of Automation, Lodz, Poland 120

Mathematical Modelling and Simulation of Vacuum Contact Drying of Porous Media in the Constant Rate Period
F. Strek and J. Nastaj, Technical University of Szczecin, Szczecin, Poland 126

Mathematical Modelling and Simulation of Vacuum Contact Drying of Porous Media in the Falling Rate Period (Boundary Condition of the First Kind)
F. Strek and J. Nastaj, Technical University of Szczecin, Szczecin, Poland 135

SECTION III DRYING OF GRANULAR MATERIALS

Calculation of Heat Transfer on Vibrating Conveyors
D.U. Ringer, Technical University Munich, West Germany 144

Process Development of a Fluidized Drying Scheme for Nitrile Rubber
J.P. Lenczyk, University of Akron, Akron, Ohio, U.S.A. and C.R. Sarkar, B.F. Goodrich Chemical Co., Avon Lake, Ohio, U.S.A. 152

Energy Use in Paddle Dryers
William L. Root, III and Edward M. Cook, Stork Bowen Engineering Inc., Somerville, N.J., U.S.A. 158

Unsteady Heat and Mass Transfer in a Packed Bed of Fine Particles with an Endothermic Process
M. Hasatani and N. Arai, Nagoya University, Nagoya 163

Drying Some Objects in Fluidized Bed Under Reduced Pressure
K. Yamamoto and Y. Kawamura, University of Hiroshima, Hiroshima, Japan 170

Drying Characteristics of Tea Fluidised on a Vibrating Bed (Part - I)
Dr. Rohit M. Shah and Suresh K. Goyel, Macneill & Magor Limited, Bombay, India ... 176

Theoretical Investigation of Drying Conditions of the Fluidized Bed Granulation
T. Vajda, Research Institute for Technical Chemistry of the Hungarian Academy of Sciences, Budapest 182

Analysis of the Role of a Microwaves Energy Contribution in Drying Porous Media
A. Le Pourhiet, Centre d'Etudes et de Recherches de Toulouse, Toulouse, France and S. Bories, Institut de Mécanique des Fluides, Toulouse, France 186

Mechanism of the Vapour Transfer in a Moist Granular Bed Under a Temperature Gradient
M. Kuramae, Hokkaido University, Sapporo, Japan 195

Drying of Granular Materials in a Vibrated Fluidized Bed
R. Gupta, P. Leung and A.S. Mujumdar, McGill University, Montreal, Canada 201

The Influence of Aerodynamics of a Vibrated Fluid Bed on Heat Transfer During Drying Process at Low Air Velocities
Z. Pakowski and C. Strumillo, Lodz Technical University, Lodz, Poland 208

Hydrodynamic Characteristic of Pneumatic Flash Dryers
A. Kmiec and S. Mielczarski, Inst. Chem. Eng. Technical University of Wroclaw, Wybrzeze Wyspianskiego 27, Poland 213

Heat and Mass Transfer in Packed Beds
M. Parti, Technical University, Budapest, Hungary 219

SECTION IV DRYING OF FOODSTUFFS AND GRAINS

Rates for Freeze Drying
A.I. Liapis, University of Missouri-Rolla, Rolla, Missouri, U.S.A. 224

Prediction of Heat and Mass Transfer Within a Grain Kernel - A Finite Element Application
Shahab Sokhansanj, University of Saskatchewan, Saskatchewan, Canada, and R.J. Gustafson, University of Minnesota, St. Paul Minnesota, U.S.A. 229

Concentration Dependent Diffusion Coefficients Derived From Experimental Drying Curves
K.Ch.A.M. Luyben, J.J. Olieman and S. Bruin, Agricultural University, Wageningen, The Netherlands 233

Continuous Vacuum Drying for Highly Viscous and Heat Sensitive Foods
E. Kumazawa, Y. Saiki, Y. Ishioka, S. Taneya, and H. Hayashi, Snow Brand Milk Products Co., Ltd., Saitama, Japan 244

Kinetics of Soybean Drying
C. Suarez, P. Viollaz and J. Chirife, Universidad de Buenos Aires, Buenos Aires, Argentina 251

Parameters Required in the Analysis of Rough Rice Drying
J.F. Steffe, Michigan State University, East Lansing, Michigan, U.S.A. and
R.P. Singh, University of California, Davis, California, U.S.A. 256

Concurrent Flow Drying of Food Grains
R.C. Brook and F.W. Bakker-Arkema, Michigan State University, E. Lansing,
Michigan, U.S.A. 263

A Study of the Heat Transfer Parameters for Drying by Immersion in a Heated
Granular Media
P. Richard and G.S.V. Raghavan, Macdonald Campus of McGill University, Ste.
Anne de Bellevue, Québec, Canada 272

Drying Characteristics of Parboiled Rice
A.S. Bakshi, University of Minnesota, St. Paul, Minnesota, U.S.A. and
R. Paul Singh, University of California, Davis, California, U.S.A. 282

Drying of Heavily Salted Codfish
Ingvald Strommen, The Technical University of Norway, Trondheim, Norway 289

Drying and Cooling Properties of Milk Powder by Using a Fluidized Bed
H. Hayashi and T. Wada, Snow Brand Milk Products Co., Ltd. Saitama, Japan 294

SECTION V DRYING OF PULP AND PAPER

Steam Drying of Pulp
Claes Svensson, MoDo-Chemetics AB, Ornskoldsvik, Sweden 301

Airfoil Dryer: Principles of Operation and Application
R.A. Bennett, Overly Inc., Neenah, Wisconsin, U.S.A. 308

A Mathematical Model of the Contact Drying Process
M. Soininen, Abok Akademi, Turku, Finland 315

Results from On-Line Investigations of Paper Contact Drying Process
M. Karlsson, Abo Akademi, Turku, Finland 322

A Literature Review of Drying Research in the Pulp and Paper Industry
R.R. McConnell, The Institute of Paper Chemistry, Appleton, WI, U.S.A. 330

Improvement of Moisture Profile on Paper Machines by RF Compensating Drying
H.C. Grassmann, Siemens AG Manufacturing Division, Erlangen, West Germany 338

Challenges of Drying the Printed Web
N.R. Eldred and T.A. Fadner, Graphic Arts Technical Foundation,
Pittsburgh, PA, U.S.A. 343

A New Vacuum-Drying Method for Paper, Board and Other Permeable Mats
J.A. Lehtinen, Tampella Engineering Works, Tampere, Finland 347

New CD Moisture Profile Correction Hood Reduces Energy Consumption and
Production Costs in High Speed Tissue Drying
H. Holik, Escher Wyss GmbH, Ravensburg, F.R.G. and R. Pinter, Maschinenfabrik
Andritz, Graz, Austria 355

Energy Consumption and Drying Costs in High Speed Tissue Drying
R. Pinter, Maschinenfabrik Andritz, Graz, Austria and H. Holik, Escher Wyss GmbH, Ravensburg, F.R.G. 362

The Effect of Air Flow on Heat Consumption in Contact Dryer
A. Strawinski, The Pulp and Paper Research Institute, Lodz, Poland 369

SECTION VI ENERGY ASPECTS

System of Drying Plaster Blocks Using a Heat Pump
R. Gauthier, R. Legoff and C. Bassac, Electricité de France - Direction des Etudes et Recherches, Moret-sur-Loing, France 374

Energy Saving in Dryers
K. Richardt, ANHYDRO A/S, Copenhagen, Denmark 379

Preconcentration of Whey: Results from Use of an Evaporator Equipped with Mechanical Recompression of Steam
G. Deschamps, A. Gauthier and R. Legoff, E.D.F. Etudes et Recherches - Centre des Renardieres, S/Loing, France 387

Approaches to More Economical Drying of Particles and Lumps
O.E. Potter, Monash University, Melbourne, Australia 396

SECTION VII SPRAY DRYING

Spray Drying in Environmental Control with Special Reference to Flue Gas Desulphurization
K. Masters, A/S Niro Atomizer, Denmark 401

Mathematical Model of Spray Drying Reckoning with Droplet Size Distribution
J. Topar, Technical University, Budapest, Hungary 405

Assessment of Numerical Models for Spray-Drying
G. Arnason and C.T. Crowe, Washington State University, Pullman, Washington, U.S.A. 410

Effect of Vane Geometry on Droplet Size and Size Distribution in Spray Dryer
I. Filkova and J. Weberschinke, CVUT, Faculty of Mechanical Engineering, Praha, Czechoslovakia 417

SECTION VIII DRYING OF COAL

The Kinetic Behavior of Subbituminous Coal Drying; Effects of Confining Pressure
L.F. Brown, B.A. Kashiwa, N.E. Vanderborgh, Los Alamos Scientific Laboratory, Los Alamos, NM, U.S.A., and R.C. Corlett, University of Washington, Seattle, WA., U.S.A. 425

Studies on Lignite Drying
B. Kisakürek, McGill University, Quebec, Canada and S. Yesil, Middle East Technical University, Turkey 434

SECTION IX SOLAR DRYING

Cost-Benefit Analysis of Solar Grain Drying and Its Policy Implications
O.Y. Kwon and P.J. Catania, University of Regina, Saskatchewan, Canada 443

Digital Simulation of a Solar Hay-Drying System
L. Imre, L. Kiss, T. Kornyey and K. Molnar, Technical University, Budapest, Hungary 446

A Simulation Model for Convective Solar Drying
C.L. Gupta and T.A. Reddy, Tata Energy Research Institute, Pondicherry, India ... 453

SECTION X NONTHERMAL METHODS

Rejection of Suspending Liquid from Fine Particles by Agglomeration Methods
C.E. Capes, National Research Council, Ottawa, Ontario, Canada and
R.J. Germain, The Steel Company of Canada, Hamilton, Ontario, Canada 460

Displacement Drying with Fluorocarbon Solvents: A Status Report
T. Devine, Du Pont de Nemours International S.A., Geneva, Switzerland 467

SECTION XI GENERAL TOPICS

The Removal of Solvent from Nitrocellulose/Nitroglycerine Mixtures
R.P. Ayerst, Propellants, Explosive and Rocket Motor Establishment,
Waltham Abbey, Essex, England 472

Thermal Degradation of Pyrethrins During Drying of Pyrethrum Flowers
P.M. Githinji, University of Nairobi, Nairobi, Kenya 478

Drying Since the Millenniums
K. Kröll, Bad Hersfeld, F.R. Germany; A.S. Mujumdar and A.S. Menon, McGill University, Montreal, Canada 485

Energy Management for Drying Systems by a Computer - Based Decision Aid
M.H. Waller, Miami University, Oxford, Ohio, U.S.A. and S.C. Curtis,
Raytheon Company, Norwood, Massachusetts, U.S.A. 495

Psychrometrics as the Thermodynamics of Moist Air
John A. Goff, Philadelphia, Pennsylvania, U.S.A. 500

Use of Simulation Techniques to Evaluate Strategies for Improvement of Industrial Multizone Through-Circulation Trolley Dryer
J.C. Ashworth, University of Birmingham, Birmingham, England and
M.C. Hill, Foseco International Ltd., Birmingham, England 508

Measurements of Heat and Mass Transport Within a Sheet of Papermaking Fibers During Drying
P. Lee and J. Hinds, Weyerhaeuser Technology Center, Tacoma, Washington, U.S.A. 523

AUTHOR INDEX 529

SUBJECT INDEX 531

PREFACE

This book, DRYING '80, Volume 2, consists of selected papers presented at the Second International Symposium on Drying held at McGill University, Montreal, Canada, July 6-9, 1980. My prime objectives in founding the biennial Symposia in Drying were to provide a truly international forum for exchange of ideas, and to foster university-industry interaction in the interdisciplinary field of drying of solids. The first Symposium held in August 1978 and now the second one did meet these objectives as a result of the strong support and encouragement of both industry and academia. Encouraged by these successes it has been decided tentatively to continue this biennial symposium series through the 80's, preferably alternating the sites between North America and Europe with an occasional meeting held in some other geographic location.

I wish to thank the authors for their time and effort in the preparation of their manuscripts. With a few exceptions the manuscripts appear in this volume essentially in the form originally prepared by the authors.

I wish to acknowledge with thanks the editorial assistance provided by Mr. Anil S. Menon and Mr. Rahul Gupta. I would like to record my deep appreciation of the assistance provided by Purnima Mujumdar and Karen Brown in the preparation of this Proceedings volume. Thanks are also due to Professor R. Toei, Dr. H. Hayashi, Professor W.J.M. Douglas, members of the Advisory Panel for the Symposium and the session cochairmen for their contributions, both direct and indirect, to the success of DRYING '80. Finally, I am indebted to Mr. William Begell, Hemisphere Publishing Corporation, New York, for accomplishing the publication of this book and its companion volume (DRYING '80, Vol. 1) in a remarkably short period of time.

A.S. Mujumdar
Editor

Department of Chemical Engineering
McGill University
Montreal, Quebec, Canada

THE SECOND INTERNATIONAL SYMPOSIUM ON DRYING

McGill University, Montreal, Canada

July 6-9, 1980

PROGRAM CHAIRMAN AND EDITOR

A.S. Mujumdar, Chemical Engineering Department, McGill University, Canada

CO-SPONSORS OF DRYING '80

Canadian Society for Chemical Engineering, American Institute of Chemical Engineers, Japanese Society for Chemical Engineering, Institution of Chemical Engineers (London), U.K., McGill University

INDUSTRIAL CO-SPONSORS

DuPont (USA), Kraft, Inc. (USA), Midland-Ross Air Systems (Canada), Douwe Egberts-Jacobs Research Co. (Utrecht, The Netherlands), International Paper Co. (USA), Snow Brand Milk Products Co. (Japan), Westvaco.

ADVISORY PANEL

J.C. Ashworth, U.K; D.J. Barr, England; G. Brunello, Brazil;
J. Chirefe, Argentina; M. Combarnous, France; R. Daane, U.S.A.;
W.J.M. Douglas, Canada; S. Endrényi, Hungary; I. Filkova, Czechoslovakia;
H. Hayashi, Japan; L. Imre, Hungary; V.K. Jindal, Thailand;
B. Kisakürek, Turkey; M. Lamvik, Norway; R.B. Keey, New Zealand;
J. Kelly, Ireland; H.G. Kessler, W. Germany; C.J. King, U.S.A.;
M.A. Mandil, S. Arabia; O.G. Martynenko, U.S.S.R.; O.E. Potter, Australia;
D. Reay, U.K.; E. Rotstein, Argentina; E.U. Schlünder, W. Germany;
R. Shah, India; C. Strumillo, Poland; A. Sorensen, Denmark;
H. Thijssen, The Netherlands; R. Toei, Japan.

AN ANALYSIS OF THE IRREVERSIBLE THERMODYNAMICS MODEL FOR COUPLED HEAT AND MOISTURE TRANSFER IN UNSATURATED POROUS MEDIA

R. J. Parikh[1]
J. A. Havens[2]

1. University of Nebraska, Lincoln, Nebraska 68588 USA
2. University of Arkansas, Fayetteville, Arkansas 72701 USA

ABSTRACT

The Irreversible Thermodynamics-based model for coupled heat and moisture transfer in porous media, attributed to Taylor and Cary, was analyzed. The transport coefficients required for the model equations were experimentally measured as a function of moisture content, and the equations were numerically integrated to predict temperature and moisture content profiles for a spherically symmetric, closed system of water-unsaturated 250 μ glass beads.

A one-dimensional (spherical) water-unsaturated glass bead medium was subjected to known heat flow rates, and steady state temperature and moisture profiles were measured. The data indicated the validity of the Irreversible Thermodynamics model predictions and support the Onsager reciprocal relation for this system over the range studied. The coupling coefficient relating thermal gradients to moisture flux was found to be strongly moisture dependent. The coupling coefficient relating moisture content gradient to heat flux was found to be extremely small, and the heat flux associated with the moisture gradient was found to be negligible.

NOMENCLATURE

D = coefficient of diffusivity of liquid water, cm^2/day

J_q = heat flux, cal/cm^2 day

J_w = moisture (liquid) flux, g/cm^2 day

K = hydraulic conductivity, cm/day

L_{11} = phenomenological coefficient, λ, cal/cm day K

L_{12} = phenomenological coefficient, $\rho_w D \beta$, cal/cm day

L_{21} = phenomenological coefficient, $D \beta^*/T$, cm^2/day K

L_{22} = phenomenological coefficient, D, cm^2/day

Q = heat rate, cal/day

R_1, R_2 = radial distances, cm

r = radius, cm

T = temperature, K

T_1, T_2 = temperature at R_1, R_2, K

β = coupling coefficient, $d\psi/d \ln T$, cal/gm

β^* = coupling coefficient, $d\theta/d \ln T$, dimensionless

θ = volumetric moisture content, cm^3 water/cm^3 medium

θ_1, θ_2 = volumetric moisture content at R_1, R_2, cm^3 water/cm^3 medium

λ = thermal conductivity, cal/cm day K

ρ_w = density of water, gm/cm^3

ψ = water potential, $dynes/cm^2$

∇ = gradient operator, cm^{-1}

INTRODUCTION

This paper describes initial efforts to assess the applicability of the Taylor and Cary (1) equations for simultaneous flow of heat and moisture in unsaturated porous media. The Taylor and Cary model, derived from the theory of Irreversible Thermodynamics and incorporating Onsager's reciprocal relation, provides simultaneous differential equations for heat and moisture transfer. Application of the equations requires evaluation of three phenomenological coefficients along with Onsager's Relation to determine the remaining "cross" coefficient. The phenomenological coefficients are strong functions of moisture content in unsaturated porous media systems, and the equations generally require numerical boundary value problem solution techniques.

Although evaluations of the Taylor and Cary model for soil heat and moisture transfer have been reported (2, 3) in which the "cross"

phenomenological coefficients have been determined, the model does not appear to have been tested by solving the equations with well defined boundary conditions, conducting a corresponding laboratory experiment with an unsaturated porous media system, and comparing the predicted and experimental results. Furthermore, uncertainty regarding the importance of complex effects in soils, such as adsorption and non-uniform solid particle size/geometry, which are not accounted for in the Taylor and Cary model, make more difficult the definitive evaluation of the assumptions which are incorporated.

This paper describes an evaluation of the theory of Irreversible Thermodynamics, as developed by Taylor and Cary, for the prediction of steady-state moisture and temperature profiles in a closed, water-unsaturated glass bead system subjected to a known heat flux.

DESCRIPTION OF MODEL

The Taylor and Cary model equations for coupled heat and liquid moisture transfer in unsaturated porous media are (1):

$$J_q = -\rho_w D \beta \nabla \theta - \lambda T \nabla \ln T \qquad (1)$$

$$J_w = -\rho_w D (\nabla \theta + \beta^* \nabla \ln T) \qquad (2)$$

For steady-state heat transfer in a closed, spherically symmetric, unsaturated porous medium, Equations (1) and (2) become

$$J_q = \frac{Q}{4\pi R^2} = -\lambda \frac{dT}{dr} - \rho_w D \beta \frac{d\theta}{dr}$$

$$= -L_{11} \frac{dT}{dr} - L_{12} \frac{d\theta}{dr} \qquad (3)$$

$$J_w = 0 \quad = -D \left(\frac{\beta^*}{T} \frac{dT}{dr} + \frac{d\theta}{dr}\right)$$

$$= L_{21} \frac{dT}{dr} + L_{22} \frac{d\theta}{dr} \qquad (4)$$

Equations (3) and (4) can be solved for the gradients of temperature and moisture content to give

$$\frac{dT}{dr} = \frac{L_{22} Q}{4\pi r^2 (L_{21}L_{12} - L_{11}L_{22})} \qquad (5)$$

$$\frac{d\theta}{dr} = \frac{L_{21} Q}{4\pi r^2 (L_{11}L_{22} - L_{21}L_{12})} \qquad (6)$$

For a known heat transfer rate Q, and initial conditions of T and θ at the boundary, Equations (5) and (6) can be integrated to predict temperature and moisture content profiles for a closed system if the phenomenological coefficients (L_{ij}) are known.

EXPERIMENT

A spherically symmetric porous media system was studied. The media (nominal 250 μ spherical glass beads, water and air) was contained in the annular space between a 30.48 cm ID, 0.47 cm thick copper sphere and a 10.0 cm OD, internally heated, copper sphere which was centered inside the outer sphere. Details of the inner and outer sphere assembly and porous media loading procedure are given in Parikh's dissertation (4). An electrical resistance heater imbedded in the inner sphere provided steady heat flows through the annular porous media of 1.5×10^5 cal/day to 3.0×10^5 cal/day in experiments described here.

Temperatures were measured with thermocouples at 1.25 cm intervals in the annular porous media, and moisture content was determined at 1.25 cm intervals by extraction of samples followed by gravimetric moisture determination. The details of the moisture content sample extraction equipment, reported previously by Moore (5), are given in Parikh's dissertation. Temperatures were also measured, with thermocouples, at the outer surface of the inner (heated) sphere, and the inner surface of the outer sphere. The sphere assembly was housed in a constant temperature air bath, which indirectly fixed the inner (R_1) and outer (R_2) temperatures for a given heater output. Figure 1 indicates the temperature boundary conditions thus measured.

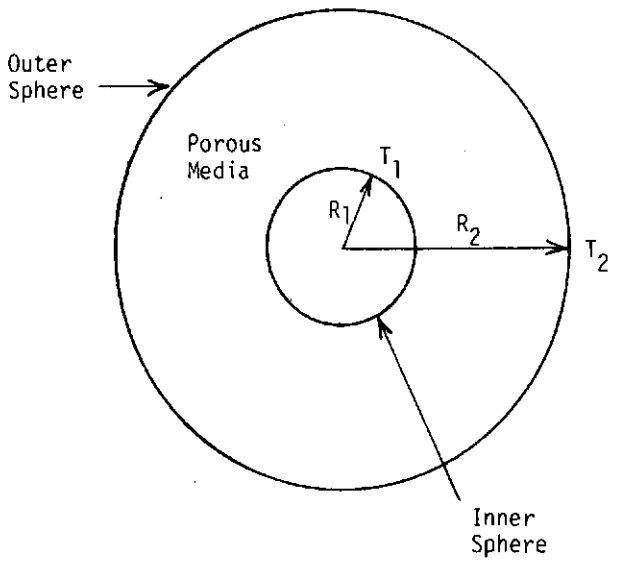

Figure 1. Spherical Porous Media System

An experimental run consisted of loading the annular region of the sphere assembly with glass beads of uniform (predetermined) moisture content, allowing the system to reach steady state at a given heater output, and measurement of temperature and moisture content distribution

as described above.

Determination of Phenomenological Coefficients

The phenomenological coefficients required are

$L_{11} = \lambda$ (thermal conductivity)

$L_{12} = \rho_w D \beta$ (cross coefficient relating moisture gradient to heat transfer)

$L_{21} = D \beta^*/T$ (cross coefficient relating temperature gradient to moisture transfer)

$L_{22} = D$ (diffusivity)

All of the phenomenological coefficients were assumed to be functions of moisture content only.

Thermal Conductivity. Thermal conductivity of the 250 μ glass bead-air-water media was determined as a function of moisture content using a transient method (6) which precluded moisture transfer effects. Figure 2 gives the measured thermal conductivity vs. moisture content.

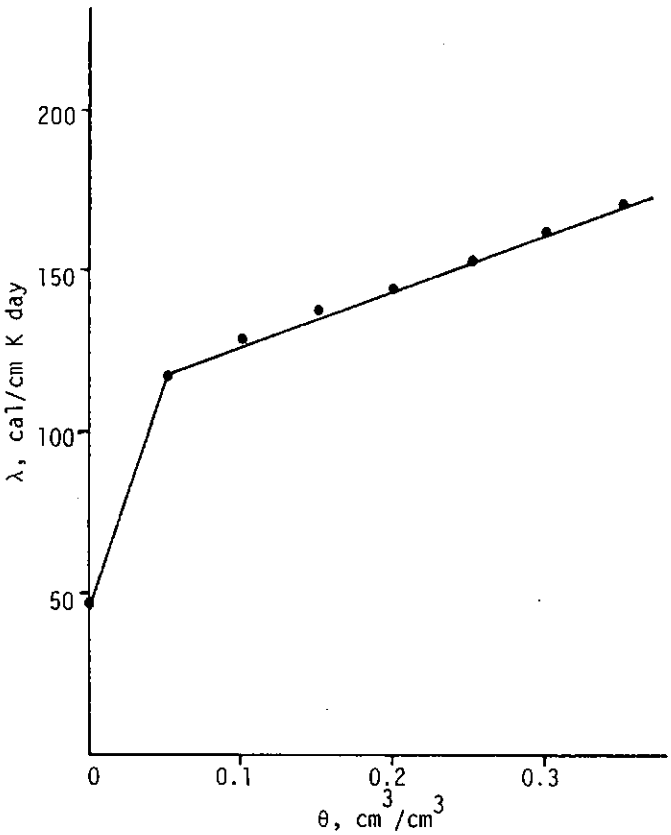

Figure 2. Thermal Conductivity vs. Moisture Content

Diffusivity. The diffusivity was determined as the product of the unsaturated hydraulic conductivity and the derivative of water potential with respect to moisture content ($D = K\, d\psi/d\theta$). The water retention curve, from which $d\psi/d\theta$ was determined graphically, was measured using the pressure plate method (7). The hydraulic conductivity was calculated as a function of moisture content using the method of Green and Corey (8) along with a value of the saturated hydraulic conductivity obtained in the laboratory assuming Darcy's Law. Figure 3 shows the diffusivity versus moisture content.

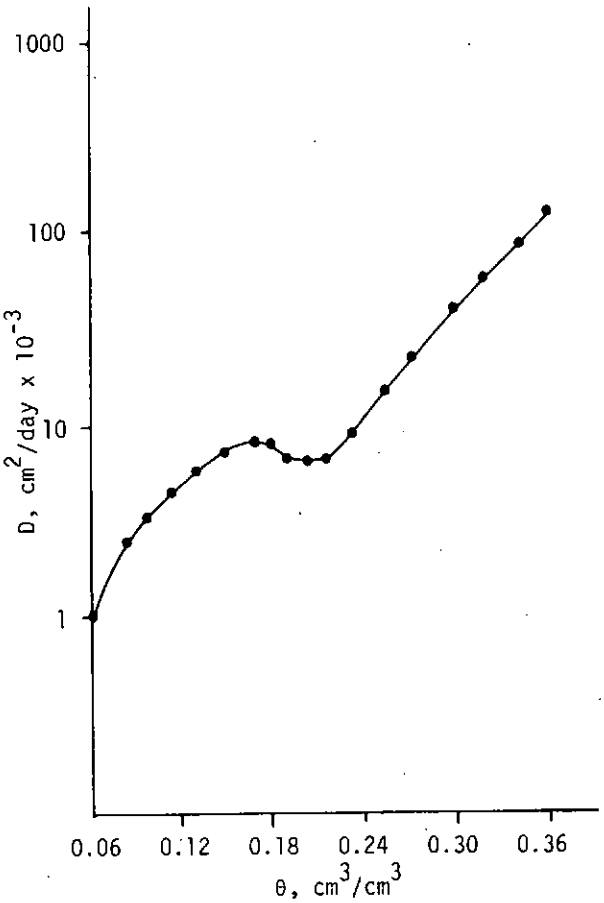

Figure 3. Diffusivity vs. Moisture Content

Cross Coefficients. β^*, which is defined as $\nabla\theta/\nabla \ln T$, was determined from steady-state temperature and moisture content profiles measured in the annulus of the sphere-porous media assembly described above. Figure 4 shows β^* as a function of moisture content determined with a heater output of 3.1×10^5 cal/day. The coefficient β, which is defined as $\nabla\psi/\nabla \ln T$ and incorporates Onsager's Relation, is shown in Figure 5 to be extremely small.

RESULTS AND DISCUSSION

Figure 6 shows the measured steady-state temperature and moisture content profiles in the annular porous media system obtained for a medium with initially uniform moisture content $\theta = 0.32$ and a heater output of 3.1×10^5 cal/day. Measurements were made along three different radii to check the expected spherical symmetry. The dotted lines represent 2D order

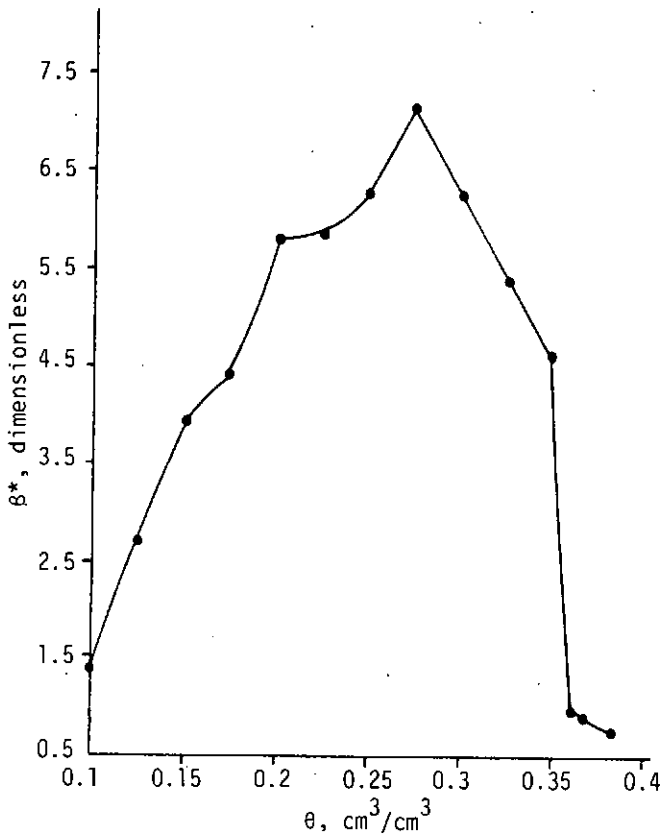

Figure 4. Coupling Coefficient β* vs. Moisture Content

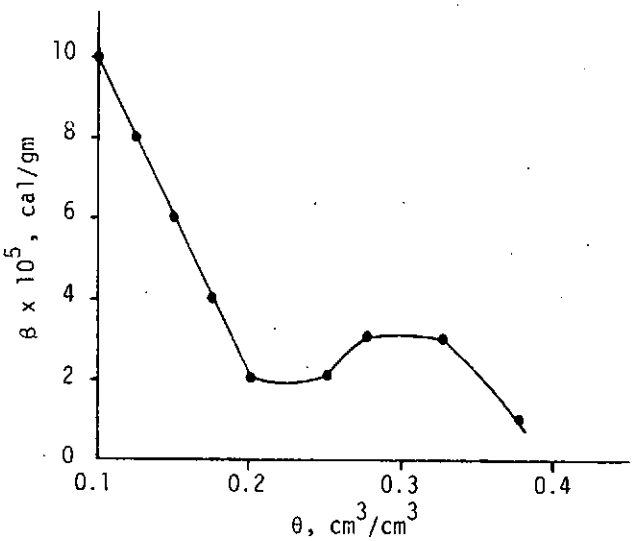

Figure 5. Coupling Coefficient β vs. Moisture Content

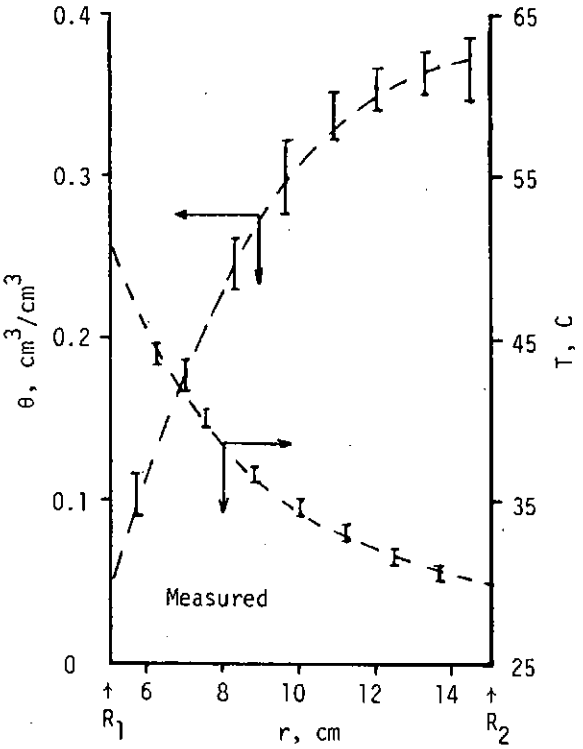

Figure 6. Temperature and Moisture Content Profiles for $Q = 3.1 \times 10^5$ cal/day, $\theta_I = 0.32$

polynomial least squares fits of the data. These curves were used to graphically determine values of $\nabla \ln T$ and $\nabla\theta$ which were then used to determine β^* as shown in Figure 4. It is an implicit assumption of the Irreversible Thermodynamics theory that β^* is not a function of the gradients in temperature or moisture content.

Using the phenomenological coefficients, including β^* and β as described above, Equations (5) and (6) were integrated to predict the moisture content and temperature profiles for other heater inputs and initial moisture contents as follows. Using the inside sphere (outer surface) temperature and an assumed moisture content, along with the heat flux as initial conditions, Equations (5) and (6) were simultaneously integrated to the outer radius R_2. The predicted moisture content profile thus obtained was integrated to get the corresponding total moisture content of the annular section. If the moisture content thus obtained was not equal to the amount of moisture initially loaded into the sphere assembly, the initial moisture content (θ_1 at $r = R_1$) was iterated until the predicted moisture profile satisfied the required mass balance. The resulting profiles were compared with measurements made for several runs at different initial moisture contents and heater outputs. General agreement was obtained as exemplified by the predicted vs. experimental results

shown in Figure 7 for an initial moisture content of $\theta = 0.3$ and a heater output of 1.58×10^5 cal/day.

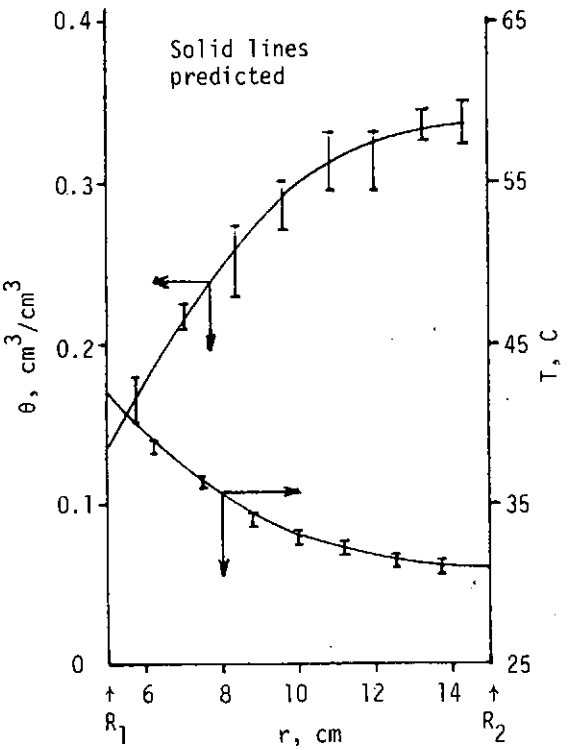

Figure 7. Temperature and Moisture Content Profiles for
$Q = 1.6 \times 10^5$ cal/day
$\theta_I = 0.30$

The range of initial moisture contents and heat fluxes was restricted in this study, so as to minimize vapor phase transfer, by keeping the moisture content above $\theta = 0.1$. It is not expected that the Taylor and Cary model would describe vapor phase moisture transfer. Within the restricted range of heat transfer studied the model appears to describe the redistribution of moisture in a closed system subjected to temperature gradients. The coupling coefficient β, which determines the effect of moisture content gradient on heat flux, is predicted to be extremely small. As a numerical check, the model equations were also solved assuming $\beta = 0$, and no change was observed in the predicted temperature and moisture content profiles. This constitutes an indirect verification of the Onsager Relation since the determination of β derives therefrom.

ACKNOWLEDGEMENTS

This work was supported in part with funds from the U.S. Department of Interior, Office of Water Research and Technology, under Public Law 88-375, as amended.

The use of equipment developed by Dr. N. Moore, the Jet Propulsion Laboratory, Pasadena, California, and Professor H. Wolf, Mechanical Engineering Department, University of Arkansas, is gratefully acknowledged.

REFERENCES

1. Taylor, S. A. and J. W. Cary, "Linear Equations for the Simultaneous Flow of Matter and Energy in a Continuous Soil System," SSSA Proceedings, 28: 167-172 (1964).
2. Gee, G. W., "Water Movement in Soils as Influenced by Temperature Gradients," Ph.D. Thesis, Washington State University, Pullman (1966).
3. Jury, W. A., "Simultaneous Transport of Heat and Moisture through a Medium Sand," Ph.D. Thesis, University of Wisconsin, Madison (1973).
4. Parikh, R. J., "An Analysis of the Irreversible Thermodynamics Model for Coupled Heat and Moisture Transport Phenomena in Unsaturated Porous Media," Ph.D. Thesis, University of Arkansas, Fayetteville (1979).
5. Moore, N. R., Jr., "Simultaneous Heat and Mass Transfer in Moist Porous Media," Research Report Series--No. 16, Engineering Experiment Station, University of Arkansas, Fayetteville (1972).
6. Parikh, R. J., J. A. Havens, and H. D. Scott, "Thermal Diffusivity and Conductivity of Moist Porous Media," SSSA Journal, 43: 1050-1052 (1979).
7. Hillel, D., "Soil and Water, Physical Principles and Processes," Academic Press, New York (1971).
8. Green, R. E. and J. C. Corey, "Calculation of Hydraulic Conductivity: A Further Evaluation of Some Predictive Methods," SSSA Proceedings, 35: 3-8 (1971).

AN APPROXIMATE METHOD FOR DETERMINATION OF THE SUBLIMATION LIMIT IN SIMPLE GEOMETRICAL POROUS BODIES

S. Lin[1]
Y.Y. Lin[2]
C.L. Wang[3]

1. Concordia University, Montreal, Que., H3G 1M8
2. Concordia University, Montreal, Que., H3G 1M8
3. University of Regina, Regina, Sask., S4S 0A2

ABSTRACT

Sublimation of frozen moisture in porous bodies having a plane plate, a cylindrical or a spherical form, is investigated. Initially the porous body is at a uniform sublimation temperature. The investigation is concentrated on the temperature and moisture distributions in the vapour region. The quasi-steady-state approximation is used to determine the temperature and moisture distributions as well as the location of the moving sublimation front. By making use of a position coordinate transformation, the temperature distribution, as well as the moisture distribution, is expressed in a unique form for the three different geometrical bodies. At the moving sublimation front, there is a discontinuity of the moisture content. The upper limit of the sublimation process is determined.

NOMENCLATURE

a = thermal dissusivity

a_m = moisture dissusivity

h = heat transfer coefficient

k = thermal conductivity

L = latent heat of sublimation

Lu = Luikov number defined by equation (31)

n = characteristic number, defined in Eqs. (1),(2)

Pn = Posnov number defined by equation (32)

R = dimensionless position coordinate defined by equation (27)

s = position of sublimation front

S = transformed position of sublimation front defined by equation (12)

t = time

T = temperature

T_v = sublimation temperature

T_∞ = temperature of hot fluid

u = moisture content (kg of moisture/kg of dry porous medium)

u_o = moisture content in frozen region

u_s = moisture content at the surface $x = x_o$

U = dimensionless moisture content defined by equation (35)

x = position coordinate

x_o = position through which heat is supplied

y = transformed position coordinate defined by equation (11)

Z = dimensionless position of sublimation front defined by equation (28)

Z_o = dimensionless surface position defined by equation (41)

δ = thermal gradient coefficient

θ = dimensionless temperature defined by equation (26)

ν = dimensionless latent heat of sublimation defined by equation (33)

ρ_p = density of dry porous medium

τ = dimensionless time defined by equation (37)

INTRODUCTION

Sublimation of frozen moisture in a porous medium has wide applications, such as separation processes, food technology, etc. An increase in the temperature above the sublimation point of moisture builds a moving sublimation front in a porous medium. The location of the moving front is unknown and has to be determined as a part of the solution. The coupled heat and mass transfer problems with moving phase front are nonlinear and solutions involve considerable mathematical difficulties. Exact solutions of such problems are limited to only a few idealized situations [1,2,3,4].

The sublimation problem considered in [4] is limited for the case that the coupled heat and mass transfer take place in a porous half-space with its heating surface maintaining at a constant temperature. In the present study, sublimation processes taking place in porous bodies having a plane plate, a cylindrical or a spherical form, are considered, and a more general boundary condition with convective heat transfer is used.

In order to obtain an analytical solution and to illustrate the parameters of significance for the sublimation process and how these parameters interact, the quasi-steady-state approximation is used to determine the temperature and moisture content distributions as well as the position of the moving sublimation front.

In the sublimation process, the moving sublimation front separates the vapour region from the frozen region in the porous body. In the vapour region, the temperature gradient is in the opposite direction to the moisture content gradient, and creates an effect to prevent the moisture diffusing away from the vapour-solid interface. Therefore, there is a limitation for the heating process. Over a certain value of heat supply, the sublimation front moves so fast that the moisture is unable to diffuse away from the sublimation front. It results in an increase of pressure, and a liquid phase will be formed at the phase front. For such a case, the sublimation process stops. One of the subjects of the present study is to determine the condition for the limitation of the sublimation process.

MATHEMATICAL FORMULATION

Consider a frozen humid porous body having a plane plate, a cylindrical or a spherical form, which is initially at a uniform moisture content u_o and a uniform sublimation temperature T_v. The porous body is sublimated by maintaining the surface at $x = x_o$ at a constant moisture content u_s and by supplying heat at $x = x_o$ from a hot flowing fluid having a temperature T_∞ which is higher than the sublimation temperature T_v. For analysis the following assumptions are made:

1. In the frozen region $0<x<s(t)$, there is no moisture movement, where $x = s(t)$ locates the sublimation front. In the vapour region $s(t)<x<x_o$, there are coupled heat and moisture flows.
2. The convective terms in the vapour region are small and may be neglected.
3. The pressure in the porous body during the sublimation process is constant.
4. The material properties remain constant.

The following differential equations describing the heat and moisture transfer in the vapour region can be obtained from the Luikov system [5] for the case $\varepsilon = 0$:

$$\frac{\partial T}{\partial t} = a \left(\frac{\partial^2 T}{\partial x^2} + \frac{n}{x} \frac{\partial T}{\partial x} \right) \quad , \quad s(t)<x<x_o \tag{1}$$

$$\frac{\partial u}{\partial t} = a_m \left(\frac{\partial^2 u}{\partial x^2} + \frac{n}{x} \frac{\partial u}{\partial x} \right) + a_m \delta \left(\frac{\partial^2 T}{\partial x^2} + \frac{n \partial T}{x \partial x} \right), \quad s(t)<x<x_o \tag{2}$$

with $n = 0$ for the plate, $n = 1$ for the cylindrical, and $n = 2$ for the spherical body. The initial condition for the vapour region can be described as

$$s(t = o) = x_o \tag{3}$$

The boundary conditions at the surface $x = x_o$, through which heat is supplied and moisture is removed, are as follows:

$$k \frac{\partial T(x_o,t)}{\partial x} = h \left[T_\infty - T(x_o,t) \right] \tag{4}$$

$$u(x_o,t) = u_s \tag{5}$$

On the sublimation front, the temperature is equal to the sublimation temperature

$$T(s,t) = T_v \tag{6}$$

The heat and moisture mass balance at the sublimation front can be expressed as

$$-k \frac{\partial T(s,t)}{\partial x} = u_o \rho_p L \frac{ds(t)}{dt}$$

$$a_m \left[\frac{\partial u(s,t)}{\partial x} + \delta \frac{\partial T(s,t)}{\partial x} \right] = \left[u_o - u(s,t) \right] \frac{ds(t)}{dt} \tag{8}$$

THE QUASI-STEADY-STATE APPROXIMATION

In the quasi-steady-state approximation, the temperature and moisture content distributions in the vapour region are assumed to be instantaneously in steady states. Under this assumption, the differential equations, Eqs. (1) and (2), become

$$\frac{\partial^2 T}{\partial x^2} + \frac{n}{x} \frac{\partial T}{\partial x} = o \quad , \quad s(t)<x<x_o \tag{9}$$

and

$$\frac{\partial^2 u}{\partial x^2} + \frac{n}{x} \frac{\partial u}{\partial x} = o \quad , \quad s(t)<x<x_o \tag{10}$$

In order to obtain a unique solution for the plate ($n = 0$), the cylindrical ($n = 1$), and the spherical ($n = 2$) problems, the following position coordinate transformation is introduced:

$$y = x_o^n \int_{x_o}^{x} \frac{dr}{r^n} \tag{11}$$

The position of the sublimation front s is similarly transformed by

$$S = x_o^n \int_{x_o}^{s(t)} \frac{dr}{r^n} \tag{12}$$

With these transformations, we obtain from Eqs. (9), (10) and (3) to (8) a new system of equations in y-t coordinate system:

$$\frac{\partial^2 T}{\partial y^2} = o \quad , \quad S(t)<y<o \tag{13}$$

$$\frac{\partial^2 u}{\partial y^2} = o \quad , \quad S(t)<y<o \tag{14}$$

$$S(t = o) = o \tag{15}$$

$$k \frac{\partial T(o,t)}{\partial y} = h \left[T_\infty - T(o,t) \right] \tag{16}$$

$$u(o,t) = u_s \tag{17}$$

$$T(S,t) = T_v \tag{18}$$

$$-k \frac{\partial T(S,t)}{\partial y} = u_o \rho_p L \left(\frac{s(t)}{x_o}\right)^{2n} \frac{dS(t)}{dt} \tag{19}$$

$$a_m \left[\frac{\partial u(S,t)}{\partial y} + \delta \frac{\partial T(S,t)}{\partial y}\right] = \left[u_o - u(S,t)\right] \left(\frac{s(t)}{x_o}\right)^{2n} \frac{dS(t)}{dt} \tag{20}$$

The solutions of Eqs. (13) and (14) can be expressed respectively as

$$T(y,t) = a + by \tag{21}$$

and $$u(y,t) = A + By \tag{22}$$

where a, b, A and B are functions of time, which have to be determined. By making use of Eqs. (16) and (18), a and b are obtained as follows

$$a = T_v - \frac{h(T_\infty - T_v)\, S(t)}{k - hS(t)} \tag{23}$$

and

$$b = \frac{h(T_\infty - T_v)}{k - hS(t)} \tag{24}$$

The temperature distribution, Eq. (21), can then be written in the following dimensionless form:

$$\theta = \frac{R - Z(t)}{1 - Z(t)} \tag{25}$$

where

$$\theta = \frac{T(y,t) - T_v}{T_\infty - T_v} \tag{26}$$

$$R = hy/k \tag{27}$$

and $$Z(t) = hS(t)/k \tag{28}$$

For the determination of A and B, Eqs. (17), (19) and (20) are used,

$$A = u_s \tag{29}$$

$$B = \frac{1 + Lu \cdot \nu \cdot Pn}{(1 + Lu \cdot \nu)\, Z(t) - Lu \cdot \nu} \left(u_o - u_s\right) \frac{h}{k} \tag{30}$$

where

$$Lu = \text{Luikov number} = \frac{a_m}{a} \tag{31}$$

$$Pn = \text{Posnov number} = \frac{(T_\infty - T_v)}{u_o - u_s} \delta \tag{32}$$

$$\nu = \frac{a\, u_o\, \rho_p\, L}{k(T_\infty - T_v)} \tag{33}$$

The moisture content distribution, Eq. (22), is then expressed in the dimensionless form.

$$U = \frac{1 + Lu \cdot \nu \cdot Pn}{(1 + Lu \cdot \nu)\, Z(t) - Lu \cdot \nu} R \tag{34}$$

where

$$U = \frac{u(y,t) - u_s}{u_o - u_s} \tag{35}$$

In Eqs. (25) and (34), Z(t) is the dimensionless location of the moving sublimation front which is unknown and has to be determined from Eq. (19). Substituting Eq. (25) into Eq. (19) we obtain

$$\left(\frac{s(t)}{x_o}\right)^{2n} \frac{dZ}{d\tau} = - \frac{1}{\nu(1 - Z)} \tag{36}$$

with

$$\tau = \left(\frac{h}{k}\right)^2 a\, t \tag{37}$$

Because the characteristic number n appears in Eq. (36), the value of Z has to be determined separately for the plate, the cylindrical, and the spherical bodies. For the purpose of integrating Eq. (36), the factor $(s/x_o)^{2n}$ is expressed in terms of Z, following the definition equation, Eq. (12), as follows:

$$\text{for } n = 0: \quad \left(\frac{s}{x_o}\right)^{2n} = 1 \tag{38}$$

$$\text{for } n = 1: \quad \left(\frac{s}{x_o}\right)^{2n} = e^{2S/x_o} = e^{2Z/Z_o} \tag{39}$$

and

$$\text{for } n = 2: \quad \left(\frac{s}{x_o}\right)^{2n} = \frac{1}{(1 - S/x_o)^4} = \frac{1}{(1 - Z/Z_o)^4} \tag{40}$$

$$\text{where } Z_o = \frac{h x_o}{k} \tag{41}$$

Integrating Eq. (36) and utilizing the initial condition, Eq. (15), we obtain the following results after the back transformation from Eq. (12):

$$\text{for } n = 0, \quad \frac{h(x_o - s)}{k} = \sqrt{2\tau/\nu + 1} - 1 \tag{42}$$

$$\text{for } n = 1, \quad \tau/\nu = \frac{Z_o(2 + Z_o)}{4} \left[1 + \left(\frac{2Z_o}{2 + Z_o} \ln \frac{s}{x_o} - 1\right) \cdot \left(\frac{s}{x_o}\right)^2\right] \tag{43}$$

and for n = 2,

$$\tau/\nu = \frac{Z_o(1 - Z_o)}{3} \left[1 - \left(\frac{s}{x_o}\right)^3\right] + \frac{Z_o}{2} \left[1 - \left(\frac{s}{x_o}\right)^2\right] \tag{44}$$

Figure 1 represents the relationship between hs/k and τ/ν with $x_o = 0$ from Eq. (42). Figures 2 and 3 represent the relationship between s/x_o and τ/ν with Z_o as a parameter from Eqs. (43) and

(44) respectively.

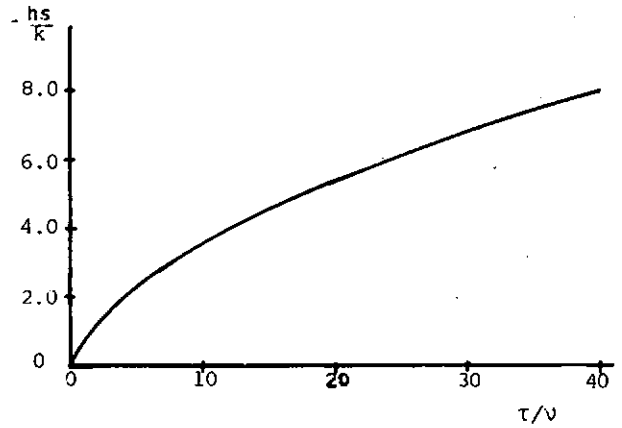

Figure 1 hs/k as a function of τ/ν with $x_o = 0$ for sublimation process taking place in a plane porous plate (n = 0).

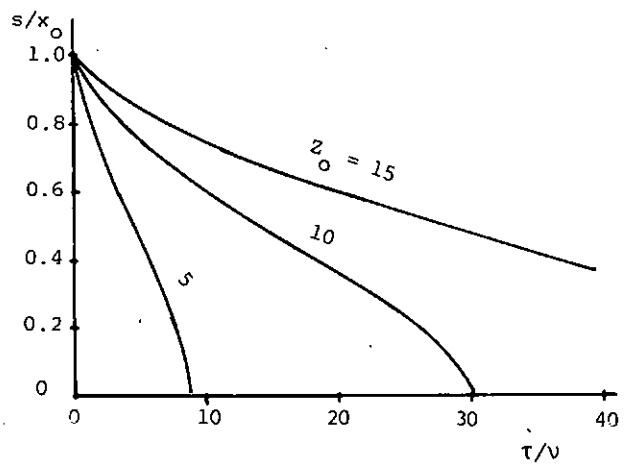

Figure 2 s/x_o as a function of τ/ν with Z_o as a parameter for sublimation process taking place in a cylindrical porous body (n=1).

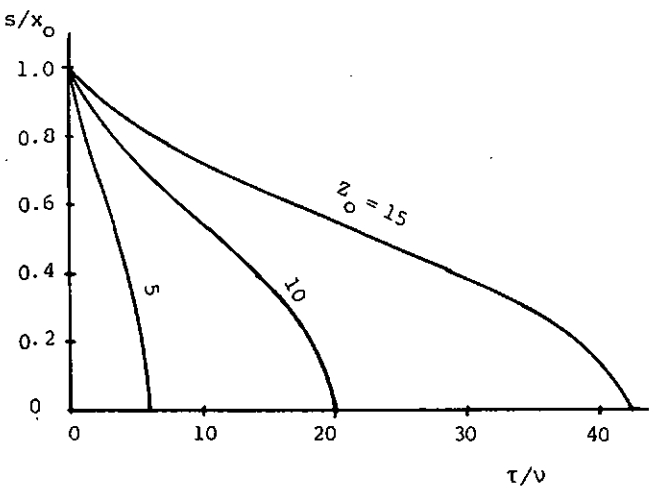

Figure 3 s/x_o as a function of τ/ν with Z_o as a parameter for sublimation process taking place in a spherial porous body (n=2).

MOISTURE CONTENT AT THE SUBLIMATION FRONT

In the sublimation process, the moisture content in the solid phase is normally much higher than that in the vapour phase. Therefore, there exists a discontinuity of the moisture content at the sublimation front, which can be obtained from Eq. (34) by letting R = Z,

$$U_{R=Z} = \frac{1 + Lu\cdot\nu\cdot Pn}{1 + Lu\cdot\nu - (Lu\cdot\nu)/Z(t)} \qquad (45)$$

Figures 4 and 5 show the dimensionless moisture content at the sublimation front, $U_{R=Z}$, as a function of Z with Pn and $Lu\cdot\nu$ as a parameter, respectively.

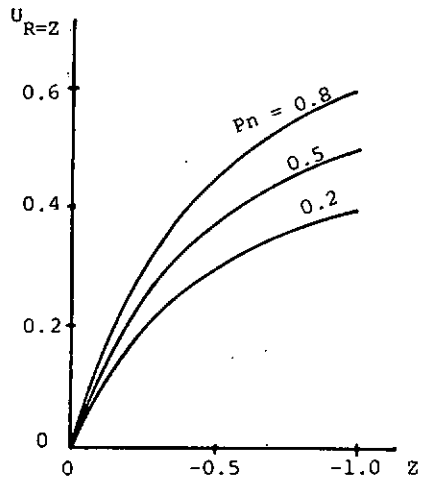

Figure 4 The dimensionless moisture content at the sublimation front, $U_{R=Z}$, as a function of Z with Pn as a parameter for $Lu\cdot\nu = 1.0$.

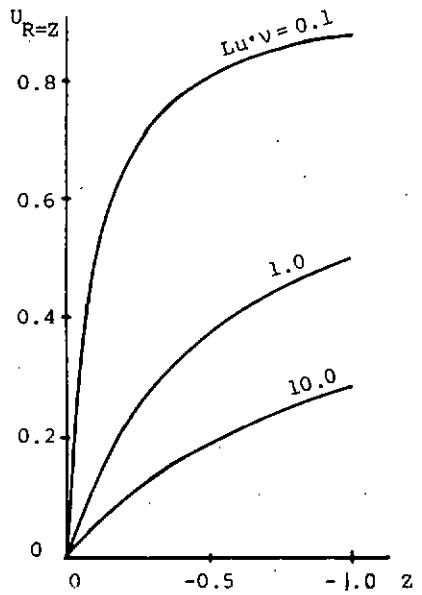

Figure 5 The dimensionless moisture content at the sublimation front, $U_{R=Z}$, as a function of Z with $Lu\cdot\nu$ as a parameter for Pn = 0.5.

Following the definition of the dimensionless moisture content, Eq. (35), U has a maximum value of one at R = Z or y = S. Therefore there is no sublimation process, when $U_{R=Z} > 1$. From Eq. (45) with Z(t) = hS(t)/k, the condition for no sublimation process can be expressed as

$$Pn > 1 - \frac{1}{hS(t)} \qquad (46)$$

For the case of the heat transfer coefficient h approaching infinite, the boundary condition at the heating surface ($x = x_o$) reduces to one that the surface temperature remains constant. Under this condition, the limitation of the sublimation process can be written as,

$$Pn_{max} = 1 \qquad (47)$$

which is identical with that given in [4] for the upper limit condition of the sublimation process.

DISCUSSION AND CONCLUSIONS

By making use of the position coordinate transformation, Eqs. (11) and (12), the temperature distribution, Eq. (25), and the moisture content distribution, Eq. (34), are expressed in unique relations for the sublimation process taking place in porous bodies having a plane plate (n = 0), a cylindrical (n = 1), or a spherical (n = 2) form. However, the location of the moving sublimation front is dependent on the geometry of the porous bodies as shown in Figures 1, 2 and 3 for n = 0, 1 and 2, respectively.

The parameter ν represents the dimensionless heat of sublimation. A larger heat of sublimation ν yields slower the sublimation process. It results in a longer time required for sublimating a fixed layer from a frozen humid porous body. From the quasi-steady-state approximation, it is shown that only the ratio, τ/ν, has an effect on the location of the moving sublimation front. The larger the ratio of τ/ν, the deeper is the propagation of the sublimation front as showen in Figures 1, 2, and 3. For a plane porous plate, the location of the moving sublimation front is only a function of the ratio τ/ν. For a cylindrical or spherical porous body, because of the change of the cross-section area, a parameter Z_o has therefore an effect on the rate of the moving sublimation front. Because Z_o represents the dimensionless diameter of the porous body, the larger the value of Z_o, the time required for sublimation is therefore longer.

The dimensionless moisture content in the vapour region, described by Eq. (34), has two parameters Pn and $Lu \cdot \nu$. The Posnov number, Pn, represents the ratio of the overall thermal potential effect on the moisture diffusion to the overall moisture potential. In the sublimating process, the temperature gradient in the vapour region is in the opposite direction to the moisture content gradient, and creates an effect to prevent the moisture diffusing away from the vapour-solid interface. Therefore the higher the value of Pn, the higher is the moisture gradient (or the higher is the value of the moisture content at the sublimation front obtained from the quasi-steady-state approximation) required to diffuse the moisture away from the phase front. This phenomenon is shown in Figure 4. The Luikov number, Lu, represents the ratio of the moisture diffusivity to the thermal diffusivity in the vapour region. The higher the value of Lu, the higher is the capability of the moisture diffusing away from the sublimation front. The parameter ν, as described above, represents the dimensionless heat of sublimation. The higher the value of ν, the slower is the sublimation process, or the smaller is the rate of the vapour moisture produced at the sublimation front. From the quasi-steady-state approximation, only the product of these two parameters, $Lu \cdot \nu$, has a common effect on the moisture content as shown in Eq. (34). Figure 5 shows the effect of the product $Lu \cdot \nu$ on the moisture content at the sublimation front.

The moisture content gradient at the sublimation front calculated from the quasi-steady-state approximation is larger than that in the real case. This means that, with the quasi-steady-state solution, the amount of moisture diffusing away from the sublimation front is more than the real amount of moisture which can diffuse. Therefore, Eq. (46) represents only the upper limit condition of the sublimation process.

ACKNOWLEDGEMENT

The present work is being supported by the Natural Sciences and Engineering Research Council of Canada under grant No. A7929.

REFERENCES

1. Cho, S.H., An Exact Solution of the Coupled Phase Change Problem in a Porous Medium, Int. J. Heat Mass Transfer, Vol. 18, pp. 1139-1142 1975.
2. Mikhailov, M.D., Exact Solution of Temperature and Moisture Distributions in a Porous Half-Space with Moving Evaporation Front, Int. J. Heat Mass Transfer, Vol. 18, pp. 797-804, 1975.
3. Mikhailov, M.D., Exact Solution for Freezing of Humid Porous Half-Space, Int. J. Heat Mass Transfer, Vol. 19, pp. 651-655, 1976.
4. Lin, S., An Exact Solution of the Sublimation Problem with Coupled Heat and Mass Transfer in a Porous Medium, Submitted to J. of Heat Transfer.
5. Luikov, A.V., Systems of Differential Equations of Heat and Mass Transfer in Capillary-Porous Bodies, Int. J. Heat Mass Transfer, Vol. 18, pp. 1-14, 1975.

MECHANICS AND THERMODYNAMICS OF DRYING
A SUMMARY

M.J. Lampinen

Valmet Oy Pansio Works, Turku, Finland

ABSTRACT

A short summary of a general theory of mechanics and thermodynamics of drying is presented. New results derived from the entropy equation are presented, the most important of which are the vapor pressure equation for hygroscopically bound water, and the shrinking pressure and capillary pressure equations. It is shown that the vapor pressure equation can be regarded as a generalization of Clausius-Claperon's equation as well as of so-called Kelvin's equation. New equations are presented for the resistance forces which appear between solid, liquid and gas phases in porous materials. It turns out that these equations include Fick's and Darcy's equations as special cases. Some examples illustrating the applications of these equations are presented.

NOMENCLATURE

$a^{(1)}$ = surface area of the 1-β interface per unit mass of constituent 1, m^2/kg

$a^{2'}$ = surface area of the 2-β interface per unit mass of constituent 2, m^2/kg

$a^{2''}$ = surface area of the 1-2 interface per unit mass of constituent 2, m^2/kg

$a^{(2)}$ = see $f_2^s a^{(2)}$, $h_2^s a^{(2)}$, $\varepsilon_2^s a^{(2)}$, $\mu_2^s a^{(2)}$

$c_\alpha = \rho_\alpha/\rho$, mass fraction of constituent α

D_{34} = diffusion coefficient, m^2/s

d_α = real density of constituent α, kg/m^3

f_1^s = Helmholtz free energy of surface $a^{(1)}$, J/m^2

$f_{2'}^s$ = Helmholtz free energy of surface $a^{2'}$, J/m^2

$f_{2''}^s$ = Helmholtz free energy of surface $a^{2''}$, J/m^2

$f_2^s a^{(2)} = f_{2'}^s a^{2'} + f_{2''}^s a^{2''}$, J/kg

$\bar{g}$, g_i = acceleration due to gravity, $9.82\ m/s^2$

$h_\alpha = \varepsilon_\alpha + p^{(\alpha)} v^{(\alpha)}$, enthalpy of constituent α, J/kg

$h_2^s a^{(2)} = h_{2'}^s a^{2'} + h_{2''}^s a^{2''}$, J/kg

I_α = strength of the mass source or sink of constituent α, $kg/m^3 s$

k_β = permeability of humid air - moist solid, m^2

l_0 = heat of vaporization of free water, J/kg

l = heat of vaporization of hygroscopically bound water, J/kg

M_α = molar mass of constituent α, kg/kmol

$\bar{m}_\alpha$, m_i^α = resistance body force per unit mass of the mixture, N/kg

$p^{(\alpha)}$ = real pressure of constituent α, N/m^2

$p_\alpha = \phi_\alpha p^{(\alpha)}$, partial pressure (pressure contribution) of constituent α in the mixture, N/m^2

$p_0^{(\alpha)}$ = equilibrium real pressure of constituent α, N/m^2

$p_v^{(\alpha)}$ = vortex pressure, N/m^2

R = gas constant, $8.314 \cdot 10^3$ J/kmol

s_1^s = entropy of surface $a^{(1)}$, J/m^2K

$s_{2'}^s$ = entropy of surface $a^{2'}$, J/m^2K

$s_{2''}^s$ = entropy of surface $a^{2''}$, J/m^2K

T = temperature, K

t = time, s

$\bar{t}_\alpha$, t_{ij}^α = stress tensor of constituent α, N/m^2

$\bar{u}_\alpha$, u_i^α = diffusion velocity of constituent α with respect to the mass-averaged velocity $\bar{v}$, m/s

$u_Y = \rho_2/\rho_1$, moisture content

$v^{(\alpha)} = 1/d_\alpha$, specific volume of constituent α, m^3/kg

$\bar{v}_\alpha$, v_i^α = velocity of constituent α, m/s

$\bar{v}$, v_i = barycentric velocity of the mixture, $\bar{v} = \sum_{\alpha=1}^{4} c_\alpha \bar{v}_\alpha$, m/s

$\bar{x}$, x_i = position vector, rectangular coordinate system, m

$\alpha_{12}, \ldots, \alpha_{\beta 2}$ = hydraulic resistances, $1/m^2$

α_{34}, α_{43} = hydraulic resistances, $1/m^2$

$\bar{\Gamma}_\alpha$, Γ_i^α = vorticity moment density vector, Nm/kg

ε_α = specific internal energy of constituent α, J/kg

$\varepsilon_1^s = h_1^s$, internal energy of surface $a^{(1)}$, J/m^2

$\varepsilon_{2'}^s = h_{2'}^s$, internal energy of surface $a^{2'}$, J/m^2

$\varepsilon_{2''}^s = h_{2''}^s$, internal energy of surface $a^{2''}$, J/m^2

η_α = dynamic viscosity of constituent α, kg/ms

$\bar{\kappa}_\alpha$, κ_i^α = coefficients, defined by (1)

$\mu_\alpha = h_\alpha - Ts_\alpha$, chemical potential of constituent α, J/kg

$\mu^s_{2a^{(2)}} = \mu^s_{2,}a^{2'} + \mu^s_{2,,}a^{2''}$, J/kg

$\nu_\alpha = \eta_\alpha/d_\alpha$, kinematic viscocity of constituent α, m^2/s

ρ_α = partial density of constituent α, kg/m^3

$\rho = \sum_{\alpha=1}^{4} \rho_\alpha$, density of the mixture, kg/m^3

$\phi_\alpha = \rho_\alpha/d_\alpha$, volume fraction of constituent α

ψ = relative vapor pressure

$\bar{\Omega}_\alpha$, Ω^α_i = vorticity vector, 1/s

Sub- and superscripts

α = 1, solid phase
= 2, water
= 3, water vapor
= 4, dry air
= β, humid air

s denotes surface quantities

SOME CONCEPTS AND DEFINITIONS

Porous materials capable of binding water are here termed hygroscopic. The hygroscopic material consists of four components: solid material (α = 1), liquid water (α = 2), water vapor (α = 3), and dry air (α = 4). Often, however, we prefer to regard the mixture as being composed of three components: solid material, liquid water and humid air (α = β). The humid air is, of course, a mixture of the components α = 3 and α = 4.

The balance equations are formulated using the twice continuously differentiable density functions, for example $\rho_\alpha(x,t)$ is the partial density on constituent α in the mixture at place x and time t ($\rho_\alpha = dm_\alpha / dV$, where dm_α is the mass of constituent α in a volume dV of the mixture). In "normal" drying problems it is usually enough to formulate the initial state in such a way that the mixture is homogeneous (during the drying process it is, of course, no longer homogeneous). However, in contact drying, where the solid is pressed against a hot surface, it might be better to distribute the mass of the solid according to the results of surface profile measurements. This is illustrated by Figure 1. In this way we get a more realistic picture of contact drying and the boundary condition of temperature becomes clear, i.e. $T(x=0) = T_\beta$ = temperature of the hot surface (the heat transfer "coefficient" between the solid and the hot surface, which is difficult to determine, is not then needed).

After the initial state is given, the task of the drying theory is to describe the motions of constituents and the temperature field $T(\underline{x},t)$, which is assumed to be the same for all constituents at the same place x.

The main concepts used in the theory (1) are the partial density $\rho_\alpha(\underline{x},t)$ described above, the "real" density $d_\alpha(\underline{x},t)$ (= dm_α/dV_α, where the real volume

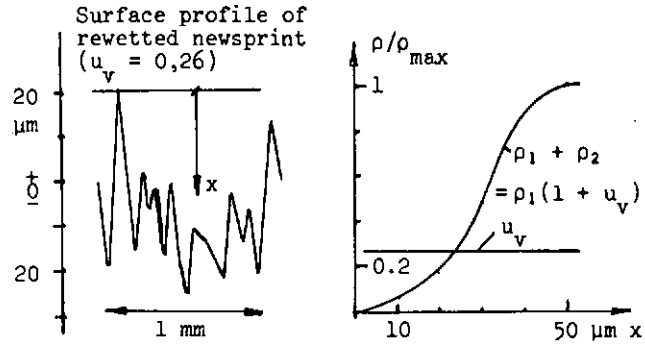

Figure 1 Distribution of the masses of the components (initial state)

occupied by dm_α is dV_α), the velocity $\bar{v}_\alpha(\underline{x},t)$ and the stress tensor $\underline{t}_\alpha(x,\underline{t})$. Hereafter we omit to mark the dependence of x and t unless necessary.

The volume fraction of constituent α is defined by an equation $\phi_\alpha \equiv \rho_\alpha/d_\alpha$. It is easy to verify that ϕ_α can also be interpreted as a volume part or as a perforated part of the total cross-section of the mixture. It is also immediately observed that $\phi_1 + \phi_2 + \phi_\beta = 1$ and $\phi_3 = \phi_4 = \phi_\beta$. Instead of the variable ϕ_2 we may also use the moisture content u_v, which is defined by $u_v \equiv \rho_2/\rho_1$. Hence the connection between the variables ϕ_2 and u_v is $u_v = (d_2/d_1)(\phi_2/\phi_1)$. The theoretical considerations become easier when we use the variable ϕ_2 instead of u_v, whereas in practical calculations u_v may be more convenient. Figure 2 shows the volume fractions at various moisture contents for timber.

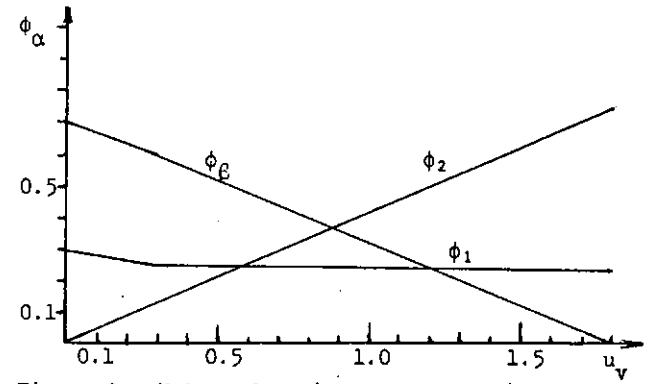

Figure 2 Volume fractions as a function of moisture content for a pine wood (T = 293 K)

Since our aim is to follow the movements of components and above all the removal of water, it is obvious that the balance equations should be considered in such a way that the role of components is central. Therefore, all the balance equations: mass, momentum, angular momentum, energy and entropy balances are formulated for each constituent of the mixture. The corresponding mixture balances are then obtained by summing over components.

When the moisture content of the material decreases, an increasing part of the water is located at the water - solid and water - air interfaces. Since this surface water is different from

normal water, it follows that at lower moisture contents the water as a whole has exceptional properties which have to be taken into account. These exceptional properties are decribed by surface functions or correction functions, as we may also call them. For instance, let ut consider the internal energy of the mixture (ε_K) in the equilibrium state. If the surfaces did not affect the internal energies, then $\varepsilon_K = c_1\varepsilon_1 + c_2\varepsilon_2 + c_\beta\varepsilon_\beta$ where $\varepsilon_\alpha(\alpha=1,2,\beta)$ are the usual "free state" internal energies of constituents. However, the surfaces affect the values of internal energies and, to get correct results, and still using the "simple" functions ε_α, we have introduced the correction functions $\varepsilon^s_{1a}{}^{(1)}$ and $\varepsilon^s_{2a}{}^{(2)}$ so that $\varepsilon_K = c_1(\varepsilon_1 + \varepsilon^s_{1a}{}^{(1)}) + c_2(\varepsilon_2 + \varepsilon^s_{2a}{}^{(2)}) + c_\beta\varepsilon_\beta$ is valid. In a similar way surface entropies have been introduced. We have regarded the surface internal energies and enthalpies as equal concepts since the surfaces "do not occupy any volume", i.e. $h^s_\alpha{}^{(\alpha)} \equiv \varepsilon^s_\alpha{}^{(\alpha)}$. The natural definition of the surface chemical potential is $\mu^s_\alpha{}^{(\alpha)} \equiv h^s_\alpha{}^{(\alpha)} - Ts^s_\alpha{}^{(\alpha)}$ and since $h^s_\alpha{}^{(\alpha)} \equiv \varepsilon^s_\alpha{}^{(\alpha)}$, we may also write $\mu^{s\alpha}_\alpha{}^{(\alpha)} \equiv f^s_\alpha{}^{(\alpha)}$.

A MECHANICAL VIEWPOINT OF CAPILLARY FLOW

By the capillary flow we man the flow of fluid in general when the interface is moving at the same time. It has been shown that the movement of the water - air interface on the surface of a solid may be compared with a rolling motion and hence the angular momentum equation is needed in capillary flow analysis (Ch. 13, (1)). Let us consider an advancing capillary flow in a tube. Due to the viscosity, the velocity profile behind the interface (sufficiently far from it) is not uniform; for example in laminar flow the velocity profile is parabolic, so that in the middle of the tube the velocity is higher than the mean velocity (in the laminar case twice as high). But the mean velocity is the same as the advancing velocity of the interface so that the water particles flowing in the middle of the tube behind the interface would sooner or later go "through" the interface if their streak lines were not curved. Hence behind the interface the flow is rotational, which will cause a force effect against the water - air surface which can be seen from the changes in the curvature of the surface. To describe the growth term in rotational momentum the following constitutive equation is suggested (Ch. 13, (1)):

$$\rho\Gamma^\alpha_i = -\eta_\alpha\kappa^\alpha_i\frac{d\phi_\alpha}{dt} \quad (\alpha = 1,2,\beta) \tag{1}$$

where the dimensionless coefficients κ^α_i (i = 1,2,3) depend on the volume fractions ϕ_1 and ϕ_2, and they describe the "direction" of the angular velocity (or rolling rate) $d\phi_\alpha/dt$.

ENTROPY BALANCE

The entropy balance equation plays a central role in obtaining many important results, among which are the following (Ch. 15, 16, (1)):

$$\mu_3 + \frac{u_3{}^2}{2} = \mu_2 + \frac{u_2{}^2}{2} + \mu^s_{2a}{}^{(2)} \tag{2}$$

$$p^{(\beta)} - p^{(1)} = (p_v^{(\beta)} - p_v^{(1)}) - \rho_1\frac{\partial(f^s_{1a}{}^{(1)})}{\partial\phi_1} - \rho_2\frac{\partial(f^s_{2a}{}^{(2)})}{\partial\phi_1} \tag{3}$$

$$p^{(\beta)} - p^{(2)} = (p_v^{(\beta)} - p_v^{(2)}) - \rho_1\frac{\partial(f^s_{1a}{}^{(1)})}{\partial\phi_2} - \rho_2\frac{\partial(f^s_{2a}{}^{(2)})}{\partial\phi_2} \tag{4}$$

where $p_v^{(\alpha)} = -\eta_\alpha\bar{\kappa}_\alpha \cdot \bar{\Omega}_\alpha$ ("vortex pressure" against the interface).

A geometrical interpretation of Eq. (4) in a certain specific case shows that it gives the well-known equation of capillarity. Also an analogous equation to Gibb's adsorption equation can be derived from (3) and (4). Equation (3) may be regarded as a "shrinking pressure" equation since it describes the force which causes the shrinking of the solid material.

Together with some other equations achieved with the aid of the entropy balance equation, the following vapor pressure equation can be derived from Eq. (2):

$$v^{(3)}\frac{dp^{(3)}}{dt} = \frac{(h_3 + \frac{u_3{}^2}{2}) - (h_2 + \frac{u_2{}^2}{2} + h^s_{2a}{}^{(2)})}{T}\frac{dT}{dt} + v^{(2)}\frac{dp^{(2)}}{dt} + \{\frac{d(f^s_{2a}{}^{(2)})}{dt}\}_T \tag{5}$$

In the equilibrium state, when $\bar{u}_\alpha = \bar{0}$, we get from (5):

$$v^{(3)}dp^{(3)} = \frac{h_3 - (h_2 + h^s_{2a}{}^{(2)})}{T}dT + v^{(2)}dp^{(2)} + \{d(f^s_{2a}{}^{(2)})\}_T \tag{6}$$

In the case of "free" water we have $h^s_{2a}{}^{(2)} = f^s_{2a}{}^{(2)} = 0$ and if $p^{(2)} = p^{(3)}$, then we obtain from (6):

$$dp^{(3)} = \frac{h_3 - h_2}{v^{(3)} - v^{(2)}}\frac{dT}{T} \tag{7}$$

which is the Clausius-Clapeyron equation. The more interesting case is naturally the one where $h^s_{2a}{}^{(2)} \neq 0$ and $f^s_{2a}{}^{(2)} \neq 0$. When the temperature is kept constant, i.e. $dT \equiv 0$, we get from (6)

$$v^{(3)}dp^{(3)} = v^{(2)}dp^{(2)} + \{d(f^s_{2a}{}^{(2)})\}_T \tag{8}$$

which describes the sorption isotherm of water in hygroscopic material in the equilibrium state. Using the ideal gas equation and by integrating (8) we obtain

$$\ln\frac{p^{(3)}}{p_0^{(3)}} = \frac{M_3}{RT}(v^{(2)}(p^{(2)} - p_0^{(2)}) + f^s_{2a}{}^{(2)}) \tag{9}$$

where $p_0^{(3)}$ is the vapor pressure at which the vapor is in equilibrium with free water at pressure $p_0^{(2)}$ and at temperature T. If $p_0^{(2)}$ is the pressure of saturated free water we have $p_0^{(2)} = p_0^{(3)}(T)$ and $\psi \equiv p^{(3)}/p_0^{(3)}$ is called the relative vapor pressure.

From (9) we may see that the vapor pressure is changed for two reasons: 1) the pressure of water

is lower than in the usual free state due to the curved surfaces (Eq. (4)), and 2) the energetic state has also been changed, which is described by $f_{2a}^{s(2)}$. Together the two terms on the r.h.s. of (9) present the total change of chemical potential of hygroscopically bound water compared to free water. The pressure difference $p^{(2)} - p_0^{(2)}$ can be greater than, say, 1 bar, which means that water as a whole is under tensile strain ($p^{(2)} < 0$). But this also means that water is then obviously no longer in the usual state and the correction functions, as we have also called the surface functions, are needed. Therefore the term $f_{2a}^{s(2)}$ is very important and has to be taken into account.

Since the surface functions are so important attention is also paid to instructions on how to measure these. A great deal of this is presented in connection with rheological studies (Ch. 21, (1)). However, in the following we present the equations by which we can calculate the surface energies $f_{1a}^{s(1)}$, $f_{2a}^{s(2)}$ and the pressure of water $p^{(2)}$ at various moisture contents and at various temperatures on the basis of calorimetric measurements and sorption isotherms (Eq. (21.1a-c), (1)):

$$f_{2a}^{s(2)} = v^{(2)} \int_{T_0}^{T} \frac{1}{T v^{(2)}} \left((1 - l_0) + \left(1 - \frac{T}{v^{(2)}} \frac{\partial v^{(2)}}{\partial T}\right) \frac{RT}{M_3} \cdot \right.$$

$$\left. \cdot \ln \psi\right) dT \qquad (10)$$

$$\rho_1 f_{1a}^{s(1)} + \rho_2 f_{2a}^{s(2)} = \frac{RT}{M_3} d_2 \int_{\phi_{2,0}}^{\phi_2} \ln \psi \, d\phi_2 \qquad (11)$$

$$p_0^{(3)}(T) - p^{(2)} = \int_{T_0}^{T} \frac{1}{T v^{(2)}} \left((1 - l_0) + \left(1 - \frac{T}{v^{(2)}} \frac{\partial v^{(2)}}{\partial T}\right) \frac{RT}{M_3} \cdot \right.$$

$$\left. \cdot \ln \psi\right) dT - \frac{1}{v^{(2)}} \frac{RT}{M_3} \ln \psi \qquad (12)$$

where T_0 is chosen sufficiently high so that $\psi = 1$, i.e. $f_{2a}^{s(2)} = 0$, at this temperature. The smaller ϕ_2-values are to be studied, the higher T_0 has to be chosen (even much higher than 373 K at very low moisture contents). Obviously we may find for all solids a sufficiently large value of ϕ_2 that $\psi = 1$, i.e. the surface functions are zero, and this value is denoted by $\phi_{2,0}$. The quantity $1 - l_0$ is the difference of heat of vaporizations between bound water and free water, i.e. it is the sorption heat.

Remark

In many books the following equation is presented as an accurate one

$$1 - l_0 = \frac{RT^2}{M_3 \psi} \left(\frac{\partial \psi}{\partial T}\right)_{u_v} \qquad (13)$$

It is not, however, accurate, although it is a very good approximation in many cases. We can see this by substituting (13) into (12) when it follows that

$$p_0^{(3)} - p^{(2)} = \int_{T_0}^{T} \frac{R}{M_3} \frac{\partial}{\partial T} \left(\frac{T}{v^{(2)}} \ln \psi\right) dT - \frac{1}{v^{(2)}} \frac{RT}{M_3} \ln \psi = 0$$

and hence (13) is valid only if the pressure of water is constant. Because of the slight effect of the pressure of water on sorption heat, Eq. (13) is a good approximation. However, if we wish to determine the pressure of water with the aid of thermodynamic methods, e.g. by using (12), we have to use calorimetric measurements of $1 - l_0$.

At the present time our laboratory experiments are not yet complete and therefore we have used Eq. (13) in calculating the first approximations of $f_{1a}^{s(1)}$ and $f_{2a}^{s(2)}$. Substituting (13) into (10) gives $f_{2a}^{s(2)} = (RT/M_3) \ln \psi$ and using numerical integration (Simpson's rule) in (11), the following two curves have been calculated to give the class of magnitude of the surface functions:

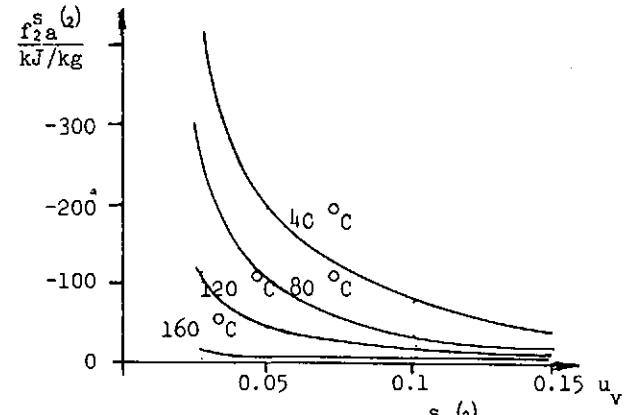

Figure 3 Helmholtz free energy $f_{2a}^{s(2)}$ of a beech wood. Sorption isotherms are taken from (2).

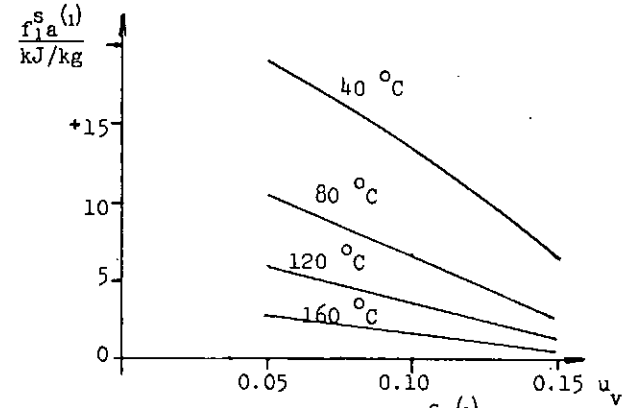

Figure 4 Helmholtz free energy $f_{1a}^{s(1)}$ of a beech wood. Sorption isotherms are taken from (2).

RESISTANCE FORCES

When a constituent of the mixture moves in relation to the other constituents, a resistance force is generated which is described by $\rho \bar{m}_\alpha$. We may assume that the forces are linearly dependent on the velocity differences between the constituents and that they depend on the dynamic viscosities. The following constitutive equations for constituents $\alpha = 1,2,\beta$ are suggested:

$$\rho \bar{m}_1 = - \eta_2 \alpha_{12} (\bar{v}_1 - \bar{v}_2) - \eta_\beta \alpha_{1\beta} (\bar{v}_1 - \bar{v}_\beta) \qquad (14)$$

$$\rho \bar{m}_2 = - \eta_2 \alpha_{21} (\bar{v}_2 - \bar{v}_1) - \eta_2 \alpha_{2\beta} (\bar{v}_2 - \bar{v}_\beta) \qquad (15)$$

$$\rho \bar{m}_\beta = - \eta_\beta \alpha_{\beta 1} (\bar{v}_\beta - \bar{v}_1) - \eta_\beta \alpha_{\beta 2} (\bar{v}_\beta - \bar{v}_2) \qquad (16)$$

where the coefficients $\alpha_{12}(T,\phi_1,\phi_2),\ldots,\alpha_{\beta 2}(T,\phi_1,\phi_2)$ may be called hydraulic resistances. Because of the equality of the action and reaction force, we have $\rho m_1 + \rho m_2 + \rho m_\beta = 0$ which implies that $\alpha_{12} = \alpha_{21}$, $\alpha_{1\beta} = \alpha_{\beta 1}$ and $\eta_2\alpha_{2\beta} = \eta_\beta\alpha_{\beta 2}$.

By taking into account Eq. (14) it is shown that the momentum equation for the humid air in a stationary state and without moisture and temperature gradients reduces to the following form (Eq. (20.3), (1)):

$$\phi_\beta v_i^{(\beta)} = -\frac{k_\beta}{\eta_\beta}\left(\frac{\partial p^{(\beta)}}{\partial x_i} - d_\beta g_i\right) \qquad (17)$$

which is actually the same as Darcy's law.

The term $k_\beta \equiv \phi_\beta^2/(\alpha_{\beta 1} + \alpha_{\beta 2})$ is called the total permeability. The left-hand side of (17) is the volume flow density (the flow of gas β divided by the cross-sectional area of the mixture). Equation (17) offers a practical way to determine the term k_β at various moisture contents and temperatures. Figure 5 is an example of this.

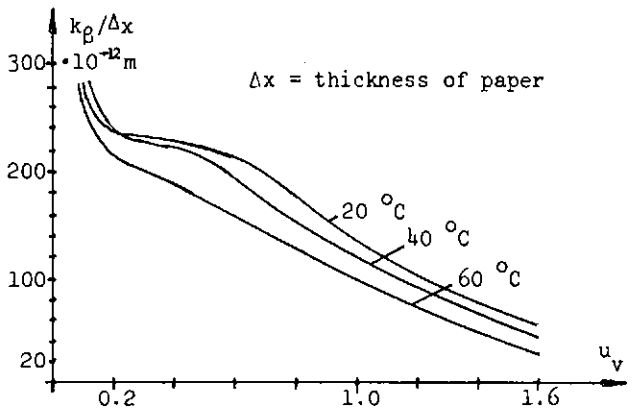

Figure 5 Permeability of rewetted newsprint (45 g/m²). Measured by P. Raatikainen, Valmet Oy (1979).

Analogously with (14), (15) and (16) constitutive equations for ρm_3 and ρm_4 are formulated:

$$\rho\bar{m}_3 = -\eta_3\phi_\beta\alpha_{34}(\bar{v}_3 - \bar{v}_4) - \frac{\rho_3}{\rho_\beta}\eta_\beta\alpha_{\beta 1}(\bar{v}_3 - \bar{v}_1) - \frac{\rho_3}{\rho_\beta}\eta_\beta\alpha_{\beta 2}(\bar{v}_3 - \bar{v}_2) \qquad (18)$$

$$\rho\bar{m}_4 = -\eta_4\phi_\beta\alpha_{43}(\bar{v}_4 - \bar{v}_3) - \frac{\rho_4}{\rho_\beta}\eta_\beta\alpha_{\beta 1}(\bar{v}_4 - \bar{v}_1) - \frac{\rho_4}{\rho_\beta}\eta_\beta\alpha_{\beta 2}(\bar{v}_4 - \bar{v}_2) \qquad (19)$$

where $\alpha_{34} = \alpha_{34}(T,p^{(3)},p^{(4)})$ and $\alpha_{43} = \alpha_{43}(T,p^{(3)},p^{(4)})$. On the other hand $\rho m_3 + \rho m_4 = \rho m_\beta$ and hence it follows from (16), (18) and (19) that $\eta_4\alpha_{43} = \eta_3\alpha_{34}$.

Using Eq. (18) it can be shown that the momentum equation for the water vapor in a stationary state and when $\phi_\beta = 1$, leads to an analogous equation with Fick's law. The following relation between the hydraulic resistance α_{34} and the diffusion coefficient D_{34} is then found (Eq. (20.25), (1)):

$$\eta_3\alpha_{34} = \frac{d_3 d_4}{M_3 M_4}\frac{M_\beta}{d_\beta}\frac{RT}{D_{34}} \qquad (20)$$

Since the permability and the hydraulic resistance are inverse quantities we may with good reason call diffusion coefficient D_{34} the permeability of water vapor through dry air.

Let us then consider the diffusion of water vapor through the solid. Neglecting other forces than the resistance force and the pressure gradient, the momentum equation gives $\rho\bar{m}_3 = \nabla p_3$ (see Eq. (19.1a), (1)). Since the inertia forces are omitted, it is obvious that we have to write $\nabla p_3 = \phi_\beta\nabla p^{(3)}$. Assuming that velocities $\bar{v}_1$ and $\bar{v}_2$ are small we get from (18):

$$\phi_\beta\nabla p^{(3)} = -\eta_3\alpha_{34}\phi_\beta(\bar{v}_3 - \bar{v}_4) - \frac{\rho_3}{\rho_\beta}\eta_\beta(\alpha_{\beta 1} + \alpha_{\beta 2})\bar{v}_3$$

In the usual contact and air drying methods dry air flows into the solid only because the space of evaporated water is replaced by air. Due to the small specific volume of liquid water, this flow is very small and with good accuracy we may then assume that $\bar{v}_4 = 0$. (In through drying this of course is not valid.) Taking this fact into account and using Eq. (20) and the relation $k_\beta \equiv \phi_\beta^2/(\alpha_{\beta 1} + \alpha_{\beta 2})$ it follows from the equation above that

$$\rho_3\bar{v}_3 = -\frac{\phi_\beta}{1 + \frac{p^{(\beta)}}{p^{(\beta)} - p^{(3)}}D_{34}\frac{M_3}{RT}\nu_\beta\frac{\phi_\beta}{k_\beta}} \cdot \frac{p^{(\beta)}}{p^{(\beta)} - p^{(3)}} \cdot \frac{M_3}{RT}D_{34}\nabla p^{(3)} \qquad (21)$$

where we have also used the ideal gas equation, i.e. $d_\beta/d_4 = p^{(\beta)}M_\beta/p^{(4)}M_4$, and the relation $p^{(4)} = p^{(\beta)} - p^{(3)}$.

Let us use the notation

$$\varepsilon_D' = \frac{\phi_\beta}{1 + \frac{p^{(\beta)}}{p^{(\beta)} - p^{(3)}}\frac{M_3}{RT}D_{34}\nu_\beta\frac{\phi_\beta}{k_\beta}} \qquad (22)$$

which can be called a diffusion resistant coefficient. The term ε_D' defined by (22) is slightly different from ε_D used in (1) (see (20.29), (1)) due to the pressure terms. We can see that even though no resistance force α_β exists, i.e. $k_\beta \to \infty$, the resistance coefficient ε_D' is smaller than one, namely $\varepsilon_D' = \phi_\beta$. This is easy to understand, since ϕ_β describes that part of the cross-sectional area of the mixture through which the vapor can diffuse. We can also see that there is no need to make separate measurements for the diffusion resistance coefficient; knowing the total permeability of air is enough. This is very natural since both the air and the water vapor flow through the same "holes" and via the same "bends".

Neglecting gravity force $\bar{g}$ and taking into account that $\rho_\beta v_\beta = \rho_3 v_3$ as $\bar{v}_4 = 0$ we obtain from Eq. (17)

$$\rho_3\bar{v}_3 = -\frac{k_\beta}{\nu_\beta}\nabla p^{(\beta)} \qquad (23)$$

Assuming that vaporization is uniform across the thickness of paper (in contact drying), let us calculate the pressure differences $\Delta p^{(\beta)} = p^{(\beta)}(x=0) - p^{(\beta)}(x=\Delta x)$ and $\Delta p^{(3)}$. Using Eq. (22) we obtain from (21)

$$\Delta p^{(3)} = -\int_0^{\Delta x} \frac{p^{(\beta)} - p^{(3)}}{p^{(\beta)}} \frac{RT}{M_3} \frac{1}{\varepsilon_D' D_{34}} \rho_3 v_3 \, dx \cong$$

$$\cong -\frac{p^{(\beta)} - p^{(3)}}{p^{(\beta)}} \frac{RT}{M_3} \frac{1}{\varepsilon_D' D_{34}} I_3 \Delta x \frac{\Delta x}{2}$$

and from (23)

$$\Delta p^{(\beta)} = -\int_0^{\Delta x} \frac{\nu_\beta}{k_\beta} \rho_3 v_3 \, dx \cong -\frac{\nu_\beta}{k_\beta} I_3 \Delta x \frac{\Delta x}{2}$$

Example

Newsprint, $\Delta x = 10^{-4}$ m, T = 333 K, $u_v = 1.2$ and the evaporation rate $I_3 \Delta x = 2.78 \cdot 10^{-3}$ kg/m²s (= 10 kg/m²h).

$\phi_1 = \rho_1/d_1 = 450/1560 = 0.29$
$\phi_2 = \rho_2/d_2 = u_v \rho_1/d_2 = 1.2 \cdot 450/1000 = 0.54$
$\phi_\beta = 1 - (0.29 + 0.54) = 0.17$
$D_{34} = 3.6 \cdot 10^{-5}$ m²/s $\quad \nu_\beta = 19 \cdot 10^{-6}$ m²/s
$p^{(3)} = 19.9 \cdot 10^3$ N/m² $\quad p^{(\beta)} = 10^5$ N/m²
$k_\beta = 7.5 \cdot 10^{-15}$ m²

$$\varepsilon_D' = \frac{0.17}{1 + \frac{1}{1-0.199} \cdot \frac{18}{8.314 \cdot 10^3 \cdot 333} \cdot 3.6 \cdot 10^{-5} \cdot \frac{19 \cdot 10^{-6} \cdot 0.17}{7.5 \cdot 10^{-15}}} =$$

$$= 0.15$$

$$\Delta p^{(3)} = -\frac{10^5 - 19.9 \cdot 10^3}{10^5} \frac{8.314 \cdot 10^3 \cdot 333}{18} \frac{1}{0.15 \cdot 3.6 \cdot 10^{-5}} \cdot$$

$$\cdot 2.78 \cdot 10^{-3} \cdot \frac{10^{-4}}{2} = -3200 \text{ N/m}^2$$

$$\Delta p^{(\beta)} = -\frac{19 \cdot 10^{-6}}{7.5 \cdot 10^{-15}} \cdot 2.78 \cdot 10^{-3} \cdot \frac{10^{-4}}{2} = -400 \text{ N/m}^2$$

The pressure curves $p^{(3)}$ and $p^{(\beta)}$ are sketched in Figure 6 below.

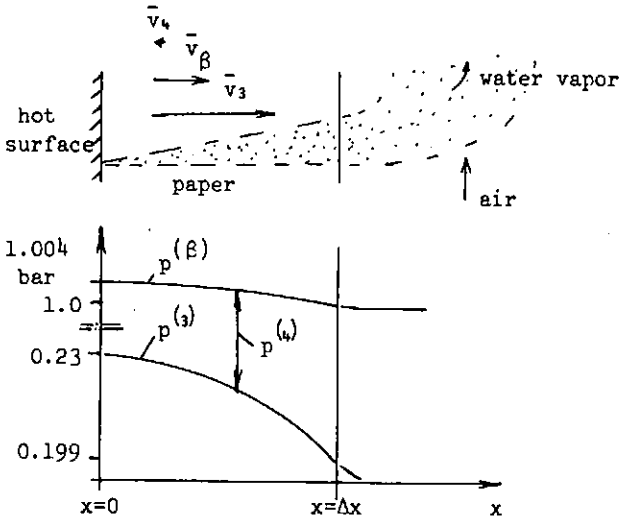

Figure 6 Pressure contributions of humid air, dry air and water vapor across a paper.

The minimum pressure by which the paper has to be stretched against the hot surface, by fabric for instance, is thus in this example 0.004 bar. If it is less than this the paper as a whole will be slightly detached from the hot surface.

ACKNOWLEDGEMENTS

The author wishes to thank all his friends and colleagues at Valmet Oy's Pansio Works and Rautpohja Works for their help, suggestions and many discussions concerning this work.

REFERENCES

1. Lampinen, M., Mechanics and Thermodynamics of Drying, Acta Polytechnica Scandinavica, Mechanical Engineering Series No. 77. Helsinki 1979. 104 pp.
2. Engelhardt, F., Untersuchungen über die Wasserdampfsorption durch Buchenholz im Temperaturbereich von 110 bis 170 °C, Holz als Roh- und Werkstoff 37 (1979), pp. 99-112.

KINETICS OF MASS TRANSFER IN A CAPILLARY WITH ACCOUNT FOR MOVABLE ADSORBED LAYERS

O.G. Martynenko, V.V. Levdansky, N.V. Pavlyukevich

Heat and Mass Transfer Institute, Minsk, U.S.S.R.

ABSTRACT

When describing mass transfer in a porous body it is very important for the theory of drying to correctly determine both the volumetric and the surface mass fluxes from capillaries and distribution of moisture content. Usually, an assumption is made on the local equilibrium between the gaseous and adsorbed phases at each location in the channel. However, such an approach is not correct (for short capillaries, in particular). The paper deals with a kinetic approach to simultaneously describe mass transfer in adsorbed and gaseous phases. The gas flow is considered to be a free molecular one. That the distribution of the adsorbed substance over the length of the capillary be determined, an integro-differential equation is obtained which takes into account the presence of the boundary layers on its ends. An approximate expression is obtained for the total flow of substance from a capillary.

NOMENCLATURE

I_d^+ = flux density of desorbed molecules, $\frac{1}{m^2}$;
I^- = flux density of falling molecules, $\frac{1}{m^2}$;
j_a = flux density of molecules in an adsorbed phase, $\frac{1}{m}$;
j_g = flux density of molecules in a gaseous phase, $\frac{1}{m^2}$;
k = Boltzmann constant, J/K;
L = capillary length, m;
m = mass of a molecule, kg;
$\tilde{M}$ = molecular weight, kg/mol;
n_a = density of adsorbed molecules, $\frac{1}{m^2}$;
n_o = density of molecules in a completely filled monolayer, $\frac{1}{m^2}$;
p_e = saturated vapor pressure, N/m^2;
$\tilde{R}$ = gas constant, J/mol K;
R = capillary radius, m;
S = thickness of a polymolecular film, m;
T = temperature, K;
x = coordinate related to L, $l = L/R$;
η = dynamic viscosity, kg/ms;
ρ = mass density of the film substance, kg/m^3;
τ = adsorption time, s;

Subscripts

1 = parameters at the entrance to the capillary (x=0);
2 = parameters at the exit from the capillary (x=1);
a = adsorbed phase;
g = gaseous phase.

In free molecular gas flow, when the effect of intermolecular collisions can be neglected, the main factor which determines the laws governing the transport processes is the type of interaction of a gas molecule with the solid surface. When striking the surface, the molecule can undergo reflection back into the gas phase or be absorbed on the surface either monomolecularly or polymolecularly (depending on the time ratio between the adsorption in the first and the subsequent adsorbed layers). When being on the surface in adsorbed state, the molecules can move along the surface either through the agency of surface diffusion (in the case of monomolecular diffusion) or in the flowing film in much the same way as a conventional viscous liquid flow. In these cases the mass transport through the channel is accomplished both in the gas phase and in the adsorbed layer. These processes are usually described on the assumption that there is a local equilibrium between the gas and adsorbed phases at each location in the channel, while the flow of molecules in the gas phase is expressed in the form of the Fick law (1,2).

This approach is not always a correct one since it provides no possibility for rather an adequate determination of the adsorbed substance distribution over the channel length and of the resultant mass flow at the exit from the channel. The kinetic approach is more correct because the transfer phenomena and the processes of interaction with the surface are not treated separately, as is the case in a phenomenological approach, but are described by a system of interrelated equations. The continuity equation for an adsorbed layer element in the steady-state case is of the form

$$-\mathrm{div}\, j_a = I_d^+ - \alpha I^- \quad , \qquad (1)$$

where α is the probability that the molecule striking the surface will succeed in not being reflected into the gas phase. For a cylindrical channel, the flux of escaping molecules I^+, which incorporates the desorbed and reflected molecules I_-, and the flux of the falling molecules I^- are interrelated by the following expression (3):

$$I^-(x) = \int_0^l I^+(x') U_1(|x-x'|)\,dx' + I_0^- U(x) +$$

$$+ I_1^- U(1-x) \, . \qquad (2)$$

Here, the reflected and desorbed molecules are assumed to be distributed according to the cosine law; I_0^- and I_1^- are the densities of the fluxes of molecules entering the capillary at x=0 and x=1; U and U_1 are the functions which characterize the probability that the molecule will succeed in travelling from one surface element to the other (3). The flux of molecules escaping from the capillary is composed of the molecules in the form of the gas phase and those in the form of the mobile adsorbed layer

$$J = \pi R^2 j_g + 2\pi R j_a \, , \qquad (3)$$

where j_g has the form

$$j_g = I_0^- U_2(l) + 2l \int_0^l I^+ U(1-x)\,dx \, , \qquad (4)$$

in which

$$\frac{dU_2}{dx} = -2l\,U, \quad l = \frac{L}{R} \, .$$

The actual form of the quantities j_a, I_d^+, α in (1) is determined by the type of adsorption (monomolecular or polymolecular). Equations (1)-(3) make it possible to calculate the total amount of the substance adsorbed in the channel, its distribution over the channel length as well as the fluxes of molecules at the exit from the channel.

a) Consider now the case of polymolecular adsorption at the pressure in the gas phase being nearly equal to the saturation pressure (the evaporation process is close to that at equilibrium). In this case, the coefficient α has the meaning of the ordinary condensation factor which is assumed to equal the coefficient of evaporation. The density of the surface flux of molecules can be written in the form (2):

$$j_a = \frac{\rho S^3}{3\eta m L} \frac{d}{dx} \left(\frac{A}{S^\mu} \right) \, , \qquad (5)$$

in which the constants A and μ characterize the interaction of molecules of the film on a substrate. The expression for I_d^+ is of the form

$$I_d^+ = \frac{\alpha p_e}{\sqrt{2\pi m k T}} \exp\left\{ - \frac{A}{S^\mu} \frac{\tilde{M}}{\tilde{\rho} \tilde{R} T} \right\} . \qquad (6)$$

Using equations (1),(2),(5),(6) for S(x) we obtain the following (here it is assumed for simplicity that $\alpha = 1$):

$$\frac{\rho A \mu}{3\eta j m L^2} \frac{d}{dx} \left(S^{-\mu+2} \frac{dS}{dx} \right) = \exp\left\{ - \frac{B}{S^\mu} \right\} -$$

$$- \int_0^l \exp\left\{ - \frac{B}{S^\mu} \right\} U_1(|x-x'|)\,dx' - \frac{I_0^-}{j} U(x) -$$

$$- \frac{I_1^-}{j} U(1-x), \qquad (7)$$

where

$$B = \frac{\tilde{M} A}{\tilde{\rho} \tilde{R} T} \, , \quad j = \frac{p_e}{\sqrt{2\pi m k T}} \, .$$

As is evident from (7), it is an integro-differential equation of the second order which is obtained for the adsorbed substance distribution over the channel length. Therefore, for the problem to have a complete formulation, it is necessary to have two additional conditions. We can write down equations (1) on the end faces of the channel and then join the solutions of equations for the end faces and the central portion of the channel. Note that the differential term in equation (7) contains the parameter the value of which is usually much smaller than unity. This allows the domain of variation of x to be divided into the internal zone, where the effect of the differential term can be neglected, and narrow boundary layers, where the complete integro-differential equation should be solved. In this case, when calculating distribution of the adsorbate

in the "body of the film"(excluding the edge effects) as well as the adsorptional capacity of the channel, the differential term can be neglected (these terms are naturally equal to zero in the case of immovable adsorption layers). This simplification seems to be also true in calculation of the flux of molecules escaping from the channel as a gaseous phase. However, in order to calculate j_a (1) one must have the solution of the complete equation, since the value of j_a is determined by the derivative of the adsorbate distribution over the end face x = 1. In the general case, equation (7) can be solved only numerically. Here, we shall consider some specific cases. First, we shall find the film thickness distribution in the central portion of the capillary (without regard for the boundary layers). Equation (7) yields for the quantity $f(x)=\exp\left\{-\frac{B}{S^{\mu}}\right\}$ the following integral equation

$$f(x)=\int_0^1 f(x')U_1(|x-x'|)dx' + \frac{I_0^-}{j}U(x) + \frac{I_1^-}{j}U(1-x) . \qquad (8)$$

From the solution of equation (8) obtained with exponential approximation of U, U_1 (4) for S(x) we find

$$S(x) = \left(\frac{A\tilde{M}}{\rho\tilde{R}T\ln\left\{j(l+2)\Big/\left[I_0^-(l+1)+I_1^-(l-x)-(I_0^--I_1^-)lx\right]\right\}}\right)^{1/\mu}$$

where we assume that $\mu = 3$, $A = 10^{-14}$ erg (2). Now, let us discuss the results obtained from the above approach for the total flux of the substance escaping from the capillary. An approximation is usually used when the both fluxes (in the form of the film and in the gas phase form) are calculated separately while the total flux is considered as the sum of the both (2). In this case the expression of the total flux of substance, escaping from the capillary, is of the form

$$J = \pi R^2\delta\frac{p_0-p_1}{kT\cdot L} + \frac{2\pi RA\rho}{\eta lm}\ln\frac{S_0}{S_1} , \qquad (9)$$

where, in the considered case of free-molecular gas flow, δ is the Knudsen diffusion coefficient which has the form

$$\delta = \frac{8}{3}\left(\frac{kT}{2\pi m}\right)^{1/2}\cdot R .$$

Now let us find the expression for the flux of substance, escaping from the capillary, on the basis of the above kinetic description at $\varepsilon = \frac{\rho A\mu}{3\eta jmL^2} \ll 1$. As has been noted above, the presence of thin boundary layers can be neglected in this case when calculating the flux escaping from the capillary as a gaseous phase. Then, with regard for (4), we obtain for j_g:

$$j_g = \frac{2}{2+l}\cdot\frac{p_0-p_1}{\sqrt{2\pi mkT}} . \qquad (10)$$

Equation (10) at $l\to\infty$ acquires the form of the Knudsen law (instead of 8/3 we have here the factor 2 owing to the approximate values of U, U_1, U_2). Then equation (10) coincides with the first term on the right-hand side of equation (9). The value of the flux j_{a_3} is proportional to the derivative of $1/S^3$ at x=1 the value of which is determined by the presence of the boundary layers. Let us estimate the value of such a flux. In order to find an approximate solution in the boundary layer in the vicinity of the point x=1, we shall employ the substitution $y = \frac{1-x}{\sqrt{\varepsilon}}$ (5). Then in terms of the new variables we have

$$\frac{d^2}{dy^2}(\ln S) = 0 ,$$

or

$$\frac{d}{dy}(\ln S) = C = \text{const} , \qquad (11)$$

i.e., the value of the derivative of lnS is constant not over the entire length of the capillary but only in the region of the boundary layer. The flux of molecules escaping from the capillary as a film is

$$2\pi Rj_a = \frac{2\pi R\rho A}{\eta Lm}\cdot\frac{1}{\sqrt{\varepsilon}}\cdot C . \qquad (12)$$

In general, the constant C should be determined from the solution of equation (7). Here, we shall qualitatively estimate C from equation (11) having integrated it over the boundary layer length which is approximated to be equal to $\sqrt{\varepsilon}$. The value of S in the beginning of the boundary layer can be determined approximately by extrapolating S(x) in the interior of the capillary to x=1 (this can be done due to weak dependence of S on x in the central portion of the capillary and small width of the boundary layer) (Fig.1). Thus, we obtain for C

$$C = \ln\left[S(1)/S_1\right] , \qquad (13)$$

where

$$S(1)=\left(A\tilde{M}/\rho\tilde{R}T\ln\frac{j(l+2)}{I_0^- + I_1^-(l+1)}\right)^{1/3} .$$

With the aid of equations (10),(12),(13)

the expression for the total flux of molecules through the channel is written down as

$$\dot{J} = \pi R^2 \frac{2}{2+l} \frac{p_o - p_1}{\sqrt{2\pi mkT}} + \frac{2\pi R\rho A}{\eta L m \sqrt{\varepsilon}} \times$$

$$\times \ln \left[\frac{\left(A\tilde{M}/\rho\tilde{R}T \ln \frac{j(l+2)}{I_o^- + I_1^-(l+1)}\right)^{1/3}}{S_1} \right] . \quad (14)$$

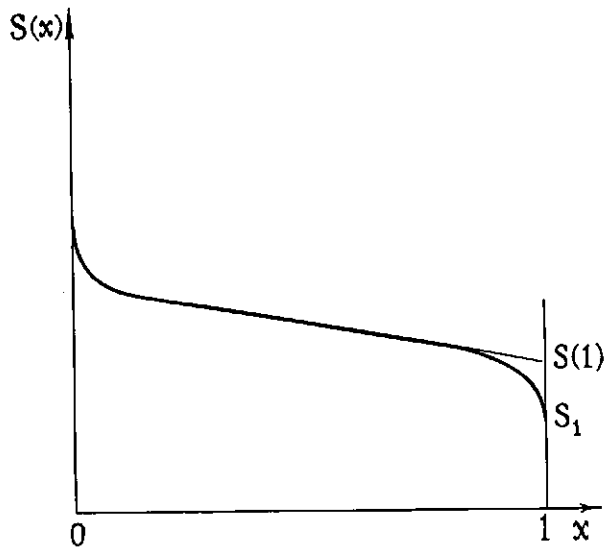

Figure 1 Dependence of the film thickness S on the dimensionless coordinate (schematic)

It follows from (14) that the amount of the substance escaping from the capillary as a film will differ from that calculated by (9).

b) Now let us briefly consider the case of monomolecular adsorption. The quantities j_a and I_d^+ in (1) will have the form

$$j_a = -\frac{1}{L}\delta_a \frac{dn_a}{dx} \quad , \quad I_d^+ = \frac{n_a}{\tau} . \quad (15)$$

Using the assumptions employed in the derivation of the Langmuir adsorption isotherm we obtain from (1),(2),(15):

$$\frac{1}{L^2}\frac{d}{dx}\left(\delta_a \frac{dn_a}{dx}\right) = \frac{n_a}{\tau} - \left(1 - \frac{n_a}{n_o}\right) \times$$

$$\times \left[\int_0^1 \left(\frac{n_a}{\tau} + I \right) U_1(|x-x'|)dx' + I_o^- U(x) + \right.$$

$$\left. + I_1^- U(1-x) \right] , \quad (16)$$

$$I = \frac{n_a}{n_o} \int_0^1 \left(\frac{n_a}{\tau} + I \right) U_1(|x-x'|)dx' +$$

$$+ I_o^- U(x) + I_1^- U(1-x), \quad (17)$$

where I is the density of the flux of molecules escaping from the surface on having been reflected from the adsorbed molecules. The physical meaning of separate terms of the above equations will be interpreted with equation (16) used as an example. The term on the left-hand side of equation (16) is due to the surface diffusion of molecules, the first term on the right describes the density of the flux of desorbed molecules, the expression in the square brackets characterizes the flux of molecules striking the element of the inner surface of the channel in the neighbourhood of the point x which includes the molecules coming directly through the ends of the channel (without colliding with the walls), as well as the molecules coming into the vicinity of the point x on having been desorbed or reflected from the channel surface. At $(n_a/n_o) \ll 1$ the system of equations (16),(17) reduces to one equation for the density of the adsorbed molecules. It is seen from the solution of this equation (6), that, as would be expected, at $(\tau\delta_a/L^2) \ll 1$ the presence of the boundary layers at the ends of the capillary is distinctly manifested.

REFERENCES

1. Sears, G.W., J.Chem.Phys., Vol. 22, No. 7, 1954.
2. Starov, V.M., and Churaev, N.V., Jr. Engng Physics, Vol. 29, No.6, 1975.
3. Clausing, P., Ann. Phys., Vol.12, p. 961, 1932.
4. Ivanovsky, A.I., Proceedings of the Central Aerological Obs., No. 56, 1964.
5. Van Dyke, M., Perturbation Method in Fluid Mechanics, Academic Press, New York, 1964.
6. Luikov, A.V., Perelman, T.L., Levdansky, V.V., Leitsina, V.G., and Pavlyukevich, N.V., Int. J. Heat Mass Transfer, Vol. 17, No. 9, 1974.

A THEORETICAL MODEL FOR SOLAR-DEHUMIDIFICATION DRYING OF WOOD

W. A. Helmer[1]
H. N. Rosen[2]
P. Y. S. Chen[2]
S. W. Wang[1]

[1]Dept. of Thermal & Env. Eng., South. Ill. Univ., Carbondale, Ill.
[2]North Cent. For. Exp. Stn., USDA For. Serv., Carbondale, Ill.

ABSTRACT

Solar energy collection and dehumidification with heat pumps are two techniques currently used by the lumber industry to reduce the energy costs of drying wood. A computer simulation model has been developed to predict the performance of a combined solar-dehumidification wood drying system. When input data (solar collector, drying chamber, wood, and dehumidifier characteristics) and ambient weather conditions (dry bulb temperature, wet bulb temperature, and solar radiation) are known, the model will predict the wood moisture content, air temperature and humidity, and energy consumption at any time during the drying process. The computer simulation model accurately predicted the kiln dry bulb temperature, kiln relative humidity, and wood moisture content for the operation of an existing solar wood dryer. For a hypothetical 60 m^3 wood dry kiln, the model predicted that the solar-dehumidification system could dry wood at a rate equal to or faster than a conventional dry kiln with only one-third of the energy consumption.

NOMENCLATURE

A = Surface area, m^2

B = Wood-water bond energy, J/Kg-K

C = Specific heat at constant volume, J/Kg-K

E = Electrical energy, Kwh

H = Enthalpy, J/Kg

I = Solar insolation rate, W/m^2

m = Mass, Kg

q = Heat transfer, J

R = Wood drying resistance, hr/Kg-dry air

T = Temperature, C

$\bar{U}$ = Overall heat transfer coefficient, W/m^2-C

U = Internal energy, J

w = Mass flow rate, Kg/hr

X = Wood moisture content, %

Y = Humidity ratio, Kg vapor/Kg dry air

η = Efficiency, %

λ = Latent heat of vaporization, J/Kg

τ = Time, hr

Subscripts

a = Dry air

am = Ambient

cd = Condenser

cm = Compressor motor

cp = Compressor

db = Dry bulb

e = Evaporator

f = Fan

fm = Fan motor

i = Inlet

k = Kiln

m = Air-water vapor mixture in kiln

o = Oven dry

s = Saturation conditions at T_{db}

sc = Solar collector

v = Water vapor

vt = Vent moist air

w = Water

wb = Wet bulb

wd = Wood

INTRODUCTION

In recent years society has been made aware of the definite limitations of energy resources, particularly oil and natural gas. All industries are now seeking better methods for energy utilization in all of their plant operations. This is particularly true for industries such as the lumber industry that must dry their product before marketing. The lumber industry alone consumes about 0.1 percent of the total energy requirement of the United States (1).

Although solar wood drying kilns have been available for more than 20 years, few commercial dryers are in operation (2). Drying lumber with solar energy requires longer drying times than conventional kiln drying because of limited kiln temperatures (generally less than 50 C), lack of heat supply at night or during cloudy weather, and unpredictable drying conditions due to changes in the weather. Dehumidification-type wood dry kilns, whereby moist air from the lumber is drawn over refrigerator coils to condense out the water, have been commercially popular in Europe for more than a decade but are just gaining acceptance in North America. Dehumidification kilns dry slower (especially below 20 percent moisture content), dry at lower temperatures, and use less energy than conventional kilns (3).

The combination of solar and dehumidification drying offers advantages not found when each of these methods are used separately: initial heat-up of the kiln and wet lumber charge would be faster, drying times shorter, and drying conditions less dependent on changes in the weather. Also, the performance of the dehumidifier could be improved if a nonconventional refrigerant (e.g., Freon R-114) were used, thereby allowing higher operating temperatures.

This paper presents a mathematical model for a combined solar-dehumidification wood drying system that is able to operate up to 82 C. If the characteristics of the wood, kiln, and dehumidifier along with the weather conditions are known, the model will predict the electrical energy consumption and wood moisture content at any drying time. This information would enable a lumber company to choose the optimum dehumidifier size and collector size for a given kiln size and wood species.

MODEL DEVELOPMENT

System Description

In a solar-dehumidification dryer the wood is dried on a batch basis (Figure 1).

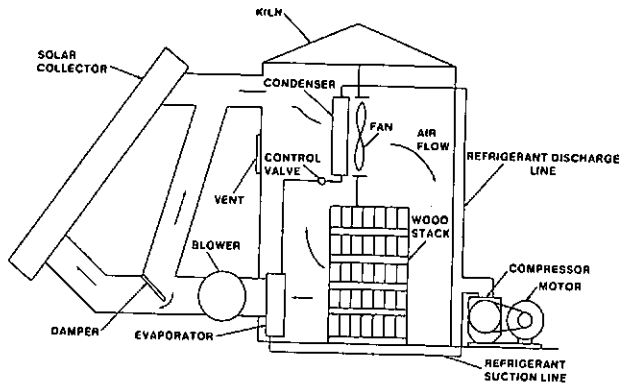

Figure 1. Solar-dehumidification dry kiln schematic.

The fan at the top of the kiln circulates the air through the wood stack to absorb moisture from the wood, and the moisture is removed from the air mainly by condensation on the cold heat exchanger of the dehumidifier (evaporator) and partially by venting. The air can be heated by being circulated through the solar collector or by being passed through the hot heat exchanger of the dehumidifier (condenser). The system is controlled such that the solar collector blower is activated whenever the outlet air temperature of the solar collector exceeds the dry bulb temperature in the drying chamber. The dehumidifier operates only when the relative humidity in the chamber exceeds a preset value and shuts off when the relative humidity goes below that value or when the temperature in the kiln exceeds a minimum or maximum allowed temperature.

Theory

A determination of the temperature and humidity conditions in the kiln can be made from a mass and energy balance on the air and wood. The most important assumptions are that (a) the dry bulb temperature of the air is equal to the temperature of the wood and (b) the properties of the wood and the properties of the air are uniform at any time period.

Energy Balance. An energy balance on the air-water vapor mixture and the green wood over a time period, $d\tau$, assumes that the net heat input to the kiln must equal the change in internal energy of the air, water, and wood. In terms of the present

system this balance becomes

$$-dq_k + dq_{sc} + dq_{cd} - dq_e - dq_{vt} + dE_f = dU_m + dU_{wd} + dU_w. \quad (1)$$

The heat loss from the kiln is calculated from

$$dq_k = \bar{U}A_k\,(T_{db,m} - T_{db,am})d\tau. \quad (2)$$

The heat supplied to the air from the collector is

$$dq_{sc} = \eta_{sc} I A_{sc}\, d\tau \quad (3)$$

where

$$\eta_{sc} = C_1 - C_2\,(T_{sc,i} - T_{am})/I. \quad (4)$$

The constants C_1 and C_2 are determined from a graph of experimental data (Figure 2).

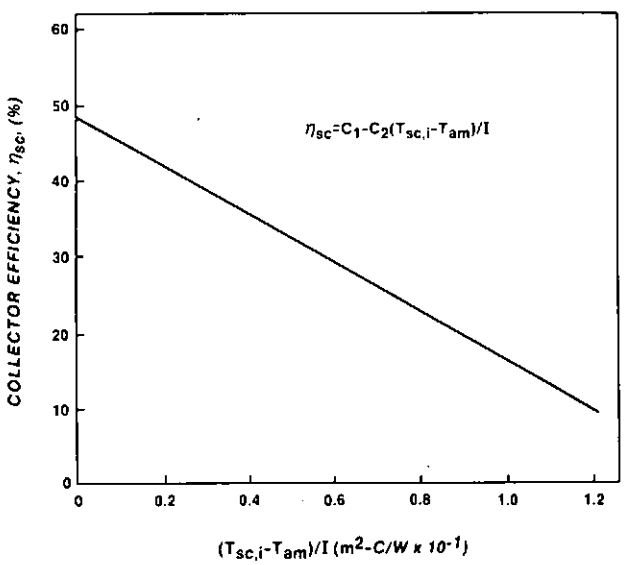

Figure 2. Typical solar collector performance curve.

A separate computer subprogram was used to calculate the heat transfer in the condenser, dq_{cd}, and in the evaporator, dq_e (4). The subprogram models the performance of a typical dehumidifier or heat pump but was modified to account for water vapor condensation on the surface of the evaporator coils (Figure 3). A typical dehumidifier operates in the following manner. Heat is absorbed in the evaporator as the refrigerant is boiled and the air is cooled and moisture removed. The refrigerant is compressed to a high temperature and high pressure in the compressor. This high temperature fluid is then cooled and condensed while the kiln air is heated up as it passes over the condenser.

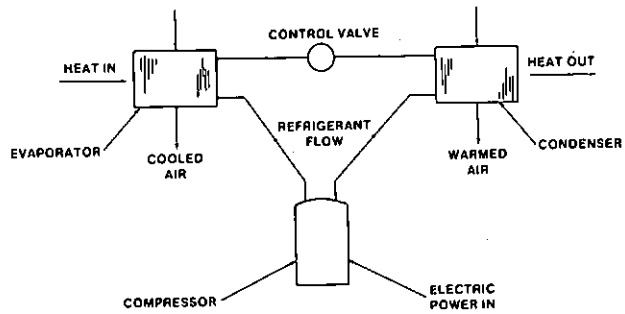

Figure 3. Typical dehumidifier schematic.

The electrical energy supplied to the compressor is calculated from

$$dE_{cp} = \frac{dq_{cd} - dq_e}{\eta_{cm}}. \quad (5)$$

The energy lost due to venting the hot moist air from the kiln is

$$dq_{vt} = (w_m H_m - w_{am} H_{am})d\tau. \quad (6)$$

The properties of the air, H_m and H_{am}, as well as other moist air properties are calculated from the ASHRAE Handbook of Fundamentals (5). The energy added to the air as it is circulated by the fans and blowers, dE_f, is calculated from

$$dE_f = \frac{(\text{Input Power})d\tau}{\eta_{fm}}. \quad (7)$$

The input power for the motor is the rated power at the given operating conditions. The motor efficiency is usually between 0.80 and 0.85.

The change in internal energy of the moist air can be calculated from the specific heat of the mixture,

$$C_m = C_a + Y_m C_v \quad (8)$$

and

$$dU_m = m_m C_m dT_{db,m}. \quad (9)$$

The change in internal energy of the moist wood is

$$dU_{wd} = m_{wd} C_{wd} dT_{wd} \quad (10)$$

where m_{wd} is the mass of the dry wood plus the mass of the liquid water in the wood. The specific heat of the wood, C_{wd}, is given as (6):

$$C_{wd} = \frac{C_o + X/100}{1 + X/100} + B \quad (11)$$

where C_o is

$$C_o = 1127 + 4.52\ T_{db}. \quad (12)$$

The change in internal energy of the water evaporated from the wood is given by

$$dU_w = dm_w \lambda \quad (13)$$

where λ is the latent heat of vaporization (7).

Mass Balance. A mass balance on the moist air in the kiln gives

$$dm_{w,wd} - dm_{v,vt} - dm_{v,e} = m_a\ dY_m. \quad (14)$$

The amount of water vapor given off by the wood is dependent upon the drying rate of the wood. Drying data for yellow-poplar wood were obtained to determine a rate relationship for the loss of water from wood (Figure 4) (8,9,10). The drying data were

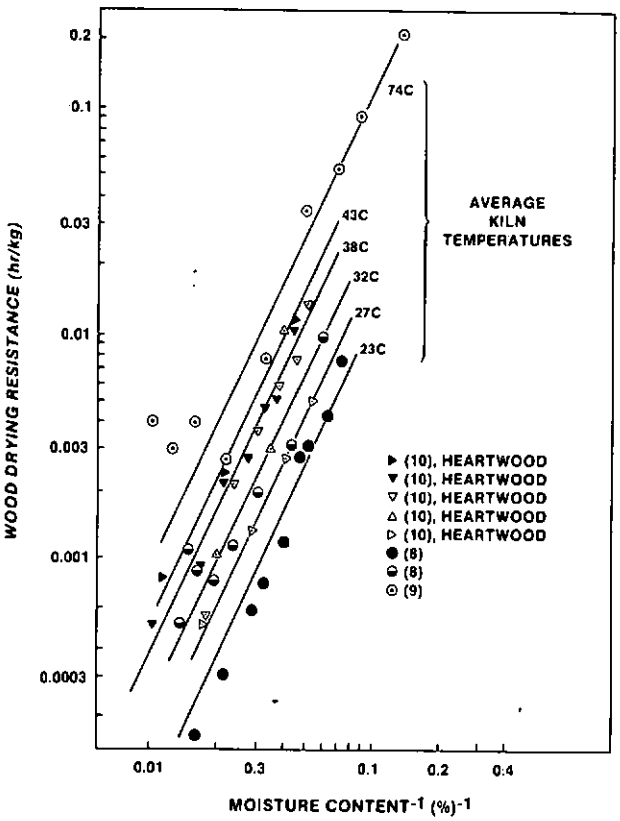

Figure 4. Yellow-poplar drying data represented as the log of wood drying resistance versus the log of reciprocal moisture content. Lines are contours of constant kiln temperatures.

obtained at both constant and varying conditions of temperature and humidity. The amount of water evaporated from the wood is given by

$$dm_{w,wd} = \frac{(Y_{m,s} - Y_m)d\tau}{R}. \quad (15)$$

The drying resistance of the wood, R, is a function of moisture content and dry bulb temperature (Figure 4). For the data shown, the correlation for the resistance is

$$R = X^{-2.38}\ (0.268\ T_{db} - 4.18). \quad (16)$$

The water vapor lost during venting is given by

$$dm_{v,vt} = Y_m dm_m - Y_{am} dm_{am}. \quad (17)$$

The amount of water vapor condensed on the evaporator coils, $dm_{v,e}$, is calculated from the dehumidifier subprogram.

Figure 5 shows the input and output factors for the main program. Knowing the

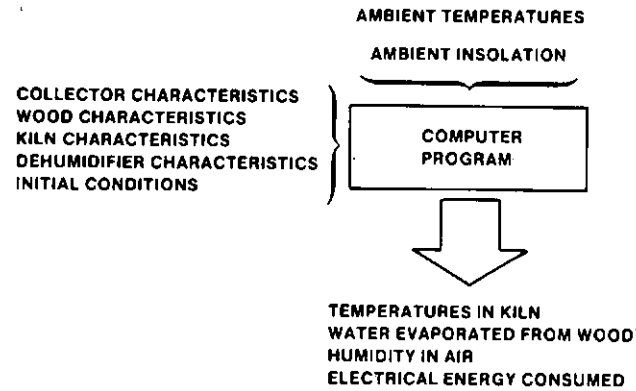

Figure 5. Computer program input and output.

ambient weather conditions, the dehumidifier parameters, the kiln geometry, the type of solar collector, and the initial conditions of the wood and air, the change in air humidity and air dry bulb temperature can be calculated after any time period, $d\tau$, using Equations (1) and (14). Wood moisture content, air temperature and humidity, and electrical energy consumption can also be calculated.

RESULTS

Model Verification for Solar Drying Only

No experimental data are published for a solar-dehumidification wood drying system. However, data are available for dry kilns using solar energy alone. The data of Chen and Rosen (8) are for a 1.2 m^3 kiln drying yellow-poplar lumber with a 11.3 m^2 air solar collector. The venting on the kiln was controlled so that the vent fans would turn on whenever the relative humidity exceeded a maximum set value according to the following schedule:

R.H. Maximum	Moisture content
80	>50
75	40
65	35
50	30
35	25
20	<25

The computer simulation was run using their weather data, kiln and collector geometry, and initial conditions.

Figures 6 to 9 show the computer results compared to the experimental data. The

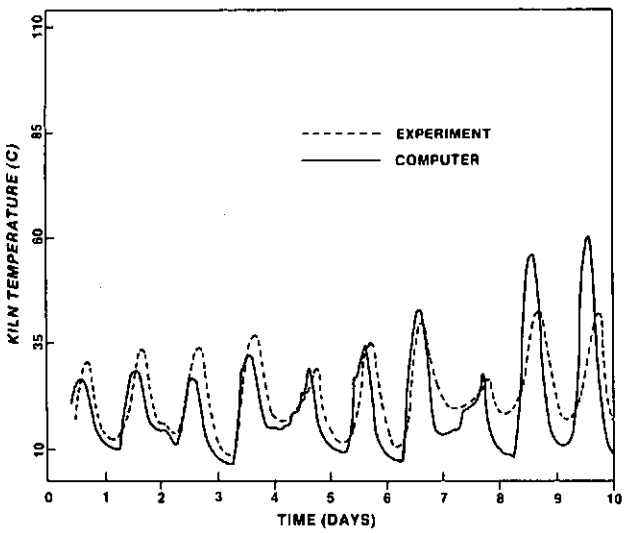

Figure 6. Kiln dry bulb temperature using solar collector only--comparison of computer model with experimental data from a 1.2 m^3 kiln (8).

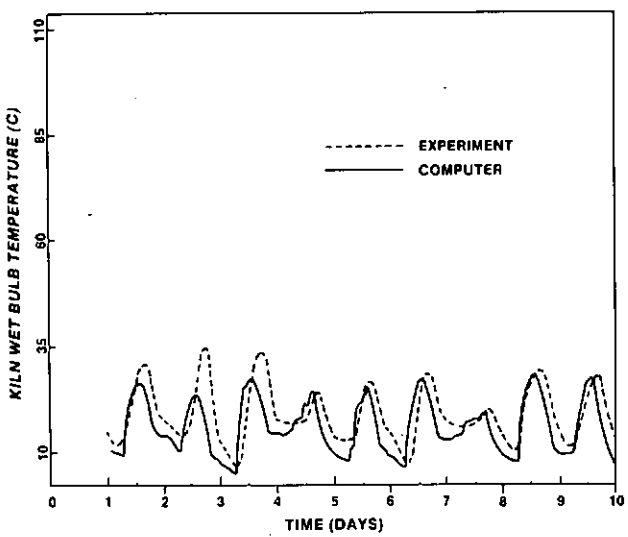

Figure 7. Kiln wet bulb temperature using solar collector only--comparison of computer model with experimental data from a 1.2 m^3 kiln (8).

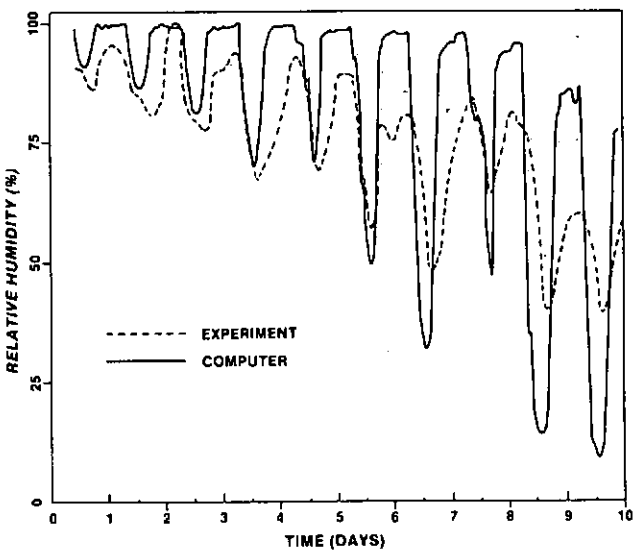

Figure 8. Kiln relative humidity using solar collector only--comparison of computer model with experimental data from a 1.2 m^3 kiln (8).

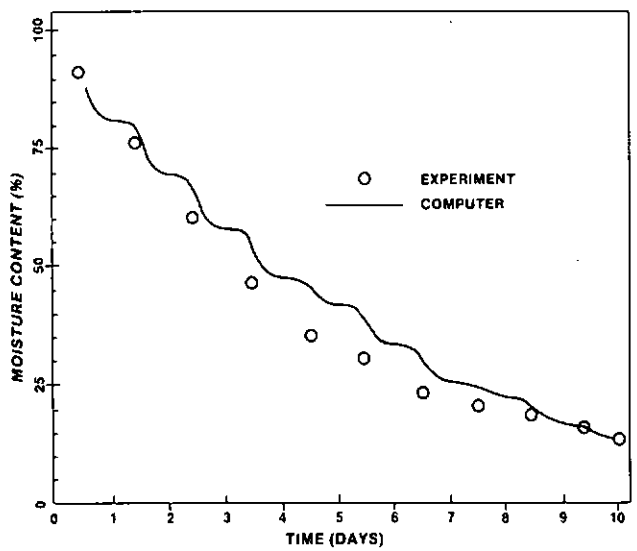

Figure 9. Drying curve using solar collector only--comparison of computer model with experimental data from a 1.2 m^3 kiln (8).

model accurately calculates the kiln dry bulb temperature except for the last 2 days. The assumption that the air temperature and wood temperature are uniform and equal to each other may cause the model to predict higher dry bulb temperatures than were measured. This difference is also illustrated in the relative humidity plot in which the model predicts lower relative humidities than were measured (Figure 8). The model does, however, calculate wet bulb temperatures that are close to the measured temperatures (Figure 7). Very

good correlation between the experiment and theory is indicated for the wood moisture content during the drying time (Figure 9). These results indicate that the model is sufficiently accurate to predict wood drying times when solar energy provides the only source of heat in the kiln.

Model Prediction for 60 m^3 Solar-Dehumidification Kiln

The computer model was used to simulate the operation of a wood dry kiln with the following conditions:

60 m^3 yellow-poplar lumber of 25 mm thickness

91 percent initial wood moisture content

356 m^3 drying chamber

30 Kw dehumidifier

0.75 Kw circulation fans (total of 8)

16 cm fiberglass kiln wall insulation

565 m^2 solar collector area

Late summer weather conditions in Carbondale, Illinois, U.S.A.

Figures 10 to 13 present the drying results assuming that the dehumidifier and the solar collectors are used separately or together to dry the wood. Using the dehumidifier alone, the system is controlled such that the vent blowers are turned on whenever the dry bulb temperature in the kiln exceeds 57 C. However, when the solar collectors are used with the dehumidifier, the solar collectors are turned on whenever the collector outlet temperature is greater than the kiln dry bulb temperature. When operated in this mode, the dehumidifier is operated only when there is no insolation and when the kiln temperature is below 57 C. A better utilization of solar energy occurred when the kiln operating temperature was limited to 57 C.

The highest dry bulb temperature in the kiln is obtained using both the solar energy and the dehumidifier system (Figure 10). Solar energy by itself is unable to get the average temperature over 35 C except for the last few days of drying.

The dehumidifier by itself does not appreciably reduce the relative humidity in the kiln (Figure 11). The lowest relative humidity occurs when the solar collector and the dehumidifier are used together. So the greatest drying occurs when the dehumidifier operates with the collectors (Figure 12). After 10 days of operation,

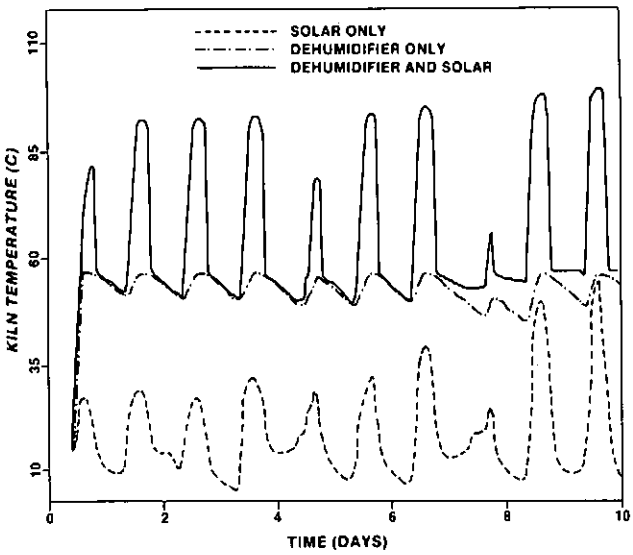

Figure 10. Comparison of kiln dry bulb temperatures when drying with the solar collectors only, the dehumidifier only, and with a combination solar-dehumidification system for a 60 m^3 kiln.

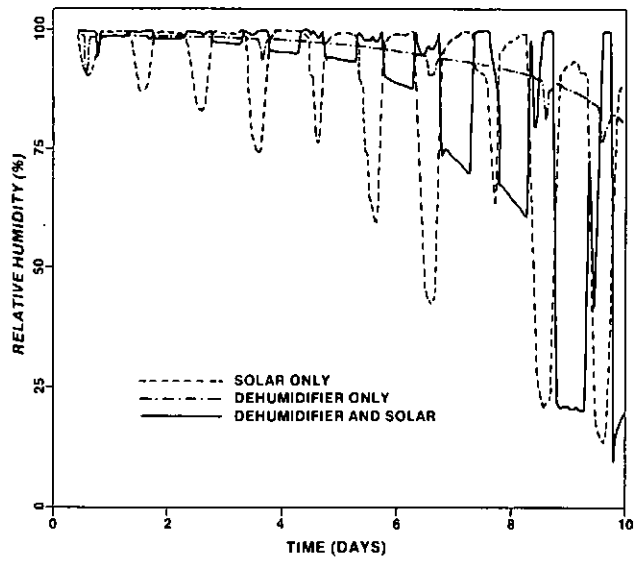

Figure 11. Comparison of kiln relative humidity when drying with the solar collectors only, the dehumidifier only, and with a combination solar-dehumidification system for a 60 m^3 kiln.

the kiln using only solar collectors had dried the wood to 16 percent moisture content, the kiln using only the dehumidifier had dried the wood to 26 percent moisture content, and the combined solar-dehumidification system had reduced the wood moisture content to less than 5 percent.

As shown below, the combined solar-dehumidification system dried yellow-poplar lumber from 90 to 12 percent moisture

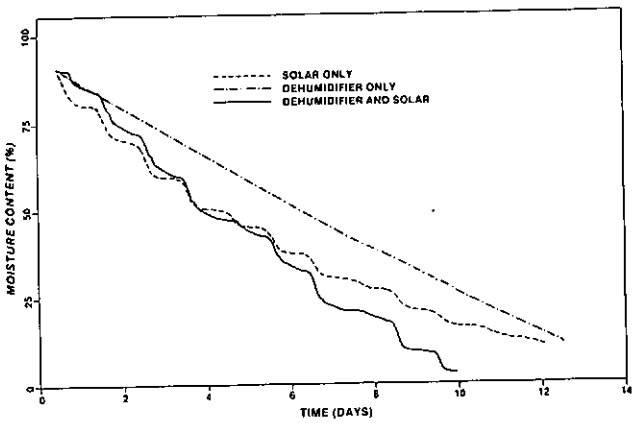

Figure 12. Comparison of drying curves when drying with the solar collector only, the dehumidifier only, and with a combination solar-dehumidification system for a 60 m^3 kiln.

content in less time and with less energy than either system alone (Figure 13).

Drying system	Drying time (days)	Total energy consumption (Kwh)
Solar	11.5	9,840
Dehumidification	12.5	19,300(10,000)[1]
Solar and dehumidification	8.2	8,770(3,620)[2]

[1]Includes 1,300 Kwh of initial resistance heating.
[2]The numbers in parentheses refer to the compressor energy consumption.

We compared these results to the energy and drying data of a commercial dehumidification wood drying system (11). Drying a similar type of wood (25 mm white pine) in a 60 m^3 kiln from 55 to 12 percent moisture content using a 7.5 Kw dehumidifier took 14 days and 110 Kwh/m^3 of energy. For the same moisture content range, the present solar-dehumidification system would use 27 percent less energy (83.8 Kwh/m^3) in a drying time of only 5 days. A conventional steam-fired dry kiln would use about 233 Kwh/m^3 of energy (1), based on assuming twice the amount of energy required to evaporate the moisture in the wood.

CONCLUSIONS

The computer simulation model accurately predicts the drying time for a solar energy lumber dry kiln. The computer results for a typical wood drying operation indicate that electrical energy consumption can be reduced by about 25 percent and drying time by more than 50 percent

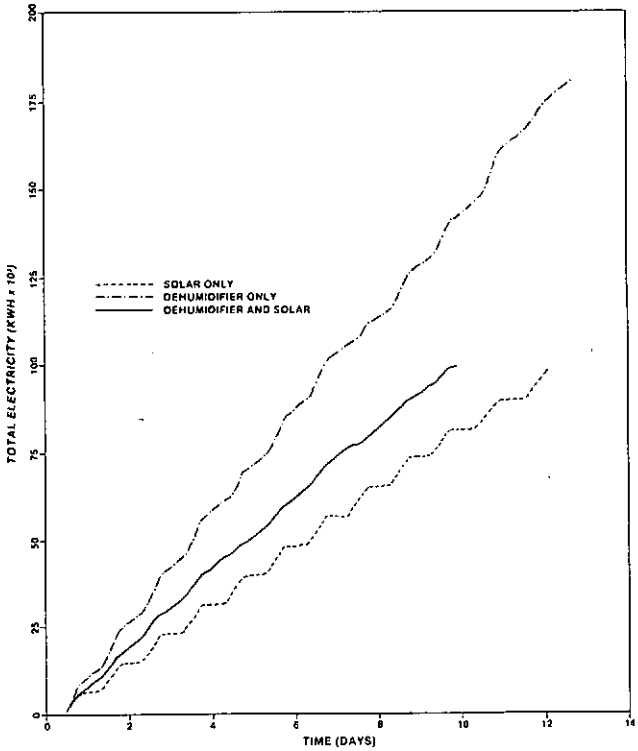

Figure 13. Comparison of electrical energy consumption when drying with the solar collectors only, the dehumidifier only, and with a combination solar-dehumidification system for a 60 m^3 kiln.

using this solar-dehumidification system compared to using dehumidification alone. This represents an energy reduction of about two-thirds over a conventional steam dry kiln during an equivalent drying time.

ACKNOWLEDGMENT

The authors wish to thank the USDA Forest Service for financial assistance in the project.

REFERENCES

1. Skaar, C., Energy requirements for drying lumber, In Practical Application of Solar Energy to Wood Processing, Workshop Proceedings, Virginia Polytechnic Institute and State University, Blacksburg, Virginia, p. 29-32, 1977.
2. McMillen, J. M. and Wengert, E. M., Drying eastern hardwood lumber, Forest Products Laboratory, USDA Forest

Service, Madison, Wisconsin. Agric. Handb. No. 528, p. 70, 1978.
3. Huber, H. A., Dehumidification drying of wood, Woodworking and Furniture Digest 79(5): 51-52, 1977.
4. Freeman, T. L., Computer simulation of heat pumps and the simulation of solar energy-heat pump systems, M.S. Thesis, Solar Energy Lab, University of Wisconsin, Madison, Wisconsin, 1975.
5. Anonymous, American Society of Heating, Refrigerating and Air Conditioning Engineers, ASHRAE Handbook of Fundamentals, Ch. 6, ASHRAE, New York, New York, 1967.
6. Eckelman, C. A. and Baker, J. L., Heat and air requirements in the kiln drying of wood, Research Bulletin 933, Agricultural Experiment Station, Purdue University, West Lafayette, Indiana, March 1976.
7. Van Wylen, G. J. and Sonntag, R. E., Fundamentals of classical thermodynamics, John Wiley and Sons, Inc., New York, New York, Second Edition, p. 649, 1972.
8. Chen, P. Y. S. and Rosen, H. N., Drying yellow-poplar in a highly efficient solar kiln, In Proceedings Annual Western Dry Kiln Clubs Meeting, Coeur d'Alene, Idaho, May 10, 1979.
9. Rosen, H. N., Establishing a schedule for jet drying of 4/4 yellow-poplar, Forest Prod. J. (In press), 1980.
10. Vick, C. B., Drying rate curves for one-inch yellow-poplar lumber in low temperature forced air dryers, Forest Prod. J. 15(12): 500-504, December 1965.
11. Townsend, K., Private communication, Irvington-Moore Co., Jacksonville, Florida, June 1979.

MODELLING AND CALCULATION OF THE DRYING PROCESS OF CAPILLARY POROUS MATERIALS

S. Szentgyörgyi
K. Molnár
M. Örvös

Department of Chemical and Food Engineering, Technical University
Budapest, Hungary

ABSTRACT

Experimental measurements carried out on capillary porous materials have proved for the major part of cases that the density of source of internal evaporation is $\sigma_V = 0$, during the drying period of free moisture, i.e. the moisture arrives in state of liquid-phase to the surface of the wet material and evaporates there. This enables to determine drying velocity and drying time for this region by aid of a relatively simple procedure (1). It also could be stated that in the region of the so-called "falling rate period of drying" an unstable, intermediate zone will develop first, where local recondensations occur, too; $\sigma_V < 0$. Following to this intermediate zone of relatively short duration, the wet material separates into an outer zone of low and an inner zone of higher moisture content which we consider as second falling rate period in the course of our investigations. Evaporation proceeds at the interphase boundary surface, lying between both zones. Moisture arrives from the inner parts of the material to the interphase surface by liquid diffusion and after evaporation it penetrates into the main mass of the drier zone by vapor diffusion. The boundary surface of the wetter zone moves towards the inside of the material as a function of time and the drying process is slowing down accordingly.

NOMENCLATURE

A = surface area, m^2
c = specific heat, J/kgK
Δh_V = evaporation heat, J/kg
L = thickness, m
M = mass, kg
$\mathfrak{M}_W$ = mole weight of moisture, kg/kmol
$\dot{m}$ = mass flux density /drying velocity/ kg/m^2s
$\Delta \bar{m}_L$ = specific moisture reduction, kg/m^2
p = pressure, N/m^2
$\dot{q}$ = heat flux density, W/m^2
$\mathfrak{R}$ = universal gas constant, 8.3443 J/molK
s = slope of the tension curve, N/Km^2
T = temperature, K
t = time, s
V = volume, m^3
v = velocity, m/s
W = mass of moisture, kg
X = moisture content of dry material, kg/kg
Z = thickness of non-moving dry bed, m
z = co-ordinate, m
α = heat transfer coefficient, W/m^2K
β = mass transfer coefficient, m/s
δ = eigenvalue
δ_{eff} = effective diffusion coefficient, m^2/s
κ = thermal diffusivity, m^2/s
Γ = temperature factor, according to Eq.(17)
λ = thermal conductivity, W/mK
ξ = location co-ordinate, m
Ω = value, determined by Eq.(24)
φ = degree of saturation
ϑ = non-dimensional temperature value
ρ_{OS} = density of the dry material, referred to the volume of the wet material, kg/m^3

Non-dimensional numbers

Bi = Biot number
Fo = Fourier number

Subscripts

I = dried region
II = wet region
a = asymptotic state

b = dew point /modified/
cr = critical
F = surface area
G = gas-phase
h = heat transfer
hm = simultaneous heat and mass transfer
j = leap of moisture content
L = liquid-phase
ℓ = lower approximation
m = mass transfer
0 = initial state; and for surface: value at the location z=0, resp.
S = saturated
u = upper approximation
V = vapor-phase
W = moisture
Z = thickness, referring to non-moving dry bed
ξ = evaporation front of layer of varying thickness

Superscripts

I = dried region
II = wet region
~ = average
* = equilibrium

INTRODUCTION

The method described in (2) has been extended to the above mentioned second falling rate period of drying. The comparison of calculated and measured results clearly show that temperature distributions as well as time requirements in the second falling rate period can be determined by the aid of our calculation method to a rather close approximation. —

There exists a certain group of materials among those ones which are submitted to drying, in the case of which an evaporation front penetrates into the deeper lying layers of the drying material, during the falling rate period of drying.

Figure 1 demonstrates a plate of gypsum--pearlite of 80 to 20% by volume, where the location of the front at different time values can be observed well by the temperature distribution.

From the starting time t_0 of the front on, the relationship between the average moisture content of the material and the location of the front is linear for a while, as shown in Figure 2.

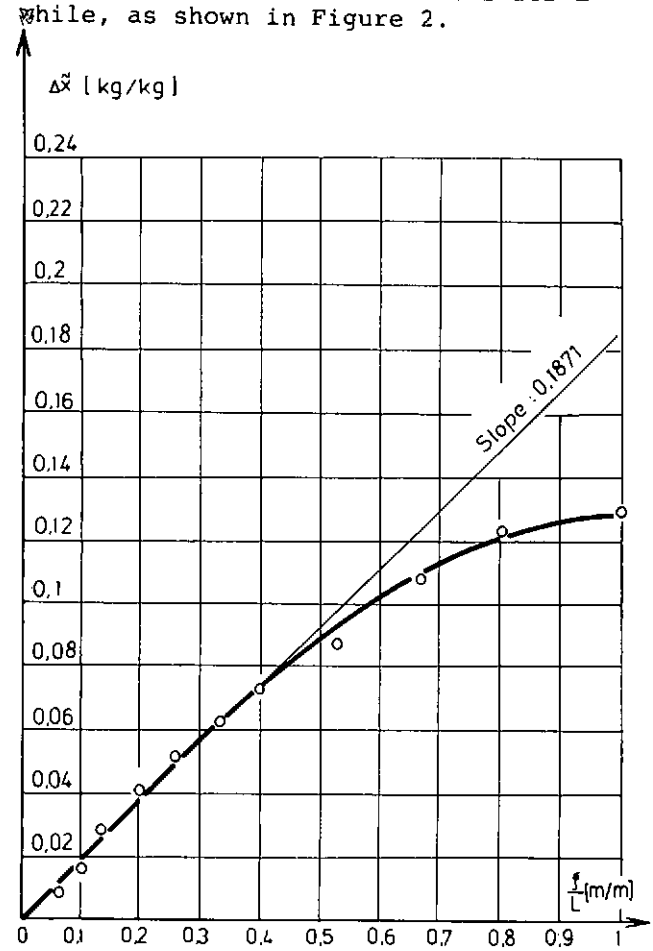

Figure 2

Hence, in the linear section for which

$$m = \text{const},$$

the slope of the straight line is

$$\Delta\bar{x} = \bar{x}_0 - \bar{x} = m\frac{\xi}{L} \qquad (1)$$

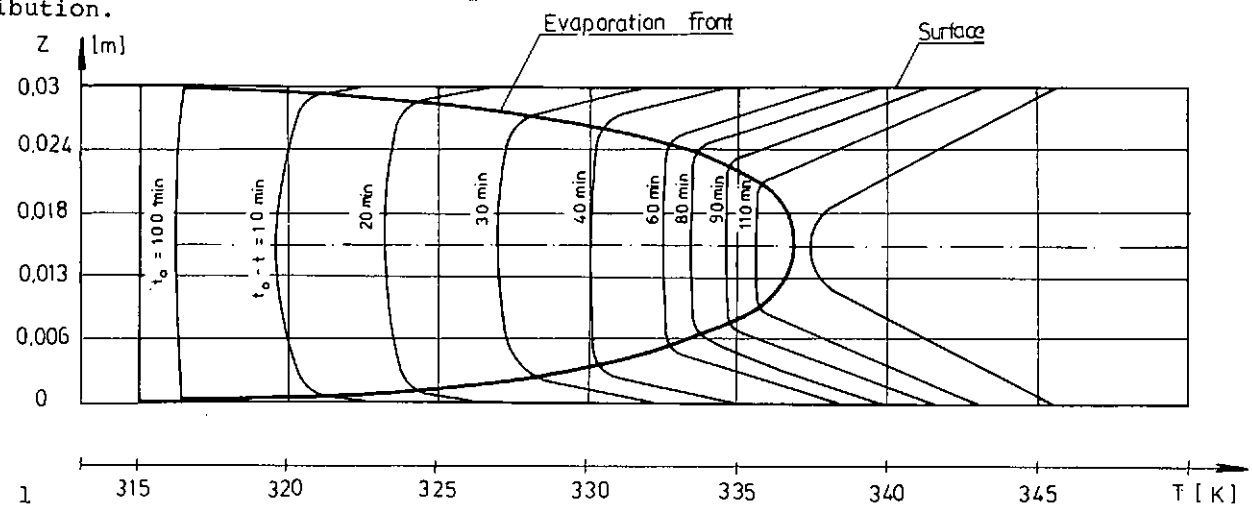

Figure 1

It follows from Eq. (1) that in the linear section a drier zone of moisture content: (zone I) X^{I} = const precedes the evaporation front, while a wetter zone of moisture content: (zone II) X^{II} = const succeeds it. At the evaporation front, however, a leap of the moisture content can be observed, i.e.

$$m = (\Delta X)_j = X^{II} - X^{I} = \text{const} \quad . \qquad (2)$$

Our above mentioned considerations are shown in Figure 3.

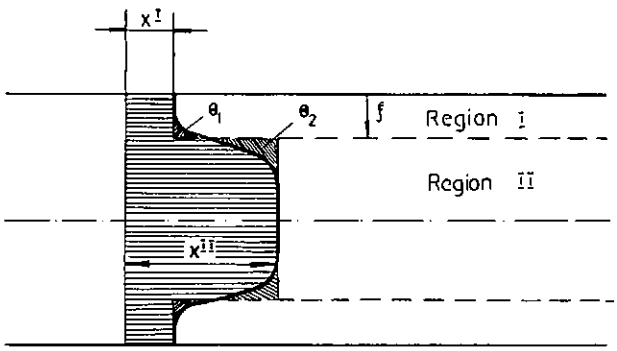

Figure 3

These considerations can be acknowledged, since

$$\Delta\tilde{X} = \tilde{X}_0 - \tilde{X} = \frac{M_{LO} - M_L}{M_S} \qquad (3)$$

according to the definition.

On the basis of Figure 3

$$M_{LO} = M_S X^{II} = \rho_{OS} LAX^{II} - \rho_{OS} A(\theta_1 - \theta_2) \qquad (4)$$

can be written, while

$$M_L = \rho_{OS} LAX^{I} + \rho_{OS}(L-\xi)\, A(X^{II} - X^{I}) - \rho_{OS} A(\theta_t - \theta_2). \qquad (5)$$

Analyzing the drying velocity curve of the examined material (Figure 4), it follows that the leap of the moisture content $(\Delta X)_j$ is just equal to the difference of the critical and the equilibrium moisture content, i.e.

$$m = (\Delta X)_j = \tilde{X}_{cr} - \tilde{X}^{*} \quad . \qquad (6)$$

Thus, from Eqs (4), (5) and (6) by application of Eq. (3), Eq. (1) can be obtained.

All these considerations also mean that in the linear section moisture content which precedes the evaporation front is at equilibrium, while that one which succeeds it, is the critical moisture content, i.e.

$$X^{I} = \tilde{X}^{*} \quad , \quad X^{II} = \tilde{X}_{cr} \, .$$

Mathematical Model of the Linear Section

Since the terms X^{I} and X^{II} are both constant, the energy-balance of both zones can

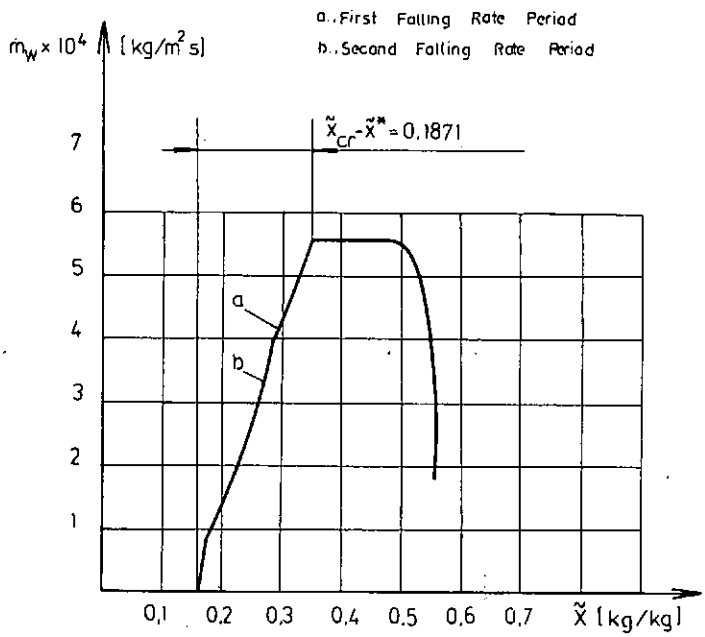

Figure 4

be written as (1):

$$\frac{\partial T^{I}}{\partial t} = \kappa_{I} \frac{\partial^2 T^{I}}{\partial z^2} \qquad (7)$$

and

$$\frac{\partial T^{II}}{\partial t} = \kappa_{II} \frac{\partial^2 T^{II}}{\partial z^2} \qquad (8)$$

according to the denotations of Figure 5.

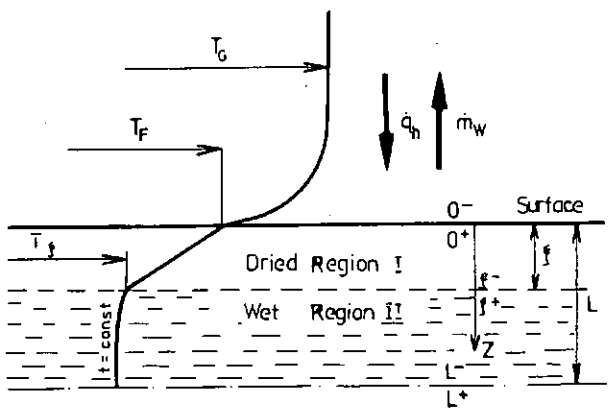

Figure 5

Uniqueness Conditions

Following to Figure 1, the initial condition is:

$$T^{I}(z,0) = T^{II}(z,0) = T_0 \cong \text{const} \qquad (9)$$

The boundary conditions are:

1. In the median /symmetry/ plane, at the

location z = L:

$$\left.\frac{\partial T^{II}}{\partial z}\right|_{z=L} = 0 \qquad (10)$$

2. At the evaporation front, at the location $z = \xi$:

$$\dot{q}\Big|_{z=\xi^-} = -\lambda_I \left.\frac{\partial T^I}{\partial z}\right|_{z=\xi^-} = -\lambda_{II} \left.\frac{\partial T^{II}}{\partial z}\right|_{z=\xi^+} +$$

$$+ \dot{m}_W \Delta h_V \qquad (11)$$

3. At the surface of the material, at the location z = 0:

$$\dot{q}\Big|_{z=0} = \alpha_G (T_G - T_F) = -\lambda_I \left.\frac{\partial T^I}{\partial z}\right|_{z=0^+} \qquad (12)$$

On the basis of Eq. (1) the drying velocity can be written as:

$$\dot{m}_W = \frac{M_S}{A}\frac{d\bar{X}}{dt} = \rho_{OS}\,(\Delta X)_j \frac{d\xi}{dt} \qquad (13)$$

Thus, boundary condition (11) can also be expressed by the penetration velocity of the front, i.e.:

$$\dot{q}\Big|_{z=\xi^-} = -\lambda_I \left.\frac{\partial T^I}{\partial z}\right|_{z=\xi^-} = -\lambda_{II} \left.\frac{\partial T^{II}}{\partial z}\right|_{z=\xi^+} +$$

$$+ \rho_{OS}(\Delta X)_j \frac{d\xi}{dt} \Delta h_V \qquad (14)$$

Considering the uniqueness conditions (9), (10), (12) and (14), the Eqs (7) and (8) can be solved by the aid of the numerical solution published in Ref. (2,3).

Approximate Solutions

According to the steps published in details (2,3), for the linear section the following relation between drying velocity and location of the front can be obtained:

$$\Delta t = t_\xi - t_0 = \frac{\rho_{OS}(\Delta X)_j \Delta h_V}{T_G - T_b}\left(\frac{1}{\alpha_G} + \frac{RT_G}{\beta M_W s \Delta h_V}\right)\xi +$$

$$+ \frac{\rho_{OS}(\Delta X)_j \Delta h_V}{T_G - T_b}\left(\frac{1}{\lambda_I} + \frac{RT_\xi}{\delta_{eff} M_W s \Delta h_V}\right)\frac{\xi^2}{2} +$$

$$+ \int_0^t \Gamma_{Za}(t)\vartheta_\xi dt \qquad (15)$$

Here

$$s = \frac{p_{V\xi} - p_{VG}}{T_\xi - T_b} \cong \text{const} \qquad (16)$$

if we assume the relation between p_V and T_ξ to be linear in the discussed section. Then, T_b is the value of this straight line, taken at p_{VG}.

Furthermore,

$$\Gamma_{Za} = \frac{T_0 - T_{Za}}{T_b - T_{Za}} \qquad (17)$$

and

$$\vartheta_\xi = \frac{T_\xi - T_{Za}}{T_0 - T_{Za}} \qquad (18)$$

In Eqs (17) and (18), T_{Za} represents the temperature, in case of a double layer material of external layer-thickness: Z = const. The evaporation front at the location Z can be written as:

$$\dot{q}_a = \dot{m}_{Wa}\,\Delta h_V \qquad (19)$$

for the asymptotic /equilibrium/ state (2, 3).

Since, from Eqs (1) and (3)

$$\xi = L\frac{\Delta\bar{X}}{(\Delta X)_j}, \quad \text{therefore,} \qquad (20)$$

from Eq. (15)

$$\frac{\Delta t}{\Delta\bar{X}} = \rho_{OS} L \frac{\Delta h_V}{T_G - T_b}\left(\frac{1}{\alpha_G} + \frac{RT_G}{\beta M_W s \Delta h_V}\right) +$$

$$+ \frac{\rho_{OS} L^2}{2(\Delta X)_j}\frac{\Delta h_V}{T_G - T_b}\left(\frac{1}{\lambda_I} + \frac{RT_\xi}{\delta_{eff} M_W s \Delta h_V}\right)\Delta\bar{X} +$$

$$+ \frac{1}{\Delta\bar{X}}\int_{t_0}^{t_\xi} \Gamma_{Za}(t)\vartheta_\xi dt \qquad (21)$$

The right hand side of Eq.(21) consists of three terms: i.e. of one constant term, one term which is varying linearly with $\Delta\bar{X}$ and one transcendent term.

A lower and an upper approximation has been deduced for the numerators of the third terms of Eq. (21), as described in Ref. (2, 3).
Hence,

$$\Gamma_{0a}\int_{t_0}^{t_{\vartheta\xi}} \vartheta_0 dt < \int_{t_0}^{t_\xi} \Gamma_{Za}(t)\vartheta_\xi dt \leq \Gamma_{Za}\int_{t_0}^{t_{u\xi}} \vartheta_z dt \qquad (22)$$

where

$$\Gamma_{Za}\int_{t_0}^{t_{\vartheta\xi}} \vartheta_z dt = \Gamma_{Za}\frac{(L-Z)^2}{\kappa_{II}}\frac{1}{Bi_{hmZ}}\Omega_Z \qquad (23)$$

Here, Ω_Z is the value of the transcendent correlation:

$$\Omega = f(Fo, Bi_{hm}) =$$

$$= \sum_{k=1}^{k=\infty} 2\frac{\sin\delta_k}{\delta_k^2 + \delta_k \sin\delta_k \cos\delta_k}(1 - \delta_k^2 Fo_k) \qquad (24)$$

considered

for the variables Bi_{hmZ} and F_{OZ}, the solution of which is given in Figure 6.

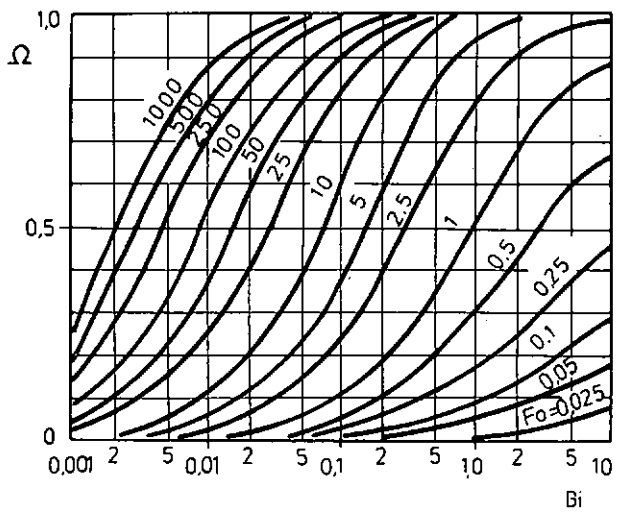

Figure 6

Now

$$Bi_{hmZ} = \frac{1}{\frac{\lambda_{II}}{L\alpha_G} + \frac{Z}{L}\frac{\lambda_{II}}{\lambda_I}} \left[1 + \frac{s\Delta h_V \left(\frac{1}{\alpha_G} + \frac{Z}{\lambda_I} \right)}{\frac{RT_G}{\beta M_W} + Z\frac{RT_\xi}{\delta_{eff} M_W}} \right] \quad (25)$$

$$Fo_Z = \frac{\kappa_{II}\, \Delta t_u}{(L - Z)^2} \quad (26)$$

while the values of δ_k represent the solutions of the transcendent equation:

$$\delta_k = \operatorname{ctg} \delta_k Bi_{hm} \quad . \quad (27)$$

Furthermore,

$$\Gamma_{Za} = \frac{T_O - T_{Za}}{T_b - T_{Za}} \quad . \quad (28)$$

In the Fourier number, the term

$$\Delta t_u = t_{u\xi} - t_O \quad (29)$$

is the time interval, required for the reduction of moisture content

$$\Delta \bar{X} = \bar{X}_O - \bar{X} \quad (30)$$

in case of the upper approximation. For the reduction of moisture content $\Delta\bar{X}$, the value $Z=\xi$ which can be calculated from Eq. (20) must be substituted into the above mentioned equations.

From certain Fourier numbers on, the upper approximation can be achieved rather well, applying the values obtained for $\Omega_Z = 1$, by Eq. (23), as was shown in Figure 6.

The lower approximation can be calculated according to Eqs (23) to (28), although Z=0 must be substituted. The term

$$\Delta t_\ell = t_{\ell\xi} - t_O \quad (31)$$

being the time interval required for the reduction of moisture content $\Delta\bar{X}$, considered equal to the upper approximation, must be substituted for the Fourier number, into Eq. (26).

In case of both, upper and lower approximation, the values which have to be substituted for the Fourier number, must be determined by aid of trial and error so that Δt figuring at the left hand side of the balance corresponding to Eq. (21) should be equal to the difference of the integral limits which appear in the third term at the right hand side.

The determination of the relationship between temperature T_ξ at the evaporation front and partial pressure $p_{V\xi}$ of moisture vapor can be regarded as the most difficult problem of the solution. The sudden change of moisture content at the evaporation front also means that there the relative moisture content of equilibrium considered according to the isotherm of sorption, will change suddenly, too. Some kind of average value can be obtained for it from $p_{V\xi}$ at the evaporation front.

For the examined model

$$\varphi_\xi = \frac{p_{V\xi}}{p_{VS}} \cong 0.55$$

has been obtained from measurement results in the linear range of the front.

Thus, in our calculations the values for s and T_b have been obtained by linear approximation of the curve of degree of saturation; i.e.:

$$\varphi = 0.55 = \text{const} \quad .$$

Comparison of Measured and Calculated Results

The studied model has been a plate of gypsum-pearlite of 80 to 20% per volume, as already mentioned above, its size being 0.1 x 0.1 x 0.03 m.

The plate was dried in a drying channel, by means of warm air, while its weight and temperature distribution according to thickness has been measured as a function of time.

The state characteristics of drying air are:

$$T_G = 354 \text{ K}$$
$$P_{VG} = 3\,166.57 \text{ N/m}^2$$
$$v_G = 1.96 \text{ m/s}$$

The state characteristics of the wet material are:

$$T_O = 316.5 \text{ K}$$
$$\tilde{X}_O = 0.288 \text{ kg/kg}$$
$$\rho_{OS} = 780 \text{ kg/m}^3$$

Temperature distribution obtained from the measured results is demonstrated in Figure 7, while $\Delta t/\Delta\tilde{X}$ vs. $\Delta\tilde{X}$, is shown in Figure 8.

Calculations were carried out by using the following data:

$$\alpha_G = 26.74 \text{ W/m}^2\text{K}$$
$$\beta = 0.0319 \text{ m/s}$$
$$\lambda_I = 0.2758 \text{ W/mK}$$
$$\lambda_{II} = 0.78 \text{ W/mK}$$
$$\delta_{eff} = 2.63 \times 10^{-5} \text{ m}^2/\text{s}$$
$$\kappa_I = 2.44 \times 10^{-7} \text{ m}^2/\text{s}$$
$$\kappa_{II} = 7 \times 10^{-7} \text{ m}^2/\text{s}$$
$$R = 8.3143 \text{ J/molK}$$
$$s = 394.3 \text{ N/m}^2\text{K}$$
$$L = 0.015 \text{ m}$$
$$T_b = 326.16 \text{ K}$$
$$\Delta h_V = 2375.172 \text{ kJ/kg}$$
$$M_W = 18 \text{ kg/kmol}$$

The transport and material characteristics have been determined by measurements. The results of the calculations are contained in Figures 7 and 8, too.

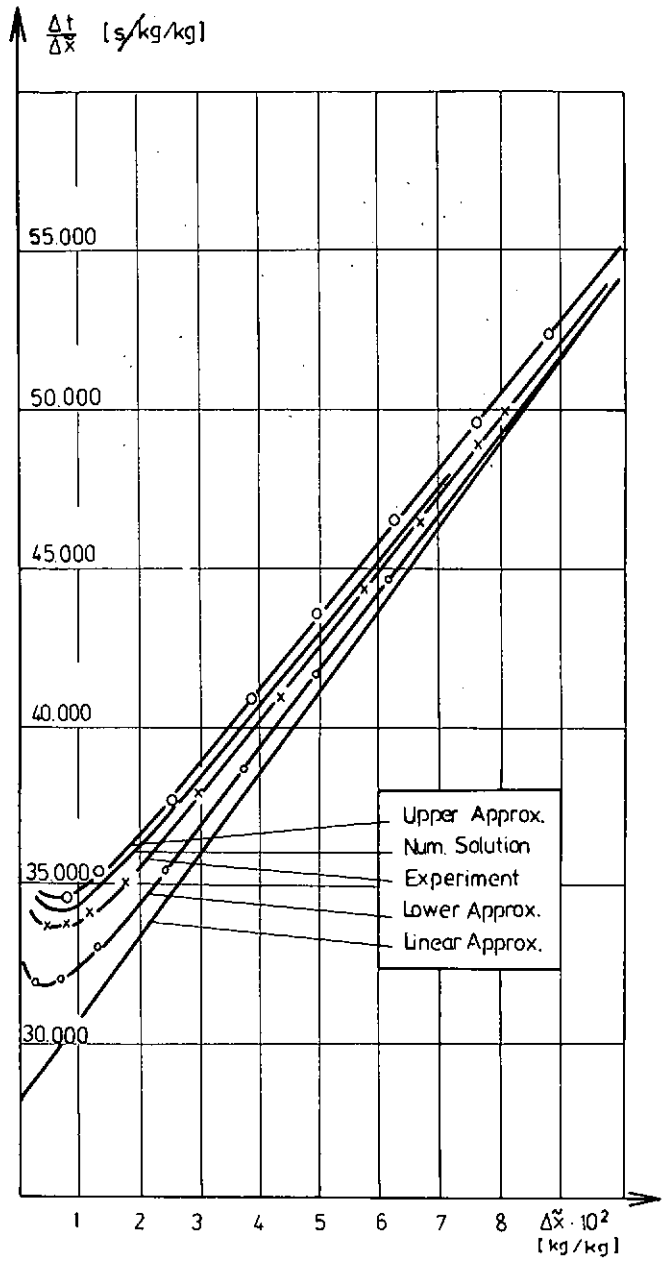

Figure 7

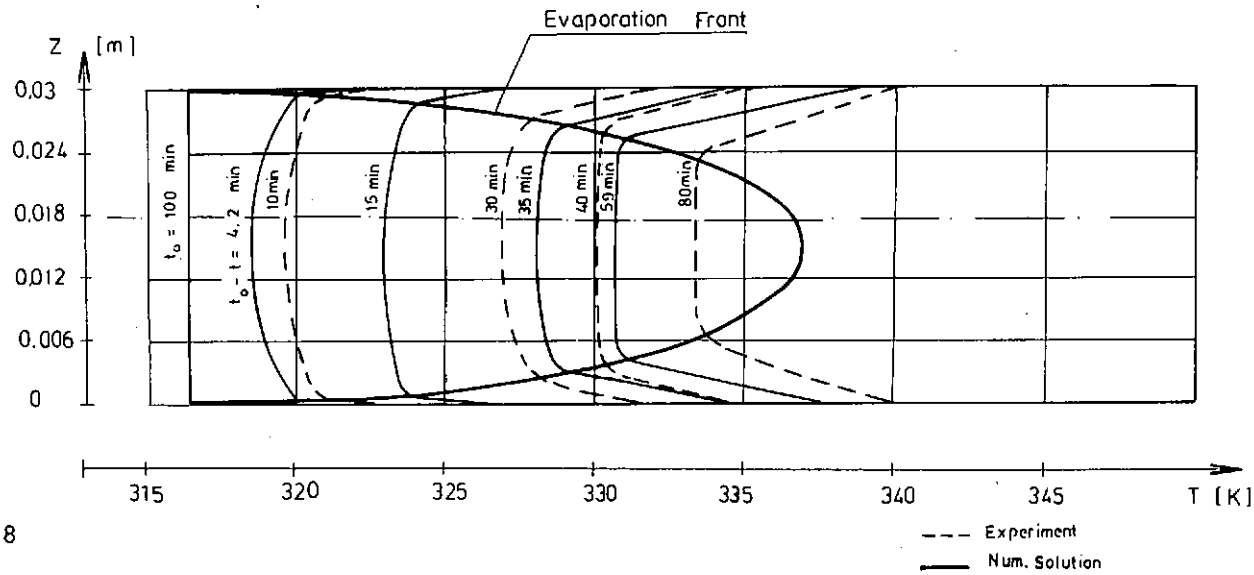

Figure 8

From Figures 7 and 8 it can be seen, that the calculation methods agree well with the measurement results.

If we wish to know temperature distribution, too, it is worth to apply the numerical solution obtained by aid of computer, while the application of the lower and upper approximations is advisable if only the determination of the time requirement of drying is desired. A satisfactory approximation /see Fig.8/ can be achieved rather quickly, if the curve of the lower or the upper approximation obtained for $\Omega=1$, is accepted as result.

REFERENCES

1. Luikov,A.V., Heat and Mass Transfer in Capillary-Porous Bodies, Pergamon Press, Oxford, 1966

2. Szentgyörgyi,S., and Molnár K., Calculation of Drying Parameters for the Penetrating Evaporation Front, Proc. of 1st Int.Symp. on Drying, Science Press, Montreal, 1978

3. Szentgyörgyi,S., and Molnár K., Acta Technica, 88, 3-4 /in print/

FIGURES

Figure 1 Evaporation Front vs. Time and Temperature

Figure 2 Relation between Moisture Content and Location of Front

Figure 3 Model of Moisture Content Distribution

Figure 4 Drying Velocity of Examined Model

Figure 5 Denotations of Examined Model

Figure 6 Ω vs. Biot Number and Fourier Number

Figure 7 Comparison of Experiments and Numerical Solutions

Figure 8 Evaporation Front vs. Time and Temperature for the Numerical Solution

PHENOMENOLOGICAL COEFFICIENTS FOR HEAT AND MASS TRANSFER EQUATIONS IN WET POROUS MEDIA

M.A. Roques[1] and A.R.H. Cornish[2]

1. Institut National Polytechnique de Lorraine, Nancy, France
2. Imperial College of Science and Technology, London, England

ABSTRACT

The transport equations generally used for studying the drying of moist solids under isobaric conditions are derived from general conservation equations and from specific constitutive equations. Whatever format is used to express the constitutive equations: classical or non-equilibrium thermodynamics, the evaluation of the phenomenological co-efficients remains the key-point for any simulation or modelisation.

This paper compares the expressions for those coefficients as found by the authors (1) with those existing in the literature. The use of thermodynamics of irreversible processes, leads to an acceptance of the presence of a new reciprocal effect in the heat flux equation. It is shown that the existence of this effect is linked to the variation of water chemical potential with temperature and that the effect remains small under normal circumstances for wetted beds of sand.

NOMENCLATURE

Roman Letters

D	: diffusion coefficient of water vapour in air.
$D_{L\theta}, D_{V\theta}$	:coefficients for moisture-induced liquid and vapour flow
D_{LT}, D_{VT}	:coefficients for temperature-induced liquid and vapour flow
j_L, j_V	:mass fluxes of liquid and vapour
j_q	:heat flux.
k	:relative permeability of liquid water in pores
L_{ij}	:Onsager coefficients
P	:total pressure
p_a, p_V	:partial pressure of air and water vapour.
p_s	:saturation pressure of liquid water
r	:radius of pore
R	:gas constant for water
T	:temperature
u	: moisture content per unit mass of dry body.
X	:driving force

Greek Letters

ε	:gas phase volumetric content
θ	:liquid water volumetric content
λ_{eq}	:equivalent thermal conductivity
Λ	:enthalpy change for vaporization of pure water.
μ	:chemical potential per unit mass
ν	:kinematic viscosity of liquid water.
ρ_L, ρ_V, ρ_s	:density of liquid water, water vapour and solid
σ	:surface tension
τ	:tortuosity factor for diffusion of gases in porous media.
ψ	:capillary potential
∇	:nabla
ΔH_V	:enthalpy change for desorption

ΔH_W :enthalpy change for wetting.

Subscripts

a	air
L	liquid water
V	water vapour
q	heat
s	solid
W	water
T	temperature

INTRODUCTION

A porous medium, which contains a degree of moisture, can be subjected to a set of gradients which will cause heat or mass to be transferred. These gradients are water vapour partial pressure, local humidity, temperature, total pressure and gravity. If one disregards the last two, the governing equations for heat and mass transfer must be derived and reasonable values for the coefficients must be found either from the structural properties of the medium or from experiments.

There are only two approaches which can be used to express the constitutive equations for such a problem:

Continuum mechanics as in the pioneering work of Philip and de Vries (2) and Luikov (3) followed by the more elaborate works of Slattery (4)(5) and Whitaker (6).

Linear thermodynamics of irreversible processes (T.I.P.) as in the early works of Cary and Taylor (7) and Valchar (8) and in the recent paper of Rogues and Cornish (9) and Fortes and Okos (9).

The procedure which leads to the constitutive equations by means of linear T.I.P. is adapted from Prigogine (10) and described in the last two references. It is important to note the limitations on the use of T.I.P. The well-established theories of transport phenomena treated by T.I.P. deal with monophase continua (11). The extension to multi-phase quasi continua has not yet received complete approbation. For the problem of heat and mass transfer in an unsaturated moisture bearing medium, two extensions to the field of application of T.IP. must be made:

$\{E^1\}$ the medium contains three phases (solid, liquid, gas)

$\{E^2\}$ the scale of homogeneity of the medium is far greater

than the molecular scale of the classical phenomena treated by T.I.P. In the present case, the scale is the diameter of a sphere in which there is no appreciable change in the variables of state describing the local situation (T, p_V, θ). In other words, this sphere is the averaging volume used by Slattery (4)(5), Whitaker (6) and Shapiro and Moran (12) in order to derive the transport equations from classical continuum mechanics. Even if the possibility of making such extensions to T.I.P. is admitted, the practical value of its use is still to be assessed.

CONSTITUTIVE EQUATIONS AS DERIVED FROM T.I.P.

The two approaches to the derivation can be compared, even when the problem is deliberately simplified with the following assumptions:

$\{A^1\}$ the total pressure is constant (no filtration)

$\{A^2\}$ the influence of gravity is negligible.

$\{A^3\}$ the inert gas velocity is negligible (stagnant air)

These assumptions are currently made for drying under moderate conditions. A more fundamental assumption is widely advanced, although not always clearly stated:

$\{A^4\}$ there is local equilibrium between vapour and liquid: This means that there are no heat and mass transfer co-efficients between the two phases within the medium. Thus the fluxes of pure heat, liquid water and water vapour may be written as follows:

$$\{1\}\quad \begin{aligned} j_q &= L_{qq} X_q + L_{qL} X_L + L_{qV} X_V \\ j_L &= L_{Lq} X_q + L_{LL} X_L + L_{LV} X_V \\ j_V &= L_{Vq} X_q + L_{VL} X_L + L_{VV} X_V \end{aligned}$$

This set of equations contains nine coefficients which fall into four categories:-

-three direct coefficients L_{qq}, L_{LL} and L_{VV},

-two typical cross coefficients L_{LV} and L_{VL},

representing the interaction between phases;

-two Dufour-like coefficients L_{qL} and L_{qV}, which characterise the flow of heat induced by a gradient in vapour or liquid potential;

-two Soret-like coefficients L_{Lq} and L_{Vq}, which characterise the flows of matter induced by a temperature gradient.

The corresponding set of driving forces may be written:

$$X_q = - \nabla T/T^2$$

$$\{2\} \qquad X_L = - \frac{1}{T} \nabla_T \mu_L$$

$$X_V = - \frac{1}{T} \nabla_T \mu_V$$

In equations {2}, the subscript T refers to an isothermal gradient. The local equilibrium assumption {A4} implies that the chemical potentials of water in the vapour and the liquid phases are equal. This equality has the following important consequence:

$$\{3\} \qquad X_L = X_V$$

In practice, a single gradient of chemical potential, hereafter referred to as X_W, is used to replace the gradients of water vapour partial pressure and of liquid water content. This sole fact should encourage the use of the T.I.P. format to express the constitutive equations. The form of equations {2} can then be simplified. It is effectively impossible and irrelevant to make any distinction between the fluxes $L_{LL}X_W$ and $L_{LV}X_W$; the coefficients can be combined into L_{LW}. Similarly, the coefficients L_{VL} and L_{VV} can be combined in the form L_{VW}. Hence, the linear relationships between fluxes and forces become:

$$j_q = L_{qq}X_q + (L_{qL} + L_{qV})\ X_W$$

$$\{4\} \quad j_L = L_{Lq}\ X_q + L_{LW}\ X_W$$

$$j_V = L_{Vq}\ X_q + L_{VW}\ X_W$$

The Onsager symmetry relation provides the further simplifications:

$$\{5\} \quad L_{qL} = L_{Lq} \text{ and } L_{qV} = L_{Vq}$$

DESCRIPTION OF THE STATE OF WATER

The two basic variables necessary to describe the state of bound water in the porous medium are the water content u, expressed as mass of water per unit mass of dry solid, or the volumetric liquid moisture content θ and the temperature. The total water content u is equal to the sum of liquid water content u_L plus water vapour content u_V. Generally the description of a wet medium is precise enough when one assumes:

$$\{A^5\} \quad u \simeq u_L \text{ or } u \simeq \frac{\rho_L \theta}{\rho_s(1-\epsilon_{dry})}$$

The two variables T and u will determine without ambiguity any chosen thermodynamic function. Usually this macroscopic function is taken to be the water activity or the capillary potential depending on the state of the moisture. It appears that the formulation of the equations with chemical potential μ_W as a state function of u and T will be more compact and will cover a wider range of situations. Nevertheless, the evaluation of this potential will have to be made differently for the two basic states of bound moisture: hygroscopic and non-hygroscopic. The situation can be summarised in a table in the following manner.

State of moisture	Thermodynamic function	Type of experiment
Hygroscopic	Water activity	Sorption-desorption isotherm
Non-hygroscopic	Capillary potential	Suction experiment. Capillary rise and drain

For the hygroscopic state, the chemical potential of bound liquid μ_L, or that of water vapour in equilibrium with the liquid μ_V, is linked to the chemical potential of pure liquid water at the same temperature: μ_L^*

$$\{6\} \quad \mu_V = \mu_L \simeq \mu_L^* + RT \ln (p_V/p_s)$$

where p_V/p_s is the liquid water activity.

For the non-hygroscopic state, the water vapour pressure reduction is negligible if the pore radii are larger than

10^{-7}m. This means that although the water is bound by weak forces, precise knowledge of these binding energies is essential because their spatial gradients may be important. A capillary drain curve or a suction experiment will give the chemical potential as a function of moisture content (3). Here, the expression for the chemical potential of water takes the following form:

{7} $\mu_V = \mu_L \simeq \mu_L^* - \psi$ where ψ is the capillary potential.

The potential ψ for a single pore of radius r is given by:

{8} $$\psi = \frac{2\,\sigma \cos \sigma}{\rho_L r}$$

and for a porous body submitted to a drainage experiment by:

{9} $\psi = \frac{h}{\rho_L}$, where h is the height above the level of free water. In spite of the fact that the vapour pressure reduction is not experimentally measurable, one can still write:

{10} $RT \ln (p_V/p_s) = -\psi$

One can see that it is not correct to oppose the use of capillary potential or liquid water activity (9), since they are two forms of the same function of state, in so far as the common driving force for liquid and vapour can always be written:

{11} $X_W = \frac{1}{T} \nabla_T \psi$

COMPARISON OF THE VARIOUS CONSTITUTIVE EQUATIONS

The classical constitutive equations are as follows:

{12} $j_q = -\lambda_{eq} \nabla T$ Fourier's law

{13} $j_L = \frac{k}{\nu} \rho_L \nabla \psi$ form of Darcy's law

{14} $j_V = -\varepsilon\tau \frac{P}{P_a} D \nabla \rho_V$ Fick's law

In equation {12}, λ_{eq} is the equivalent heat conductivity of the wetted bed. It takes into account conduction in the three phases. However, it must be emphasised that it does not include contributions from the effects of convection or from evaporation-condensation cycles.

Since j_V is a mass flux per unit cross-sectional area of medium, the gas phase volumetric fraction ε must be taken into account using Dupuit's expression. Note that ε varies with water content i.e. the extent to which the pore volumes are filled. The mass concentration of vapour in the voids is given by

{15} $\rho_V = \frac{p_V}{RT}$

Most authors, using a mechanistic approach, (2)(3)(6)(12)(13)(14) write the Darcy and Fick's laws in their non-isothermal forms and obtain a set of constitutive equations expressed with T and u or θ as variables. This procedure cannot produce a second term in the heat flux equation {12}, such as $(L_{qL}+L_{qV})X_W$ in equation {3}. So the second feature of T.I.P. is to introduce into the heat flux equation a contribution arising from a water activity gradient. For this reason, the authors suggest that the original work of Luikov(2) and of those using Luikov's model be regarding as belonging to the classical approach.

In general, the system of constitutive equations are written as follows: (12)(13)(14)

{16}
$$j_q = -\lambda_{eq} \nabla T$$
$$j_L = -\rho_L (D_{L\theta} \nabla_T \theta + D_{LT} \nabla T)$$
$$j_V = -\rho_L (D_{V\theta} \nabla_T \theta + D_{VT} \nabla T)$$

The two approaches pretend to describe the same physical reality so that it is tempting to identify the coefficients of equations {4} with {12} {13} and {14}. This has been done systematically by Roques and Cornish (1) followed by Fortes and Okos (9). Without making any assumptions, the following equivalences can be written:

{17}
$$D_{L\theta} = -\frac{k}{\nu}\frac{\partial \psi}{\partial \theta}; \qquad L_{LW} = \frac{k}{\nu}\rho_L T$$
$$D_{LT} = -\frac{k}{\nu}\frac{\partial \psi}{\partial T}; \qquad L_{Lq} = -\frac{k\rho_L T^2}{\nu}\frac{\partial \psi}{\partial T}$$
$$D_{V\theta} = \frac{D\varepsilon\tau P}{\rho_L P_a}\frac{\partial \rho_V}{\partial \theta}; \qquad L_{VW} = -\frac{TD\varepsilon\tau P}{P_a}\frac{\partial \rho_V}{\partial \psi}$$
$$D_{VT} = \frac{D\varepsilon}{\rho_L}\tau\frac{P}{P_a}\frac{\partial \rho_V}{\partial T}; \qquad L_{Vq} = T^2 D\varepsilon\tau\frac{P}{P_a}\frac{\partial \rho_V}{\partial T}$$

At constant total pressure and humidity, the partial derivative $\partial\psi/\partial T$ is linked to the enthalpy of wetting ΔH_W whatever the situation: hygroscopic or not. One can write:

{18} $\frac{\partial \psi}{\partial T} = \frac{\psi}{T} - \frac{\Delta H_W}{T}$ with $\Delta H_W = \Delta H_V - \Lambda$

ΔH_V and Λ are the enthalpy changes for desorption of water in the solid and for vaporisation of pure water. The other partial derivatives can be written:

$$\{19\}\quad \frac{\partial \rho_V}{\partial T} = \frac{P_V}{RT^2}\left[\frac{\Lambda}{RT} - 1\right] + \frac{P_V}{R^2T^2}\left[\frac{\psi}{T} - \frac{\partial \psi}{\partial T}\right]$$

$$\{20\}\quad \frac{\partial \rho_V}{\partial \theta} = -\frac{\partial \psi}{\partial \theta}\,\frac{P_V}{R^2T^2}$$

$$\{21\}\quad \frac{\partial \rho_V}{\partial \psi} = -\frac{P_V}{R^2T^2}$$

Since ρ_V not only depends on temperature but also on ψ, equation {19} may be transformed by making use of {18} into:

$$\{22\}\quad \frac{\partial \rho_V}{\partial T} = \frac{P_V}{RT^2}\left[\frac{\Lambda}{RT} - 1\right] + \frac{P_V}{R^2T^2}\left[\frac{\Delta H_W}{T}\right] = \frac{P_V}{RT^2}\left[\frac{\Delta H_V}{RT} - 1\right]$$

The ways of determining the transport coefficients from experiments are different according to the state of moisture. For hygroscopic conditions, one uses the various experimental enthalpy changes. In the particular case of food products, the fact that the curve ψ vs θ is rather insensitive to temperature has led some authors (9) to make the assumption $\frac{\partial \psi}{\partial T} = 0$ or $\psi = \Delta H_w$. This assumption should be considered with circumspection, since, although it will not alter calculations of the transport of energy very much, some coefficients will be greatly affected. One will obtain, for example: $L_{Lq} = 0$.

As it is common knowledge that $L_{Lq} >> L_{Vq}$ for most situations, the typical reciprocal effect introduced by T.I.P. will not exist under this hypothesis and the use of T.I.P. will be pointless. Returning to high-moisture content situations, where water is in a capillary state, the variation of ψ with temperature at constant θ can be attributed to the variation of surface tension, providing the porous medium is not deformed. In this case, one finally obtains:

$$L_{qq} = \lambda_{eq}T^2$$

$$L_{qL} = L_{Lq} = -\frac{T^2 k \rho_L}{\nu}\cdot\frac{\tau^1}{\tau}\psi$$

$$\{23\}\quad L_{LW} = \frac{k\rho_L T}{\nu}$$

$$L_{VW} = D\varepsilon\tau\frac{P}{p_a}\,\frac{p_v}{R^2T}$$

$$L_{qV} = L_{Vq} = D\varepsilon\tau\frac{P}{p_a}\,\frac{p_V}{R}\left[\frac{\Lambda}{RT} - 1 + \frac{\psi}{RT} - \frac{\psi}{R}\,\frac{\sigma^1}{\sigma}\right]$$

where $\sigma^1 = \partial\sigma/\partial T < 0$.

ACCESS TO NUMERICAL VALUES OF COEFFICIENTS

A set of curves θ vs ψ at different temperatures will provide all the necessary thermodynamic information. As has already been pointed out, two types of experiments will be necessary: desorption for low values of p_V/p_s and capillary drain experiments for $\frac{p_V}{p_s} \simeq 1$. The thermokinetic data to be collected are essentially σ, ν, k and D. The structural properties of the porous body are basically ε and τ.

Many authors prefer to evaluate directly these transport coefficients from simple kinetic experiments. Bories et al (14) confirm that the liquid conductivity k and the ratio ψ/σ depend only on the structure of the porous body and on θ.

THE RECIPROCAL EFFECT ($L_{qL} + L_{qV}$)

To assess the importance of this effect, one must evaluate the coefficients and then compare the two terms of the heat flux equation:

$$\{24\}\quad j_q = -T^2\lambda_{eq}\frac{\nabla T}{T^2} + (L_{Lq} + L_{vq})\frac{1}{T}\nabla_T\psi$$

or taking into account {17}

$$\{\{25\}\quad j_q = -\lambda_{eq}\nabla T + \rho_L T\,(D_{LT} + D_{VT})\,\nabla_T\psi$$

In the literature one can find results on the transport of heat and mass in wetted beds of fine sand (3) (9) (13) (14). For this situation, the order of magnitude of the coefficients are found to be:

$$\lambda_{eq} \simeq 1 Wm^{-1}K^{-1}$$

$$10^{-10} m^2 s^{-1} K^{-1} < D_{LT} < 10^{-7} m^2 s^{-1} K^{-1}$$

$$D_{VT} \simeq 10^{-11} m^2 s^{-1} K^{-1}$$

Taking, for example, the data from reference (14), one finds that for a volumetric saturation of 15% and a temperature of 50°C the heat transport equation can be written:

$$\{26\}\quad j_q = -2.1\ \nabla T + 2.9 \times 10^{-3}\ \nabla_T \psi$$

For the second term to be significant, one should have high water chemical potential gradients and simultaneously low thermal gradients. Such situations are not likely to be frequent. Again from (14), typical gradients are:

$$\nabla T \simeq 90\ Km^{-1}$$

$$\Delta_T \psi = \frac{\partial \psi}{\partial \theta} \nabla_T \theta \simeq 1.5\ m.s^{-2}$$

Under these circumstances, the reciprocal effect is negligible. The theoretical expressions {23} applicable to capillary conditions can also be used to evaluate the term $(L_{Lq} + L_{Vq})$. The liquid conductivity $D_{L\theta}$ is taken from (14) and, as $L_{Lq} >> L_{Vq}$, the second term in equation {26} can be estimated to have a value of about $6.9 \times 10^{-3}\ \nabla_T \psi$. So, it is again very small in comparison with the conduction term.

More data on different systems in different conditions are required in order for a decision to be made on whether or not the reciprocal effect should be incorporated in the heat transport equation. It is, however, obvious that only under drastic conditions with high moisture content gradients could the consideration of such a term be justified but then, application of linear T.I.P. would be questionable.

CONCLUSION

The use of linear T.I.P. to express the constitutive equations of heat and mass transfer in wet porous bodies, throws light on two facts: the two driving forces for the water vapour and the liquid water have a single expression since the chemical potential for those two phases is the same, the constitutive equation for heat transport contains a reciprocal term which indicates that there is a heat flux induced by the water potential gradient.

The first of these two facts is merely a convenient way of writing the equations. Only the second fact could justify the use of T.I.P. and bring different results from the classical approach. If one accepts the identification procedure between T.I.P. and classical approaches, one can evaluate this reciprocal term. It appears to be very small under normal circumstances for wetted beds of sand. Direct evaluations of this effect are still necessary because one cannot justify the addition of a supplementary term in the energy transport equation based on the fitting of experimental and theoretical moisture and temperature profiles alone.

REFERENCES

(1) ROQUES M.A. and CORNISH A.R.H., 1977, A fundamental study of the transport equations for wet porous media. The Second Pacific Chemical Engineering Congress, Denver, 516-521.

(2) PHILIP J.R. and de VRIES D.A., 1957, Moisture movement in porous materials under temperature gradients. Trans. Am. Geophys. Union 38, 222-232.

(3) LUIKOV A.V., 1966, Heat and mass transfer in capillary porous bodies, Pergamon Press, Oxford.

(4) SLATTERY J.C., 1967, Flow of visco elastic fluids through porous media. A.I.Ch.E.J. 13, 1066-1071.

(5) SLATTERY J.C., 1970, Two-phase flow through porous media. A.I.Ch. E.J. 16, 345-354.

(6) WHITAKER S. 1977, Simultaneous heat, mass and momentum transfer in porous media. A theory of Drying, Adv. Heat. Transf. 13, 119-203.

(7) CARY J.W. and TAYLOR S.A., 1962 . The interaction of simultaneous diffusion of heat and water vapour, Soil Sci. Am. Proc. 28. 167-172.

(8) VALCHAR, J., 1966, Heat and moisture transfer in capillary porous materials from the point of view of the thermodynamics of irreversible processes. Third Int., Heat, Transf. Conf., Chicago, 1, 409-418,

(9) FORTES M., and OKOS M.R., 1978, A non-equilibrium thermodynamics approach to transfer phenomena in capillary porous media. Proceedings of the First Int. Symp. on Drying Montreal. Science Press, 100-109.

(10) Prigogine I., 1961, Introduction to thermodynamics of irreversible processes, Interscience Pub., J. Wiley & Sons, New York.

(11) MILLER D.G., 1969, The experimental verification of the Onsager relations. in TRANSPORT PHEOMENA IN FLUIDS Ed. Hanlel J.M., DEKKER N., 377-432.

(12) SHAPIRO H.N. and MORAN M.J., 1978, Simultaneous heat and mass transfer in soil with application to waste heat utilization, Sixth Int. Heat Transf. Conf. Toronto, paper E.N-4

(13) PREECE R.J. and HITCHCOCK J.A., 1978, Simultaneous diffusion of heat and moisture through isotropic porous media with varying physical properties.

Sixth Int. Heat Transf. Conf., Toronto, paper HM-2.

(14) BORIES S., CRAUSSE P., GAUDU R. and BACON G., 1978, Etude experimentale et simulation numerique des transferts de chaleur et de masse dans les milieux poreux non saturés. Sixth Int., Heat Transf., Conf., Toronto, paper HM-1.

STUDIES ON THE DRYING KINETICS

R.Z.Tudose[1]
Gh.Cristian[1]

1.Polytechnic Institute , Jassy,Romania

ABSTRACT

In the present paper the drying process modelling is reported of the material layers consisting of unporous grains bathed on the surface by the drying agent.The drying mechanism is determined by the moisture migration in liquid state.During drying a migration zone might form within the material with a thickness varying between zero and the material layers thicknees.The modelling was based on the criterion of moisture migration zone thickness.The fact was made evident experimentally that the moisture in liquid state migrates within certain materials while within other does not.The drying mechanism and implicitly the drying model depend on the thickness of migration zone. One general and two particular drying models are advanced for drying of the materials under study.According to the general model the drying takes place in three stages:namely the stages of migration zone formation,shifting and disappearance, respectively.Calculating relations of the drying rate and time were obtained for each stage.The following particular models are proposed:the model with complete zone of moisture migration,according to which the drying takes place in two stages,and the model without moisture migration, according to which the drying proceeds in one stage.

NOMENCLATURE

D = diameter of grains,m
g_n = acceleration of gravity,m/s^2
K_{Sh}= Sherwood comparator
K_m = dimensionless number
l = current length,m
l_o = length of the zone with initial moisture,m
l_u = length of the wet zone,m
$\dot{m}$ = rate of drying,kg/m^{2}s
$\dot{m}_c$ = rate of drying in the constant period,kg/m^{2}s
p = partial pressure,N/m^2
p_a = partial vapour pressure in air,N/m^2
p_v = partial vapour pressure the evaporation surface,N/m^2
$\bar{R}$ = universal gas constant,j/mol K
S = total thickness of the material layer,m
S_m = thickness of the moisture migration zone,m
S_d = thickness of the dry zone,m
S_o = thickness of the initial moisture zone,m
t = drying time,s
t_a = air temperature,^oC
T = thermodynamic temperature,K
v_a = air velocity,m/s
x = moisture,kg/kg
x_{cr}= critical moisture,kg/kg
x_e = equilibrium moisture,kg/kg
x_i = moisture at the evaporation surface kg/kg
x_o = initial moisture,kg/kg
β = mass transfer coefficient,m/s

δ_l = the coefficient of moisture migration in liquid state, m^2/s

δ_v = the effective coefficient of vapours diffusion through the layer, m^2/s

ρ = density, kg/m^3

Superscript

+ = dimensionless thickness

INTRODUCTION

The studies on the material drying kinetics evidenced this process to be complex due to the different physico-chemical characteristics of the materials as well as to a simultaneous heat and mass transfer. In spite of the great deal of efforts a generally accepted theory of the material drying has not been developped yet.

The drying process proceeding is determined by the moisture shifting within the material, the evaporation energy required as well as by the internal and external diffusion of vapours.

The theoretical and experimental investigations on the material drying were aimed to elucidate numerous aspects. Some of them were directed towards the elucidation of the mechanism aspects. In this connection, some reported papers approached the modelling of the material drying process (1...11). Toei and Hayashi (1) have developed a model accounting for the drying mechanism in the second stage of the drying rate decreasing. Toei and Okazaki (2) have developed a model of capillary-porous material drying. Other investigators (3,4) concluded the moisture transfer during drying process to take place in vapour state. The proposed mechanism consists in the vapour diffusion from an internal front located between the dry and the wet zones, the moisture migration in liquid state being neglected. A series of papers (5...11) report a drying process modelling assuming the moisture migration in liquid state to be essential. From this point of view materials were found for which the migration rate is zero as well as materials for which the migration rate is larger than zero. It was made evident experimentally that in function of the migration rate of moisture the thickness of migration zone can vary between zero and the layer thickness, the drying mechanism depending on the migration zone thickness (7,9). In the present paper a drying process modelling is reported in function of the moisture migration zone thickness in liquid state. One general and two particular drying models are presented. With each model relations for calculating the drying rate and time were settled. The models were derived for drying of the material layers consisting of unporous grains and bathed on the surface by the drying agent.

MODELLING OF DRYING PROCESS

The theoretical and experimental studies on the drying kinetics revealed that the drying of layers of unporous unadsorbent materials takes always place on the surface and that in the material layer three zones can coexist, namely:

- the dry zone, at the material surface bathed by the drying agent;
- the moisture migration zone in liquid state, inside;
- the zone with initial moisture at the layer basis.

In the first stage the evaporation takes place on the external surface and in the following stages on the interface between the dry and the moisture migration zones. The thickness of the moisture migration zone corresponds to the range of humidity variation, from the initial value till the equilibrium humidity and can take values comprised between zero and the material thickness.

The modelling of drying process of unadsorbent unporous materials bathed on

the surface by the drying agent was derived in function of the thickness of the moisture migration zone, S_m. Based on this criterion a general and two particular drying models are advanced. The general drying model, refered to as the model with limited moisture migration zone corresponds to the case when the moisture migration zone thickness is comprised between zero and the material thickness, $0 < S_m < S$. For the moisture migration zone thickness equal to the material thickness, $S_m = S$, a particular model is obtained, namely the model with complete moisture migration zone. The second particular model, named the model of drying without moisture migration corresponds to the moisture migration zone thickness equal to zero, $S_m = 0$. Models analogous to those previously discussed were developed by means of which the drying curves may be reproduced experimentally (9).

Physical Models

According to the general model the drying proceeds in three stages (Figure 1). In the first stage - of migration zone formation - Figure 1a, the moisture migration toward the material surface takes place due to the moisture gradient occuring by the moisture evaporation at the surface. The moisture migration zone thickness, S_m, is continously increasing. In the material there are the external moisture migration zone and the internal zone of initial moisture, S_o. When the moisture at the material external surface equals the equilibrium moisture the moisture migration zone thickness is maximum, the first stage is finished and the second begins. The first stage is characterized by a constant drying rate, the vapour diffusion through the external boundary film being the determining elementary process.

In the second stage - of migration zone shifting - Figure 1b, the drying surface shifts within the material, so that three zones coexist: the external dry zone, S_d, the moisture migration zone, S_m, and, finally, the zone of initial moisture, S_o, at the layer basis. In this stage the migration zone shifts inside the material and the evaporation takes place at the interface between the migration zone and the

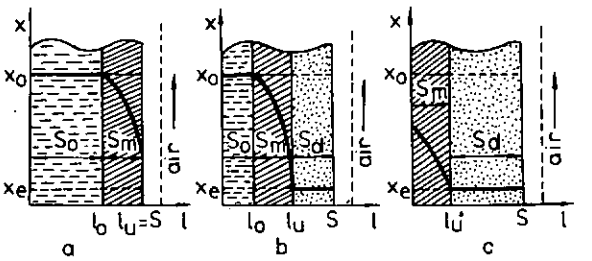

Figure 1. The drying mechanism according to the general model.

dry zone. The thickness of the dry zone increases continously while the thickness of the zone of initial moisture decreases In this stage the drying rate decreases continously since the resistance towards the vapour diffusion through the dry zone adds to the resistance of the external boundary layer. The second stage is finished when the zone of initial moisture disappears. In the third stage - that of migration zone disappearance - Figure 1c, there are two zones within the material: an external dry zone, S_d, and an internal migration zone, S_m. The migration rate of the moisture in liquid state largely diminishes as a result of the wet zone disappearance which causes the dry zone thickness and, hence, the resistance towards vapour diffusion through this zone to increase rapidly and the drying rate to decrease markedly. The drying is considered finished when the humidity of the whole layer equals the equilibrium humidity. The inflexions on the drying curves during the periods of decreasing rates may be caused not only by the passing from the second to the third

stage but also by the modifications of rate of moisture migration in liquid state

A particular case of the general model is obtained for a moisture migration zone thickness equal to that of the material (Figure 2).The material drying according

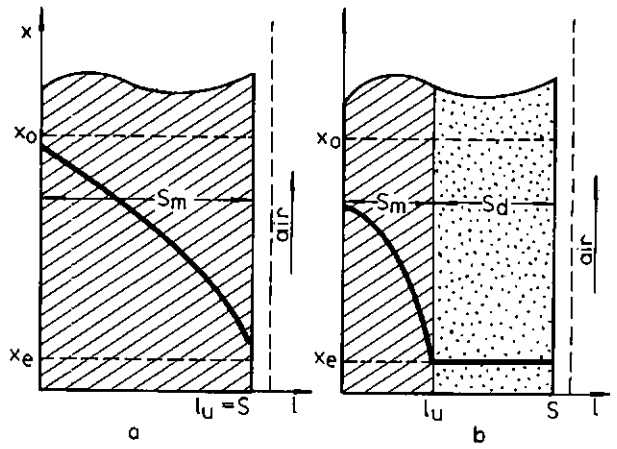

Figure 2.The drying mechanism according to the model with complete moisture migration zone.

to the model with complete moisture migration zone takes place in two stages: that of migration zone formation and disappearance,respectively.In the first stage the migration of the moisture in liquid state from the whole material thickness towards the evaporation surface takes place.Within the material only the moisture migration zone exists,S_m,Figure 2a.The drying rate keeps constant from the very begining till the material moisture on the surface bathed by the drying agent equals the equilibrium moisture.In the second stage the evaporation surface shifts within the material.The rate of moisture migration in liquid state is much lower than that in the first stage.There are two zones within the material:the external dry zone,S_d,and the internal migration zone,S_m,Figure 2b. The drying rate decreases continously since the resistance to the vapour diffusion through the dry zone,which becomes determining in process,adds to the resistance of the external boundary layer.

Another particular case of the general model is obtained for the migration zone thickness equal to zero,which corresponds to a coefficient of migration in liquid state equal to zero (Figure 3).In this case the moisture does not migrate in li-

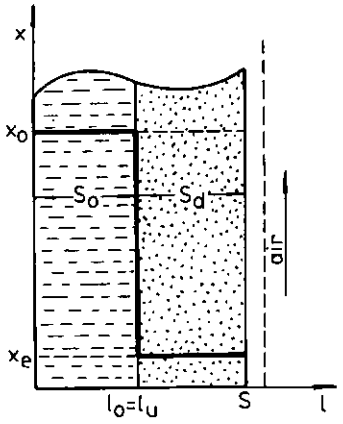

Figure 3.The drying mechanism according to the model without moisture migration.

quid state,the drying proceeding with a continously decreasing rate,that is the drying period with constant rate lacks. There are two zones within the material the external dry zone,S_d,and the internal zone of initial moisture,S_o.The moisture evaporation proceeds at the interface between the two zones.

A picture of the drying mechanism and models according which the process proceed is depicted in Figure 4.The drying starts in corner $\overset{*}{S}_o = 1$ and ends in corner $\overset{*}{S}_d = 1$.The material drying might proceed by three different ways namely;

- for $0 < \overset{*}{S}_m < 1$,in there stages,according to the general model;
- for $\overset{*}{S}_m = 1$,in two stages according the model with complete zone of moisture migration,and
- for $\overset{*}{S}_m = 0$,in a single stage according to the model without moisture migration.

Theory

Based on the physical model, shown in Figure 1, the moisture distribution within the material was calculated and relations for the drying rate and time were derived. Relation for the moisture distribution, drying rate and time were also obtained for the particular cases of the general model.

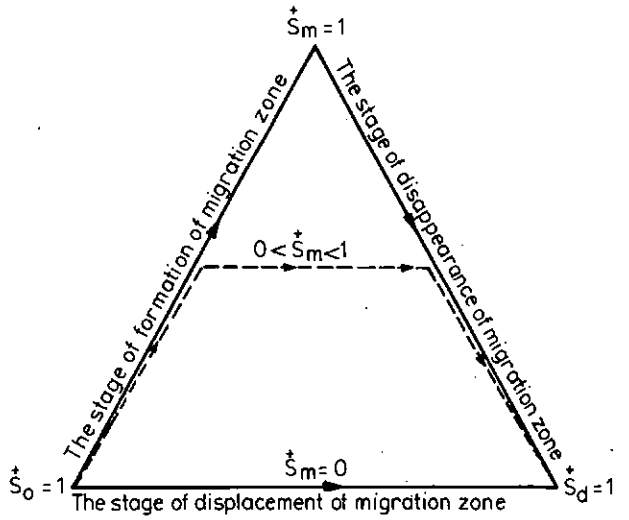

Figure 4. The triangle representation of the drying process.

The stage of the migration zone formation

In this stage the moisture migration rate from the inside towards the surface is high enough to ensure the moisture feeding to the surface. The drying rate keeps constant since the moisture evaporation takes place at the surface and the moisture of the material surface is larger than the equilibrium moisture. In this stage the drying rate is calculated with the relation (7):

$$\dot{m} = \dot{m}_c = \frac{\beta}{RT}(p_v - p_a) \qquad (1)$$

The moisture distribution within the migration zone is given by a differential equation of a form similar to the diffusion equation, which for unidirectional migration can be written as:

$$\frac{\partial x}{\partial t} = \delta_l \frac{\partial^2 x}{\partial l^2} \qquad (2)$$

The moisture variation in time within the migration zone is given by:

$$-\frac{\partial x}{\partial t} = \frac{\dot{m}}{(S - l_o)\rho} \qquad (3)$$

From the relations (1)...(3) one obtains:

$$\frac{d^2x}{dl^2} = -\frac{\dot{m}_c}{\delta_l (S - l_o)\rho} \qquad (4)$$

In equation (4) the coefficient of moisture migration in liquid state intervenes which depends on the moisture content (12)...(15). It can be integrated, by assuming the coefficient of moisture migration in liquid state constant, with the following boundary conditions:

$$\frac{dx}{dl} = 0 \text{ at } l = l_o \text{ and } x = x_i \text{ at } l = S \qquad (5)$$

where x_i denotes the moisture at the material surface, and varies from the moisture x_o till the equilibrium moisture x_e. By integrating the moisture distribution within the migration zone is obtained:

$$\frac{x}{x_o} = 1 - \frac{K_{\dot{m}}}{2} \frac{(\overset{*}{S} - \overset{*}{S}_o)^2}{1 - \overset{*}{S}_o} \qquad (6)$$

where $K_{\dot{m}} = \dot{m}_c S / x_o \delta_l \rho$ - dimensionless number.

For the drying model without moisture migration the stage of migration zone formation does not exist and the material moisture in the wet zone is equal to the initial one, $x = x_o$. The current drying time in the first stage is derived by integrating the equation (3) by means of boundary conditions (5) and the equation (6) of moisture distribution. In dimensionless form the equation (7) is obtained:

$$\frac{t_1}{t_o} = (1 - \overset{*}{S})\left(\frac{1 + \overset{*}{S}}{2} - \overset{*}{S}_o\right) \qquad (7)$$

where $t_o = S^2/\delta_l$, has time dimension

For the overall drying time in the first

stage one obtains:

$$\frac{t_{1t}}{t_o} = \frac{1}{2}(1 - \overset{*}{S}_o^2) \qquad (8)$$

For the drying model with complete zone of moisture migration the moisture distribution within the migration zone is obtained from equation (6) for $\overset{*}{S}_o = 0$:

$$\frac{x}{x_o} = 1 - \frac{K_{\hat{m}}}{2}\overset{*}{S}^2 \qquad (9)$$

In case of the model with complete zone of moisture migration the current and the overall drying times are obtained by using the equations (7) and (8) for $\overset{*}{S}_o = 0$:

$$\frac{t_1}{t_o} = \frac{1 - \overset{*}{S}^2}{2} \qquad (10)$$

$$\frac{t_{1t}}{t_o} = \frac{1}{2} \qquad (11)$$

The stage of shifting the moisture migration zone

At the end of the first stage the moisture at the material surface equals the equilibrium moisture and the evaporation surface shifts within the layer. Three zones occurs within the material: the external dry zone, the internal zone of moisture migration and the zone of initial moisture at the layer basis. In this stage the resistance to the vapour diffusion through the dry zone adds to the resistance of the external boundary layer, which results in drying rate decreasing.

The drying rate in the second stage can be be determined starting from the equation of vapour diffusion through the dry zone:

$$\hat{m} = -\frac{\delta_v}{RT}\frac{dp}{dl} \qquad (12)$$

The partial pressure gradient of moisture vapours is obtained starting from the distribution equation of the vapour partial pressure through the dry zone:

$$\frac{\partial p}{\partial t} = \delta_v \frac{\partial^2 p}{\partial l^2} \qquad (13)$$

By assuming quasi-stationary conditions and a constant diffusion coefficient of the vapours through the dry zone the equation (13) may be integrated by means of the boundary conditions written for the interface between the dry and migration zones:

$$-\delta_v \frac{dp}{dl} = \beta(p - p_a) \quad \text{at} \quad l = S$$
$$p = p_v \quad \text{at} \quad l = l_u \qquad (14)$$

By integrating the equation (13) by means of the boundary conditions (14) the vapour partial pressure distribution through the dry zone is obtained:

$$p = p_v - \frac{\beta(p_v - p_a)}{\delta_v + \beta(S - l_u)}(l - l_u) \qquad (15)$$

By introducing the expression for the presure gradient, resulting from equation (15), in equation (12) one obtains:

$$\frac{\hat{m}}{\hat{m}_c} = \frac{1}{1 + K_{Sh}(1 - \overset{*}{S}_u)} \qquad (16)$$

where K_{Sh} is a dimensionless number, named Sherwood comparator since it compares that resistances to the vapour diffusion through the external boundary layer and through the material dry zone.

From the equations (2), (3) and (16) one obtains:

$$\frac{d^2x}{dl^2} = -\frac{\hat{m}_c}{1 + K_{Sh}(1 - l_u/S)\delta_l(l_u - l_o)} \qquad (17)$$

If the coefficient of moisture migration in liquid state is assumed constant the equation (17) can be integrated by means of the following boundary conditions:

$$x = x_e \quad \text{at} \quad l = l_u$$
$$x = x_o \quad \text{at} \quad l = l_o \qquad (18)$$

By integrating the equation (17) the moisture distribution within the migration is obtained:

$$\frac{x_o - x}{x_o - x_e} = \left\{1 + \frac{K_{\dot{m}}(\overset{*}{S} - \overset{*}{S}_u)}{2[1+K_{Sh}(1-\overset{*}{S}_u)]}\right\}\frac{\overset{*}{S} - \overset{*}{S}_o}{\overset{*}{S}_u - \overset{*}{S}_o} \quad (19)$$

where $K_{\dot{m}} = \frac{\dot{m}_c S}{\delta_l (x_o - x_e)\rho}$

The drying time in the second stage is obtained by integrating the equation (3), using equations (16) and (19):

$$\frac{t_2}{t_o} = \frac{1}{2}(1 - \overset{*}{S}_o)^2 - \frac{1}{4}(\overset{*2}{S}_u - \overset{*2}{S}_o) + \frac{1 + K_{Sh}(1 - \overset{*}{S}_u)}{K_{\dot{m}}}(\overset{*}{S}_u - \overset{*}{S}_o) \quad (20)$$

The overal drying time in the second stage results from the equation (20) for $\overset{*}{S}_o = 0$:

$$\frac{t_{2t}}{t_o} = \frac{1}{2} - \frac{1}{4}\overset{*2}{S}_u + \frac{1+K_{Sh}(1 - \overset{*}{S}_u)}{K_{\dot{m}}}\overset{*}{S}_u \quad (21)$$

In case of model without moisture migration for the current drying time, the following relation was obtained:

$$\frac{t}{t_o} = (1 - \overset{*}{S}_u)\left[1 + \frac{K_{Sh}}{2}(1 - \overset{*}{S}_u)\right] \quad (22)$$

The overall drying time is obtained from equation(22) for $\overset{*}{S}_u = 0$:

$$\frac{t_t}{t_o} = 1 + \frac{K_{Sh}}{2} \quad (23)$$

<u>The stage of disappearance of the moisture migration zone</u>

In this stage the drying rate continues to decrease due to the fact that resistance to vapour diffusion through dry zone increases continously, becoming the rate determining step. There are two zones in the material: the external dry zone and the internal zone of moisture migration. The distribution of vapour partial pressure within the dry zone is given by the equation (15). The drying rate is calculated by means of the equation (16). The moisture distribution within the migration zone is given by the equation (3) in which the following equation may be substituted for the moisture variation in time:

$$-\frac{\partial x}{\partial t} = \frac{\dot{m}_c}{\rho l_u} \quad (24)$$

Combining the equations (3) and (4) one obtains:

$$\frac{d^2x}{dl^2} = -\frac{\dot{m}_c}{\delta_l l_u \rho} \quad (25)$$

The equation (25) can be integrated by assuming a constant coefficient of moisture migration, using the following boundary conditions:

$$x = x_e \quad \text{at} \quad l = l_u$$
$$\frac{dx}{dl} = 0 \quad \text{at} \quad l = 0 \quad (26)$$

By integration, the moisture distribution within the migration zone is obtained:

$$\frac{x - x_e}{x_o - x_e} = \frac{K_{\dot{m}}}{2\overset{*}{S}_u}\left[\frac{\overset{*2}{S}_u - \overset{*2}{S}}{1+K_{Sh}(1 - \overset{*}{S}_u)}\right] \quad (27)$$

The equation (27) is also valid for the model with complete zone of moisture migration, in the second stage, that of migration zone disappearance.

The drying time in the third stage of the general model is obtained by integrating the equation (24). In dimensionless form it results:

$$\frac{t_3}{t_o} = \frac{1}{2}(1 - \overset{*2}{S}) + \frac{1}{4}\overset{*2}{S}_u + \frac{1+K_{Sh}(1-\overset{*}{S}_u)\overset{*}{S}_u}{K_{\dot{m}}} \quad (28)$$

For the overall time this relation becomes:

$$\frac{t_{3t}}{t_o} = \frac{1}{2} + \frac{1}{4}\overset{*2}{S}_u + \frac{1 + K_{Sh}(1-\overset{*}{S}_u)\overset{*}{S}_u}{K_{\dot{m}}} \quad (29)$$

The drying might be considered finished when the moisture at the layer basis equals the equilibrium moisture.

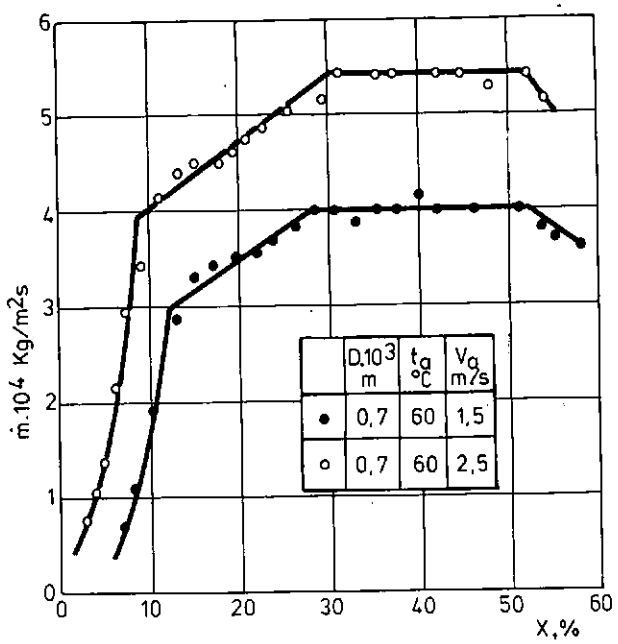

Figure 5.Drying curves of the copolymer layers.

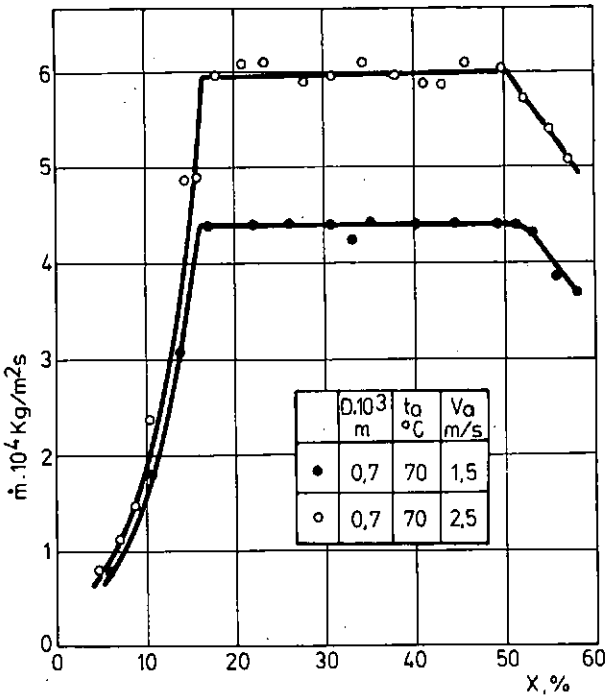

Figure 6.Drying curves of the polystyrene layers.

EXPERIMENTALS

The materials subjected to drying consisted of layers of styrene-divinylbenzene copolymers,polystyrene pearls and quartz sand.The drying was carried out by passing the drying agent over the material surface The experimental equipment was reported elsewhere (7).The obtained experimental results were plotted as drying rate versus moisture (Figures 5,6 and 7).

The copolymer and sand layers show three drying periods while the styrene ones only two.The drying rate during the first period is significantly influenced by the rate of drying agent since the process is controlled by the external diffusion of water vapours.In case of drying the quartz sand layers,Figure 7-curves 1 and 2,the experimental results are indicative of a three stages drying mechanism.The period of constant drying rate is characterized by an intensive migration of the moisture in liquid state.To study the influence of the moisture migration on drying a new experimental procedure was applied namely non-

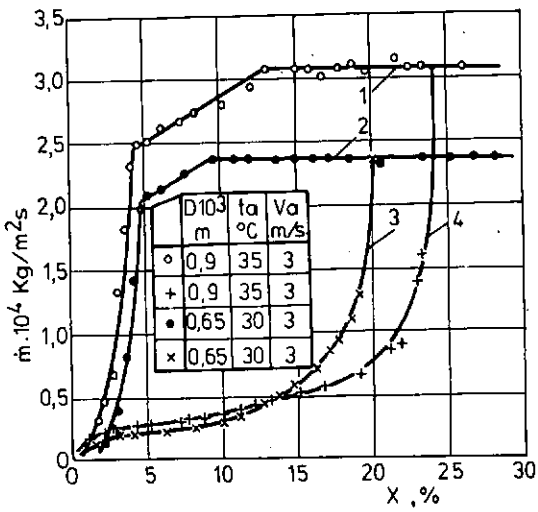

Figure 7.Drying curves of the quartz sand layers.

wettability of the sand particules.In this purpose the sand grains were covered with an extremely thin wax film.The sand thus treated was wetted with such a water amount as to obtain a sand moisture higher than the first critical moisture attained in drying the untreated sand.

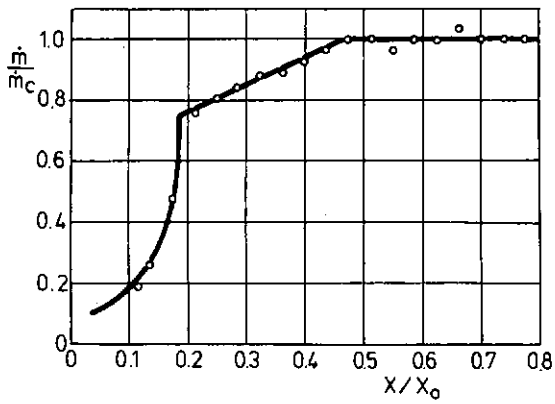

Figure 8.Comparison of the experimental results and the theoretical values in case of drying the copolymer layers;
o -experimental;- -theoretical

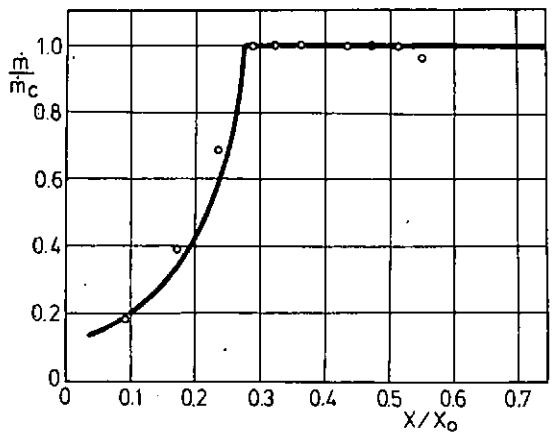

Figure 9.Comparison of the experimental results and the theoretical values in case of drying the polystyrene layers;
o - experimental
- - theoretical

Curves characteristic of a continously decreasing drying rate were thus obtained, Figure 7 - curves 3 and 4,which indicates the process to take place according to the drying model without moisture migration.

COMPARISON OF THE EXPERIMENTAL AND THEORETICAL RESULTS

To compare the theoretical values and the experimental results the dimensionless drying rate was calculated and plotted versus the dimensionless material moisture (Figures 8 and 9).The theoretical values have been calculated by means of the equations for the drying rate in each process stage.The experimental results are depicted as points in Figures 8 and 9.

The drying rate during the stage of constant rate was calculated with the equation (1).The mass transfer coefficient was determined experimentally (9).

The drying rate in the first stage of rate decreasing was calculated with equations (16) in which the dimensionless thickness of the moisture zone intervenes. To calculate this amount the curves of the moisture distribution were plotted for both the copolymer and polystyrene pearl layers.

The drying rate in the second stage of rate decreasing for the copolymer layers and in the stage of rate decreasing,for the polystyrene pearls,were calculated by means of equation (16).In this equation,the relative thickness of the migration zone intervenes.Starting from the facts that in this stage there are only two zones in the material, the external dry zone and the internal migration zone, and that the shifting of the migration zone within the material may proceed in three ways,the equation of Toei and coworkers has been used (1).By using the calculating equation for the relative thickness of the moisture migration zone, the relation (16) becomes:

- for the copolymer layers;

$$\frac{\dot{m}}{\dot{m}_c} = \frac{1}{1 + K_{Sh}\left(1 - \frac{x}{x_{cr2}}\right)} \qquad (30)$$

- for the polystyrene layers;

$$\frac{\dot{m}}{\dot{m}_c} = \frac{1}{1 + K_{Sh}\left[1 - \left(\frac{x}{x_{cr}}\right)^{1/3}\right]} \qquad (31)$$

The mass transfer coefficients as well as those of vapour diffusion through layer which intervene in Sherwood comparator have been determined experimentally (15).

The theoretical values of the drying rate,in the three stages of the process, determined by means of the derived equations are plotted in Figures 8 and 9.A good accordance is noticed between the theoretical and experimental values in case of the two material layers.

REFERENCES

1.Toei,R.,and Hayashi,M.,Memoirs of the Faculty of Engineering,Kyoto Univ., Vol.25,p.457,1963

2.Toei,R.,and Okazaki,M.,Eng.Phy.J.,Vol.19 3,p.464,1966

3.Garside,J.,Lord,L.W.,and Reagon,R.,Chem. Eng.Sci.,Vol.25,7,p.1133,1970

4.Hideguki,S.,Kogaku Kagaku,Vol.28,7, p.585,1964

5.Tudose,R.Z.,and Cristian,Gh.,Rev.de chimie,Vol.22,9,p.550,1971

6.Tudose,R.Z.,and Cristian,Gh.,Rev.de chimie,Vol.25,6,p.456,1974

7.Tudose,R.Z.,and Cristian,Gh.,Bul.Inst. Polit.Iaşi,XX (XXIV),3 - 4,p.25,1974

8.Tudose,R.Z.,and Cristian,Gh.,Bul.Inst. Polit.Iaşi,XXII (XXVI),1 - 2,p.43,1976.

9.Cristian,Gh.,Doctoral Thesis,Polyt. Inst.,Jassy,1976

10.Tudose,R.Z.,and Cristian,Gh.,Rev.de chimie,Vol.28,6,p.555,1977

11.Cristian,Gh.,Tudose,R.Z.,and Popovici, L.,Bul.Inst.Polit.Iaşi,XXIV (XXVIII), 1-2,p.39,1978

12.Meier,E.,Chem.Ing.Tech.,Vol.41,7,p.472, 1969

13.Akbar,M.,and Gorling,P.,Chem.Ing.Tech. Vol.33,9,p.619,1961

14.Meier,M.,Chem.Ing.Tech.,Vol.42,5,p.327, 1970

15.Cristian,Gh.,and Tudose,R.Z.,Rev.de chimie,Vol.27,10,p.858,1976

THE THERMOKINETICS OF THE MOISTURE TRANSPORT IN SOLIDS DURING DRYING

J.Valchářová

J.Valchář

National Research Institute for Machine Design, Prague, ČSSR

ABSTRACT

The paper presents the analysis of the simultaneous heat and moisture transport in solid disperse systems with bound moisture. Using the methods of the thermodynamics of irreversible processes, the choice of conjugated thermodynamic fluxes and forces describing this process and of the system of differential equations determining the non-stationary temperature and moisture fields have been taken. Further, this system of equations is simplified for certain simpligying assumptions and the algorithm of the numerical solution applying the finite element method is described.
The concluding part of the paper suggests the possibility of applying the program to mathematical modelling of the hygrothermical parameter effects upon the temperature and moisture fields in dried solids.

NOMENCLATURE

The following tabulation lists all symbols used in the text except those employed occasionally and specifically defined in the text.

c = heat capacity, J/kg K

c_u = isothermal mass capacity, kg/kg M

j_k = moisture-transfer flux, kg/m^{2}s

j_Q = heat-transfer flux, W/m^2

l = characteristic dimension, m

r = specific heat of evaporation of the liquid phase of moisture, J/kg

t = temperature /Celsius scale/, ^oC

u = moisture content /dry basis/ of solid, kg/kg

x = Carthesian coordinate, m

y = Carthesian coordinate, m

z = Carthesian coordinate, m

L = phenomenological transport coefficient

M = mass, kg

T = temperature /Kelvin scale/, K

V = volume, m^3

α_Q = heat transfer coefficient, W/m^2

α_w = mass transfer coefficient, kg/m^{2}s^oM

$\gamma_x, \gamma_y, \gamma_z$ = direction cosine

Γ = boundary

δ = effective moisture thermodiffusivity, $\delta_{M/K}$

ε = phase change parameter after Luikov

θ = mass transfer potential or degrees of moistness after Luikov, ^oM

λ_Q = thermal conductivity, W/mK

λ_w = effective moisture diffusivity, kg/ms^oM

μ = chemical potential, J/kg

ϱ = density, kg/m^3

τ = time, s

ω_{12} = rate of local production of vapour phase of moisture due to phase change from the liquid phase of moisture, kg/m^{3}s

Subscripts

B = boundary conditions
I = initial conditions
Q = heat
W = moisture in general
0 = solid skeleton
1 = liquid phase of moisture
2 = vapour phase of moisture
3 = inert gas

INTRODUCTION

From the point of view of inquiring into the drying process, the processes that occur within the dried material during the drying are of the most principal significance, since they are affected by the moisture-solid relationships. The study of these processes can be based on physical chemistry which, using physical

methods describes and explaines such processes in all fields of chemistry associated with physics, either through their nat ure or the method of investigation. Out of the whole of physical chemistry, coloid chemistry is most important for the study of the moisture-solid bond, which being based on general physical-chemical principles, investigates systematically disperse systems; moist material can also be considered a disperse system, formed by moisture and solid.

At present, the following sections can be classified as fundamental in the drying theory:

1. The theory of moisture-solid bond and the theory of the thermodynamic equilibrium of the wet material and the environment. This part of the drying theory is sometimes called the moist material thermodynamics,or also the statics of drying.
2. The theory of the energy /heat/ and moisture mass transport in disperse solids.
3. The heat and mass transfer in the boundary layer at the dried material surface.
4. Theoretical basis of the drying process technology.

The following section of this paper will present a survey of the results in the theory of the energy /heat/ and moisture mass transport in disperive solids, as achieved by individual authors.

The theory of transport processes in moist solids

Simultaneous heat and mass transport in disperse solids with bound moisture represents a complex, irreversible process, which is inseparable from the transfer processes occuring on the dried solid surface. The mathematical model of this complex process is illustrated schematically in Fig. 1.

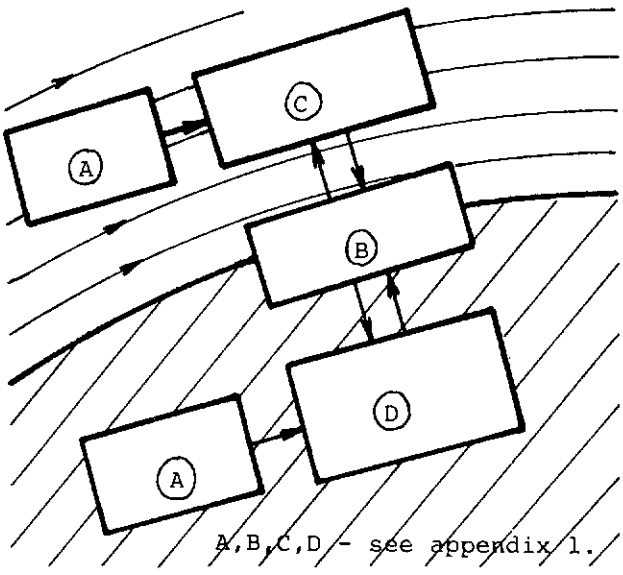

Figure 1 The mathematical model of the transport processes occuring during drying

The mathematical model is thus determined by a system of differential equations for simultaneous energy and mass transport in disperse solids and by a system of differential equations for transfer processes in the boundary layer, supplied with corresponding boundary and initial conditions of the solution Simultaneous solution of both equation would be essentially possible using numerical methods; although, from the partice point of view, such solution would be considerably difficult.

Further, the problems of calculating the non-stationary temperature and specific moisture content fields in the dryed solid will be subject to particular analysis, with respect to some simplifying assumptions concerning particularly the assessment of the boundary conditions, or even some further subsystems of the mathematical model.

Simultaneous heat and mass transfer in disperse solids with bound moisture represents a complex irreversible process. For its theoretical description, rigorous choice of the system of conjugated thermodynamic fluxes and that of thermodynamic forces is of primary importance, with respect to direct and cross efects affecting the heat and moisture transport. The choice can be made using the methods of the thermodynamics of irreversible processes /1, 2/.

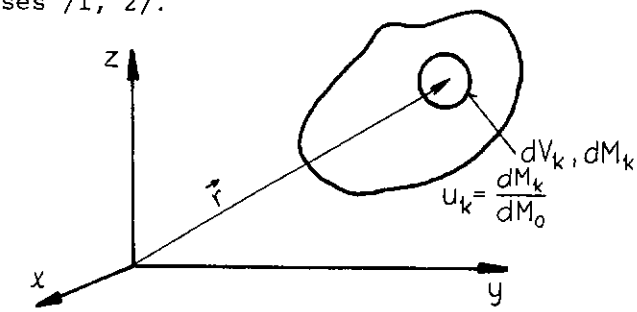

Figure 2 Moist solid composition

index: k = 0 solid skeleton
1 moisture liquid phase
2 moisture vapor phase
3 inert gas

For the disperse system illustrated in Fig. 2, eqs.

$$\vec{j}_k = -\frac{L_{kQ}}{T}\nabla T - \sum_{i=1}^{3} L_{ki}\nabla_T \mu_i \,, \qquad /1/$$

$$\vec{j}_Q = -\frac{L_{QQ}}{T}\nabla T - \sum_{i=1}^{3} L_{Qi}\nabla_T \mu_i \qquad /2/$$

were determined for the thermodynamic fluxes of heat $\vec{j}_Q$ and moisture in singular phases $\vec{j}_k$. Eqs. /1/ and /2/ represent 1+3 linear relations between the thermodynamic fluxes $\vec{j}_Q$, $\vec{j}_\varepsilon$ and thermodynamic

forces. The thermodynamic force for the direct effect of the heat flux has been determined as $\nabla_T |T|$ and the generalized force for the direct effect of the moisture flux has been determined as $\nabla_T \mu_k$/index T at the gradient operator stands for T = const./. The quantities L in eqs. /1/ and /2/ are so-called kinetic or phenomenological coefficients. The phenomenological coefficients L_{QQ} and L_{lk} /for l = k/ characterize so-called direct effects. The phenomenological coefficient L_{QQ} characterizes the direct thermal conductivity effect /determined by the Fourier law/

$$(\vec{j}_Q)' = -\frac{L_{QQ}}{T}\nabla T = -\lambda \nabla T \quad , \qquad /3/$$

whre $(\vec{j}_Q)'$ is the component of the heat flux corresponding to the direct effect. The phenomenological coefficient L_{kl} /for k = l/ gives the characteristics of the direct diffusion effect given by the component of the moisture flux corresponding to the chemical potential gradient $\nabla_T \mu_k$, i.e.

$$(\vec{j}_k)' = -L_{kk} \nabla_T \mu_k \quad , \qquad /4/$$

whre $(\vec{j}_k)'$ is the component of the flux of the k-th phase of moisture belonging to the direct effect.
The phnenomenological coefficients L_{Qk}, L_{kQ}, L_{kl} /for $l \neq k$ / characterize so-called cross effects.
The coefficient L_{kQ} characterizes thermal diffusion /called sometimes the Soret effect/, which, according to Fitts /3/, can be defined as the maintainging the gradient of the chemical potential through the temperature gradient. The coefficient L_{Qk} characterizes the diffusive heat flux /called sometimes the Dufour effect/, which, according to Fitts, can be defined as the maintaining the temperature gradient as an effect of the chemical potential gradient.
The coefficient L_{kl} /for $l \neq k$/ charakterizes co-diffusion given by the component of the diffusive flux galling to the chemical potential gradient /e.g. part of the moisture flux in the vapor phase caused by the moisture chemical potential gradient in the liquid phase/.
The quadratic matrix of the phenomenological coefficients L is of the 4 rank and is symmetric according to Onsager theorem /3/.
Using eqs. /1/ and /2/ and applying the first thermodynamic law respecting the phase changes, we can derive a system of differential equations describing the nonstationar temperature and speciffic moisture content fields in wet solids during simultaneous heat and mass transport /1/.

$$\rho_0 c_0 \frac{\partial T}{\partial \tau} + \nabla\left[-\frac{L_{QQ}}{T}\nabla T - \sum_{l=1}^{3} L_{Ql}\nabla_T \mu_l\right] - r_1 \omega_{12} = 0 \quad /5/$$

$$\rho_0 \frac{\partial u}{\partial \tau} + \sum_{k=1}^{3} \nabla\left[-\frac{L_{kQ}}{T}\nabla T - \sum_{l=1}^{3} L_{kl}\nabla_T \mu_l\right] = 0 \quad . \qquad /6/$$

The last member in eq. /5/ respects the energy expended on the phase change which occurs in moist solids /evaporation of the liquid phase of moisture/; the quantity ω_{12} [kg/m^{3}s] is the rate of local production of vapor phase of moisture as a consequence of the liquid phase evaporation.
Since eqs. /5/ and /6/ will be utilized further on, their rearrangement is necessary, in terms of the specification of the thermodynamic force /or the chemical potential/ of the moisture bound in particular phases. For the disperse system with moisture bound in a polycapillar porous system, which is most frequent to occur, eqs. /5/ and /6/ were in transformed into

$$\rho_0 \frac{\partial u}{\partial \tau} + \sum_{k=1}^{3} \nabla\left[-L'_{kQ}\nabla T - (L'_{k_1}\nabla u_1 + L'_{k_2}\nabla u_2)\right] = 0 \quad , \qquad /7/$$

$$\rho_0 c_0 \frac{\partial T}{\partial \tau} + \nabla\left[-L'_{QQ}\nabla T - (L'_{Q_1}\nabla u_1 + L'_{Q_2}\nabla u_2)\right] - r\omega_{12} \quad . \qquad /8/$$

In rearranging the differential eqs. /5/ and /6/ into /7/ and /8/, the generalized thermodynamic forces for the mass flux, expressed as the gradients of the chemical potential $\nabla_T \mu_k$, were substituted by thermodynamic forces, experessed as the gradients of relative masses of the disperse system components. The phenomenological coefficients L'_{k1}, L'_{k2}, L'_{Qk}, L'_{kQ} /k = 1, 2, 3/ appearing in eqs. /7/ and /8/ can ben expressed as depending on the original kinetic coefficients L_{kl}, L_{kQ}, L_{Qk} . In transforming eqs. /5/ and /6/ into /7/ and /8/, also the number of the kinetic coefficients decreased.
A more detailed analysis can be found in /5/. The differential equations /7/ and /8/ can be simplified further, if one assumes the kinetic coefficients being constant for a definite extent of specific moisture content and temperatures. For this case, the differential equations /7/ and /8/ can be rearranged into the form

$$\frac{\partial u}{\partial \tau} = k\nabla^2 u + \delta_u \nabla^2 T \quad , \qquad /9/$$

$$\frac{\partial T}{\partial \tau} = a\nabla^2 T + \delta_{Q_1}\nabla^2 u_1 + \delta_{Q_2}\nabla^2 u_2 + \frac{r_1 \omega_{12}}{c_0}\frac{\delta u_1}{\delta \tau} \quad . \qquad /10/$$

The kinetic coefficients appearing in eqs. /9/ and /10/ are expressed in terms of the kinetic coefficients figuring in eqs. /7/ and /8/ and of the material properties ρ_0 and c_0 ; the coefficient $a\ [m^2/s]$ is the coefficient of the thermal conductivity of wet material and the coefficient $k\ [m^2/s]$ is the moisture diffusion coefficient. The coefficient $\delta_n, \delta_{Q1}, \delta_{Q2}$ characterize Soret and Dufour effects. Lykov /9/ calls the quantity ε_{12} the criterion of the phase change. Its relation to the rate of local production of vapour ω_{12} is given by eq.

$$\omega_{12} = \rho_0 \varepsilon_{12} \frac{\partial u_1}{\partial \tau} \quad . \qquad /11/$$

The phase change parameter ε_{12} reaches the values within the range from 0 /no moisture evaporation inside the material/ to 1 /all moisture evaporates inside the material/.
The differential equations /5/ and /6/ can in principle be rearranged also in some other way, e.g. introducing so-called experimental moisture potential θ , according to A.V.Lykov /6/, which is considered to be a function $\theta(u,T)$ and its scale is determined experimentally. Stipulating some simplifying assumptions, one can gradually rearrange eqs. /5/ and /6/ into the form which had originally been derived by Lykov /7/

$$\rho_0 c_Q \frac{\partial T}{\partial \tau} = \lambda_Q \nabla^2 T + \varepsilon_{12} r_1 \rho_0 c_w \frac{\partial \theta}{\partial \tau} \quad , \qquad /12/$$

$$\rho_0 c_w \frac{\partial \theta}{\partial \tau} = \lambda_w \delta \nabla^2 T + \lambda_w \nabla^2 \theta \quad . \qquad /13/$$

Naturally, the present analysis does not offer all possible transformations of the fundamental differential equations for the non-stationary temperature and moisture field /5/ and /6/; however, with regard to practical application in calculating the non-stationary fields, all relevant ways have been shown.

The calculation of the non-stationary temperature and moisture fields in wet solids

The system of the differential equations describing the non-stationary temperature and moisture fields in dried solids, which was derived with various modifications in the previous paragraph, can be solved either analytically or numerically, considering suitably defined boundary and initial conditions of the solution. However, the analytical method of solution is limited only to the integral domains of simple geometrical forms, and, therefore, its application in practice is fairly restricted. Out of the numerical methods, the finite element method is very promising /8,9,10/. This method has been used to set up a computing algorithm and a program for a digital computer. Eqs. /12/ and /13/ have been taken as the basis for the solution, particularly for that reason that after having been rearranged they can be transformed into a symmetric form, as it will be shown later on.

The boundary conditions of the solutions to eqs. /12/ and /13/ were, in accordance with /7/ considered i n the form

$$t = t_B \qquad \text{at} \quad \Gamma_1 \ , \qquad /14/$$

$$\lambda_Q \nabla t \vec{n} + j_Q + \alpha_Q (t - t_E) + (1-\varepsilon) r \alpha_Q (\theta - \theta_E) = 0 \qquad /15/$$

$$\text{at} \quad \Gamma_2 \ ,$$

$$\theta = \theta_B \qquad \text{at} \quad \Gamma_3 \ , \qquad /16/$$

$$\lambda_w \nabla \theta \vec{n} + j_w + \lambda_w \delta \vec{n} + \alpha_w (\theta - \theta_E) = 0 \qquad /17/$$

$$\text{at} \quad \Gamma_4 \ .$$

where $t_B, \theta_B, j_Q, j_w, \alpha_Q, \alpha_w$ are given functions at the boundary. The symbol $\vec{n}$ designates a unit vector in the direction normal to the integration boundary. The boundary conditions defined by eqs. /14/ to /17/ respect in fact all significant processes occuring at the integration boundary, particularly the influence of mass transfer upon heat transfer with regard to phase changes in wet solid and the influence of the heat transfer upon the mass transfer , while considering Soret effect. The boundary parts Γ_1 to Γ_4 can overlap or be identical.

Aiming at adapting the mathematical model for the simultaneous heat and moisture transport in solid determined by eqs. /12/ and /13/, by the boundary conditions /14/ to /17/ and by suitably chosen initial conditions of the solution based on the finite element we think it helpful to transform eqs. /13/ and /14/ into a symmetric form.To do this, it is convenient to transform these equations into a dimensionless form. Having made certain rearrangements, which are not relevant for the uderstanding of the method of the solution, we can transform eqs. /13/ to /17/ into

$$C_Q = \frac{\partial \bar{T}}{\partial \bar{\tau}} = L_Q \nabla^2 \bar{T} + L_\varepsilon \nabla^2 \bar{\theta} \quad , \qquad /18/$$

$$C_w = \frac{\partial \bar{\theta}}{\partial \bar{\tau}} = L_\delta \nabla^2 \bar{T} + L_w \nabla^2 \bar{\theta} \quad , \qquad /19/$$

$$\bar{T} = \bar{T}_B \qquad \text{at} \quad \Gamma_1 \,, \qquad /20/$$

$$L_Q\left(\frac{\partial \bar{T}}{\partial X}\gamma_x + \frac{\partial \bar{T}}{\partial Y}\gamma_y + \frac{\partial \bar{T}}{\partial Z}\gamma_z\right) + J_Q^* = 0 \qquad /21/$$

$$\text{at} \quad \Gamma_2 \,,$$

$$\bar{\theta} = \bar{\theta}_B \qquad \text{at} \quad \Gamma_3 \,,$$

$$L_w\left(\frac{\partial \bar{\theta}}{\partial X}\gamma_x + \frac{\partial \bar{\theta}}{\partial Y}\gamma_y + \frac{\partial \bar{\theta}}{\partial Z}\gamma_z\right) + J_w^* = 0 \qquad /22/$$

$$\text{at} \quad \Gamma_4 \,.$$

The dimensionless forms of the boundary conditions /21/ and /22/ have been written out into a component form. In eqs. /21/ and /22/ signifies

$$J_Q^* = A_Q(\bar{T} - \bar{T}_E) + A_\varepsilon(\bar{\theta} - \bar{\theta}_E) + J_Q \,, \qquad /23/$$

$$J_w^* = A_\delta(\bar{T} - \bar{T}_E) + A_w(\bar{\theta} - \bar{\theta}_E) + J_w \,. \qquad /24/$$

The dimensionless quantities are established by relations

$$\bar{T} = \frac{t}{t_I} \,, \qquad \bar{\theta} = \frac{\theta}{\theta_I} \,, \qquad \bar{\tau} = \frac{\tau}{\tau_I} \,, \qquad /25/$$

$$X = \frac{x}{l} \,, \qquad Y = \frac{y}{l} \,, \qquad Z = \frac{z}{l} \,.$$

As for further parameters, C are generalized capacities and L, A, J^* can be considered as the generalized parameters of mass transfer and specific fluxes.
Further, in eqs. /18/ and /19/ holds

$$L_\varepsilon = L_\delta = \frac{\varepsilon r \lambda_w \delta}{\lambda_Q} \,; \qquad /26/$$

then, the system of eqs. /18/ and /19/ is symmetric.
Further, it holds

$$C_Q = \left(\frac{\rho_0 c_Q l^2}{\lambda_Q \tau_I}\right)\left(\frac{t_I \delta}{\theta_I}\right) \,, \qquad /27/$$

$$C_w = \left(\frac{\rho_0 c_w l^2}{\theta_I}\right)\left(\frac{\varepsilon r \theta_I}{\lambda_Q t_I}\right) \,, \qquad /28/$$

$$L_Q = \left(\frac{\lambda_Q + \varepsilon r \lambda_w \delta}{\lambda_Q}\right)\left(\frac{t_I \delta}{\theta_I}\right) \,, \qquad /29/$$

$$L_w = \frac{\varepsilon r \lambda_w \theta_I}{\lambda_Q t_I} \,, \qquad /30/$$

$$J_Q = \left(\frac{j_Q l \delta}{\theta_I \lambda_Q}\right)\left(\frac{\lambda_Q + \varepsilon r \lambda_w \delta}{\lambda_Q}\right) \,, \qquad /31/$$

$$J_w = \left[\left(j_w - \frac{\lambda_w \delta}{\lambda_Q} j_Q\right)\left(\frac{l}{\lambda_w \theta_I}\right)\right]\left(\frac{\varepsilon r \lambda_w \theta_I}{\lambda_Q t_I}\right) \,, \qquad /32/$$

$$A_Q = \left(\frac{\alpha_Q l}{\lambda_Q}\right)\left(\frac{\lambda_Q + \varepsilon r \lambda_w \delta}{\lambda_Q}\right)\left(\frac{t_I \delta}{\theta_I}\right) \,, \qquad /33/$$

$$A_w = \left(\frac{\alpha_w l \varepsilon r \theta_I}{\lambda_Q t_I}\right)\left[1 - \frac{(1-\varepsilon) r \lambda_w \delta}{\lambda_Q}\right] \,, \qquad /34/$$

$$A_\varepsilon = (1-\varepsilon)\frac{\alpha_w l r \delta}{\lambda_Q}\left(\frac{\lambda_Q + \varepsilon r \lambda_w \delta}{\lambda_Q}\right) \,, \qquad /35/$$

$$A_\delta = -\left(\frac{\varepsilon r \lambda_w \delta}{\lambda_Q}\right)\left(\frac{\alpha_Q l}{\lambda_Q}\right) \,. \qquad /36/$$

The unknown functions $\bar{T}$ and $\bar{\theta}$ can be in time $\bar{\tau}$ approximated within the whole of the area solved by the relations

$$\bar{T} = \sum_{m=1}^{s} N_m(X, Y, Z)\bar{T}_m(\bar{\tau}) = \mathbf{N}\bar{\mathbf{T}} \,, \qquad /37/$$

$$\bar{\theta} = \sum_{m=1}^{s} N_m(X, Y, Z)\bar{\theta}_m(\bar{\tau}) = \mathbf{N}\bar{\boldsymbol{\theta}} \,, \qquad /38/$$

whre Nm are smooth functions on the element, and piecewise smooth functions within the entire domain of the solution. The sum index m reaches the values of 1 to s, where s equals 3 in the case of linear distribution of the temperature and moisture potential over the element. This assumption was used in setting up the computating program.

Applying the Galerkin method described in /11/ and using Green theorem for the boundary conditions of the solution, we get a set of equations for the unknown $\bar{T}_m$ and $\bar{\theta}_m$, which, in the matrix form, becomes

$$\mathbf{H}\boldsymbol{\phi} + \mathbf{G}\dot{\boldsymbol{\phi}} = \mathbf{F}(\boldsymbol{\phi}) \,, \qquad /39/$$

where **H** and **G** are symmetric matrices 2s x 2s

$$\mathbf{H} = \begin{bmatrix} H_Q & H_\varepsilon \\ H_\delta & H_w \end{bmatrix} \,, \qquad /40/$$

$$\mathbf{G} = \begin{bmatrix} G_Q & 0 \\ 0 & G_w \end{bmatrix} \qquad /41/$$

and $\boldsymbol{\phi}$, **F** are the vectors with 2s components

$$\phi = \left[\bar{T}, \bar{\Theta}\right]^T , \qquad /42/$$

$$F = \left[F_Q, F_w\right]^T \qquad /43/$$

The point in eq. /39/ represents derivation with respect to time. We get the particular matrix elements H, G, F

$$(H_{mn})_Q = \sum \int_{\Omega^e} L_Q \left(\frac{\partial N_m}{\partial X}\frac{\partial N_n}{\partial X} + \frac{\partial N_m}{\partial Y}\frac{\partial N_n}{\partial Y} + \frac{\partial N_m}{\partial Z}\frac{\partial N_n}{\partial Z} \right) d\Omega , \qquad /44/$$

$$(G_{mn})_Q = \sum \int_{\Omega^e} C_Q N_m N_n d\Omega , \qquad /45/$$

$$(F_m)_Q = \sum \int_{\Gamma^e} \left(J_Q^* + J_w^* \frac{L_\varepsilon}{L_w} \right) N_m d\Gamma , \qquad /46/$$

$$(F_m)_w = \sum \int_{\Gamma^e} \left(J_w^* + J_Q^* \frac{L_\delta}{L_Q} \right) N_m d\Gamma , \qquad /47/$$

where the indices m, n reach the values of 1 to s. The summation in eqs. /44/ to /47/ is understood as covering all the elements in the domain of integration.
Considering the boundary condition of the 3rd type as determined by eqs. /15/ and /17/, then, after some reaarangement, the expressions in brackets in eqs. /46/ and /47/ can be vritten out as

$$J_Q^* + J_w^* \frac{L_\varepsilon}{L_w} = \left(A_Q + \frac{L_\varepsilon}{L_w} A_\delta \right)\left(\bar{T} - \bar{T}_E \right) + \left(A_\varepsilon + \frac{L_\varepsilon}{L_w} A_w \right)\left(\bar{\Theta} - \bar{\Theta}_E \right) , \qquad /48/$$

$$J_w^* + J_Q^* \frac{L_\delta}{L_Q} = \left(A_\delta + \frac{L_\delta}{L_Q} A_Q \right)\left(\bar{T} - \bar{T}_E \right) + \left(A_w + \frac{L_\delta}{L_Q} A_\varepsilon \right)\left(\bar{\Theta} - \bar{\Theta}_E \right) . \qquad /49/$$

From the indicated derivation procedure it is obvious thatfor those elements, the side of which is identical with the boundary of the integration domain, to which the boundary condition of the third type applies, it is required that H and F in the expressions /40/ and /43/ preserve the form

$$H = \begin{bmatrix} H_Q + H_Q^\Gamma & H_\varepsilon + H_\varepsilon^\Gamma \\ H_\delta + H_\delta^\Gamma & H_w + H_w^\Gamma \end{bmatrix} , \qquad /50/$$

$$F = \left[F_Q + F_Q^\Gamma \quad F_w + F_w^\Gamma \right] , \qquad /51/$$

where the elements of matrices H^Γ and vectors F^Γ at the integration domain boundary can be determined from the analogical relations /44/, /46/ and /57/, in which we substitute alternatively from relations

$$\begin{aligned} L_Q^\Gamma &= A_Q + \frac{L_\varepsilon}{L_w} A_\delta , \\ L_\varepsilon^\Gamma &= A_\varepsilon + \frac{L_\varepsilon}{L_w} A_w , \\ L_\delta^\Gamma &= A_\delta + \frac{L_\varepsilon}{L_Q} A_Q , \\ L_w^\Gamma &= A_w + \frac{L_\varepsilon}{L_Q} A_\varepsilon , \end{aligned} \qquad /52/$$

$$\begin{aligned} J_Q^\Gamma &= L_Q^\Gamma \bar{T}_E + L_\varepsilon^\Gamma \bar{\Theta}_E , \\ J_w^\Gamma &= L_\delta^\Gamma \bar{T}_E + L_w^\Gamma \bar{\Theta}_E . \end{aligned} \qquad /53/$$

The matrix equation / 39/ represents a system of common differential equations for $\phi(\bar{\tau})$. The solution of this system is called "Galerkin´s approximations continuous in time" /12/. The particular form of the solution can be obtained numerically. Out of the methods possible for numerical solution, the linear one-step method has been chosen. For the solution of the matrix eq. /39/ this method can be written in a generalized form

$$\dot{a} = g(a, \tau) , \qquad a(0) = a^0 , \qquad /54/$$

where a is a general notation of the variable and a^0 is the initial condition. The point in eq. /54/ designates the derivation with respect to time. The solution /54/ can be expressed by the relation

$$a^{n+1} - a^n = \Delta\tau \left[(1-\Theta) g^{n+1} + \Theta g^n \right] . \qquad /55/$$

The necessary and sufficient condition for the absolute stability of the solution /55/ is $\Theta \leq \frac{1}{2}$. For $\Theta = \frac{1}{2}$,this method is often called a trapeziodal rule and, applying it to /39/ we get the well-known Crank-NIcholson s scheme .

$$\left(G + \frac{1}{2}\Delta\bar{\tau} H \right)\phi(\bar{\tau} + \Delta\bar{\tau}) = \left(G - \frac{1}{2}\Delta\bar{\tau} H \right)\phi(\tau) + \frac{1}{2}\Delta\bar{\tau}\left[F(\bar{\tau} + \Delta\bar{\tau}) + F(\bar{\tau}) \right] . \qquad /56/$$

Based on the indicated derivation of the computating algorithm of the non-stationary fields of temperature and moisture potential using the finite element method, a program in Fortran has been set up, for a plane problem with the use of the plane triangular element. The structure of the program is consistent with the computation procedure and the entire calculation is performed in the computer operational memory. With respect to the fact that the system matrix is not band and, in the case of the boundary condition of the third type is not even symmetric, the solution is carried out using the iterative Seidl´s method /13/. The result accuracy depends on the element network division and on the time-step length. The testing computations yielded very good results provided the network was fine enough.
The present program was used for computations according to the following input values:

$\varepsilon = 0,3$, $r = 2,5.10^{6}$ J/kg,
$\lambda_w = 6,04.10^{-8}$ kg/ms ^{o}M, $\lambda_Q = 0,44$ W/m K,
$\delta = 0,56$ ^{o}M/K, $C_Q = 879$ J/kg K,
$\rho_o = 1200$ kg/m^3, $l = 0,1$ m, $\tau_I = 10$ s,
$t_I = 10$ ^{o}C, $C_w = 1,8.10^{-3}$ kg/kg ^{o}M,
$\Theta_I = 111$ ^{o}M, $\alpha_Q = 35$ M/m^{2}K,
$\alpha_w = 8,64.10^{-6}$ kg/m^{2}s ^{o}M, $t_E = 60$ ^{o}C,
$\Theta_E = 11$ ^{o}M

The geometrical arrangement of the integration domain, the element network, the initial boundary conditions and the calculation results for times t = 3, 4 and 5 hours are seen in Figs. 3, 4 and 5. Axonometric illustration has been chosen to make the diagrams more clear.

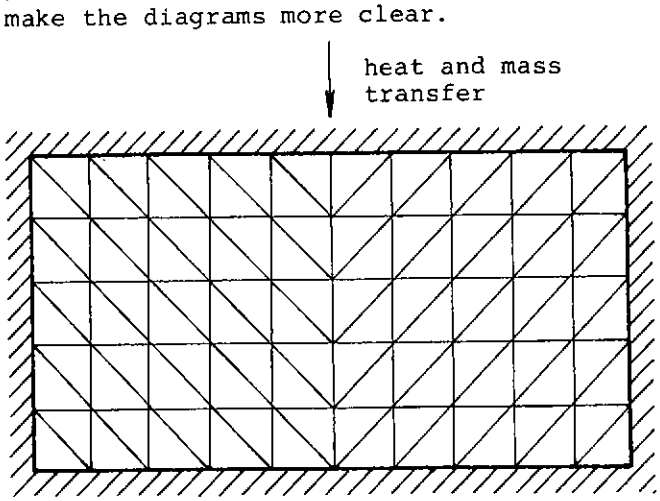

Figure 3 - The element network

An alterantive calculation for $\delta = 0,56.10^{-3}$ ^{o}M/K has also been carried out. It follows from the comparison of both cases that the influence of Soret effect was insignificant for given values.

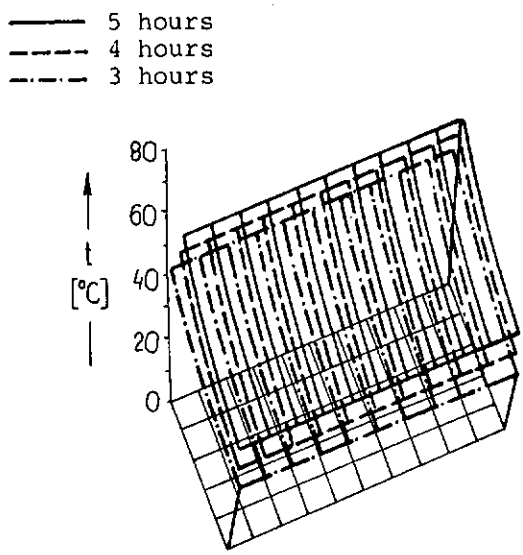

Figure 4 - The calculated results

It can be concluded that the presented calculation procedure and the program for computing the non-stationar temperature fields and the moisture potential fields are very convenient for the mathematical modelling the effect of the moist solid hygrothermic parameters and that of the boundary conditions upon the process of drying wet materials.

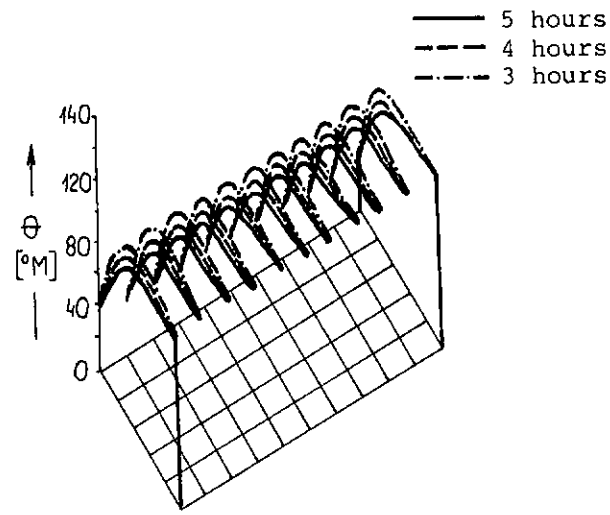

Figure 5 - The calculated results

REFERENCES

1. Valchář J., Strojírenství, Vol 22, p. 358-363, 1972
2. Valchář J., Heat and Moisture Transfer in Capillary-Porous Materials form the Point of View of the Thermodynamics of Irreversible Processes, Third Int.Heat Transfer Conf., Chicago, Vol. 1, Paper No. 40, Aug. 1966
3. Fitts, D.D., Non-equilibrium Thermodynamics, Mc Graw Hill Book Co., New York, 1962
4. Valchář J., K analizu vybora sistemy termodinamicheskih potokov i sil dlja odnovremennoy teplo- i vlagoperedachi, Teplo- i massoperenos, Vol. 9, part I, Minsk 1972
5. Valchář J., Theoretical Analysis of Nonstationary Temperature and Moisture Content Fields in Capillary Porous Materials and Binding Energy of Moisture, Int. Symposium on Heat and Mass Transfer Problems in Food Engineering, Wageningen, The Netherladns, 1972
6. Luikov A.V., Teoriyj sushki, Energiya, Moskva 1968
7. Luikov A.V., Heat and Mass Transfer in Capillary-porous Bodies, Pergamon Press, Oxford, 1966
8. Zienkiewicz O.C., The Finite Element Method in Engineering Science, Mc Graw Hill, London, 1970
9. Levi R.V., Comini G., Humpheson C., Inzhenerno-fyzicheskiy zhurnal /Journal of Engineering Physics/, Vol 29, p. 483-488, 1975
10. Valchářová /Budáčová/ J., Inzhenerno-fizicheskiy zhurnal /Journal of Engineering Physics/, Vol 33, p. 728-733, 1977
11. Demidovich, B.P., Maron J.A., Základy numerické matematiky, SNTL Praha, 1966
12. Douglas J., Dupont J.T., SIAM Journal of Numerical Analysis, Vol 7, 575-626, 1970

Appendix 1

(A) initial conditions

(B) boundary conditions

(C) eqs. of nonstationary hydrodynamic, thermal and diffusion boundary layer

(D) differential equations of nonstationary temperature and moistrue content fields

CHARACTERISING MOISTURE BOND IN MATERIALS WITH RESPECT TO DRYING USING THE STATE FUNCTION DIAGRAM

B. Čermák PhDr

National Research Institute for Maschine Design,
Praha 9 250 97

ABSTRACT

Moisture bond in materials can be thermodynamically expressed by state functions - specific enthalpy, specific entropy and potential of bound moisture. In the suggested diagram, the values of the bound moisture state functions determined experimentally in various moisture content under constant temperature and pressure form a curve characteristic for given material. Direct comparison with the theoretically significant values of the bound moisture state functions in the diagram permits objective valuation of the character of moisture bond in the material.

NOMENCLATURE

G = Gibbs function, J
H = enthalpy, J
h = specific enthalpy, J/kg
m = mass, kg
p = pressure, Pa
S = entropy, J/K
s = specific entropy, J/kg K
T = temperature, K
u = moisture content, kg/kg
μ = potential of moisture, J/kg

Subscripts

j = component j
w = moisture
wo= pure moisture in liquid phase

Superscripts

MR = real mixing

THERMODYNAMICS OF MOIST MATERIAL

Moist materials represents heterogeneous multicomponent mixture. In drying theorie there are only two components to distinguish :

dry matter and moisture /1/. The state of moist material is determined by its composition, by mutual bond of the components and by external conditions /temperature, pressure/ or rather by state functions of the mixture and its components /2/.

In the heat and moisture transfer follow-ing state functions have to be considered :

potential of moisture

$$\mu_w = \left[\frac{\partial G}{\partial m_w}\right]_{T,p,m_w \neq m_j} \quad (1)$$

specific enthalpy of moisture

$$h_w = \left[\frac{\partial H}{\partial m_w}\right]_{T,p,m_w \neq m_j} \quad (2)$$

specific entropy of moisture

$$s_w = \left[\frac{\partial S}{\partial m_w}\right]_{T,p,m_w \neq m_j} \quad (3)$$

with mutual relations

$$\mu_w = h_w - T\, s_w \quad (4)$$

$$s_w = -\frac{\partial \mu_w}{\partial T} \quad (5)$$

In relations /1/ to /3/ G designates Gibbs function, H enthalpy, S enthropy of moist material, m_j and m_w designate mass of a j-th component and material moisture respectively.

For moist material as a real mixture /2/, the state functions can be expressed in form

$$\mu_w = \mu_{wo} + \mu_w^{MR}$$

$$h_w = h_{wo} + h_w^{MR}$$

$$s_w = s_{wo} + s_w^{MR}$$

where index WO designates the value corresponding to the pure moisture in liquid phase and index MR designates a contribution resulting from actual mixing of the components, i.e. mixing with mutual bond of moisture and material.
From the viewpoint of drying :

μ_w^{MR} represents the thermodynamic potential of moisture transfer

h_w^{MR} is the heat effect of moisture bond with material ; it enters energy balance of the drying process in the sum with the heat of evaporation of the moisture

s_w^{MR} expresses changes in the configuration and mobility of moisture and material during drying

Actual values of the state functions of bound moisture in real material can be determined only experimentally.

Diagram of the state functions of bound moisture and its application

To evaluate the nature of moisture bond in material from the viewpoint of drying, the diagram of the state functions of bound moisture has been suggested /1/. In fig. 1 the diagram is demonstrated with the network of the theoretically significant values μ_w^{MR}, h_w^{MR} and s_w^{MR} for temperature T = 298 K and pressure $p = 10^5$ Pa.

Each pair of the experimentally determined values $\mu_w^{MR}(u)$ and $h_w^{MR}(u)$ for particular material moisture content u /expressed in kg of moisture per kg of dry matter/ represents in the diagram a point $\langle h_w^{MR}(u) ; \mu_w^{MR}(u) \rangle$. A set of these points expressing the change of states due to the change in material moisture under a constant temperature and pressure forms a curve characteristic for given material.

Up to now about 20 materials have been measured and 4 basic types of characteristic curves have been observed.

Basic types of characteristic curves are schematically drown in fig. 2. From the view point of drying these curves allow the following interpretation :

1 - material is stable, strongly hydrophilic
2 - material is stable, predominantly hydrophobic
3 - material is stable with unimportant phase changes of higher order
4 - material is unstable, intensified way of drying may produces a deteriorated quality of product.

The diagram of the state functions of bound moisture with characteristic curves for bentonite and potatoe flour is presented in fig. 3. The experimental points have been determined by measuring the heats of immersion and the sorption isotherms, with the equipment developed in our Institute /1/. At each point the value of moisture content /kg/kg/ is designated.

For bentonite we can conclude :

1. Notably negative values of specific enthalpy h_w^{MR} throughout the whole range of the values of the moisture content correspond to strongly hygrophilic character of bentonite.
2. The specific entrophy values s_w^{MR} correspond to the model of partially

solidified moisture and inert material throughout the whole range of the values of the moisture content.

3. The considerable values of s_w^{MR} at $\mu_w^{MR} > -10$ kJ/kg give evidence of configuration of a high degree and low mobility of water between aluminium silicate layers of montmorillonite, the chief mineralogic component in bentonite.
4. Remarkable changes in the course of the curve at higher moisture contents can be interpreted as phase changes of a higher order in various types of moisture sorption.
5. Characteristic curve is of type III, from the view point of drying, the material can be considered stable. In natural drying down to $u \doteq 0{,}12$ kg/kg the binding energy represents already more than 10 per cent of the heat of evaporation.

For potato flour there are following conclusions :

1. The material is hydrophilic, specific enthalpy is negative throughout the whole moisture content range.
2. The positive values s_w^{MR} at higher moisture contents $u > 0{,}15$ kg/kg can only be ascribed to the disturbation of material skeleton due to the moisture bound.
3. The low values s_w^{MR} and h_w^{MR} at $u < 0{,}03$ kg/kg correspond to associative chemical bonds between moisture and partially dehydrated material.
4. Characteristic curve is of type IV, from the view point of drying the material can be considered unstable. Applying intensified ways of drying at higher material moisture contents / $u > 0{,}15$ kg/kg/ can result in deteriorated quality of the product.

Using recirculation of dried material at the dryer inlet, the inlet moisture content of material can be brought down below the value $u \doteq 0{,}13$ kg/kg so the risk of wasting the product by intensified ways of drying is reduced. At the same time, the energy consumption in releasing moisture increses up to more than 15 per cent of the heat of evaporation.

CONCLUSION

Moisture bond in materials is described by state fumetions of bound moisture, values of which have to be determined experimentally.

The suggested diagram permits from experimentally determined values of specific enthalpy and potential of bound moisture a new, objective and complex evaluation of the moisture bond in materials.

REFERENCES

1. Čermák, B. : Termodynamická metoda hodnocení charakteru vazby vlhkosti v materiálech PhDr Thesis, SVÚSS, Praha 1977
2. Denbigh,K. : The principles of chemical equilibrium, Cambridge University Press, 1961

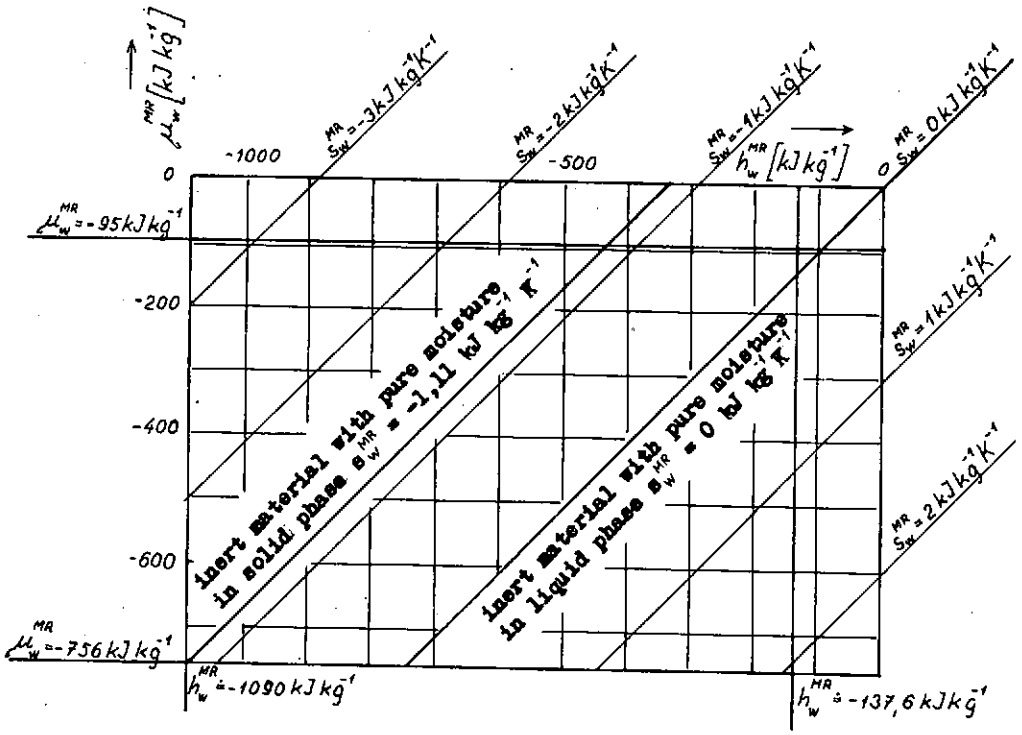

Fig 1 Diagram of the state functions of bound moisture with theoretically significant values for T = 298 K, p = 10^5 Pa

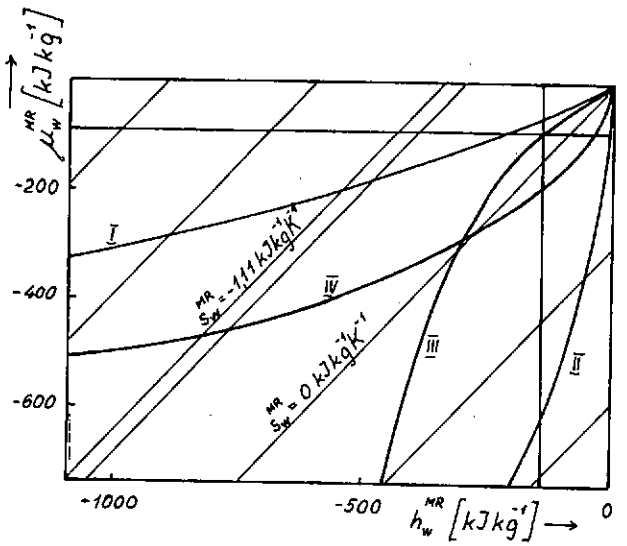

Fig 2 Basic types of characteristic curves in diagram of the state functions of bound moisture

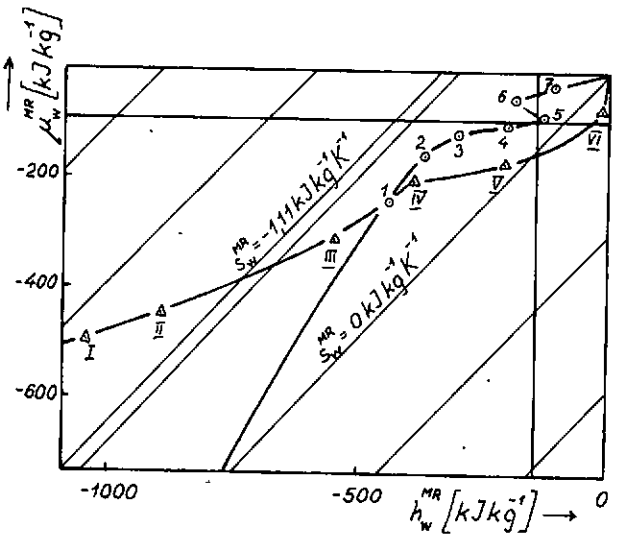

values of the moisture content u [kg kg^{-1}] at points 1 0.086; 2 0.115; 3 0.133; 4 0.152; 5 0.168; 6 0.185; 7 0.210; I 0.031; II 0.045; III 0.076; IV 0.121; V 0.135; VI 0.189

Fig 3 Diagram of the state functions of bound moisture with characteristic curves for bentonite ⊙ and potato flour △

INTERDEPENDENCE BETWEEN HEAT AND MASS TRANSFER IN DRYING

P.S.Kuts and I.F.Pikus

Luikov Heat and Mass Transfer Institute,
BSSR Academy of Sciences, Minsk, USSR

NOMENCLATURE

b = temperature coefficient of drying

B = dimensionless temperature coefficient of drying

C_g = specific heat of drying agent (gas) J/kg.deg

C_s = specific heat of dry material, J/kg.deg

F = gas - distributor area, m^2

G = mass of moist material, kg

$G_{d.s.}$ = mass of dry material, kg

Δh_v = evaporation heat of water, J/kg

k_m = moisture diffusion coefficient, m^2/s

k = thermal diffusivity, m^2/s

$\dot{m}$ = moisture flow density, kg/m^2s

N = maximum drying rate, kg/kg dry (%/dry)

$\dot{q}$ = heat flux, J/m^2s

R_v = equivalent (hydraulic) radius, m

τ = time, s

T_a = ambient (drying agent) temperature, K

T_r = radiation temperature, K

T_s = body surface temperature, K

T_w = wet - bulb temperature, K

v = drying agent velocity, m/s

X = instantaneous moisture content, kg/kg (%)

X_0 = initial moisture content of material, kg/kg (%)

X_{cr} = critical moisture content of material, kg/kg (%)

X_E = equilibrium moisture content of material, kg/kg (%)

Z = dimensionless coordinate

α_m = heat transfer coefficient for the falling-rate period, W/m^2 deg

α_{cr} = heat transfer coefficient for the constant-rate period (at critical moisture content of material), W/m^2deg

Θ = temperature of material, °C

Θ_a = ambient temperature, °C

Θ_0 = initial temperature of material, °C

Θ_g = initial temperature of drying agent, °C

ρ = density of drying agent, kg/m^3

ρ_s = density of dry material, kg/m^3

φ = relative air humidity, %

$\mathcal{H}$ = relative coefficient of drying

Bi = Biot number

Fo = Fourier number

Ki = Kirpichev number

Ko = Kossovich number

Lu = Luikov number

Nu = Nusselt number

Rb = Rebinder number

Pn = Posnov number

ε = phase transition number

Subscripts

— = mean value

• = value per unit time

INTRODUCTION

Thermal calculation of drying thermolabile materials basically implies determination of the dehydration time with allowance for the kinetics of material heating up to an ultimately admissible temperature, as the variation of material temperature and the time of its being in a heated state control the quality of the end product.

The problem of analytical study of the kinetics of heating and drying moist materials is rather complicated and requires solution of coupled parabolic or hyperbolic differential heat and mass transfer equations with appropriate boundary conditions.

A rigorous analytical theory of energy and substance transfer in drying moist materials has been developed in detail by A.V.Luikov and Yu.A.Mikhailov in their fundamental monographs (1,2). The solutions they have obtained may be used to determine instantaneous transfer potential fields in the material under drying as well as to describe and calculate the kinetics of varying mean-volume transfer potentials during drying. Unfortunately, the wide use of these rather complicated solutions in engineering practice requires a knowledge of a series of thermophysical and mass transfer properties that are too scanty in modern literature. Also, in a number of instances rigorous mathematical description of the interdependence between the surroundings and dried material surface involves great difficulties. Finally, when it is necessary to allow for the dependence of thermophysical properties of the material and transfer coefficients on moisture content and temperature, the problem becomes extremely complicated because of its substantial nonlinearity. Therefore it is a common practice in engineering design of the kinetics of moist material heating and drying to use approximate calculation methods developed, as a rule, with definite simplifying assumptions and based on the general laws established experimentally for that or another particular process.

BASIC EQUATION FOR THE DRYING KINETICS

In the general case, description of the drying kinetics requires a knowledge of the time variation of mean-volume moisture content $\bar{X}$ and temperature $\bar{\theta}$. Therefore, for analysing the interdependence between heat and mass transfer in this process, the relationships for external moisture exchange intensity $\dot{m}$ and external heat exchange intensity $\dot{q}$ might be formally used. But, sufficiently accurate calculation of $\dot{m}$ and $\dot{q}$ by the Dalton and Newton formula for the falling-rate period of drying seems to be impossible since moisture and heat transfer coefficients change with time because drying is a typical unsteady process of moisture and heat exchange. In the first approximation, the intensity of moisture transfer may be defined as (3)

$$\dot{m} = R_V \rho_S \left(\frac{d\bar{X}}{dt}\right) = \\ = R_V \rho_S K (\bar{X} - X_E) = R_V \rho_S \frac{\mathcal{K} N}{100} (\bar{X} - X_E) \qquad (1)$$

where R_V is the body volume-to-surface ratio (characteristic dimension); K the drying coefficient whose value is directly proportional to maximum drying rate N ; $\mathcal{K}$ relative drying coefficient.

The two-zone method for the drying curve calculation (4) represents further development of the previous one. It implies that the drying-rate curve for the falling-rate period is replace by a broken straight line, i.e. the falling-rate period of drying is divided into two zones with the drying rate decreasing depending on the moisture content by the linear law. In this case two values, $\mathcal{K}_1$ and $\mathcal{K}_2$, of the relative drying coefficient must be known. Some more approximate equations for the drying-rate curve are known to describe more accurately the real kinetics of moisture exchange but all of them abound with constants that are determined upon correlation of the experimental data. As a representative example, one may refer to the methods of calculating the drying-rate curve based on the analysis of the relative drying rate ($1/N \; d\bar{X}/dt$) vs instantaneous excessive moisture content of the material ($\bar{X} - X_E$) (3,5)

$$-\left(\frac{1}{N}\frac{d\bar{X}}{dt}\right) = \frac{(\bar{X} - X_E)^n}{A + D(\bar{X} - X_E)^n} \qquad (2)$$

$$-\left(\frac{1}{N}\frac{d\bar{X}}{dt}\right) = A'(\bar{X} - X_E) + D'(\bar{X} - X_E)^2 \qquad (3)$$

where A , D , n , A' and D' are constants determined experimentally.
Thus, the intensity of moisture exchange

in drying of different materials may be culculated sufficiently accurately. At the same time, the data on the moisture exchange kinetics make it possible to completely reveal the kinetics of heat transfer in drying. Indeed, since the heat supplied to material is spent for its heating and moisture evaporation,then with the energy conservation law, the relationship between heat and moisture transfer rates in drying can be established..This enables us to reduce the calculation of heat transfer to the one of moisture transfer and vice versa

$$\dot{q}(t) = \dot{m}(t)\left(\Delta h_v + c\frac{d\Theta}{d\bar{X}}\right) = R_v \rho_s \Delta h_v \left(\frac{d\bar{X}}{dt}\right)\left[1 + \frac{c}{\Delta h_v}\frac{d\bar{\Theta}}{d\bar{X}}\right] \quad (4)$$

where c is the reduced specific heat of a moist body ($c = c_s + c_m \bar{X}$).

The quantity $\frac{d\bar{\Theta}}{d\bar{X}}$ involved into relation (4) specifies a variation of the mean temperature of dried material with changing of its mean moisture content per unit for infinitesimal time. This quantity being an important characteristic of the drying kinetics is referred to as the temperature coefficient of drying " b ". The dimensionless generalized variable $b\frac{c}{\Delta h_v}$ equal to the ratio of heat for body heating to that for moisture evaporation for infinitesimal time is the basic criterion of the drying kinetics and is referred to as the Rebinder number

$$Rb = \frac{c}{\Delta h_v}\left(\frac{d\bar{\Theta}}{d\bar{X}}\right) \quad (5)$$

The Rb number depends on the temperature drying coefficient, specific heat of moist material, evaporation heat and, hence, on the forms of moisture-material bond.

Equation (4) may be written in the criterial form

$$Ki_q(t) = Ki_m(t)\, Lu\, Ko\,(1 + Rb) \quad (6)$$

where the heat and moisture exchange Kirpichev numbers are, respectively,

$$Ki_q(t) = \frac{\dot{q}(t) R_v}{\lambda T_a}; \quad Ki_m(t) = \frac{\dot{m}(t) R_v}{k_m \rho_s \bar{X}_0} \quad (7)$$

T_a is the ambient temperature, K.

The Lu number for relative moisture exchange is equal to the moisture diffusion coefficient, k_m, to the heat diffusion coefficient ($Lu = k_m/k$). The Kossovich number

$$Ko = \frac{\Delta h_v X_0}{c T_a} \quad (8)$$

is the ratio of heat for evaporation of the whole amount of moisture in the body to that for its heating from 0 to , while the Rebinder number specifies the ratio of local heat quantities for moisture heating and evaporation.The Kossovich and Rebinder numbers are related as

$$Ko = \frac{B}{Rb} \quad (9)$$

where B is the dimensionless temperature drying coefficient

$$B = b\frac{X_0}{T_a} = \frac{d\bar{\Theta}/T_a}{d\bar{X}/X_0} \quad (10)$$

In the constant-rate period of drying, the Rebinder number is zero and then

$$\dot{q}_I = \Delta h_v \rho_s R_v \frac{N}{100} = const \quad (11)$$

By denoting the ratio of a heat flux for the falling-rate period of drying, $\dot{q}(t)$, to that for the constant-rate period , $\dot{q}_I$, as $\dot{q}^*(t)$,we obtain

$$\dot{q}^*(t) = \frac{\dot{q}(t)}{\dot{q}_I} = \left(\frac{d\bar{X}}{dt}\right)^*(1 + Rb) \quad (12)$$

where $\left(\frac{d\bar{X}}{dt}\right)^* = \frac{100}{N}\left(\frac{d\bar{X}}{dt}\right)$ is the relative drying rate for the falling-rate period.

Equation (12) relates heat transfer , $\dot{q}^*$, to moisture exchange ($d\bar{X}/dt$) in terms of the Rb number. This relation is the basic equation of drying kinetics. Using this relation, heat transfer may be completely described by the data for moisture exchange.

As stated above, the variation of moisture exchange rate may be approximated by relations (1)-(3). Then the heat transfer rate, $\dot{q}(t)$, may be easily calculated by equation (12) if the dependence bet-

ween Rb and material moisture content is known. The relation $Rb = f(\bar{X})$ may be found experimentally or analytically from the solutions to simultaneous differential heat and moisture transfer equations.

The dimensionless temperature coefficient of drying

$$B = Rb \cdot Ko \qquad (13)$$

makes it possible to relate mean temperature, Θ, of the body and its moisture content, $\bar{X}$, as

$$\frac{\Theta}{T_a} = -\int \frac{B(\bar{X})}{\bar{X}_0} d\bar{X} + C_1 \qquad (14)$$

where C_1 is an arbitrary constant.

Thus, to find empirical correlations $Rb = f(\bar{X})$ and $B = \varphi(\bar{X})$ is of great interest both for calculation of drying kinetics and for drying technology because the main properties of dried material are governed by its temperature and moisture content.

ANALYSIS OF Rb NUMBERS VS MATERIAL MOISTURE CONTENT

Experimental data of the present authors and other investigators as to the kinetics of heating and dehydration of various materials made it possible to obtain the relation $Rb = f(\bar{X})$ and to analyse the effect of the governing factors on the nature of this relation.

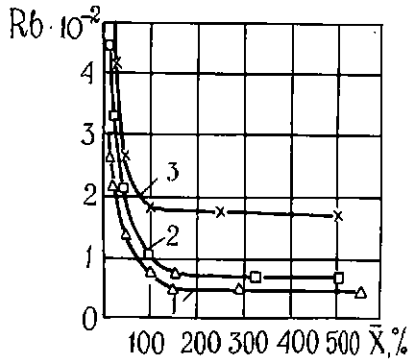

Fig.1. The Rb number vs moisture content $\bar{X}$ (%) for peat-slab drying (v =4 m/s, φ = 4%). 1, Θ_a = 100°C; 2, 150°C; 3, 200°C

Thus, in Figs 1 through 3, the above relationship is given as a representative example. These data have been obtained for convective drying of a peat slab and porous ceramics, as well as for drying of cube-cut potato in a fluidized bed under oscillating conditions. It is seen from Fig.1 that the Rb number for moisture content $1.5 < X < 5.0$ is approximately constant and then increases sharply with decreasing moisture content. This relationship can be governed by

$$Rb = A(\bar{X} - X_E)^n \qquad (15)$$

where A and n are constants.

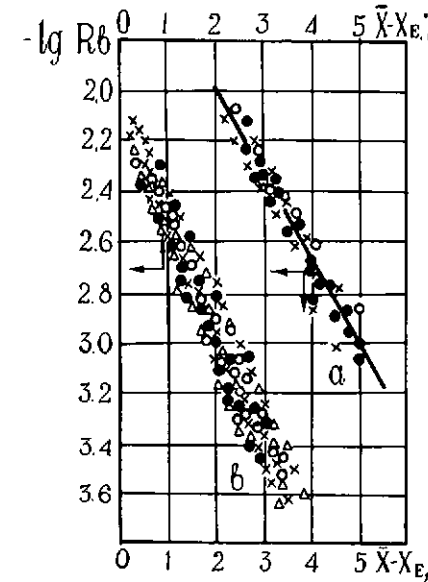

Fig.2. The lgRb vs excessive moisture content ($\bar{X} - X_E$) (%) for a moist ceramic slab (180x40x 6.5 mm) at: a - φ = 5%; v = 0 m/s; Θ_a: ● - 75°C; × - 90°C; o - 120°C; b - φ: ● - 20%, o - 40%; X - 60%; Δ - 80%

The constant n is independent of the drying regime and equals to n=-0.8. The constant A grows with increasing temperature (see Table 1). Similar results have been obtained for drying of porous ceramics, but in this case the relationship between the Rb number and material moisture content is approximated by the following empirical correlation

$$Rb = A \exp\left[-n(\bar{X} - X_E)\right] \qquad (16)$$

where A and n are experimentally determined constants (see Table 1). (Here moisture content is in %).

Table 1

A and n constants for some materials

Kind of material	Drying regimes Θ_a°C	φ %	V m/s	A	n
Peat slabs (relation 15)	100	4	4.0	0.26	-0.8
	150	4	4.0	0.40	-0.8
	200	4	4.0	0.57	-0.8
Porous ceramics (plate 80x40x 6.5 mm)	75	5	0.0	0.01	0.83
	90	5	0.0	0.01	0.83
	170	5	0.0	0.01	0.83
ρ_s= 1684 kg/m^3	120	20	0.0	0.01	1.00
(relation 16)	120	80	0.0	0.01	1.00

The treatment of the experimental data has shown that in drying of porous ceramics under free convection, variation of air temperature from 75 to 120°C and of relative air humidity from 20 to 80% does not practically affect the relationship between Rb and ($\bar{X} - X_E$).

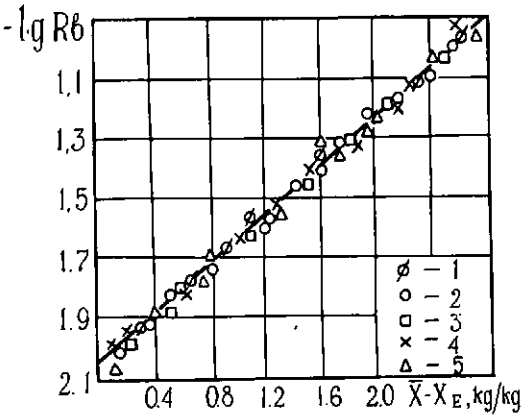

Fig.3. The lgRb vs excessive moisture content ($\bar{X} - X_E$) kg/kg for fluidized drying of cut potato under oscillating conditions ($\Theta_a - \Theta_w$ = 51°C, t_{osc} = 40 s). 1, $v\rho$ = 4 kg/m^{2}s; 2, 6; 3, 7.8; 4.5, 6 kg/m^{2}s; 1-3, R_v= 9.9 mm; 4, 12.4; 5-8 mm

It is seen from Fig.3 that for drying of potato blocks in a fluidized bed under oscillating conditions the relationship $Rb = f(\bar{X} - X_E)$ may be described by equation (15) with $n > 0$. It is worth noting that variation of the mass flow rate of the drying agent (between 4 and 7.8 kg/m^{2}s) and characteristic size of dried product particles ($Д_H$= 8-12.4 mm) did not result in any noticeable change of the considered quantity.

Difference in the Rb number vs moisture content for capillary-porous colloids and capillary-porous bodies is basically explained by different forms of moisture bonds for these materials. At the same time, vast experimental investigations have shown that in many instances the qualitative and quantitative nature of Rb variations in drying does not depend on operational parameters and characteristic size of the samples, i.e. the Rb number is a single-valued function of the body moisture content. With this in view and proceeding from the empirical correlations for the Rb number vs mean instantaneous excess material moisture content, the appropriate equations for the temperature curve may be obtained. If, for example, equation (16) is used, then the dependence between the mean temperature, $\bar{\Theta}$, of the body and its moisture content $\bar{X}$ is described by the exponential function of the form

$$\bar{\Theta} = \bar{\Theta}_0 + \frac{A\Delta h_v}{cn}\left\{\exp\left[-n(\bar{X}-X_E)\right] - \exp\left[-n(\bar{X}_0-X_E)\right]\right\} \quad (17)$$

EFFECT OF THE GOVERNING SIMILARITY NUMBERS ON THE TEMPERATURE COEFFICIENT OF DRYING

The dependence of the temperature coefficient of drying on the governing similarity numbers may be analysed by solving the system of the differential equations that describe, for example, convective drying of an infinite slab under the third-kind boundary conditions. These simultaneous heat and mass transfer differential equations in the form of generalized variables for a one-dimensional problem are as follows (1)

$$\frac{\partial T(z,Fo)}{\partial Fo} = (1+\varepsilon Ko\,Pn\,Lu)\frac{\partial^2 T(z,Fo)}{\partial z^2} - \varepsilon Ko\,Lu\frac{\partial^2 X(z,Fo)}{\partial z^2} \quad (18)$$

$$\frac{\partial X(z,Fo)}{\partial Fo} = Lu\frac{\partial^2 X(z,Fo)}{\partial z^2} - Lu\,Pn\frac{\partial^2 T(z,Fo)}{\partial z^2} \quad (19)$$

Dimensionless third-kind boundary conditions may be written for the system of equations (18) and (19) as

$$\frac{\partial T(1,Fo)}{\partial z} = Bi_q[1-T(1,Fo)] + (1-\varepsilon)Ko\,Lu\,Ki_m(Fo) \quad (20)$$

$$\frac{\partial X(1,Fo)}{\partial z} + Pn\frac{\partial T(1,Fo)}{\partial z} + Ki_m(Fo) = 0 \quad (21)$$

The most representative form of the relationship for dimensionless substance flow in convective heat and mass transfer may be

$$Ki_m = Bi_m[1 - X(1,Fo)] \quad (22)$$

i.e. substance flow on the body surface is a mass transfer potential function.The problem is considered symmetric, i.e.

$$\frac{\partial T(0,Fo)}{\partial z} = \frac{\partial X(0,Fo)}{\partial z} = 0; \quad \begin{matrix} T(0,Fo) \neq \infty \\ X(0,Fo) \neq \infty \end{matrix} \quad (23)$$

Dimensionless initial conditions are written to give

$$T(z,0) = X(z,0) = 0 \quad (24)$$

The solution of the system of heat and mass transfer equations (18) and (19) subjected to the above boundary conditions for an infinite slab has the form

$$T(z,Fo) = 1 - \sum_{n=1}^{\infty}\sum_{i=1}^{2} C_{ni}\cos(\nu_i\mu_n z)\exp(-\mu_n^2 Fo) \quad (25)$$

$$X(z,Fo) = 1 + \frac{1}{\varepsilon Ko}\sum_{n=1}^{\infty}\sum_{i=1}^{2} C_{ni}(1-\nu_i^2)\cos(\nu_i\mu_n z)\exp(-\mu_n^2 Fo) \quad (26)$$

The expressions to calculate the coefficients C_{ni}, and the characteristic equation to determine the roots μ_n, are given in (1).

Dimensionless rate of heat and substance transfer potential variation may be found by differentiating equations (25) and (26) over Fo

$$\frac{d\bar{T}}{dFo} = \sum_{n=1}^{\infty}\sum_{i=1}^{2} C_{ni}\frac{\mu_n}{\nu_i}\sin\nu_i\mu_n\exp(-\mu_n^2 Fo) \quad (27)$$

$$\frac{d\bar{X}}{dFo} = \frac{1}{\varepsilon Ko}\sum_{n=1}^{\infty}\sum_{i=1}^{2} C_{ni}\frac{\mu_n(1-\nu_i^2)}{\nu_i}\sin\nu_i\exp(-\mu_n^2 Fo) \quad (28)$$

Based on expressions (27) and (28), the temperature coefficient of drying is determined as

$$b = \frac{d\bar{T}/dFo}{d\bar{X}/dFo}$$

Thus, solution of the differential heat and moisture transfer equations enables us to analyse the dependence of the temperature coefficient of drying on a large set of heat and mass transfer similarity numbers

$$b = f(Fo, Lu, Bi_q, Ko, Bi_m, \varepsilon)$$

However, the effect of these numbers on the behavior of a process is different.

Numerical computations of equations (27) and (28) on the electronic computer "Minsk-22" made it possible to relate individual heat and mass transfer similarity numbers to the temperature coefficient of drying.

The most pronounce effect on the temperature coefficient under the conditions of convective drying has the Lu number.It is seen from Fig. 4a that the value of " b " rises with increasing Lu. The change of the " b " coefficient is most substantial for the range of moderate Fo numbers. This is because, with incipient drying, the rate of temperature variation is higher than the velocity of moisture propagation in the material.

The surface heat and mass transfer numbers, Bi_q and Bi_m, have a marked effect on the process kinetics. In Fig.4b the temperature coefficient of drying " b " is plotted vs Bi_q. The calculations suggested that with small Bi_q, the rate of heat transfer potential $d\bar{T}/dFo$ variation exceeds greatly the rate of substance transfer potential $d\bar{X}/dFo$ variation, i.e. the temperature coeffici-

ent of drying increases with decreasing Bi_q. As Bi_q grows, transfer processes are enhanced and the gradients of transfer potentials in the material increase, too. With increasing Fo, the Bi_q numbers exerts a less pronounced effect on "δ". At Fo=10 for $Bi_q > 0.4$, the temperature coefficient of drying "δ" is independent of the surface heat transfer number.

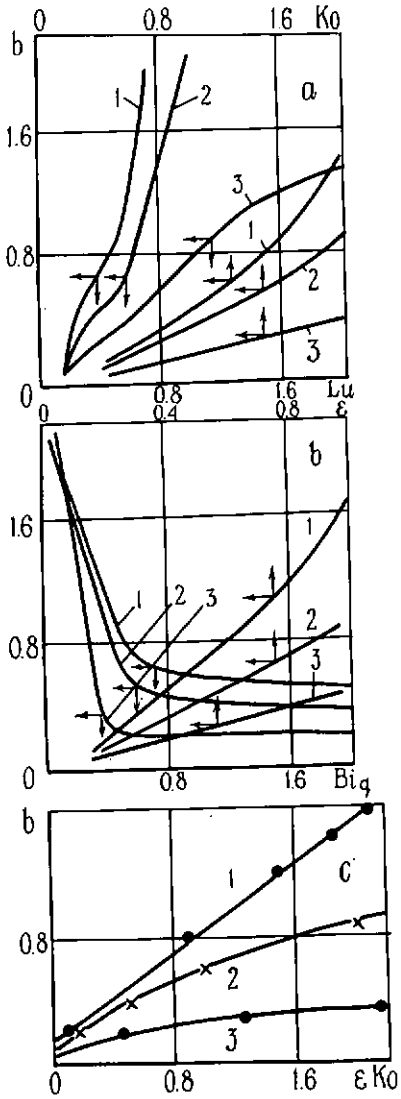

Fig.4. Temperature coefficient of drying vs Lu and Ko (a), ε and Bi_q (b); $\varepsilon \cdot Ko$ (c); 1, Fo=0.5; 2, 1.0; 3, 10

The phase conversion number ε has a similar (thus less pronounced) effect on heat and mass transfer as the Kossovich number. The plot of ε vs temperature coefficient "δ" is identical to $\delta = f(Ko)$ (Fig.4b). With increasing Ko and ε, the temperature coefficient "δ" increases, other conditions being equal.

In numerical heat and mass transfer calculations the product εKo is often encountered.

In Fig. 4c the temperature coefficient of drying vs absolute εKo is plotted. The behavior of these curves is similar to $\delta = f(\varepsilon)$ and $\delta = \varphi(Ko)$

In accordance with the analysis in (1), when calculating unsteady fields of transfer potentials, the effect of some criteria may be ignored since their influence on the evolution of temperature and moisture content fields in the material is insignificant.

Taking into account that in the second drying period in the majority of cases $Bi_q > 0.4$ and the temperature coefficient of drying, as seen from Fig.4b, is almost independent of Bi_q, then to some accuracy the reduced criterial relation for δ vs the governing similarity numbers may be presented as

$$\delta = f(Lu, Ko, \varepsilon, Fo)$$

Graphical and analytical treatment of the calculated data for the temperature coefficient of drying made it possible to obtain the criterial equation in an explicit form (7)

$$\delta = 3.55\, Ko^{0.89}\, \varepsilon^{0.89}\, Lu^{1.34}\, Fo^{-0.34} \qquad (29)$$

This expression holds for the following range of similarity numbers: $0.4 \leq Fo \leq 10$; $0.4 \leq Ko \leq 2$; $0.1 \leq \varepsilon \leq 1$; $0.15 \leq Lu \leq 1$.

EXTERNAL HEAT TRANSFER AND THE REBINDER NUMBER

As is known (3,8), the heat transfer coefficient, α_m, may be constant only within the period of a constant rate of drying, while in the falling-rate period it diminishes with decreasing moisture content.

To calculate α_m, P.D.Lebedev suggested the relationship (8)

$$\frac{\alpha_m}{\alpha_{cr}} = \left(\frac{\bar{X}}{\bar{X}_{cr}}\right)^n \qquad (30)$$

and to obtain the heat-transfer Nusselt

number, the empirical correlation

$$Nu = A\,Re^{p}\left(\frac{T_a}{T_w}\right)^{m}\left(\frac{T_z}{T_a}\right)^{\kappa}\left(\frac{\bar{X}}{\bar{X}_{cr}}\right)^{n} \quad (31)$$

We have attempted to assess the Nusselt number (Nu) for the second period using its values (Nu_{cr}) in the first period and the dimensionless rate of drying N* (9). These values can be readily found both theoretically and experimentally. As to estimate the heat transfer coefficient by relation (31), a knowledge of the surface material temperature is required. However, its exact measurement often involves great experimental difficulties.

The basic equation of the drying kinetics may be of the form

$$\dot{q}(t) = -R_v \rho_s \Delta h_v \frac{d\bar{X}}{dt}(1 + Rb) \quad (32)$$

The rate of drying in the first period may be estimated, provided that the heat flux is known, by the following formula

$$N = \frac{\dot{q}_I}{\Delta h_v R_v \rho_s} \quad (33)$$

Then the heat-transfer intensity in the first period is governed by the Newton formula

$$N = \frac{\alpha_{cr}(T_a - T_w)}{\rho_s R_v} \quad (34)$$

In the second, the drying rate is

$$\frac{d\bar{X}}{dt} = -\varkappa N(\bar{X} - X_E) \quad (35)$$

In the period of the falling rate of drying, the heat flux is specified by the Newton formula for convective heat transfer

$$\dot{q}_{II} = \bar{\alpha}(T_a - T_s) \quad (36)$$

Substituting (35) and (36) into equation (32), gives

$$\bar{\alpha}(T_a - T_s) = R_v \rho_s \Delta h_v \varkappa N(\bar{X} - X_E)(1 + Rb) \quad (37)$$

Replacing N by expression (34) yields

$$\bar{\alpha}(T_a - T_s) = \varkappa \cdot \alpha_{cr}(\bar{X} - X_E)(T_a - T_w)(1 + Rb)$$

or

$$\frac{\bar{\alpha}(T_a - T_s)}{\alpha_{cr}(T_a - T_w)} = \varkappa(\bar{X} - X_E)(1 + Rb) \quad (38)$$

Denoting

$$\Delta T^* = \frac{T_a - T_s}{T_a - T_w}; \qquad N^* = \frac{d\bar{X}/dt}{N} \quad (39)$$

and substituting the results into relation (38) we obtain

$$\Delta T^* = N^*(1 + Rb)\frac{\alpha_{cr}}{\bar{\alpha}} \quad (40)$$

or

$$\Delta T^* = N^*(1 + Rb)\frac{Nu_{cr}}{Nu} \quad (41)$$

For the materials as cloth, the Rebinder number ranges from 0.0064 to 0.04 at $\bar{X}_\delta$ = 0.02 - 0.3 kg/kg; for ceramic slab (δ = 6.5 mm), from 0.03 to 0.3 at $\bar{X}$ = 0.1 - 0.03 kg/kg and for asbestos, from 0.02 to 0.3 at $\bar{X}$ = 0.02 - 0.18 kg/kg. In case the Rebinder number is small,

$$\Delta T^* = N^*\frac{Nu_{cr}}{Nu} \quad (42)$$

but

$$\frac{Nu_{cr}}{Nu} = f(N^*)$$

As seen from Fig.5 all the experimental points for such materials as wood, felt, asbestos, ceramics, carrot and clay, irrespective of the drying regimes, fall on one curve described by equation (43) (the uncertainty being 10-15%)

$$\frac{Nu_{cz}}{Nu} = (N^*)^{-0,57} \qquad (43)$$

or

$$Nu = Nu_{cz}(N^*)^{0,57} \qquad (44)$$

Thus, formula (44) is common for many colloid capillary-porous materials and permits estimation of the Nusselt number in the second period at $Bi_q \leq 1$.

With allowance for the Rebinder number formula (43) becomes

$$(1+Rb)\frac{Nu_{cz}}{Nu} = (N^*)^{-0,57} \qquad (45)$$

Substitution of formula (45) into expression (41) yields

$$\Delta T^* = (N^*)^{0,43} \qquad (46)$$

and

$$T_s = T_a - (N^*)^{0,43}(T_a - T_w) \qquad (47)$$

The drying rate being known, equation (47) allows estimation of the material surface temperature in the second period, which is not always reasonable to obtain experimentally.

APPROXIMATE METHOD OF CALCULATING DRYING KINETICS

The above laws of drying and approximate methods of calculating the heat transfer kinetics that stem from the analysis of the experimental data on drying of a variety of capillary-porous and colloid capillary-porous materials with different modes of heat supply may serve as a basis for a relatively simple method of approximate calculation of drying kinetics.

Treatment of numerous experimental data (4) has shown that the heat-transfer intensity in the period of the falling rate of drying changes with respect to time with a sufficient accuracy according to the exponential relation

$$\dot{q}(t) = \dot{q}_I \exp(-m' t_{II}) \qquad (48)$$

where t_{II} is the drying time in the second period related to zero. The value of m' can be easily found by plotting $\dot{q}(t) = f(t)$ in semilogarithmic coordinates. Denoting the ratio of the heat fluxes in the periods of the falling and constant rates of drying by $q^*(t)$ and the ratio of the times of drying by t^*, transforms expression (48) to a dimensional form

$$q^*(t) = \frac{\dot{q}(t)}{\dot{q}_I} = \exp\left(-m\frac{t_{II}}{t_I}\right) = \exp(-mt^*) \qquad (49)$$

On the other hand, the governing equation of drying kinetics, which relates the heat-transfer q^* and moisture transfer N^*, is of the form

$$q^*(t) = \frac{\dot{q}(t)}{\dot{q}_I} = N^*(1+Rb) \qquad (50)$$

From expressions (49) and (50), we have

$$N^*(1+Rb) = \exp(-mt^*) \qquad (51)$$

The Rebinder number for many of the capillary-porous materials in a wide range of moisture contents varies from 0.01 to 0.3, its maximum values (0.2–0.3) corresponding to the end of drying (i.e. to moisture contents close to equilibrium). The neglect of small Rb results in

$$N^* = \exp(-mt^*) \qquad (52)$$

Correlation of the experimental data on drying of different materials in the form of $\lg N^* = f(t^*)$ (Fig. 6) has shown that the experimental points fall satisfactorily on the straight lines for the whole range of operating parameters (ϑ_a, φ, v) and material thickness. The constant m in formula (52) is a linear function of the moisture content ratio ($\bar{X}_0/\bar{X}_{cz}$) for the whole class of the moist materials considered (Fig. 7).

$$m = 0,67\frac{\bar{X}_0}{\bar{X}_{cz}} - 0,35 \qquad (53)$$

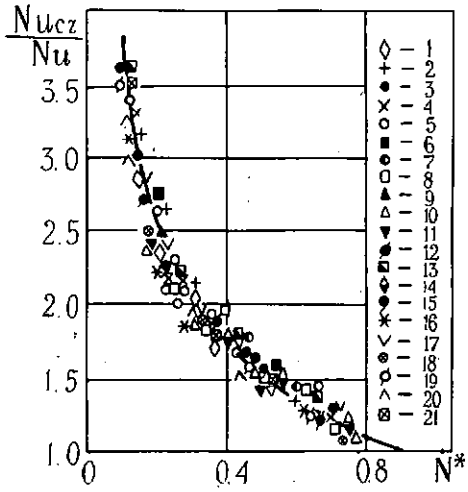

Fig.5. Nu_{cr}/Nu vs N^* for: 1, wood (pine) at Θ_a=120°C, v=10m/s, δ =10 mm; 2, felting at Θ_a= 120°C, φ =5% , δ =8 mm; 3, 3m/s; 4, 5m/s; 6, 15m/s; 7, Θ_a=150°C, v=5m/s, asbestos at Θ_a=120°C, φ =5%, δ =6 mm; 8, 3m/s; 9, 5m/s; 10, 10m/s; 11, 15m/s; 12, Θ_a=90°C, v=5m/s, ceramics at Θ_a=120°C, δ =5mm; φ =5%; 13, 3m/s; 14, 5m/s; 15, 10m/s; carrot at Θ_a=80°C, φ =5%; 16, 3 m/s; 17, 5m/s; 18, 10m/s; clay at Θ_a = 120°C, v=5m/s, φ =5%; 19, 10 mm; 20, 20mm; 21, 50 mm.

Relation (53) has been obtained for $2 \leq v \leq 5$ m/s, $90 \leq \Theta_a \leq 150$°C. Thus, equation (52) has the constant m whose meaning resembles the relative coefficient of drying . For the materials whose drying proceeds only in the period of the falling rate (carrot, beet, potato, sunflower) the experimental data are correlated by

$$N^* = \exp(-m' t) \tag{54}$$

In this case the constant m' is expressed in 1/unit time.
The drying rate in the second period can be found from equation (52)

$$-\frac{d\bar{X}}{dt} = N \exp(-m t^*) \tag{55}$$

which upon integration within the prescribed range gives

$$-(\bar{X}_{cr} - \bar{X}) = N \frac{t_I}{m} \left[\exp\left(-\frac{m}{t_I} t_{II}\right) - 1\right] \tag{56}$$

Upon transformations, we get the time of drying in the period of the falling rate

$$t_{II} = -\frac{2.3 t_I}{m} \lg\left[1 - \frac{(\bar{X}_{cr} - \bar{X}) m}{N t_I}\right] \tag{57}$$

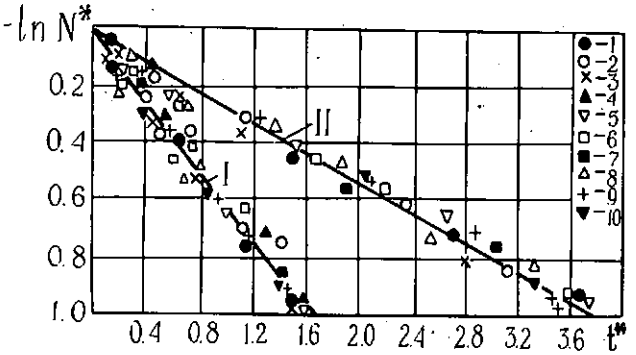

Fig.6. N^* vs t^* at forced-convection drying of asbestos (I) and felting (II) plates. 1, Θ_a=90°C; 2, Θ_a=120°C; 3, Θ_a=150°C (at v=5m/s, φ =5%, δ =8mm); 4, v = 3 m/s; 5, 10m/s; 6, 15m/s; 7, 20 m/s; 8, 25m/s (at Θ_a= 120°C; φ =5%, δ= 8mm); 9, δ =6mm; 10, δ = 12 and 18 mm (at Θ_a= 120°C; v = 3 m/s, φ = 5%).

Taking into account the drying time in the first period

$$t_I = \frac{\bar{X}_0 - \bar{X}_{cr}}{N} \tag{58}$$

we determine the overall duration of the process as

$$t = t_I + t_{II} = \frac{\bar{X}_0 - \bar{X}_{cr}}{N} \left\{1 - \frac{2.3}{m} \lg\left[1 - \frac{(\bar{X}_{cr} - \bar{X}) m}{(\bar{X}_0 - \bar{X}_{cr})}\right]\right\} \tag{59}$$

or, finally,

$$t = \frac{\bar{X}_0 - \bar{X}_{cr}}{N} \left\{1 - \frac{2.3}{m} \lg\left[1 - \frac{(\bar{X}_{cr} - \bar{X}) m}{(\bar{X}_0 - \bar{X}_{cr})}\right]\right. \tag{60}$$

where $\bar{X}$ is the instantaneous moisture content of the material.

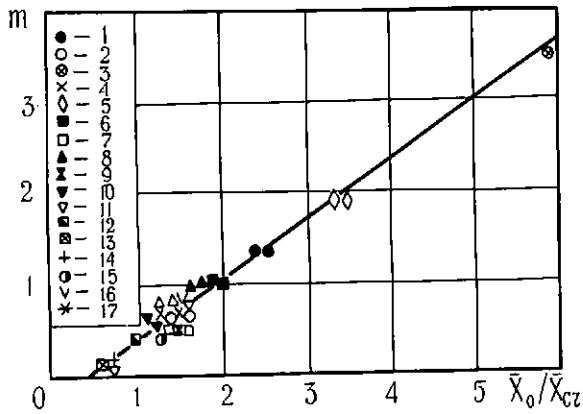

Fig.7. Constant m vs $\bar{X}_0/\bar{X}_{cr}$. 1, asbestos 2, felting; 3, grass; 4, leather; 5, felt; 6, ceramics; 7, cardboard; 8, clay; 9, peat slab; 10, yeast; 11, carrot; 12, sunflower seeds; 13, potato; 14, beet; 15, cement stone; 16, macaroni; 17, microbiological mass of lysine.

For the materials whose drying does not involve the constant-rate period, the overall drying time is determined by integrating equation (54)

$$t = -\frac{2.3}{m} \lg\left[1 - \frac{(\bar{X}_0 - \bar{X})m}{N}\right] \qquad (61)$$

where

$$N = \left(\frac{d\bar{X}}{dt}\right)_{max}$$

is the maximum rate of drying.

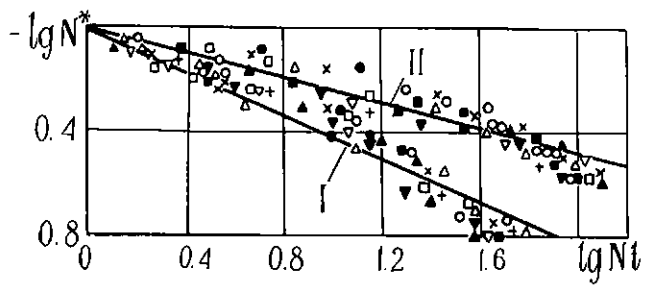

Fig.8. $\lg N^*$ vs $\lg Nt^*$ for forced-convection drying of asbestos (I) and felt (II) slabs (For notation see Fig.6)

As already noted, the analysis of the experimental data on convective drying of various capillary-porous materials enabled us to derive semiempirical correlation (47) to determine the material surface temperature . Substitution of N^* from expression (52) into (47) gives

$$T_s = T_a - \exp(-0{,}43\, m t^*)(T_a - T_w) \qquad (62)$$

Thus, equation (62), provided that the constant m is known, makes it possible to determine easily enough the material surface temperature.

Consider one more method of experimental treatment based on the relative drying rate N^* and the so-called generalized drying time Nt (4).

The value of N^* is independent of the drying regime and is a function of the moisture content alone for a particular material and for this method of drying. The variable Nt is a stable complex of quantities characteristic of a drying process and makes the study of drying more general. The generalized-curve method makes it possible to extend the data of a particular case to many instances with different regimes. This reduces the series of experiments.

The generalized-curve method implies that the generalized time Nt as well as the relative rate of drying N^* is a function of moisture content, i.e. $N^* = f(\bar{X})$ and $Nt = \varphi(\bar{X})$, and, hence, $N^* = \psi(Nt)$.

It is known that in correlation of the drying kinetics curves, the use can be made of the power-law dependence between the rate of drying and moisture content in the second period (9)

$$-\frac{d\bar{X}}{dt} = \varkappa N (\bar{X} - X_E)^n$$

The verification has suggested that the constant n is independent of the operational parameters and material thickness and is specified only by the form of moisture-material bond. It is therefore reasonable, provided that the drying curves refer to the 2nd or 3d kind in A.V.Luikov's classification (3), to seek for $N^* = \psi(Nt)$ in the form

$$N^* = (Nt)^k \qquad (63)$$

The constant k is estimated from the experimental data using the plot $\lg N^* - f[\lg(Nt)]$;

The slope of the curve obtained is numerically equal to the exponent k .

In Fig.8, logarithmic coordinates are used to plot the dependence between the relative rate of drying N^* and generalized time Nt for drying of felt and asbestos under forced convection. It follows from this figure that variation of the operational parameters and material thickness within wide ranges does not affect the exponent k .

From expression (63), the rate of drying with allowance for the sign of the exponent k is

$$-\frac{d\bar{X}}{dt} = N\,(Nt)^{-k} \qquad (64)$$

Integrating equation (64) within the prescribed limits gives the time of drying in the falling-rate period

$$t_{II} = \left[\frac{(\bar{X}_{cr} - \bar{X})(1-k)}{N^{1-k}}\right]^{\frac{1}{1-k}} \qquad (65)$$

The overall drying time

$$t = \frac{1}{N}\left\{(\bar{X}_0 - \bar{X}_{cr}) + \left[(\bar{X}_{cr} - \bar{X})(1-k)\right]^{\frac{1}{1-k}}\right\} \qquad (66)$$

Comparison of the experimental data on drying time with calculations by formulae (60) and (66) has shown that the accuracy of these methods is approximately the same but for a small segment of the drying curve at low values of moisture content close to equilibrium ones, where equation (66) does not hold. This indicates that the power-law dependence of form (63) does not fully describe the drying curve for the second period.

Equations (47) and (63) may give one more form of a calculation formula to determine material surface temperature

$$T_s = T_a - (Nt)^{-0.43k}(T_a - T_w) \qquad (67)$$

Comparison between the design relations obtained and the experimental data has shown that the maximum uncertainty in calculating the drying time and material temperature is 7-10% and 10-15%, respectively. Higher error in determining material temperature is due to superposition of two approximate methods of calculation. (As a representative example, Figure 9 gives a comparison between the experimental and calculated values of drying time and surface temperature for asbestos slabs).

Thus, the considered laws of heating and drying kinetics for various materials as well as the analysis of the interdependence between heat and mass transfer in drying allowed rather simple and convenient in practice relationships to estimate qualitative characteristics of convective drying (drying time, heat transfer intensity, material temperature).

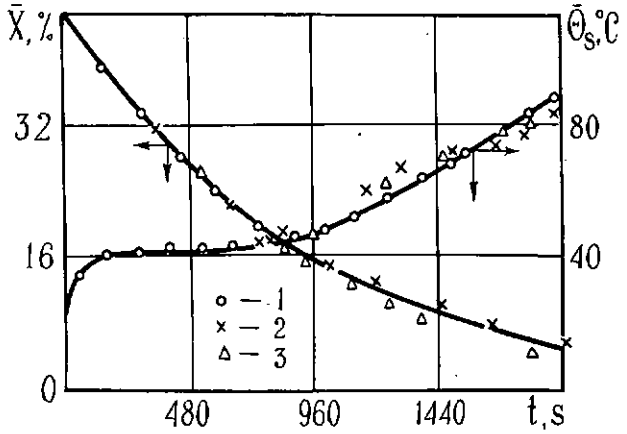

Fig.9. Comparison between experimental and calculated values of the drying time and material surface temperature for asbestos slab at Θ_a = 120°C, v= 3 m/s, φ = 5% (1, experimental data; 2, data calculated by formulae (60) and (62); 3, by formulae (66) and (67)

INTERDEPENDENCE BETWEEN THE MOISTURE CONTENT AND TEMPERATURE OF DISPERSED MATERIAL UNDER FLUIDIZED DRYING

As stated, the problem of relating uniquely the moisture content and temperature of the material under dehydration is among the most urgent ones when studying high-intensive drying of different materials. Its solution is particularly important for drying dispersed thermolabile suspended materials, specifically, in a fluidized bed. The possible enhancement of heat and mass transfer, on the one hand, as well as danger of material superheat and deterioration of the quality of the end product, on the other, requires a choice of optimum operational parameters and calculation of these devices taking account of thermolabile material heating up to maximum possible temperature.

There are some works available on a mathematical description of the kinetics for heating of moist dispersed materials in a fluidized bed under batch drying related to constant- and falling-rate periods of drying (5,10,11). We have tried to consider analytically the problem on a direct relationship between moisture content and temperature of a

dispersed material under batch drying in fluidized-bed devices.

In the general case, as is known, a rigorous analytical study of heat and mass transfer in heterogeneous dispersed systems involves insuperable difficulties. Yet, specific features inherent in fluidized-bed apparatuses and specified by intense mixing of phases through the whole test volume of the chamber allow a number of simplifying assumptions for solution of the problem. In particular, experimental verification has shown that in developing an approximate method of calculation of fluidized-bed dispersed material heating, the following simplifying approximations proved to be fairly good (5.11):

1. At every given moment, the fluidized bed of the material under drying is assumed to be isothermal, the temperature of waste drying agent leaving the bed being equal to integral temperature of particles in the bed.

2. Temperature gradient over particle cross-sections is considered negligible.

3. Under batch drying conditions, the moisture content of particles throughout the fluidized bed at one and the same time is taken constant.

Proceeding from the model adopted and ignoring heat losses to the surroundings, we may represent the initial calorimetric heat balance equation for the fluidized bed of moist dispersed material as

$$F v \rho c_g (\Theta_g - \bar{\Theta}) d\tau = G c_M d\bar{\Theta} - G_{d.s} \Delta h_v d\bar{X} \qquad (68)$$

For the constant rate of drying

$$d\tau = -d\bar{X} / N$$

Expressing the mass of dried packing and heat capacity of material for any time instant accordingly through

$$G = G_{d.s}(1 + \bar{X})$$

$$c_M = \frac{c_s + X}{1 + \bar{X}}$$

and upon some transformations, we arrive at

$$(B'\bar{\Theta} - A) d\bar{X} = (c_s + \bar{X}) d\bar{\Theta} \qquad (69)$$

where

$$B' = \frac{F v \rho c_g}{G_{d.s} N} ; \quad A = B'\Theta_g - \Delta h_v$$

Dividing the variables and integrating over the appropriate limits gives finally

$$\bar{X} = (c_s + \bar{X}_0)\left(\frac{A - B'\bar{\Theta}}{A - B'\bar{\Theta}_0}\right)^{\frac{1}{B'}} \qquad (70)$$

The fluidized-bed temperature vs instantaneous material moisture content in batch drying during a constant-rate period may be accordingly expressed as

$$\bar{\Theta} = \frac{A}{B'} - \left(\frac{A}{B'} - \Theta_0\right)\left(\frac{c_s + X}{c_s + X_0}\right)^{B'} \qquad (71)$$

In the general case, for the falling-rate drying period, the linear law of drying rate variation

$$-\frac{d\bar{X}}{d\tau} = K(\bar{X} - X_E) \qquad (72)$$

may provide sufficient design accuracy. With regard for (72), the initial differential heat balance equation for a moist dispersed fluidized bed may be given as

$$-\frac{F v \rho c_g (\Theta_g - \bar{\Theta})}{K(\bar{X} - X_E)} dX = G_{d.s}(c_s + \bar{X}) d\bar{\Theta} - G_{d.s} \Delta h_v d\bar{X} \qquad (73)$$

Ignoring intermediate transformations, we obtain

$$\frac{d\bar{\Theta}}{d\bar{X}} - \bar{\Theta}\frac{B_1'}{(\bar{X} - X_E)(\bar{X} + c_s)} = \frac{\Delta h_v (\bar{X} - X_E) - B_1'\Theta_g}{(\bar{X} - X_E)(\bar{X} + c_s)} \qquad (74)$$

where

$$B_1' = F \rho v c_g / K G_{d.s}$$

Solution to the nonuniform linear differential first-order equation (74) subjected to the initial condition gives

$$\bar{\Theta}|_{\bar{X} - \bar{X}_{cr}} = \bar{\Theta}_0'$$

$$\bar{\Theta}=\bar{\Theta}_0'\left[\frac{(\bar{X}_{cz}+C_s)(\bar{X}-X_E)}{(\bar{X}_{cz}-X_E)(\bar{X}+C_s)}\right]^m+\sum_{n=1}^{m-1}\left\{\frac{\Delta h_v}{n-m}\left[\left(\frac{\bar{X}-X_E}{\bar{X}+C_s}\right)^n-\left(\frac{\bar{X}-X_E}{\bar{X}+C_s}\right)^m\left(\frac{\bar{X}_{cz}+C_s}{\bar{X}_{cz}-X_E}\right)^{m-n}\right.\right.+\frac{B_1'\Theta_g}{m}\left[\frac{(\bar{X}-X_E)^{n-1}}{(\bar{X}+C_s)^n}-\left.\left.\left(\frac{\bar{X}-X_E}{\bar{X}+C_s}\right)^m\frac{(\bar{X}_{cz}+C_s)^{m-n}}{(X_{cz}-X_E)^{m-n+1}}\right]\right\} \quad (75)$$

where

$$m=\frac{B_1'}{C_s+X_E}$$

(when m is a fractional number, it must be rounded to the nearest integer).

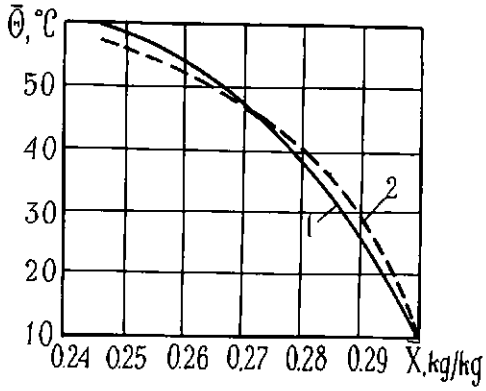

Fig.10. $\bar{\Theta}=\varphi(\bar{X})$ for fluidized drying of wheat ($v\rho$ = 1.98 kg/m²s; $G_{d.s}/F$ = 65 kg/m²; X_0=0.3kg/kg Θ_g = 80°C). 1, by relation (76); according to experimental data.

The analysis of the solution obtained shows that in practice the first term of the final sum entering into expression (75) may held to a certain accuracy. As a result, the general approximate solution may be given by the following convenient in practice formula

$$\bar{\Theta}=\left[\bar{\Theta}_0'-\frac{\Delta h_v(\bar{X}_{cz}-X_E)}{(1-m)(\bar{X}_{cz}+C_s)}-\frac{B_1'\Theta_g}{m(\bar{X}_{cz}+C_s)}\right]\times \quad (76)$$

$$\times\left[\frac{(\bar{X}-X_E)(\bar{X}_{cz}+C_s)}{(\bar{X}+C_s)(\bar{X}_{cz}-X_E)}\right]^m+\frac{\Delta h_v(\bar{X}-X_E)}{(1-m)(\bar{X}+C_s)}+\frac{B_1'\Theta_g}{m(\bar{X}+C_s)}$$

It is seen from equation (76) that at equilibrium moisture content of the product ($\bar{X}=X_E$) the integral temperature of the fluidized dispersed bed becomes equal to a heat carrier temperature, ($\bar{\Theta}=\Theta_g$). For the case when the falling-rate drying is preceded by the constant-rate drying, the value of $\bar{\Theta}_0'$ may be calculated from equation (71).

Note that the quantity m entering into expression (75) depends on the basic factors governing the kinetics of heat and mass transfer between the material and drying agent. These are, first of all, temperature, mass velocity and physical properties of drying agent, specific load of the material on the grid, as well as the initial moisture content and basic properties of the dehydrated product as a drying object. As our investigations showed, real values of the parameter m as applied to drying in a fluidized bed of such thermolabile materials as grain and cut potato range between 10 and 200. As follows from expression (75), the mathematical error due to simplification of the solution obtained is mainly specified by the simplex $(\bar{X}-X_E)/(\bar{X}+C_s)$. As the instantaneous moisture content $\bar{X}$ diminishes, this simplex (and, hence, the calculation error) decreases as well. This circumstance must be taken into account to estimate the total uncertainty of the method, because in defining $\bar{\Theta}=f(\bar{X})$, of the greates interest is the region of low moisture contents when the bed temperature approaches as much as possible a permissible maximum temperature (for technological reasons) of the product.

Finally, the difference between the calculated and real temperatures of the moist material greatly depends on the nature of the drying process and on how accurately the falling-rate drying curve is described by equation (72). This error is analysed in (41).

The validity of the suggested approximate solution is verified through comparison of the results calculated by equation (76) and the experimental data for grain drying in a wide range of operational parameters. The comparison testifies to a fair agreement between the experimental and calculated data, the deviation being no more than 12% (Fig.10).

The point to be stressed in conclusion is that the relations obtained may be used to choose reliable drying regimes for dispersed thermolabile materials in fluidized-bed dryers with account taken of admissible product temperature and to design automatic control systems for these dryers. The analytical direct relationship between the moisture content and temperature of the product may be used as a basis for the programs of automatic control of the drying process by the variation of the mean temperature of the fluidized bed of material under drying. Here, as a reference parameter, one may use the temperature of waste drying agent that can be easily measured by any thermometer.

REFERENCES

1. Luikov, A.V. and Mikhailov, Yu.A., Heat and Mass Transfer Theory. Gosenergoizdat, Moscow-Leningrad, 1963.
2. Luikov, A.V. and Mikhailov, Yu.A., Energy and Substance Transfer Theory. Izd. AN BSSR, Minsk, 1959.
3. Luikov, A.V., Theory of Drying. Energiya, Moscow, 1968.
4. Krasnikov, V.V., Conductive Drying. Energiya, Moscow, 1973.
5. Lyuboshits, I.L., Slobodkin, L.S., and Pikus, I.F. Drying of Dispersed Thermolabile Materials. Nauka i Tekh nika, Minsk, 1969.
6. Luikov, A.V., Sheiman, V.A., Kuts , P.S., and Slobodkin, L.S. An approxi- mate method of drying kinetics calcu- lation. Journ Engng Phys. 13,5, 1967.
7. Kuts, P.S., Method of determining moisture diffusion coefficient in terms of the temperature coefficient of drying. In "Heat and Mass Transfer in Drying of Various Materials". Izd. ITMO, Minsk, 1974.
8. Lebedev, P.D., Dryer Design. Gosener- goizdat, Moscow, 1963.
9. Kuts, P.S., and Olshansky, A.I. To approximate methods of calculating the convective plane-material drying kinetics. Journ. Engng. Phys. 28, 4, 1975.
10. Ginzburg, A.S., and Rezchikov, V.L., Fluidized Food Drying. Pishchev. Prom 1966.
11. Pikus, I.F., Heat and Mass Transfer in Dispersed Systems. Nauka i Tekh- nika, Minsk, 1965.
12. Kuts, P.S., and Pikus, I.F., Thermo- physics and Technology of High - Voltage Insulation Drying, Nauka i Tekhnika, Minsk, 1979.

NON-STEADY-STATE SURFACE EVAPORATION FROM POROUS BODIES WITH NON-UNIFORM PORE DISTRIBUTION

S. Endrényi

Refrigerating Works
Budapest-Jászberény, Hungary

ABSTRACT

A mathematical model is described for the surface evaporation for non-steady-state processes from porous bodies which are characterized by non-uniform pore distribution. A model is developed also for the solution of heat and mass transfer problems of non-steady-state surface evaporation in porous media. Consequently, a mathematical model of surface evaporation into the ambient gas flow of a liquid or solvent bound in a porous body is considered. Physical parameters of this process are determined and the changing transfer coefficients of simultaneous heat and mass transfer during surface evaporation described.

NOMENCLATURE

- c = specific heat of humid gas, superheated vapour
- F = Lewis factor
- i = enthalpy of humid gas, water vapour
- I = enthalpy of moist solid
- q' = from the text
- q'' = differential sorption energy
- R = integral sorption energy
- R_g = gas constant
- t,T = temperature, absolute temperature
- x,z = absolute humidity of gas
- X,Z = absolute moisture content of solid
- α = heat transfer coefficient
- Δ = symbol of difference
- η = relative mass flow rate
- ϕ = relative humidity of gas
- σ = mass transfer coefficient
- θ = temperature difference

Subscripts

- e = equilibrium
- g = superheated vapour (for specific heat)
- K = referring the wet bulb temperature (w.b.t., Kühlgrenze)
- ℓ = indicates the dry gas
- L = indicates the carrier gas, flowing gas
- m = material, solid
- o = initial state
- t = belonging to temperature, saturation temperature
- w = water, moisture, liquid

INTRODUCTION

The theory of surface evaporation phenomena from porous bodies has recently shown a gradual but considerable development (1-4). Several valuable approaches have been described. However, to date, their synthesis has not been accomplished.

The present study aims at completing this synthesis. First, a model is described for non-steady-state processes in bodies of non-uniform pore distribution. A model is developed also for the solution of heat and mass transfer problems of non-steady-state surface evaporation in porous media. Therefore, the paper will consider the mathematical modelling of surface evaporation into the ambient gas flow of a liquid or solvent bound in a porous body. Physical parameters of this process will be determined and the changing transfer coefficients of the simultaneous heat and mass transfer during surface evaporation will be described.

It will be assumed that a convective heat flux of a gas stream in quasi-stationary state flows laminarly above an infinite flat plate. This is of a capillary-porous material which has sorptive characteristics and is made up of a system of non-uniform capillary pores in a given distribution.

For this model, the following detailed assumptions will be made: (i) During the period neither the temperature nor the concentration is constant at the surface of the material; (ii) The system of capillaries at the surface of the solid is quasi-monomolecular without depth dimension. Consequently, the temperature and concentration

gradients on the surface can be disregarded; (iii) All chemical changes occurring in the porous medium are neglected.

THE MATHEMATICAL MODEL

With the symbols defined at the end of the paper and in Fig. 1 the following equations can be established:

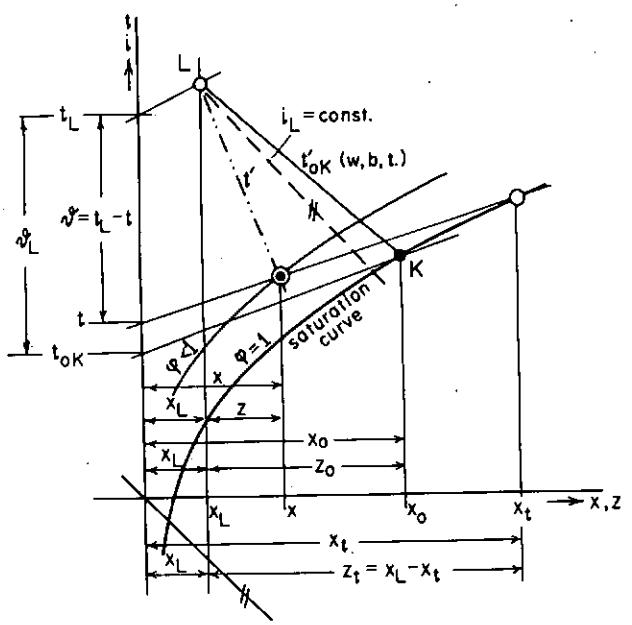

Fig. 1: State changes of the humid gas in the unsteady period.

I. For the gaseous state:

$$i = ct + r_0 x \tag{1}$$

where:

$$c = c_\ell + c_g x, \quad r_0 + c_g t = r + t$$

$$i_L = c_L t_L + r_0 x_L \tag{1a}$$

$$i_L - i = \Delta i = c\theta + (r_L + t_L)\Delta x, \text{ or}$$

$$\Delta i = c_L \theta + (r+t)\Delta x, \text{ and}$$

$$\frac{\Delta i}{\Delta x} = t' = c\frac{\theta}{z} + r_L + t_L \tag{2a}$$

$$t' = c_L \frac{\theta}{z} + r + t, \quad \text{respectively,} \tag{2b}$$

where

$$\left.\begin{aligned} &\theta = t_L - t, \quad \Delta x = z = x_L - x \\ &c_L = c_\ell + c_g x_L \\ &r_L = r_0 - (1-c_g)t_L \\ &r = r_0 - (1-c_g)t \end{aligned}\right\} \tag{2c}$$

II. For the moist material:

$$I = (c_m + c_w X)t + R(X).$$

With

$$c_w \cong 1, \; R(X) \equiv R \text{ and } C = c_m + X,$$

$$I = (c_m + X)t + R = Ct + R. \tag{3}$$

Further,

$$di = \eta dI, \quad dx = \eta dX. \tag{4}$$

The integration may be carried out between the limiting values of

$$z = x_L - x, \quad z_0 = x_L - x_0, \text{ corresponding to}$$

$$Z = X_e - X, \quad Z_0 = X_e - X_0.$$

Consequently,

$$\eta = \frac{z}{Z} = \frac{z_0}{Z_0} \; . \tag{4a}$$

From equation (4)

$$\frac{di}{dx} = \frac{dI}{dX} \; . \tag{5}$$

Substituting equation (1) and (3):

$$\left.\begin{aligned} &\frac{di}{dx} = c\frac{dt_\ell}{dx} + r + t_\ell \\ &\frac{dI}{dX} = C\frac{dt_m}{dX} - q'' + t_m = \eta C\frac{dt_m}{dx} - q'' - t_m \\ &\qquad = t_m - q' - q'' \end{aligned}\right\} \tag{5a}$$

where

$$q' = -C\frac{dt}{dX} = -\eta C\frac{dt}{dx} \; , \tag{5b}$$

$$q'' = -\frac{\partial R}{\partial X} = -R_g T_L \ell n \phi \; . \tag{5c}$$

Assuming $t_\ell = t_m$:

$$\frac{dt}{dx} = -\frac{dt}{dz} = \frac{d\theta}{dz} = \frac{r+q''}{\eta C - c} = \frac{r+q''}{\eta C_e - c - z} = \frac{r+q''}{\eta C_e - c_L - (1-c_g)z} \tag{6}$$

where

$$c=c_L-c_g z, \quad C_e=c_m+X_e \quad \text{and} \quad \eta C=\eta C_e-z$$

III. For the balance equations of energy and mass conservation:

$$\left.\begin{aligned} \alpha\theta &= -\sigma z(r+c_g\theta+q'+q''), \quad \text{or} \\ \alpha\theta &= -\sigma z(r_L+\theta+q'+q'') \ . \end{aligned}\right\} \qquad (7)$$

Introducing the Lewis factor, defined by

$$F = \frac{\alpha}{\sigma}\frac{1}{c}$$

one can write

$$\frac{\theta}{z} = -\frac{r+c_g\theta+q'+q''}{Fc} \ , \text{ or} \qquad (7a)$$

$$\frac{\theta}{z} = -\frac{r_L+\theta+q'+q''}{Fc} \ . \qquad (7b)$$

IV. For the state of psychrometric equilibrium between the gas and moist material surface:

$$\phi = \frac{0.622+x_t}{0.622+x}\cdot\frac{x}{x_t} \ . \qquad (8a)$$

Introducing the equation for the saturation curve:

$$x_t = x_t(t) \quad \text{with} \quad x_L - x_t = z_t = z_t(\theta) \qquad (9)$$

results in

$$\phi = \frac{1.61+\dfrac{1}{x_L-z_t}}{1.61+\dfrac{1}{x_L-z}} \ . \qquad (8b)$$

Finally, the sorption isotherm equation:

$$X = X(\phi)\Big|_{t_L}, \qquad z = \eta[X_e-X(\phi)]_{t_L} \qquad (10)$$

Using these equations, particularly (2a), (6), (7a), (8b), (9), (10), the following relations can be determined from the independent variables θ and/or z:

a) By z or θ: $\theta(z)$ or $z(\theta)$;

b) By z or θ: $z_t(z)$ or $z_t(\theta)$;

c) By z or θ: $\phi(z)$ or $\phi(\theta)$;

d) By ϕ : $X(\phi)$ or $Z(\phi)$;

e) By z or θ: $F(z)$ or $F(\theta)$;

f) By z or θ: $t'(z)$ or $t'(\theta)$.

In greater detail:

a) Substituting in (6) the values from (2c) and expressing ϕ with (8b), we obtain

$$\frac{d\theta}{dz} = \frac{r_L+(1-c_g)\theta-R_g T_L \ln\phi}{C_e\eta-c_L-(1-c_g)z} = f(z,\theta). \qquad (11)$$

After separating the variables and integrating the unambiguous function follows, reciprocally,

$$\theta = \theta(z) \quad \text{or} \quad z = z(\theta). \qquad (11a)$$

b) On the basis of (9), z_t can be evaluated as

$$z_t = z_t(z) \quad \text{or} \quad z_t = z_t(\theta). \qquad (12)$$

c) On the basis of (8b), a given z or θ fixes the value of ϕ as

$$\phi(z) \quad \text{or} \quad \phi(\theta) \qquad (13)$$

after z_t having been determined in b).

d) On the basis of (10), $Z(\phi)$, $X(\phi)$, can be calculated as

$$X(z), \ X(\theta) \quad \text{or} \quad Z(z), \ Z(\theta). \qquad (14)$$

e) On the basis of (7a), taking the value for q from (5b), and that of $d\theta/dz$ from (6):

$$Fc+c_g z = c\,\frac{r+q''}{\eta C-c}\cdot\frac{1}{(\theta/z)} = c\,\frac{r+q''}{\eta C_e-c-z}\cdot\frac{1}{(\theta/z)}$$

$$= c\,\frac{r+q''}{\eta C_e-c_L-(1-c_g)z}\cdot\frac{1}{(\theta/z)} \qquad (15)$$

By substituting (6), one can write

$$Fc + c_g z = c\,\frac{d\theta/dz}{(\theta/z)} \qquad (16)$$

and so

$$F = \frac{d\theta/dz}{(\theta/z)} - \frac{c_g}{c}z = \frac{d\theta/dz}{(\theta/z)} + \frac{1}{1-\dfrac{c_L}{c_g z}} \qquad (17)$$

According to (11a) the right-hand side can be expressed in terms of z or θ and so also F can be written as

$$F = F(z) \quad \text{or} \quad F = F(\theta). \qquad (18)$$

Note: When $z\to 0$ then according to (6)

$$\left.\frac{d\theta}{dz}\right|_{z\to 0} \neq 0, \quad \text{and furthermore} < 0$$

and so, corresponding to (16):

$$\left.\frac{\theta}{z}\right|_{\substack{z\to 0\\ F\to 0}} = \frac{c}{Fc+c_g z}\cdot\left.\frac{d\theta}{dz}\right|_{z\to 0} \to -\infty .$$

f) On the basis of (2b), taking the value for θ/z from (15), then using the transformation

$$Fc + c_g z = c_L - (1-F)c,$$

$$\frac{\theta}{z} = \frac{1}{Fc+c_g z}\cdot\frac{r+q''}{\eta C_e - c_L - (1-c_g)z} = \frac{c}{c_L-(1-F)c}\cdot\frac{r+q''}{\eta C - c} \tag{19}$$

and replacing it into (2b),

$$t' = t + r\left(1 + \frac{cc_L}{(Fc+c_g z)[\eta C_e - c_L - (1-c_g)z]}\right)$$

$$+ q''\frac{cc_L}{(Fc+c_g z)[\eta C_e - c_L - (1-c_g)z]} \tag{20}$$

and

$$t' = t + r\left(1 + \frac{cc_L}{[c_L-(1-F)c](\eta C - c)}\right)$$

$$+ q''\frac{cc_L}{[c_L-(1-F)c](\eta C - c)} \tag{20a}$$

With

$$\varepsilon = \frac{cc_L}{(Fc+c_g z)[C_e\eta - c_L - (1-c_g)z} = \frac{cc_L}{(Fc+c_g z)(C_e\eta - c - z)}$$

$$= \frac{cc_L}{[c_L-(1-F)c](\eta C - c)}$$

$$t' = t + (1+\varepsilon)r + \varepsilon q''. \tag{21}$$

Note: When $F\to 0$ and $z\to 0$, then in (20), $\eta C_e - c_L < 0$ and $t'\to -\infty$.

In this case $\left.\frac{\theta}{z}\right|_{\substack{z\to 0\\ F\to 0}} \to -\infty$ follows also from (2b), where when $t'\to -\infty$ then necessarily $\frac{\theta}{z}\to -\infty$. This applies generally to the case when $Fc+c_g z=0$. According to (17), when $z\to 0$, $\left.\frac{d\theta}{dz}\right|_{z\to 0}\neq 0$, and from the foregoing $\left.\frac{\theta}{z}\right|_{z\to 0} = -\infty$ and $F\to 0$. From (2a), when $t'=t=t_{ok}$, in which case $q'=0$, $q''=0$,

$$\left.\frac{\theta}{z}\right|_{t_{ok}} = -\frac{r_L+\theta_L}{c_{ok}} .$$

On the other hand, from (7b)

$$\left.\frac{\theta}{z}\right|_{\substack{t_{ok}\\ \theta=\theta_L}} = -\frac{r_L+\theta_L}{F_{ok}c_{ok}}$$

and so $F_{ok}=1$. In this case $Fc+c_g z=c_L$, so follows from (20), with $t'=t$: $\varepsilon=-1$. Consequently, $z_{ok}=C_e\eta=(c_m+X_e)\eta$, or from (20a), $\eta C|_{ok}=0$, $X|_{ok}=X_o=-c_m$. Substituting this into the equation above,

$$z_{ok} = (-X_o+X_e)\eta = Z_o\eta. \tag{22}$$

Here the value of z_{ok} turned out to be identical with its psychrometric interpretation.

REFERENCES

1. Endrényi, S., "Some problems of heat and mass transfer processes of sorptive materials", Symposium of the Japan Society of Mechanical Engineers, Tokyo, 1967.

2. Endrényi, S., "Simultaneous convection and diffusion in the drying process of porous materials of high sorptivity", Akadémiai Kiadó, Vol. 2, Budapest, 1971.

3. Endrényi, S., "Anleitung zur Erweiterung der Anwendung psychrometrischer Methoden auf Verdunstungsvorgänge besonderer Art", Verfahrenstechnik, 6, 2, 63, 1972.

4. Endrényi, S., "Mathematical modelling of the application of psychrometric methods for surface phenomena of porous bodies at simultaneous heat and mass transfer", 5th International Heat Transfer Conference, Tokyo, 1974.

A NUMERICAL MODEL OF HEAT AND MASS TRANSPORT IN WOOD DURING DRYING

G. A. Spolek and O. A. Plumb

Washington State University, Pullman, Washington 99164

ABSTRACT

During convective drying of dimensional lumber, it is commonly felt that capillary action is the dominant mechanism for moisture movement during the constant rate drying regime, while diffusive transport accounts for moisture movement during the falling rate regime. To determine the relative effect of each mechanism during wood drying, an analytical model of the heat and mass transfer is developed, resulting in a set of coupled partial differential equations for temperature and moisture content as a function of space and time. The relevant transport properties for wood, as well as their dependence on temperature and moisture content, are either available in the literature or are predicted utilizing a mechanistic structural model for wood. The governing transport equations are solved numerically and the resulting drying rate, as well as moisture and temperature distributions, are compared with experimental data available in the literature. The relative contributions of the various transport modes for heat and mass are discussed.

NOMENCLATURE

- a = Lumen width/cell width
- A = Surface area (cm^2)
- C_S = Liquid saturation coefficient ($gm/cm\ s^2$)
- C'_S = Gas saturation coefficient ($gm/cm\ s^2$)
- C''_S = Vapor concentration saturation coefficient
- C_T = Liquid temperature coefficient ($gm/cm\ s^2\ ^oK$)
- C'_T = Gas temperature coefficient ($gm/cm\ s^2\ ^oK$)
- C''_T = Vapor concentration temperature coefficient ($1/^oK$)
- c_p = Phase specific heat ($cal/gm\ ^oK$)
- C_p = Mass fraction average specific heat ($cal/gm\ ^oK$)
- D = Diffusion coefficient (cm^2/s)
- EMC = Equilibrium moisture content
- FSP = Fiber saturation point
- g = Gravitational constant (cm/s^2)
- h_h = Convective heat transfer coefficient ($cal/cm^2 s\ ^oK$)
- h_m = Convective mass transfer coefficient (s/cm)
- h'_m = Convective mass transfer coefficient ($gm/cm^2 s$)
- $h_{\ell g}$ = Latent heat of evaporation (cal/gm)
- I = Number of spatial nodes
- k = Thermal conductivity ($cal/cm\ s\ ^oK$)
- K = Permeability (cm^2)
- L = Half-width of board (cm)
- $\dot{m}$ = Rate of mass evaporation per unit volume ($gm/s\ cm^3$)
- M = Moisture content
- M_{max} = Maximum moisture content
- ΔM = Moisture content change for full saturation
- P = Pressure ($gm/cm\ s^2$)
- $\dot{q}$ = Heat transfer (cal/s)
- r = Radius of curvature (cm)
- R = Gas constant ($cal/gm\ ^oK$)
- S = Saturation as defined by equation (3)
- t = Time (s)
- T = Temperature (^oK)
- T^* = Dimensionless temperature
- ΔT = Difference of free stream and initial temperatures (^oK)
- v = Velocity (cm/s)
- w = Lumen width (cm)
- W = Cell width (cm)
- z = Distance (cm)
- Z = Permeability (cm^2)

Greek Letters

- α = Cell overlap ratio
- λ = Correction factor for thermal conductivity of bulk wood
- μ = Dynamic viscosity ($gm/cm\ s$)
- ρ = Spatial average density (gm/cm^3)
- ρ_i = Phase density (gm/cm^3)
- σ = Surface tension (gm/s^2)
- ϕ = Void fraction
- ψ = Volume fraction

Subscripts

a = Air
c = Capillary
conv = Convective
cr = Critical
g = Gas phase
∞ = Free stream
i = Spatial index
ir = Irreducible
j = Time index
ℓ = Liquid phase
o = Initial condition
s = Solid phase
S = Saturation
sat = Fully saturated condition
T = Temperature
wv = Water vapor

INTRODUCTION

Dimensional lumber must be dried from its green condition to achieve structural stability. The drying operation requires considerable energy and time, thus, efficient kiln design is crucial to maintain productivity and profit. Experience has shown that serious cracking, warping, and fiber collapse occur if the wood is dried too fast. In order to quantify the effects of these factors for optimization of kiln design and operation, researchers have developed analytic models to describe the movement of moisture in wood during drying. Sherwood (1) assumed that moisture movement through a solid porous media such as wood was due to gradients of the moisture content, and used Fick's second law of diffusion to predict the unsteady concentration of water. Good agreement with experimental data followed when the diffusion coefficient could be written as an appropriate function of moisture content and the range of moisture contents predicted was less than the fiber saturation point (FSP), which corresponds to the moisture content at which all water molecules are chemically bound to the cellulose. Gradients in moisture content correspond to gradients in binding energy, leading to a diffusive type flux.

At moisture contents greater than FSP, the additional water must exist as liquid water and as water vapor in the voids or lumens in the wood cells. These cells are long and narrow, hollow in the center, and overlap one another on ends that taper shut. On the overlapping surfaces there are small orifices or pits that provide fluid paths between adjacent cell lumens. This morphology suggests that the capillary mechanisms that allow the motion of nutrient fluids in the living tree may also control the movement of the free liquid in wood during drying (2). Luikov (3) developed a set of coupled, partial differential equations to describe the heat and mass transport in capillary porous media by assuming that the transfer of moisture is analagous to heat transfer and that capillary transport is proportional to gradients in moisture and temperature. The resulting transport coefficients are strong functions of both temperature and moisture content, as well as wood species and drying conditions. Thus, extensive experimental programs are required to determine the coefficients necessary to analyze a wide variety of woods and drying methods.

The purpose of this paper is to develop and solve a set of governing differential equations that describe both capillary and diffusive transport of moisture as well as energy transport during drying. By developing these equations from first principles, the coefficients that arise will depend on basic transport properties and wood geometry that are well documented in the literature. The solution will predict the controlling mechanisms during each drying regime.

THEORETICAL MODEL

Wood in its green state can be considered a three-phase mixture: solid cell wall material (with bound water to FSP), free liquid that partially fills the lumens, and gas bubbles containing air and water vapor that occupy the remaining lumen space. Each phase is well-defined in space and represents a continuum within its domain. As such, the theory of continuum mechanics can be used to predict phase behavior in accordance with the conservation laws for mass, momentum, energy and molecular species. The result is a different set of governing differential point equations for each phase. Although each set of equations is assuredly valid within its phase, there is no way of knowing *a priori* in which phase an arbitrary point lies and, therefore, which set of equations is appropriate. However, if each arbitrary point is associated with a surrounding volume that contains all phases and the volume average of a given phase property is associated with that point, then the volume averaged form of each set of governing equations is valid everywhere.

In order to utilize this approach to develop the governing equations of drying, certain approximations and assumptions need to be made. It is assumed that the transverse movement of heat and moisture control lumber drying so that the one-dimensional form of the governing equations are sufficient. The cell wall material is assumed to be rigid above the FSP (4) with constant density. Both liquid and gas phase motion are slow so that convective accelerations can be ignored. Within the averaging volume, the thermal conductivity is assumed to be constant, as is the specific heat so that enthalpy is a linear function of temperature. In addition, it is assumed that both reversible work and viscous dissipation are negligible, and that there is no internal heat source, although such a factor to account for electromagnetic heating can readily be included.

The behavior of the moisture in drying wood is described by the continuity equation for the liquid phase and the water vapor portion of the gas phase. The volume averaged form of these equations was developed by Whitaker (5):

$$\frac{\partial}{\partial t}(\rho_\ell \psi_\ell) + \frac{\partial}{\partial z}(\rho_\ell v_\ell) + \dot{m} = 0 \quad (1)$$

$$\frac{\partial}{\partial t}(\rho_{wv}\psi_g)+\frac{\partial}{\partial z}(\rho_{wv}v_g)-\dot{m}=\frac{\partial}{\partial z}(\rho_g D\frac{\partial}{\partial z}(\rho_{wv}/\rho_g)), \quad (2)$$

where ψ_i is the local volume fraction of phase i, and $\dot{m}$ is the local rate of evaporation per unit volume. The mass flux boundary condition based on the surface drying rate cannot be separated into liquid and vapor components, so a total moisture transport equation is generated by adding equations (1) and (2), and introducing the dimensionless liquid saturation S as

$$S = (\psi_\ell \rho_\ell + \psi_g \rho_{wv})/\phi\rho_\ell. \quad (3)$$

Then the governing differential equation for moisture becomes

$$\phi\frac{\partial S}{\partial t} + \frac{\partial}{\partial z}(v_\ell + \frac{\rho_{wv}}{\rho_\ell} v_g) = \frac{\partial}{\partial z}(\frac{\rho_g}{\rho_\ell} D \frac{\partial}{\partial z}(\frac{\rho_{wv}}{\rho_g})). \quad (4)$$

Development of the volume averaged thermal energy equation for each phase and their subsequent summation yields the total thermal energy again detailed by Whitaker (6):

$$\rho C_p\frac{\partial T}{\partial t} + (\rho_\ell c_{p_\ell} v_\ell+\rho_g c_{p_g} v_g)\frac{\partial T}{\partial z} + \dot{m}h_{\ell g} = \frac{\partial}{\partial z}(k\frac{\partial T}{\partial z}), \quad (5)$$

where ρ is the spatial average density

$$\rho = \psi_s\rho_s + \psi_\ell\rho_\ell + \psi_g(\rho_{wv} + \rho_a) \quad (6)$$

and C_p is the mass fraction average specific heat

$$C_p = (\psi_s\rho_s c_{p_s} + \psi_\ell\rho_\ell c_{p_\ell} + \psi_g(\rho_{wv}c_{p_{wv}} + \rho_a c_{p_a}))/\rho. \quad (7)$$

Arrival at this total energy equation requires the important simplifying assumption of local thermal equilibrium - locally the temperature of each phase is the same. The criteria for the validity of this assumption (5) are easily satisfied by the slow process of wood drying.

Equations (4) and (5) constitute the set of governing differential equations describing the heat and mass transfer during wood drying. Each equation includes both diffusive and convective components. In order to solve these equations, the convective liquid and gas phase velocities must be determined by solving the phase momentum equations. On dimensional grounds (7), this solution must be a form of Darcy's law, the volume average of which can be shown (8) to depend on the phase pressure gradient and the permeability, K, by

$$v_g = -\frac{K_g}{\mu_g}(\frac{\partial P_g}{\partial z} - \rho_g g) \quad (8)$$

$$v_\ell = -\frac{K_\ell}{\mu_\ell}(\frac{\partial P_\ell}{\partial z} - \rho_\ell g). \quad (9)$$

Darcy's law is known to be a good approximation for single phase flow through wood (9), and it is assumed valid for two-phase flow based on experience with unsaturated flow through other media (10). The liquid and gas phase pressures are related by the capillary pressure P_c as

$$P_c = P_g - P_\ell. \quad (10)$$

The capillary pressure is defined by the surface tension of the liquid σ and the principle radii of curvature, r_1 and r_2, as

$$P_c = \sigma(\frac{1}{r_1} + \frac{1}{r_2}). \quad (11)$$

Since σ depends on temperature while r_1 and r_2 depend on saturation, then $P_c = f(S,T)$ and by the chain rule

$$\frac{\partial P_c}{\partial z} = C_S\frac{\partial S}{\partial z} + C_T\frac{\partial T}{\partial z}, \quad (12)$$

where

$$C_S = \frac{\partial P_c}{\partial S} \quad (13)$$

$$C_T = \frac{\partial P_c}{\partial T}. \quad (14)$$

The gas phase pressure depends on the partial pressure of the air and water vapor. If the number of moles of air remains constant and the ideal gas law is used, the partial pressure of air will depend only on the temperature and gas phase volume, or saturation. Utilizing the Clapeyron-Clausius equation and the Kelvin equation, the partial pressure of the water vapor can be expressed in terms of variables that depend only on S and T. Thus, the gas phase pressure $P_g = f(S,T)$ and

$$\frac{\partial P_g}{\partial z} = C'_S\frac{\partial S}{\partial z} + C'_T\frac{\partial T}{\partial z}. \quad (15)$$

where

$$C'_S = \frac{\partial P_a}{\partial S} + \frac{\partial P_{wv}}{\partial S} \quad (16)$$

$$C'_T = \frac{\partial P_a}{\partial T} + \frac{\partial P_{wv}}{\partial T} \quad (17)$$

Since the diffusive term of equation (4) can be written in terms of partial pressures and in turn as a function of S and T, then let

$$\frac{\partial}{\partial z}(\frac{\rho_{wv}}{\rho_g}) = C''_s\frac{\partial S}{\partial z} + C''_T\frac{\partial T}{\partial z}. \quad (18)$$

Substituting equations (8), (9), (10), (12), (15), and (18) into equations (4) and (5), the governing differential equations can be expressed entirely in terms of the two dependent variables S and T:

$$\phi\frac{\partial S}{\partial t} - \frac{\partial}{\partial z}\{[\frac{K_\ell}{\mu_\ell}(C'_s-C_s)+\frac{\rho_{wv}}{\rho_\ell}\frac{K_g}{\mu_g}C'_s+\frac{\rho_g}{\rho_\ell}DC''_s]\frac{\partial S}{\partial z} +$$
$$[\frac{K_\ell}{\mu_\ell}(C'_T-C_T)+\frac{\rho_{wv}}{\rho_\ell}\frac{K_g}{\mu_g}C'_T+\frac{\rho_g}{\rho_\ell}DC''_T]\frac{\partial T}{\partial z} -$$
$$(\rho_\ell + \rho_g)g\} = 0 \quad (19)$$

$$\rho C_p \frac{\partial T}{\partial t} - \{\frac{\rho_\ell c_{p\ell} K_\ell}{\mu_\ell}[(C_s'-C_s)\frac{\partial S}{\partial z} + (C_T'-C_T)\frac{\partial T}{\partial z} - \rho_\ell g]$$

$$+ \frac{\rho_g c_{pg} Z_g}{\mu_g}[C_s' \frac{\partial S}{\partial z} + C_T' \frac{\partial T}{\partial z} - \rho_g g]\}\frac{\partial T}{\partial z} + \dot{m}h_{\ell g} =$$

$$\frac{\partial}{\partial z}(k \frac{\partial T}{\partial z}) \qquad (20)$$

While lengthy, this form of the equations allows ready comparison of liquid convection, gas convection, and diffusion. Notice that the equations are intimately coupled, and equation (20) contains several nonlinear products of differentials. Additional nonlinearities abound since most coefficients are dependent on one or both of the dependent variables. To help sort out negligible terms and the functional form of the coefficients, a mechanistic model of wood structure is developed in the next section.

MECHANISTIC MODEL

Since the analytical model depends so intimately upon prediction of flow through wood structure, a physical model based upon measured directional permeabilities has been developed. By assuming that the pit structure controls flow characteristics, Comstock (11) developed the cellular model shown in figure 1. The model accurately predicts permeability ratios and resembles observed wood cell geometry. The pits are located only on the overlapping surfaces, and the cells are square in cross section. This cell structure is assumed to be homogeneous and end effects are ignored. For any given wood species, the cell width W and the lumen width w can be measured (12), and specified as the ratio, a = w/W. The fraction of the total cell length that overlaps the next is identified by α and is determined from permeability data. Thus, the model geometry is characterized by W, a, and α

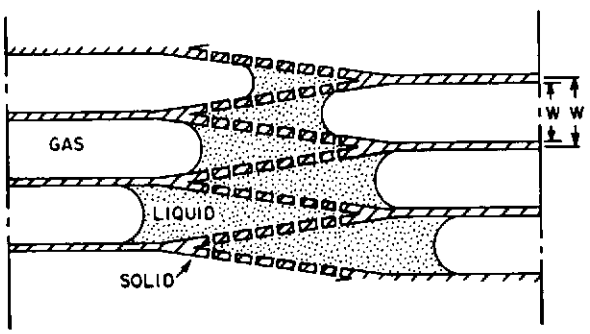

Figure 1. Mechanistic Wood Structure Model

When partial saturation of this wood model occurs, the gas phase is likely to form a single bubble centrally located in the lumen. The free liquid occupies the tapered ends of the cells as indicated in figure 1. As can be seen, the radius of curvature of the menisci formed between the two phases is controlled by the geometry. As the saturation of a cell lowers, the menisci recede toward the ends and, after entering the tapered portion, the radius of curvature decreases. The capillary pressure of equation (11) thereby increases and induces liquid motion. Simultaneously, the receding menisci progressively diminish the number of pits available for liquid passage and, therefore, the liquid phase permeability. When the menisci in adjacent cells reach the point of overlap, the continuous liquid phase path is broken and liquid permeability goes to zero. The saturation level at this point is the irreducible saturation S_{ir} and can be determined from the geometry as

$$S_{ir} = \frac{a\alpha}{4[1-(2-a)\alpha]} \qquad (21)$$

Similarly, the critical saturation S_{cr} at which the menisci first enter the tapered portion is

$$S_{cr} = 4S_{ir} . \qquad (22)$$

In arriving at these expressions, the gas phase contribution to the saturation level has been neglected so that equation (3) has been approximated by

$$S \simeq \psi_\ell/\phi. \qquad (23)$$

The void fraction is

$$\phi = a^2[\frac{1-(2-a)\alpha}{1-\alpha}] \qquad (24)$$

Using the mechanistic model geometry and assuming that all pits are of uniform size and flow resistance, the liquid permeability can be related to the measured saturated permeability K_{sat} and the saturation level as

$$K_\ell/K_{sat} = \begin{cases} 1 & S_{cr}<S<1 \\ 2(S/S_{cr})^{\frac{1}{2}}-1 & S_{ir}<S<S_{cr} \\ 0 & 0<S<S_{ir} \end{cases} \qquad (25)$$

The gas phase permeability can theoretically be predicted in the same manner, but actual drying behavior does not conform well to this model. As the liquid meniscus moves by a pit, mechanical forces on the pit structure are sufficient to aspirate or occlude about 95% of the pits (13) so that they do not allow significant gas flow between lumens. Thus, it is reasonable to assume that gas phase permeability is zero everywhere in drying wood, eliminating all gas phase convection terms from equations (19) and (20). If the diffusive replacement of air into the space evacuated by the receding water level is slow, as it probably is, the total pressure in the wood will not remain constant, and the gas phase density must be related to the partial pressure of the constituents by

$$\rho_g = (\frac{P_{wv}}{R_{wv}} + \frac{P_a}{R_a})\frac{1}{T} , \qquad (26)$$

where

$$P_a = (P_o - P_{wvo})\frac{(1-S_o)}{(1-S)}\frac{T}{T_o} \qquad (27)$$

$$P_{wv} = P_{wvo} \exp[-\frac{h_{\ell g}}{R_{wv}}(\frac{1}{T} - \frac{1}{T_o})], \qquad (28)$$

the subscript o indicating initial conditions.

Following the approach of Siau (9), the dependence of thermal conductivity on geometry and moisture content can be written

$$k = \frac{k_s[\lambda(1-S)+S][ak_g(1-S)+ak_\ell S+k_s(1-a)]}{(1-a)[ak_g(1-S)+ak_\ell S+k_s(1-a)]+ak_s[\lambda(1-S)+S]}, \quad (29)$$

where λ is a correction factor that compensates for two dimensional heat flux (14, 9).

The capillary pressure coefficients, equations (13) and (14), can be determined by expressing P_c in terms of the principle radii of curvature as

$$P_c = \begin{cases} \frac{4\sigma}{aW} & S_{cr}<S<1 \\ \frac{2\sigma}{aW}\left[1 + (S_{cr}/S)^{\frac{1}{2}}\right] & S<S_{cr} \end{cases} \quad (30)$$

This saturation dependence of the capillary pressure is compared qualitatively with that of several tests of unconsolidated sand in figure 2. The Leverett j-function (15) is a dimensionless capillary pressure and d is a characteristic dimension. For sand, Leverett used $d = (K/\phi)^{\frac{1}{2}}$, while $d = aW$ is used for wood. It can be seen that the capillary pressure predicted by the mechanistic model of wood agrees well with the experimental relationship for sand inspiring confidence in the model even though the structure of the two materials is quite different.

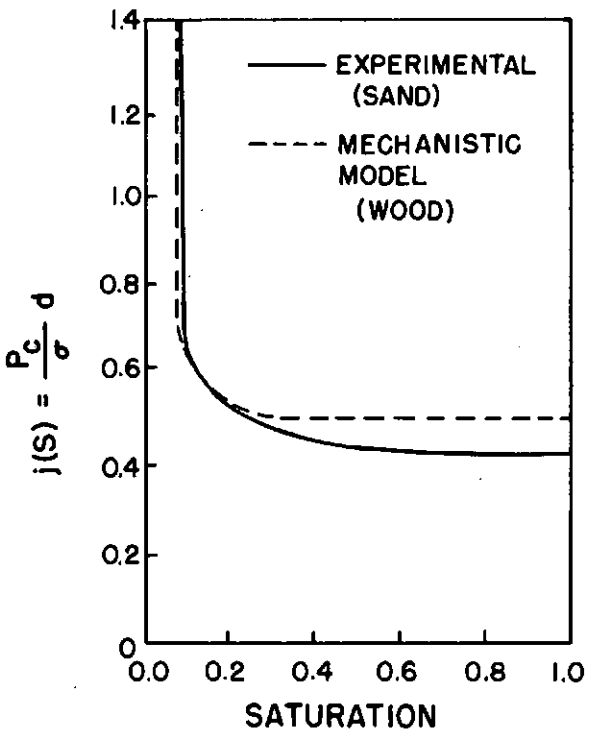

Figure 2. Comparison of dimensionless capillary pressure for sand and mechanistic wood structure.

Using an empirical relationship (16) for the surface tension dependence on temperature gives

$$C_T = \begin{cases} -\frac{0.576}{aW} & S_{cr}<S<1 \\ -\frac{0.288}{aW}\left[1 + (S_{cr}/S)^{\frac{1}{2}}\right] & S<S_{cr} \end{cases} \quad (31)$$

and

$$C_S = \begin{cases} 0 & S_{cr}<S<1 \\ -\frac{\sigma}{aW}(S_{cr}/S^3)^{\frac{1}{2}} & S<S_{cr} \end{cases} \quad (32)$$

Using equations (16), (17), (26), (27), and (28)

$$C_T' = \frac{P_a}{T} + \frac{P_{wv}h_{\ell g}}{R_{wv}T^2} \quad (33)$$

$$C_s' = \frac{P_a}{(1-S)} \quad (34)$$

$$C_T'' = -\frac{P_a}{P_{wv}}\frac{1}{T}\left(1 - \frac{h_{\ell g}}{R_{wv}T}\right)/\left(1 + \frac{P_a}{P_{wv}}\right)^2 \quad (35)$$

$$C_s'' = -\frac{P_a}{P_{wv}}\frac{1}{(1-S)}/\left(1 + \frac{P_a}{P_{wv}}\right)^2 \quad (36)$$

Using the given relationships for typical drying conditions, the hydrostatic effect on liquid flow is negligible. Also, the temperature effects on surface tension can be ignored, since $C_T << C_T'$. An additional simplification is realized from the nature of water vapor diffusion. Since it has been assumed that there is no continuous gas phase path for convection, water vapor must diffuse through a series of lumen-cell wall paths: vapor diffuses across the lumen, condenses on the cell wall surface, diffuses through the cell wall as bound water, evaporates at the next surface, and so on. As a result, there is no net latent heat absorbed in a cell; all evaporative latent heat is assumed to be consumed at the drying surface as either the final evaporation of bound water or evaporation of convected liquid. This diffusive path implies that the diffusion coefficient will be independent of moisture content at levels greater then FSP since the cell wall material cannot contain more moisture. Below the FSP, however, the diffusion coefficient varies with both temperature and moisture content (17, 18). The literature provides temperature and saturation dependencies for the phase viscosities (19,20), and specific heats (9,19,24), and the latent heat of evaporation (21).

These assumptions reduce the governing equations to

$$\phi\frac{\partial S}{\partial t} - \frac{\partial}{\partial z}\{[\frac{K_\ell}{\mu_\ell}(C_s' - C_s) + \frac{\rho_g}{\rho_\ell}DC_s'']\frac{\partial S}{\partial z} + [\frac{K_\ell}{\mu_\ell}C_T' + \frac{\rho_g}{\rho_\ell}DC_T'']\frac{\partial T}{\partial z} = 0 \quad (37)$$

$$\rho C_p\frac{\partial T}{\partial t} - \frac{\rho_\ell c_{p\ell}K_\ell}{\mu_\ell}[(C_s' - C_s)\frac{\partial S}{\partial z} + C_T'\frac{\partial T}{\partial z}]\frac{\partial T}{\partial z} = \frac{\partial}{\partial z}(k\frac{\partial T}{\partial z}) \quad (38)$$

The boundary conditions necessary for solution of this set of equations are formulated by assuming

that convective heat and mass transfer occur at the board surface and that there is no heat or mass flux through the mid-plane at a distance L from the surface.

@z=0 1. $$\left[\frac{\rho_\ell K_\ell}{\mu_\ell}(C'_s - C_s) + \rho_g D C''_s\right]\frac{\partial S}{\partial z} +$$
$$\left[\frac{\rho_\ell K_\ell}{\mu_\ell}C'_T + \rho_g D C''_T\right]\frac{\partial T}{\partial z} = \dot{m}_{conv} \qquad (39)$$

2. $$\dot{m}_{conv} h_{\ell g} - k\frac{\partial T}{\partial z} = \dot{q}_{conv} \qquad (40)$$

@z=L 3. $$\frac{\partial S}{\partial z} = 0 \qquad (41)$$

4. $$\frac{\partial T}{\partial z} = 0 \qquad (42)$$

The convective heat and mass transfer can be expressed as

$$\dot{m}_{conv} = h_m A(P_{wv}/_{z=0} - P_{wv\infty}) \qquad (43)$$

$$\dot{q}_{conv} = h_h A(T/_{z=0} - T_\infty) \qquad (44)$$

The convective heat transfer coefficient h_h can be determined from the drying conditions, and the mass transfer coefficient h_m is found from h_h by analogy. This should give satisfactory results if the drying rate is sufficiently low so that the transpiration rate at the surface does not effect the heat transfer coefficient.

NUMERICAL SOLUTION

Numerical solution of equations (37) and (38) is simplified if a dimensionless temperature is used:

$$T^* = \frac{T - T_o}{T_\infty - T_o} = \frac{T - T_o}{\Delta T} \quad . \qquad (45)$$

It is also convenient to replace fractional saturation level with fractional moisture content, M, which is conventionally used in the wood drying literature. Assuming that the cell wall remains at FSP until the free liquid is depleted, there is a linear relationship between the two variables:

$$M = (M_{max} - FSP)S + FSP = (\Delta M)S + FSP. \qquad (46)$$

The maximum possible moisture content M_{max} can be found from the wood geometry.

Since the drying process is slow, adequate linearization of the governing equations is realized by calculating all transport properties and geometric coefficients based on the temperature and moisture content at the previous time step. The temperature gradient of the convective energy term is also linearized in this manner. If i is the spatial index and j is the time index, then the fully implicit forms of the governing equations are

$$\phi\left(\frac{\partial M}{\partial t}\right)_{i,j+\frac{1}{2}} - \frac{\partial}{\partial z}\left\{\left[\frac{K_\ell}{\mu_\ell}(C'_s - C_s) + \frac{\rho_g}{\rho_\ell}DC''_s\right]_{i,j}\left(\frac{\partial M}{\partial z}\right)_{i,j+1} +$$
$$\Delta M \Delta T\left[\frac{K_\ell}{\mu_\ell}C'_T + \frac{\rho_g}{\rho_\ell}DC''_T\right]_{i,j}\left(\frac{\partial T^*}{\partial z}\right)_{i,j+1}\right\} = 0 \qquad (47)$$

$$(\rho C_p)_{i,j}\left(\frac{\partial T^*}{\partial t}\right)_{i,j+\frac{1}{2}} - \left(\frac{\rho_\ell c_{p\ell} K_\ell}{\mu_\ell}\frac{\partial T^*}{\partial z}\right)_{i,j}\left[\frac{1}{\Delta M}(C'_s - C_s)_{i,j}\right.$$
$$\left.\left(\frac{\partial M}{\partial z}\right)_{i,j+1} + \Delta T(C'_T)_{i,j}\left(\frac{\partial T^*}{\partial z}\right)_{i,j+1}\right] = \frac{\partial}{\partial z}\left[(k)_{i,j}\left(\frac{\partial T^*}{\partial z}\right)_{i,j+1}\right]. \qquad (48)$$

The boundary conditions follow directly from equations (39) to (44). Since the saturated partial water vapor pressure at the surface is non-linear with temperature, the convective mass transfer is approximated by

$$(\dot{m}_{conv})_{i,j+1} = h_m A[(P_{wv})_{i,j} - P_{wv\infty}]. \qquad (49)$$

When the surface dries to a moisture content less than FSP, the water vapor is no longer saturated at the surface temperature, and equation (49) is not valid. Following the suggestion of Luikov (3), the convective driving potential is expressed in terms of the surface moisture content and the equilibrium moisture content (EMC) of the wood with the drying air:

$$(\dot{m}_{conv})_{i,j+1} = h'_m A[(M)_{i,j} - EMC] \mid M<FSP. \qquad (50)$$

A different convective coefficient h'_m is used that assumes a continuous mass flux is maintained as the surface dries from above to below the FSP, and is assumed to remain constant.

The initial moisture and temperature distribution are assumed uniform, therefore

@ j = 0 $$(M)_{i,j} = M_o \qquad (51)$$

$$(T)_{i,j} = T_o \qquad (52)$$

For I spatial nodes, the matrix of simultaneous equations exhibits a 2I x 2I coefficient matrix. There are seven, non-zero diagonals so that a full matrix inversion scheme is required for solution.

To test the performance of the model, the wood drying literature was surveyed for lumber drying data. Surprisingly, there is very little complete and well documented data. One study that measured temperature and moisture contents at both surface and centerline of spruce boards during drying is reported by Keylworth (19). The wood can be characterized by the following parameters:

$\alpha = 0.25$; $L = 1.2$ cm ; $a = 0.8$;

$W = 23\mu m$; $FSP = 0.3$; $K_{sat} = 10^{-13}$ cm^2.

The initial conditions are given as:

$T_o = 10^oC$; $M_o = 0.86$

The flow of drying air provides:

$T_\infty = 110^oC$; $T_{wb} = 87^oC$

$EMC = 0.04$; $h_h = 5.4 \times 10^{-4}$ cal/cm^{2}s ^oC.

The convective mass transfer coefficient can be calculated from the heat transfer coefficient by analogy (20) to be

$$h_m = 2.1 \times 10^{-9} \text{ s/cm},$$

when partial pressure is expressed in units of gm/cm s^2. This analogy assumes that the evaporative surface is completely saturated, such as a pan of water. During the drying of wood, a completely wetted surface would require some physical mechanism to draw the liquid water onto the surface. The model predicts no such phenomenon. It seems more likely that the only surfaces that remain wetted and in equilibrium with saturated water vapor are the pits that are open over the free liquid; the remaining surfaces are unsaturated and, for this study, must be neglected. Stamm (21) estimates that pits cover about 1% of the total surface area of wood. Thus, for mass transfer per total area basis,

$$h_m = \begin{cases} 2.1\times10^{-11} \text{ s/cm} & S_{cr}<S<1 \\ 2.1\times10^{-11} \left[2(S/S_{cr})^{\frac{1}{2}}-1\right] & S_{ir}<S<S_{cr}. \end{cases}$$

Using spatial increments of 0.6 mm and time steps of one minute, the numerical solution of equation (47) and (48) was generated. The calculated temperature and moisture content at the surface and the centerline have been plotted in figure 3 along with the experimental values. The most important observation from figure 3 is that the capillary flow model of wood predicts qualitatively the measured drying behavior. The calculated temperature displays the same sigmoid increase and naturally approaches the wet bulb temperature, remaining at that value until the surface dries to below S_{ir}. Then the temperature rises and approaches the drying air temperature. The calculated moisture contents are of the same order of magnitude, but a steeper gradient occurs in the calculated values between 50 and 100 minutes. This increasing slope corresponds to a constant drying rate regime that is characteristic of most lumber drying curves (22). The experimental curve that conveys a constant decrease of moisture content with the logarithm of time does not show a constant rate period but rather exponentially decaying rate from the beginning. Due to this inconsistency, the accuracy of the experimental data might be questioned and it has not been used as an absolute measure of the validity of the model.

Certain physical interpretations of the moisture movement during drying can be obtained directly from equation (47). For the drying conditions modeled in figure 3, the diffusive terms for both M and T gradients are several orders of magnitude smaller than the corresponding convective terms; capillary transport is the controlling mechanism while $S>S_{ir}$. It is interesting to note from equations (33) to (36) that the convective and diffusive flux coefficients have opposite signs, or that gas

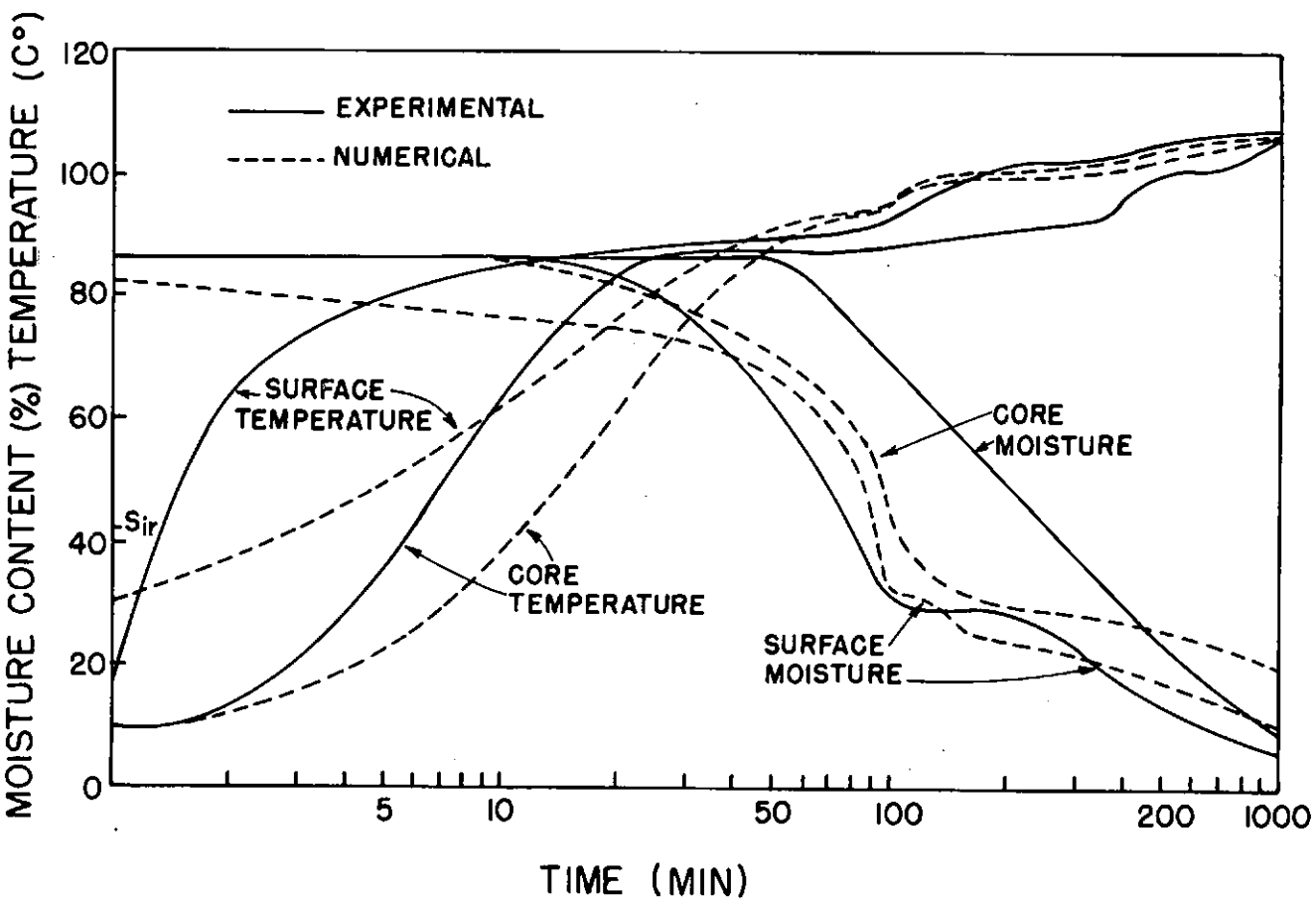

Figure 3. Comparison of numerical results with experimental wood drying data.

phase diffusion is actually in the opposite direction as the corresponding capillary induced flow. This result arises from the assumption of local mass equilibrium (5). The water vapor partial pressure increases exponentially with temperature while the partial pressure of air increases linearly. So a water vapor concentration gradient aligns with the temperature gradient. Simultaneously, as the saturation level decreases, the air volume increases so that the air density decreases; but the water vapor is saturated, the density being fixed by the temperature. The water vapor concentration is therefore greater where the saturation is lower, and the concentration gradient opposes the saturation gradient.

During convective drying, the gradient of the dimensionless temperature and the moisture content are of the same order of magnitude but of opposite sign. The direction of bulk moisture movement therefore depends on the relative magnitude of the capillary flow coefficients (if diffusive flux is negligible). These coefficients show weak moisture content dependence but strong temperature dependence. The ratio of the coefficients of the second and third terms of equation (47) is plotted as a function of temperature in figure 4. At low temperature, the ratio is less than one and the moisture content gradient induces flow toward the evaporative surface. However, the temperature gradient induced flow begins to dominate as the temperature increases, causing flow of free liquid away from the surface and toward the center of the board until sufficient moisture content gradient is established to counteract this effect. As the total board warms up and the temperature gradient thereby declines, the bulk liquid flow reverses direction and moisture is supplied to the drying surface. This phenomenon is observed in the drying curves of figure 3 where significant drying does not occur until the entire board has reached a fairly uniform temperature. During the warm up period, the numerical solution predicts a small but finite increase of moisture content in the center of the board that must delay the drying process. This phenomenon suggests the use of electromagnetic heating to initially warm the boards so that unfavorable temperature gradient induced moisture movement does not occur, after which time convective drying could be utilized to provide evaporative energy to the surface.

SUMMARY

Lumber dried from high moisture contents is modeled as a capillary porous media and the governing differential equations are developed. The mechanistic wood structure model allows calculation of the necessary transport properties. Numerical solution of the equations indicate that capillary mechanisms completely control the movement of wood moisture when free liquid exists, and the end of this regime can be predicted strictly from the wood cell geometry. As the free liquid is depleted, diffusive transport prevails as would be expected. The numerical results are in agreement, at least qualitatively, with the limited experimental data which is available. Further verification of the model awaits the development of experimental input in two specific areas. First, experimentally determined transport properties are necessary to verify those developed from the structural model and, second, accurate local temperature and moisture measurements taken during a carefully controlled drying experiment are necessary to make quantitative comparisons with the model predictions.

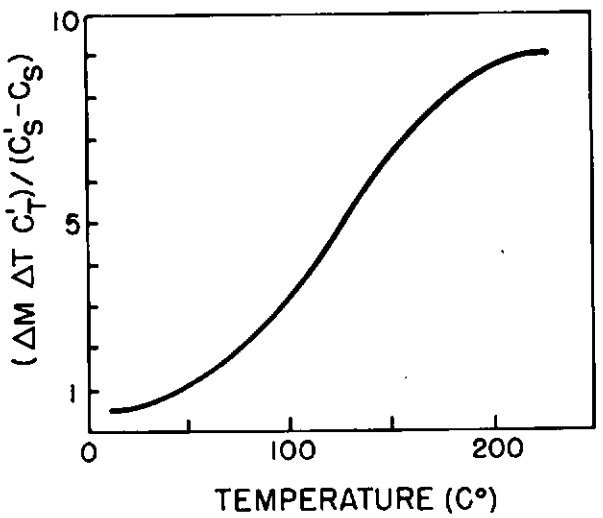

Figure 4. Temperature dependence of capillary flow coefficients

ACKNOWLEDGEMENTS

This work has been sponsored in part by the National Science Foundation under Grant No. CME-7906367. In addition, the continuous exchange of information and ideas with members of the drying research group at Weyerhaeuser Company of Tacoma, WA has been invaluable.

REFERENCES

1. Sherwood, T.K., "The drying of solids - I," Ind. Eng. Chem., V.21, No.12 (1929).
2. Hart, C.A., The Drying of Wood, Technical Report No. 27, School of Forestry, North Carolina State University (1965).
3. Luikov, A.V., Heat and Mass Transfer in Capillary - Porous Bodies, Pergamon Press, (1966).
4. Skaar, C., Water in Wood, Syracuse Univ. Press, New York (1972).
5. Whitaker, S., "Heat and mass transfer in granular porous media," to be published in Advances in Drying, V.1, A.S. Mujamdar, ed. for (1978).
6. Whitaker, S., "Simultaneous heat, mass, and momentum transfer in porous media: a theory of drying," Advances in Heat Transfer, V.13 (1977).
7. Collins, R.E., Flow of Fluids Through Porous Materials, Reinhold Publishing Corp., New York (1961).
8. Whitaker, S., "Advances in theory of fluid motion in porous media," Ind. Eng. Chem., V.61, No.12 (1969).
9. Siau, J.F., Flow in Wood, Syracuse University Press, New York (1971).
10. Bear, J., Dynamics of Fluids in Porous Media, American Elsevier Pub. Co., New York (1972).

11. Comstock, G.L., "Directional permeability of softwoods," Wood and Fiber, V.1(4) (1970).
12. Scallan, A.M. and Green, H.V., "A technique for determining the transverse dimensions of the fibres in wood," Wood and Fiber, V.5(4) (1974).
13. Meyer, R.W., "Influence of pit aspiration on early wood permeability of Douglas-fir," Wood and Fiber, V.2(4) (1971).
14. Hart, C.A., "Theoretical effect of gross anatomy upon conductivity of wood," For. Prod. J., V. 14 (1) (1964).
15. Leverett, M.C., "Capillary behavior in porous solids," Trans. AIME, V. 142(1941).
16. Fleming, R.H. and Revelle, R., Symp. Recent Marine Sediments, Ann. Ass. Pet. Soc., P.D. Trask (ed.) (1939).
17. Yao, J., "A new approach to the study of drying diffusion coefficients of wood," For. Prod. J., V. 16(6) (1966).
18. Stamm, A.J., "Combined bound-water and water-vapor diffusion in Sitka spruce," For. Prod. J., V.10(12)(1960).
19. Kays, W.M., Convective Heat and Mass Transfer, McGraw Hill Co., New York, (1966).
20. Bingham, E.C., Fluidity and Plasticity, McGraw-Hill Co., New York, (1922).
21. Keenan, J.H. and Keyes, F.G., Steam Tables, John Wiley & Sons, New York (1969).
22. Keylworth, R., "Der Verlauf der Holztemperatur wahrend der Furnier und Schnittholztrocknung," Holz als Roh-und Werkstoff, V.10(3) (1952).
23. Krieth, F., Principles of Heat Transfer, International Textbook Co., Scranton, PA (1969).
24. Stamm, A.J., Wood and Cellulose Science, Ronald Press Co., New York (1964).
25. Keey, R.B., Drying Principles and Practice, Pergammon Press, Oxford (1972).

A MATHEMATICAL MODEL FOR THE DRYING OF LATEX FILMS

N. Pramojaney[1]
G. W. Poehlein[2]
J. W. Vanderhoff[1]

1. Emulsion Polymers Institute, Lehigh University
Bethlehem, Pennsylvania 18015
2. School of Chemical Engineering, Georgia Institute
of Technology, Atlanta, Georgia 30332

ABSTRACT

The effects of temperature, relative humidity, and laminar flow velocity of drying air upon the drying rate of latexes were measured experimentally. A mathematical model was developed using simplifying assumptions, which satisfactorily described the transient and non-uniform drying behavior of a thin latex film on a flat substrate under forced-air-drying conditions. A modified gravimetric technique was used in measuring the evaporation flux of water (and other volatiles) from thin films of the monodisperse 60:40 styrene-butadiene copolymer latexes. The evaporation flux during the constant-rate (CR) stage of the drying was measured accurately; however, the flux during the falling-rate (FR) was measured less accurately, partly as a result of the non-uniform drying pattern of the latex films and the small and diminishing value of the flux. It was found that the rate of heat transfer to the drying film by radiation was significant, and, in most cases, can not be neglected. Furthermore, it was demonstrated that, in spite of the inaccuracy of the measured evaporative surface temperature, the drying flux could be estimated with reasonable accuracy by using the fundamental knowledge of simultaneous heat and mass transfer and the boundary-layer theory.

NOMENCLATURE

c = specific heat at constant pressure, J/kg-K

D = diffusion coefficient of water vapor in air, m^2/s

F_r = ratio of the experimental flux to the theoretical flux

F_{12} = view factor

h = coefficient of heat transfer, W/m^2-K

h_c = coefficient of heat transfer by convection in the presence of mass transfer, W/m^2-K

h_r = coefficient of heat transfer by radiation, W/m^2-K

H_{vap} = latent heat of vaporization for water at T_{sf}, J/kg-K

K = mass transfer coefficient, m/s

k = thermal conductivity, W/m-K

L = ending length, m

N_w = evaporation flux of water vapor, kg/m^2-s

P = atmospheric pressure, N/m^2

P_{BM} = $[(P-p_s)-(P-p_a)]/\ln[P-p_s)/(P-p_a)]$

Pr = Prandtl Number of air

p = partial pressure of water, N/m^2

R = gas constant, $m\text{-}s^2/kg\ mol$

RH = relative humidity of the air, %

Re_z = Reynolds Number expressed as: $Re_z = \rho Vz/u$

S = thickness of latex film, m (or specified otherwise)

S_g = thickness of glass slide, m

S_p = thickness of platform, m

Sc = Schmidt Number for water-air system

$solid$ = solid content of latex, % by volume

T = temperature, °C

t = time, s

u = viscosity of air, $N\text{-}s/m^2$

V = average air flow velocity, m/s

x = starting length, m

z = distance from the leading edge to a location on the film, m

Greek Symbols

ε = emissivity

ρ = density, kg/m^2

σ = Stefan-Boltzmann constant, W/m^2-K^4

Subscripts

a = air

db = dry-bulb

g = glass slide

o = initial value at time=0

p = platform

s = latex film

sf = surface of the latex film

vap = water vapor

w = water

wall = surrounding wall

wb = wet-bulb

xL = from x to L

z = at distance z from the leading edge

Superscripts

j = the j-th element

Conversion Table for SI Units

1 atm	=	101325	N/m^2
T °C	=	(T+273.15)	°K
1 cal	=	4.1868	J
1 cm	=	.01	m
1 gm	=	.001	kg
1 gm/cm^2-sec	=	10	kg/m^2-s
1 mil	=	2.54×10^{-5}	m

INTRODUCTION

Film-forming polymer latexes have been widely used in the formulation of paints, adhesives, and surface coatings. These latexes comprise submicroscopic polymer particles (100 to 300 nm in diameter) colloidally suspended in the aqueous phase. The evaporation of the aqueous phase, i.e., water and other volatiles, leads to film-formation, as the polymer particles are drawn toward one another to the point of coalescence, after which viscous flow and the diffusion of polymer chain ends consolidate the polymer particles into a continuous film [1].
In most latex applications, air-drying is used to remove the aqueous phase of the latexes, and cause the particles to coalesce. Air-drying of latex films can be divided in three consecutive stages which correspond to the constant-rate (CR) and the first falling-rate (FFR), and the second falling-rate (SFR) stages of drying, as follows: (a) the initial stage or wet stage, during which the latex particles move freely and the evaporation rate is fairly constant; (b) the intermediate stage, where the particles come into irreversible contact and the water evaporation rate drops to 5 to 10% of its initial value, as the film surface becomes progressively less saturated or covered with water; (c) the final stage or dry stage, during which the small amount of water and other volatiles remaining in the film escape slowly, by diffusion through capillary channels or through the polymer toward the film surface [2].

Despite several extensive works in the area of drying and film-formation of latexes, little attention has been paid to the evaluation of the drying rate. Furthermore, the rates reported in the literature often disagree, perhaps, owing to the different drying conditions, the geometry of the equipment, the poorly-defined parameters such as the 'zero' air flow velocity, and the non-uniform drying nature of thin latex films.

The following work was originally conducted to clarify some doubts stemming from the recent investigation by Witmeyer, et al. [3,4] on the rate of water evaporation from thin films of monodisperse 60:40 styrene-butadiene copolymer latexes, and, subsequently, to study the effect of several parameters, e.g., temperature, relative humidity, and laminar flow velocity of the drying air, on the drying of latex films. Additional information on the drying rates of formulated latexes, which may contain volatiles other than water, is given in a recent review by Patton [5] and other work of the author [6].

EXPERIMENTAL DESCRIPTION

Equipment

Thin films of the latexes were dried in a wind tunnel (Figure 1) at various temperatures, relative humidities, and laminar flow velocities of the drying air. The wind tunnel was capable of maintaining an air flow velocity from 0 to 80 m/s in the test section. The temperature and relative humidity of air being circulated inside the tunnel could be controlled at desired levels by means of electrical heating elements and injection of low pressure steam into the tunnel.

The test section consisted of a special Plexiglas platform mounted on top of a top-loading Mettler P160N balance, a 35 mm SLR camera with

close-up lenses, a remote electronic flash gun, and dry-bulb and wet-bulb mercury thermometers with 0.1 °C subdivisions. The average air flow velocity was measured with a vane anemometer (Davis Instrument Mfg. Co.).

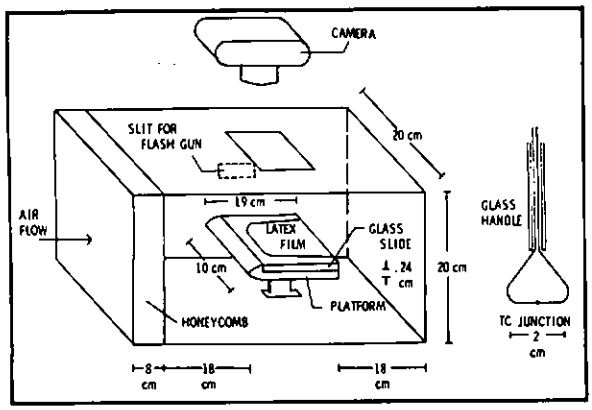

Figure 1 The Test Section & Thermocouple Assembly

Experimental Procedure

Thin films(about 3-6 mils or 0.008-0.016 cm) of the monodisperse 60:40 styrene-butadiene copolymer latex (Dow Chemical Co.) were drawn down on a 10 cm x 16.5 cm glass slide with a 6-mil-gap drawdown film applicator (Precision Gage & Tool Co.). Immediately thereafter, the glass slide was placed on the Plexiglas platform inside the test section. Extreme care was taken to level the platform so as to keep the film thickness as uniform as possible. To determine the wet area of the drying film, i.e., the non-transparent, non-coalesced, cloudy or milky, and tacky region, pictures of the drying film were taken periodically. At the same time, the weight of the film and platform was recorded as a function of the elapsed time.

Thicker films (about 40 mils or 0.1 cm) were prepared by spreading a sufficient amount of latex inside a crayon-marked rectangular area on the glass slide. The temperature of the drying films were measured with a 20-mil copper-constantan thermo-couple junction, shaped as shown in Figure 1 to minimize heat conduction through the wire. Since the temperature varies between different locations in the film, the temperature at the middle portion of the film was taken as the average film temperature in subsequent calculations. To obtain the evaporation flux or the drying rate per unit area of evaporative surface, the drying rate computed from the slope of the weight loss versus time curve was simply divided by the corresponding wetted area.

It should be noted that the surface tension of Dow monodisperse 60:40 styrene-butadiene copolymer latexes (with solid content of about 40% wt) were adjusted to 35 dyne/cm (3.5×10^{-2} N/m) by addition of sodium dodecyl sulfate. The thickened latexes used in some experiments contained about 0.5% wt of methyl cellulose thickening agent (Dow Methocel HG 1500cp).

Experimental Results

The drying rates (fluxes) of the drawndown latex film were determined gravimetrically using a procedure similar to that employed previously by Witmeyer [3]. Typical drying flux versus time curves are given in Figure 2. In general, the measured evaporation flux, which was expected to remain relatively constant during the CR stage of drying and then decrease to a very low level in the subsequent FR stage, characteristically dropped to a certain level, remained somewhat constant for a period of time, and then rose to a very high level at the end of the drying run, until the flux became too small to be detected accurately.

To explain this increase in the evaporation flux at the end of the drying run, Witmeyer suggested that the transparent portion of the film presumed to be completely dry may still have contained considerable water which evaporated slowly but sufficiently to affect the calculated flux, especially at the end of the experiment when the dried area became much larger than the remaining wetted area. Similar results were observed by Isaacs [7], who proposed that the increase in the evaporation flux was due to gelation of the system and the possible increase in the effective evaporative surface area from increased surface roughness as the water level receded into the particle matrix.

Because of the variations in the evaporation flux, particularly the unexplained rise near the end of the drying run, it was decided to carry out an in-depth analysis of the experimental system. The mathematical model used in this analysis will be described in the following section.

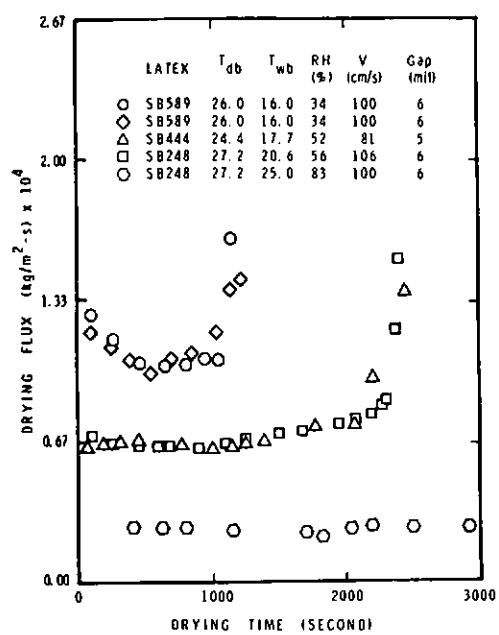

Figure 2 Experimental Drying Flux Versus Time Plots

MATHEMATICAL MODELING OF THE SYSTEM

Careful examination of the system indicated that the drying of a thin latex film is a transient process. Figure 3 clearly demonstrates that the surface film temperature (T_{sf}) is a function, not only of the drying time but also of the position on the drying film. Moreover, another transient aspect of the drying of a thin latex film on a flat substrate is shown by the increase in the starting length (x) as the film becomes dried from front to back in the direction of air flow, as shown in Figure 4.

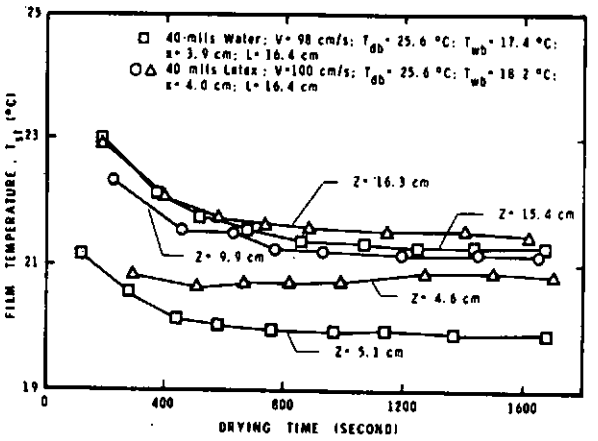

Figure 3 Film Temperature (T_{sf}) Measured at Various Locations (z) as a Function of Time.

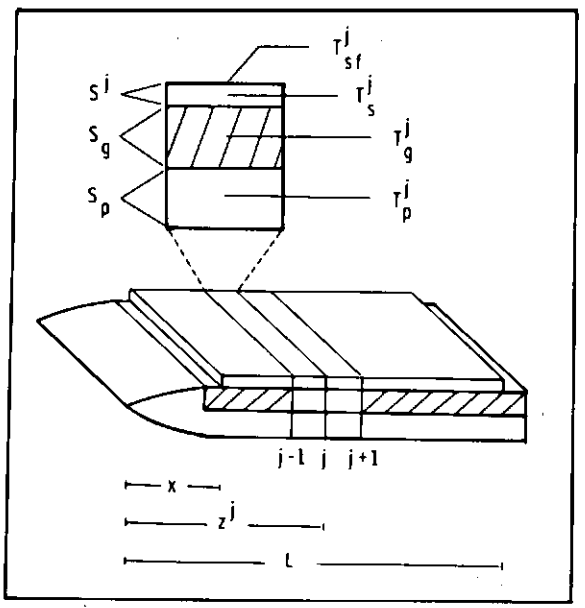

Figure 4 A Schematic Representation for the Latex Film, Glass Substrate, and Platform, Showing the j-th Film Element for Mathematical Modeling

Since the momentum, heat, and mass transfer boundary layers do not coincide in the presence of the starting length (x), the theoretical expression for the local heat transfer coefficient (h_z) derived by Pohlhausen [8,9] from boundary-layer theory is applicable:

$$h_z = 0.332\ k_a Pr^{1/3} Re_z^{1/2} [1-(x/z)^{3/4}]^{1/3} \quad (1)$$

The average heat transfer coefficient (h_{xL}) from x to L may be obtained by integration of Equation (1):

$$h_{xL} = 0.664\ k_a Pr^{1/3} (\rho_a V/u)^{1/2} [L^{3/4}-x^{3/4}]/(L-x) \quad (2)$$

Likewise, the corresponding expression for the average mass transfer coefficient (K_{xL}) can be given as:

$$K_{xL} = 0.664\ D\ Sc^{1/3} (\rho_a V/u)^{1/2} [L^{3/4}-x^{3/4}](L-x) \quad (3)$$

The average evaporation flux (N_w) may be calculated [10]:

$$N_w = 18.016\ K_{xL} (P/P_{BM}) (p_{sf}-p_a)/R(T_a+273.15) \quad (4)$$

Estimation of N_w from Equation (4) is possible only if the temperature of the evaporative surface (T_{sf}), from which p_{sf} can be directly computed, is known. Furthermore, it is imperative that an accurate value of T_{sf} must be used in Equation (4), since the value of T_{sf} may increase N_w by more than 25% of its original value.

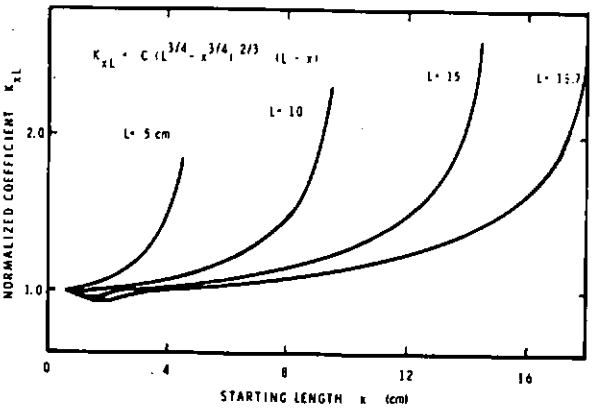

Figure 5 Normalized Mass Transfer Coefficient (K_{xL}) as a Function of the Starting Length (x) and the Ending Length (L).

The effect of the starting length (x) on K_{xL} is illustrated in Figure 5, where several curves of K_{xL} versus x at different values of L are presented. Note that the rise of the curves as x approaches L corresponds to the rise in the evaporation flux measured at the end of the drying experiment.

Figure 4 shows the cross-section of the experimental system divided into the elements used as a basis for the mathematical modelling. It was assumed that the latex film was so thin that T_{sf}

approaches the average film temperature (T_s), and that the flow of water between these two elements is negligible. The following ordinary differential equations were developed to describe the transient behavior of the thickness (S^j) and surface film temperature (T_s^j) of the j-th film element.

From mass balance:

$$dS^j/dt = N_w^j/\rho_s \quad (5)$$

From energy balance in the film:

$$\rho_s c_s\, d(S^j T^j)/dt=(T_a-T_s^j)(h_c^j+h_r^j)-N_w^j H_{vap}(T_s^j)+(T_g^j-T_s^j)/2(S^j/k_s+S_g/k_g)+[k_s S^j/(z^j-z^{j-1})][-dT_s^j/dz+dT_s^{j+1}/dz] \quad (6)$$

From energy balance in the glass slide:

$$\rho_g c_g S_g dT/dt_g^j/dt = (T_p^j-T_g^j)/2(S_g/k_g+S_p/k_p)-(T_g^j-T_s^j)/2(S_g/k_g+S^j/k_s)+[k_g S_g/(z^j-z^{j-1})][-dT_g^j/dz+dT_g^{j+1}/dz] \quad (7)$$

From energy balance in the platform:

$$\rho_p c_p S_p\, dT_p^j/dt = (T_a-T_p^j)/[1/(h^j+h_r^j)+S_p/2k_p] - (T_p^j-T_g^j)/2(S_p/k_p+S_g/k_g) + [k_p S_p/(z^j-z^{j-1})][-dT_p^j/dz+dT_p^{j+1}/dz] \quad (8)$$

Other expressions necessary for the evaluation of the foregoing ordinary differential equations:

$$N_w^j = 18.016\, K^j (P/P_{BM})(p_s^j-p_a)/R\ (T_a+273.15) \quad (9)$$

$$K^j = 0.664\, D\, Sc^{1/3}(\rho_a V/u)^{1/2} [[(z^j)^{3/4}-x^{3/4}]^{2/3}-[(z^{j-1})^{3/4}-x^{3/4}]^{2/3}]/(z^j-z^{j-1}) \quad (10)$$

$$p_s^j = p_{sf}^j = p_s(T_s^j) \quad (11)$$

$$h^j = 0.664\, k_a Pr^{1/3}(\rho_a V/u)^{1/2} [[(z^j)^{3/4}-x^{3/4}]^{2/3}-[(z^{j-1})^{3/4}-x^{3/4}]^{2/3}]/(z^j-z^{j-1}) \quad (12)$$

$$h_r^j = F_{12}\varepsilon\sigma[(T_{wall}+273.15)^4-(T_{sf}^j+273.15)^4]/(T_{wall}-T_{sf}^j) \quad (13)$$

$$h_c^j = N_w^j c_{vap}/[1-\exp(-N_w^j c_{vap}/(h^j+h_r^j))] \quad (14)$$

The relative humidity and thus p_a of the drying air can be conveniently computed from the measured dry-bulb temperature (T_{db}) and wet-bulb temperature (T_{wb}) using Dropkin's method [11].

Numerical Approach

A semi-implicit Euler integration technique was used to compute the numerical solutions of the above set of simultaneous O.D.E.'s. Sufficiently small time increments were used, while the width of the j-th element (z^j-z^{j-1}) was kept small at the front portion of the film and increased toward the back portion, since x tended to increase more slowly during the initial period of drying. The model predictions to be presented in the following section were obtained by using a total of 25 film elements and a time increment of 2.5s.

It is important to emphasize that the evaporative surface temperature (T_{sf}^j) was assumed to equal the average film temperature (T_s^j) for a very thin film of latex. Finite difference approximation was applied in the calculation of the temperature gradients:

$$dT_s^j/dz = (T_s^j-T_s^{j-1})/(z^j-z^{j-1}) \quad (15)$$

$$dT_g^j/dz = (T_g^j-T_g^{j-1})/(z^j-z^{j-1}) \quad (16)$$

$$dT_p^j/dz = (T_p^j-T_p^{j-1})/(z^j-z^{j-1}) \quad (17)$$

RESULTS AND DISCUSSION

Figures 6 to 10 show the variation of the theoretically predicted evaporation flux with time under different drying conditions. Generally, the model predictions and the experimental results were in good qualitative agreement. The experimental evaporation flux versus time curves, however, tend not to be so smooth, since the actual film, not being rectangular and uniform, dries not only from front to back, but also from both side edges towards the middle.

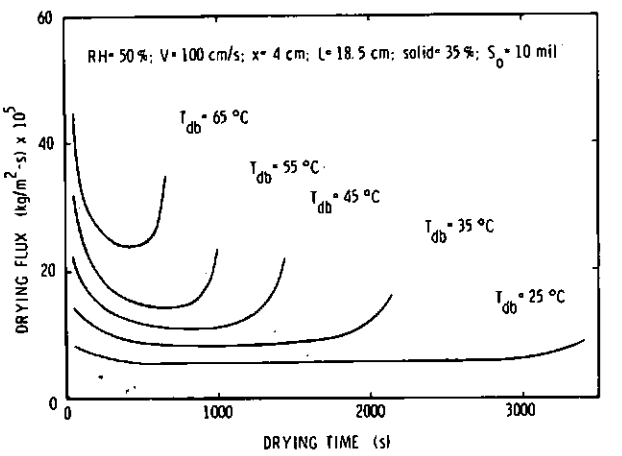

Figure 6 Model Predictions Showing the Influence of Air Temperature (T_{db})

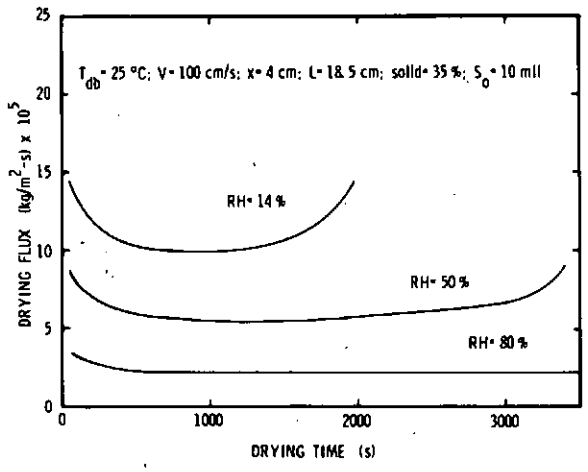

Figure 7 Model Predictions Showing the Influence of Relative Humidity (RH)

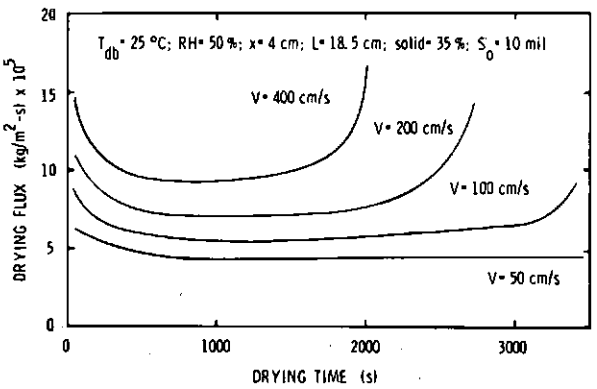

Figure 8 Model Predictions Showing the Influence of Air Flow Velocity (V)

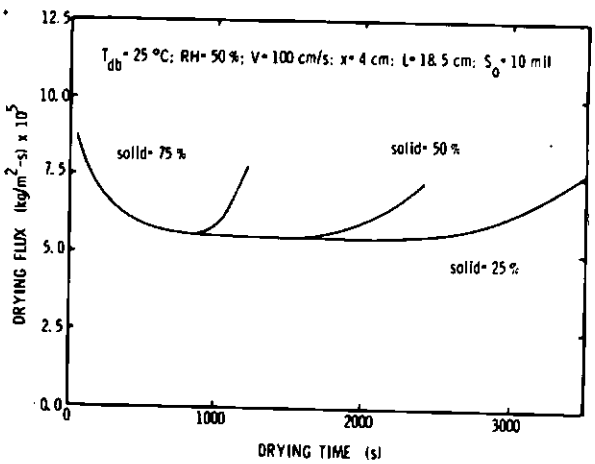

Figure 9 Model Predictions Showing the Influence of Solid Content in the Latex

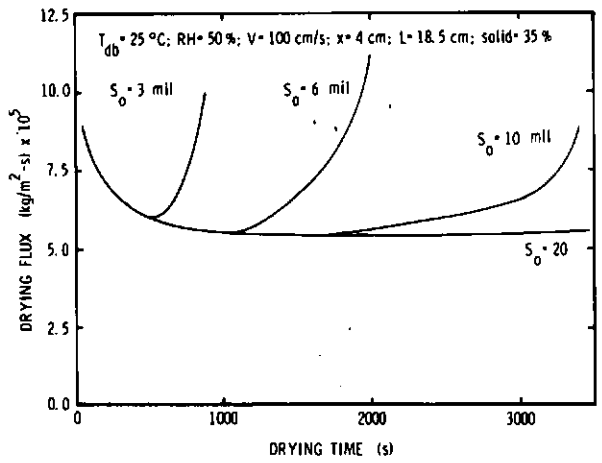

Figure 10 Model Predictions Showing the Influence of the Initial Film Thickness (S_o) (S_o in mil=2.54x10^{-5}m)

The model predictions confirmed that there exist certain temperature and moisture gradients from the front to the back of the drying film, as shown in Figure 11. The reasons for the fact that T_{sf} is always greater than T_{wb} are simply that the heat transferred by conduction through the substrate to the drying film seems to be substantial, e.g., it may be as high as 50% of the total heat flow from both sides to the evaporative surface, and that heat transferred by radiation from the surroundings (wall) to the evaporative surface may amount to 20-50% of that by convection.

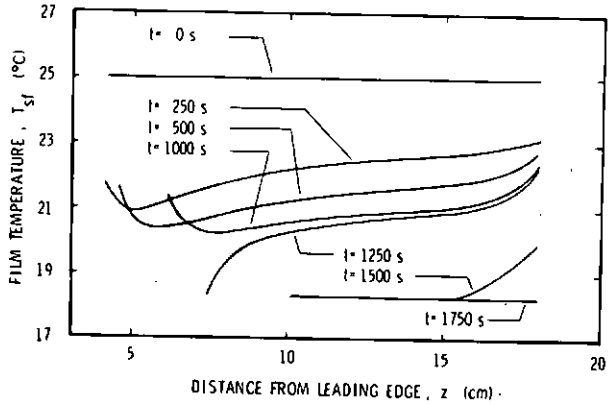

Figure 11 Model Predictions Showing Film Temperature (T_{sf}) as a Function of Position (z) and Drying Time (t); T_{db}=25°C; T_{wb}=18.3°C; RH=50%; x=4 cm; L=18.5 cm; solid=35%; S_o=6 mil.

Figure 12 shows that, not only were the starting length (x) versus time plots reasonably reproducible for drawndown latex films made from thickened latexes, but also similar curves were predictable from the theoretical model.

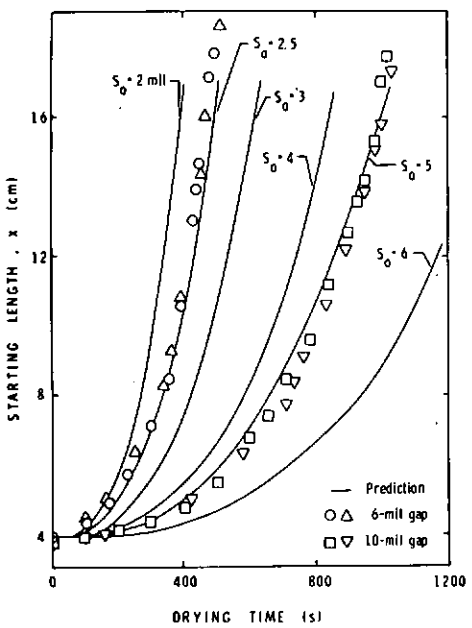

Figure 12 Starting Length (x) as a Function of Drying Time: V=100 cm/s; T_{db}=24.8°C; T_{wb}=12.6°C; solid=30%; x=4.0 cm; L=18.5 cm (S_o in mil=2.54x10^{-5} m)

It is evident that the rise in evaporation flux at the end of a drying run is to be expected. The flux may remain quite constant for a period of time, providing that the evaporation rate is kept low, e.g., by increasing the relative humidity, or the initial film is sufficiently thick to keep the film wet for a longer period of time. As a result, a simpler, more reproducible method was developed in which the rate of water evaporation was determined from the non-drawndown, rectangular latex films of about 0.1 cm (40 mils) thickness. Selected data obtained from these experiments are given in Table I.

It can be seen that Equation (4) yields accurate predictions of the evaporation flux for thin films of water over wide ranges of air temperature, humidity, and air flow velocity, as judged by a comparison of the experimental and theoretical values as well as the correction factor (F_r), i.e., the ratio of the experimental flux to the predicted flux. These results also show that water evaporates from a latex film at about the same rate as it would from a film of water under the same conditions. Furthermore, the particle size of the latex did not substantially influence the drying rate, in contrast with the earlier finding[3,4] that the rate of drying increased with increasing latex particle size. It is suspected that the apparent dependence of the evaporation flux on latex particle size may arise from the higher values of T_{sf}, which were not measured by Witmeyer [3], perhaps due to the differences in the rheological and convective heat transfer properties of latexes with different particle sizes.

CONCLUSIONS

It has been shown that a mathematical model can be used to predict the constant-rate evaporation flux of a drying latex film. This seemingly simple process is actually complicated and care must be taken not to oversimplify the process by using unjustifiable assumptions. This model offers a powerful tool for developing a suitable experimental design and obtaining a meaningful analysis of the data.

ACKNOWLEDGEMENT

This study was supported by the Emulsion Polymers Liaison Program.

Table 1 Selected Experimental Drying Fluxes

Sample	T_{db} (°C)	T_{wb} (°C)	RH %	T_{sf} (°C)	V (cm/s)	x (cm)	L (cm)	Flux x 10^5 (kg/m^2-s) Exprmt	Predct	F_r
Water	25.86	17.90	43	21.51	96	3.9	16.44	7.57	7.38	1.026
Water	26.04	17.95	43	20.40	195	3.9	16.44	9.16	8.78	1.043
Water	26.48	18.28	44	20.45	300	3.9	16.44	10.69	10.44	1.024
Water	43.45	38.35	72	38.80	97	4.7	16.65	3.89	3.92	0.992
Water	41.64	25.20	24	29.18	84	4.7	16.65	13.75	13.11	1.049
Water	44.54	26.00	21	29.75	175	4.7	16.65	20.13	19.69	1.022
Water	43.50	35.10	57	35.48	350	4.7	16.65	9.76	9.59	1.018
SB165	24.65	17.20	45	20.00	98	4.5	16.45	6.72	6.31	1.065
SB346	24.93	18.25	50	20.95	99	4.0	17.2	5.81	5.83	0.997
SB589	25.05	18.50	51	21.30	99	3.3	17.0	5.90	5.89	1.002
Lucite Paint	42.40	25.73	24	29.41	124	3.2	17.8	14.97	14.66	1.021

Note: SB346 = styrene-butadiene copolymer latex with an average particle diameter of 346 nm

REFERENCES

1. Vanderhoff, J. W., British Polym. J., 2, p 161 (1970)
2. Vanderhoff, J. W., Bradford, E. B., Carrington, W. R., J. Polym. Sci. Symp. Ser. No. 41, p 155 (1973)
3. Witneyer, R. J., "Drying Rates of 60:40 Styrene-Butadiene Latexes", M. S. Research Report, Chem. Engr. Dept., Lehigh Univ., 1973
4. Poehlein, G. W., Vanderhoff, J. W., Witmeyer, R. J., Polymer Preprints, 16(1), p 268 (1975)
5. Patton, T. C., Paint Flow and Pigment Dispersion, Wiley-Interscience, N.Y., 1979
6. Pramojaney, N., "Drying Rates of Latex Films," M.S. Research Report, Chem. Engr. Dept., Lehigh Univ., 1977.
7. Isaacs, P. K., J. Macromol. Chem., 1, p 163 (1966)
8. Kays, W. M., Convective Heat & Mass Transfer, McGraw-Hill, N.Y., 1966
9. Eckert, E. R., & Drake, R. M., Jr., Analysis of Heat & Mass Transfer, McGraw-Hill, N.Y., 1972
10. Sherwood, T. K., Pigford, R. L., & Wilke, C.R., Mass Transfer, McGraw-Hill, N. Y., 1975
11. Dropkin, D., Cornell Univ. Engr. Exprmtl. Station Bulletin No. 23 (1936) and Bulletin No. 26 (1939)

SEARCH METHODS THROUGH SIMULATION FOR PARAMETER OPTIMIZATION OF DRYING PROCESS

R. BERTIN, Z. SROUR

G.R.A.I. Université de Bordeaux I
TALENCE - FRANCE

ABSTRACT

The paper is concerned with parameter optimization through simulation of drying process. These types of problems arise in two areas :-(i) search of unknown parameters by identification methods (fitted parameters).(ii) search of optimum parameters for optimizing dryer operation.
In this paper, we carry out the search of the optimal production capacity of a tunnel-dryer. The production of dried foodstuffs is studied versus tray loading and truck speed. We take into account as constraints, the product quality using the maximum temperature and the final water content of the product. The results shown are in agreement, with similar results deduced from experimental optimization (on different foodstuffs), given in literature.

NOMENCLATURE

a = Surface area per unit volume (m^2/m^3)
Bi = Biot number ($\alpha R_f/\lambda$)
C = Specific heat ($J/kg°C$)
d_w = Product desorption coefficient (-)
f_1^w to f_5 = functions of product water content (-)
G = Dry gas flow (kg/s)
J = Criterion
l = lenght of the truck (m)
L = Dry solid flow rate (kg/s)
P = Total air pressure (N/m^2)
p = Parameter vector or pressure (N/m^2)
R_f = Dry product external radius (m)
T = Normalized temperature (-)
t = Normalized time (-)
u = Truck speed ($\bar{u}$ averaged over time) (m/s)
v = Air velocity (m/s)
W = Normalized water content of the product (-)
w = Normalized water content of the air (-)
x = Normalized longitudinal coordinate (-)

Greek letters

α = Normalized heat transfer coefficient (-)
β = Normalized mass transfer coefficient (-)
Δh_v^m = Latent heat of vaporization (J/kg)
Δh = Normalized latent heat of vaporization (-)
λ = Steplenght
ρ_s = Density of bone-dry solids (kg/m^3)

Subscripts

a = Air
g = Gas phase
i = Initial or indice
j = Indice
k = Indice
n = Value used to normalize
p = Product
s = Dry solid
sat = Satured water vapor
surf = Surface

Supercripts

exp = Experimental value
th = Theoretical value
$\hat{}$ = Optimal value
A, a, B, b, c, d, e, g, U, β_k are defined in the following equations of the paper.

INTRODUCTION

Drying processes are energy-consuming, so the problem of their optimization is very important (1)
In this paper we try to give guidelines to optimize dryer operation. The criteria which may be chosen by the process analyst are production and/or profit, and/or quality, and/or energy consumption. In fact we must take into account several of them, firstly by a weighted sum of these partial criteria or secondly as constraints as in this paper.
In order to design and/or optimize dryer operation it is necessary to get a mathematical model and often to identify some unknown parameters of this model (model fitting) these methods are known as identification methods (2), (3), (4), (5). These last methods use the same computational techniques as optimization methods (6), (7), (8). In identification methods we search the unknown parameters and to reach this goal we take a weighted least squares criterion between experimental data and model values.
There are many papers and books about identification methods (2), (3), (4), (5) but few deal with the identification of drying process (9), (10), (11). On other hand there are many papers about optimization of drying process (12), (13), (14).
In this paper, we present the two steps that we find in practice. Identification of unknown para-

meters of the model, before the second step, optimization of the criterion. Here we take it, as production capacity of a co-current dryer. The quality of the product is taken into account as constraints.

PROBLEM FORMULATION

To carry out an optimization problem of a drying process we must known : its mathematical model, the criterion to be optimized and the different constraints.
An search algorithm is used to change the parameters towards their optimum corresponding to the optimal criterion (Maximum or minimum), without violating any constraints. The Figure 1 shows the optimization method through simulation.
We make a slight difference between identification methods (model fitting), as shown in Figure 2, and optimization methods.

Problem statement

When we optimize (maximize or minimize) the following criterion :

$$\text{Max (or Min) } P_j = J_j (p_1, - - - p_n) \qquad (1)$$

subject to the constraints :

$$a_i \leq p_i \leq b_i \quad i \in [1,n] \qquad (2)$$

The constraints a_i to b_i $i \in [1, n]$ are known. However $J_j(p)$, with vector $p = [p_1 - p_n]^T$, must be calculated through simulation.
When there are several partial criteria, the criterion function is given by :

$$\text{Max (or Min) } P_j = \sum_{j=1}^{m} c_j J_j (p) \qquad (3)$$

Where c_j are the weighting coefficients, there are usually normalized, the sum is equal to 1.

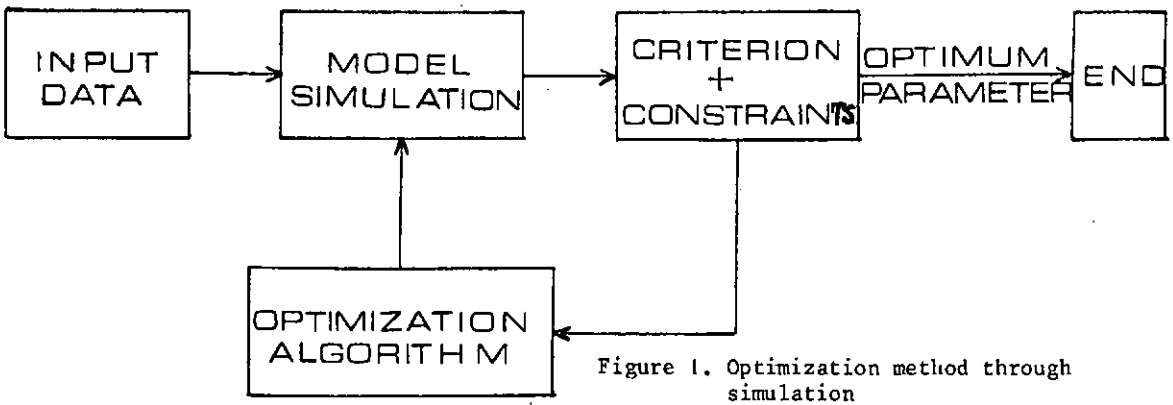

Figure 1. Optimization method through simulation

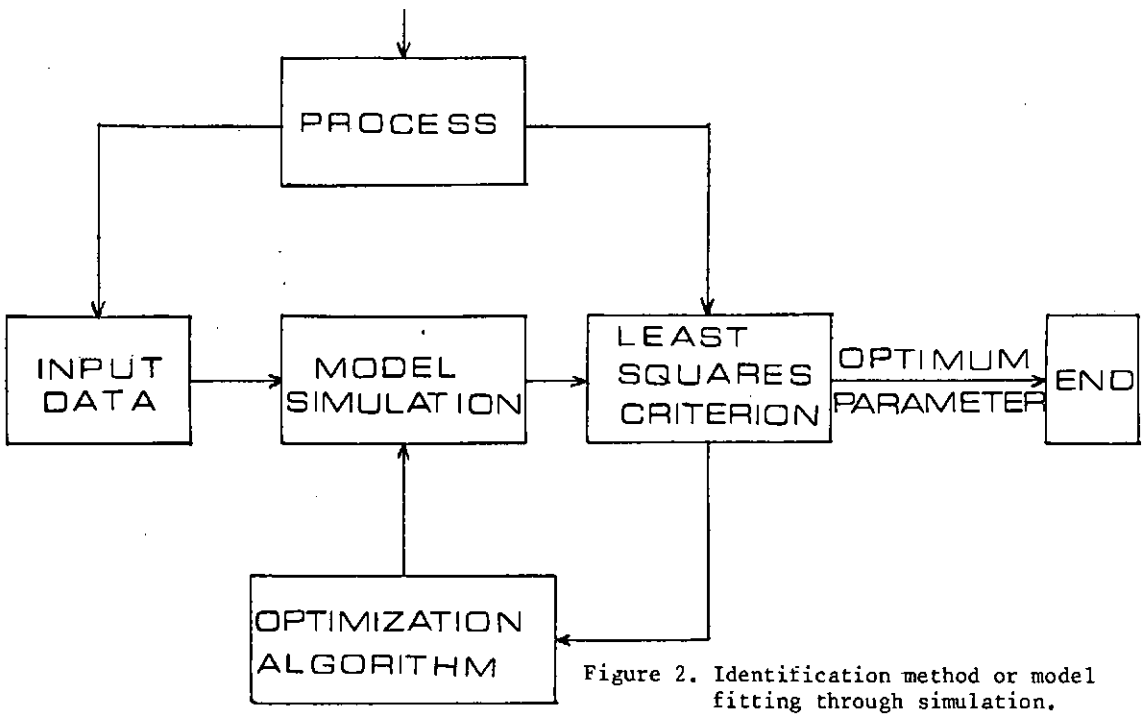

Figure 2. Identification method or model fitting through simulation.

When there are some criteria to be maximized and others to be minimized we obtain :

$$\text{Max } P = \sum_{j=1}^{s} c_j J_j(p) - \sum_{j=s+1}^{m} c_j J_j(p) \quad (4)$$

Optimization methods

We only summarize the usual computational methods. Hence there are many books and papers about this subject (6), (7), (8). Among these methods we must point out two classes :

- (i) Direct search methods

- (ii) Gradient methods

The first methods use different algorithms to progress from point to point. The main algorithms are: coordinate search, pattern search of Hooke-Jeeves (6), rotating coordinate of Rosenbrock (15), Simplex of Nelder and Mead (16)
The second methods require to calculate the derivatives of the function taken as criterion . The search towards the optimum is the gradient direction .The main methods are : steepest descent (or ascent for a maximum), conjugate gradient methods. The disadvantages of steepest descent is that the average rate may be very slow.Therefore there are conjugate gradient which are highly efficient search techniques as the Fletcher-Reeves method (7) to accelerate convergence. This method, by acceleration step search, is not time-consuming on digital computer.
We must indicate also the Powell's method (7) which uses conjugate directions but it does not require evaluation of derivatives.

- Steepest descent method. Let J(p) the criterion to optimize, it is a function of the vector parameters p from a current point p(k) the algorithm is given by :

$$p(k+1) = p(k) - \lambda(k) \nabla J(p(k)) \quad (5)$$

Where $\lambda(k)$ is the steplength, the simulation permits to estimate the gradient direction $\nabla J(p(k))$. Simulation trials are then conducted, along this direction to a new point p (k + 1)
- Precise sequences of the algorithm :
1/ Identify the known experimental region
$a_i \leq p_i \leq b_i$
2/ Initialization
3/ Perform simulation trials at each step. Calculate the gradient vector $\nabla J(p)$

4/ Apply the appropriate optimization technique to locate the next point
5/ Repeat procedure from step 3 until there is no change from iteration to iteration. It is possible to choose a variety of "stopping rules".
- Fletcher-Reeves method. The algorithm for minimizing a function is :
1/The initial step is in the direction of steepest descent $d_1 = - g_1$ with g_1 equal to the gradient $\nabla J(p)$ which is calculated
2/ Compute $p(k+1) = p(k) + \lambda(k)\, d_k$ (6)
3/ Compute the gradient vector g_{k+1} and

$$\beta_k = g^2_{k+1} / g^2_k \quad (7)$$

4/ Compute the new direction given by :

$$d_{k+1} = - g_{k+1} + \beta_k d_k \quad (8)$$

where d_{k+1} and g_{k+1} are vectors
We must know that these different computational techniques must be easy get from the library subroutines of the computer used ; or from different code centers (Argonne Code Center. U.S.A., Harwell Library, England ; N.E.A. DATA BANK, France).

Identification methods

In this case the algorithms used are the same ones as optimization methods. The criterion to be minimized, in this case, is the weighted least squares criterion, between experimental data and model values (Model fitting). The criterion, weighting by variables, is the following one :

$$J(p) = \sum_{k=1}^{K} c_k \sum_{i=1}^{I} e^2_{i,k} \quad (9)$$

In the last formula c_k are the weighting coefficients by variables for K variable number and $e_{i,k}$ is the difference between experimental and model values taken in the same conditions. They depend of the variables and their measurement number is equal to I for each. The procedure was shown on Figure 2.

EXAMPLE : CO-CURRENT DRYER

Modeling

In different papers, we have described the tray and truck dryers of co-current type (18), (19). The truck loading consists of entering by batch operation trucks at feed time. We must know two types of models, firstly the dryer model itself and secondly the product drying model (fruits in our case). These models are described in several papers by the authors (17), (13) and can be deduced from different books (18), (20) and paper (21). These models are deduced from energy and mass balances at two scales : (i) the dryer itself (ii) the product.
We obtain in normalized from :

$$\left.\begin{aligned} \frac{\partial T_p}{\partial t} &= b_1 \\ \frac{\partial W}{\partial t} &= b_2 \end{aligned}\right\} \text{ Drying Model} \quad (10), (11)$$

$$\left.\begin{aligned} \frac{\partial T_a}{\partial t} + \frac{\partial T_a}{\partial x} &= b_3 \\ \frac{\partial w}{\partial t} + \frac{\partial w}{\partial x} &= b_4 \end{aligned}\right\} \text{ Dryer Model Itself} \quad (12), (13)$$

The coefficients b_1 to b_4 are functions of all the variables.The dimensionless variables are obtained by dividing its by characteristic values. Hence we get for the coefficients :

$$b_1 = f_1 \left[\alpha (T_a - T_p) + \Delta h\, f_2\, b_2\right] \quad (14)$$

$$b_2 = - f_3 \beta_m (w_{surf} - w) \quad (15)$$

$$b_3 = \mu \sigma (\Delta h\, b_2 - f_4\, b_1) \quad (16)$$

$$b_4 = - \mu\psi\, b_2 \quad (17)$$

The dimensionless variables x and t are obtained from coordinate and time respectively by dividing its by (1/v) and 1 then we obtain the main dimensionless coefficients :

$$\alpha = \hat{\alpha}\ 1\ a\ /\ v\rho_s\ C_s \quad (18) \qquad \beta_m = \hat{\beta}_m\ 1\ a\ w_n / v\rho_s W_n \quad (19)$$

$$\Delta h = \Delta h_v\ W_n / C_s\ T_{an} \quad (20) \qquad \mu = (L/G)\ (v/\bar{u}) \quad (21)$$

$$\sigma = C_s / C_g \quad (22) \qquad \psi = W_n / w_n \quad (23)$$

For more details see APPENDIX
The functions f_1 to f_4 take into account shrinkage effect and the variation of specific heat of the product versus water content of the product d. b. By identification with the equations (10) to (13) we can put this model according to the following simple form

$$\frac{\partial U}{\partial t} + A(U) \frac{\partial U}{\partial x} = B(U) \quad (24)$$

for $(x,t) \in]0,1] \times]0,t_f[$
The vector U is equal to $[T_p, W, T_a, w]^T$
T indicates transposed vector, A is a 4 x 4 matrix and B an vector whose elements are b_1 to b_4
The initial and boundary values are :

$$U(x,0) = U_i(x) \qquad x \in [0,1] \quad t = 0 \quad (25)$$

$$U(0,t) = U_o(t) \qquad t \in [0,t_f] \quad x = 0 \quad (26)$$

Identification of parameters

The parameter identification or model fitting consists, for our example, in deducing the heat and mass transfer coefficients from the experimental data. The results are performed through computational techniques of optimization i. e. by comparison between experimental data and model results. The criterion to be optimized is the following weighted least squares criterion :

$$J_{(p)} = \sum_{k=1}^{4} c_k \sum_{i=1}^{I} \sum_{j=1}^{J} e^2_{i,j,k} \quad (27)$$

p is the parameter vector equal to $(\alpha, \beta_m)^T$

T indicate transposed vector, c_k are weighting coefficients. In our case k varies from 1 to 4 because we have four variables and we have a double sum with indices i and j from measurements versus time and space. The value $e_{i,j,k}$ is given by the difference :

$$e_{i,j,k} = U^{exp}_k (x_j, t_i) - U^{th}_k (x_j, t_i, p) \quad (28)$$

In this study the measurements by sensors give the temperature and water content of both air and product.
The mathematical model is simulated on computer DEC. PDP 11/50 using the method of lines (discrete space and continuous integration in time). The continous integration is carried on by a predictor - corrector algorithm with step size control. The optimum values $\hat{\alpha}$ and $\hat{\beta}_m$ are searched using the discrete conjugate gradient method because of its fast convergence. By this way we have obtained:

$$\hat{\alpha} = 63\ W / m^2\ °C \qquad \hat{\beta}_m = 4.8\ 10^{-3}\ kg/m^2\ s$$

We can note that we have a better sensitivity versus the mass transfer coefficient than the heat transfer coefficient.

Optimization of the dryer production

To carry on an optimization problem of a process we must know:
- Its mathematical model and the values of its paramaters.
- The criterion to be optimized and the different constraints of the process.
- Some parameters must be deduced from measurements at small scale and the others are obtained by identification methods (model fitting). The choice for optimizing criterion of drying process may be : Production, Energy consumption, Quality of the product, Profit. In practice we take into account several of them as partial criteria, or one as criterion and the others as constraints. For example, in this paper we take capacity production of the tunnel dryer as the only criterion and the quality of the product as constraint. The product temperature must not exceed 76° C to keep good quality and the final water content of the product must stay under an average value of 0.3 Kg/kg d.b. In a next step we shall take into account energy consumption as partial criterion together with capacity production. In this study, we take the production as criterion, because it is very important to dry a large amount of fruit during a short time.

We optimize the capacity production of the dryer with certain parameters equal to constants ; because they have small influence or they are difficult to change in industrial conditions. Experimental measurements in laboratory oven and in industrial dryer are used, as initial data, for these parameters.
We study the variation of the production which depends on truck speed and tray loading (or mass of product per truck). The input air temperature is controlled to get the input product temperature equal to the constraint during the final time. While the velocity and humidity of the input air are equal to constants, so is the dryer length.
The main numerical values taken in the program are the following ones :
- Relative humidity 15 %
- Air velocity 3 m/s
- Tunnel length 9 m (corresponding to nine trucks)

The search towards optimum value of the product uses the discrete conjugate gradient algorithm, given by library routine. This search is performed through model simulation without violating any constraints (22). The simulation is carried out by mean of integration algorithm, the method of lines since the mathematical model is a partial differential equations system. The method of lines changes the last system to an ordinary

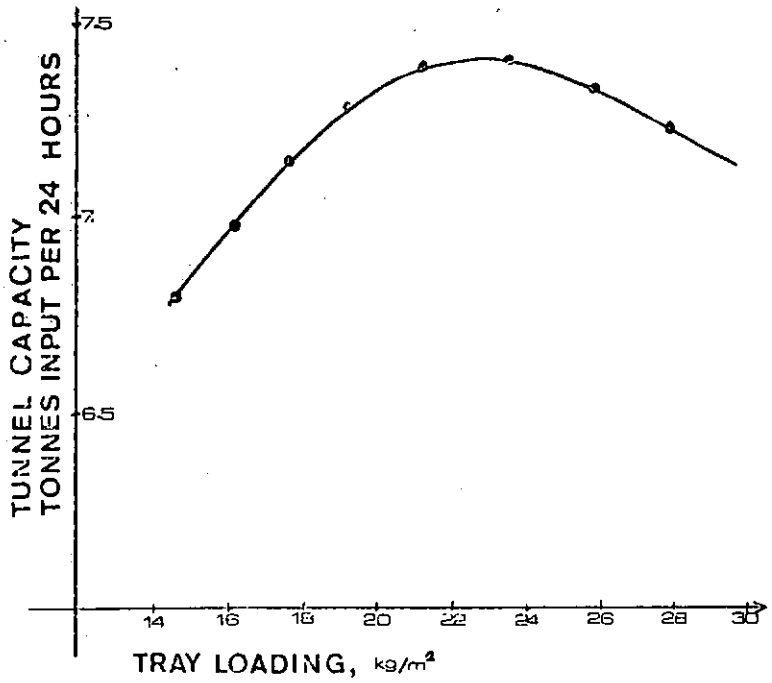

Figure 3. Effect of tray loading near the maximum upon tunnel capacity in dehydrating prunes co-current tunnel 9 trucks, drying to 0.3 kg/kg d.b. moisture. Results obtained from model simulation.

differential equation system which is integrated by a predictor-corrector algorithm (23).
Other study had been carried out with a simpler model (ordinary differential equations system) if we suppose continuous loading (13).
We obtain a maximum for the production capacity versus tray loading by variation of truck speed. The results obtained are in agreement with experimental optimization on similar industrial dryers, for different foodstuffs, given by Kilpatrick et al (19). On other hand we obtain with slight differences the same results using the simple model. The Figure 3 shows the results near the maximum.

CONCLUSION

This paper has shown the different search methods for optimizing parameters through simulation and using computational techniques. These methods may be carried on for identification of unknown parameters (Model fitting) and for production optimization of co-current dryer. The integration and optimization programs used may be get from different routine libraries.
On other hand this study may be applied to others dryers and with several criteria.
The theoretical search for optimal capacity production versus tray loading permits to give guidelines towards an overall optimization of the dryer. Our next step could be optimization by taking into account energy consumption.
The optimization results can also help optimal design and give the set points for an optimal automatic control.

REFERENCES

1. Flink, J.M., Energy analysis in dehydration processes, Food Technology, Vol.31, p. 77-84, 1977.
2. Eykhoff, P., System Identification., J. Wiley, N.Y., 1974.
3. Bard, Y. Nonlinear parameter estimation, Academic Press, N.Y., 1974.
4. Sage, A.P., and Melsa, J.L., System Identification, Academic press, N.Y., 1971.
5. Richalet, J., Rault, A., and Pouliquen, R., Identification des processus par la méthode du modèle, Gordon et Breach, London, 1971.
6. Cooper, L., and Steinberg, D., Introduction to methods of optimization, W.D. Saunders Company, London, 1970.
7. Walsh, G., R., Methods of optimization, J., Wiley, N. Y., 1975.
8. Pierre, D. A., Optimization Theory With Applications, J., Wiley, N.Y., 1969.
9. Kacki, F., and Niewierowicz, T., A hybrid System of Identification of industrial processes of mass and heat transfer, Digital Computer Applications to Process Control, IFAC and North Holland, P. 607-615, 1977.
10. Bertin, R., and Srour , Z., Identification of a distributed process of heat and mass transfer using multilevel, Preprints 5th IFAC, Symposium on Identification and Systems Parameter Estimation, Darmstadt, Germany, p. 1257-1263, 1979.
11. Beckwith, W.F., Beard, J.N. and Gross, R.L., The Optimization of Textile Tenter Fram Dryer Operations, Presented at 1st Symposium on Drying, p. 168-174, 1978.
12. Bolvary-Zahn, W.D., Optimierung von Bandtrocknern, Chem. Ing. Tech., Vol.39, p. 254-259, 1967.
13. Bertin, R., Blazquez, M., and Cazaubon, C.,

Modeling and optimization of a dryer, J.A.E.R., (to appear).
14. Niewierowicz, T., Application of hybrid computers to optimization of drying process, AICA Symp. on Hybrid Computation in dynamic systems design, Rome, 1974.
15. Rosenbrock, H.H., An automatic method for finding the greatest or least value of a function, comput. J., Vol. 3., p. 175-184, 1960.
16 Nelder, J.A., and Mead, R.A., Simplex method for function minimization, comput. J., Vol., p. 308-313, 1965.
17. Bertin, R., Pierronne,F., and Combarnous, M., Modeling and simulating a distributed parameter tunnel-drier, J. Food Sci., Vol. 45, p. 123-125, 1980.
18. Keey, R.B., Introduction to industrial drying operations, Pergamon Press, Oxford, 1978.
19. Kilpatrick, P.W., Lowe, E., and Van Arsdel, W.B., tunnel dehydrators for fruits and vegetables, Advance in Food research, Vol. 6, p. 314-359, 1955.
20. Luikov, A.V., Heat and Mass Transfer in Capillary Porous Bodies, Pergamon Press, Oxford, 1966.
21. Babukha, G.L., and Shraiber, A.A., Interphase heat transfer in poly-disperse gas suspension flows 5th Int-Transfer Conference, Tokyo, Vol. 5, p. 69-73, 1974.
22. Biles, E.W., Strategies for optimization of multiple reponse simulation models, Presented at Winter Simulation Conference, p. 135-142, 1977.
23. Gear, C. W., Numerical Initial Value Problems in Ordinary Differential Equations. Prentice Hall, N.J., 1971.

APPENDIX

Dimensionless functions :

$$T_{surf} = T_p + (Bi / 5\alpha)\, f_5\, b_1$$

$$p_{surf} = p_{sat}\,(T_{surf})\, d_w / P$$

$$w_{surf} = D\, p_{surf} / w_n$$

where D is taken as a constant.

TOWARD AUTOMATIC CONTROL BY MICROPROCESSOR FOR CONVECTIVE DRYER SYSTEMS

C. CAZAUBON, R. BERTIN, and M. BLAZQUEZ

GRAI, Université de Bordeaux 1
Talence, France

ABSTRACT

The aim of this paper is to present a control scheme for a tunnel-dryer. This study is applied to discontinuous dryers with trucks and trays used for foodstuffs (fruits in our case).
The automatic control is obtained from two steps : (i) off line : data from simulation and optimization using a dryer model, data from simulation of the model of the heating system. (ii) on line : automatic control by microprocessor of the dryer.
We take the maximum production as a criterion and the optimization problem has to satisfy some constraints, for example the final product quality.
The maximum capacity of the dryer is obtained by the simulation of a mathematical model (system of differential equations).
From the results of the optimization, a microprocessor system can change on line the set points of the drying system. On the same way, the model of the heating system gives data to regulate temperature and humidity at the input dryer through the microprocessor system.
With the set of measurements on line, the knowledge of parameters on line and the knowledge of data obtained off line, it is so possible to control the drying process by taking into account the criterion of maximum production.

NOMENCLATURE

b = fruit number corresponding to unit of weight
Bi = Biot number
f_1 to f_6 = functions of product water content
F = energy variation
G = air flow rate
l = length of the dryer
m = mean of inverse weight of sample
M = mass product per truck
N = truck position
Q = probability density function of fruit number
RH = relative humidity of air
t = time
$t(y)$ = drying time
T = normalized temperature
u = truck speed
v = air velocity
w = normalized water content of air (d.b.)
W = normalized free water content of product (d.b.)
x = normalized longitudinal coordinate
y = fruit number per unit of weight
z = distribution of fruit number per unit of weight
α = normalized heat transfer coefficient
β_m = normalized mass transfer coefficient
Δh_v, Δh = normalized latent heats of vaporisation
μ = mean value of y
μ_s = flow rate of dry product to dry air
σ = y standart deviation
σ_s = specific heat ratio of dry product to air
ψ = given constant
θ = air temperature
τ = feed time

Subscripts

a = air
f = final
fr = fresh
i = initial
p = product, plum
r = recycled
surf = surface

Superscripts

Λ = optimum value

INTRODUCTION

The aim of this paper is to point out that automation of process permits to solve some problems of knowledge and control of drying process for a given product.
In the field of drying, there are numerous papers about the knowledge of operating conditions of the process at industrial scale, i.e. for tunnel dryer (1), (2), (3), (4), and at small scale in laboratory oven about the product drying (5), (6). At the opposite, few studies deal with the optimal control of drying process (7), (8). This paper takes as an example a co-current discontinuous tunnel dryer for fruits. The dryer consists of two compartments (1), (2) : the heating system with fans and a heater, the drying system with trays and trucks. For solving an optimization problem, it is necessary to have a mathematical model of the dryer and to know the management directives in order to take into account a

criterion and the constraints. An automatic control by minicomputer is too complex to put on the system and requires a too high financial investment. So we chose a simple automatic control by microprocessor.

THE OFF-LINE OPTIMIZATION PROBLEM

The mathematical model of the process, the criterion to be optimized and the different constraints have to be known for the solution of the off line optimization problem.

Modeling of a tunnel dryer

Two models have been worked out (6), (4). The first one is a simple model for giving an average value of its operation. The second, more complete, gives transient regimes and variations of different temperatures and humidities versus time, at a given place of the dryer. But this last one is too complex (hyperbolic system) ; also for this study, we use the simple one. In this case, we must make some hypotheses to simplify : loading is considered as continuous, input loading and output unloading of trucks are not taken into account. The mathematical simple normalized model is a system of non linear ordinary differential equations (8) :

$$\frac{dTp}{dx} = f_1\left[\alpha(T_a - T_p) + \Delta h_v f_2 \frac{dW}{dx}\right] / \left[1 + (Bi/5) f_6\right] \quad (1)$$

$$\frac{dW}{dx} = - f_3 \beta_m (w_{surf} - w) \quad (2)$$

$$\frac{dT_a}{dx} = \mu_s \sigma_s (\Delta h \frac{dW}{dx} - f_4 \frac{dTp}{dx}) \quad (3)$$

$$\frac{dw}{dx} = - \mu_s \psi \frac{dW}{dx} \quad (4)$$

We add the initial conditions (x = 0)

$$T_p\ (x = 0) = T_{pi} \qquad W(x = 0) = W_i$$
$$T_a\ (x = 0) = T_{ai} \qquad w(x = 0) = w_i \quad (5)$$

and the formula for the normalized surface temperature of the product :

$$T_{surf} = T_p + (Bi/5\alpha)\ f_5 \frac{dTp}{dx} \quad (6)$$

Criterion

To take into account the fact that an important amount of fruit is dried during a short time (drying season), the criterion is the production capacity of the dryer.

Constraints

The two main constraints to satisfy are the final water content of the dried product and the fruit temperature. The first one must be equal to 0.3 Kg/Kg d.b., the last one must not exceed 74° C to keep a good fruit quality.

Optimization parameters

The variables used as control are :
(1) temperature, velocity and relative humidity of inlet air
(2) tray loading or mass of product per truck
(3) truck speed
(4) dryer length (or number of trucks)

Experimental results have shown that optimal relative humidity of inlet air is found to be between 10 % and 20 % ; also we have taken a mean value of 15 %. Moreover a sensitivity analysis has been performed.
The dryer and fruit parameters that we cannot change or have a small influence on the drying process have been kept constant. Their values have been given by experimental results.

Problem resolution

The numerical method for solving this problem uses two algorithms (8) : the first one simulates the mathematical model ; the second one gives the optimum value of the dry product flow, to this end it computes the initial temperature of air and the speed of the trucks to satisfy constraints for different masses of wet fruits on trucks.
The numerical solution is computed on P.D.P. 11/50. These algorithms used for various lengths of dryers and air velocities lead to diagrams (8). The theoretical results obtained are in good agreement with experimental results (2) for different products like foodstuffs.

THE HEATING SYSTEM

Modeling of the heating system

In order to carry on an automatic control of the overall tunnel dryer (dryer and heating system) we make a simple model of the heating system. For this goal, we take into account continuity principle, perfect gas law, and Ramzin formula. The experimental analysis of the heating system operation shows, when the product loading is put :
(1) the air flow rate varies slowly
(2) the air volume necessary to burn the gas is small in comparison with the overall air flow rate.

On other hand, the temperature of the mixture of air is low, hence we can take it as a perfect gas. Then we obtain :

$$RH_i = f\ (G_r, G_{fr}, \theta_r, \theta_{fr}, RH_r, RH_{fr}) \quad (7)$$

for a temperature θ_i given. By this way we get :
(1) the relative influence of the fresh and recycled air flow rate on the humidity of input air (Fig. 1)
(2) the energy consumption (losses are supposed small) (fig. 2)

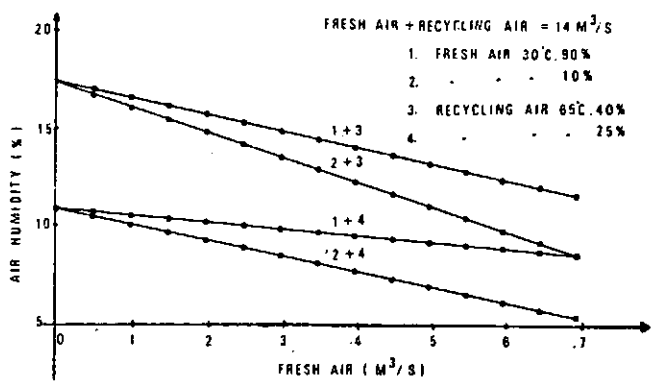

Fig. 1 - Air humidity variation vs fresh and recycling air flow

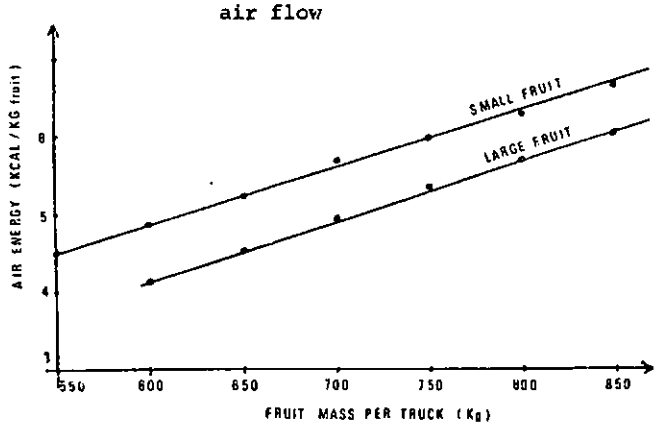

Fig. 2 - Air energy variation vs fruit mass per truck

Automatic regulation

From the model structure we can obtain a classical automatic regulation problem. High values of the time constants of the system permit to carry on a single input regulation by digital P.I.D. regulators (Fig. 3)

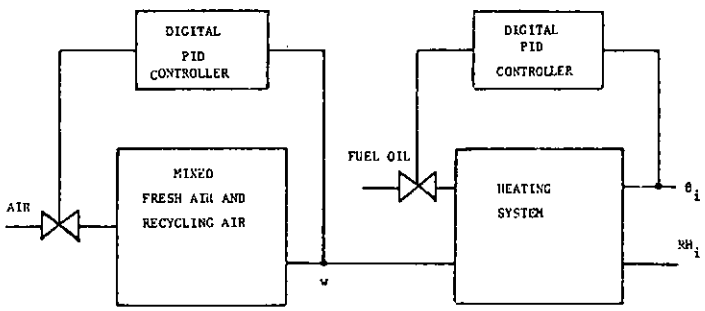

Fig. 3 - Heating system regulation

A more complicated system of automatic regulation does not give better results about overall energy efficiency.

AUTOMATIC CONTROL

The analysis of the results obtained from the optimization problem off-line permits to put the set points at their optimum values for the drying process. This analysis shows the relative influence of the control parameters and the perturbation parameters.

Analysis of the results

-sensitivity study

A study of sensitivity has been carried out on relative humidity of inlet air and on the parameters of the fruit, i.e. weight, water content and initial temperature. Variations of these parameters imply more or less variations of the optimum conditions (speed truck or dry product flow, inlet air temperature).

- Choice of size product

The optimal conditions of drying vary versus the size product. It is necessary to chose the size of fruit to give the best conditions of drying for a maximum of fruits. If we sort out the fruit between two sizes, we must define the boundary between small and large size. For this, we consider the distribution of fruit number by unit of weight, and the energy consumption.
The distribution may be approached by a Gauss' curve (9) :

$$z(y) = \frac{b}{\sqrt{2\pi}} \exp\ (-\ y^2/2) \text{ with } y = \frac{m-\mu}{\sigma} \qquad (8)$$

The energy consumption is a complex function of the product size. In the case without recycled air and near optimum, energy is proportional to drying time.

$$\text{Let } Q(y) = \int_y^{\infty} \frac{b}{\sqrt{2\pi}} \exp\ (-\ \sigma^2/2)\ d\sigma \qquad (9)$$

the probability fruit density and t(y) the drying time. If y_1 is the value of y for getting Q(y) = 0.99, hence $t(y_1)$ is the drying time of largest fruits with 1 % of loss product. In this case

$$F(y) = t(y_1)\left[\ 0.99 - Q(y)\right] + t(y).Q(y) \qquad (10)$$

represents the energy variation. We can find in this way y_0, the value of y which is the boundary between the two fruit sizes, by minimizing this function. The minimum value is get by a simple calculation on computer.

- Speed truck influence

For a given size, drying conditions are optimum only for a well defined weight of fruit. It is necessary to change these conditions to get a correct drying for the whole fruits of the considered size. Analysis of the results shows that we are near optimum values, for the two chosen sizes, with the following conditions :

θ_i = 82 to 85° C RH_i = 15 % v = 4 m/s
M = 700 Kg l = 12 m
u = 0.5 m/hr (small size) or
u = 0.4 m/hr (large size).

We note the influence of the trucks. We can use this result to carry on a simple automatic control after regulating other parameters near indicated values.

Automatic control scheme

From the choice of the size and water content of the fruits we can obtain the optimum values of the drying : temperature and humidity of the input air, air velocity and truck speed. These values are used as automatic control variables.
The sensitivity analysis about the humidity and velocity of the air shows that these values can be taken as constant during the drying time. On other hand when we carried on the study of the heating system we showed that it was necessary to increase or decrease the flow rate ratio of fresh to recycled air to increase or decrease the relative humidity of air. Then, the humidity of air is regulated by a digital P.I.D. controller.
If we take into account the truck loading of the tunnel-dryer, the air velocity varies slowly, then we do not regulate it.
The analysis carried out in the last paragraph shows that the truck speed is very important in comparison with the temperature of input air. Hence, the truck speed is chosen to carry on a simple automatic control by a microprocessor ; the air temperature versus truck speed is regulated near its set point. The chart flows of Fig. 4 and Fig. 5 indicate the automatic control.

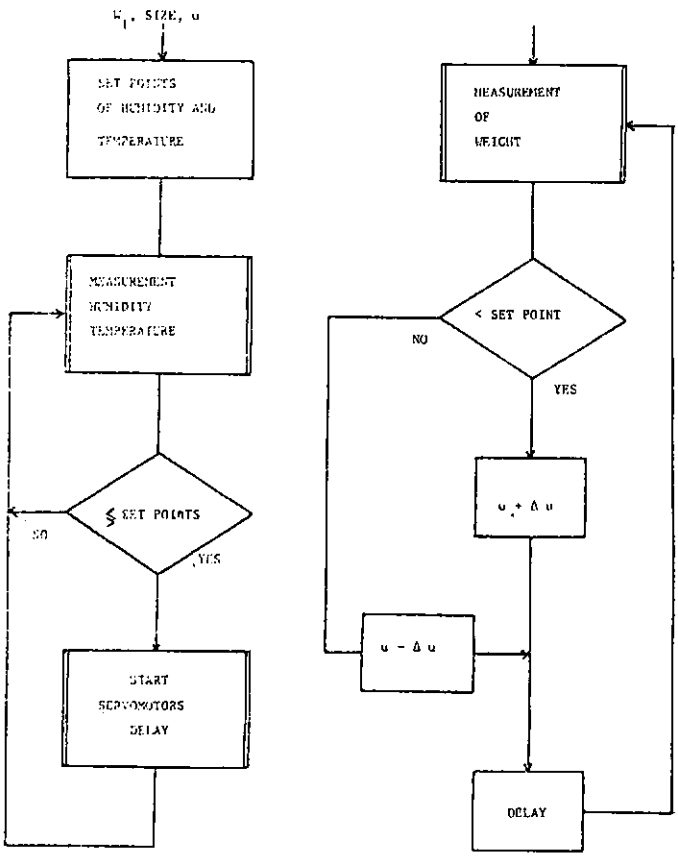

FIGURE 4 : TEMPERATURE, HUMIDITY OF INPUT AIR AND TRUCK SPEED REGULATIONS

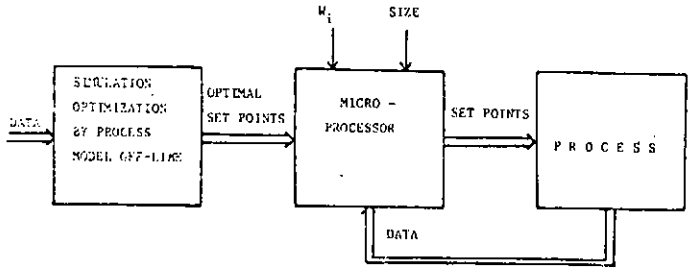

FIGURE 5 : OVERALL AUTOMATIC CONTROL

AUTOMATIC CONTROL BY MICROPROCESSOR

Practical control scheme

The simulation and the last automatic control are get from a simple model : we suppose a continuous loading of the trucks.
In the real case of the process, fruits are put on trays and the trucks enter the tunnel by a batch operation. Hence it is necessary to change the set points to this real case. The changes are carried on the truck speed and the input air temperature.
The truck speed u is replaced as variable by the feed time τ. The procedure used is the following one : the measurement of the truck weight is carried on at the position N (corresponding at the tunnel length), from this result we increase or decrease τ by $\Delta\tau$; the truck at position N is then put at the position N + 1 or taken off.
For the input air temperature we have taken a staircase function whose mean value is equal to the optimum value calculated (Fig. 6).

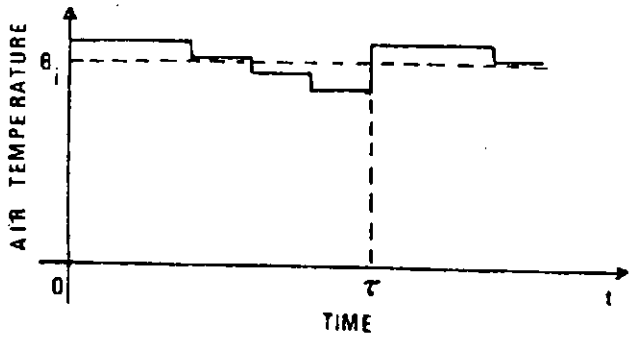

Fig. 6 - Shape of the input air temperature control

The duration of the first step is more large to take into account the perturbation of the input of a new truck.

Simulation of the automatic control by microprocessor

The drying process is simulated in a laboratory oven controlled by the T.D.S. Motorola system.

The temperature and humidity of air, the final weight of the samples are measured by gauges to get analog values proportional to their variations. These gauges are connected to peripheral interface adaptator by mean of a 8 bit analog digital converter. The conversion is carried on by the microprocessor system.
The large values of time constants of the process permit to examine by polling the different measured variables and to carry on the different automatic control and regulation. Time is measured independently by a timer which controls the running of the main program by an interrupt service routine. The initialization sequence puts into the routine the values of set points, if the product size and the final weight of the samples are known.
The block diagram and the flow chart are given by Fig. 7 and Fig. 8.

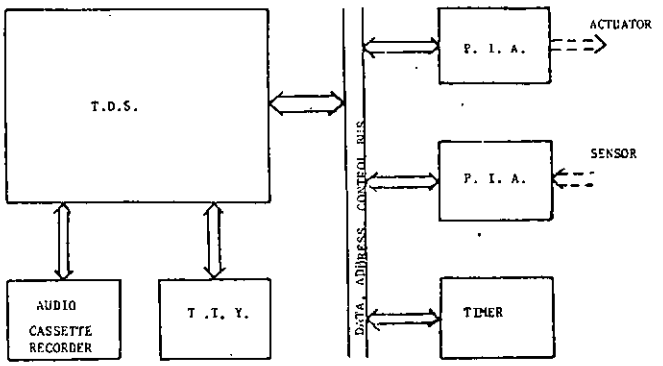

FIGURE 7 : AUTOMATIC CONTROL SIMULATION BY MICROPROCESSOR

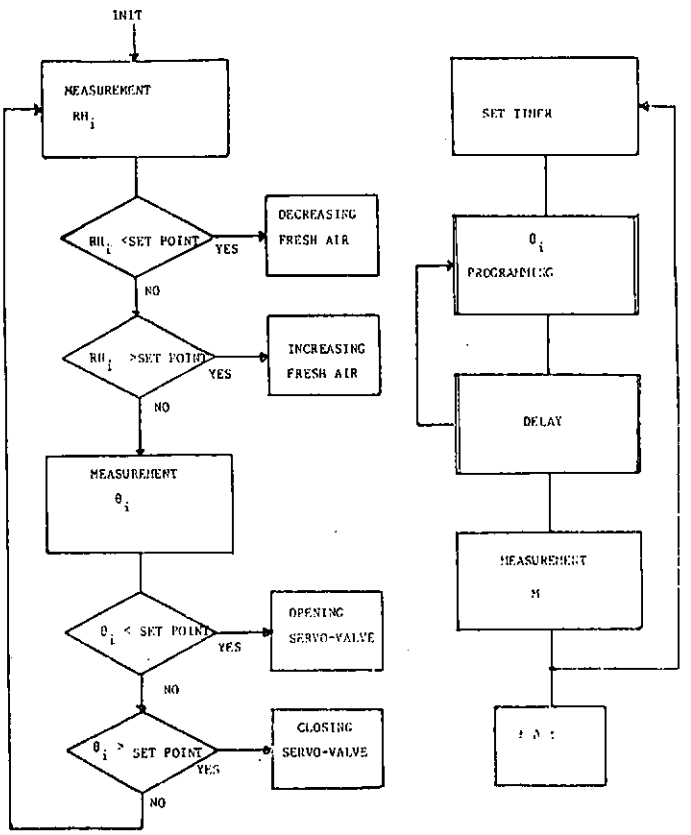

FIGURE 8 : AUTOMATIC CONTROL BY MICROPROCESSOR

CONCLUSION

The results of this study are in fact only suboptimal conditions of drying in comparison with the process itself. We have used simplifying hypotheses to elaborate the mathematical model. We have considered the actual structure of a tunnel-dryer and, in this case, we can only control the input parameters ; a distributed control would be more convenient. Finally the results given for two sizes come in fact from two well defined weight classes.
The theoretical search of optimal operation of dryer shows the different parameters which influence the production capacity and gives their optimum values. The study may be extended to dryers of different types (counter-current and conveyor dryers).
Using a microprocessor system on these dryers it is possible first to regulate the set points, then to change their values according to the perturbations of inlet air and fruit size.

REFERENCES

1. Gentry, J.P., Miller, M.W., and Claypool, L.L., engineering and fruit quality aspects of prune dehydration in parallel and counter-flow tunnels, Food Technology, Vol. 9, p. 121-125, 1965
2. Kilpatrick, P.W., Lowe, E., and Van Arsdel, W.B., Tunnel dehydrators for fruits and vegetables, Advance in food research, vol. 6, p 314-359, 1955
3. Keey, R.B., Introduction to industrial drying operations, Pergamon Press Oxford, 1978
4. Bertin, R., Pierronne P., and Combarnous, M., Modeling and simulating a distributed parameter tunnel drier, Journal of Food Science, vol. 45, p 122-125, 1980
5. Perry, R.L., Heat and Vapor transfer in the dehydration of prunes, Trans. A.S.M.E., vol. 66 p 448-456, 1944
6. Bertin, R., Pierronne F., and Combarnous M., determination des paramètres de séchage de certains fruits compacts, Ann. Technol. Agric., vol. 27, p 489-500, 1978
7. Bolvary-Zahn, W.D., Optimierung von Bandtrocknern, Chem. Ing. Tech., vol. 39, p 254-259, 1967
8. Bertin, R., Blazquez, M., and Cazaubon C., Modelling and optimisation of a dryer, J.A.E.R., (to appear)
9. Bertin, R., Blazquez, M., Cazaubon, C. and Letang G., étude du séchage de la prune d'Ente en séchoir tunnel, GRAI Laboratory report, 1977

THE MATHEMATICAL MODEL OF FINAL TEMPERATURE BEHAVIOUR FOR TEXTILE MATERIALS IN A DRYING CHAMBER

J. Spirnek

Research and Development Centre
of Automation and Instruments of Precision, Łódź, Poland

ABSTRACT

The present paper deals with the analysis of relationships between the kinetic and dynamic characteristics of the industrial drying process for textile materials. It is the aim of this paper to formulate differential equations describing dynamic behaviour of the final temperature θ_k of the material subjected to drying after coming out of a drying chamber and to give on this basis a simple method for the identification of the control channel of the process (the velocity of the dried material v - the increase of final temperature θ_k). Relationships will be derived between the longitudinal temperature distribution of the drying material due to the final temperature behaviour of this material which is the result of the disturbances or planned changes of the process parameters. This paper is a continuation of the article (5).

NOMENCLATURE

A = heat transfer area, m^2

c_{MW} = specific heat of the dried material, J/kG^oC

c_{MS} = specific heat of the dry material, J/kG^oC

D_1 = dimension of the dried material, m

h = specific latent heat of vaporization J/kG

$K_{II}(t)$ = time function for the time interval of the falling drying rate period, 1/s

l_s = length of drying zone drying chamber , m

q_s = density of the stream of heat supplied to the dried material, W/m s

q_{MW} = the amount of heat flow required for the phase change and amount of heat flow required for moisture and vapour transfer in the dried material, W/m s

t = time, s

t_c = heat delay time interval, s

$\bar{t}_T$ = transportation delay, s

$\bar{t}$ = time constant or time interval characterizing the drying curve and transient characteristics, s

V = velocity of the movement of the dried material in the drying chamber, m/s

$\hat{V}$ = volume of the drying zone, m^3

X = average moisture content in the measuring zone of dimensions D_1 D_2 D_3, %

X_k = final moisture content, %

X_{KR} = critical moisture content, %

X_R = equivalent moisture content, %

x,y,z = space coordinates

α_{MW} = heat transfer coefficient of the dried material, $W/m^{2o}C$

ε = factor accounting for the increase of the evaporation surface caused by its roughness.

j_W = mass of moisture transferred in the dried material, kG

j_P = mass of vapour transferred in the dried material, kG

θ_M = temperature of the dried material, ^oC

θ_{MW} = wet bulb temperature, ^oC

θ_k = final temperature of the dried material leaving the drying chamber, ^oC

$\hat{\theta}$ = temperature of the material at any point $\hat{\theta}(x,y,z,t)$, ^oC

ρ_{MS} = specific mass of the dry material, kG/m^3

ρ_{MW} = specific mass of the dried material, kG/m^3

τ = time measured from the moment the material leaves the drying chamber, s

ϕ_o = final temperature component, ^oC

$\mathcal{H}$ = moisture transfer factor, m^2/s

$1(t)$ = unit function

INTRODUCTION

One of the controllable parameters of the drying process is the temperature of the material leaving the drying chamber, Θ_k. Among others it is useful in the case when a direct measurement of the final moisture content X_k (e.g. loose textile fibres) is not possible, and thanks to the measurement of the final temperature we can infer, on the basis of the function $X_k = f(\Theta_k)$, about the value and changes X_k of the basic and controllable parameters of the process. Another reason is the temperature limits resulting from the physical properties of a material and set by technologists, either to protect the material from damage, or to maintain thermic stabilization. At the present stage of knowledge a controllable process should take the optimal course. The essential condition of the optimal control is the knowledge of the process expressed as a mathematical model. The basis for constructing a mathematical model is a description of the heat and moisture transfer taking place in a material being dried. This paper deals, from the point of view of the drying process control, with the temperature changes of the dried material resulting from heat transfer.

THE EQUATION OF HEAT BALANCE IN THE DRIED MATERIAL

The heat balance for the area A_v of the volume V and the heat transfer area A_s of the dried material moving through the drying space at constant velocity v, in a given time unit, can be expressed by the following equation:

$$\iiint_{\hat{V}} \frac{\partial(c_{MW}\rho_{MW}\Theta_M)}{\partial t}\,d\hat{V} = \iint_{\hat{A}} q_s\,dA - \iiint_{\hat{V}} v\frac{\partial(c_{MW}\rho_{MW}\Theta_M)}{\partial y}\,d\hat{V} + \iiint_{\hat{V}} q_{MW}\,dV. \qquad (1)$$

where:

$\iiint_{\hat{V}} \frac{\partial(c_{MW}\rho_{MW}\Theta_M)}{\partial y}\,d\hat{V}$ - storing the heat energy in the area A of the dried material of the volume $\hat{V}$ and heating transfer area A in a given time unit,

$\iint_{\hat{A}} q_s\,dA$ - the heating medium flow rate passing through the heating transfer area A of the area A in a given time unit,

$\iiint_{\hat{V}} \frac{\partial(c_{MW}\rho_{MW}\Theta_M)}{\partial y}\,d\hat{V}$ - heat variation caused by the convection of heat energy of the dried material A_v area with velocity v, together with this material in a given time unit

$\iint_{\hat{A}} q_{MW}\,dA$ - heat energy necessary for moisture liberation and phase change in a given time unit, taken from area A of the dried material,

where:

$\rho_{MW} = \rho_{MS}(1+X)$ - specific mass of the dried material

$c_{MW} = \frac{c_{MS} + X}{1 + X}$ - specific heat of the dried material

$q_s = \alpha_{MW}\nabla\Theta_M$ - density of the stream of heat supplied to the dried material

$$q_{MW} = \underbrace{h\varepsilon\rho_{MS}\frac{\partial X}{\partial t}}_{\text{the amount of heat given back at the phase change}} + \underbrace{c_W j_W \nabla\Theta_M + c_p j_p \nabla\Theta_M}_{\text{the amount of heat used for moisture and vapour transfer in the dried material}}$$

j_w - mass of moisture transferred with material through equipotential surface unit within time unit (density of mass stream)

j_p - as above, but according to vapour.

Taking the following into consideration:

$\iint_{\hat{A}} q_s\,dA = \iiint_{\hat{V}} \nabla q_s\,dV$ according to Ostrogradski-Gauss, law

$c_W j_W \nabla\Theta_M = c_W v_W \rho_W \nabla\Theta_M$,

$c_p j_p \nabla\Theta_M = c_p v_p \rho_p \nabla\Theta_M$,

v_W - velocity of moisture transfer in the material,

v_p - velocity of vapour transfer in the material,

the heat balance can be expressed by the following equation:

$$\rho_{MW}c_{MW}\frac{\partial\Theta_M}{\partial t} - \alpha_{MW}\nabla^2\Theta_M + v\rho_{MW}c_{MW}\frac{\partial\Theta_M}{\partial y} + c_W v_W \rho_{MW}\Delta\Theta_M + c_p v_p \rho_{MW}\nabla\Theta_M + h\varepsilon\rho_{MS}\frac{\partial X}{\partial t} + c_W\rho_{MS}\Theta_M\frac{\partial X}{\partial t} = 0. \qquad (2)$$

The method of material drying in industrial convection dryers results in uniformity of the moisture transfer process in the direction of longitudinal axis z and transversal axis y, i.e. moisture translocates in the direction of the material axis x

(see (5) Fig. 1, 2). For the dried materials the amount of heat given out together with moisture and vapour transfer in the material is small in comparison with the amount of heat given out for the change of phase (according to (2), p.67). Taking the above into account and combining the statements

$$\frac{\partial \hat{\theta}_M}{\partial t} + v \frac{\partial \hat{\theta}_M}{\partial y} - k_\theta \frac{\partial \hat{\theta}_M}{\partial x^2} + k_w \frac{\partial \hat{X}}{\partial t} = 0 \quad (3)$$

where:

$$k_\theta = \frac{\alpha_{MW}}{(c_{MS} + c_w X)\rho_{MS}},$$

$$k_w = \frac{h\varepsilon + c_w \theta_M}{c_{MS} + c_w X}$$

KINETIC CHARACTERISTICS

The differential equation (3) presenting changes of temperature in the material has different solutions for different drying periods (Fig. 1).

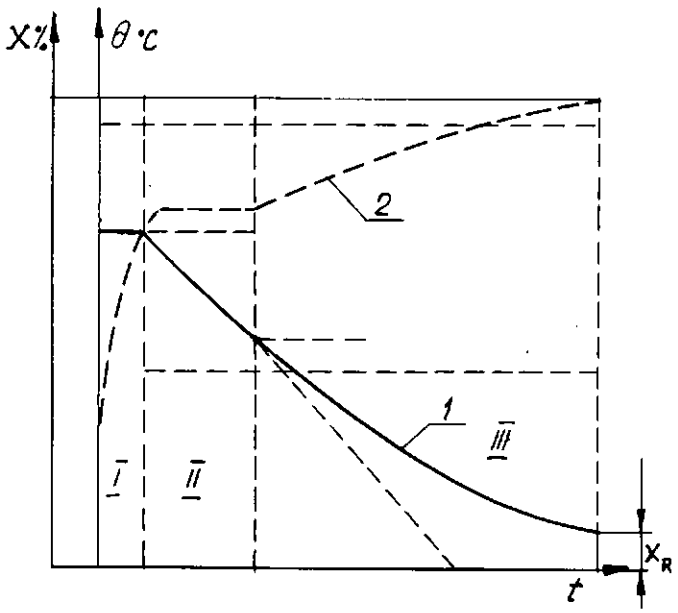

Figure 1. Graphic representation of
1) drying curve,
2) temperature of the drying material
I heating period
II constant drying rate period
III falling drying rate period

During the material warming up period from $t = 0$ up to $t = t_c$ we have

$$\frac{\partial X}{\partial t} \cong 0.$$

Thus equation (3) takes the form:

$$\frac{\partial \theta_M}{t} + V \frac{\partial \theta_M}{y} - k_0 \frac{\partial^2 \theta_M}{x^2} = 0 \quad (4)$$

The boundary conditions:

$$-\alpha_{MW}\left(\frac{\partial \theta_M}{\partial x}\right)_{x = D_1} + q_s = 0,$$

$$\left(\frac{\partial \theta_M}{\partial x}\right)_{x = 0} = 0. \quad (5)$$

For the mean temperature values

$$\theta_M = \theta_M(y,t) = \frac{1}{D_1}\int_0^{D_1} \hat{\theta}(x,y,t)\, dx$$

we have:

$$\frac{\partial \theta_M}{\partial t} + V \frac{\partial \theta_M}{\partial y} - k_\theta \left[\left(\frac{\partial \theta_M}{\partial x}\right)_{x = D_1} - \left(\frac{\partial \theta_M}{\partial x}\right)_{x = 0}\right] = 0,$$

thus,

$$\frac{\partial \theta_M}{\partial t} + V \frac{\partial \theta_M}{\partial y} - k_\theta \frac{q_s}{\alpha_{MW}} = 0. \quad (6)$$

Because of

$$q_s = \alpha_{MW}(\theta_s - \theta_{Mp}) \quad (7)$$

where:

θ_s - temperature of heating medium

θ_{mp} - temperature of the surface of the dried material

and

$$\theta_{Mp} = k_p \theta_M$$

$$\theta_s = \theta_{SMX} - (\theta_{sMx} - \theta_z)\exp\left(-\frac{t}{t_p}\right)$$

θ_z - temperature of the air around the drying chamber

$\bar{t}_p$ - time constant of the heating medium.

Having taken the above into account we obtain the equation:

$$\frac{\partial \theta_M}{\partial t} + V \frac{\partial \theta_M}{\partial y} = k_\theta\left[\theta_{SMX} - (\theta_{SMX} - \theta_z)\exp\left(-\frac{t}{t_p}\right) - k_p \theta_M\right], \quad (8)$$

and its solution:

$$\Theta_M = \frac{1}{k_p}\left[1 - \exp\left(-\frac{t}{\bar{t}_c}\right)\Theta_{SMX} + \right.$$

$$+ \frac{\bar{t}_p}{\bar{t}_p - \bar{t}_c}\left(\Theta_{SMX} - \Theta_z\right)\left[\exp\left(-\frac{t}{\bar{t}_c}\right) - \exp\left(-\frac{t}{\bar{t}_\theta}\right)\right] +$$

$$+ \Theta_z \exp\left(-\frac{t}{\bar{t}_c}\right), \qquad (9)$$

where:

$$\bar{t}_\theta = \frac{\bar{t}_p\,\bar{t}_c}{2\bar{t}_p - \bar{t}_c},$$

$$\bar{t}_c = \frac{1}{k_p k_\theta}$$ - time constant of the heated material.

The warming up period for the dried material is over after $t = t_c$, when dried material reaches the wet bulb temperature. The temperature will remain constant during the period of constant drying rate, i.e. from the moment when material moisture reaches the critical moisture content X_{KR} (Fig. 2).

In the period of falling drying rate differential equation (2) for the mean temperature value Θ_M will take the form:

$$\frac{\partial \Theta_M}{\partial t} + V\frac{\partial \Theta_M}{\partial y} - k_\theta\left[\left(\frac{\partial \Theta_M}{\partial x}\right)_{x=D_1} - \left(\frac{\partial \Theta_M}{\partial x}\right)_{x=0}\right] +$$

$$+ k_w\frac{\partial X}{\partial t} = 0. \qquad (10)$$

Taking the boundary conditions into account

$$-\alpha_{MW}\left(\frac{\partial \Theta_M}{\partial x}\right)_{x=D_1} + q_s - h\left(1 - \varepsilon\right)j_p = 0,$$

$$\left(\frac{\partial \Theta_M}{\partial x}\right)_{x=0} = 0 \qquad (11)$$

and the initial conditions $(t = 0)$

$X(0) = X_{KR}$, $\Theta_M(0) = \Theta_{MW}$,

we have:

$$\frac{\partial \Theta_M}{\partial t} + V\frac{\partial \Theta_M}{\partial y} - k_\theta\left[\Theta_s(y) - \Theta_{Mp}\right) -$$

$$\frac{h}{\alpha_{MW}}\left(1 - \varepsilon\right)\Big]j_p - k_w\frac{\partial X}{\partial t} = 0. \qquad (12)$$

Furthermore, if we take into account (5) (formulae (3), (4) and (11)) we have:

$$\frac{\partial X}{\partial t} = -K_{II}(t)\left(X_{KR} - X_R\right)\exp\left(-\int_0^t K_{II}(t)\,dt\right), \qquad (13)$$

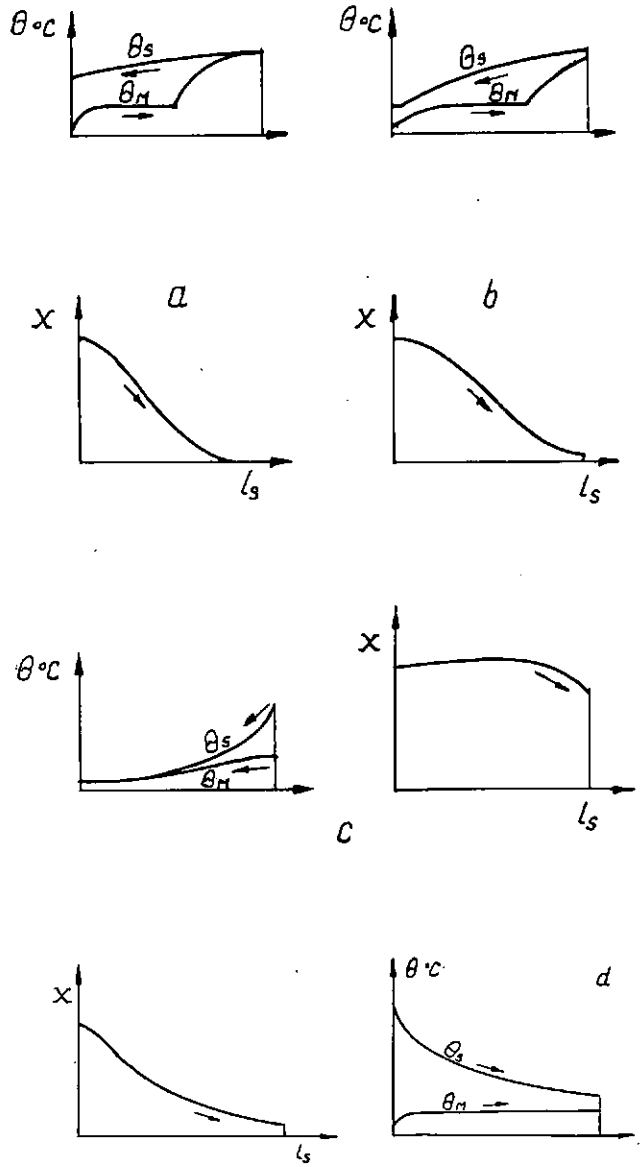

Figure 2. Changes of temperature Θ_s - drying air, Θ_M - dried material
a,b,c - for parallel flow,
d - for counter flow according to (1)

so we have:

$$\frac{\partial \Theta_M}{\partial t} + V\frac{\partial \Theta_M}{\partial y} - k_\theta\left[\left(\Theta_s(y) - k_p\Theta_M\right) -\right.$$

$$+ \frac{h}{\alpha_{MW}}\left(1 - \varepsilon\right)D_1K_{II}(t)\left(X_{KR} - X_R\right)\times$$

$$\times\exp\left(-\int_0^t K_{II}(t)\,dt\right) - k_wK_{II}(t)\left(X_{KR} -\right.$$

$$\left.\left. - X_R\right)\left[\exp\left(-\int_0^t K_{II}(t)\,dt\right)\right] = 0 \qquad (14)$$

or

$$\frac{\partial \theta_M}{\partial t} + V \frac{\partial \theta_M}{\partial y} - k_\theta \left[\left(\theta_s(y) - k_p \theta_M \right) + k_R \left(X_{KR} - X_R \right) \left[\exp\left(- \int_0^t K_{II}(t)\, dt \right) \right] \right] = 0, \quad (15)$$

where:

$$K_R = K_e \frac{h}{\alpha_{MW}} \left(1 - \varepsilon \right) \rho_{MS} D_1 + k_w .$$

In the further discussion we shall not take into consideration the changes of the coefficient in a given time unit,

$$- \int_0^t K_{II}(t)\, dt = - \frac{t}{\bar{t}_a} \text{ at}$$

applying the approximation given by Lykov ((2), p.116, Fig.2-21), i.e.

$$\int_0^t K_{II}(t)\, dt = \frac{t}{\bar{t}_s} , \quad \bar{t}_s = \text{const.}$$

So the equation (15) will take the form:

$$\frac{\partial \theta_M}{\partial t} + V \frac{\partial \theta_M}{\partial y} - k_\theta \left[\left(\theta_s(y) - k_p \theta_M \right) - \left(X_{KR} - X_R \right) \frac{k_p}{\bar{t}_s} \exp\left(- \frac{t}{\bar{t}_s} \right) \right], \quad (16)$$

and its solution at the initial conditions:

$$\theta_M(0) = \theta_{MW}$$

and taking the average values into consideration:

$$k_\theta , \; k_w \quad \text{and} \quad \theta_s(y) = \theta_{SMx} - \theta_L(y) ,$$

takes the form:

$$\theta_M = k_p \theta_{SMx} \left[1 - \exp\left(- \frac{t}{\bar{t}_p} \right) \right] + k_\theta \left[\theta_L(0) \exp\left(- \frac{t}{\bar{t}_p} \right) - \theta_L(y) \right] + k_R \frac{\bar{t}_p - 2\bar{t}_s}{\bar{t}_p \bar{t}_s} \left(X_{KR} - X_R \right) \left[\exp\left(- \frac{t}{\bar{t}_p} \right) - \exp\left(- \frac{t}{\bar{t}_\theta} \right) \right] + \theta_{MW} \exp\left(- \frac{t}{\bar{t}_p} \right), \quad (17)$$

where:

$\theta_L(y)$ - function describing the temperature distribution in the drying chamber caused by natural factors (heater contamination, fresh air supply etc) or caused by the intentional temperature distribution in the drying chamber,

$$\bar{t}_\theta = \frac{\bar{t}_p \bar{t}_s}{\bar{t}_p - 2\bar{t}_s} .$$

The first part of the equation illustrates the influence of moisture evaporation from the dried material, diminishing progressively as time passes, on the dried material temperature. The equation holds in the period of time $0 < t \leqslant t_k$, assuming t_{KR} - for the initial moment ($t = 0$).
The temperature course described by equations (9) and (17) is presented in Fig. 1. For different conditions of temperature distribution in the drying chamber Kröll (1) gives temperature curves presented in Fig. 2.

THE STEADY STATE CHARACTERISTICS

The limited velocity of material transfer through the drying chamber, the constant material temperature in the period of constant drying rate influence the range of final temperature changes in the function of dried material transfer velocity. In order to describe these changes we use equation (17) replacing t (time) by $t_s = l_s/V$ where l_s is the drying chamber length corresponding to the section with a falling drying rate, so

$$\theta_{MR} \leqslant \theta_{MK} \leqslant \theta_{MW}$$

where: θ_{MR} - material temperature corresponding to equivalent moisture content X_R for drying chamber.

Hence we have:

$$\theta_{MK} = k_p \theta_{SMx} - \left[k_p \theta_{SMx} - \theta_{MW} - \theta_L(0) \right] \exp\left(- \frac{l_s}{V \bar{t}_p} \right) + k_R \frac{\bar{t}_p - 2\bar{t}_s}{\bar{t}_p \bar{t}_s} \left(X_{KR} - X_R \right) \left[\exp\left(- \frac{l_s}{V \bar{t}_p} \right) - \exp\left(- \frac{l_s}{V \bar{t}_\theta} \right) \right] - \theta_L(y). \quad (18)$$

The graph of the above equation is presented in Fig. 3.
If necessary, the forms of equations describing the steady state characteristics of moisture and the final temperature of the dried material can be simplified by substituting less complicated forms appropriate for calculating purposes.
When discussing the changes $\theta_{MK} = f(V)$ the influence of evaporation can be left out of account, so we have:

$$\theta_{MK} = k_p \theta_{SMx} - k_p \left[\theta_{SMx} - \theta_{MW} - \theta_L(0) \right] \exp\left(- \frac{l_s}{V \bar{t}_p} \right) - \theta_L(y) \,. \qquad (19)$$

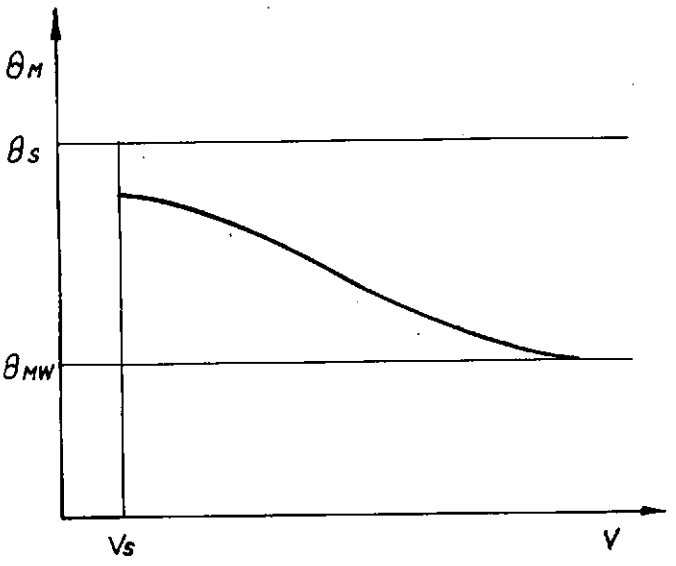

Figure 3. Steady state characteristics $\theta_{MK} = f(V)$ of textile materials

THE DYNAMIC BEHAVIOUR $\Delta\theta_K = \mathcal{C}(t)$ FOR CHANNEL $\Delta V - \Delta\theta_K$

Equation (17), taken as the initial one, will be modified as follows:

$$\theta_{MK} = \frac{1}{k_p} \theta_{SMx} + \underbrace{\left[\theta_{MW} - \theta_{SMx} + k_\theta \theta_L(0) + k_R \frac{\bar{t}_p - 2\bar{t}_s}{\bar{t}_p \bar{t}_s} \left(X_R - X_{KR} \right) \right]}_{\phi_o} \exp\left(- \frac{t}{\bar{t}_p} \right) + - k_R \frac{\bar{t}_p - 2\bar{t}_s}{\bar{t}_p \bar{t}_s} \left(X_{KR} - X_R \right) \exp\left(- \frac{t}{\bar{t}_\theta} \right) - \theta_L(y). \qquad (20)$$

We assume that at the moment $t = 0$ (i.e. at the beginning of the period of falling drying rate), the velocity V_o has been replaced by $V_1 = V_o + \Delta V$, when

$$V_o = \frac{l_s}{t_o} \,, \quad V_1 = \frac{l_s}{t_1} \,.$$

It will result in static change of temperature from θ_{MK_o} to $\theta_{MK_1} = \theta_{MK_o} + \Delta\theta_{MK}$.

We shall evaluate the dynamic changes, taking into consideration the temperature θ_{My} of the point moving in the drying chamber, as shown in Fig. 4. l_s is the length of the drying chamber corresponding to the section with a falling drying rate period.

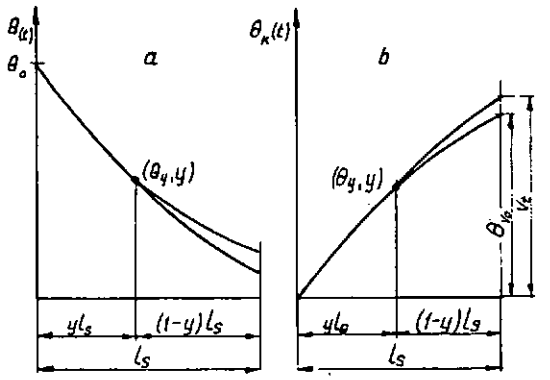

Figure 4. Dynamic characteristics of the process: $\phi = f_1(t)$ at $\Delta\dot{V} = 0$
$\theta_K = f_2(t)$ at $\Delta\dot{V} = 0$

Let us consider only the components of equation (20), being the time function, as they are responsible for dynamic changes of temperature θ_{MK}

First we shall consider the component:

$$\phi = \phi_o \exp\left(- \frac{t}{\bar{t}_p} \right) \qquad (21)$$

The final temperature component, corresponding to the drying time

$$t_o = \frac{l_s}{V_o}$$

will be:

$$\phi_{K_o} = \phi_o \exp\left(- \frac{t_o}{\bar{t}_p} \right). \qquad (22)$$

The component ϕ_y of a point with the coordinate (y, ϕ_y) will be:

$$\phi_y = \phi_o \exp\left(-y \frac{t_o}{\bar{t}_p} \right). \qquad (23)$$

The final temperature component after the velocity change:

$$\phi_{Kt} = \phi_y \exp\left[- \left(1 - y \right) \frac{t_1}{\bar{t}_p} \right]. \qquad (24)$$

Reconsidering equation (22) we obtain:

$$\phi_o = \phi_{K_o} \exp\left(\frac{t_o}{\bar{t}_p} \right). \qquad (25)$$

Substituting it to (23), we have:

$$\phi_y = \phi_{K_o} \exp\left(\frac{t_o}{\bar{t}_p}\right) \exp\left(-y \frac{t_o}{t_p}\right) =$$

$$= \phi_{K_o} \exp\left[\left(1 - y\right) \frac{t_o}{t_p}\right]. \qquad (26)$$

Substituting (26) to (24) we have:

$$\phi_{kt} = \phi_{K_o} \exp\left[\left(1 - y\right) \frac{t_o}{t_p} - \left(1 - y\right) \frac{t_1}{t_p}\right] =$$

$$= \phi_{K_o} \exp\left[\left(1 - y\right) \frac{t_1}{\bar{t}_p} \frac{t_o - t_1}{t_1}\right]. \qquad (27)$$

Taking into account that

$$\frac{t_o - t_1}{t_1} - \frac{V_1 - V_o}{V_o} = \frac{\Delta V}{V_o}$$

and

$$\tau = \left(1 - y\right) t_1 ,$$

for the observer positioned at the end of the process we obtain:

$$\phi_{K_t} = \phi_{K_o} \exp\left(\frac{\tau}{t} \frac{\Delta V}{V_o}\right).$$

Because

$$\Delta \phi_K(t) = \phi_{Kt} - \phi_{K_o} = \theta_{Kt} - \theta_{K_o} =$$

$$= \theta_{K_o}\left[\exp\left(\frac{\tau}{t_p} \frac{\Delta V}{V_o}\right) - 1\right]. \qquad (28)$$

The above are the dried material final temperature changes evaluated without taking into account the influence of moisture evaporation which is described by the component:

$$k_R \frac{\bar{t}_p - 2\bar{t}_s}{\bar{t}_p \bar{t}_s}\left(X_{KR} - X_R\right) \exp\left(-\frac{t}{t}\right),$$

of equation (20).
We shall consider the effect of this component on the temperature changes including equation (28) formula 48 (5) multiplied by an appropriate coefficient.
Finally the dried material temperature changes resulting from the change of its transfer velocity in the drying chamber can be expressed by the following equation:

$$\Delta\theta_K(t) = -\operatorname{sign} \Delta V\left[\theta_{K_o}\left(\exp\left(\frac{\tau}{\bar{t}_p} \frac{\Delta V}{V_o}\right) - 1\right) - K_R \frac{\bar{t}_p - 2\bar{t}_s}{\bar{t}_p \bar{t}_s}\left(X_{K_o} - X_R\right)\left[\exp\left(\frac{\tau}{t_p} \frac{\Delta V}{V_o}\right) - 1\right]\right]. \qquad (29)$$

The equation expresses only the temperature changes in the drying chamber, i.e. in the period 0, t_k and does not take into account the heat time delay and the influence of temperature changes on the drying process. As in the case of final moisture changes the temperature changes reflect the kinetics of the process, as expressed by equation (17). Having left the drying chamber, the material has a constant temperature for some time. Thus we assume that the temperature of the material is constant from the moment the material leaves the drying chamber to the moment of temperature measuring. Taking the above into consideration we can express the final temperature changes by the equation:

$$\Delta\theta_K(\tau) = c_1^x \exp\left(-\frac{\tau}{\bar{t}_1}\right) - c_2^x \exp\left(-\frac{\tau}{\bar{t}_2}\right) + c_1^x - c_2^x + k_T\left[c_2 \exp\left(-\frac{\tau}{\bar{t}_{VS}}\right) - c_1 \exp\left(-\frac{\tau}{\bar{t}_c}\right) + c_1 - c_2\right]. \qquad (30)$$

The values c_1^x, c_2^x, $\bar{t}_1$, $\bar{t}_2$ as in Fig. 5 according to (5) Fig. 12 and Table T-1 item 2.
The differential equation of the dependence (30) will have the following form:

$$\begin{bmatrix}\dot{\theta}_1 \\ \dot{\theta}_2\end{bmatrix} = \begin{bmatrix}0 & 1 \\ -\frac{1}{\bar{t}_1\bar{t}_2} & -\frac{\bar{t}_1+\bar{t}_2}{\bar{t}_1\bar{t}_2}\end{bmatrix}\begin{bmatrix}\theta_1 \\ \theta_2\end{bmatrix} + \begin{bmatrix}0 & 1 \\ \frac{k_T}{\bar{t}_{VS}\bar{t}_c} & -k_T\frac{\bar{t}_{VS}+\bar{t}_c}{\bar{t}_{VS}\bar{t}_c}\end{bmatrix}\begin{bmatrix}X_1 \\ X_2\end{bmatrix} + \begin{bmatrix}0 \\ \frac{K_V}{\bar{t}_1\bar{t}_2} & \frac{K_{VW}}{\bar{t}_{VS}\bar{t}_c}\end{bmatrix} V \qquad (31)$$

where:

$$\theta_1 = \Delta\theta_k(\tau), \quad \theta_2 = \theta_1, \quad K_{Vw} = \frac{\Delta X_k(\tau)}{\Delta V},$$

$$V = \Delta V(\tau), \quad X_1 = \Delta X_k(\tau), \quad X_2 = \dot{X}_1,$$

$$K_{V\theta} = \frac{\Delta\theta_K(\tau)}{\Delta V}.$$

For the materials of small mass we can disregard the effect of moisture evaporation. Then we shall obtain

$$\begin{bmatrix} \dot{\theta}_1 \\ \dot{\theta}_2 \end{bmatrix} = \begin{bmatrix} 0 & 1 \\ -\frac{1}{\bar{t}_1\bar{t}_2}, & -\frac{\bar{t}_1+\bar{t}_2}{\bar{t}_1\bar{t}_2} \end{bmatrix} \begin{bmatrix} 0_1 \\ 0_2 \end{bmatrix} + \begin{bmatrix} 0 \\ \frac{K_{v\theta}}{\bar{t}_1\bar{t}_2} \end{bmatrix} v \quad (32)$$

and $$\Delta\theta_k(\tau) = \begin{bmatrix} 1, & 0 \end{bmatrix} \begin{bmatrix} 0_1 \\ 0_2 \end{bmatrix}.$$

The equation coefficients as in Fig. 5.

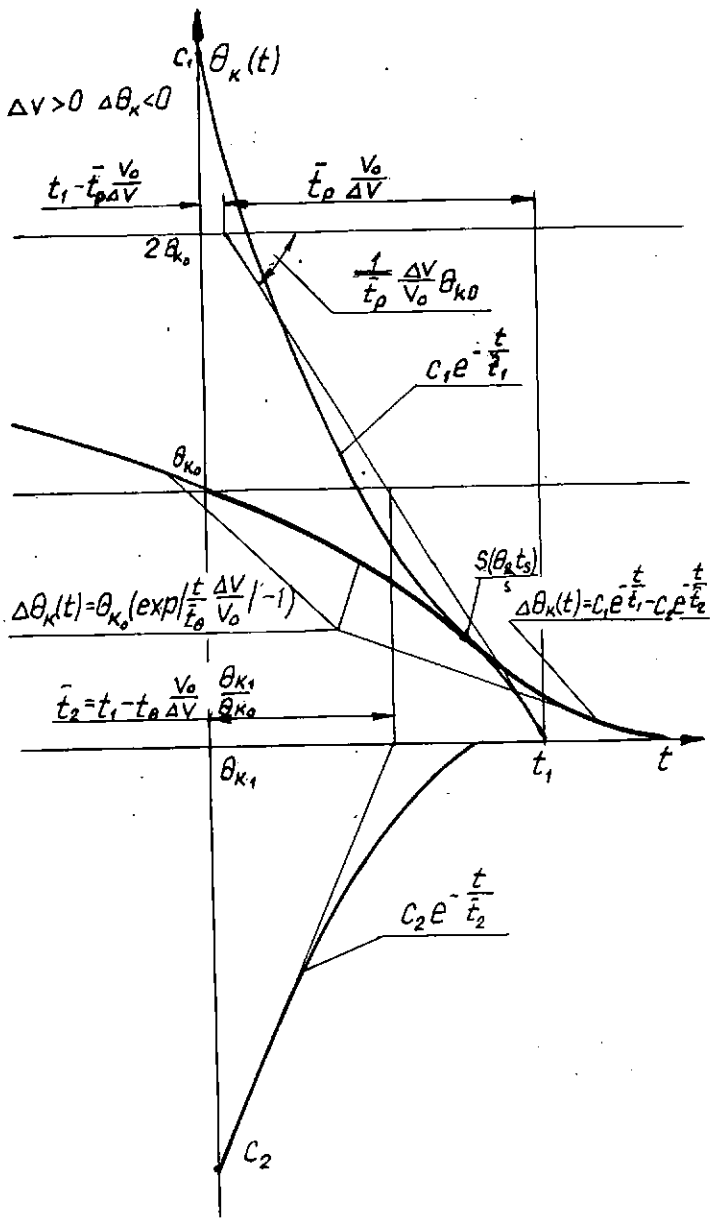

Figure 5. Graphic representation of equation (30) ($k_T = \theta$)

$$C_1^x - C_2^x = \theta_{K_o} - \theta_{K_1}$$

$$C_1 \exp\left(-\frac{t_s}{\bar{t}_1}\right) =$$

$$= \theta_{K_o}\left(\exp\left(\frac{t_s}{\bar{t}_1}\frac{\Delta V}{V_o}\right) - 1\right)$$

Combining the equations which describe the changes of final moisture 5 and final temperature we obtain for the equation in Table T-1, item 2 :

$$\begin{bmatrix} \dot{X}_1 \\ \dot{X}_2 \\ \dot{\theta}_1 \\ \dot{\theta}_2 \end{bmatrix} = \begin{bmatrix} 0 & 1 & 0 & 0 \\ -\frac{1}{\bar{t}_{vs}\bar{t}_c}, & -\frac{\bar{t}_{vs}\bar{t}_c}{\bar{t}_{vs}\bar{t}_c} & 0 & 0 \\ 0 & 0 & 0 & 0 \\ \frac{K_T}{\bar{t}_{vs}\bar{t}_c}, & k_T\frac{\bar{t}_{vs}+\bar{t}_c}{\bar{t}_{vs}\bar{t}_c}, & -\frac{1}{\bar{t}_1\bar{t}_2} & -\frac{\bar{t}_1+\bar{t}_2}{\bar{t}_1\bar{t}_2} \end{bmatrix} x$$

$$\begin{bmatrix} X_1 \\ X_2 \\ \theta_1 \\ \theta_2 \end{bmatrix} + \begin{bmatrix} 0 \\ \frac{K_{vw}}{\bar{t}_{vs}\bar{t}_c} 1(\tau - \bar{t}_r) \\ 0 \\ \frac{K_v}{\bar{t}_1\bar{t}_2} 1(\tau - t_r) \end{bmatrix},$$

$$\begin{bmatrix} \Delta X_k(\tau) \\ \Delta\theta_k(\tau) \end{bmatrix} = \begin{bmatrix} 1, & 0, & 0, & 0 \\ -k_T, & 0, & 1, & 0 \end{bmatrix} \begin{bmatrix} X_1 \\ X_2 \\ \theta_1 \\ \theta_2 \end{bmatrix}. \quad (33)$$

Symbols as in equation (32) and Table T-1, item 2 (5). We assume the regulation channel is non linear and monotonic but can be described by linear differential equation for the step of velocity ΔV .

REFERENCES

1. Krischer O., Kroll, Die wissenschaftlichen Grundlagen der Trocknungstechnik, Springer Verlag 1959
2. Lykov A.V., Teoria Sushki, Energiya, Moskva 1968
3. Lykov A.V., Teplo i Massoobmen v Processakh Sushki, G.E.J. 1956, Moskva, Leningrad
4. Spirnek J., Dynamika i regulacja procesu suszenia tkanin. Ph.D. Thesis, Łódź Technical University 1972
5. Spirnek J., The Mathematical Model of Drying Chamber for Textile Materials. I International Symposium on Drying, McGill University, Montreal, Aug.3-4, 1978

A METHOD OF DETERMINATION OF AN OPTIMUM TEMPERATURE DISTRIBUTION ALONG A DRYING CHAMBER

I. Dziubiński [1]
J. Spirnek [2]

1. Technical University, Łódź, Poland
2. Research and Development Centre of Automation, Łódź

ABSTRACT

The paper determines a control method of temperature distribution along a drying chamber assuming minimal use of thermal energy and drying time (efficiency of the drying chamber). The considerations are based on a mathematical model of the drying process.
The authors designed the mathematical model according to the requirements of control. The model determined heat and mass transfer which is observed during the drying process of textile fabrics in the drying chamber. The operation of the drying chamber is considered for minimum energy criterion with boundary conditions to temperature and efficiency (drying time). Basing on the results the authors proposed the temperature distribution and the method of adjusting temperature regulators along the drying chamber.

NOMENCLATURE

$\mathbb{A}, \mathbb{B}, \mathbb{C}, \mathbb{D}, \mathbb{E}, \mathbb{V}, \mathbb{X}, \mathbb{Y}$ = matrix of the state equations
D = dimension of the dried material, m
$G(s)$ = transient function
$I(k)$ = object function
K = static gain
k = coefficient of differential equations
L_o = length of the drying zone, m
M_L = mass flow rate of drying air, kg/s
Q = total flow rate, W/s
t = time, s
t = time constant, s
u = manipulated variable, ^oC
v = velocity of the movement of the dried material in the drying chamber, m/s
$X_{(x,y,z)}$ = moisture content of the material at any point, %
X_k = final moisture content, %
$\mathbb{X}$ = moisture content, %
x,y,z = space coordinate
$\mathbb{Y}$ = humidity of the drying air, %
$\Theta_M(x,y,z)$ = temperature of the dried material, ^oC
Θ_3 = temperature of the heating medium, ^oC
$\varkappa$ = moisture transfer factor, m^2/s

INTRODUCTION

Until now the requirements regarding the drying process control systems have been limited to maintaining the constant value of the final moisture content of the dried material. But as the heating energy has become more and more expensive, it pays to use control systems to control the process in an optimal way. The object function is to minimize the consumption of energy.

$$I(u) = \int_0^T \int_0^A \left[X(xt) - X_c(t)\right]^2 dx dt + \lambda \int_0^T u^2(t)\, dt .$$

One of the conditions of the optimal course of the process is the proper distribution of drying air temperature in the 'dry' section of a drying chamber. This problem is the subject of the present paper. The starting point will be to present a mathematical model of the control channel (drying air temperature - final moisture content).

THE MATHEMATICAL MODEL OF THE DRYING ZONE AND TRANSFER FUNCTION BETWEEN THE TEMPERATURE OF HEATING MEDIUM AND THE MOISTURE CONTENT REMOVED FROM THE DRIED MATERIAL

As this paper is written for technologists and constructors of dryers, it is necessary to give some information on the terminology applied in the theory of regula-

tion. The mathematical model of a control object is a set of information concerning the controlled process, limitations, aim of control (object function), given in the form of mathematical interrelations. Its useful form is a signal flow diagram classifying the physical variables (i.e. controlled variables) and the relationships between them. Below we present the signal flow diagram of a drying zone (drying nozzles) of a convection dryer for textile materials as in (8) (Fig. 1).

The limited extent of this paper does not allow us to present the considerations which have led to the synthesis of dynamic behaviour inside the drying chamber and to the construction of the model. A detailed analysis presented in equations of mass and energy balances (in an undefinable condition) is included in (7),(8).

The basic assumption for constructing the model is taking into consideration the average values of process parameters in the drying chamber of such values as to ensure the same duration of the process as in industrial dryers in which the parameters of the drying factor are changeable in time and drying chamber. We also assume that partial derivatives of the process parameters, resulting from linearization of mass and energy balance equations in dynamic behaviour change very slowly and can be approximated by introducing their individual average values.

Due to these simplifying assumptions the process taking place in the drying chamber can be expressed by means of linear differential equations. Laplace transformation also holds in the case of two non-linear equations presenting the changes of the final moisture content X_K, temperature Θ_M of the dried material in the function of the correcting variable (the velocity of the material being dried), provided that every time we take into consideration the change of velocity ΔV - the increase of velocity (the equation coefficients are functions of ΔV).

Our aim is to present the relationships between drying air (heating medium) temperature Θ_s and moisture content in the material being dried. Such a statement will be a basis for discussing the optimal temperature distribution inside a drying chamber, and precisely in its 'dry' section, i.e. in the falling drying rate period.

Having considered Fig. 1 we have:

$$\frac{X(s,t)}{\Theta_s(t)} = \frac{\Delta G(s,t)\,(1+s\bar{t}_8)}{(1+s\bar{t}_8)\,(1+s\bar{t}_c)\,(1+s\bar{t}_w)+sK_8K_7K_3\Delta G(s,t)} \qquad (1)$$

where:

t_c - time constant of time delay. In this case $t_c = 0$ the textile after the constant drying rate period

$\bar{t}_8$ - time constant describing the inertia of the changes of moisture content in the drying air

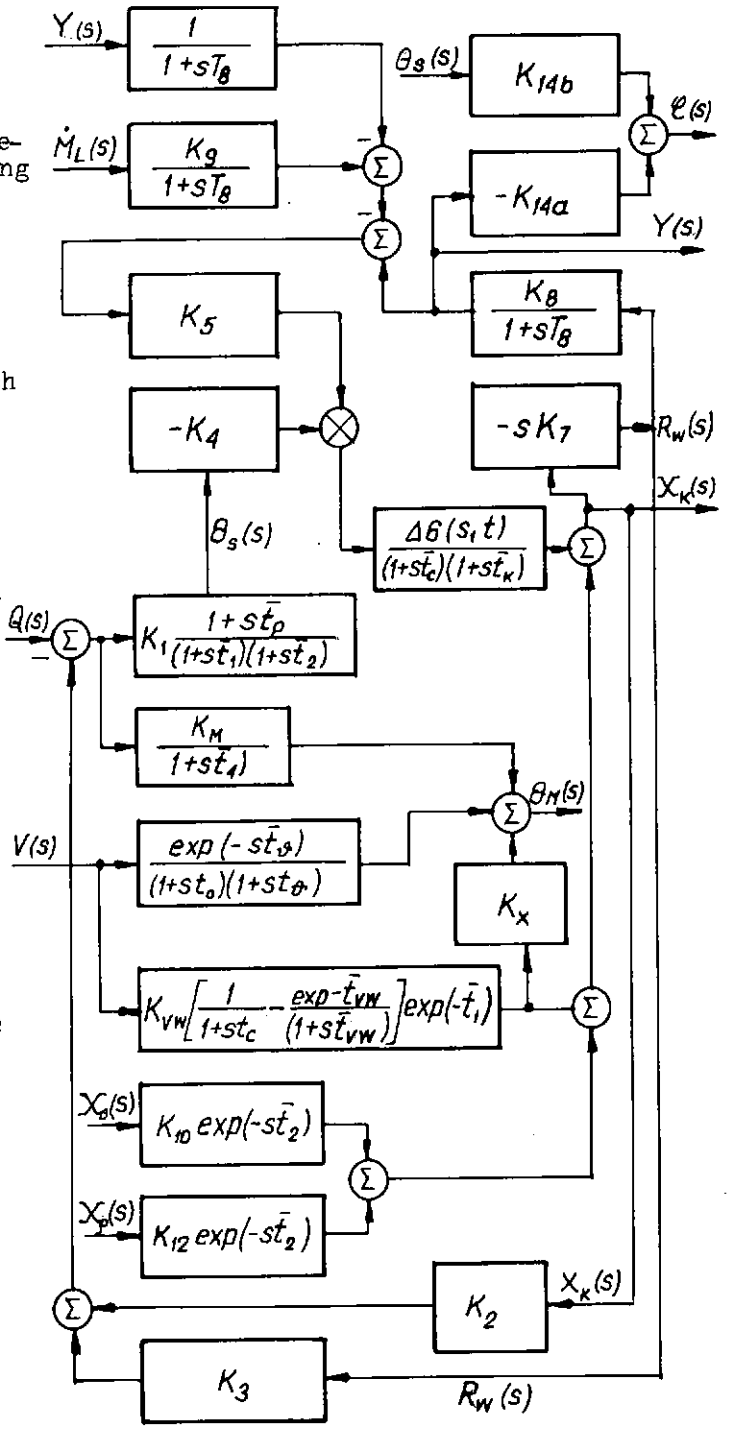

Figure 1. Signal flow diagram for drying zone of a drying chamber

K_8 - static gain equal to the transfer function describing the velocity of drying air humidity change ($Y(s)$) in relation to velocity change of moisture evaporated from the textile ($R_w(s)$)

$\bar{t}_w(t)$ - differential equation coefficient

K_5 - static gain of the transfer function which characterizes the change of drying conditions determined

by the parameter X_A, together with the air humidity change ΔX

K_7 - static gain of the transfer function describing the change of moisture (R_w) evaporation velocity from the textile, according to the change of moisture content ΔX in a textile.

$$\bar{G}(s,t) = \frac{s\,\bar{t}_w\,\dot{\bar{t}}_w}{(1+s\bar{t}_w\dot{\bar{t}}_w)^2} + \frac{3s^2\bar{t}_w^2\dot{\bar{t}}_w^2}{(1+s\bar{t}_w)^4} - \frac{s(\bar{t}_w\dot{\bar{t}}_w^2 + \bar{t}_w^2\ddot{\bar{t}}_w)}{(1+s\bar{t}_w)^3} \qquad (2)$$

The component of the transfer function characterizing the inertia of moisture transfer in textile material takes into account the change of equation coefficient (1) $\bar{t}_w(t)$ in a unit of time (according to formula 15 (8)). Assuming that $\bar{t}_w$ is constant we have $\Delta\bar{G}(s,t) = 1$. Because of the low inertia of the process of moisture content changes in the air, in relation to the changes of moisture content in the textile material, the time constant T_8 can be disregarded, so finally equation (1) will take the form:

$$\frac{X(s)}{\Theta_s(s)} = \frac{1}{1+s\underbrace{(\bar{t}_w+K_8K_7K_5)}_{\bar{t}_x}} \qquad (3)$$

or

$$\bar{t}_x\,\frac{dX(t)}{dt} + X(t) = \Theta(t) \qquad (4)$$

If a textile moves in a drying zone at constant velocity v in the direction of the axis y, then moisture content X is the function of axis y and time t, i.e. X(y,t). The process is described by the equation:

$$\bar{t}_x\,\frac{D}{Dt}\,X(y,t) + X(y,t) = \Theta(y,t) \qquad (5)$$

where the hydrodynamic time derivative is

$$\frac{D}{Dt}\,X(y,t) = \frac{\partial X(y,t)}{\partial t} + \frac{\partial X(y,t)}{\partial y}\,\frac{dy}{dx} =$$

$$= \frac{X(y,t)}{\partial t} + v\,\frac{X(y,t)}{\partial y} \qquad (6)$$

Thus, finally the equation describing the dynamic behaviour takes the form:

$$\bar{t}_x\left(\frac{\partial X(y,t)}{\partial t} + v\,\frac{\partial X(y,t)}{\partial y}\right) + X(y,t) = \Theta(y,t) \qquad (7)$$

where $v = \frac{dy}{dt}$ - velocity of textile band transfer in the drying zone

$0 \leqslant y \leqslant L$, $0 \leqslant t \leqslant T$

L - length of the drying chamber

$\bar{t}$ - time of observation, according to the length L.

Our aim is the optimal temperature distribution in the drying chamber (in its 'dry' section), so the manipulated variable will be equal to zero, thus the initial equation presenting the distribution of average material moisture content in the 'dry' section of the drying chamber takes the form:

$$\frac{\partial X(y,t)}{\partial t} + v\,\frac{\partial X(y,t)}{\partial y} + \frac{1}{\bar{t}_x}\,X(y,t) = 0. \qquad (8)$$

The distribution and transfer of moisture inside the textile material are not taken into account in this equation. For heavy materials (of large volume) such an approximation is too big when we consider that kind of control.

The problem of moisture distribution in the material was considered in (8), Fig. 3. In a similar manner we can finally obtain the initial equation for discussing the optimal temperature distribution:

$$\frac{\partial X(x,y,t)}{\partial t} + v\,\frac{\partial X(x,y,t)}{\partial y} - \varkappa_x\,\frac{\partial^2 X(x,y,t)}{\partial x} = 0 \qquad (9)$$

where:

$$\varkappa_x = \frac{1}{\bar{t}_x} = \frac{1}{\bar{t}_w+K_8K_7K_5}.$$

Equation (9) is identical to the equation of diffusion describing the changes of moisture content in the material being dried, as given, among others, in (1),(2). Only the factor $\varkappa_x$ diminishes (according to time passing) which results from feedbacks caused by the drying process taking place in the drying chamber.

As in the case of moisture content changes we can find the correlations describing the dried material temperature changes. Anyhow, we shall confine ourselves to the statement that in such a case the coefficients k_Θ and k_w of the equation decrease:

$$\frac{\Theta_M(x,y,t)}{\partial t} + v\,\frac{\Theta_M(x,y,t)}{\partial y} - k_\Theta\,\frac{\partial^2\Theta_M(x,y,t)}{\partial x^2} +$$

$$+ k_w\,\frac{\partial X(x,y,t)}{\partial t} = 0. \qquad (10)$$

As in the above case it is the result of a feedback caused by the process (mainly by the change of air temperature and humidity content in the air caused by the evaporation of moisture from the dried material).

A METHOD OF DETERMINATION OF AN OPTIMUM TEMPERATURE DISTRIBUTION ALONG THE DRYING ZONE

The phenomena of heat and mass transfer in moist materials taking place during the drying process are expressed by the following system of differential equations:

$$\frac{\partial \theta_M}{\partial t} + v\frac{\partial \theta_M}{\partial y} - k_v\frac{\partial^2 \theta_M}{\partial x^2} + k_w\frac{\partial X}{\partial t} = 0$$

$$\frac{\partial X}{\partial t} + v\frac{\partial X}{\partial y} - \varkappa_x\frac{\partial^2 X}{\partial x^2} = 0 \qquad (11)$$

with initial conditions

$$\theta_M(x,y,0) = \theta_o^* = \text{const}$$

$$X(x,y,0) = X_o^* = \text{const}, \qquad (12)$$

where

$$\theta_M(x,y,t) = \theta_M$$

$$X(x,y,t) = X$$

and boundary conditions

$$\theta_M(x,0,t) = \theta_o^* = \text{const}$$

$$X(x,y,0) = X_o^* = \text{const}$$

$$\frac{\partial \theta_M}{\partial x}\Big|_{x=D} = \left[u(y,t) - \theta_M(D,y,t)\right]$$

$$\frac{\partial \theta_M}{\partial x}\Big|_{x=0} = 0 \qquad (13)$$

$$\frac{\partial X}{\partial x}\Big|_{x=D} = \delta\frac{\partial \theta_w}{\partial x}\Big|_{x=s}$$

$$\frac{\partial X}{\partial x}\Big|_{x=0} = 0$$

$0 \leq x \leq D$, $0 \leq y \leq L$, $0 \leq t \leq T$

δ - thermogradient coefficient

$\varkappa = Nu\,\frac{\lambda_p}{L}$ Nu - Nusselt number
λ_p - coefficient of thermal conductivity of damp air.

We shall assume some restrictions

$A_1 \leq u(y,t) \leq A_2$ A_1, A_2 - taken arbitrarily.

As a criterion of appreciation of the system we take the following object function:

$$I(u) = \int_0^T\int_0^D\int_0^L \left[X(x,y,t) - X_C(t)\right]^2 dxdydt +$$

$$+ \lambda\int_0^T\int_0^L u^2(y,t)\,dydt \qquad (14)$$

X_C - the requested distribution of moisture in the material during the drying process ($0 \leq t \leq T$)

$\lambda > 0$ - weight.

Assuming that the speed of material passage through the drying chamber is constant ($y = vt$, $0 \leq y \leq L$) we obtain the following form of initial equations

$$\frac{\partial \theta_M}{\partial t} = k_v\frac{\partial^2 \theta_M}{\partial x^2} - k_w\varkappa_x\frac{\partial^2 X}{\partial x^2}$$

$$\frac{\partial X}{\partial t} = \varkappa_x\frac{\partial^2 X}{\partial x^2} \qquad (15)$$

with initial conditions

$$\theta_M(x,o) = \theta_o^* = \text{const}$$

$$X(x,0) = X_o^* = \text{const} \qquad (16)$$

and boundary conditions

$$\frac{\partial \theta_M}{\partial x}\Big|_{x=D} = \varkappa\left[u(t) - \theta_M(S,t)\right]$$

$$\frac{\partial \theta_M}{\partial x}\Big|_{x=0} = 0, \qquad (17)$$

$$\frac{\partial X}{\partial x}\Big|_{x=D} = \frac{\partial \theta_w}{\partial x}\Big|_{x=0},$$

$$\frac{\partial X}{\partial x}\Big|_{x=0} = 0.$$

The object function assumes the form:

$$I(u) = \int_0^T\int_0^D \left[X(x,t) - X_C(t)\right]^2 dxdt +$$

$$+ \int_0^T u^2(t)dt\,. \qquad (18)$$

Because of unattainability of the analytical solution of the problem we approximate the system with distributed parameters by the system with lumped parameters.

$$\frac{d\mathbb{X}}{dt} = \mathbb{A}\mathbb{X} + \mathbb{B}u(t),$$

$$\mathbb{X}(0) = \mathbb{X}_o \qquad (19)$$

with the object function

$$I(u) = \int_0^T (\mathbb{X}(t) - \mathbb{X}_C(t))'\,\mathbb{D}(\mathbb{X}(t) -$$

$$- \mathbb{X}_C(t)\Big]dt + \lambda \int_0^T u^2(t)dt \qquad (20)$$

denotes transposition, where

$$\mathbb{X} = \begin{bmatrix} \Theta_{M1} \\ \Theta_{M2} \\ \vdots \\ \Theta_{MN} \\ X_1 \\ X_2 \\ \vdots \\ X_N \end{bmatrix}, \quad \mathbb{B} = \begin{bmatrix} 0 \\ 0 \\ \vdots \\ n \\ 0 \\ 0 \\ \vdots \\ s \end{bmatrix}, \quad \mathbb{X}_o = \begin{bmatrix} \Theta^*_{M_o} \\ \Theta^*_{M_o} \\ \vdots \\ \Theta^*_{M_o} \\ X^*_o \\ X^*_o \\ \vdots \\ X^*_o \end{bmatrix}, \quad \mathbb{X}_C(t) = \begin{bmatrix} 0 \\ 0 \\ \vdots \\ 0 \\ X_C(t) \\ X_C(t) \\ \vdots \\ X_C(t) \end{bmatrix}$$

$$\mathbb{A} = \left[\begin{array}{cccc:cccc} -k_v & k_v & 0 & \dots & k_w\mathcal{K}_x & -k_w\mathcal{K}_x & 0 & \dots \\ k_v & -2k_v & k_v & \dots & -k_w\mathcal{K}_x & 2k_w\mathcal{K}_x & -k_w\mathcal{K}_x & \dots \\ 0 & k_v & -2k_v & \dots & 0 & -k_w\mathcal{K}_x & 2k_w\mathcal{K}_x & \dots \\ \hdashline 0 & 0 & 0 & \dots & 0 & 0 & 0 & \dots k_w\mathcal{K}_x \\ 0 & 0 & 0 & \dots & -\mathcal{K}_x & \mathcal{K}_x & 0 & \dots \\ 0 & 0 & 0 & \dots & \mathcal{K}_x & -2\mathcal{K}_x & \mathcal{K}_x & \dots \\ \hdashline 0 & 0 & 0 & \dots r & 0 & 0 & 0 & \dots -\mathcal{K}_x \end{array}\right]_{2N\cdot 2N}$$

$$\mathbb{D} = \begin{bmatrix} 0 & \vdots & 0 \\ \cdots & \vdots & \cdots \\ 0 & \vdots & \begin{matrix} 2 & 0 \\ 1 & \ddots \\ 0 & 1 \end{matrix} \end{bmatrix}_{2N \times 2N}$$

$$\Theta_{Mi}(t) = \Theta_M(X_i,t), \quad X_i(t) = X(x_i,t) \quad i=0,1,\dots N+1$$

$$\Theta_{Mi}(0) = \Theta^*_o, \qquad X_i(0) = X^*_o,$$

$$n = h\left(\frac{k - k_w\mathcal{K}_x h_{\mathcal{K}}\delta}{1 + h\mathcal{K}} - k_w\mathcal{K}_x\delta\right)$$

$$s = h\mathcal{K}\left(k_x\delta - \frac{k_v h\mathcal{K}\delta}{1+h\mathcal{K}}\right)$$

$$m = \frac{k_v + k_w\mathcal{K}_x h\delta}{1+h\mathcal{K}} - 2k_v$$

$$r = -\frac{\mathcal{K}_x h\mathcal{K}\delta}{1+h\mathcal{K}}$$

Algorithm for Calculating the Optimum Control

We introduce new variables

$$\begin{cases} \mathbb{Y}(t) = \mathbb{X}(t) - X_C(t), \mathbb{Y}_o = \mathbb{X}_o - \mathbb{X}_C(0) \\ \mathbb{V}(t) = \mathbb{A}\mathbb{X}_C(t) - \dfrac{d\mathbb{X}_C(t)}{dt} \end{cases}$$

System (19) with the object function (20) assumes the form

$$\begin{cases} \dfrac{d\mathbb{Y}(t)}{dt} = \mathbb{A}\mathbb{Y}(t) + \mathbb{B}u(t) + \mathbb{V}(t) \\ \mathbb{Y}(0) = \mathbb{Y}_o \end{cases} \qquad (21)$$

with the object function

$$I(u) = \int_0^T \left\{\mathbb{Y}(t)'\mathbb{D}\mathbb{Y}(t) + \lambda u^2(t)\right\}dt \qquad (22)$$

Algorithm:

1. Solve the matrix equation

$$\begin{cases} \dfrac{d\mathbb{E}(t)}{dt} = \mathbb{D} - \mathbb{A}'\mathbb{E}(t) - \mathbb{E}(t)\mathbb{A} - \dfrac{1}{\lambda}\mathbb{E}(t)\mathbb{B}\mathbb{B}'\mathbb{E}(t) \\ \mathbb{E}(T) = 0 \qquad \dim \mathbb{E}(t) = 2N \times 2N \end{cases}$$

2. Solve the vector equation

$$\begin{cases} \dfrac{d\mathbb{H}(t)}{dt} = -\left[\dfrac{1}{\lambda}\mathbb{E}(t)\mathbb{B}\mathbb{B}' + \mathbb{A}\right]\mathbb{H}(t) - \mathbb{E}(t)\mathbb{V}(t) \\ \mathbb{H}(T) = 0 \end{cases}$$

3. Calculate $\mathbb{H}^*(t)$

$$\mathbb{H}^*(t) = \frac{1}{\lambda}\mathbb{B}'\mathbb{H}(t)$$

4. Calculate $\mathbb{E}^*(t)$

$$\mathbb{E}^*(t) = \frac{1}{\lambda}\mathbb{B}'\mathbb{E}(t)$$

5. Solve the equation

$$\begin{cases} \dfrac{d\mathbb{Y}}{dt} = \mathbb{A}\mathbb{Y}(t) + \mathbb{B}\left[\mathbb{H}^*(t) + \mathbb{E}^*(t)\mathbb{Y}(t)\right] + \mathbb{V}(t) \\ \mathbb{Y}(0) = \mathbb{Y}_o \end{cases}$$

6. Determine the optimum control

$$u^o(t) = \mathbb{H}^*(t) + \mathbb{E}^*(t)\mathbb{Y}(t)$$

7. If needed

$$\mathbb{X}(t) = \mathbb{Y}(t) - \mathbb{X}_C(t)$$

$\mathbb{X}(t)$ - temperature and moisture distribution in the material.

REFERENCES

1. Lykov, A.V., Teplo i Massoobmen v Processakh Sushki. G.E.J. 1956, Moskva Leningrad
2. Lykov, A.V., Teoria Sushki. Energiya, Moskva 1968
3. Lions, J.L., Contrôle optimal de systèmes gouvernés par des équations aux dérivées partielles. Dunod, Paris 1968
4. Lions, J.L., Magenes, E., Problémes aux limités non homogénes et applications. Vol.1, Dunod, Paris 1968
5. Lee, E., Markus, L., Osnovy Teorii Optimalnovo upravlenija. Nauka, Moskva 1972

6. Temam, R., Sur la stabilité et la convergence de la mèthode des pas fractionnaires. Thèse, Paris 1968
7. Spirnek, J., Dynamika i regulacja procesu suszenia. Ph.D. Thesis, Łódź Technical University, 1972
8. Spirnek, J., The Mathematical Model of Drying Chamber for Textile Materials. I International Symposium on Drying. McGill University, Montreal, August 3-4 1978

MATHEMATICAL MODELLING AND SIMULATION OF VACUUM CONTACT DRYING OF POROUS MEDIA IN THE CONSTANT RATE PERIOD

F. Stręk
J. Nastaj

Department of Chemical Engineering
Technical University of Szczecin, Szczecin, Poland

ABSTRACT

The process of vacuum contact drying in which dried porous medium adheres closely to the hot surface is considered. The investigations were carried out in the most intensive i.e. boiling region. These investigations dealt with drying of porous media with internal porosity (molecular sieve, aluminiumoxid, silicagel, kieselgel). Different wetting liquids (water, methyl alcohol, n-propyl alcohol, n-butyl alcohol) were used. The process was realised either at constant temperature of the hot surface or at constant heat flux density supplied to this surface. Analysis of most significant characteristics of the process and identification of the static characteristics e.g. critical moisture content were performed. General mathematical model of the process has been proposed which enables the process simulation in the constant rate period for three, important from technical point of view, methods of process performance, i.e. for known functional relationships:

1. of the hot surface temperature from time;
2. of heat flux density supplied to the hot surface from time;
3. of temperature of surroundings of the hot surface from time and known constant value of convective heat transfer coefficient.

The theory was checked experimentally giving very good agreement in the wide range of process parameters.

NOMENCLATURE

A = surface area, m^2

c_p = specific heat of liquid, J/kgK

D = particle diameter, m

Δh_v = specific latent heat of vaporization, J/kg

$\dot{m}$ = mass flux density (evaporation rate per unit hot surface, $\dot{m} = dU/dt$), kg/m^2s

M = mass, kg

n = ratio of specific surfaces ($n = D_e \varrho_s o/6$), -

N = noises (disturbances, Figure 5)

o = specific surface of porous medium, m^2/kg

p = total pressure, N/m^2

$\dot{q}$ = heat flux density, W/m^2

$\bar{r}$ = equivalent radius of pores of porous medium particles, m

S = layer thickness of dried bed, m

t = time, s

T = thermodynamic temperature, K

ΔT = temperature difference ($T_o - T_b$), K

T_∞ = thermodynamic temperature of surroundings of hot surface, K

U = moisture content of dried bed per unit hot surface ($U = M_{ld}/A_o$), kg_{ld}/m^2

V = volume, m^3

V_μ = specific volume of micropores and transitory pores, m_p^3/kg

x = position coordinate in dried bed, m

x^* = dimensionless space coordinate ($x^* = x/S$), -

X = moisture content of dried bed (volumetric saturation, $X = V_{ld}/V_p$), m_{ld}^3/m_p^3

$\bar{y}$ = average value of dependent variable (in general)

Y = moisture content of dried bed (dry basis, $Y = M_{ld}/M_{dm}$), kg_{ld}/kg_{dm}

α = heat transfer coefficient from hot surface to dried bed defined by equation (1), W/m^2K

α_∞ = convective heat transfer coefficient, W/m^2K

ε = total porosity of dry bed, m_p^3/m^3

η = dynamic viscosity of liquid, kg/ms

λ = thermal conductivity of liquid, W/mK

ρ = mass density, kg/m^3

σ = surface tension, N/m

$\bar{y}$ = standard deviation residual of dependent variable in general

Subscripts

1,2 = indices

b = at boiling point of liquid

bu = bulk of bone dry porous medium

cr = critical

dm = bone dry porous medium

e = equivalent

eI = equivalent in first drying period

eII = equivalent in second drying period

i = initial

ld = liquid

o = hot surface

p = pores

s = solid (without voids)

I-II = separating first drying period from second one

INTRODUCTION

The purpose of this work is to obtain a mathematical model for the process of vacuum contact drying of porous media (especially for porous media with internal porosity) in the constant rate period, which can be used in design calculations and the process simulation. The term "porous medium" means here the granular bed as opposed to porous material e.g. ceramics, paper, fabric. Porous medium with internal porosity is the one which solid phase is porous material. A vacuum drying is irreplaceable in these cases in which dried material is temperature sensitive. The reduction of pressure in contact drying causes the decreasing of the process temperature and reduces the rate of harmful chemical processes i.e. chemical decomposition and oxidation. The process of vacuum contact drying differs from other methods of drying in high intensity and high watt-hour efficiency (1,2). It has been found that papers concerning directly this subject are very scarce. The majority of these papers refer either to technological variants or equipment of this process. Only in a few works the qualitative analysis of the effect of different parameters upon the process has been performed (3, 4, 5,6). A simplified mathematical model of the process of vacuum contact drying of porous media without internal porosity, which is valid for comparatively little range of the process parameter variability, has been derived by the authors(7,8). The authors(9,10,11) have presented applicability of the Han's theory (12) to generalization of their own investigations of contact drying of the layers of sand, filter paper and fabrics at atmospheric pressure. Moreover, this model is valid for low and medium intensity region of the process and for the only method of the process realization i.e. at T_o = const. For these reasons it has the limited range of application. In the most intensive process region, i.e. the boiling region, almost the whole vapor flux appears in the so-called "hot layer" and flows to the exposed surface of a dried bed as hydraulic flux under the influence of the gradient of total pressure (13). In the dried layer the equilibrium between liquid and vapor is not achieved. It is only established on the exposed bed surface. Liquid is transported under the influence of forces of gravity and capillary forces with friction forces hampering the flow being taken into consideration. From our own investigations (14) it results that kinetics of the process of vacuum contact drying in boiling region is divided into three periods. The first and the second ones are constant drying rate periods and differ from one another in the pattern of variation of the equivalent heat transfer coefficient α_e. In the present paper an attempt of identification of the following statical (independent of time) characteristics of the process: transition points on characteristic drying curve X_{cr} and X_{I-II} and the equivalent heat transfer coefficient α_e has been made. The possibility of occurate prediction of these quantities is of great importance in forming a comprehensive mathematical model of the process of vacuum contact drying of porous media in the boiling region. In this work, the mathematical model of the process in the first and the second drying periods has been presented.

EXPERIMENTAL EQUIPMENT AND METHODOLOGY

General Description of the Experimental Equipment

The container for a dried porous medium was the main part of the experimental equipment (Figure 1). It was made of Teflon in the shape of a cylinder, closed by a brazen bottom being a hot surface. Heat flux density supplied to the hot surface was controlled by changing the voltage of stabilized alternating current supplying a heating coil. The heating coil was carefully insulated from all

sides but the upper one and the insulation was reheated with the help of a reheating coil to eliminate the existence of temperature gradient in the insulation. In this way, the heat losses from the heating coil were prevented. In order to prevent bed

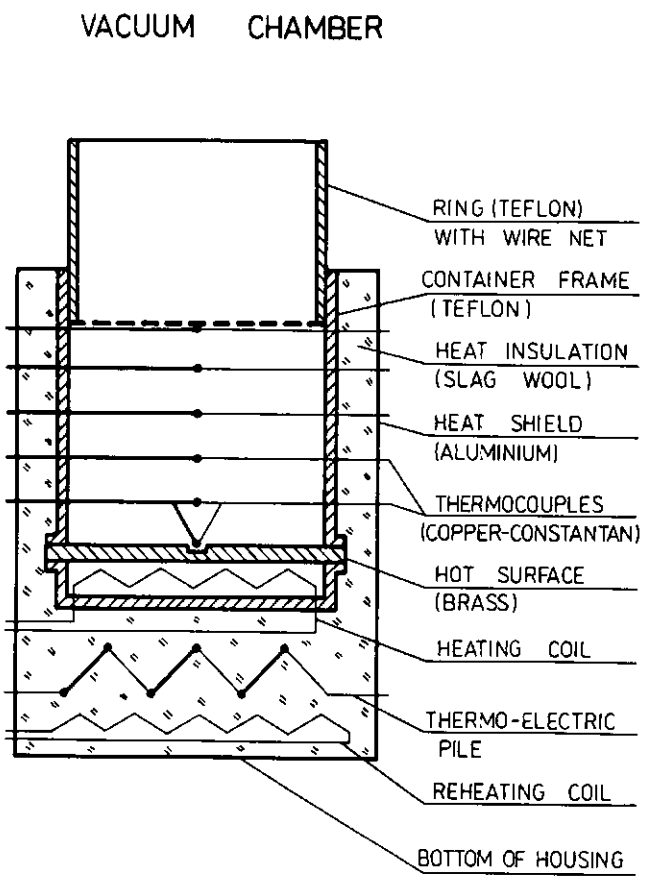

Figure 1 Sketch of Container

expansion and displacement, during experiment, of porous medium particles, a set ring with a wire net was fixed over the bed surface. Such a performance of the container provided

(a) the close contact between a dried bed and the hot surface;
(b) unilateral heat supply to the investigated sample;
(c) thermal resistance to about 600 K ;
(d) minimization of heat losses;
(e) prevention of bed fluidization.

The container with the investigated moist bed sample was suspended on the gravimetric transducer arm, inside the vacuum chamber. The decrease of dried bed moisture content was continuosly monitored and recorded by means of the gravimetric transducer. The hot surface temperature and temperatures inside the dried bed were measured and continuosly recorded, using six thermocouples placed at the container axis. Inside the vacuum chamber, the temperature was kept equal to the boiling point of the wetting liquid at the given total pressure with the help of the internal thermostating by the heating-cooling jacket. Vacuum in the experimental system was maintained by the vacuum pump. It was measured by the electronic vacuum gauge and controlled by the use of control valves.

Characteristic of Porous Media and Liquids Used in the Experiments

The analysis of a drying process requires the best possible knowledge of mechanical - structural and physical properties of a dried body. For this reason the best possible knowledge of structure and physical properties of dry porous media used for drying experiments is necessary. Physical properties of liquids constituting moisture content in the investigated process should also be known. In such experiments artificial porous beds particles of which are composed of metal or glass uniform spheres are usually used. Because of the lack of such beds, in the case of porous media with internal porosity, drying experiments were conducted making use of chromatographic column packing chemically neutral in relation to liquids used for experiments. For all considered packings, i.e. silicagels, molecular sieves, aluminiumoxid, chromosorb, kieselgel, etc. the following values V_μ, ρ_{bu}, ρ_s, o, $\bar{r}$ were determined. In addition, integral and differential curves of pores volume distribution depending on capillaries radius were determined by the porosimetric method. On the basis of these determinations, porous media with internal porosity characterized by a large volume fraction of micropores and transitory pores were distinguished. Finally, six porous media were choose for the investigations. Table 1 presents their basic physical properties. The choice of liquids used in experiments was made from the point of view of the highest possible physical properties variation in relation to water. Methyl alcohol, n-propyl alcohol and n-butyl alcohol with high degree of purity were used. In the case of water, distilled water was used. Physical properties of liquids are presented in Table 2.

Experimental Methodology

Porous media which had been previously dried to the constant weight in a vacuum drier were stored in hermetically closed vessels. Next, the right quantity of liquid was poured into the container for dried porous medium and the previously prepared portion of porous medium was then slowly added to it. Everything was mixed and rammed in order to get the constant, characteristic to the given

Table 1. Basic Physical Properties of Porous Media

Porous Medium	Physical Property						
	$10^3 D_e$ (m)	ε (m_p^3/m^3)	$10^{-4} n$ (-)	$10^{10} \bar{r}$ (m)	$10^{-3} o$ (m^2/kg)	ρ_{bu} (kg/m^3)	ρ_s (kg/m^3)
Silicagel	0.120	0.68	2.31	9.37	540	692	2135
Silicagel	0.230	0.67	4.66	9.44	587	681	2070
Kieselgel	0.345	0.75	5.47	34.00	457	517	2080
Molecular Sieve	0.390	0.64	5.21	10.88	403	714	1988
Molecular Sieve	0.785	0.59	9.70	11.20	371	815	2000
Molecular Sieve	1.200	0.61	13.30	38.10	330	798	2019

Table 2. Physical Properties of Liquids[1]

Liquid	Physical Property					
	ρ_b (kg/m^3)	$10^3 \eta_b$ (kg/ms)	$10^3 \sigma_b$ (N/m)	$10^{-3} c_{pb}$ (J/kgK)	λ_b (W/mK)	$10^{-3} \Delta h_v$ (J/kg)
Water	959-998	0.29-1.26	59.0-72.4	4.20-4.23	0.579-0.682	2260-2475
Methyl Alcohol	753-825	0.34-1.10	19.0-26.2	2.39-2.78	0.204-0.215	1100-1225
n-Propyl Alcohol	736-807	0.49-2.65	17.5-24.2	2.36-3.19	0.151-0.169	687-796
n-Butyl Alcohol	739-802	0.42-2.24	16.4-23.7	2.44-3.37	0.138-0.151	594-679

[1]The range of variability of any physical property results from the change of total pressure used in the experiments.

porous medium, bed porosity ε . This way of sample preparation eliminates air bells retention in the bed which would otherwise increase their volume and violently expand at the pressure decrease. It was noticed, particularly at the preparation of the sample with water, that a great quantity of heat connected with heat of wetting of a given porous medium is released. Hence, before experiment, the whole sample was cooled by leaving it for some time in a freezer. This gave additional prevention from liquid superheating and vapor bubbles expansion at pressure decrease to the total pressure of experiment p. The container was placed inside the vacuum chamber on the gravimetric transducer arm. Then, the chamber was closed, the vacuum pump was switched on, the required pressure was attained and controlled, the hot surface heating was switched on and the run of the process was recorded from that moment.

ANALYSIS OF SOME CHARACTERISTICS OF THE PROCESS

Because of the lack of publications dealing with investigations of vacuum drying of porous media with internal porosity, two series of preliminary experiments have been carried out. They differed from the point of view of the method of realization the process (the first series at T_o = const; the second one at q_o = const). Preliminary runs of the process were made on the basis of the factorial design of experiments, changing: the kind of porous medium, thickness of layer of dried bed, total pressure, hot surface temperature T_o or heat flux density supplied to this surface, the kind of liquid saturating the porous medium. All trials were made in the most intensive region of the process (boiling region). The analysis of obtained results showed that runs of the process for T_o = const and $\dot{q}_o$ = const can be, irrespective of factors combination, presented as in Figure 2 and Figure 3.

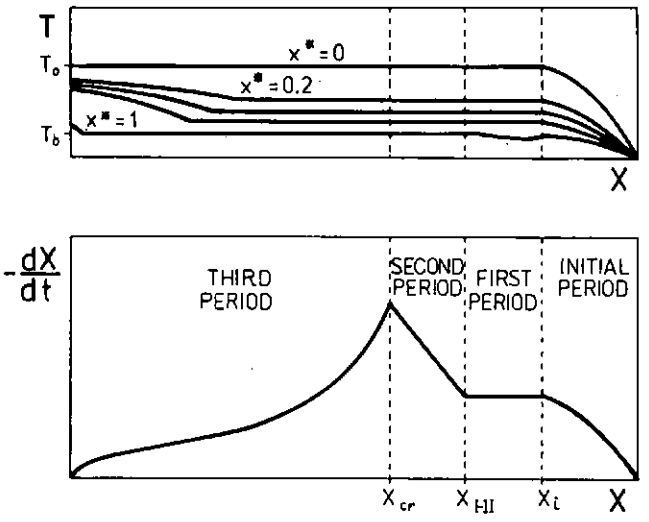

Figure 2. Temperature Profiles and Drying Rate Versus Moisture Content for T_o = const

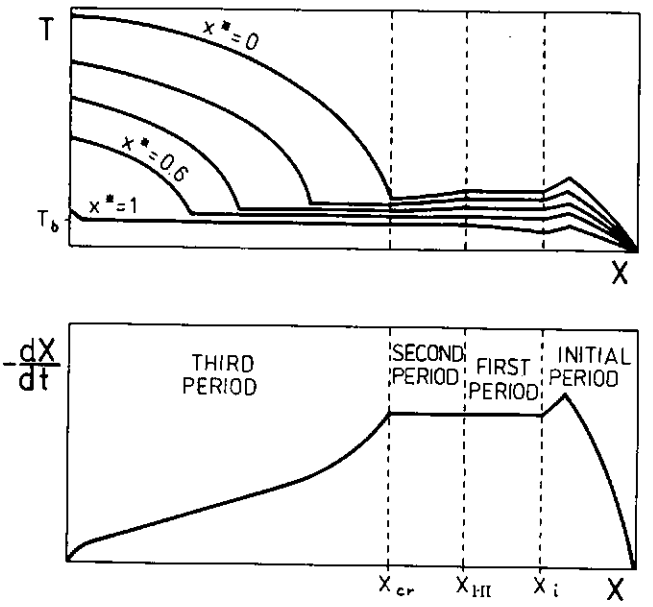

Figure 3. Temperature Profiles and Drying Rate Versus Moisture Content for $\dot{q}_o$ = const

The drying period for $X_{cr} \leq X \leq X_i$, called in literature the period of constant rate is in the case of vacuum contact drying of porous media divided into two periods. The pattern of variation of the equivalent heat transfer coefficient α_e defined as:

$$\alpha_e = \frac{\dot{q}_o}{T_o - T_b} = \frac{-\frac{dX}{dt} S \varepsilon \varrho_b \Delta h_v}{T_o - T_b} \qquad (1)$$

is the criterion of the division. The first period, for $X_{I-II} \leq X \leq X_i$, is the period of constant α_{eI}. The second period of drying for $X_{cr} \leq X \leq X_{I-II}$ is the period of the increasing α_{eII}. As the result of the analysis of the process three cases equivalent to three different methods of carrying out the process in a boiling region (Figure 4) were distinguished.

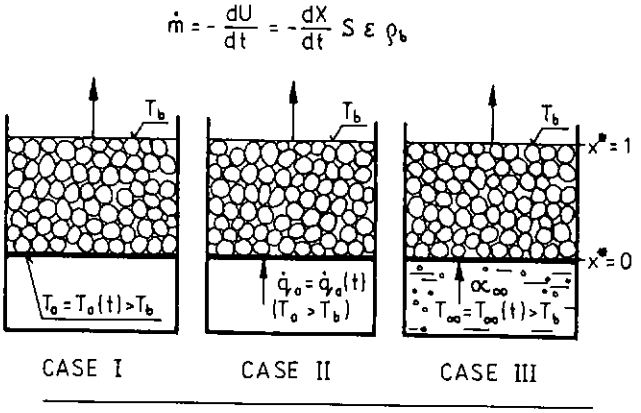

Figure 4. Physical Situation of Modelling Object for Moisture Content Range of Bed $X_{cr} \leq X \leq X_i$

The process of vacuum contact drying of porous media in the boiling region can be performed by the three following methods:

1. at $T_o = T_o(t)$, where the temperature of hot surface $T_o(t)$ is known time function;
2. at $\dot{q}_o = \dot{q}_o(t)$, where heat flux density supplied to the hot surface $\dot{q}_o(t)$ is known time function;
3. at $T_\infty = T_\infty(t)$ and α_∞ = const, where the temperature of the heating medium $T_\infty(t)$ is known function of time.

The process of vacuum contact drying of porous media with internal porosity (investigated object) has a few characteristics (outputs). They can be obtained from the single run of the process. The average drying rate $-dX/dt = -dX/dt(t)$, the average bed moisture content $X = X(t)$ and temperature in any point of the dried bed $T = T(x,t)$ are exemplary dynamic characteristics (dependent on time). Analogically, the distinctive moisture content of the bed X_{I-II} and the equivalent heat transfer coefficient in the first drying period α_{eI} are exemplary static characteristics of the investigated object. In the investigated process the whole bed, for the moisture content range $X_{cr} \leq X \leq X_i$, is wet (Figure 4). Evaporation of the moisture take place, almost completely, on the hot surface. The change of this physical situation occurs after reaching the critical moisture content X_{cr} by the bed. Then, the dry layer of the bed appears directly at the hot surface. Evaporation of the moisture take place on plane moving bounda-

ry and the falling drying rate period (third period) begins from this moment.

MATHEMATICAL MODELLING OF VACUUM CONTACT DRYING FOR MOISTURE CONTENT RANGE $X_{cr} \leq X \leq X_i$

Identification of the Static Characteristics of the Investigated Object

It results from the analysis of the static characteristics that they are dependent mainly on the following groups of input parameters (Figure 5):

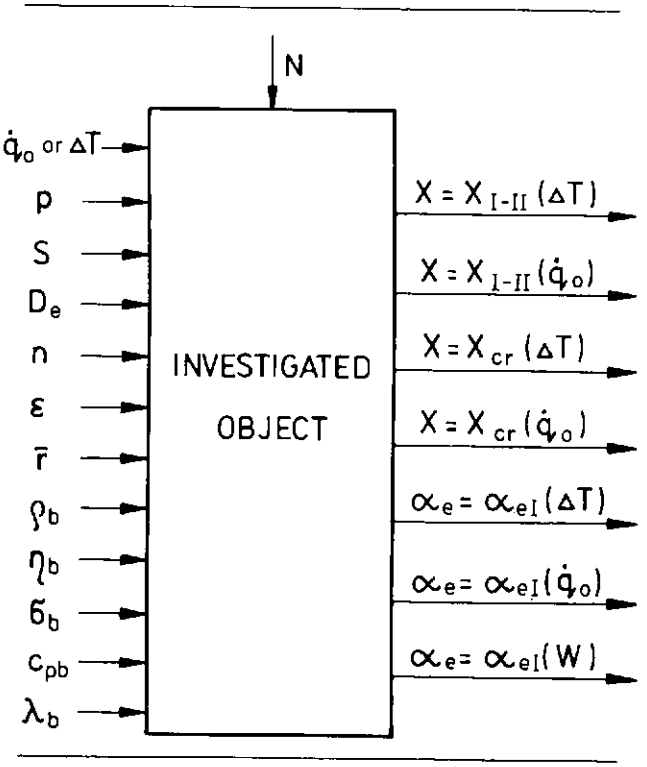

Figure 5. General Scheme of Mathematical Models of Identified Static Characteristics

1. state variables of the process (ΔT or $\dot{q}_o$, p);
2. physical properties of the bone dry bed (S, D_e, n, ε, $\bar{r}$);
3. physical properties of the liquid saturating the dried bed (ρ_b, η_b, σ_b, c_{pb}, λ_b).

Parameters p, $\dot{q}_o$, S and ΔT are measurable and controllable. The others are measurable and uncontrollable. Because the relationships between particular static characteristics of the investigated object and investigated input parameters are unknown, the identification of mathematical models of characteristics X_{I-II}, X_{cr}, α_{eI}, α_{eII} should be carried out. They are so-called the "black box" models. For modelling the process of vacuum contact drying and comparison model solutions with experimental results, the program of proper investigations comprising two experimental series was made. The main series of investigations consisting of 384 experiments and comprising the full factorial experiment was made for the case II $\dot{q}_o$ = const. In particular trials the following input parameters were changed:

(a) kind of the porous medium (all six media choosen for investigations);
(b) kind of the wetting liquid (water, methyl alcohol, n-propyl alcohol, n-butyl alcohol);
(c) q_o on two levels: 5000 and 14000 W/m^2;
(d) S on two levels: 0.005 and 0.025 m;
(e) p on four levels: 1333; 33330; 67993 and 97323 N/m^2;

The second series consisting of 108 experiments and comprising incomplete factorial experiment was made for the case I T_o = const. In particular trials, instead of $\dot{q}_o$, ΔT on four levels 5; 10; 15 and 20 K was changed. The others input parameters were changed in the same way as in the main experimental series. Functional relationships between the static characteristics and input parameters of the object can be approximated (identified) in general case by numerical equations. To determine the optimum form of these equations the algorithm of stepwise regression analysis [15] was used. The exemplary mathematical models of particular characteristics [16] obtained for $\dot{q}_o$ = const are presented below.

$$X_{I-II} = 12.349 + 42700 D_e^2 - 0.114\varepsilon - 7.02\times10^{-7} n - 1.08\times10^{-2} \rho_b + 2.57\times10^{-4} \eta_b^{-1} + 144\,\sigma_b^2 + 0.106 c_{pb}^2 + 4.63\,\lambda_b^2 + 1.53\times10^{-3} S^{-1} - 9.10\times10^{-4} \dot{q}_o^{0.5} - 1.081\log p \qquad (2)$$

The ratio of standard deviations (residual) to the mean value of dependent variable which is the average relative error of identification is evaluated (in percentages) as:

$$\frac{\bar{\sigma}_y}{\bar{y}} 100 = 9.88\%$$

$$X_{cr} = 27.659 + 69.90 D_e + 4.25\times10^{-2}\varepsilon + 3.37\times10^{-7} n - 9.571\log \rho_b + 11.70\,\eta_b + 0.4681\log \sigma_b + 3.021\log c_{pb} - 6.10\times10^{-2}\lambda_b + 6.31\times10^{-4} S^{-1} + 2.26\times10^{-3}\dot{q}_o^{0.5} \qquad (3)$$

where: $\frac{\bar{\sigma}_y}{\bar{y}}$ 100=11.98%

$$\log \alpha_{eI} = -1.741 + 2.18\times10^{-6} D_e^{-1} - 2395 n^{-1} + 4477\, \varrho_b^{-1} + 7.33\times10^{-5} \eta_b^{-1} + 5.09\times10^{-3} \sigma_b^{-1} - 4.39 c_{pb}^{-1} + 1.32\, \lambda_b^2 - 294 S^2 + 8.92\times10^{-3} q_o^{0.5} - 411 p^{-1} \quad (4)$$

where $\frac{\bar{\sigma}_y}{\bar{y}}$ 100=17.24% (related to the α_{eI}, not to the $\log \alpha_{eI}$)

Similar equations were obtained for the characteristics X_{I-II}, X_{cr} and α_{eI} for the case I T_o= const in which ΔT exists without $\dot{q}_o$. In the second drying period the identification of the characteristic α_{eII} should be done. It was proved that the best generalization of experimental results is obtained assuming linear increase of the characteristic α_{eII} in relation to the characteristic α_{eI}.

$$\alpha_{eII} = \alpha_{eI}\left(1 + 1.11 \frac{(X_{I-II} - X)}{(X_{I-II} - X_{cr})}\right) \quad (5)$$

The average relative error of identification, determined for $X=X_{cr}$, with assumption α_{eI} free of error is evaluated as:

$\frac{\bar{\sigma}_y}{\bar{y}}$ 100=18.6%

The equation (5) for α_{eII} holds for both methods of process performance.

General Mathematical Model of the Process for the First and the Second Drying Periods

Having identified the static characteristics, the general mathematical model of the process valid in the first and the second drying periods should be considered. From the overall heat balance equation:

$$\dot{q}_o(t) = -\frac{dX}{dt}(t)\, S\, \varepsilon\, \varrho_b\, \Delta h_v = \alpha_{eI}(T_o(t) - T_b) = \alpha_\infty (T_\infty(t) - T_o(t)) \quad (6)$$

drying rate and, after some calculations, the average moisture content of the bed in any arbitrary moment of time t can be determined for all the three methods of carrying out the process. Equations of particular dynamic characteristics will be by way of example presented for the case III $T=T_\infty(t)$; α_∞=const (Figure 4). This is the most difficult case to calculate because either temperature T_o or value $\dot{q}_o$ are unknown a priori. Thermal resistance of hot surface (temperature drop on the wall separating a heating medium from the dried bed) was neglected. The error caused by this simplifying assumption does not exceed a few per cent. To simplify the notation the equations will be presented for the particular way of the case III realization i.e. T_∞=const.

The first period $X_{I-II} \le X \le X_i$

Making use of the previously defined static characteristic α_{eI}, the following balance equations can be written:

$$-\frac{dX}{dt}\, S\, \varepsilon\, \varrho_b\, \Delta h_v = \alpha_\infty (T_\infty - T_o) \quad (7)$$

and

$$\dot{q}_o = \alpha_\infty (T_\infty - T_o) = \alpha_{eI}(T_o - T_b) \quad (8)$$

The static characteristic α_{eI} can be calculated from the equation for T_o=const as well as from that for $\dot{q}_o$=const. The drying rate equation directly results from rearrangement of the relationships (7) and (8)

$$-\frac{dX}{dt} = \frac{\alpha_\infty (T_\infty - T_o)}{S\, \varepsilon\, \varrho_b\, \Delta h_v} = \frac{\alpha_{eI}(T_o - T_b)}{S\, \varepsilon\, \varrho_b\, \Delta h_v} \quad (9)$$

By separation of variables in equation (9) and integration, one obtains

$$-\int_{X_i}^{X} dX = \frac{\alpha_\infty (T_\infty - T_o)}{S\, \varepsilon\, \varrho_b\, \Delta h_v} \int_{t_i}^{t} dt \quad (10)$$

If we assume initial conditions $t_i=0$ for X_i, we obtain the equation of the characteristic $X = X(t)$

$$X(t) = X_i - \frac{\alpha_\infty (T_\infty - T_o)}{S\, \varepsilon\, \varrho_b\, \Delta h_v} t \quad (11)$$

Assuming temperature gradient linearity $\frac{dT}{dx}$ = const, the following expression for temperature in any arbitrary point of the dried bed can be received (characteristic $T(x^*)$):

$$T(x^*) \cong T_o - x^*(T_o - T_b) \quad (12)$$

The above assumption is very close to the real physical situation. Substituting the expression for T_o obtained from (8) into

(12), two equivalent equations for the characteristic $T(x^*)$ one gets

$$T(x^*) \cong \frac{\dot{q}_o}{\alpha_\infty}(x^*-1) + T_\infty (1-x^*) - x^* T_b \qquad (13a)$$

$$T(x^*) \cong \frac{\dot{q}_o}{\alpha_{eI}}(1-x^*) + T_b \qquad (13b)$$

In the above equations $\dot{q}_o$ is unknown in any evident form. It can be evaluated making use of the both equations for the characteristic α_{eI} i.e. equation (4) for $\dot{q}_o$= const or that one for T_o= const, which was not cited here. Equations, one of two things for α_{eI} e.g. (4) and (8) are solved together by trial and error method on a digital computer. The proposed method of computation enables the direct evaluation of the characteristic $T(x^*)$ from (12) also valid for the case I.

The second period $X_{cr} \leq X \leq X_{I-II}$

The drying rate characteristic $-dX/dt = -dX/dt(t)$, the characteristics $X = X(t)$ and $T(x^*)$ can be obtained from the solution of the following system of equations:

$$-\frac{dX}{dt} = \frac{\alpha_\infty}{S\,\varepsilon\,\varrho_b\,\Delta h_v}\left(T_\infty - T_o(X)\right) \qquad (14a)$$

$$\dot{q}_o(X) = \alpha_{eI}\left(T_o(X) - T_b\right) = \alpha_\infty\left(T_\infty - T_o(X)\right) \qquad (14b)$$

$$T(x^*) = \frac{\dot{q}(X)\left(X_{I-II} - X_{cr}\right)}{\alpha_{eI}\left(X_{I-II} - X_{cr} + 1.11\left(X_{I-II} - X\right)\right)} \times (1-x^*) + T_b \qquad (14c)$$

Equations (14a) and (14b) are immediately obtained from the equations (9) and (8) respectively, after considering the fact that $T_o = T_o(X)$ and α_{eII} replaces α_{eI} in the second period of the case III. The equation (14c) is evaluated after introducing $\dot{q}_o(X)$ instead of $\dot{q}_o$ and the term on the right-hand side of (5) instead of α_{eI} into (13b). It is to be noted that α_{eI} for (14b) and (14c) is to be calculated from the identified equations for the first period e.g. from (4). The initial conditions for the system (14) are established as follows: $X = X_{I-II}$ and $T_o(X) = T(x^*=0) = T_o$= const from the first drying period for $t = t_{I-II}$. The differential equation (14a) can be integrated by any arbitrary numerical method (e.g. Euler's one) in the range of bed moisture content $X_{cr} \leq X \leq X_{I-II}$ and the characteristic $X = X(t)$ is obtained. Simultaneously, the values $T_o(X)$ and $\dot{q}_o(X)$ should be determined for each step of integration. They can be evaluated by trial and error method from (14b) while making use of one of two things for α_{eI} e.g. (4) and $T(x^*)$ can be also obtained from (14c). The simultaneous system (14) is solved numerically and the computations are done on a digital computer. It is understood that equations of the dynamic characteristics will undergo a certain modification if the process is carried out with known functional relationships $T_o = T_o(t)$; $\dot{q}_o = \dot{q}_o(t)$ or $T_\infty = T_\infty(t)$ and α_∞ = const. The evaluation a priori of the static characteristics X_{I-II}, X_{cr} and α_{eI} is of certain difficulty at that time. In this instance the corresponding integral values, to calculate these characteristics from the identified equations e.g. from (2), (3) and (4) should be taken into account, for example:

$$T_o = \frac{\int_{t_1}^{t_2} T_o(t)\,dt}{t_2 - t_1} = \text{const} \qquad (15a)$$

and

$$T_\infty = \frac{\int_{t_1}^{t_2} T_\infty(t)\,dt}{t_2 - t_1} = \text{const} \qquad (15b)$$

The relationships between different definitions of bed moisture content which can be easily derived, enable recalculations.

$$U = XS\,\varepsilon\,\varrho_b \qquad (16)$$

$$Y = X\frac{\varrho_b\,\varepsilon}{\varrho_{bu}} = X\frac{\varrho_b\,\varepsilon}{\varrho_s(1-\varepsilon)} \qquad (17)$$

Comparison with Experimental Data

The verification of the computational solutions of the model equations with the results of own experimental data showed a good agreement with the accuracy equal to that of identified equations for the characteristics α_{eI} and α_{eII}. It was done on many conditions of vacuum contact drying and the numerical procedure always results in a good simulation of the experimental drying data. The deviations of $-dX/dt(t)$, $X(t)$ and $T(x^*)$ between the observed and the numerically calculated values were ± 18% (at most) in the first

drying period, independently of the method of the process performance. In the second drying period the deviations are a little more significant that is, estimated values differ from the observed ones about ± 23% (at most), independently of the method of the process performance. The agreements are within the satisfactory accuracy from the practical point of view over the wide range of process parameters.

CONCLUSIONS

In order to simulate the process of vacuum contact drying of porous media with internal porosity for the bed moisture content range $X_{cr} \leq X \leq X_i$, some theoretical considerations and experiments were performed. The three cases equivalent to the three different methods of the process performance were distinguished. The drying period for $X_{cr} \leq X \leq X_i$, called in literature the period of constant rate is in the case of vacuum contact drying of porous media divided into two periods. The patern of variation of the equivalent heat transfer coefficient α_e is the criterion of the division. The identification of the static characteristics of the investigated object and modelling of its dynamic characteristics allowed us to distinguish all these parameters, from among state variables: p, $\dot{q}_o$ or ΔT, bone dry bed and wetting liquid parameters, which significantly influence the process. The process of vacuum contact drying of porous media with internal porosity, in the boiling region, was represented as the pool boiling process of a liquid on the hot surface, in presence at it of the solid phase particles. The developed general mathematical model is the versatile one, i.e. it is adequate both for vacuum contact drying of porous media without internal porosity and porous materials. Application of the model for the different methods of the process performance yielded a good agreement between predicted and experimental values over the wide range of process parameters.

ACKNOWLEDGEMENT

The authors wish to acknowledge the financial assistance of the Polish Academy of Sciences.

REFERENCES

1. Strumiłło, C., Fundamentals of Theory and Technique of Drying. WNT, Warszawa, 1975
2. Keey, R.B., Drying. Principles and Practice. Pergamon Press, London, 1972
3. Kessler, H.G., Chem. Ing. Techn., Vol. 41, p. 463, 1969
4. Kneule, F., Vakuumtechnik, Vol. 11, p. 115, 1962
5. Toei, R., et al., Vol. 24, p. 289, 1960
6. Kirschbaum, E., and Baumann, R.F., Chem. Ing. Techn., Vol. 23, p. 520, 1956
7. Stręk, F., and Dudczak, J., Inż. Chem., Vol. 4, p. 113, 1974
8. Stręk, F., and Dudczak, J., Inż. Chem., Vol. 4, p. 487, 1974
9. Ziołkowski, Z., and Kmieć, A., Inż. Chem., Vol.2, p. 129, 1972
10. Ziołkowski, Z., and Kmieć, A., Inż. Chem., Vol. 2, p. 357, 1972
11. Ziołkowski, Z., and Kmieć, A., Inż. Chem., Vol. 2, p. 691, 1972
12. Han, S.T., Pulp und Paper Magazine of Canada, Dec., T-537, 1964
13. Bunin, O.A., Osobiennosti Kontaktnoj Suski Poristych Materialov. Gosenergoizdat, Moskva, 1958
14. Stręk, F., et al., Vacuum Contact Drying of Porous Media, Second All Polish Symposium on Drying, Warszawa, Proceedings, p. 65, 1975
15. Draper, N.R., and Smith, H., Applied Regression Analysis. PWN, Warszawa, 1973
16. Stręk, F., and Nastaj, J., Some Aspects of Investigations of Vacuum Contact Drying of Porous Media with Internal Porosity, Third All Polish Symposium on Drying, Łódź, Proceedings, p. 215, 1978

MATHEMATICAL MODELLING AND SIMULATION OF VACUUM CONTACT DRYING OF POROUS MEDIA IN THE FALLING RATE PERIOD (BOUNDARY CONDITION OF THE FIRST KIND)

F. Stręk
J. Nastaj

Department of Chemical Engineering
Technical University of Szczecin, Szczecin, Poland

ABSTRACT

A versatile mathematical model of vacuum contact drying of porous media in the falling rate period is proposed. The process of vacuum contact drying of porous media was presented as the moving boundary problem of the plane of moisture evaporation. Boundary condition of the first kind (Dirichlet boundary condition) for the known functional relationship of the hot surface temperature from time was considered. The solution of this problem was resolved itself into a system of ordinary nonlinear differential equations. The process simulation for combinations of process parameters (i.e. total pressure, temperature of hot surface, physical properties of porous medium bed and moisture), which occur in experimental investigations was performed. System of differential equations was solved numerically and values of drying rate, integral moisture content of the bed, moving boundary position as well as temperature in any point of the bed and at any moment of time were obtained. Comparison of the results of the process simulation with the own experimental data was performed. Applicability of the presented model for purposes of design, optimisation and control of the process was stated.

NOMENCLATURE

A = surface area, m^2

A', B', C' = coefficients in equation (in general)

c_{pm} = specific heat capacity of bone dry porous medium, J/kgK

Δh_v = specific latent heat of vaporization including heat of wetting, J/kg

H = moving boundary position of moisture evaporation in cartesian coordinate system, m

$\dot{H}^* = dH^*/dt$, s^{-1}

k = function symbol

M = mass, kg

N = number of differential equations in system (14)

p = total pressure, N/m^2

$\dot{q}$ = heat flux density, W/m^2

S = layer thickness of dried bed, m

t = time, s

T = thermodynamic temperature, K

$\bar{T}^*$ = dimensionless quantity in the Equation (13) and the system (14), -

U = moisture content of dried bed per unit hot surface ($U = M_{ld}/A_o$), kg_{ld}/m^2

V = volume, m^3

x = cartesian coordinate in dried bed, m

X = moisture content of dried bed (volumetric saturation, $X = V_{ld}/V_p$), m^3_{ld}/m^3_p

Z = surface bounding (Figure 1)

ε = total porosity of dry bed, m^3_p/m^3

κ = thermal diffusivity of dried bed, m^2/s

λ = thermal conductivity of dried bed, W/mK

ϱ = mass density, kg/m^3

τ_d = dimensionless time of complete drying, -

τ_i = dimensionless initial time, -

Subscripts

A = region A (dry)

b = at the boiling point of liquid

B = region B (moist)

bu = bulk of bone dry porous medium

cr = critical

eA = equivalent of the A (dry) region

l = local

ld = liquid

o = hot surface

p = pores

Superscripts

- = averaged quantity

Dimensionless Numbers

$$\Delta h_v^*(\tau) = \frac{X_l(H^*)\,\varepsilon\,\varrho_l\,\kappa_{eA}\,\Delta h_v}{(T_o(H^*)-T_b)\,\lambda_{eA}}$$

dimensionless parameter in the system (11) and (14)

$$H^*(\tau) = \frac{H(t)}{S}$$ dimensionless position of moving boundary

$$q^*(H^*) = \frac{\dot{q}(H^*)\,S}{\lambda_{eA}(T_o-T_b)}$$ dimensionless heat flux density

$$T_A^* = \frac{T_A-T_b}{T_b-T_o(t)}$$ dimensionless temperature of region A

INTRODUCTION

In the process of vacuum contact drying carried out in the most intensive i.e. boiling region, we deal with unsteady-state heat transfer from hot surface to a moving boundary of moisture evaporation changing its position in time. This phenomenon occurs in the falling rate period of the process after reaching the critical moisture content X_{cr} by the dried bed.

The essential feature of this problem is the existence of a moving boundary usually as a result of change of phase the location of which is unknown a priori and is in itself dependent upon the amount of heat or mass which has been brought up to it in the past. In the investigated process, the three methods of the process realization in the third period ($0 \le X \le X_{cr}$) equivalent to the three boundary conditions at the hot surface (boundary of the investigated region) are particularly important from the technological point of view. These three standard boundary conditions for the problem of unsteady-state heat transfer with the moving boundary of moisture evaporation correspond to the three cases (methods of the process realization) considered at the modelling of the process in the constant drying rate period [1]. Different kinds of problems within a given boundary condition at the hot surface result from different boundary conditions at the moving boundary and at the exposed surface of the dried bed. In this paper only the boundary condition of the first kind (Dirichlet boundary condition) at the hot surface has been considered. At present, the specified boundary condition should be discussed in details to carry out a modelling of the process of vacuum contact drying in the falling rate period.

MATHEMATICAL MODEL

Assumptions

A physical model of the investigated object in the falling rate period of drying is presented in Figure 1.

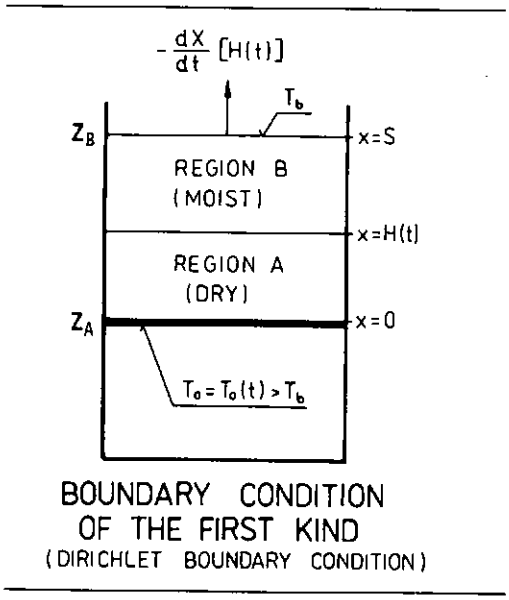

Figure 1. Physical Model

Let us consider two regions separated at any time t by an interface H (t) position of which in space is an unknown function of time. The two regions are bounded in space by the two surfaces Z_A and Z_B equations of which relative to a conveniently chosen three dimensional coordinate system have the form $Z_A(x) = 0$, $Z_B(x) = S$. Surfaces Z_A and Z_B being fixed in space will be called the fixed interfaces. The interface H(t) the position of which is function of time will be called the "moving boundary". The majority of physical problems are described as one dimensional problems in rectangular coordinate system. In these instances the moving boundary is described geometrically as a plane moving boundary and the problem may be described by only two variables: time and a single

position variable. A dry porous medium occupies the region A bounded by Z_A and $H(t)$, a wet porous medium occupies the region bounded by $H(t)$ and Z_B. In both regions a diffusant (e.g. heat) is present. Diffusional processes cause transport of the diffusant relative to the cartesian co-ordinate x, and transfer from one region to another. It is theoretically assumed that two regions are stagnant in the sense that they are free from convection currents, but which may be in relative bodily motion along the normal to the surface $H(t)$, and they are a continuous phase. If heat conduction occurs in one region (e.g. region A) this is one-region problem, otherwise this is two-region problem. The acceptance of these assumptions is justified by the fact that one dimensional mathematical models describe the real physical situation in a relatively simple but at the same time detailed enough way to predict the process running. Assuming in simplification that a porous medium:

(a) is a continuous phase described by equivalent quantities;
(b) has constant thermal properties;

and

(c) lacks of distributed energy or mass sources;

the appropriate transport equations for each region can be written. The boundary conditions at the fixed interfaces Z_A and Z_B may be represented in terms of the Dirichlet, Neumann or mixed Dirichlet-Neumann type. In the boundary condition of the first kind (Dirichlet boundary condition) the field is prescribed along the boundary surface, and for the general case it is a function of both time and position coordinate; i.e.,

$$T = f(x,t) \tag{1}$$

The function T satisfies two boundary conditions at the moving boundary. The first one is a Dirichlet type boundary condition which can be expressed as

$$T\left(H(t),t\right) = k(t) \tag{2}$$

where $k(t)$ is a function of time determined by the physical conditions of the problem. Occasionally this may be written as $k\left(H(t)\right)$ to emphasise that k is a functional which is to say that it is a function of the unknown function $H(t)$, The second boundary condition on T at the moving boundary accounts for interface transport; i.e., gives an energy balance at the moving boundary. The initial temperature field in both regions is specified function of position and can be generally expressed by the following equation

$$T(x,0) = k(x) \tag{3}$$

The initial position of the moving boundary; i.e., $H(0)$ is also specified. It is stated, in practice, that equilibrium moisture content for the process of vacuum contact drying of porous media is equal to zero.

Statement of the Problem

At time $t=0$ the hot surface is brought to some temperature $T_o > T_b$ and held as $T_o = T_o(t) > T_b$ thereafter. Let the average moisture content of a dried bed of porous medium be e.g. $X = X_{cr}$ at time $t=0$, and temperature in the whole bed region $0 \le x \le S$ is equal to $T(x,0) = T_b$. The particular kind of this problem, for which own experimental work was made, is the one for T_o = const. Assuming that one dimensional and one-region problem of the plane moving boundary is considered, the appropriate differential equation and associated boundary conditions, which were mentioned in the previous section, may be written as follows:

$$\kappa_{eA}\frac{\partial^2 T_A}{\partial x^2} = \frac{\partial T_A}{\partial t}$$

$$\text{in} \quad 0 \le x \le H(t), \; t > 0 \tag{4a}$$

$$T_A = T_o(t)$$

$$\text{at} \quad x = 0, \; t > 0 \tag{4b}$$

$$T_A = T_b$$

$$\text{at} \quad x = H(t), \; t > 0 \tag{4c}$$

$$\lambda_{eA}\frac{\partial T_A}{\partial x} = -X_1(H)\,\varepsilon\,\varrho_b\,\Delta h_v\frac{dH}{dt}$$

$$\text{at} \quad x = H(t), \; t > 0 \tag{4d}$$

$$\frac{\partial T_A}{\partial x} = 0$$

$$\text{at} \quad x = S, \; t > 0 \tag{4e}$$

From the equation (4d) while making use of the following definition $X_1(H)\,\varepsilon\,\varrho_b dH/dt = dU/dt$ one obtains:

$$\frac{dU}{dt} = -\frac{\lambda_{eA}}{\Delta h_v}\frac{\partial T_A}{\partial x} \quad \text{at } x = H(t), \; t > 0 \tag{5}$$

Introducing the expression for U, which was cited in (1), i.e. $U = XS\varepsilon\rho_b$ into (5), the additional equation for the average moisture content of the bed is obtained. The result is

$$\frac{dX}{dt} = -\frac{\lambda_{eA}}{S\varepsilon\rho_b\Delta h_v}\frac{\partial T_A}{\partial x} \quad \text{at} \quad x = H(t), \; t>0 \tag{6}$$

This equation should be added to the system of equations (4). This problem is cast into a more convenient form by defining the following dimensionless variables:

$$x^* = \frac{x}{S} \tag{7}$$

$$\tau = \frac{\kappa_{eA}t}{S^2} \tag{8}$$

$$H^*(\tau) = \frac{H(t)}{S} \tag{9}$$

$$T_A^* = \frac{T_A - T_b}{T_b - T_o(t)} \tag{10}$$

For practical reasons it is also convenient to replace the variable $T_o(\tau)$ by the equivalent variable $T_o(H^*)$. It means that $T_o(\tau) \equiv T_o(H^*)$. The problem then runs as follows:

$$\frac{\partial^2 T_A^*}{\partial x^{*2}} = \frac{\partial T_A^*}{\partial \tau} \quad \text{in } 0 \le x^* \le H^*(\tau), \; \tau>0 \tag{11a}$$

$$\frac{dX}{d\tau} = -\frac{X_1(H^*)}{\Delta h_v^*}\frac{\partial T_A^*}{\partial x^*} \quad \text{at} \quad x^* = H^*(\tau), \; \tau>0 \tag{11b}$$

$$T_A^* = -1 \quad \text{at} \quad x^* = 0, \; \tau>0 \tag{11c}$$

$$T_A^* = 0 \quad \text{at} \quad x^* = H^*(\tau), \; \tau>0 \tag{11d}$$

$$\frac{dH^*}{d\tau} = \frac{1}{\Delta h_v^*(\tau)}\frac{\partial T_A^*}{\partial x^*} \quad \text{at} \quad x^* = H^*(\tau), \; \tau>0 \tag{11e}$$

$$\frac{\partial T_A^*}{\partial x^*} = 0 \quad \text{at} \quad x^* = 1, \; \tau>0 \tag{11f}$$

where

$$\Delta h_v^*(\tau) = \frac{X_1(H^*)\,\varepsilon\,\rho_b\,\kappa_{eA}\,\Delta h_v}{(T_o(H^*)-T_b)\,\lambda_{eA}} = \frac{X_1(H^*)\,\varepsilon\,\rho_b\,\Delta h_v}{(T_o(H^*)-T_b)\,(\rho_{bu}c_{pm})_{eA}} \tag{12}$$

The particular case of the dimensionless parameter $\Delta h_v^*(\tau)$ is the one in which $T_o(H^*) = T_o = \text{const}$ and, e.g., $X_1(H^*) = X_{cr} = \text{const}$. At that time the parameter $\Delta h_v^*(\tau)$ is constant (independent of dimensionless time τ) over the range of integration and it should be indicated as Δh_v^*. The quantities $X_1(H)$ or $X_1(H^*)$ mean for the general case a local moisture content distribution in the bed at the moment when moving boundary passes any position co-ordinate H or H^* respectively. Solutions of the system (11) are expected within the range of $0 \le H^* \le 1$.

Solution of the Problem

Using the finite integral-transform technique (2,3), the solution of this problem takes form:

$$T_A^* = \frac{2}{H^*}\sum_{j=1}^{N-2}\bar{\bar{T}}_{Aj}^*(\tau)\times\sin\frac{j\pi x^*}{H^*} \tag{13}$$

where $\bar{\bar{T}}_{Aj}^*(\tau)$ and $H^*(\tau)$ are determined from the following system of ordinary, first-order, nonlinear differential equations

$$\frac{d\bar{\bar{T}}_{Aj}^*}{d\tau} = \frac{j^2\pi^2}{H^{*2}}\bar{\bar{T}}_{Aj}^* - \frac{j\pi}{H^*} - \frac{2j}{H^*}\frac{1}{H^*}\sum_{i=1}^{N-2}\bar{\bar{T}}_{Ai}^* B_{ij} \quad j=1,2,3,\ldots,N-2 \tag{14a}$$

$$\frac{dH^*}{d\tau} = \frac{2\pi}{\Delta h_v^*(\tau)\,H^{*2}}\sum_{i=1}^{N-2}(-1)^i i\,\bar{\bar{T}}_{Ai}^* \tag{14b}$$

$$\frac{dX}{d\tau} = -\frac{2\pi X_1(H^*)}{\Delta h_v^*(\tau)\, H^{*2}} \sum_{j=1}^{N-2} j\bar{\bar{T}}_{Aj}^*(\tau) \cos j\pi \tag{14c}$$

$$B_{ij} = \begin{cases} \frac{i}{i^2-j^2}(-1)^{i+j+1} & \text{for } j \neq i \\ -\frac{1}{4j} & \text{for } j = i \end{cases} \tag{14d}$$

and N is the number of differential equations in the system (14). Equation (14c) is immediately obtained substituting the partial derivative $\partial T_A^*/\partial x^*$ in (11b) by its value obtained from the differentiation of analytical solution (13). The initial conditions are given e.g. by

$$H^*_{|\tau=0} = 0 \tag{14e}$$

$$\bar{\bar{T}}^*_{Aj}\Big|_{\tau=0} = 0 \tag{14f}$$

$$X_{|\tau=0} = X_{cr} \tag{14g}$$

The functions on the right-hand side of equations (14a), (14b) and (14c) are indeterminate at $H^*=0$, and so system (14) cannot be integrated numerically starting from $\tau=0$. However, a solution to (11) for small τ may be obtained by noticing that for small values of τ the thickness H^* of the dry layer of the bed is thin enough so that the temperature profile in the dry region is essentially of the steady-state type; i.e. linear. Hence, we have

$$T_A^* = \frac{x^*}{H^*} - 1 \tag{15}$$

and

$$\frac{dH^*}{d\tau} = \frac{1}{\overline{\Delta h}_v^*(\tau)\, H^*} \tag{16}$$

Integrating (16) while making use of (14e) and assuming that the parameter $\overline{\Delta h}_v^*(\tau)$ is constant quantity averaged over the integration range i.e.

$$\overline{\Delta h}_v^*(\tau) = \frac{\bar{X}_1(H^*)\, \varepsilon\, \varrho_b\, \kappa_{eA}\, \Delta h_v}{\left(\bar{T}_o(H^*) - T_b\right) \lambda_{eA}} \tag{17}$$

where

$$\bar{T}_o(H^*) = \frac{\int_0^{H^*(\tau_o)} T_o(H^*)\, dH^*}{H^*(\tau_o)} \tag{18}$$

and

$$\bar{X}_1(H^*) = \frac{\int_0^{H^*(\tau_o)} X_1(H^*)\, dH^*}{H^*(\tau_o)} \tag{19}$$

one obtains

$$H^{*2} = \frac{2}{\overline{\Delta h}_v^*(\tau)}\, \tau_o \tag{20}$$

The similar asymptotic solution given by equations (15) and (20) has been derived and used elsewhere (4). This asymptotic solution may then be used to compute suitable initial conditions for system (14). The initial conditions for system (14) may then be written as follows

$$H^*(\tau_o) = \left[\frac{2\,\lambda_{eA}\left(\bar{T}_o(H^*) - T_b\right)}{\bar{X}_1(H^*)\, \varepsilon\, \varrho_b\, \kappa_{eA}}\, \tau_o\right]^{\frac{1}{2}} \tag{21a}$$

$$\bar{\bar{T}}^*_{Aj}(\tau_o) = \frac{H^*(\tau_o)}{j\pi} \tag{21b}$$

$$X^*(\tau_o) = X_{cr} - H^*(\tau_o)\, \bar{X}_1(H^*) \tag{21c}$$

The value of τ_o can be chosen in a vay that always made e.g. $H^*(\tau_o) = 0.01$ or $H^*(\tau_o) = 0.05$. These values of $H^*(\tau_o)$ were found to be small enough so that the assumption of using the asymptotic solution to start the solution of system (14) is valid.

SIMULATION OF THE PROCESS

Computer Results

A computer subroutine, which solves a general system of first-order ordinary differential equations with given initial values, was used for the solution of system (14) with the initial conditions (21). This subroutine uses the predictor-corrector equations of R.L. Crane (5), which have a wide range of stability. The necessary backpoints are initially calculated with the Runge-Kutta-Gill single step

method. At each step the calculation procedure gives an estimate for the local truncation error; thus, the procedure is able, without significant additional calculation time, to choose and change the step size. Therefore, control of accuracy and adjustment of step size is done automatically. The initial time step was set equal to 0.05 , and this was automatically adjusted during the whole computation by halving or doubling so that the maximum error at each step remained less than 10^{-4}. Since only finite systems can be solved numerically the value of N in system (14) was set equal to a finite value and was allowed to increase. Calculations were made for N = 5,7,11,15. In all these cases the computations were stopped when H^* reached unity. This numerical analysis showed that the subsequent approximations converge quickly beginning with N = 5. The solutions of system (14), for different values of $\overline{\Delta h_v^*}(\tau)$ which appear in vacuum contact drying, were obtained with N = 5 ; this being considered an appropriate balance between accuracy and execution time on a digital computer. The results were simultaneously obtained in the dimensional and dimensionless variables. The system (14) was numerically integrated for the same conditions as in own experiments i.e. $T_o(H^*)=T_o$= const was taken to calculate $\Delta h_v^*(\tau)$ in each step of integration. Values of $X_1(H^*)$ were calculated from the expression of the type:

$$X_1(H^*) = A' H^{*2} + B' H^* + C' \qquad (22)$$

which had been previously derived on the basis of own experimental investigations. It results from performed identification of coefficients A', B', C' that they are exclusively dependent on these parameters which influence value X_{cr}. The conditions of carrying out the process in the first and second period, causing special distribution of moisture content in the bed at X_{cr}, are here of great importantce apart from physical parameters of the bed and liquid. If drying concerns the beds of low moisture content $X_i < X_{cr}$ which were not submitted to foregoing drying in the first or the second period, X_i= const should be taken as $X_1(H^*)$. For the simulation purpose of the investigated process over the experimental range of total pressure variation p it is necessary to predict the boiling point of liquid under given pressure p and then to predict physical properties of liquid ϱ_b and Δh_v as the function of this temperature. The boiling point of given liquid as the function of pressure p was calculated from Antoine'a equation (6). The relationship of the given liquid density from temperature was approximated by a linear function and the one of the heat of vaporization without heat of wetting by a quadratic function. The identification of the thermal properties λ_{eA}, κ_{eA}, for dry porous media used in experiments, was separately done on the basis of own measurements within the wide range of pressure and temperature variability. A establishing the temperatures at which values λ_{eA} and κ_{eA} should be accepted creats a some dificulty in the above calculations. No essential influence of temperature on κ_{eA} (contrary to the essential influence of pressure p) for porous media with internal porosity was proved. The values λ_{eA} were accepted in the average temperature $T=(T_o+T_b)/2$ = const. The exemplary results of numerical integration of system (14) with initial condition (21) for different values of Δh_v^* (constant value over the range of integration) or $\overline{\Delta h_v^*}(\tau)$ are shown in Figures 2 through 7.

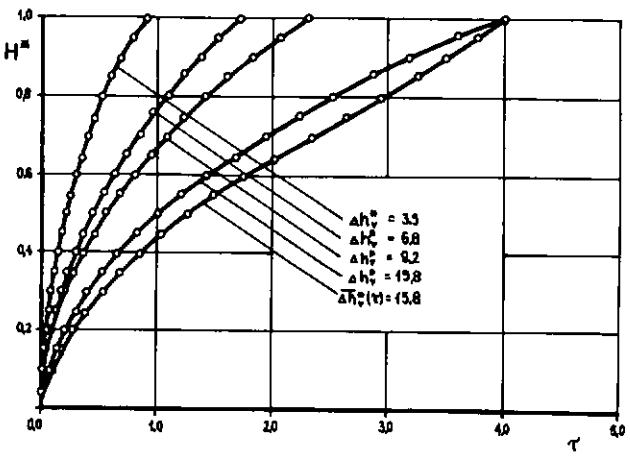

Figure 2. Position of the Dry Front Versus Dimensionless Time, for Different Values of Δh_v^* or $\overline{\Delta h_v^*}(\tau)$

In Figures 2 and 3 the dry front location is plotted versus τ for various values of Δh_v^* or $\overline{\Delta h_v^*}(\tau)$ ranging from 3.5 to 131.2 . The plots for the reciprocal of the dimensionless heat flux density $\lambda_{eA}(T_o - T_b) / \dot{q}(H^*)S$ at the hot surface x = 0, for different values of $\overline{\Delta h_v^*}(\tau)$, are shown in Figure 4. In Figures 5 and 6 calculated characteristics $X = X(\tau)$ for different values of $\overline{\Delta h_v^*}(\tau)$ are shown.

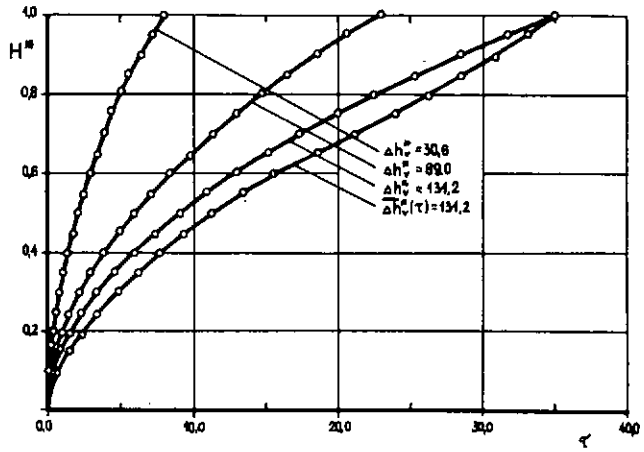

Figure 3. Position of the Dry Front Versus Dimensionless Time, for Different Values of Δh_v^* or $\overline{\Delta h}_v^*(\tau)$

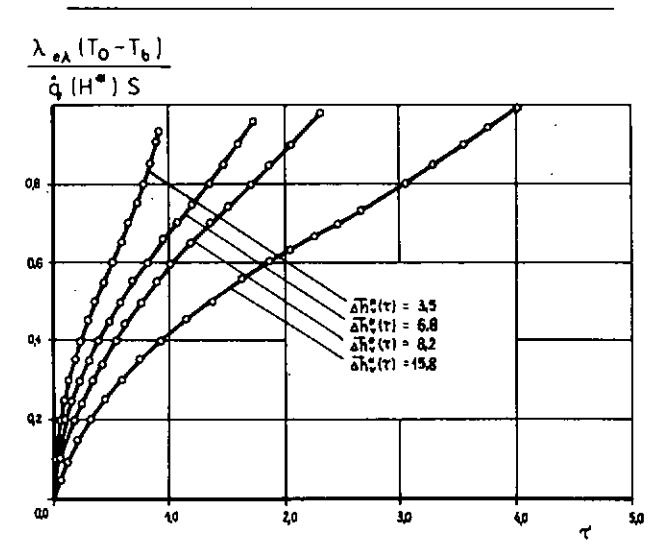

Figure 4. Plot of the Reciprocal of the Dimensionless Heat Flux Density Versus Dimensionless Time, for Different Values of $\overline{\Delta h}_v^*(\tau)$

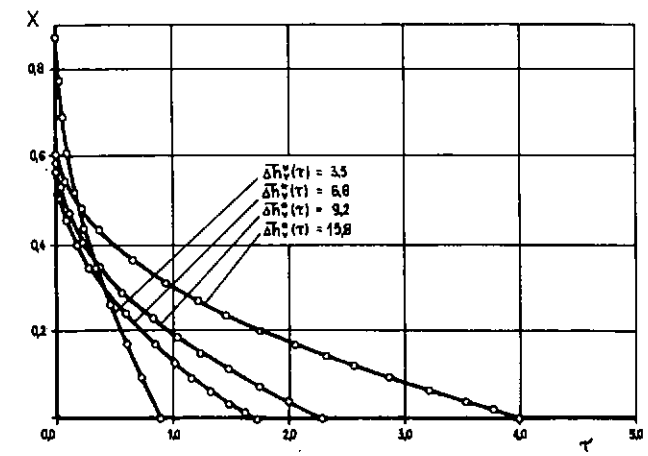

Figure 5. Moisture Content of the Bed Versus Dimensionless Time, for Different Values of $\overline{\Delta h}_v^*(\tau)$

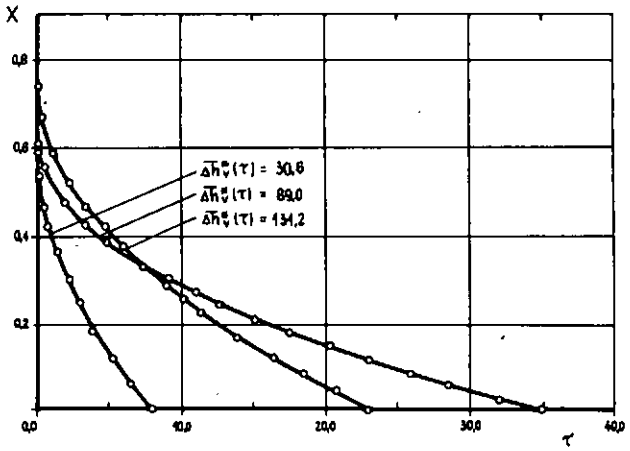

Figure 6. Moisture Content of the Bed Versus Dimensionless Time, for Different Values of $\overline{\Delta h}_v^*(\tau)$

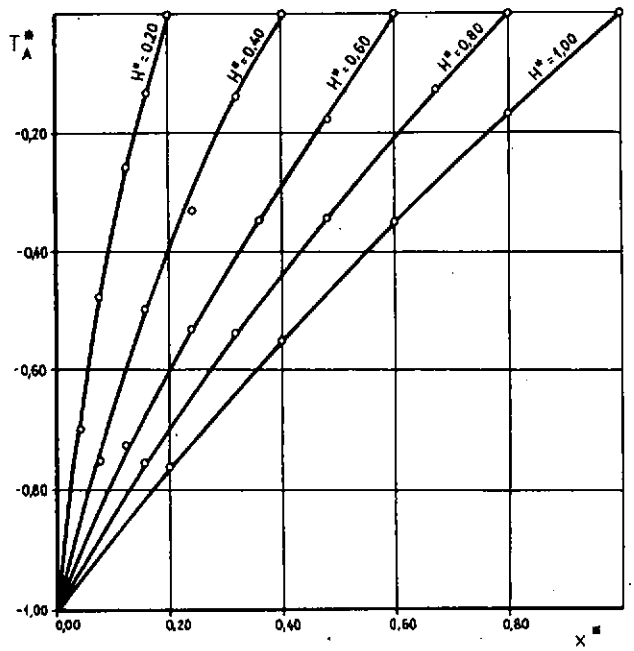

Figure 7. Temperature Profiles for Vacuum Contact Drying of Porous Media at T_o = const; $\overline{\Delta h}_v^*(\tau) = 3.5$

In Figure 7 a sample set of temperature profiles for $\overline{\Delta h}_v^*(\tau) = 3.5$ is shown.

Comparison with Experimental Data

In Figures 8 and 9 the comparison of the characteristics $X = X(t)$, obtained from computer simulation, with the corresponding experimental characteristics is presented. In Figure 10 the complete durations of vacuum contact drying τ_d in the falling rate period (the third period) are shown. It also includes the comparison between simulated and experimental data. The adequacy of the developed mathematical model to the purpose of the

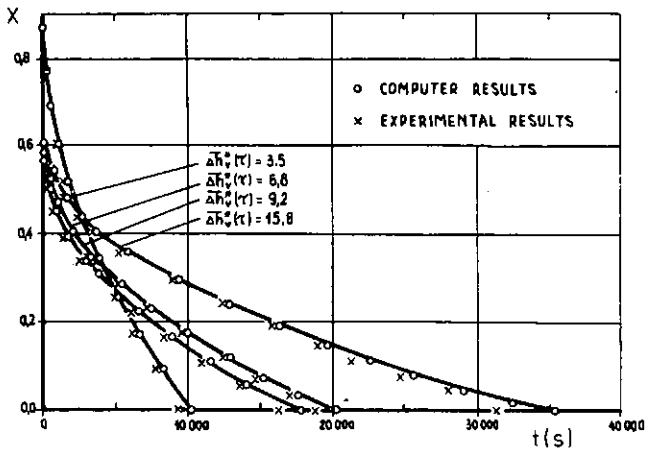

Figure 8. Moisture Content of the Bed Versus Time, for Different Values of $\overline{\Delta h}_v^*(\tau)$

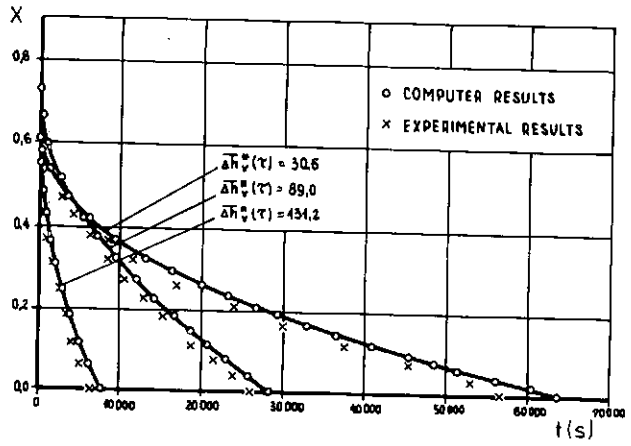

Figure 9. Moisture Content of the Bed Versus Time, for Different Values of $\overline{\Delta h}_v^*(\tau)$

particular characteristics prediction of the process must be stated, as the result of performed simulation and comparison with own experimental data. The own experiments were done for the same range of input parameters of the process, as was presented in (1). The mathematical model developed here enables to compute the most important characteristics of the process with the relatiwe error not exceeding 15% , over the wide range of input parameters variability. The mathematical model may then be used for purposes of design, optimisation and control of the process.

CONCLUDING REMARKS

A general model of unsteady-state heat transfer with moving boundary of moisture evaporation in the dried bed was presented in application to the Dirichlet boundary condition. This model is the versatile one i.e. should also apply to remaining boundary conditions at the hot surface i.e.

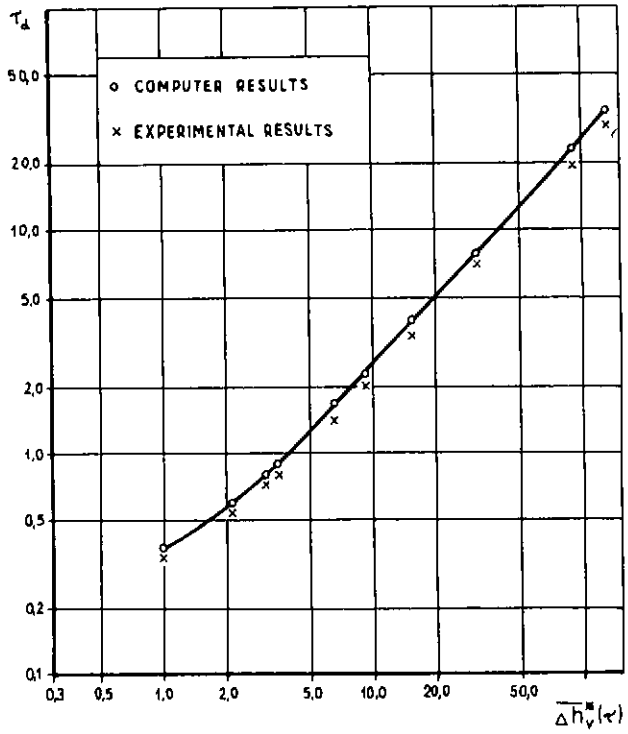

Figure 10. Complete Durations of the Vacuum Contact Drying of Porous Media at T_o = const in the Falling Rate Perid

to boundary conditions of the Neumann or Dirichlet-Neumann type. It should be useful to predict the performance of vacuum contact drying of the layers of porous media without internal porosity and porous materials. Application of the integral transform method to a moving boundary problem removes the space variable from the partial differential equation and reduces the problem to a system of ordinary differential equations which may be solved by numerical means. The numerical solutions yielded good agreement between predicted and experimental values.

ACKNOWLEDGEMENT

The authors wish to thank the Polish Academy of Sciences for the financial support given this research.

REFERENCES

1. Stręk, F., Nastaj, J., Mathematical Modelling and Simulation of Vacuum Contact Drying of Porous Media in the Constant Rate Period, Paper accepted at the Second International Symposium on Drying, McGill University, Montreal, Canada July 6-9 1980
2. Doetsch, G., Math. Ann., Vol. 112, p. 52, 1936
3. Selim, M.S., and Seagrave, R.C., Ind. Eng. Chem. Fundam., Vol. 12, p.1, 1973

4. Ingersoll, L.R., et al., Heat Conduction with Engineering and Geological Applications, McGraw-Hill, New York, 1948
5. Crane, R.L., and Lambert, R.G., J. Ass. Comp. Mach., Vol. 9, p. 104, 1962
6. Perry, J.H., Chemical Engineers Handbook, McGraw-Hill, New York, 1963

CALCULATION OF HEAT TRANSFER ON VIBRATING CONVEYORS

D.U. Ringer

Technical University Munich
West Germany

ABSTRACT

Vibrating conveyors with internals for heat transfer are used in the chemical and allied industry for cooling, heating and drying of particulate solids, especially when transport and heat transfer should be carried out simultaneously. Until now, conveyors of this type have been constructed on the basis of practical experience. In this paper, a model for the calculation of the heat transfer on those conveyors is presented, also results about raising the heat transfer efficiency on them.
Starting from physically reasonable models for the motion of the granulate and the heat transfer from the conveyor trough to it, a system of equations is developed for the calculation of the heat transfer coefficient. It can be easily solved numerically. Hence, with knowledge of the physical properties of the granulate (effective thermal conductivity, heat capacity, density, void fraction, thermal conductivity of the gas in the void fraction) and the conveyor operating parameters (amplitude, frequency), the calculation of the heat transfer on vibrating conveyors is possible. Comparison between theoretical and experimental data shows good agreement. The experimental tests were performed on industrial scale equipment. They have shown, that the heat transfer coefficient between the heat transferring area and the particulate solids is mainly influenced by the particle diameter at short residence times and by the heat penetration values at longer times.
As experiments have shown, there is almost no mixing of the particulate solid on the conveyor. Therefore, the heat transfer coefficient decreases continuously along the conveying track. So test were carried out to raise the effiency of heat transfer by using mixing elements for the granulate. These results are also presented.

NOMENCLATURE

a = thermal diffusivity, m^2/s
A = area, m^2
b = heat penetration value, $W \cdot \sqrt{s}/m^2K$
B = width of the granular bulk, m
c_p = heat capacity, J/kgK
C = trajectory constant, 1/s
C_s = radiation constant of black body (value see /12/), W/m^2K^4
d_p = particle diameter, m
$d_{p,50}$ = average particle diameter, m
D = damping constant
f = frequency of vibration, 1/s
Fo = Fourier-Number, $(= a \cdot t/L^2)$
g = gravitational acceleration, m/s^2
h = thickness of gas layer, m
H = height of granular bulk, m
L = lenght, m
M = mass, kg
p = pressure, N/m^2
r,s = lenght variables, m
t = time, s
v = conveying velocity, m/s
w_B = superficial gas velocity, m/s
x,y = coordinates, lenght variables, m
X = amplitude, m

Greek Symbols

α = heat transfer coefficient (htc), W/m^2K
γ = accommodation coefficient (value see /12/)
Γ = characteristic trajectory value $(= \omega^2 \cdot X/g)$
ε = void fraction
ε^* = emissivity (value see /12/)

η = viscosity, kg/ms

ϑ = temperature, K

λ = thermal conductivity, W/mK

λ_G^* = reduced thermal conductivity of gas in narrow gaps, W/mK

Λ = mean free path of gas molecules (value see /12/), m

ρ = density, kg/m^3

τ = dimensionless time (= $\omega \cdot t$)

φ = covering factor

$\dot{\phi}$ = heat flux, W

ω_o = angular velocity of the conveyor trough (= $2\pi f$), 1/s

Subscripts

A = area

B = bulk (upper side)

AB = bulk (lower side)

exp. = experimental

E = end of flight

F = beginning of flight

G = gas

GG = gas gap

max = maximum

O = surrounding

op = one vibration period

R = radiant

S = solid

theor. = theoretical

tot = total

1. INTRODUCTION

In the chemical and allied industry many raw materials, intermediate and end products are present as granular solids. During the transport of these materials it is often required to subject them to heating, drying or cooling. It is therefore advantageous to use the transport apparatus vibrating conveyor as a heat exchanger too. Conveyors of this type have until now been constructed on the basis of practical experience. The object of the present investigation was to study, both theoretically and experimentally, the heat transfer to granulate, transported in this type of conceyor.

2. THEORY

2.2. Model

Experiments /1, 2/ have shown, that the flow of the particulate solids in the conveyor trough is practically piston flow. Mixing of the particles can be neglected and hence the bulk of the granulate can be regarded as a fixed bed, which moves steadily along the conveying track.

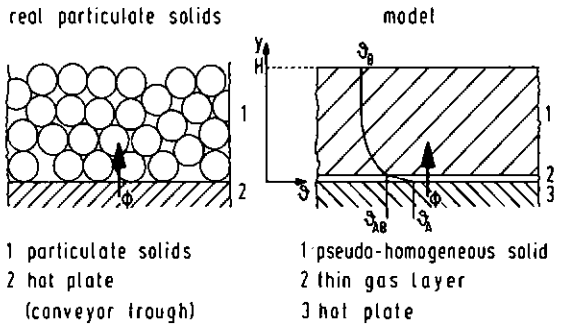

Fig. 1: Model for the heat transfer vibrating conveyor-particulete solids. Temperature profile in the case of heating

If a bulk of particulate solids with uniform temperature comes in contact with the heat transferring surface, an institutionary temperature change starting from the surface will take place. Gabor /3/ has shown, that the isothermal lines in such a case are nearly parallel to the surface. Therefore, the bulk of particulate solids and gas can be represented as a pseudo-homogeneous solid, whose physical properties are the effective values of the mixture of solids and gas. The pseudo-homogeneous solid is separated from the surface by a thin gas layer, which is produced by vibration and therefore changes periodically (Fig. 1). Heat transfer from the heat transferring area to the pseudo-homogeneous solid or reverse is considered as occuring in two stages. The first stage is the transfer across the thin gas layer, the second the spread of heat inside the pseudo-homogeneous solid.

2.2. Thickness of the Gas Layer

For the first stage, the calculation of heat transfer across the thin oscillating gas layer, it is essential to know the thickness of the layer. It is assumed here that the trough of the conveyor is horizontal and its vibration is a sinus-

odial oscillation. The vertical part of the oscillation causes the formation of the gas layer, the horizontal part the conveying velocity. For heat transfer, only vertical motion is of interest. The granulate should exhibit an ideally plastic behaviour (Fig. 2). Hence the vertical motion of the conveyor can be expressed by:

$$x = X \cdot \sin(\omega_o \cdot t) \qquad (1)$$

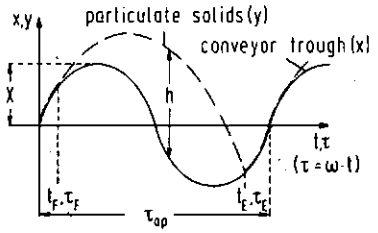

Fig. 2: Model for the vertical motion of conveyor trough and particulate solids.

As long as the vertical acceleration of the conveyor trough is smaller than gravitational acceleration, granulate and trough remain in direct contact. When the acceleration of the trough exceeds the gravitational acceleration, the solid is thrown up into the gas and performs a damped trajectory motion. After falling back on the trough, the process starts again. During the throw the following equilibrium of forces applies to the solid:

$$M \cdot \ddot{y} + M \cdot g + \Delta p \cdot A + D \cdot M \cdot \omega_o (\dot{y} - \dot{x}) = 0 \qquad (2)$$

Mass force $M \cdot \ddot{y}$ and gravity $M \cdot g$ need no explanation. The pressure force $\Delta p \cdot A$ is caused by the pressure drop of the gas, flowing through the bulk into and out of the oscillating gas layer. During the flight, friction and bumps of the particles at the side-walls and among each other act as a damping force, which is proportional to the velocity difference between particles and conveyor trough.
If we assume laminar gas flow, we get for the pressure drop (see /4/).

$$\frac{\Delta p}{H} = 180 \, \frac{\eta_G \cdot (1-\varepsilon)^2 \cdot w_B}{d_p^2 \cdot \varepsilon^3} \qquad (3)$$

If the pressure drop Δp is small in comparison with athmospheric pressure p_o ($\Delta p / p_o < 1\%$), the gas can be regarded as incompressible. From the continuity equation then follows:

$$w_B = (\dot{y} - \dot{x}) \qquad (4)$$

Deriving the conveyor velocity $\dot{x}$ from equation (1) and dividing equation (2) through the mass of the solid in the conveyor trough, we get:

$$\ddot{y} = - C \cdot \dot{y} + C \cdot X \cdot \omega_o \cdot \cos(\omega_o \cdot t) - g \qquad (5)$$

with

$$C = D \cdot \omega_o + 180 \cdot \frac{\eta_G \cdot (1 - \varepsilon)}{d_p^2 \cdot \varepsilon^3 \cdot \rho_s} \qquad (6)$$

Equation (5) must be solved with the initial conditions:

$$y = x; \quad \ddot{y} = \ddot{x} = - g; \quad \text{at} \quad t = t_F \qquad (7)$$

The thickness of the gas layer is given by:

$$h = y - x \qquad \text{for} \quad h \geq 0 \qquad (8)$$

Solution of Eq. (5) combined with Eqs. (1) and (8) results in the following expression for the thickness:

$$h = \frac{g}{C \cdot \omega_o} \left[(\tau_F - \tau) + \left(\frac{\omega_o}{C} + \sqrt{\Gamma^2 - 1} \right) \cdot \left[1 - \frac{1}{\frac{C^2}{\omega_o^2} + 1} \cdot e^{\frac{C}{\omega_o}(\tau_F - \tau)} \right] \right] - X \left[\frac{\frac{C}{\omega_o} \cdot \cos\tau + \sin\tau}{\frac{C^2}{\omega_o^2} + 1} \right] \qquad (9)$$

With equation (9) the thickness of the gas layer and the period of flight can be calculated. The beginning of flight is given by Eq. (1) for $t = t_F$, the end by Eq. (9) for $h \leq 0$ and $t > t_F$. For the calculation the value of the damping constant D is required. Therefore a comparison with experimental data for flight periods was undertaken (see Fig. 3).

The best result was obtained with

$$D = \frac{2H}{B} \cdot 0{,}4 \qquad (10)$$

which should be used for the calculation of the thickness of the gas layer.

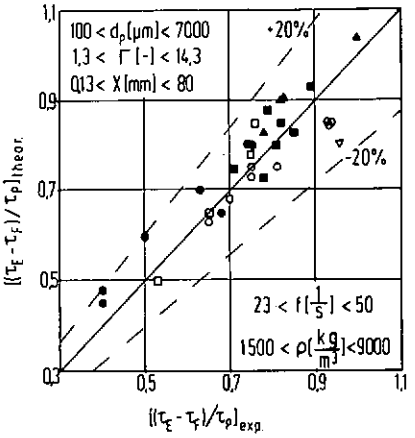

Fig. 3: Comparison of flight times. Theoretical versus experimental data Böttcher /1/ ● , Peschl, Schmid /5/ ■ , Gray, Rhodes /6/ □ , Gutman /7/ ▽ , Kroll /8/ ▲ , Sakaguchi /9/ ○ .

2.3. Heat Transfer Surface-Spherical Particle

The heat transfer across the gas layer takes place between the surface and the first (lowest) layer of the particulate solids. The grains should be regarded as spherical. As previously indicated, the bulk moves as a fixed bed, i.e. there is nearly no relative motion of particles with respect to one another. So it is sufficient to regard one sphere. According to Carslaw/Jaeger /10/, the temperature profile in a gas layer bounded by two solids is linear for Fourier-Numbers greater than 0,5 (here $Fo = a_G \cdot t/h^2$). The analysis of Eq. (9) shows, that during one oscillation period for ordinary operating parameters and particulate solids, no Fourier-Numbers greater than 0,5 appear.
Basing on the model of Schlünder /11/, the differential equation for the pseudo-stationary heat flux by conduction from a heating surface to a spherical particle at distance h from the surface (see Fig. 4)

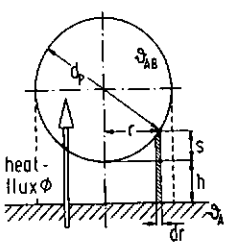

Fig. 4: Model of the heat transfer from a (heating) surface to a spherical particle at distance h from the surface

is given by:

$$d\phi = \frac{\lambda_G^*}{s+h} \cdot (\vartheta_A - \vartheta_{AB}) \cdot 2\pi r \cdot dr \qquad (11)$$

In the case of direct contact (h = 0) and even during the flight, reduced thermal conductivity of the gas because of the narrowness of the gas layer must be taken into account (see /4/). It is given by:

$$\frac{\lambda_G^*}{s+h} = \frac{\lambda_G}{s+h+\sigma} \quad \text{with } \sigma = 2\Lambda \cdot \left(\frac{2-\gamma}{\gamma}\right) \qquad (12)$$

There σ is a factor, which takes into account the reduction of thermal conductivity as soon as the gas layer thickness reaches the order of magnitude of the mean free path of the gas molecules.
With reference to the surface of projection of the sphere, the htc is given by:

$$\alpha_1 = \frac{4 \cdot \int_A d\phi}{\pi d_P^2 (\vartheta_A - \vartheta_{AB})} \qquad (13)$$

and by integration α_1 becomes:

$$\alpha_1 = \frac{4 \cdot \lambda_G}{d_P} \cdot \left[\left(\frac{2(\sigma + h)}{d_P} + 1 \right) \cdot \ln \left(\frac{d_P}{2(\sigma + h)} + 1 \right) - 1 \right] \qquad (14)$$

α_1 depends on the thickness of the gas layer and therefore changes periodically, too. As long as λ_G and σ do not change very much, the periodical alternation of α_1 is the same for every period. During the time of one oscillation period, no great change of the temperature in the pseudo-homogeneous body will take place. It is therefore useful to do further calculations not with the exact temporal value of α_1 but with an average value over one oscillation period.

$$\overline{\alpha_1} = f \cdot \int_0^{1/f} \alpha_1 \cdot dt \qquad (15)$$

Aside from heat conduction, heat is also transported by other kinds of heat transfer across the gas layer. They are all expressed as htc's for one oscillation period.
The first kind of these processes is heat transported by radiation. It can be expressed by (see /12/):

$$\alpha_R = \frac{0,04}{\frac{2}{\varepsilon^x} - 1} \cdot C_s \cdot \left(\frac{\vartheta_A + \vartheta_{AB}}{200} \right) \qquad (16)$$

The second is the convection of gas which

flows into and out of the oscillating gas layer. Here we get (see /13/):

$$\alpha_G = \frac{h_{max} \cdot \rho_G \cdot c_{p,G} \cdot f}{2} \qquad (17)$$

The third is energy conversion when the particles rebound against the trough. But this part can usually be neglected in reference to the others.
Eq. (14) and (17) refer to the surface of projection of a sphere. However, the sum of these surfaces of the particles of the first bulk is not the whole heat transferring area. Therefore, a covering factor φ is introduced. As an intermediate value between quadratic and rhombic covering is $\varphi = 0{,}846$, which is assumed here. The whole htc for the heat transfer surface-spherical particle is then given by:

$$\alpha_{GG} = \varphi \cdot (\overline{\alpha_1} + \alpha_G) + \alpha_R \qquad (18)$$

2.4. Transfer of Heat Inside the Pseudo-homogeneous Solid

As already stated, the whole heat transfer surface-pseudo-homogeneous solid is an unstationary process which can be divided into two parts. As just seen, the first part, the heat transfer across the gas layer, can be regarded as a steady process. So the instationary process remains only for the second part. For Fourier-Numbers of less than 0,2 (here $Fo = a_B \cdot t/H^2$), as obtained in this investigation and used in practice, the pseudo-homogeneous solid can be regarded as semi-infinite. If we assume constant heat flux into the solid, as it was given by the performed tests, the well known rules for non-steady heat transfer (see /4/) can be applied. The following equation then gives the htc into the pseudo-homogeneous solid with reference to the temperature difference $\vartheta_{AB} - \vartheta_B$ (see Fig. 1):

$$\alpha_2 = \frac{\sqrt{\pi}}{2} \cdot b \cdot \frac{1}{\sqrt{t}} \qquad (19)$$

2.5. Overall Heat Transfer Coefficient

Taking both parts of the heat transfer process into consideration, and thus a driving force equal to the difference between the temperature of the heat transferring surface ϑ_A and the initial bulk temperature ϑ_B (remainig constant at the bulk's upper side), the overall htc is obtained as:

$$\frac{1}{\alpha_{tot}} = \frac{1}{\alpha_{GG}} + \frac{1}{\alpha_2} \qquad (20)$$

This htc α_{tot} has a maximum value given by α_{GG} for very small residence times and decreases with increasing time.

For the calculation of htc's measured effective physical properties for the particulate solids were used. But is also possible to calculate them by equations given in literature /12/.

3. EXPERIMENTAL EQUIPMENT

3.1. General Description

The tests were performed in an industrial scale equipment (Fig. 5). In the trough of an off-the-shelf industrial vibrating

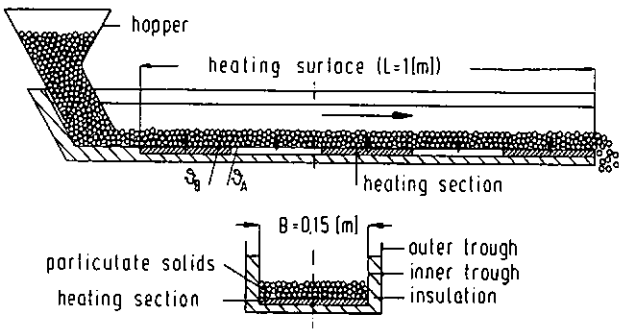

Fig. 5: Experimental Equipment (schematic)

conveyor, another trough was installed for the purpose of heat transfer. The inner trough was insulated on the outside in order to reduce heat losses. The base of the inner trough was divided into 5 electrically heated sections of similar size which were insulated from each other. The total length of the heating plate was one meter, and each section could be separately regulated. This construction of the heating surface permitted constant heat flux over the whole cross-section.
The granulate flowed at uniform temperature from a hopper into the trough of the vibrating conveyor, where it was transported with constant speed. After a short entrance section the material came into contact with the heating surface and from then on absorbed heat continuously. By means of further equipment the solids were returned to the hopper whilst being cooled, so that a steady-state re-circulation of the material was attained.
Because of the piston flow of the particulate solids, vibrating conveyors for heat transfer are frequently equipped in practice with mixing elements for the granulate, for instance with simple steps. So test were performed in a vibrating conveyor with such internals (Fig. 6).
The angle against horizontal was 3°, the mixing elements were steps. The rims of the steps could be changed. Here 8 heating elements were installed.

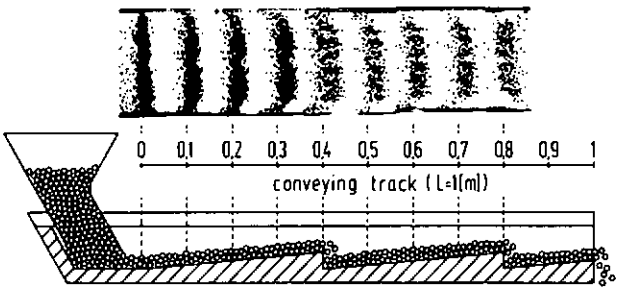

Fig. 6: Vibrating conveyor with mixing elements (steps) for the particulate solids (schematic). Above: photographed flow profiles.

3.2. Measurement of Heat-Transfer-Coefficient

Heat transfer between the heating sections and the solids is a non-steady process. Therefore, the relevant parameter is the instantaneous htc α given by the equation:

$$\alpha = \frac{\phi}{A \cdot \Delta\vartheta} \qquad (21)$$

The heat flux ϕ was calculated from the supplied electrical energy. The heat exchange area A was known from the geometry of the heating sections. In all experiments, the Fourier-Number of the bulk was less than 0,2. This indicates, that the temperature ϑ_B of the top layer remains constant along the conveying track. Therefore, the value $\vartheta_A - \vartheta_B$ was assumed as the characteristic temperature difference $\Delta\vartheta$ (see Eq. (21)). ϑ_A was measured with thermocouples inside the heating sections, ϑ_B with an infrared thermometer. This temperature difference and hence the htc was measured at the centre of each heating section. Residence time of the solids with respect to each measurement point was obtained from the time of the run and the geometry of the trough, for the material flowed with constant velocity. The run time was measured with the aid of tracer particles and a stop watch.

4. EXPERIMENTAL RESULTS

The variation of the conveyor's operating parameters (amplitude, frequency) and the main physical properties of the particulate solids (particle diameter, heat penetration value) produced the results illustrated in the Figs. 7, 8, 9 and 10 (for further results see /13/). At the used apparatus the conveying velocity was varied at constant frequency by different amplitudes. Increasing amplitude thus results in increasing velocity and trajectory value. In the diagrams. the conveying velocity is used as the interesting conveying parameter.

Fig. 2 shows results for glass spheres of different diameter at high and low conveying velocities. It can bee seen, that the htc falls with increasing residence time (= time required for a particle to pass from the point of entry into the heating area to the measurement location). The larger the particles, the smaller are the htc values, particularly at short residence times. Furthermore, the difference between the data points for large and small particles grows smaller with increasing time.
The effect can be easily explained by the presented theory. For small residence times, the htc is limited by heat transfer across the thin gas layer, which is greatly influenced by particle diameter (see Eqs. (14), (18)). For increasing time, heat transmission to the pseudo-homogeneous solid becomes dominant, where heat penetration value b is, aside from time, the main factor. b itself is not influenced by particle diameter.

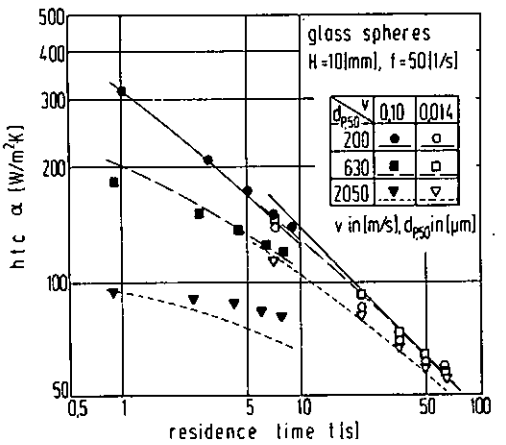

Fig. 7: Effect of particle diameter on htc; lines: theoretical prediction for Γ = 3,0 and 1,1, ϑ_B = 40 [°C], Eq. (20)

Fig. 8 shows experimental data for two particulate solids of comparable diameter but different heat penetration values (Granal = spheres of 99% Aluminium). As theoretically predicted, the main influence of heat penetration values is given at great residence times. There, the ratio of experimental data is the same as the ratio of the heat penetration values. Both particulate solids have nearly the same htc value α_{GG} for heat transfer across the gas layer. It is therefore not astonishing that the experimental data for small residence times flow together to a mutual point and the influence of the heat penetrations value on the htc diminishes rapidly.
The operating parameters of the conveyor only have an influence on the htc at great

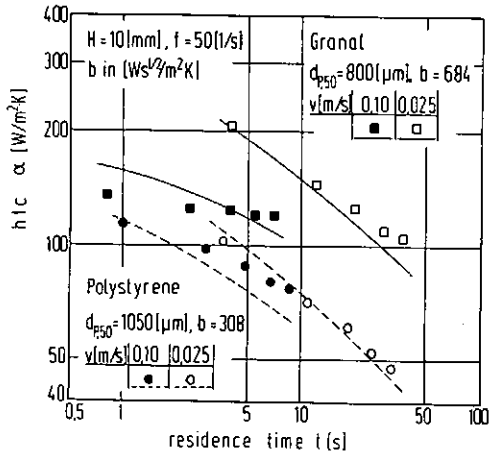

Fig. 8: Effect of heat penetration value on htc; lines: theoretical prediction for Γ = 3,0 and 1,4, ϑ_B = 40 [°C]

particle diameters and small residence times (see /2/, /13/). In all cases, the agreement of experimental data and theoretical prediction is good.
Figs. 9 and 10 show results for a vibrating conceyor with steps as mixing elements for the granules. Previous investigations have shown that steps with straight-line rims only do little mixing and the effect on the decreasing htc is not sufficient. So we used a jagged tim. Flow profiles for these investigations are shown in Fig. 6. It can be seen, that at the point of the rims, mixing of particles takes place, but it is not ideal. Fig 9 shows htc values for glass of small and great particle diameter and great (left) and small (right) conveying velocities. After each rim, residence time starts again at zero, so that the steps are comparable. It can be seen, that the values of the first step are not reached by the following, particularly at

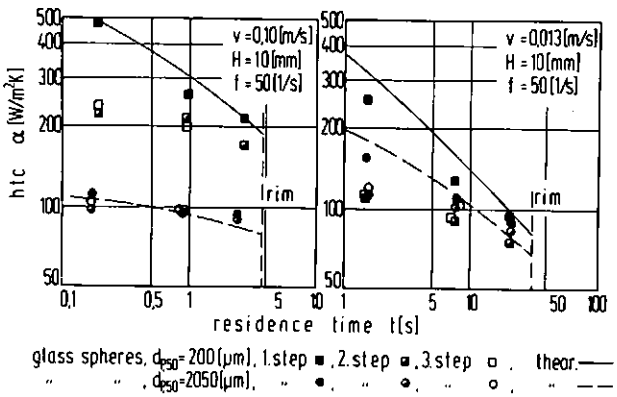

Fig. 9: Effect of mixing elements on htc. Comparison of the steps; lines: theoretical prediction for unmixed granulates with Γ = 3,0 and 1,1· ϑ_B = 40 [°C], Eq. (20)

small particle diameters and small residence times. The values of the second and third step are nearly the same.
From Figs. 6 and 9 we can conclude, that mixing by the rims is not ideal. Therefore, the amount of the htc on the first step can not be reached by the next. But the mixing by the rims is the same on each one so for the second and third step the same values for the htc are obtained. The decrease of the htc therefore can be periodized by using mixing elements, and a high average htc can be obtained. This average htc is about the local htc when the first rim appears. The same we can conclude from Fig. 10, where the same data as in Fig. 9 is used, but with residence time running from the start of the first step. The lines represent htc values for unmixed conveying tracks as predicted by theory.

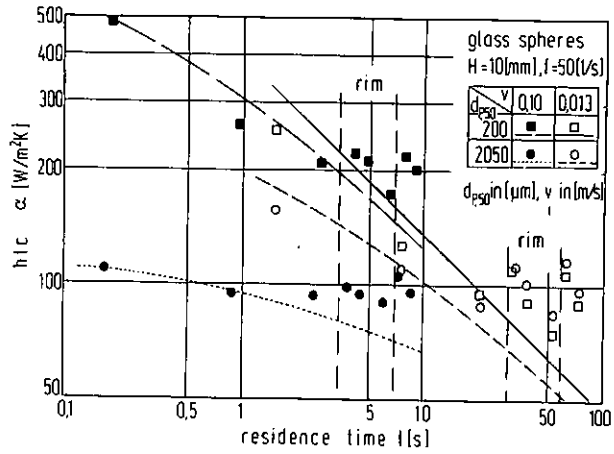

Fig. 10: Effect of mixing elements on htc. Comparison with theoretical prediction for unmixed conveying track (lines), Γ = 3,0 and 1,1, ϑ_B = 40 [°C], Eq. (20)

As previously shown, the theoretical values are in good accordance with experimental data. It can be seen, that htc values on conveyors with mixing elements decrease periodically. The average htc value for the whole residence time is much higher on conveyors with mixing steps than on flat ones. Therefore, the efficiency of the heat transfer process can be elevated by using mixing elements for the particulate solids.

REFERENCES

1. Böttcher, S., Dissertation. T.H. Hannover 1957
2. Ringer, D.U., Ger. Chem. Eng. 1(1978), 361-365
3. Gabor, J.D., Chem. Engng., Prog. Symp. Ser., 66, No. 105. 76-86
4. Krischer, O., Kröll, K. Trocknungstechnik Vol. 1, Springer Verlag,

Berlin-New York 1956
5. Peschl, J., Schmid, W., fördern und heben, (1965)8, 606-613
6. Gray, W.A., Rhodes, G.T., Powder Technology, 6(1972), 271-281
7. Gutman, R.G., Trans. Inst. Chem. Engnrs., 54(1976), 174-183
8. Kroll, W., Forschung auf dem Gebiete des Ingenieur-Wesens, 20(1954)1, 2-16
9. Sakaguchi, Bull. of JSME, 20(1977)143, 554-560
10. Carslaw, H.S., Jaeger, J.C., Conduction of Heat in Solids, Oxford University Press, 1959
11. Schlünder, D.U., Chem. Ing. Techn., 43(1971)11, 651-654
12. VDI-Wärmeatlas. VDI Verlag, Düsseldorf 1974
13. Ringer, D.U., Dissertation TU München 1980

PROCESS DEVELOPMENT OF A FLUIDIZED DRYING SCHEME FOR NITRILE RUBBER

J. P. Lenczyk[1]
C. R. Sarkar[2]

1. University of Akron, Akron, OH 44325
2. B. F. Goodrich Chemical Co., Avon Lake, OH

ABSTRACT

The results from the batch fluid-bed drying of NBR crumb were used to design a commerical dryer. The batch experiments were carried out from a 60% initial moisture content to less than 0.5% final moisture content. At the inlet air temperature of 366K and a mass velocity of 7646 kg/hr m^2 a heat transfer coefficient was calculated to be 34.74×10^4 J/hr m^2 K along with a mass transfer coefficient of 255 kg/hr m^2 (kg/kg).

The batch drying parameters were used in the design and scale-up of a commercial batch dryer at 910 kg/batch and a three-stage continuous drying process of 910 kg/hr. For the batch process, the designed dryer diameter and height would be 2.44 m and 3.66 m respectively. For the first-stage of the continuous dryer the diameter and height of the dryer would be 2.59 m and 3.66 m respectively. Both the second and last stage of the continuous drying process would be 1.30 m in diameter. However, the dryer height of the second stage would be about 6.10 m and 3.66 m for the last stage. The energy consumption for the continuous drying process (4.64×10^9 J) would be more than that for the batch dryer (4.10×10^9 J).

NOMENCLATURE

A = Slope of the moisture content-time plot during the constant rate period of drying

B = An arbitrary constant in the falling rate period

C = An arbitrary constant in the falling rate period

C_p = Heat capacity at constant pressure

C_v = Heat capacity at constant volume

d = Column diameter

$E(t)$ = Residence Time Distribution Function

F = Mass of condensed phase

G_o = Superficial mass velocity of air

H_g = Humidity of air

h_p = Heat transfer coefficient

k_p = Mass transfer coefficient

$\dot{m}_g$ = Mass flow rate of air

P = Air pressure

T_g = Air temperature

T_g^* = Logarithmic mean air temperature

t = Drying time

$\overline{t}_c$ = Mean residence time of solids in the constant rate period of continuous drying

$\overline{t}_f$ = Mean residence time of solids in the falling rate period of continuous drying

U_o = Superficial air velocity

W = Mass of vapor phase

$\dot{W}$ = Power

X_{f_i} = Initial moisture content

$\overline{X}_c$ = Critical moisture content

X_{i_f} = Initial moisture content in the falling rate period

$\bar{X}_f$ = Final moisture content

X_i = Mass fraction of solids in the size interval i in the bed

y = Mass fraction of water vapor in air

γ = Ratio of heat capacities of air

ε = Bed voidage

ρ = Density of crumb particles

η = Efficiency of blower or compressor

λ = Latent heat of vaporization of water

τ = Batch drying time

τ_c = Batch drying time to the end of the constant rate period

INTRODUCTION

Feasibility studies on the fluidized-bed drying of NBR latex crumb were done (1, 2) and only the results are presented. The Alum Method of coagulation (5% to 6% Alum) produced very uniformly sized crumb particles of 1.6 mm to 3.2 mm in diameter with a moisture content of 60% on a wet basis. The Sauter mean diameter, $\bar{d}_p$, was calculated to be 2.8 mm from data obtained by sieving the dry crumb.

The Ergun (3) equation modified with an apparent density, ρ_a, was used to calculate the minimum fluidization velocity $\bar{U}_{mf}$. The terminal velocity U_t was calculated by using the Levenspiel & Kunii (4) correlation in each flow regime, and again these were modified with use of ρ_a.

The pressure drop through the bed, ΔP_{bed}, and distributor plate, $\Delta P_{distr.}$, were measured as a function of the inlet air velocity, G_o. Predictably, the ΔP_{bed} is unaffected by G_o and the $\Delta P_{distr.}$ increases with G_o. The heat transfer coefficient between the air and the crumb particles for the constant rate period is calculated from temperature, area, and axial temperature profile data. With the inlet gas temperature, T_{g_i} at 366 K and G_o = 7646 kg/hr m^2 a heat transfer coefficient, h_p, was determined to be 34.75x10^4 J/hr m^2 K. The mass transfer coefficient, k_p, was determined from the dynamic equilibrium established between heat transfer and mass transfer and was found to be 255 kg/hr m^2 (kg/kg) for the same conditions. It was also concluded that the higher T_{g_i} the shorter is the drying time and likewise as G_o is increased the drying rate increases. The critical moisture content $\bar{X}_c$, was found to be about 0.16 (dry basis) and was uneffected by G_o and T_{g_i}.

Batch Dryer Scale-Up

The quantities affecting the performance of the laboratory fluid-bed dryer are basically the same as those in the case of a commercial batch fluid-bed dryer. The commercial batch dryer scale-up design is based on 910 kg/batch of dried crumb. A schematic of the material balance for the process is given in Figure 1. The material balance equations are (1):

Overall Balance:

$$F_i + W_i = F_o + W_o \qquad (1)$$

Moisture Balance:

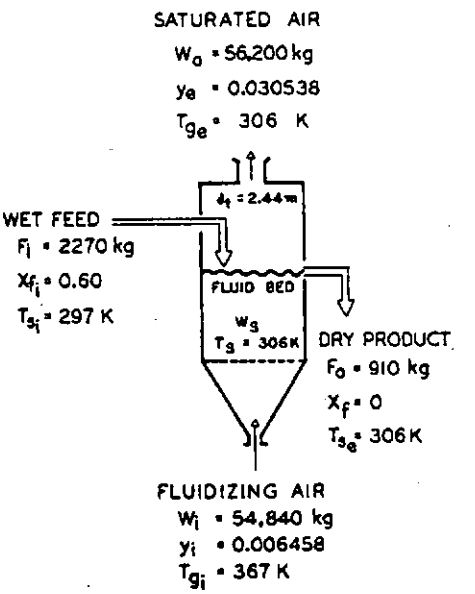

FIGURE 1: COMMERCIAL BATCH FLUID-BED DRYER SHOWING THE MATERIAL BALANCE FOR 4500 SECONDS OF DRYING TIME

$$F_i X_{f_i} + W_i Y_i = F_o(X_f) + W_o(Y_e) \quad (2)$$

and Energy Balance Equation:

$$\dot{m}_g C_{p_g}(T_{g_i} - T_s)t_d = F_1[\lambda + C_{p_\ell}(T_s - T_{s_i})] + F_2 C_{p_s}(T_s - T_{s_i}) \quad (3)$$

The dry air requirement based on the material balance would be 12.1 kg/s. Calculations showed that the bed area required would be about 4.645 m^2 corresponding to a bed diameter of 2.42 m. Therefore a bed diameter of 2.44 m was recommended. The actual energy required for fluidization was calculated using the following expression for power requirement (4):

$$\dot{W}_{sa} = \left(\frac{\gamma}{\gamma - 1}\right) P_e U_e \left[1 - (P_i/P_e)^{\frac{\gamma-1}{\gamma}}\right] \frac{1}{\eta} \quad (4)$$

where $\gamma = C_p/C_v$ = Ratio of heat capacities for air = 1.4

P_i and P_e = Inlet and exit air pressure

U_e = Exit volumetric flow rate of air

and η = Efficiency of the blower or compressor equals approximately 0.8

The total energy required for fluidizing and heating the air would be 4.18×10^9 J.

Continuous Drying

In a continuous drying, the bed consists of a small fraction of wet particles interspersed in a bed of almost dry solids. The moisture content of the solids may differ and the interparticle interaction may be important. Thus the analysis of drying may differ significantly and require a more rigorous design and scale-up.

Mean Residence Time of Solids

In a continuous drying operation it is of primary importance to know the mean residence time of the solids, $\bar{t}$, in the dryer. For complete mixing, the product stream leaving the dryer is representative of the solids in the dryer. The residence time distribution (RTD) function for the solids is represented by Levenspiel and Kunii (4):

$$E(t) = \frac{1}{\bar{t}} \exp(t/\bar{t}) \quad (5)$$

where $E(t)dt$ is the fraction of solids with the residence time in the bed between t and t + dt. For a bed weight of W_s and a product withdrawal rate of F_o, the mean residence time of solids, $\bar{t}$, in a single feed continuous fluid-bed dryer becomes

$$\bar{t} = W_s/F_o \quad (6)$$

Examining a single spherical wet crumb particle at a temperature T_s and assuming that its rate of drying is determined by its thermal interaction with the neighboring fluid at a temperature T_g^*, the change in moisture content, X_f, with time is given by:

$$-dX_f = \frac{6h_p(T_g^* - T_s)}{\rho_s \bar{d}_p \lambda} dt \quad (7)$$

During the constant rate period, Equation (7) can be integrated for a constant ΔT and $X_f = X_{f_i}$ at t = 0. This leads to:

$$X_{f_i} - X_f = \frac{6h_p(T_g^* - T_s)}{\rho_s \bar{d}_p \lambda} t \quad (8)$$

or,

$$X_f = X_{f_i} - At \quad (9)$$

where $$A = \frac{6h_p(T_g^* - T_s)}{\rho_s \bar{d}_p \lambda} \quad (10)$$

The critical moisture content or the average moisture content of the leaving solids at the end of the constant rate period, $\bar{X}_c$, is defined by

$$\bar{X}_c = \int_0^{\tau_c} X_f E(t)dt \quad (11)$$

where τ_c = Batch drying time in the constant rate period and integrating, we have (12):

$$X_{f_i} - \bar{X}_c = A\bar{t}_c - [A(\bar{t}_c + \tau_c) - X_{f_i}]\exp(-\tau_c/\bar{t}_c) \quad (12)$$

Equation (12) relates $\bar{X}_c$ and X_{f_i} to τ_c and $\bar{t}_c$ during the constant rate drying period in continuous operation.

During the falling rate period, h_p and k_p decrease. The functionality of this decrease is not explicitly known but assumed that h_p decreases linearly with time during the falling rate period in the following manner:

$$h_{p_f} = h_p(1-Bt) \quad (13)$$

where h_{p_f} is the heat transfer coefficient during the falling rate period, h_p is the heat transfer coefficient obtained from the constant rate drying batch data and B is determined from the falling rate drying data. Combining Equation (7), (10), and (13), we have

$$-dX_f = A(1-Bt)dt \quad (14)$$

Integrating Equation (14) with $X_f = X_{i_f}$ at $t = 0$ and rearranging leads to:

$$X_f = X_{i_f} - At + Ct^2 \quad (15)$$

where $C = AB/2$ (16)

Combining Equation (5), (11) and (15) and using the falling rate period notations, we can write

$$\bar{X}_f = \int_0^{\tau_f} (X_{i_f} - At + Ct^2)(1/t_f)\exp(-t/\bar{t}_f)dt \quad (17)$$

Equation (17) can be integrated by parts to give

$$X_{i_f} - \bar{X}_f = A\bar{t}_f - [A(\bar{t}_f + \tau_f) - X_{i_f}]\exp(-\tau_f/\bar{t}_f) - 2C\bar{t}_f^2[1-\{1+(\tau_f/\bar{t}_f) - \tfrac{1}{2}(\tau_f/\bar{t}_f)^2\}\exp(-\tau_f/\bar{t}_f) \quad (18)$$

The mean residence time of solids during the falling rate period, $\bar{t}_f$, can be calculated using Equation (18) knowing the other parameters obtained from the batch drying data.

Continuous Dryer Scale-Up

The continuous dryer design and scale-up were divided into two parts: first for the constant rate period and then the falling rate period. Using the mean residence times of the solids as calculated from Equations (12) and (18), the specifications for each dryer were obtained. The design calls for a three-stage drying process. The first-stage drying (I) is for the constant rate period and the following two stages (II) and (III) are for the falling rate period. All three stages are shown in the form of a flow diagram in Figure 2. All the corresponding identification of each process stream are given in Table 1.

Dryer I was designed for a product withdrawal rate of 0.300 kg/s at 16% moisture content. This corresponds to a final production capacity of 0.252 kg/s of dry product having 0.2% moisture content. In the second-stage dryer the moisture content would be reduced from 16% to 2%, and in the third-stage dryer the moisture content would be reduced to 0.2%. The important design parameter for the three-stage drying process are given in Table 1.

Comparison of the Batch and Continuous Dryers

Both the batch and continuous drying processing are designed for a 910 kg/batch or 0.252 kg/s of production capacity for dry NBR crumb. The pertinent design variables are given in Table 2. Both these processes are industrially feasible. In batch drying only one dryer would be required as compared to three dryers in continuous process. As the diameter of the dryer increases so does the cost. In addition all the necessary equipment with each dryer would obviously increase the capital investment cost. Also it can be

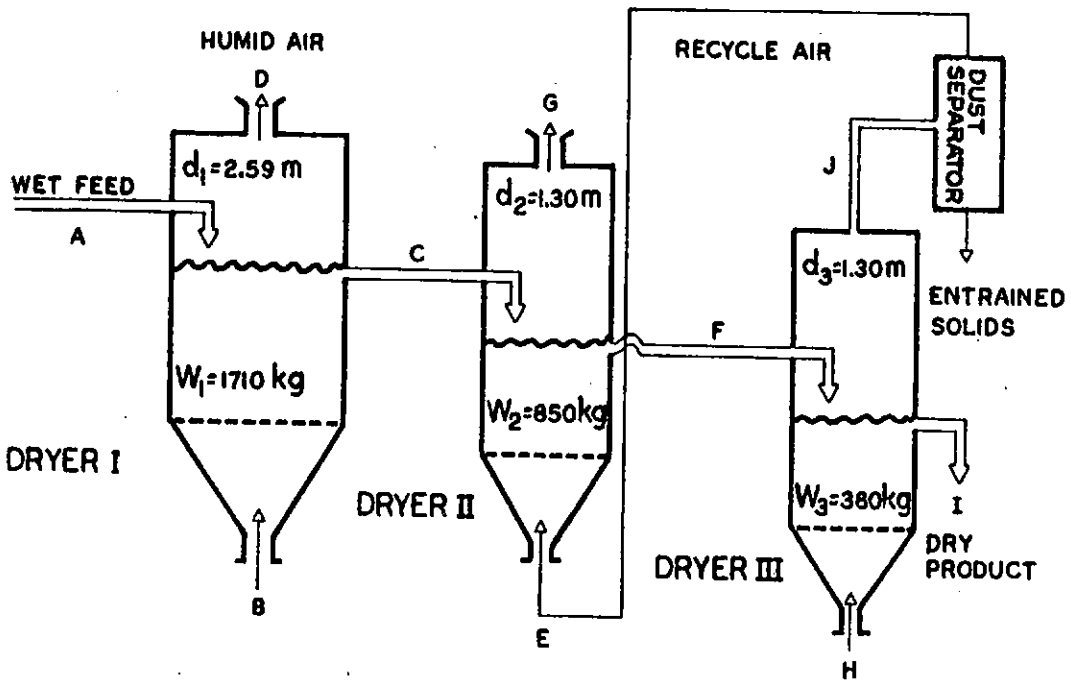

FIGURE 2: FLOW DIAGRAM OF THE COMMERCIAL CONTINUOUS FLUID-BED DRYING PROCESS

TABLE 1

Process Streams for Continuous Drying Process (Figure 2)

STREAM / COMPONENT	A	B	C	D	E	F	G	H	I	J
Bone Dry Crumb (kg/s)	0.252		0.252	0	0	0.252	0	0	0.252	0
Moisture (kg/s)	0.378	0.086	0.048	0.416	0.019	0.005	0.062	0.015	0.0005	0.019
Dry Air (kg/s)	0	13.20	0	13.20	2.22	0	2.22	2.22	0	2.22
Total (kg/s)	0.630	13.29	0.30	13.62	2.24	0.26	2.28	2.23	0.25	2.24
Humidity (kg H_2O/kg dry air)	–	0.0065	–	0.0315	0.0086	–	0.0280	0.0065	–	0.0086
Temperature (K)	297	366	305	305	359	311	333	366	353	359

TABLE 2

Comparison of Batch and Continuous Fluid-Bed Dryers

Process Variables	Batch	Continuous Dryer I	Dryer II	Dryer III
Dry Air Requirement, $\dot{m}_g$ (kg/s)	12.10	13.20	2.22	2.22
Inlet Air Humidity, H_{g_i} (kg H_2O/kg dry air)	0.0065	0.0065	0.0086	0.0065
Exit Air Humidity, H_{g_e} (kg H_2O/kg dry air)	0.0315	0.0315	0.0280	0.0086
Inlet Air Temperature, T_{g_i} (K)	366	366	359	366
Bed Temperature, T_s (K)	305	305	311	353
Residence Time of Solids, $\bar{t}$ (s)	4500	5700	3300	1500
Dryer Diameter, d_t (m)	2.44	2.59	1.30	1.30
Settled Bed Depth, L (m)	0.61	0.79	1.91	0.90
Active Bed Depth, L_f (m)	1.46	1.88	4.57	2.13
Bed Height Including Freeboard (m)	3.66	3.66	6.10	3.66
Pumping Energy (J)	1.46×10^9	1.38×10^9	0.31×10^9	0.24×10^9
Heating Energy (J)	2.72×10^9	2.32×10^9	–	0.39×10^9
Total Energy (J)	4.18×10^9	3.70×10^9	0.31×10^9	0.63×10^9

seen from Table 2 that the total energy requirements for the continuous process (about 4.64×10^9 J total for all three dryers) would be slightly higher than that for the batch process (4.18×10^9 J).

Conclusions

One of the most important outcomes of this work was the preparation of free-flowing NBR crumb. This product in dried crumb or powder form has a tremendous savings potential in subsequent processing steps (5, 6). It offers a greater economic advantage by eliminating the grinding of the baled polymer currently done by the Mills and Banburys in industry.

REFERENCES

1. Sarkar, C. R., Doctoral Dissertation, Dept. of Chem. Egn., Univ. of Akron, Dec. 1977.
2. Sarkar, C. R. and J. P. Lenczyk, 72nd Annual Meeting A.I.Ch.E. Nov. 1979, San Francisco, Ca.
3. Ergun, S., Chem. Engr. Prog., 48, 2, 89 (1952).
4. Levenspiel, O. and Kunii, D., "Fluidization Engineering" J. Wiley and Sons, Inc., N. Y., 1969.
5. Goshorn, T. R., Jorgensen, A. H. and Woods, M. E., Rubber World, 161 (1), 66 (1969).
6. Woods, M. E., and Whittington, W. H., Rubber Age, 107 (10), 39 (1975).

ENERGY USE IN PADDLE DRYERS

William L. Root, III and Edward M. Cook

STORK BOWEN ENGINEERING INC.
Somerville, NJ - U.S.A.

ABSTRACT

This paper discusses the energy related characteristics of horizontal, indirectly heated agitator dryers of the hollow paddle type and related designs, such as the hollow disc, hollow screw and steam tube dryers. These units are used for various processing duties, but drying is their principal use and the one on which they are generally evaluated. Heat transfer rates for drying range from approximately 300 BTU/hr-ft^2-°F (1700 J/s-m^2-°C) in a boiling mode to 10 BTU/hr-ft^2-°F (57 J/s-m^2-°C) for essentially sensible heating of materials with poor heat transfer characteristics.

Paddle dryers decouple the heat transfer rate and residence time, making it easier to optimize operating conditions. They also give greater localized mixing, which improves heat transfer rate and avoids overheating the product.

A major heat loss from directly heated dryers is in their exhaust air. Indirect dryers practically eliminate this loss because they use little or no air. Heat requirements are generally about 1200 btu/lb water evaporation (2.83 x 10^6 J/kg) compared to 1500-2500 btu/lb water evaporation (3.49 x 10^6 - 5.80 x 10^6 J/kg) for directly heated dryers.

INTRODUCTION

Indirectly heated agitated dryers are of increasing interest because of their comparatively low energy use, which results principally from the use of little or no air (or other gas) flow. A better understanding of the practical aspects of their heat transfer mechanisms should lead to broader applications of the equipment, especially where reduced energy use is a dominant factor.

Our particular concern is a specific design of horizontal paddle dryer with heated jacket and heated paddle agitators. This general class of equipment also includes heated hollow screw and heated disc types. All have stationary trough-shaped containment vessels, which are jacketed for heating. The designs are all characterized by loading, or holdup, of the process mass so as to cover 50% to 100% of the heated agitator. Air flow, if any, is used for sweeping over the bed of drying material to aid in removal of the evaporated moisture.

Discussion of this type of dryer generally has been omitted from handbooks and overview articles in engineering journals, perhaps because its energy conserving traits have not been understood or appreciated until recently.

Rotary steam tube dryers have somewhat similar characteristics and action on the product being dried, but the mechanical design is quite different because of the rotating shell, low holdup (typically 3-5%) and higher air flow.

In indirectly heated dryers there are two (2) basic energy considerations:

1. The method of heat transfer from metal surface directly and indirectly to the product.
2. The amount of energy consumed as heat and power, compared to other types of dryers.

HEAT TRANSFER ACTIVITY

Flow of heat in agitated dryers is initiated by conduction from heated surface to the material, then between particles or from one part of the material mass to another. Convection also plays a part - evaporated vapor recondenses on cooler material, also any air present transfers heat from warmer to cooler parts of the material. The magnitude of these effects is not known, and even less is known of the influence of radiation.

The aim of design innovation in these units is to minimize equipment size and cost by optimizing the effectiveness of the heated surfaces - both trough and agitator. This means maximizing product side heat transfer coefficient and degree of holdup.

A second purpose is to improve residence time - temperature relations, i.e., give each particle about equal time and heat exposure. The ideal result is difficult to achieve, however, because good mixing (rather than plug flow) is required to give good heat distribution, but mixing tends to spread out the time distribution. Intensive local mixing is needed, without encouraging short circuiting of product.

A distinction should be made between average residence time and residence time distribution. The average residence time (typically 10 minutes to 4 hours) can be determined by volume of the dryer divided by volumetric flow rate of material. Residence time distribution is the range of residence times of all particles and can be represented by a normal distribution curve.

Residence time in the dryer can be adjusted in several ways. The agitator can push the material, as in the case of screw designs. However, heat transfer rates and degree of mixing are then tied to the desired residence time, so that reaching ideal conditions is difficult.

Other designs rely on "hydraulic head" of process mass to force product flow toward and over an outlet weir - this allows an intensive local mixing pattern without affecting the degree of holdup. Tilting of the unit is also effective in some applications.

Heat transfer rates influence dryer size as they do heat exchanger size. The amount of heating surface required, A (total of jacket plus agitator heated surfaces) is a function of heat load, Q, mean temperature difference, MTD, and the effective heat transfer rate, U. Heat transfer rate for the agitator surface is several times greater than for the trough, sometimes as much as tenfold.

The equation $A = Q/(U \times MTD)$ can be averaged for drying over the entire unit, but it is more accurate to use it to represent conditions at points or at logical segments of the operation. This is especially true for widely varying changes in product consistency throughout the dryer. The MTD is calculated from heating medium and product temperatures. It is sometimes difficult to determine because of phase change and removal of solvent and, at low moisture content, the heating of the solids above the boiling point, or introduction of air into the bed of material. The heat transfer rate can only be calculated from the measured values of the other variables. Any inaccuracy in measuring temperatures and calculating MTD yields uncertainty in heat transfer rates. To determine required surface and/or heat transfer rates it is customary for manufacturers to run tests on small sized equipment. Requirements for commercial production rates are scaled up from the test data.

Mass and heat transfer in these units involves mechanical mixing of the wet solids with release of the vapor through the mass of solids. Characteristics of materials vary from granular, free flowing, even powdery solids to pasty masses to mixtures of solids in boiling solvent - and all possibilities in between. Calculation of heat transfer rates and design scale-up is especially complex when more than one of these conditions occurs in a single drying operation. Also, fouling of heat transfer surface can reduce dryer performance.

AGITATION

The basic purpose of agitation is to minimize the heated surface required. It separates heated material from hot surfaces so that cooler particles can move in; this avoids over-exposure to heat. Mixing also improves contact between particles of different temperature, increasing the effective heat transfer rate.

Multiple agitator shaft designs are often used. Sometimes the use of two (2) inter-meshing agitator shafts will improve mixing and self cleaning ability. The use of two or four shaft design increases heating surface per unit volume.

Lifting flights on agitator blades move the material adjacent to the trough. They also add to the general mixing effect, which is additionally needed to avoid stagnation of product below the weir.

DESIGN TYPES

Among the available heated agitator dryers, there are some important variations. The main difference is in the agitator design and how each contacts and mixes the material.

Jacketed hollow screw conveyor dryers were a natural development from the simple, practical screw conveyor. The screw heats the material and moves it in essentially plug flow. Multiple screw designs tend to break up plug flow, or "roping", giving somewhat better mixing, thus better heat transfer into the bed. Residence time can be lengthened by reducing screw speed, but this lowers heat transfer rates and degree of mixing.

The hollow disc design having no positive forwarding transport action (as found in the screw units) can promote some local mixing, which enhances heat transfer rate. This design provides holdup that often can be only 2/3 or less of the heated surface. Better control of residence time is afforded, however, because travel of material from inlet to outlet is governed principally by the feed rate. One of the available designs has multiple shafts with product flow perpendicular to the shafts. Utilization of heat transfer surface is improved because the unit can be operated close to its flooded condiiton, i.e., 100% holdup. However, the mechanical drive is necessarily more complex.

A further development in this class of heated agitator dryers has cut flight paddles, designed to improve heat transfer, mixing and particle distribution vs. residence time. The paddles cut through the material and then allow it to fold in on itself, thus enhancing the mixing action and motion of particles to and from the heated surface. One such design is shown in Figure 1.

Agitator speed is typically 10-40 rpm - the optimum for a given material must be found by testing. Heat transfer rates increase at increasing speed in the lower range, but it is well below a linear relationship. Values of heat transfer rate vs. speed flatten out and finally decline, because fluidization, with greater gas entrainment, is approached at higher speeds. Residence time can be varied from a few minutes to several hours, depending on needs of the product.

The paddles in this unit have a cuneiform, or wedge shape that plows through the material. See Figure 2. Pressure against the material is equal on both sides and the shape induces a scouring action of particles against the metal that retards the formation of a fouling layer. Heat transfer rate on the agitator surface is typically 5-10 times greater than on the trough surface.

ENERGY CONSUMPTION

The principle advantage of indirect drying, related to energy, is the absence of air (or other carrier gas) for supplying the necessary heat. Some air is used in some designs, depending on the application, to aid in removing the evaporated moisture by sweeping across the bed of material. It does not travel through the material as in direct dryers.

A major energy loss in direct drying is in the flow of air, which is exhausted at typically 160°F to 350°F. Only a portion of this heat loss is recoverable and to date few installations have found it economically justifiable.

In a direct dryer the driving force for evaporation is the drying air temperature difference from inlet to outlet. Greater temperature difference gives both smaller equipment size and lower energy use. For an indirect dryer, the evaporative driving force is the temperature difference between the heating medium (in the agitator and jacket) and the substance being dried. This temperature difference affects only equipment size; energy use is a function of required evaporation, sensible heat difference between feed and dry product, and heat loss - plus whatever heat is added to any sweep air used.

Table 1 lists three (3) specific materials that were tested on a paddle dryer. For comparison, similar applications were estimated from test data on direct heated dryers. It should be noted that for most applications both direct and indirect types cannot be used successfully - for some others both types are not economically feasible. At very high capacities indirect dryers are relatively less cost effective because of size limits. Also, they are not heated by the products of combustion as direct dryers often are.

No sweep air was used for the paddle dryers listed in Table 1. Steam evolved in such a design is removed by a condenser and, if necessary, a vacuum source. Powder separating equipment is seldom required with this arrangement. However, when an air sweep is used, a fan and dust collector are required, and condensation usually must be avoided. Energy use is somewhat higher as a result of the heat in the exhaust air.

Generalizations about power requirements cannot be made, except that total power for agitated dryers is usually 60-85% of that for direct dryers on those applications that have been compared. The power is of less concern because fuel costs are 5-20 times greater.

Figure 3 illustrates the power requirement vs. material consistency for a typical application. Area under the curve represents the total power required. Path through the dryer is from right to left.

For the equipment user the important relation is energy per unit of product. However, the equipment designer is more concerned with energy per unit of evaporation, because evaporation requirement has the dominant influence on equipment sizing and energy use. Also, it is a value that is useful in comparing similar applications. For agitated dryers this heat requirement is typically 1,200-1,250 btu/lb of evaporation. This compares with values for direct dryers of typically 1,500-3,500.

SUMMARY

The importance of energy use continues to escalate upward and no change of this trend is in sight. In addition to having to factor this into his designs, the equipment manufacturer has the added concern of assuring that his designs will have the maximum possible success on a wide range of products. This requires that the equipment will make satisfactory product and will operate with minimum maintenance and cleaning problems. Nevertheless, energy concerns will play an increasingly important role in the design of equipment and systems, especially in the drying industry.

TABLE 1

Paddle Dryer vs Direct Dryer for Specific Application

Energy Use Comparison

Product Name:	Diatomaceous Earth		Aluminum Hydroxide		Organic Intermediate	
Product Rate, lb/hr:	2,300		3,500		2,250	
Evaporation Rate, lb/hr:	1,230		2,230		692	
Feed Moisture, %:	36.5		45		23.5	
Product Moisture, %	2.5		10		0.5	
Dryer Type:	Paddle	Direct Ht.	Paddle	Direct Ht.	Paddle	Direct Ht.
Avg. U btu/hr-ft^2-°F:	27	--	56	--	30	--
Installed cost, $1,000	276	216	276	260	174	156
M btu/hr	1.516	2.213	2.717	3.917	0.863	1.540
btu/lb evap'n.	1,233	1,800	1,218	1,757	1,247	2,225
HP	25	45	30	46	14	35

TABLE 2

Conversion of Units

Unit or Symbol	To Convert From U.S. Customary Units	To SI Metric Units	Multiply by
U	btu/hr-ft^2-°F	J/s-m^2-°K	5.6764
A	ft^2	m^2	0.092902
Q	btu/hr	J/s	0.29297
Length	inches	m	0.025400
Weight Flow Rate	lb/hr	kg/s	.0001260
Heat Load	M btu/hr	J/s	.29297 x 10^6
Heat Ratio	btu/lb	J/kg	2325.2
Power	HP	W	746.00

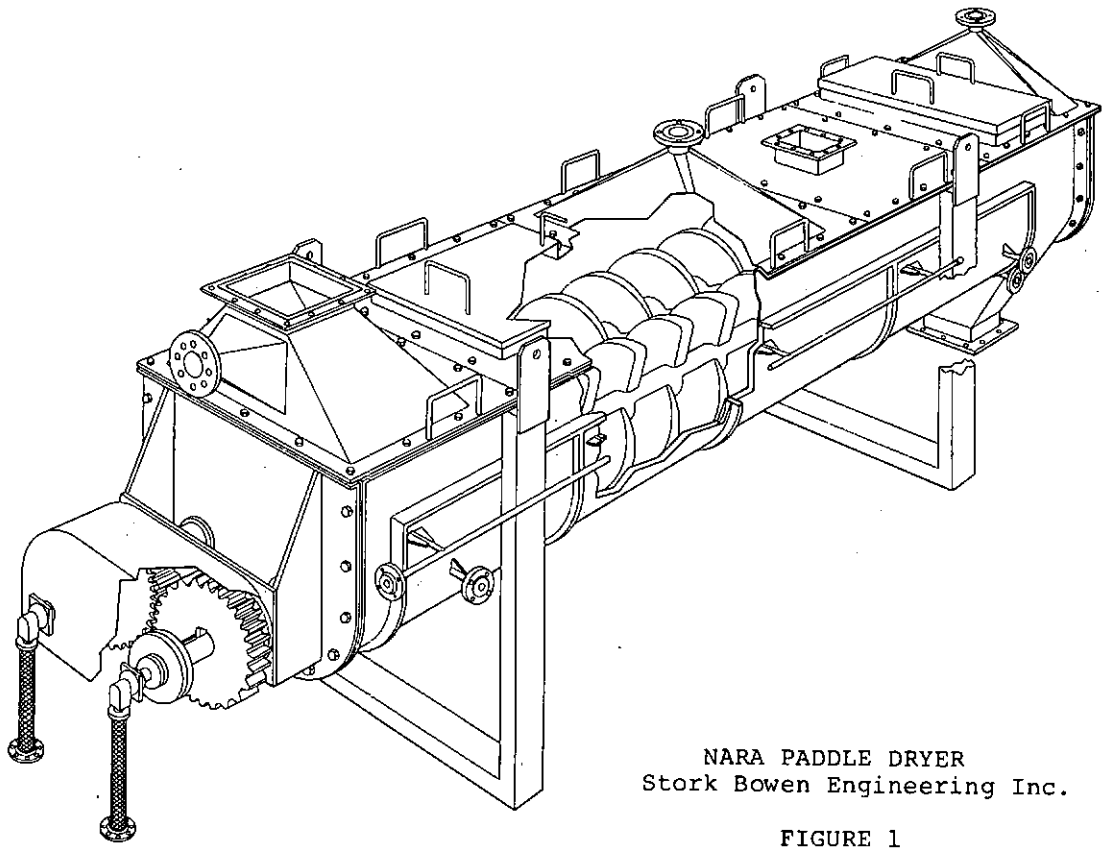

NARA PADDLE DRYER
Stork Bowen Engineering Inc.

FIGURE 1

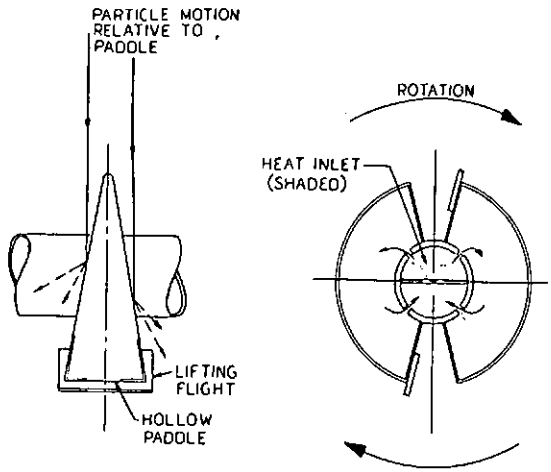

PADDLE DESIGN - NARA PADDLE DRYER

FIGURE 2

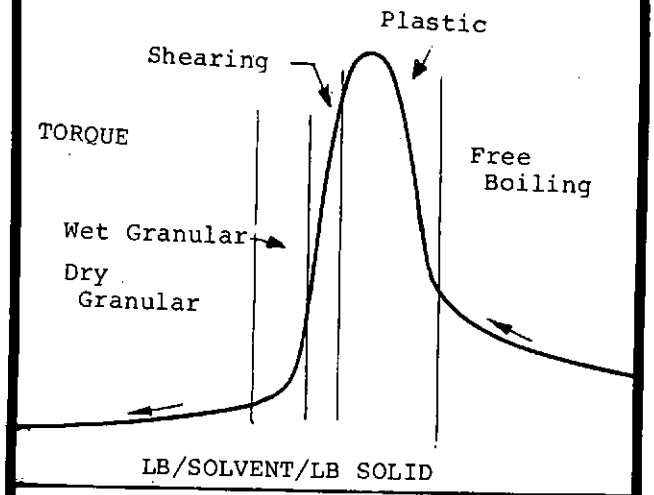

POWER vs PHYSICAL CHARACTERISTICS
Typical material in an agitated dryer

Figure 3

UNSTEADY HEAT AND MASS TRANSFER IN A PACKED BED OF FINE PARTICLES WITH AN ENDOTHERMIC PROCESS

M. Hasatani
N. Arai

Department of Chemical Engineering,
Nagoya University, Nagoya

ABSTRACT

The basic differential equations controlling the temperature and concentration field in a packed bed of fine particles are derived and solved for the general case in which an endothermic process of particles takes place under the non-isothermal and non-isoconcentrate conditions. The time-changes for fluid- and particle-temperature and concentration of fluid(humidity) are calculated by a numerical method, assuming that the rate of the endothermic process can be expressed by a first-order rate equation and that the fluid flow through the bed is of a piston flow type. In order to examine the applicability of the present theoretical analysis, the experiments are conducted for the drying of silica-gel and the two-stage dehydration of natural gypsum. It has been found that the calculated results show a satisfactory agreement with the measured data within the range of the experimental conditions employed.

NOMENCLATURE

a_p = surface area of particle per unit bed volume, m^2/m^3
c = specific heat, $J/kg \cdot K$
$D_{e,r}$ = radial effective-diffusivity of humid air m^2/sec
D_p = particle diameter, m
f_i = rate constant of endothermic process on the i-stage , $1/sec$
H_g = air humidity, $kg\text{-}H_2O/kg\text{-}dry \cdot air$
H_i = endothermic heat, J/kg
H_p = vapor concentration in the pore within particle, $kg\text{-}H_2O/kg\text{-}dry \cdot air$
h_p = heat transfer coefficient, $W/m^2 \cdot K$
k_p = mass transfer coefficient, $kg\text{-}dry\ air/m^2 \cdot sec$
R_p = radius of cylindrical bed, m
Re_p = particle Reynolds number
r = radial distance in cylindrical coordinate, m
t = particle temperature, °C,K
t_w = wall temperature, °C,K
u_g = superficial velocity of fluid, m/sec
w = moisture content of particle, $kg\text{-}H_2O/kg\text{-}dry \cdot solid$
Z = total bed height, m
z = axial distance in cylindrical coordinate, m
γ_i = fractional conversion
ε = void fraction
θ = time, sec
λ = thermal conductivity, $W/m \cdot K$
λ_r^o = radial effective-thermal conductivity of the bed, $W/m \cdot K$
ρ = density, kg/m^3
ψ = fluid temperature, °C,K

Subscripts

0 = initial or entrance
B = bed
g = fluid
p = particle

Superscript

$-$ = dimensionless quantity

INTRODUCTION

In the drying of hydrophilic materials, such as silica-gel and calcium chloride, the water which is directly vaporized inside is removed outside the solid in the state of vapor. And also the drying of capillary porous materials during the falling rate period(in particular, its second-stage period) is not under the measurable influence of liquid phase transfer. Thus, the course of drying under this condition(i.e., little influence of liquid phase transfer) has a high similarity to other heterogeneous endothermic processes, for instance, the dehydration of natural gypsum($CaSO_4 2H_2O$),calcium hydroxide($Ca(OH)_2$),iron sulfate ($FeSO_4 7H_2O$) and so on. The basic difference between the two processes is that drying is a physical process, while dehydration is a chemical one; it can be treated as a difference in the rate expression of an endothermic process as will be described in detail later. Therefore, they can be all analysed systematically and theoretically as a problem of simultaneous heat and mass transfer with an endothermic process.

Development of a systematical and theoretical analysis as mentioned above makes possible a relative comparison with the analyses that have been dealt with independently in industrial operation. And , at the same time, we can make a theoretical approach appropriate to newly-arisen problems on engineering, for example, heat recovery and storage by making use of the endothermic and exothermic cycle. In the previous paper concerning the heat and mass transfer in a single solid particle

with an endothermic process, the authors(1) made it clear that in a fundamental sense the theoretical analysis based on this idea was of great significance for the systematical treatment of the problem. Recently, the necessity for batch or discontinuous operation has been revalued in each industrial field. It is supposed that in heat recovery and storage the theoretical analysis with an expectation of batch operation gives a more applicable solution. However, as all the phenomena become unsteady in batch operation, a theoretical treatment is so complicated that a lot of questions may remain unsolved.

In the present study, a mathematical model which can be dealt systematically with the unsteady characteristics of the phenomena is presented for the heat and mass transfer with an endothermic process in a packed bed, as in a typical batch operation. It is assumed that in the present mathematical model the packed solid particles are fine and so the heat and mass transfer resistance within particles is neglected. And the rate expression of an endothermic process is simplified to where it can be applied to the drying of hydrophilic materials, the dehydration of metallic salts and so on. The numerical solution of the basic differential equations derived from the present mathematical model is compared with the experimental results on the drying of silica-gel and the two-stage dehydration of natural gypsum, in order to clarify the applicability of the present theoretical analysis. And also the unsteady heat and mass transfer rates are correlated with the operation parameters of a packed bed by discussing the characteristics of the solution.

MATHEMATICAL MODEL

The four following fundamental assumptions are made for the mathematical model developed in the present study:

(i) The endothermic process takes place successively within the range of the respective temperature on multiple stages. Its rate expression is all of first order and the endothermic process does not accompany with liquid phase transfer.

(ii) The heat and mass transfer resistance of packed solid particles is taken into account only on the boundary surface between particles and fluid. For that reason the resistance within particles is neglected.

(iii) The fluid flows through the bed by the piston flow type with a uniform velocity distribution, and the rate of transfer due to diffusion and mixing in the axial direction is extremely small as compared with that due to flow.

(iv) The values of physical properties and the structure of a packed bed(void fraction, particle diameter and so on) do not undergo changes in the course of endothermic process.

Heat and Mass Transfer Equation for Packed Particles

When solid particles at arbitary positions of a cylindrical packed bed(r=r, z=z) come into contact with the fluid of temperature ψ and absolute humidity H_g and bring about the endothermic process on the n-stage, the following differential equations can be produced from the infinitesimal heat and mass balance equations for solid particles:

$$c_p\rho_p(1-\varepsilon_B)\frac{\partial t}{\partial\theta} = \lambda_r^0\left(\frac{\partial^2 t}{\partial r^2}+\frac{1}{r}\frac{\partial t}{\partial r}\right)+h_p a_p(\psi-t) - \sum_{i=1}^{n} H_i\rho_p(1-\varepsilon_B)\frac{\partial\gamma_i}{\partial\theta} \quad (1)$$

$$-\rho_p(1-\varepsilon_B)\frac{\partial w}{\partial\theta} = \sum_{i=1}^{n}\rho_p(1-\varepsilon_B)y_{i,0}\frac{\partial\gamma_i}{\partial\theta} = k_p a_p(H_p-H_g) \quad (2)$$

where, γ_i is the fractional conversion(γ_i=0~1.0) of an endothermic process on the i-stage, and by using the moisture content $w_{i,f}$ and $w_{i-1,f}$ at the completion of an endothermic process on the i- and (i-1)- stage ,

$$\gamma_i = \frac{w_i-w_{i,f}}{w_{i-1}-w_{i,f}} = \frac{w_i-w_{i,f}}{y_{i,0}} \quad (3)$$

And H_i shows the endothermic heat of the i-stage (the latent heat of evaporation or the heat of hydration).

The initial and boundary conditions are:

$$\theta = 0,\quad 0\le r\le R;\quad t = t_0,\quad H_p = H_{g,0},\quad \gamma_i = 0 \quad (4)$$

$$\theta > 0,\quad r = 0;\quad \frac{\partial t}{\partial r} = 0 \quad (5)$$

$$\theta > 0,\quad r = R;\quad t = t_w(=\psi_0) \quad (6)$$

By introducing the following dimensionless parameters,

$$\Theta = \frac{\lambda_r^0\theta}{c_p\rho_p(1-\varepsilon_B)R^2},\quad \omega = \frac{r}{R},\quad p_1 = \frac{h_p a_p R^2}{\lambda_r^0},$$

$$p_{2,i} = \frac{k_p a_p c_p R^2 H_{g,0}}{y_{i,0}\lambda_r^0},\quad \bar{t} = \frac{t}{\psi_0},\quad \bar{\psi} = \frac{\psi}{\psi_0},$$

$$\bar{H}_p = \frac{H_p}{H_{g,0}},\quad \bar{H}_g = \frac{H_g}{H_{g,0}},\quad \bar{H}_i = \frac{H_i}{\psi_0 c_p},$$

Equations(1) and (2) are rewritten as follows:

$$\frac{\partial\bar{t}}{\partial\Theta} = \frac{\partial^2\bar{t}}{\partial\omega^2}+\frac{1}{\omega}\frac{\partial\bar{t}}{\partial\omega}+p_1(\bar{\psi}-\bar{t})-\sum_{i=1}^{n}\bar{H}_i\frac{\partial\gamma_i}{\partial\Theta} \quad (7)$$

$$\sum_{i=1}^{n}\frac{\partial\gamma_i}{\partial\Theta} = p_{2,i}(\bar{H}_p-\bar{H}_g) \quad (8)$$

In the same way,

$$\Theta = 0,\quad 0\le\omega\le 1;\quad \bar{t} = t_0/\psi_0\ \text{(known)},\quad \bar{H}_p=1,\quad \gamma_i=0 \quad (9)$$

$$\Theta>0,\quad \omega = 0;\quad \frac{\partial\bar{t}}{\partial\omega} = 0, \quad (10)$$

$$\theta>0, \quad \omega = 1 \; ; \quad \bar{t} = 1 \tag{11}$$

Heat and Mass TransferEquation for Flowing Fluid

For the fluid flowing through the void in a packed bed, the following equations are produced from the infinitesimal heat and mass balance equations, taking the same viewpoint as in Equations(1) and (2):

$$\varepsilon_B c_g \rho_g \frac{\partial \psi}{\partial \theta} + c_g \rho_g u_g \frac{\partial \psi}{\partial z} = \lambda_g \left(\frac{\partial^2 \psi}{\partial r^2} + \frac{1}{r} \frac{\partial \psi}{\partial r} \right) - h_p a_p (\psi - t) \tag{12}$$

$$\varepsilon_B \frac{\partial H_g}{\partial \theta} + u_g \frac{\partial H_g}{\partial z} = D_{e,r} \left(\frac{\partial^2 H_g}{\partial r^2} + \frac{1}{r} \frac{\partial H_g}{\partial r} \right) + \frac{k_p a_p}{\rho_g} (H_p - H_g) \tag{13}$$

The initial and boundary conditions for the equations above are:

$$\theta = 0, \quad 0 \le r \le R, \quad z = 0 \; ; \quad \psi = \psi_0, \quad H_g = H_{g,0} \tag{14}$$

$$\theta > 0, \quad r = 0, \quad 0 \le z \le Z \; ; \quad \frac{\partial \psi}{\partial r} = 0, \quad \frac{\partial H_g}{\partial r} = 0 \tag{15}$$

$$\theta > 0, \quad r = R, \quad 0 \le z \le Z \; ; \quad \psi = t_w (= \psi_0), \quad \frac{\partial H_g}{\partial r} = 0 \tag{16}$$

where, by introducing new variables η and τ like $z=\eta$ and $\theta = \tau + (\varepsilon_B \eta / u_g)$, Equations(12) and (13) are rewritten as follows:

$$\frac{\partial \psi}{\partial \eta} = \frac{\lambda_g}{c_g \rho_g u_g} \left(\frac{\partial^2 \psi}{\partial r^2} + \frac{1}{r} \frac{\partial \psi}{\partial r} \right) - \frac{h_p a_p}{c_g \rho_g u_g} (\psi - t) \tag{17}$$

$$\frac{\partial H_g}{\partial \eta} = \frac{D_{e,r}}{u_g} \left(\frac{\partial^2 H_g}{\partial r^2} + \frac{1}{r} \frac{\partial H_g}{\partial r} \right) + \frac{k_p a_p}{u_g \rho_g} (H_p - H_g) \tag{18}$$

Furthermore, assuming that the analogous relation exists between heat and mass transfer,

$$X = \frac{\lambda_g \eta}{u_g \rho_g c_g R^2} = \frac{D_{e,r} \eta}{u_g R^2}, \quad p_3 = \frac{h_p a_p R^2}{\lambda_g}, \quad p_4 = \frac{k_p a_p R^2}{\rho_g D_{e,r}}$$

By using the dimensionless parameters above, Equations(12) to (16) are finally transformed as follows:

$$\frac{\partial \bar{\psi}}{\partial X} = \frac{\partial^2 \bar{\psi}}{\partial \omega^2} + \frac{1}{\omega} \frac{\partial \bar{\psi}}{\partial \omega} - p_3 (\bar{\psi} - \bar{t}) \tag{19}$$

$$\frac{\partial \bar{H}_g}{\partial X} = \frac{\partial^2 \bar{H}_g}{\partial \omega^2} + \frac{1}{\omega} \frac{\partial \bar{H}_g}{\partial \omega} + p_4 (\bar{H}_p - \bar{H}_g) \tag{20}$$

The initial and boundary conditions are:

$$X = 0, \quad 0 \le \omega \le 1 \; ; \quad \bar{\psi} = 1, \quad \bar{H}_g = 1 \tag{21}$$

$$X > 0, \quad \omega = 0 \; ; \quad \frac{\partial \bar{\psi}}{\partial \omega} = 0, \quad \frac{\partial \bar{H}_g}{\partial \omega} = 0 \tag{22}$$

$$X > 0, \quad \omega = 1 \; ; \quad \bar{\psi} = 1, \quad \frac{\partial \bar{H}_g}{\partial \omega} = 0 \tag{23}$$

Rate Expression of Endothermic Process

The rate of each endothermic process, ($\partial \gamma_i / \partial \theta$:i.e. the changing rate of the moisture content of packed particles by an endothermic process on the i-stage) is expressed as follows based on the assumption(i),

$$\frac{\partial \gamma_i}{\partial \theta} = \alpha_i (H_p^* - H_p)(1 - \gamma_i) \tag{24}$$

where, H_p and H_p^* indicate the vapor concentration and equilibrium vapor concentration in the pore within packed particles respectively, and α_i is a fixed rate constant which can be determined as an inherent characteristic value of packed particles. Because H_p^* can be treated as a function of temperature, we can also express Equation(11) approximately as follows:

$$\frac{\partial \gamma_i}{\partial \theta} = f_i (t, H_p)(1 - \gamma_i) \tag{25}$$

By introducing the following dimensionless rate constant,

$$\bar{f}_i (\bar{t}, \bar{H}_p) = f_i (t, H_p) \frac{c_p \rho_p (1 - \varepsilon_B) R^2}{\lambda_r^0}$$

Equation(25) is rewritten:

$$\frac{\partial \gamma_i}{\partial \theta} = \bar{f}_i (\bar{t}, \bar{H}_p)(1 - \gamma_i) \tag{26}$$

NUMERICAL CALCULATIONS

By solving the simultaneous differential equations of Equations (7),(8),(19),(20) and (26), we get theoretically the unsteady temperature and concentration distributions in a packed bed of fine particles with an endothermic process on the n-stage. The given simultaneous differential equations are transformed into the simultaneous difference equations in consideration of the initial and boundary conditions of Equations (9) to (11) and (21)to(23) and are solved numerically by the successive integration method. In the numerical calculation within the range of the experimental conditions Equation (26) is approximated by the following linear equation,

$$f_i(t,H_p) = A_i t + B_i H_p + C_i \qquad (27)$$

and the integral intervals of time and space are limited to $\Delta\theta$=1∿5 sec and $\Delta r=\Delta z=(2.5\sim5)\times10^{-3}$m respectively.

EXPERIMENTAL APPARATUS

The schematic drawing of the experimental apparatus in the present study is shown in Figure 1. The inner tube (6×10^{-2} m in diameter), made of stainless steel, is attached with bolts the outer tube (8.2×10^{-2} m in diameter) with 100 mesh wire -netting on its bottom. A packed bed is formed within the inner tube and removed easily with it after the experiment has been finished.
The apparatus itself is a type of a radiative electric furnace with a SiC heater. The packed bed is placed in the center of this furnace and the wall temperature of the bed is kept steady and uniform throughout the period of the experiment. The air used as heating fluid is pre-heated to a given temperature by an electric heater with the maximum load of 12 KW. Figure 2 shows the testing section in detail. C.A. thermocouples of 300 μ in diameter are placed at the nine points in the bed -- three points in the radial direction(r=0,0.01 and 0.02 m) and three points in the axial direction(z=0.05,0.1 and 0.15 m), through which the time-change of the temperature distribution in the bed can be measured continuously. As for the air humidity, the time-change of the cross-sectional average humidity at the exit of the bed is measured by a hygrometer(made by Yokogawa Electric Works Ltd., Dew-cell type).

Procedures and Other Details

After first confirming that the temperature and humidity of the heated air have become steady and uniform over the entire bed in the state of the empty tube, weighed sample particles are packed into the inner tube quickly, while the heated air being blown into it is stopped for a short time. The packed weighed sample particles is 0.65 kg and so the bed height is about 0.2 m. The flow velocity of the heated air is adjusted to a given value again and the time-change of the temperature at the respective positions in the bed and the air humidity at its exit are measured continuously by the method mentioned above until the endothermic process has finished. After that, the packed bed

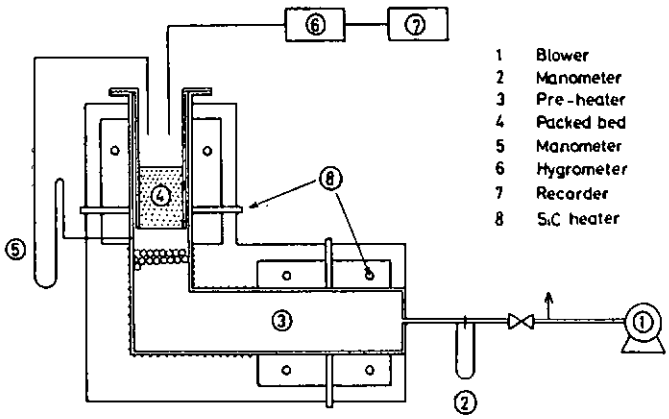

Figure 1 Experimental Apparatus

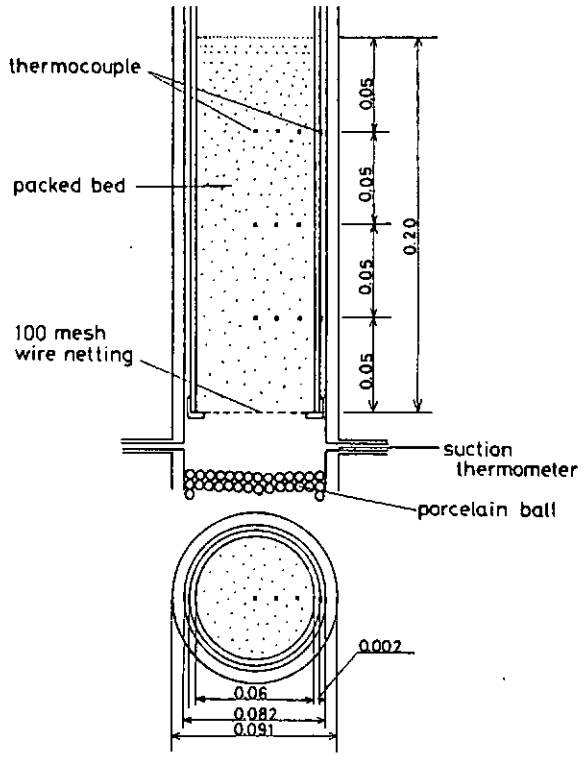

Figure 2 Details of Testing Section

is taken out of the furnace to measure the bed height and the weight of sample particles.
The range of the present experimental conditions in the case of natural gypsum(purity of more than 98 % ,from Africa) is as follows:
ψ_0= 220-450°C, Re_p= 1-15, ε_B= 0.43-0.53, $H_{g,0}$= 0.005-0.02 kg-H_2O/kg-dry·air, D_p=(0.25-1.25) $\times10^{-3}$ m.
And dehydration of gypsum takes place by heating in the two step as follows:

$$CaSO_4\cdot 2H_2O \xrightarrow{110\sim140°C} CaSO_4\cdot 1/2H_2O$$

$$CaSO_4\cdot 1/2H_2O \xrightarrow{160\sim190°C} CaSO_4 + 1/2H_2O$$

RESULTS AND DISCUSSION

Property Determination and Calculated Results

An example of the calculated results on natural gypsum is shown in Figure 3, where the changes of the particle temperature, the air temperature, the air humidity and the moisture content at a given position in the bed are plotted with the elapsed time. The values of physical properties and characteristics used in numerical calculation of the basic equations derived before are obtained by calculation or measurement as follows:

λ_p(thermal conductivity of packed particles): an arithmetic average of both the results measured before and after an endothermic process by a hot-wire method (2).

H_i(in natural gypsum): the value measured by Southard(3) was used.

h_p and k_p (heat and mass transfer coefficient between particles and fluid): h_p was calculated from the empirical equation by Kunii& Smith(4) and k_p was calculated from h_p by applying the analogy rule.

λ_r^0(effective thermal conductivity in the radial direction of a static bed): calculated from the theoretical equation by Kunii & Smith(5).

$f_i(t,H_p)$: measured by the same procedure which the authors (1) reported in the previous paper. The measured values of $f_{i=1,2}(t,H_p)$ for natural gypsum are:

$$f_1(t,H_p) = 6.11 \times 10^{-5} - 13.6\left(\frac{\rho_g \varepsilon_p}{\rho_p}\right)H_p - 5.14 \times 10^{-3} \quad [1/\text{sec}]$$

$$f_2(t,H_p) = 1.94 \times 10^{-4} - 13.6\left(\frac{\rho_g \varepsilon_p}{\rho_p}\right)H_p - 3.06 \times 10^{-2} \quad [1/\text{sec}] \qquad (28)$$

where, ε_p=0.3(the value measured by the air displacement method after dehydration has finished). It is found from Figure 3 that the difference between particle and fluid temperature is much more than that of the case without an endothermic process, and that the temperature and concentration have a large distribution not only in the axial direction but also in the radial direction. This suggests that, in analyzing theoretically the heat and mass transfer of a packed bed with an endothermic process, the two-dimensional mathematical model with the transfer resistance on the boundary surface between particles and fluid taken into consideration is often necessary, even though a packed bed is composed of fine particles as in the present experiment.

Comparison Between Experimental Data and Calculated Results

The experimental results of the time-change of the temperature distribution in the bed and the air humidity at its exit are compared with the calculated results to examine the applicability of the present theoretical analysis.

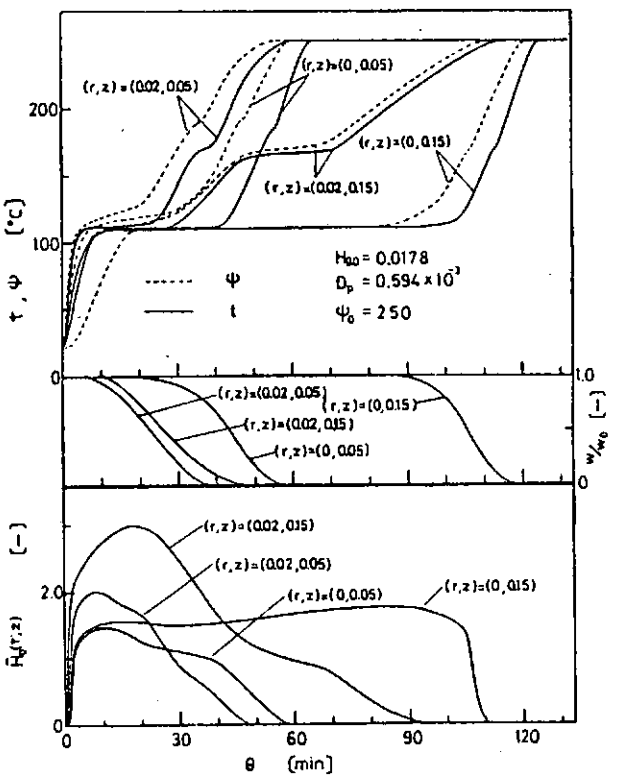

Figure 3 An Example of Calculated Results on Natural Gypsum

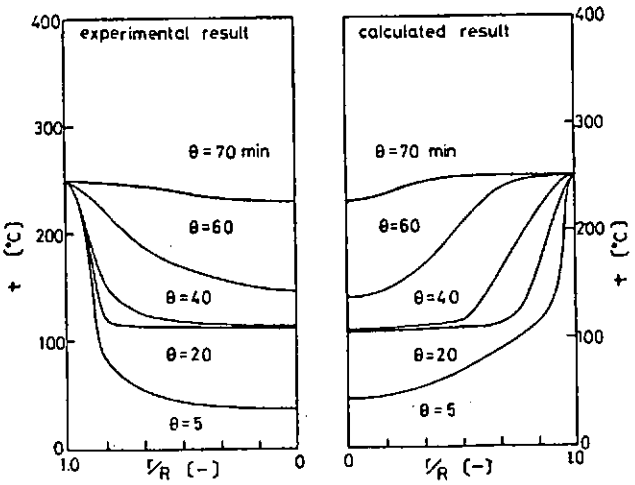

Figure 4 Comparison between Calculated- and Experimental Results for Unsteady Temperature Distribution in the Bed (Experimental conditions are the same as in Fig.3)

(1) Unsteady Temperature Field in the Bed

Figure 4 shows the time-change of the temperature distribution in the radial direction at the position z=0.1 m. Figures 5 and 6 show the time-change of the temperature distribution in the axial direction in the center of the bed.

In these figures, the calculated results are compared with the experimental ones. The temperature measured by a thermocouple is an intermediate value between the particle temperature and the air temperature. Within the range of the experimental conditions employed, the temperature curve for the measured value is approximate to the calculated particle temperature, so that in Figures 4 to 6 the measured temperature is compared with the calculated particle temperature. As seen in these figures, the particle temperature is gradually rising with elapse in time toward the center of the upper part of the bed from its lower part and the tube wall. And because of the endothermic process of natural gypsum on the first and second stage, the rising rate of the temperature is extremely slow in the vicinity of 110°C and 160°C. There is good agreement between the experimental and the calculated results for these trends. All these facts are also found when the experimental conditions of the particle diameter, the heating temperature, the flow velocity of the air and so on are changed within the range employed.

(2) Unsteady Air Humidity at the Exit of the Bed

Figures 5 and 6 show an example of the comparison between the calculated and the experimental results on the time-change of the air humidity at the exit of the bed. The time-change of the measured air humidity is remarkably similar to the response curve in the falling rate period which the authors (6) obtained in the packed bed drying of porous particles(brick particles). In this case, the influence of the two stage endothermic process is not so clear as found in the temperature distribution of the bed. It is likely that this is because the water removed in the second stage is one-third of that in the first stage and the air humidity at the exit of the bed appears as an integral value of the average rate of dehydration in the entire bed. However that may be, the calculated results agree well with the experimental ones for the air humidity as well as the temperature distribution as mentioned above. Therefore, it is concluded that the theoretical approach proposed in the present study of heat and mass transfer in a packed bed of fine particles with an endothermic process is of great use.

(3) Effect of Entrance Air Humidity on the Endothermic Process

Figure 7 shows the calculated results of the time-change of the particle temperature in the center of the bed, in a case where only $H_{g,0}$ is changed in the experimental conditions of Figure 5. In a case with $H_{g,0}$= 10 kg-H_2O/kg-dry·air, even in natural gypsum which is expected to be under the little influence of $H_{g,0}$, it is found that the first stage dehydration-temperature becomes about 10°C higher than that in a case with $H_{g,0}$=0.

ACKNOWLEDGEMENT

The authors wish to express their thanks to Prof. S.Sugiyama(Aichi Institute of Technology) for his helpful advices and suggestions, to Mr.S.Taniguchi

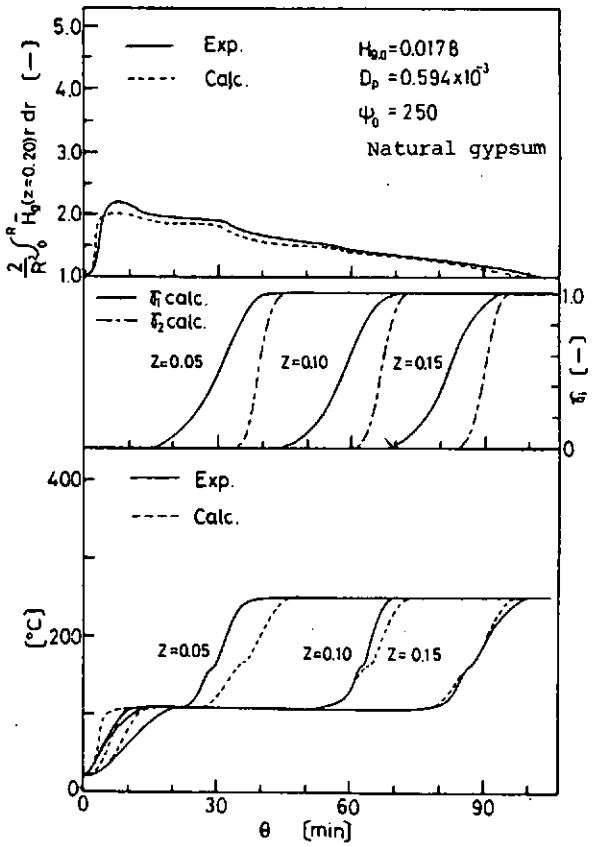

Figure 5 Comparison between Calculated- and Experimental Results

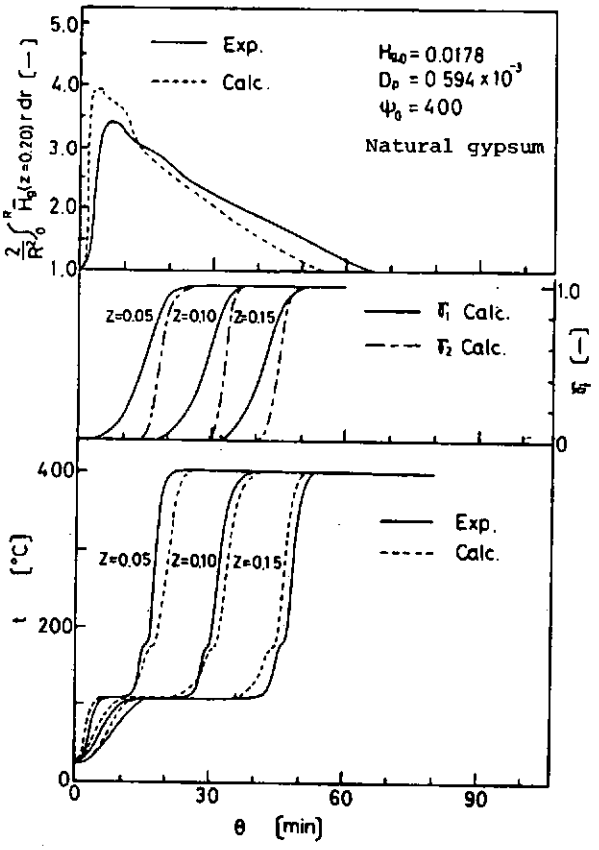

Figure 6 Comparison between Calculated- and Experimental Results

for his help with experiments.

REFERENCES

1. Kondo,T.,Hasatani,M. and Sugiyama,S., Kagaku Kogaku,Vol.31,p.806-811,1967
2. Nagasaka,K.,Shimizu,M. and Sugiyama,S., J.Chem. Eng.Japan,Vol.6,p.264-268,1973
3. Southard,J.C.,Ind.Eng.Chem.,Vol.32,p.442-445, 1940
4. Kunii,D. and Smith,J.M.,AIChE J.,Vol.6,p.71-78, 1960
5. Kunii,D. and Smith,J.M., ibid.,Vol.7,p.29-34, 1961
6. Arai,N.,Hori,I.,Hasatani,M. and Sugiyama,S., J.Chem.Eng.Japan,Vol.13, No.2,1980(in press)

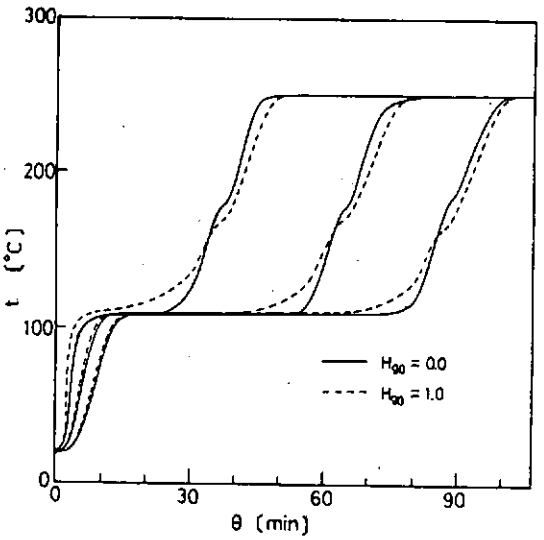

Figure 7 Effect of Entrance Air Humidity on Unsteady Temperature Distribution in the Bed (Calculated result; calculated conditions are the same as in Fig.5 except $H_{g,0}$)

DRYING SOME OBJECTS IN FLUIDIZED BED UNDER REDUCED PRESSURE

Kazumi YAMAMOTO, Yuji KAWAMURA

University of Hiroshima, Hiroshima, JAPAN

ABSTRACT

The heat transfer coefficient between the gas-fluidized bed and the plates immersed in the bed was measured under reduced pressure from 10^4 to 8×10^4 Pa (80 to 600 Torr) by means of cooling of the hot plate. On the other hand, the heat and mass transfer coefficient was measured by means of drying of wet asbestos plates in the same condition.

It became clear through the experimental results that the heat transfer coefficient did not change remarkably with operating pressure, but the mass transfer coefficient increased with the decreace of pressure. It can be considered as the fluidizing particles contribute to maintenance of the heat transfer between the object and circumference, and the decreasing of the air in operating circumference and fluidized particles contribute to the increace of the mass transfer on the object. This means that the operation in fluidized bed under reduced pressure becomes a useful method for drying.

NOMENCLATURE

A = surface area of plate, m^2
c = specific heat of plate, J/kg·K
d_p = diameter of fluidized particles, mm
h_w = heat transfer coefficient between the bed and the plate, $kW/m^2 \cdot K$
h_w' = $h_w^o(k_w/k_w^o)$, estimated heat transfer coefficient between the gas flow and the plate in fluidized bed, $kW/m^2 \cdot K$
h_w^o = heat transfer coefficient between the gas flow and the plate calculated from Eq. (5), $kW/m^2 \cdot K$
k_w = mass transfer coefficient on the plate in fluidized bed, $kg/m^2 \cdot s \cdot Pa$
k_w^o = mass transfer coefficient on the plate calculated from Eq. (4), $kg/m^2 \cdot s \cdot Pa$
L = length of the plate, mm
P = total pressure, Pa
p_f = vapor pressure in the fluidized bed, Pa
p_w = equilibrium vapor pressure on the surface of plate, Pa
R_c = drying rate in constant drying period, $kg/m^2 \cdot s$
Re = Reynolds number, -
Sc = Schmidt number, -
T, T_o = temperature of plate, K
T_f = temperature of fluidized bed, K
u = gas velocity based on hollow bed, cm/s
u_{mf} = superficial fluid velocity at minimum fluidizing conditions, cm/s
V = volume of plate, m^3
ε = void fruction, -
ρ = density of plate, kg/m^3
θ = time, s

1. INTRODUCTION

The many studies on the heat and mass transfer coefficient between the fluidized bed and the object immersed in the bed have been carried out up to the present. In the every case of these, the fluidized bed was operated under atmospheric pressure, and the study which was operated under reduced pressure as this work has not been reported in the literature.

It was reported in the last symposium (1) that the fluidized bed could be operated satisfactorily under reduced pressure even several ten Torr as well as at atmospheric pressure. Ziegler et al. (2) suggested that 85 ∿ 95 % amount of heat was transported by fluidized particles and the contribution of flowing gas was less than 20 % on the heat transfer between the bed and the object. It, therefore, may be thought that even the operation under reduced pressure gives the same effect on heat transfer as the operation at atmospheric pressure, if the good fluidized situation is held certainly. On the other hand, it was suggested by Shirai et al. (3) that the transportation of water and/or water vapor by fluidized particles could be neglected. Therefore, the mass transfer on the object in fluidized bed is affected only the diffusion of vapor through the surface gas film, and it means that the mass transfer coefficient was influenced considerably by the operating pressure. As the fluidized particles always have contact with surface of the object and disturb the surface gas film, this effect may be appeared besides the above mentioned effect on the heat and mass transfer coefficient.

In this paper, the heat transfer coefficient between the fluidized bed and the plate immersed in the bed was measured by means of cooling of the hot copper plate. On the other hand, the heat and mass transfer coefficient was measured by means of drying of wet asbestos plate in the same condition. The investigation on how influence of the operating pressure appears is the subject in this work. Accordingly the experiments were done under

the condition of various reduced pressures to about 133×10^2 Pa (100 Torr), but the other conditions maintain constant.

2. EXPERIMENTAL EQUIPMENT AND PROCEDURE

2.1 Experimental Equipment

The schematic diagram of experimental equipment is shown in Fig. 1. The main column of fluidized bed (225 mm I. D., 600 mm height) is made from transparent plastics (PVC), and it is surrounded with water cooling jacket, which maintains the fluidized bed at constant temperature. The bottom plate of bed is made from perforated brass plate, felt sheet and brass mesh (80 mesh), and it is confirmed experimentally that the uniform fluidization is secured.

The fluidizing air is introduced to the fluidized bed 4 after passing the flow meter (Orific meter) 1, and the control valve 2. The passed air over the fluidized bed goes through the filter 3, and the control valve 9, and is exhausted by the rotary vacuum pump 11. The operating pressure is measured by mercury manometer. The sands which have the characteristic values as show in Table 1 were used to fluidizing particles after classified by screens. The packing hight of fluidizing particles was kept 150 mm for all the experiments.

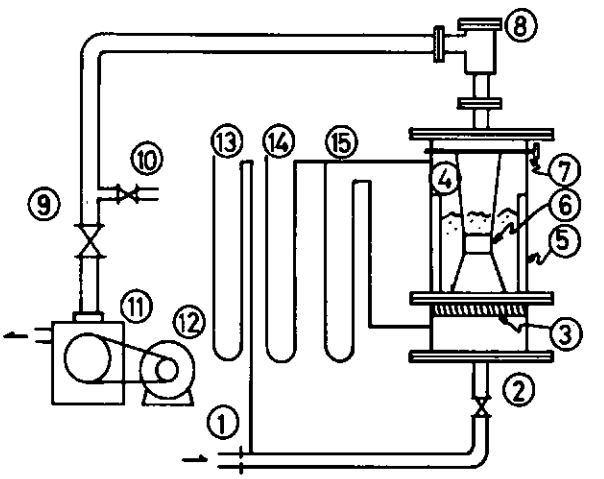

1. orifice meter
2. vacuum cock
3. distributer
4. main body
5. jacket
6. sample board
7. handle
8. filter
9. valve
10. valve
11. vacuum pump
12. moter
13. manometer
14. manometer
15. manometer

Fig. 1 Experimental apparatus

2.2 Experimental Method and Arrangement Procedure

2.2.1 Experiment of Heat Transfer

The heat transfer coefficients between wall and bed, h_w, were determined by the following procedure. The copper plate was submerged in fluidized bed after preheated uniformly, and the temperature of hot plate was measured continuously with copper-constantan thermo-couples set on the surface of the plate. The dimension of the heating plates is shown in Table 2. The cooling jacket kept fluidized bed at a constant temperature between 10 ∿ 20 °C during measurement. Since the thermal conductivity of the plates was large, the temperature in it could be neglected. Therefore the following Newton's equation can be used for determing the heat transfer coefficients between bed and wall, h_w, under these conditions.

$$\frac{T - T_f}{T_o - T_f} = \exp\left(-\frac{h_w A}{\rho c V}\theta\right) \qquad (1)$$

2.2.2 Experiment of Drying

Asbestos plates were used for drying sample. The dimensions of the plate are also shown in Table 2. An example of the drying characteristic curve of these asbestos plates is shown in Fig. 2. These plates were submerged in fluidized bed at about 60 % of water content, and the measurement of weight loss and surface temperature were performed in the period of constant drying rate. Drying rate, R_c, was determined by measuring the weight loss during the experiment*. The surface temperature of plate was measured with several copper-constantan thermo-couples set on the surface of plate, and the bed temperature was measured with the coveringless thermo-couples immersed in the bed. These temperature were kept at constant through measurements except for a short time at the beginning, and the difference of the measured surface temperatures were bound to be less than 1 °C. Therefore, the avarage of these temperatures was used in the calculations. Using the equilibrium vapor pressure p_w at this average

Table 1 Characteristic values of fluidizing particles

particles (mm)	density (g/cm^3)	shape factor (-)	voidage (-)	specific heat ($J/kg \cdot K$)	thermal conductivity ($W/m \cdot K$)	minimum fluidization velocity (cm/sec)
sand d_p=0.277	2.63	0.85	0.44	0.71×10^3	0.79	7.8
sand d_p=0.329	2.62	0.93	0.45	0.71×10^3	0.79	9.2

* The unavoidable unstational drying period at the beginning was so short that it could be disregarded.

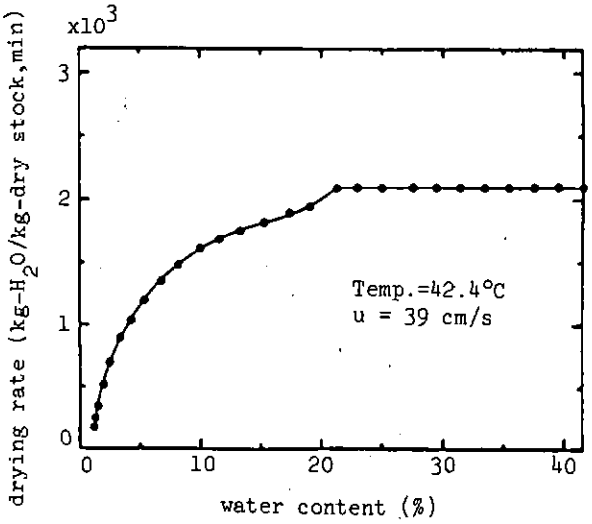

Fig. 2 Drying characteristic curve at atmospheric pressure

Table 2 Dimension of the plate

material	length (mm)	width (mm)	thickness (mm)
experiment of cooling			
copper	75	110	5
experiment of drying			
asbestos	30	80	3
	60	80	3
	120	80	3

surface temperature and the vapor pressure p_f in bed, which can be determined from the humidity of inlet air**, the mass transfer coefficients, k_w, can be determined from the following equation.

$$R_c = k_w(p_w - p_f) \qquad (2)$$

For reference, the experiments of drying for the same sample were performed in parallel air stream in the empty column. Since those experiments were done in reduced pressure, and the amount of heat supply from flowing gas was little, heater surrounding the plate was used additionally for heat supply much enough.

2.2.3 Determination of Gas Velocity

The previous paper (1) suggested that fluidizing situation was fairly effected by gas velocity. The effect of gas velocity, u, on the heat transfer coefficient between the bed and the plate, h_w, was shown in Fig. 3. The h_w increased with u, but approached a constant value at the velocity condition ($u/u_{mf} \gtrsim 4$). Also, it was confirmed that the

** In this experiment, the change of the vapor pressure in gas flow for evaporating from the plate is so little that it could be ignored.

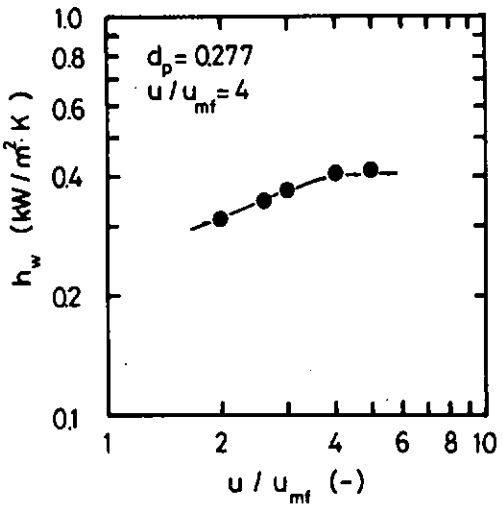

Fig. 3 Increasing of h_w with u/u_{mf} at the reduced constant pressure 5.32×10^4 Pa (400 Torr)

condition of ($u/u_{mf} \gtrsim 4$) gave a satisfactory fluidizing situation to 1.1×10^4 Pa (80 Torr). In the following experiment the velocity condition was applied $u/u_{mf} = 4$.

3. EXPERIMENTAL RESULTS AND CONSIDERATION

3.1 Drying Experiment in Empty Column

The experimental result which varied the operating condition of the plate length in flow direction (height), gas velocity, and pressure was shown in Fig. 4. The solid line in Fig. 4 showed the mass transfer coefficient calculated from the following Pohlhausen's equation. This equation can be applied to parallel laminar flow to the plate.

$$Sh = 0.664\ Re^{1/2}\ Sc^{1/3} \qquad (3)$$

Reynolds number consists of the length of plate, gas velocity, and pressure, as being independent, but it is found that the results of experiments

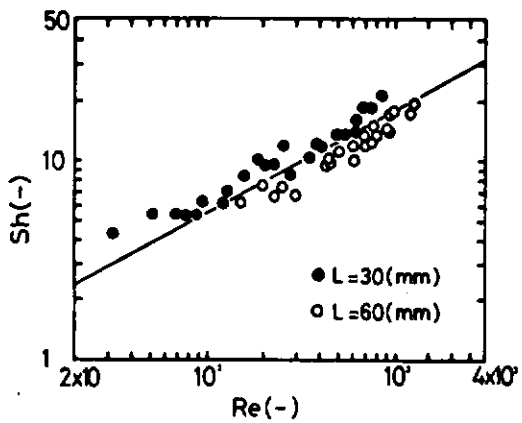

Fig. 4 Mass Transfer Coefficient in Empty Column

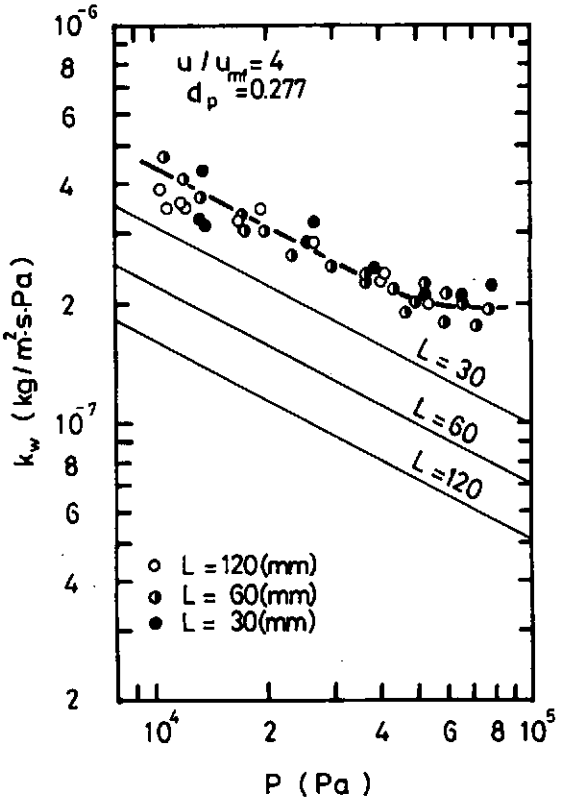

Fig. 5 Mass Transfer Coefficients in Fluidized Be

agree with Eq. (3), as shown in Fig. 4. This result is afterward used for considering mass and heat transfer coefficients in the fluidized bed.

3.2 Mass Transfer Coefficients on the Plate Surface in Fluidized Bed

3.2.1 Contribution of the Pressure

The relation between mass transfer coefficients, k_w which is based on the experiment about drying and pressure, P, is shown in Fig. 5. In the range of low pressure, k_w decreases in proportion to about $P^{-1/2}$ with increace of P, but with closing the atmospheric pressure the slope becomes gentle gradually.

3.2.2 Mechanism of Mass Transfer in Fluidized Bed

If it is generally proper that the contribution of flowing gas about transport phenomena in fluidized bed may be expressed by correcting by void fraction of fluidized bed, ε, the result which obtained for parallel flow in empty column, the following equation is applied for mass transfer on the flat plate in laminar flow region.

$$Sh = 0.664(Re/\varepsilon)^{1/2} Sc^{1/3} \qquad (4)$$

The thin straight lines in Fig. 5 show the calculated value by Eq. (4). These lines are separated by the dimension of plate, because the dimension of plate is chosen the characteristic length of Re. The experimental results in fluidized bed being compared with Eq. (4), in the range

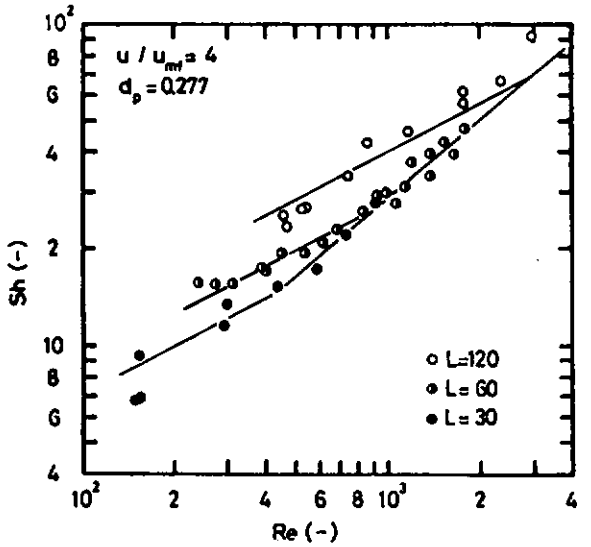

Fig. 6 Mass Transfer Coefficients Rewritten by Sh and Re in Fluidized Bed

of low pressure, it is evident that the slope of k_w vs. P (correspond generally to Re) is equal to that of Eq. (4), and while experimental results show the value 1.5 ∿ 3 times as much. The above results are explained as follows; collision of fluidizing particles against all the surface of plate decreases the resistance of gas boundary layer. Since the effective action of particles on the plate is the same everywhere, it is an interesting fact that the dimension of plate has no longer effect on mass transfer, and the relation between k_w and P plotted on one line in spite of the dimension of plate.

Fig. 6 is that the above experimental results are rewritten by Sh and Re on the basis of the dimension of plate. From Fig. 6 and Fig. 5, it is found that Sh in fluidized bed is in proportion to $Re^{1/2}$ in the range of low Re, but Sh is in proportion to $Re^{0.8}$ in the range of high Re. Not being concerned in the length of plates, it shows one straight line. This is similar to the relation in turbulent boundary layer formed from the edge of plate, and is paid attention to a sign of contribution of fluidizing particles to the boundary layer.

The ratio of k_w^o to k_w is shown in Fig. 7, the values of k_w^o (which show the contribution of only gas flow) are calculated from Eq. (5). The operation in fluidized bed is more favorable than usual drying (by direct contact with hot gas) for mass transfer, as is obvious from Fig. 7.

3.3 Characteristics on Heat Transfer between Bed and Plate

3.3.1 Contribution of the Pressure

The results on the heat transfer coefficient measured by cooling of the hot object in fluidized bed are shown in Fig. 8. The value of h_w decreases only slightly with decreace of pressure, P under good fluidizing condition. It is evident from Fig. 8 that the relation between h_w and P gives almost straight lines on log-log graph, and

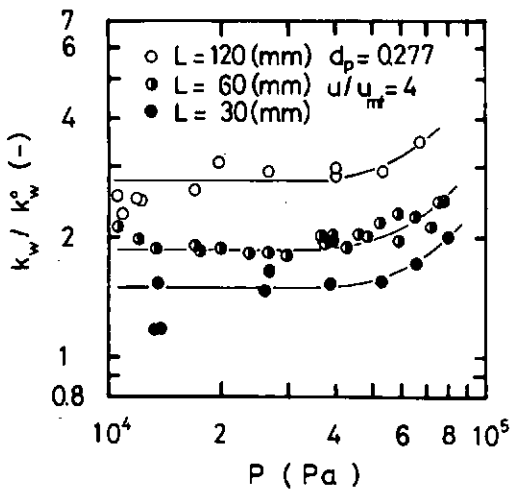

Fig. 7 The Ratio k_w° to k_w

these slopes are 0.056 in average for sand particles. And the value of h_w also increases as the diameter of fluidized particles decreases such as known on normal operation.

Fig. 9 shows the same relationship as Fig. 8 measured by drying, and the solid lines in this figure show the relation of Fig. 8. Since the measured temperature differences between the bed and the plate were so little in the experiment of drying, the obtained values of h_w lie considerably scattered but show generally the same result, comparing with Fig. 8. Also, these values are about 30 % higher than ones of Fig. 8. This phenomenon is similar to the fact that h_w measured by drying (i.e. an operation of simultanious heat and mass transfer) is higher than that by only heat transfer, but the definite consideration has never found.

3.3.2 Mechanism of Heat Transfer in Fluidized Bed

As mentiond in introduction, it has been known about heat transfer on the surface of immersed object in fluidized bed that greater part of heat is transported by fluidizing particles, and the remainder can be attributed to the flowing gases.

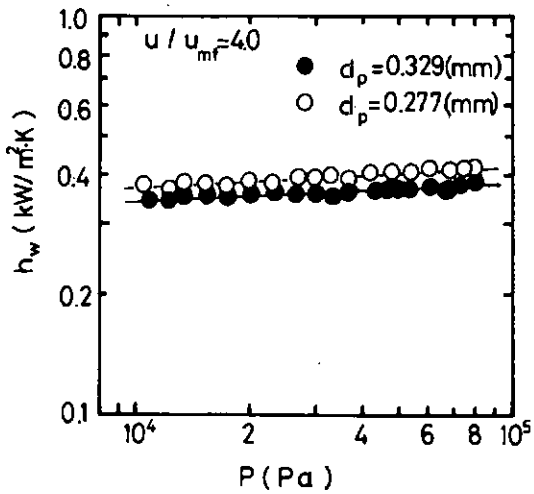

Fig. 8 Situation of h_w under Reduced Pressure

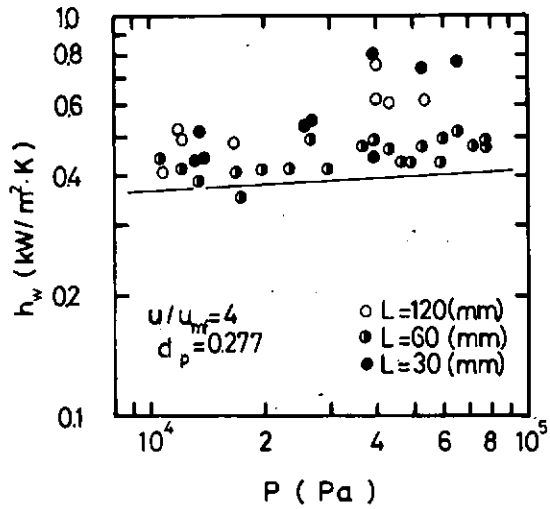

Fig. 9 h_w Measured by Drying

The contribution of flowing gases decreases with the decreasing pressure in the operation under reduced pressure, but the contribution of fluidizing particles will be unchanged. It, therefore, is understandable that the change with the operating pressure has little effect on the value of h_w.

The modified Pohlhausen's equation which expresses the contribution of flowing gas on the heat transfer as the same as Eq. (5) is follows;

$$N_u^\circ = 0.664(Re/\epsilon)^{1/2} Pr^{1/3} \quad (5)$$

But actual heat transfer coefficient in fluidized bed is larger than the calculated value according to above equation because of the effect of fluidizing particles.

If the analogy holds between heat and mass transfer, it is satisfactory to consider that the ratio of h_w' to h° is equal to that of k_w' to k°. The calculated values of h_w' based on the above analogy are shown in Fig. 10, and, of course, h_w' means the contribution of flowing gases on heat transfer coefficient in fluidized bed. h_w' in Fig. 10 being comparing with h_w in Fig. 8 or 9, it is

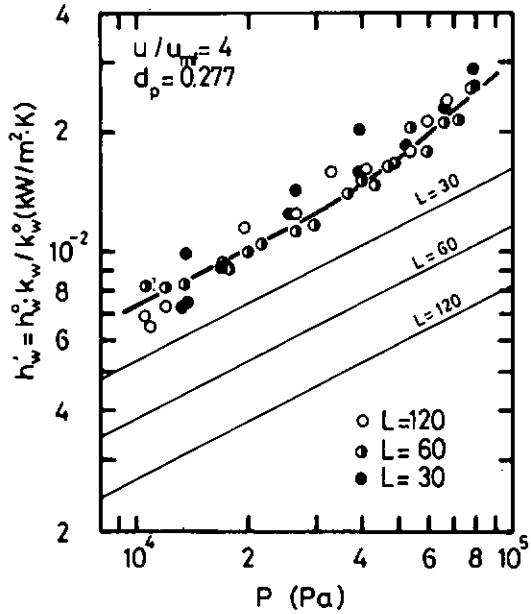

Fig. 10 Calculated Values of h_w'

Table 3 Contribution of fluidizing particles to heat transfer

P (Pa)	h_w (kW/m^{2}K)	h_w' (kW/m^2·K)	$(h_w - h_w')/h_w$ (%)
1.33×10^4	349×10^{-3}	7.9×10^{-3}	98
7.98×10^4	370×10^{-3}	27×10^{-3}	93

found that the contribution of fluidizing particles to heat transfer is very large (see Table 3).

Accordingly the difference of the mechanism of transfer owing to position on the plate is so little, the dimension of object does not also take part in heat transfer in practical application as well as mass transfer.

CONCLUSION

Heat and mass transfer coefficients on the object immersed in the fluidized bed were measured by means of cooling of the pre-heated plate and drying of wet asbestos plate under reduced pressure. The following mechanisms on transport phenomena in fluidized bed became evident through the experimental results.

1. The mass transfer coefficients decrease in proportion to about $P^{-1/2}$ with increase of the operating pressure, P. It is similar to the fact that the mass transfer coefficients on a flat plate in laminar flow are in proportion to $Re^{-1/2}$. But in the range of higher pressure approaching the atmospheric pressure, the dependence of pressure on mass transfer becomes weak, and it is considered that the transport mechanism moves toward similar behavior in turbulent boundary layer formed from the front edge of plate.
2. Experimental results show that the mass transfer coefficients in the fluidized bed are 1.5 ∿ 3 times as much as those estimated briefly from Eq. (4), and the dimension of plate has no longer effect on the mass transfer coefficient in fluidized bed. These results are explained that collision of fluidizing particles against all the surface of plate decreases the resistance of gas boundary layer, and this effective action on the plate is the same everywhere.
3. The values of h_w decrease only slightly with decrease of pressure. This result is considered that greater part of amount heat is transported by fluidizing particles, and the remainder can be attributed to the flowing gases. Because the contribution of flowing gases decrease with the pressure decreasing but the contribution of fluidizing particles is unchanged.
4. The contribution of flowing gases on heat transfer was calculated by assuming the analogy between heat and mass transfer. This value is only 2 ∿ 7 % of the overall heat transfer coefficient, therefore the contribution of fluidizing particles to heat transfer is evidently very large. Being analogous to the case of mass transfer, the dimension of object does not also take part in heat transfer.
5. It may be mentioned through the above results that the operation is fluidized bed under reduced pressure becomes a useful method for drying.

REFERENCES

(1) Y.Kawamura, T.Imada, "Developments in drying", Vol.1 Science Press. (1979)
(2) E.N.Ziegler, L.B.Koppel, and W.T.Brazelton, Ind.Eng.Chem.Fundamentals, 3, 94, (1964)
(3) T.Shirai, H.Yoshitome, Y.Shoji, S.Tanaka, K.Hojo, and S.Yoshida, Kagaku Kogaku (Chem. Eng.Japan), 29, 880 (1965)

DRYING CHARACTERISTICS OF TEA FLUIDISED ON A VIBRATING BED (PART-I)*

Dr. Rohit M. Shah[1]
Suresh K. Goyel[2]

1. Macneill & Magor Limited, Bombay, India
2. Macneill & Magor Limited, Bombay, India

ABSTRACT

In an endeavour to improve the quality of tea and develop a better and more efficient drying system, it was necessary to study the drying characteristics of tea on a vibrating-fluidised bed and its impact on the quality of tea in terms of its flavour, liquor characteristics, colour, fibre content, bloom and briskness, all of which are known to be influenced by the type of dryer. Therefore a pilot plant was installed in the field to study feasibility of fluidising and drying tea, study effect of operating parameters, analyse the quality of teas produced and optimise the parameters like frequency, amplitude, geometry of perforated plates, air velocity, pressure drops and bed heights etc. Design data was collected for producing a commercial size drying system.

NOMENCLATURE

D = Distributor Plate

E = Excitation, $(mm)(sec)^{-1}$

f = Frequency, $cycles(sec)^{-1}$

M = Moisture (wet basis), %

T = Temperature, ^{o}C

t = Time, min.

INTRODUCTION

Tea is conventionally dried in a through-flow multideck apron type conveyor dryers. This is an age old design and the dryer has numerous moving parts with associated maintenance problems. The thermal efficiency of the system is also low.

Several attempts have been made to fluidise tea but have failed mainly due to the fact that wet tea cannot be brought to the state of fluidisation without some aid. Besides, drying characteristics seem to have overwhelming effect on the quality of tea produced.

Drying of tea is not just removal of moisture from wet product, as tea has numerous important characteristics which contribute to its quality and value. These are its flavour, liquor, bloom, texture, colour and briskness. Drying has a very significant effect on these characteristics and the same can be established only by tea experts.

Processing Tea and its Types

Green tea leaves are plucked and then withered in conditioned air. The withered leaves are rolled in rolling machines, shredded, and thereafter left for fermentation in conditioned air before feeding into the dryer. Tea being very perishable in nature and susceptible to growth of bacteria, delays are not acceptable at any stage of processing. Withering, rolling and fermentation time are of great importance.

Rolled tea leaves are passed through a sifter to sort out orthodox tea and the residue in the sifter is sent to shreder to produce CTC tea. CTC tea is coarse in nature whereas orthodox tea is fibrous.

The method of drying seriously affects the characteristics of tea, and a few undesirable phenomena like balling, casehardening etc. have to be guarded against. Tea is said to undergo 'Caramelisation' when dried under proper conditions.

A Pilot Plant in the Field

Because of the above characteristics of tea, it cannot be made available in a laboratory on a regular basis and also dried tea cannot be tasted by anybody but by tea experts. It is for this reason that bench scale experiments for tea are not feasible in a laboratory and studies have to be carried out in the field.

Another necessity of field experiments is because of simulating initial processing conditions like rolling, fermenting times and comparison of quality of tea with that produced by other methods. The teas are tasted in accordance with methods and standards laid down. The quality of teas to be tasted should be consistant and quantity enough to have sufficient data on a continuous through - put basis. But a full scale dryer was not advisable as this would not only be expensive because of provisions for varying operating parameters, but also would result in a huge wastage of tea.

The above considerations called for a pilot plant experimentation at a tea garden where processed tea would be regularly available and the tea samples could be tasted.

Scale-up Analysis

In order to achieve proper simulation between the drying characteristics of 'pilot plant' to that of 'full scale plant' it was necessary to maintain the folloiwing parameters, of the pilot plant as well as of full scale plant, constant :

a) Fluidisation velocity of air

b) Temperature profile of inlet air

c) Bed height of the product

would be directly proportional to the bed area of the product.

A pilot plant was designed with a bed area of one-ninth of the full scale plant. The capacity of the pilot plant therefore, would be one-ninth of the full scale plant.

Drying characteristics of both CTC and orthodox teas were studied under various sets of parameters. Both teas fluidised and dried under more than one set of parameters, but acceptable quality of tea was produced with a particular excitation, distributor plate and airflow. Batch and continuous,both types of experiments were conducted and all possible data collected. Samples of teas were collected at various time intervals to prepare drying characteristics. Samples of dried tea were collected to analyse and establish the quality of tea to study the effect of various parameters.

DESCRIPTION OF THE PILOT PLANT

The pilot plant was capacity-wise one-ninth and geometry-wise one-third of fullscale commercial unit. It comprised of a hot air generator, a fully balanced twin-mass excitation system, dryer and plenum chambers, a cyclone separator,

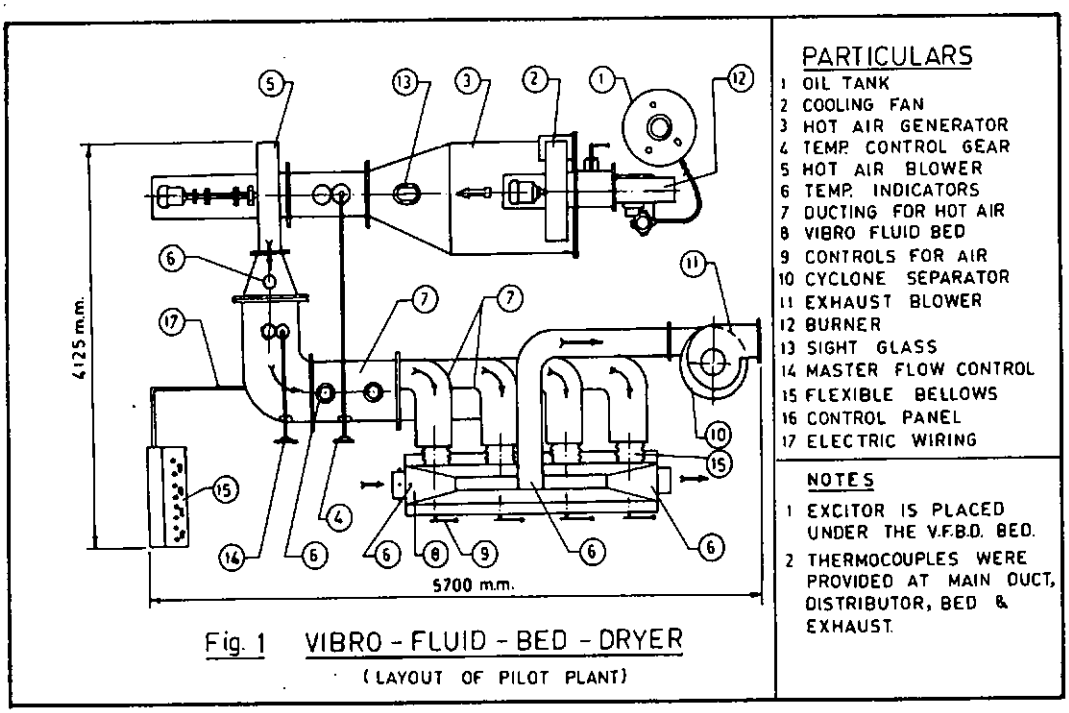

Fig. 1 VIBRO - FLUID - BED - DRYER
(LAYOUT OF PILOT PLANT)

d) Frequency of excitation

e) Amplitude of vibrations.

Then the capacity of the pilot plant

ductings and a control panel. The hot air generator consisted of an oil fired burner, a combustion chamber, a hot air blower, ductings and allied accessories

The dryer part comprised of a 300 mm X 2100 mm bed from underneath of which hot air was passed from four independent plenum chambers. Please refer to fig.- 1 The bed was visible from sides and top through sight glasses. Moisture-ladenair was collected from the top of the bed by a cyclone separator. Air flow was controlled in the main duct as well as in the four plenum chambers by control levers. Temperature could be varied between 60° to 200°C by varying the mix of hot air and cold air entering into the hot air blower.

The exciter provided vibrations to the entire bed including the plenum chamber and exhaust hood. The excitation frequency was varied by a control wheel on the variable speed drive and amplitude by a double eccentric.

The distributor plate was replaceable and could be changed as a series of them were available. Temperature, amperage, voltage and on-off were monitored through the control panel. Temperatures were recorded at inlet, bed, outlet and exhaust.

EXPERIMENTATION

Fluidisation and drying characteristics of CTC and orthodox teas were studied under various sets of parameters. The variables were frequency, amplitude, distributor plate, airflow, and bed height. The temperature was varied between 82°C to 104°C and time between 14 minutes to 30 minutes, as it was learnt that acceptable quality of tea is produced only under these ranges of temperature and time. For a few experiments the temperature of air was around 150°C. Four sets of distributor plates were used for varying the percentage openings of the vibrated bed. The excitation Γ (= $2xf$) could be varied from 10 $(mm)(sec)^{-1}$ to 160 $(mm)(sec)^{-1}$.

Batch and continuous-through put, both types of experiments were conducted. Suitable combinations of operating variables were determined by batch experimentation. Continuous through-put trials were conducted under suitable sets of parameters, and tea was dried in three passes, and in some cases more, depending upon the excitation, distributor plate, and bed height. A few experiments were conducted under different excitation when tea was dried only in a single pass.

The degree of fluidisation was varied by pushing in more air through the bed and effect studied on the quality of tea produced. Samples of tea were collected during the process of drying at different time intervals and after drying.

Drying characteristics were prepared and quality of tea tasted by recognized tea tasters. Various phenomena like balling case hardening, bloom and distribution of particle size etc. were studied.

OBSERVATIONS

Tea required careful handling & drying under controlled conditions. Tea can be effectively dreid on a vibratory fluidised bed under specific conditions of time, temperature, excitation percentage openings and airflow Air requirements were found less as compared to the conventional methods of drying. Vibro-fluidised bed provided an extremely uniform exposure of tea to hot air. Thus carameli-sation could take place without any formation of balls, loss of bloom and casehardening, and thereby quality teas could be produced.

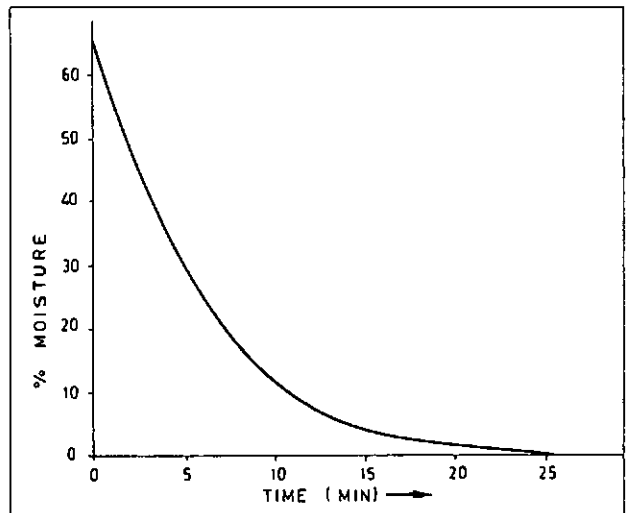

FIG. 2 IDEAL DRYING CURVE FOR TEA.

Fig. 2 shows the ideal curve for tea without affecting its flavour, colour and liquor characteristics. It was verified that if actual drying curve approached this curve, good teas would be produced.

It was observed that good quality of teas are produced only when the temperature during 'falling-rate period' is kept below 93°C and the total drying time remains within the range of 15 to 24 minutes depending upon the type of tea and initial moisture content.

Fig. 3 illustrates as to how the degree of fluidisation and quality index (QI) vary with the change in excitation (Γ). It is observed that good quality of tea is produced within a certain range of excitation, and when excitation is continuously increased the quality is impaired. (Quality Index: QI, is a composite quantitative representation of

liquor characteristics of tea).

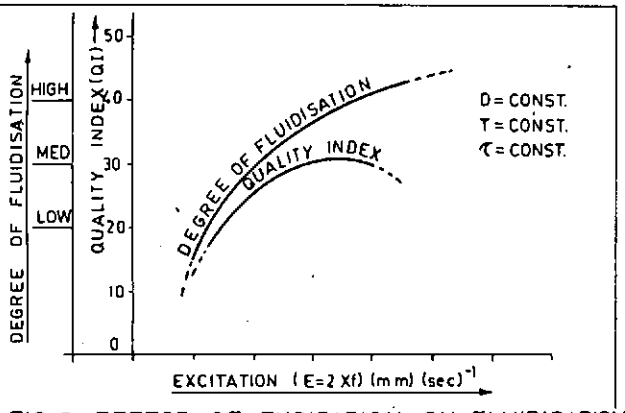

FIG. 3, EFFECT OF EXCITATION ON FLUIDISATION & QUALITY OF TEA.

The percentage openings in the distributor plate affect the drying process and the quality of tea produced.

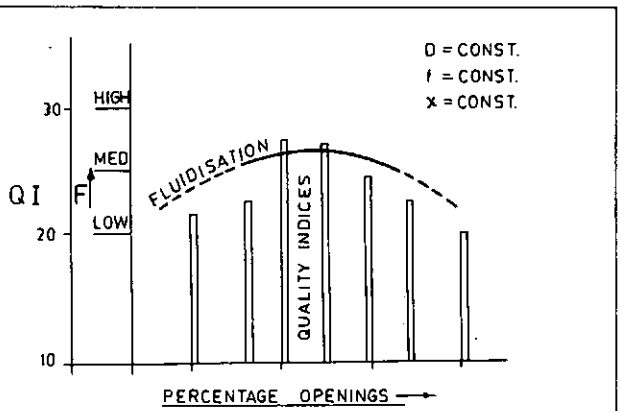

FIG. 4, EFFECT OF PERCENTAGE OPENINGS ON FLUIDISATION & QUALITY OF TEA

The degree of fluidisation also varies with the percentage openings. Fig. 4 and 5 represent the effect graphically.

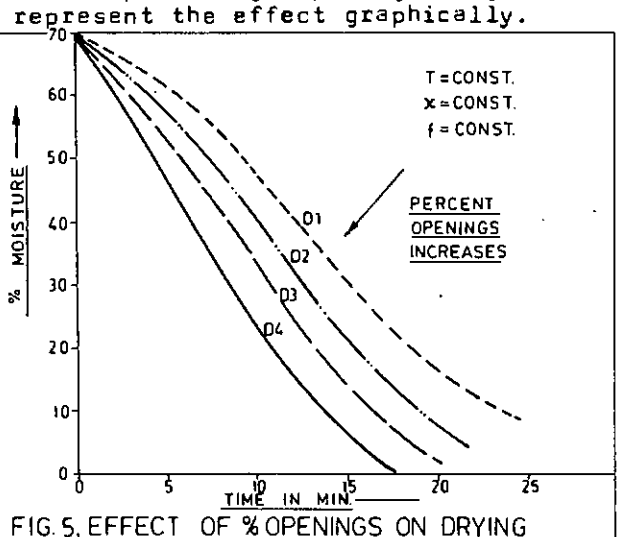

FIG. 5, EFFECT OF % OPENINGS ON DRYING

The rate of drying is directly proportional to the percentage openings.

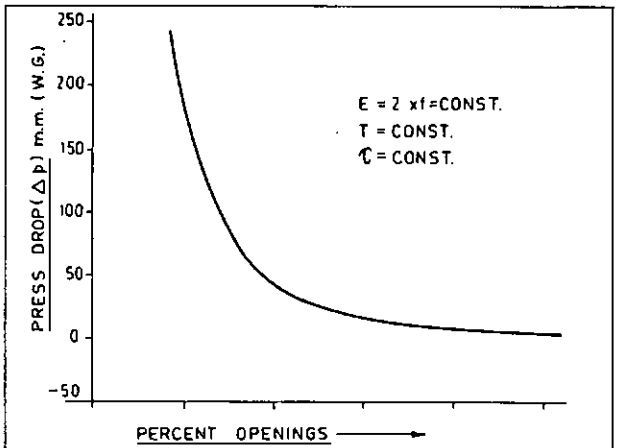

FIG. 6, VARIATION OF PRESSURE DROP WITH % OPENINGS IN THE DISTR. PLATE

But fluidisation and drying of tea were seriously impaired at very high and low values of percentage openings.

Fig. 6 illustrates the effect of per - centage openings in the distributor plate on the pressure drop a c r o s s the vibro-fluidised-tea bed.

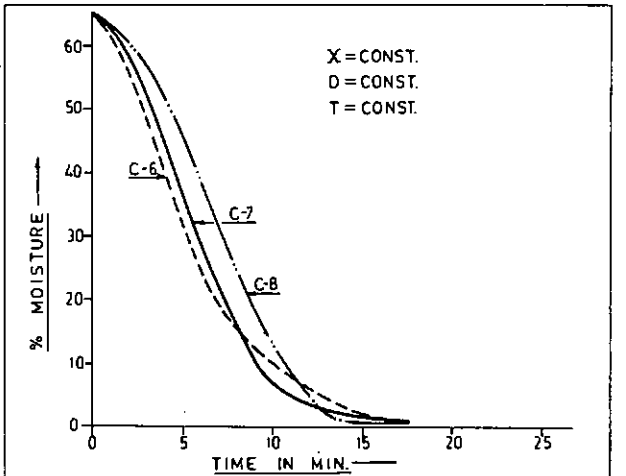

FIG. 7, EFFECT OF FREQUENCY ON DRYING CHARACTERSTICS

Fig. 7 illustrates the effect of frequency of excitation (f) on the process of drying tea, whereas fig. 8 shows the variation of quality index (QI) with the frequency.

It is observed that for given values of amplitude and percentage openingsin the distributor plate, the quality index (QI) declines on very low and high values of frequency.

Fig. 7 shows how the rate of drying is retarded in the 'constant-rate period , with increase in frequency. This effect is reversed in the 'falling-rate period'

Amplitude of excitation has a significant effect on the process of drying.

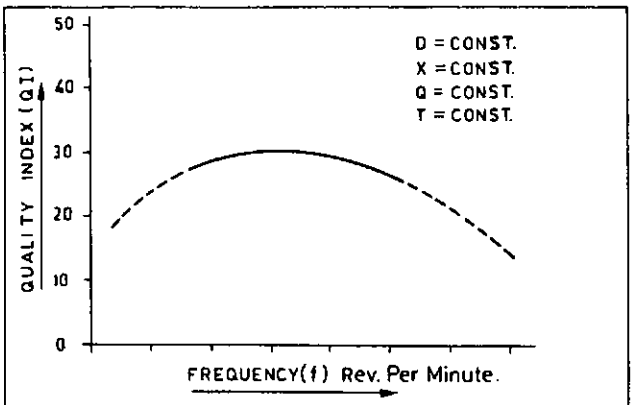

FIG.8 EFFECT OF FREQUENCY ON QUALITY OF TEA

Fig. 9 shows how the time-moisture curve tends to shift towards left with the increase in the amplitude of excitation.

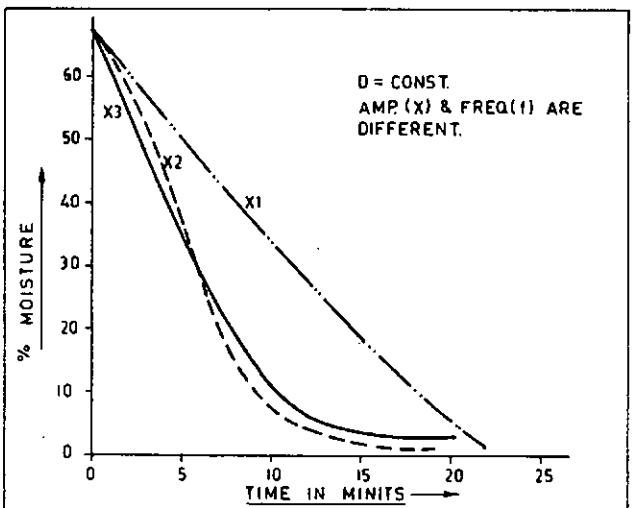

FIG.9 EFFECT OF AMPLITUDE ON DRYING CHARACTERSTICS

The behaviour is note-worthy in the falling-rate period.

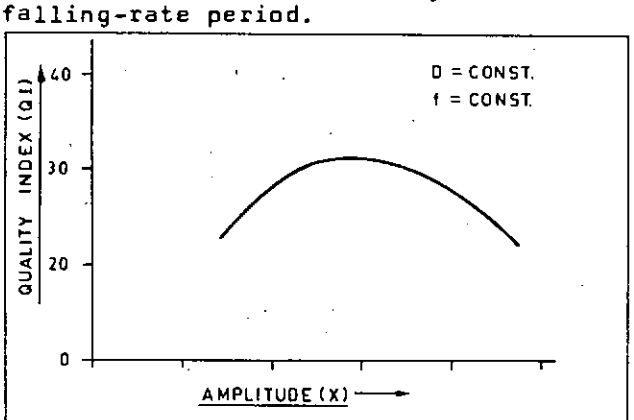

FIG.10. EFFECT OF AMPLITUDE ON QUALITY OF TEA

Fig. 10 shows variation of quality-index (QI) with aplitude (x). Higher values of amplitude are detrimental to the process of drying since 'case-hardened' teas are produced and bloom is also lost.

Bed heights were varied under controlled conditions of temperature and time. The quality of tea was affected with change in bed height beyond a particular range when excitation (E) is fixed. This was because of varied rates of derivation of moisture. An optimum range of values of bed heights was established. At very low bed heights the vibro-fluidised bed had a tendency to become unsteady or it gives rise to 'casehardening' because of too rapid derivation of moisture.

CONCLUSIONS

Following conclusions are drawn from the above pilot-plant studies:

1. Wet tea can be effectively fluidised with the aid of vibrations.
2. Vibratory as well as process parameters have an overwhelming effect on the quality of tea produced.
3. The quality of tea produced is superior to that produced by conventional dryers.
4. Separation of tea fibres is an incidental advantage in a vibro-fluidised-bed dryer.

LIMITATIONS

1. Temperature and time parameters were not studied in a wider range with a view to limit the scope of present study. Otherwise variable parameters would have been too many.
2. In continuous-through put trials only average drying time was noted since exact residence time could not be determined.
3. Tea was dried in three to four passes since the length of pilot plant dryer was limited. This would have also adversely affected the quality of tea.
4. The feed rate was controlled manually as no postive method dof measurement was employed.
5. There is no scientific way to measure the quality of tea produced and the results are always

subjective opinions based on the judgement of tea tasters.

ACKNOWLEDGEMENT

The authors express their sincere gratitude to Mr. J.M. Trinick, Tea Taster and Manufacturing Adviser, of M/s. George Williamson & Company Ltd London, for his valuable suggestions & tasting of teas during the course of above pilot plant studies.

The authors would like to thank also Mr. S. S. Jamwal, Manager, Pertabghur Tea Estate, Assam, India, for his keen interest and assistance during the course of above studies.

NOTE * : This paper constitutes the first phase of a continuing research programme for developing and improving drying systems for applications in Tea Industry, undertaken by Macneill & Magor Limited, India.

THEORETICAL INVESTIGATION OF DRYING CONDITIONS OF THE FLUIDIZED BED GRANULATION

T. Vajda

Research Institute for Technical Chemistry of the Hungarian Academy of Sciences, Budapest

ABSTRACT

A model for the drying process of the fluidized bed granulation has been worked out with several simplifying conditions. In order to describe the granulation we applied empirical tools. The change of the moisture content of the charge has been assumed independent from the effective granulation process. We characterized the drying operation by finding on appropriate source term in the mass balance equation. The results obtained reliably agree with the practical experiences.

NOMENCLATURE

- a = median parameter of the lognormal distribution, m
- b = parameter of the lognormal distribution's dispersion
- r = grain radius, m
- s = density function of the surface distribution, m
- S = total surface, m²
- t = time parameter, s
- u = mass rate of the spraying of the solution of binding material, kg/s
- v = effective volume of granulate, m³
- V = volume of equipment, m³
- w = density function of the weight distribution, m^{-1}
- X = moisture content during the granulation, kg/m³
- X' = moisture content during the drying, kg/m³
- α = mass transfer coefficient, m/s
- β = proportionality factor
- γ = specific mass of granulate, kg/m³
- ε = volume quotient
- ν = density function of the number distribution, m^{-1}

INTRODUCTION

Of the methods of the chemical industry serving for a similar purpose, granulation in a fluidized bed is known to be applied in a wide field only in the last decade. Though granulation in a fluidized bed can be carried out by various methods, in the pharmaceutical, food and detergent industries in the first line the process based on spraying a binding material became widespread /1-6/.

An essential feature of this process is to spray an adequate binding material in a dissolved state into the fluidized bed formed from the substance to be granulated. In the course of this process, partially parallel to each other, the admixture of both media, the moistening of the grains of the substance to be granulated, then their sticking together and lastly the evaporation of the solvent from the developed granulates take place. Of the aforementioned four partial processes we desire now to discuss in the first line the investigation of the last one, thus in general the investigation of the moisture content of the formed granulates.

THE PHYSICAL - MATHEMATICAL MODEL

Fig. 1 shows a schematic sketch of the equipment for carrying out the process.

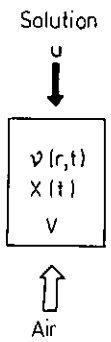

Figure 1 Schema of the Equipment

The volume of the equipment is V. Let us imagine in its inside, in a uniformly distributed and completely mixed-up, fluidized state the substance to be granulated whose quantity is given by the density function of the number distribution $\nu(r,t)$ referred to the total number of grains. The solution containing the binding material and inducing the granulation is sprayed-in at the top of the equipment at a mass rate of u. The moistening of the granulates due to this treatment is measured by the moisture content $X(t)$ referred to unit volume. The maintenance of the fluidized state and the drying of the granulates are carried out by air blown-in at the base of the equipment.

The relationship representing the change of the quantity $X(t)$ can be obtained apparently by writing down the balance equation of the moisture content of the equipment. The rate of drying can be considered to be proportional to the total surface S and to the moisture content of the granulates. Of these the former is considered to be known already in a factual form on the basis of experimental and theoretical results relating to the density function of the number distribution /6/. On taking into account also that in the system the solvent of the sprayed-in binding material serves as a source of moisture, and presuming this to be a dilute solution with a source intensity of similarly u, the above mentioned balance equation is as follows:

$$V\frac{dX}{dt} = -\alpha S X + u . \qquad /1/$$

DETERMINATION OF THE TOTAL SURFACE AND THE MOISTURE CONTENT

As already mentioned, it is known that the density function $\nu(r,t)$ can be derived at a fair approximation and in an arbitrary moment of the granulation process from the lognormal distribution /7/:

$$\nu(r,t) = \frac{1}{br\sqrt{2\pi}}\, e^{-\frac{\ln^2\left(\frac{r}{a}\right)^{1/b}}{2}} , \qquad /2/$$

wherein the changes in time of the parameters a and b during the granulation process should be considered as given in the following way:

$$a = a_1 - a_2 e^{-a_3 t} , \qquad b = b_1 - b_2 e^{-b_3 t} . \qquad /3/$$

The graph of a density function describing a real granulation process is shown in Fig. 2 to which the following system of parameters corresponds:

$a_1 = 1{,}8.10^{-3}$m, $a_2 = 1{,}75.10^{-3}$m,
$b_1 = 1$, $b_2 = 0{,}3$,
$a_3 = b_3 = 0{,}003\ s^{-1}$.

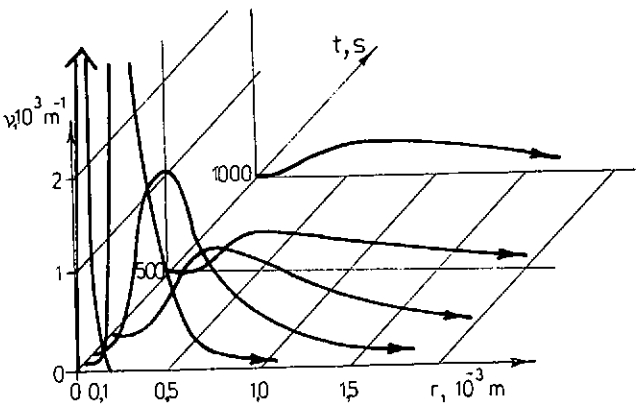

Figure 2 Number Distribution

On determining the total surface it must be taken into account that in the course of the process, instead of the number of grains rather the weight of the charge is constant /neglecting the quantity of binding material/, and thus the density function of the weight distribution referred to unit weight is:

$$w(r,t) = \frac{r^3}{a^3 e^{9/2} b^2}\,\nu(r,t) , \qquad /4/$$

further, from formula /4/, on introducing the factual volume v of the granulates the surface distribution's density function referred to the total charge is:

$$s(r,t) = 3v\gamma\,\frac{w(r,t)}{4\pi r^3 \gamma}\,4\pi r^2 , \qquad /5/$$

wherein the grains of the granulated product were considered as being spherical. Now the whole surface is obtained, on applying formulas /2/, /4/ and /5/, as follows:

$$S = S(t) = \int_0^\infty s(r,t)\,dr =$$

$$= \frac{3v}{a^3 b e^{9/2 b^2}\sqrt{2\pi}} \int_0^\infty r e^{-\frac{\ln^2\left(\frac{r}{a}\right)^{1/b}}{2}}\,dr = \frac{3v}{a e^{5/2 b^2}} . \qquad /6/$$

For the sake of simplicity and since the qualitative result is apparently hardly affected by this, in formula /6/ only a is considered to be a function of time, and thus introducing the adequate average $\beta = e^{5/2 b^2}$ the total surface will be on the basis of formula /3/:

$$S = \frac{3v\beta}{a_1 - a_2 e^{-a_3 t}} \qquad /7/$$

Let us now substitute the result given in formula /7/ into formula /1/ which affords the following equation for the change of moisture content during the granulation process:

$$V \frac{dX}{dt} = - \frac{3\alpha\beta v}{a_1 - a_2 e^{-a_3 t}} X + u \quad , \qquad /8/$$

and for the subsequent simple drying under fluidization the equation:

$$V \frac{dX'}{dt} = - \frac{3\alpha\beta v}{a_1} X' \quad . \qquad /9/$$

Equation /8/ is solved by introducing the volume quotient of the solid material $\varepsilon = v/V$

$$X = \frac{u}{a_3 V} \left(a_1 e^{a_3 t} - a_2\right)^{-\frac{3\alpha\beta\varepsilon}{a_1 a_3}} \int_{a_1 - a_2}^{a_1 e^{a_3 t} - a_2} \frac{\tau^{\frac{3\alpha\beta\varepsilon}{a_1 a_3}}}{a_2 + \tau} d\tau, \qquad /10/$$

the solution of equation /9/ having the following form:

$$X' = \frac{u a_1}{3V\alpha\beta\varepsilon} e^{-\frac{3\alpha\beta\varepsilon}{a_1} t} \quad , \qquad /11/$$

wherein $X(t=0) = 0$ and $X'(t=0) = X(t=+\infty)$ were taken into account as initial conditions /the time scale was begun also in equation /9/ with the value $t=0$ /. It can be understood easily that on evaluating the integration in /10/ at the comlex value $\frac{3\alpha\beta\varepsilon}{a_1 a_3} = 0{,}0{,}5, n; \; n = 1, 2, \ldots$ the function in time of the moisture content will be /8/:

$$X_0(t) = \frac{u}{V} t \qquad X_{0,5}(t) = \frac{2u}{V a_3} \left(1 - \right.$$

$$\left. - \frac{\sqrt{a_2}\,\mathrm{arc\,tg} \sqrt{\frac{a_1 e^{a_3 t} - a_2}{a_2}} - \sqrt{a_1 - a_2} + \sqrt{a_2}\,\mathrm{arc\,tg} \sqrt{\frac{a_1 - a_2}{a_2}}}{\sqrt{a_1 e^{a_3 t} - a_2}} \right),$$

/12/

$$X_n(t) = \frac{u}{V a_3} \left\{ \sum_{k=1}^{n} \frac{(-a_2)^{n-k}}{k} \left[\left(a_1 e^{a_3 t} - a_2\right)^k - \right.\right.$$

$$\left.\left. - (a_1 - a_2)^k \right] + a_3 (-a_2)^n t \right\} \left(a_1 e^{a_3 t} - a_2\right)^{-n} ,$$

on the basis of which results it is already possible to establish the behaviour of the multitude of the solution curves.

DISCUSSION AND CONCLUSION OF THE MODEL

In Fig. 3 a graphic presentation of the system of the $X(t)$ functions during the actual granulation is compiled on the basis of the relationships /12/. Also the curve corresponding to the case of $n = +\infty$ is given. For the calculations, besides the values already presented, also the values

$$u = 1{,}8 \cdot 10^{-3} \text{ kg/sec}$$

and

$$V = 3 \cdot 10^{-3} \text{ m}^3$$

were chosen which correspond to an equipment of laboratory scale. In Fig. 4, in turn, the changes in the moisture content of the charge are shown during the entire process. Here the earlier results and the relationship /11/ were used.

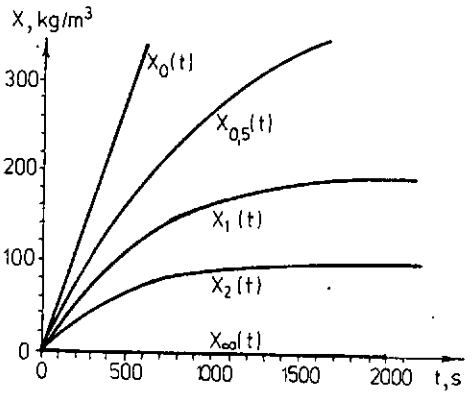

Figure 3 System of X Functions

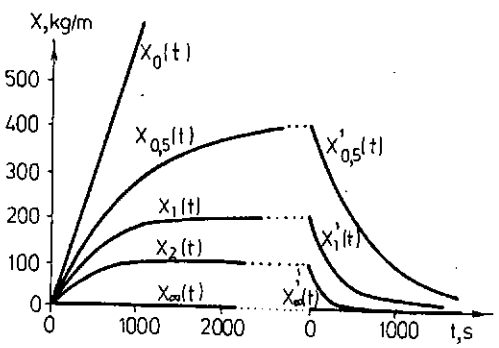

Figure 4 The Moisture Content

It can be stated the solving curve $X(t)$ corresponding to the arbitrary positive real value

$$0 < \frac{\alpha \beta \varepsilon}{a_1 a_3} < +\infty$$

of the complex tends to saturation and to an asymptote between zero and infinite. Thus the obtained results correspond to expectation as regards the nature of the curves. The relatively very high moisture contents observed at low complex values indicate, in turn, that concordant results by the measurements can be obtained only at complex values of an order of magnitude of about ten which represents a sort of limitation for the parameters of the model. Concerning the two sections of the process it deserves attention that the continuations $X'(t)$ of the $X(t)$ curves which attained lower saturation values exhibited more abrupt decreases. This indicates here the more intensive nature of the mass transfer processes.

REFERENCES

1. Wurster, D. E., J. Pharm. Sci. 49 82 /1960/
2. Rankell, A. S. et al., J. Pharm. Sci. 53 320 /1964/
3. Contini, S. et al., Pharm. Ind. 28 144 /1966/
4. Wolf, G., Pharm. Ind. 30 552 /1968/
5. Pilpel, N., Chem. and Proc. Eng. 50 67 /1969/
6. Ormós, Z. et al., Hung. J. Ind. Chem. 1 207, 307 /1973/
7. Fáy, G. et al., Energia és Atomtechnika /Hung./ 13 333 /1960/
8. Gröbner, W. et al., Integraltafeln, Springer Verlag, Wien, 1961.

ANALYSIS OF THE ROLE OF A MICROWAVES ENERGY CONTRIBUTION IN DRYING POROUS MEDIA

A. LE POURHIET[1]

S. BORIES[2]

1. Centre d'Etudes et de Recherches de Toulouse, Dépt. Automatique (ONERA-CERT-DERA), 2, av. E. Belin, Toulouse, France
2. Institut de Mécanique des Fluides, Associé au CNRS, 2, rue Ch. Camichel, Toulouse, France

ABSTRACT

The need to increase the velocity of industrial drying processes is clearly felt and many experiments have been made in this way by means of microwaves energy. The present study concerns the global analysis of drying in porous media when this energy is used simultaneously with the conventional hot air. Theoretical considerations, based on physical equations of heat and mass transfers, lead to fundamental relations between the dissipated energy and the decrease of the drying time. Moreover a microwave performance ratio is computed taking into account some loss of the efficiency of the hot air when electromagnetic energy is used. For purpose of later economical decisions, one defines a conventional drying process equivalent to the combined one. At last, a border line of economical profitability is computed for the use of microwaves energy contribution. Simulations of drying process are obtained by numerical solutions of the physical equations and they confirm the results of this analysis.

NOMENCLATURE

$a_m(\omega,\theta)$ = moisture diffusion coefficient, m2/sec.

$a_m\delta(\omega,\theta)$ = moisture diffusion coefficient due to a temperature gradient, m2/sec.K

$C_p(\omega)$ = isobaric specific heat of porous material, J/Kg.K

h = heat transfer coefficient, W/m2

L = half thickness of the slab, m

$p_{mo}(x,t)$ = ponctual thermal power dissipated by microwaves, W/m3

$P_{mo}(t)$ = total thermal power dissipated by microwaves, W/m2

$Q(\theta)$ = latent heat of vaporisation of the fluid, J/Kg

t = time

T_c = time of drying without microwaves, sec.

T_{mo} = time of drying with microwaves, sec.

ΔT = $T_c - T_{mo}$, gain of time for a drying with microwaves, sec.

x = space dimension, m

$W_c(t)$ = energy given by convection until the time t, J/m2

$W_{mo}(t)$ = total microwaves energy thermaly dissipated until the time t, J/m2

$\omega(x,t)$ = humidity content : mass of water/ mass of the dry body, %

$\theta(x,t)$ = temperature, K

$\theta_s(t)$ = (0,t) temperature of the surface, K

ω_o = (x,0), initial humidity content, %

θ_o = (x,0), initial temperature, K

$\omega_{moy}(t)$ = Mean humidity, %

$\theta_{moy}(t)$ = Mean temperature, K

θ_a = airstream temperature, K

ϕ_a = relative humidity of the airstream, %

θ_s^* = equilibrium temperature of the surface, K

α = mass transfer coefficient, m/sec.

ρ_o = density of dry material, Kg/m3

$\lambda(\omega)$ = thermal conductivity coefficient, W/m.K

γ = condensation and evaporation coefficient

$\rho_{vs}(\theta)$ = density of saturated vapor at θ, Kg/m3

$\mu(\theta)$ = $\dfrac{d\rho_{vs}}{d\theta}$

$\Delta\rho(\theta_a,\phi_a,\theta_s) = \phi_a\,\rho_{vs}(\theta_a) - \rho_{vs}(\theta_s)$

DEFINITIONS AND FORMULAS

$$\omega_{moy}(t) = \frac{1}{2L}\int_0^{2L} \omega(x,t)\,dx \qquad (1)$$

$$\theta_{moy}(t) = \frac{1}{2L}\int_0^{2L} \theta(x,t)\,dx \qquad (2)$$

$$P_{mo}(t) = \int_0^{2L} p_{mo}(x,t)\,dx \qquad (3)$$

$$W_{mo}(t) = \int_o^t P_{mo}(\tau)\, d\tau \qquad (4)$$

$$W_c(t) = \int_o^t h(\theta_a - \theta_s) d\tau \qquad (5)$$

$$Q(\theta) = 439.7 - 0.58\theta \quad (J/Kg, \theta \text{ in } ^\circ K) \qquad (6)$$

$$\rho_{vs}(\theta) = 1000 \exp(48.013 - 6848./\theta - 6.282 \operatorname{Log}(\theta)) \quad (Kg/m3, \theta \text{ in } ^\circ K) \qquad (7)$$

INTRODUCTION - BALANCE WITHOUT MICROWAVES

The aim of this study is to give some elements of quantitative conclusion concerning the interest of the use of microwaves to increase the rapidity of drying processes. As drying is often a limiting step in the manufacturing of certain products, the need to reduce its duration is clearly felt in the industry and the research of methods bringing this improvement are in progress.

For some years the use of microwaves energy as a supplementary energy has been at the origin of many experimental studies. The interest for this type of energy is mainly due to the properties of microwaves to dissipate the heat inside the material and so to increase the mass flow towards the surface of the product. In order, to improve the knowledge of the mecanisms of microwaves on drying and so to estimate its technical interest on the monitoring of the evolution of the process, a more precise analysis must be developped.However due to the high cost of this energy, comparisons with conventional energy must be done in order to maximise the global profitability of the setting up ; thus we look for an optimum between the energetic cost and the production increase due to the safe of time of operation.

In order, to study the microwaves influence on drying, a mathematical model describing the physical laws of heat and mass transfer and taking into account the electromagnetic power dissipated in the material has been used. Established by LUIKOV [3 to 6] and experimentaly validated by S. BORIES [7 to 10] , this model obtained through mass and energy balances is

$$\frac{\partial \omega}{\partial t} = \frac{\partial}{\partial x}\left(a_m \frac{\partial \omega}{\partial x} + a_m \delta \frac{\partial \theta}{\partial x}\right) \qquad (8)$$

$$\rho_o C_p \frac{\partial \theta}{\partial t} = \frac{\partial}{\partial x}\left(\lambda \frac{\partial \theta}{\partial x}\right) + \gamma \frac{\partial \omega}{\partial t} + p_{mo}(x,t) \qquad (9)$$

It has been numerically resolved in order to study, in the unidirectional case, the drying of a slab of porous material having 2L thickness, the surfaces of which (i.e. x = 0 and x = 2L parallels to the median plane) being heated by an airstream. Due to the symmetry of the system the boundary conditions are

$$-\rho_o\left(a_m \frac{\partial \omega}{\partial x} + a_m \delta \frac{\partial \theta}{\partial x}\right)_{x=0} = \alpha \Delta\rho(\theta_a, \phi_a, \theta_s) \qquad (10)$$

$$h(\theta_a - \theta_s) = -\lambda\left(\frac{\partial \theta}{\partial x}\right)_{x=0} - \alpha\, Q(\theta_s)\Delta\rho(\theta_a, \phi_a, \theta_s) \qquad (11)$$

$$\left(\frac{\partial \omega}{\partial x}\right)_{x=L} = 0 \quad \text{and} \quad \left(\frac{\partial \theta}{\partial x}\right)_{x=L} = 0 \qquad (12)$$

Equation (11) is the balance energy equation on the surface x = 0 : (heat flux furnished by hot airstream) = (rate of energy input by conduction) + (rate of energy used for evaporating moisture from convection). This last term is egal to the product of the mass flux on the surface ($-\alpha\,\Delta\rho$) by the latent heat of vaporisation $Q(\theta_s)$. The surface being submitted to the heating of the hot airstream and to the cooling due to evaporation, when microwaves are absent θ_s tends evidently to a limit θ_s^* ($\theta_o < \theta_s^* < \theta_a$) which characterizes the thermal equilibrium of the system in steady state:

$$\theta_a - \theta_s^* = -\frac{\alpha}{h}\Delta\rho(\theta_a, \phi_a, \theta_s^*) \cdot Q(\theta_s^*) \qquad (13)$$

Then from (1) the velocity of drying is given by:

$$\frac{d\omega_{moy}}{dt} = \frac{1}{L}\left[a_m \frac{\partial \omega}{\partial x} + a_m \delta \frac{\partial \theta}{\partial x}\right]_0^L = \frac{\alpha \Delta\rho(\theta_a, \phi_a, \theta_s)}{\rho_o L} \qquad (14)$$

In the figure (1) we show for θ_a given$\Delta\rho$ with respect to ϕ_a and θ_s with the evaporative ($\Delta\rho < 0$) and the condensing ($\Delta\rho > 0$) areas. On the same figure are drawn the curves converging to the point ($\Delta\rho = 0$, $\phi_a = 1$, $\theta_s = \theta_a$) which gives with respect to α/h and ϕ_a the solution θ_s^* of (13).

Example : $\theta_a = 90^\circ$, $\phi_a = 0.1$, $\alpha = 0.005$ m/s, $h = 10$ W/m$^2{}^\circ$K, L = 5 cm, $\rho_o = 1660$ kg/m3. On the figure (1) we can read $\theta_s^* = 48^\circ$, $\Delta\rho(\theta_o, \phi_a, \theta_s^*) = -35$ g/m^3 ; then the velocity of drying in thermal equilibrium is given by (14) :

$\frac{d\omega_{moy}}{dt}$ = 0,71 % an hour.

In order to verify this result, numerical solution of equations (8 to 12) is used. The coefficients a_m, $a_m \delta$, C_p, λ are determined for sand [7] and are represented on figures (2) and (3). The numerical solution given on figure (4) allows to verify the validity of (14). In the numerical simulation, the coefficient γ has been neglected due to the range of the humidity content in which this study has been made, ($\omega > 4\ \% \Rightarrow \gamma \simeq 0$).

BALANCE WITH MICROWAVES

Global energetic balance

Taking into account (11) and (12) the integration of (9) with respect to x gives

$$\int_0^L \rho_o C_p \frac{\partial\theta}{\partial t}\,dx = h(\theta_a-\theta_s) + Q(\theta_s)\alpha\Delta\rho(\theta_a,\phi_a,\theta_s) + \frac{1}{2}P_{mo} \qquad (15)$$

hence

$$\rho_o C_p L \frac{d\theta_{moy}}{dt} = -(\lambda\frac{\partial\theta}{\partial x})_{x=0} + \frac{1}{2}P_{mo} \qquad (16)$$

Taking into account (4), (5) and (14) an another integration with respect to t gives then

$$L\left(-\rho_o Q(\theta_s)(\omega_{moy}-\omega_o) + \rho_o C_p(\theta_{moy}-\theta_o)\right) = \frac{1}{2}(W_c + W_{mo}) \qquad (17)$$

Let us assume that the temperature of the surface tends again to an equilibrium and

$$\rho_o C_p L \frac{d\theta_{moy}}{dt} << (\lambda\frac{\partial\theta}{\partial x})_{x=0} \qquad (18)$$

(hypothesis verified at 5 % by the numerical simulation ; see figures 5 and 6) ; we have then

$$(\lambda\frac{\partial\theta}{\partial x})_{x=0} = \frac{1}{2}P_{mo} \qquad (19)$$

By eliminating $(\lambda\frac{\partial\theta}{\partial x})_{x=0}$ from (19), (10) and (11) we obtain

$$\theta_a-\theta_s^* = -\frac{P_{mo}}{2h} - \frac{\alpha}{h}Q(\theta_s^*)\,.\,\Delta\rho(\theta_a,\theta_a,\theta_s^*) \qquad (20)$$

$$\frac{1}{2}P_{mo} = -\left[\frac{\alpha\lambda\Delta\rho}{\rho_o a_m\delta}\left(1+\frac{a_m\rho_o}{\alpha\Delta\rho}\frac{\partial\omega}{\partial x}\right)\right]_{x=0,\theta=\theta_s^*} \qquad (21)$$

θ_a, ϕ_a, α and h being given, (20) is used to calculate θ_s^* in fonction of P_{mo} (fig. 7). As it can be observed on this figure the temperature θ_s^* corresponding to the thermal equilibrium of the surface determined by (20) is in good agreement with the value obtained, through the numerical integration of (8) and (9) (fig. 6). This result justifies a posteriori the validity of the approximation (18) used to define the global energy balance. (See fig. 10, for thermal dissipation of microwave energy versus x).

Monitoring of the humidity profile

If we consider the equation governing the mass flux in the material i.e.

$$\vec{J}_e = -(a_m\frac{\partial\omega}{\partial x} + a_m\delta\frac{\partial T}{\partial x}) \qquad (22)$$

it generally appears that in a drying process the temperature and mass gradients have opposite directions. In order to increase the mass flux towards the surface or, this value being known, in order to control the humidity profile, it is useful to modify, whenever possible, the temperature gradient. By internal energy generation, microwaves are able to provide this modification and so, have to be tested to avoid the appearance of a dried zone near the surface. The relation between $(\partial\omega/\partial x)_{x=0}$ and P_{mo} is given by (21). For $(\partial\omega/\partial x)_{x=0} = 0$ this relation gives

$$P_{mo} = -\left[\frac{2\alpha\,\lambda\,\Delta\rho(\theta_s,\phi_a,\theta_s)}{\rho_o a_m\delta}\right]_{x=0,\theta_s=\theta_s^*} \qquad (23)$$

Figure (4) shows a result in which the microwave power has been monitored according to (23) to obtain a uniform distribution of the humidity in the slab. As the coefficient $a_m\delta$ decreases rapidly when the humidity decreases, one can see that P_{mo} becomes very large and thence induces a high temperature inside the material. In the case of thick materials this result prove that it is not easy, even with microwaves, to avoid the appearance of a dried zone near the surface.

When microwaves are not used, P_{mo} does not exist and we have

$$(\frac{\partial\omega}{\partial x})_{x=0} = -\left[\frac{\alpha\,\Delta\rho\,(\theta_s,\phi_a,\theta_s)}{a'_m\,\rho_o}\right]_{x=0,\theta_s=\theta_s^*} \qquad (24)$$

with $a'_m = ka_m$. The validity of this relation has been tested for different values of k (i.e. for different porous media), by the numerical resolutions of (8) and (9). The cases represented on figure (4) correspond to k = 0.05 : this small value has been chosen in order to visualize a non-uniform humidity profile and so, to appreciate the influence of microwaves.

EQUIVALENT OUTSIDE HOT AIRSTREAM

This section is devoted to the research of the characteristics of an outside airstream giving the same drying velocity as the conjugate heating by microwaves and hot airstream ; we have then

$$R \triangleq \Delta\rho(\theta_a,\phi_a,\theta_s^*) - \Delta\rho(\theta'_a,\phi'_a,\theta_s^{*\prime}) = 0 \qquad (25)$$

where the superscript′concerns the equivalent standard drying. θ_a, ϕ_a and θ_s^* being known, computation of θ'_a, ϕ'_a and $\theta^{*\prime}$ is then developped as follows ; we first determine

$$\theta'_a = \theta'_s - \frac{\alpha}{h}Q(\theta_s^{*\prime})\,.\Delta\rho(\theta_a,\phi_a,\theta_s^*) \qquad (26)$$

then

$$\phi'_a = \phi_a\frac{\rho_{vs}(\theta_a)}{\rho_{vs}(\theta'_a)}\frac{\theta_a}{\theta'_a} \quad \text{(perfect gaz law)} \qquad (27)$$

and finaly minimise (R) with respect to $\theta_s^{*\prime}$ by using an iterative algorithm. On figure 7 we have drawn

the curves giving $\theta_s^{*'}$, θ_a', θ_s^{*}, ϕ_a' with respect to the dissipated microwaves power for different values of ϕ_a. We may observe that we always obtain

$$\theta_s^{*} \simeq \theta_s^{*'} \quad \text{and} \quad \frac{P_{mo}}{2h} \simeq \theta_a' - \theta_a \qquad (28)$$

These relations canalso be theoretically demonstrated (annexe 2) and are closely verified by the numerical simulations.

By combining (23), (25) and (28) we can also write

$$\left(\frac{\partial \omega}{\partial x}\right)_{x=0} - \left(\frac{\partial \omega'}{\partial x}\right)_{x=0} = \frac{1}{2}\frac{\delta}{\lambda} P_{mo}$$

For $\delta = 2.10^{-4}$, $\lambda = 2$ W/m°K, $P_{mo} = 2000$ W this difference is about 0,5 % for a 5 cm thickness. This small discrepency confirms the validity of the results presented in the second section about the opportunity of the use of microwaves in the monitoring of the humidity profile.

GAIN OF DRYING TIME

In order to determine the time of operation which can be saved by the use of microwaves, we will start from the numerical observation concerning the evolution of the temperature at the surface of the material. As we may observe on figures (4) and (5) this evolution approximatively obey at a first order equation

$$\tau \dot{\theta}_s + \theta_s = \theta_s^{*} \qquad (29)$$

Let us now consider two drying regimes corresponding to the same outside hot airstream with different microwave power. If for both regimes we suppose that the microwaves are absent after the time t_e the temperature profiles and the decrease rate of the global humidity for the time $t_f = t_e + \tau$ are the same. Taking (14) into account, differentiating (17) gives then

$$\frac{1}{2}(\Delta W_{mo} + \Delta W_c) + Q(\theta_s^{*}).\alpha.\Delta\rho(\theta_a, \phi_a, \theta_s^{*})\ \Delta T = 0 \qquad (30)$$

relation in which $\Delta\theta_{moy}$ has been neglected. This simplification, justified by the numerical simulation, will be justified by the results obtained through this analysis. ΔW_{mo} and ΔW_c correspond respectively to the electromagnetic and convective energy variation which together give the safe of time ΔT.

As we can observe on the figure 5, ΔT is only function of $(\Delta W_{mo} + \Delta W_c)$ and does not depend on the way W_{mo} is brought in the material.

The microwaves energy increases the surface temperature and thus reduces the standard energy given by the outside hot airstream : when θ_a, ϕ_a, α and h are constant the increase of ΔW_{mo} gives the following ΔW_c (see annexe 1)

$$\Delta W_c = -\frac{\Delta W_{mo}}{1 - \frac{\alpha}{h} Q(\theta_s^{*}) \cdot \mu(\theta_s^{*})} \qquad (31)$$

For a given ΔW_{mo} the variation of energy provided to the material is then

$$(\Delta W_{mo} + \Delta W_c) = R_i\ \Delta W_{mo}$$

with

$$R_i = \left[1 - \frac{h}{\alpha\ Q(\theta_s^{*})\ \mu(\theta_s^{*})}\right]^{-1} \qquad (32)$$

then the equation (30) can be written

$$E \triangleq \frac{\Delta T}{\Delta\left(\frac{W_{mo}}{h}\right)} = \frac{1}{2\Delta\rho(\theta_a, \phi_a, \theta_s^{*}).\left[Q(\theta_s^{*})\frac{\alpha}{h} - \frac{1}{\mu(\theta_s^{*})}\right]} \qquad (33)$$

R_i is defined as the "intrinsec performance" and the non dimensional coefficient E gives the time which can be saved by dissipating ΔW_{mo} into the material. On figure (8) E and R_i are represented with respect to θ_a and ϕ_a when α/h is given. The thick line curves correspond to an air heated from ($\theta_a = 20°$, $\phi_a = 0{,}05$) obeying to the perfect gas law. For $\alpha = 5.10^{-3}$ m/sec, h = 10 W/m2, $\theta_a = 90°$, $\phi_a = 0{,}1$ we can read $R_i = 0{,}82$, E = 10 and thence ΔT = 1 h/Kwh. This result is very close to the one obtained from the numerical simulations (fig. 4 and 5) an then justifies the hypothesis which have been made. Coefficient R_i includes the loss of conventional energy when microwaves are used. Generalisation of this result for a complete dryer would let us know the microwaves energy used to heat the airstream.

ECONOMICAL EFFECTS OF MICROWAVES

The equivalence which exists between the internal energy generation and the increasing of the temperature by a standard drying has been demonstrated in the last section ; consequently for the same velocity of drying the choice between the two types of methods must be done with respect to economical criteria.

In this section we are going to suppose that the mixed regime has been chosen and we will examine if the advantages due to the use of electromagnetic power may compensate the additional cost that it involves. This analysis is very schematic but may be used to draw a more complete industrial approach.

Nomenclature

P_{max} = useful microwaves power in place (watts) ; it corresponds to the maxi-

mum total power which may be dissipated on thermal energy in the material

k_u = relative cost per hour of the running of the dryer, without energetic cost relative to microwaves

$K_c T_c$ = energetic cost for a standard drying without microwaves

$K'_c T_{mo}$ = energetic cost for standard drying with microwaves

W_{mo} = microwaves energy dissipated for the time T_{mo}, (Kwh)

$k_{mo} W_{mo}$ = energetic cost for microwaves really dissipated in thermal energy into the material

$k_i T_{mo} P_{max}$ = cost of microwaves installation

J_c = cost of drying phase in the price of conventionaly dried material

J_{mo} = cost of drying phase in the price of a material dried with mixed regime

$\mathcal{J}_c = (k_i P_{max} + k'_c - k_c) T_c + J_c$

$J'_{mo} = k_{mo} T_c / h E$

$D = \mathcal{J}_c - J'_{mo}$

$N = \mathcal{J}_c - J_{mo}$

Mathematical formulation

The financial profit ΔR realized by unit of time (hour) by using the mixed regime

$$\Delta R \triangleq \left[\frac{J_{mo} - k_i P_{max} T_{mo} - k'_c T_{mo} - k_{mo} W_{mo}}{T_{mo}} - k_u\right] - \left[\frac{J_c - k_c T_c}{T_c} - k_u\right] = \frac{D - N}{T_c - h E W_{mo}} - \frac{D}{T_c}$$

Considering the algebric values of N and D, four cases are to be examined in view to analyse the influence of W_{mo} on ΔR. The case ($N > 0$, $D > 0$) is the most interesting and is only presented here (fig. 9). We may observe that ΔR increases with W_{mo}, the values of which being defined between

$$\Delta R > 0 \quad \text{and} \quad W_{mo} \leq P_{max} T_{mo} = P_{max}(T_c - hEW_{mo}) \quad (34)$$

whence

$$(W_{mo})_{min} \triangleq \frac{T_c}{hE} \frac{N}{D} < W_{mo} < \frac{P_{max} T_c}{1 + hEP_{max}} \triangleq (W_{mo})_{max}$$

The condition of the existence of W_{mo} writes

$$(W_{mo})_{min} < (W_{mo})_{max}$$

$$J_{mo} > \frac{hEP_{max} J'_{mo} - \mathcal{J}_c}{1 + hEP_{max}} \quad (35)$$

The profitability of microwaves implies that the part of drying in the cost of the dried product exceeds a certain level. As the relation (35) indicates, this level must be as small as possible, i.e. k_i and k_{mo} small and E large. These conditions are true only for $T_c \gg \Delta T$ i.e. in the range of validity of the equation (32). For $P_{mo}(t) = P_{max}$ (33) gives $\Delta T = (T_c\ h\ E\ P_{max})/(1 + h\ E\ P_{max})$; we will so choose $\Delta T \simeq T_c/2$ and $h.E\ P_{max} \simeq 1$.

CONCLUSION

Many theoretical relations concerning the drying of porous materials by microwaves energy have been put in evidence through this study. Starting from the global equations governing the coupled heat and mass transfer phenomena, these relations have been established by taking into account some hypothesis posteriorly validated by numerical simulations of local equations.

The most important results mainly concern :

1./ For non hygroscopic materials, as long as the surface is wet, the humidity contain linearly decreases with respect to time. The velocity of drying depends, only in this case, on the characteristics of outside airstream and on surface temperature.

2./ The time which can be saved by using electromagnetic energy as a supplement of energy does not depend on the way this energy is used ; thence the optimization with respect to time of the power which is dissipated is out of interest.

3./ In the steady state, i.e. when the temperature of the surface is close to the equilibrium, the amount of microwaves energy actually used for heating the material is very low (approximatively 5 %), the residual energy being only used for evaporation.

4./ The heating by microwaves reduces the efficiency of drying by outside airstream and thence an "intrinsec performance" has been defined.

5./ For a given standard drying it is possible to determine the time ΔT which can be saved by using a supplementary microwave energy ΔW_{mo}.

6./ For a given microwave power it is possible to determine the gradient of humidity at the surface and thus to use this power for monitoring the humidity profile. This monitoring is particularly interesting at the end of drying to avoid the appearance of a dried zone which in some cases deteriorate the material ; nevertheless this monitoring uses high microwaves power and induces high temperature inside the material.

7./ For a given microwave power one can determine the equivalent outside airstream temperature which would give, without microwaves, the same velocity of drying.

All the relations established in this study take explicitely into account the microwaves power, the

temperature and humidity of the outside airstream, the transfer coefficients α and h and the density of the saturated vapour. The abacus drawn give the characteristics of drying in function of these parameters and then may be used to define any such experimental context.

As the whole results obtained through this analysis have been validated by numerical simulations we think that this study may be useful in the design of a drying process involving microwave energy. The conclusion 7 is particularly important because for a given gain of time it is possible to choose between the use of microwaves and the heating of the outside airstream. In this case the decision must be analysed from an economical point of view. In the same context, by assuming that the choice of microwaves has been made, we have determined the minimum cost of drying which, by considering the gain of time as a unique performance index yields profitability of the electromagnetic power.

ACKNOWLEDGEMENT

The authors wish to acknowledge the financial assistance of Electricité de France, Department Optimisation et Automatisation des Processus (Monsieur SOLIGNAC). They thank Professor LEFEUVRE, Messieurs PARESI and BOSCHET (Ecole Nationale Supérieure d'Electronique, d'Informatique et d'Hydraulique de Toulouse) for writing the model of microwave dissipation.

REFERENCES

1. Solignac M., Diagramme de Mollier et séchage par air chaud. Application au fluidisé (Document EDF, MC 342 T 208)
2. Le Pourhiet A., Bories S., Analyse du rôle d'un appoint d'énergie microondes pour le séchage des corps poreux - Rapport final, contrat EDF-CERT (EDF EP 31 - GB/EF 118), Juin 1979
3. Philip J.R., De Vries D.A., Moisture movement in porous materials under temperature gradient - Trans. Am. Geo. Union, vol. 38, N° 2, Avril 1957 pp. 222-232
4. Luikov A.V., Heat and mass transfer in capillary porous bodies, Pergamon Press (1966)
5. Defay R., Prigogine I., Bellemans A., Everest D. H., Surface tension and adsorption - Longmains, Greens and Co (1966)
6. Krisher S., Kroll K., Bases scientifiques sur la technique du séchage - (Traduction du Centre Technique des Industries Aérauliques et Thermiques)
7. Bories S., Crausse P., Nguyen Tan H., Thermomigration en milieu poreux - Etude des coefficients de diffusion capillaire - CRAS t. 284, B, Sept. 1977, pp. 17-19
8. Bacon G., Bories S., Crausse P., Gaudu R., Thermomigration en milieu poreux - Etude expérimentale et simulation numérique des transferts en phase liquide - CRAS t. 285, B, Oct. 1977, pp. 191-194
9. Bories S., Crausse P., Gaudu R., Bacon G., Etude expérimentale et simulation numérique des transferts de chaleur et de masse en milieu poreux - 6ème Congrès International des Transferts de Chaleur et de Masse - Toronto - Août 1978 - Publication HM 1, pp. 317-321
10. Bacon G., Crausse P., Zarcone C., Détermination des coefficients de diffusion massique aux faibles teneurs en humidité - Note interne G.Et. 39, IMF Toulouse
11. Jolion M.,Applications industrielles des hautes fréquences et hyperfréquences - Activités de recherches menées à l'EDF (Document EDF, ME 142 T 298)
12. Jollion M., Introduction théorique au chauffage électrique haute fréquence et microondes (Document EDF, ME 142 T 302)
13. Lefeuvre S., Hyperfréquences, Dunod Université. Paris.

ANNEXE I - DEMONSTRATION OF THE RELATION (31)

We want calculate ΔW_c corresponding to ΔW_{mo} ; (30) gives

$$h\tau(\theta_s^*-\theta_o)_{t=t_f} + h\int_o^{t_f}\theta_s\,dt = h\int_o^{t_f}\theta_s^*\,dt \qquad (36)$$

or by differenciating and taking into account $(\Delta\theta_s^*)_{t=t_f} = 0$

$$-\frac{1}{2}\Delta W_c = h\int_o^{t_f}\Delta\theta_s^*\,dt \qquad (37)$$

As $Q(\theta_s)$ and $\mu(\theta_s)$ are few variable for both regimes, the differenciation of (20) gives

$$\Delta\theta_s^*\left[-1+\frac{\alpha}{h}Q(\theta_s^*)\,\mu(\theta_s^*)\right] = -\Delta\left(\frac{P_{mo}}{2h}\right)$$

whence

$$\int_o^{t_f}\Delta\theta_s^*\,dt = \frac{1}{1-\frac{\alpha}{h}Q(\theta_s^*)\mu(\theta_s^*)}\,\frac{\Delta W_{mo}}{2h} \qquad (38)$$

and so (31) by comparing (37) and (38).

ANNEXE II - DEMONSTRATION OF RELATIONS (28)

By subtracting (26) of (11) we obtain

$$h(\theta'_a-\theta_a)-h(\theta'^*_s-\theta_s^*)=\frac{1}{2}P_{mo}+\alpha\Delta\rho(\theta_a,\phi_a,\theta_s^*).[Q(\theta_s^*)-Q(\theta'^*_s)]$$

or since Q does not largely depends of θ

$$h(\theta'_a-\theta_a)-h(\theta'^*_s-\theta_s^*)\simeq\frac{1}{2}P_{mo} \qquad (28a)$$

It is easy to verify that $(\theta'^*_s-\theta_s^*)/(\theta'_a-\theta_a)\ll 1$

Since by taking into account (27) this inequality may be written

$$\frac{\theta'^{*}_s - \theta^{*}_s}{\rho_{vs}(\theta_s) - \rho_{vs}(\theta'^{*}_s)} \ll \frac{\theta'_a}{\phi_a\, \rho_{vs}(\theta_a)}$$

or approximatively

$$\frac{d\ \rho_{vs}(\theta)}{d\theta} \gg \frac{\phi_a\, \rho_{vs}(\theta_a)}{\theta'_a} .$$

This relation being largely verified in the problem considered we have so an identity between (28a) and (28).

CAPTIONS OF FIGURES

Figure 1 : Evaporation capacity $\Delta\rho$ with respect to θ_a, ϕ_a, θ_s and equilibrium surface temperature $\theta^{*}_s(\theta_a, \phi_a, \frac{\alpha}{h})$. We read for instance $\theta^{*}_s(90°, 0.1, 5.10^{-4}) = 48°C$.

Figure 2 : Variation of physical coefficient a_m and $a_m\,\delta$ versus humidity ω and temperature θ .

Figure 3 : Variations of the thermal conductivity λ and $\rho_o\, C_p$ versus the humidity.

Figure 4 : Evolution of thermal and humidity contain states

—— without microwaves

---- uniform humidity profile given by the relation (23)

Figure 5 : Evolution of the mean humidity contain and of the surface temperature for differents values of $P_{mo}(t)$. We observe that ΔT = 2h/2Kwh. The equilibrium surface temperatures 48°, 55° and 62° are in good agreement with the theory (see fig. 6 and 7).

Figure 6 : Evolution of humidity profiles for a continue power $P_{mo}(t)$ = 1000 W/m2.

Figure 7 : Characteristics θ'_a, ϕ'_a and θ'^{*}_s of the equivalent standard regime with respect to θ_a, ϕ_a, $\frac{\alpha}{h}$ and $\frac{P_{mo}}{2h}$. Comparison of θ^{*}_s and θ'^{*}_s.

Figure 8 : Intrinsec profitability R_i and gain of drying time E with respect of θ_a, ϕ_a, $\frac{\alpha}{h}$.

Figure 9 : Cost of drying versus dissipated microwave energy

Figure 10 : Local microwaves power dissipated (——) versus humidity profile (----). P_{mo} = 1000 W/m2.

RESUME

Le besoin d'accroître la rapidité des processus de séchage industriel est clairement ressenti et de nombreuses expériences ont été réalisées dans cette voie à l'aide des microondes. La présente étude concerne l'analyse du séchage des corps poreux lorsque cette énergie est utilisée conjointement avec l'air chaud conventionnel. Des considérations théoriques, basées sur les équations physiques des transferts couplés de chaleur et de masse, conduisent à des relations fondamentales reliant l'énergie dissipée, le gain de temps de séchage et les modifications des profils d'humidité et de température. Un "rendement intrinsèque" est défini qui tient compte de la baisse d'efficacité de l'air chaud en présence des microondes; dans le but d'aide future à la décision économique on calcule les caractéristiques du séchage conventionnel équivalent au régime combiné ; enfin un seuil de rentabilité économique est calculé pour l'utilisation de l'appoint électromagnétique. De nombreuses simulations numériques visualisent la sensibilité du processus à différents paramètres et confirment les résultats fondamentaux de cette étude.

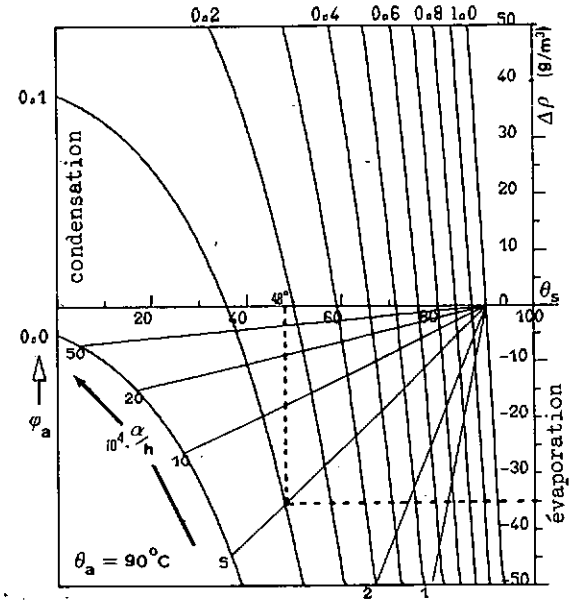

FIGURE 1

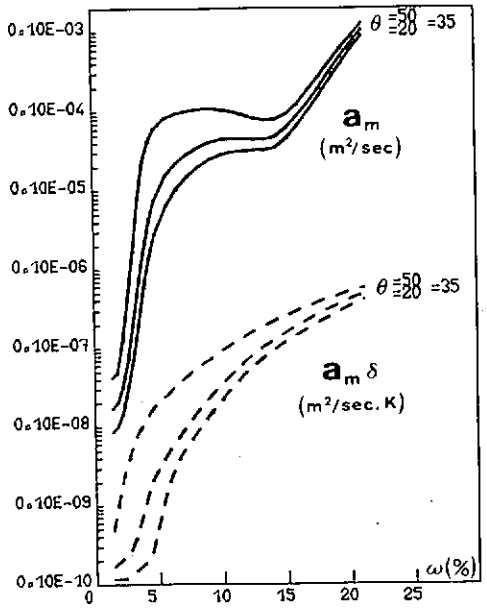

FIGURE 2

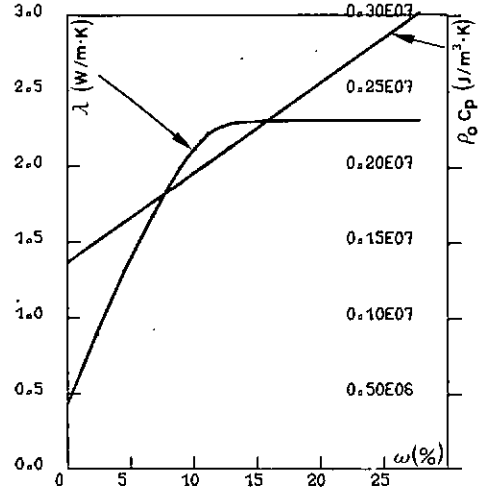

FIGURE 3

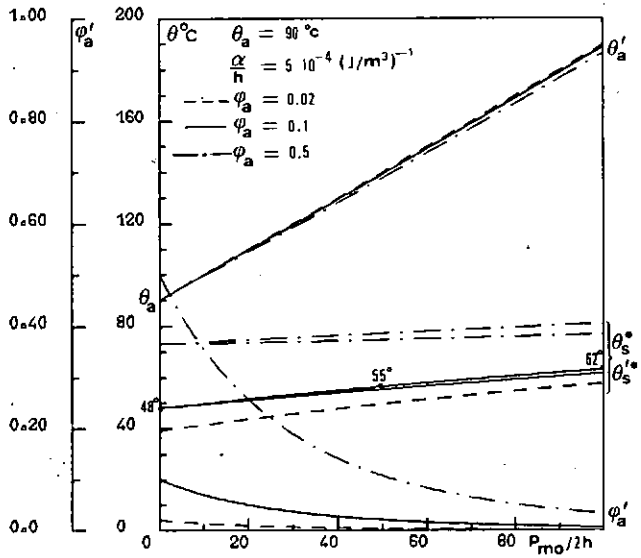

FIGURE 7

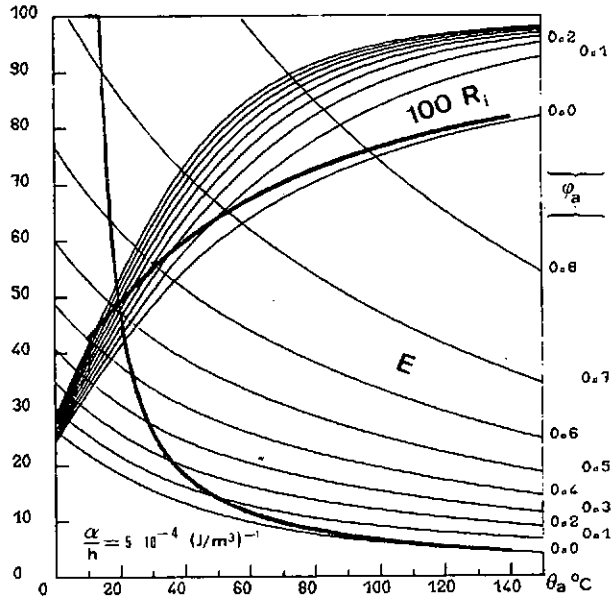

FIGURE 8

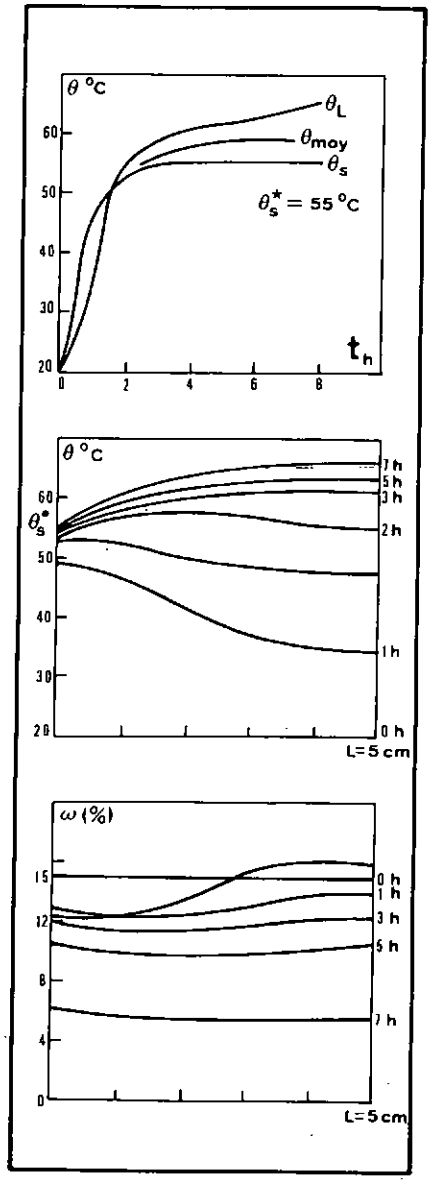

FIGURE 6

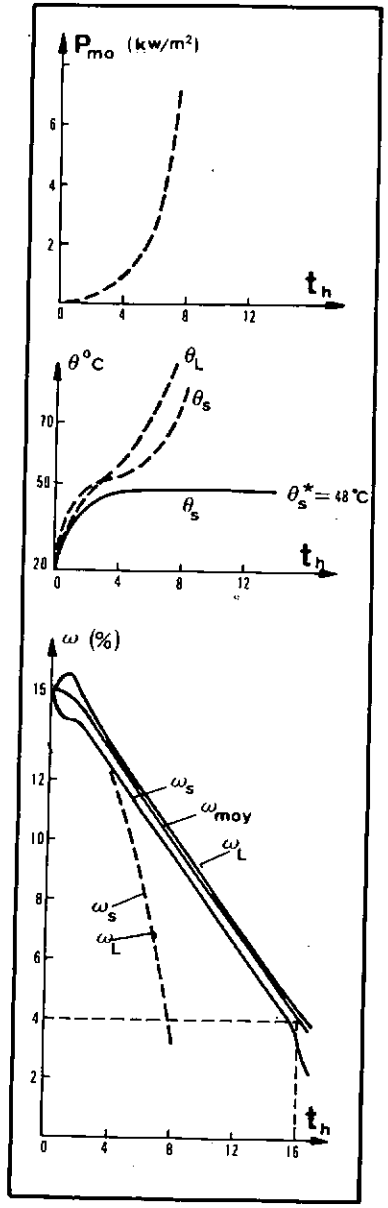

FIGURE 4

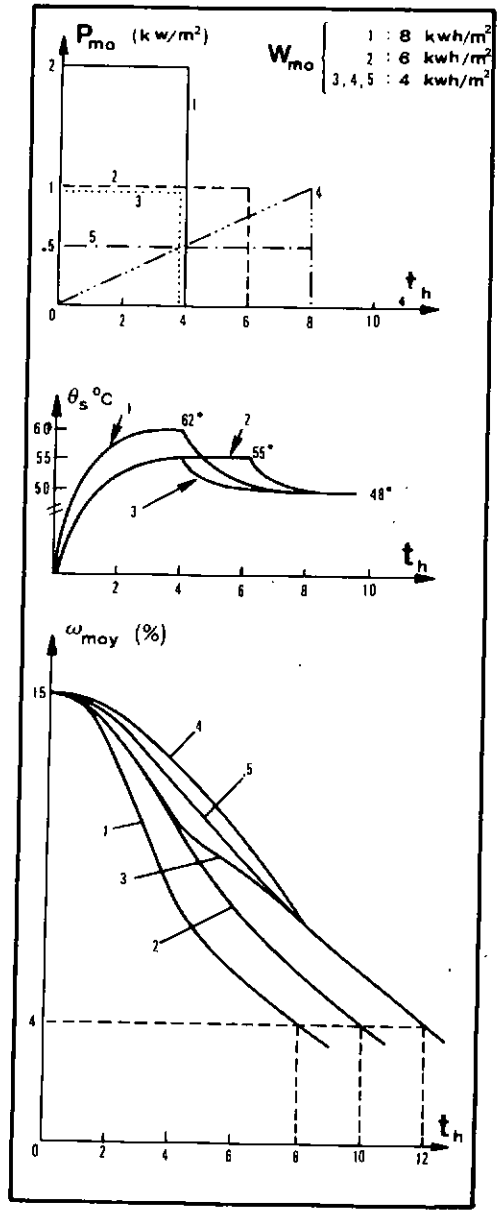

FIGURE 5

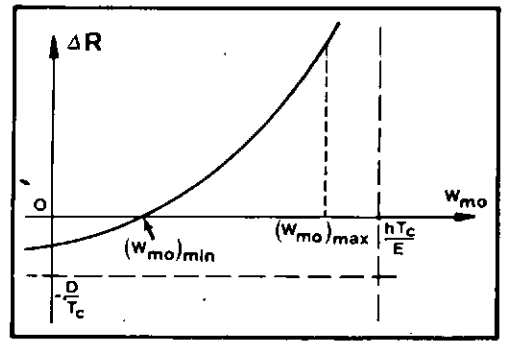

FIGURE 9

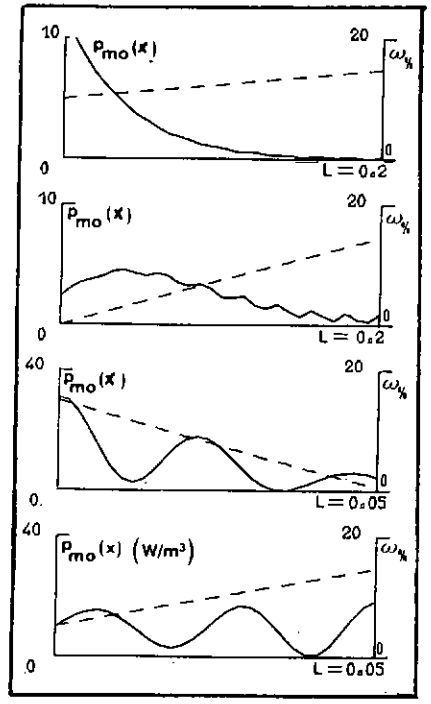

FIGURE 10

MECHANISM OF THE VAPOUR TRANSFER IN A MOIST GRANULAR BED UNDER A TEMPERATURE GRADIENT

M. Kuramae

Hokkaido University, Sapporo, Japan

ABSTRACT

This paper deals with the problem of the vapour transfer mechanism in a moist granular bed under a temperature gradient. First, temperature gradient ratio ξ was defined as the ratio of the temperature gradient in air filled void to that of the overall granular bed. Then, the dependence of the properties of the composite materials, its porosity, liquid content and temperature on ξ was analyzed by the series-parallel heat conduction model. Moisture flow experiments under a temperature gradient were also performed by using NaCl as the tracer. As the results, it was suggested that the value of the ξ has a significant effect on the vapour transfer rate in a partially saturated granular bed, where the transfer takes place accompanied with repeated vaporization and condensation.

NOMENCLATURE

A = sectional area, m^2

a = parameter

D = diffusion coefficient, m^2/hr

e = rate of NaCl transfered from low temperature region to high temperature region

G = vapour transfer rate, kg/m^2hr

L = depth of the bed, m

P = vapour pressure, Kg/m^2

P = saturated vapour pressure, Kg/m^2

R = gas constant, Kgm/mole°C

S = saturation

T = temperature, °C

x = distance, m

β = coefficient

ε = porosity

λ_e = thermal effectivity, kcal/mhr°C

ξ = temperature gradient ratio

τ = time, hr

Subscripts

p = parallel

s = series

1 = solid

2 = liquid

3 = vapour

exp= experiment

INTRODUCTION

The phenomena of vapour flow or diffusion in porous medium such as a granular bed are extensively studied in the fields of drying or reaction engineering. Generally, its transport mechanism has been devided into (A) molecular diffusion due to concentration gradient, (B) Knudsen diffsion, (C) flow due to pressure gradient, (D) surface diffusion, (E) thermal diffusion due to temperature gradient, etc. Especially, for the mechanism (A) which is most commonly observed, the flow rate has been usually estimated by the modified version of diffusional equation based on the diffusion in an air space. For example, the flow rate of water vapour in an partially saturated granular bed under a temperature gradient was estimated by the following equation based on the Stefan's unidirectional diffusion.

$$G_D = -\beta \frac{D_v}{RT} \varepsilon (1-S) \frac{P}{P-P_s} \frac{dP_s}{dT} \frac{dT}{dx} \qquad (1)$$

In this equation, temperature gradient dT/dx is adopted as the driving force of the vapour transfer, G_D is the vapour flow rate, P and P_s are respectivity total and partial vapour pressure, D_v, diffusional coefficient of water vapour in air space, ε, porosity and S is liquid saturation. The term $\varepsilon(1-S)$ expresses the rate of effective diffusional area and β is the correction factor to account for the zigzag nature of the vapour flow path, and its value is said to depend on void structure of porous media and always less than unity.(1) (2) However it is doubtful whether the vapour transfer rate is estimated correctly from this simple relationship because the mechanism of heat and moisture transfer in partially saturated porous bodies is supposed to be extremely complicated. In fact, experimental results not to be explained by Eq.(1) have been reported.(3),(4),(5) In this paper, we reexamine the mechanism

of vapour flow in partially saturated granular bed under a temperature gradient and intend to evaluate the appropriateness of Eq.(1).

VAPOUR TRANSFER MECHANISM UNDER A TEMPERATURE GRADIENT

The partial vapour pressure of air filled pores in granular bed at equilibrium state is thought to be constant and if the granular bed is sufficiently wetted, it will be saturated. If temperature gradient exists, difference of partial vapour pressure occurs and vapour diffuses from high to low temperature section because the saturated vapour pressure depends upon the temperature significantly. Although the occurence of vapour diffusion tends to break the equilibrium relationship between the vapour pressure and the temperature, it will be restored immediately by the vaporization and condensation. In other words, rate of phase change in porous media is supposed to be sufficiently rapid as compared with that of vapour diffusion except for case in which the porous bodies are not so wetted or the temperature is extremely high and the temperature gradient is very steep as is the case with drying at elevated temperature.
As the results, the phenomena of vapour transfer in partially saturated granular bed under a temperature gradient are thought to occur by the difference of vapour pressure induced by the temperature gradient in an air filled pore. But a question does arise here as to the validity of the use of the overall, not local, temperature gradient as the driving force in Eq.(1). In actuality, if the thermal conductivity of air filled pore is different from that of liquid and solid phases, the temperature fields within them are not to be equal and temperature gradient in the air filled pore is naturally different from that of the overall bed.

INVESTIGATION BASED ON THE HAET CONDUCTION MODEL

How different the temperature gradient of the overall bed is from that of the air filled pores is extensively investigated by a heat conduction model of a partially saturated granular bed. Generally the heat transfer mechanism of a partially saturated granular bed is very complicated as many factors exist. Several heat conduction models have been suggested previously, (6), (7), (8), (9), (10), but here we assume that the investigation of the three phases of the granular bed is expressed by series and parallel model shown in Fig.1(c). Here the thermal effectivity λe of the bed is given by the following equation. (9)

$$\lambda e = \frac{1}{\frac{a}{\lambda ep} + \frac{1-a}{\lambda es}} \qquad (2)$$

in which λs and λp are the thermal effectivities for the series and parallel models shown respectively in Fig.1(a) and (b). Analytical expressions for these models are

$$\lambda es = \frac{1}{\left[\frac{(1-\varepsilon)}{\lambda_1} + \frac{\varepsilon S}{\lambda_2} + \frac{\varepsilon(1-S)}{\lambda_3}\right]} \qquad (3)$$

$$\lambda ep = (1-\varepsilon)\lambda_1 + \varepsilon S\lambda_2 + \varepsilon(1-S)\lambda_3 \qquad (4)$$

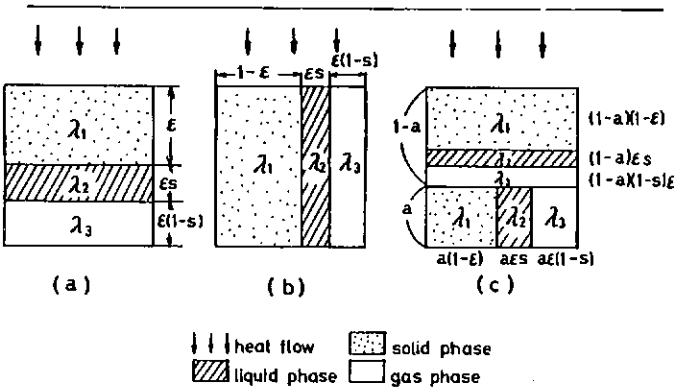

Figure 1 Heat Conduction Model

in which $\lambda_1, \lambda_2, \lambda_3$ are thermal conductivities of the solid, liquid and gas phase. Next, we define the temperature gradient ratio ξ which is the ratio of the temperature gradient of air filled pore to that of the overall bed.

$$\xi = \frac{(\text{temperature gradient of air filled pore})}{(\text{temperature gradient of overall bed})} \qquad (5)$$

By use of the model in Fig.1(c), ξ is expressed by the following equation. The derivation is shown in Appendix

$$\xi = \frac{1}{1 + \frac{\lambda ep}{\lambda es}\frac{(1-a)}{a}} + \frac{1}{\frac{a}{(1-a)}\frac{\lambda_3}{\lambda ep} + \frac{\lambda_3}{\lambda es}} \qquad (6)$$

If we eliminate parameter " a " in Fig.1(c) from Eqs.(2) and (6), ξ is expressed in term of thermal effectivity.

$$\xi = \frac{\left(1 - \frac{\lambda e}{\lambda ep}\right)}{\left(\frac{\lambda ep}{\lambda es} - 1\right)} + \frac{\left(1 - \frac{\lambda e}{\lambda ep}\right)}{\left(\frac{\lambda_3}{\lambda ep} - \frac{\lambda_3}{\lambda es}\right)} \qquad (6)'$$

Accordingly ξ depends upon thermal conductivities and composition of each phase. From Eq.(6) it is clear that if the thermal conductivities of the three phases are different, the temperature gradient in the air filled void is not equal to the overall value provided a≠1. Since ξ is thought to be an effective conductivity which consists not only of thermal conductivity but also of equivalent conductivity due to the latent heat transfer by vapour flow, it, accordingly ξ too, depends upon the temperature significantly. (11)

EXPERIMENTAL INVESTIGATION

Experimental apparatus and measurement

To investigate the above problems, experiments for measuring vapour transfer rate were proposed. The ξ, defined by Eq.(3), was measured to examine its dependence on the temperature and moisture content. Experimental apparatus are shown in Fig.2. 4 acryle rings ① were pilled up and glass beads partially saturated with dilute NaCl solution, about 3 % of the saturation concentration, were uniformly packed in it so that its porosity is constant. The granular bed was then sealed by

winding tapes so as not to let moisture escape and the bakelite standard plates ② were placed at both ends.

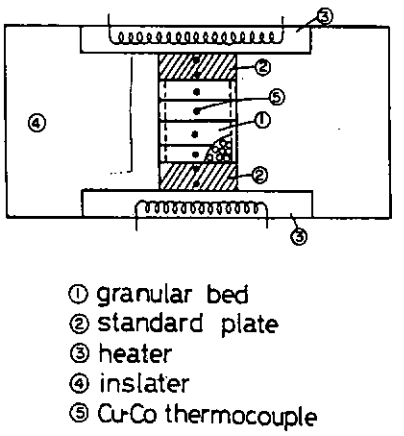

Figure 2 Experimental Apparatus

The granular bed was held vertically and the upper and the bottom ends were kept at constant temperatures with plate type heater ③. Insulator ④ was applied to the side to prevent the heat loss. Temperature in the granular bed was measured by 0.3mm Cu-Co thermocouples ⑤ inserted into the rings. The temperature of the standard plates were also obtained by thermocouples at constant intervals. After about two days from the start of the experiment, the granular bed was cut apart into 4 rings and the moisture content was measured by absolute drying method. Then the content of each ring was diluted with water and NaCl concentration was estimated by measuring electrical conductivity of the solution. From the experimental data of NaCl concentration vapour flow rate G_{vexp} is estimated by the following equation, which is derived based on the mass balance with assumption that the NaCl migrates only when moisture transfers in liquid phase and NaCl diffusion through the liquid is negrigible.[1]

$$G_{v\exp} = \frac{eS\varepsilon L}{2\tau} \qquad (7)$$

Here, L is the depth of the bed and e, the rate of NaCl transfered from upper half section (low temperature) to lower half section (high temperature) in time interval τ. Accordingly, if avarage temperature, moisture content, porosity and avarage temperature gradient are given, ζ is calculated by Eqs. (1) and (7). Here we assume that D_{v} is estimated from Krischer's experimental equation (9) and β in Eq.(1) is 1/1.57 (12).

1) If we designate with A, the sectional area of granular bed and with C_o, the initial concentration of NaCl, the rate of NaCl which have been transfered from upper half section (low temperature) and deposited to lower half section (high temperature) is $G_{v\exp} A\tau C_o$ and the amount of NaCl which existed at initial state is $1/2L\varepsilon SA$. Accordingly, the rate of NaCl transfered to the lower half section in time interval τ is $e = G_{v\exp} A\tau / \frac{1}{2} L\varepsilon SA$

Experimental REsults

Fig.3 shows experimental results for the relationship between ζ and moisture content. In this Figure solid line —— designates calculated value of ζ from Eq.(6) and the broken line ---- the predicted value from Philip's model (13).

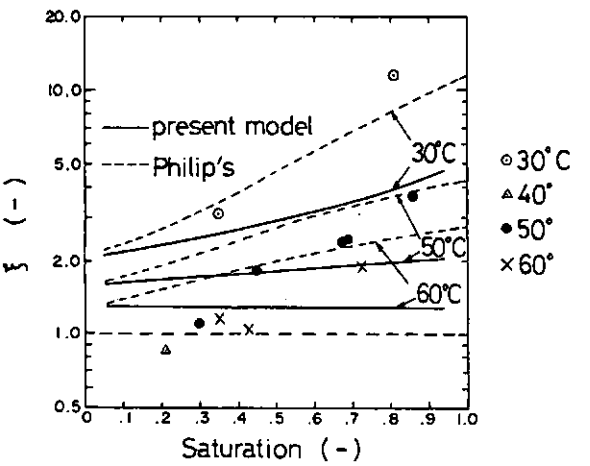

Figure 3 Experimental Results

Philip et all (13) suggested that for not fully wetted soil, the vapour transfer rate is determined by series or parallel flow of the vapour and liquid from one isolated liquid island to the other, under the influence of the temperature gradient in an air filled pore. For wetted soil, they supposed that the number of the liquid islands decreases in proportion to the percentage of air filled void. But their model differs from the one proposed here. They consider that the flow within an island contributes to the total vapour flow. So far as the results in Fig.3, Philip's results seem to be fairly well. However since the phenomena of heat and moisture transfer in partially saturated porous media are very complicated and since neither the heat conduction model in this analysis nor the experiment can be expected to be very accurate, we must very careful in making a judgement. Our experimental results show that ζ depends upon moisture content more heavily than our predicted values. But they are in accord with the predicted values by the Philip's theory as well as ours in the following aspects; ζ is larger than unity and increases with decreasing temperature and increasing moisture content. These seem to justify our supposition that, for partially saturated granular bed under a temperature gradient, the difference of the temperature gradient between the air filled pore and overall bed significantly affects the estimation of the rate of vapour transfer.
Fig.4 shows the comparison of ζ_{calc}, which is calculated from thermal effectivity of bed by Eq.(6). (which are shown in Fig.5 with Ohtani's data(14)) with ζ_{exp}, the experimental results.

INVESTIGATION FOR VAPOUR TRANFER MECHANISM

Effect of Characteristics of Composite Materials

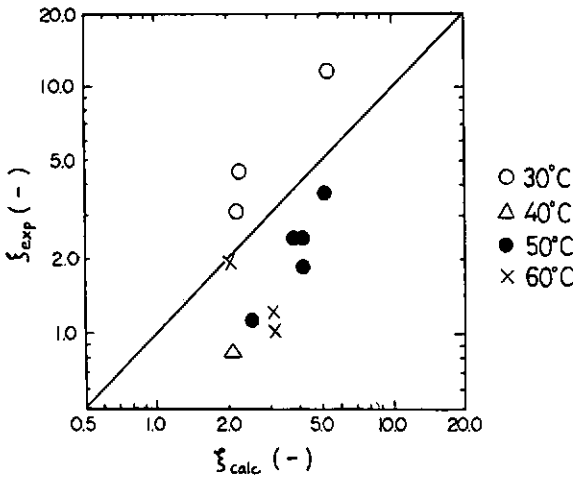

Figure 4 Correlation between and

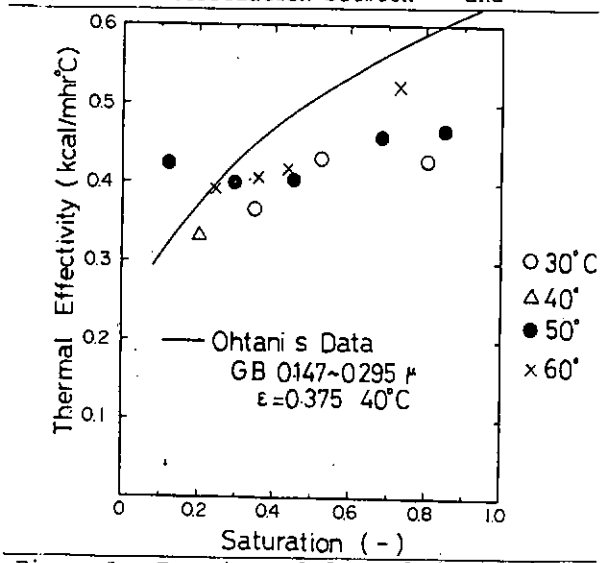

Figure 5 Experimental data of thermal effectivity

Fig. 6~9 show theoretical of the dependence of the temperature and moisture content on ξ when the characteristics of composite materials and its porosity are changed. The values of thermal conductivity of these materials used in the calculation are shown in Table.1.

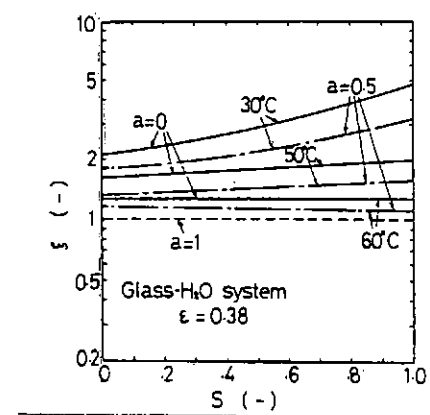

Figure 6 Calculated Results

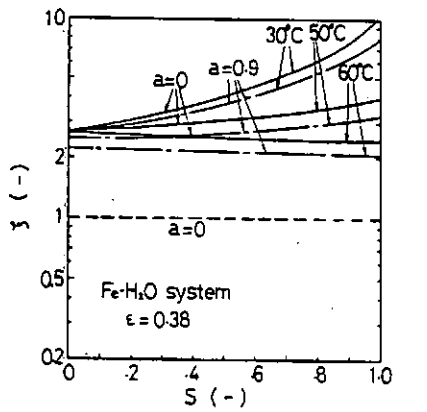

Figure 7 Calculated Results

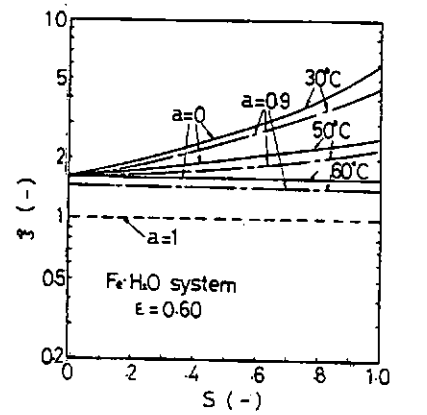

Figure 8 Calculated Results

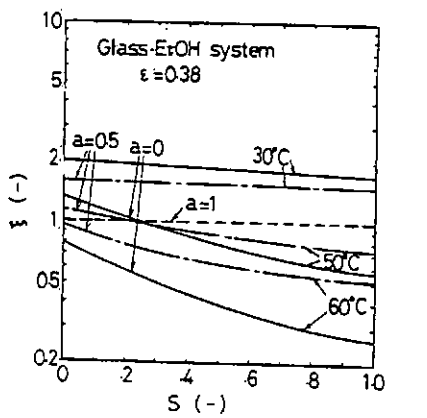

Figure 9 Calculated Results

By comparison with Fig.6 and Fig.7, it is evident that use of metal (iron) particles of large termal conductivity makes the value of ξ much larger than unity. Comparison with Fig.7 and Fig.8 shows the dependence of the ξ on the porosity of the bed. Fig.9 which is the results with C_2H_5OH used in place of water (the latent heat for vaporization is larger), shows that increase in the rate of latent heat transfer makes the value of ξ decrease. Especially, for higher temperature(50~60°C), the equivalent thermal conductivity of the gas phase exceeds that of solid and liquid phases for C_2H_5OH.

Table 1 Thermal Conductivity of Materials

Material \ Temperature °C	20	30	50	60
glass sphere	0.839	0.903	0.922	0.932
H_2O(liquid)	0.510	0.519	0.547	0.563
" (vapour)	0.0173	0.0176	0.0180	0.0185
" (latent heat)	0.069	0.120	0.335	0.565
air	0.0221	0.0224	0.0230	0.0237
C_2H_5OH	0.155			
" (latent heat)		0.166	0.556	1.200
Fe		61.6	62.5	63.4

Table 2 Classification of Vapour Transfer

	Temperature	Liquid content	Mechanism	Example
(1)	constant	various	Ⓐ	isothermal reaction
(2)	under temperature gradient	high	Ⓑ	wetted soil conduction drying
(3)	"	low	Ⓐ/Ⓑ	dry soil convection drying
(4)	"	extremly low	Ⓐ	nonisothermal reaction

Conclusion and Discussion

From the results shown in Figs.3~4 or Figs.6~9, it appears that the mechanism of vapour transfer in a partially saturated granular bed is closely related to that of the heat transfer, and that the value of ξ can be fairly greater than unity depending upon the characteristics of the composite materials, porosity, temperature and moisture content. These indicate that quantitative estimation of the vapour transfer rate is seriously affected by ξ even if compared with the behavior of the value of tortuous factor β which is nearly unity(2),(6),(12). But these are applicable only to the case where the vapour in a granular bed is saturated and transfers accompanied by repeated vaporization and condensation, and not applicable to the cases where noncondensable gas diffuses or the vapour transfers in a dried media. For example, in the analysis of decreasing drying period, the correction of ξ will not be neccesary to the estimation of vapour transfer rate from inner evaporating plane to the surface. From these viewpoints, the phenomena of vapour transfer in porous bodies will be generally classified in Table.2. In this table, Ⓐ indicates that vapour transfers according to our suggested mechanism and Ⓑ ordinary mechanism. In description of the phenomena Ⓐ, a new correction factor, which is affected by the heat transfer mechanism should be introduced in Eq.(1). If this correction factor is designated by ξ', Eq.(1) should be modified as;

$$G_D = -\beta \xi' \frac{D_v}{RT} \varepsilon (1-S) \frac{P}{P-P_s} \cdot \frac{dP_s}{dT} \cdot \frac{dT}{dx} \qquad (1)'$$

Should we discrive this phenomenon in the form of Eq.(1), β ought to be treated as, not a constant depending only upon the porosity and the value of which is less than unity, but a constant, the value of which is also dependent upon thermal conductivity of composite materials, moisture content and temperature as well as thermal conductivity of the bed (14).

REFERENCES

1. Brakel J.V and P.M. Heertjes., Analysis of diffusion in macroporous media in terms of a porosity, a tortuosity and a constrictivity factor, Int. J. Heat Mass Transfer, Vol 17, p.1093, 1974
2. Schecter, R.S., The Variational Method in Engineering, p.213, McGraw-Hill, New York, 1967
3. Hadley,W.A., and R. Eisenstadt., Thermally actuated moisture migration in granular media, Trans. Amer. Geophys. Uni., Vol.36, p.615, 1955
4. Rollins, R.L., M.G. Spangler and D. Kirkham., Movement of soil moisture under a thermal gradient, Highway. Res. Board. Proc., Vol 33, p.492, 1954
5. Taylor, S.A and L. Cavazza., The movement of soil moisture in response to temperature gradient, Soil. Sci. Soc. Amer., Vol.18, p.351, 1954
6. Brailsford, A.D and K.G. Major., The thermal conductivity of aggregates of several phases, including porous materials, Brit. J. Appl. Phys., Vol.15, p.313, 1964
7. Endo,A., I.Shishido., M.Suzuki and S.Ohtani., Estimation of critical moisture content, A. I. Ch. E. J, Vol.73, No.163, p.57, 1977
8. Kimura, M.,Thermal effectivity of partially saturated packed bed, Kagaku Kogaku, Vol.23 p.502, 1959
9. Krischer, o and H. Esdorn., Die Wärmeübertragung in feucher, porigen stoffen verschiedener, VDI-Forsch Heft, Vol.22, p.1, 1956
10. Nissan, A.H., D. Hausen and J.L. Walker., Heat transfer in porous media containing a volatile liquid, Chem. Eng. Progr. Simpo, Ser., Vol.59 p.114, 1963
11. Saito, T and O. Okagaki., Heat transfer characteristics of partially saturated media, Nihon Kikai Gakkaishi, Vol.62, p.75, 1959
12. Krischer, o., Vörgange der stoffbewegung durch haufwerke und porige guter bei deffusion, molekularbewegung sowie laminarer und turbulenzartiger strömung, Chem. Ing. Tech., Vol.34 p.154, 1962

13. Philip, J.R and D. A. de Vries., Moisture movement in porous materials under temperature gradient, Trans. Amer. Geophs. Uni., Vol.38, p.222 1957
14. Yamakawa, N., Y. Sasaki., T. Okada and S. Ohtani Thermal effectivity of partially saturated granular bed, Kagaku Kogaku, Vol.36, p.1432, 1972

APPENDIX

By using heat conduction model represented in Fig.10 we write heat flux q by the following equation.

$$q = \lambda e \frac{\Delta T}{\Delta x} = \lambda ep \frac{\Delta Tp}{a\,\Delta x} = \lambda es \frac{\Delta Ts}{(1-a)\Delta x} \qquad (A\text{-}1)$$

Accordingly

$$\Delta Tp = \frac{a\lambda e}{\lambda ep}\Delta T \qquad (A\text{-}2\text{-}1)$$

$$\Delta Ts = \frac{(1-a)\lambda e}{\lambda es}\Delta T \qquad (A\text{-}2\text{-}2)$$

If we assume that vapour transfer rate was descrived in term of temperature gradient as the driving force, the vapour transfer rate in parallel and series part of Fig.10 are respectively

$$Gp = a\,G\,\frac{\Delta Tp}{a\,\Delta x} \qquad (A\text{-}3\text{-}1)$$

$$Gs = (1-a)\,G\,\frac{\Delta Tsg}{(1-a)\,\varepsilon(1-S)\Delta x} \qquad (A\text{-}3\text{-}2)$$

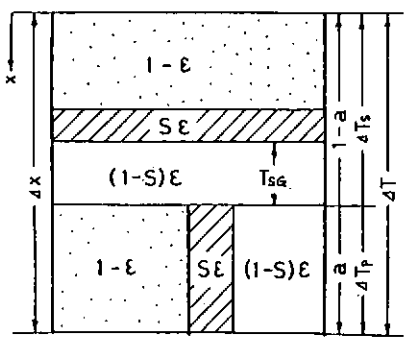

Figure 10 Heat Conduction Model

in which

$$G = \frac{\beta\varepsilon D_v}{RT}(1-S)\frac{P}{P-P_s}\cdot\frac{dP_s}{dT} \qquad (A\text{-}4)$$

Accordingly, total vapour transfer rate G_D is

$$G_D = G_p + G_s = G\frac{\Delta Tp}{\Delta x} + \frac{G}{\varepsilon(1-S)}\cdot\frac{\Delta T_{sg}}{\Delta x} \qquad (A\text{-}5\text{-}1)$$

Then, by using Eqs.(A-2-1) and (A-2-2)

$$G_D = G\left[a\frac{\lambda e}{\lambda ep} + (1-a)\frac{\lambda e}{\lambda g}\right]\frac{\Delta T}{\Delta x} \qquad (A\text{-}5\text{-}2)$$

Appearent vapour transfer rate G_D' is

$$G_D' = G\cdot\frac{\Delta T}{\Delta x} \qquad (A\text{-}6)$$

Accordingly ξ is

$$\xi = \frac{G}{G_D'} = a\frac{\lambda e}{\lambda ep} + (1-a)\frac{\lambda e}{\lambda g} \qquad (A\text{-}7)$$

and by use of Eq.(A-5-2), the following equation is obtained.

$$\xi = \frac{1}{1+\frac{\lambda ep}{\lambda es}\frac{(1-a)}{a}} + \frac{}{\frac{a}{(1-a)}\frac{\lambda_3}{\lambda ep}+\frac{\lambda_3}{\lambda es}} \qquad (A\text{-}8)$$

DRYING OF GRANULAR MATERIALS IN A VIBRATED FLUIDIZED BED

Rahul Gupta, Peter Leung and A.S. Mujumdar

Department of Chemical Engineering
McGill University, Montreal

ABSTRACT

Results of an experimental study on the drying characteristics of a vertically vibrated fluidized bed of cross section 0.2 m x 0.2 m are presented and discussed. Variables studied included: air velocity, air temperature, amplitude of vibration, bed height, frequency of vibration, particle size and the particle shape.

Effect of vibration parameters on the constant rate drying of molecular sieve and silica gel particles is discussed in a semi-quantitative manner.

NOMENCLATURE

a	= amplitude	m
C_p	= heat capacity	$J\ kg^{-1}k^{-1}$
d_p	= particle diameter	m
f	= frequency of vibration	s^{-1}
g	= gravitational acceleration	ms^{-2}
G	= air flow rate	kgs^{-1}
h	= heat transfer coefficient	$Wm^{-2}k^{-1}$
L	= bed height	m
m	= moisture content in solid	$kgkg^{-1}$
m_c	= critical moisture content	$kgkg^{-1}$
P	= air pressure	$N\ m^{-2}$
Q	= rate of heat transfer	W
T	= temperature	K
U	= superficial air velocity	ms^{-1}

Greek Letters

ε	= bed porosity	-
θ	= time interval	s
ϕ	= particle shape factor	-
λ	= heat of evaporation	Jkg^{-1}
ρ	= density	kgm^{-3}
ω	= angular frequency of vibration	s^{-1}

Subscripts

b = bulk solid particles

c = constant rate period

in = at inlet to dryer

mf = minimum fluidization conditions

mm = minimum mixing conditions

out = at outlet to dryer

s = non-vibrated

v = vibrated

w = wet bulb

Dimensionless Groups

Ar = Archimedes Number

Nu = Nusselt Number

Pr = Prandtl Number

Re = Reynolds Number

INTRODUCTION

The term 'Vibrated Fluidized Bed' (VFB) generally refers to a shallow rectangular fluidized bed wherein the complete assembly is vibrated at a relatively high frequency and with a small amplitude. The vibration vector is generally at a small angle to the horizontal in order to facilitate solids movement towards the discharge. In addition to simultaneous accomplishment of drying, cooling and conveying of granular solids, other advantages offered by the VFB include:

reduced air flow requirements, better control over the particle residence time, plug flow operation, lack of dead pockets and ability to fluidize agglomerating and sticky materials (8). Some typical applications of the VFB include the thermal processing of asbestos fibres, clays, detergents, foodstuffs (milk powder, cocoa, coffee), granulated fertilizers, organic chemicals, pharmaceuticals etc.

During the last two decades, over one hundred publications, primarily originating in Russia, have appeared in the literature. These deal with various aerodynamic and heat transfer aspects of the VFB behaviour. Comprehensive reviews of the available literature may be found in Gupta (10), Gupta and Mujumdar (11), and Strumillo and Pakowski (20). In addition, two books dealing exclusively with VFB's are available (5,7) in the Russian language.

PRIOR WORK

Most prior work on VFB drying is confined to experimental studies of the effect of the vibration parameters (amplitude and frequency) on constant rate drying and to heat transfer from immersed heated surfaces to the bed. The aeration rates used were generally very low; many heat transfer studies were conducted in non-aerated beds. Furthermore, a significant number of papers pertain to range of operation where the vibration factor, $a\omega^2/g$, was in excess of 5, which is of little industrial interest. Many researchers reported existence of optimal values for the vibration parameters for drying. Both increases and decreases in heat transfer with vibration have been reported.

Osiniskii et al (17), Ginzberg (9), Zaitsev et al (25) and Chlenov and Mikhailov (6) have reported several fold increases in drying rates as a result of applied vibration, the comparison being with a non-fluidized bed operating under identical conditions of temperature, air velocity etc. For aerated beds operated at $a\omega^2/g > 3$, Zelepuga et al (26) found the drying rate to increase monotonically with increase in the vibrational acceleration.

The effect of air velocity on drying rate in a fluidized bed was reported by Kavetskii et al (14) to be less pronounced in the presence of vibration. Sugiyama and Arai (21) postulated that the influence of vibration may be incorporated in the form of an equivalent air velocity.

The effect of bed height on the drying rates in VFB's has been studied by Zelepuga et al (26) and Ovchinikov et al (18); both reported monotonic decrease in the drying rate with increase in bed depth. For very shallow beds, however, Volovik et al (23) found that an optimum value of the bed height existed.

As far as the effect of vibration on the critical moisture content is concerned, at least two groups of researchers report a decrease in the critical moisture content with applied vibration (2, 15). No physical explanation was offered in support of this observation.

Finally, it is interesting to note that Bukareva et al (2) and Tamarin and Kal'tman (22) observed that for agglomerating granular solids a minimum excitation vibration frequency must be exceeded before vibration aids the drying process.

Gupta and Mujumdar (12) have proposed that for efficient operation of a VFB, the air velocity must exceed a 'minimum mixing velocity', U_{mm}, which they correlated as follows:

$$\frac{U_{mm}}{(U_{mf})_s} = 1.952 - 0.275\left(\frac{a\omega^2}{g}\right) - 0.686\left(\frac{a\omega^2}{g}\right)^2 \qquad (1)$$

where $(U_{mf})_s$ is the theoretically computed minimum fluidization velocity for non-vibrated beds.

They also presented the following correlation for the bed pressure drop in the presence of vibration

$$\frac{(\Delta P_{mf})_v}{(\Delta P_{mf})_s} = 1 - 0.935\left(\frac{dp}{L}\right)^{0.946}\left(\frac{a\omega^2}{g}\right)^{0.606}(\phi)^{1.637} \qquad (2)$$

This paper presents the results of drying experiments carried out in the same apparatus as used for the aerodynamic investigation reported in (10, 12).

EXPERIMENTAL APPARATUS AND TECHNIQUE

Figure 1 is a schematic of the equipment used in the present experimental study. The instrumentation and control scheme is also shown in this figure.

The fluidized bed consisted of a chamber of rectangular cross-section, 0.2m x 0.2m, equipped with 23 percent open area perforated plate distributor. The entire bed was vibrated sinusoidally in the vertical plane by means of a variable eccentricity (and hence variable amplitude) drive mechanism. The frequency of vibration was regulated with an SCR-controlled DC motor. The fluidized bed chamber and the connecting ducts were insulated to minimize heat losses.

Table 1

Material	d_p (μm)	ρ_b (kgm^{-3})	ϕ	C_p ($Jkg^{-1}k^{-1}$)	m_c ($kgkg^{-1}$)
Molecular Sieve	2200	887	1.00	0.962	0.240
	3100	887	1.00	0.962	0.240
	3900	887	1.00	0.962	0.240
Silica gel	550	865	0.77	0.920	0.160
	2200	865	0.77	0.920	0.160

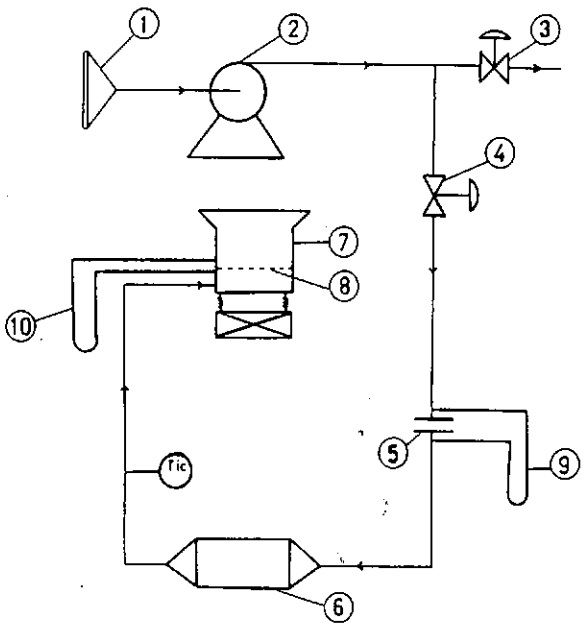

Figure 1: Experimental Setup
(1) Air Filter (2) Blower (3) Bypass Valve (4) Control Valve (5) Orifice Plate (6) Heater (7) Fluidized Bed (8) Distributor Plate (9) Inclined Tube Manometer (10) Inclined Tube Manometer

The ranges of operation are listed in Table 1, along with the experimental uncertainty associated with the measurement of each variable. The test materials selected were molecular sieve and silica gel granules of different size fractions. The physical properties of these test materials are tabulated in Table 2.

The VFB dryer was operated batchwise. Drying rate curves were constructed by withdrawing small samples of solids from the bed at short intervals and determining their moisture content. Over 150 sets of drying rate curves were obtained under various conditions of operation. The parameters which were varied systematically were: the frequency and amplitude of vibration, air velocity, inlet air temperature, mean particle size, bed height and the type of distributor. Most of the observations were taken under constant drying rate conditions; the effect of vibration on the falling rate period was observed to be negligible within experimental error.

Table 2

Variable	Range of Operation Minimum	Maximum	Measurement Uncertainty	Units
w	0	105	0.2	s^{-1}
a	0	4.25×10^{-3}	0.1×10^{-3}	m
L	12.5×10^{-3}	100×10^{-3}	0.25×10^{-3}	m
dp	0.55×10^{-3}	3.9×10^{-3}	0.25×10^{-3}	m
uo	0.3	2.5×10^{-3}	0.06	ms^{-1}
m_s	0	0.45	0.001	$kgkg^{-1}$
R_c	0	20×10^{-4}	0.25×10^{-4}	$kgkg^{-1}s^{-1}$

RESULTS AND ANALYSIS

Figure 2 is a typical set of drying curves obtained for a fluidized bed of molecular sieve granules at various vibration frequencies under fixed conditions of air temperature, humidity, air flow rate, vibration amplitude, bed height and particle size. Results for a non-vibrated bed are also plotted for comparison (Curve 1). It is clear that vibration causes no appreciable change in the shape of the drying rate curve. The similarity of the shape of the curves indicates that the mechanism of drying in the falling rate period is probably not affected by vibration. The small change in the observed critical moisture content was found to be random and hence is attributed to experimental uncertainty.

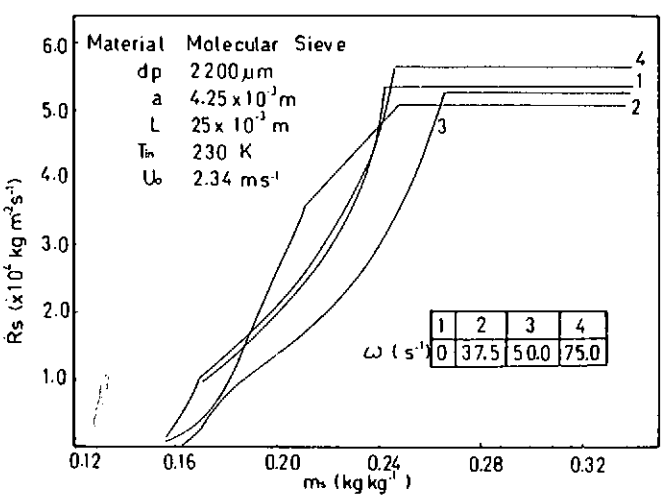

Figure 2: Drying Curves at Different Vibration Frequency

Referring back to Figure 2 it may be observed that over the lower range of vibration frequency, the measured rate of drying, R_c, is lower than that for a non-vibrated bed while for higher frequencies it is greater than that for the non-vibrated bed. This effect is more clearly illustrated in Figure 3 where R_c is plotted against ω at various amplitudes. Figure 3a presents drying rate data for larger size molecular sieve particles (d_p = 2200 μm) while Figure 3b presents the same for the smaller silica gel particles (d_p = 550 μm). It is interesting to note that R_c exhibits a minimum within the frequency range considered, for both materials and at all amplitudes of vibration. Figure 3c illustrates the same effect for other particle sizes also.

The interacting effects of vibration frequency and amplitude can also be seen from Figure 3. The frequency corresponding to the minimum drying rate increases as the vibration amplitude is reduced. It is interesting to note that this minimum drying rate always occurs at $a\omega^2/g = 1$, regardless of the values of ω and a. For $a\omega^2/g < 1$, vibration decreases the rate of drying, while for $a\omega^2/g > 1$ a monotonic increase in R_c is observed with increase in the vibration frequency. It should be noted that this increase in R_c with vibration, beyond $a\omega^2/g = 1$ is consistent with the earlier findings of Bukareva et al (2) and Zaitsev et al (25).

The effect of the amplitude of vibration on R_c at a given frequency is found to be more complex than the effect of frequency at given amplitude; this is apparent from Figure 3. While for molecular sieve particles, the highest amplitude gives consistently higher drying rates compared with the values at other amplitudes, for the smaller size silica gel particles the trend is quite the opposite. For clarity, these results are replotted in Figure 4 with the amplitude of vibration as the abscissa. For the smaller particles of silica gel, a maximum in R_c is observed at the higher frequency (75 s^{-1}) indicating the existence of an optimum amplitude of vibration (for a given bed and frequency). For the other conditions (for the larger particles and lower frequency range of the smaller size particles), the maximum probably exists, but lies beyond the range of amplitude considered for the study. It is felt that this highly non-linear behaviour with respect to vibration amplitude arises from two counteracting effects of the amplitude: while the reduction in distributor-to-particle contact time with increasing amplitude improves the local unsteady state heat transfer coefficient, a simultaneous reduction in contact area itself offsets this advantage to an extent which is dependent on the vibration parameter.

The rate of drying in the VFB was found to decrease considerably with increase in bed height; the same effect was also observed in nonvibrated beds. Figure 5 is a plot of the rate of drying, R_c, vs. the inverse of the bed height, 1/L. It is clear from this figure that the rate of drying is proportional to 1/L at all frequencies. Under

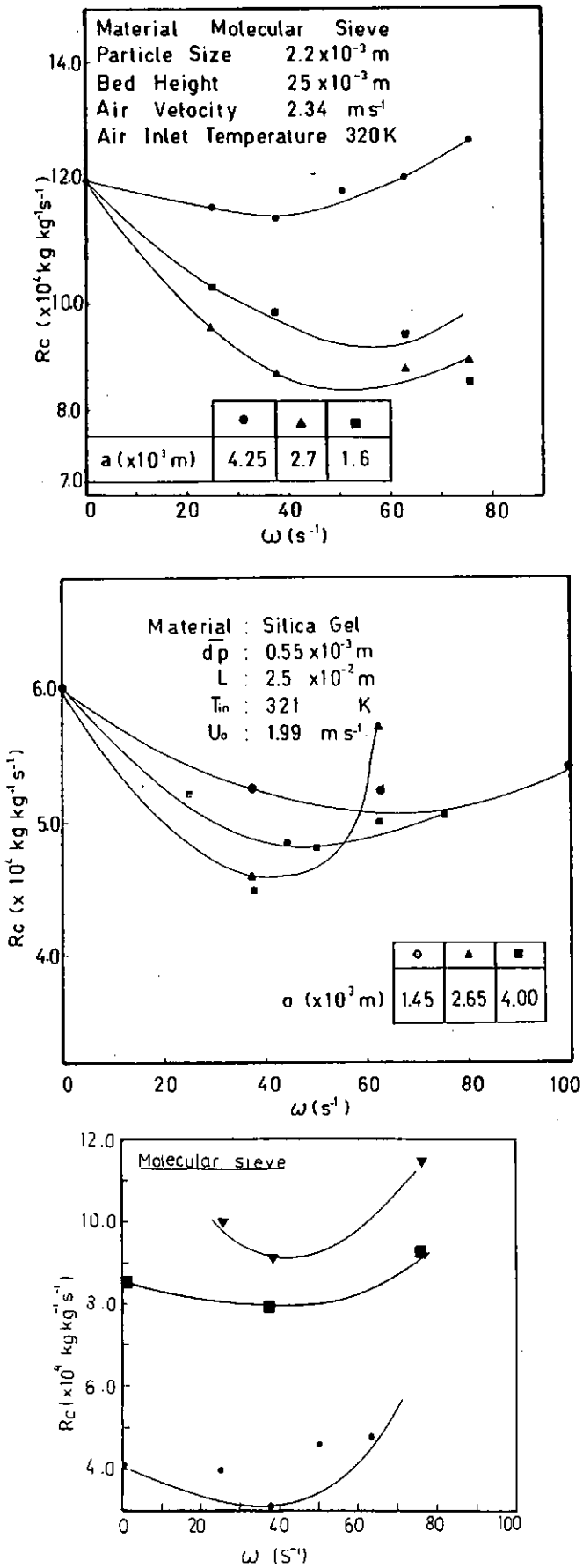

Figure 3: Effect of Frequency on Rate of Drying

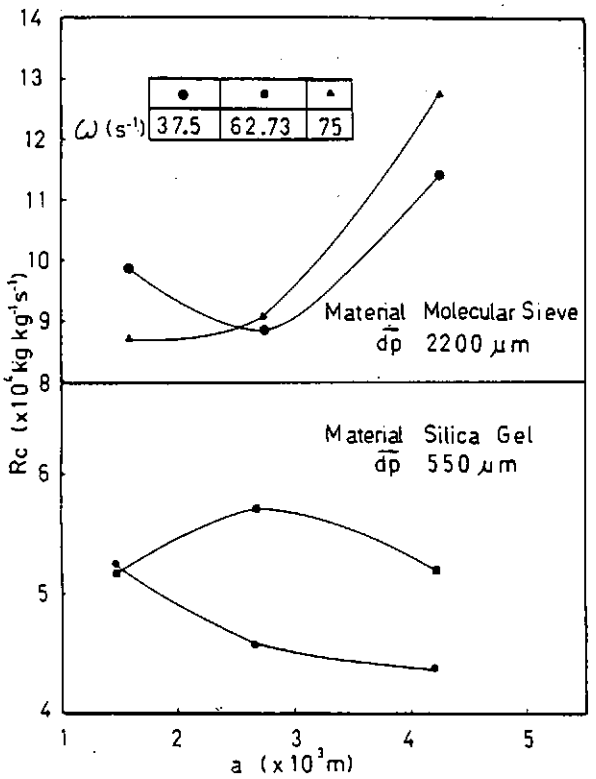

Figure 4: Effect of Amplitude on Rate of Drying

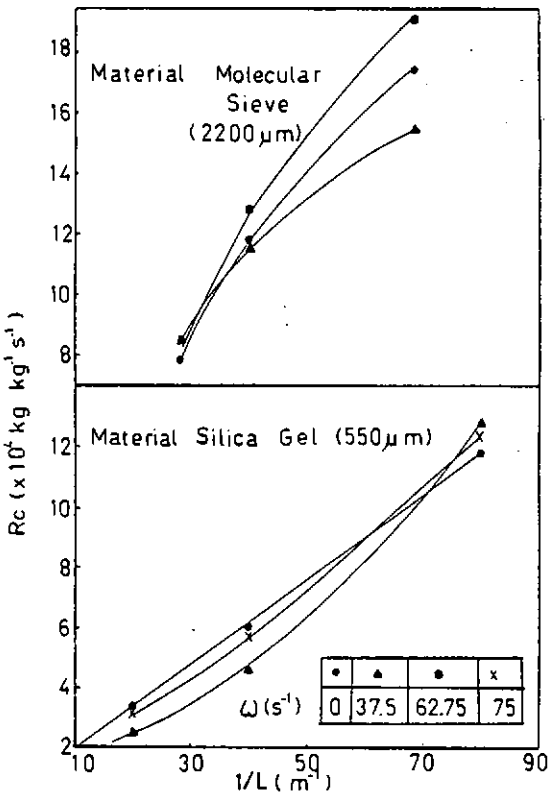

Figure 5: Effect of Bed Height on Rate of Drying

constant rate drying conditions, the overall heat transfer rate, Q, is given by:

$$Q = (R_c)(AL\rho_b)(\lambda).$$

The experimental results ($R_c \alpha 1/L$) therefore indicate that the heat transfer rate, Q, is independent of bed height. This is consistent with observations of earlier workers that most of the heat transfer in a fluidized bed takes place within the first few millimeters of the bed above the distributor. It is believed (13, 16, 24) that for such shallow beds, convective heat transfer between the gas and the solids is small and the bulk of the heat transfer takes place by conduction of heat to the particles from the gas distributor. This explains the lack of dependence of the overall heat transfer rate on the bed height.

The rate of drying was also found to be strongly influenced by the particle size d_p. A bed of smaller size particles, by virtue of much higher heat transfer area per unit volumetric holdup than an equivalent bed of larger size particles would be expected to display a higher overall heat transfer rate. This is clear from Figure 6a for silica gel particles of size d_p = 550 μm and d_p = 2200 μm respectively; the smaller particles exhibit upto 50 percent higher heat transfer rates than the larger ones. To compare the relative influence of vibration on the two particle sizes, these results are replotted in Figure 6b, in terms of the normalized drying rate, $(R_c)v/(R_c)s$. It is clear that vibration is more detrimental to the drying rate of beds of smaller particles. No physical explanation could be offered for this behaviour.

The effect of the inlet air temperature on the rate of drying is shown in Figure 7, where R_c is plotted against $(T_{in} - T_{out})$, yielding a linear dependence. This is consistent with the energy balance around the dryer, for no heat losses and only evaporative load, i.e.

$$Q = R_c LA\rho_b\lambda = GC_{pf}(T_{in} - T_{out}).$$

Within the range of air velocities considered, the air flow rate was found to have a strong influence on the drying rate. Figure 8 is a plot of the rate of drying, R_c, against the air

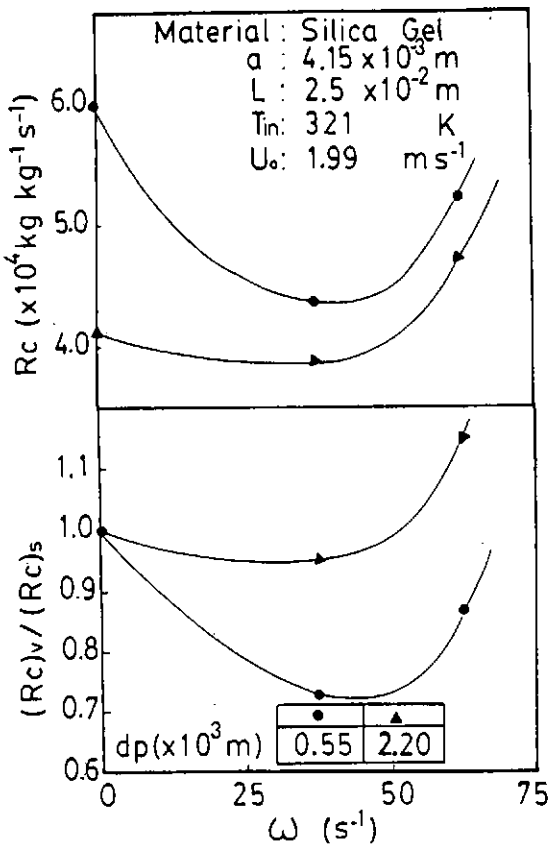

Figure 6: Effect of Particle Size on Rate of Drying

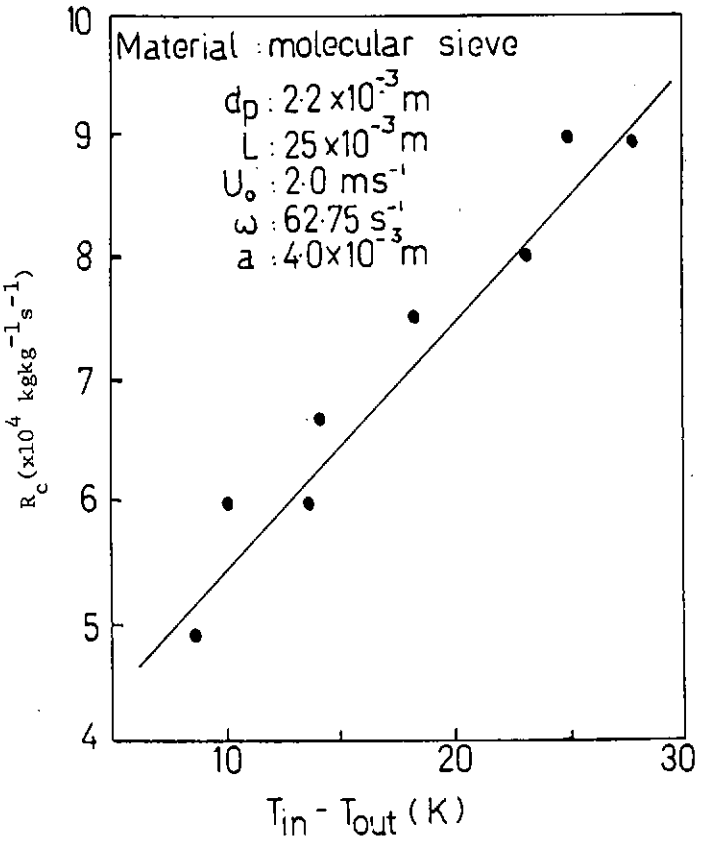

Figure 7: Effect of Air Temperature on Rate of Drying

velocity u_o. The following dependence of R_c on u_o is exhibited:

$R_c \alpha u_o^{1.034}$ for $u_o < 1.85$ m/s,

$R_c \alpha u_o^{1.8}$ for $u_o > 1.85$ m/s.

It is of interest to note that the exponent is independent of the vibration frequency. Moreover, the exponent is lower than the corresponding value for non-vibrated beds (1.130 for $u_o < 1.85$ and 2.40 for $u_o > 1.85$), indicating the reduced influence of air velocity on drying in vibrated beds.

CONCLUSIONS

(1) For non-agglomerating particles, with operation in excess of $(U_{mf})_s$, no measureable change in either the shape of the rate of drying curve, or in the critical moisture content was observed as a consequence of vibration.

(2) Minimum rates of drying were found for operation at the vibration acceleration of $a\omega^2/g = 1$. A monotonic decrease in the drying rate occured with increase in the vibration frequency below this level. Optimum conditions of amplitude (corresponding to highest drying rate) were observed.

(3) In addition to the vibration parameters, other factors influencing the drying rate were found to be: the inlet air temperature, bed height, air flow rate and particle size. The effect of air velocity was found to be less significant in a VFB than in non-vibrated beds.

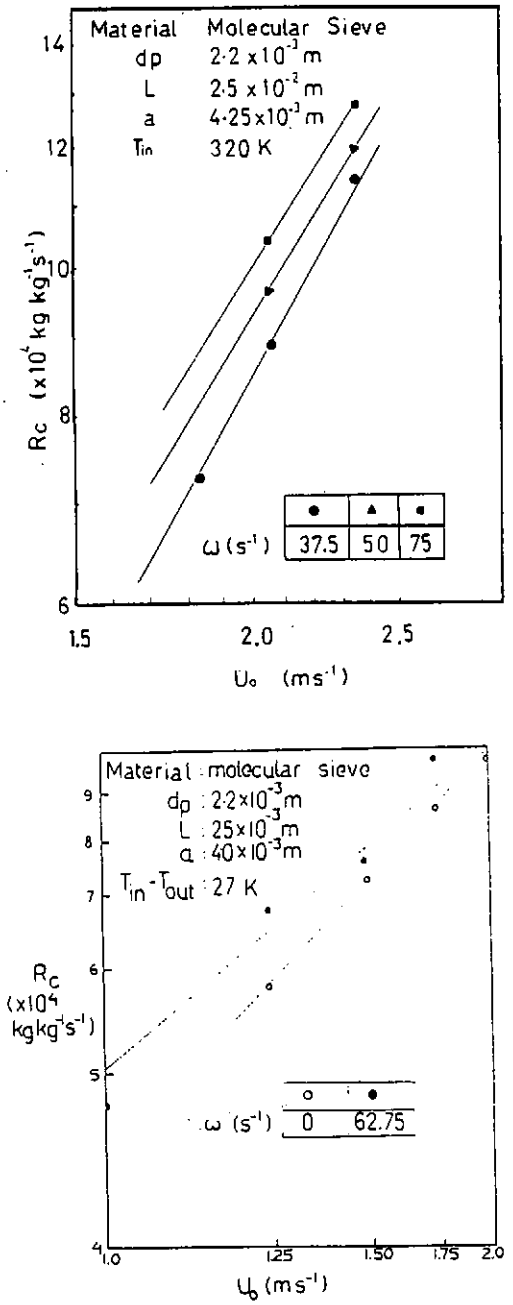

Figure 8: Effect of Air Velocity on Rate of Drying

REFERENCES

1. Arai, N., and Sugiyama, S., Kagaku Kogaku 38 (1), 15 (1974)
2. Bukareva, M.F., Chlenov, V.A., and Mikhailov, N.V., Porosh. Met. 7, 85 (1967)
3. Bukareva, M.F., Chelnov, V.A., and Mikhailov, N.V., Int. Chem. Eng. 9, 119 (1969)
4. Ciberowski, J., and Roszar, Inzh. Fiz. Zhur 1, (12), 8 (1958)
5. Chlenov, V.A., and Mikhailov, N.V., 'Drying of Free Flowing Materials in Vibrated Fluidized Bed' Stroyizdat Press, Moscow (1967)
6. Chlenov, V.A., and Mikhailov, N.V., J. of Eng. Phy. 9, 137 (1965)
7. Chlenov, V.A., and Mikhailov, N.V., 'The Vibro Fluidized Bed', Nauka Press, Moscow (1967)
8. Danielson, S., and Howmand, S., 'Development in Drying', ed. A.S. Mujumdar, Hemisphere Publishing Corp, N.Y. (1980)
9. Ginzburg, A.S., and Syroedov, V.I., J. Eng. Phy. 9, 455 (1965)
10. Gupta, R., M.Eng. Thesis, McGill University, Montreal (1979)
11. Gupta, R., and Mujumdar, A.S., 'Development in Drying', ed. A.S. Mujumdar, Hemisphere Publishing Corp., N.Y. (1980)
12. Gupta, R., and Mujumdar, A.S., Presented at C.S.Ch.E. Conference, Sarnia (1979)
13. Heertjes, P.M., Chem. Eng. Sc., 2(3), 97 (1953)
14. Kavetskii, G.D., Nikonov, L.V., and Krohin, N.G., Chem. Tech. Fuel. Oil, 13, 126 (1977)
15. Kazanchinskaya, N.V., and Bilik, O.I., Heat Tr. Sov. Res. 7(6), 146 (1975)
16. Leva, M., 'Fluidization' (1959)
17. Osinskii, V.P., Sazhin, B.S., and Chuvpilo, E.A., Chem. Petrol. Eng. 11, 866 (1969)
18. Ovchinnikov, S.A., Borisov, G.N., and Egorava, V.I., Pharm. Chem. J. 10, 1380 (1976)
19. Shenkovskaya, P.T., J. Eng. Phy. 9, 144 (1965)
20. Strumillo, C., and Pakowski, Z., 'Development in Drying', ed. A.S. Mujumdar, Hemisphere Publishing Corp., N.Y. (1980)
21. Sugiyama, S., and Arai, N., Kagaku Kogaku 1, 598 (1975)
22. Tamarin, A.I., and Kal'tman, I.I., J. Eng. Phy. 20, 197 (1971)
23. Volovik, V.I., Moseychuk, G.G., and Isahov, N.A., Heat Tr. Sov. Res. 7(6), 146 (1975)
24. Zabrodski, S.S., 'Hydrodynamics and Heat Transfer in Fluidized Beds', M.I.T. Press (1966)
25. Zaitsev, E.D., Redekop, V.I., Shuetsov, V.V., Pharm. Chem. J., 10, 354 (1976)
26. Zelepuga, V.I., Stroit Mater 11, 35 (1975)

THE INFLUENCE OF AERODYNAMICS OF A VIBRATED FLUID BED ON HEAT TRANSFER DURING DRYING PROCESS AT LOW AIR VELOCITIES

Z. Pakowski
C. Strumiłło

Łódź Technical University, Łódź, Poland

ABSTRACT

Experimental results of effective heat transfer coefficient during drying of calcium carbonate spheres (d_e = 0.328 mm) in 140 mm I.D. vibrated fluid bed (VFB) 55 mm high for frequency 8.42 to 24.8 Hz, amplitude 0.75 to 4.75 mm and superficial air velocity 0.08 to 0.24 m/s have been presented.
The dependence of the measured heat transfer coefficient on the maximum height of bed throw (which was measured by means of photographic technique) has been given in graphical form.

NOMENCLATURE

- A_t - total area of heat exchange, m^2
- A - vibration amplitude, m
- d_e - equivalent particle diameter, m
- f - vibration frequency, Hz
- Δh_v - specific latent heat of vaporization, kJ/kg
- M_B - mass of the bed, kg
- $\dot{N}$ - drying rate, kg/s
- p_L - temporary value of pressure under the bed, N/m^2
- s - temporary value of bed throw height, m
- s_o - peak value of bed throw height, m
- t - time, s
- u - superficial air velocity, m/s
- u_{mf} - minimum non-vibrated fluidization velocity, m/s
- u^* - pulsatile air velocity, m/s

Greek

- α_e - effective heat transfer coefficient, W/m^2K
- ρ_p - particle material density, kg/m^3

Subscripts

- m - logarithmic mean value

INTRODUCTION

Many advantages of application of vibration to fluid bed of granular materials have focussed the attention of investigators on this technique for a certain time. Promising results allowed for application of vibrated fluid bed (VFB) to many industrial processes. The reference literature on this subject is quite vast (i.e. (1) to (3)). The main advantages of VFB in comparison with typical fluid bed are as follows:

- appropriate vibrations can make the bed "flow" at low air velocity or even without gas flow at all. Thus matching vibrations with air flow it is possible to obtain a bed with good internal mixing at any gas flow rate;
- vibration reduces pressure drop in the bed in comparison with typical fluid bed at the same flow rate;
- vibration can serve as a transporting agent for material under treatment.

Application of VFB technique to the drying process results in considerable technological and economical profits when compared with traditional fluid bed technique.
Although there is a wide variety of papers on VFB theory and application (most of them were recently reviewed by Gupta and Mujumdar (4) and Strumiłło and Pakowski (5)) an explanation of the influence of vibration on convective heat transfer in VFB is still lacking.
The objective of this paper is to explain the influence of some aerodynamic bed parameters on the convective heat transfer during drying in VFB.

PRIOR WORK

Drying Many papers on drying granular material either in vibrated bed with contact heat supply or VFB with contact and/or convective heat supply report the dependence of drying rate on vibration parameters. As they were already abstracted in details (5) here only the most significant ones will be presented.
In the case of contact drying in vibrated bed Chlenov and Mikhajlov (6) reported the negative pressure to be formed under a vibrated bed (in the gap between the

bed and the vessel bottom plate during the flight period). The pressure was found to be dependent on frequency and amplitude of vibration. Apart from that a linear dependence of drying rate in the I period on this pressure was given in graphical form. In field of convective drying in VFB the paper of Sinz and Lund (7) is worth noticing. They carried out experiments with drying of some vegetable products (carrot and potato cubes, peas, corn etc.). Nearly linear dependence of drying rate on vibration amplitude was observed. Curvilinear dependence of drying rate on vibration frequency was found, having a maximum at $f = 10.1$ Hz (at $A\omega^2/g \cong 5$). Surprising effect of decrease of drying rate with increase of air velocity in the range of investigated parameters was noticed.
Some other authors report there is a range of optimal vibration parameters in which drying is the most effective. Osinski et al. (8) found this range between 1.8 to 2.9 g and Mushtayev et al. (9) between 2 and 3 g. The above cited results enable us to state that heat and mass transfer phenomena during drying are closely associated with bed dynamics and should be explained in terms of this dynamic behaviour of the bed.

The Influence of Bed Dynamics on Heat Transfer The concept of basing heat transfer in the bed on bed dynamics fully succeeded in the analysis of contact heat transfer in vibrated bed done by Gutman (10). A scoured film model was evaluated by him which forecasted a linear dependence of contact heat transfer coefficient (from a vertical surface immersed in a vibrated bed) on the maximum height of the bed throw s_o. The model was fully verified in course of the experiments.
Yamazaki et al. (11) for the same type of heat exchange but in VFB presented a different approach. He correlated the results of contact heat transfer coefficients vs. total gas velocity being a sum of mean superficial u and pulsatile u* gas velocities. The pulsatile gas velocity u* was calculated from a model of gas flow through the bed. The model allowed for calculation of u* if the pressure fluctuations under the bed were known from experiments. All results correlated in this way resulted approximately in one curve except for larger air velocity and smaller particles. Although a convincing scoured film mechanism of contact heat transfer does not include any direct connection between gas velocity $u + u^*$ and heat transfer coefficient, on the other hand the maximum bed throw height s_o is coupled with pressure fluctuations under the bed p_L. This probably explains why Yamazaki's correlation succeeded.
The close connection between s_o and p_L was observed for example by Kroll (12) and Gutman (13). They presented mathematical models describing bed trajectory $s = f(t)$ and pressure changes under the bed $p_L = f(t)$ for vibrated beds and for the case when the bottom plate of the vessel was not gas permeable.
In the case of VFB drying when low air velocities are applied (i.e. $u \leqslant u_{mf}$) bed dynamics similar to that reported for vibrated beds is observed. There is also a gap between the bed and the bottom plate formed and pulsations of air velocity observed. Taking into account that pressure fluctuations reported by Kroll for vibrated bed are of order of 0.1 atmospheric pressure in magnitude the process of gap formation can influence the air velocity in the bed thus affecting convective heat exchange in it. To prove this the following experiments were performed.

EXPERIMENTAL PART

The experiments were carried out in 140 mm I.D. cylindrical vessel with perforated bottom plate (gas distributor). As the gas distributor served 1 mm thick brass plate with drilled 1 mm orifices (8% of free area ratio). Gas distributor was covered with fine nylon mesh to protect particles against falling into the orifices. The vessel was mounted on helical springs and attached to the adjustable excentric driven by a D.C. motor.

Drying Experiments For drying experiments the vibrated glass vessel was equipped with gas supply system and thermocouples for temperature measurements (Fig.1).

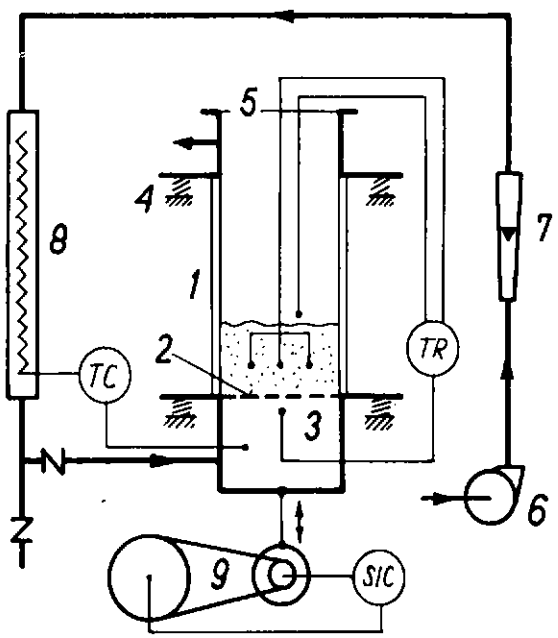

Fig.1. Scheme of the experimental equipment.
1- glass tube, 2- gas distributor,
3- plenum chamber, 4- springs,
5- hatch, 6- fan, 7- rotameter,
8- heater, 9- drive

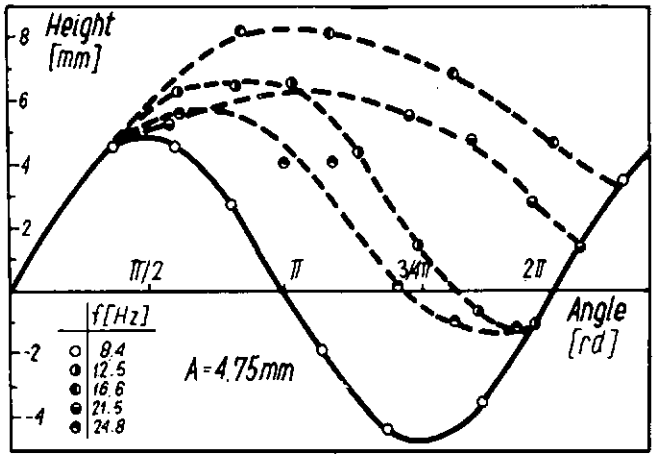

Fig. 6. Bed trajectories for different frequency at higher amplitude

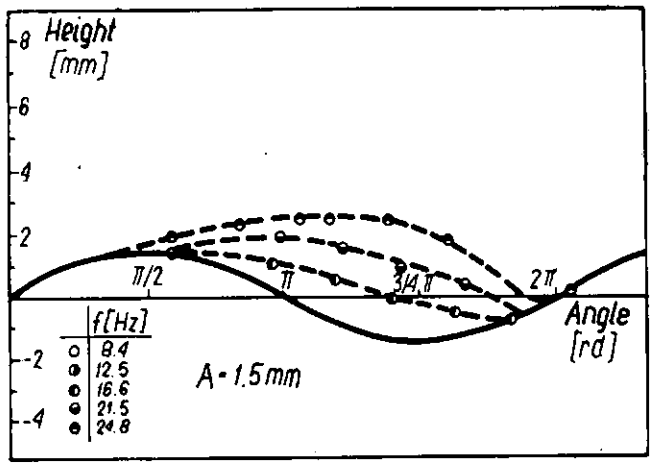

Fig. 7. Bed trajectories for different frequency at lower amplitude

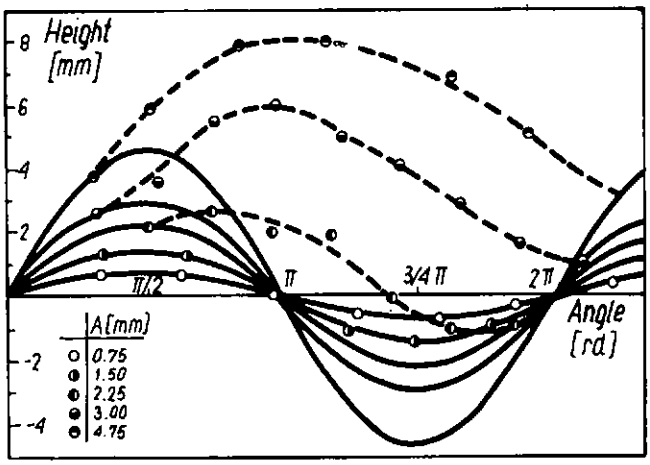

Fig. 8. Bed trajectories for different amplitudes

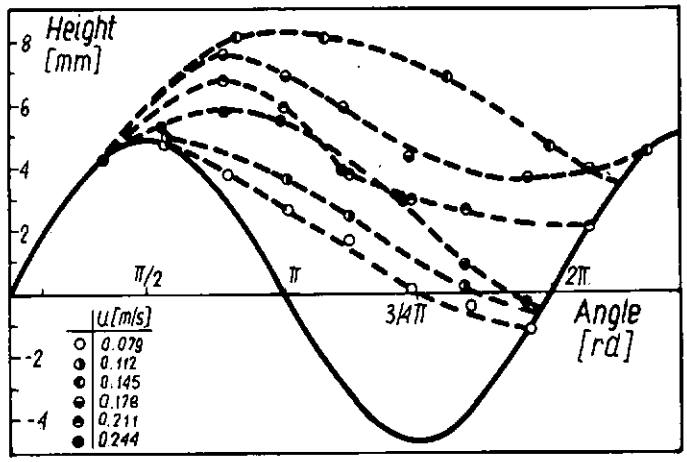

Fig. 9. Bed trajectories for different air velocity

constant voidage fraction and particle circulation streams are observed. At the same time bed constantly jumps up and falls down reaching the peak throw height of order of 2·A (if only the frequency is great enough to obtain vibrofluidization regime).
During the flight period the air under the bed is periodically compressed and decompressed.
As we know there is a close relationship between maximum throw height s_o and pressure under the bed p_L (the latter governs the air velocity in the bed). The assumption that heat transfer coefficient in VFB (α_e) is dependent on relative bed-air velocity results in the dependence of α_e on s_o.
The peak throw height s_o was then read from the bed trajectories and plotted vs. the same parameters as an effective heat transfer coefficient. The curves obtained in this way are shown in Figs. 10 - 13.
The results of measured heat transfer coefficient were plotted vs. measured maximum throw height (Fig. 14) showing there

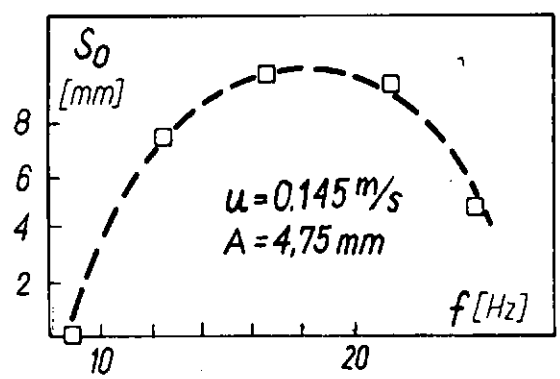

Fig. 10. Dependence of s_o on frequency for higher amplitude

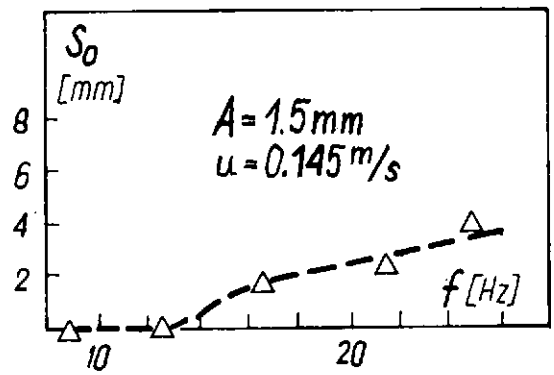

Fig. 11. Dependence of s_o on frequency for lower amplitude

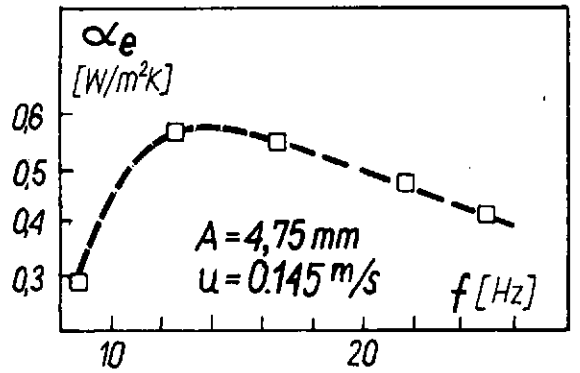

Fig. 2. Dependence of α_e on frequency for higher amplitude

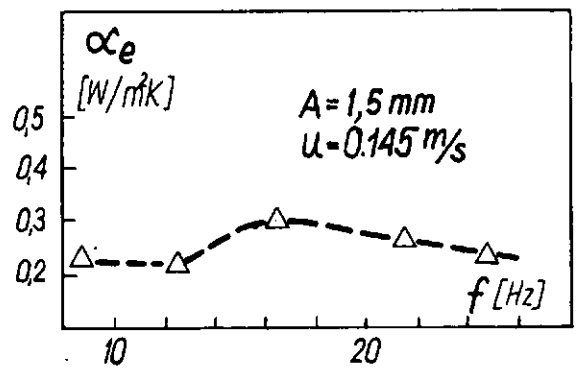

Fig. 3. Dependence of α_e on frequency for lower amplitude

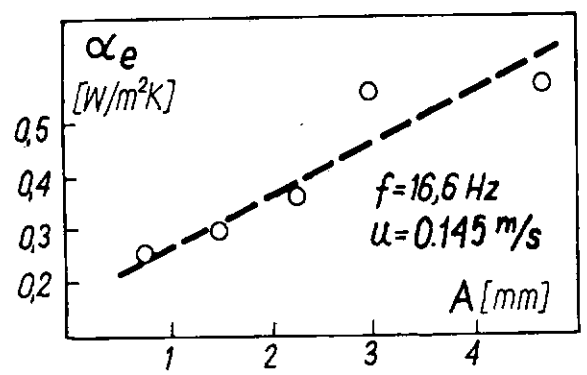

Fig. 4. Dependence of α_e on amplitude

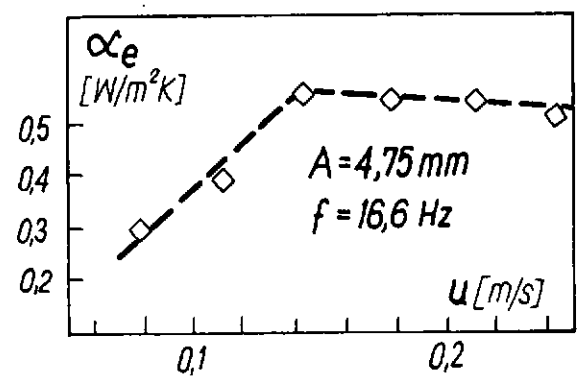

Fig. 5. Dependence of α_e on air velocity

The outer wall of the vessel was heat insulated with thin transparent foil, in such a way that a thin (~5 mm) air space between the glass and foil was left. The experiments were carried out on the 55 mm high bed of calcium carbonate spheres (d_e = 0.328) having 2% of initial water content. Temperature of air entering the apparatus was kept constant at 378 K. Drying curves were drawn by plotting the moisture content of samples collected from the bed vs. time. Drying rate in the period of constant drying rate was calculated from the drying curves. Temperature of the bed was measured by means of 3 bare thermocouples. Temperature of gas under the distributor and just above the bed was also measured. This allowed for calculation of the effective heat transfer coefficient on the basis of the following formula

$$\alpha_e = \frac{\dot{N}\,\Delta h_v}{A_t\left(T_G - T_B\right)_m} \qquad (1)$$

where

$$A_t = \frac{6 \cdot M_B}{\rho_p\, d_e} \quad \text{- total area of particles contained in the bed} \qquad (2)$$

The experimental results are given in Figs. 2 - 5.

Bed Dynamics Experiments For this purpose the same apparatus as for drying experiments was used. Only the vessel was changed into a 140 mm I.D. perspex tube having the gas ditributor installed at a certain height to make the region of the bed close to the distributor clearly visible. For the same parameters as used in drying studies the bed trajectory was measured for the bed having 2% of water content (earlier bed aerodynamical properties were found constant within the range of moisture content which corresponds to the I period of drying). For this purpose a photographic technique invented by Kroll (12) was used. The gap under the bed was photographed using a flash lamp. The lamp could be activated by an adjustable switch at any given angle of vibration cycle. Thus a series of 10 photographs could be taken covering the whole vibration cycle from which bed trajectory could be read. The measured trajectories are shown in Figs. 6 - 9 as dotted lines together with the vessel trajectories (full lines).

ANALYSIS OF RESULTS

Experiments show that for low air velocity (for $u \leqslant u_{mf}$) heat transfer in VFB is seriously dependent on vibration parameters. In that range filtration of gas through the bed is observed. No great air bubbles which cause vigorous mixing in the bed are present. Bed structure is homogeneous,

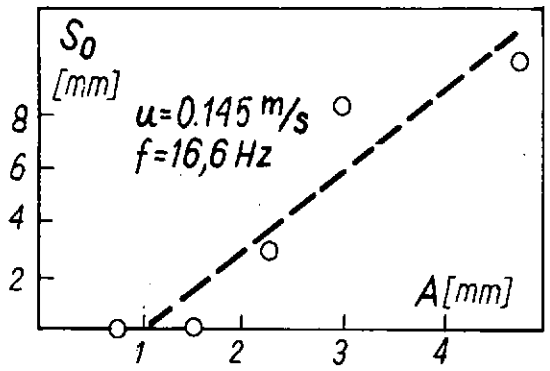

Fig. 12. Dependence of s_o on amplitude

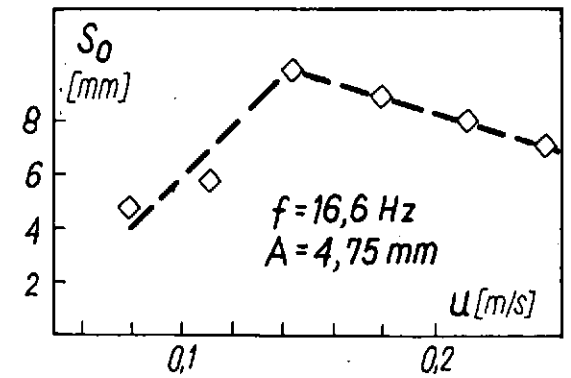

Fig. 13. Dependence of s_o on air velocity

is a correlation between these two.

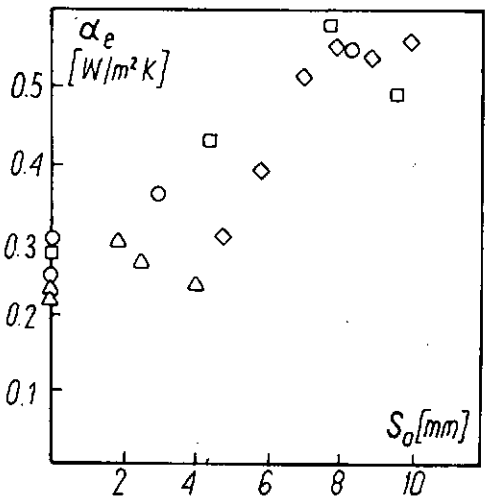

Fig. 14. Correlation of effective heat transfer coefficient on maximum bed throw height

As an analytical approach to that problem a mathematical model of bed dynamics (based on the incompressible gas model) was elaborated. The model allows for calculation of both functions $s = f(t)$ and $p_L = f(t)$. The solution of the model and comparison of the theoretical results with presented here experimental results require further studies.

CLOSURE

Experimental results of convective heat transfer coefficient α_e measurements correlated with bed peak throw height s_o show the dependence of α_e on s_o. Having in mind that s_o can be calculated from a mathematical model of bed dynamics, a way of choice of optimum for drying vibration parameters seems to be possible in theoretical calculations.

REFERENCES

1. Chlenov V.A., Mikhajlov N.V., Vibrokipiaschii sloi, Nauka, Moscow, 1972
2. Karmazin V.D., Technika i primenenie vibriruyushchego sloya, Naukova Dumka, Kiev, 1977
3. Goncharevich I.F., Urev N.B., Taleysnik M.A., Vibracyonnaya technika v pishchevoi promyshlennosti, Pishchevaya Promyshlennost, Moscow, 1977
4. Gupta R., Mujumdar A.S., Dev. in Drying ed. A.S. Mujumdar, Science Press, Princeton (NJ) 1978
5. Strumiłło C., Pakowski Z., (same as above)
6. Chlenov V.A., Mikhajlov N.V., Sbornik: Fiziko-khim. mekh. dissp. struktur, Moscow, 1966
7. Sinz R., Lund D.B., Proc. Biochem., 6, 1974, 27
8. Osinski V.P., Sazhin B.S., Chuvpilo E. A., Khim. Neft. Mashinostr., 11, 1969, 13
9. Mushtaev V.I., Chevilenko B.M., Korotkov B.I., Teoret. Osn. Khim. Technolog. VII, 6, 1972, 866
10. Gutman R.G., Trans.Inst.Chem.Engrs., 54, 1976, 532
11. Yamazaki R., Kanagawa Y., Jimbo G., Journ.Chem.Eng.Jap., 5, 1974, 373
12. Kroll W., Forsch. auf dem Gebiete des Ingenieurwessens, 20, 1, 1954,2
13. Gutman R.G., Trans.Inst.Chem.Engrs, 54, 3, 1976,176

HYDRODYNAMIC CHARACTERISTIC OF PNEUMATIC FLASH DRYERS

A. Kmieć
S. Mielczarski

Inst. Chem. Eng. Technical University of Wrocław,
50-370 Wrocław, Wybrzeże Wyspiańskiego 27 /Poland/

ABSTRACT

Investigations of the hydrodynamics of a pneumatic flash dryer with two different types of spouting chamber are reported. Relations of pressure drop, residence time of particles and slip velocity have been determined and verification of particle - wall friction factors has been carried out.

NOMENCLATURE

A = cross - sectional area of pipe or chamber, m^2
D = diameter of pipe or maximum diameter of chamber, m
F = volume flow rate of gas, m^3/s
f = friction factor,
g = acceleration due to gravity, m/s^2
h = height, m
L = pipe length, m
m = mass flow rate, kg/s
Δp = pressure drop, Pa
S = volume flow rate of solid, m^3/s
w = superficial gas velocity, m/s
ε = voidage fraction,
ρ = density, kg/m^3
$\tau_{p(g)}$ = shear stress, Pa
$\tau_{k(r)}$ = time, s

Subscripts

f = fluid
g = gas
j = unit
k = chamber
p = particle
r = pipe
s = solid
t = terminal

INTRODUCTION

Pneumatic flash dryers constitute a group of dryers being a modification of pneumatic dryers. The basic element that makes distinctive pneumatic flash dryers is a chamber placed between two vertical pipe sections. As a result of the velocity decrease in the chamber particles transported by gas are recirculated. Because of this phenomenon the residence time of particles increases considerably. For given flow conditions, it is possible to keep the assumed moisture content of outlet particles in an apparatus with shorter pipe sections and thus a lower height. The above properties of the apparatus also offer the prospect of limiting of heat losses to the environment: this may constitute a considerable component of energy balance in the case of dryers (1-3). Earlier papers (3,4) provided a basis for continuation of hydrodynamic investigations of a pneumatic flash dryer with spouting chambers of various shapes and dimensions. In this paper dependences of pressure drop, residence time and slip velocity are reported and particle - wall friction factors have been varified.

REVIEW OF PREVIOUS WORK

The complicated character of hydrodynamics in pneumatic flash dryers results from interrelations of various phenomena such as agglomeration and recirculation of particles (4,5), stream turbulence (6), distributions of mass and linear velocity of particles (4,7). Under the conditions of steady - state pneumatic transport the pressure drop is described by the following equation (3,12,14)

$$-\frac{dp}{dz} = (1-\varepsilon)\rho_p g + \frac{4}{D}(\tau_g + \tau_p) \qquad (1)$$

The particle - wall friction term (τ_p) is defined by analogy with the gas - wall friction term:

$$\tau_p = \frac{1}{2} f_p \rho_p (1-\varepsilon)\left[\frac{S}{A(1-\varepsilon)}\right]^2 \qquad (2)$$

The relation between particle concentration and the slip velocity of particles may be expressed by Richardson-Zaki

equation (8,9)

$$\frac{F}{A} = \frac{S\,\varepsilon}{A(1-\varepsilon)} + w_t\,\varepsilon^n \qquad (3)$$

At first this equation was obtained for fluidized and settling particles but later (9-11) it has been shown that this formula is useful for the description of pneumatic transport dynamics where porosities are close to unity (ε= 0,95-1,0). Hence eq. (3) may be simplified to the following form

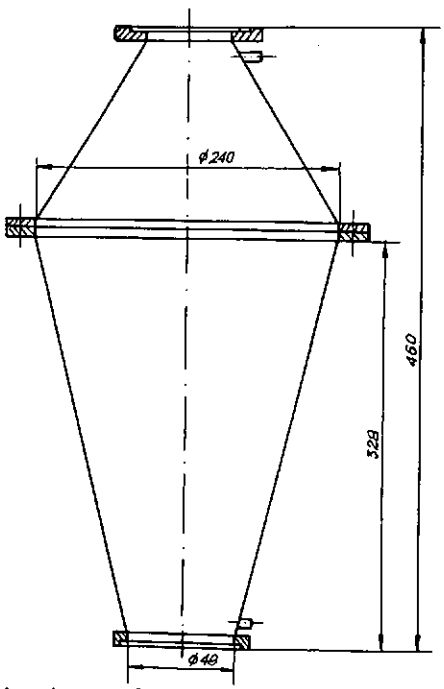

Fig. 1. Chamber of KD type

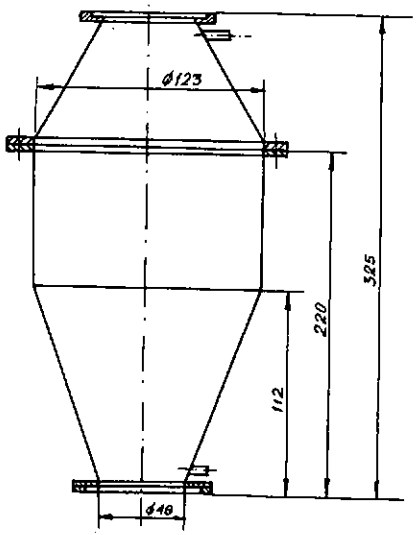

Fig. 2. Chamber of KM type

$$\frac{F}{A} = \frac{S}{A(1-\varepsilon)} + w_t \qquad (4)$$

This means that the slip velocity of particles is equal to the terminal free falling particle velocity. Capes and Nakamura (12) carried out an analysis of experimental data using the formula (4) which showed that the tangent of the inclination angle of the line was in the range of one to two but the constant was approximately equal to the terminal velocity. In some cases the aerodynamic slip velocity of particles was then higger than the terminal free falling particle velocity. Such results were also obtained earlier (13). In general these

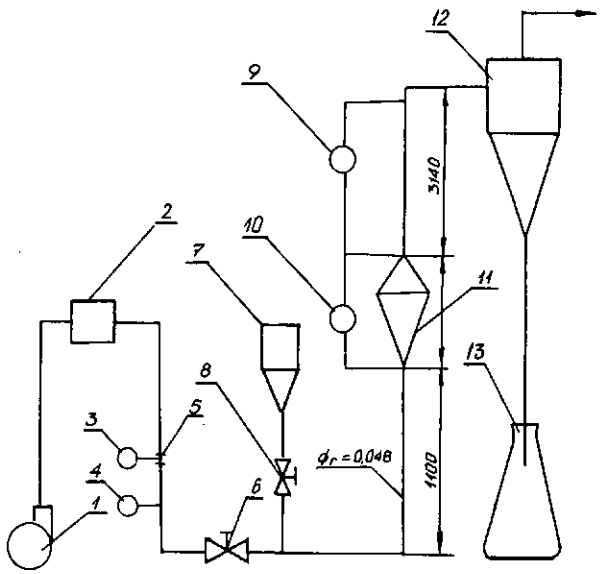

Fig. 3. Schematic diagram of apparatus. 1 - blower, 2 - buffer tank heater , 3 - U-manometer, 4 - thermometer, 5 - calibrated double orifice, 6 - valve, 7 - hopper, 8 - valve, 9,10 - optic manometers, 11 - spouting chamber, 12 - cyclone, 13 - container.

effects may be explained only be the assumption of particle recirculation and the resulting particle - wall friction.

EXPERIMENTAL EQUIPMENT

Hydrodynamic characteristics of a pneumatic flash dryer has been determined for an apparatus with two different spouting chambers. The details and dimensions of the chambers are shown in Fig. 1 and 2. Experiments have been performed using the equipment shown in Fig. 3. The main part of it is a dryer with a chamber at the end divided by hand values in order to measure the particles holdup. The pipe diameter was 4.8 cm and the total height of the unit was about 5 m.

Operating procedure

After turning on the blower the gas flow rate was set by valve adjustment and presseure drop measurement on a calibrated double orifice. Pressure drops on respective parts of the drier were measured with optic water manometers with an accuracy of 0,01 mm water. Next, the valve under the tank with solids was opened and the particles were fed into an air streem. The pressure drops ware measured again. At the end of the measurement, after 10 min., the three valves were closed simultaneously and the solids trapped were blown out through the tee at bottom of the line. By opening the consecutive valves the solids which had been trapped in the test section were removed and their weight recorded.

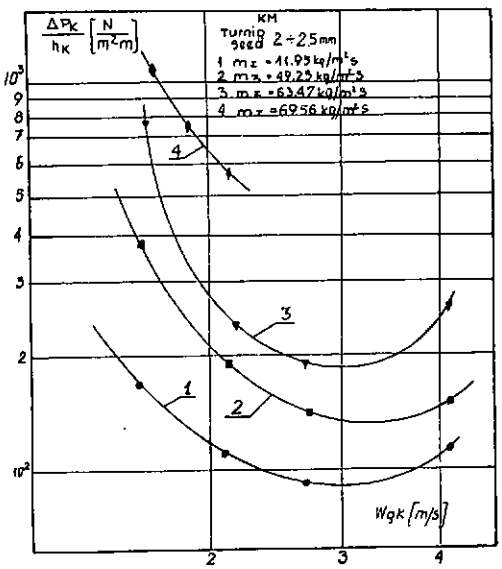

Fig.4. Dependence of unit pressure drop on superficial gas velocity for the KD chamber

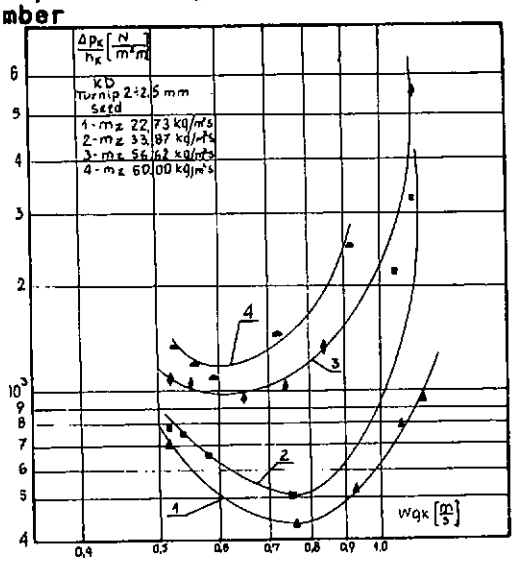

Fig.5. Dependence of unit pressure drop on superficial gas velocity for the KD chamber.

Properties of particles

The materials investigated consisted of 2 fractions of turnip seed and a fraction of silica gel. The physical properties are summarized in Table 1. The solid density was determined pycnometrially with water. The particle diameter d_p of the fractions was calculated from the geometrical average of the diameters of adjacent screens. The particle density was

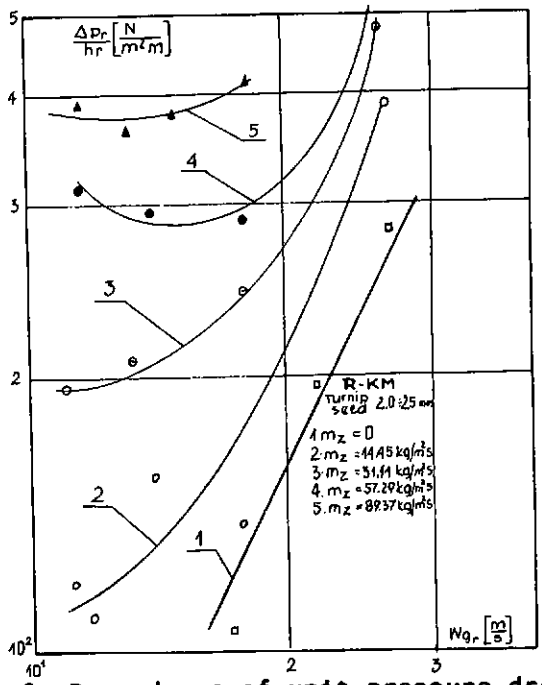

Fig.6. Dependence of unit pressure drop on superficial gas velocity for pipe section working with the KM chamber.

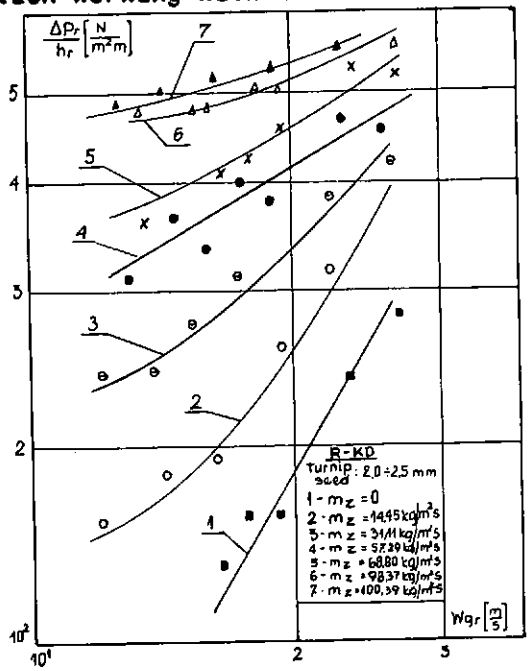

Fig.7. Dependence of unit pressure drop on superficial gas velocity for a pipe section working with the KD chamber.

calculated from measurements of the weight and volume of a number of particles.

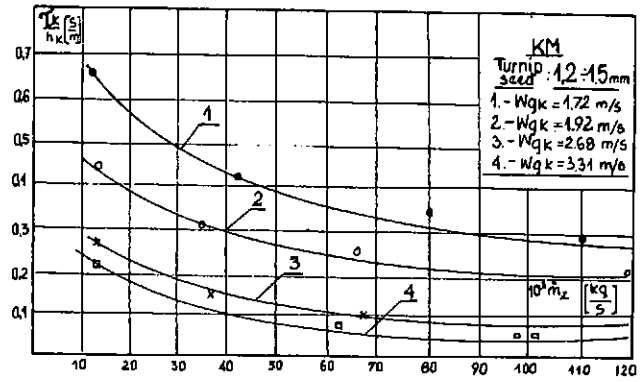

Fig.8. Dependence of unit mean residence time in the KM chamber.

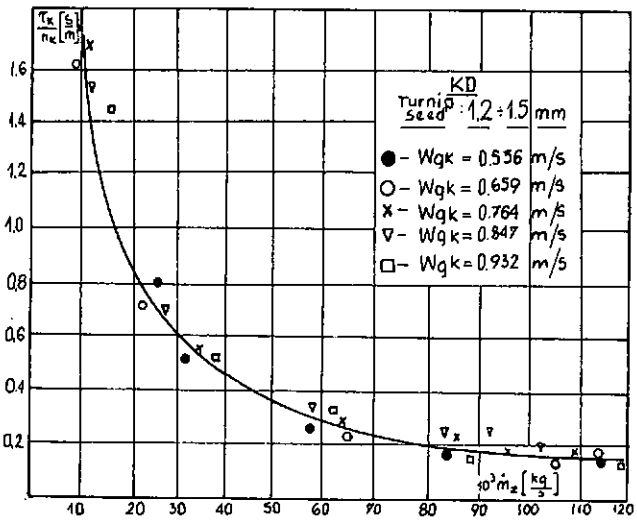

Fig.9. Dependence of unit mean residence time in the KD chamber.

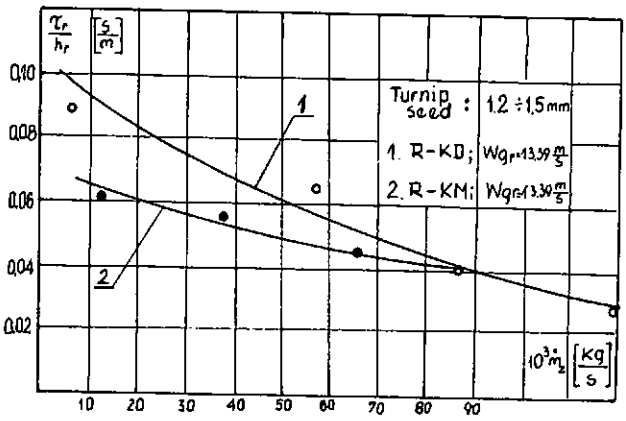

Fig.10. Dependence of unit mean residence time in a pipe section.

EXPERIMENTAL RESULTS AND DISCUSSION

Based on measurements the following parameters were determined: pressure drops on a unit length of the pipe section and a chamber, mean residence times, particle - wall friction factors, linear velocity of solid ($w_p = S/[A(1-\varepsilon)]$). For the conical - cylindrical - conical chamber these parameters were calculated assuming a pipe shape with a total length L and a larger diameter D.

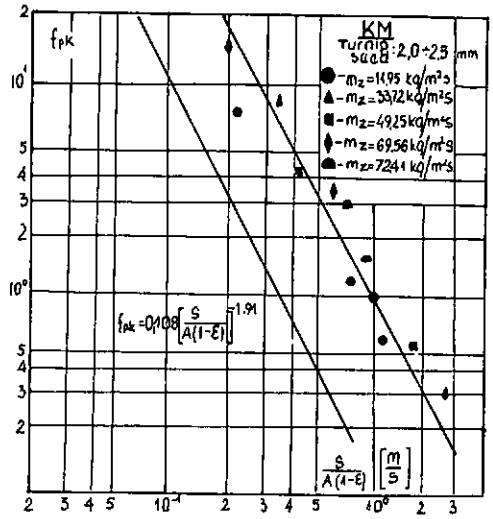

Particle - wall friction factor as a function of particle velocity for the KM chamber.

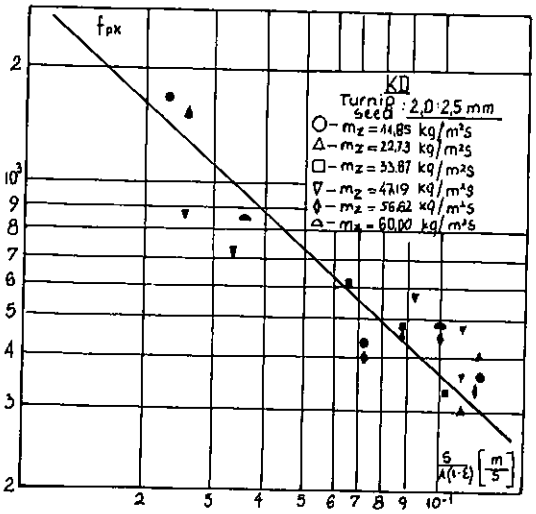

Fig.12. Particle - wall friction factor as a function of particle velocity for the KD chamber.

The experimental results of pressure drops in the chambers of both types KM and KD as a function of superficial gas velocity and a solid phase mass flow rate are shown in Figs. 4 and 5.
The respective curves are shifted upwar-

ds with solids load increase and all of them have the characteristic minimum of the pressure drop. As one could expect, the pressure drops in the chamber of KD

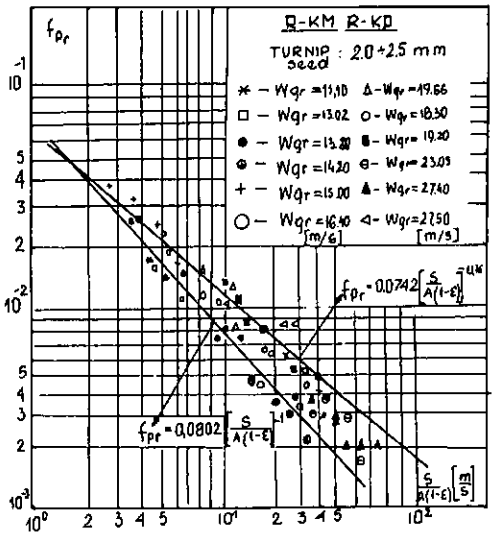

Fig.13. Particle - wall friction factor as a function of particle velocity for a pipe section.

Table 1. Properties of the particles

Material	Fraction ($x10^{-3}$m)	Particle diameter d_p ($x10^{-3}$m)	Particle density ρ_p (kg/m^3)
Turnip seed	2,5-2,0 1,5-1,2	2,24 1,34	802,0 802,0
Silica gel	4 - 3	3,46	1154,0

type are higher than those in the chamber of KM type. This results from a higher concentration of solids in the chamber KD for a given gas flow rate. The pressure drops measured on the upper pipe section working with both chambers respectively are shown in Figs 6 and 7. It is seen from Fig. 7 that higher pressure drops in the pipe section are present in the case of the chamber KD only for very high solid flow rates.
Mean residence times of particles are shown in Figs 8 and 9 as a function of the solid flow rate and superficial gas velocity. The mean residence time of particles decreases in the chamber KM with both the solid flow rate and gas velocity but for the chamber KD, only the effect of the solid flow rate is important. In the case of the chamber KD, the values of the mean residence time are higher than those for the case of the chamber KM. It appears that the presence of the chamber also influences the mean residence time of particles in the pipe section (Fig.10) For low solid flow rates, mean residence times in the pipe section are higher in the case of the chamber KD. This effect results from the fact that for this arrangement the length of particle acceleration is longer because most of the particles have lost their velocity in the chamber.
The analysis of particle - wall friction factors in chambers (Fig. 11 and 12) shows that their values are 40 - 50 times higher for the chamber KD than in the chamber KM. This may be accounted for by a higher rate of particle recirculation in the chamber KD. The particle - wall friction factors measured in the pipe section working with both chambers are shown in Fig. 13. As can be seen the results may be approximated by the equation

$$f_p = 0{,}0742\left[\frac{S}{A\,(1-\varepsilon)}\right]^{-0{,}75} \qquad (5)$$

which has been obtained recently (3) for a pneumatic flash dryer with smaller dimensions. Based on the results of Van Swaaij et al (14) the equation obtained

$$f_p = 0{,}0802\left[\frac{S}{A\,(1-\varepsilon)}\right]^{-1{,}0} \qquad (6)$$

gives only slighly lower values.
Correlations of gas and particle velocity for all solids are given in Table 2. These equations describe the slip velocity of particles and thus their mean residence time in the respective sections of the apparatus. The slope of the lines obtained from these relations is in general lower than in the case of a typical pneumatic system. This effect results from the action of spouting chambers.

CONCLUSIONS

1. Pressure drops in the spouting chambers of a pneumatic flash dryer depend on the flow rates of both phases and they increase with the ratio of the chamber diameter to the riser pipe diameter.
2. For high loads of solids the pressure drop in the pipe section of a pneumatic flash dryer is higher than the respective one in a pneumatic riser.
3. The mean residence time of solids in the chamber of KM type decreases with an increase in the flow rates of both phases, whereas in the chamber of KD type the effect of solids load is an important one.
4. The dependence of gas velocity on particle velocity is in general slighter

Table 2. Correlations of superficial gas velocity and particle velocity ($w_p = \frac{S}{A(1-\varepsilon)}$)

The chamber of KM type		
Turnip seed: 1,5-1,2 mm	w_{gk}=0,454	w_{pk}+0,912
Turnip seed: 2,5-2,0 mm	w_{gk}=0,550	w_{pk}+1,12
Silica gel: 4 - 3 mm	w_{gk}=0,487	w_{pk}+1,63
The chamber of KD type		
Turnip seed: 1,5-1,2 mm	w_{gk}=0,425	w_{pk}+0,475
Turnip seed: 2,5-2,0 mm	w_{gk}=0,480	w_{pk}+0,340
Silica gel: 4 - 3 mm	w_{gk}=0,804	w_{pk}+0,230
Pipe section - KM		
Turnip seed: 1,5-1,2 mm	w_{gr}=0,204	w_{pr}+10,0
Turnip seed: 2,5-2,0 mm	w_{gr}=0,309	w_{pr}+8,34
Silica gel: 4 - 3 mm	w_{gr}=1,01	w_{pr}+5,68
Pipe section - KD		
Turnip seed: 1,5-1,2 mm	w_{gr}=0,215	w_{pr}+12,55
Turnip seed: 2,5-2,0 mm	w_{gr}=0,333	w_{pr}+11,44
Silica gel: 4 - 3 mm	w_{gr}=0,885	w_{pr}+ 8,69

than in the case of a pneumatic riser.

1. G. Nonhebel and A.A.H. Moss, Drying of Solids in the Chemical Industry, Butterworths, London, 1971, chap. 12.
2. Cz.Strumiłło, Bases of theory and technique of drying, WNT, Warsaw, 1975, chap. 8 (in Polish).
3. A.Kmieć, S.Mielczarski, J.Pająkowska, Powder Technol., 20 (1978) 67.
4. A.Kmieć, S.Mielczarski, J.Sobesto,Inż. Ap. Chem. 4 (1978) 10.
5. J.W. Van Breugel, J.J.M. Stein, R.J. de Vries, Proc. Instn. Mech . Engrs, 148 (3C),(1969) 70, 18.
6. R.G. Broothroyd, Trans. Instn. Chem. Engrs., 45 (1967) 297.
7. C.S. Rao, A.E. Dukler, IEC Fund., 10 (1971) 520.
8. J.F. Richardson, W.N. Zaki, Trans.Inst. Chem. Engrs., 35 (1954) 35.
9. C.E. Capes, Can. J. Chem. Eng. 49 (1971) 182.
10. L.S. Leung, R.J. Wiles, D.J. Nicklin, IEC Proc. Des. Dev. 10 (1971) 183.
11. R.M. Ormiston, Ph.D. Thesis, Univ. of Cambridge (1966).
12. C.E. Capes, K.Nakamura, Can. J. Chem. Eng., 51 (1973) 31.
13. J.D. Doig, G.H. Roper, Aust. Chem. Eng., 4, 4 , (1963), 9.
14. W.P.M. Van Swaaij, C.Buurman, J.W. Van Breugel, Chem. Eng. Sci., 25 (1970) 1818 .

HEAT AND MASS TRANSFER IN PACKED BEDS

M. Parti

Department of Chemical and Food Engineering, Technical University
Budapest, Hungary

ABSTRACT

Packed beds of granular solid materials are used extensively in various chemical operations, such as drying, extraction, adsorption and heat regeneration. In order to determine the heat and mass transfer coefficients necessary in design and analysis of these operations, numerous studies have been carried out mainly on laboratory size equipment. To recover deficiency, some research measurements were performed by laboratory and semi-plant apparata. Flow-through drying has been chosen for experimental examinations. The transfer factors were determined by adaption of experimental results and solution of mathematical models. - The error function has been applied, determined by means of the critical drying time, different from routine up to now. The experimental results can be described by the following relations:

$$\psi j_M = 0.78\ Re^{-0.5}$$

$$j_H = 1.1\ j_M$$

which can be used within the range $70 < Re < 900$. The received results correspond well with those ones mentioned in literature. For our examinations, the heat transfer factor can be estimated by knowledge of the friction factor of packed layers and by help of the analogy, set up in our previous studies.

NOMENCLATURE

a_p = specific surface, m^2/m^3
C = constant
c = specific heat, Wh/kgK
D_p = particle size, m
e^p = non-dimensional roughness--size
f = friction coefficient
G = mass flux density of the drying medium, kg/m^2h
$j_H = \frac{\alpha}{GC_n} Pr^{2/3}$ = factor of heat transfer
$j_M = \frac{\beta_x}{G} Sc^{2/3}$ = factor of mass transfer
n = exponent
α = heat transfer coefficient, W/m^2K
β_x = mass transfer coefficient, kg/m^2h
ρ = density, kg/m^3
ψ = porosity, m^3/m^3
μ = dynamic viscosity, kg/mh

Dimensionless numbers

Pr = Prandtl number
$Re = \frac{GD_p}{\mu}$ = Reynolds number
St = Stanton number

Subscripts

H = heat transfer
M = mass transfer
p = particle

INTRODUCTION

Examination of heat and mass transfer processes in packed columns, determination of heat and mass transfer coefficients of particle/gas-systems have been carried out first by Gamson (1) in 1943. He has evaporated water from porous particles and has determined transfer coefficients from constant drying velocity. Subsequently, many inventions were published on these problems and several authors have applied Gamson's method for experimental determination of transfer coefficients. This method assumed the thickness of the packed layer to be smaller than the length of the desorption zone. Then, during the

evaporation of surface moisture, drying occurs simultaneously at the total thickness of the layer: the surface of transfer is the total bed-surface. The state characteristics of the drying medium leaving the packed layer remain constant during the evaporation of surface moisture. Drying velocity and transfer coefficients, respectively, can be calculated on the basis of measurements of state characteristics. Furthermore, the temperature of the evaporating particles (surface) had to be measured, too, or assumptions had to be made to estimate this value.

The layers examined by this method had a thickness of several centimeters. Application of obtained results for thick beds, however, are brought into challenge by several authors, due to the inlet and outlet effects. We have carried out experimental measurements with thick beds for elimination of existing deficiencies, (the thickness of the beds surpassed the length of the desorption zone). The results of the measurements are reported in this present paper.

1. EXPERIMENTAL EXAMINATION METHOD

The flow-through drying method has been chosen for experimental examinations, the drying medium was air. Following dimensions have been applied: the diameters of the flow-through dryers were 400 mm and 80 mm, resp., bed-heights varied between 50 mm and 700 mm. Three types of particles have been used for our experiments, i.e. two kinds of tabletted adsorbents (trade-name: "Agelon") and wooden balls. These particles are very hygroscopic, their wetting has been achieved by soaking them in water. The main characteristics of the particles and the packed bed, respectively, are listed below:

Particle	Shape	D_p mm	a_p m^2/m^3	ψ m^3/m^3	ρ_p kg/m^3	c_p kJ/kgK
wooden ball	sphere	18	187	0.467	739	1.47
Agelon	tablet	8	504	0.328	747	0.84
Agelon	sphere	7.16	500	0.40	1916	0.84

For the sake of elaboration of measurements and determination of the transport coefficients, information has to be acquired on the drying process. That means, measurements for the state characteristics of the process have to be carried out. These measurements may concern temperature and moisture content of the drying medium and also of the material to be dried.

In the course of our investigations the following characteristics have been continuously measured:

- temperatures of inlet and outlet drying media, measured by means of thermocouples;
- moisture content of inlet and outlet drying media, partly by measuring dew-point temperature and partly by measuring wet temperature;
- temperature of the drying bed, measured by means of thermocouples built in the particles.

Measurement series have been carried out, too, by which the moisture content of the packed layer has been measured almost continuously, at some points of different heights. The measuring sensor has indicated electric capacity of the packed layer and its variation, respectively. Electric capacity of the packed layer is a function of moisture content and temperature. Above the critical moisture content, however, the temperature of the evaporating medium can be regarded as practically constant; hence, there exists an univocal relationship between electric capacity and moisture content.

The experimental measurements were carried out in the following way: the volume of the drying air and the desired heating power have been adjusted. After having started the fan and the calorifer, the system has been operated until the state characteristics of air turned steady; thus, the system and its environment were in equilibrium. After this, the previously wetted particles of volume measured in advance, have been placed into the drying chamber and measurements could be started. The investigated state characteristics were fixed, according to the foregoing considerations and the measurements have been continued until the temperature of the outlet drying medium approached the value of that one measured in the entering cross section. Then the mass of the bed, consisting of dried particles has been measured and its moisture content has been determined. The heat and mass balance of the experimental examinations have been carefully checked; the maximum error concerning the mass balance has been 5% and that one of the heat balance 4%.

2. EVALUATION METHOD OF EXPERIMENTAL MEASUREMENTS

The evaluation of experimental measurements could not be achieved neither by application of Gamson's (1) nor other recently developed methods (2), since the drying procedure of beds being thicker than the desorption zone, differs

essentially from drying of short layers. In case of thick particle layers evaporation of the surface moisture into the warm gas stream occurs within a relatively narrow band and this band moves on slowly, in the flow direction of the drying medium. This band is named the desorption zone (3). The outlet drying gas grows practically saturated when reaching the adiabatic saturation temperature. The state characteristics of the drying gas leaving the system will remain unchanged until the desorption zone rests within the wetted particle layer. If this desorption zone reaches the edge of the particle layer, the state characteristics of the outlet drying medium will change, i.e. the gas leaves in a more and more saturated state. The period of our investigations, until which the state characteristics (temperature, moisture content) of the outlet drying material remain practically constant, is called critical time.

While drying such beds, the thickness of the simultaneously evaporating particle layer is not known in advance; and on the other hand, the temperature of the wet evaporating bed varies along the bed-height.

Thus, a new evaluation method had to be elaborated to which the previously developed mathematical model has been applied (4). The basic idea for the determination of the transfer coefficients has been the following:

- the response of the examined system (drying wet material, drying medium) has been determined by measurements of given inlet values;
- accepting the mathematical model of the process as correct, the "response" of the model is adapted to that one of the system, by variation of the requested transport coefficients;
- in the course of adaption, the minimum value of the error function is aimed at.

According to computerized processing of experimental results, we have stated that it seems most expedient to use critical time as error signal for the error function. Critical time is highly responsive to the variation of requested transport coefficients in every range, having the special advantage that it is the linear function of these coefficients. Critical time can be determined from experimental measurements with relatively high accuracy.

3. RESULTS OF EXPERIMENTAL EXAMINATIONS

Heat and mass transfer coefficients of experimental measurements have been determined by aid of the method described in the foregoing chapter and then, the non-dimensional factors of heat and mass transfer, too. The results, determined for two series of the experimental examinations have been summarized in Tables 1 and 2. The values given in Table 1 refer to experimental measurements carried out in larger size equipments, while those ones given in Table 2 refer to experimental results, carried out in smaller size equipments. Some values given in Table 2 represent the mean value of several measurements of approximately equal parameters. The transfer factors have been shown as functions of the Reynolds number.

On the basis of the diagrams it can be definitely stated that the transfer factors referring to different porosity values are functions different from the Reynolds number, although the measured values can be described well by power functions. Accordingly, the received correlation is:

$$j_i = C\ Re^{-n} \qquad (1)$$

where the constants are:

ψ	C_H	n_H	C_M	n_M
0.328	1.23	0.373	1.09	0.378
0.400	2.77	0.555	2.51	0.553

Table 1

ψ = 0.328

Serial Nos:	Re	α W/m^{2}K	β_x kg/m^{2}h	j_H	ψj_H	j_M	ψj_M
1/1	426	174	610	0.127	0.0418	0.117	0.0384
2/1	450	172	590	0.119	0.0391	0.107	0.0351
3/1	542	192	660	0.109	0.0368	0.098	0.0323
4/1	866	267	920	0.095	0.0312	0.086	0.0281
5/1	700	244	840	0.107	0.0350	0.096	0.0315
6/1	860	273	940	0.097	0.0319	0.087	0.0287
7/1	717	244	840	0.104	0.0342	0.094	0.0308
8/1	677	227	780	0.104	0.0341	0.093	0.0307
9/1	444	173	600	0.119	0.0393	0.109	0.0357
10/1	377	165	565	0.136	0.0447	0.122	0.0401
11/1	443	180	620	0.132	0.0432	0.119	0.0390

Table 2

$\psi = 0{,}400$

Serial Nos:	Re	α W/m^{2}K	β_x kg/m^{2}h	j_H	ψj_H	j_M	ψj_M
1-6/2	251	127	437	0.135	0.0539	0.121	0.0485
7-8/2	191	110	380	0.145	0.0580	0.131	0.0525
9-13/2	152	107	368	0.170	0.0681	0.153	0.0613
14/2	78	81	280	0.258	0.1030	0.233	0.0933
15/2	113	93	320	0.209	0.0837	0.189	0.0754
16/2	139	98	336	0.180	0.0719	0.162	0.0646
17/2	163	102	352	0.162	0.0649	0.147	0.0589
18/2	186	105	360	0.149	0.0598	0.134	0.0537
19/2	203	110	380	0.145	0.0580	0.131	0.0525
20/2	218	119	408	0.143	0.0572	0.128	0.0513

The product of transfer factors and porosity, however, are already unique functions of the Reynolds number:

$$\psi j_H = 0.792\ Re^{-0.483} \qquad (2)$$

and

$$\psi j_M = 0.748\ Re^{-0.492} \qquad (3)$$

According to close approximation, the exponents can be considered as (-0.5) and hence, the above functions can be written as:

$$\psi j_H = 0.88\ Re^{-0.5} \qquad (4)$$

and

$$\psi j_M = 0.78\ Re^{-0.5} \qquad (5)$$

thus

$$j_H = 1.1\ j_M \qquad (6)$$

Figure 1 shows the product of transfer factors and porosity as a function of the Reynolds number, and the functions corresponding to Eqs (4) and (5).

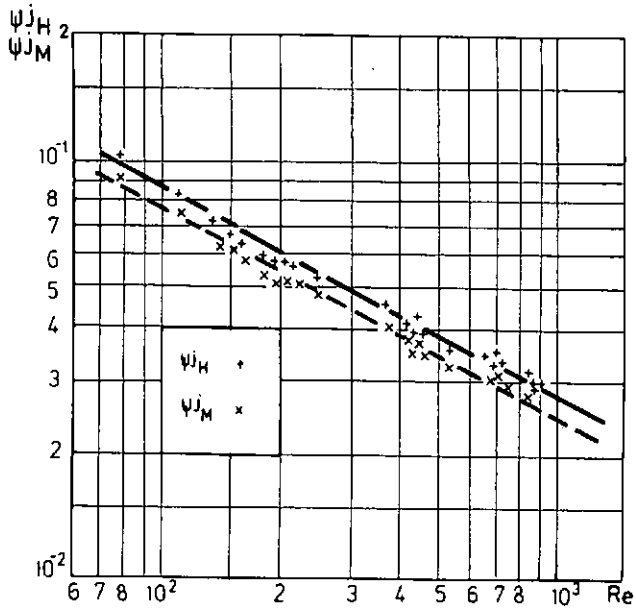

Figure 1 Product of Heat Transfer and Mass Transfer Factors and Porosity vs. Reynolds Number

The range of applicability of the measurement results is:

$$70 < Re < 900$$

$$0.328 < \psi < 0.4$$

Eqs (4) and (5) correspond well to the results in the references, measured at laboratory conditions. Hence, e.g. according to Beek (5):

$$\psi j_M = (0.6 \pm 0.10)\ Re^{-0.43} \qquad (7)$$

if

$$50 < Re < 2000$$

or

$$\psi j_M = (0.81 \pm 0.05)\ Re^{-0.5} \qquad (8)$$

if

$$5 < Re < 500$$

and by aid of computerized processing of the data taken from literature, Dwivedi(6) has obtained the following results:

$$\psi j_M = 0.4548\ Re^{-0.4069} \qquad (9)$$

if

$$Re < 10$$

Thus, on the basis of our investigations, the experimental results obtained in laboratory-size equipment and for short packed layers are definitely applicable to long beds and large-scale equipment, too. In the course of our investigations no re-

lation could be established between thickness of the packed layer and transfer coefficients. According to our examinations, checking the dependency on porosity, the results applied to the earlier statements in the references, too. The results of Rowe (7) were used on this occasion.

The analogy between transfer coefficients of transport processes developing in packed columns, is still a debated question. In our opinion, in such cases there must exist some direct relation between the transfer coefficients, e.g. between the heat transfer and friction coefficients. For the sake of setting up a relation between the transfer coefficients, a new geometrical model has been applied to the packed layer, i.e. the packed bed has been replaced by a capillary tube-bundle of rough surface. The diameter of the capillaries is equal to Carman's hydraulic equivalent diameter, roughness-size has been determined by geometrical examination of the packed bed. The hydraulic theory of rough tubes has been applied to this geometrical model and by the aid of the friction coefficients of packed layers given in literature, the modified friction law of Prandtl-Nikuradse (8) for packed beds has been deduced.

The friction law (9) for packed layers can be written as:

$$\sqrt{\frac{6}{f}} = 2.5 \ln\left(\frac{Re}{1-\psi}\sqrt{\frac{f}{6}}\right) - 6.32\left(\frac{Re}{1-\psi}\right)^{0.135} + 2.2 \qquad (10)$$

Hereupon, a physical model was set up for the heat transfer process of packed layers.

For the relation of heat transfer and friction coefficient the following equation has been obtained:

$$\psi St = \frac{\sqrt{\frac{f}{6}}}{2.12 \ln\left(\frac{Re}{1-\psi}\sqrt{\frac{f}{6}}\right) + \beta(Pr,e^+)} \qquad (11)$$

where

$$\beta(Pr,e^+) = 4.9 - 5.37\left(\frac{Re}{1-\psi}\right)^{0.135} - 2.7\psi^{0.5}\left(Re\sqrt{\frac{f}{6}}\right)^{-0.5} + 0.158\left(\frac{Re}{\psi}\sqrt{\frac{f}{6}}\right)^{0.5}(3Pr^{2/3}-1) \qquad (12)$$

According to our examinations Eqs (10), (11) and (12) can be applied satisfactorily to the determination of friction coefficient and heat transfer coefficient of packed layers. Their application to our experimental results are demonstrated in Figure 2.

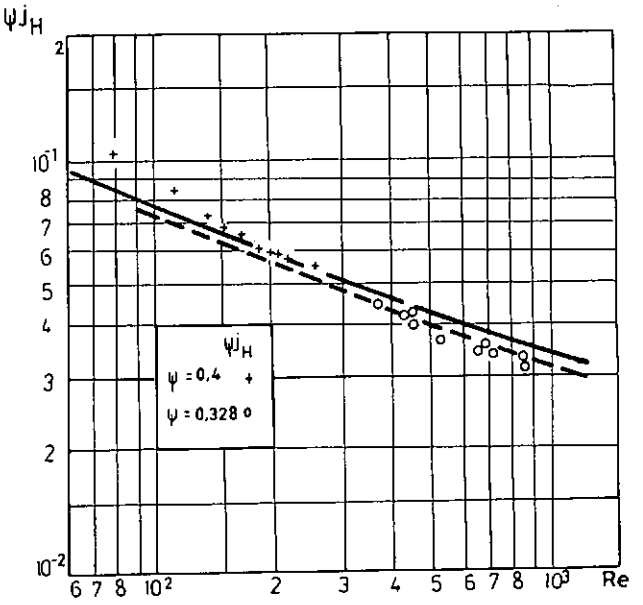

Figure 2 Comparison of Experimental Results and Analogy

SUMMARY

The present paper deals with the results obtained by experimental examinations of thick beds (considerably thicker than the desorption zone). According to our investigations it is univocal that the earlier results, received for laboratory conditions, can be applied satisfactorily to the determination of transfer coefficients of thick beds. Our studies on analogy were also briefly mentioned from which we have stated that analogy can be applied to transfer coefficients of packed layers, too.

REFERENCES

1. Gamson,B.W. et al., Trans.Am.Inst. Chem.Engrs, 39,1 (1943)
2. Wakao,M.-Funazkri,T., Chem.Eng.Sci. 33,p.1375 (1978)
3. Treybal,R.E., Mass Transfer Operations, McGraw Hill Book Co., (1963)
4. Palácz,B.-Parti,M., Acta Technica, 74, p.441 (1973)
5. Davidson,J.F.-Harrison,D., Fluidization, Academic Press, London, (1971)
6. Dwivedi,P.N. et al., Ind.Eng.Chem., PDD., 16,p.157 (1977)
7. Rowe,P.N.-Claxton,K.T., Trans.Inst. Chem.Eng. 43, T321 (1965)
8. Reynolds,A.J., Turbulent Flow in Engineering, John Wiley, London, (1974)
9. Parti,M., Periodica Polytechnica, 23, 3. (1979)

RATES FOR FREEZE DRYING

A. I. Liapis

Department of Chemical Engineering
University of Missouri-Rolla, Rolla, Missouri 65401 USA

ABSTRACT

A mathematical model which describes the nonsteady state heat and mass transfer operations during the freeze drying process is presented. Both sublimation and adsorption are permitted to take place simultaneously so that a sorbed moisture concentration gradient is predicted to occur across the porous layer as drying proceeds. Numerical solutions to these adsorption-sublimation model equations are shown to agree quite closely with experimental data over the entire drying period. It is also shown by comparison with experimental data that the adsorption-sublimation model predicts the experimental terminal drying rates quite more accurately than the sublimation (1), and the uniformly retreating ice front (URIF), (3), models.

NOMENCLATURE

C_{pI}, C_{PII}, C_{pg}, C_{PIe} = heat capacities

C = weight fraction of bound water in dried layer

C_{01} = constant dependent only upon structure of porous medium and giving relative D'Arcy flow permeability

C_1 = constant dependent only upon structure of porous medium and giving relative Knudsen flow permeability

C_2 = constant dependent only upon structure of porous medium and giving the ratio of bulk diffusivity within the porous medium to the free gas bulk diffusivity, dimensionless

$D_{w,in}$ = free gas mutual diffusivity in a binary mixture of water vapor and inert gas

$D^o_{w,in} = D_{w,in}P$

$f(T_x)$ = water vapor pressure-temperature functional form = $133.32 \exp(23.9936 - 2.19\ \Delta H/T_x)$, N/M^2

k = thermal conductivity

k_1 = bulk diffusivity constant = $C_2 D^o_{w,in} K_w / (C_2 D^o_{w,in} + K_{mx} P)$

k_2, k_4 = self diffusivity constant = $K_w K_{in} / (C_2 D^o_{w,in} + K_{mx} P) + (C_{01}/\mu_{mx})$

k_3 = bulk diffusivity constant = $C_2 D^o_{w,in} K_{in} / (C_2 D^o_{w,in} + K_{mx} P)$

K_g = internal mass transfer coefficient for desorption

K_w = Knudsen diffusivity, $K_w = C_1 \sqrt{(RT/M_w)}$

K_{in} = Knudsen diffusivity, $K_{in} = C_1 \sqrt{(RT/M_{in})}$

K_{mx} = mean Knudsen diffusivity for binary gas mixture, $(K_{mx} = y_w K_{in} + y_{in} K_w)$

L = sample thickness

M = molecular weight

N_t = total flux $(N_t = N_w + N_{in})$

N_w = water vapor flux

N_{in} = inert gas flux

P = total pressure in dried layer

P_T = total pressure in drying chamber

P_o = drying chamber pressure at surface of dried layer

P_w = partial pressure of water vapor

P_{in} = partial pressure of inert gas

q = radiant energy flux

R = universal gas constant

$T°$ = sample temperature at $t = 0$

T = temperature

t = time

V = velocity of interface

X = position of frozen interface

y_w = mole fraction of water vapor

y_{in} = mole fraction of inert gas

Greek Symbols

α = thermal diffusivity

ε = voidage fraction

ΔH = enthalpy of sublimation

μ = viscosity

ρ = density

Superscripts

0 = initial value at time zero

* = equilibrium value

Subscripts

e = effective value

g = gas

in = inert

Mx = mixture

w = water vapor

X = interfacial value

0 = surface value

I = dried region

II = frozen region

INTRODUCTION

Freeze drying is the process whereby water vapor is removed by sublimation from a frozen material (often a food stuff), usually under the condition of low pressure and the action of radiant heat. The advantages of such a separation process lie in the high quality of the product and they are discussed extensively in (3). Figure 1 is a diagram of the process. Radiant energy is incident at the surface, and is conducted through a dried layer to the interface, where the ice sublimes directly to vapor. Moisture passes through the dried region countercurrent to the heat flow, and eventually condenses onto a refrigerated plate some distance from the sample. The presence of inert gas in the chamber enhances heat flux but at the expense of mass transfer; and operating constraints of interface and surface temperatures exist.

A number of freeze drying models have been published (1, 2, 4, 5, 6), with the earliest due to King (3), who postulated the uniformly retreating ice front (URIF) model. These models are intended to describe drying rates during the removal of the first 60 - 90% of the moisture. The remaining moisture is present due to mechanisms of (i) physical adsorption, (ii) chemical absorption, (iii) water of crystallization. In addition, moisture may be physically trapped within pockets in the material, from which it can leave only via small channels offering a high resistance to mass transfer. Although this 'bound' water constitutes a small proportion of the total, its effect is significant as it frequently takes as long to remove as the free water (7, 8). Sheng and Peck (7) have proposed a model which takes bound water into account. This model is limited, however, by the assumptions

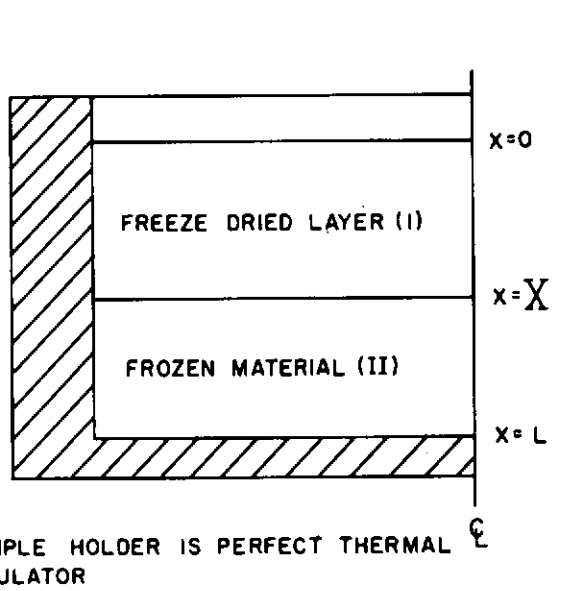

Figure 1 Schematic of Freeze Drying Process

(i) of constant surface and interface temperatures, (ii) of a heat transfer controlled process, and (iii) that bound water leaves only after all the ice has sublimed. The model presented in this paper does not suffer from the above restrictions and in particular, allows desorption and sublimation to take place simultaneously, so that a sorbed moisture gradient will occur across the dried layer as drying proceeds. This is in accordance with the experimental data reported in (9, 10).

MATHEMATICAL MODEL

The one-dimensional system considered in this section is shown in Figure 1. A heat source is positioned above a slab of material of thickness L, which has a frozen and a porous dried region. The boundary between the dried region and frozen region is termed the sublimation interface. The following assumptions have been made in the development of the mathematical model: (1) Only one-dimensional heat and mass flows, normal to the interface and surface are considered. (2) Sublimation occurs at an interface parallel to, and at distance X from, the surface of the sample. (3) The thickness of the interface is taken to be infinitesimal. This assumption has been validated for most applications by Harper (16). (4) A binary mixture of water vapor and inert gas flows through the dried layer. (5) At the ice interface, the concentration of water vapor is in equilibrium with the ice. (6) As the interface recedes, it leaves behind a partially dried layer having a moisture content substantially greater than the equilibrium value at that pressure and temperature. In the porous region, the solid matrix and the enclosed gas are in thermal equilibrium. However, the partial pressure of water vapor is not necessarily in

equilibrium with the solid phase concentration. (7) The frozen region is considered to be homogeneous, of uniform thermal conductivity, density and specific heat, and to contain an insignificant proportion of dissolved gases. (8) The sides and the bottom of the slab are assumed to be perfectly insulated against the transfer of mass and heat.

The model consists of the unsteady state energy and material balances in the dried (I) and frozen regions (II):

$$\frac{\partial T_I}{\partial t} = \alpha_{Ie} \frac{\partial^2 T_I}{\partial x^2} - \frac{N_t C_{pg}}{\rho_{Ie} C_{pIe}} \frac{\partial T_I}{\partial x} - \frac{T_I C_{pg}}{\rho_{Ie} C_{pIe}} \frac{\partial N_t}{\partial x} + \frac{\Delta H \rho_I}{\rho_{Ie} C_{pIe}} \frac{\partial C}{\partial t}, \quad 0 \leq x \leq X \tag{1}$$

$$\frac{\partial T_{II}}{\partial t} = \alpha_{II} \frac{\partial^2 T_{II}}{\partial x^2}, \quad X \leq x \leq L. \tag{2}$$

In the dried layer effective parameters are considered which include the physical properties of both the gas and solid, which have been considered to be independent of space. The initial and boundary conditions are:

$$T_I = T_{II} = T_x = T°(x) \text{ at } t = 0, \ 0 \leq x \leq L \tag{3}$$

$$q = k_{Ie} \frac{\partial T_I}{\partial x} \text{ at } x = 0, \ t > 0 \tag{4}$$

$$k_{II} \frac{\partial T_{II}}{\partial x} - k_{Ie} \frac{\partial T_I}{\partial x} + V(\rho_{II} C_{PII} T_{II} - \rho_I C_{PI} T_I) + N_t C_{pg} T_I = -\Delta H N_t$$

$$\text{at } x = X, \ 0 < t \leq t_{X=L} \tag{5a(i))}$$

$$T_I = T_{II} = T_x \text{ at } x = X, \ 0 < t \leq t_{X=L} \tag{5a(ii))}$$

or

$$\frac{\partial T_I}{\partial x} = 0 \quad \text{at } t > t_{X=L} \tag{5b}$$

$$\frac{\partial T_{II}}{\partial x} = 0 \quad \text{at } x = L. \tag{6}$$

The boundary condition, equation (5), couples the energy equations in the two layers. The continuity equations for the dried region are:

$$\frac{1}{R} \frac{\partial}{\partial t} \left(\frac{P_w}{T}\right) = -\frac{1}{M_w \epsilon} \frac{\partial N_w}{\partial x} - \frac{\rho_I}{\epsilon M_w} \frac{\partial C}{\partial t} \tag{7}$$

$$\frac{1}{R} \frac{\partial}{\partial t} \left(\frac{P_{in}}{T}\right) = -\frac{1}{M_{in} \epsilon} \frac{\partial N_{in}}{\partial x} \tag{8}$$

$$\frac{\partial C}{\partial t} = K_g (C^* - C). \tag{9}$$

C^* is the weight fraction of water in the solid which would be in local equilibrium with the partial pressure of water vapor. A relationship for C^* was fitted by flexible pattern search to the data of King, et al. (11) for freeze dried turkey. It was, however, found impossible to fit an isotherm to the data both below and above 0°C, and separate isotherm expressions were developed. These were based on the Sips type II adsorption isotherms and are:

$$C^* = \frac{2.32 \times 10^{-4} \exp(962.779/T) P_w^{0.1594}}{1 - 0.0101 \exp(962.779/T) P_w^{0.1594}} \tag{10}$$

and

for $T > 0°C$

$$C^* = \frac{1.766 \times 10^{-4} \exp(1035.786/T) P_w^{0.267}}{1 - 3.69 \times 10^{-3} \exp(1035.786/T) P_w^{0.267}} \tag{11}$$

for $T < 0°C$

The standard deviation in the values of C^* was 0.009 for equation (10) and 0.012 for equation (11).

The expressions for the adsorption isotherm of reconstituted instant nonfat milk are reported in (12). It should be noted that model simulations are performed for turkey and reconstituted instant nonfat milk as the foodstuffs.

The diffusion equations of Evans, et al. (9), and the D'Arcy equation for viscous flow, can be used to develop the following equations for the fluxes N_w and N_{in}:

$$N_w = -\frac{M_w}{RT} \left[k_1 \frac{\partial P_w}{\partial x} + k_2 P_w \left(\frac{\partial P_w}{\partial x} + \frac{\partial P_{in}}{\partial x}\right)\right] \tag{12}$$

$$N_{in} = -\frac{M_{in}}{RT} \left[k_3 \frac{\partial P_{in}}{\partial x} + k_4 P_{in} \left(\frac{\partial P_{in}}{\partial x} + \frac{\partial P_w}{\partial x}\right)\right] \tag{13}$$

Equations (12) and (13) can be substituted into equations (7) and (8) and the resulting expressions solved using the following boundary and initial conditions:

$$P_w = P_{wo}, \ P_{in} = P_o - P_w \text{ at } x = 0 \tag{14}$$

$$P_w = P_w^o, \ 0 < x \leq X \quad \text{at } t \leq 0 \tag{15}$$

$$P_{in} = P_{in}^o, \ 0 < x \leq X \quad \text{at } t \leq 0 \tag{16}$$

$$P_w = f(T_X), \ \frac{\partial P_{in}}{\partial x} = 0$$

$$\text{at } x = X, \ 0 < t \leq t_{X=L} \tag{17a}$$

or

$$\frac{\partial P_w}{\partial x} = 0 \qquad \text{at } t > t_{X=L} \tag{17b}$$

$$C = C^0, \quad 0 < x < X, \qquad t \leq 0. \tag{18}$$

The variable P_{wo} above, is the chamber water vapor pressure, usually determined by the condenser design, and assumed constant within the chamber. The model is completely specified by a material balance at the interface which defines its velocity as:

$$V = \frac{dX(t)}{dt} = - \frac{N_w}{\rho_{II} - \rho_I} \tag{19}$$

Equations (1 - 19) represent the adsorption-sublimation model which involves a moving boundary (the position of the interface). These model equations are solved using the numerical method in (13, 14). External transport resistances can be easily incorporated in this model by including the equations presented in (1). In a well designed freeze-dryer the external mass and heat transfer resistances should not be significant.

RESULTS

Figures 2 - 3 show the results obtained from the adsorption-sublimation model simulations using turkey and nonfat milk as the foodstuffs being freeze dried. The values of the model parameters of these foodstuffs are given in (13, 14). It is seen that the adsorption-sublimation model predicts the experimental data better than the sublimation model (1), whose predictions are more accurate than those of the URIF model (3). The URIF and the sublimation models do not account for the heat of sublimation of the bound water phase, and also neglect the adsorption-desorption processes which occur in the dried layer. The adsorption-sublimation model predicts a slower moving interface because part of the heat supplied at the surface of the sample is used for the sublimation of bound water, thus resulting to slower drying rates than those predicted by the other two models. It is important to note the ability of the adsorption-sublimation model in predicting the terminal drying rates quite more accurately than the sublimation and the URIF models.

The adsorption-sublimation model can provide product temperatures and moisture contents as a function of time and geometric location. Since destruction rates of various important nutrients (as well as activation energies) are a function of temperature and moisture content, knowledge of temperature and moisture profiles inside a piece of food during processing is extremely important for predicting the extent of quality deterioration for particular process conditions. This is necessary for determining optimal processing policies (15).

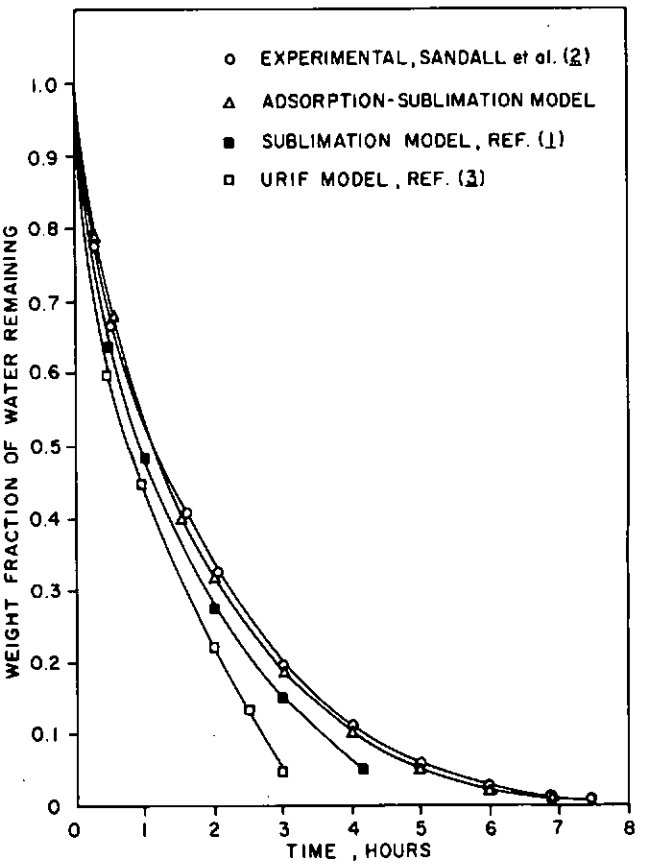

Figure 2 Freeze Drying of Turkey Meat
$K_g = 17.65 \times 10^{-5} s^{-1}$

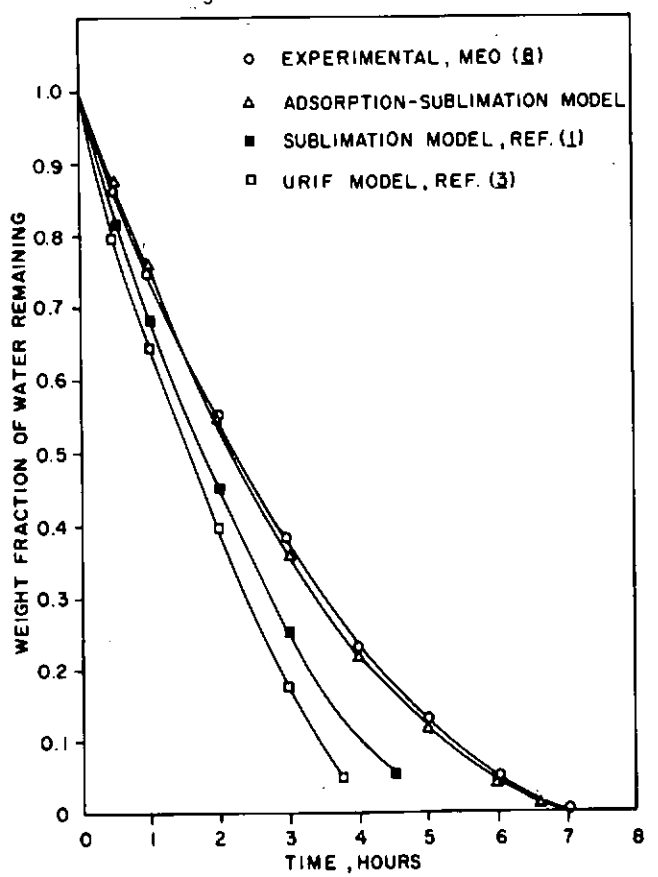

Figure 3 Freeze Drying of Instant Non-Fat Milk
$K_g = 11.08 \times 10^{-5} s^{-1}$

CONCLUSIONS AND REMARKS

The adsorption-sublimation model permits adsorption and sublimation to take place simultaneously, so that a sorbed moisture concentration gradient is predicted to occur across the porous layer as drying proceeds. It was shown by comparison with experimental data that this model predicts the overall drying times, and especially the terminal drying rates quite more accurately than the sublimation and the URIF models. When kinetic data on product deterioration are available, the adsorption-sublimation model may be used with optimal control theory (1) to provide the operating conditions, during freeze drying, that minimize the total drying time as well as the deteriorative changes.

REFERENCES

1. Liapis, A. I., and Litchfield, R. J., Chemical Engineering Science, Vol. 34, p. 975-981, 1979
2. Sandall, O. C., King, C. J., and Wilke, C. R., AIChE Journal, Vol. 13, p. 428-438, 1967
3. King, C. J., Freeze-Drying of Food Stuffs, C.R.C. Critical Review Series, 1971
4. Clark, J. P., and King, C. J., Chemical Engineering Progress Symposium Series, No. 108, Vol. 67, p. 102-111, 1971
5. Moraine, R. A., M.S. Thesis, Illinois Institute of Technology, Chicago, 1953
6. Ginzburg, A. S., and Lyakhovisky, Using Infrared Radiation to Intensify the Freeze Drying Process, Proceedings of the XII International Congress of Refrigeration, Madrid, Spain, 1969
7. Sheng, T. Y., and Peck, R. E., AIChE Symposium Series, No. 163, Vol. 73, p. 124-130, 1977
8. Meo, D., M.S. Thesis, The University of Rochester, Rochester, 1972
9. Meffert, H. T., Freeze-Drying: Physical Aspects, IBVT (now Sprenger Inst.) Annual Report, Wageningen, The Netherlands, 1965
10. Gentzler, G. L., and Schmidt, F. W., Transactions of the ASAE, Vol. 16, p. 179-182, 1973
11. King, C. J., Lam, W. K., and Sandall, O. C., Food Technology, Vol. 22, p. 100-106, 1968
12. Aguilera, J. M., and Flink, J. M., Journal of Food Technology, Vol. 9, p. 391-396, 1974
13. Liapis, A. I., and Litchfield, R. J., Numerical Solution of Moving Boundary Transport Problems in Finite Media by Orthogonal Collocation, Computers in Chemical Engineering (in press)
14. Litchfield, R. J., and Liapis, A. I., Chemical Engineering Science, Vol. 34, p. 1085-1090, 1979
15. Labuza, T. P., Nutrient Losses During Drying and Storage of Dehydrated Foods, C.R.C. Critical Reviews in Food Technology, Vol. 3, p. 217-240, 1972
16. Harper, J. C., AIChE Journal, Vol. 8, p. 298-302, 1962

PREDICTION OF HEAT AND MASS TRANSFER WITHIN A GRAIN KERNEL - A FINITE ELEMENT APPLICATION

Shahab Sokhansanj[1]
R.J. Gustafson[2]

1. University of Saskatchewan, Saskatoon, Sask. S7N 0W0
2. University of Minnesota, St. Paul, Minn 55108

ABSTRACT

The finite element method was utilized to solve the coupled heat and mass transfer equations. The equations describe temperature and moisture distributions within a single kernel of drying cereal grain. Simulated drying rate of a corn kernel with spatially variable mass diffusion coefficients were compared to the available experimental data. Kernel's temperature gradients with and without the vapor diffusion effect were analysed. During the initial stages of drying, kernel's temperature was found to be nearly independent of the vapor diffusion. Temperature and moisture gradients within a rice kernel were concentrated in the area of the bran and the endosperm interface.

NOMENCLATURE

C = specific heat, J/kgK

D = diffusion coefficient, m^2/s

h = heat transfer coefficient, W/m^2K

h_{fg} = heat of vaporization of water, J/kg

h_m = mass transfer coefficient, m/s

K = thermal conductivity, W/mK

ℓ = direction cosine

M = moisture content, kg/kg

M_e = equilibrium moisture content, kg/kg

M_o = initial moisture content, kg/kg

T = temperature, ^oC

T_o = initial temperature, ^oC

T_a = air temperature, ^oC

T_s = surface temperature, ^oC

t = time, s

x = x direction

y = y direction

ρ = density, kg/m^3

Subscripts

M = related to moisture

s = at the surface

T = related to temperature

t = time

INTRODUCTION

Many current grain drying systems utilize high air temperatures to expedite the moisture removal process. It is well documented that the quality of cereal grains that are exposed to high temperatures will deteriorate. One of the most severe damages is caused by hydro-thermal stress cracking. Hydro-thermal stresses are the result of elevated temperatures and/or moisture gradients within a kernel. To develop processes that limit these stresses requires an understanding of temperature and moisture distributions within a grain kernel during drying.

The objective of this investigation was to estimate temperature and moisture gradients within a drying grain kernel using a finite element technique.

BACKGROUND

Three theories have been developed by various researchers to explain the physical phenomenon of moisture transfer in porous media; namely, the theories of diffusion, capillary flow, and evaporation-condensation. Depending upon the structure of the porous medium, and the moisture content, one of these transfer mechanisms will dominate. Whitaker (1), in reviewing drying theory has explained the applicability of each of these theories to a specific situation.

Heat and mass transfer mechanisms within a grain kernel have been investigated by several researchers (2, 3, 4). There is a general agreement that a grain kernel dries at a rate that decreases with time. However, different theories have been utilized to explain the moisture transfer.

Bakker-Arkema et al. (4) have assumed, for the practical analysis of cereal grain drying, that the process is an isothermal one that can be described by a mass transfer equation of the form:

$$\frac{\partial M}{\partial t} = D\left(\frac{\partial^2 M}{\partial x^2} + \frac{\partial^2 M}{\partial y^2}\right) \quad (1)$$

Other researchers (2, 3) have shown that the moisture movement within a grain kernel is in the form of vapor diffusion and is temperature dependent. In that case the appropriate heat flow equation is of the form:

$$C\frac{\partial T}{\partial t} = K\left(\frac{\partial^2 T}{\partial x^2} + \frac{\partial^2 T}{\partial y^2}\right) + h_{fg}\,\rho\,\frac{\partial M}{\partial t} \quad (2)$$

It should be noted that the coupled mass and heat transfer equations (Eqs. 1 and 2) are written for a smaller zone of the kernel over which the parameters D, K, ρ and C are assumed to be constant.

The dependence of the diffusion coefficient, D, on moisture and temperature has been shown by Chu and Hustrulid (5) and by Steffe and Singh (6). In addition, the diffusion coefficient is dependent also upon the various constituents of the kernel (bran, germ, endosperm). Determination of the diffusing coefficient is a complex procedure. Nonetheless Steffe and Singh (6) have determined diffusion coefficient values for the bran, germ and endosperm of a rice kernel.

NUMERICAL SOLUTION BY FINITE ELEMENTS

The finite element method has been applied to two-dimensional heat and mass transfer problems by Comini and Lewis (7). They demonstrated that the method is both viable and versatile for the solution of practical applications of a system of heat and mass transfer equations. Haghighi and Segerlind (8) applied the finite element technique using cylindrical coordinates, to the analysis of heat and mass transfer in a soybean kernel.

For the drying process, the following equations are the appropriate initial and boundary conditions to be applied to Eqs. 1 and 2 to obtain a solution.

Initial equations:

$$M(x, y, t = 0) = M_o \quad (3)$$
$$T(x, y, t = 0) = T_o \quad (4)$$

Boundary conditions:

$$\left(\ell x\frac{\partial M}{\partial x} + \ell y\frac{\partial M}{\partial y}\right)\Big|_s = h_m\,(M_s - M_e) \quad (5)$$

$$\left(\ell x\frac{\partial T}{\partial x} + \ell y\frac{\partial T}{\partial y}\right)\Big|_s = h\,(T_s - T_a) \quad (6)$$

The finite element method of solution of Eqs. 1 to 6 is based on the dividing of a cross section of the grain kernel into small triangular elements. Temperature and moisture distributions are approximated by simple continuous functions over each element. The assembly of these functions forms two systems of algebraic equations that describe the temperature and moisture profiles over the entire two-dimensional domain. The process of setting up of the systems of algebraic equations is well documented. The procedure outlined by Segerlind (9), for a two dimensional simplex (triangular) element, was used in this analysis.

In finite element form, Eqs. 1 to 6 take on the following form:

$$(C)_M\frac{\partial}{\partial t}\{M\} + (K)_M\{M\} + \{f\}_M = 0 \quad (7)$$

$$(C)_T\frac{\partial}{\partial t}\{T\} + (K)_T\{T\} + (C)\frac{\partial}{\partial t}\{M\} + \{f\}_T = 0 \quad (8)$$

The (C) matrices contain the capacitance terms, while the (K) matrices contain the material properties for each element. The vectors {f} contain the initial and boundary conditions. Subscripts T and M represent the temperature and moisture related parameters, respectively.

The systems of linear equations resulting from Eqs. 7 and 8 were solved by substituting the approximation

$$\frac{\partial}{\partial t}\{M\} = \frac{\{M\}_{t+\Delta_t} - \{M\}_t}{\Delta t} \quad (9)$$

and then solving Eq. 7, followed by Eq. 8, for a time step of Δt.

Cross sections of kernels of corn and rice are shown in Fig. 1. Each kernel has been divided into three structurally distinctive sub-regions. Thermal and mass transfer properties of each sub-region have been estimated from the available experimental data (11, 12).

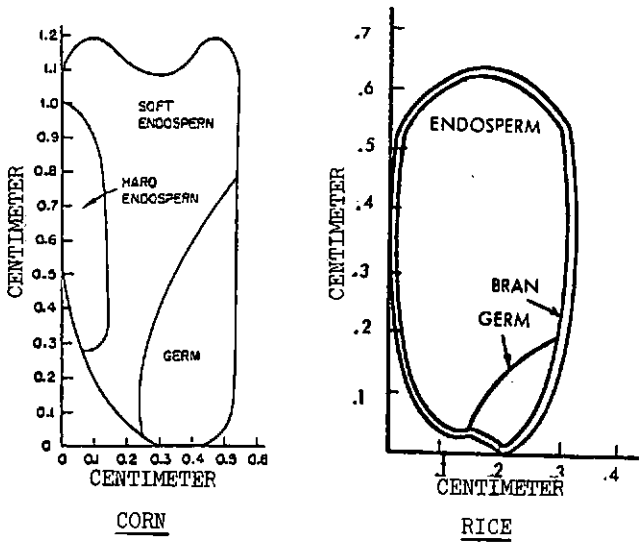

Figure 1 Corn and Rough Rice Kernels' Cross Section

Table 1 is a list of the material properties used in this analysis. Figure 2 shows computer generated finite element meshes. The corn and the rice kernels contained 198 and 192 triangular elements; respectively. Nodal coordinates and

elemental material properties were stored for later use in the simulation analysis.

Table 1. Thermal and mass transfer properties of rice and corn kernels.

Property	Unit	Rice			Corn		
		Endosperm	Bran	Germ	Hard Endosperm	Soft Endosperm	Germ
Thermal conductivity (K)	$\frac{W}{m.k}$	.105	.100	.110	.17	.16	.18
Specific heat x density (C)	$\frac{J}{m^3.k}$	$.25 \times 10^7$	$.24 \times 10^7$	$.28 \times 10^7$	$.169 \times 10^7$	$.161 \times 10^7$	$.197 \times 10^9$
Convective transfer coeff. (h)	$\frac{W}{m^2.k}$	33.0	33.0	33.0	33.0	33.0	33.0
Convective mass transfer coeff. (h_m)	$\frac{m}{s}$	.03	.03	.03	.03	.03	.03
Diffusion coefficient (D)	$\frac{m^2}{s}$	$.94 \times 10^{-10}$	$.28 \times 10^{-10}$	$.94 \times 10^{-10}$	$.36 \times 10^{-10}$	$.14 \times 10^{-9}$	$.22 \times 10^{-9}$

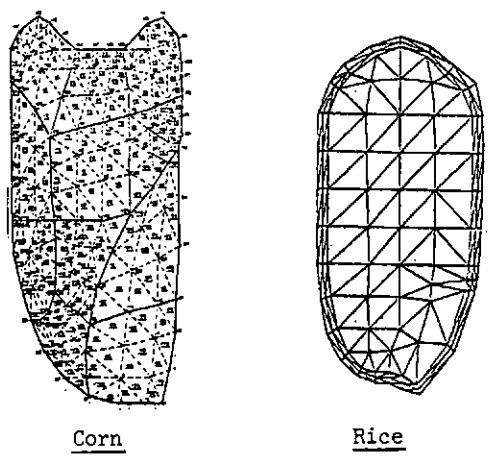

Figure 2 Finite Element Grids

The finite element solutions were compared to the experimental data that were available.

Figure 3 shows a comparison between experimental corn drying data of Chu (10) and simulations using the three subregions of the kernel with different properties, and the entire kernel with one overall property. During the first hour of drying, both simulations approximate the experimental data closely, however, during later stages of drying neither simulations match the experimental data. This likely indicates that the value of the diffusion coefficient should be varied as a function of the grain's moisture content.

Figure 4 shows the temperatures at the surface of the corn kernel, and at the center of the kernel, as a function of time as simulated using Eq. 2 in its entirety and as simulated when the $\partial M/\partial t$ term was neglected. Although in the early stages of drying there was little difference between the two simulations, in the later stages the complete model did predict temperatures that were somewhat lower.

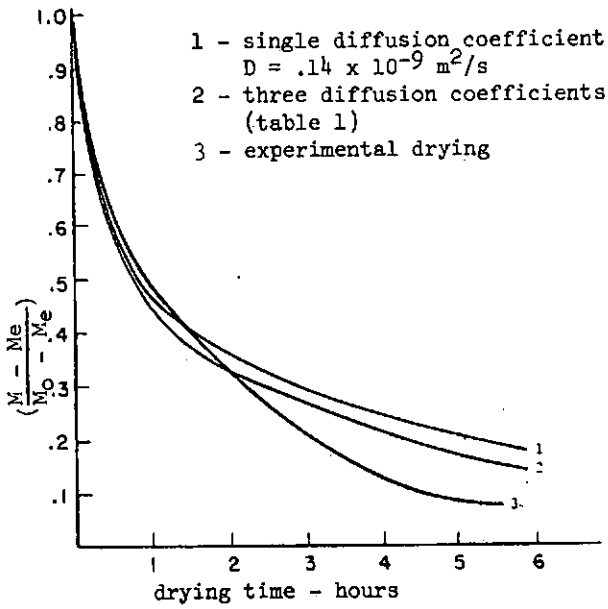

Figure 3 Experimental and simulated drying of a corn kernel.

Figure 4 also shows that the internal temperature gradient between the surface and the center of the kernel is at maximum within the interval of 20 to 60 seconds. This temperature gradient could result in high stresses within the kernel.

Figure 5a shows temperature profiles within a rice kernel that is heated for 30 seconds. The largest gradients are along the bran and the endosperm interface, an area that is most susceptible to thermal expansion and consequently thermal stresses.

Figure 5b shows moisture profiles within a rice kernel that is exposed to isothermal drying for one hour. As in the thermal expansion situation,

the largest gradients are concentrated at the interface of the bran and endosperm. These moisture gradients will cause shrinkage of the bran. The volumetric changes within the grain kernel will result in fissures and cracks.

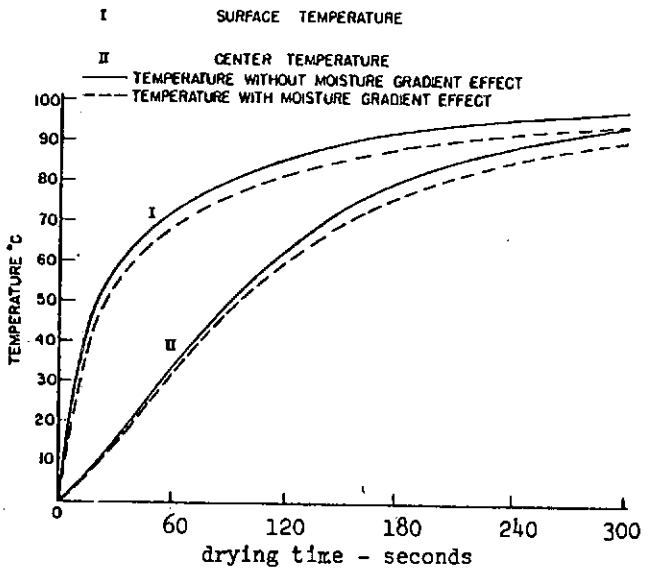

Figure 4 Temperatures of two locations within a corn kernel.

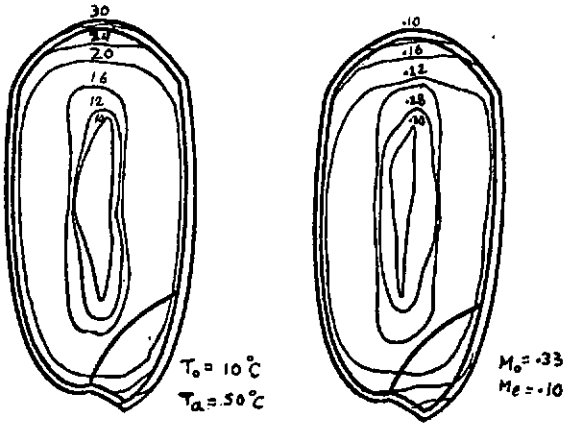

a. Temperatures Elapsed time: 30 seconds

b. Moisture Elapsed time: 1 hour

Figure 5 Temperature and moisture profiles in the rice kernel.

CONCLUSION

The finite element technique offers a viable method for the study of temperature and moisture distribution within a grain kernel. With this method; Spatial material properties and the non-geometrical shapes associated with the cereal grain can be considered.

The simulation results showed that the inclusion of $\partial M/\partial t$ in the heat transfer equation slightly affected the grain temperature during the early stages of drying. As the moisture gradients within the kernel became larger, the effect of $\partial M/\partial t$ became more pronounced. The total heat of vaporization associated with $\partial M/\partial t$ is provided by the grain and as a result the temperatures are lower.

The method of finite element predicted the location of largest temperature and moisture gradients within a kernel. The magnitude of temperature and moisture gradients would correspond to the hydro-thermal stresses. In the case of the analysed rice kernel, the location of maximum hydro-thermal stresses were between the bran and the endosperm.

REFERENCES

1. Whitaker, S. Simultaneous heat, mass, and momentum transfer in porous media: A theory of drying. Advances in Heat Transfer 1977.
2. Young, J.H. Simultaneous heat and mass transfer in a porous hygroscopic solid. TRANS. ASAE, 1968, Vol. 12: 720-725.
3. Husain, A., Chen, C.S., Clayton, J.t. and Whitney, L.F. Mathematical simulation of mass and heat transfer in high moisture foods. TRANS. ASAE, 1972, Vol. 15: 732-736.
4. Bakker-Arkema, F.W., Brook, R.C. and Lerew, L.E. Cereal grain drying. In: Advances in Cereal Science and Technology. 1977 Vol. II. American Society of Cereal Chemists. Minneapolis, Minn.
5. Chu, S.T. and Hustrulid, A. Numerical solution of diffusion equations 1968, Vol. 11: 705-715.
6. Steffe, J.F. and P.R. Singh, Liquid diffusivity of rough rice components 1979, ASAE 79-6006. American Society of Agricultural Engineers, St. Joseph, MI.
7. Comini, G. and Lewis, R.W. A numerical solution of two dimensional problems involving heat and mass transfer. 1976. Int J. Heat and Mass Transfer Vol. 19: 1384-1392.
8. Haghighi, K. and Segerlind, L.D. Computer simulation of stress cracking of soybeans, 1978, ASAE 78-3560 American Society of Agricultural Engineering, St. Joseph, MI.
9. Segerlind, L.J. 1976. Applied Finite Element Analysis.John Wiley and Sons. Inc., New York, NY.
10. Chu, S.T. 1966. A theoretical and experimental study of the effects of size and shape of kernels on the drying rate of shelled corn. Ph. D. Thesis. Univ. of Minnesota, St. Paul, Minn.
11. Gustafson, R.J. Thompson, D.R. and Sokhansanj, Shahab. Temperature and stress analysis of corn kernel-finite element analysis. 1979, TRANS. ASAE 22: 955-958.
12. Sokhansanj, Shahab, and Gustafson, R.J. Finite element predictions of rice cracking during drying. 1979, ASAE 79-3547 American Society of Agricultural Engineers, St. Joseph MI.

CONCENTRATION DEPENDENT DIFFUSION COEFFICIENTS DERIVED FROM EXPERIMENTAL DRYING CURVES

K.Ch.A.M. Luyben,
J.J. Olieman, S. Bruin.

Department of Process Engineering,
Agricultural University, Wageningen, the Netherlands.

ABSTRACT

Desorption behaviour was measured for a number of materials in a diffusion cell under carefully controlled boundary conditions. The experimental set-up is described.

Using the *regular regime* method developed by Schoeber (1), it is possible to determine the concentration dependence of the effective water diffusivity from measured drying curves.

Drying curves of glucose, coffee extract, skim milk, apple tissue, potato tissue and an animal feed formulation are presented, together with data on the concentration dependence of the effective water diffusivity and of the activation energy of diffusion, derived from these drying curves.

NOMENCLATURE

A	= parameter in eqn. for activation energy
B	= parameter in eqn. for activation energy
C	= parameter in eqn. for activation energy , kJ/mole
d	= density , kg/m^3
$\mathbb{D}_o \rho^2_{s,o}$	= dimensional constant (see eqn. 1), kg^2/m^4s
$\mathbb{D}_r$	= reduced diffusivity ($= \mathbb{D}_w \rho_s^2 / \mathbb{D}_o \rho^2_{s,o}$)
$\mathbb{D}_{w,e}$	= effective water diffusivity , m^2/s
E_D	= activation energy for diffusion, kJ/mole
E_F	= activation energy for flux parameter , kJ/mole
F	= flux parameter (see eqn. 1)
j	= drying flux , kg/m^2s
R	= gas constant , kJ/mole K
R_s	= dry solids radius , m
$\overline{Sh}_d$	= average Sherwood number (see eqn. 3)
T	= absolute temperature , K
ρ	= mass concentration , kg/m^3
ω'	= mass fraction (dry solids basis) , kg/kg

Subscripts

e	= effective
i	= interface
p	= pure
r	= reduced
s	= solids
w	= water
o	= initial
1	= condition 1
2	= condition 2
$\bar{}$	= average

INTRODUCTION

Knowledge of the (effective) diffusivity of the components transferred in a system, is necessary in the design of mass transfer processes like drying, extraction, ad- and absorption, ion-exchange etc. However, the determination of the diffusion coefficient, and especially its concentration dependence, usually is a rather cumbersome and laborious task. A large number of methods for the determination of diffusion coefficients have been proposed in the literature.

Reviews on measuring techniques and data-reduction were presented, among others, by Johnson & Babb (2), Crank & Park (3) and Crank (4). These methods can be summarized as follows :

1. Methods in which the mobility of diffusing molecules is measured directly.
2. Methods in which a stationary or transient gradient is applied.

Examples of the first group are : spin-spin relaxation in nuclear magnetic resonance and quasi-elastic light scattering. The relatively complex and expensive equipment needed for these techniques, is however an important disadvantage. In the second group the stationary methods like permeation through a membrane or diaphragm are usually rather simple, but time consuming, especially in the case of very low diffusion coefficients.

Instationary methods are most widely used for the determination of diffusion coefficients. From these, desorption methods are particularly relevant for drying processes. In this paper we will therefore apply a method proposed by Schoeber (1) based on a desorption experiment.

This method has previously been applied to determine the concentration dependence of the (effective) water diffusivity in glucose (5,6), maltodextrine (7), potato (8), and skim milk (9). For all of these materials with exception of skim milk experimentally determined isothermal drying curves have been used.

In this paper we will present the concentration dependence of the effective water diffusivity in three liquid food materials (coffee-extract, skim milk and glucose) and three structured materials (apple, potato and an animal feed formulation). The temperature dependence of the determined diffusivities will be given in the form of a concentration dependent activation energy. A relatively simple piece of equipment for measuring drying curves, will be described. Isothermal *regular regime* curves for a constant surface concentration, needed to determine the diffusivity, will be calculated from experimentally determined non-isothermal drying curves.

METHOD

Schoeber analyzed by numerical calculations, the influence of the variation in the concentration dependence of the diffusion coefficient on drying behaviour, for the case of constant surface concentration. The results of this analysis offer the procedure described in this chapter to calculate the complete concentration dependence of the (effective) diffusion coefficient over the concentration interval over which the *regular regime* curve has been determined experimentally. So a prerequisite for the method is the knowledge of the *regular regime* curve at the desired temperature for the case of constant surface concentration. The regular regime period can be explained as follows : Some time after the beginning of an instationary diffusion process in a homogeneous (binary) mixture, one will find that the shape of the concentration profile and its change in time, has become independent of the initial concentration profile. We then say that the instationary diffusion process has reached its regular regime. This means that, when plotted in the right way, all drying curves of various initial moisture contents of the same material at one temperature and for the same geometry merge into each other. They form one general curve : the regular regime curve. For systems with a constant diffusion coefficient this can be shown analytically from the solutions of the diffusion equation. The regular regime, which is a well known phenomenon in mass transfer theory, can numerically and experimentally also be found in systems with a strong concentration dependent diffusivity. For a more detailed description of regular regimes in systems with concentration dependent diffusion coefficients the reader is referred to the thesis of Schoeber (1).

To facilitate a further explanation of the method the following parameters are introduced :

- *the flux parameter :*

$$F = \frac{j_{w,i}\, d_{s,p}\, R_s}{\mathbb{D}_o\, \rho^2_{s,o}} \qquad (1)$$

in which $j_{w,i}$ is the flux of water relative to the moving interface ; $d_{s,p}$ is the density of the pure dry solids ; R_s is the solids radius ; and $\mathbb{D}_o \rho^2_{s,o}$ is a dimensional constant with numerical value 1, introduced for similarity reasons.

- *the average reduced diffusion coefficient :*

$$\overline{\mathbb{D}}_r = \frac{1}{(\bar{\omega}'_w - \omega'_{w,i})} \int_{\omega'_{w,i}}^{\bar{\omega}'_w} \mathbb{D}_r \, d\omega' \qquad (2)$$

in which ω'_w is the moisture content on dry basis (i refers to the interface) ; and $\mathbb{D}_r$ ($= \mathbb{D}_w \rho^2_s / \mathbb{D}_o \rho^2_{s,o}$) is the reduced diffusivity.

- *the average Sherwood number for the dispersed phase :*

$$\overline{Sh}_d = \frac{2F}{(\bar{\omega}'_w - \omega'_{w,i})\, \overline{\mathbb{D}}_r} \qquad (3)$$

From many numerical calculations for different concentration dependences of the diffusion coefficient, Schoeber found that the average Sherwood number as a function of $d \ln F / d \ln (\bar{\omega}'_w - \omega'_{w,i})$ was hardly dependent on the concentration dependence of the diffusivity. Fig. 1 gives a relation between $\overline{Sh}_d$ and $d \ln F / d \ln (\bar{\omega}'_w - \omega'_{w,i})$ for the case of a slab with or without shrinkage and for non-shrinking cylinder and sphere. The curve given here represents a sort of average for a wide number of concentration dependences of the diffusion coefficient.

To explain the calculation procedure, suppose we have got a regular regime curve (RR-curve) expressing the flux parameter (F) as a function of the average moisture content minus the interfacial moisture content $(\bar{\omega}'_w - \omega'_{w,i})$, for a constant surface concentration $(\omega'_{w,i})$.

Now the concentration dependent (effective) diffusivity can be determined as follows :

1. Differentiation of the RR-curve gives $d \ln F / d \ln (\bar{\omega}'_w - \omega'_{w,i})$ as a function of $\bar{\omega}'_w$.
2. Determine $\overline{Sh}_d$ as a function of $\bar{\omega}'_w$ by means of Fig. 1 . In case of a shrinking cylinder or sphere the following corrections have to be applied :

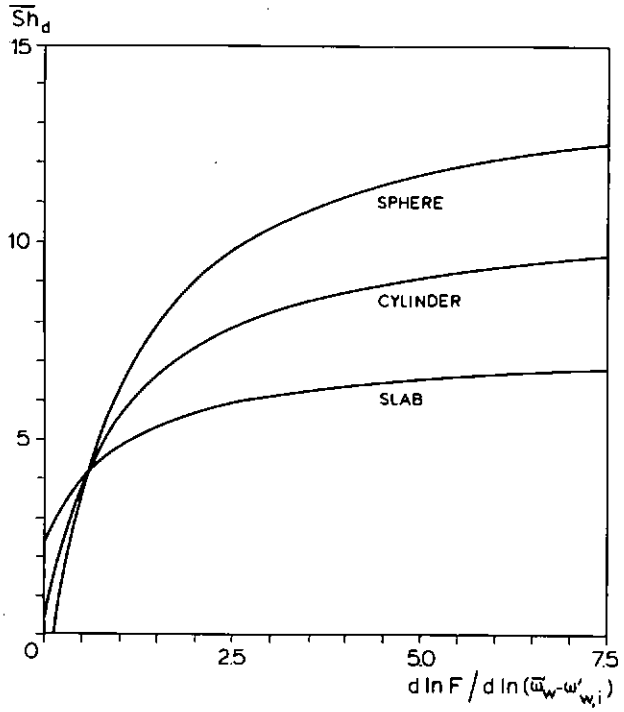

Fig. 1. Average $\overline{Sh}_d$ relations for shrinking or non-shrinking slab, non-shrinking cylinder and non-shrinking sphere.

2. continued.

$$\overline{Sh}_d = \overline{Sh}_{d,\text{non-shrinking}} + \Delta\overline{Sh}_d \qquad (4)$$

where for a cylinder :

$$\Delta\overline{Sh}_d = 10.87\ \{(1 + \frac{\bar{\omega}'_w\ d_s}{1000})^{\frac{1}{2}} - 1\} \qquad (5)$$

and for a sphere :

$$\Delta\overline{Sh}_d = 14.39\ \{(1 + \frac{\bar{\omega}'_w\ d_s}{1000})^{\frac{2}{3}} - 1\} \qquad (6)$$

3. Combination of eqn. 2 and eqn. 3 gives :

$$\int_{\omega'_{w,i}}^{\bar{\omega}'_w} \mathbb{D}_r\ d\omega'_w = \frac{2\ F}{\overline{Sh}_d} \qquad (7)$$

For every $\bar{\omega}'_w$ of the RR-curve the left-hand side of this equation can be evaluated, because F is known from the RR-curve and $\overline{Sh}_d$ is known from step 2.

4. Differentiating the definite integral obtained in step 3 with respect to $\bar{\omega}'_w$ (upper boundary of the integral), gives the reduced diffusivity ($\mathbb{D}_r$) as a function of the integration variable ω'_w :

$$\mathbb{D}_r(\omega'_w) = \frac{d}{d\bar{\omega}'_w}\left\{\int_{\omega'_{w,i}}^{\bar{\omega}'_w} \mathbb{D}_r\ d\ \omega'_w\right\} \qquad (8)$$

5. The concentration dependent (effective) diffusivity is finally obtained by use of eqn. 9.

$$\mathbb{D}_{w,e} = \mathbb{D}_r/\rho_s^2 \qquad (9)$$

EXPERIMENTAL SET-UP

Fig. 2 shows schematically the experimental set-up and the data-acquisition system used for the experiments. Helium gas flows via a flow sensor and controller through both thermal conductivity cells as a reference gas stream. Then the helium gas passes an injection point and after this can either flow back immediately, or through a humidifier, in which a certain water concentration in the helium gas is generated, depending on temperature and pressure in this humidifier. Now the inlet concentration is measured and the gas enters the diffusion cell. Finally the gas passes the second detector to measure the outlet concentration. Both detectors, the diffusion cell and the humidifier are built together in a brass block. This block is placed in a thermostatic bath. For the experiments described in the following the humidifier is not used, resulting in a zero inlet concentration.

Diffusion cell

The diffusion cell has a cylindrical shape, with a tangential inlet and an anti-tangential outlet. The volume of the cell can be changed by means of cylindrical rings to be placed between the brass block and the lid of the cell. Residence time distribution measurements showed that the gasphase in the cell is ideally mixed, even without stirring. In order to be able to vary the gasphase mass transfer coefficients without changing the He-gas flow rate, the gasphase can be stirred. In the diffusion cell the sample is placed on the bottom (slab), or suspended by a thin thermocouple (cylinder, sphere or arbitrary geometry). In the first case an isothermal drying curve is measured if the sample has good thermal contact with the bottom and in the second case non-isothermal drying curves are measured.

Data acquisition and process control system

In the lower part of Fig. 2 a schematical picture of the data acquisition and process control system is given. This system basically consists of a CAMAC-CRATE with various modules (timer, multiplexer, ADC, DAC etc.) controlled by a MACAMAC-controller. Input takes place by multiplexing a number of channels from which the information is fed via an analog-digital converter to the microprocessor. Processed output is sent to a

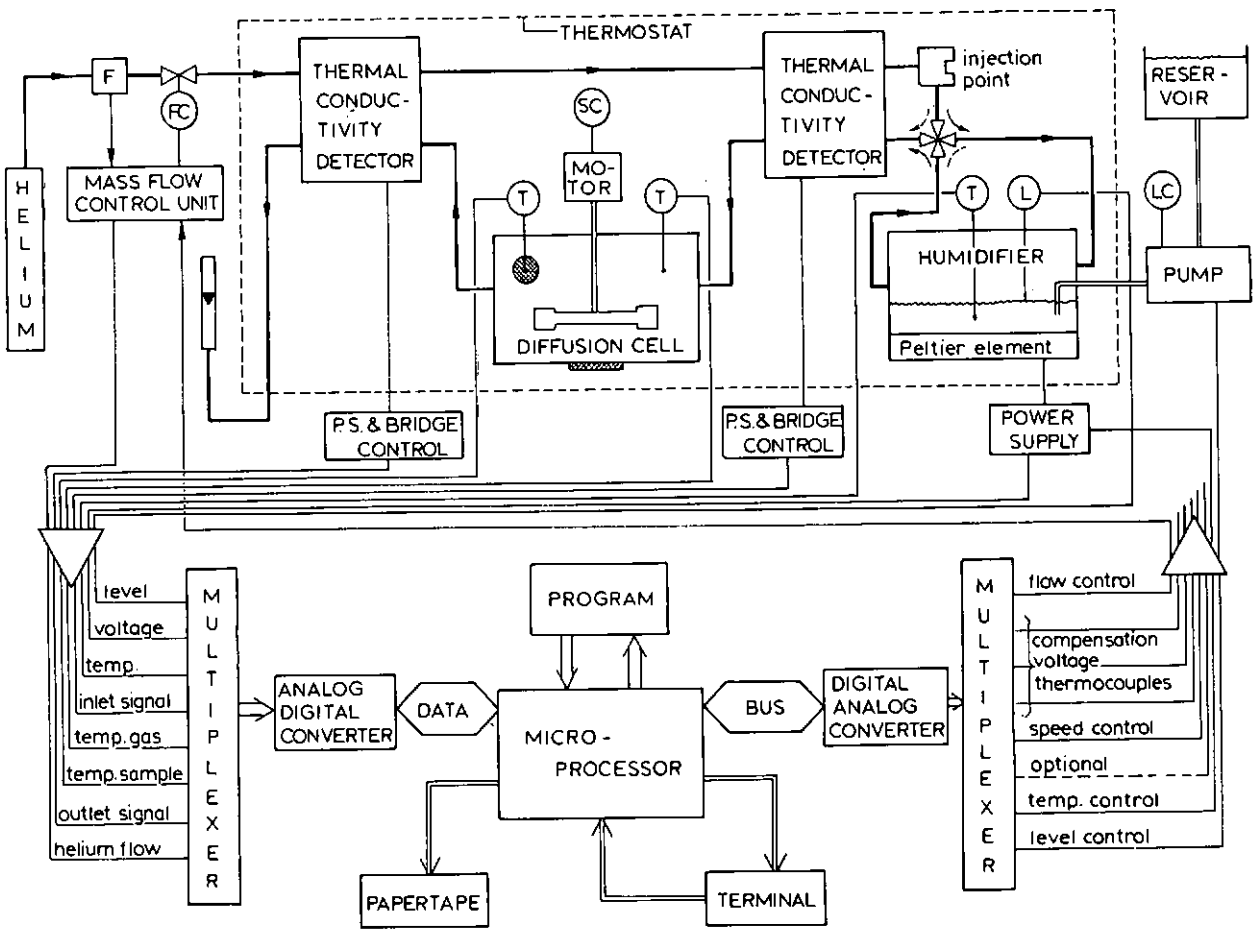

Fig. 2. Experimental set-up, data-acquisition and process control system.

terminal and punched on papertape. Control output is sent via a digital-analog converter (containing a memory) and a multiplexer back to the system. The whole operation is controlled by a basic computer program residing in RAM-memory. After an experiment the measured data (punched on papertape) are further processed using the data reduction programs described in the following chapter.

An important advantage of the measuring technique using thermal conductivity cells, is the direct determination of the drying flux. From this drying flux the average moisture content is determined by an integration procedure. In case of weighing the sample to be dried, the weight at every moment is a measure for the average moisture content. However in that case the signal has to be differentiated to obtain the flux. Since integrating generally reduces errors, while differentiating induces errors, the first is to be preferred. An advantage of weighing is the possibility to measure very low fluxes, where in case of the thermal conductivity cells the signal gets lost into noise. By reducing the gasflow substantially the influence of noise can however be postponed considerably.

DATA REDUCTION

In Fig. 3 a schematic representation is given of the data reduction applied to the measurements. In this chapter this scheme is followed roughly.

Since the time constant of the drying process is large compared to that of the perfectly mixed diffusion cell, the measured outlet concentration multiplied by the gasflow gives the total drying flux directly. From this total drying flux, the fluxparameter is calculated assuming homogeneous shrinkage throughout the drying process. This assumption cannot always be justified, as we will see in the DISCUSSION. Integration of the total drying flux starting from the final moisture content, results for an isolated sample in a non-isothermal drying curve expressed as the fluxparameter (F) versus the average moisture content ($\bar{\omega}'_w$). From measurements at different temperature levels (different gasphase temperatures) followed, as also stated by Schoeber, that the temperature dependence of the fluxparameter can by good approximation be described by the Arrhenius equation, for as well the regular regime period as the penetration period.

$$F_2 = F_1 \exp\{\frac{-E_F}{R}(\frac{1}{T_2} - \frac{1}{T_1})\} \qquad (10)$$

in which E_F is the concentration dependent activa-

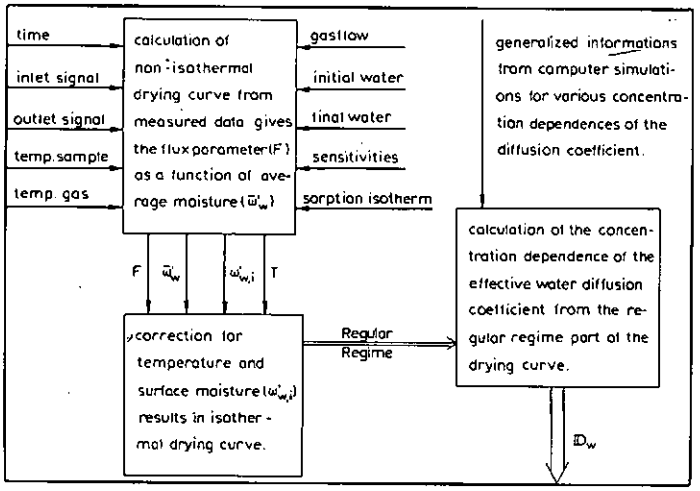

Fig. 3. Data reduction scheme.

tion energy.
Using eqn. 10 it is possible to determine this concentration dependent activation energy from the curves measured at different temperature levels and to calculate isothermal drying curves.

During the experiment the water concentration in the diffusion cell drops gradually. So during the experiment the interfacial moisture concentration in the dispersed phase will not be a constant. In order to obtain a curve for constant surface concentration the following correction of the RR-curve is applied :

$$F(\bar{\omega}'_w, 0) = F(\bar{\omega}'_w, \omega'_{w,i}) + F(\omega'_{w,i}, 0) \qquad (11)$$

where the parameter indicates the average moisture content and the second moisture concentration at the interface. Assuming that the interfacial concentration is effectively zero at the end of a drying experiment using dry helium gas, eqn. 11 can be used to calculate the regular regime curve for the case of zero surface concentration. Because the interface concentration generally is fairly low compared to the average concentration, this correction has only a minor influence on the fluxparameter.

From the now obtained RR-curve for constant surface concentration, the concentration dependence of the diffusivity is calculated, using the previously described steps. With regard to this calculation, the following remarks can be made :

1. For convenient manipulation of the F-curve and its derivatives , the regular regime part of the measured drying curve is fitted with an analytical equation. For this purpose we used a multiple knots cubic spline approximation (10).
2. The obtained definite integral (eqn. 7) is fitted again with an equation from which the derivative can easily be determined. For this we also used a cubic spline approximation.
3. The temperature dependence of the diffusion coefficient is described with a Arrhenius equation. The activation energy in this equation is by good approximation equal to that for the fluxparameter, as will be shown here.

The temperature dependence of $\overline{\mathbb{D}}_r$ is equal to that of F, since $\overline{Sh}_d$ is hardly dependent on temperature. So :

$$\overline{\mathbb{D}}_{r,2} = \overline{\mathbb{D}}_{r,1} \exp\{\frac{-E_F}{R}(\frac{1}{T_2} - \frac{1}{T_1})\} \qquad (12)$$

The concentration dependence of E_F is described by the following equation (see next chapter) :

$$E_F = A.\ \exp(-B\,\bar{\omega}'_w) + C \qquad (13)$$

in which A, B and C are parameters.
Taking the derivative of eqn. 12 with respect to $\bar{\omega}'_w$ gives :

$$\mathbb{D}_{r,2} = \{\mathbb{D}_{r,1} \frac{dE_F}{d\bar{\omega}'_w} \cdot \frac{\overline{\mathbb{D}}_{r,1}}{R}(\frac{1}{T_2} - \frac{1}{T_1})\} \cdot \exp\{\frac{-E_F}{R}(\frac{1}{T_2} - \frac{1}{T_1})\} \qquad (14)$$

Using eqn. 13 gives :

$$\mathbb{D}_{r,2} = \{1 + \frac{\overline{\mathbb{D}}_{r,1}}{\mathbb{D}_{r,1}} \frac{AB}{R}(\frac{1}{T_2} - \frac{1}{T_1}) \exp(-B\bar{\omega}'_w)\}.\ \mathbb{D}_{r,1} \cdot \exp\{\frac{-E_F}{R}(\frac{1}{T_2} - \frac{1}{T_1})\} \qquad (15)$$

For the values of A and B and for the temperature and moisture ranges of interest it can easily be shown that :

$$1 >> \frac{\overline{\mathbb{D}}_{r,1}}{\mathbb{D}_{r,1}} \frac{AB}{R}(\frac{1}{T_2} - \frac{1}{T_1}) \exp(-B\bar{\omega}'_w) \qquad (16)$$

So :

$$\mathbb{D}_{r,2} = \mathbb{D}_{r,1} \exp\{\frac{-E_D}{R}(\frac{1}{T_2} - \frac{1}{T_1})\} \qquad (17)$$

with

$$E_D \simeq E_F \qquad (18)$$

4. Because of non-perfect and non-homogeneous shrinkage (see DISCUSSION), the effective diffusivity resulting from the above given calculational procedure, contains not only effects like liquid diffusion, vapor diffusion, capillary flow, evaporation-condensation etc., but also the effect of non-perfect and/or non-homogeneous shrinkage.

To test the data reduction programs, and to check if no artificial concentration dependence was created, a drying curve calculated numerically for a constant diffusivity was used as input data. The diffusivity calculated by the data reduction programs from this, was constant well within 15 %. The small dependence found, is caused by three effects :

- use of the average relation for $\overline{Sh}_d$ (see Fig. 1) instead of a constant $\overline{Sh}_d$-value ;
- use of the shrink correction, for $\overline{Sh}_d$, from an extremely concentration dependent diffusivity (eqn. 6), which is slightly different from that for a constant diffusivity ;
- small differences between the calculated F-values and those fitted by cubic spline approximation.

MEASUREMENTS AND RESULTS

Drying experiments were performed with three liquid foods and three solid food materials. The liquid materials were gelled with approximately 1 weight percent of agar-agar on water basis and injected into a spherical mould to cool off. The solids were formed to be desired shape by cutting. In the following the materials we measured will be discussed successively.

Glucose

Glucose has been measured as a reference, because the concentration dependence of the diffusivity for this material is well known (11, 1). In Fig. 4 the isothermal drying curves for zero surface concentration are shown. These curves have been calculated from non-isothermal drying curves of spherical particles with an initial diameter of 1 centimetre, using gasphase temperatures of 30,50 and 70 degrees centigrade respectively.

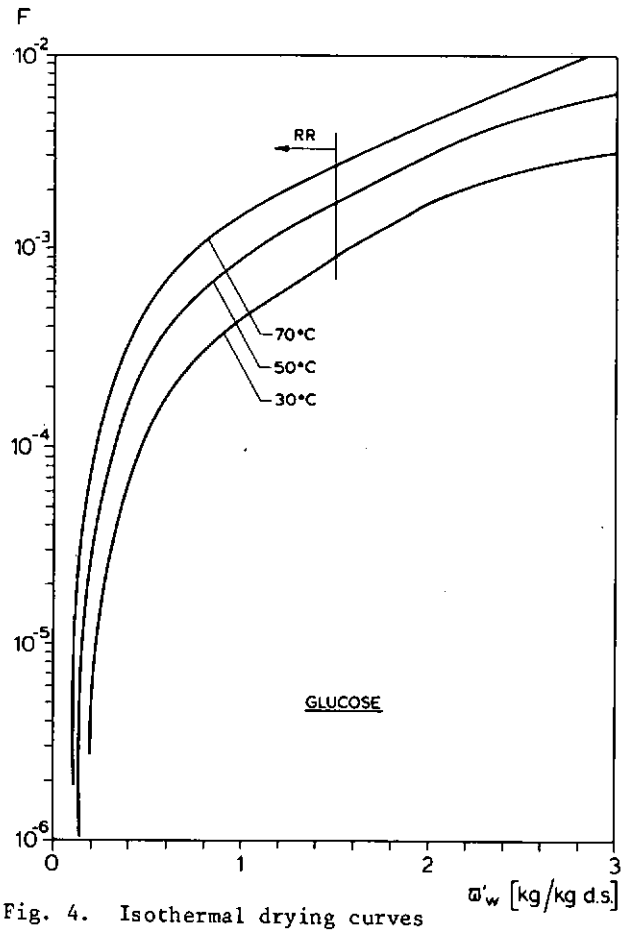

Fig. 4. Isothermal drying curves of glucose for zero surface concentration.

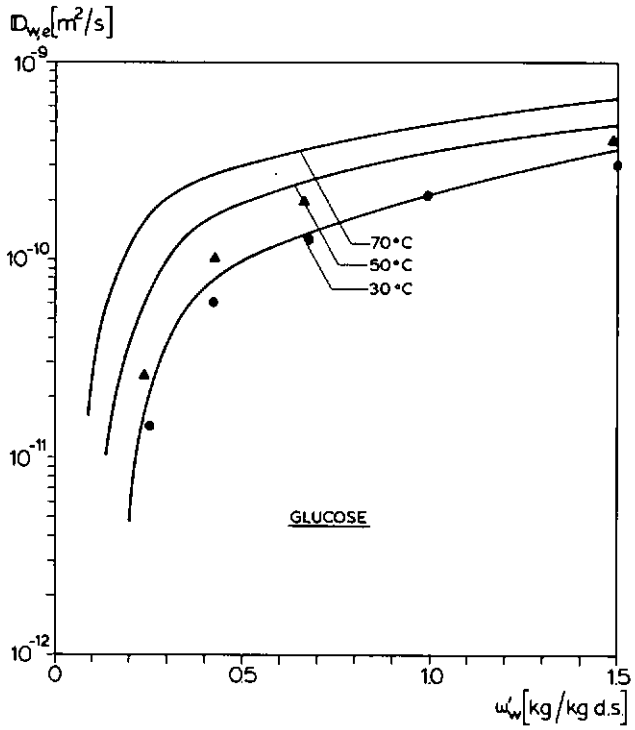

Fig. 5. Concentration dependence of water diffusivity for glucose. Measurements by Gladden & Dole : ● 25 °C ; ▲ 35 °C .

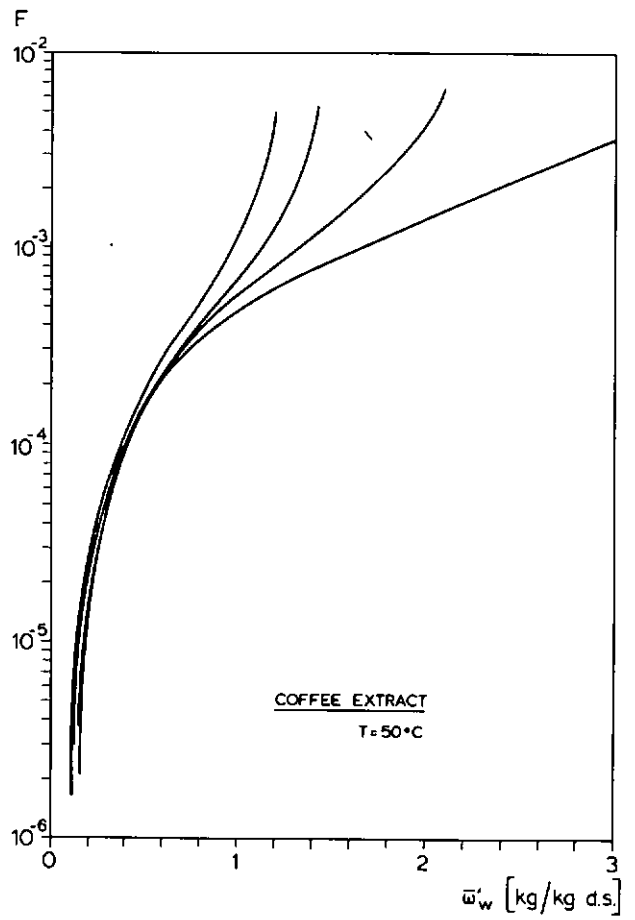

Fig. 6. Isothermal drying curves of coffee extract for different initial moisture contents.

In Fig. 5 the diffusion coefficients, calculated from the regular regime parts of these drying curves, are given. In this figure also the data measured by Gladden & Dole (11) at 35 °C (▲) and 25 °C (●) have been depicted. Parameters for the concentration dependence of the activation energy (eqn. 13) are given in Table 1.

Coffee extract

Coffee extract has been measured most amply. Fig. 6 shows the fluxparameter as a function of the average moisture content, for four different initial moisture contents, calculated using eqn. 10 and eqn. 11 to correct for temperature and surface concentration respectively. Measurements were performed using spherical particles with an initial diameter of 1 centimetre and a gasphase temperature of 50 °C. This figure clearly illustrates how different penetration curves merge into one single *regular regime* curve, as expected from theory. Fig. 7 gives the influence of geometry on the regular regime. Although the flux (per square metre per second) increases going from sphere to slab, the reversed behaviour is shown by the fluxparameter because of its definition. Fig. 8 gives three RR-curves for zero surface concentration, from which the diffusivities depicted in Fig. 9 have been calculated. Parameteres for the concentration dependent activation energy are given in Table 1.

Skim milk

The drying curves of skim milk, represented in Fig. 10 , have been constructed by linking two measurements (one with high and one with low initial flux) together. The reason for this is the tedious shrinking behaviour of skim milk spheres (see DISCUSSION). In Fig. 11 the diffusion coefficients calculated from these curves are given.

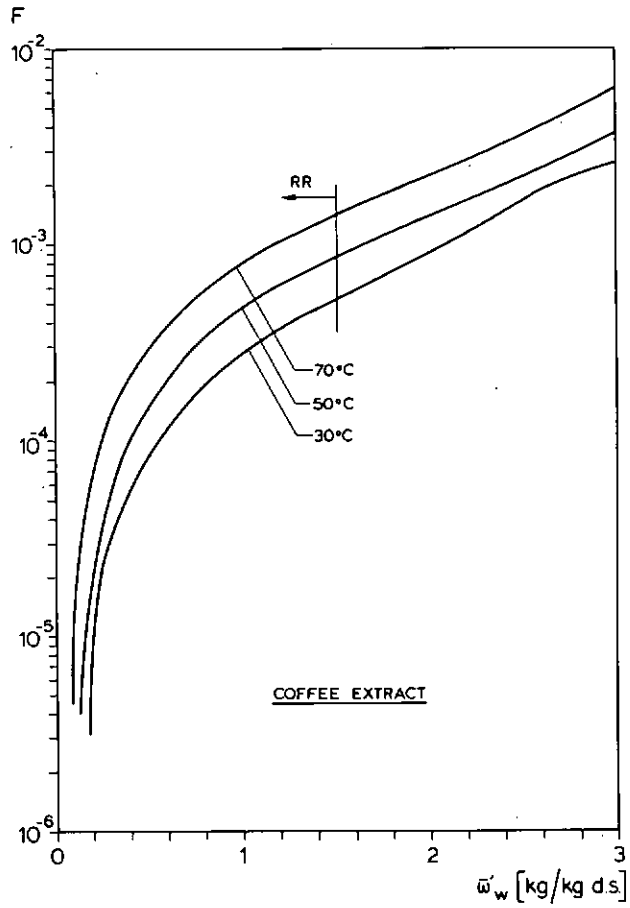

Fig. 8. Isothermal drying curves of coffee extract for zero surface concentration.

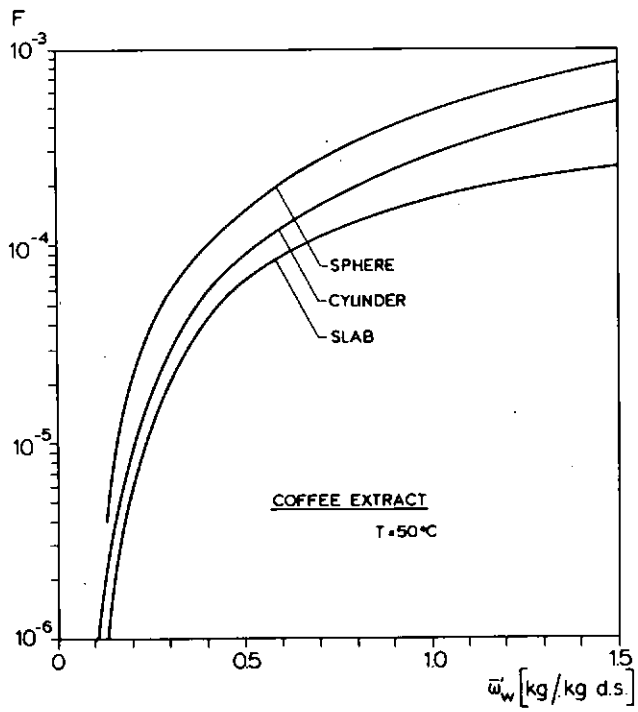

Fig. 7. Influence of geometry on fluxparameter in the regular regime period for coffee extract.

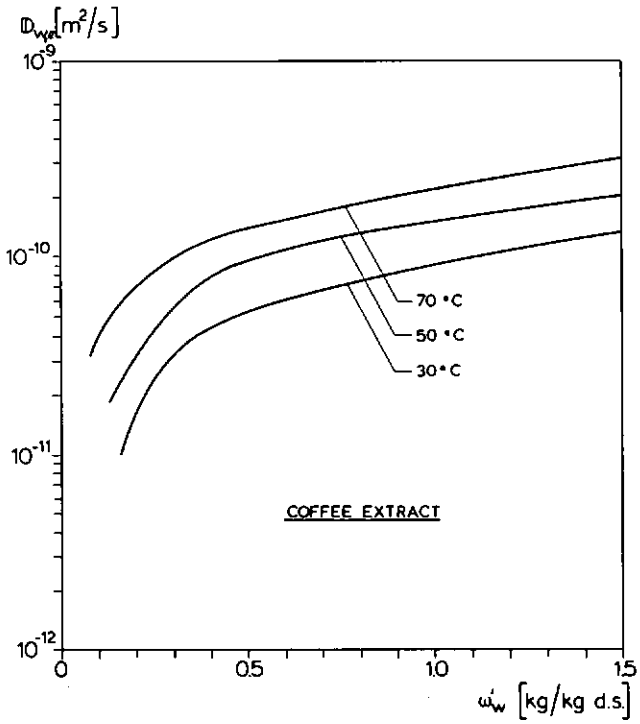

Fig. 9. Concentration dependence of water diffusivity for coffee extract.

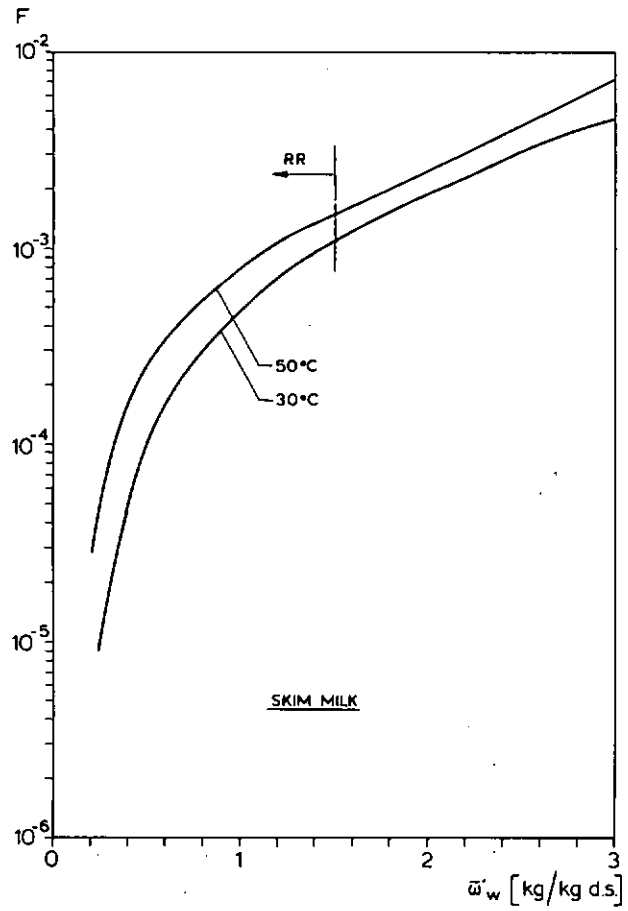

Fig. 10. Isothermal drying curves of skim milk for zero surface concentration.

The dashed parts in Fig. 11 represent the added measurements of 30 °C and 50 °C.

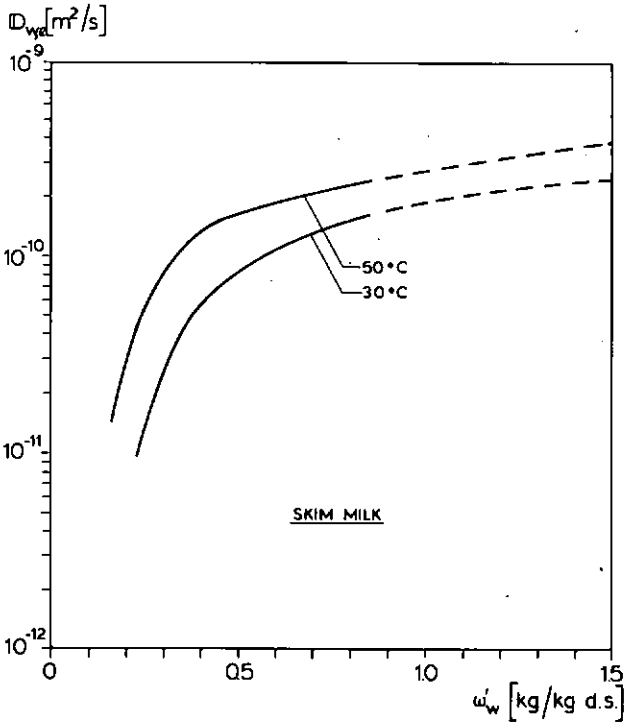

Fig. 11. Concentration dependence of water diffusivity for skim milk.

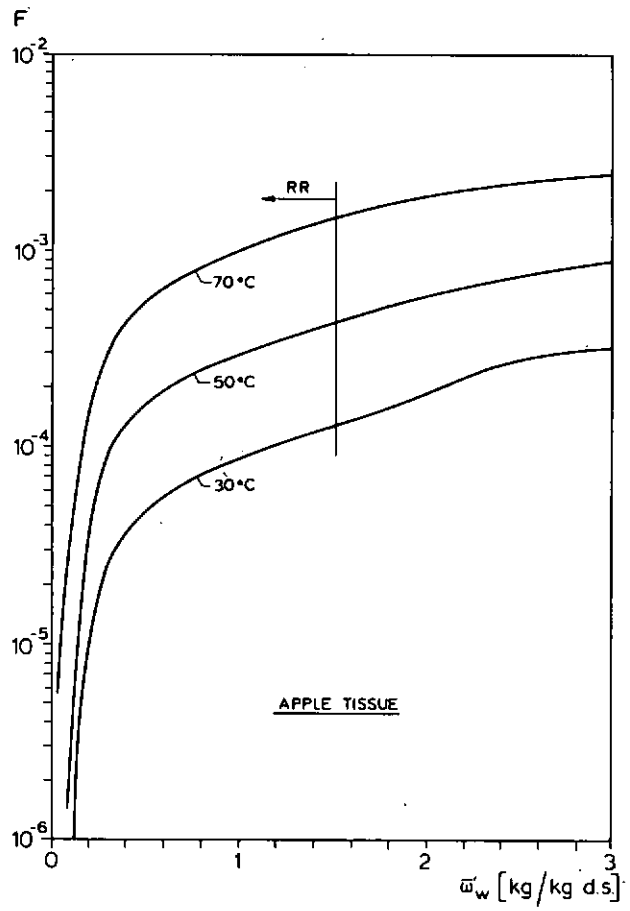

Fig. 12. Isothermal drying curves of apple tissue for zero surface concentration.

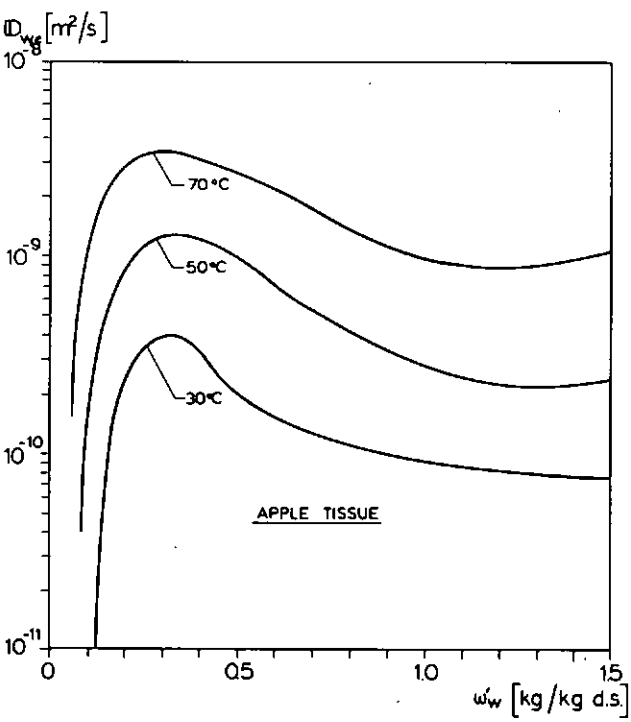

Fig. 13. Concentration dependence of the effective water diffusivity for apple tissue.

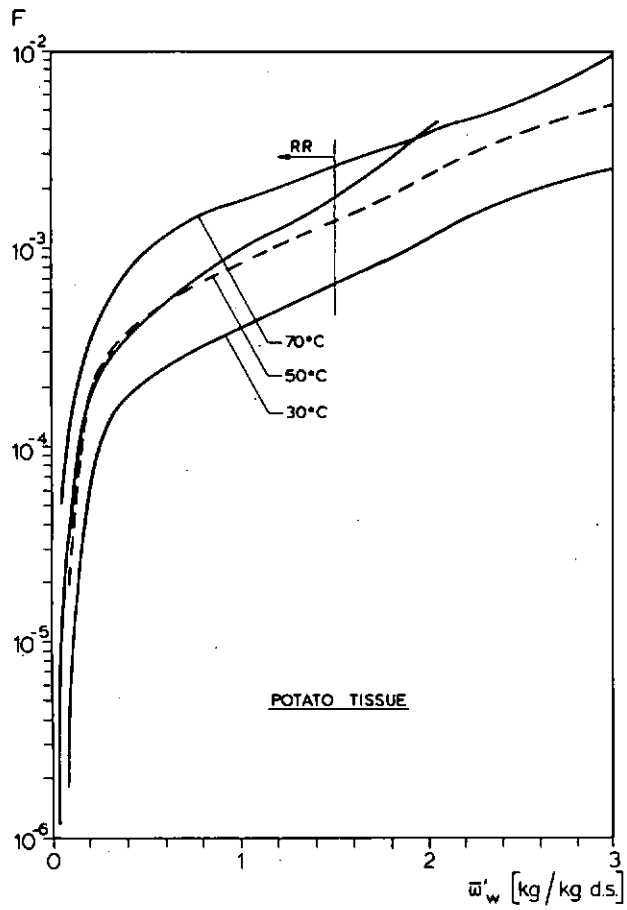

Fig. 14. Isothermal drying curves of potato tissue for zero surface concentration , (- - - : calculated).

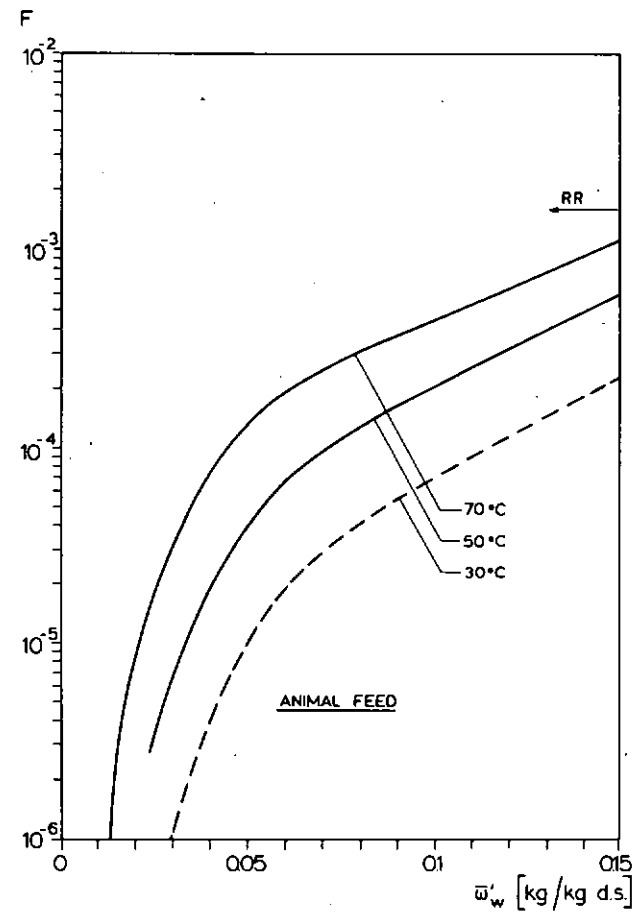

Fig. 16. Isothermal regular regime curves of an animal feed for zero surface concentration, (- - - : calculated).

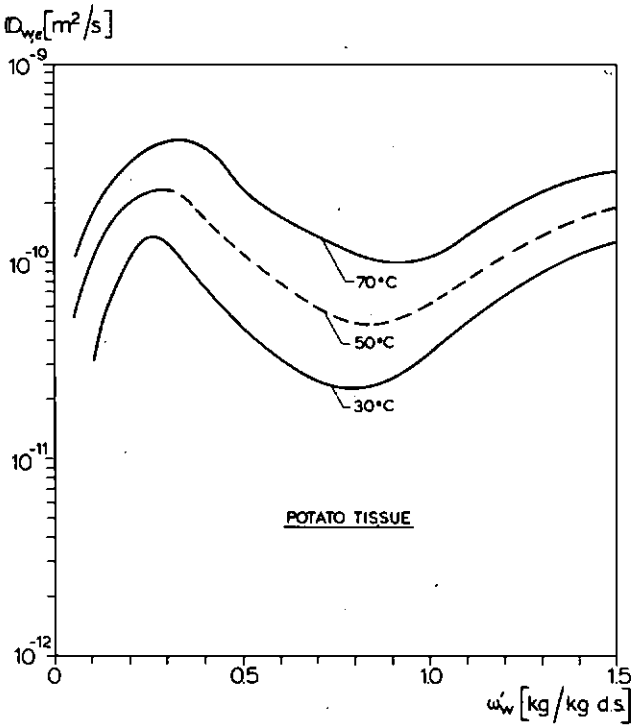

Fig. 15. Concentration dependence of the effective water diffusivity for potato tissue.

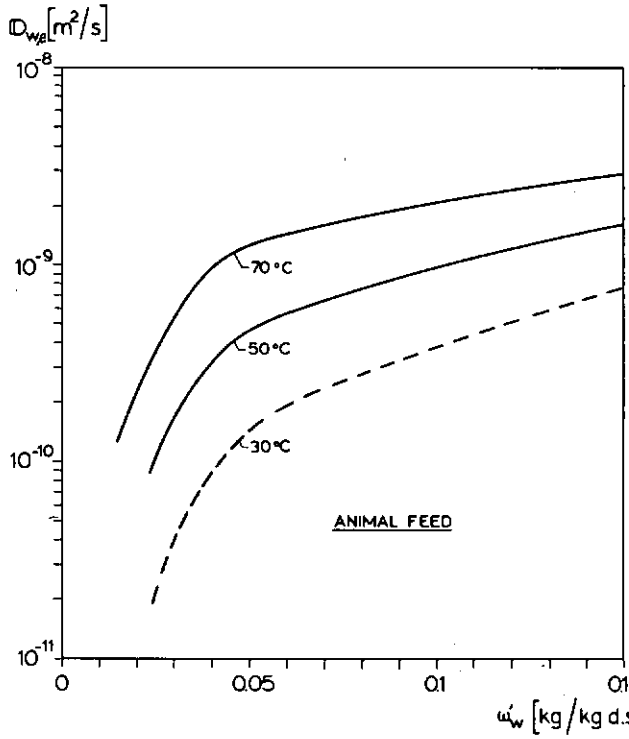

Fig. 17. Concentration dependence of the effective water diffusivity for animal feed.

Apple tissue

Spherical particles with a diameter between 1 and 1.5 centimetre were cut from the tissue of fresh apples. Isothermal drying curves calculated from the measurements are shown in Fig. 12. Effective water diffusivities calculated from the regular regime part of these drying curves are shown in Fig. 13. Parameters for the activation energy can be found in Table 1.

Potato tissue

Samples were prepared similar as for apple tissue. Fig. 14 gives the drying curves corrected for temperature and surface concentration in the described way. For the measurement at 50 °C the penetration period continues till well below 1.5 [kg/kg d.s.] because of the low initial moisture content, therefore we used in our calculations the dashed curve which is computed from the measurements at 30 °C and 70 °C. Fig. 15 gives the results from the calculation of the diffusivities, in which the curve for 50 °C is also dashed for the above mentioned reason. Parameters for the activation energy are given in Table 1.

Animal feed

For the experiments cylindrically shaped animal feed pellets have been used, which were closed at both ends. Fig. 16 gives the regular regime curves and Fig. 17 shows the diffusivities computed from these. Measurements were performed at 70 °C and 50 °C only and the curves for 30 °C were computed from these. Parameters for the activation energy can again be found in Table 1.

MATERIAL	A	B	C	RANGE
Glucose	146	6.64	24	0.10 - 2
Coffee extract	268	11.5	23	0.10 - 2
Skim milk	110	27.0	11	0.15 - 2
Apple tissue	110	12.3	51	0.05 - 2
Potato tissue	168	15.4	30	0.05 - 2
Animal feed	96	32.0	37	0.01 - 0.15

$$E_D \simeq E_F = A \exp(- B \omega'_w) + C \text{ [kJ/mol]}$$

Table 1. Parameters for the concentration dependence of the activation energy.

DISCUSSION

An important restriction to the results presented in the previous chapter is the fact that in all the calculations perfect homogeneous shrinkage was assumed. As already mentioned, for most of the materials we worked with, this assumption however, is not correct. In Fig. 18 the various types of shrinking behaviour we actually observed are reproduced schematically. For animal feed a small concentration range was measured and only very slight

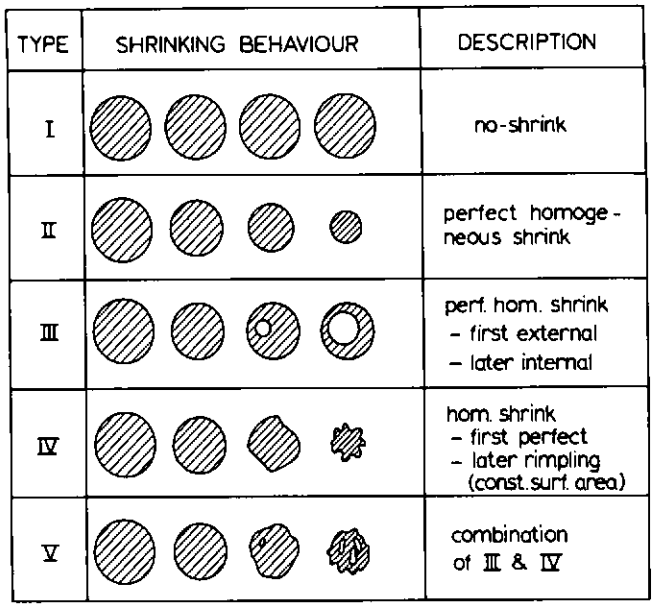

Fig. 18. Schematic representation of the various types of shrinking behaviour observed.

shrinkage occurred, so this can be described by either type I or II behaviour. Glucose was the only material which clearly showed a type II behaviour. Skim milk and coffee extract showed in the case of high initial fluxes a type III behaviour. Skim milk further gave the complication of cracks in these situations, but in case of very mild drying conditions a perfect homogeneous shrinking behaviour was observed for a longer period of time. Apple tissue exhibited type IV behaviour and potato tissue type V. In cases of the more complex type of shrinking behaviour the following simplifications may proof helpful. If shrinking does not occur from the inside (type II and IV) calculations can be based on perfect homogeneous shrinkage. An indication for this is the fact that for these materials no significant influence of initial radius was observed. If after some period of external shrinking a skin is formed and shrinkage progresses from the inside (type III and V) corrections can possibly be based on Sh_d, which in this case should be obtained from numerical calculations with a constant outer radius and a changing inner radius.

The effective diffusivities found for apple and potato tissue (not monotone with concentration) can be explained by the addition of two effects, prevailing vapor diffusion in the low concentration range and liquid diffusion at higher concentrations (12).
It is of importance to realize, that the diffusion coefficients presented in the previous chapter, are not to be interpreted as molecular diffusion coefficients. As already mentioned in the chapter DATA REDUCTION, these effective diffusivities can contain several effects like liquid diffusion, vapor diffusion (see above), surface diffusion, capillary flow, evaporation-condensation etc. Moreover, because we assumed perfect homogeneous shrinkage, also the effect of non-perfect and/or non-homogeneous shrinkage is incorporated in the diffusivities presented.

Finally a remark should be made on the accuracy of the diffusivities. During the calculations it was clearly found that fitting the F and $\overline{D}_r$ values and using the derivatives of these was the limiting factor. Using different splines (3 - 8 knots) could easily result in diffusivities differing by a factor of two, especially in the range from 0.6 till 1.2 [kg/kg d.s.]. The results presented have been obtained by taking the average of many different spline approximations.

REFERENCES

1. Schoeber, W.J.A.H., *Regular regimes in sorption processes*. Ph.D. Thesis, Eindhoven (1976)
2. Johnson, P.A. & Babb, A.L., Chem. Rev., 56 (1956), 387-
3. Crank, J. & Park, G.S., *Diffusion in Polymers*. Academic Press, London (1968)
4. Crank, J., *The mathematics of diffusion*. 2nd ed., Claridon Press, Oxford (1975)
5. Warmoeskerken, M.M.C.G., M.Sc. Thesis, Eindhoven (1975)
6. Franke, A.C., M.Sc. Thesis, Wageningen (1978)
7. Weys, A.R.S., M.Sc. Thesis, Eindhoven (1976)
8. Jansen, S.M., M.Sc. Thesis, Eindhoven (1977)
9. Aarts, G.J., M.Sc. Thesis, Eindhoven (1977)
10. International Mathematical and Statistical Libraries, *IMSL Library 2*, 6th ed., Houston, Texas (1977)
11. Gladden, J.K. & Dole, M., J. Am. Chem. Soc., 75 (1953), 3900 - 3904
12. Keey, R.B., *Drying principles and practice*, Pergamon Press, Oxford (1972).

CONTINUOUS VACUUM DRYING FOR HIGH VISCOUS AND HEAT SENSITIVE FOODS

Eitaro Kumazawa
Yukihiro Saiki, Yozo Ishioka, Shinichi Taneya, Hiromichi Hayashi

Snow Brand Milk Products Co., Ltd
Technical Research Institute
1-2, Minamidai 1-chome, Kawagoe, Saitama, 350 Japan

ABSTRACT

Improvements are made on the continuous vacuum drying method so as to enable application to foods of considerably high viscosity such as fresh fish meat paste and natural cheese.
By applying the model of the uniform retreating ice front to continuous vacuum drying, an optimization of heating temperature was attained through developing a correlation between drying conditions and product quality.
The overall heat transfer coefficient of the dryer was found to be around 23 $W/M^2 \cdot K$.

NOMENCRATURE

A_1, A_2 = areas of tube inside, outside, respectively (m^2)

A_{ln} = logarithmic mean area of A_1 and A_2 (m^2)

e = emissivity (-)

h = heat transfer coefficient (W/M^2K)

k = thermal conductivity of dried material ($W/M \cdot K$)

N = length of string-like material (m)

n = division number (-)

Q = total heat flow rate (J/sec)

Qc = heat flow rate by conduction (J/sec)

Qi = heat flow rate across evaporating front (J/sec)

Qr = heat flow rate by radiation (J/sec)

r = radius position of evaporating front (m)

R = radius of material (m)

T = temperature (k)

t = time (sec)

Td = drying time (sec)

Θ = contact angle (rad)

δ = stefan-boltzmann constant (W/M^2K^4)

ΔH = latent heat of evaporation of water (J/N)

Vw = volume occupied by unit water (m/N)

ΔP = pressure loss (Pa)

U = overall heat transfer coefficient ($W/M^2 \cdot K$)

Wo = initial moisture content (% WB)

Wr = moisture content at r position of evaporating front (% WB)

Wcal = moisture content obtained by calculation (% WB)

Wobs = moisture content observed by experiment (% WB)

Subscripts

h = heater

i = evaporating front

s = surface

INTRODUCTION

Selection of drying method is important for drying high viscous and heat sensitive foods. Vacuum puff-drying is considered as a suitable method for drying of such foods. According to several research reports,[1) 2) 3)] it results in products having porous structure, little deterioration of original flavour, and ready dispersibility in cold water. However, since this method was developed only through practical application, the actual theoretical basic mechanisms have as yet not been established, and problems of determination of the temperature and moisture content of the material in a drying chamber while in motion under vacuum remained.
In this study, a theoretical basic mechanism was developed for application of the continuous vacuum drying to foods of considerably higher viscosity. It was found that the temperature and moisture content of the material could be estimated by applying the model of the uniform retreating ice front, making possible the optimization of drying

conditions and the application of these estimated values to attain superior product quality.

THEORETICAL ANALYSIS

Uniform Retreating Model of Evaporating Front

Since in the drying of highly viscous material, movement of water from the internal areas of the material to the surface is difficult, we assumed a theoretical model, similar to that which occurs in the phenomenon of sublimation of frozen material having a gradually retreating evaporating front which starts from the surface and retreats into the interior as the drying progresses. We have applied this model, as shown in Fig.1, to continuous vacuum drying with the assumptions being;

1) Evaporating front retreats from the surface to the center of the drying material in an uniform manner.
2) The temperature at the evaporating front is equal to the saturation temperature corresponding to the operating pressure. (vacuum)
3) Extruded material diameter remains unchanged without shrinkage throughout drying process.
4) The material is uniformly extruded at the same speed as the moving belt.
5) The sensible heat of evaporation is considered as being negligible.
6) Emissivity of the material is 0.5.

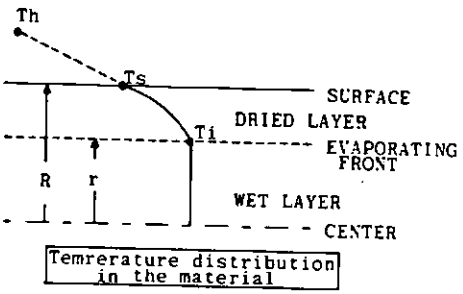

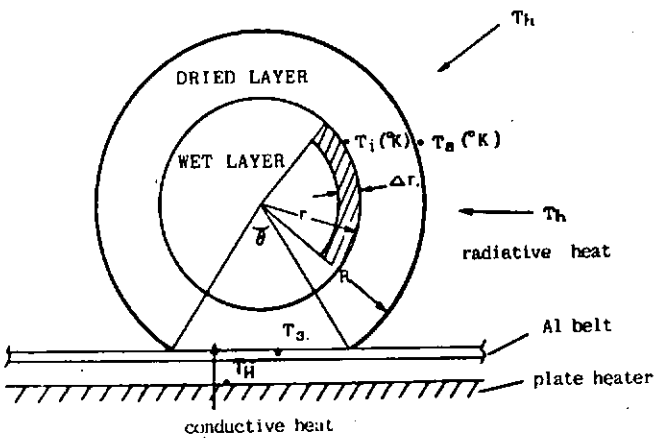

Fig.1 Uniform retreating model of evaporating front

Both radiative and conductive heat are applied to the material by an electric heater. Radiative heat is represented by the following equation(4th power law of radiation).

$$Qr = 2\pi R\ N\ e\delta\ (Th^4 - Ts^4) \quad \text{---------(1)}$$

The heat quantity passing to the material through the belt from the heater is represented as ;

$$Qc = h\ (2\pi R\ N)\theta/2\pi(Th - Ts) \quad \text{-------(2)}$$

($h\theta/2\pi = U$, U represents the overall heat transfer coefficient.)

The total heat quantity given to the material is;

$$Q = 2\pi R\ N\ \{e\delta(Th^4 - Ts^4) + U\ (Th - Ts)\} \quad \text{----(3)}$$

The heat quantity which passes through the developing dried layer from the material surface is given by the following equation as;

$$Qi = -2\pi k\ r\ N \frac{dT}{dr} = \frac{2\pi k\ N\ (Ts - Ti)}{\ln\ (R/r)} \quad \text{----(4)}$$

Since Q is equal to Qi, the following 4th power equation regarding Ts can be obtained.

$$Ts^4 + Ts\ \left(\frac{U}{e\delta} + k\ A\right) - \left(Th^4 + \frac{U\ Th}{e\delta} + k\ A\ Ti\right) = 0 \quad \text{---(5)}$$

where $A = 1/(R\ e\delta\ \ln\ (R/r))$

If Th corresponding to any given r is known, Ts can be obtained. Also, since Q is consumed as latent heat of evaporation, the following equation can be established.

$$Q = \frac{\Delta H}{Vw} \cdot (2\pi r\ N)\frac{dr}{dt} \quad \text{----------(6)}$$

By equalizing and integrating the equations (4) and (6), the time required for the evaporating front to retreat from the surface to r is obtained by;

$$t = \frac{\Delta H}{Vw\ k} \int_R^r \frac{r \cdot \ln\ (R/r)}{Ts - Ti}\ dr \quad \text{----------(7)}$$

EXPERIMENTAL APPARATUS AND PROCEDURE

Pre-treatment

1) fish meat paste
First class frozen fresh fish meat, used as starting material, is stored at 5°C for 18 hours to reach a semi-thawed condition and is then crushed using a slicer and a chopper, while adding ice to attain a moisture content of 20% and is further processed into paste in a colloid mill and used in the subject tests.
2) cheese
A 1:1 mixture of Gouda cheese and Chedder cheese (both were made in Australia) is used as starting material. The cheeses are chopped and blended. The blend is heated to 60°C and, with water being added to attain a total solid content of 45%, it is mechanically emulsified without emulsifying agent.

Measurement of Thermal Conductivity

It is reported [4) 5)] that the thermal conductivity of a dried material is affected by the pressure and nature of the gas surrounding it. The thermal conductivity of the dried materials in this work is measured by using the experimental apparatus as shown in Fig.2. The thermal conductivity, k,

of the dried material is calculated by the following equation,

$$k = Q (r_2 - r_1)/\{A_{1n} (T_2 - T_1)\}$$

where $Q = I^2 R$ (I = input current in ampere, R = resistance of the heat wire in ohm)

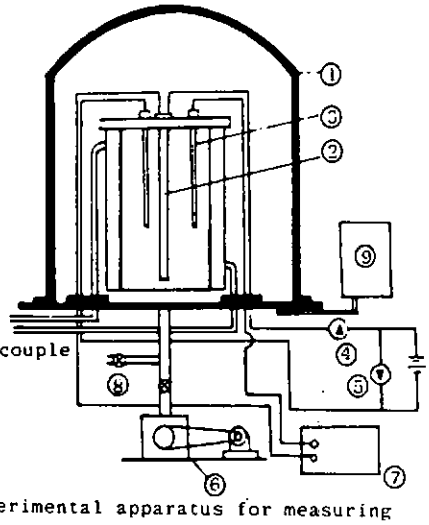

Fig.2. Experimental apparatus for measuring the thermal conductivity of the products in vacuum

Experimental Apparatus for Vacuum Drying

The experimental apparatus is shown in Fig.3. The device mainly consists of a supply section, a drying section, a product discharging section and a vacuum exhaust section. The material is charged into a cylinder and extruded under pressure from a piston into the feed nozzle. The emerging string-like material, which is extruded onto the moving belt, passes through the drying section and is dried to the desired moisture content. The drying section consists of a stainless steel pipe (78 mm in diameter, 6 m in length), wound around with a band heater and insulation. The belt guider is installed lengthwise inside the pipe with the plate heaters placed under the guider. The heater element (band and plate heater) is divided into 6 independent equal stages for the entire length of 6 m. The temperature of each stage can be controlled individually. The dried material is cut in lengths of about 5 cm by rolling cutter in vacuum chamber and passes out through the product discharging section. These 5 cm pieces are further pulverized into powder.

Feed Nozzle

The feed nozzle used is shown in Fig. 4. The shape of the nozzle developed after various preliminary tests is designed so that no dried material accumulates around the nozzle in long operations. The multi-orifices are placed in concentric circles to attain same linear velosities of the emerging extrusions for uniform product quality.

RESULTS AND DISCUSSION

Thermal Conductivity

Fig.5 shows the respective relation between pressure and thermal conductivity of fish meat powder and dried cheese powder. In these cases, the thermal conductivity increases with the increase of pressure. It is assumed that the thermal conductivities at less than 10 Pa in pressure approach their specific values. Because under very low pressure, the mean free path of gas molecules, which exists in pores of materials is larger than the diameters of pores, thermal conductivity becomes an unvarying inherent specific value.

As the pressure raises, the mean free path of gas molecules decreases and becomes comparable to pore diameters. Then, the thermal conductivity increases and is gradually leveling off at 10,000 Pa in pressure. For exampe, the thermal conductivity of dried cheese is 0.035 W/MK at 40 Pa and 0.055 W/MK at 1000 Pa, respectively.

In general, a vacuum dryer is usually operated at about 1,000 Pa and a freeze dryer, at less than 10 Pa. Therefore, the drying rate of a vacuum dryer is higher than that of a freeze dryer because of the difference in thermal conductivities of the dried material in the different pressure ranges.

Analytical Procedure

(a) Heating temperature is approximated using 3rd power equation of distance traversed from nozzle. Because measuring points of temperature are at the centers of each stage plate heater and each heater is closely connected, the temperature does not break in a stepwise manner, resulting in the use of a moderated curve in approximation.

(b) Read thermal conductivity corresponding to vacuum degree in Fig.5.

(c) Make assumption for U value.

(d) Divide material radius R into n equal parts ($\Delta r = R/n$), and calculate from the surface towards the center of the material ($R - \Delta r$, $R - 2\Delta r$, ... $R - i\Delta r$, ... Δr, 0) in step with gradual retreating of evaporating front.

Assuming that the portion through which evaporating front has passed is in a completely dried state and the remaining portion has the same solid content as originally, moisture content in r position can be calculated from the following equation;

$$Wr = Wo \left(\frac{r}{R} \right)^2$$

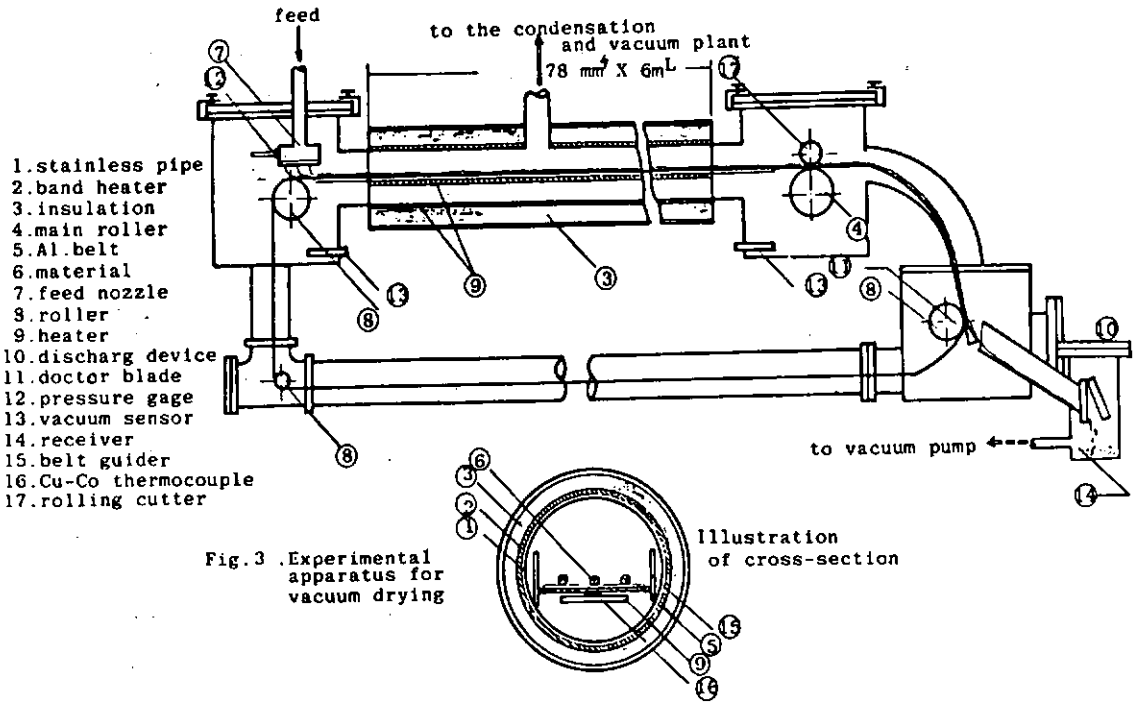

Fig.3 .Experimental apparatus for vacuum drying

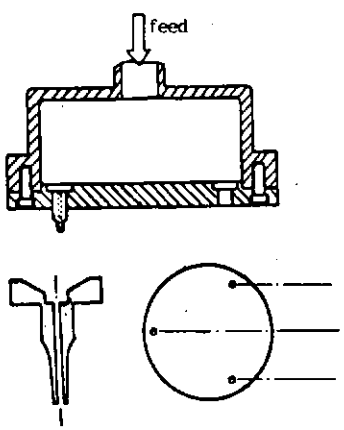

Fig.4. Illustration of feed nozzle

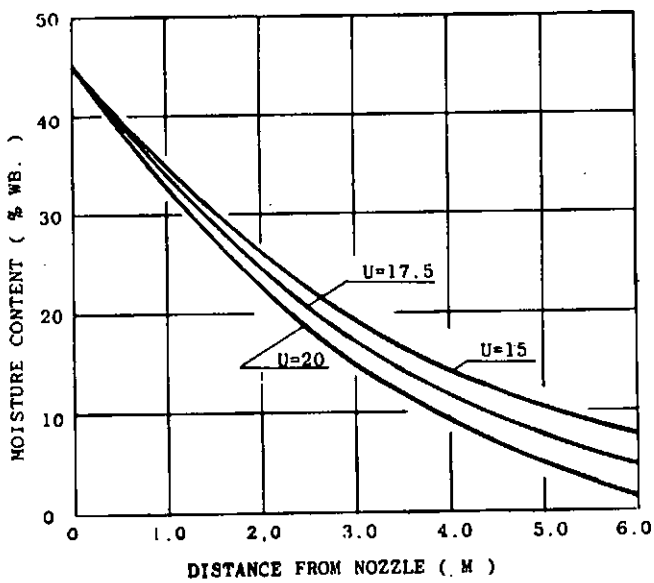

Fig. 6 . Effect of U value on the change of the moisture content of the material

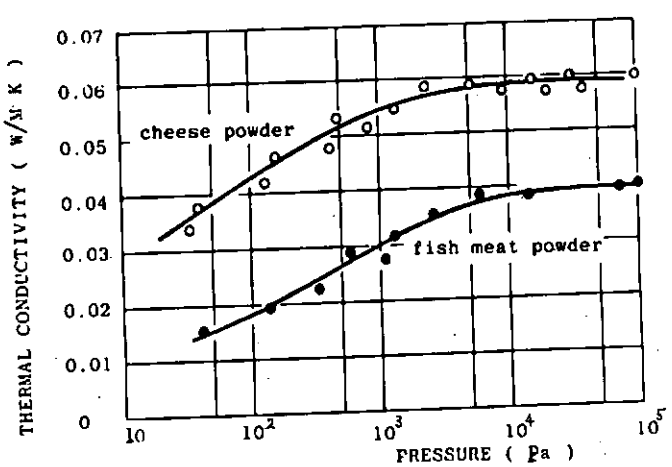

Fig.5. Effect of pressure on thermal conductivity

(e) Calculation of Ts
In the 4th power equation (5) regarding Ts, if evaporating front position is given, all the coefficients become known. Using incremental approximation, the equation (5) can be solved by computer calculation to obtain Ts.
(f) With Ts obtained as above, increment time (Δt), which evaporating front takes to retreat a minute distance (Δr), can be calculated from the equation (6).
(g) Thus, the time in which evaporating front position retreats from R to r is obtained and, as a result, the position of material in drying tube of evaporating front when at r can be calculated. Here, the time Td in which material passes through

6 m of drying tube is obtained through tests. By repeating calculation of (d) to (g), until t = Td, the change of surface temperature, the change of moisture content in material and the heat accumulation at material surface can be obtained. Above procedure is programmed and calculated are made using a computer. From this calculation, the moisture content of final product(Wcal), corresponding to any given U value, can be calculated This calculation, using arbitrarilly assumed U values, is repeated until the thus calculated Wcal and Wobs as observed in test become equal ; the U value at this point becoming the sought for U value. In this case, as shown in Fig.6, Wcal decreases with the increase in U value. This is, as understood from equation(3), because, with an increase in U value, input heat (Q) to material increases and accordingly drying rate increases.

Performance of Vacuum Drying

Experimental and analysed results are shown in Table. 1 and Table. 2 for the cheese and the fish meat paste, respectively. The heating temperature was lowered to minimize the heat accumulation on the surface of the material because conductive resistance increases with the thickening of dried layer at the surface.
Generally, the moisture content of final products is the net result of the solid content in the raw material, vacuum degree, drying time, heating temperatures, etc.
The six heaters, here, can control individually the heat input of the respective stages but the surface temperature and moisture content of the material can not be acculately controlled at 2nd and following stages due to residual heat effects of the preceeding stages on the drying rates of individual stages. Therefore, the required heating temperature has to be determined by analysing experimental data concerning the moisture content of final products; the experimental data obtained here being analysed by a computer based on the model in previous Theoretical Analysis.
In the calculations, n = 100, namely, division width of 0.01 is used.

1) Fig. 7 is a calculation example of drying performance of fish meat paste. As a result of calculations, Wcal is equal to Wobs at the U value of 29 W/M^2K. In the early stages of drying, the dried layer is as yet thin and resistance to conductive heat is small, therefore, even if heated to such a high temperature as 250°C, input heater to the material is mainly used as latent heat and surface temperature does not rise noticeably.
However, as drying progresses, the dried layer thickens and resistance to conductive heat becomes larger. If high temperature heating is continued, surface temperature increases quite noticeably. Therefore, as shown in Fig. 7, the heating pattern which reduces the temperature is chosen and the rise in surface temperature is consequently suppressed. In this example, this is achieved by reducing the temperature of 3rd and 4th heaters.

2) Fig.8 shows a calculation example of the drying performance of cheese. In this instance, in spite of adoption of a heating pattern quite similar to

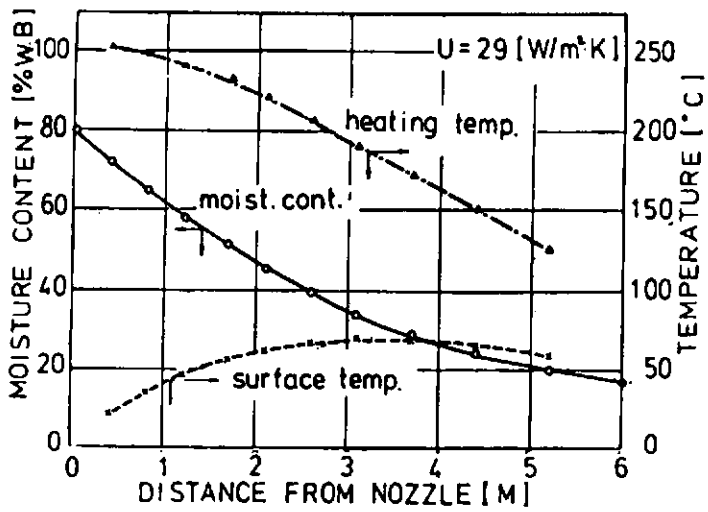

Fig.7. A calculation example of drying performance for fish meat paste

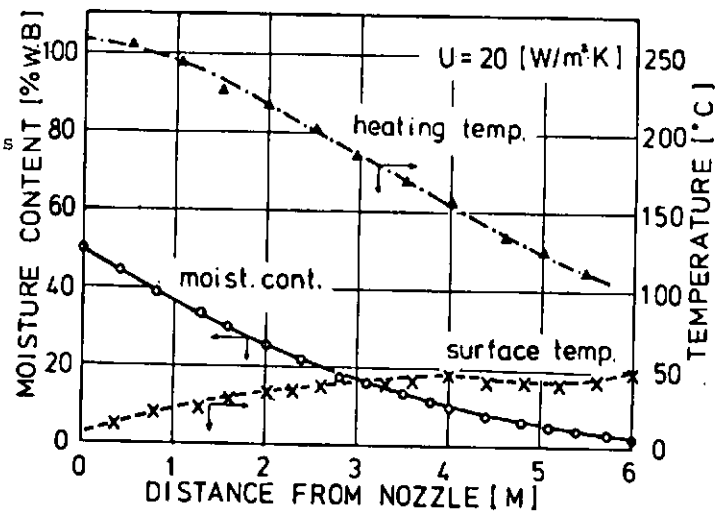

Fig.8. A calculation example of drying performance for cheese

that of 1), the maximum surface temperature is only 45°C and, moreover, the drying rate is faster than that of fish meat paste. This is because, as seen in Fig. 5, apparent thermal conductivity of dried cheese is higher than that of fish meat powder.

3) The calculated value of Qc divided by Qr is about 3 in all the tests. Therefore, it is assumed that heat for this drying is mainly transferred by conduction through the moving belt. Fig. 9 shows the relation between U and belt speed. As far as determined through our tests, U values remain between 15 and 33 W/M^2K, so long as belt speed remains below 200 m/hr. This is because, in this test, the moving belt contacts the plate heater and contact efficiency between belt and plate heater decreases with increase of belt speed, which in turn results in reduction of U value. Hence, in designing the dryer, the belt speed had better be below 200 m/hr; otherwise, heat efficiency of the dryer will be reduced.

Table 1. Experimental condition and analysed results for cheese

Exp.condition / Exp. No.	orifice dia.	chamber press.	drying time	initial moist.	heating temperature (°C)						Wobs.	U	Wcal.
					1st	2nd	3rd	4th	5th	6th			
	mm	Pa	sec.	%							%w.b.	W/m²K	%w.b.
1	1.5	670	107	45	257	227	205	170	130	113	1.25	20	2.0
2	1.5	670	106	45	241	215	192	147	110	75	8.2	30	8.0
3	2.0	1340	145	45	212	187	164	124	99	68	19.3	15	18.9
4	2.0	2700	184	45	241	210	179	140	109	85	6.5	22	6.8
5	2.0	2700	162	45	217	191	158	118	88	65	14.1	20	12.5
6	2.0	2700	154	45	210	183	141	109	79	54	17.0	20	18.0
7	2.0	2700	150	45	216	181	166	143	115	85	9.6	20	10.6
8	2.0	2700	154	45	238	191	158	126	100	78	10.0	20	9.7
9	2.0	2700	165	45	237	195	170	153	116	94	4.0	20	4.5

Table.2 Vacuum Drying Condition and Product Quality for Fish Meat Paste

Cond.and quality / Exp.No.	orifice dia.	chamber press.	drying time	heating temperature (°C)						final moist.	ATPase activity
				1st	2nd	3rd	4th	5th	6th		
	mm	Pa	sec							%WB	P-μmol/g.min
1	1.5	1000	96	243	229	215	195	151	115	30.0	91.7
2	1.5	1000	97	234	225	219	196	147	116	17.0	43.9
3	1.5	1300	90	211	202	187	162	138	117	51.9	107.8
4	1.5	1300	112	210	203	188	159	135	116	28.5	94.0
5	1.5	1300	135	211	206	190	158	134	115	16.6	84.9
6	1.5	1300	90	240	224	201	171	139	118	45.8	117.5
7	1.5	1300	153	245	243	242	234	195	201	5.0	20.5
8	1.5	1300	115	260	214	189	147	111	72	34.1	78.7
9	1.5	1300	119	252	245	240	225	130	69	22.6	50.9
10	1.5	1300	90	246	244	244	223	125	68	40.7	67.5
11	1.5	1300	130	210	190	169	140	96	60	39.4	80.8
12	1.5	1300	171	211	194	173	186	103	68	13.4	70.4

4) Correlation of heat accumulation on material surface and ATPase activity (Adenosine Tri Phosphatase)

Degree of heat denaturation which dried material receives may be estimated from heat accumulation associated with time factor rather than the maximum temperature which material reaches. As seen in Fig.1, which indicates temperature distribution inside material during drying process, material surface always has the highest temperature and is the place which receives heat denaturation most easily. For this reason, heat accumulation on material surface is calculated and its relation with product quality is examined.

Noticing that fish meat protein is far more heat sensitive than that of cheese and, therefore, fish meat will exhibit more conspicuous tendencies, test results of fish meat are analysed. Fig. 10 shows the relation between accumulated heat and ATPase activity. In Sample 1 and Sample 2, different

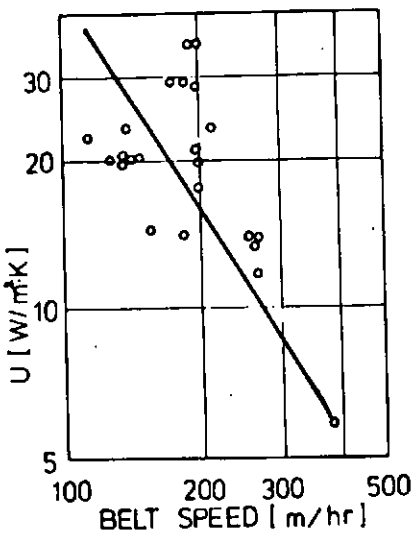

Fig.9. Relation between U and belt speed

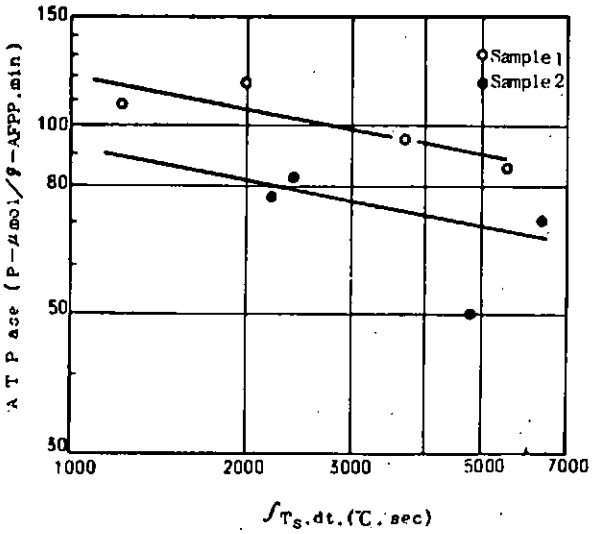

Fig.10. Relation between accumulated heat and ATPase activity

correlations are present. In other words, with increase of accumulated heat on material surface, ATPase activity tends to decrease. This result suggests that the ATPase activity which the material will have when dried in any given drying condition can be predicted by measuring the ATPase activity at the raw material stage.
The optimum drying condition necessary for obtaining a high quality product can also be determined by repeatedly calculating the accumulated heat on the surface until it becomes minimum.

CONCLUSION

Applying the model of uniform retreating ice front, changes of material surface temperature, moisture content and heat accumulation during the drying process are calculated and their correlations with final product quality are determined.
Hitherto, drying conditions have been selected through trial and error methods, but, by using this analytical procedure, optimization becomes possible.

REFERENCES

1. F.Fixari, W.Conley, and G.Bard. Continuous high vacuum drying techniques. Food Tech. March, 1959, P.217-220
2. N.C.Aceto, H.I.Sinnamon, E.F.Shoppet, and R.K.Eskew. Continuous vacuum drying of whole milk foam. J.Dairy Science, 45(4) P.501-507 (1962)
3. G.K.Notter, J.E.Brekke, and D.H.Taylor. Factors affecting behavior of fruit and vegetable juice during vacuum puff-drying. Food Tech. June, P.341-345 (1959)
4. G.L.Gentzler and F.W.Schmidt. Determination of thermal conductivity values of freeze-dried evaporated skim milk. J.of Food Sci. 37, 554 (1972)
5. T.A.Triebes, and C.J.King. Factors influencing the rate of heat conduction in freeze-drying. I&EC Process Design And Development. 5(4) Oct, P.430(1966)

KINETICS OF SOYBEAN DRYING

Constantino Suarez, Pascual Viollaz,
and Jorge Chirife

Facultad de Ciencias Exactas y Naturales,
Universidad de Buenos Aires, Dto. Industrias,
1428 Buenos Aires, Argentina

ABSTRACT

The solution of Fick's second law for diffusion out of spheres was succesfully applied to describe the kinetics of soybean drying. It was found that the diffusivity of water in soybean was fairly constant in the approximate range of moisture content 29 - 7 % (dry basis). The classical Arrhenius type temperature dependency of moisture diffusivity was found, the energy of activation being 8.7 kcal/g mole. It was observed that oil content of soybean affects the kinetics of drying.

INTRODUCTION

Various studies have been made on the rate of moisture diffusion through cereal grains and others field crops, mainly in connection with problems of drying. Diffusion models have been considered for the drying of, wheat (Becker and Sallans, 1955), corn (Chu and Hustrulid 1968), rice (Steffe and Singh, 1979) and sorghum (Suarez et al. 1980), among many others. This work examines the application of a constant diffusivity model to interpret the kinetics of moisture movement during air drying of a thin-layer of soybeans.

EXPERIMENTAL PART

Laboratory drier

It consists of a centrifugal fan which blows the air over twelve 0.75 kW electric bar elements into a chamber at the base and then upwards through a vertical duct. The vertical duct has a flow-smoothing section of small glass spheres. A metal cup with screened bottom and lid served as drying chamber and was mounted on the outlet of the duct. A high constant air velocity (about 10 - 13 m/sec) was used in all experiments in order to eliminate external resistances to the moisture loss. This through-flow of air produced a vigorous fluidizing action in the grain sample. The inlet air dry bulb temperature was regulated ($\pm$ 0.1°C) by an electronic proportional controller; wet and dry bulb thermometers were fitted in the drying chamber. Relative humidity of the drying air was calculated from the wet bulb depression. A single layer of grain (about 20 g) was used for each drying experiment the progress of which was followed by weighing the sample periodically in a precision balance ($\pm$ 0.001 g). For this purpose, the drying cup was removed, rapidly weighed and replaced in the drier at regular intervals.

Materials

A local variety of soybean having an average oil content of 21 % was used in most experiments. Some drying runs were also performed using a different variety having an oil content of 15 %. Oil content was determined using a soxhlet apparatus. The soybean was received with an average moisture content of about 10 - 11 % (dry basis).
It was neccesary to add water to the soybean for the drying experiments. This was done by humidification over a saturated solution of barium chloride which provided a constant relative humidity of about 90 %. The grain was placed in evacuated vacuum dessiccators

containing the saturated salt solution and kept at 7°C until equilibrium was reached. The grains were irradiated with UV light in order to prevent (or delay) the growth of microorganisms during the equilibration period (about 2 weeks). This method of humidification gave more satisfactory results than the usual procedure of adding liquid water (Becker and Sallans 1955, Steffe and Singh 1979) to the grains.
Moisture content of grains at equilibrium was found to be 29 % (dry basis) and this value was used as initial and uniform moisture content of the grains in the drying runs.
The grains were screening prior to humidification and drying in order to obtain samples of uniform size. Size distribution of the samples utilized in the drying experiments ranged between 0.70 - 0.75 cm. Volumetric tests were conducted to obtain radius estimates of the soybean grains. The total volume of a large lot of grains was measured using a pycnometer (with chlorobencene as the fluid). The average grain volume was calculated by dividing the total sample volume by the total number of grains. The equivalent spherical radius was then computed from the formula for the volume of a sphere ($V = 4\pi r^3/3$) using the average grain volume.
Moisture content of the grains was determined gravimetrically using a vacuum oven method at 70°C over magnesium perchlorate.

Determination of equilibrium moisture content

Selected values of equilibrium moisture content at the various drying temperatures were determined by equilibration against saturated salt solutions which provided known constant relative humidities. The measurements corresponded to the desorption branch of the isotherm. The details of the experimental technique have been published elsewhere (Iglesias et al. 1975).

RESULTS AND DISCUSSION

Figure 1 shows the effect of two different air velocities on the drying curve of soybean. It can be seen that increasing air velocity does not affect the drying rate, which means that the internal transfer of moisture is likely to be the main resistance to the rate of loss of moisture (Vaccarezza et al. 1974). Assuming that the simultaneous heat transfer which accompanies mass transfer may be neglected, (Alzamora et al., 1979), the solution of Fick's second law for diffusion out of spheres may be used to fit the experimental drying data of soybean

$$m^* = \frac{\bar{m} - m_e}{m_o - m_e} = \frac{6}{n^2\pi^2} \sum_{n=1}^{\infty} \exp(- n^2\pi^2 D_{eff} \theta / r^2) \qquad (1)$$

where $\bar{m}$ is the average moisture content (dry basis), m_o is the uniform initial moisture content, m_e is the equilibrium moisture content (at the air dry bulb temperature), r is the radius of grain, θ is the drying time, and D_{eff} is the moisture diffusivity.
Diffusion coefficients for water in soybean were found by comparing actual and predicted (equation 1) drying curves.
Equilibrium moisture contents to be used in equation 1, were determined experimentally for the various drying runs; Table 1 shows some of the values obtained. The diffusion coefficients were calculated by means of a non-lineal regression method which minimizes the sum of the squared deviation between the actual and theoretical curve.
Typical results comparing the predicted and measured drying curves for soybean at three different temperatures are shown in Figure 2. These curves indicate that the diffusion theory with constant diffusivity predicts very well the drying behaviour of soybean.
In order to obtain the influence of temperature on the diffusion coefficient, values of log D_{eff} are plotted versus 1/T, as shown in Figure 3. It can be seen that the plot is essentially a straight line, from which an activation energy for diffusion may be estimated from the Arrhenius equation

$$D_{eff} = A \exp(- E_a/RT) \qquad (2)$$

The activation energy calculated from the slope of the straight line in Figure 3 was found to be, E_a = 8.7 kcal/g mole. Table 2 compares the activation energy for water diffusion in soybeans, with literature values for other field crops in similar ranges of moisture content.
The influence of oil content on the drying rate of soybean may be observed in Figure 4 which shows the drying behaviour at 53 °C and 60°C of soybean having 21 % and 15 % oil content respectively . It can be seen that increasing oil content decreases the rate of drying at both temperatures studied. Other authors also found that the drying behaviour of foods was influenced by its fat/oil content. Palumbo et al. (1977), Jason (1965) and Alzamora and Chirife (1980) found that the diffusion coefficients of water in pepperoni, fish muscle and avocado pulp, respectively, were inversaly correlated with the fat/oil content. These effects were attributed to the hydrophobic character of fat which imposes a resistance to the flow of water.

CONCLUSIONS

As found by many workers who studied the drying of various field crops (Becker and Sallans 1955, Steffe and Singh 1979, Suarez et al. 1980), the internal diffusion equation with constant diffusivity predicts very well the drying behaviour of soybean in the moisture range of most practical interest. It was also observed that the rate of drying was negatively affected (decreased) by the oil content.
It is interesting to note that the ability to mathematically represent the single-particle drying behavicur is a preliminary requisite for the successful application of modeling techniques to large masses of grain undergoing drying.

ACKNOWLEDGMENTS

The authors acknowledge the financial support from the Secretaría de Estado de Ciencia y Tecnología de la República Argentina (Programa Nacional de Tecnolcgía de Alimentos).

REFERENCES

1. Alzamora, S.M., Chirife, J. and Viollaz, P. (1979). J. Food Technol., 14 : 369
2. Alzamora, S.M. and Chirife, J. (1980) J. Food Science (in press).
3. Becker, H.A. and Sallans, H.R. (1955). Cereal Chem., 32 : 212
4. Chu, S. and Hustrulid, A. (1968). Trans. ASAE, 11 : 705
5. Jason, A.C. (1965). J. Sci. Fd. Agric., 16 : 281
6. Palumbo, S.A., Komanowsky, M., Metzger, V.and Smith, J.L. (1977). J. Food Sci., 42 : 1029
7. Steffe, J.F. and Singh, R.P. (1979). Diffusivity of starchy endosperm and bran of fresh and rewetted rice. Paper Nº 53, 39 th. Annual IFT Meeting, St. Louis, June 10, 1979.
8. Suarez, C., Viollaz, P. and Chirife, J. (1980). "Diffusional analysis of air drying of grain sorghum". Submitted for publication.
9. Vaccarezza, L.M., Lombardi, J.L. and Chirife, J. (1974). J. Food Technol., 9 : 317

Table 1. Equilibrium moisture content of soybean for various drying conditions.

Run Nº	Air temperature (°C)	RH (%)	m_e (dry basis)
1	60.0	7	0.006
2	53.0	4.5	0.008
3	41.5	18	0.034
4	70.8	2.1	0.000
5	53.0	17	0.022
6	60.0	12	0.010

Table 2. Activation energies for water diffusion during drying of various cereal grains and soybeans.

	Moisture range (dry basis)	E_a (kcal/g-mole)	Reference
Rice[a]	0.34-0.15	6.8	Steffe & Singh (1979)
Sorghum	0.21-0.06	7.5	Suarez et. al (1980)
Soybean[b]	0.29-0.07	8.7	This work
Weat	0.30-0.12	12.9-14.6	Becker & Sallans (1955)

LEGENDS FOR FIGURES

Figure 1. Effect of air flow rate on drying curves of soybean (21% oil content)

Figure 2. Comparison of measured and predicted drying curves for soybean (21% oil content) at various air dry bulb temperatures.

Figure 3. Effect of temperature on the diffusion coefficient of water in soybean having 21% oil content.

Figure 4. Comparison of drying kinetics of soybean with different oil content.

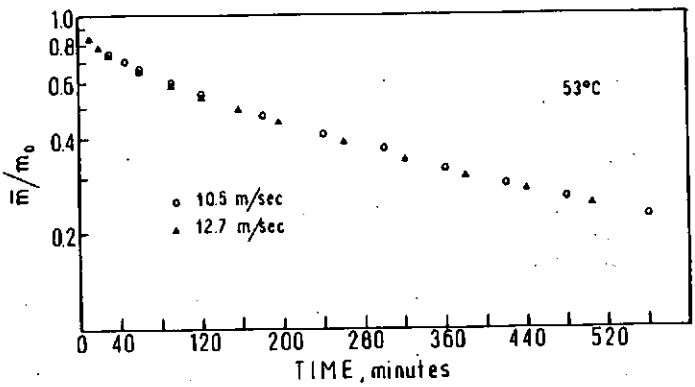

FIGURE 1

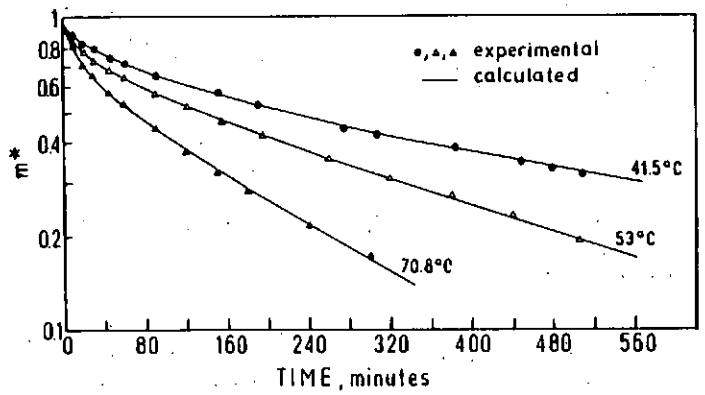

FIGURE 2

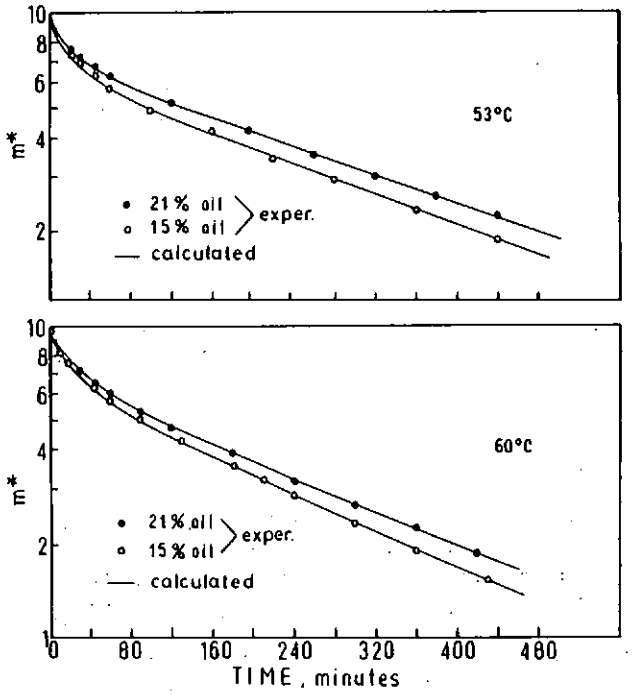

FIGURE 4

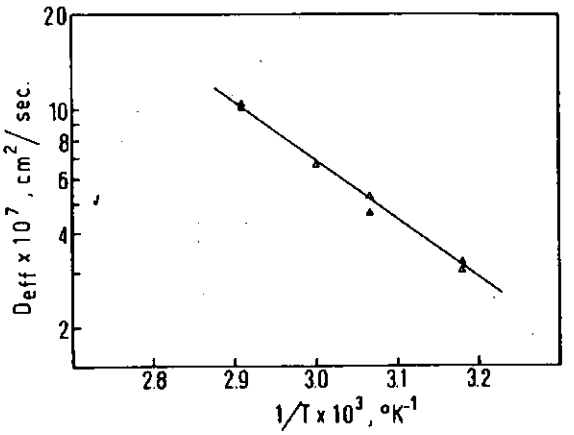

FIGURE 3

PARAMETERS REQUIRED IN THE ANALYSIS OF ROUGH RICE DRYING

J.F. Steffe[1]
R.P. Singh[2]

1. Michigan State University, East Lansing, MI
2. University of California, Davis, CA

ABSTRACT

Parameters required in the analysis of rough rice drying are reviewed and recent research related to these parameters is summarized. Equations describing the following rough rice variables are presented: basic thermal and physical properties; convective heat transfer coefficient; equilibrium moisture content; thin-layer drying; and mass diffusion coefficients. Curves describing the pressure drop through a bed of rough rice are also given for numerous rice varieties.

NOMENCLATURE

D = diffusivity (m^2/h)

G = airflow rate (kg dry air/$s \cdot m^2$)

h = convective heat transfer coefficient ($J/m^3 \cdot s \cdot K$)

h_{fg} = latent heat of vaporization (kcal/kg)

M = moisture content (percent wet basis)

M_d = moisture content (decimal dry basis)

M_e = equilibrium moisture content (percent dry basis)

M_o = initial moisture content (percent dry basis)

M_p = moisture content (percent dry basis)

r = statistical correlation coefficient

RH = relative humidity (decimal)

t = time (h)

t' = tempering time (h)

T_a = absolute temperature (^oK)

T_a' = absolute temperature (^oR)

T_c = temperature (^oC)

V = volume (mm)

ΔM = moisture reduction in one drying pass (percent dry basis)

Δt = length of one drying period

INTRODUCTION

Rice constitutes a major segment of the world food supply. The grain is generally harvested at a high moisture content and must be dried to insure preservation. Rice may be dried in a batch or continuous type system which may include numerous flow or mixing patterns. The analysis of rough rice drying is a prerequisite for optimizing the design and operation of rice dehydration equipment.

OBJECTIVE

The purpose of this paper is to summarize the current information available on the parameters required in the analysis of rough rice drying. The following parameters were considered: kernel dimensions, kernel volume, specific gravity, bulk density, surface area, porosity, pressure drops through a bed of rough rice, equilibrium moisture content, diffusion coefficients, specific heat, bulk thermal diffusivity, bulk thermal conductivity, latent heat of vaporization, convective heat transfer coefficient, thin-layer drying equations and tempering time.

ROUGH RICE CLASSIFICATION

The varieties of rice grown in the United States may be divided into three types depending on the size and shape of the grain. The groups of rice are referred to as short (Pearl), medium, and long grain types. The size and shape classification based on the brown rice kernels (dry) are as follows (USDA (1)):

	Average Length (mm)	Average Length/ Width Ratio
Long grain	6.61 to 7.5	over 3.0
Medium grain	5.51 to 6.6	2.1 to 3.0
Short grain	5.50 or less	Up to 2.1

The principle rice varieties grown in the United States are listed in Table 1. It should be noted that new varieties are regularly introduced into the agricultural market and many new rice varieties have been developed (such as short grain S6 and medium grain CSM5) since the information in Table 1 was first developed.

ROUGH RICE DRYING PARAMETERS

Table 1. Principle rice varieties grown in the United States (USDA(1)).

Grain type & variety	FAO* number	Registration** number
Short-grain:		
Caloro	211	5
Colusa	213	8
Medium-grain:		
Arkrose	207	1
Calrose	1013	6
CS-M3	-	34
Nato	1133	13
Nova 66	-	30
Saturn	1415	29
Zenith	206	19
Long-grain:		
Belle Patna	1334	27
Bluebelle	-	32
Bluebonnet 50	1012	3
Dawn	-	33
Della (aromatic)	-	-
Rexoro	214	14
Starbonnet	-	31
Toro	1134	18
TP 49	1020	17

*Accession number, World Catalogue of Genetic Stocks - Rice. Food and Agriculture Organization of the United Nations.

**Registration number, American Society of Agronomy - U.S. Department of Agriculture.

Table 2. Dimensions of short, medium and long grain rough rice.

Dimension = A + B(M)

where M = Moisture Content in Percent Wet Basis

Dimension (cm)		Short* Grain	Medium** Grain	Long† Grain
Length	A	.7318	.899	.894
	B_2	.00122	.00013	.00584
	r^2	.98	.99	.96
Width	A	.3358	.302	.239
	B_2	.00089	.00076	.00165
	r^2	.99	.60	.96
Thickness	A	.2187	.184	.177
	B_2	.00089	.00089	.00114
	r^2	.99	.89	.85
Approximate Range of M		11-22	12-18	12-18

* Morita and Singh (2): Rice variety is Caloro
** Wratten et al. (3): Rice variety is Saturn
† Wratten et al. (3): Rice variety is Bluebonnet -50

Dimensions

Dimensions of rough rice kernels are determined by making physical measurements of the length, width and thickness. Equations which describe the variation (with moisture content) in the principle dimensions of short, medium and long grain rough rice are summarized in Table 2. The length and width equations for the short grain rough rice were determined by Morita and Singh (2) from the measurements of individual kernels made with a calibrated microscope. Wratten et al. (3) based the length and width equations for the medium and long grain rough rice on the measured length of 10 kernels (placed tip to tip or side to side). A micrometer was used to measure the thickness for all grain types.

Generally, the regression equations given in Table 2 are a good representation of the original data. However, the equation to describe the width of the medium grain rough rice has a particularly low coefficient of correlation. The correlation coefficients for the thicknesses of the medium and long grain rice types are also low.

Volume

Wratten et al. (3) have formulated linear equations expressing volume as a function of moisture content (Table 3). Data from Steffe (4) was used to formulate the following linear regression equation to describe the volume of a short grain, smooth hulled variety of rough rice (S6):

$$V = 19.29 + .1684\ M_p \qquad [1]$$

$$r^2 = .93$$

Steffe and Singh (5) found that a volumetric reduction of 10.7% could be expected in reducing the moisture content of short grain rough rice from 30 to 15 percent moisture content dry basis. The data of Steffe and Singh (5) also indicate that the volumetric reduction of the hull may be less than the volumetric reduction of the brown rice kernel during rough rice drying. This unequal shrinkage may have a significant influence on the drying characteristics of the grain.

The volumetric data discussed above was determined with the use of an air-comparison pycnometer. The specific volume of a certain number of kernels was measured and the average volume per kernel was calculated from the resulting data.

Surface Area

The following four methods have been used to determine the surface area of rough rice:

--Method 1 was reported by Wratten et al. (3). Individual kernels of grain were embedded in wax and sliced into sections with a microtome cutting machine. The perimeters of the grain body sections were found by assuming an elliptical shape and the surface area was calculated by multiplying the section thickness by the perimeter (average of both sides). The surface

areas of the kernel ends were calculated by assuming them to be right circular cones. Total surface area was determined by adding the areas found for the individual sections.

Table 3. Constants required in the equations to calculate various rough rice parameters.

Quantity = A + B(M)

where M = Moisture Content in Percent Wet Basis

Quantity (Units)		Short* Grain	Medium** Grain	Long† Grain
Volume (mm)	A	-	9.73	15.40
	B_2	-	.508	.229
	r^2	-	.95	.95
Bulk Density (g/cm^3)	A	.5836	.4997	.5194
	B_2	.00427	.00833	.00528
	r^2	.95	.99	.94
Specific Gravity (True)	A	1.421	1.465	1.436
	B_2	-.00564	-.0076	-.0042
	r^2	.94	.94	.95
Porosity (Percent)	A	-	69.05	65.55
	B_2	-	.885	.475
	r^2	-	.99	.95
Specific Heat (Cal/g°C)	A	.3032	.2201	-
	B_2	.00833	.01301	-
	r^2	.93	.81	-
Bulk Thermal Conductivity (W/m°K)	A	.09999	.0866	-
	B_2	.01107	.00133	-
	r^2	.65	.87	-
Bulk Thermal Diffusivity (m^2/hr)	A	.000451	.000486	-
	B_2	5.58×10^{-6}	8.96×10^{-6}	-
	r^2	.99	.99	-
Approximate Range of M		11-22	12-18	12-18

*Morita and Singh (2): Rice variety is Caloro
**Wratten et al. (3): Rice variety is Saturn
†Wratten et al. (3): Rice variety is Bluebonnet-50

--Method 2 was reported by Hosokowa and Motohashi (6). The hull of the rough rice kernel was removed and flattened between two glass slides. The total surface area of the grain was measured by using a planimeter on a magnified picture of the flattened hull.

--Method 3 was reported by Morita and Singh (2). The surface area was determined with the use of a scanning electron microscope and a geometrical analysis. This method accounts for the many small ridges found on the surface of rough rice. The dimensions, density and shape of the ridges were determined from electron microscopic pictures. Mathematical functions which described the side and end views of the ridges were formulated to determine the area per ridge. The basic hull area was found by Method 2 mentioned above. Total surface area was computed by multiplying the surface area per ridge (cm^2/ridge) times the number of ridges per unit basic area (ridges/cm^2) times the total basic area (cm^2).

--Method 4 was reported by Bakshi and Singh (7). This method involves coating a known number of rough rice kernels and glass beads with a thin layer of varnish and nickel power. The surface area of the rice is calculated from the known surface area of the glass beads and the measured amounts of metal powder adhering to the rice and beads respectively.

The surface area values reported from using Methods 1 and 2 are related to the projected area of the rough rice kernel because they do not account for the ridges found on the rough rice hull. Bakshi and Singh (7) found that Method 4 gives erroneous results when measuring the surface area of rough rice due to the irregular hull surface. They conclude that Method 3 gives the best estimate of the actual rough rice surface area. Morita and Singh (2), using Method 3, have reported the total surface area of short grain rough rice (at 18 percent moisture content wet basis) as .8723 cm^2. This surface area value is 80 to 100 percent larger than those values reported by researchers using Methods 1 and 2. No equations giving rough rice surface area, found using Method 3, as a function of moisture content are available.

Bulk Density

Equations which describe the variation in bulk density with moisture content have been developed for each major type of rough rice (Table 3). The data was found by determining the weight of a sample which could fill a container of known volume. However, the container filling methods were significantly different for the three types of rice. The data for short grain rice represents a packed fill because Morita and Singh (2) tapped their sample container numerous times to achieve a maximum capacity fill. The bulk density data for medium and long grain rice given by Wratten et al. (3) represents a loose fill situation. All data are for clean rough rice which is devoid of straw, dirt and other foreign matter.

Specific Gravity

An equation (Table 3) giving the specific gravity as a function of moisture content for short grain rough rice was developed by Morita and Singh (2). This data was collected using a toluene-glass pycnometer method. Similar equations (Table 3) have been reported for medium and long grain rough rice. However, Wratten et al. (3) used an air-comparison pycnometer to obtain the specific gravity information. The above mentioned methods of collecting specific gravity data may yield different results because rough rice may absorb a significant amount of toluene.

Porosity

Wratten et al. (3), have reported linear equations (Table 3) giving porosity as a function of moisture content for medium and long grain rough rice. These equations are for a loose fill situation and the data was obtained from sample weights and air-comparison pycnometer volumetric measurements. Porosity for a packed fill of short grain rough rice can be estimated from the specific gravity and bulk density information given in Table 3.

Specific Heat

Equations are available to describe the specific heat of short and medium grain rough rice as it varies with moisture content (Table 3). The equations are based on data obtained by the method of mixtures. This method involves measuring the temperature change of a solution (water in this case) contained in a calorimeter when a known quantity of rough rice (at a higher temperature) is added to it.

Bulk Thermal Conductivity

Bulk thermal conductivity equations for short and medium grain rough rice are summarized in Table 3. The data for these equations were determined from the mathematical expression for transient heat flow in an infinite mass which is initially at a uniform temperature and is heated by a line source of constant current. Transient temperature information was collected and graphical methods were used to compute the bulk thermal conductivity. The statistical correlation coefficients (Table 3) obtained for the bulk thermal conductivity equations are low for both equations mentioned.

Bulk Thermal Diffusivity

Bulk thermal diffusivity equations have been reported for short and medium grain rough rice (Table 3). The data for these equations was calculated from the following expression:

$$\text{Thermal Diffusivity} = \frac{\text{Bulk Thermal Conductivity}}{\text{Specific Heat} \times \text{Bulk Density}} \qquad [2]$$

The information required on the righthand side of Equation [2] represents the same parameters which have been previously discussed. The bulk thermal diffusivity data was highly correlated with moisture content as shown by the correlation coefficients given on Table 3.

Equilibrium Moisture Content (EMC)

Zuritz et al. (8) developed the following equation to give the EMC of rough rice as a function of absolute temperature and relative humidity:

$$M_e = \left(\frac{\left[-\ln (1 - RH)\right] T_a}{\left[1 - \frac{T_a}{641.7}\right]^{-23.4380}} \right)^{\left(\frac{1}{4.000 \times 10^5 \ (T_a^{-2.1166})}\right)} \qquad [3]$$

Equation [3] was developed for a smooth hulled medium grain rice variety (CSM5) from desorption isotherms using static equilibrium moisture content data. The equation covers a temperature and relative humidity range of 10 to 40°C and 11.2 to 92.5 percent respectively.

Pfost et al. (9) formulated a more general EMC equation for rough rice as

$$M_e = (.325535 - .046015 \ln (-1.987(T_c + 35.703) \ln(RH))) \times 100 \qquad [4]$$

Equation [4] was developed using a collection of data from many sources (numerous rice varieties considered) and includes both desorption and adsorption information.

Thin-Layer Drying Equations

Thin-layer or single-layer drying equations are empirically derived expressions which describe the change in moisture content (over time) of a single-layer of grain as a function of the initial grain moisture content and the drying conditions. Agrawal and Singh (10) reported an equation for short grain rough rice (Caloro variety) as

$$\frac{M - M_e}{M_o - M_e} = \exp (- x \, t^{\,y}) \qquad [5]$$

where the constants x and y are

$$x = 0.02958 - 0.44565(RH) + 0.01215(T_c) \qquad [6]$$

$$y = 0.13365 + 1.93653(RH) - 1.77431(RH)^2 + 0.009468(T_c) \qquad [7]$$

Equation [5] was determined from temperatures ranging from 32 to 51°C and relative humidities ranging from 18.75 to 85 percent.

Wang and Singh (11) formulated a thin-layer drying equation for medium grain rough rice (CSM5 variety) expressed as

$$\frac{M - M_e}{M_o - M_e} = 1 + 60At + 60Bt^2 \qquad [8]$$

where the constants A and B are defined as

$$A = -0.001308(T_c^{.4687})\ (RH^{-.3187}) \quad [9]$$

$$B = .00006625(T_c^{.03408})\ (RH^{-.4842}) \quad [10]$$

Equation [8] was developed considering temperatures ranging from 30 to 55°C and relative humidities from 15 to 95 percent. It should be mentioned that the quadratic nature of Equation [8] causes the moisture content to approach infinity as drying becomes long. However, the equation closely approximates the thin-layer data in the short time periods generally required in modeling rough rice drying. Wang and Singh (11) also presented an exponential approximation of their thin-layer data as

$$\frac{M - M_e}{M_o - M_e} = a \exp(-60bt) \quad [11]$$

where

$$a = .96 - .00008826(T_c) + .02324(RH) \quad [12]$$

$$b = .002814 + .0001267(T_c) - .003620(RH) \quad [13]$$

Equation [11] does not have the time limitation of Equation [8] and may be used for approximating moisture reduction over long drying periods.

Moisture Diffusion Equations

Equations are available which give the liquid diffusivity of rough rice and rough rice components as a function of absolute temperature. These equations (Table 4) were formulated by assuming rough rice to be a solid sphere (whole rough rice) or a solid sphere surrounded by concentric shells (starchy endosperm surrounded by the bran and hull respectively). Husain et al. (13) have reported diffusion coefficients for a rough rice drying model which considers the coupled heat and moisture diffusion equations. An equation, giving these coefficients as a function of temperature and moisture content, is

$$D = A \exp(BM_p) \quad [14]$$

where

$$A = 9.8787 \times 10^{-3} \exp(-7730.65/(T_a')) \quad [15]$$

$$B = 8.83 \times 10^{-4}(T_a') - .3788 \quad [16]$$

Equation [14] was developed from data for whole long grain rough rice (Bluebelle variety) and was formulated by considering the following range of conditions: temperatures from 48.8 to 82.2°C; 20 to 60 percent relative humidity; and 26 to 32 percent moisture content (dry basis).

Convective Heat Transfer Coefficient

Wang et al. (14) formulated an equation to predict the convective heat transfer coefficient in a packed bed of medium grain rough rice (variety not specified but believed to be CSM5). The equation, found by comparing experimental and theoretically predicted heating curves, was reported as

$$h = 8.69 \times 10^4\ G^{1.30} \quad [17]$$

The airflow rate parameter (G) represents the superficial air mass velocity through the bed of rice. The units for h are $J/m^3 \cdot s \cdot K$ and this parameter actually represents a volumetric convective heat transfer coefficient. The values of h were determined by calculating the surface convective heat transfer coefficient and incorporating this with the surface area per unit volume of rough rice (a constant value of 10.38 cm^2/cm^3 was used).

Table 4. Diffusion coefficients for rough rice and rough rice components.

$D = A \exp(B/T_a)$

Diffusivity (m^2/hr)	A	B
Rough Rice Hull*	2.57×10^{-3}	-2880
Rough Rice Bran*	7.97×10^{-1}	-5110
Rough Rice Starchy Endosperm*	4.84×10^{2}	-7380
Whole Rough Rice Kernel**	9.83×10^{-3}	-4151

*Steffe and Singh (12): Short grain smooth hulled rice variety (S6).

**Wang and Singh (11): Medium grain smooth hulled rice variety (CSM5).

Latent Heat of Vaporization

Wang and Singh (15) developed an equation to describe the latent heat of vaporization of rough rice as a function of grain temperature and moisture content. The equation is

$$h_{fg} = (415.6734 - .6495T_c)\ M_d^{-.308} \quad [18]$$

This equation was formulated from the equilibrium moisture content data determined by Zuritz et al. (6) for a medium grain smooth hulled rice variety (CSM5).

Brook and Foster (16) have reported an equation for the latent heat of vaporization which utilized the rough rice equilibrium moisture content data summarized by Pfost et al. (9). The equation, which incorporates data from many different varieties of rice, is

$$h_{fg} = .5555(1094 - 1.026(T_c + 17.78))\ (1 + 2.4962\exp(-21.7330M_d)) \quad [19]$$

Equations [18] and [19] were developed using the plotting technique described by Othmer (17). This technique is based on the Clausius-Clapeyron

equation (Heldman (18)) and involves a comparison between the latent heat of vaporization of free water and the latent heat of vaporization of grain.

Pressure Drop Through A bed of Rough Rice

Empirical data giving the pressure drop necessary to achieve a particular air flow through a bed of rough rice is given in Figure 1. These data were summarized by Steffe et al. (19) and represent numerous rice varieties at various moisture contents with varying degrees of foreign matter contamination. Data shown by the curves in Figure 1 are for a loosely filled bed of grain.

Rough Rice Tempering

Steffe and Singh (20) have developed equations to estimate the minimum holding time (or tempering time) required between passes when drying rough rice in a multipass drying system. The equation giving tempering time as a function of drying air temperature, drying air relative humidity, initial grain moisture content and the moisture reduction

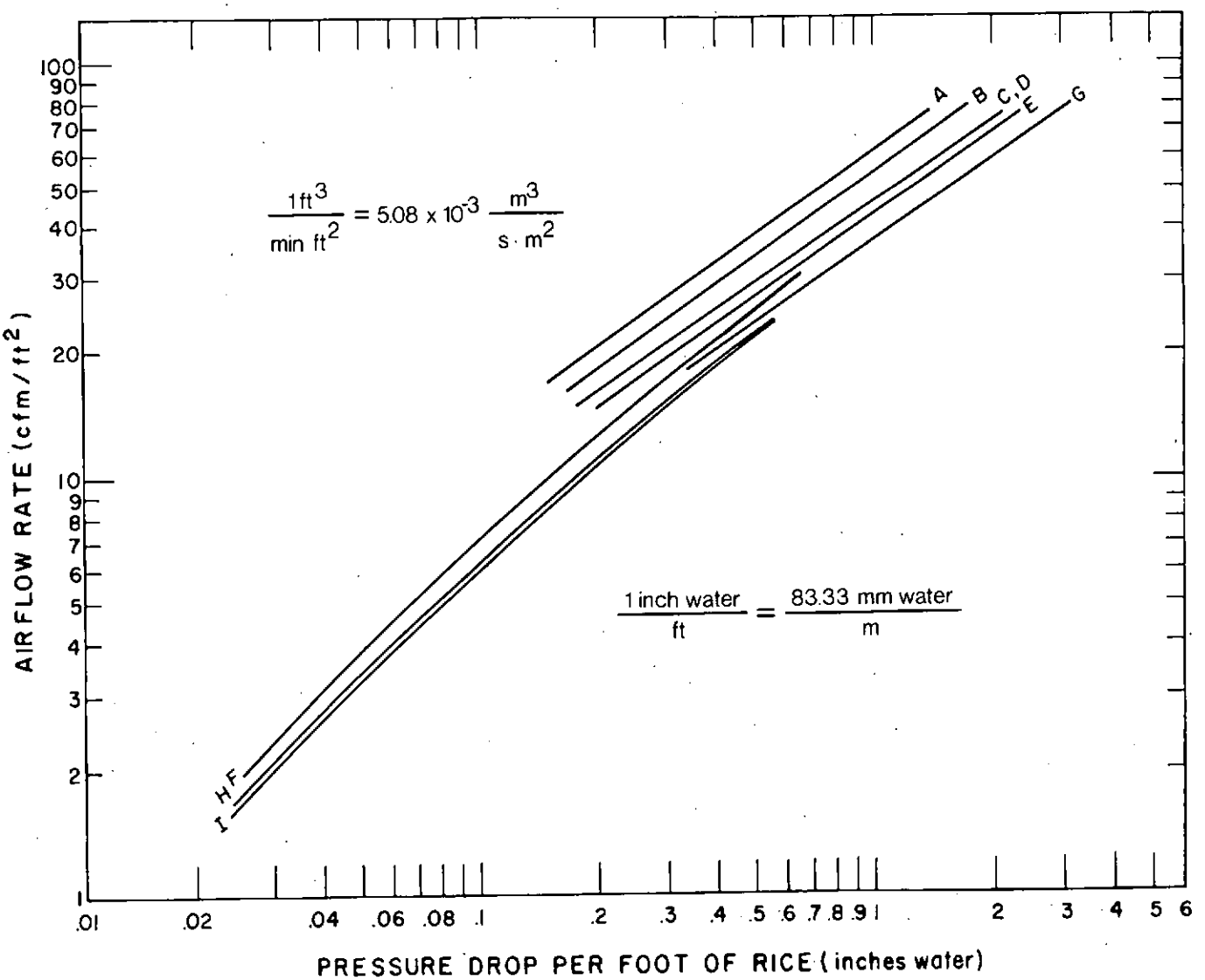

A. Calrose, Medium Grain, Rough hulled (with trichomes), 24.4% MC wb*, .66% Foreign matter.
B. Same as A but 12.7% wb.
C. CSM3, Medium Grain, Smooth hulled (glabrous), 27.6% MC wb, .88% Foreign matter.
D. Caloro, Short Grain, Dry (exact MC unknown), Clean.
E. Same as C but 12.7% MC wb.
F. Bluebonnet Long Grain, 13.4% MC wb, Clean.
G. CSM3, Dry (exact MC unknown), Clean.
H. Belle Patna, Long Grain, 15.2% MC wb, Clean.
I. Nato, Medium Grain, 16.5% MC wb, Clean.
* MC wb = Moisture Content (wet basis).

Figure 1. Resistance of rough rice to airflow. Source: Steffe et al. (19).

during drying is

$$t' = 24.145 - 5.344\ \ell n(T_c) + .253\ \ell n(\Delta M) - .287(RH) + 1.096(M_o) \quad [20]$$

A complementary equation giving the tempering time in terms of the drying period is

$$t' = 21.5373 - 4.899\ \ell n\ (T_c) + .131\ \ell n(\Delta t) - .491(RH) + 2.132(M_o) \quad [21]$$

The center and surface moisture content of the kernel is reduced to less than .05 percent dry basis. Equations [20] and [21] are based on experimental data and a theoretical analysis of rough rice tempering which assumes a uniform initial kernel moisture content.

SUMMARY

The information presented in this paper has been for specific rice varieties under a specified range of conditions. All the parameters discussed would not be required in a particular drying analysis and applications for required parameters may deviate from the data collection conditions. However, existing data should give reasonable estimates for the parameters required in solving most rice drying problems.

REFERENCES

1. USDA. 1973. Rice in the United States: Varieties and Production. Agriculture Handbook No. 289. Agricultural Research Service, United States Department of Agriculture, Washington, D.C.
2. Morita, T. and R.P. Singh. 1979. Physical and thermal properties of short-grain rough rice. Trans. of the ASAE 22 (3): 630-636.
3. Wratten, F.T., W.D. Poole, J.L. Chesness, S. Bal, and V. Ramarao. 1969. Physical and thermal properties of rough rice. American Society of Agricultural Engineers Paper No. 68-909. ASAE, St. Joseph, MI.
4. Steffe, J.F. 1979. Moisture diffusion and tempering in the drying of rough rice. Unpublished Ph.D. Thesis. Agricultural Engineering Department, University of California, Davis, CA.
5. Steffe, J.F. and R.P. Singh. 1979. Volumetric reduction of short grain rice during drying. Cereal Chemistry. Accepted for publication.
6. Hosokawa, A. and K. Motohashi. 1975. Constant drying rate of a single paddy grain. Nogyo-Kikai Gjakkaishi 37(3): 326-330.
7. Bakshi, A.S. and R.P. Singh. 1979. Surface area measurements of rough rice. American Society of Agricultural Engineers Paper No. 79-3549. ASAE, St. Joseph, MI.
8. Zuritz, C., R.P. Singh, S.M. Moini, and S.M. Henderson. 1979. Desorption isotherms of rough rice from 10°C to 40°C. Trans. of the ASAE 22 (2): 433-436.
9. Pfost, H.B., S.G. Maurer, D.S. Chung, and G.A. Milliken. 1976. Summarizing and reporting equilibrium moisture data for grains. American Society of Agricultural Engineers Paper No. 76-3520. ASAE, St. Joseph, MI.
10. Agrawal, Y.C. and R.P. Singh. 1977. Thin-layer drying studies on short-grain rough rice. American Society of Agricultural Engineers Paper No. 77-3531. ASAE, St. Joseph, MI.
11. Wang, C.Y. and R.P. Singh. 1978. A single layer drying equation for rough rice. American Society of Agricultural Engineers Paper No. 78-3001. ASAE, St. Joseph, MI.
12. Steffe, J.F. and R.P. Singh. 1979. Liquid diffusivity of rough rice components. American Society of Agricultural Engineers Paper No. 79-6005. ASAE, St. Joseph, MI.
13. Husain, A.C., C.S. Chen and J.T. Clayton. 1970. Coupled heat and moisture diffusion in porous food products. American Society of Agricultural Engineers Paper No. 70-833. ASAE, St. Joseph, MI.
14. Wang, C.Y., T.R. Rumsey, and R.P. Singh. 1979. Convective heat transfer coefficient in a packed bed of rice. American Society of Agricultural Engineers Paper No. 79-3040. ASAE. St. Joseph, MI.
15. Wang, C.Y. and R.P. Singh. 1978. Computer-aided simulation of rice drying. Paper presented at 71st Annual Meeting of American Institute of Chemical Engineers, Miami Beach, FL. Nov. 12-16.
16. Brook, R.C. and G.H. Foster. 1979. Cereals and Feed Grains, Including Soybeans. Chapter 2. In: E.E. Finney (ed). Transportation and Marketing, Section E, CRC Handbook Series In Agriculture. CRC Press, Inc., West Palm Beach, FL. In Press.
17. Othmer, D.F. 1940. Correlating vapor pressure and latent heat data. Ind. Eng. Chem. 32 (6): 841-856.
18. Heldman, D.R. 1975. Food Process Engineering. AVI Publishing Co., Westport, CT.
19. Steffe, J.F., R.P. Singh and G.E. Miller. 1979. Harvesting, drying and storage of rough rice. Chapter 8. In: B.S. Luh (ed). Rice: Production and Utilization. AVI Publishing Company, Westport, CT.
20. Steffe, J.F. and R.P. Singh. 1979. Rough rice tempering. American Society of Agricultural Engineers Paper No. 79-3548. ASAE, St. Joseph, MI.

CONCURRENT FLOW DRYING OF FOOD GRAINS

R.C. Brook
F.W. Bakker-Arkema

Agricultural Engineering Department
Michigan State University, E. Lansing, MI

ABSTRACT

A simulation model for concurrent flow drying of food grains was developed. Multi-stage concurrent flow dryers with intermediate tempering were simulated. Moisture transfer was based on diffusion within spherical products. Grain quality factors were considered. The model matched previous experimental results well enough for use in the design of multi-stage concurrentflow dryers.

NOMENCLATURE

a = specific surface area of grain, m^2/m^3

c = heat capacity, $J/g-^oC$

D = diffusion coefficient, m^2/h

G = dry weight flow rate, $g/h-m^2$

h = convective heat transfer coefficient, $J/h-m^2-^oC$

h_{fg} = latent heat of vaporization, J/g

H = air humidity ratio, decimal d.b.

M = local moisture content, decimal d.b.

$\bar{M}$ = average kernel moisture content, decimal d.b.

r = kernel radial coordinate, m

t = time, h

T = air temperature, ^oC

x = dryer length coordinate, m

ρ = grain density, g/m^3

θ = grain temperature, ^oC

Subscripts

a = air

p = grain

v = water vapor

w = water liquid

INTRODUCTION

Grains are economically important for human food in the United States for both domestic consumption and export. Food products from corn include corn grits, corn starch and corn oil. Soybeans are used to produce soybean oil and soy protein products. Wheat is used for baking breads and cookies. Rice, after milling, and navy beans are stand-alone food products.

These grains are often harvested at moisture contents above those desirable for storage. The crossflow dryer has been the predominant technology for removing the excess moisture. The concurrent flow dryer has advantages over the crossflow dryer because of its improved energy efficiency, high grain quality characteristics, and favorable pollution qualities.

The objective of this paper was to develop a simulation model for the drying process in a multistage concurrent flow dryer. A multistage dryer includes intermediate tempering stages and a counterflow cooler, as illustrated in Figure 1. The simulation model can then be used for designing a dryer for the several grains considered.

CONCURRENT FLOW DRYERS

Öholm(1) first described the principle of concurrent flow drying. Concurrent flow dryers have only recently become available commercially. In a concurrent flow dryer the air and the grain flow in the same direction; the hottest air encounters the wettest grain (see Figure 1). Drying air temperature in a concurrent flow dryer can be as high as 260°C (500°F). The high rate of evaporation cools the air rapidly and prevents excessive grain kernel temperatures. As the grain moves downward, its temperature increases, then decreases along with the decrease in the drying air temperature (Figure 2). Thompson (2) found that air introduced at 148°C (300°F) was cooled to 82°C (180°F) in traveling 5 cm (2 in.) into corn at 25% moisture w.b. Energy utilization of betwen 4185-5120 kJ/kg of water evaporated is common for a single-stage concurrent flow dryer; crossflow dryers average about 7500 kJ/kg of water evaporated (3).

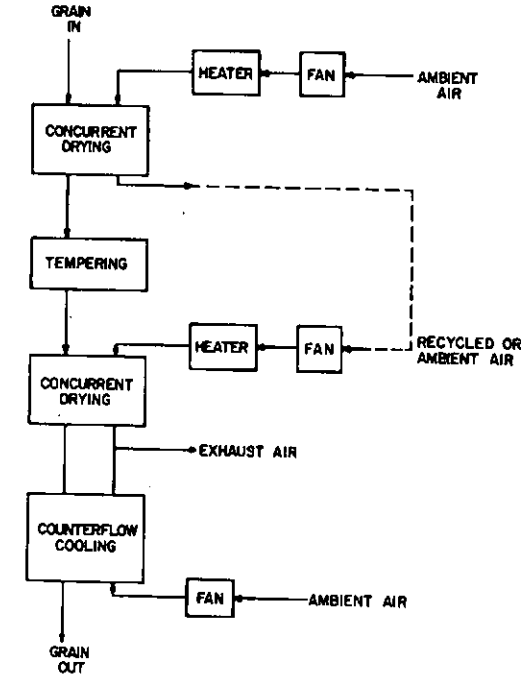

Figure 1 Block diagram of a two-stage concurrent flow dryer with counterflow cooler

The concurrent flow dryer subjects all grain kernels to the same drying treatment, thus avoiding nonuniformity in moisture content inherent in crossflow dryers (4). The grain temperature continually decreases through the last portion of the drying bed (Figure 2); therefore, the driest grain is also the coolest grain. This helps reduce stress cracks and subsequent mechanical damage when the grain is handled. The quality of several grains dried in a concurrent flow dryer have been shown to have improved and more uniform grain quality than grain from a comparable capacity crossflow dryer (5).

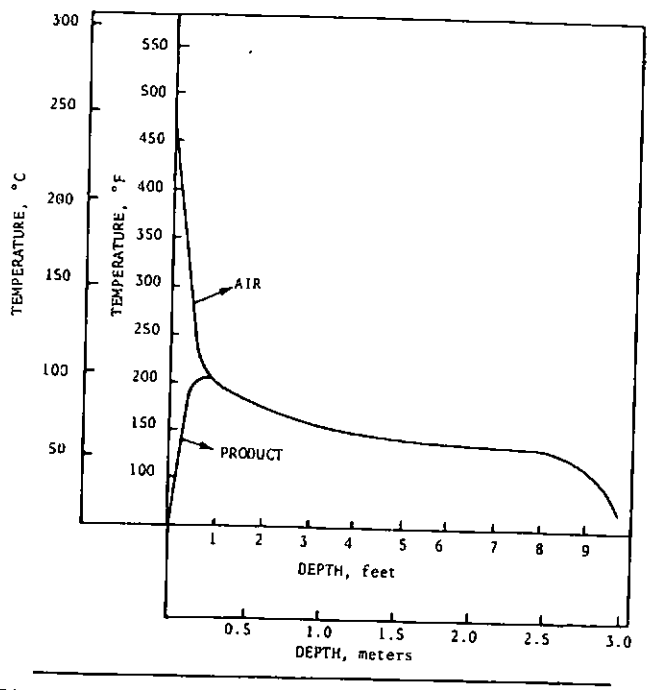

Figure 2 Air and product temperatures versus depth for a single-stage concurrent flow dryer

The Clean Air Act of 1970 has established standards that must be adhered to by the grain handling industry. The pollution characteristics of the various dryer types differ, partially due to differences in the quantities of air discharged to the atmosphere. The air exhausted from a crossflow dryer is eight to ten times as large as in a comparable concurrent flow dryer (6).

LITERATURE REVIEW

The optimal design of a concurrent flow dryer has been studied using computer simulation (2,7,8,9) Thompson (2,10) compared the performance characteristics of crossflow and concurrentflow grain dryers using general performance graphs for each dryer type. Baughman (7) simulated the drying of shelled corn in a concurrent flow dryer based on radical diffusion in an assumed spherical kernel. Drying parameters were studied for the purpose of controlling the moisture of the grain leaving the dryer. Farmer (8,11) developed a dynamic programming algorithm for a single-stage concurrent flow dryer with a counterflow cooler. The objective function considered energy costs and employed grain quality constraints. The results indicated that the concurrent flow dryer should be operated at higher air temperatures and lower airflow rates (to increase the relative humidity of the outlet air). Brook (9) was the first to consider multistaging of concurrent flow dryers. The multistage dryer can be expected to produce better quality dried grain at a reduced energy cost over a crossflow dryer.

Grain quality is an important constraint on the design of any drying equipment. Drying air temperature in a concurrent flow dryer of less than 121°C (250°F) gave acceptable wet millability for corn (10). Increasing temperatures resulted in continually decreasing millability. Only slight changes in nutritive value of corn dried in a single-stage concurrent flow drier have been noted (12).

A multi-stage concurrentflow dryer will result in better grain quality. The quality of pea beans was found to be directly affected by drying rate and drying air temperature, and inversely by dryer throughput rate (13). A concurrent flow dryer can operate as safely (with respect to grain quality) at 121°C (250°F) as a crossflow model at 32°C (90°F). Rice is susceptible to cracking during drying and milling. No significant changes in head yield were found for drying rice from 17 to 13% moisture w.b. at temperatures up to 121°C (250°F) in one pass (14). Wheat, dried in a single-stage dryer (15) and a multi-stage dryer (16), showed no sifnificant changes in flour yield or baking characteristics. Soybeans, dried in multi-stage dryers at temperatures up to 323°C (450°F), have shown no deterioration in the quality of the oil extracted (17). Germination decreases and the percentage of cracked beans in-

creased (17,18); however, these quality characteristics are not considered important in an oil extraction plant.

Experimental studies, in addition to the research reported above, have helped to understand the advantages, design and operation of concurrent flow dryers (19,20,21,22).

MODEL DEVELOPMENT

The phenomena of heat and mass transfer in a concurrent flow dryer was modeled from the viewpoint of the individual kernels involved. Thin layer models are available for corn and a few other products (23,24). Thin layer models suffer from the severe limitation that they do not consider what is occurring within the kernel. The degree of damage during drying is affected by many variables. Previous research indicates that moisture variations within the kernel may be significant (25,26).

The grain kernels were assumed to be represented by a sphere of equivalent radius (27,28) which exchanges moisture with the air by diffusion. A diffusion model has a number of advantages. First, it is easily applicable to a number of agricultural products for which a diffusion coefficient is known. Second, the assumed shape of the kernel can be easily changed to represent a sphere, cylinder, or other shape. Third, the diffusion model can be used to approximate moisture distribution within the kernel.

The transfer of heat and moisture within the kernel occurs by diffusion; at the surface by convection with the surrounding air. For most agricultural products, no thermal gradient exists within the kernel, even though the kernel temperature may change with time (29). The diffusion of moisture within the kernel was represented by the diffusion equation for a sphere (30):

$$\frac{\partial M}{\partial t} = \frac{D}{r^2}\left(r^2 \frac{\partial M}{\partial r^2}\right) \qquad (1)$$

The second order partial differential equation was transformed into a set of coupled ordinary differential equations (ODE's) using the method of lines with a linear central difference approximation. The diffusion was assumed to be symmetric about the center of the sphere. At the surface, the diffusion or moisture exchange was calculated by assuming the existance of a pseudo-point outside the kernel with a moisture content equal to the equilibrium moisture content of the surrounding air.

The conditions of the air and the grain vary from the inlet point through the length of the dryer. The heat and mass exchange at the surface of the kernel was described using mass and energy balances previously developed (23):

$$\frac{dT}{dx} = \frac{-ha\,(T-\theta)}{G_a\,(c_a + c_v H)} \qquad (2)$$

$$\frac{d\theta}{dx} = \frac{ha(T-\theta)}{G_p(c_p+c_w\bar{M})} - \frac{h_{fg} + c_v\,(T-\theta)}{G_p(c_p+c_w\bar{M})} G_a \frac{dH}{dx} \qquad (3)$$

$$\frac{dH}{dx} = \frac{\rho_p}{G_a}\frac{\partial M}{\partial t} \qquad (4)$$

A digital computer solution is obtained using a fourth-order Runge-Kutta integration algorithm featuring automatic step size adjustment and relative error checking.

The solution of the ODE's requires knowledge of several grain and air properties. Diffusion coefficients were assumed to be independent of location within the kernel; i.e. the kernel was assumed to be homogeneous with respect to moisture diffusion. Diffusion equations for corn (27), pea beans and soybeans (31), wheat (28) and rice (32) were used. Equilibrium moisture content of the grains was calculated using equations presented by Pfost (33). The changing air properties were calculated from psychrometric equations written in SI units (24). Other properties (e.g. specific heats and equivalent kernel radius) change only with the type of grain being dried and were summarized by Brook (34).

Tempering of warm grain from the concurrent flow dryer sections was estimated using the ODE's described (equation 1,2,3,4). The derivatives at the surface of the kernel were set to zero, assuming that the kernel does not change temperature or average moisture during tempering (35). During tempering, the moisture within the kernel is redistributed and equalized by diffusion.

MODEL VALIDATION

Single-Stage Drying of Shelled Corn

The single-stage concurrent flow dryer has previously been studied for shelled corn (2,7,12,20). Comparison between randomly selected experimental results from several of these studies and the simulation results are presented in Table 1. The average deviation in moisture content was 0.9% w.b.; in outlet dryer temperature 6°C.

Multi-Stage Drying of Food Grains

Shelled corn was dried in two- and three-stage concurrent flow dryers (13). The test conditions are presented in Table 2. Drying air temperatures ranged 149-218°C; initial corn moistures ranged 25-30% moisture w.b.. The experimental and simulation results are presented in Table 3. The average deviation in the outlet moisture content was 2.3% w.b.; in the outlet grain temperature 5°C using an appropriate cooling estimation. Representative grain moisture and temperature profiles are presented in Figure 3.

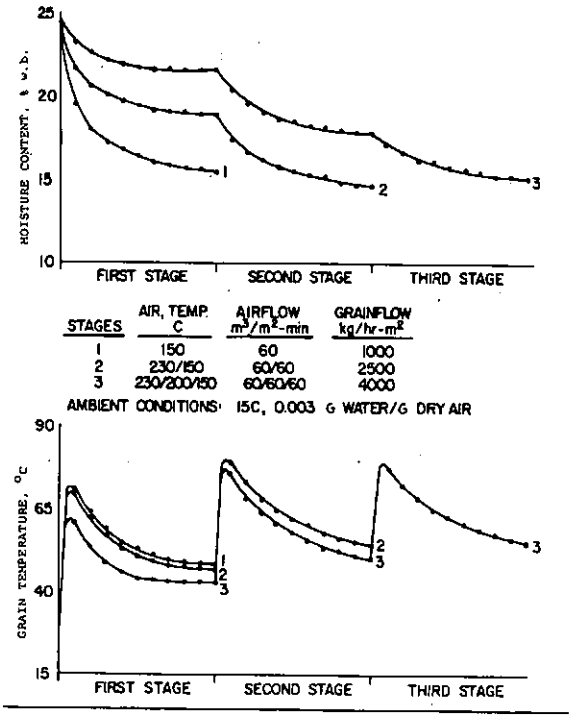

Figure 3 Corn Moisture and temperature profiles for 1,2, and 3 stage concurrent flow dryers. Each stage 2 m long followed by 3.5 m tempering.

Pea beans were dried in two- and three-stage concurrent flow dryers (13). The test conditions are presented in Table 4. Drying air temperatures ranged 52-121°C; initial bean moistures ranged 20-23%. The experimental and simulation results are presented in Table 5. The average deviation in the outlet moisture content was 0.9% w.b.; in the outlet grain temperature 3°C.

Other Grains: Soft white spring wheat was dried in a single-stage concurrent flow dryer (15), with the compared experimental and simulated conditions presented in Table 6. The average deviation in outlet moisture content was 0.6% w.b.; in outlet grain temperature 9°C. Hard red spring wheat was dried in a two-stage dryer (16), with the compared experimental and simulated conditions presented in Table 7. The average deviation in outlet moisture content was 0.6% w.b.. Rice was dried in one-, two- and three-stage dryers. Experimental tests for a two-stage dryer are presented in Table 8; a representative simulation result is presented in Table 9. Soybeans have to be dried in one- and two-stage dryers (17,18) with representative experimental conditions presented in Table 10. While final simulation results are not yet available, preliminary results are very encouraging.

EFFECT OF TEMPERING

Increased drying capacity and improved grain quality have been noted when tempering is included in a crossflow dryer (35,36). During tempering in a concurrent flow dryer, the moisture within the kernel redistributes as shown in Figure 4.

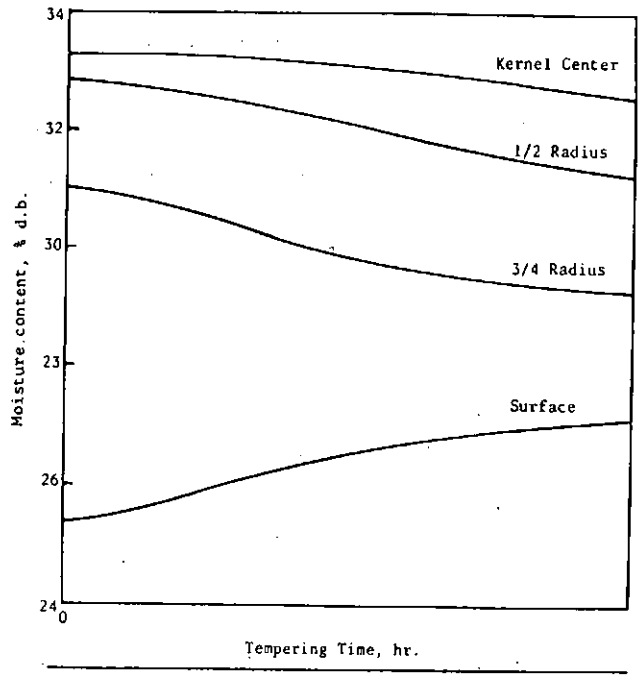

Figure 4 Moisture content versus tempering time for shelled corn after drying from 25.0% w.b. in a concurrent flow dryer. Kernel temperature during tempering 51°C

As the tempering time increases, the moisture concentration at any point within the kernel asymptomatically approaches an average value. This can also be seen in the data for rice drying presented in Table 9. Since the moisture loss occurs only at the surface, the moisture concentration increase would increase the drying rate following tempering. This can be seen from the data for corn drying in Figure 3. Tempering times greater than 1.25 hours appear to have a negligible effect on the final moisture content and temperature of corn. This is less than the optimal 6-8 hours following crossflow drying (35). The concurrent flow dryer requires less tempering time because of the uniformity of moisture and temperature among kernels after concurrent flow drying.

CONCLUSIONS

The multi-stage concurrent flow drying model, based on uniform diffusion within an assumed spherical kernel, has been developed. Simulation results match experimental results well enough for the model to be extremely useful for the design of these dryers. The model is constructed to be useful for several agricultural products. Grain quality factors can be considered through monitoring grain temperature and drying rates. The multi-stage concurrent flow dryer can be expected to produce a better quality dried product at a reduced energy cost over a crossflow dryer.

ACKNOWLEDGMENTS

The authors express sincere thanks to Westlake

Agricultural Engineering, St. Marys, Ontario, Canada for assistance during the experimental tests. The partial financial support of Westlake Agricultural Engineering and the Anderson Agricultural Research Fund, Columbus, OH was appreciated.

REFERENCES

1. Öholm, G.V. 1955. Method and arrangement for drying grain and the like in drying silos provided with direct heat supply. US Patent No. 2, 706, 343.
2. Thompson, T.L. 1967. Predicted performance and optimal designs of convection grain dryers. Ph.D. Thesis, Purdue Univ., W. Lafayette, IN
3. Muhlbauer, W. and Isaacs, G.W. 1975. Wärmeruck gewinnung bei Kärmer fruchttrocknungslagen. Landtechnik 11:3160-3165.
4. Graham, D.L. 1970. Concurrent flow grain dryer design study and proposal. Special Report, MSW Gear Co., Gibson City, IL
5. Bakker-Arkema, F.W., Brook, R.C., Walker. L.P. Kalchik, S.J., and Ahmadnia, A. 1977. Concurrent flow grain drying - grain quality aspects. Corn Quality Res. Conf. Proc., Univ. of Ill., Urbana, IL.
6. Bakker-Arkema, F.W. Brooker, D.B., and Hall, C.W. 1972. Comparative evaluation of crossflow and concurrent flow grain dryers. ASAE Tech. Paper 72-849. Am. Soc. Agr. Engr., St. Joseph, MI.
7. Baughman, G.R., Barre, H.J., and Hamdy, M.V. 1973. Experimental study and simulation of concurrent flow dryers. Trans ASAE 16: 890-894.
8. Farmer, D.M. 1972. Optimization techniques for grain dryer design and analysis. Ph.D. Thesis, Mich. State Univ., E. Lansing, MI
9. Brook, R.C., Bakker-Arkema, F.W. 1978. Simulation for design of commerical concurrent flow grain dryers. Trans. ASAE 21:978-981.
10. Thompson, T.L., Foster, G.H., and Peart, R.M. 1969. Comparison of concurrentflow, crossflow and counterflow grain drying methods. Market Res. Rpt. 841, USDA, Washington, D.C.
11. Bakker-Arkema, F.W., Farmer, D.M. and Lerew, L.E. 1973. Optimum dryer design through simulation. In: Preservation of Wet Harvested Grains, Ed. by J.L. Multon and A. Builbot. Ins. Nat. Recherche Agronomique, Paris, France.
12. Muhlbaer, W., Scheuerman, A., Mauer, K., and Blumel, K. 1971. Trocken von Körnermais im Glerchstromverfahren mittles haher Luftemperaturen. Grundl. Landtech. 21:1-5.
13. Brook, R.C. 1977. Design of multi-stage grain dryers. Ph.D. Thesis, Mich. State Univ., E. Lansing, MI.
14. Walker, L.P. 1977. Concurrent flow rice drying. Ph.D. Theis, Mich. State Univ., E. Lansing, MI.
15. Ahmadnia-Sokhansanj, A. 1977. Quality of soft wheat dried in a concurrent-countercurrent dryer. MS Thesis, Mich. State Univ. E. Lansing, MI.
16. Bakker-Arkema, F.W., Ahmadnia-Sokhansanj, A., and Green, G. 1977. High temperature wheat drying. ASAE Tech Paper 77-3527, Am. Soc. Agr. Engr., St. Joseph, MI
17. Kalchik, S.J. 1977. Drying of soybeans in a pilot scale concurrent-flow grain dryer. MS Thesis, Mich. State Univ., E. Lansing, MI.
18. Dalpasquale, V.A. 1979. Continuous flow drying of soybeans. MS Thesis, Mich. State Univ., E. Lansing, MI.
19. Anderson, R.J. 1972. Commercial concurrent flow heating-counterflow cooling grain dryer. ASAE Tech. Paper 72-846. Am. Soc. Agr. Engr., St. Joseph, MI.
20. Carrano, J.A., Bickert, W.G., and Bakker-Arkema, F.W. 1971. Design and testing of a laboratory scale concurrent-counterflow high temperature corn dryer. ASAE Tech. Paper 71-320. Am. Soc., Agr. Engr., St. Joseph, MI.
21. Meiering, A.G., and Hoefkes, H.J. 1977. Dryer performance and energy use in corn drying. Can. Agr. Engr., 19:49-54.
22. Westelaken, C.M. 1977. Concurrent flow commercial grain dryers - The Westelaken models. ASAE Tech. Paper 77-3016. Am. Soc. Agr. Engr. St. Joseph, MI.
23. Brooker, D.B., Bakker-Arkema, F.W., and Hall, C.W. 1974. Drying Cereal Grains. AVI Publ. Co. Westport, CN.
24. Bakker-Arkema, F.W., Brook, R.C., and Lerew, L.E. 1978. Cereal grain drying. In: Advances in Cereal Science and Technology, Vol. II, ed. by Y. Pomeranz. Am.Assoc. Cer. Chem., St. Paul, MN.
25. Thompson, R.A., and Foster, G.H., 1963. Stress cracks and breakage in artificially dried corn. Mrkt. Res. Rpt. 631, USDA, Washington, D.C.
26. Hammerle, J.R., White, R.K., and Mohsenin, N.N. 1971. The rheological properties of corn horny endosperm. Cer. Sci. Today 16:60-68,72.
27. Chu, S.T. and Hustralid, A. 1968. Numerical solution of the diffusion equation. Trans. ASAE 11:705-710,715.
28. Ingram, G.W. 1976. Deep bed dryer simulation with intra-particle moisture diffusion. J. Agr. Engr. Res. 21:263-272.
29. Young, J.H., and Whitaker, T.B. 1971. Numerical analysis of vapor diffusion in a porous composite sphere with concentric shells. Trans. ASAE 14:1051-1057.
30. Crank, J. 1974. The Mathematics of Diffusion. Clarendon Press, Oxford, England.
31. Sabbah, M., Meyer, G.E., Keener, H.M., and Roller, W.L. 1976. Reversed-air drying for fixed bed of soybean seed. ASAE Tach. Paper 76-3023, Am. Soc. Agr. Engr., St. Joseph, MI.
32. Husain, A.C., Chen, C.S. and Clayton, J.T. 1970. Coupled heat and moisture diffusion in porous food products. ASAE Tech. Paper 70-833. Am. Soc. Agr. Engr., St. Joseph, MI
33. Pfost, H.B., Mauer, S.G., Chung, D.S., and Milliken, G.A. 1976. Summarizing and reporting equilibrium moisture data for grains. ASAE Tech. Paper 76-3520, Am. Soc. Agr. Engr., St. Joseph, MI.
34. Brook, R.C. and Foster, G.H. 1980. Drying, cleaning and conditioning. In: CRC Handbook Series in Agriculture, Sec. E - Transportation and Marketing, ed. by E.E. Finney. CRC Press, Boca Raton, FL. IN PRESS.
35. Sabbah, M.A., Foster, G.H., Haugh, C.G., and Peart, R.M. 1972. Effect of tempering after drying on cooling on shelled corn. Trans. ASAE 15: 763-765.
36. Katic, Z. 1975. Drying of different corn varieties and hybrids. Mühle & Mischfuttert. 112: 561-568.

Table 1 --Comparison of simulated drying conditions with single-stage experiement drying tests reported in the literature. Drying only, no cooling.

Test Number*	T24	T34R	T45	T207	T309	T359	C2	C4	C6A	B10	B11	Bf.4
Ambient Conditions:												
Temperature, °C	16	16	16	16	16	16	28	29	29	25	21	11
Humidity, decimal	.010	.010	.010	.010	.010	.010	.015	.017	.014	.007	.005	.006
Drying Conditions:												
Temperature, °C	93	149	204	93	149	177	232	232	96	83	82	121
Airflow, m/min	21.4	24.1	30.5	21.3	27.4	27.4	21.3	21.3	33.5	30.5	32.9	24.4
Grainflow, kg/hr-m^2	230	266	770	162	419	654	494	1223	799	254	226	273
Length, m	0.61	1.22	0.61	0.61	0.61	0.61	0.34	0.34	0.34	0.61	0.61	0.61
Initial Conditions:												
Temperature, °C	16	16	16	16	16	16	28	29	29	25	21	11
Moisture, % w.b.	17.8	25.2	18.1	23.6	24.7	21.5	26.3	20.3	20.6	25.2	24.7	25.0
Experimental Results:												
Temperature, °C	55	52	79	54	--	75	61	54	32	38	38	43
Moisture, % w.b.	12.5	15.0	13.6	12.7	16.5	14.6	15.2	17.1	17.4	16.5	15.3	15.1
Simulated Results:												
Temperature, °C	54	59	86	48	57	65	71	70	51	41	44	51
Moisture, % w.b.	12.4	12.0	12.1	14.1	15.8	15.0	16.5	17.4	18.4	17.1	15.9	15.4

*T25, T34R, T45 from Thompson (1967), drying tests for 1964 harvest season. T207, T309, T359 from Thompson (1967), drying tests for 1965 harvest season. C2, C4, C6A from Carrano et al. (1971), drying tests for 1970 harvest season. B10, B11, Bf.4 from Baughman et al. (1971), drying tests for 1970 harvest season.

Table 2 CORN DRYING TEST CONDITIONS

Test Number	1	2	3	4	5	6	7	8
Ambient Conditions:								
dry bulb temperature, °C	3	1	8	3	6	8	8	2
wet bulb temperature, °C	1	-3	3	2	3	5	4	-1
Airflow (all stages, m^3/min	61.6	61.6	61.6	61.6	61.6	65.2	65.2	65.1
Drying air temperatures, °C								
stage 1	163	191	191	218	177	163	177	177
stage 2	163	191	191	218	177	163	149	149
stage 3	163	177	191	218				
Grainflow, kg/h	3790	3450	2790	3030	1750	1450	1230	1520
Inlet grain conditions								
temperature, °C	17	10	12	8	11	16	14	15
moisture, % w.b.	27.5	24.8	28.4	28.1	28.7	28.4	30.0	30.7
BCFM,%	0.8	0.5	0.6	0.6	0.6	0.7	0.5	0.6
Stein Breakage,%	15.2	16.3	10.2	11.5	17.3	15.8	21.0	26.6

Table 3 SIMULATION AND EXPERIMENTAL RESULTS FOR CORN DRYING TESTS

Test Number	1	2	3	4	5	6	7	8
Simulation Results								
Stage 1								
temperature, °C	36	39	40	41	40	41	43	41
moisture, % w.b.	25.2	21.5	24.5	24.0	22.2	20.2	19.7	22.6
Stage 2								
temperature, °C	41	49	46	50	53	60	56	49
Moisture, % w.b.	21.8	16.9	18.8	17.8	14.0	11.3	11.9	14.3
Stage 3								
temperature, °C	44	60	58	66				
moisture, % w.b.	18.1	12.8	13.1	11.8				
Cooler[1]								
temperature, °C	23	23	28	24	27	29	23	17
moisture, % w.b.	17.3	11.6	12.0	10.5	13.1	10.3	10.8	13.2
Experimental Dried Corn Results								
Temperature, °C	21	27	19	23	25	18	30	20
Moisture content, % w.b.	18.2	11.1	16.7	16.9	15.5	15.1	12.6	16.1
BCFM,%	0.7	0.6	0.7	0.6	0.8	0.7	0.9	0.7
Breakage	12.8	20.7	13.6	17.3	34.3	23.8	24.8	42.5
Heat damage,%	---	---	0.5	0.7	0.3	0.6	1.5	0.1
Efficiency, kJ/kg H_2O[2]	3778	4197	3738	3910	3832	3981	3853	3986

[1]Cooler airflow 14.9 m^3/min test 1-4, 7.4 m^3/min test 5-9.

[2]Does not include the energy used or the moisture removed during cooling.

Table 4 -- Pea bean drying test conditions

Test Number	2	3	4	5	6	8	9	10	11	12
Ambient Conditions										
dry bulb temperature, °C	17	11	18	20	20	13	18	21	21	18
wet bulb temperature, °C	13	9	14	13	14	12	14	16	16	14
Airflow (all stages), m^3/min	45.3	45.3	45.3	45.3	45.3	45.3	45.3	45.3	45.3	45.3
Drying air temperatures, °C										
stage 1	52	74	93	93	107	121	107	79	121	107
stage 2	52	74	93	74	93	107	93	107	107	93
stage 3								93	93	93
Grainflow, kg/hr	3100	2480	2480	2480	3100	3690	2740	2740	4280	3690
Inlet grain conditions										
temperature, °C	19	19	20	20	21	17	18	18	18	18
moisture,% w.b.	20.6	21.2	20.1	21.0	21.0	22.3	22.6	21.9	22.3	22.1
cracks, %	1.3	1.3	1.0	1.0	1.7	0.6	0.7	0.8	1.2	0.6
splits, %	0.3	0.3	0.3	0.2	0.1	0.1	0.2	0.1	0.3	0.2

Table 5: Simulation and experimental results for pea bean drying tests.

Test Number	2	3	4	5	6	8	9	10	11	12
Simulation Results										
Stage 1										
temperature, °C	24	29	35	33	35	33	33	29	32	32
moisture, %w.b.	20.3	20.4	19.2	20.0	20.1	21.5	21.5	21.2	21.7	21.4
Stage 2										
temperature, °C	28	34	41	36	40	39	37	38	38	36
moisture, %w.b.	19.8	19.4	17.8	18.9	19.0	20.4	20.2	19.8	20.8	20.5
Stage 3										
temperature, °C								41	40	39
moisture, %w.b.								18.4	19.9	19.5
Cooler										
temperature, °C	23	21	22	24	28	21	23	27	32	27
moisture, %w.b.	19.8	18.7	17.3	18.6	18.7	19.8	19.7	18.1	19.7	19.2
Experimental Results										
Stage 1										
temperature, °C	22	22	32	31	36	32	33	29	35	35
moisture, %w.b.	20.0	20.9	18.6	19.3	19.0	20.9	20.5	21.1	20.8	20.7
cracks, %	1.4	1.7	5.1	3.6	3.4	1.3	2.3	1.3	2.0	1.5
splits, %	0.5	0.3	0.4	0.4	0.2	0.1	0.1	0.1	0.2	0.2
Stage 2										
temperature, °C	23	29	37	34	39	42	39	36	36	33
moisture, %w.b.	19.3	17.7	16.7	17.0	16.9	18.8	18.6	19.5	19.8	20.3
cracks, %	2.2	5.2	8.8	10.1	9.6	8.7	7.2	5.3	2.4	2.2
splits, %	0.4	0.3	0.4	0.7	0.4	0.1	0.4	0.1	0.2	0.2
Stage 3*										
temperature, °C								40	39	38
moisture, %w.b.								17.8	18.7	18.9
cracks, %								11.8	4.2	3.6
splits, %								0.1	0.2	0.1
Efficiency, kJ/kg water	4989	4417	5277	3726	3675	4500	4191	5456	4675	5696

*Cooler outlet conditions for test 12 were 28°C/19.7% w.b./2.9%/0.2%

Table 6: Experimental & simulated results of drying tests with soft spring white wheat in a one-stage concurrent flow dryer.

Air temp (°C)	Experimental Wheat temp (°C)	Experimental MC (%wb)	Simulated Wheat temp (°F)	Simulated MC (%wb)
121	37	16.4	39	15.6
149	40	15.9	44	15.1
177	44	14.3	49	14.6
204	46	14.0	54	14.1
232	--	12.8	61	13.7

Table 7: Experimental & simulated results of drying tests with hard spring red wheat in a commercial two-stage concurrent-flow dryer.

Test No.	Stage No.	Air temp (°C)	Grain Flow m/hr	MC in (%wb)	MC Out (%wb) Exp.	MC Out (%wb) Sim.
1	1	204	4.2	19.8		17.5
	2	163			12.3-14.3	14.1
2	1	218	5.9	17.5		15.5
	2	177			13.1-14.1	13.1
3	1	149	5.9	17.2		16.4
	2	149			13.0-14.0	14.1
4	1	218	7.0	17.7		16.6
	2	177			13.4-14.2	14.3
5	1	196	8.9	16.8		16.2
	2	163			13.6-14.1	14.4

Table 8: Head yield changes of rice dried in a two-stage concurrent-flow grain dryer.

MC (%)	MC (%)	Airflow m^3/m^2-min	Grain m/hr	Tempering (hr)	Head (%)
* 17.5	13.2	26.5	2.0	--	-1.4
* 17.0	13.0	26.5	2.0	2	-1.8
**16.9	14.3	20.1	2.9	0	-3.0
**17.1	13.7	19.2	2.4	2	-0.6

* Air temperature 93°C
**Air temperature 121°C

Table 9: Simulation results of two-stage concurrent-flow rice drying (drying air temperature 121°C).

Stage	Depth (m)	Rice temp °C	Kernel MC (%db) Avg.	Max.	Min.
Drying	0	25.6	28.2	28.2	28.2
	0.3	38.5	26.0	28.2	21.9
	0.9	31.8	24.6	27.9	20.7
	1.5	28.5	23.9	27.4	20.3
Tempering	1.5	28.5	23.9	27.4	20.3
	3.0	28.5	23.9	26.1	22.9
	4.5	28.5	23.9	25.1	23.4
Drying	4.5	28.5	23.9	25.1	23.4
	4.8	43.1	23.1	24.2	18.1
	5.5	36.7	20.8	24.2	17.1
	6.1	34.8	20.4	23.6	17.1

Table 10: Germination and oil analysis of soybeans dried in a one- and two-stage concurrent-flow grain dryer.

MC in (%)	MC out (%)	Air Temp (°F)	Germ (%)	Crude Fat (%)	FFA[1] (%)
13.6	---	control	99	18.1	0.19
13.6	11.4	177	66	18.2	0.18
11.4	9.3	149	51	---	---
12.5	--	control	99	16.9	0.18
12.5	10.6	232	57	17.1	0.20

[1]FFA- free fatty acids as oleic

A STUDY OF THE HEAT TRANSFER PARAMETERS FOR DRYING BY IMMERSION IN A HEATED GRANULAR MEDIA

P. Richard
G.S.V. Raghavan

Department of Agricultural Engineering
Macdonald Campus of McGill University
Ste. Anne de Bellevue, Québec H9X 1C0
Canada

ABSTRACT

Granular foodstuff can be dried by immersion in an agitated and heated granular medium with high efficiency and very high drying rates. By this method, large quantities of heat are exchanged and high heat transfer coefficients are obtained. Data from the literature describing heat transfer obtained by this agitation method were compared with another independent experiment where heat transfer between a flowing granular medium and objects immersed in it was measured. This comparison allowed separation of the heat transfer properties of the particulate media from the effect on the heat transfer pertaining to the stirring and mixing action occurring in the drum. Analytical models for both situations are presented.

NOMENCLATURE

d	:	diameter (m)
D	:	thermal diffusivity (m^2/s)
h	:	distance between the surface of the bed and the centre of the drum (m)
$\bar{h}$	:	dimensionless h
H	:	contact resistance (W/m^2C)
ℓ	:	thickness of the sliding layer (m)
L	:	dimensionless ℓ
r	:	radius of the drum (m)
t	:	time of contact (s) residence time (s)
v	:	speed of the sliding layer (m/s)
V	:	dimensionless v
α	:	heat transfer coeffcient (W/m^2C)
β	:	angle between the surface normal and a drum radial
β_0 β_1	:	parameters of equation (4)
ε	:	porosity
λ	:	thermal conductivity (W/mC)
ω	:	drum angular velocity
χ	:	contact resistance parameter
{ }	:	function of

Subscripts

b	:	bed
g	:	gas
p	:	particle
s	:	sliding layer
B	:	bulk layer

INTRODUCTION

Most of the operations which involve the drying and/or heat processing of granular foodstuff use hot air as the agent of convection. Air is a practical, non-contaminating medium and easy to handle, but offers low heat transfer coefficents and becomes saturated with moisture before all the available heat is extracted from it. These factors are particularly important for harvesting and storage operations of agricultural crops, where slow drying and low efficiency create bottlenecks, often resulting in partial loss of the crop.

A solid, granular, inert medium can be used in combination with air to greatly enhance the heat transfer rates, resulting in faster drying. In such a technique, granular foodstuff is mixed with such a material and then vigorously agitated until it is dried; the separation can be made through a simple sieving process. The agitation can be done by fluidizing the mixture, but most of the experiments making use of the technique provided the agitation using some kind of mechanical action. Such a heat transfer technique is termed as particle-particle heat transfer. Even though it is a very promising technique with a wide range of potential applications, so far it has been studied only in a few experimental processes in which grain or other food products were either dried, roasted or puffed successfully. One of the reasons why this process has not been studied in more detail and has not found extensive commercial applications yet may be due to a lack of basic design data. Numerous parameters affect the performance of such a system and the relative importance of each of them are still to be assessed in more detail before reliable design information, based on analytical studies, could be used.

The purpose of the present paper was to study some of the parameters influencing the heat transfer in a simple unflighted drum. The following approach was followed: first, the heat transfer between a hot metallic ball and the granular medium was investigated in a situation where the flow pattern of the granular medium was known. An apparatus was built to test the analytical model of that situation. A model for the flow pattern of a mixture of metallic balls and granular media in a rotating drum was then developed so that the heat transfer could be predicted. This model was tested using the experimental data of Downs et al. (1).

REVIEW OF LITERATURE

Several researchers have published the results of drying experiments using particle-particle heat transfer. Khan et al. (2), Raghavan and Harper (3), Lapp et al. (4) have dried grains using rotary drums. They investigated the effects of various parameters such as residence time, drum rotating speed and angle, type and particle size of granular media, and mass ratio of cereal to granular medium on the drying performance. Richard and Raghavan (5) have published a review of the existing information on these dryers.

Uhl and Root (6) published a comprehensive review of the information available on heat transfer to granular solids in agitated units. The kinds of apparatus surveyed included stirred beds, cut-flight agitators and rotating drums. Several researchers, such as Sass (7), analyzed the heat transfer situation in a rotary kiln. Berntsson (8) designed a rotating drum heat exchanger for indirect heat transfer between two streams of granular solids. Even though there was no contact between the two types of solids, the principle of the drum action was based on enhanced agitation and larger heat transfer surfaces and, therefore, the heat transfer coefficients achieved were fairly high.

Numerous researchers have published models of the mixing mechanism in rotary drums (Abouzeid and Fuerstenau (9) and Hehl et al. (10)). Fan and Shin (11) have studied the segregation problems that occur while mixing particles of different sizes. Chaudhuri and Fuerstenau (12) reported that, when balls were added in a drum mixer, higher rates of mixing resulted. However, all these studies deal with axial mixing rather than transverse mixing.

Lehmberg et al. (13) analyzed the transverse mixing in a horizontal rotary drum reactor. They used hot particles as tracers to show how the mixing occurred. They also studied the transfer of heat between the bulk of the particles and the wall of the drum. Kroger et al. (14) used this data to study heat transfer and chemical reaction of powders in a drum reactor. Bozatli et al. (15) and Downs et al. (1) studied the heat transfer from hot metallic balls to different granular materials in a rotating drum.

Several researchers have analyzed the heat transfer between a surface and flowing granular material when the flow pattern is known. Harakas and Beatty (16) studied the heat transfer between a flat plate and a rotating granular medium. Raghavan et al. (17), in a study similar to this one, analyzed the heat transfer from a metallic ball to a stream of granular medium flowing in a pipe. Sullivan and Sabersky (18) studied the heat transfer from a flat plate with a similar type of flow situation. Wunschmann and Schlünder (19) studied the heat transfer from a flat plate to a static and a stirred bed of particles. In the case where heat is transferred to a flowing granular medium of which flow pattern is known, existing analytical models describe the data satisfactorily (Richard and Raghavan, (20)).

HEAT TRANSFER IN A CONTROLLED FLOW SITUATION

Theory

The simplest situation to analyze is the case of a bed of granular material flowing at a uniform speed past a heated flat plate as shown in Figure 1. This situation can be modelled using the following assumptions: (a) the flow of heat is unidimensional, perpendicular to the plate; (b) the penetration of heat is proportional to the time because the flow of particles past the plate is "laminar"; (c) there is a finite contact resistance; the heat transfer coefficient has a maximum limiting value. Many authors (8, 13, 18, 19, 20) have shown that this model represents adequately the physical situation existing in their experiments. The analytical solution to such a situation is well known and can be found, for instance, in Carslaw and Jaeger (21).

Sullivan and Sabersky (18) have shown that the expression for the heat transfer coefficient, α, obtained in such a situation can be replaced by the following, numerically approximate solution:

$$\alpha = [H^{-1} + \lambda_b^{-1} (\tfrac{\pi}{4} Dt)^{1/2}]^{-1} \qquad (1)$$

In this equation, λ_b and D are respectively the thermal conductivity and thermal diffusivity of the bed of the particles. In the case of a flowing bed, the time of contact, t, is defined as the length of the heated surface divided by the velocity of the bed. H is the contact resistance, which becomes equal to α, when the time of contact tends to zero.

The existence of the contact resistance has been explained by the presence of a layer of gas between the heated surface and the bulk of the bed of particles. It is assumed that no convection takes place in this layer, in such a way that the contact resistance is a function only of the thickness of the gas layer and of the gas conductivity, λ_g. This is expressed by:

$$H = \lambda_g (\chi \cdot d_p)^{-1} \qquad (2)$$

where χ is the ratio of the thickness of the gas

layer over the diameter of the bed of particles, d_p. It is doubtful whether there actually exists a uniform gas layer between the plate and the particles, preventing a direct contact between the former and the latter. However, it is well known that there is an increase in porosity of a bed of particles at the surface of contact of the bed and a plate or a wall restraining it (22). This increase in porosity creates more resistance to the heat flow (since the gas is a much better insulator than the particles) and this, therefore, results in the same effect as a uniform gas layer. The porosity at the vicinity of the wall is also a function of the overall porosity of the bed and, therefore, the authors were able to analyze the data of the authors (16, 17, 18, 19) and obtain the following correlation between χ and the porosity, ϵ, of the bed:

$$\chi = 5.16\ \epsilon^{5.06} \qquad (3)$$

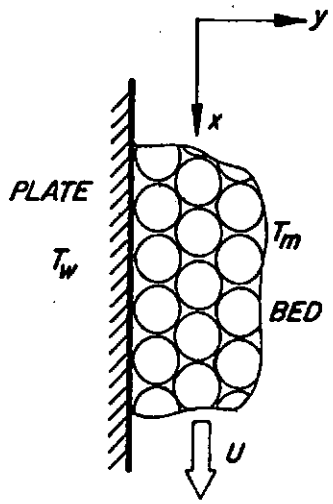

Figure 1. Model of heat transfer past the flat plate.

In the rotating drum experiment, the heat transfer surface used was a sphere rather than a plate. Here, it was also assumed that the bed was flowing past the sphere with a tangential velocity that varied with the angle in such a way that the downward component of the speed past the sphere would be equal to the speed of the bulk of the bed, as shown in Figure 2.

Experimental Setup

The setup shown in Figure 3 consisted of a vertical pipe in the middle of which a steel ball, diameter 1.267 cm, was placed. The ball was heated with a torch and the internal temperature was recorded continuously with an iron-constantan thermocouple. Granular material was flowing in the pipe from a hopper and the rate of flow was controlled by a gate at the bottom. The heat transfer coefficient was calculated by measuring the temperature of the ball and by calculating the rate of cooling of the ball. Since the Biot number was very small, the heat transfer coefficient was calculated according to the Newtonian law of cooling. Three types of salt and two kinds of sand were used as granular material; their main properties are given in Table 1.

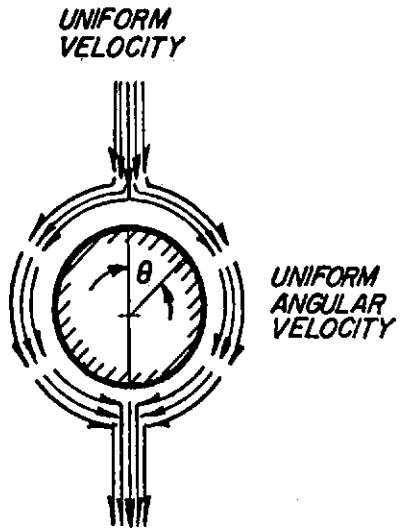

Figure 2. Model of the flow of granular material past a sphere.

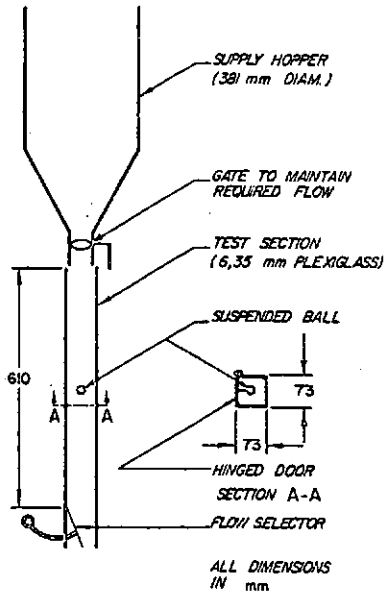

Figure 3. Experimental apparatus.

Results

The results of the experiments with the five different materials are shown in Figures 4, 5, 6, 7 and 8, where the heat transfer coefficients are plotted against the contact time. The solid line on these graphs represents the best fit curve of the form:

$$\alpha^{-1} = \beta_1 \sqrt{t} + \beta_0 \qquad (4)$$

Comparing equation (1) and (4):

$$\beta_1 = (2 \cdot \lambda_b)^{-1} \sqrt{\pi D} \quad \text{and} \quad \beta_0 = \chi d_p \cdot \lambda_g^{-1} \qquad (5)$$

In Table 2 are shown the values of β_1, β_0 and the coefficient of determination, r^2.

TABLE 1. Properties of the granular materials in the flowing bed experiment

Material	Particle size (mm)	Density (kg/m^3)	Porosity	Heat capacity (J/m^3C)	Thermal conductivity (W/mC)
Coarse sand	0.515	1436	0.347	1.17×10^6	0.20
Fine sand	0.210	1444	0.344	1.18×10^6	0.20
Crystal salt	0.221	1076	0.502	0.95×10^6	0.27
Granulated salt	0.348	1252	0.420	1.10×10^6	0.29
Topping salt	0.778	1055	0.512	0.93×10^6	0.24

However, the equivalence between the values obtained for β_1 and the values calculated from the particle data were significantly different. In every case, the calculated values were greater than the experimental ones. Various factors can explain this discrepancy; one of them is the fact that the steel ball was interfering with the flow of the particles and, therefore, the porosity of the bed may not be the same in the vicinity of the ball as that in the bulk of the bed. Such a decrease in porosity would increase the thermal conductivity and the heat capacity of the bed, therefore lowering β_1. A similar type of effect appears also in the experiments of Raghavan et al. (17) and Harakas and Beatty (16) where objects were immersed in a flowing bed, therefore constraining the flow in the vicinity of the immersed objects and consequently decreasing the porosity.

Table 2 also shows the value of χ that was derived from β_0, as well as the values predicted by equation (3). The difference between the predicted values of χ and the experimental ones for salt is within reasonable limits. On the other hand, equation (3) predicts χ values for the sand particles that are much smaller than the experimental results. However, equation (3) was established using experimental data of material having higher porosities than those of the sands used here. Consequently, this equation gives aberrant results outside the extreme values for which it was established. Another factor that may have had its importance is the fact that salt had a very narrow particle size distribution, and sand had a much wider one. Since χ is a proportionality factor between the particle size and the thickness of the gas layer, one would suspect that the presence of many sizes of particles in a granular bed would have some effect on χ. Further research is currently taking place to assess the importance of these factors and to derive an analytical model of the contact resistance.

HEAT TRANSFER IN A HORIZONTAL, UNFLIGHTED ROTARY DRUM

Theory

In this section, the situation is analyzed where metallic balls and a granular material are mixed together in a rotating horizontal drum. If the relative motion of the balls with respect to the granular medium could be determined, then the average time of contact between the balls and the particles of the bed could be analyzed and equation (1) could be applied to predict the heat transfer coefficient obtained.

First, it will be assumed that the balls are well mixed and that no segregation occurs, so that all the surface of each ball is available for transferring heat with the granular bed. Downs et al. (1) have analyzed in detail the different flow regimes occurring in the drum. At low angular velocities, the bed tends to slip down the surface of the drum and no mixing actually occurs within the bed. As the velocity increases, the angle of the bed in the drum reaches the angle of repose of the particles and so the particles start to roll from the top of the bed to the bottom. At higher velocities, centrifugal forces carry the material high on the side of the drum from where it "showers" into the main bed. At faster speeds, the carry-over is complete and the material constantly sticks to the side of the drum. In this analysis, it is assumed that rolling is the dominant regime.

Downs et al. (1) have shown that the rolling motion can be analyzed by making a balance of the mass passing across a drum radial to yield the following expression for the thickness of the sliding layer, ℓ:

$$L = \cos\beta \cdot (V^2\cos^2\beta + 2\bar{h}V + \ell)^{1/2} - V\cos^2\beta - \bar{h} \quad (6)$$

where: $V = v/(r\omega)$, $L = \ell/r$, $\bar{h} = h/r$ and v is the velocity of the sliding layer, h is the distance between the surface of the bed and the centre of the drum, β is the angle between the surface normal and a drum radial, r is the drum radius and ω, the angular velocity, as shown in Figure 9. Lehmberg et al. (13) analyzed the transverse mixing in a rolling situation and found no mixing as the material was carried up by the drum, but there was intense mixing in the sliding layers. On the basis of this information, calculation can be made for the time during which an individual particle stays in the bulk of the bed and in the sliding layer. The average time of residence was calculated by dividing the bed into layers ($\Delta\ell$), as shown in Figure 9, and performing a numerical integration, for different angular velocities, when $V = 5$ and $\bar{h} = 0.5$.

The heat transfer coefficient obtained in the bulk of the bed can then be calculated using the residence time in the bulk of the bed as the

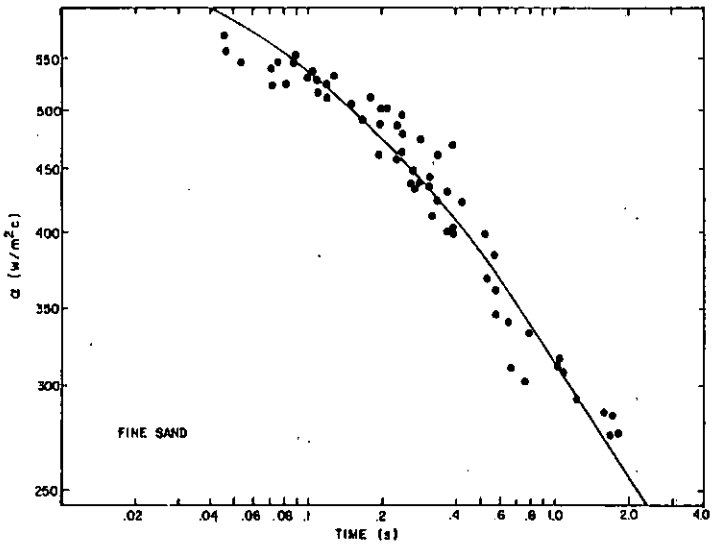

Figure 4. Heat transfer coefficient vs. contact time for fine sand.

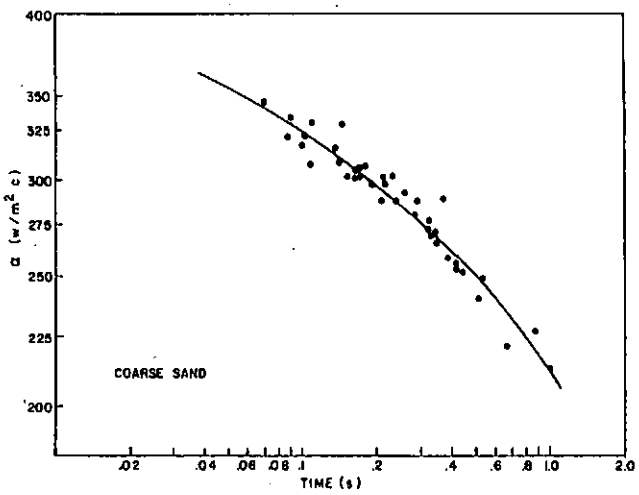

Figure 5. Heat transfer coefficient vs. contact time for coarse sand.

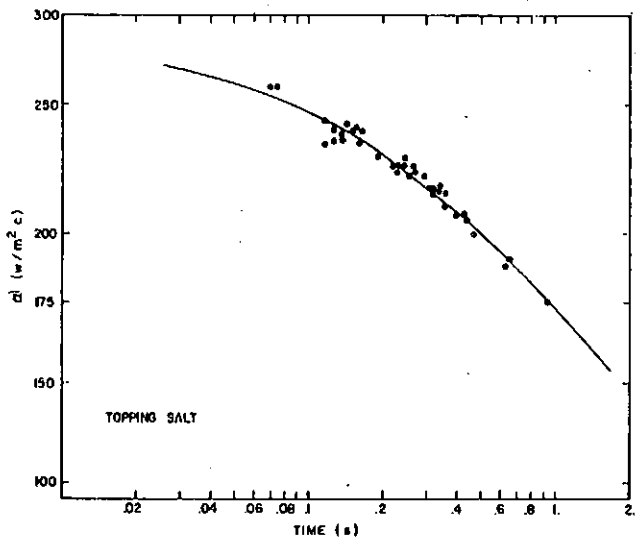

Figure 6. Heat transfer coefficient vs. contact time for topping salt.

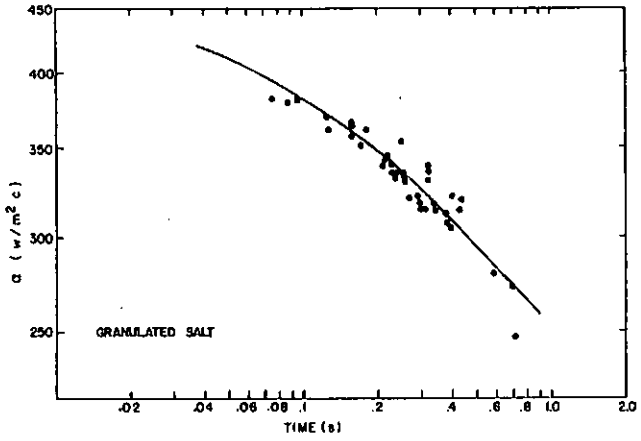

Figure 7. Heat transfer coefficient vs. contact time for granulated salt.

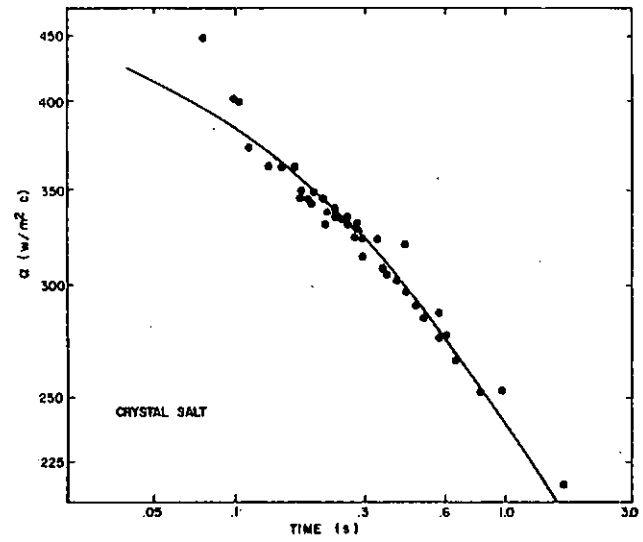

Figure 8. Heat transfer coefficient vs. contact time for crystal salt.

contact time. In the sliding layer, high mixing occurs and, therefore, the contact time cannot be made equivalent to the residence time. Therefore, it was assumed that all particles (and hence the balls) moved with the speed, v, with respect to each other. This resulted in very short contact times (equal to the ball diameter divided by the speed); however, at such short contact times, the heat transfer quickly apporaches a maximum value as the parameter χ becomes dominant. The overall heat transfer coefficient was calculated as the average of the heat transfer coefficients in each region weighted over the time spent. The reason for using this type of average is that the probability of an individual ball being in each region is equal to the fraction of the total time that is spent in that region. This is expressed by:

$$\alpha_{avg} = \frac{\alpha(t_B) \cdot t_B + \alpha(d_p/v) \cdot t_s}{(t_B + t_s)} \qquad (7)$$

where $\alpha(t_B)$ is equation (1) and t_B and t_s are the residence time in each layer as given in Table 3.

TABLE 2. Experimental and calculated regression parameters for equation (4) in the flowing bed experiment

Material	$\beta_1$exp	$\beta_1$calc*	$\beta_0$exp	χexp	χcalc†	r^2
Coarse sand	0.00237	0.00183	0.00231	0.126	0.02	0.928
Fine sand	0.00184	0.00182	0.00129	0.172	0.02	0.952
Crystal salt	0.00226	0.00175	0.00188	0.238	0.16	0.975
Granulated salt	0.00213	0.00157	0.00194	0.156	0.06	0.908
Topping salt	0.00248	0.00188	0.00329	0.118	0.17	0.955

*calculated from equation (1).
†calculated from equation (3).

TABLE 3. Residence time of a particle in the mixing layer section and bulk section of a rotating drum per drum rotation

RPM	Mixing layer section t_s (s)	Bulk section t_B (s)
10	0.124	1.66
20	0.062	0.83
30	0.041	0.55
40	0.031	0.41
50	0.025	0.33
60	0.021	0.28
70	0.018	0.24
80	0.015	0.21

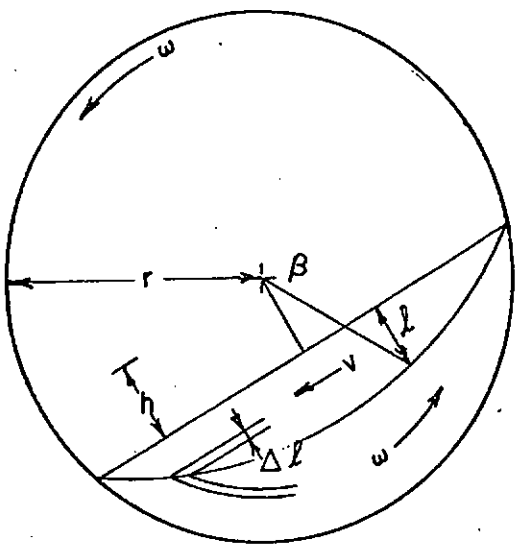

Figure 9. Model of the flow of granular material in a rotary drum.

Experimental Results

The data analyzed here were obtained from the experiment of Downs et al. (1). They used a rotary drum of 60 cm diameter with heated steel and aluminum balls having diameters of 1.905 and 1.270 cm. The characteristics of the particulate materials used in these experiments are given in Table 4. Details of their experimental apparatus are given by Downs et al. (1) and Bozatli et al. (15).

Figure 10 shows the heat transfer obtained with various types of salt and balls. Aluminum balls with fine salt gave the highest heat transfer coefficients. Equation (1) shows that the finer type of granular material should have a smaller contact resistance and thus favouring higher rates of heat transfer. The density of the aluminum balls was, in every case, close to the density of the particulate material, contrary to the steel balls. Hence, segregation problems probably occurred in the case of the steel balls, preventing all the available surface from being exposed to heat transfer. Therefore, only the data obtained with aluminum balls were analyzed using equation (7).

The average residence time in each region, t_s and t_B, of the rotating bed was determined using values of $V = 5$ and $h = 0.5$ as shown in Table 3. These values of V and h seemed to be most realistic. A computer simulation was run with other values of h (0 to 0.5) and V (1 to 5) and found that these parameters of the model did not greatly affect the values of α for drum speeds of 20 rpm and over.

The data obtained for both sizes of aluminum balls and the various granular materials are shown in Figures 11, 12, 13, 14 and 15. These results were compared with the theoretical model using various values of the parameter χ. The solid curve on these figures shows the results at which the parameter χ minimizes the error with the data. The value of χ in each case is shown in Table 5.

TABLE 4. Properties of granular materials in Downs et al. (1) experiment

Material	Particle size (mm)	Density (kg/m^3)	Porosity	Heat capacity (J/m^3C)	Thermal conductivity (w/mC)
Coarse salt	1.80	1250	0.43	1.10×10^6	0.291
Fine salt	0.35	1300	0.40	1.14×10^6	0.291
Coarse sand	1.80	1370	0.46	1.12×10^6	0.356
Fine sand	0.35	1220	0.47	0.99×10^6	0.356
Glass	0.35	1530	0.36	1.15×10^6	0.865

TABLE 5. Experimental and calculated values of contact resistance parameters for the experiment of Downs et al. (1)

Material	χcalc*	χexp
Coarse salt	0.07	0.045
Fine salt	0.053	0.085
Coarse sand	0.103	0.065
Fine sand	0.109	0.185-0.2
Glass	0.028	0.12

*calculated from equation (3).

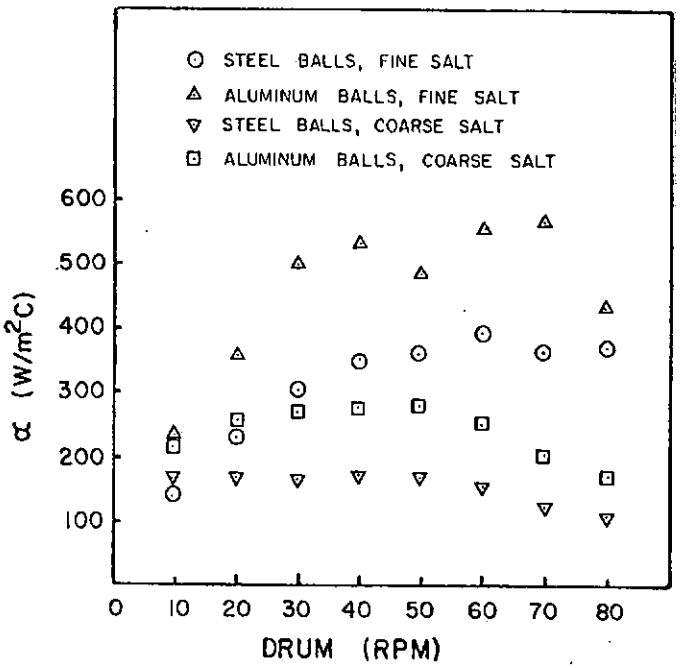

Figure 10. Heat transfer coefficient vs. rotating speed after (1).

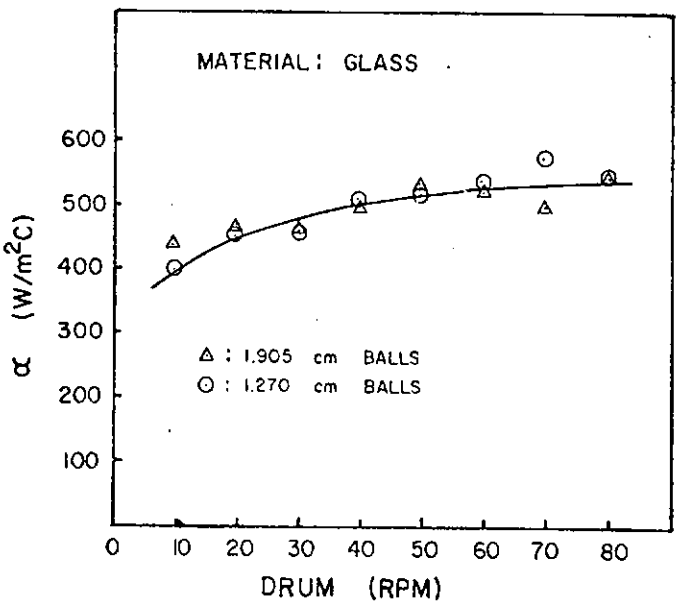

Figure 11. Heat transfer coefficient vs. rotating speed using glass, after (1).

For all of the material except glass, it is obvious that irregularities in the flow regime of the drum occur. Slippage seems to exist for fine salt at low speed. This would result in the bulk of the bed not turning as fast as the drum itself and, thus, the reduced heat transfer coefficients. Centrifugation occurs in most materials at speeds higher than 60 rpm, resulting again in lower heat transfer coefficients due to the fact that the material stays longer in the bulk of the bed without mixing. It is also interesting to note that there is very little variation between the heat transfer obtained with the two sizes of balls, as was predicted by the theoretical model.

The values of χ are the same for both sizes of balls, as shown in Table 5, except for fine sand which has two close values of χ. This table also gives the theoretical value of χ obtained from equation (3). The values given by this equation are of the same magnitude as those determined experimentally; however, this equation fails to

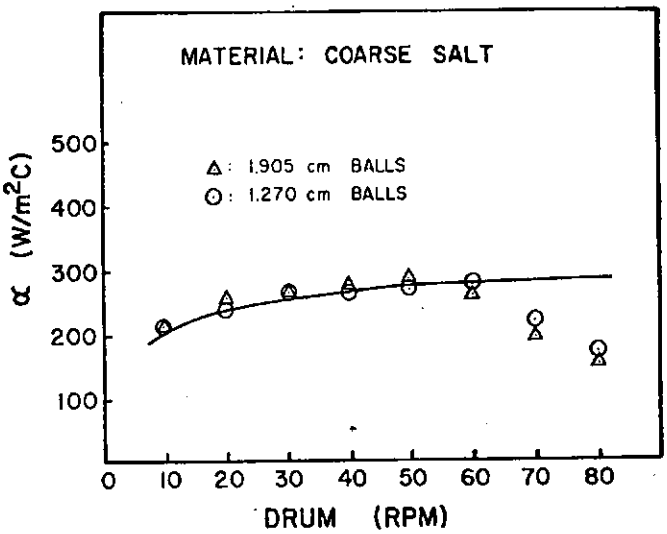

Figure 12. Heat transfer coefficient vs. rotating speed using coarse salt, after (1).

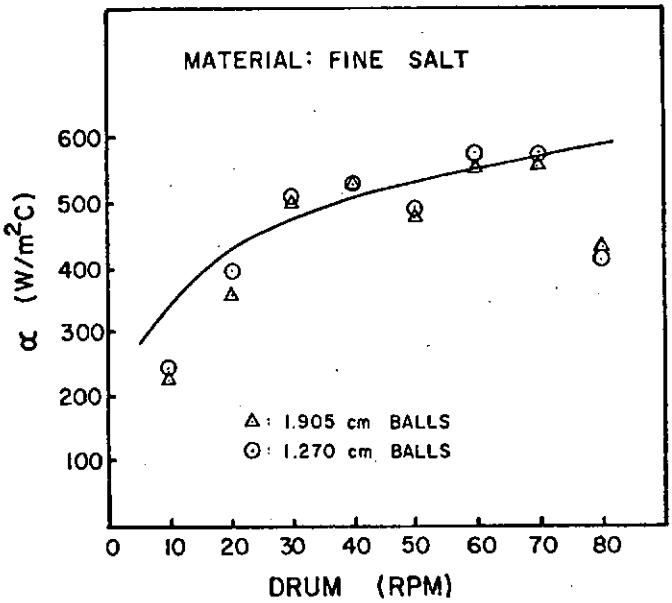

Figure 13. Heat transfer coefficient vs. rotating speed using fine salt, after (1).

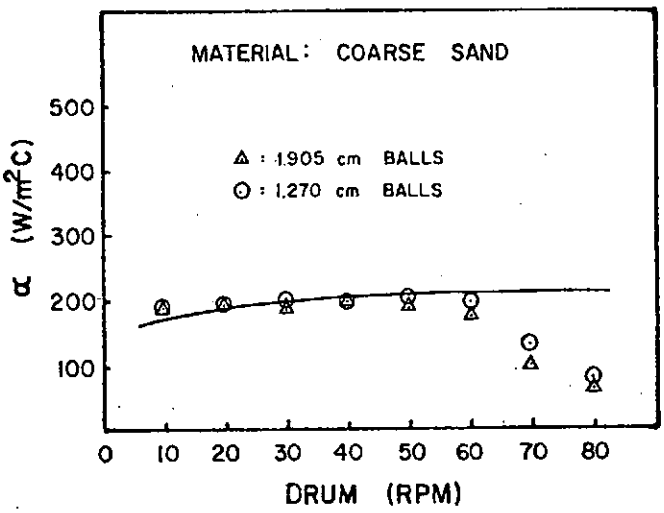

Figure 14. Heat transfer coefficient vs. rotating speed using coarse sand, after (1).

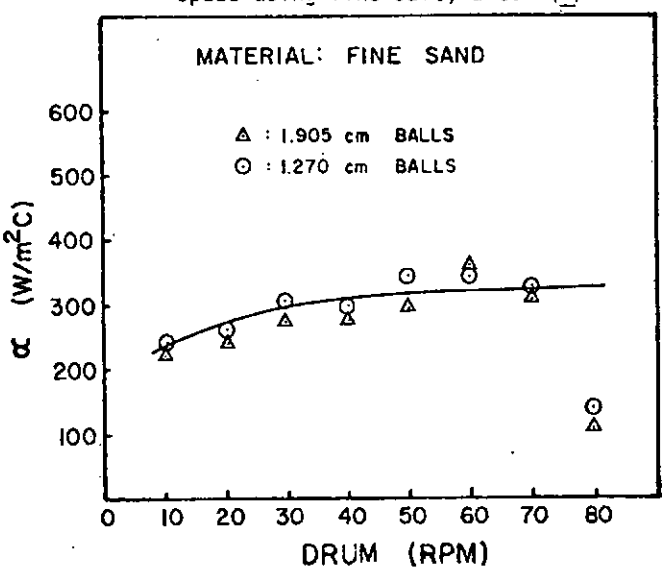

Figure 15. Heat transfer coefficient vs. rotating speed using fine sand, after (1).

give an accurate prediction of the actual values of χ. Consistently, the prediction is too high for coarse particles and too small for fine particles.

Porosity values used in equation (3) were measured in static conditions. Under dynamic conditions, it is quite probable that the porosity of the rotating bed would be increased, therefore increasing the contact resistance between the particles and the balls. Another factor of importance is the shape of the particles. For instance, according to (1), fine sand had a value of 1.5 for shape factor. This factor, as defined by McCabe and Smith (23), gives an indication of the surface to volume ratio and is higher than unity for particles of irregular shape. Therefore, it is suspected that the bed of fine sand will tend to get a higher porosity under dynamic conditions due to the irregular shape of the particles. This factor also implies that the diameter of the particles, determined by sieving, is most probably the second diameter of the particle rather than the biggest. Both of these factors tend to increase the value of χ. Fine sand has a higher χ than the other materials following the above argument; but the lower experimental values of χ for coarse particles contradicts the argument. It is, therefore, necessary to find some other mechanism to explain this contradiction. Further research is needed towards this end.

CONCLUSIONS

The problem of obtaining an anlytical model for the drying of granular foodstuff in rotary drums using particle-particle heat transfer has to be resolved in a multi-step approach. In this paper, it was assumed that the rate of heat transfer is the limiting factor of the drying

operation and, consequently, only the heat transfer aspects of drying were analyzed here.

Granular foodstuff can be thought of as spheres and so the heat transfer between a flowing granular medium and a metallic sphere was analyzed. It was found, as expected, that there is a finite contact resistance that limits the heat transfer coefficient that can be obtained. This contact resistance can be expressed by a single parameter, χ. A reasonable approximation of χ was predicted by using the particle size and the porosity of the material. The experimental evaluation of the contact resistance, as was carried out here, has immediate applications to particle-particle heat transfer but is also very valuable to other areas of research such as fluidized-bed heat transfer.

The second step consisted of a theoretical model of the transverse motion of a mixture of particles in a rotating drum. Two types of motion occur in a rotating drum; in one type, there is no relative motion, nor mixing, between the particles and the metallic balls; in the second type of motion, there is intense mixing and it was assumed that the relative motion of the particles and the balls is of the same nature as that encountered in a situation of controlled flow as in the first step. The time of contact for each type of motion was predicted using numerical techniques. It was shown that the heat transfer in the rotary drum could be successfully analyzed using the model developed as long as rolling motion was prevalent in the drum.

In summary, this paper presents analytical models of heat transfer from spheres immersed in granular medium flowing at a uniform speed or in drum-type flow conditions. These models describe successfully experimental data and, therefore, outline the parameters that are of importance in drying apparatus design using particle-particle heat transfer.

ACKNOWLEDGEMENTS

The authors wish to thank Professor Harper of Colorado State University for kindly communicating his results. The financial support of the NSERC, without which this study would not have been feasible, is also gratefully acknowledged.

REFERENCES

1. Downs, H.W., J.D. Kellerby, J.M. Harper, R.D. Haberstroh and W.D. Marlatt, Heat transfer by contact between agitated particles, Unpub. final report, Colorado State Univ., 1977.
2. Khan, A.U., A. Amilhussin, J.R. Arboleda, A.S. Manola and J.W. Chancellor, Accelerated drying of rice using heat conduction media, ASAE Paper No. 73-321, 1973.
3. Raghavan, G.S.V., and J.M. Harper, High temperature drying using a heated bed of granular salt, Trans. ASAE, Vol. 17, p. 108-111, 1974.
4. Lapp, H.M., G.S. Mittal and J.S. Townsend, Cereal grain drying and processing with solid heat transfer media, ASAE Paper No. 76-3524, 1976.
5. Richard, P., and G.S.V. Raghavan, Particle-particle heat transfer applications to drying and processing - a review, in: Developments in Drying, Science Press, Princeton, 1979.
6. Uhl, V.W., and W.L. Root, Heat transfer to granular solids in agitated units, Chem. Eng. Prog., Vol. 63, p. 81-92, 1967.
7. Sass, A., Simulation of the heat-transfer phenomena in a rotary kiln, Ind. Eng. Chem. Process Des. Dev., Vol. 6, p. 532-535, 1967.
8. Berntsson, T., Heat transfer in a new type of heat exchanger for divided solids, Powder Techn., Vol. 22, p. 101-111, 1979.
9. Abouzeid, A.Z.M., and D.W. Fuerstenau, On the contribution of convective dispersion and diffusion mechanisms to the dispersion of particulates in rotating drums, Ind. Eng. Chem., Process Des. Dev., Vol. 15, No. 1, p. 14-15, 1976.
10. Hehl, M., H. Kroger, H. Helmrich and K. Schugerl, Longitudinal mixing in horizontal rotary drum reactors, Powder Techn., Vol. 20, p. 29-37, 1978.
11. Fan, L.T., and S.H. Shin, Stochastic diffusion model of non-ideal mixing in a horizontal drum mixer, Chem. Eng. Sci., Vol. 34, p. 811-820, 1979.
12. Chaudhuri, P.K., and D.W. Fuerstenau, The effect of mixing aids on the kinetics of mixing in a rotating drum, Powder Techn., Vol. 4, p. 146-150, 1970.
13. Lehmberg, J., M. Hehl and K. Schugerl, Transverse mixing and heat transfer in horizontal rotary drum reactors, Powder Techn., Vol. 18, p. 149-163, 1977.
14. Kröger, H., M. Hehl, H. Helmrich and K. Schugerl, Decomposition of powders in horizontal rotary drum reactors, Powder Techn., Vol. 22, p. 1-10, 1979.
15. Bozatli, A.N., R.D. Haberstroh and J.M. Harper, Heat transfer by contact between agitated particles, ASME Paper No. 76-HT-61, 1976.
16. Harakas, N.K., and K.O. Beatty, Moving bed heat transfer, C.E.P. Symposium Series, Vol. 59, p. 122-218, 1963.
17. Raghavan, G.S.V., J.M. Harper and R.D. Haberstroh, Heat transfer study using granular media, Trans. ASAE, Vol. 17, p. 589-592, 1974.
18. Sullivan, W.N., and R.H. Sabersky, Heat transfer to flowing granular media, Int. J. Heat Mass Transfer, Vol. 18, p. 97-107, 1975.
19. Wunschmann, J., and E.V. Schlünder, Heat transfer from heated plates to stagnant and agitated beds of spherical shaped granules, Proc. 5th Int. Heat Transfer Conf., Vol. 5, p. 49-53, 1974.
20. Richard, P., and G.S.V. Raghavan, Heat transfer between flowing granular materials and immersed objects, submitted for publication, Trans. ASAE.
21. Carslaw, H.S., and J.C. Jaeger, Conduction of heat in solids, 2nd ed., Oxford University Press, Oxford, 1959.

22. Botterill, J.S.M., Fluid bed heat transfer, Academic Press, London, 1975.
23. McCabe, W.L., and J.C. Smith, Unit operations of chemical engineering, 2nd ed., McGraw-Hill Book Company, New York, 1967.

DRYING CHARACTERISTICS OF PARBOILED RICE

A. S. Bakshi[1]
R. Paul Singh[2]

1. University of Minnesota, St. Paul, MN
2. University of California, Davis, CA

ABSTRACT

A study was conducted to obtain information on drying rates of parboiled rice. Parboiled rice was dried under controlled air conditions to allow measurement of mass diffusivities and develop drying equations. It was found that there was no constant rate period of drying in parboiled rice. The drying rates of parboiled rough rice and parboiled brown rice were the same. The diffusivities dependence on temperature can be expressed as Arrhenius type relationships.

NOMENCLATURE

a	Radius, m
D	Mass diffusivity, m^2/hr
h_{fg}	Heat of evaporation, kJ/kg
M	Moisture content, decimal (dry basis) at any time t
M_e	Equilibrium moisture content, decimal (dry basis)
M_o	Initial moisture content, decimal (dry basis)
P	Parameter in thin layer equation
Q	Parameter in thin layer euqation
r	Variable radius, m
SSD	Sum of squared deviation
RH	Relative humidity, percent
t	Time, hr
T	Temperature, ^oC
T_p	Rice temperature, ^oC
T_a	Absolute temperature, ^oK
const	Constants in parameters P and Q

INTRODUCTION

Rice is consumed by more than half the world's population. It is obtained from rough rice by milling process. To reduce breakage during milling, rice is parboiled. Parboiling is a hydrothermic treatment, given to rough rice before milling to accomplish gelatinization of starch and thus imparting hardness to rice. Parboiling process consists of soaking in hot water, steaming and drying of rice. At the end of soaking and steaming operation, the rice attains a moisture content of about 60 percent dry basis (Bakshi and Singh, 1979). This high moisture is not encountered in raw rough rice (without parboiling). Thus, drying characteristics of parboiled rice are expected to be different from that of raw rice. In the recent years drying characteristics of raw rice are discussed by Wang and Singh (1978), Bakshi et al. (1978) and Steffe (1979). A discussion on the effect of drying conditions on the milling yield is given by Bhattacharya and Swamy (1967). However, published information on the drying characteristics of parboiled rice is lacking. Thus, a study was planned with the following objectives:

1. To obtain information on the drying rates of parboiled rice.
2. To calcuate mass diffusivities in rough and brown parboiled rice.
3. To develop drying equations for parboiled rough and brown rice.
4. To compare energy required for the drying of parboiled rice with that of raw rice using a computer-aided model.

In a study on the kinetics of rice parboiling process, Bakshi and Singh (1979) observed that it is possible to dehusk rough rice before parboiling to reduce energy input. Thus, in the present study drying rates of parboiled brown rice (dehusked rough rice) are also determined. The drying characteristics of parboiled rice are compared with that of raw rice. The drying equations developed in this study will be useful in modeling and drying process for parboiled rice. Using drying equations developed in this study and computer aided model of a crossflow dryer, the energy required for the drying

of parboiled rice is compared with that of raw rice.

METHOD AND EQUIPMENT

Raw Material Preparation

Short grain rough rice (S6) was obtained from the Rice Growers Association. This is a smooth-hull variety. The foreign matter, broken and immature kernals were separated by hand. A clean sample was used for the drying study.

Parboiling

Rough rice was soaked for 2 1/2 hours in water at 70°C and steamed at 5 psig for 15 minutes. Brown rice was soaked for 45 minutes at 70°C and then steamed for 10 minutes. These time and temperature combinations were found to accomplish complete parboiling (Bakshi and Singh, 1979). The soaking and steaming was done in model rice parboiling apparatus as shown in Figure 1.

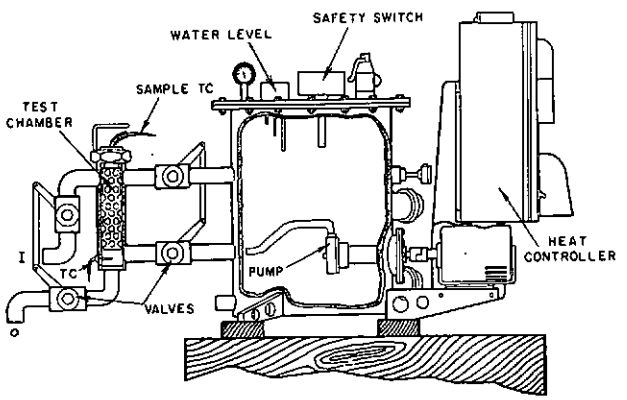

Figure 1. Schematic of a rice parboiling apparatus.

This apparatus allows for a high rate of water flow around the rice sample enclosed in the sealed test chamber. The following procedure was used in all the experiments. Desired water temperature was achieved by adjusting the dial on the heat controller. A 120 g sample of rice was placed in the perforated cylinder, which was then attached to the cap. This assembly was secured to the empty test chamber and hot water introduced into the chamber. The sample was soaked in water for the desired length of time. Then the hot water was turned off and steam was introduced into the chamber from port I. The sample was then removed from the perforated cylinder and surface moisture was removed.

Drying

The experimental setup and procedure was the same as described by Agrawal and Singh (1977) and Steffe (1979). A single layer of rice kernal was placed on trays. Air at constant temperature and humidity was allowed to pass through the grain. Aminco Aire unit (Model J45590A) was used as source of air supply. A change in weight as a function of time was recorded by a strip chart recorder using a load cell output. The data from strip chart was digitized using a Hewlett-Packard Digitizer (Model 9864A). The summary of drying conditions are shown in Table 1 for both rough parboiled and brown parboiled rice. Only parboiled rice was dried in the current study. The data for raw rice drying was obtained from Steffe (1979).

THEORETICAL CONSIDERATIONS

Diffusion Coefficient

Newman (1931) and Sherwood (1931) proposed the application of Fick's law of diffusion to the drying of solids during falling rate period. The Fick's law in three-dimensional rectangular coordinates can be expressed as:

$$\frac{\partial M}{\partial t} = \frac{\partial}{\partial x}\left(D\frac{\partial M}{\partial x}\right) + \frac{\partial}{\partial y}\left(D\frac{\partial M}{\partial y}\right) + \frac{\partial}{\partial z}\left(D\frac{\partial M}{\partial z}\right)$$

The solution to the above equation is given by Crank (1975). In case of sphere, the solution of the diffusion equation can be expressed as:

$$\frac{M - M_e}{M_o - M_e} = \frac{6}{\pi^2} \sum_{n=1}^{\alpha} \frac{1}{n^2} \text{Exp}\left(\frac{-n^2 \pi^2 D}{r^2}\right)t \qquad [1]$$

Boundary Conditions

$$\frac{\partial m}{\partial r} = 0,\ r = 0,\ t \geq 0$$

$$M = M_e,\ r = a,\ t \geq 0$$

$$M = M_o,\ 0 \leq r \leq a,\ t = 0$$

Assumptions

1. The mechanism of moisture movement is liquid diffusion.
2. Diffusion coefficients are independent of moisture concentration.
3. Rice drying is considered as isothermal process.
4. Rice is considered as sphere.
5. Shrinkage during drying is neglected.

Table 1. Rice Thin-Layer Drying Conditions and Mass Diffusivity

	Temperature °C		M_o	M_e	Diffusivity
	Dry bulb	Wet bulb	(decimal db)	(decimal db)	(m^2/hr x 10^{-7})
Raw Rough	54.8	47.8	.3120	.1290	1.2960
	49.9	42.8	.3130	.1370	0.8146
	40.2	29.4	.3200	.1590	0.3694
Raw Brown	54.8	47.8	.2850	.1360	2.3675
	50.0	42.2	.3090	.1400	1.8410
	40.8	34.5	.2790	.1630	1.1620
Parboiled Rough	56.1	46.1	.6032	.1054	2.4886
	51.1	42.2	.6141	.1132	1.9068
	40.6	36.7	.6375	.1512	0.8863
	50.1	42.0	.3015	.1126	1.8840
Parboiled Brown	56.1	46.1	.6414	.1136	2.4720
	51.1	42.2	.6400	.1516	1.9295
	40.2	36.4	.6376	.1292	0.8326

The mechanism of moisture movement during grain drying is diffusion as stated by Crank (1975). The movement of moisture could be in the liquid or vapor state. Chhinnan (1976) compared vapor and liquid diffusion equations for describing the drying of peanuts. He found that the liquid model gave a better fit during most of the drying period. However, both the liquid and vapor diffusion model gave an adequate prediction of the drying curve.

The diffusion coefficients are assumed to be independent of moisture concentration. Steffe (1979) found that the diffusion coefficient in rice was independent of moisture concentration in the moisture range of 13 to 30 percent dry basis. In the present research, this assumption is tested for parboiled rice. The result indicate the validity of this assumption.

Heat transfer equations were neglected in the current study because the resistance to heat flow is small as compared to resistance to mass flow. Young (1969) concludes that heat transfer can be neglected if the Lewis number is greater than 60. Steffe (1979) estimated a Lewis number of 7446 for rice drying. Thus, this assumption holds good.

The biological products are not defined by a common geometric shape. However, for simplified mathematical analysis it is necessary to assume a simple configuration. Hosokawa and Motohashi (1973) found that the shape of rice kernal could be assumed spherical during drying. More over a short grain variety of rice was used in the current research, thus making this assumption more reasonable.

Shrinkage of rice kernal is neglected during drying. An average value of equivalent radius of a sphere is used for the determination of diffusion coefficient.

The above equation which gives the moisture ratio at any time, was programmed on a computer (Burroughts 6700). A nonlinear optimization technique based on steepest descent method is used in conjunction with Equation [1] to find the diffusion coefficients. The optimization program estimates a set of parameters in a mathematical model which give a minimum value of the sum of squares of the deviation between the observed and the estimated values. The technique is described in detail by Chhinnan (1976).

Thin Layer Equation

Page (1949) suggested the following equation relating moisture ratio during drying to the relative humidity and dry bulb temperature of air:

$$\frac{M - M_e}{M_o - M_e} = \text{Exp } (-P\ t^Q)$$

$$P = \text{const}_1 + \text{const}_2 \times T - \text{const}_3 \times RH$$

$$Q = \text{const}_4 + \text{const}_5 \times T + \text{const}_5 \times RH$$

The advantages of this thin layer equation over the other thin layer equations available in literature were discussed by Wang (1978). The values of the constants were determined as in the case of diffusion coefficient.

Rice Drying Simulation

Wang (1978) modified the MSU corn drying computer program (Bakker-Arkema, et al., 1974) for rice drying. He tested this program against actual drying of rice in a crossflow dryer. Rice drying in a crossflow dryer was simulated using the thin layer equations developed in this study. The drying conditions for a simulation study were:

Dry bulb temperature - 50°C

Relative humidity - 62%

In the current study the simulation was used only to examine energy requirements of the drying of parboiled and raw rice for both rough and brown rice.

RESULTS AND DISCUSSION

Drying Rate

Drying curves for parboiled rice are plotted in Figure 2. The upper curve is for drying at 56°C and lower is at 40°C. It can be seen that there is no constant rate drying period. The drying rate is not constant even at the high moisture content of 0.60 (db). All the drying in case of rice takes place in the falling rate period. Thus, Fick's law of moisture diffusion may be used for modelling the entire drying period for parboiled rice.

Examination of Figure 2 also reveals that the drying rates at the two temperatures are different. This is expected due to the difference in drying potential. For the top curve, the difference in dry bulb and wet bulb temperature is 10°C and for the lower one it is only 4°C.

It is also clear from Figure 2 that there is no difference in the drying rates of rough and brown parboiled rice. This can be attributed to the splitting of husk during parboiling (Bakshi and Singh, 1979). Thus, parboiled rough rice behaves like brown rice as husk after splitting offers practically no resistance to drying.

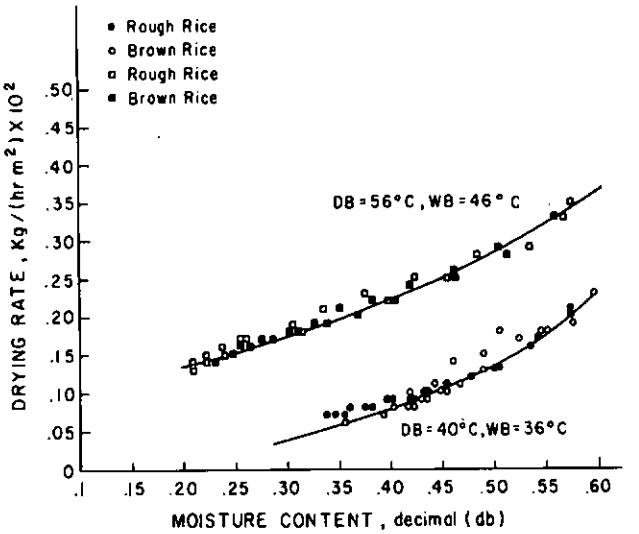

Figure 2. Drying curves for parboiled rice.

The drying rate of parboiled rice is compared with the drying rate of raw rough and brown rice in Figure 3. The closeness of drying curves for parboiled rough rice supports the above observation that resistance of husk in parboiled rice is negligible. It can also be safely said that parboiling does not result in changing resistance to moisture movement. In the case of raw rough rice the husk offers considerable resistance in drying as is indicated by the low drying rate of raw rough rice (Steffe, 1979).

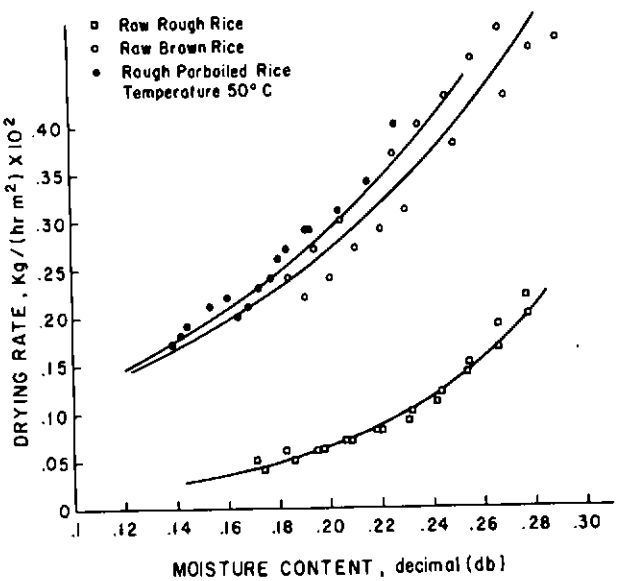

Figure 3. Comparison of drying rates of raw and parboiled rice.

Table 2. Arrhenius Relations for Rice Mass Diffusivities

	Diffusivity m^2/hr	r^2
Raw Rough	$D_{rr} = 3.3029 \times 10^4 \text{ Exp } (-8.6243 \times 10^3/Ta)$	.99
Raw Brown	$D_{rb} = 0.7979 \text{ Exp } (-4.9333 \times 10^3/Ta)$	.91
Parboiled Rough	$D_{pr} = 4.1186 \times 10^2 \text{ Exp } (-6.9777 \times 10^3/Ta)$	.98
Parboiled Brown	$D_{pb} = 4.0162 \times 10^2 \text{ Exp } (-6.7436 \times 10^3/Ta)$	.97

Table 3. Thin Layer Drying Equations for Rice

$$\frac{M - M_e}{M_o - M_e} = \text{Exp } (-p\ t^Q)$$

		SS D
Raw Rough	P = .744982 + .0002615 T - .0003335 RH	.337
	Q = .094070 + .005984 T - .0113465 RH	
Raw Brown	P = .438957 + .0002748 T - .0006705 RH	.240
	Q = .093302 + .007272 T - .01551836 RH	
Parboiled Rough	P = .503265 + .0002734 T - .0001760 RH	.331
	Q = .064445 + .0046369 T - .0147194 RH	
Parboiled Brown	P = .016538 + .000173684 T + .0064722 RH	.174
	Q = -.7766099 + .001417332 T + 0.07367 RH	

Values of P and Q for raw rice are calculated from the data of Steffe (1979).

Diffusivity

The diffusion coefficients at various drying temperatures for parboiled and raw rice are given in Table 1. The raw rough rice has the lowest value of diffusion coefficient, indicating high resistance to moisture movement. The diffusion coefficient of parboiled rough rice was determined at two initial moisture contents of 0.3015 and 0.6141 at a drying air temperature of about 50°C. This was done to determine the effect of moisture concentration on diffusivity. The value of diffusion coefficient in two cases is about the same being 1.8840×10^{-7} and 1.9068×10^{-7} m^2/hr. Thus indicating diffusion coefficient is independent of concentration even at the high moisture content of 0.6 (db). In studying wheat drying, Becker (1959) found that diffusion coefficients were independent of moisture content in the range of .13 to .25 (db). Steffe (1979) confirmed this in the case of white rice.

The Arrhenius type relations for the effect of temperature on diffusion coefficients as calculated from Figure 4 are shown in Table 2. The curves for raw and parboiled rice slope in a similar manner, indicating that the diffusivity changes of both are similar with respect to the temperature.

Energy for Drying

The thin layer equations as developed from the drying data for raw and parboiled rice are given in Table 3. Rice drying was simulated in a crossflow dryer. The following equation as developed by Wang (1978) for rice from the data of Zuritz and Singh (1978) was used to calculate the heat of evaporation at each stage of drying in the computer model.

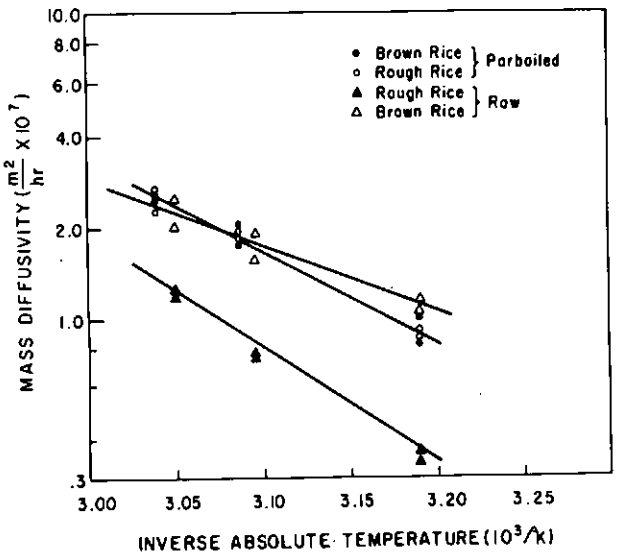

Figure 4. Diffusion coefficients of raw and parboiled rice.

$$h_{fg} = (1547.84 - 1.46\ T_p)M^{-0.346}$$

The results of the simulation study are shown in Figure 5. To evaporate one kg of water from rice in the moisture range of .3 to .16 (db), it takes 5017 kJ for parboiled rough rice and 6533 kJ for raw rough rice. The energy input for the drying of parboiled rice is less due to the splitting of husk during parboiling. However, the moisture content of parboiled rice is 0.6 (db) at the start of drying, whereas, for raw rice initial moisture content is about 0.3 (db). To dry this additional moisture, it takes more energy. To get 100 kg of rough rice at 0.16 moisture content (db), a total of 129000 kJ are required for parboiled rice as compared to 89900 kJ for raw rice.

The thin layer equations developed in the current research can be used to model drying of parboiled rice in different types of dryers a.g. deepbed dryer, crossflow dryer, concurrent flow dryer etc. These modeling studies will give information on the time required for the drying of parboiled rice and can help in the selection of type and dimensions of dryer to reduce energy input. In conclusion;

1. There is no constant rate drying in rice even at a high moisture content of 60% (db).
2. Drying rates of parboiled rough rice, parboiled brown rice and raw brown rice are about the same.
3. Drying rate of raw rough rice is lower due to the presence of the husk.
4. Arrhenius type relation holds for the diffusivities and drying air temperature for parboiled rice.
5. Energy required to evaporate one kg of water in parboiled rice is less than raw rice in the same moisture content range.

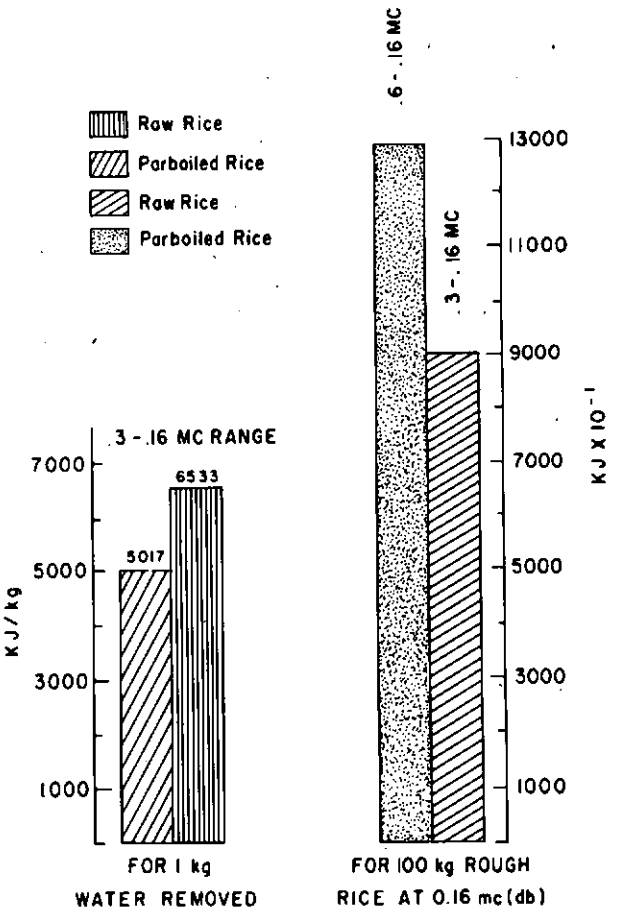

Figure 5. Energy requirements for the drying of raw and parboiled rough rice.

REFERENCES

1. Agrawal, Y. C., and Singh, R. P., Thin-layer drying studies for short grain rice, ASAE Paper No. 77-3531, ASAE, P.O. Box 410, St. Joseph, MI 49085, 1977.
2. Bakker-Arkema, F. W., Lerew, L. E., DeBoer, S. F., and Roth, M. G., Grain dryer simulation, Res. Rept. 224, Mich. State Univ., Agric. Exp. Sta., 1974.
3. Bakshi, A. S. and Singh, R. P., Kinetics of water diffusion and starch gelatinization during rice parboiling, Paper No. 259, 39th Annual IFT Meeting, St. Louis, MO, June 10-13, 1979.
4. Bakshi, A. S., Singh, R. P., Wang, C. Y., and Steffe, J. F., Energy cost of a conventional and air recycling crossflow rice dryer. ASAE Paper No.

78-3011, ASAE, P.O. Box 410, St. Joseph, MI 49085, 1978.
5. Becker, H. A., A study of diffusion in solids of arbitrary shape, with application to the drying of wheat kernal, J. Applied Polymer Science, 1(2):212-226, 1959.
6. Bhattacharya, K. R. and Swamy, Y. M. I., Conditions of drying parboiled paddy for optimum milling quality, Cereal Chem 4(6):592-600, 1967.
7. Chhinnan, M. S., Bulk thin-layer models for drying of peanuts in pods, Unpublished Ph.D. Thesis, North Carolina State Univ., Raleigh, 1976.
8. Crank, J., The Mathematics of Diffusion, Second Edition, Oxford Univ. Press, Ely, House, London, W.I., 1975.
9. Hosokawa, A. and Motohashi, K., Drying characteristics of a single grain of unhulled rice, J. Soc. Agr. Mach. Japan, 34(4):372-378, 1973.
10. Newman, A. B., The drying of porous solids: diffusion calculations, AIChE, Interim publication of August 1, 1931:310-333, 1931.
11. Page, G. E., Factors influencing the maximum rates of air-drying shelled corn in thin layers, Unpublished M.S. Thesis, Purdue Univ., Lafayette, Indiana, 1949.
12. Sherwood, T. K., Application of theoretical diffusion equation to the drying of solids, AIChE 27:190-202, 1931.
13. Steffe, J. F., Moisture diffusion and tempering in the drying of rough rice, Unpublished Ph.D. Thesis, Univ. of Calif., Davis, CA 95616, 1979.
14. Young, J. H., Simultaneous heat and mass transfer in a porous hygroscopic solids, Transactions of the ASAE, 12(2):720-725, 1969.
15. Wang, C. Y., Simulation of thin-layer and deep bed drying of rough rice, Ph.D. Thesis, Univ. of Calif., Davis, CA 95616, 1978.
16. Wang, C. Y. and Singh, R. P., A single layer drying equation for rough rice, ASAE Paper No. 78-3001, ASAE, P.O. Box 410, St. Joseph, MI 49085, 1978.
17. Zuritz, C. A. and Singh, R. P., Desorption isotherms of rice from 10°C to 40°C, ASAE Paper No. 78-6006, ASAE, P.O. Box 410, St. Joseph, MI 49085, 1978.

DRYING OF HEAVILY SALTED CODFISH

Ingvald Strømmen

Institute of Refrigeration,
the Technical University of Norway, Trondheim

ABSTRACT

The artificial drying of heavily salted codfish is an important side of Norwegian fish industry. From drying experiments in a pilot plant a mathematical model to describe drying curves under different conditions, is set up. The model is used to simulate the industrial drying of codfish in a heat pump plant. Energy considerations and drying procedures, for instance batch versus continously, are being specially studied. Because of the nature of the fish, continously drying shows up to be a much better principle than batch drying. By using a heat pump system, continously, one reduces the energy costs by 2/3 of the costs in a traditional petroleum dryer.

The mathematical model is semi-empirical. It has its basis in the theory of drying of capillary-porous bodies, and it includes, somewhat simplified, transport processes in the fish. These processes are being studied separately. They involve the migration of salt and water, the evaporation, and transport of vapour, during a drying experiment.

NOMENCLATURE

A = area of drying surface, $[m^2]$
α = heat transmission number $[W/m^2K]$
β = mass transfer number $[-]$
c_p = specific heat of the air $[J/kgK]$
D = diffusion number, water vapor in air $[m^2/s]$
ϕ = relative humidity of air $[-]$
G_d = drying speed $[kg/s]$
G = weight loss in the first drying period $[kg]$
h = enthalpy of the air $[J/kg]$
λ = thermal conductivity, dry layer $[W/mK]$
μ = diffusion resistance in dry layer $[-]$
p_d = water vapor pressure $[N/m^2]$
Q_d = latent heat transport $[W]$
Q_k = convective heat transport $[W]$
r = heat of evaporation $[J/kg]$
R_d = gas constant, water vapor $[J/kgK]$
s = thickness of dry layer $[m]$
σ = mass transfer coefficient $[kg/m^2s]$
t = temperature $[^oC]$
T = absolute temperature $[K]$
w = air velocity $[m/s]$
X = moisture constant $[kgH_2O/kg$ dry air$]$

Subscripts

o = on the outer surface
L = in the surrounding air
s = on the irride drying front

INTRODUCTION

Heavily salted fish has been dried in Norway for more than 400 years. The fish used belongs to the Cod family and includes Cod, Lang, Tusk, Haddock and Coalfish.
Nowadays all the fish are being dried artifically in tunnels with heated air. The heating of the outdoor air takes place in a heat exchanger with electricity or petroleum as the heat source. Fish and air are moving in counter-current direction through the tunnel. Recommended drying conditions and processing schemes has its background in the wish to dry the fish as fast and cheap as possible without quality defects.
The energy crises has created the need to reduce energy costs. The heat pump has two advantages: It is energy saving and it regulates the drying conditions independent of the outdoor air.

This work intend to describe what is optimal drying conditions with respect to temperature, relative humidity and air velocity. Further, what is the best drying procedure, utilization, of a heat pump system.

EXPERIMENTAL EQUIPMENT

Drying experiment

The influence of temperature, relative humidity and air velocity on the drying is studied. A heat

pump pilot plant is used to create the desired drying conditions. This is shown on Figure 1.

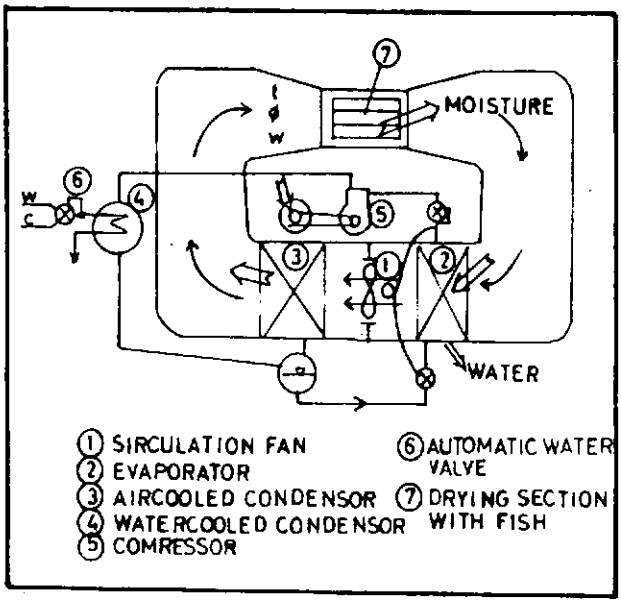

Figure 1. Heat pump pilot plant.

The fish is placed in a tunnel where the air is sirculating in a closed loop. A fan with speed regulation is giving the desired air velocity. The air is reaching the drying section with a given condition. In passing the fish heat is taken from the air to evaporation of water. Reaching the evaporation in the refrigerating plant the air is cooled and water is condensing on its surface. In this process heat is preserved by the evaporation of a refrigerant. The tunnel condensor is heating the air to the desired temperature and the excess heat is removed in a water cooled condensor.
The desired temperatures and relative humidity can be obtained with the heat pump.

The highest humidities is obtained by irrigating water on the tunnel condensor.

Temperatures is measured with Cu/Con termocouples and relative humidities with Vaisala Humicap Humidity Meter. Air velocity is measured with a Schiltknecht velocity meter. The accuracies is $\pm$ 0,5°C, $\pm$ 2,0 R.H. and $\pm$ 0,2 m/s. Temperatures during experiments have been between 11°C and 26°C, relative humidities between 30% and 70% R.H. and air velocity between 1 m/s and 4 m/s.

Transport phenomena

In this part transport of water and salt during a drying experiment, will be examined. For this use a test cylinder is utilized to cut out cylindrical fish samples. The fish cylinders are cut in thin slices and examined on water and salt content. Water content is determined by drying at 105°C in 24 hours. Salt content is found by leaching the bone dry fish/salt sample in a certain amount of water and then analyzed on chlorid content. This is done by titration with $AgNO_3$.

RESULTS

Drying experiments

Several lots of fish has been examined. Before drying, the salt fish is usually washed, press-piled in stacks and resalted. The fish used in the experiments are of equal size and are being handled equally. Both unwashed/cleaned and washed/resalted fish has been dried.
The highest temperature used in the experiments, 26°C, has been chosen to ensure not "burning" the fish. "Burning" is an irreversible and unwanted quality defect appearing at too high temperatures. The upper limit for codfish is found to be 27°C (1). In another article the same limit is found (80°F) (2).

The water content during drying moves from 55 to about 45 percent wet basis. At a given water content drying speed increases with increasing temperature and decreasing relative humidity. An example of drying curves are shown on Figure 2.

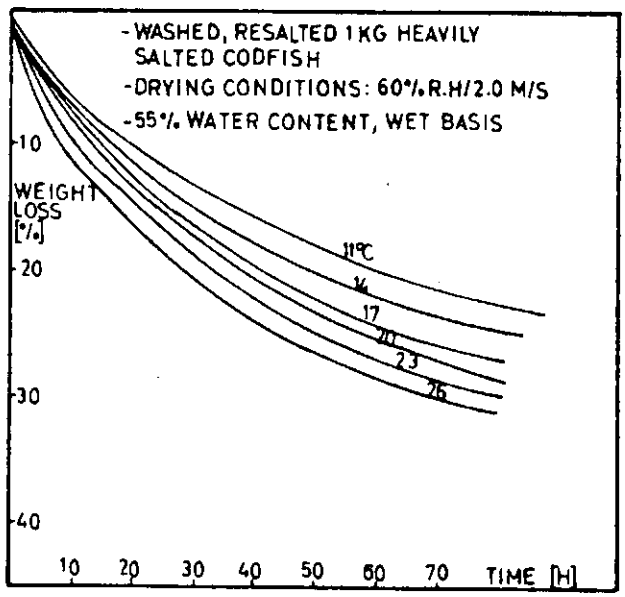

Figure 2. Example of drying curves.

With respect to air velocity drying curves are almost coinciding for velocities over 2 m/s.

Transport phenomena

When heavily salted fish is drying dry layers are formed on both sides of the fish, while the water content in the core is lowered with some few per cent, wet basis. There is no qualitative differences in the water profile whether the drying potensial has been high or low, whether the fish

used has been washed/unwashed, big (2,4 kg) or small (1 kg). An example of the time development of the water profile is shown on Figure 3.

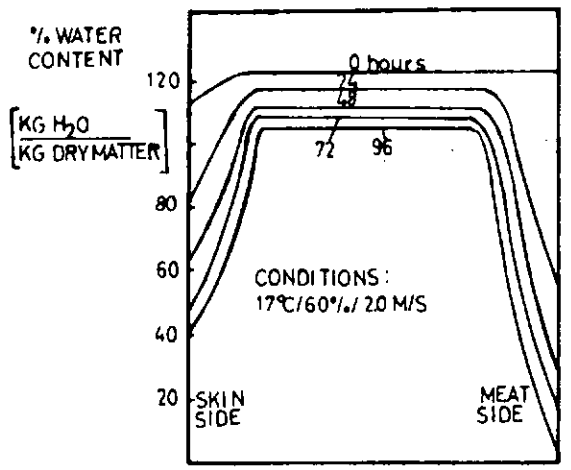

Figure 3. Time development of water profile.

Time development of the salt profile for the same experiment is shown on Figure 4.

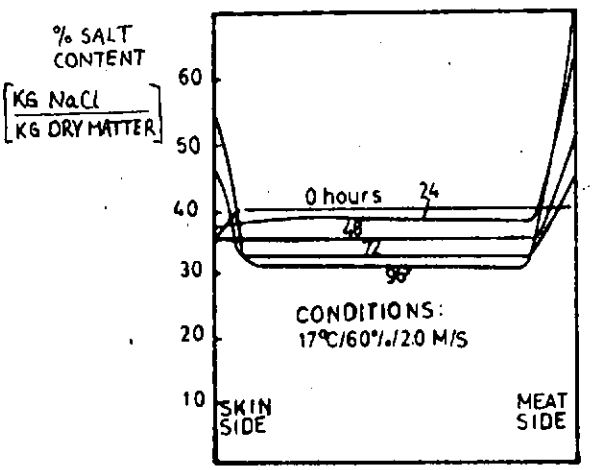

Figure 4. Time development of salt profile.

From Figure 3 and 4 it is apparent that water is transported in the liquid phase from the core, and that evaporation takes place in the outer dry layers.

MATHEMATICAL MODEL

There is a need for predicting the drying curve for certain drying conditions. When evaporated quantity of water from one fish is known, air condition after the fish can be calculated and the condition of the air along a tunnel can be determined. In this way drying procedures may be simulated and energy need calculated.

The drying is divided into two phases. In the first we have drying from a wet surface. The potensial in this mass transfer is the vapor pressure difference between the surface and the surrounding air:

$$G_d = \sigma \cdot A \, (X_o - X_L) = \frac{B \cdot A}{R_d \cdot T} (p_{do} - p_{dL}) \qquad (1)$$

Heat of evaporation:

$$Q_d = G_d \cdot r \qquad (2)$$

The necessary heat of evaporation is taken from the air itself:

$$Q_k = \alpha \cdot A \cdot (t_L - t_o) \qquad (3)$$

The Lewis relationship combines heat and mass transfer:

$$\sigma = \frac{\alpha}{c_p} \qquad (4)$$

Thermal equilibrium gives:

$$Q_d = Q_k \qquad (5)$$

$$h_L = h_o \qquad (6)$$

The surface temperature will be given of equation (6) and the fact that water activity for heavily salted fish is 0,76.

In the second period dry layers are formed. We now make the assumption that evaporation takes place from a drying front inside the fish, and water are being transported by diffusion through the dry layers. The following equations describe the mass transport:

$$G_d = \frac{D \cdot A}{\mu \cdot S \cdot R_d \cdot T} (p_{ds} - p_{do}) \qquad (7)$$

$$G_d = \frac{\beta \cdot A}{R_d \cdot T} (p_{do} - p_{dL}) \qquad (8)$$

Elimination of p_{do}:

$$G_d = \frac{1}{R_d T} \frac{A}{\frac{1}{\beta} + \frac{\mu \cdot S}{D}} (p_{ds} - p_{dL}) \qquad (9)$$

Heat transfer is being described by:

$$Q = \alpha \cdot A \cdot (t_L - t_o) \qquad (10)$$

$$Q = \frac{\lambda}{S} \cdot A \cdot (t_o - t_s) \qquad (11)$$

Elimination of t_o:

$$Q = \frac{A}{\frac{1}{\alpha} + \frac{S}{\lambda}} \cdot (t_L - t_s) \qquad (12)$$

Neglecting the heat capacity, air condition on the outer surface will remain on the same enthalphy as

he surrounding air. The following choice of constants and phycial relations have been made:

$$R_d = 462 \text{ J/kgK}$$

$$D = 2{,}61 \cdot 10^{-5} \text{ m}^2/\text{s}$$

$$\lambda = 0{,}1 \text{ W/mK}$$

$$p_d = \phi \cdot 10^{(11{,}232 - 2305{,}3 \frac{1}{T})} \quad (13)$$

$$\alpha = 9{,}05 \cdot w^{0{,}8}$$

$$h = |1{,}005 \cdot t + X\,(2500 + 1{,}86 \cdot t)| \cdot 10^3 \quad (14)$$

The model is calculating a theoretical drying curve on this basis. The fish stays in phase 1 until a certain amount of water, ΔG, is lost. In the second drying period a growing dry layer with a certain resistance factor μ is formed. A plotting routine is comparing the measured curve with the theoretical one for a certain choice of the parameters μ and ΔG. For a given lot of fish one is registrating the choices of ΔG and μ giving fitting curves. In this way differences between the real drying process and the theoretical one are included in the choice of the parameters.
The air condition meeting the next row of fish along a tunnel can now be calculated. Thusboth air and fish condition can be calculated everywhere in the tunnel. In this way drying procedures and energy need can be simulated. The model is used to simulate a heat pump system. The principles of such a system are shown in Figure 1 but the tunnel has a certain length in where the fish is placed on wheeled racks. Condition of the air along the tunnel is assumed to follow the isentalpic line on the humidity chart.

When the tunnel dimensions and amounts of fish are known for an industrial plant several processing relations can be simulated. Here, three examples will be mentioned: Figure 5 is showing the production rate in tons/24 hours as a function of regrigarator capacity and the inlet temperature of the tunnel. The processing sheme here used is the principle "1 out/1 in". That means: When the first row of racks has reached a certain degree of dryness it is removed from the tunnel and a new wet row is pushed in from behind. Further, the production rates shown on Figure 5 are those appearing 750 hours after drying start. If a production of 10 tons/24 hours is aquired at 20°C inlet temperature a plant with 200 kW refrigator capacity is necessary. At 26°C inlet temperature a plant of 150 kW is sufficient.
Figure 6 gives the production rate as a function of total number of wheeled racks in the tunnel. The ever increasing curves has its explanation in a lowering of the ratio $\frac{dh}{dx}$ for the air passing the evaporator. In Figure 7 production rate for two drying principles, 1 out/1 in, 8out/8in is shown for a plant of 150 kW cooling load. At 26°C inlet temperature the production rate is 13% higher with the principle 1out/1in. Drying with a "batch" principle, fill the tunnel with wet fish and dry it all complete falls out as an unacceptable drying procedure. This may easily be explained from the fact: the more fish in the second drying period the higher ratio $\frac{dh}{dx}$ for the air passing the evaporator.

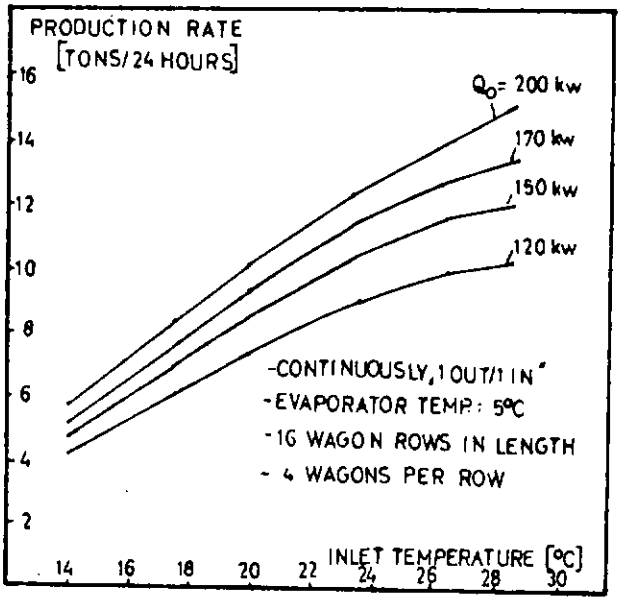

Figure 5. Production rate as a function of refrigeration capacity, and inlet temperature.

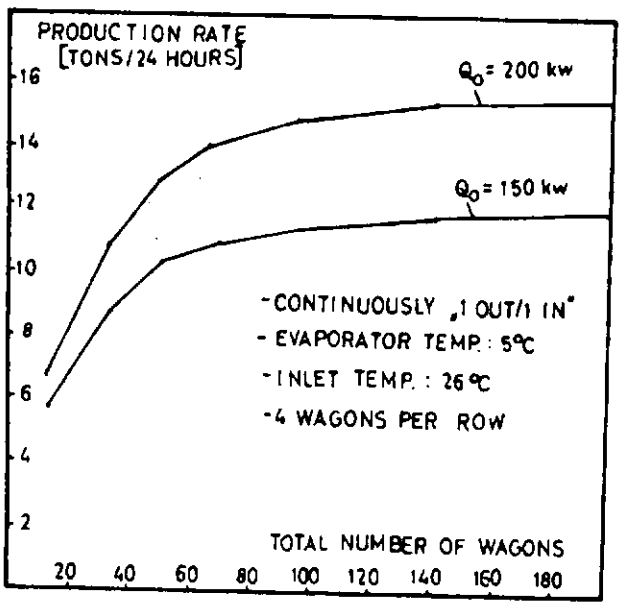

Figure 6. Production rate as a function of total number of waggons.

The energy need for a plant of 150 kW cooling load at 26°C inlet temperature, 5°C evaporator temperature is calculated. The refrigerant is R22, total efficiency of the compressor 0,67, evaporation temperature is set to 0°C and condensation temperature to 35°C. This will give a compressor work of 39 kW. Power consumption per ton fish produced is 86 kWh, alternatively 0,46 kWh per kg water evaporated. With oil prices from 1. sept. 1979 the energy costs for drying is 3,4 times higher with a traditional petroleum dryer. If

capital costs are included, a heat pump system will still come out as the best alternative, even though it is about 4 times more expensive. [1]

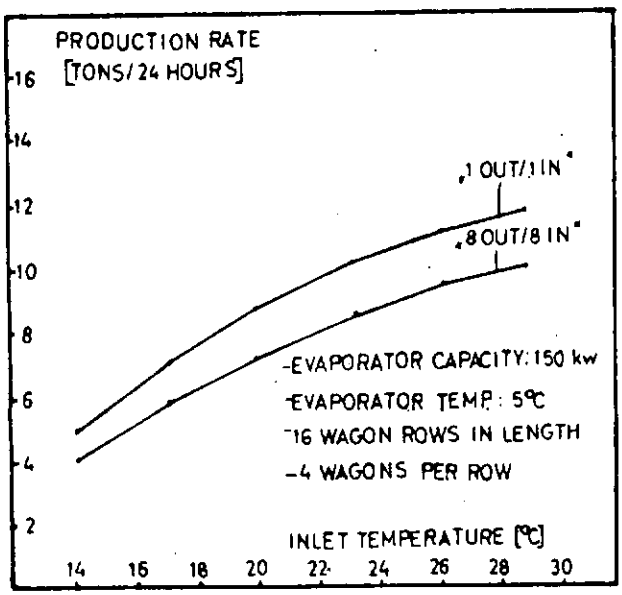

Figure 7. Production rate as a function of drying principle and inlet temperature.

CONCLUSIONS

When heavily salted fish is drying the drying speed at a certain water content of the fish increases with increasing temperature and decreasing relative humidity. Further, dry layers are formed, and these are qualitatively equal whether the drying potensial has been high or low. Optimal drying seems therefore to be as warm and dry as possible, within certain limits, not "burning" the fish.

A mathematical model is formed on this basis. Using it on a heat pump dryer several drying procedures are simulated and energy need calculated. Continuously drying shows up to be a much better principle than batch drying. A traditinal petroleum dryer uses today 3-4 times more for energy costs than the heat pump. In times to come with increasing oil prices, the advantages of the heat pump will become even more important.

REFERENCES

1. Strømmen, I., Drying of heavily salted codfish. Thesis for the degree dr.ing. Institute of Refrigeration, the Technical University of Norway, Trondheim, 1980.
2. Legendre, R., The artificial drying of Lightly Salted Codfish. J. Fish. Res. Bd. Canada 12 (1) 1955.

DRYING AND COOLING PROPERTIES OF MILK POWDER BY USING A FLUIDIZED BED

Hiromichi Hayashi
Tsuneo Wada

Snow Brand Milk Products Co., Ltd.
Technical Research Institute
1-2, Minamidai 1-chome, Kawagoe, Saitama, 350 Japan

ABSTRACT

The thermal efficiency of a spray dryer and the quality of milk powder could be improved if a fluidized bed combined with a spray dryer in milk powder processing. This research has studied the drying properties in the 2nd stage falling rate period of drying, the cooling and the fluidizing properties for skim milk powder by using a fluidized bed. The results are summarized as follows:
1) For obtaining good fluidization of the milk powder, the air velocity should be 9cm/sec, and the bed expansion ratio be 1.7~1.8.
2) The suitable hot air temperature for minimizing the thermal denaturation is 85°~100°C, to dry the moisture content from 7% to 4%.
3) The volumetric heat transfer coefficient for the fluidized bed is 700~1600 W/m^{3}K in cooling the 80°C the milk powder with the residence time of 35~78 minutes.
4) Fine particles of the milk powder entrained by air are collected in a cyclone. The fractional recovery of the separated fine particles is 6~12%.

NOMENCLATURE

A = area of material m^2

Af = area of fluidized bed m^2

a = specific surface area m^2/m^3

C_H = specific heat of moist air kJ/kg°C

C_{mf} = fluidized coefficient

C_s = specific heat of bone dryed material kJ/kg°C

C_w = specific heat of water kJ/kg°C

F = free moisture content

F_c = critical moisture content

G_o = air mass flow rate, kg/hr m^3

G = dry air flow rate, kg/hr

g = gravity acceration, m/sec

g_c = convert coefficient of gravity, kg-m/kg-sec^2

h = heat transfer coefficient, W/m^{2}K

ha = volumetric heat transfer coefficient, W/m^{3}K (kcal/m^{3}hr°C)

L_o = height of fluidization, m

Nu = Nusselt number

ΔP_f = pressure loss of fluidized bed, Pa(mmAq)

q = heat transfer capacity, kJ/kg

Q = air flow rate through distribution plate, cm^3/sec

R_{ep} = Reynolds number

r_w = latent heat of steam at tw°C kJ/kg

t = dry bulb temperature °C

t_w = wet bulb temperature °C

$(\Delta t)_m$ = logarithmic mean temperature difference between particle and air (°C)

U_{mf} = air velocity for fluidization, m/sec

V = volume of static fluidized bed, m^3

v = air velocity, m/sec

W = feed rate of bone dry material , kg/hr

W_s = packed weight, kg

w = moisture content

Greek symbole

θ = time, min

$\bar{\theta}$ = mean resident time of particle, min

Suffix

1 = inlet

2 = outlet

m = material

g = air

mf, f = fluidization

o = static state

INTRODUCTION

Two stage drying of milk powder is preferred both for its superior economy and for the improved product quality obtained by this system. The steam consumption in a two stage drying plant is 15~ 20% lower than in an equivalent single stage drying plant. Higher inlet air temperature and milk solid are allowed by two stage drying process which further reduces it's drying cost. Due to the above advantage for two stage drying, the drying and cooling properties of milk powder that has been discharged from a spray dryer with a fluidized bed has been investigated.

THEORETICAL CONSIDERATIONS

Drying Process in a Spray Dryer

In spray drying process, liquid droplets and hot air are passing through a dryer, influencing each other, i.e., varying their temperatures, air humidity and solid moisture content. Hence, the theoretical treatment of unsteady drying mechanism is needed for analysing the process.
If adiabatic heating is assumed for the drying process within a parallel flow dryer, the following equations should hold (2).

$$hA\,(t_g - t_m)\,d\theta = -G\,C_H\,dt_g \qquad (1)$$

and, at any section,

$$W\,(-dw)/A\,d\theta = h(t_g - t_w)F/r_w F_c \qquad (2)$$

(3)

eliminating $d\theta$ from Eq. (1) and (2), we have

$$dt_g/dw = \frac{W\,r_w\,(t_g - t_w)\,F_c}{G\,C_H(t_g - t_w)\,F} \qquad (4)$$

eliminating $d\theta$ from Eqs. (2) and (3) gives

$$dt_m/dw = \left\{ r_m - \left(\frac{t_g - t_m}{t_g - t_w}\right) \frac{r_w\,F_c}{F} \right\} \Big/ (C_s + C_w\,W) \qquad (5)$$

By the use of Runge-Kutta numerical integration method, we can solve Eqs.(4) and (5) simultaneously with respect to t, t_m and F, which indicate the interrelationship among the changing air temperature, powder temperature and its moisture content during the spray-drying process.

Calculating the overall heat transfer coefficient of a fluidized bed

Overall heat transfer coefficient ha of a fluidized bed is defined in Eq.(6), as in general type of heat exchangers.

$$q = ha\ v\ (\Delta t)m \qquad (6)$$

However, how to determine $(\Delta t)m$, the mean temperature difference, has not yet been consistent up until now, resulting in the scattered values of ha reported by past investigators. Two examples will therefore be examined in the following.

Cross-flow fluidized bed model

Suppose a laterally expanded fluidized bed, in which particles are continuously moving in horizontal direction in cross-flow with fluidizing gas. Assuming that the particles in the bed are fully mixed only in the vertical direction but no back mixing in the horizontal direction, ha can be given by the following equations(2) :

$$ha\,L_o = G\,C_H \Big/ \left\{ \left\{ \frac{G_o\,C_H\,Af}{W\,C_s} \Big/ \ln \Delta t \right\} - 1 \right\} \qquad (7)$$

$$(\Delta t)lm = t_{m2} - t_{m1} / \ln \left\{ t_{g1} - t_{m1} / t_{g1} - t_{m2} \right\} \qquad (8)$$

$$q = W(w_1 - w_2)r_w + W(C_s + C_w\,w_2)(t_{m2} - t_{m1}) \qquad (9)$$

$$q = Af\ G\,C_H(t_{g_1} - t_{g_2}) \qquad (10)$$

In practice, however, a corrective term should be added to Eq.(9), taking into account the cooling effect of powder temperature during the passage from dryer's exit to fluidized bed.
These equations are used in general for evaluating ha of a fluidized bed. But, in the case of a direct feed of the solid particles from a spray dryer to a fluidized bed, it is impossible to measure the inlet and outlet temperatures of solid materials, as a matter of fact. Therefore, one has to calculate or estimate them with reference to Eqs.(4) and (5).

Fully mixing flow model

Contact area between particles and gas in a fluidized bed is so large that the exit-air temperature t_{g2} becomes nearly equal to the particle temperature t_m even in a shallow bed.
In this case, both the particles and the gas are fully mixed, respectively, so that the temperature of heating air entering the fluidized bed should instantaneously become equal to t_{g_2} ; the air is to leave the bed at the same temperature.
Since the temperature of solids as well as that of air are constant, respectively, there is obtained

$$\Delta t_m = t_{g_2} - t_m \qquad (11)$$

The maximum temperature rise of the milk powder observed was as small as 1.3°C in the present experiment, in which the moisture content was varied from 7% at the inlet to 4% at the exit.
Consequently, t_m in Eq.(11) can be replaced by t_f, the temperature of the fluidized bed.
Furthermore, it is also hard to measure t_{g_2}, so that $(t_{g_1} - t_m)$ would be used as the driving force for heat transfer, as was dealt with by Inoue et al (6).
Then a very simple form of equation can be obtained as below.

$$q = ha\ V(t_{g_1} - t_f) \qquad (12)$$

Since $t_{g_2} = t_m$ is assumed here, the following relationship is also obtained from Eqs.(10) and (12).

$$(ha)cal = G\,C_H / L \qquad (13)$$

EXPERIMENTAL APPARATUS AND PROCEDURE

Flow sheet of the present experiment is shown in Fig.1 and the fluidized bed used is detailed in Fig.2. Skim milk powder, manufactured by use of a laboratory scale vertical spray dryer (standard capacity = 50 kg powder/hour), was discharged from the dryer system through a cyclone 6 and a butterfly value 11. Further, the powder was supplied to a fluidized bed 10 (1 m in inside diameter and 0.5 m in effective height); air from blower was blown, Fig.2, in the fluidized chamber through perforated plate 7. The perforated plate was of 1 mm diameter hole, 12 mm pitch, and 5400 number of holes. Fluidization of the milk powder in the bed was promoted by using a stirrer-puddle coupled with a variable speed controller motor. The rotating speed was, however, kept constant at 36 R P M. The milk powder, fed through a feed pile 1, left spontaneously the fluidized bed through exit 4 after a definite holding time, which was controlled by varying the height of weir 3. Exhaust air from the fluidized bed was drawn out through exit pipe 12 accompanied by fine particles, which were separated by cyclone 17. Spray drying was carried out at temperature 150°C of the heating air. When the continuous cooling process was performed in the fluidized bed, a spray nozzle (orifice No. 60 and 1.02 mm diameter core No. 17), the pressure of 150 Kg/cm^2 and the exhaust air temperature of 82~83°C were used, while, on the other hand, a nozzle (orifice No. 56, 1.18 mm diameter core No. 21), the pressure of 70 Kg/cm^2, and the exhaust air temperature of 74°C were used when the secondary drying was carried out. Moisture contents of the milk powder at the exit of the spray dryer for both cases mentioned above became 3.6 % for the former and 7.0~8.9 % for the latter, and the production capacities were 53.5 Kg/hr and 62.1 Kg/hr, respectively. Particle size of the powder at the exit of the spray dryer were about 80~90 μm in Sauter mean diameter.

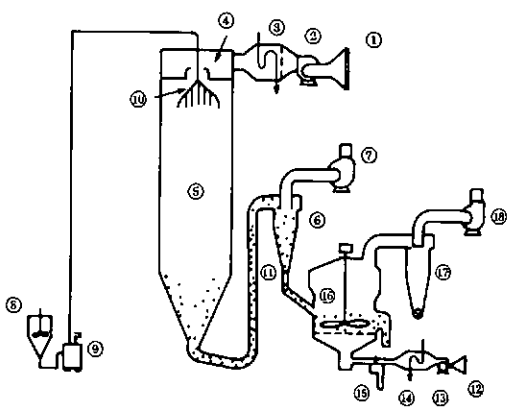

Fig. 1. Flow sheet of drying and cooling process for dry milk.

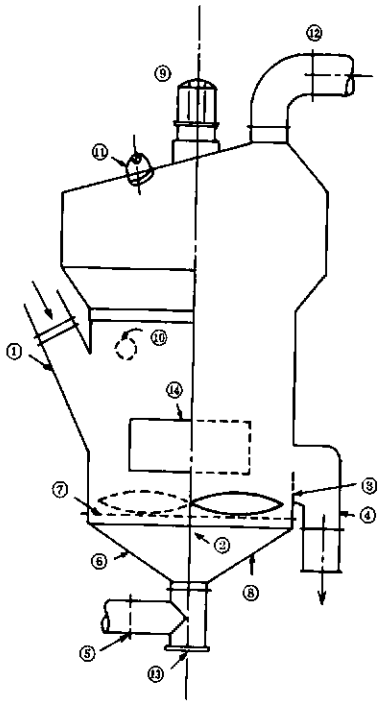

Fig. 2. Fludized bed.

RESULTS AND DISCUSSIONS

Fluidization air velocity

Expansion ratio, i.e., the ratio of height of expanded fluidized bed to that of the static bed, was related to the air velocity, as shown in Fig.3. The ratio increased with increasing air velocity, but an approximately constant value (1.7~1.8) was reached when the air velocity exceeded 7 cm/sec. Some data exhibited particularly higher values of the expansion ratio, suggesting rather uniform fluidization occurring over the whole bed.

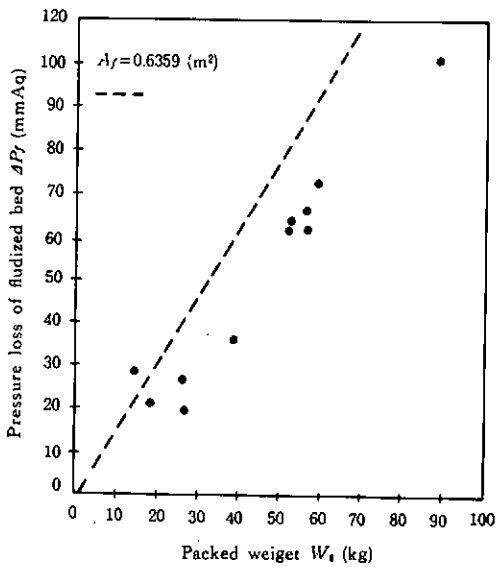

Fig. 3. Relation between packed weight and pressure loss of fludized bed.

Secondary drying properties in continuous process

Skim milk powder of high moisture content (7~8.3%) at the exit of the spray dryer was directly and continuously supplied into the fluidized bed for the secondary drying to satisfy a definite level of moisture content of the milk product. In case of this continuous process it is necessary to know t_f, the temperature within the fluidized bed, in order to use Eq.(12). Fig. 4 represents the relationship between t_f and the inlet temperature of the heating air. In Fig. 4, $t_g < t_f$ refers to the case of cooling process.

In the region of secondary drying at $t_{g_1} > t_f$, hold up of particles had no effects upon t_f so long as the inlet air temperature was below 90°C. However, if the latter became higher than 100°C, the smaller the quantity of hold up, the higher became t_f, leading to partial color changes of the milk powder because of the heat. Both the mean residence time of particles and the inlet air temperature t_{g_1} were plotted against the moisture content of discharge in Fig. 5 and Fig. 6, respectively. These figures show that the exit moisture content of milk powder relies largely upon the inlet air temperature, and is scarcely influenced by the residence time. Consequently, the moisture content of the product can be controlled only by the inlet air temperature. Appropriate air temperature for obtaining 4% of the product moisture content was 85°~100°C.

Calculated ha from Eq. (12) was plotted against the inlet air temperature in Fig. 7 as well as against the residence time in Fig. 8. ha thus calculated decreased with increasing inlet air temperature. This was caused by the fact that the temperature rise of the fluidized bed was rather small at higher inlet air temperature, as represented in Fig. 4, and therefore the temperature difference, i.e., the temperature driving force became larger. This effect suggests that the heat and mass transfer efficiencies are lowered with increase of the inlet air temperature towards the end of the secondary drying stage. Judging from the both figures, the residence time is of considerable importance as a controlling factor upon ha.

The dotted line in Fig. 8 refers to the theoretical values according to Eq.(13). The experimental data became somewhat higher than the theory for the cooling process, whereas somewhat lower for the drying process. However, Eq.(13) can still be used for both cases. It should be noted here that ha calculated from Eqs.(7) and (8) by estimating t_{m_1} and t_{m_2} becomes several times (1.2~3.1) as much as that calculated from Eqs.(12) and (13), so that how to take the driving force in calculating ha should clearly be noted.

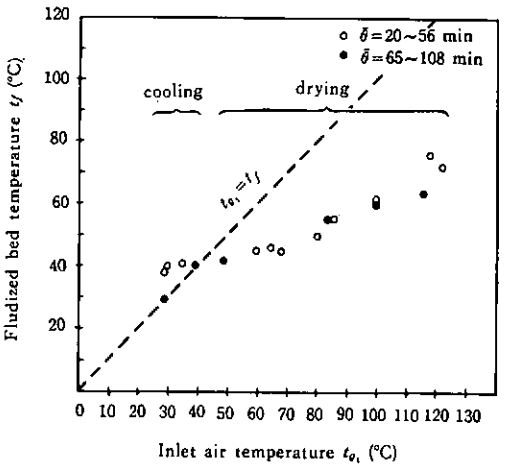

Fig. 4. Relation between inlet air temperature and bed temperature in fludized bed.

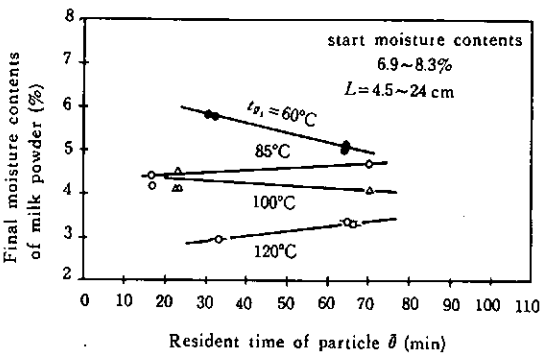

Fig. 5. Relation between mean resident time in fludized bed and final moisture contents of milk powder.

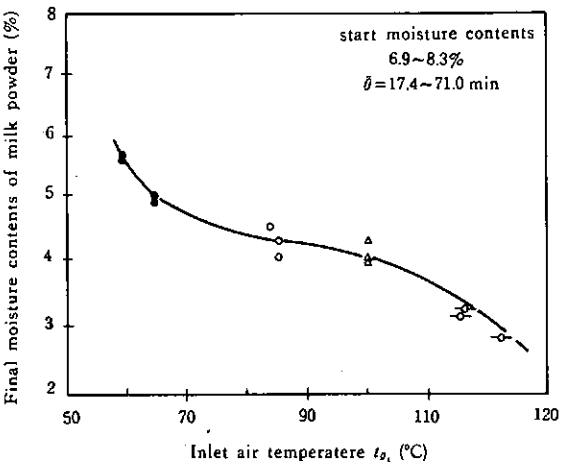

Fig. 6. Relation between inlet air temperature in fludized bed and final moisture contents of milk powder.

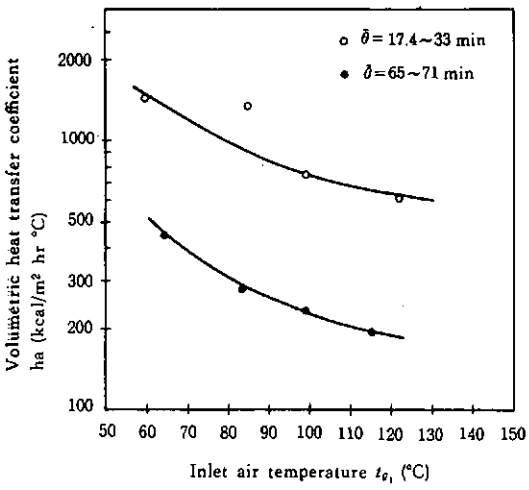

Fig. 7. Relation between inlet air temperature and the volumetric heat transfer coefficient.

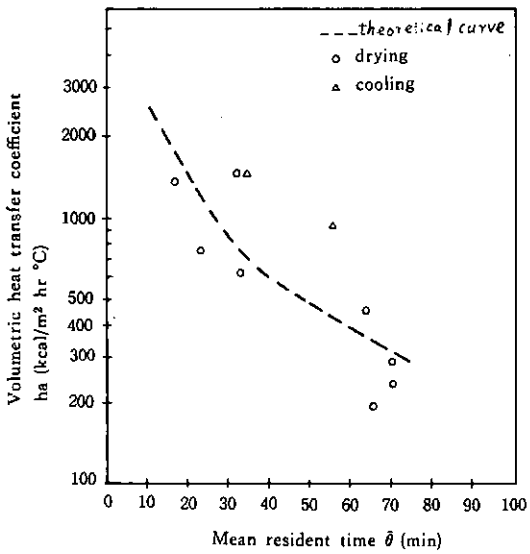

Fig. 8. Relation between mean resident time and volumetric heat transfer coefficient.

Cooling properties of skim milk powder

Batch cooling process

With milk powder in a spray dryer, the solid temperature increases gradually as the vaporization of the moisture content proceeds. (the region of falling rate of drying.) The temperature of air and milk powder and the relations to the moisture content in this case were calculated from Eqs.(4) and (5). Four examples of them were shown in Fig. 9, from which the milk powder temperature turned out to be nearly equal to the exhaust air temperature at around 4% of moisture content of the product.

To examine the cooling properties of a batch fluidized bed, the milk powder discharged from the spray dryer was fed into the fluidized bed, through which heated air of 80°C flowed, and the bed temperature was maintained constant until a definite amount of milk powder was accumulated in the fluidized bed. After that, by a step change from high temperature to the room temperature for the inlet air, the cooling responses were measured and plotted against the lapse of time, see Fig. 10. The temperature drop was remarkable at the starting 40 minutes but the rate of drop was likely to decline afterwards. Fig. 11 indicates the packed mass of skim milk powder per the integrated mass of air, i.e., the mixing ratio of particles to air in relation to the total heat leaving the fluidized bed. It was found that heat treated in a fluidized bed increased linearly with increasing load at the mixing ratio over 0.1. This suggests that a fluidized bed has a comparatively wide range of thermal processing capacity with a little amount of air required. This should be a remarkable feature of fluidization process.

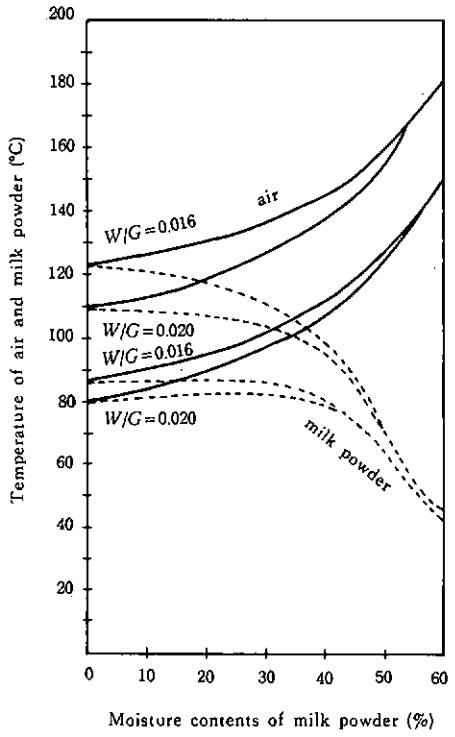

Fig. 9. Relation between air temp., milk powder temp., and moisture contents of milk powder.

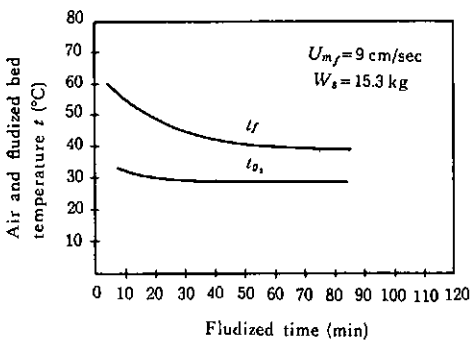

Fig. 10. Cooling curve of milk powder.

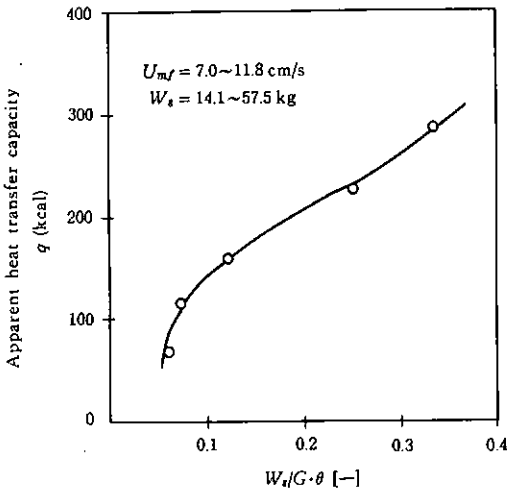

Fig. 11. Relation between cooling capacity of skim milk powder and mixing ratio ($W_s/G\cdot\theta$)

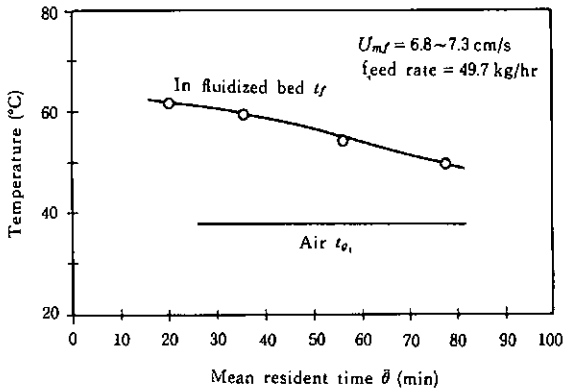

Fig. 12. Relation between mean resident time and temperature of fludized bed.

Continuous cooling process

Skim milk powder discharged from spray dryer was fed into fluidized bed, to which air was supplied at the room temperature; then the milk powder was fluidized and cooled for a period of definite time and was discharged from another exit.
A relation between the mean residence time of the particles and the degree of cooling was shown in Fig. 12. Temperature inside the fluidized bed was still higher at residence time of 20 minutes, but was approaching that of the cooling air at residence time of 80 minutes. In this case, the measured temperature of the discharged milk powder was about 3°C higher than that of the fluidized bed, t_f. This result shows that 60~80 minutes should be needed as the mean residence time of particles in bed, in order for the skim milk powder of 80°C to be cooled down to the level of room temperature.
The overall heat transfer coefficient calculated by applying Eq.(13) to those results mentioned above was represented as a function of $\bar{\theta}$ in Fig. 13. In this figure, two models were depicted at the same time; i.e., one is calculated from Eqs.(7) and (8), and the other from Eq.(12). Eq.(13) is surely simple and easy to handle, but some attentions should be paid since ha based on Eq.(12) can be evaluated a little bit smaller. Stirring was not always needed in case of cooling process. Additionally, drying did not proceed appreciably at the present experimental run, as evidenced by the moisture contents only varied from 4.7% at the inlet to 4.46~4.67% at the exit.

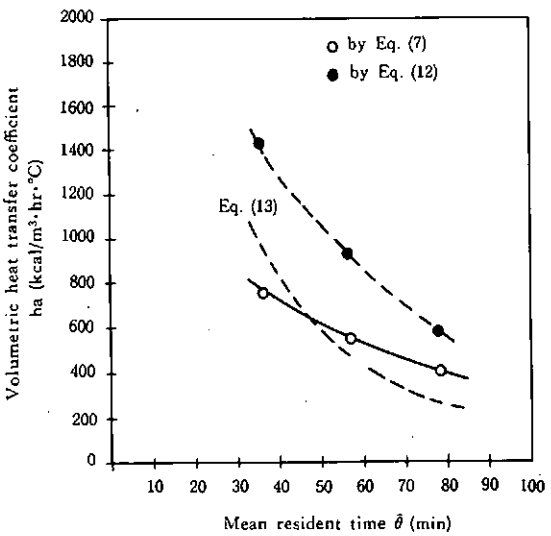

Fig. 13. Relation between mean resident time and volumetric heat transfer coefficient in the cooling process.

CONCLUDING REMARKS

Using a fluidized bed in direct connection with a laboratory scale spray dryer, experiments of the secondary drying and the continuous cooling of skim-milk powder were carried out. The results were summarized as follows:

Properties of the fluidized bed

Good fluidization of skim milk powder was available at the air velocity of 9 cm/sec, where the bed expansion ratio was found to be 1.7~1.8.

Secondary drying properties

Moisture content of the milk powder from the fluidized bed was primarily controlled by the temperature of inlet air, and not so much by the residence time of solids. In case of the inlet

moisture content of 7~8%, use of 85~100°C of the inlet air should be recommended, in order to maintain the exit moisture content 4%. Over 100°C, somewhat colored milk powder was produced. Overall heat transfer coefficient increased with lowering the inlet air temperature, and particularly with increasing residence time.

Continuous cooling

To have the milk powder coming from spray dryer cooled immediately down to the room temperature, the mean residence time of 60~80 minutes for solids would be necessary. Experimental data of ha were 700~1600 W/m^3K in accordance with Eq.(7), whereas 460~780 W/m^3K with Eq.(12), both of which were greater than the theoretical values.

Others

The present fluidized bed turned out satisfactory for its application to skim milk powder production. However, as to the whole milk powder and whey milk powder which are of poor fluidization properties, vibrating or various mechanisms other than the perforated plate construction should be devised in the future.

REFERENCES

1. Wada, T., and H. Hayashi., Report of Research Institute, Snow Brand Milk Products Co., Ltd. Tokyo, Japan No.116 1973
2. Toei, R., Transaction of Japanese Chemical Engineering Vol. 23, No. 10 1959
3. Toei, R., Proceedings of Chemical Engineering. Conference in Tokuyama district 1970
4. Kamei, S., Transaction of Japanese Chemical Engineering Vol. 18, No. 3 1954
5. Shirai, S., Fluidized Bed,Kagakugijitsushya 1965
6. Inoue, S., Chemical Engineering in Japanese, April, 1968

STEAM DRYING OF PULP

Claes Svensson

MoDo-Chemetics AB, S-891 01 ÖRNSKÖLDSVIK, Sweden

ABSTRACT

Market pulp is dried by the use of oil, gas and/or steam in flash or web dryers. The energy consumption in pulp dryers corresponds to 1.5-3 tonnes of steam per ton of evaporated water, and usually no or very little energy can be economically recovered. The oil prices today imply energy costs of $ 15-20 per ton of pulp. A new drying technique has been developed at Chalmers University of Technology, Gothenburg (Professor Bengt Hedström) in cooperation with MoDo-Chemetics AB, Örnsköldsvik, Sweden. The principle is to work with indirectly heated pressurized superheated steam as drying medium. The system is called the Steam Dryer system or the Backpressure Drying system and fits very well in the sulphate pulp mill steam balance. The dryer works under pressure, meaning that pulp is fed against a pressure of 0.2-0.5 MPa (backpressure). The heating steam, for indirect use, has a pressure of 0.7-1.5 MPa (extraction steam pressure). The steam generated from drying the pulp is bled from the dryer as process steam (0.2-0.5 MPa) and can be used elsewhere in the pulping process. As a consequence the net steam consumption is reduced to about 0.3 tonnes per ton of evaporated water thus saving about $ 10 per ton of pulp. There are several other advantages. High heat transfer coefficient which is implying small heating surfaces and low investment cost. Low specific power consumption because of small circulated gas volumes. No diffusion controlled drying rates (no air) which makes it possible to dry with short retention time giving no or minor quality effects on the fibres.

NOMENCLATURE

A = area m^2

a = specific heat transfer area, m^2/kg

c_p = specific heat capacity, kWs/kg K

D = diffusivity, m^2s

d = diameter, m

dT = small temperature change, K

dx = small length, m

dX = small change in moisture ratio,

M = molecular weight

m = solid mass fraction

P = pressure, bar

P_G = partial pressure of steam in bulk air

P_c = partial pressure of steam in inside porous material

R = universal gas constant, kJ/kmol K

r = heat of vaporization, kWs/kg

s = material thickness, m

T = temperature, K

α = coeff. of heat transfer, kW/m^2K

β = coeff. of mass transfer, m/s

δ = boundary layer thickness, m

λ = thermal conductivity, kW/mk

μ = diffusion resistance, -

μ' = "drying resistance" for drying in steam,

π = pi, to calculate radius

ρ = density, kg/m^3

Subscripts

c = centrum

cell = cellulose fibres

d = refers to diameter

G = transport gas, steam

H = heating steam

In = inert gases

M = medium

S = saturation

INTRODUCTION

In pulp and paper industry the use of steam for process heating and power generation is very common. Most of the heat for steam generation comes from burning cooking liquor, bark and wood-waste. However, the use of oil is necessary in boilers to balance the heat demands and in some special applications; for instance in the lime kiln and for flash drying market pulp. Drying consumes about 20-30% (1) of the total heat consumption in the production of market pulp and there exists a natural incentive to develop new drying techniques, which would be less energy consuming and which would not use oilfired air heaters. Figure 1 shows the principle of a modern oil fired flash dryer for pulp. Some steam is used in the second stage and air is recirculated to the air heater. Energy consumption is usually between 3.0-3.5 GJ per ton of pulp (ptp).

Figure 1 - Oil-fired Flash Dryer for Pulp

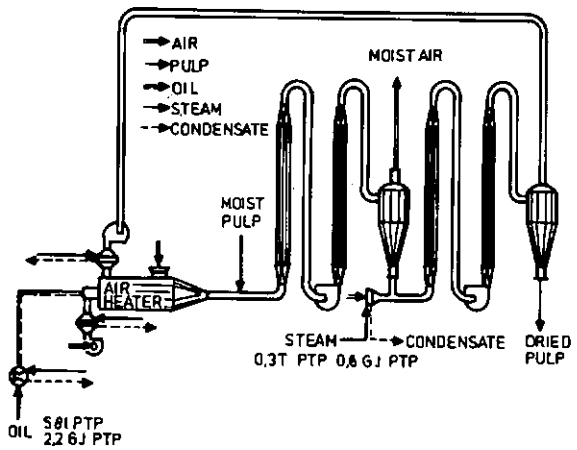

The use of less air reduces exhaust losses and this is possible if the air is heated indirectly during the drying process. Preferably, steam is used for heating and the problem then becomes how the heat exchanger shall be designed to permit cellulose fibres to pass through it without clogging. Nevertheless a drying system using indirectly steam heated surfaces for pulp-air suspensions has been patented. Energy consumption is reduced to about 2.6 GJ ptp by this system (2).

The next step, which we believe will become very important in the future for the pulp and paper industry, is to use steam as drying medium instead of air. The system which we call the backpressure system or the steam drying technique is shown in figure 2 (3).

Figure 2 - Backpressure System for Pulp Drying

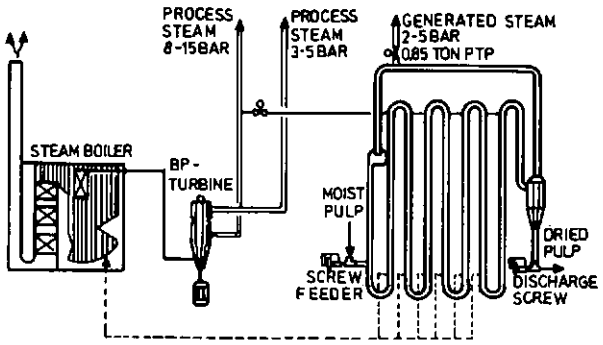

STEAM DRYING PRINCIPLE AND ECONOMY

Steam for indirect heating is extracted from a backpressure turbine at a pressure of 8-15 bar. This steam is condensed in the dryer heat exchangers and the condensate is pumped back to the boiler. In the dryer, which is a pressurized system (2-5 bar) superheated steam is circulated by fans. This steam is used both as transport and drying medium for the moist material. During its way through the dryer, the suspension passes through the heat exchangers where heat for drying is transferred. After separation and discharge of the dried material, this steam is recirculated. The moisture removed during drying forms steam and, to maintain the pressure constant, this excess is bled off as process steam from the dryer. In most cases this steam can replace fresh steam without need for cleaning, but for general purposes, steam from feedwater can be regenerated at somewhat lower pressure.

The first Steam Dryer was erected at the Rockhammar Mill, Sweden and it has now been running successfully for about a year. The dryer, figure 3 is designed to produce various grades of dry mechanical pulp at a rate of 150 ton/24h.

The pulp is mechanically dewatered to a dry content of about 45% and thoroughly fluffed (desintegrated) before drying and the dried pulp is baled at about 85-90% dry content.

Although the drying principle and basic design is the same when drying different materials, some modifications have to be made in order to get an optimal design. This is especially the case with equipment for feeding and discharge of the material being dried.

Figure 3 - Rockhammar Dryer for Pulp

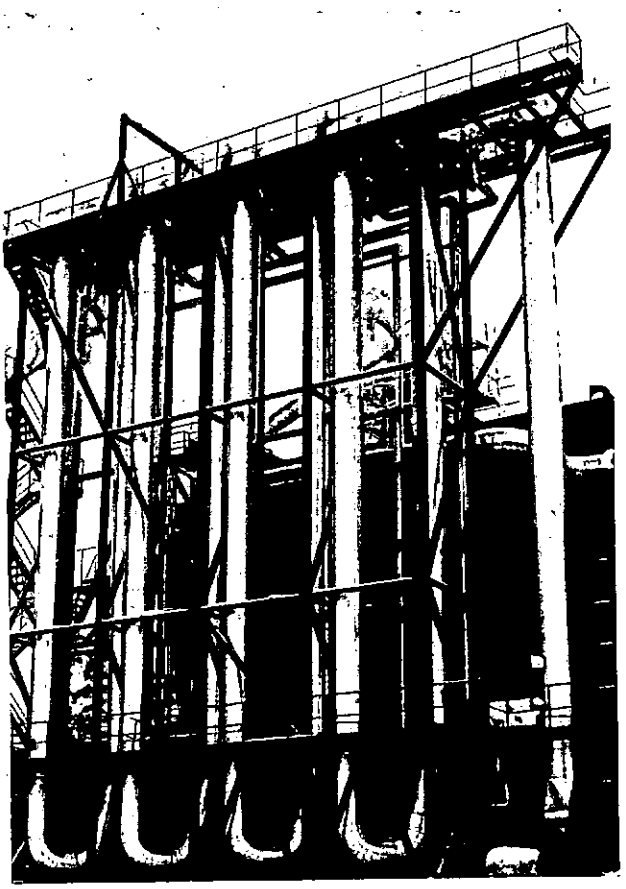

When drying pulp plug compression screws are used, but when drying bark and hog fuels, rotary valves are a competitive alternative.

Experiences and heat balance measurements from the first industrial dryer have shown a very low net energy consumption (0.4-0.5 GJ ptp), if the generated steam can be used as process steam. In Rockhammar, fresh steam is replaced in lumber drying, preheating of combustion air etc. Example of a heat balance is shown in table 1.

Table 1 - Heat Balance for a Backpressure Dryer

Figures are presented per bone-dry ton of pulp.

Heating steam, ton		1.28
Heating steam, pressure, bar		9.3
Generated excess steam, ton		1.0
Generated excess pressure, bar		3.2
Energy in		
Steam	GJ	2.6
El. power	GJ	0.3
Pulp (50°C)	GJ	0.3
Total		3.2

Table 1 - (Cont'd)

Energy out		
Heat losses by radiation,	GJ	0.2
Steam leakage,	GJ	0.05
Dried pulp (125°C)	GJ	0.2
Generated excess steam	GJ	2.75
Total	GJ	3.2

Compared to conventional flash dryers, the use of steam drying reduces the drying costs by approximately US$ 10 ptp, see table 2.

Table 2 - Energy Costs for a Conventional Flash Dryer and a Backpressure dryer

Energy costs per ton of air dry pulp

	Conventional Flash Dryer US$	Steam Dryer US$
Steam (11.8 $/ton)	3.50	14.10
Oil (188 $/m^3)	11.1	-
Electrical power (0.05 $/kWh)	4.25	2.80
Gross energy cost	18.85	16.90
Value of generated steam	-	9.40
Loss of back pressure power generation	-	1.80
Alt 1: Net energy cost (with turbine)	18.85	9.30
Alt 2: Net energy cost (without turbine)	18.85	7.50

THEORY OF DRYING

Basic engineering and testing is made in cooperation with the Department of Chemical Engineering Design, Chalmers University of Technology, Gothenburg. In a pilot plant, heat exchangers and transport pipes are tested in all relevant aspects, drying rates are investigated for different materials and models for design are developed.

The drying rates in superheated steam depend mainly on heat transport mechanisms even if the moist material is porous. Due to the high temperatures, equilibrium moisture content will be low and often of less importance, see figure 4. When calculating drying times in superatmospheric steam drying. Compared to drying of pulp in air, average drying rates in superheated steam under pressure are 2-3 times higher. Assuming that the mean temperature difference is 10 times higher using air than steam (150 versus 15) this indicates the total coefficient of heat- (and mass-)-transfer

in steam is 20-30 times higher. Diffusion rates are ratedeterming when drying capillary, porous materials in air atmosphere of inert gases (air).

Figure 4 - Equilibrium Moisture Content for Wood Pulp

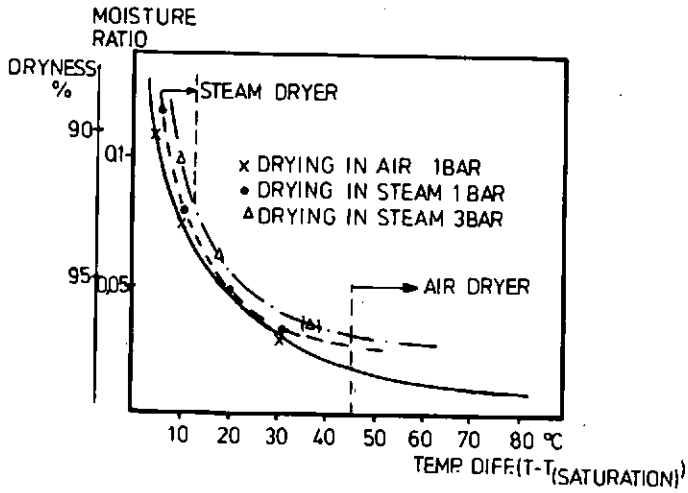

Referring to classical drying theory (4) (5) diffusion resistance controls the final stage of drying, see equation (1): (see figure 5).

$$(T_G - T_c) = \frac{M \cdot r_c}{RT_M} \cdot \frac{\beta}{\alpha} \cdot \frac{1 + \frac{\alpha \cdot s}{\lambda}}{1 + \frac{\mu s \beta}{D} \cdot \frac{P_{In}}{P}} \cdot (P_c - P_G) \qquad (1)$$

Figure 5 - Heat and Mass Transfer when Drying Porous Air and for Superheated Steam

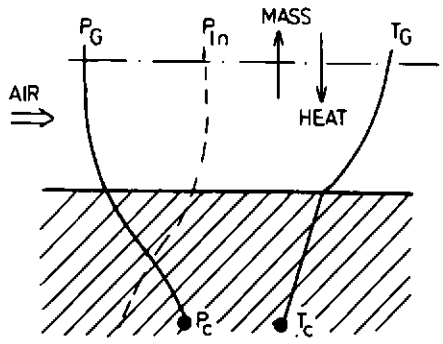

The temperature and partial pressure gradients are calculated by knowing heat- and mass transfer coefficients, β/α and physical data of the drying goods. Essential for this theory of counter-current flow of mass and heat is the Stefan flow indicated by the term P_{In}/P. The local partial pressure of inert gases plus pressure of water vapor must equal the total pressure in the system at every point.

Cellulose fibre surfaces are not wetted over approx. 55-60% dry content. Diffusion resistance ($5<\mu<10$) and heat conductivity of the material starts to determine the drying rate. Temperature of the fibres will start to increase above the wet bulb temperature of the drying air.

However, when drying in pure superheated steam there is no diffusion resistance because diffusion cannot exist. Heat and mass flows are counter-current to each other, as in figure 6, and resistances result only from a poor heat conductivity of the dried material near the surface and from the requirement of a pressure drop for moving the evaporated water from the inner regions of the material out to the surface via capillaries and pores.

Figure 6 - Heat and Mass Transfer when Drying with Superheated Steam

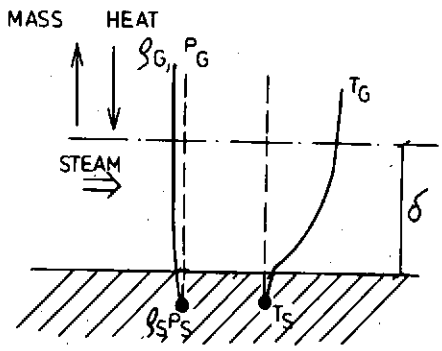

Assuming Ficks' law, equation (2), and steam as an ideal gas, we can calculate an analogous equation to that when drying in air.

$$-D \cdot \frac{d}{dy} \approx \frac{D}{\delta}(\rho_S - \rho_G) = \beta(\rho_S - \rho_G) \qquad (2)$$

$$\frac{\alpha}{r_S}(T_G - T_S) = \frac{\beta}{\mu'}(\rho_S - \rho_G) \qquad (3)$$

$$\rho = {}^{P \cdot M}/_{RT};\ P_S \approx P_G = P \text{ and } T_S \approx T_G = T_M$$

$$\frac{\alpha}{r_S}(T_G - T_S) = \frac{\beta}{\mu'} \frac{P \cdot M}{RT_M^2} \cdot (T_G - T_S) \qquad (4)$$

The simple equation includes μ' which expresses the total resistance for drying at higher dryness compared to drying of wet material. From experiments we have found μ' to be between 1.1 to 1.5 for thoroughly fluffed pulps between 80 and 90% dryness.

We assume that heat conductivity of the cellulose material can mostly explain the decrease in rate of evaporation.

When calculating α/β for air drying, the Lewis-coefficient, or similar, is calculated. This is normally found to be about 1 kWs/m^3K at normal temperatures and pressured, see equation (5). From (4) we can calculate α/β for steam drying

assuming $\mu' = 1$, equation (6). In table 3 a rough comparison is made between drying in steam at different pressures and drying in air at 1 bar.

$$\frac{\alpha}{\beta} \approx \rho \cdot c_p \quad \text{(for turbulent boundary layer)} \qquad (5)$$

$$\frac{\alpha}{\beta} = \rho_M \cdot \frac{r_s}{T_M} \qquad (6)$$

Table 3 - Heat and Mass Transfer Coeff. for Air and Superheated Steam

medium	pressure	temp.	relative values α/β	α	β
			$\frac{kWs}{m^3K}$	$\frac{kW}{m^2K}$	m^2/s
	(bar)	(°C)			
Air	1	0-100	~1	1.3	1.3
Steam	0.5	80	2.0	0.6	0.30
	1	100	3.6	1	0.28
	2	120	6.3	1.7	0.27
	5	150	13.0	3.4	0.26

Drying with air at 1 bar gives higher evaporation rates than if steam is used, assuming the same temperature difference. However, if diffusion resistance is a significant rate controlling factor then steam drying can be favourable. This perhaps explain some results from experiments found in the literature (6) and (7).

DRYING SIMULATION AND DESIGN

The complex theory of drying is not applicable in detail when designing an industrial backpressure dryer for pulp, bark or peat. Pilot tests instead give information about drying rates which can be used for scaling up. Much of the time for design is spent calculating flow rates, heat exchanger construction to prevent clogging, cyclone and fan design, discussions about material of construction etc. One big problem is often to choose the right equipment for feeding and discharge.

The design parameters and their limits are discussed below. The discussion refers to pulp drying.

Inlet moisture content: This should be as low as possible since mechanical dewatering often is cheaper than drying. Due to clogging risks, more than 30-35% water content cannot be accepted.

Outlet moisture content: Between 85 to 90% dry content is normal. Higher dryness can damage the quality, but lower dryness can be economical if transport distances are short.

Drying capacity: Maximum is about 25 ton evaporated per hour.

Steam pressures: Heating and drying steam pressures are often determined by the process steam pressures, for example 10 and 3 bar.

Heat exchanger surface: This is calculated from results in the pilot plant. Not only the size of the heat exchangers is important but also the optimal place for them in the system. This is discussed below. The hydraulic diameter is chosen to prevent clogging while keeping a short drying time.

Transport velocity: From given pressures of steam, the most economical velocity can be calculated to transport the pulp in the dryer. Usually this is between 20 and 40 m/s depending on heat exchanger cost and cost for power consumption in transport fans. Lower than about 20 m/s cannot be used because of clogging risks.

Dry pulp to steam ratio: This should be as high as possible to save transport energy but not more than ~0.4 kg/kg to prevent clogging. Depending on the degree of fluffing (pulp quality) and drying steam pressure there is a limit where heat exchanger area determines the length of the dryer.

Height of drying stages: From a practical point of view, the maximum height is usually between 20 and 30 m. However, for bark and peat the maximum height can be 40 to 60 m if the dryer is erected outside a boiler building.

When designing a dryer in detail, a computer program is used and some equations from this are shown below. The equations can be explained by looking at figure 7.

Figure 7 - Incremental Section of Dryer, dx (m) for Data Calculations.

7.a. - Heat Exchanger

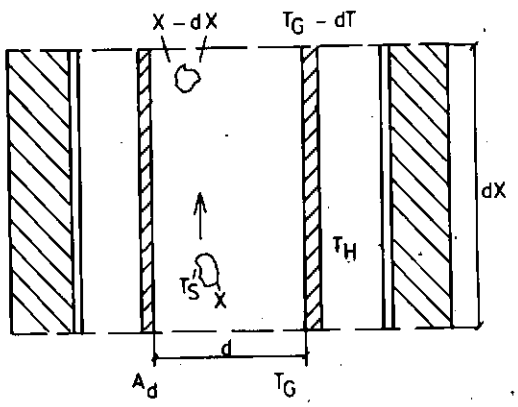

7.b. - Without Exchanger

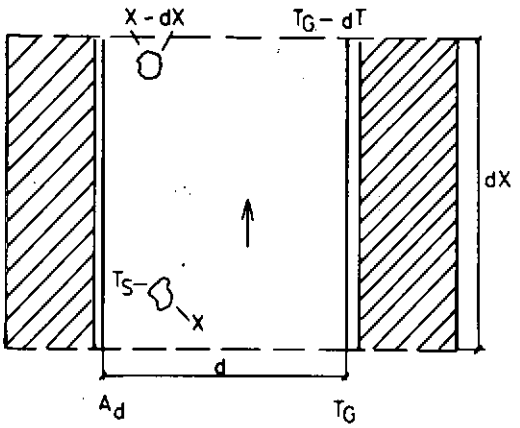

$$\frac{\alpha \cdot \pi \cdot d \cdot dx \cdot dT \cdot dt}{\ln \frac{T_H - T_G}{T_H - T_G - dT}} \qquad (7)$$

Heat from transport steam:

$$A_d \cdot dx \cdot c_p \cdot \varrho \cdot dT \qquad (8)$$

Heat to drying:

$$m(-dX)\ c_p(T_G + dT - T_S) + r) \qquad (9)$$

(7), (8) and (9) can be combined to (10)

$$dT = \frac{t \cdot \alpha \cdot \pi \cdot d \cdot dx \cdot (T_H - T_G) + 2 \cdot m \cdot dX \cdot (c_p(T_G - T_S) + r)}{t \cdot \alpha \cdot \pi \cdot d \cdot dx + 2A_d \cdot dx \cdot c_p \cdot \varrho - 2m \cdot dX \cdot c_p} \qquad (10)$$

The change in moisture ratio is calculated by the equation:

$$-dX = \frac{(\alpha \cdot a)\text{cell}}{r} (T_G - T_S) \cdot t \qquad (11)$$

To calculate the changes in a pipe without heating surfaces there is a more simple equation:

$$dT = \frac{m \cdot dX(c_p(T_G - T_S) + r)}{A_d \cdot dx \cdot \varrho \cdot c_p - m \cdot dX \cdot c_p} \qquad (12)$$

By putting all economical limit in the design program it is possible to calculate where to finish the heating surface. The relative cost between 1 meter of heat exchanger and 1 meter of empty pipe, including power consumption costs, usually gives a 15 to 25 m heat exchanger length. A typical example is shown in figure 8.

From pilot trials and industrial measurement, coefficients of heat transfer to cellulose fibres have been determined. In figure 9 results are shown as a function of dry content for various pulps. Since the heat transfer area of fibres cannot be properly determined, we have defined the product $(\alpha \cdot a)_{cell} = \frac{kW}{m^2 K} \cdot \frac{m^2}{kg\ dry\ cellulose}$

Figure 8 - Results from Simulating Drying of Pulp

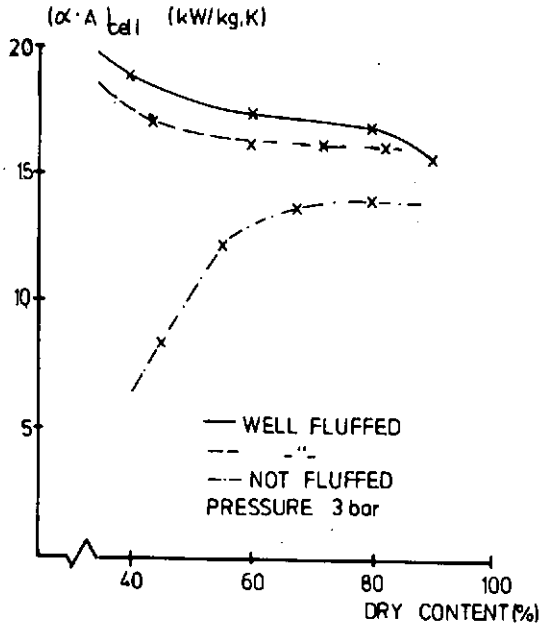

Figure 9 - Example of Heat Transfer Coefficient for Pulp

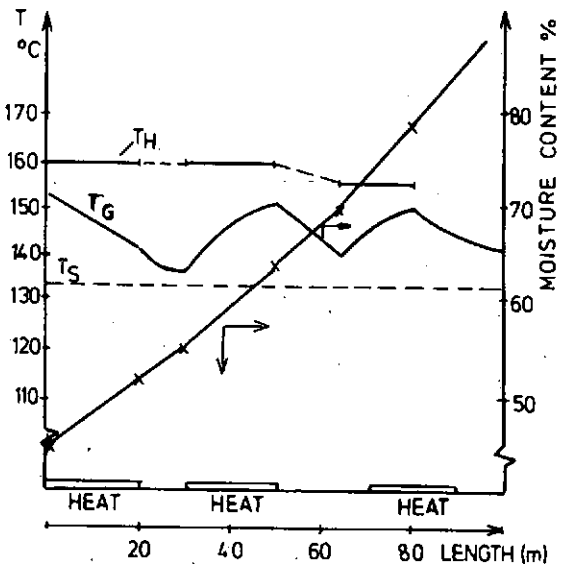

It is very important that the pulp is well fluffed to give as much surface as possible. If unfluffed pulp is fed in the heat transfer coefficient can be observed to increase during drying due to the mechanical treatment in the dryer.

REFERENCES

1. Wahlman, Markku; Pulp & Paper International, Nov 1974, p. 60
2. U.S.Pat. Apr. 30 1974, No 3,808,093, B.O.A. Hedström. "Method and apparatus for drying pulp including heat exchange and temperature equilizing zones".
3. U.S.Pat. Aug. 23 1977, No 4,043,049, B.O.A. Hedström. "Process and apparatus for flash drying fluffed cellulose pulp".
4. Kneule "Das Trocknen", Aarau: Sauerländer & Co (1975)
5. Krischer "Die Wissenschaftlichen Grundlagen der Trocknungs-technik, Springer-Verlag (1956)
6. Yoshida, T.; Hyodo, T; Food Engineering, Apr. 1966, p. 86.
7. Trommelen, A.M., Crosby, E.J. AICLE Journal, Sept. 1970, p. 858.

AIRFOIL DRYER: PRINCIPLES OF OPERATION AND APPLICATION

R. A. Bennett

Overly Inc., Neenah, Wisconsin

ABSTRACT

The basic concept upon which the Airfoil is designed and the careful application of the Bernoulli principle. Airflow pattern resulting from the orifice aspect ratio, nozzle surface and air temperature. Effect of the turbulent air condition as it passes along the nozzle and sheet surfaces. Heat transfer resulting from the high temperature differential and continual boundary layer breakdown due to scrubbing action of air. Changes in quality of coating as a result of controlled binder migration. Comparison of physical quality of sack kraft grades dried on cylinders. Cost comparison for air drying to conventional drying. Useful heat recovery from economizers applied to an integrated air drying system.

NOMENCLATURE

c = specific heat, BTU/LB

h = enthalpy of water, BTU/LB

·F = logarithmic mean degrees

H_t = coefficient of heat transfer, BTU/SQ FT/HR/·F

R_w = evaporation rate, LB H_2O/SQ FT/HR

T_{si} = sheet temperature into dryer, ·F

T_{so} = sheet temperature dryer exit, ·F

$\Delta T_s = T_{si} - T_{so}$, ·F

T_a = supply air temperature, ·F

$\Delta T_1 = T_a - T_{si}$, ·F

$\Delta T_2 = T_a - T_{so}$, ·F

ΔT_{lm} = logarithmic mean temperature

$= \Delta T_1 - \Delta T_2 / \ln (\Delta T_1 / \Delta T_2)$, ·F

Applied equations for calculations:

Water in basestock [lb/(hr)/(ft)] = [(coater speed)(basestock a.d. wt)(% moisture in basestock)(60)]/[(3000)(100)] (1)

Water in coating applied [lb/(hr)/(ft)] = [(coater speed)(o.d. coating wt)(60)(100)/(3300)(% coating solids)] - [(coater speed)(o.d. coating wt)(60)/(3300)] (2)

Water in sheet exiting dryer [lb/(hr)/(ft)] = [(coater speed)(coated sheet o.d. basis wt)(% moisture out of dryer)(60)]/[(100 - % moisture out of dryer)(3300)] (3)

Water removed by dryer [lb/(hr)/(ft)] = Eq. 1 + Eq. 2 - Eq. 3 (4)

Water removal rate [lb/(hr)/(ft^2)] = (water removed by dryer)/(effective drying length) (5)

Sensible heat transferred to coating [Btu/(hr)/(ft)] = (0.25) [o.d. coating wt applied/(hr)/(ft)](ΔT_s) (6)

Sensible heat transferred to sheet [BTU/(hr)/(ft)] = (0.35) [o.d. basestock wt/(hr)/(ft)](ΔT_s) (7)

Sensible heat transferred to water in sheet [Btu/(hr)/(ft)] = (1.0)(water in basestock) (ΔT_s) (8)

Sensible heat transferred to water in coating [Btu/(hr)/(ft)] = (1.0)(water in coating applied)(ΔT_s) (9)

Latent heat transferred [Btu/(hr)/(ft)] = (water removed by dryer)(h) (10)

Total heat load transferred [Btu/(hr)/(ft)] = Eq. 6 + Eq. 7 + Eq. 8 + Eq. 9 + Eq. 10 (11)

Overall heat-transfer coefficient [Btu/(hr)/(ft^2)(F·)] = (total heat load transferred)/(heat transfer area)(ΔT_{lm}) (12)

Note: All calculations based upon one (1) foot width and effective length in feet. Evaporation rates R_w are based upon projected dryer area.

INTRODUCTION

Although the basic elements of drying have remained a problem of fundamental physics, the techniques have been molded into many shapes and arrangements. Other speakers will describe the designs and attributes of the method of drying in which they exhibit their own expertise. Many drying methods overlap the same process areas creating some degree of confusion in the user's thinking and a more serious conflict among the designers and builders of drying systems As a result, a clear understanding of strengths and weaknesses of any given system as applied to a particular drying requirement may not be possible due to reluctance to risk change in a capital intensive industry, unwillingness to change from an "acceptable" method or possibly the inability of management to fully explain and instruct the operators in the handling and advantages of an unfamiliar system. But these objections are the province of marketing and sales. Our interest is in evaluating a specific drying system known as the Airfoil dryer. This air floating dryer design will be described and analyzed in concept, construction, application, performance and efficiency.

Conduction drying had been considerd for many years as the means of evaporating water or solvents from various matrices. Because of the acceptance of steam cylinders as the drying method on paper machines, the natural step to take was to use the same means in the field of coating. Events quickly proved the error of this expediency. Flaws in the coating due to non-uniform drying were evident in casual observation and became the bane of the printer's effort. As a result, more gentle drying with warm air was conceived in the form of long tunnels with slat conveyors. The coat quality was of high caliber but production speeds painfully slow and costs high. High velocity impingement air dryers were used in combination with cylinders. Here again, serious drying-related quality problems forced the coater operator to limit the rate of drying. Designs with impinging air directed at a felt-supported sheet followed in the normal course of system development. The next step in the progression was the two-side impingement air dryer. Direct involvement with the manufacture of high velocity impingement drying of both one- and two-side designs led to the Airfoil.

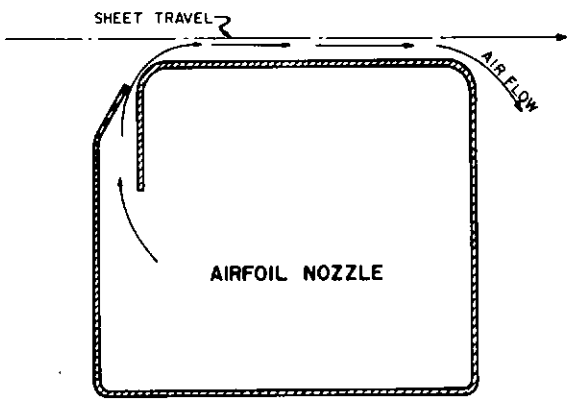

Figure 1

Figure 1 shows a simplified cross-sectional view of the Airfoil nozzle. Air enters the body of the nozzle which acts as a plenum distributing the air in its approach to the orifice throat. As the air emerges from the orifice at the desired velocity, the flow clings to the nozzle wall, turns on the curved portion and travels along the top surface. The moving air draws the sheet due to the negative pressure created by the fluid flow as set forth in the Bernoulli theorem. A sandwich of the sheet, air and nozzle surface is formed. The turbulent air scrubs the boundary layer of the sheet and coating surface resulting in a high drying rate. The phenomonen of air scrubbing as opposed to impinging has a marked effect on binder migration. This will be discussed later. When experiments revealed that the nozzle did in fact support the sheet, the next step was to arrange the nozzles in the most economic configuration.

Figure 2 is a schematic cross-sectional elevation of a short one-side dryer. Note close spacing of the nozzles. The air flowing across the nozzle area may pass in the direction of or opposite to the substrate travel. This feature takes advantage of the energy furnished by the coater or machine drive. Because there is no lateral airflow, the unsupported sheet passes along with dryer without need for guiding. The need for

one-side dryers is based upon available space in rebuilds and special binder holdout requirements on heavier coated grades including cover stock. Limitation of the one-side unit is lower drying rates and inability to control temperature of the substrate. Advantages of the one-sider are use in limited space, position on coated or uncoated side, and board grades. The one-side Airfoil was among the first units to be produced, meanwhile, the two-side dryer was undergoing intensive trials.

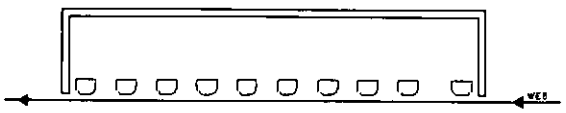

Figure 2

Figure 3 represents a cross-sectional elevation view of a two-side dryer. Note the staggered spacing, designed to allow the sheet to pass from the nozzle on one side to the other without conflict of forces. The two-side dryer is the most widely used design incorporating many features unavailable to other drying methods. One of the unique capabilities of the Airfoil is that the velocity on one side can be greater or less than the opposite. This feature is effective in controlling drying rate of coated and uncoated sides. In special cases, separate temperature zones are used. Thus, ink holdout, binder penetration into the substrate, binder migration, ink receptivity, mottle, sheet curl (correctible with drying rate differential) and stress strain characteristics are properties this dryer will affect favorably. But before covering these areas in detail, an overall view of a typical system will be helpful.

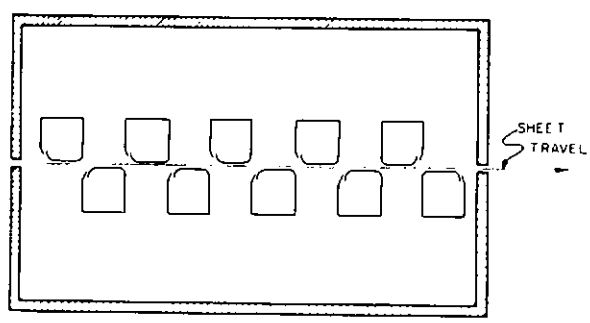

FIG.3 TWO SIDE AIRFOIL FLOATER DRYER

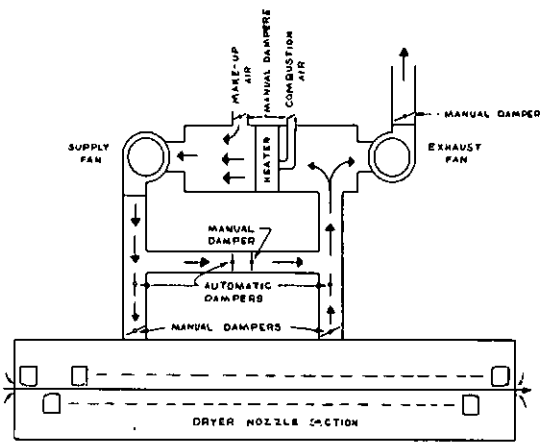

Figure 4

For those of you unfamiliar with the Airfoil dryer, Figure 4 represents a typical two-side dryer assembly. The burner chamber, designed for direct-fired gas, propane or No. 2 fuel oil or indirect steam heated operation, is mounted on a platform upon which the supply and exhaust fans and drives are mounted. The assembly is complete with ductwork, control dampers, an automatic by-pass system and controls. Supply air velocity is controlled with the supply damper at each hood. Figure 5

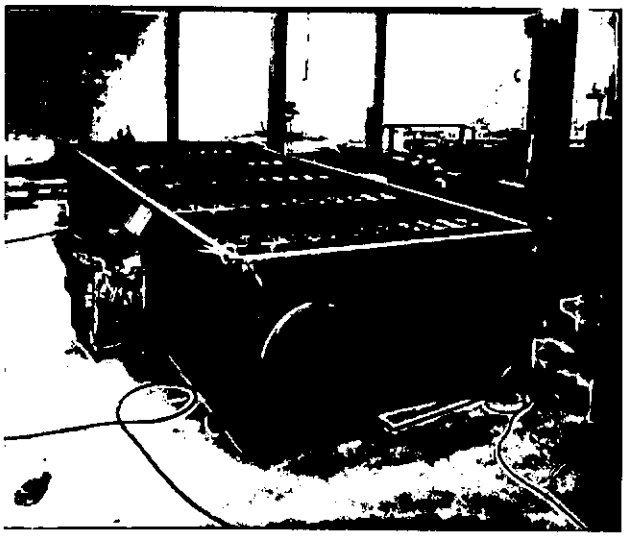

Figure 5

is a photograph of a hood of a two-side dryer under construction. The supply air enters the hood through the cross-header and is fed into the supply bulkheads. The nozzles are mounted on top of the bulkheads. Figure 6 shows the completed assembly of a one-side dryer with the nozzles in position. The basic hood design is similar but nozzle configuration and spacing differ. Another design variation is in nozzle width. Two standard width nozzles are used depending upon available supply air temperature and physical space. Since most of the Airfoil installations have been for drying various coatings, most of the data which has been compiled is in this field.

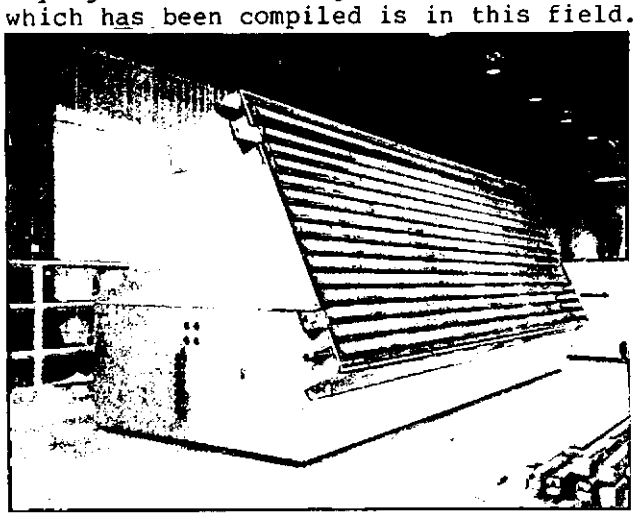

Figure 6

The two factors directly affecting dryer operation are air temperature and velocity. A family of curves can be developed using nozzle air velocity as the ordinates and evaporation rates as the abscissa. Figure 7 shows three curves. The curve to the left is for a one-side dryer and the other two are for a two-side unit. The displacement of the center curve shows the increase in in heat transfer of a two-side unit compared to a one-sider operating at the same temperature. The displacement to the left of the third curve demonstrates the increase in energy transfer due to temperature increase from 350°F. supply air to 500°F. As indicated on the curve, air temperature is in degrees Fahrenheit, air velocity is in feet per minute and evaporation rate is in pounds of water per square foot of dryer using its effective area. The effective length of a dryer is determined by the number of nozzles per side. A theoretical effective length is assigned to each nozzle depending upon dryer condiguration. A breakdown of these curves to a useful form is possible if a heat transfer factor can be developed. In order to do this, a curve was plotted based upon a series of tests taken at various supply air velocities and at a constant temperture. An H_t factor versus air velocity at a temperature of 470°F. is shown in Figure 8. Since H_t equals BTU/hr./ft.^{2} /°F., the total heat transfer per hour per square foot is equal to $H_t \times \Delta T_{lm}$. The log mean temperature difference is based upon the difference between supply air temperature and entering and leaving sheet temperature. The difference between

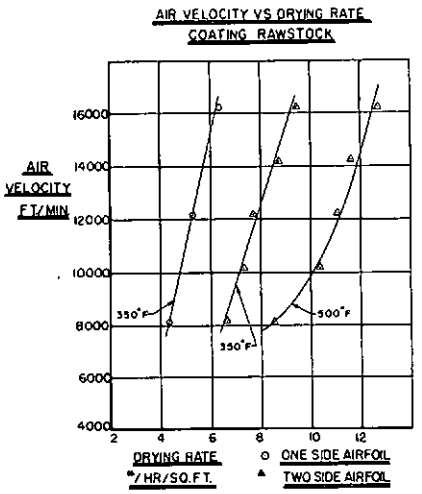

Figure 7

these quantities is divided by the natural log of the entering temperature difference divided by the leaving. The curve of total heat transfer/sq.ft./hr. versus air velocity at 470°F. is shown in Figure 9.

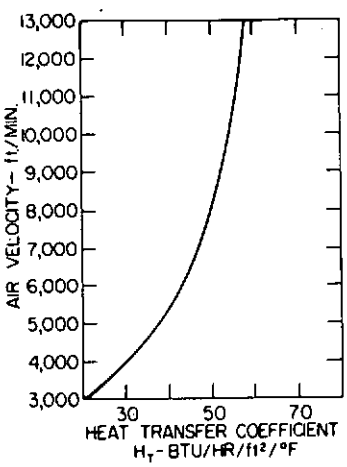

Figure 8

A typical single point calculation based upon trials on a merchant grade run by Mr. Ronald E. Johns is shown in Table I. This series of calculations has made it possible to determine a heat transfer coefficient for the selected grade operating at low and medium velocity range. The equipment used for these trials was two and one-half (2½) inch nozzles on six (6) inch centers. A significantly higher drying

rate was attained compared to an impingement air dryer without evidence of binder migration on grades ranging from 50 to 80 lb/ream C-2-S (25" x 38" - 500) with coatings of all synthetic, starch/PVAc and protein/styrene-butadiene latex binders. Evaporation rates ranging from 8.8 to 9.8 lbs./sq.ft./hr. are actually beyond the levels for which we design and recommend. It should also be noted that the exit sheet moisture is 8.2% (91.8% B.D.). This fact points to a significant feature of air drying.

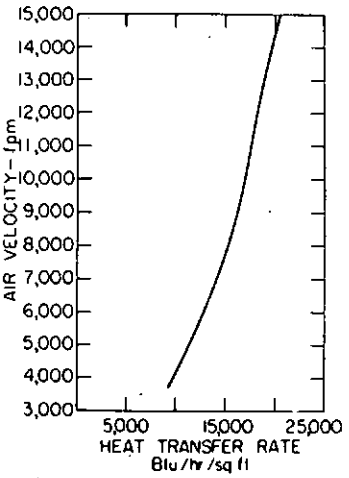

Figure 9

The traditional drying cycle of high temperature while the sheet is in contact with the cylinder and the immediate drop as the sheet travels across the draw is non-existent in the Airfoil. Figure 10 represents a moisture/temperature curve. In the early section of the drying cycle, the heat transferred is absorbed as sensible and latent heat. In the center zone extending to 92% B.D., almost the entire energy transferred is absorbed as latent heat. This large temperature difference between air at 600°F. and the sheet at 165°F. produces a high evaporative driving force. And the final phase is a return to a combination of sensible and latent heat. At 95 to 96% B.D., exit temperatures range from 200 to 210°F. To the designer, sheet moisture conditions become a vitally important consideration when determining the dryer length needed for a coater line, size press or primary drying application. The moisture/temperature curve could be readily interpreted into an evaporation rate/moisutre curve with a high drying rate extending to the 92% B.D. level and then a drop-off to compensate for the increase in sensible heat. Because of to the constant sheet temperature condition throughout the major portion of the drying cycle, air drying presents an interesting drying phenomenon.

Data	
Coater speed, ft/min	1,210
Temperature, °F	
Low-velocity supply	600
Low-velocity return	390
Medium-velocity supply	575
Medium-velocity return	380
Web into dryer	85
Web exiting dryer	150
Nozzle velocity,ft/min	
Low-velocity	7,200
Medium-velocity	10,000
Rawstock a.d. basis wt, lb/ream	54.0
Rawstock moisture, %	6.5
Coating wt (o.d.), lb/ream	8.2
Coating solids, %	60.6
Coated o.d. basis wt, lb/ream	58.6
Coated sheet moisture exiting dryer, %	8.2
Calculations	
Water, lb/(hr)/(ft)	
In basestock (1)	77.2
In coating applied (2)	117.3
In sheet exiting dryer (3)	115.2
Removed by dryer (4)	79.3
Water removal rate, lb/(hr)(ft^2)(5)	8.8
Sensible heat transferred, Btu/(hr)/(ft)	
To coating (6)	2,932
To sheet (7)	25,271
To water in sheet (8)	5,018
To water in coating (9)	7,624
Laten heat transferred, Btu/(hr)/(ft) (10)	79,950
Total heat load transferred, Btu/(hr)/(ft) (11)	120,795
Overall heat-transfer coefficient, Btu/(hr)/(ft^2)(F°) (12)	28.6

Table I: Sample Dryer Calculation for Airfoil Dryer

On lightweight coated grades being dried in a two-side Airfoil system, the heat penetrates the coating from the coated side and the substrate from the uncoated side. Water is vaporized beginning at the coated surface, and simultaneously, the heat penetrating the rawstock begins to vaporize the coatng at the interface of the coating and rawstock. The water vapor readily passes through the voids in

the substrate. A ratio of 60% from the coated side and 40% from the uncoated side are average evaporation conditions following the first coater station. The ratio changes to about 70/30 on the second side. The effect of two-side drying is to allow the maximum allowable drying to be done from the coated side compatible with quality requirements and added capacity from the back-side drying. Binder shrinkage can be controlled to avoid dusting and picking. Similar capability may be realized with respect to binder penetration into the rawstock. Sufficient penetration can be realized to achieve a good binder "hooking" action into the base sheet.

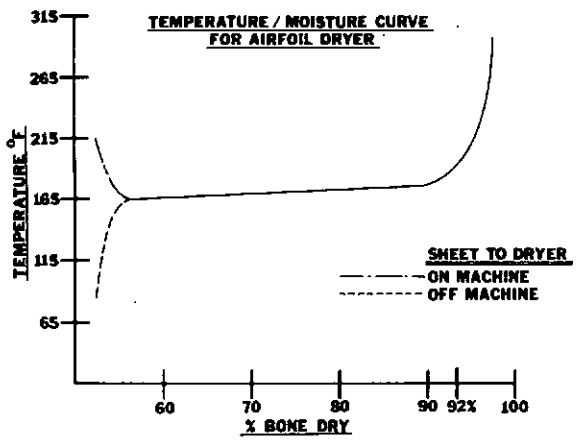

Figure 10

Having reached the design level of providing systems capable of speeds up to 4,000 fpm for off-machine coaters and up to 3,000 fpm on-machine and ranging up to 300 inch trim widths, the obvious area to challenge is drying on the paper machine. Primary drying is particularly attractive because this segment of the paper machine remains basically unchanged with little improvement over the years. The first step in this direction was to set up a trial run at Blandin Paper Company on the No. 3 machine.

Data compiled from trials run with a 40 lb. rawstock taken from the reel at 77.5% B.D., then air dried to 96.2% B.D., were used as the basis of comparison to the drying rates normally achieved on the machine. Machine data was developed by taking samples at 75% B.D. from the halfway point in the dryer section and at the reel at 96.2% B.D. Under these conditions, the TAPPI standard evaporation rate on the machine was 0.92 lb/sq.ft./hr. as compared to 9.4 lbs. for the two-side Airfoil dryer. Figure 11 represents the drying rate curve of the machine. One of the most notable features of the curves is the point at which the evaporation rate drops sharply in the dryer section. The sheet is at 75% B.D. at the midway point of the dryer section and the remaining

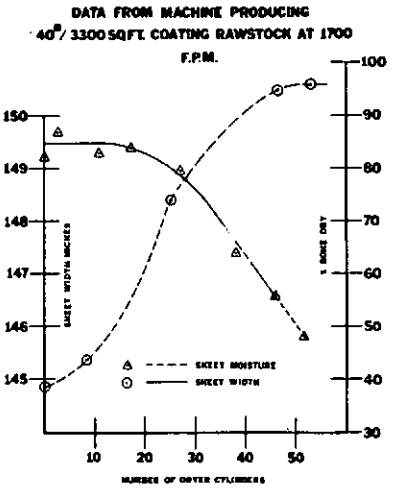

Figure 11

twenty-five (25) dryers are required to complete the evaporation at the typically poor rate for this grade. These trials clearly reveal differences in the drying characteristics of Airfoil versus cylinder operation. It should be noted that physical properties of the test samples before and after coating showed no significant differences due to air drying the rawstock. The results of these tests led to the exciting possibility of expanded use of the Airfoil dryer on the machine.

In order to justify such a change to the traditional configuration of the dryer section of a paper machine, an analysis of operating efficiency was necessary. Figure 11 represents the material and heat balance of a gas-heated system designed for partial drying of a 50#/3000 sq.ft. multiwall sack kraft and to increase the machine speed from 1700 to 2250 fpm. This

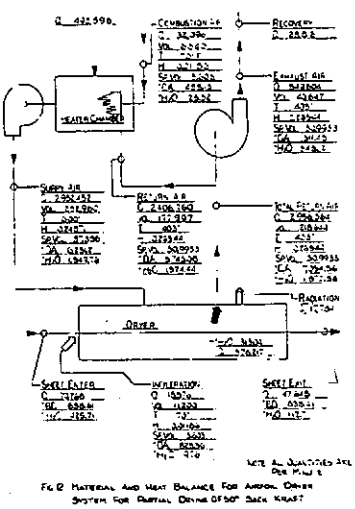

Figure 12

would be an ideal air drying application due to the fact that the sheet would enter the dryer, following the first two cylinder sections, at a moisture of 60.0% B.D. and leave the dryer at 85% B.D. The four (4) dryers, each 14'-0" long, would evaporate 1,024.5 lbs. water/ft. width/hr. (a total of 18,785 lbs.) at an R_W of 19.70 lbs. water/sq.ft./hr. With the sheet entering and leaving the dryer at approximately the adiabatic saturation point temperature, a negligible quantity of energy is transferred to sensible heat, resulting in an unusually efficient system of 71.5%. This high efficiency is due not only to the minimal sensible load but readily available water, which makes high evaporation rates possible. Under these most suitable conditions, the specific heat consumption is 1.577 BTU/lb. of water evaporated. Since the energy is generated in a direct-fired gas or oil system, the only losses are from radiation and infiltraton. Any comparison of alternate drying efficiencies must be considered on the basis of fuel heating value and consumption in order to have validity and not only on the basis of energy consumption at the point of drying. In addition to the fuel energy consumed, the system requires a total operating horsepower of 460 for the supply and exhaust fans, which equivalent to 19,512 BTU/minute.

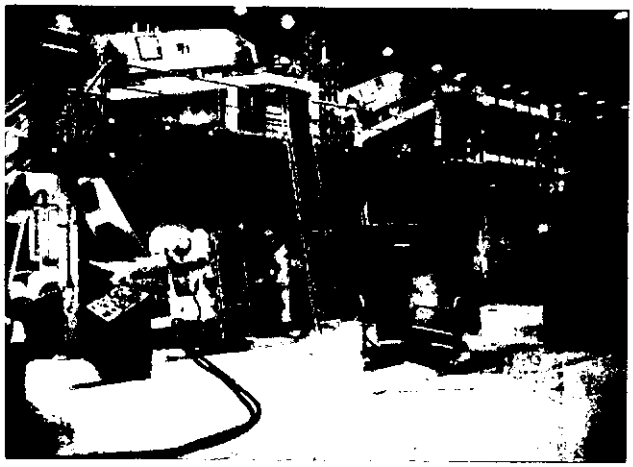

Figure 13

In summary, air drying has come into the paper and converting and graphics industries in a practical and readily acceptable manner with the invention of the Airfoil dryer shown in Figure 12. Coating drying, both on- and off-machine has commanded the most attention because of the great need for quality improvement. Air-supported drying has proven to be ideally suited because of the uniformity of heat transfer in cross-machine direction and its high gentle rate of evaporation due to the air-flow pattern. In the case of primary drying on the machine, the unrestrained drying results in high tear and T.E.A. in kraft multiwall, lack of curl retention of crepe in towelling or tape backing and, of course, the savings in building length and economy of operation. Since energy has had such a cost impact and will continue to escalate, reeling newsprint at higher moisture levels becomes most attractive and the Airfoil a most suitable drying method because of its inherent moisture profiling. Certainly, the future appears bright for air drying.

A MATHEMATICAL MODEL OF THE CONTACT DRYING PROCESS

Mauri Soininen

Åbo Akademi, Turku, Finland

ABSTRACT

Two simultaneous differential equations are derived from the heat balance and mass balance equations. Two subdivisions, pores and fibres, are treated separately in order to allow the application of this model to the through-drying process. The boundary conditions are derived using modifications of the "Lewis' relation" and the "enthalpy method".

In order to present the usefulness of the model, two computational results are given graphically, Figs. 4 and 5.

The nature and boundary conditions of the through-drying process are discussed briefly.

NOMENCLATURE

a = thermal diffusivity

A = surface

b = constants

D = diffusion coefficient

F = flow area

h = specific enthalpy

$\dot{H}$ = enthalpy flow

$\dot{m}$ = mass flow

p = pressure, partial pressure

r = heat of evaporation

R = gas constant

t = time

T = temperature

x = air humidity

y = coordinate

z = sheet moisture content

w = air velocity

α = heat transmission coefficient

δ = thickness

ε = porosity

κ = moisture diffusivity

λ = thermal conductivity

ρ = density, concentration

ϕ = heat flow

Subscripts

a = air

c = cylinder surface

d = dry fibres, drying air

D = diffusional

F = fibres

P = pores

s = apparent, screen

v = vapor

w = water

z = at moisture content z

δ = at $y = \delta$

0 = at $0^{\circ}C$, at $y = 0$

Superscripts

' = at saturation, at water surface

" = density of mass flow

INTRODUCTION

The scope of the work presented here and made by a rather small research group at the Plant Design Laboratory of Åbo Akademi (Turku, Finland) is to develop a model of the contact drying process, which can be applied especially for the study of the drying intensity in conventional paper machines and, also, in quite new drying machine concepts.

Equations governing the process are produced by writing mass and energy balances for an element of the sheet. Due to the small thickness of the sheet, differentials but in one direction, perpendicular to the sheet, have to be regarded.

Consider an element of the drying sheet, Fig. 1. The differential thickness of the element is dy. Two subdivisions of the element are inspected separately, e.g., subdivision "F" comprising fibres with both mechanically bound and hygroscopic water, and subdivision "P" comprising gas-filled pores. The inner surface A_F of the web element, between the subdivisions F and P, is assumed to be immense in comparison to the cross-sectional area F ($= F_P+F_F$) of the element. The local mean temperatures inside the subdivisions are T_P and T_F. In most cases the difference between T_P and T_F is very small and may be neglected.

Geometrically the system according to Fig. 1 will be characterized with three constants b, b_P and b_F:

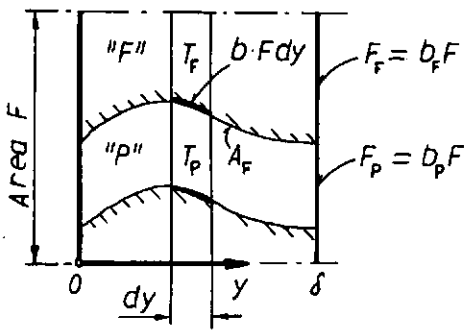

Figure 1

$$A_F = bV = b\delta F \;,\; A_F/F = b\delta >> 1 \qquad (1)$$

$$F_P = b_P F \;,\; F_F = b_F F \;,\; b_P+b_F = 1 \qquad (2)$$

THE MASS BALANCE EQUATIONS (Table 1)

Table 1 Mass flow quantities

Subdiv.	Entering at y	Leaving at $y+dy$	Description
P	$\dot{m}_a$	$\dot{m}_a$	Air mass flow
	$\dot{m}_v$	$\dot{m}_v+\frac{\partial \dot{m}_v}{\partial y}\cdot dy$	Vapor mass flow
	$a\cdot Fdy\cdot \dot{m}''$		Evaporation from F
F	$\dot{m}_w$	$\dot{m}_w+\frac{\partial \dot{m}_w}{\partial y}\cdot dy$	Liquid water mass flow
		$a\cdot Fdy\cdot \dot{m}''$	Evaporation to P

Subdivision P

Due to the low density and, also, the low heat capacity of subdivision P, all time-dependent derivatives, i.e., the accumulation terms, can be neglected.

If there exists a pressure drop across the sheet, a gas flow is generated through the pores. The flow of air, $\dot{m}_a$, is, of course, constant. The flow of water vapor, $\dot{m}_v$, is increased with the rate of evaporation at the inner surface A_F. If the mass flow density of this evaporation is denoted with $\dot{m}''$, the mass balance equation becomes

$$\frac{\partial \dot{m}_v}{\partial y} = aF\cdot \dot{m}'' \qquad (3)$$

Subdivision F

Equating the difference between the entering and leaving mass quantities with the moisture content change, $\rho\cdot Fdy\cdot\frac{\partial z}{\partial t}\cdot dt$, during the time interval dt, we obtain

$$\rho F\frac{\partial z}{\partial t} = -\frac{\partial \dot{m}_w}{\partial y} - aF\cdot m'' \qquad (4)$$

For the liquid water flow we write

$$\dot{m}_w = -\kappa F\cdot\frac{\partial z}{\partial y} \qquad (5)$$

THE ENERGY BALANCE EQUATIONS (Table 2)

Subdivision P

The energy or heat balance for subdivision P is written by equating the sum of the entering contributions to the sum of the leaving contributions:

$$aF\cdot \dot{m}'' h_{vF} - aF\cdot\alpha(T_P-T_F) - \frac{\partial}{\partial y}(\phi_P+\dot{H}_a+\dot{H}_v) = 0 \qquad (6)$$

Using (3) the first term can be expressed as

$$aF\cdot \dot{m}'' h_{vF} = h_{vF}\cdot\frac{\partial \dot{m}_v}{\partial y}$$

and, further,

$$\phi_p = -\lambda_p\frac{\partial T_p}{\partial y}\cdot F_p \qquad (7)$$

$$\dot{H}_a = \dot{m}_a h_a \qquad (8)$$

$$\dot{H}_v = \dot{m}_v h_v \qquad (9)$$

Table 2 Energy flow quantities

Sub-div.	Entering at y	Leaving at $y+dy$	Description
P	ϕ_P	$\phi_P+\frac{\partial\phi_P}{\partial y}\cdot dy$	Conduction heat flow
	$\dot{H}_a$	$\dot{H}_a+\frac{\partial\dot{H}}{\partial y}\cdot dy$	Enthalpy flow of air
	$\dot{H}_v$	$\dot{H}_v+\frac{\partial\dot{H}}{\partial y}\cdot dy$	Enthalpy flow of vapor
	$a\cdot F dy\cdot\dot{m}''\cdot h_{vF}$		Enthalpy flow of evaporation
		$a\cdot F dy\cdot\alpha(T_P-T_F)$	Convection heat flow over A_F
F	ϕ_F	$\phi_F+\frac{\partial\phi_F}{\partial y}\cdot dy$	Conduction heat flow
	$\dot{H}_w$	$\dot{H}_w+\frac{\partial\dot{H}_w}{\partial y}\cdot dy$	Enthalpy flow of liquid water
		$a\cdot F dy\cdot\dot{m}''\cdot h_{vF}$	Enthalpy flow of evaporation
	$\alpha\cdot F dy\cdot\alpha(T_P-T_F)$		Convection heat flow over A_F

Subdivision F

The difference between the entering and leaving energy quantities in accumulated as internal energy in the sheet element. In the foregoing, in fact, we already have assumed that the amount of the fibres in the sheet element remains unchanged during the process (see, e.g., the derivation of (4)). This means that we have allowed small movements of the boundaries due to small density changes which are produced by temperature and moisture variations. The corresponding work done by the moving boundaries must be added to the internal energy, the sum being the enthalpy of the matter in the sheet element.

Thus we obtain the energy balance for F

$$\rho F\cdot\frac{\partial h_F}{\partial t} = -aF\cdot\dot{m}''h_{vF}+aF\cdot\alpha(T_P-T_F)-\frac{\partial}{\partial y}(\phi_F+\dot{H}_w) \quad (10)$$

We assume that the specific enthalpy of the fibres, h_F, can be written as the sum of the enthalpies of the dry fibres, h_d, and of the water, zh_w:

$$h_F = h_d+zh_w \quad (11)$$

The differentiation of (11) gives

$$\frac{\partial h_F}{\partial t} = (c_d+zc_w)\frac{\partial T_F}{\partial t}+h_w\frac{\partial z}{\partial t} = c_z\frac{\partial T_F}{\partial t}+h_w\frac{\partial z}{\partial t}$$

Inserting this into (10) and using the mass balance equations (3) and (4) we get

$$\rho Fc_z\frac{\partial T_F}{\partial t} = -aF\cdot\dot{m}''h_{vF}+aF\cdot\alpha(T_P-T_F)-\frac{\partial}{\partial y}(\phi_F+\dot{H}_w)+$$
$$+h_w(\frac{\partial\dot{m}_v}{\partial y}+\frac{\partial\dot{m}_w}{\partial y}) \quad (12)$$

where

$$\phi_F = -\lambda_F\frac{\partial T_F}{\partial y}\cdot F_F \quad (13)$$

$$\dot{H}_w = \dot{m}_w h_w \quad (14)$$

THE CONTACT DRYING PROCESS

Differential equations

In the contact drying process $\dot{m}_a = 0$, $\dot{H}_a = 0$ and $T_P = T_F = T$. By summing the energy equations (6) and (12) it is found that

$$\rho Fc_z\frac{\partial T}{\partial t} = -\frac{\partial}{\partial y}(\phi+\dot{H}_v+\dot{H}_w)+h_w(\frac{\partial\dot{m}_v}{\partial y}+\frac{\partial\dot{m}_w}{\partial y}) \quad (15)$$

where according to (7), (13) and (2)

$$\phi = \phi_P+\phi_F = -(\lambda_P b_P+\lambda_F b_F)\frac{\partial T}{\partial y}\cdot F = -\lambda\frac{\partial T}{\partial y}\cdot F$$

As a first approximation we set $b_P = \varepsilon$ (= the sheet porosity), $b_F = 1-\varepsilon$. This includes an error caused by varying cross sections of the subdivisions, by the

tortuosity of the flow paths, and by the heat flow resistances, which are partly coupled in parallel and partly in series.

Into (15) we insert

$$\dot{H}_v+\dot{H}_w = \dot{m}_v h_v+\dot{m}_w h_w = \dot{m}_v r'+(\dot{m}_v+\dot{m}_w)h_w$$

and get

$$\rho F c_z \frac{\partial T}{\partial t} = -\frac{\partial}{\partial y}(\phi+\dot{m}_v r')-(\dot{m}_v+\dot{m}_w)\frac{\partial h_w}{\partial y} \qquad (16)$$

The vapor flow, $\dot{m}_v$, in the pores is created by diffusion, the magnitude of the flow conforming to the well known Stefan-equation

$$\dot{m}_v = -\varepsilon F \cdot \frac{D}{R_v T}\cdot\frac{p}{p-p_v}\cdot\frac{\partial p_v}{\partial y} \qquad (17)$$

The quantity group $\phi+\dot{m}_v r'$ in (16) we call "apparent heat flow" ϕ_s, its expression being

$$\phi_s = \phi+\dot{m}_v r' = -(\lambda+\varepsilon\cdot\frac{Dr'}{R_v T}\cdot\frac{p}{p-p_v}\cdot\frac{\partial p_v}{\partial T})\frac{\partial T}{\partial y}\cdot F =$$

$$= -(\lambda+\varepsilon\lambda_D)\frac{\partial T}{\partial y}\cdot F = -\lambda_s\cdot\frac{\partial T}{\partial y}\cdot F \qquad (18)$$

In a wet sheet, above the fiber saturation the apparent thermal conductivity, λ_s, is a function of the temperature only. The derivative $\partial p_v/\partial T$ may be obtained from a steam table. Using the notation of (18) the energy balance equation may be written thus:

$$\rho c_z \frac{\partial T}{\partial t} = \lambda_s\frac{\partial^2 T}{\partial y^2}+\frac{\partial T}{\partial y}\cdot\frac{d\lambda_s}{dy}-(\dot{m}_v+\dot{m}_w)c_w\cdot\frac{\partial T}{\partial y}$$

or, finally

$$\rho c_z \frac{\partial T}{\partial t} = \lambda_s\frac{\partial^2 T}{\partial y^2}+\frac{d\lambda_s}{dT}\left(\frac{\partial T}{\partial y}\right)^2-(\dot{m}_v+\dot{m}_w)c_w\cdot\frac{\partial T}{\partial y} \qquad (19)$$

The last right hand side term is often very small and negligible. The remaining equation is principally the basic heat conduction equation for conduction in a material with temperature dependent heat conductivity.

Combining (3) and (4) the mass balance equation becomes

$$\rho F\frac{\partial z}{\partial t} = -\frac{\partial \dot{m}_w}{\partial y}-\frac{\partial \dot{m}_v}{\partial y} \qquad (20)$$

The boundary conditions (Figs. 2 and 3)

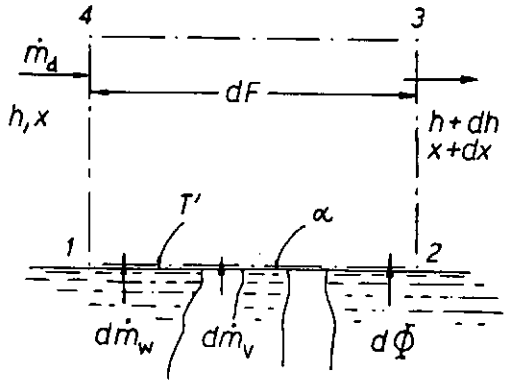

Figure 2

The boundary 12 of the control volume 1234 follows the outer surface of the drying sheet. The differential size of the surface is dF, its temperature T' and it is passed by a differential heat flow $d\phi$ and by two water flows, viz. $d\dot{m}_v$ (= vapor through pores) and $d\dot{m}_w$ (= evaporating water). The drying air flow, $\dot{m}_d$, has entering parameters h, x, (T), and leaving parameters $h+dh$ etc.

The energy balance equation will be

$$\dot{m}_d dh = d\phi+d\dot{m}_w\cdot c_w T'+d\dot{m}_v(r_0+c_v T')$$

Differentiating the specific enthalpy equation $h = c_a T+(r_0+c_v T)x$ we get the dependence between the differentials dh, dT and dx:

$$dh = (c_a+xc_v)dT+(r_0+c_v T)dx \qquad (21)$$

Inserting dh and $\dot{m}_d dx = d\dot{m}_w+d\dot{m}_h$ into the energy balance equation (20) we find that

$$d\phi-\dot{m}_d(c_a+xc_v)dT = d\dot{m}_w(r_0+c_v T-c_w T')+d\dot{m}_v\cdot c_v(T-T') \qquad (22)$$

Here the right side terms represent the rate of heat which is needed for the evaporation of $d\dot{m}_w$ and for the heating of all vapor, $d\dot{m}_w+d\dot{m}_v$, from the surface temperature T' to the drying air temperature T. This demand of heat is satisfied by the entering heat flow $d\phi$ and by a convective heat flow, $-\dot{m}_d(c_a+xc_v)dT$, which is delivered by the drying air flow $\dot{m}_d$. Denoting the heat transfer coefficient at the evaporating surface with α', we hence write

$$\alpha'(T-T')dF = -\dot{m}_d(c_a+xc_v)dT \qquad (23)$$

Examining the psychrometric Mollier-chart, Fig. 3, we find $h'-h = (x'-x)(r_0+c_v T)-(c_a+x'c_v)(T-T')$ from which we solve

$$T-T' = \frac{r_0+c_v T-\Delta h/\Delta x}{c_a+x'c_v}(x'-x) \qquad (24)$$

where $\frac{\Delta h}{\Delta x} = \frac{h'-h}{x'-x}$.

Multiplying (21) with $\dot{m}_d$ we get

$$-\dot{m}_d(c_a+xc_v)dT = (r_0+c_v T-dh/dx)(d\dot{m}_w+d\dot{m}_v) \qquad (25)$$

For the total evaporation we write

$$d\dot{m} = d\dot{m}_w+d\dot{m}_v = \dot{m}_d \cdot dx \qquad (26)$$

and insert (24) and (25) into (23), which after a slight modification results in

$$\frac{d\dot{m}}{dF} = \frac{\alpha'}{c_a+x'c_v}\cdot\frac{r_0+c_v T-\Delta h/\Delta x}{r_0+c_v T-dh/dx}\cdot(x'-x)$$

At least at turbulent flow of the drying air the change of state, which is characterized by the quotient dh/dx, is directed towards the point (h',x') of the saturation curve. With quite satisfactory accuracy we write $dh/dx = \Delta h/\Delta x$, and find that

$$\frac{d\dot{m}}{dF} = \frac{\alpha'}{c_a+x'c_v}(x'-x) \qquad (27)$$

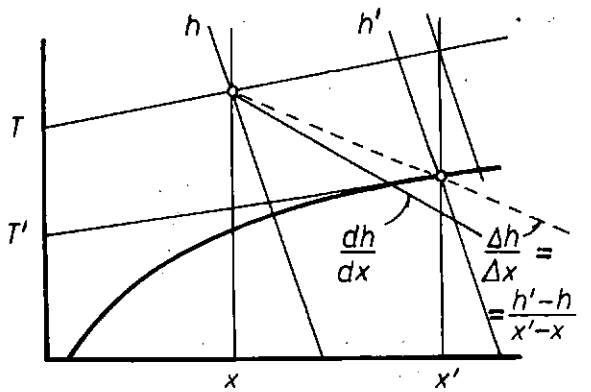

Figure 3

Combining (21), (22) and (26) we get

$$\frac{d\phi}{dF}+\frac{d\dot{m}}{dF}\cdot c_w T'+\frac{d\dot{m}_v}{dF}(r_0+c_v T'-c_w T') = \frac{\dot{m}_d dx}{dF}\cdot\frac{dh}{dx}$$

Here $r_0+c_v T'-c_w T' = r'$ = heat of evaporation at T'. If we integrate the equation over so small a surface F that all values of the parameters are unchanged, we get

$$\phi+\dot{m}_v\cdot r'+\dot{m}\cdot c_w T' = \frac{\alpha'}{c_a+x'c_v}(h'-h)\cdot F \qquad (28)$$

Using the energy balance equation, the thermodynamic properties of humid air and the definition of a coefficient of heat transmission at simultaneous heat and mass transfer (23) we, hence, have found equations similar to the "Lewis' relation" (27) and to the "enthalpy method" (28). The latter will be slightly modified:

$$\phi+\dot{m}_v r' = \frac{\alpha'}{c_a+x'c_v}\left((h'-h)-(x'-x)c_w T'\right)\cdot F \qquad (29)$$

Now, comparing (18) and (29) we now find the boundary condition at $y = \delta$:

$t > 0$, $y = \delta$:

$$-(\lambda_s\cdot\frac{\partial T}{\partial y})_\delta = \frac{\alpha'}{c_a+x'c_v}\left((h'-h)-(x'-x)c_w T'\right) \qquad (30)$$

For $y = 0$ is simply written:

$$t > 0,\ y = 0:\ \alpha_c(T_c-T_0) = -(\lambda_s\cdot\frac{\partial T}{\partial y})_0 \qquad (31)$$

Finally the initial condition shall be defined:

$$t = 0,\ 0 \leq y \leq \delta:\ T = T(0,y) \qquad (32)$$

The boundary condition at screen-covered paper surfaces

A very approximate method will be developed. In (29) we replace α' with the overall heat transmission coefficient k, this being

$$\frac{1}{k} = \frac{\delta_s}{\varepsilon_s\lambda_a}+\frac{1}{\alpha_s} \qquad (33)$$

where δ_s and ε_s are the screen thickness and porosity, respectively, and α_s the heat transfer coefficient on the screen. Thus

$t > 0$, $y = \delta$:

$$-(\lambda_s\frac{\partial T}{\partial y})_\delta = \frac{k}{c_a+x'c_v}\left((h'-h)-(x'-x)c_w T'\right) \qquad (34)$$

Applications

The system of equations governing the contact drying process can not, of course, become solved analytically. A program for the numerial solution has been developed.

A couple of worked examples are presented in Figs. 4 and 5. The main characteristic parameters are given in the figures. The left hand side subfigure shows the temperature profiles of the sheet at various instants of a contact drying cycle comprising two phases, viz. the contact period of the sheet with a cylinder, and the free travel between two cylinders. The right hand side subfigure gives the

temperature graphs of both sheet sides during one drying cycle.

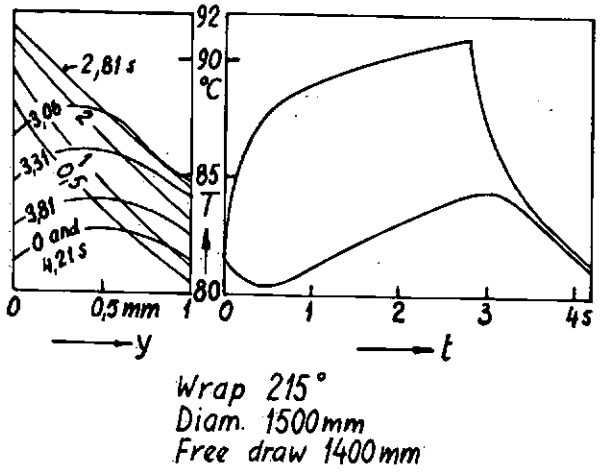

Figure 4

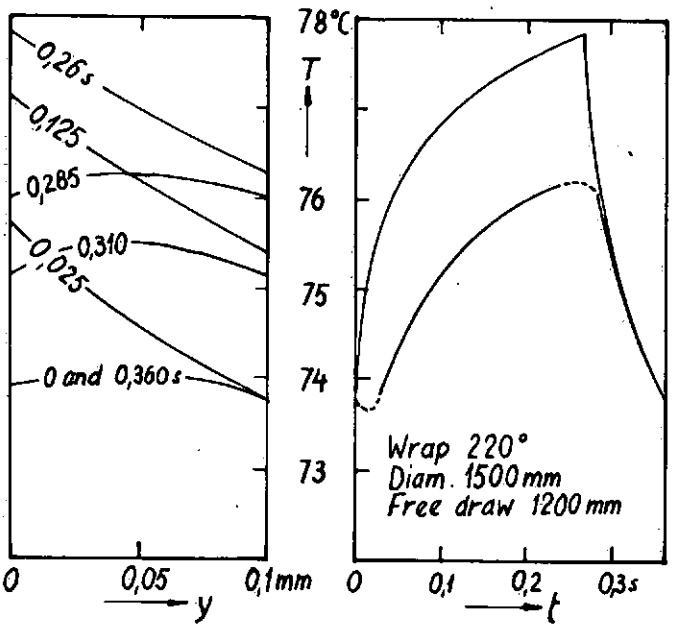

Figure 5

A prerequisite for the use of the developed model is that the several parameters appearing in the equations are known. Efforts have been made in order to measure the heat transfer coefficients between the sheet and the drying air during the free travel, and between the cylinder surface and the sheet during the contact period. This work has been done on operating production machines producing light weight grades (1).

The through-drying process

The subdivisions P and F were treated separately in order to get a model which would be applicable for the study of the through drying process. The numerical treatment of the problem has, however, not yet been carried out.

The entering gas side boundary condition is of special interest. For the temperature T of the entering gas outside the sheet surface the differential equation (35) holds true (w = gas velocity, a = thermal diffusitivity):

$$w\frac{dT}{dy} - \frac{d^2T}{dy^2} = 0 \qquad (35)$$

Using the boundary conditions

$y = -\infty$, $T = T_a$

$y = 0$, $T = T_0$

we find the solution

$$T = T_a - (T_a - T_0)e^{yw/a} \qquad (y < 0) \qquad (36)$$

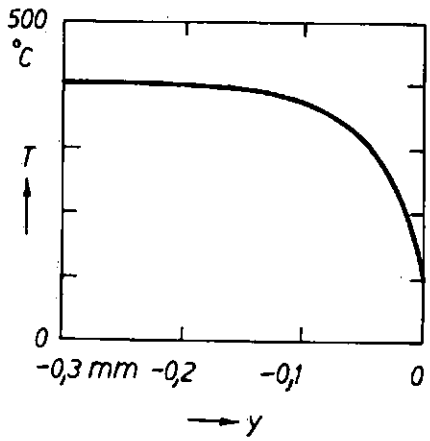

Figure 6

As an example, the air temperature before penetration into the sheet has been given graphically in Fig. 6. The air mass flow density is 1 kg/(m^{2}s), and we see that during a travel length of 0,2 mm before entering the sheet, the air temperature drops from 400°C to the sheet temperature, which, at least in the beginning, is less than 100°C. Also a partial pressure boundary layer is formed in an analogous way.

The very large heat flow according to the given example, due to the great drop in air temperature immediately before entering the sheet, creates in the sheet a very large heat flow by conduction. The convection in the pores is less important

because the temperature drop of air in the pores is less than that before the air enters the wet sheet.

REFERENCE

1. Karlsson, Markku, Results of On-line Investigations of Paper Contact Drying Process, Second International Symposium on Drying, July 7-9, 1980

RESULTS FROM ON-LINE INVESTIGATIONS OF PAPER CONTACT DRYING PROCESS

Markku Karlsson

Åbo Akademi, Turku, Finland

ABSTRACT

On-line measurements have been made on several paper machines having operation speeds of about 300, 500 and 800 m/min respectively in order to get values of the heat transfer coefficients between the cylinder surface and the sheet and between the sheet and the drying air during the sheet free travel. The sheet temperatures in the free travel (both sides) and the cylinder temperatures were recorded.

The numerical values of the heat transfer coefficients have been calculated by comparing the measured temperatures with the theoretical model of the process.

The heat transfer coefficient between the sheet and the drying air depends on the relative velocities of the sheet and the air. It is, hence, also a function of the machine ventilation air rate.

Some single-screen machines are also studied. Measurements of the sheet temperatures and of the drying air condition show that cylinders in contact with the screen are essentially ineffective. The drying intensity of the cylinders in contact with the sheet is greatly improved due to the large temperature drop of the sheet and due to the improved ventilation.

NOMENCLATURE

A = surface, m^2
c = specific heat, kJ/kg ^oC
h = specific enthalpy, kJ/kg d.a.
l = length, m
m = mass flow, kg/s
M = basis weight, g/m^2
N = perpendicular force, N
Nu = Nusselt number
Pr = Prandtl number
q = specific heat consumption, kJ/kg H_2O
r = regression coefficient
Re = Reynolds number
t = time, s
T = temperature, ^oC, K
u = induced air velocity, m/s
v = sheet velocity, m/s
x = air humidity, kg H_2O/kg d.a.
y = coordinate
z = sheet moisture content, kg H_2O/kg d
α = heat transfer coefficient, $W/m^2{}^oC$
δ = thickness, mm
ϵ = emissivity
λ = thermal conductivity, W/m^oC
μ = friction factor
ρ = density, kg/m^3
ϕ = heat flow, kJ/s

Subscripts

a = air
c = cylinder surface
d = dry fibres
s = sheet
v = vapor
w = water
z = at moisture content z

Superscripts

' = at saturation
- = average

INTRODUCTION

The increased speeds on fast machines have lately caused serious operating problems in paper mills. It is apparent that, with present double-screen systems, the operation speed can not be increased any further. In practice this has resulted in increasing conversions to single-screen dryers.

It is hardly possible to calculate the efficiency of a modern multi-cylinder dryer or to compare alternative geometries and production strategies without a good mathematical model for the contact drying process. The most important parameters in such a model are the heat transfer coefficients. To estimate the numerical values of these parameters and to verify the model, a series of surveys have been carried out on single- and double screen paper machines. In this paper the results of these investigations are presented, first for double screen dryers and then for single screen dryers.

2. ON-LINE SURVEY ON A DOUBLE-SCREEN SYSTEM

This survey has included three production paper machines, whose operating speeds were approximately 300, 500 and 800 m/min respectively. A few free travel zones were measured along each machine, and about twenty succesful series of measurement were obtained. Many series of measurement were spoiled by either a web break or a change in operating conditions.

2.1 Method of measurement

Considering the high temperature and humidity of the drying air, and the poor accessibility, a prerequisite for measuring the temperature drop at a free travel zone in a multi-cylinder drying machine was to design special equipment for carrying out the measurements. For the temperature sensing element, a resistor wire sensor touching the sheet lightly was used. A measuring error was, however, produced. It was caused by frictional heat increasing the sheet temperature, and the prevention, of evaporation at the sensor. The maximal magnitude of this error is obtained by assuming that the sensor is externally insulated and that the contact resistance between the sheet and the sensor equals zero. Hence, the boundary condition at the surface in contact with the sensor, in the differential equation (1 ; eq. 18), is expressed

$$\mu N v = -\lambda\left(\frac{\partial T}{\partial y}\right)A \quad ; \; y = 0, \; t > 0 \qquad (2.1.1)$$

Considering the initial and boundary conditions, the differential equation yields the sheet temperature increase. Fig. 2.1.1 shows the increase in temperature when using a sensor 7 cm long. When the sheet touches the sensor, its initial temperature is 78.0°C, and when the sheet 0.0053 seconds later parts from the sensor its temperature is 78.1°C. At the same time, the temperature of the free sheet surface has dropped to 77.5°C, as evaporation has taken place unobstructedly. From this example it is seen that the sheet temperature increase caused by sensor contact is insignificant. Due to the great mass flow in the sheet, the heat caused by friction is not capable of heating the sheet.

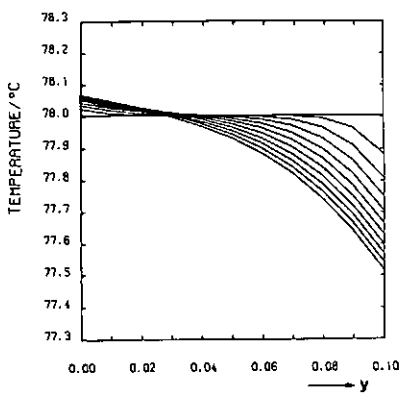

Figure 2.1.1 Temperature drop in sheet in contact with temperature measuring device.

2.2 Measuring apparatus

A general view of the apparatus used for measuring the temperature of the paper web and the condition of the drying air surrounding it is shown in Fig. 2.2.1. The measuring bracket holding the measuring beam has been mounted parallel to the sheet run. The measuring heads required for measuring the sheet temperature and air humidity have been mounted at the end of the measuring beam.

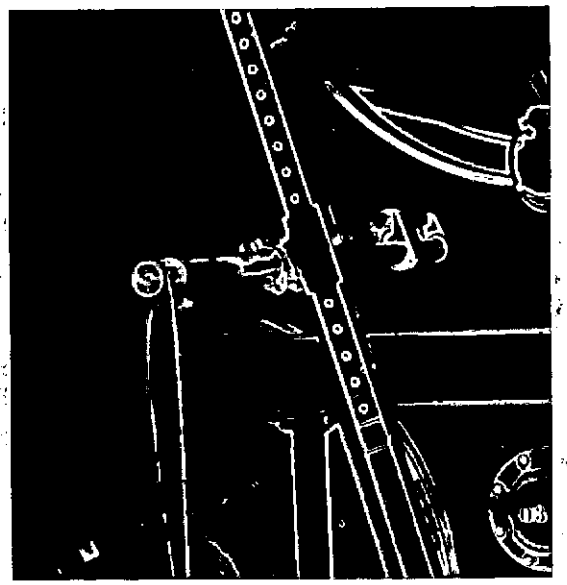

Figure 2.2.1 General view of temperature measuring apparatus.

The measuring apparatus further includes a cylinder surface thermometer.

2.3 Measuring procedure

In most cases the temperature measurement of the sheet free draw was done measuring the temperature of one side of the sheet twice, to establish the repeatability of the measuring operations. To avoid the edge effect, a measuring point at a distance of about 50 cm from the sheet tending side edge was selected. The dry and wet bulb temperatures of the drying air were measured at a distance of 3-4 cm from the sheet surface. In addition to the measurement of the sheet free draw temperature drop and the drying air condition, each series of measurement included a measurement of the surface temperature of the adjacent cylinders, at the same distance from the sheet edge as the sheet temperature had been measured. As the cylinder surface temperature varied only a few tenths of a degree, the temperature obtained at the free surface holds also for the surface covered by the sheet. The total time required for accomplishing one series of measurement was, due to the multi-cylinder dryer geometry and the simple construction of the measuring apparatus, several hours.

2.4 Examples of temperature measurements

The total temperature drop was obtained by extra-

polation as the temperature of the free draw between the cylinders could be measured only at the free draw middle. In each machine, the lengths of the free draws were assumed to be equal, i.e., independent of the sheet tension. In the following, a few typical measuring results are studied:

At the machine speed range of about 300 m/min, the measurements were taken at the production of 95 g/m^2 cable paper. The results of the measurements on the free draw between cylinders 32 and 33 are shown in Fig. 2.4.1. These results are each shown in three diagrams. The left hand side diagram shows the sheet temperature and the dry bulb and wet bulb temperatures of the drying air. As an indication of evaporation efficiency, these figures also show the difference between the saturation ratio of air at sheet temperature and the moisture ratio of the surrounding air, $x' - x$, (middle diagram), and the difference between specific enthalpies, $h' - h$, of saturated air at the sheet temperature, and drying air (right hand side diagram). Further, the diagrams have been divided with a horizontal line into two sections, the top section showing condition above the sheet and the sheet top and the bottom section, correspondingly, the conditions on the wire side. The horizontal coordinate axis represents the length of the free draw so that the parting point coincides with the origin and the end of the free draw falls on the vertical line.

A point on the sheet requires 0.25 seconds to travel from one end of the free draw to the other. Temperature drops of 9.4°C (9.6°C) and 9.0°C take place in the sheet, on the top side and wire side resectively, in the free draw between cylinders 32 and 33. The corresponding temperature drops in the free draw between cylinders 18 and 19 are 4.7°C on the top side and 4.1°C on the wire side (not shown) They are smaller than those between cylinders 32 and 33 because the heat capacity flow is dependent on the sheet water content. Especially on the wire side, the changes in drying air condition are notable. At the end of the free draw, the sheet cooling is reduced. This is caused by the heating effect of the adjacent wire side cylinder, also of the high humidity of the drying air.

The measurements at the speed range of about 800 m/min were carried out on a newsprint machine. The machine speed was 780 m/min and the sheet basis weight was 50g/m^2. Fig. 2.4.2 show the results obtained from measurements taken between cylinders 17 and 18. To travel the length of the free draw, the sheet requires 0.12-0.13 s. During this time the sheet temperature drops 6.4°C on the wire side and, on the top side, 4.8°C. The air moisture ratio changes on the wire side from 0.128 to 0.148 and, on top side, from 0.227 to o.289, as counted from the point of departure. As the differences in x and h are greater on the wire side of the sheet, also evaporation is greater on the wire side. The diagrams show that the condition of the surrounding drying air at this speed range has been more stable than the drying air condition at the 300m/min speed range. This is explained by the increased pumping action of the screens, at higher speeds. The temperature difference between the cylinder surface and the paper web contact surface was 4.1 °C between cylinders 17 and 18.

2.5 Distribution of evaporation

The local specific evaporation for a free draw may be calculated when the heat released by the sheet is known. To establish this, an equation is written for the mass flow thus:

$$\dot{m}_s = M l v \tag{2.5.1}$$

and for its specific enthalpy,

$$h_s = c_z T' \tag{2.5.2}$$

where

$$c_z = c_d + z c_w \tag{2.5.3}$$

Equation (2.5.3) is valid only above the fiber saturation point, where the water and dry substance form a mechanical mixture. As the heat flow by radiation from the cylinders is negligible compared with the heat flow due to sheet cooling, the energy balance for the sheet and the drying air in its immediate vicinity may be written in the form

$$-\dot{m}_s dh_s = \dot{m} dh \tag{2.5.4}$$

where

$$dh_s = c_z dT' + c_w T' dz \tag{2.5.5}$$

By inserting (2.5.5) into (2.5.4) and integrating over the whole free draw, one obtains

$$-\dot{m}_s \bar{c}_z \Delta T' - \dot{m}_s c_w \bar{T}' \Delta z = \dot{m} \Delta h \tag{2.5.6}$$

where

$$\bar{c}_z = c_d + \bar{z} c_w \tag{2.5.7}$$

Using the heat flow released by the sheet one may write

$$\phi \approx -\dot{m}_s \bar{c}_z \Delta T' \tag{2.5.8}$$

Hence, by inserting (2.5.8) into (2.5.6), one obtains

$$\phi = \dot{m} \Delta h + \dot{m}_s c_w \bar{T}' \Delta z \tag{2.5.9}$$

Then, dividing (2.5.9) by the water balance

$$\dot{m}_w = -\dot{m}_s \Delta z = \dot{m} \Delta x \tag{2.5.10}$$

yields the specific heat consumption

$$q = \frac{\phi}{\dot{m}_w} = \frac{\Delta h}{\Delta x} - c_w \bar{T}' \tag{2.5.11}$$

Consequently the evaporation at the free draw may be obtained by dividing the value of ϕ obtained from (2.5.8) by the value of q obtained from (2.5.11). Relation $\Delta h/\Delta x$ may be determined from relation $(\bar{h}' - \bar{h})/(\bar{x}' - \bar{x})$ with sufficient accuracy. Further, by dividing the free draw evaporation so

obtained, by the cylinder surface, one may write for the specific evaporation:

$$\frac{\dot{m}_w}{A} = \frac{\phi/l}{\pi Dq} = -\frac{\dot{m}_s c_z \Delta T'}{\pi DLq} \qquad (2.5.12)$$

After this, the distribution of evaporation may be calculated as a relation between the free draw local specific evaporation based on measurements, and the total specific evaporation. The total specific evaporation may be determined when the machine speed, basis weight, water content of the sheet entering and leaving, and number of cylinders in operation are known.

The value of ϕ obtained from equation (2.5.8) is correct only if the sheet may be considered thin, i.e., no appreciable difference exists between the surface temperature and average temperature of the sheet. The temperature differences of a thin sheet were m thematically found to be only a few tenths of a degree (1, Fig. 5)

The accuracy of the calculation performed depend essentially on how accurately the sheet free draw temperature drop can be extrapolated and the sheet moisture content determined. Due to insufficient means for determining sheet moisture, estimations on moisture content had to be done based on drying characteristics for corresponding machines, obtained from machine manufacturers, when calculating the evaporation distribution. Standardizing the drying characteristics, and their application with due consideration to random moisture samples, have been of advantange in estimating sheet moisture contents at the free draws. As a result of said inaccuracies, the calculations made of the evaporation distribution are somewhat inaccurate.

In table 2.5.1 below, the calculated specific evaporations are shown. The percentage in the last column indicates the free draw portion of the total evaporation.

Table 2.5.1 Evaporation distribution

Mach. nr.	v m/min	Basis weight g/m²	Paper	x kg/kg	Cyl's nr	Evaporation kg/(hm²) total	free draw	%
1	780	49,1	news print	1,0	11-12		4,4 ; 5,0	
	"	49,6	"	0,9	17-18		5,2	
	"	49,1	"	0,7	21-22	11,8	4,6 ; 4,3	39
	"	49,6	"	0,6	29-30		4,4 ; 4,3	
	795	49,3	"	0,5	31-32		4,8 ; 4,8	
2	531	79,0	writings	1,1	9-10	22,4	6,0	27
	532	71,5	"	0,7	15-16	19,7	6,4 ; 7,7	36
3	510	44,5-46,9	diagr.pap.	0,7	18-19	11,5	3,3 ; 2,8	27
	487	48,5	perg.pap.	0,7	18-19	11,6	4,5	35
	489	48,0	"	0,4	26-27		3,9 ; 3,8	
	297	92,8-93,3	cable pap.	1,3	10-11		2,6	
	299	94,7-95,0	"	1,0	18-19	10,9	3,6	34
	292	92,4	"	0,7	26-27		3,9 ; 4,4	
	308	94,9-95,4	"	0,4	32-33		4,0 ; 4,0	

It is found that the part of the total evaporation which takes place at the free draw is particularly sensitive to machine speed. When the speed is increased, the time of sheet and cylinder contact is shortened, and the sheet reheating takes a relatively greater portion of the contact time. For this reason, the evaporation at the free draw increases in relation with the evaporation at the cylinder surface. A higher speed also leads to an increase in the heat and mass transfer coefficient between the sheet and drying air. The comparability of the results is impaired by the scarcity of available data and the dissimilarity of machines, screens, steam pressures, paper grades, etc. For example, with few exceptions the cylinder surface temperatures on machines 1 and 3 ranged from 85 to 100°C, whereas on machine number 2the surface temperatures varied between 105 and 110°C, which is also reflected in the high specific evaporation. Generally speaking, the evaporation at the free draw is relatively lower than what could be expected on the grounds of surveys made on felted machines or the information available in literature on machines with drying screens. The screen impairs evaporation on the cylinder very little. However, no secondary evaporation occurs from the screen as from a felt as the screen does not become wet.

2.6 Heat transfer coefficient in free draw

Water evaporating from the sheet consumes the sheet heat energy. As a result of this, the sheet temperature drops, in proportion to the evaporation taking place. As the heat capacity flow of a wet sheet is higher than that of a dry sheet, the wet sheet temperature drops less.

Assuming that the sheet is so thin that there is no appreciable difference between average temperature and surface temperature and writing an energy balance for the free draw length element dy applying the enthalpy method one obtains

$$\frac{\alpha}{c_a + x' c_v}(x' - x)\left(\frac{h' - h}{x' - x} - c_w T'\right)\cdot 2dy \simeq -\rho c_2 v \delta dT' \qquad (2.6.1)$$

The flow of steam diffusing from the inside of the sheet into the surface is neglible and has not been considered. Separating the factors

$$-\frac{dy}{\rho c_2 v\delta/2\alpha} = \frac{c_a + x' c_v}{h' - h - (x' - x)c_w T'}\, dT' \qquad (2.6.2)$$

is obtained, where the right hand side is a function of sheet temperature only and can be integrated as such. Writing $y/\rho c_2 v\delta/2\alpha = \eta$ where η is dimensionless distance of y, and whereas the term $(x' - x)c_w T'$ usually can be neglected, one obtains

$$\eta_2 - \eta_1 = \int_{T_2'}^{T_1'} \frac{c_a + x' c_v}{h' - h}\, dT' \qquad (2.6.3)$$

The solution of equation (2.6.3) is shown in Fig. 2.6.1 for some drying air conditions. It is observed that if the average drying air condition

remains unchanged, the free draw temperature drop may be determined as a function of sheet water content and temperature just by evaluating term $\rho c_z v\delta/2\alpha$. For various drying air conditions, separate curve may be drawn.

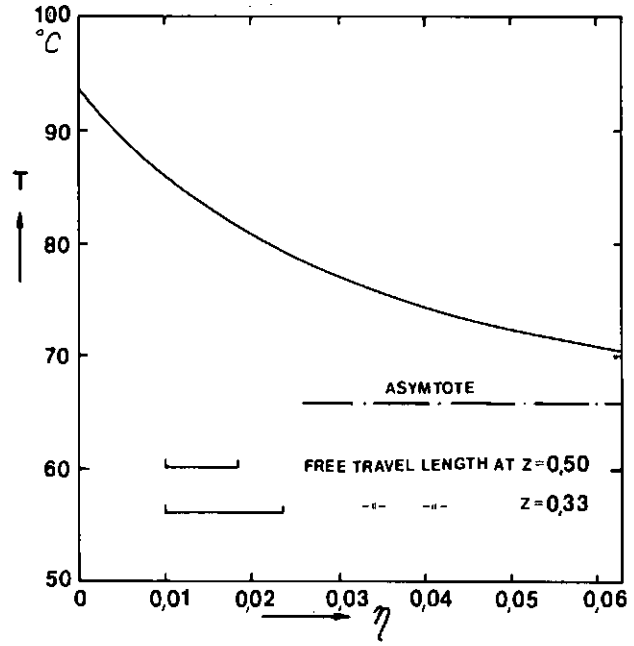

Fig. 2.6.1 Temperature drop in free draw

The heat transfer coefficient for heat transfer from the sheet to the surrounding air may be determined based on equation (2.6.2), as x' and h' are known functions of T', and the drying air condition, sheet density, machine speed, and the sheet water content may be measured or estimated. When processing the measuring results, the right hand side of (2.6.2) has been calculated as an average of conditions of both sides of the sheet. Due to its neglible change, c_z has been assumed constant within a single free draw.

The values of heat transfer coefficients calculated from the measuring results have been grouped in Fig. 2.6.2 by speed ranges. The figure also includes the heat transfer coefficient calculated theoretically according to equation (2.6.4).

$$Nu = 0.057\, Re^{0.78} Pr^{0.78} \qquad (2.6.4)$$

When air at 80°C flows along a plane surface 1-1.5 m long, it is observed that the heat transfer coefficients obtained by measurement are smaller than those obtained for parallel blow. This is due to the fact that the sheet induces by frictional forces an air flow unidirectional with the sheet. Thereby the relative air velocity $\Delta u = v-u$ becomes smaller than the sheet velocity. At lower sheet velocities the induced air flows are almost nonexistent, and the relative velocity, $\Delta u \approx v$, but at higher velocities $\Delta u < v$.

Considering the assumptions made, i.e., that the heat transfer coefficient on both sides of the sheet are equal and that the results are not comparable with each other because of variations in operating conditions, it is not possible to give a

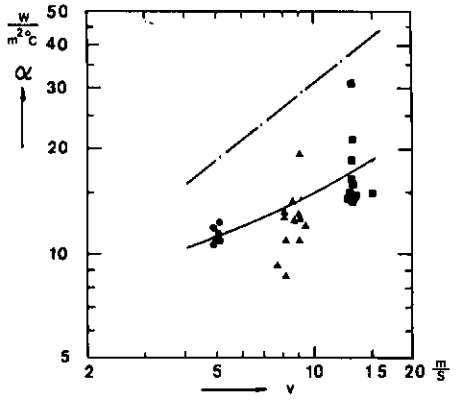

Figure 2.6.2 Calculated heat transfer coefficients compared with coefficients obtained for parallel blow.

representative expression of the interdependence between Nusselt's, Reynold's and Prandtl's numbers. It may, however, be stated that the results obtained can, with fair accuracy ($r^2 = 0.96$), be expressed with equation

$$\alpha / \frac{W}{m^2 °C} = 5.3 \left(\frac{v}{m/s}\right)^{0.46} \qquad (2.6.5)$$

In equation (2.6.5), it is assumed that the heat transfer coefficient is a function of sheet velocity only. This is, however, not quite true. The value of the heat transfer coefficient depends, besides the sheet velocity and machine configuration, also on operating conditions, particularly the ventilating air rate. At a low ventilation air rate, the frictional forces induced by the sheet affects a small mass flow only whereby the relative velocity decreases resulting an a decrease in the heat transfer coefficient. The evaporation decreases together with the heat transfer coefficient, also because of the high ventilation air humidity. Moreover, the pumping action of the screens tend to decrease the heat transfer coefficient: with open screens, the relative velocity decreases because of the pumping effect.

2.7 Heat transfer coefficient between cylinder and sheet

The heat transfer coefficient is defined by eq (2.7.1).

$$\alpha_s = \frac{q\dot{m}}{A_s} / (T_c - \overline{T}_s) \qquad (2.7.1)$$

where q = specific heat consumption of machine
$\dot{m}/A_s$ = specific evaporation of machine calculated for the cylinder surface covered by paper
T_c = cylinder surface temperature, nearly constant
$\overline{T}_s$ = paper surface temperature on cylinder contact side

The heat flow from cylinder to air has, in relation with the heat flow from cylinder to sheet, not been considered. As the specific heat con-

sumption (∿3000 kJ/kg H_2O)
may be estimated and the evaporation per unit paper covered cylinder surface calculated, the heat transfer coefficient for the heat flow from the cylinder to the sheet may be obtained from (2.7.1). The avarage temperature T_s of the cylinder side sheet surface may be calculated with sufficient accuracy based on drying phases obtained with the aid of a mathematical model (1, Fig. 5), as the extrapolated free draw initial temperatures are known.

The heat transfer coefficients calculated from the results obtained with measurements are shown in Fig. 2.7.1. Heat transfer coefficients obtained from lit erature have been grouped in Fig. 2.7.1. These are valid mostly for small pilot machines.

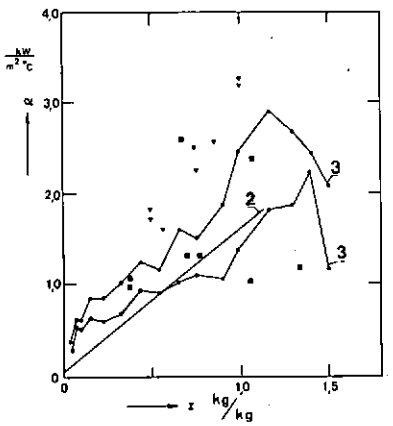

Fig. 2.7.1 Heat transfer coefficient between cylinder and sheet α_s.

The variance of the measuring results obtained is considerable as the heat transfer coefficient in heat flow from cylinder to sheet is not a function of sheet water content only but depends on many factors. These include screen tension, cylinder surface smoothness and cleaness, sheet porosity, and screen weaving, to mention those most important. In addition to above factors, the method of calculation with its approximations tends to further increase the scatter.

The results obtained may be expressed with formula ($r^2 = 0.70$)

$$\alpha_s / \frac{kW}{m^2 {}^{o}C} = 0.29 + 2.56z$$

2.8 Conclusions

When studying the results above, one should note the factors which impair their general applicability and comparability. The operating conditions of the three machines under observation, such as steam pressures, screen tensions and types, paper grades, etc. were varying. Further, due to deficiencies in instrumentation, some readings are inaccurate, some even missing, e.g., local moisture data of the sheet were not available.

In spite of these differences in operating conditions, configurations, etc., extensive similarities are seen in the results of these measurements. The curves for T, Δx and Δh have their characteristic shape in relation to each other. The method of determining the evaporation distribution, based on the sheet temperature drop, has yielded dependable results. The heat transfer coefficients calculated from the measurement readings for the sheet free draw are clearly shown depend on the machine speed. Correspondingly, the heat transfer coefficient for the heat flow between cylinder and sheet depends on the sheet water content. Simple calculation methods, which have been used to determine the heat transfer coefficients, have produced quite dependable results and have thereby proved their usefulness.

3. ON-LINE SURVEY ON A SINGLE-SCREEN SYSTEM

Single-screen drying groups have lately gained much popularity. In a single-screen system, the one and same screen winds around both the upper and lower cylinders. The paper sheet then travels alternatingly between the cylinder surface and the screen, and outside the screen (generally on the lower cylinders). A screen run of this type has been used. mainly for experimental purposes, on a few drying groups following the press section in some fast paper machines in production, for improving the runnability. When a single-screen concept is used on a drying group, it is obvious that the drying group specific evaporation and the thermal process of the whole dryer change. To establish and analyze these changes, some sheet temperature measurements carried out on single-screen drying groups are treated in the following.

3.1 Method, apparatus and procedure

Instead of the sensor which lightly touches the sheet, an infrared radiation thermometer was used to measure the temperature. The high dynamic accuracy of these instruments and the facility of the measuring operations have spoken for replacing the measuring devices used before with an IR thermometer. The accuracy obtained with this measuring system depends on the magnitude of the sheet emissivity and its variation. Seeking a temperature difference, the temperature reading change caused by a change in the emissivity may be calculated using equation (3.1.1)

$$\frac{\Delta(\Delta T_s)}{\Delta T_s} \simeq -\frac{\Delta \varepsilon_s}{\varepsilon_s} \qquad (3.1.1)$$

when $T_a / T_s \simeq 1$

Hereby the IR thermometer is well suited for determining temperature differences. On the other hand, when attempting to measure absolute temperatures with an IR thermometer, the emissivity must be known. For a wet sheet, this may only be established by calibrating the IR thermometer against another type of thermometer.

The IR thermometer used was a Heimann KT-16. For cooling, the instrument is mounted in an enclosure, the enclosure is placed in a carriage running

on a track mounted around a lower cylinder. Outside the carriage, at a distance of 2-3 cm from the sheet surface a psychrometer is attached.

Measurements were made on two machines, the speeds of which were approximately 640 m/min and 230 m/min resectively. The latter of the two was a board machine. On both machines the sheet temperature was measured at a few lower cylinders, from the merging point to the parting point. The points measured were located on the cylinder periphery, 10 cm apart, about 50 cm away from the sheet drive side edge. The measuring apparatus used did not allow measuring of the free draws.

3.2 Measuring results and conclusions

An example of results is shown in the form of a diagram in Fig. 3.2.1. These results were obtained from the machine operated at a speed of 634 m/min and where the sheet basis weight was 56 g/m^2 (printing paper)

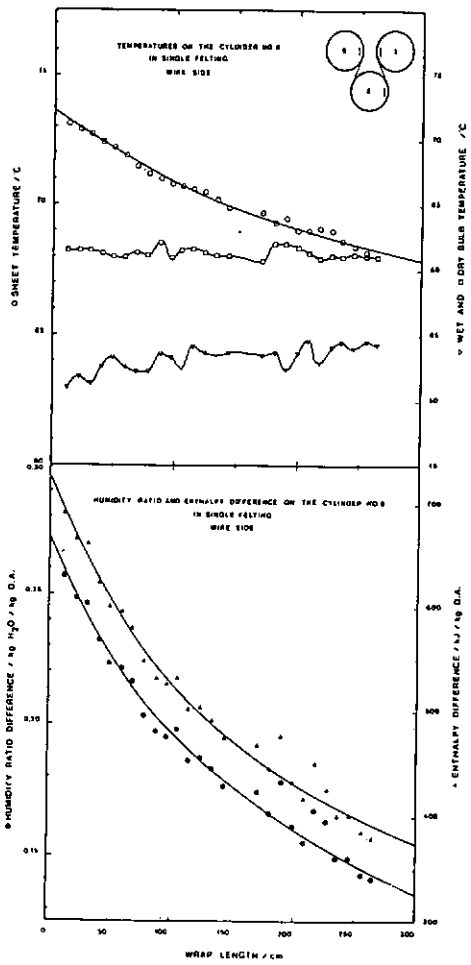

Fig. 3.2.1 Sheet cooling on "inactive" cylinder

The horisontal line dividing the figure into a top section and bottom section represents a sheet traveling from left to right and intersecting the ordinate at the merging point. The primary measuring results have been arranged in the top section of the figure. The difference between air saturation moisture ratio at sheet temperature and the moisture ratio of surrounding air, $x' - x$, and difference between the specific enthalpies of saturated air at sheet temperature and the drying air, $h' - h$, are shown in the bottom section of the figure.

A temperature drop of approx. 6 °C is indicated by the measurements, on lower cylinder No 8, and about 7 °C, on lower cylinder No. 10, (not shown) during a time period of 0,27 s. As indicated by the air temperature measurements, the moisture ratio of air in contact with the sheet changes at cylinder No. 8 from 0.09 kg H_2O/kg d.a. to 0.1. This humidity is considerably below the average humidities encoutered at double-screen drying groups.

On cylinders where the screen runs between the cylinder and the sheet, the cooling of the sheet in fast machines indicates that the sheet contact time is too short and the contact resistance too great to allow the heat flow through to the sheet. Thereby the heat obtained from these cylinders has only an indirect effect in evaporation, as it mainr causes a temperature rise of a few degrees to the screen and the drying air surrounding the cylinder.

Based on the foregoing, one could conclude that the specific evaporation in single-screen drying groups would drop to about half of the original as the heat transfer surface is nearly reduced to half (the wrap angle at the upper cylinders increases sligtly). However, this is not the case. Specific evaporations measured on operating machines show a decrease of about 30% only as compared with a normal double-screen drying group. This is due to the temperature amplitude of the single-screen group. It is higher than that of a conventional group and causes an increased heat flux at conventional cylinders. The high temperature amplitude in the sheet, on the other hand, results from an excessively long free draw and the good ventilation qualites of the single-screen As compared with a single-screen group, the air humidity in a conventional group is often twice as high.

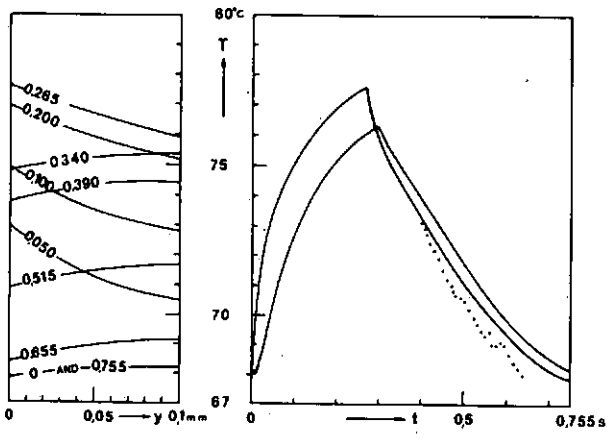

Fig. 3.2.2 A single-screen paper drying cycle
Points indicate measured sheet temperatures on the "inactive" cylinder.

The sheet temperature behaviorin a single-screen group is best demonstrated by Fig. 3.2.2. The figure shows a sheet drying cycle, obtained by means of a mathematical model, as the sheet travels the distance from cylinder No.7 to 9 in a single-screen group. Fig.3.2.2 shows that the temperature amplitude is 10°C. Corresponding temperature amplitude for a double-screen group is 4°C (1, Fig. 5) In simulations, the same cylinder surface temperature (81°C) has been assumed to occur in both conventional and single-screen groups. In reality,this is not quite true unless the pressure of the steam supplied to the single-screen group is increased.

Based on the example described above, the agreement between results obtained from a mathematical model and those obtained from field measurements seems satisfactory,

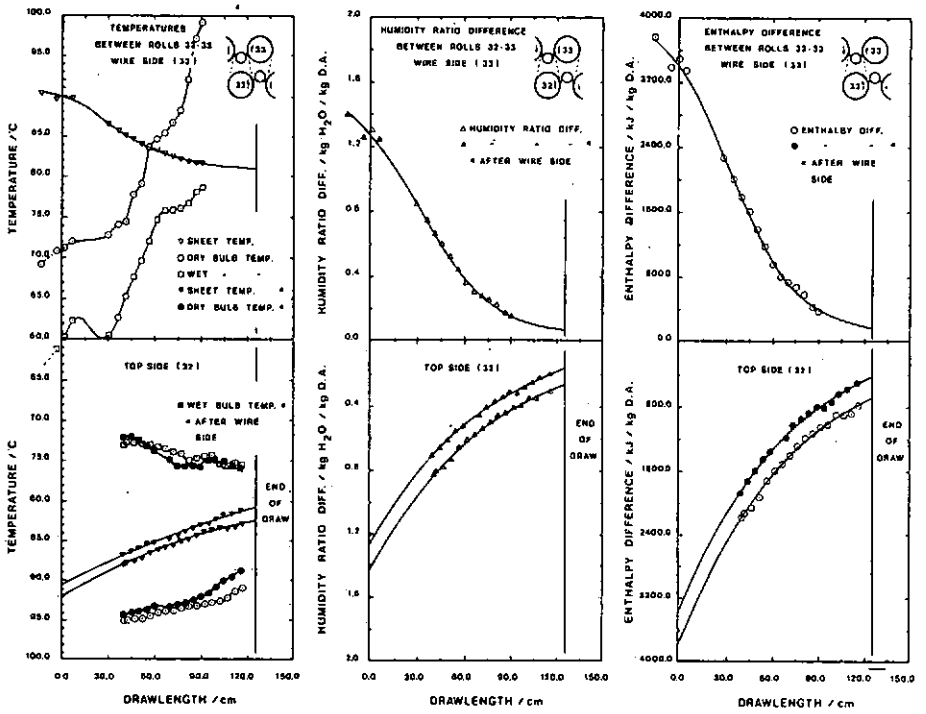

Fig: 2.4.1 Measuring results, between cylinders 32 -33

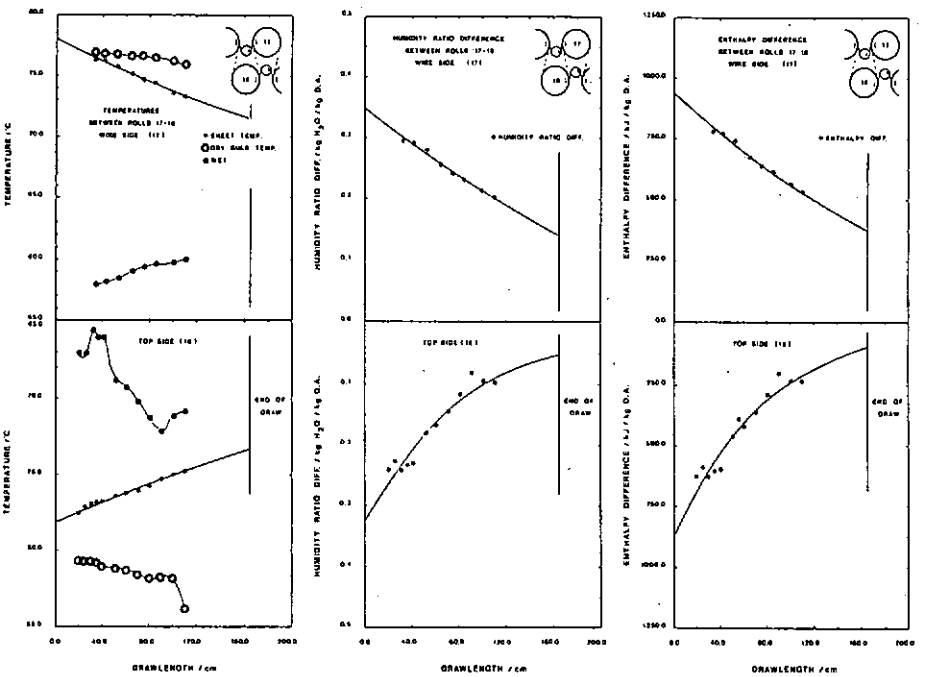

Fig. 2.4.2 Measuring results, between cylinders 17 -18

REFERENCES

1. Soininen, M., A mathematical model of the contact drying process, Second Int. Symposium on Drying

2. Göttsching,L. and Rhodius, D., Der Trocknungsverlauf von Papier und Pappe in Abhängigkeit von Trocknungstechnischen und Papiertechlogischen Parametern, Part IV, Das Papier, Heft 1,1979

3. Lemaitre, A., Perron, M. and charvel,R., Modélisation et simulation du sèchage du papier sur cylinders pour la conception de sécheries a` hautes performances, XVII EUCEPA-Conference, Vienna, 1977.

A LITERATURE REVIEW OF DRYING RESEARCH IN THE PULP AND PAPER INDUSTRY

R. R. McConnell

The Institute of Paper Chemistry, Appleton, WI 54912

ABSTRACT

The main dryers used in the United States pulp and paper industry are drum section, impingement and Yankee dryers. Research has been done on each of the dryer types and their components. The most thoroughly researched area is convective drying. The areas that have had the least work are dryer dynamics, ventilation systems and overall dryer performance evaluation.

INTRODUCTION

Drying is an important unit operation in the pulp and paper industry. The production of over 60-million tons of paper per year, in the United States, requires the removal of over 80-million tons of water by dryers. Many types of dryers are used in the industry. An estimate of the distribution of dryer types is shown in Table 1. First, the percent water removed was assumed proportional to the product produced. Thus, about 7% of the industry water removal is in pulp drying, 6% in tissue drying, 34% in paper drying, 51% in paperboard drying and 2% in coatings drying. Next, the distribution of the types of dryers for each application was estimated. For example, in pulp drying it is estimated that 70% of the pulp is dried in impingement (floater) dryers, 15% in flash dryers and 15% in vacuum dryers. After the dryer distribution for each application was determined, the total percentage water removed on each of the types of dryers was determined by multiplying the percent of the dryer distribution by the fraction of water removed in the corresponding application. This shows that 80-85% of the industry's drying is done on conventional drum dryers. Approximately 5-10% of the drying is done on impingement dryers. About 4-5% of the drying is done on Yankee dryers. Less than 3% of the drying is done on infrared dryers. Through, flash and vacuum dryers each account for about 1% of the drying. Finally, almost no drying is done on dielectric and microwave dryers. Thus we see that the conventional drum dryer is dominant in the industry. The impingement dryer is the next most important but is used mainly for drying pulp and coatings. Yankee dryers follow in importance and dominate tissue drying. Thus drum, impingement and Yankee dryers are important to the industry, and much has been written about them.

TABLE I

U.S. PAPER INDUSTRY DRYER DISTRIBUTION

	Paper Industry Drying Application					Totals, %
	Pulp	Tissue	Paper	Board	Coating[a]	
	Water Removed, %					
	7	6	34	51	2	100.00
	Dryer Distribution, %					
Drum section dryer		15	95	95	35	82.35
Impingement dryer	70		2	2	50	7.60
Yankee dryer		70				4.20
Infrared dryer			3	3	15	2.85
Through-dryer		15				0.90
Flash dryer	15					1.05
Vacuum dryer	15					1.05
Dielectric dryer						
Microwave dryer						
Totals	100	100	100	100	100	100.00

[a]This includes both on and off machine coating operations.

REVIEW OF DRYING

There is relatively little written on a unified treatment of paper drying. The book by Keey (1) covers all aspects of industrial drying but has little specifically on the drying of paper. The chapter by Coveney and Robb (2) on the dryer section is mostly descriptive of equipment and has a little analytical treatment of dryers. The book edited by Gavelin (3) is the best available on the drying of paper, but suffers from the fact that it is a series of articles and not a unified text by one author. Other similar, but less complete, article series were edited by Cirrito (4-14) and Blundell (15-21).

There have been several reviews of drying that are helpful. The review by Han (22) discusses work on modeling the transport phenomena occurring in the dryer. The reviews by Burgess (23,24) compare the principles and economics of several drying methods: conventional drum section, high velocity hoods, dielectric and microwave, radiant, fluidized beds, and through-dryers. Most of the other articles on drying describe a particular type of application for a dryer.

Drum Dryers

Several workers have analyzed conventional drum dryers. However, all the past web modeling work has been done for evaporation at one atmosphere in air. Nissan (25-29) was the first person to model a conventional drum dryer section. The drying process was modeled by a dynamic thermal diffusion equation with time-varying boundary conditions. The work by Snow (30) extended this model by including the transient moisture flow in the web. He included the capillary flow of liquid and the diffusion of vapor. The model by Holm (31) incorporated earlier work by Han (32,33). This model included moisture flow by capillary, diffusion and pressure gradients. Thus, these models emphasized the temperature and moisture profiles in the web.

Other researchers have not included as much detail about the transport phenomena in the web but have emphasized other subsystems. The best example of this is in the model developed by Knight and Kirk (34) based on Knight's thesis (35). Their model includes the drum steam and condensate dynamics as well as pocket ventilation. Kirk (36) has used the model to study the effect of different pocket ventilation flow patterns on the cross direction (CD) moisture profile. Depoy (37) and Meisel (38) have used an analog computer to simulate a dryer section using a model similar to that developed by Nissan. Other examples of models based on Nissan's work are those by Strong and Powell (39) and Lehtikoski (40). Rhodius and Gottsching used a similar model (41) but did extensive experimental work (42-44) determining the parameters that affect drying rate. Their experimental technique is similar to that used by Lee and Hinds (45) to determine the effect of wet pressing, refining and surface texture on drying. Thus, a good start has been made on understanding conventional drum dyers. However, a thorough study should be undertaken to determine the transport coefficients to predict drying rates and energy efficiency. Also, methods to improve CD moisture profiles are needed.

Yankee Dryers

The main components in a Yankee dryer are the steam heated drum and the high velocity hood. Researchers have worked on characterizing the heat transfer from both of these sources. Zabel (46) used an analog computer to simulate the heat transfer in a Yankee dryer shell. His results agreed with earlier experimental work by Brauns and Jansson (47) showing that most of the temperature changes occur under the press roll and in a thin layer of the shell next to the web. Their experimental technique was extended by Sundberg, et al. (48) for use in mill operation. Schiel and Zurn (49) used calculations of the thermal resistances of the paper, shell and condensate to determine the capacity of Yankee drums with plain shell, plain shell with spoiler bars and grooved shell.

Most of the work on Yankee dryers has been concentrated on the high velocity hood. Spraker, et al. (50) used a simple lumped-parameter model to relate heat and mass fluxes to the temperature and humidity differences. Rounds and Wedel (51) calculated the theoretical drying rate and specific energy consumption of a Yankee hood as a function of the supply air humidity and temperature, and the impingement velocity and open area.

Several investigators have studied the heat transfer in air-impingement drying. Daane and Han (52) correlated the turbulent heat transfer coefficient to the Reynolds number, Prandtl number, and geometrical factors for single and multiple round jets and slots. Larsson (53) compared several impingement heat transfer correlations and high velocity hood designs. Han and Seely (54) analyzed the heat transfer from single and multiple round jets by similarity with momentum transfer, using the Blasius Law for turbulent flow in a pipe. Mujumdar and Douglas (55) surveyed the literature on the heat transfer characteristics of two dimensional slot-jets, single and arrays of round jets impinging on flat and curved surfaces. Other correlations for impingement heat transfer are given by Batsis and Schukow (56) and Christ and Weinmann (57). A summary of the state of the art in impingement heat and mass transfer is given by Martin (58). Other authors have emphasized the practical aspects of Yankee hood applications. Andersson (59) gives an overview of the design and use of high velocity hoods. Villalobos (60) has discussed blow-through and draw-through fan arrangements, the importance of humidity levels and the relative merits and problems of heat recovery. Methods are also available (61) for evaluating high velocity dryers. Finally, Villalobos (62) has discussed the use of a gas turbine with a Yankee dryer to improve the utilization of available work.

Thus, much work has been done on Yankee dryers. The analysis of Yankee dryers is more advanced than that of conventional drum dryers.

Convection and Through-Dryers

Two of the most active areas of drying research in recent years have been convective and through drying. Holik (63) discussed the main considerations in through drying and developed a simple drying model. In a later paper, Holik (64) presented a review of convection drying.

Villalobos has written three papers on through drying. In the first (65), he discussed the main factors in the design and operation of through dryers. The second (66) pointed out the benefits of operating through dryers at low temperatures. The third (67) described the through-drying processes used in the manufacture of tissue and toweling.

Several models of convective and through drying have been developed. Crotogino (68) reviewed

the factors governing the drying rates attainable with impingement and through-drying in his survey of convective drying. Crotogino and Galatone (69) modeled a Papridryer by adding the impingement and through-drying rates. Gardiner has written three papers discussing his through-dryer model. In the first (70), he outlined the model and describes the sensitivity of design and operating parameters on dryer capacity, drying rates and operating costs. The second (71) showed the effects of hood temperature and humidity on energy efficiency as well as describing through dryer applications. The third (72) developed the general relations between energy consumption and drying capacity for convective dryers. Wedel and Chance (73) developed a distributed-parameter model of through-drying and used it to predict the drying rate and energy consumption. The operation of convection and through-dryers is fairly well understood. The ongoing research in this area seems to be adequate.

Ventilation

The work on ventilation can be divided into hood air systems and pocket ventilation. Most of the articles on hood air systems have been qualitative instead of quantitative. Marshall (74) gave an overview of dryer hood selection and use. Walker (75) described some of the benefits of a well designed air handling system. Reed (76) discussed the design considerations for an air handling system. Walker (77) outlined some energy conservation measures in air handling systems. There have been many articles on pocket ventilation, but most have been descriptive. Kottick (78) gave a short overview of pocket ventilation. Soininen (79) analyzed the air flow patterns caused by permeable dryer fabrics. Soininen and Nurminen (80) described how a pocket ventilation system can level the web moisture profile. Kottick (81) discussed the use of pocket ventilation on a high-speed newsprint machine. Several authors (82,83,84) show examples of how pocket ventilation improves the web moisture profile. Grott (85) discussed the fuel and power costs of pocket ventilation. Metcalfe (86) outlined the types of pocket ventilation equipment that are available. Gardner has written several papers (87,88,89) describing the principles involved in pocket ventilation and the moisture profile leveling advantages. Future ventilation research should quantify the interaction among the web, dryer fabrics and ventilation system. Improved ventilation systems should do much to improve productivity and moisture profile uniformity.

Dryer Fabrics

The two main innovations in dryer fabrics have been the change from felts to open weave fabrics and the development of single felting. The open weave fabrics were discussed in some of the pocket ventilation articles (78-82).

Single felting is the term used to describe the use of serpentine dryer fabric in the first section to reduce web flutter. Sahay (90) and Josef (91) described applications of single felting to reduce flutter problems. Palazzolo (92) discussed the advantages and problems with single felting. Bringman and Jamil (93) compared single felting and impingement drying as solutions to the web flutter problem. Schlipf (94) measured the air temperatures and humidities in a single felting application. Wheeldon and Ashworth (95) measured the cylinder and sheet temperatures in single felting and conventional applications.

Steam and Condensate Systems

The proper design and operation of steam and condensate systems are important in conventional and Yankee dryers. Much experimental and analytical work has been done on these systems. Simmons (96) gave an overview of dryer condensate removal and steam pressure control. Daane (97) presented the results of experimental work relating pressure differential, condensate flow rate, blow-through steam flow rate, dryer speed and steam pressure for stationary and rotating siphons. Wahlstrom and Larsson (98) investigated the general characteristics of rotating and stationary siphons when in series with condensate piping. Gardner (99) calculated the minimum pressure differentials required for a rotary siphon. Appel and Hong (100) derived equations for the distribution of condensate rimming in a dryer and verified the results with experiments on a five foot model. Calkins (101) has shown the effect of syphon clearance and dryer heat transfer. Hurm (102-104) has written several articles on the principles of operation of dryer drainage systems. Hart (105) discussed steam and condensate system design considerations to reduce maintenance problems.

Dryer Measurements and Evaluation

Most of the articles on dryer surveys have either focused on instrumentation or survey results. Allan, et al. (106-108) discussed the instrumentation they developed and adapted for paper machine surveys. The instrumentation was used to measure moisture, basis weight, steam flow, condensate flow, air flow, dryer surface and sheet temperatures, and pocket wet and dry bulb temperatures. Luce, et al. discussed the use of infrared thermography (109) and video tape systems (110) in analyzing the performance of paper machines. Bennett (111), Fraser-Clark (112) and Rhorer (113) discussed the use of microwave moisture meters in analyzing moisture profile problems.

Other authors have emphasized the results of dryer tests. Montgomery (114) presented the results of moisture and temperature profile measurements from 40 different drying tests. Hoecke (115) reported the correlation between drying rate and steam pressure for linerboard and corrugating medium. Urbas (116), Wiseman (117) and Kerr (118) reported on surveys of Canadian newsprint machines. Garvin and Pantaleo (119) presented the survey methods and results of several dryer section testing programs. Chalmers (120) and Mardon, et al. (121) discussed to methodology of dryer heat and energy balances. Mardon, et al., (122-124) described the results of paper machine surveys.

Other authors (125-127) have investigated the factors that affect CD moisture profiles.

CONCLUSION

As can be seen from the above, work has been done on most aspects of paper drying. Convective drying (including through, impingement and floater drying) is the area that is best understood. The transport phenomena are well documented, and much experimental work has been done to correlate the transport coefficients.

Also, much analytical and theoretical work has been done on steam pressure regulation and condensate removal. However, little has been done on the dynamics and control of the steam/condensate system.

Very little analytical work has been done on dryer ventilation and the effects of dryer fabrics on drying. Most of the work has been empirical and fragmented. A thorough analytical and experimental program is needed to quantify the effect of ventilation and fabrics on drying in a conventional drum dryer.

The instrumentation is available for conducting an adequate dryer survey. Much has been published on paper machine surveys, however, no suitable dryer model has been developed for comparing the thermal performance of dryers.

REFERENCES

1. Keey, R.B., Introduction to Industrial Drying Operations Pergamon Press (1978).

2. Coveney, D.B. and Robb, G.A., "The Dryer Section," Chapter 9 in Pulp and Paper Manufacture, Volume III. Papermaking and Paperboard Making, Edited by R.G. MacDonald and J.N. Franklin, McGraw-Hill (1970).

3. Gavelin, G. (editor), Drying of Paper and Paperboard, Lockwood (1972).

4. Cirrito, A.J., "Paper Drying: Part I - Differential heat flow measurements in cylinder drying," Paper Industry, October 1962, p. 397-401, 426.

5. Cirrito, A.J., "Paper Drying: Part IA - Surface temperature variations in cylinder dryers and measurement technique," Paper Industry, November 1962, p. 469-470.

6. Cirrito, A.J., "Paper Drying: Part IB - The effects of noncondensible gases and superheat on heat transfer," Paper Industry, January 1963, p. 593-595.

7. Cirrito, A.J., "Paper Drying: Part IC - Determination of the steamside and shell heat transfer coefficients and their effects on the drying rate," Paper Industry, February 1963, p. 645-646, 658.

8. Cirrito, A.J., "Paper Drying: Part II - External factors," Paper Industry, April 1963, p. 27-29 and May 1963, p. 86-87.

9. Cirrito, A.J., "Paper Drying: Part IIA - Elements of Mass Transfer," Paper Industry, June 1963, p. 139-142.

10. Cirrito, A.J., "Paper Drying: Part IIB - The zone of nearly constant evaporation rate," Paper Industry, August 1963, p. 251-252 and September 1963, p. 319-322.

11. Cirrito, A.J., "Paper Drying: Part III - Air Jet Impingement," Paper Industry, November 1963, p. 433-435.

12. Cirrito, A.J., "Paper Drying: Part III-A - Controlling Quality and Heat Rate in Impingement Drying," Paper Industry, January 1964, p. 548-550 and February 1964, p. 599-601.

13. Cirrito, A.J., "Paper Drying: Part IV - The Falling Rate Zones," Paper Industry, May 1964, p. 115-118 and June 1964, p. 203-206.

14. Cirrito, A.J., "Paper Drying: Part V - Radiation," Paper Industry, August 1964, p. 407-409, September 1964, p. 499-501, November 1964, p. 744-747, and December 1964, p. 842-845.

15. Wells, G.K., "Getting the best out of your drying cylinders," Paper Industry, vol. 183, no. 2 (1975), p. 74-75, 78-79.

16. Nuki, R.P., "Heating of drying cylinders," Paper, Vol. 183, no. 3, 1975, p. 126, 128-131.

17. Whittaker, J.D., "Trends in modern high velocity hood applications," Paper, Vol. 183, no. 3, 1975, P. 132-133, 135, 142.

18. Smith, J.C., "Paper Mill Ventilation," Paper Vol. 183, no. 4, 1975, p. 190, 192-193.

19. Kirk, L.A., "Exotic methods of paper drying," Paper Vol. 183, no. 5, 1975, p. 246, 249-250, 252, 260.

20. Palmer, P.J., "Developments in infrared drying," Paper, Vol. 183, no. 6, 1975, p. 331-334.

21. Blundell, K.D., "Gauges, the computer and the dry part," Paper Vol. 183, no. 6, 1975, p. 340, 343, 345.

22. Han, S.T., "Drying of Paper," Tappi, Vol. 53, no. 6: 1034-1046, 1970.

23. Burgess, B.W., "The Drying of Web Materials," Pulp and Paper Mag. Can. T-303-309, June 1961.

24. Burgess, B.W., "Future Trends in Drying," Paper Technology, Vol. 12, no. 6: 459-472, 1971.

25. Nissan, A.H., and Hansen, D., "Heat Transfer and Water Removal in Cylinder Drying: I. Unfelted Cylinders," Tappi, Vol. 43, no. 9: 753-756, 1960.

26. Nissan, A.H., Hansen, D. and George, H.H., Jr., "Heat Transfer and Water Removal in Cylinder Drying, II. Felted Cylinders," Tappi, Vol. 45, no. 3: 213-218, 1962.

27. Nissan, A.H. and Hansen, D., "Fundamentals of Drying Porous-Materials," Tappi, Vol. 44, no. 8: 529-534, 1961.

28. Nissan, A.H. and George, H.H., "Heat and Mass -- Transients in Cylinder Drying: Part 1. Unfelted Cylinders," AIChE Journal, Vol. 6, no. 4: 606-611, 1960.

29. Nissan, A.H. and George, H.H., "Heat and Mass Transfer Transients in Cylinder Drying: Part II. Felted Bylinders," AIChE Journal, Vol. 7, no. 4: 635-641, 1961.

30. Snow, R.H., "Studies of Drying in Paperboard Machines," IITRI Project C877, May 1964, May 1965.

31. Holm, R.A. and Hung, J.Y., "A Study of the Drying of Linerboard," IPC Project 2693 August 1971.

32. Han, S.T., "Heat and Mass transfer in hot-surface drying of fibre mats," Pulp Paper Mag. Can. Vol. 65, no 12: T537-549 December 1964.

33. Han, S.T. and Matters, J.F., "Vapor transport in fiber mats during drying," Tappi, Vol. 49, no. 1: 1-4 January 1966.

34. Knight, R.L.C. and Kirk L.A. "Simulation of the Papermachine Drying Section," International Water Removal Symposium, London, 1975.

35. Knight, R.L.C., "Some theoretical considerations of paper machine dryer sections," Ph.D. Thesis, University of Manchester Institute of Science and Technology, September 1972.

36. Kirk, L.A., "Digital simulation of the ventilation of a paper machine dryer section," Proceedings of the Second Pacific Chemical Engineering Congress, Vol. II Denver, 1977.

37. Depoy. J.A., "Analog computer simulation of paper drying: a workable model," Pulp Paper Mag. Can., Vol. 73, no. 5: 67-74, May 1972.

38. Meisel, R.M. "Analog computer simulation of paper drying," Tappi Vol. 60, no. 1: 160-162, January 1977.

39. Strong, A.B. and Powell, T. "An analysis of drying on conventional paper machines," Pulp Paper Mag. Can., Vol. 75, no. 3: 71-78, March 1974.

40. Lehtikoski, O.I. "A mathematical model of the dryer section," Papper och Tra, no. 2: 63-65, 68-72, 1970.

41. Rhodius, D. and Gottsching, L., "Course of drying of paper and board as a function of drying techniques and paper parameters. Part 4: Drying in the multicylinder dryer section," Das Papier, Vol. 33 no. 1: 1-8, 1979.

42. Rhodius, D., Part 1: Survey and discussion of testing methods for convective drying," Das Papier, Vol. 31, no. 10A-419-427, October 1977.

43. Rhodius, D., Part 2: Dependence of drying on paper parameters," Das Papier Vol. 32, no. 2: 49-58, February 1978.

44. Rhodius, D., Part 3: Level of critical moisture content," Das Papier, Vol. 32, no. 6: 234-242, June 1978.

45. Lee, P.F. and Hinds, J.A., "Optimizing dryer performance: A technique for measuring the drying characteristics of fiber webs," Tappi, Vol. 62, no. 4: 45-48, 1979.

46. Zabel, L.W., "The application of an analog computer to a paper manufacturing problem." Tappi, Vol. 42, no. 8: 687-690, August 1959.

47. Brauns, O. and Jansson, A.L., "Heat transmission in the drying of paper on a Yankee cylinder," Svensk Papperstidning, Vol. 60, no. 17, September 1957.

48. Sundberg, T., Andersson, N. Lofgren, K. and Osterberg, L., "Heat transfer in MG Drying," Svensk Papperstidning, Vol. 71, no. 8, 1968, p. 317-324.

49. Schiel, C. and Zurn, G., "Thermal capacity of high-performance creeping dryers," STFI Yankee Dryer Symposium, February 4-5, 1976, Stockholm, Sweden.

50. Spraker, W.A., Wallis, G.B. and Yaros, B.R., "Analysis of heat and mass transfer in the Yankee dryer," Pulp and Paper Mag. Can., January 3, 1969, p. 55-59.

51. Rounds, D.A., and Wedel, G.L., "Drying rate and energy consumption for an Air Cap dryer system," First International Symposium on Drying, Science Press, Princeton, N.J., 1978, p. 185-191.

52. Daane, R.A. and Han, S.T., "An analysis of air-impingement drying," Tappi, Vol. 44, no. 1, 1961, p. 73-80.

53. Larsson, T. "Comparing high velocity dryers—aspects of theory and design," Paper Trade Journal, September 17, 1962, p. 36-41.

54. Han, S.T. and Seely, T. "Heat transfer from a solid surface under air impingement," Tappi Vol. 48, no. 12, 1965, p. 705-708.

55. Mujumdar, A.S. and Douglas, W.J.M., "Impingement heat transfer: A literature survey," TAPPI Meeting, New Orleans, October 1972, p. 107-136.

56. Batsis, C., and Schukow, V., "Characteristics of high velocity air jets for Yankee dryer system,", presented at the First International Symposium on Drying, Montreal, August 3-5, 1978.

57. Christ, A., Weinmann, M. and Weinmann, A., "Berechnungsgrunslagen zur konvektionstroknung von papier mit dusenhauben," Escher Wyss Mitterlungen, no. 1, 1977, p. 11-16.

58. Martin H., "Heat and mass transfer between impinging gas jets and solid surfaces," Advances in Heat Transfer, Vol. 13, 1977, Academic Press.

59. Andersson, K.H., "Design, use and limitations of high velocity air hoods," Paper Trade Journal, August 17, 1970, p. 36-41.

60. Villalobos, J.A., "Yankee air system engineering," Tappi, Vol. 49, no. 9, 1966, p. 406-409.

61. "Methods of evaluating high velocity dryers," TAPPI Technical Information Sheet 14.15, 1970.

62. Villalobos, J.A. "The effective use of energy in the paper drying process," presented at the First International Symposium on Drying, Montreal, August 3-5, 1978.

63. Holik, H. "Air-through-drying of paper," Das Papier, Vol. 26, no. 4, 153-161, 1972,

64. Holik, H., "Convection drying," Wochenblatt fur Papierfabrikation, Vol. 102, no. 2: p. 52-62, 1974.

65. Villalobos, J.A., "Engineering considerations in through drying," Paper Technology and Industry, October 1975, p. 290-302.

66. Villalobos, J.A., "Through-drying—new developments in a growing field," Tappi, Vol. 59, no. 4, 1976, p. 76-80.

67. Villalobos, J.A., "Through-drying in tissue and toweling," Tappi, Vol. 60, no. 1, 1977, p. 137-139.

68. Crotogino, R.H., "The growing significance of air-drying," Paper Technology and Industry, August 1975, p. 247-258.

69. Crotogino, R.H. and Galatone, V., "A mathematical model of the Papridryer process," CPPA Annual Meeting Reprints 65B91-101, 1979.

70. Gardiner, F.J., and Rohrer, J.W., "Through-drying; heat transfer mechanism and machine system response," Tappi, Vol. 59, no. 4, 1976, p. 82-87.

71. Gardiner, F.J. and Dietl, R., "Progress in through-drying techniques," Das Papier, Vol. 30, no. 10A, p. 118-127, 1976.

72. Gardiner, F.J., "Design of convective dryers for best efficiency and productivity," Tappi, Vol. 60, no. 7, 1977, p. 90-93.

73. Wedel, G.L., and Chance, J.L., "Analysis of through-drying," Tappi, Vol. 60, no. 7: 82-85, 1977.

74. Marshall, H., "Dryer hoods and ventilation - how they affect costs and paper quality," Paper Trade Journal, October 26, 1970, p. 48-53.

75. Walker, D., "Ventilation and air systems," Paper Technology, Vol. 12, no. 5: 392-397, 1971.

76. Reed, D.L., "Energy requirements of air systems," Paper Technology and Industry.

77. Walker, P.J., "Some fundamental principles of paper mill energy optimization," Canadian Pulp and Paper Industry, February 5, 1977, p. 32-34.

78. Kottick, G.J., "Trends and developments in paper machine pocket ventilation," Paper Trade Journal, September 21, 1970, p. 78-79.

79. Soininen, M.A., "Air flow and pocket ventilation," Chapter II in Drying of Paper and Paperboard, edited by G. Gavelin, Lockwood, 1972.

80. Soininen, M. and Nurminen, J., "An orientation to the pocket ventilation design in a drying section with open mesh fabrics," Papper och Tra, no. 4a: 281-294, 1974.

81. Kottick, G.J., "Synthetic dryer clothing combined with a moisture profiling air system on high-speed newsprint machines," Pulp and Paper Mag. Can., February 21, 1969, p. 55-65.

82. Race, E. and Wheeldon, J.B., "A practical comparison of pocket ventilating systems," Pulp and Paper Mag. Can., January 3, 1969, p. 60-64.

83. Janett, L.G., "Profile correction and economics in drying of paper," Tappi, Vol. 53, no. 6, p. 981-988, 1970.

84. West, A.O. and McMullen, D.W., "Application of modern pocket ventilation systems to the conventional dryer section," Tappi, Vol. 59, no. 4, p. 88-91, 1976.

85. Grott, R.W., "The economics of pocket ventilation systems," American Paper Industry, April 1976, p. 14-17.

86. Metcalfe, W.K., "What pocket ventilation systems can do - and what they cannot," Pulp and Paper, February 1970, p. 95-97.

87. Gardner, T.A., "Pocket ventilation and applied fundamentals spell uniform drying," Paper Trade Journal, January 22, 1968, p. 46-52.

88. Gardner, T.A., "Pocket ventilation does work," American Paper Industry, February 1970, p. 44-46, 48-50.

89. Gardner, T.A., and West, A.O., "PV system improves web profile," Pulp and Paper, October 1971, p. 89-94, 143.

90. Sahay, A., "Single fabric in first dryer section ends sheet flutter lowers breaks," Canadian Pulp and Paper Industry, March 5, 1977, p. 36-37.

91. Josef, M.J., "Draw free sheet transfer in first dryer section proves advantageous," Pulp and Paper, May 1977, p. 156-159.

92. Palazzolo, S., "Positive and negative aspects of serpentine felt drying-benefits outweigh detriments," Paper Trade Journal, May 16, 1978, p. 33-35.

93. Bringman, D.J., and Jamil, Q.H., "Engineering considerations for lightweight paper drying in high speed machines," Paper Technology and Industry, August 1978, p. 194-197, 200.

94. Schlipf E., "Drying conditions with single felting in the cylinder dryer section," CPPA Annual Meeting Preprints 65B:185-189, 1979.

95. Wheeldon, J.B., and Ashworth, T.N., "Single felting - its effect on the drying rate," CPPA Annual Meeting Preprints, 65B:119-124, 1979.

96. Simmons, T., "Dryer condensate removal and steam pressure control," Paper Trade Journal, August 3, 1970, p. 32-40.

97. Daane, R.A., "An experimental study of some drier drainage siphons," Tappi, Vol. 42, no. 3, p. 208-218, 1959.

98. Wahlstrom, P.B. and Larsson, K.O., "Factors determining condensate removal," Pulp and Paper Mag. Can., Vol. 64, no. 5:T203-T210, 1964.

99. Gardner, T.A., "Minimum pressure differentials required for dryer drainage," International Symposium on Water Removal at the Presses and Dryers, CPPA, Montebello, QUE., 1964, p. 154-155.

100. Appel, D.W. and Hong, S.H., "Condensate distribution and its effects on heat transfer in steam-heated dryers," Pulp and Paper Mag. Can., February 21, 1969, p. 66-77.

101. Calkins, D.L., "The effects of siphon clearance on dryer performance," The Johnson Corporation, 1966, 20 p.

102. Hurm, R.B., "Factors affecting drier cylinder uniformity," Tappi, Vol. 46, no. 9, p. 531-533, 1963.

103. Hurm, R.B., "Paper machine dryer drainage systems: past, present, future," Pulp and Paper, October 1974, p. 62-65.

104. Hurm, R.B., "Improving paper drying with the right steam condensate system," Pulp and Paper, November 1974, p. 134-138.

105. Hart, R.H., "Spotlight on maintenance: paper machine steam and condensate systems," American Paper Industry, November 1971, p. 38, 40.

106. Allan, R.S., Rutland, D.F., and Skeet, C.W., "Evaluating papermachine press dryer performance," Pulp and Paper Mag. Can., Vol. 74, no. 6, p. 67-74, 1973.

107. Allan, R.S., and Kerr, R.B., "Evaluating paper machine press and dryer performance-update," CPPA Annual Meeting, February 1978 p. B147-B153.

108. Allan, R.S. and Kerr, R.B., "The measurement of paper machine press and dryer section variables," TAPPI Paper Makers Conference, 1978, p. 53-61.

109. Luce, J.E., Atkins, J.W. and Vickery D.E., "Infrared thermography as an aid to solving paper machine moisture profile problems," TAPPI Paper Makers Conference, 1978, p. 39-51.

110. Luce, J.E., "High speed video tape analysis of paper machines," TAPPI Paper Makers Conference, 1977, p. 125-127.

111. Bennett, P.G. "The use of a microwave moisture meter for process investigations," Appita, Vol. 26, no. 4, p. 267-272, 1973.

112. Fraser-Clark, D. "The use of portable microwave moisture meters on paper machines," Paper Technology and Industry, December 1975, p. 382-388.

113. Rhorer, C.R., "Diagnosis and correction of moisture profile problems of paper machines," Tappi, Vol. 54, no. 1, p. 43-46, 1971.

114. Montgomery, A.E., "Variation of drying rates of individual driers through to drier section," Tappi, Vol. 37, no. 1, p. 1-13, 1954.

115. Hoecke, D.A., "Drying rates on paper machines with high-pressure dryers," Tappi, Vol. 53, no. 4, p. 664-666, 1970.

116. Urbas, J.C., "Steam consumption and dryer performance on Canadian newsprint machines," Pulp and Paper Mag. Can., Convention Issue, 1962, T-87-92, 101.

117. Wiseman, N., "Dryer performance of North American newsprint machines," CPPA Annual Meeting, February 1978, B173-178.

118. Kerr, R.B., "Newsprint machine energy balance," CPPA Annual Meeting, February 1978, B131-145.

119. Garvin, S.P., Jr., and Pantaleo, P.F., "Measurements and evaluation of dryer section performance," TAPPI Engineering Conference, 1976, p. 125-133.

120. Chalmers, G.J., "Performance testing the dryer section of a paper machine," Pulp and Paper Mag. Can., Convention Issue, 1954, p. 236-243, 274.

121. Mardon, J., Turnbull, J.A. and Monahan, R.E., "The organization, carrying out and end results of heat and material balances on papermaking and coating machines," Pulp and Paper Mag. Can., January 1966, T-37-46.

122. Mardon, J., O'Brien, G.O., Dempsey, J.G., Marshall, H., Urbas, J.C., and Wahlstrom, B., "Examples of the use of heat and material balances in the study of the drying of pulp, paper and board: Part II - Paper machines," Norsk Skogindustri, no. 4, p. 136-150, 1963.

123. Mardon, J., Campbell, D., Marshall, H. Urbas, J.C., Sailer C.H., and Wahlstrom, B., "Examples of the use of heat and material balances in the study of the drying of pulp, paper and board: Part III - Drying and ventilating survey of a board machine," Norsk Skogindustri, no. 10, p. 395, 398-406, 1963.

124. Mardon, J., Smook, G.A., Stokes, T.W., Howe, B.I., and Monahan, R.E., Drying investigations on large paper machines," Papper och Tra, no. 7: 445-450; no. 8: 481-483, 486-495, 498-500; no. 9, p. 559-561, 565-570, 1970.

125. Lachmann, T.E., and Welch, J.W., "Factors that influence cross-machine reel moisture profiles," Tappi, Vol. 51, no. 4, p. 47A-53A, 1968.

126. Grimwood, K., "Towards a better understanding of dryer sections," Pulp and Paper Mag. Can., June 20, 1969, p. 70-76.

127. Hazelwood, E., "The investigation and correction of the cross direction moisture profiles on two fine paper machines," TAPPI Engineering Conference, 1970, p. 291-306.

IMPROVEMENT OF MOISTURE PROFILE ON PAPER MACHINES BY RF COMPENSATING DRYING

Hans Christian Grassmann

Siemens AG Manufacturing Division, Erlangen, West Germany

Summary

After intensive development in the laboratory and long-time test runs with a 600 kW RF prototype, the largest industrial RF dryer with a capacity of 900 kW RF power was delivered to a paper mill in the Netherlands in 1977.

With the RF dryer, the drying capacity of the paper machine was increased by up to 25 % and the moisture profile evened out from ± 1.5 % to ± 0.5 %. The paper machine in question was 5 m wide, ran at a speed of 450 m/min, and was in floating production.

The system, cylinder dryer and RF dryer are described.

Energy consumption and running costs are compared with those of the conventional drying system.

Two years of experience have shown that the RF dryer is an economical and highly reliable piece of equipment.

Paper presented

1. IMPORTANCE OF THE MOISTURE EVENING-OUT EFFECT

Outstanding basis weight and moisture profiles can be obtained today with modern paper machines. However, deviations in the moisture profile frequently increase over a maintenance interval.

Moisture deviations therefore necessarily result in overdrying in the drying section and cause significantly higher energy costs. The running properties during subsequent processing are thus seriously impaired.

Due to the inherent delay time of the controlled system, the problems cannot be resolved with the conventional heating processes, so that new solutions must be found.

2. REQUIREMENTS ON AUXILIARY COMPENSATING DRYERS

Based on theoretical considerations, the following requirements must be met by this new type of auxiliary dryer:

1. Installation of the auxiliary dryer must be possible at the end of the cylinder dryer.
2. The inlet temperature must be as high as possible.
3. Because of the high rate of power change and the high evaporative power, unsupported web sections must be available to allow unrestricted evaporation.

The RF dryer meets these requirements. Irrespective of their change with respect to time, moisture variations in the longitudinal and transverse profile are well evened out by the RF dryer, thereby increasing the drying capacity of a paper machine by up to 20 %.

3. MODE OF OPERATION OF RF DRYERS

If wet paper is placed in an electrode field to which a high-frequency voltage of several thousand volts is applied at a frequency of 13.56 MHz, the water molecules are moved about their rest position in synchronism with the frequency change by the alternating high-frequency field. The result of this movement is that heat is generated. The energy consumption of paper in an electrode field rises over-proportionally with increasing moisture. The reason for this is that the dielectric losses are dependent on moisture content.

The RF dryer comprises a dryer compartment through which hot air flows. The compartment contains a large number of rod-shaped electrodes arranged crosswise to the web (Fig. 1).

These electrodes are connected to the poles of an RF generator at alternating polarity. Generators of this type have an Output of up to 600 kW at a frequency of 13.56 MHz.

When the web is guided past these electrodes, the alternating electrical field between the individual rods causes rapid heating of the paper.

Steam vapours at the boundary layer are removed by the flow of hot air (approx. 120 °C). The hot exhaust air is blown under the drying hood.

The RF dryer is installed in the basement at the end of the conventional cylinder dryer (Fig. 2). The RF oscillator is flange-mounted to the side of the dryer compartment.

The paper is guided past the electrode fields over deflection rollers.

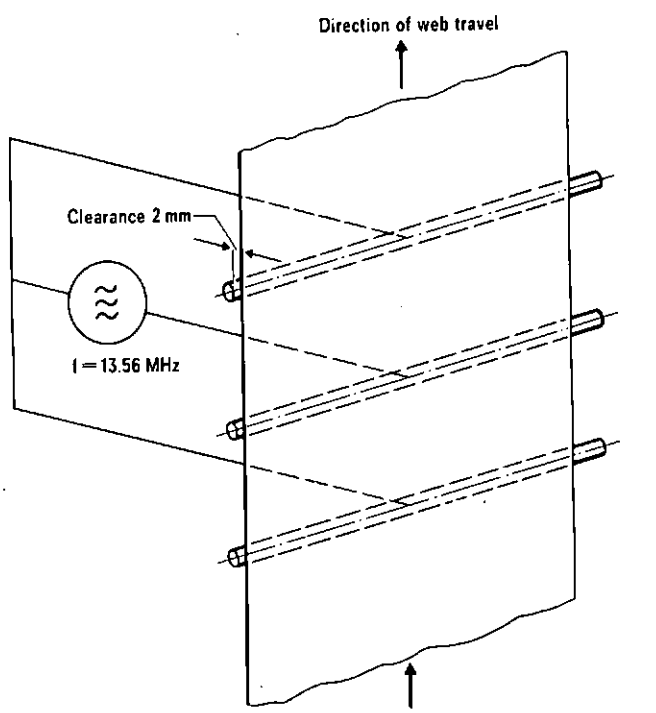

Fig. 1 RF dryer with stray-field electrodes

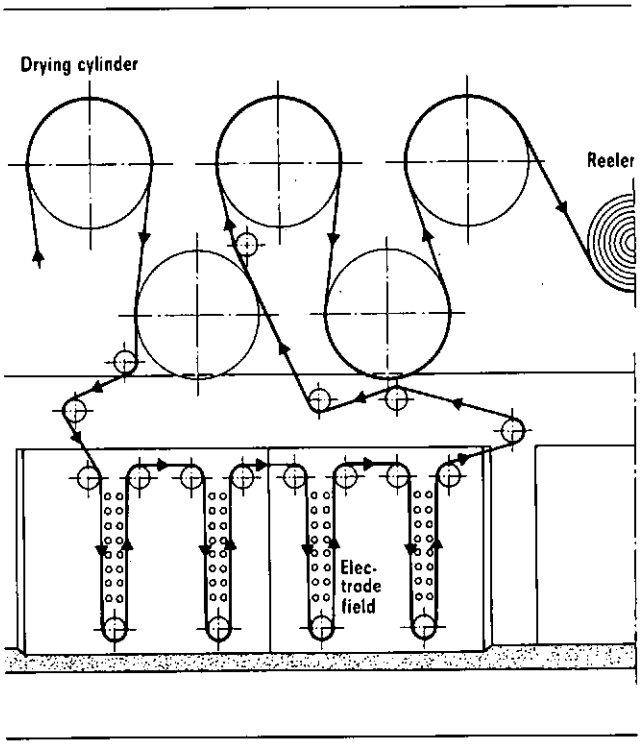

Fig. 2 Installation of the RF dryer under the cylinder dryer

Fig. 3 shows the paper dryer at the Roermond paper mill. The RF power is 900 kW with the doors open.

Since the dielectric losses are a function of the moisture content, wet areas in the paper web absorb significantly more power than dry areas. The specific evaporation power of the electrode field versus the input moisture content in the RF dryer is shown in the graph (Fig. 4). It can be seen that with decreasing RF input moisture the evaporation power decreases considerably, whereas it only diminishes slowly in the range under 10 %.

Given, for example, an RF dryer input moisture of 15 % and an output moisture of 9 %, it can be seen that the actual evaporation power at the beginning is approximately 3 times greater than with the output moisture of 9 %. The evaporation power of a cylinder dryer of the same overall length is shown for comparison.

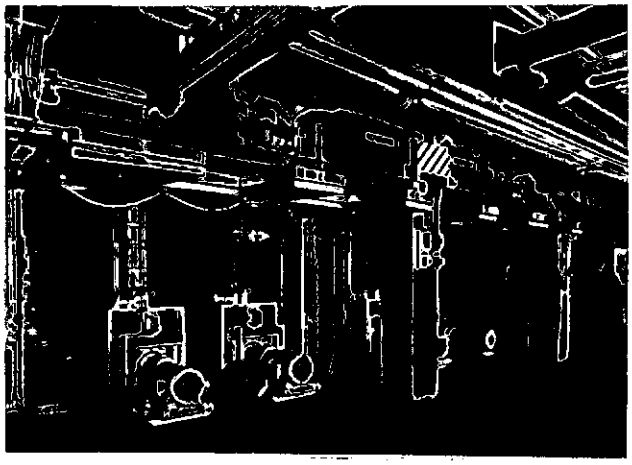

Fig. 3 RF dryer with compartment doors open

If it is now assumed that with a final moisture of 7 % on a machine, a deviation of ± 1.5 % appears in the moisture profile, the error deviation calculated on the basis of an analog model for the RF input moisture of 15 % is ± 2 %.

If the evaporation power with these deviations is considered, it can be seen that this change in input moisture of ± 2 % causes a change in evaporation power of approximately ± 10 kg_2H_2O/m^2 h at a mean value of 30 $kg\ H_2O/m^2$ h. The percentage of water evaporated increases or decreases accordingly. Variations in input moisture of approx. ± 2 % are thus reduced to variations smaller than ± 0.5 % for an RF output moisture of 9 %.

It can be clearly seen from the graph that, in order to take full advantage of the self-regulating characteristic, the RF dryer should not be located directly at the end of the cylinder drying section, since with moisture contents under 9 % there is no significant difference between the performance of the RF dryer and that of the cylinder dryer.

Drying from 9 to 7 % is thus performed by cylinders arranged behind the RF dryer.

The improved evening-out effect obtained by the RF dryer is dependent on the degree of moisture removal in the RF dryer and on the moisture-dependent power characteristic of the individual types of paper.

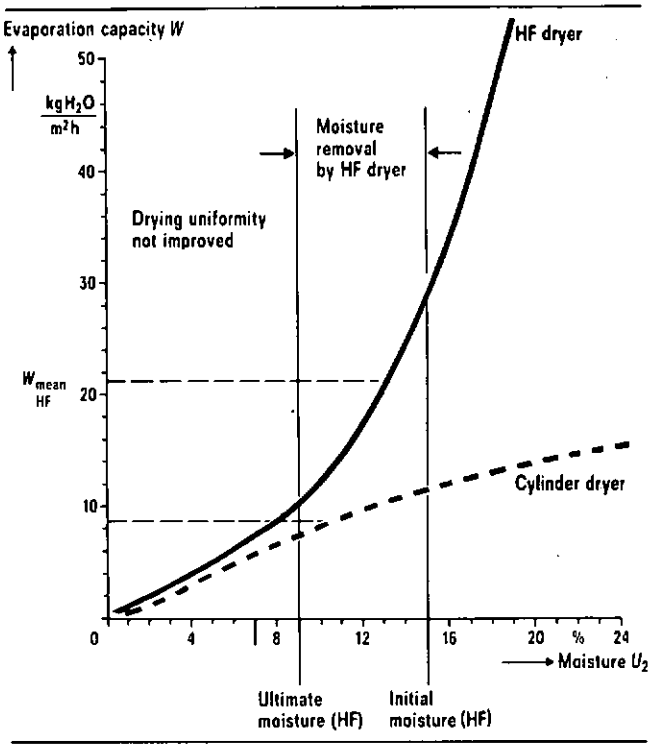

Fig. 4 Comparison of the evaporation power of RF dryers and cylinder dryers

RF dryers make it possible to attain moisture profiles with tolerance limits 2 to 3 times smaller than those attainable with cylinder dryers alone.

4. INCREASE IN DRYING CAPACITY

The upper part of Fig. 5 shows the drying characteristic of a cylinder dryer versus time. The final moisture U_4 is attained at time t = 100 %. If the steam pressure on the machine is held constant and its speed increased, the output moisture also increases. If, for example, the speed is raised by 20 % and the drying time shortened to 83 %, the output moisture rises from 9 % to 15 %. The same final moisture can now be attained by RF dryer evaporation of the difference ΔU_{HF} from 15 % to 9 % = 6.0 %.

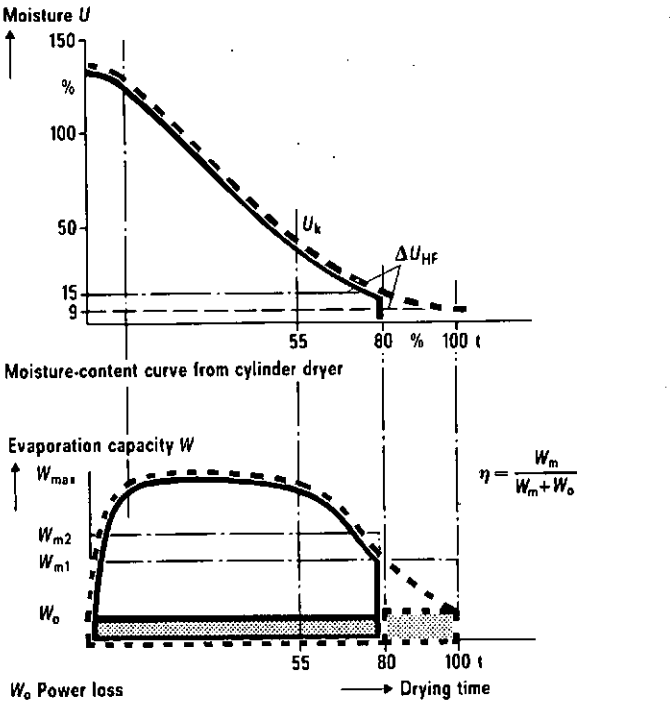

Fig. 5 Moisture curve and evaporation power of cylinder dryers

The graph below shows the curve of the evaporation power at the individual cylinders versus the drying time. It can be seen that in the first drying stage up to critical moisture U_K, the evaporation power remains practically constant and then drops in an approximately linear manner. If the drying time is now reduced from t = 100 % to t = 83 % and the output moisture increased, a higher mean evaporation power W_{m2} results from the improved heat transfer. If it is assumed that the power losses W_o as well as the maximum evaporation W_{max} do not change an improvement in efficiency

$$(\eta = \frac{W_{m2}}{W_{m2} + W_o}) \text{ is obtained.}$$

5. ENERGY CONSUMPTION AND COSTS

A comparison of the energy costs is made in Fig. 6 for the selected example. It can be seen that cost savings are made when the ratio of the cost per thermal unit of steam to electric current drops below 1 : 3.8. With a cost ratio of more than 1 : 3.8, a slight increase in energy costs can occur unless the user generates his own electricity. This increase, however, is more than compensated for by the cost-saving advantages of the RF dryer.

With capital costs of approx. DM 100 000 for the RF dryer, including reinforcement for the other parts of the machines, the invested capital is amortized in approx. 2.5 years.

The RF dryer can be installed in the cellar under the paper machine without interrupting production, so considerable savings in stoppage time are achieved in comparison with conventional dryer extension.

6. FOR WHAT KINDS OF PAPER SHOULD RF DRYERS BE USED?

As a consequence of the possible quality improvement brought about by a better moisture profile, the RF dryer is particularly suitable for:

Newsprint

Fine paper (also with a final moisture of 2 - 4 % for a subsequent coating process)

Corrugated board raw paper

Cardboard

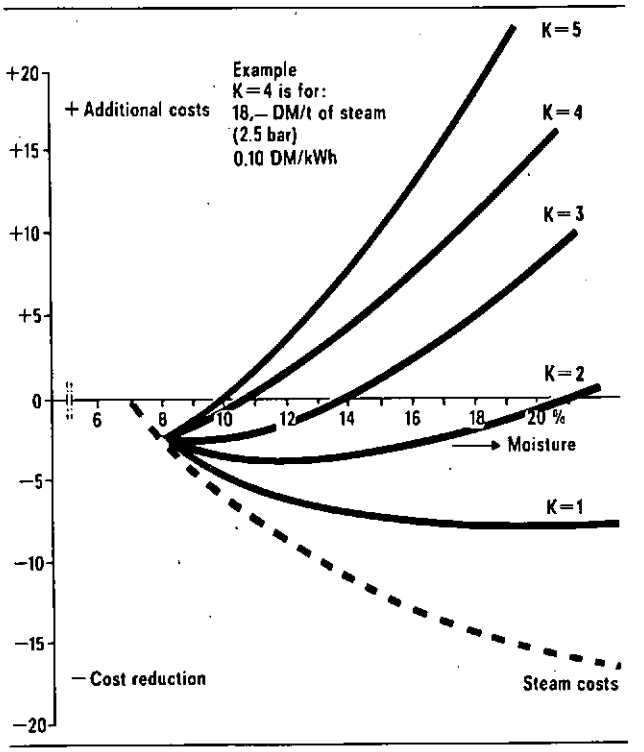

Fig. 6 Specific energy costs

Preferred basis weights are above 35 g/m^2. The overall length of the RF dryer is significantly reduced with increasing basis weight.

7. RF DRYING IN PRACTICAL OPERATION

After wide-ranging experiments at the research centre of Siemens AG and with the experience gained with a large prototype paper machine, the world's largest RF dryer with a power of 900 kW was delivered in 1977 to the Roermond paper mill in the Netherlands for a paper machine with an operating width of 5 m. The system is used to increase the drying capacity by up to 20 % and improve the moisture profile. It has been operating successfully for more than 2 years.

Fig. 7 shows a typical comparison of the moisture profile with and without RF drying.

The increase in drying capacity for a portion of the paper production is significantly higher than planned.

When a new production unit is put into operation, it is most important that the usual high degree of operating reliability of paper machines is quickly attained.

The average availability of the RF dryer in the first year of service was 97 %.

A distinct improvement in paper quality was noticed by discerning customers, so that now only this quality of paper is accepted.

8. CONCLUSION

After intensive development and testing, two years of service on a large paper machine have demonstrated that the RF dryer is a reliable and economic unit for increasing and improving paper production.

Due to its method of operation, the RF dryer for the first makes possible a significant reduction in moisture deviations in the longitudinal and transverse profile without additional means of control.

The HF dryer provides the paper manufacturer with the means of increasing his share of the market by improving product quality and raising output.

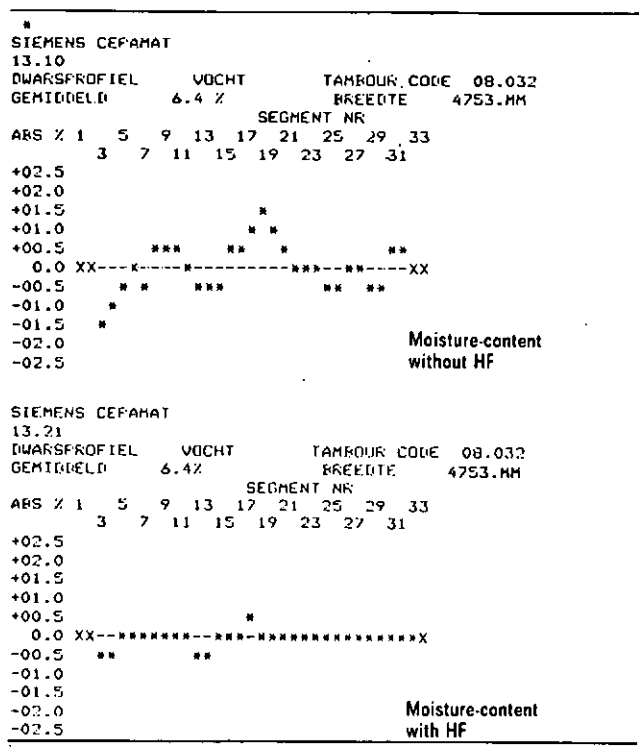

Fig. 7 Moisture profiles with and without RF

Index of figure captions for the paper RF drying on paper machines

Fig. 1 RF dryer with stray-field electrodes

Fig. 2 Installation of the RF dryer under the cylinder dryer

Fig. 3 RF dryer with compartment doors open

Fig. 4 Comparison of the evaporation power of RF dryers and cylinder dryers

Fig. 5 Moisture curve and evaporation power of cylinder dryers

Fig. 6 Specific energy costs

Fig. 7 Moisture profiles with and without RF

CHALLENGES OF DRYING THE PRINTED WEB

Nelson R. Eldred[1]
Thomas A. Fadner[2]

Graphic Arts Technical Foundation
Pittsburgh, PA

ABSTRACT

Conventional printing techniques require an ink that can be converted from a fluid to a solid in a fraction of a second after it has been applied to the web. Conversion of inks on printed webs of paper, board, plastic, or metal occur by one or more of four mechanisms: absorption, evaporation, polymerization, or solidification of a melt. Although current technology is, obviously, viable, a number of problems remain to challenge scientists and engineers. Among these are product performance, print quality, the efficient use of energy, environmental problems including pollution and health, and, always, cost.

DEFINITIONS

Letterpress: printing from a raised-image plate.

Lithography: printing from a flat plate in which the image and non-image areas are differentiated by their ability to be wet with water or by ink. Offset lithography is commonly called "offset."

Gravure/rotogravure: printing from a recessed image (engraved plates.) Most gravure printing is accomplished from engraved (rotary) cylinders.

Flexography: letterpress printing from flexible elastomeric plates.

INTRODUCTION

Printing is done either with sheetfed or with web processes. Sheetfed inks dry by a complicated chemical reaction, but web inks dry by simpler, physical processes. Web printing is a continuous, in-line operation. Web printing has the advantages of economy and speed, while sheetfed printing offers greater versatility and adaptability. In printing, as is generally true throughout industry, economy and speed tend to drive out versatility. Effectively all of the gravure printing and about two-thirds of lithographic printing in North America is now done on the web press.

In printing a web by lithography, the printer must not only have an ink that works with water and transfers properly to the substrate, but he must apply energy to the ink to dry it, he must chill the melted ink film to solidify it, and he must be concerned about the solvents that are evaporated. All of this must be done rapidly. Web speeds of 1000 feet per minute (5 meters per second) are common in lithography and speeds of 2000 feet per minute (10 meters per second) are common in gravure.

The printing ink business is a relatively small volume business, only $1,100 million in the U.S. in 1978, and little research has been carried out. Most of the knowledge of printing inks has been generated by people or companies interested in paints. Printing, by itself, has likewise supported very little basic research. Most of the new technology used in printing has come from other industries. This is the first challenge: more basic research is needed in drying processes and especially in the very rapid transformation of liquids to pseudo-solid phases.

Compounding the problem is the fact that much of the color printing that is turned out is done by "process color" in which various amounts of four different inks: yellow, magenta, cyan, and black are laid down on a web or sheet to create the appearance of all colors.

Stability is also required in the ink. The desired stability requires a liquid ink that becomes solid after it has been applied to paper, paperboard, metal, or plastic, but remains a stable liquid on the press. Dry toners (powders) that are dry before they are applied to paper have not yet proved practical for commercial printing. Therefore, we must solidify the liquid ink by evaporation or by chemical reaction.

Chemical reactions requiring several minutes to a few hours for completion are well known in printing inks and in paints, but they are not suitable for printing webs. Drying or solidification times of less than one second are required, after which the printed web will be folded, perforated, die cut, sheeted and otherwise handled as it comes off the press.

Other problems including press performance, end-use requirements, and environmental requirements must also be solved, presenting additional challenges to the chemist and to the engineer.

At the present time, inkmakers and printers take advantage of five different drying mechanisms and combinations of them to meet these needs.

ABSORPTION

News inks used for letterpress do not really dry, but as the liquid, mineral oil portion of the ink is absorbed by the paper, the pigment becomes sufficiently immobile to preserve the image for the relatively short lifetime that the product must serve.

In the narrowest sense, there is really no drying problem with news inks, but there is an end-use problem. Letterpress news inks are primarily a dispersion of carbon black in a hydrocarbon oil, and this provides no mechanism for true drying or curing. The ink is easily rubbed off from the paper. Any commercial success in eliminating rub-off must be achieved at a low price, equivalent to that of carbon black and hydrocarbon oils. Newspaper publishers are unwilling to pay for already available inks that will solve the problem at a greater cost. Other printed products require at least some rub resistance, and although there is no drying problem, news inks are not acceptable for other products.

In addition to letterpress, newspapers are printed by web offset and rotogravure. News inks for printing by web offset resemble letterpress news inks. The inks have a higher level of pigmentation and consequently sell for a higher price. Rotogravure inks used to print Sunday supplements and long-run magazines printed on uncoated paper, contain a film-forming resin dissolved, usually, in a hydrocarbon oil. Because they are formulated differently than letterpress news inks, web offset and rotogravure news inks offer at least some resistance to rub-off.

The challenge with the absorption mechanism is to provide a low-cost ink that does not rub off. It should be obvious that such an ink will find uses far beyond the printing of newspapers. An ink that dries by absorption to form a rub-resistent film would help overcome problems of air pollution and the use of expensive energy, problems characteristic of other printing processes.

One promising solution is to provide water-based inks. There are two challenges that must be met: the relatively large amount of water used to dissolve the binder causes problems when water is absorbed by the paper, and a low-cost, high-performance, water-soluble binder is required. Water soluble binders generally have given printed ink films with poor gloss. Furthermore, although water-soluble inks overcome air pollution problems, they are not useful in lithography and they require large amounts of energy for drying on most substrates.

EVAPORATION AND SOLIDIFICATION

With the exception of most news inks, all inks contain a film-forming binder which holds the pigment in place on the web thereby preventing rub-off. Some ink binders, such as nitrocellulose are precipitated as a solid when the solvent evaporates. Hydrocarbon resins and modified rosins used in web letterpress and web offset inks are liquids when the web leaves the drier, and the print must be solidified by passing over chill rolls.

Most of the ink that is printed on paper webs is dried by evaporation and solidification, parts of a mixed mechanism to be considered in more detail later. Printed flexible packaging, such as polyethylene or cellophane, is usually dried simply by evaporation. Freezing, solidification, or "cold setting" may also be required depending on the nature of the binder, the substrate, and the boiling range of the solvent.

Gravure and flexographic inks are dried by evaporation at relatively low temperature, often by steam heat. A dryer is used after each color is applied. Lithography and letterpress involve paste inks that require extensive working of the ink on open rollers on the press to enable transfer of a thin film to the substrate. For this reason, the solvents must not have significant volatility at room temperature, and consequently, web offset lithography and letterpress require higher temperatures to dry than gravure and flexography. Webs printed by lithography and letterpress are dried after all of the colors have been printed. The amount of energy required to dry litho and letterpress webs has been greatly reduced by improved design of high-velocity hot-air dryers. Heat exchange units further reduce the energy requirements for drying.

Flexographic and rotogravure presses are relatively closed, and the inks can contain solvents that evaporate fairly rapidly at room temperatures.

After they have been printed, they evaporate readily with the use of little energy, but it it is difficult to recover the solvents to prevent air pollution problems. Gravure inks are printed from a metal cylinder and often contain ester or ketone solvents to improve adhesion to plastic substrates. Flexo inks are printed from rubber or metal plates and must not contain solvents that swell or dissolve the plate. Water and alcohols are appropriate solvents, acceptable under governmental guidelines. In these cases, shellac, styrene-maleic resins and other alkali-soluble polymers are used as binders. Water-based systems are attracting attention currently and provide immediate, major challenges. The challenges in printing with flexo and gravure inks are to develop practical means for solvent recovery, to find improved water-based inks, to develop water-resistant paper, or perhaps to develop a satisfactory water-based driographic ink. ("Driography" is a planographic printing process in which the plate itself resists wetting and therefore does not require a water phase to separate the image from the non-image area.)

POLYMERIZATION

Thermally reactive inks have been used for printing paper and board. For instance, modified isocyanates, activated with heat, provided one mechanism for the process. The inks showed poor working properties, they yielded low-gloss films, but they showed good scuff resistance. Basic thermodynamics is the challenge: how can we make an ink that will remain stable in the can and on the press and yet react in a fraction of a second when it is warmed to a temperature that will not damage the paper?

Use of infrared radiation to polymerize inks on the web is not yet successful owing to the relatively low energy levels of infrared radiation. Radiation in the near infrared, which is the most energetic, is abosrbed differently by inks of different colors. Black prints can be charred while yellow prints are scarcely warmed. If we are to apply infrared more broadly, we must find a route around these impasses.

It should be noted that, in sheetfed printing, infrared radiation provides heat that speeds up the slow oxidative drying reaction.

Polymerization of acrylic oligomers with ultraviolet rays or electron beams has caught the fancy of the chemist, and, in fact, a fair amount of printing is dried or cured in this manner. In 1975, there were 27 web offset presses in North America equipped with ultraviolet driers.

One of the chief uses of radiation-initiated polymerization is the printing of cans for packaging soft drinks, beer, and aerosol sprays. Acrylic varnishes, applied to printed paperboard or cans and cured with UV, provide high gloss and resistance to scuffing, abrasion, chemicals, and oily products. The ultraviolet radiators are fairly expensive when the entire equipment package is considered, and the radiator must be shielded to protect the crew from the ultraviolet rays and ozone. In addition, the inks are two to three times as costly as conventional inks. One of the most serious complaints is that of skin sensitivity to the acrylic formulation.

Because little energy is required to initiate this reaction, the amount of energy required is significantly less than that required to dry evaporative inks, but the cost of electrical energy often outweighs the savings of the energetically efficient UV system. In metal decorating (printing of metal cans), savings are substantial, but most UV systems waste large amounts of energy as heat, and herein lies an additional challenge.

Electron beam generators are more expensive and more hazardous than ultraviolet lamps. Owing to their high electron energy, electron beams generate X-rays and large quantities of ozone, and workers must be protected. Photoinitiators, incorporated into ultraviolet curing inks, are not required for the higher-energy electron beam systems, and the inks are, correspondingly, somewhat less costly. The chief benefit of electron beam curing resides in its penetrating power which cures thick films or films on both sides of the sheet of paperboard. The unit would allow simultaneous curing of several webs at once if there were any practical way of feeding such webs past the electron beam.

We know of one electron beam unit installed on a printing press in North America on sheetfed equipment, and there is one being installed on a web-fed paperboard press.

The electron beam is generated in a curtain rather than as a scanning electron beam, and it produces a beam of a few kilovolts intensity. It takes relatively little power to operate the unit. This approach is a high-capital, low-energy response to the challenges in drying inks on a printed web.

GELATION

Most inks used for printing paper webs depend on gelation as part of the mechanism for converting the liquid to a solid. A gel varnish is incorporated into the ink formulation, and sufficient

solvent is added to reduce its viscosity enough to give good press performance. When the ink reaches the paper, the solvent is absorbed by the sheet, and the gel structure in the ink recovers rapidly giving a "quick-set" ink, but the body or viscosity is far too low to provide a "dry" sheet.

New acrylic resins showing limited solubility in heatset oils are used to provide quick setting, that is, quick formation of a near-solid gel structure on the paper surface. Heatset oils are low viscosity, fractionated hydrocarbon solvents, used to formulate lithographic inks for web printing.

The challenge is to use this gel mechanism and to provide rub resistance without using heat and without the expense of radiation curing.

MIXED MECHANISMS

As a matter of fact, most inks dry by a combination of the preceding mechanisms. When paper or paperboard is printed, absorption almost always plays a role, and gelation is used increasingly to provide quick setting. The solvent evaporates, and letterpress or web offset prints are often chilled to solidify the ink.

Disposal of the solvent is troublesome, regardless of the printing method. It has been common practice to use afterburners to incinerate solvents from web offset heatset inks, but use of natural gas to burn valuable solvents has obvious drawbacks. Solvent recovery and heat recovery present challenges to the printer and the equipment manufacturer.

The Graphic Arts Technical Foundation has conducted a major, confidential, study of heatset web offset drying to describe and measure low-energy alternatives to heatset drying.

Rotogravure and flexographic printing have the advantage of drying rapidly at modest temperatures, but this causes solvent-recovery problems which are now plaguing the package printing industry since new government regulations prevent discharging even small amounts of these solvents into the air. Low boiling solvents are especially difficult to recover economically. This problem is complicated because many different solvents are frequently used in many small printing plants. Recovery, collection and separation of small batches of mixed solvents from many plants is not an attractive opportunity. The challenge here goes far beyond thermodynamics and engineering and includes environmental problems.

SUMMARY

Although it is one of the nation's largest, the printing industry has lagged in the application of new technology. There are many opportunities, including opportunities to improve the performance of printing inks. Challenges of drying the printed web include:

Conduct more basic research in drying processes, notably in rapid transformation of a liquid to a solid film.

Develop inks that remain liquid on the press but dry quickly when they are applied to a substrate.

Develop low cost inks that show good resistance to rubbing.

Discover low-cost, high-performance water-soluble binders.

Develop inks that cause no air-pollution problems.

Find low-cost, low-energy solutions to ink drying.

Find better ways to recover solvents from rotogravure inks.

A NEW VACUUM-DRYING METHOD FOR PAPER, BOARD AND OTHER PERMEABLE MATS

J.A.Lehtinen

Tampella Engineering Works, Tampere, Finland SF-33101

ABSTRACT

A general description of a new vacuum drying method for paper, and other permeable webs, is given. Experiments are described for determining the drying rates obtainable under various drying conditions and for different webs, as well as for determining the effects of the drying process on the web quality.

When the heating surface temperature is 175 C, with 300...450 g/m^2 board the drying rate is 150...200 kg/(h·m^2) if the web is dried from 40 % to 91 % dry content. While drying, the web presses onto a hot metal surface with almost the pressure of the atmosphere. Thus, there is a loss of web bulk relative to normal cylinder drying, but there is also a considerable increase in bond. The fibers pressed against the hot surface flatten and weld together. Consequently, improved surface smoothness and strength are obtained, and the stiffness of board grades increases appreciably. As the web dries being held fixed in the MD- and CD-directions, much more web isotropy is obtained than in webs dried under MD-tension.

A possible construction for a commercial paper machine dryer is presented. Drying economics that would result from its use are considered.

INTRODUCTION

The principle of drying in a near vacuum has been applied to the drying of paper on a commercial scale in the Minton Vacuum Dryer. Several of these were built for paper and pulp machines about 50 years ago, but to the author's knowledge only some Minton pulp dryers are still operating. Although the vacuum ambient of the Minton improved the drying rate in an otherwise ordinary cylinder dryer section to the extent that the total length of the dryer section was reduced to about a quarter of the normal, there were difficulties. The vacuum hood was massive, expensive, and clumsy. There were sealing problems, and problems with sheet breaks.

In any evaporative drying process heat must be supplied to the evaporating water, and the generated vapor must be carried away. In order for the drying process to be rapid, the resistances to both of these constituent processes must be low. In vacuum drying the molecules that are able to leave the liquid phase are much less liable to be bounced back into the liquid as a result of a molecular collision in the surrounding gas phase, than are those escaping molecules when the partial pressure of air in the ambient is high.

The purpose of this presentation is to describe a new vacuum drying method for permeable webs or mats, and to consider its potentialities on an industrial scale. Basically, the transfers of heat and mass occur in this new vacuum drying process (Fig. 1) almost as in the so-called heat pipe, with the exception that the condensate is not allowed to move back to the evaporation zone, while in the heat pipe this movement is necessary for continuous operation.

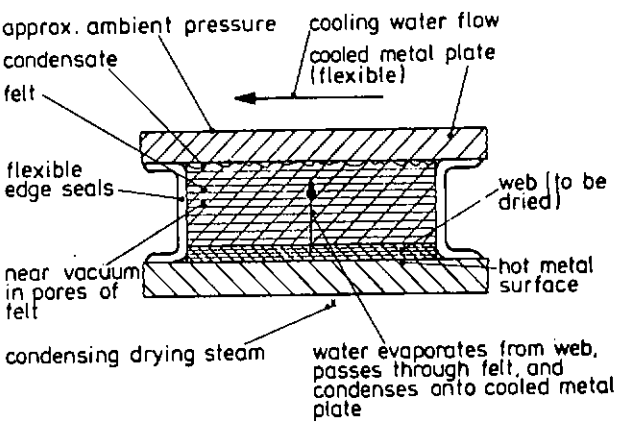

Figure 1 Principle of Convac Drying

In this new process the wet web is placed on a heatable metal surface. Onto the web is placed a permeable felt or mat, which is then covered by an impermeable metal sheet. Before the drying process starts, air is removed from the pores of the wet web and from those of the felt to as great an extent as practical. The metal sheet on top is cooled from the outside. When the heatable metal surface is heated, water readily evaporates from the wet web into the surrounding near vacuum. The vapor passes through a portion of the web, and through the felt, and condenses onto the cooled metal sheet. The small amount of air remaining in the "sandwich" between the heated metal surface and the cooled metal sheet collects to a layer next to the condensate on the cooled metal sheet. While the drying process is going on, the pressure in the pores of the felt is mainly determined by the temperature of the cooled metal sheet. Thus, a quite low pressure prevails. This means that the web is being pressed onto the heated metal surface with almost the pressure of the atmosphere.

Consequently, very good thermal contact is obtained between the heated metal surface and the web lying on it. Also, this same pressure causes more fiber to fiber contact points, and more contact area, to be formed within the web, and results in a higher effective thermal conductivity for the web, as well as in web strength improvement.

As the vacuum between the hot surface and the cold plate is being maintained by continuously condensing the vapor that evaporates from the web, one may think of the operation as "vacuum maintained by condensation". For this reason a working name for the drying process involved has evolved as CONVAC drying. That name will be used in the following.

The fact that thick, wet webs, or thick, wet mats of porous material, dry so rapidly with the Convac method is very attractive from the practical, economic, viewpoint. In order to reach such drying rates as to be able to compact the drying section onto a single, 6.2 m diameter drying cylinder, it will be necessary to use surface temperatures in the range 170...180 C. This high a temperature causes welding of the surface fibers together, as well as the usual flattening collapse of those fibers, also experienced at lower temperatures. Experiments have been carried out to determine some of the effects of this surface welding, and will be described.

The generally very positive effects of the Convac drying process on the qualities of newsprint and of board grades are probably attributable to the factors just discussed above, as well as to the increased number and strength of fiber to fiber contacts within the web. The improved isotropy of the web in the MD- and CD-directions is also a valuable result.

A negative feature is the one-sidedness of the web dried with the process. One side of the web faces the heated smooth metal surface, the other the relatively cool felt or permeable mat, which marks the side of the web facing it. In an industrial process it is thought that the web can be passed first over one drying cylinder with one side facing the cylinder, and then over another cylinder with the other side facing the cylinder, if the same smoothness is desired for both sides.

The design that has been worked out for a commercial Convac dryer must, no doubt, be further evolved on the basis of operating experience from a full-speed, narrow test machine, yet to be built. In Fig. 2 is shown an outline of what the dryer may look like.

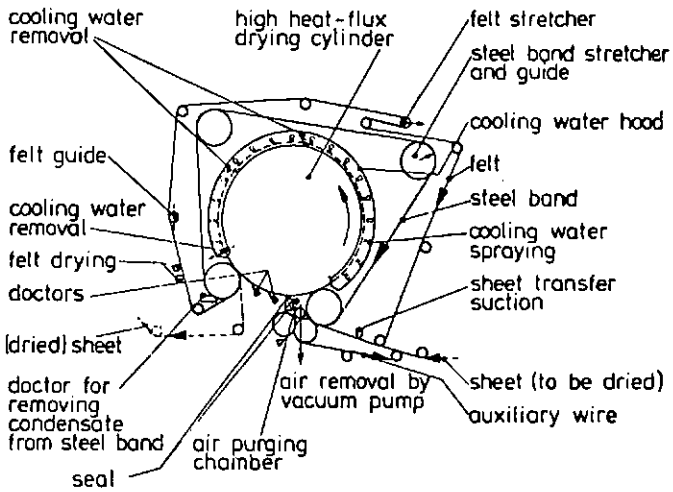

Figure 2 Proposed Commercial Convac Dryer

In order to reach cylinder surface temperatures in the range 170...180 C, one would have to use steam pressures inside the cylinder in the range 0,8...1,05 MPa. From the economic viewpoint this would mean a loss in the available turbine power, as the back pressure exhausted by the turbine would have to be raised from its usual level. However, the heat losses from the Convac drying section would be much smaller than they are today. Overall, the cost of the steam for drying would be in Convac drying slightly less than, or about equal to, what it is today, depending on the grade being dried.

STATIC EXPERIMENTS

Static laboratory experiments to determine drying rates and quality effects were carried out using the device of Fig. 3.

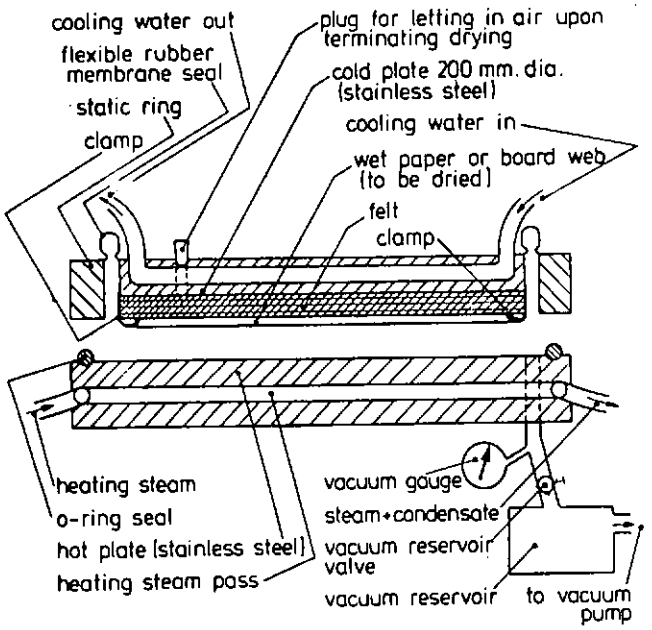

Figure 3 Laboratory Static Convac Dryer

The hot plate, with nothing on it, is first heated up to temperature. The felt, or other permeable mat, is placed onto the underside of the cold plate (with cooling water passing through continually), and the wet web onto the underside of the felt. Both are fixed into place by means of small, flexible, side clamps on the cold plate. The assembly consisting of the just described "sandwich" and the encircling static ring is then lowered onto the hot plate. The cold plate can move up and down like a piston inside the encircling static ring. At the instant when the O-ring seal touches the static ring, the vacuum reservoir valve is opened. Air is thus sucked out of the space between the hot and the cold plates, the web is pressed against the hot surface, and drying begins. The vacuum reservoir valve is closed after three or four seconds (when a steady vacuum level has been reached in the drying space), but it makes no noticeable difference on the drying rate whether the valve is thus closed, or remains open for the duration of drying. The wet web sample and the felt have in the tests always been of nearly the same diameter as the cold plate. Thus, the pressure with which the web is being pressed onto the hot plate during drying has been nearly the atmospheric minus the pressure in the drying space.

For terminating drying a hole in the cold plate is opened, letting ambient air into the drying space, and the assembly of parts above the hot plate is lifted off.

The water which has evaporated from the web is now mostly on the cold plate, and in its immediate proximity in the felt.

It has been roughly determined that if the air partial pressure remaining between the hot and cold plates is higher than 8 kPa, there is already a noticeable decrease in the drying rate. No quantitative values are available. The evacuation arrangement used (normally) brings the air partial pressure down to the range 4...6 kPa, and no drying rate variations have been observed within this range. There are factors which influence the drying rate much more than these variations in the air partial pressure.

DRYING RATE RESULTS

Fig. 4 gives measured drying rate results for paper and board as total drying time vs. surface temperature when drying from 38 % to 91 % dry content. There is an effect of the freeness of the stock that should be taken into account, as well as an effect due to the pressing history of the web. No quantitative results are yet available in this connection.

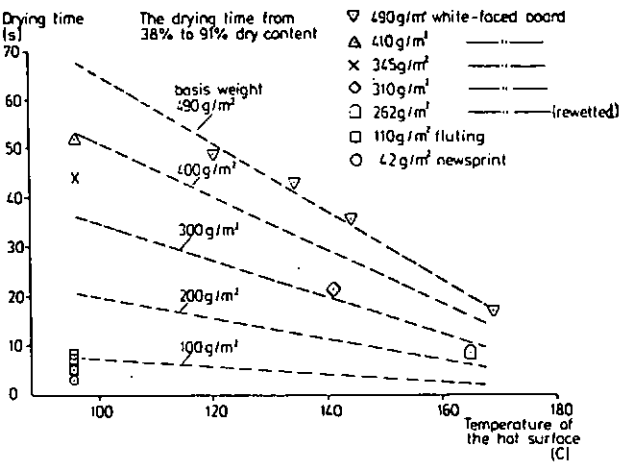

Figure 4 Convac Drying Time for Various Grades As Function of Surface Temperature

For 320 g/m^2 board and 100 C surface temperature the Convac drying time is about 1/3 of that measured on a real board machine with ordinary drying cylinders and ventilation (the drying time meaning time in cylinder contact). With practical applications in mind, however, it may be noted that if 170 C surface temperatures can be used, the Convac drying time

drops to about 1/4 th of what it is at 100 C, and would, then, be about 1/12th of that in an ordinary drying section with 100 C cylinder surface temperatures.

The test points in Fig. 4 each represent the average of several (usually more than 4) drying tests. The tests done with the light grades - fluting and newsprint - give a very unreliable drying time due to difficulties with the static drying apparatus. Namely, after the web has touched the hot surface it takes a few seconds before fully effective drying occurs. This is due to the slow air removal from the felt. Similarly, it takes about a second for the air to rush in upon termination of drying. As the amount of air strongly influences the drying rate, and as the total drying time for 50 g/m^2 paper with 95 C surface temperature is 3...4 seconds, the error ensueing is very great. For the 490 g/m^2 board points the error is less than ± 5 %.

Fig. 4 has been constructed by first fairing a curve on a separate graph through the data points at 95 C. The terminal points, with the hot surface at 95 C, of the curves on Fig. 4 are from that curve. Then, after drawing a curve on Fig. 4 through the 490 g/m^2 data points, the other b.w. curves have been drawn, assuming that the same proportionality is maintained between them as at the surface temperature of 95 C.

In no test with newsprint has there been difficult adhesion of the web to the drying surface even with drying times as short as 0.3 s. There has been some adhesion of the board grades, but only when the sample web has not been dried to the terminal 91 % dryness.

EFFECTS OF CONVAC DRYING PROCESS ON PAPER AND BOARD PROPERTIES

For evaluating the effects of the Convac process on web properties, wet web was obtained directly from the appropriate location in a paper or a board machine. Simultaneously, a comparison sample was taken from the dry end of the machine, both before the calender section and from the reel, with all coating, sizing and glueing operations turned off.

To begin the survey, a test series will be described, the purpose of which was to test two hypotheses. Firstly, it was believed that when using high surface temperatures in the Convac process, welding together of the surface fibers would occur on the web surface contacting the heating surface. This hypothesis had already been supported by the fact that when drying board from press section to reel dryness, much higher stiffness values had been obtained with the surface at 141 C than at 95 C.

Secondly, it had been observed that with higher surface temperatures worse web surface smoothness was obtained. This was believed to be principally due to supersaturation vaporization explosions in the capillary water on, and near, the web surface. There should be more of these explosions, and they should be stronger, at higher metal surface temperatures - causing the observed higher Bentsen roughness values. This hypothesis was strongly corroborated by the more "pot-marked" appearance (under microscope) of the Convac dried board surface obtained with higher metal surface temperatures.

In order to check the above hypotheses, white-faced board web of 365 g/m^2 b.w. was taken leaving the press section of a board machine at 38 % dry content. Three series of tests were run on the static Convac dryer with this web: series A, in which the drying was done with the white side facing the hot metal surface for 30 s; series B, with the gray side first facing the metal for 10 s, and then the white side for 20 s; and series C, with the gray side facing for 15 s, and then the white side for 15 s.

In some tests (marked with the letters IH in Table Ia) of series B and C the white surface was pressed lightly (as on an ordinary drying cylinder) against a smooth metal surface at 100 C for 3...4 s between the Convac dryings. A comparison series V was dried on an ordinary laboratory drum dryer from 38 % dryness for 2 h. Table Ia gives the results.

In Table Ib the caliber, stiffness and tensile values of Table Ia have been corrected for deviations in b.w. to the same standard b.w. of 365 g/m^2. The correction has been done assuming stiffness to be proportional to the third power of b.w. This is roughly correct if the bulk remains constant. In Table Ic the stiffness results of Table Ib have been corrected to the same standard caliper of 0,600 mm, again assuming stiffness proportional to the third power of caliper.

It is evident from the Bentsen roughness values of Table Ia that the predrying of the white side of the web (the IH-runs) at 100 C before being pressed against the Convac dryer's metal at about 145 C greatly improves the final white surface smoothness. This supports the hypothesis about the vaporization explosions, since the predrying drives capillary water away from the white surface into the inner regions of the web.

Table Ia Test Results for 365 g/m^2 White-faced Board with the Static Convac Device

Note: In the "Sample" column the numbers in parentheses correspond to Convac drying time with the gray side facing the hot surface and the white side facing the hot surface, respectively. IH between the numbers means that the white side of the board has been pressed lightly for 3...4 s against a metal surface at 100 C. The Comparison series has been dried on a laboratory drum dryer for about 2 h.

Sample	Metal surface temp. C	Bas. wt. g/m^2	Caliper mm	Bulk factor cm^3/g	Roughness Bentsen 75 wg ml/min	Stiffness (Taber) mN·m MD	CD	Ratio	Tensile strength kN/m MD	CD	Ratio
Series A	about										
A1(0-30)	147	362	0,552	1,52	430	29,4	13,5	2,18	24,5	9,8	2,50
A2(0-30)	147	361	0,553	1,53	415	25,8	16,2	1,59	24,7	10,5	2,35
A3(0-30)	140	357	0,539	1,51	425	28,4	14,7	1,93	23,8	10,4	2,29
Series B											
B1(10-20)	140	364	0,541	1,49	>500	28,2	13,5	2,09	24,5	9,9	2,47
B2(10-IH-20)	145	357	0,530	1,48	210	29,7	14,2	2,09	24,3	11,1	2,19
B3(10-IH-20)	148	358	0,547	1,53	330	28,7	15,5	1,85	25,2	10,8	2,33
Series C											
C1(15-15)	140	357	0,532	1,49	>500	28,4	13,3	2,14	24,8	10,7	2,32
C2(15-IH-15)	140	360	0,532	1,48	280	30,2	15,5	1,95	22,9	9,9	2,31
C3(15-15)	145	361	0,549	1,52	>500	27,7	13,5	2,05	24,2	10,3	2,35
C4(15-IH-15)	145	357	0,536	1,50	290	29,7	14,5	2,05	23,4	10,3	2,27
Comparison Series V											
V1	100	378	0,678	1,79	>500	34,5	17,4	1,98	20,7	8,2	2,52
V2	100	376	0,677	1,80	>500	33,6	16,2	2,07	19,4	8,1	2,40
V3	100	378	0,687	1,82	>500	35,0	15,4	2,27	20,8	8,1	2,57
V4	100	379	0,703	1,85	>500	37,0	17,2	2,15	20,9	7,5	2,79
V5	100	379	0,698	1,84	>500	36,3	16,4	2,21	21,5	7,7	2,79

Table Ib The Calipers, Stiffnesses, and Tensile Strengths of Table Ia Corrected to the Same Basis Weight (365 g/m^2)

Sample	Caliper mm	Stiffness mN·m MD	CD	Tensile strength kN/m MD	CD
A1	0,5566	30,14	13,84	24,70	9,88
A2	0,5591	26,67	16,74	24,97	10,62
A3	0,5511	30,35	15,71	24,33	10,63
Av.		29,05	15,43	24,67	10,38
B1	0,5425	28,43	13,61	24,57	9,93
B2	0,5419	31,74	15,18	24,84	11,35
B3	0,5577	30,42	16,43	25,69	11,01
Av.		30,20	15,07	25,03	10,76
C1	0,5439	30,35	14,21	25,36	10,94
C2	0,5393	31,48	16,15	3,22	10,04
C3	0,5550	28,62	13,95	4,47	10,41
C4	0,5480	31,74	15,50	23,92	10,53
Av.		30,55	14,95	24,24	10,48
Comparison Series V					
V1	0,6547	31,06	15,67	19,99	7,92
V2	0,6572	30,74	14,81	18,83	7,86
V3	0,6634	31,51	13,87	20,08	7,82
V4	0,6770	33,05	15,36	20,13	7,22
V5	0,6722	32,42	14,65	20,71	7,42
Av.		31,76	14,87	19,95	7,65

Table Ic The Stiffnesses of Table Ib Corrected to the Same Caliper (0,600 mm)

Sample	Stiffness mN·m MD	CD
A1	37,75	17,34
A2	32,96	20,69
A3	39,17	20,27
Av.	36,63	19,43
B1	38,46	18,41
B2	43,08	20,60
B3	37,88	20,46
Av.	39,81	19,82
C1	40,74	19,08
C2	43,35	22,24
C3	36,16	17,63
C4	41,66	20,34
Av.	40,48	19,82
Comparison Series V		
V1	23,91	9,28
V2	23,39	11,27
V3	23,31	10,26
V4	23,01	10,69
V5	23,06	10,42
Av.	23,34	10,38

Table II Effects of Convac Drying on 306 g/m^2 White-faced Board; Drying Surface at 141 C

Property	Convac-dried. In parentheses b.w. corrected (to 306 g/m^2)	Normally dried (in machine) Before calender BC	Normally dried (in machine) After calender AC	% change resulting from Convac-drying (using b.w. corrected values) Compared with BC	% change resulting from Convac-drying (using b.w. corrected values) Compared with AC
Basis Weight (g/m^2)	303,6	306	305		
Bulk. fact. (cm^3/g)	1,55	1,55	1,41	0,0	+ 9,9
Stiffness (mN·m)					
MD	16,5 (17,1)	16,2	14,7	+ 5,6	+ 16,3
CD	7,6 (7,8)	6,0	5,4	+ 30,0	+ 44,4
Ratio	2,14 (2,17)	2,72	2,72		
Tensile Str. (kN/m)					
MD	16,7 (16,9)	19,8	20,7	- 14,6	- 18,4
CD	7,7 (7,7)	6,7	6,8	+ 14,9	+ 13,2
Bond (Scott) (J/m^2)	196	165	140	+ 18,8	+ 40,0
Burst (Mullen) (kPa)	652 (660)	675	685	- 2,3	- 3,6
Stretch (%)					
MD	2,7	2,0	2,1	+ 35,0	+ 30,0
CD	3,2	3,8	3,9	- 15,8	- 17,9
Roughness (Bentsen) 150 wg with wt.	> 500	245	100		

Table III Effect of Convac Drying on 66 g/m^2 Newsprint with Drying Surface at 172 C

Property	0 normal drying	a 2-sided Convac	b 1-sided Convac
Bas. wt. (g/m^2)	66,5	64,7	67,2
Opacity (%)	95,9	95,5	96,2
Light Scatt. Coeff. (m^2/kg)	65,1	65,3	67,2
Tens. Index (N·m/g)			
MD	35,6	36,3	
CD	14,8	16,9	15,9
Stretch (%) MD	1,2	1,4	
CD	1,5	1,9	1,5
Tear Index (mN·m^2/g)			
MD	4,89	4,95	
CD	6,56	6,36	6,49
Burst Index (kPa·m^2/g)	1,22	1,34	

In Table Ic, in which the deviations due to b.w. differences and caliper differences have been removed, one can readily see the greatly beneficial effect that Convac drying has on the structural strength in comparison with drum drying. This strength improvement is most likely due to both welding of the surface fibers together, and to more and stronger interfiber contacts within the web. Adding together the MD- and CD-values of stiffness in the A, B, and C-series in Table Ic one can see that there is, indeed, an improvement in stiffness due to drying the web two-sidedly against the hot metal surface (B and C) relative to drying it one-sidedly (A). This follows, naturally, if the surface fibers weld together.

Although the number of samples in the above tests has been quite small, it is believed that the trends brought out in the discussion are sufficiently definite to be qualitatively accepted.

In Table II is given a comparison of results between Convac dried 306 g/m^2 white-faced board, taken at 39 % dry content leaving the third press, and comparison lots taken at the same time before the calenders, and at the reel. Every value in Table II is the average of at least eight test results. The Convac dryer surface temperature was about 141 C, and the drying time varied, 18...22 s. In every case a final dry content above 93 % was

reached.

There is a strong increase in the stiffness, and especially in the CD-stiffness, that results from the Convac-process, in comparison with normal cylinder drying. There is also a very strong increase in the bond. These may be explained as being a result of the greater number of, and stronger, inter-fiber bonds within the web. The changes in the tensile strength and in the stretch may be explained as being principally due to the web being fixed laterally while drying. More nearly equal values are thus obtained in the MD- and CD-directions - also stiffness values.

Table II shows that poor smoothness is obtained with the Convac process at this temperature. As was explained in connection with Table Ia, it is possible to improve the smoothness a great deal by predrying the web surface at a relatively low temperature.

In other tests it was determined that if the Convac dryer surface temperature is 95 C instead of 141 C as for Table II, the Convac process does not fare nearly as well in comparison with ordinary cylinder drying, as far as strength values are concerned. The CD-stiffness increases by roughly 30 %, but the MD-stiffness decreases by 20 %, when compared with the reel sample. Similarly, the bond only increases by about 20 %. The smoothness, in contrast, is almost as good directly out of the Convac dryer as that of the calendered sheet from the reel.

No board web strength or smoothness results are so far available with the Convac drying surface temperature at the level 170...180 C, where, it is visualized, it would be in a commercial dryer.

Results (Table III) at the high-temperature level have been obtained, however, for newsprint. The Convac hot surface temperature was 172 C. Each value in column a, which is for two-sided Convac drying, is the average of about 8 tests, while the values in column b, which is for one-sided Convac drying, stand only for 2 tests. The comparison samples were taken from the same lot leaving the 3rd press as were the Convac samples.

The comparison samples were dried in an ordinary, though slow, laboratory cylinder dryer section, and were taken to be measured uncalendered. The results appear in column 0.

For making the tests of column a it was necessary to dry the web first from one side in the Convac device for as short a while as possible: usually about 0,3... 0,7 s. The web was then turned over and dried from the other side for about 1,0... 1,3 s. The web was always finally superdry. Only thus dried samples which finally had almost the same smoothness on both sides were accepted. In these tests a fine Yankee press felt was used.

In other tests, using a very fine paper machine wire between the felt and the web, it has been determined that as a result of two-sided Convac drying of newsprint at 155 C the resultant Bentsen roughness on both sides may be had in the range 280...370. This is very much lower than on newsprint before calendering on an ordinary machine, where values in the range 900...1100 are typically obtained.

Table III shows that the Convac process has a beneficial effect on most of the important strength values. There has, however, been a slight decrease in the CD-tear index.

The very few surface strength measurements so far made with newsprint dried with the high-temperature Convac process gave much higher IGT-surface strengths than measurements from normally dried newsprint, but more results are needed before conclusions can be drawn. Slightly lower surface air permeabilities were also obtained than with normally dried newsprint, as might be expected on the basis of the previously considered Convac drying effects on the web surface.

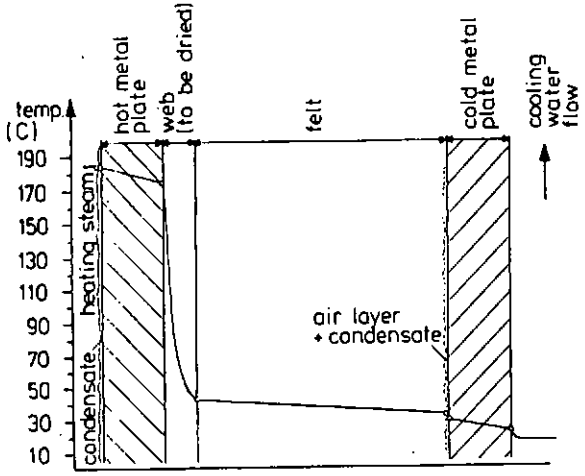

Figure 5 Temperature Distribution during Convac Drying

DRYING PROCESS

It is difficult to calculate the temperature distribution in the web during high surface -temperature Convac drying. There are numerous theoretical analyses of hot

surface drying of paper, but these have many simplifying assumptions which are invalid in the conditions of Convac drying. There are at least three physical phenomena, not adequately considered in these previous analyses, which, it is believed, play a major role in the heat and mass transfers within the web in high surface-temperature Convac drying.

Firstly, since there is a strong temperature gradient in the fibers near the heated metal surface in the direction perpendicular to the surface, there is also a strong surface tension gradient in the capillary water wetting these fibers, acting in the direction as to cause the capillary water to spread from the inside of the wet web toward the heated metal surface. Secondly, the same temperature gradient causes strong Marangoni convections to be set up in the contact, or proximity, areas between fibers, if wetted by capillary water. Thirdly, there are local vaporization explosions of superheated water, causing forced movements in the capillary water and the inter-fiber vapor.

The temperature distribution within the web shown in Fig. 5 results from these considerations, as well as from a few thermocouple measurements. Ordinary heat and mass transfer calculations account for the other temperatures in the figure.

CONSTRUCTION OF A COMMERCIAL DRYER

The configuration visualized for a commercial dryer utilizing the Convac method (Fig. 2) is a cylinder with a high heat flux outer mantle, with the wet web passing onto the cylinder, a felt onto the web, and a steel band passing outermost. The steel band would be cooled from the outside by water showers inside a hood encircling the cylinder. The web and the felt would pass through an air purging chamber before going onto the surface of the cylinder. The vacuum in the air purging chamber would be maintained by means of a vacuum pump. After passing over the cylinder the felt and the steel band would be separated from each other. Most of the water which had evaporated from the web and condensed onto the steel band would come out on the steel band. It could be removed therefrom by doctoring. The rest of the condensate could be removed from the outer surface of the felt by a suitable means.

The success of the drying process on the cylinder would depend on the success of the seals. The space in which the web and the felt would be between the surface of the cylinder and the steel band would have to be sealed against air leaking in from both sides of the machine.

ECONOMIC CONSIDERATIONS

Big capital cost savings would result if the drying section would be reduced to a single 6,2 m diam. Convac cylinder, or to two smaller cylinders. The shortening of the machine hall by 40...80 m would, alone, mean savings of the order of US $ 1.5... 3.3 million. The price of the dryer section, itself, would be reduced by at least 33 %.

The heat losses in Convac drying would be very small, but counteracting this effect would be the higher price of the Convac steam (0,8 MPa) than for today's drying (about 0,4 MPa). Overall, the steam and electricity costs for Convac drying would be roughly what they are today.

It is thought that the Convac dryer section could be operated almost with no dryer section breaks at all. The economic value of this varies from situation to situation, and also depends on the method of accounting.

The improved quality of Convac dried products would mean firstly, that one could sell the products at a higher price, and secondly, that one might get along with less, or cheaper, stock, or lower cost of stock preparation.

CONCLUSIONS

The Convac process seems to improve the quality of paper and board in several, economically important, ways. This conclusions, based only on laboratory tests with a static Convac device, is believed to be quite reliable in the case of folding boxboard grades, and as far as the tests went, with newsprint. The Convac effects on newsprint printability can only be determined with a full-speed pilot Convac machine.

It is possible that entirely new types of products could also be developed, as the Convac drying process differs very much from ordinary cylinder drying.Especially, the high surface temperature of the Convac cylinder, the fact that the web is being pressed with a pressure close to that of the atmosphere during drying, and the fact that the web cannot move laterally during drying cause interesting quality effects.

Economically, the Convac process looks quite good. Big capital cost savings could be expected. The cost of energy would, overall, remain about the same as in the very best machines of today, but there would be some small variations, depending on the type of product.

NEW CD MOISTURE PROFILE CORRECTION HOOD REDUCES ENERGY CONSUMPTION AND PRODUCTION COSTS IN HIGH SPEED TISSUE DRYING

Dipl.-Ing. H. Holik[1]
Dr. techn. R. Pinter[2]

1. Escher Wyss GmbH, Ravensburg / F.R.G.
2. Maschinenfabrik Andritz, Graz / Austria

1. INTRODUCTION

The improved design of today's tissue machines enables machine speeds of above 1500 m/min to be reached. However, the economic advantages of this increase in production speed are often balanced out by an increase in specific energy consumption at the wet end and in the dryer section (Fig. 1).

Since stock pumping energy depends only on machine speed, throughput and pipework, energy consumption can be reduced (but only to a limited extent) by increasing stock consistency.

In the dryer section there are a large number of parameters affecting specific energy consumption and drying costs and they often have an influence on each other.

In the first part of this paper, the different methods of reducing energy consumption and production costs in the dryer section is discussed and the implementation of improvements suggested.
In the second part, a new high temperature hood with a special CD moisture profile correction facility is presented. The system's correction potential is described and its design features explained.

2. REDUCTION IN SPECIFIC PRODUCTION COSTS OF TISSUE DRYING

The specific production costs of drying can be reduced in general by:

- lower specific energy costs of drying
- increased production
- lower specific raw material input.

The basic information needed for work on cost reduction is:

- the drying curve of the tissue web
- the influence of design and operating parameters on drying rate and energy consumption
- energy costs, i.e. costs of hood burner fuel, steam and electricity.

The drying curve (Fig. 2) shows the changing rate in sheet moisture reduction for one revolution of the tissue cylinder. This basic information was obtained by detailed investigation of the dryer sections of several high speed tissue machines /1/. This represents the most useful single source of information for all further cost reduction work.

2.1 Reduction in Energy Costs

2.1.1 Reduction of the Amount of Water to be Evaporated

The first step in reducing energy costs is to minimize the amount of water to be evaporated. This is done by effective dewatering at the first and second presser roll and by running the machine at the highest admissible final moisture content (Fig. 2).

2.1.2 Use of the Cheapest Form of Energy

A further reduction in drying costs is achieved by using the most economical form of drying energy (i.e. minimize energy costs and maximize efficiency in the use of the fuel for water evaporation). In most cases, steam drying energy is cheaper than forced convection drying energy.
Fig. 3 shows the drying costs for a given situation in relation to machine speed. Steam pressure is varied by about 1 bar. The diagram shows that in this case the operating steam pressure, i.e. the drying rate of the cylinder should always be the highest admissible. A ribbed dryer with its increased drying

rate will improve drying economy further. However, it should be remembered that the specific drying costs always depend on the prevailing cost of energy.

2.1.3 Optimized Hood

A further contribution to energy cost saving is the installation of a highly efficient hood. The efficiency is related to the fan power required to effect heat and mass transfer.

Fig. 4 shows some of the results of a detailed investigation into hood patterns. For a given constant heat transfer coefficient α, the required fan power is plotted against the spacing of the nozzle plate to the paper using different nozzle patterns. For a spacing in the range of 15 to 25 mm the round nozzle type 1 represents the most economic design.

This type of nozzle design is shown in Fig. 5, in a triangular nozzle distribution pattern. The exhaust slots run parallel to the cylinder axis.

Depending on the energy cost situation at the paper mill, there is an optimal combination of air temperature and air velocity in the nozzle for a required drying rate (Fig. 6). Given the local cost situation, the optimal layout can be found from the k = const lines.

2.1.4 The Air Flow System

The applied air flow system has some special features (Fig. 7):

- no throttling of the re-circulated air stream and a
- small additional inlet air fan.

This results in less fan energy consumption and an independent control facility for blow air humidity as well as for the pressure in the space between nozzle and cylinder.

2.1.5 Optimizing Hood Operating Conditions

The fuel consumption of a high temperature air impingement hood is also dependant on the h e a t r e c o v e r y system. By installing a larger heat exchanger, which results in a lower temperature difference between the inlet and outlet air flow at the hot end of the heat exchanger, fuel efficiency can be slightly increased /1/.

Increased a i r h u m i d i t y also results to some extent in a higher fuel efficiency /1/. The limitations are:

- the necessary amount of fresh air for burning the fuel to effect a desired drying rate
- the cylinder drying rate will be decreased by this operating condition, thus partly balancing out the advantage of a higher fuel efficiency for air heating.

2.1.6 Quantitative Evaluation

Fig. 8 gives a rough estimation of the results of adjustment of hood and cylinder operation. It shows the influence of an approximately 50% variation in adjustment on the specific energy consumption. The energy consumption is here related to the production rate (evaporated water) dried by the cylinder respectively hood. The results can vary from negligible (less than 1%) to worse or better by up to 5 to 10% and more.

2.2 Increased Productivity

A further means of reducing specific production costs is to increase production i.e. machine productivity.

An increase in production can be obtained by:

- running the machine faster
  - operating at the highest admissible drying rates which may be limited by safety factors in the dryer section (and by economy factors)
  - lowest possible moisture content after the press section
- reducing machine "downtime", i.e.
  - increase intervals between doctor blade changing
  - reduce time required for actual doctor blade changing or
  - reduce broke production.

A similar analysis as undertaken for specific energy consumption was carried out with measures to increase the drying rate. Fig. 9 shows the results of this rough estimation.

As mentioned before, the improvement in drying rate may adversely affect the specific energy consumption.
Only the measures "reduce spacing of hood to paper" and "increase steam pressure in the cylinder" result in an im-

provement of both drying rate and energy consumption whereas all other measures to increase the drying rate are followed by an increase in specific energy consumption, albeit small.

2.3 Lower Specific Raw Material Input

The last means of reducing specific production costs to be discussed in the following is to reduce the specific raw material input, i.e. leave more water in the product which is sold by weight.

Here the aim is to raise the moisture content at the reel to the highest possible level allowed by quality and by converting.

In this respect an even moisture profile is the predominant requirement.

Wet and dry streaks

- increase specific energy consumption
- reduce machine productivity
- increase specific raw material consumption.

The potential origins of wet streaks are manifold and it is really worthwhile searching for the origins in each specific case. On the other hand, for economic reasons, production must be continued for as long as possible. A means of continuous moisture profile correction is therefore a significant practical help.

2.4 Escher Wyss - Andritz High Temperature Hood with Moisture Profile Correction System

2.4.1 Description of the General Design

A moisture profile correction system has recently been developed for incorporation into the proven existing design of our high temperature hood. In Fig. 10 a hood is shown being works erected. The hood consists of a number of nozzle chambers extending across the machine width. Fig. 11 shows an end view of a single nozzle chamber.

The nozzle chambers are welded to two rings at each side thus forming a rigid and stiff construction with a well defined geometry (Fig. 12). The "flexible" side and separating walls of the hood are bolted to this construction. This design ensures the avoidance of high stresses in the hood due to temperature differences.

Even distribution of the blow air is assured by the symmetrical feed into the nozzle chambers and by the relatively low air velocities inside the hood. The exhaust slots are equally distributed around the hood wrap and assure uniform pressure distribution over the whole circumference of the hood.

A special feature of the described hood pattern is the low dependency of the heat transfer coefficient on the spacing of nozzle plate to paper at constant air velocity (Fig. 13). This ensures a uniform cross machine drying rate even with slight cross machine differences in nozzle plate to paper spacing.

2.4.2 Moisture Profile Correction System

On beginning the development of our moisture profile correction system, we defined the following requirements:

- control wet streaks
- control dry streaks
- no loss in overall drying capacity
- no increase in specific energy consumption.

The principle used in the moisture profile control system is to increase or reduce the open area of the nozzle pattern thus increasing or reducing the drying rate. The nozzle plate is provided with holes of two different diameters. Inside the nozzle chamber a perforated control plate can be moved, thus opening additional holes or closing all holes (Fig. 14). The width of these control plates is less than 500 mm. The special feature of this system is that it works by locally re-distributing the drying potential provided by the fan.

A photo of the control system with nozzle chamber and movable control unit is shown in Fig. 15.

Fig. 16 gives a view of the nozzle side of the hood. It shows the control pattern with the indicated sections including a control unit. Each nozzle chamber is provided with 4 control areas. The number of control areas aligned in the machine direction determine the overall correction potential. In the free areas of the nozzle chambers the standard nozzle pattern is provided.

The potential for cross machine moisture profile correction is plotted in Fig. 17 against the moisture content of the wet streak, and in Fig. 18 against the mois-

ture content of the dry streak. The control potential depends to a great extent on this moisture content which can be explained by the drying curve of the paper web showing a decreasing slope at low moisture contents. The contribution of the hood to the overall drying rate also has a significant influence on the correction potential.

An approximate economy evaluation demonstrates that the pay-back period for the return on investment for such a control installation is only a few months, thus showing the significant economical advantage of such a CD moisture profile control hood.

3. SUMMARY

It has been shown that there are different measures in the drying section to reduce production costs (Fig. 19). The paper mill should select an optimized cylinder and hood design when installing a new dryer section.

By selecting optimum operating conditions, further economic advantages can be realized, e.g.: by increasing the dewatering effect of the presser rolls; by increasing the paper web moisture content at the reel; by running the cylinder at the maximum admissible drying rate as well as by optimizing the humid air exhaust of the hood. These measures ensure increased production at lower specific drying energy costs.

Savings in raw material by running the web at a high moisture content and an even CD moisture profile are easily gained with the new CD moisture profile control hood explained here. It is therefore possible to increase tissue machine speeds whilst at the same time reducing drying costs.

4. LITERATURE

/1/ R. Pinter, H. Holik

"Energy Consumption and Drying Costs in High Speed Tissue Drying"

2nd International Symposium on Drying
McGill University, Montreal,
July 6 - 9, 1980

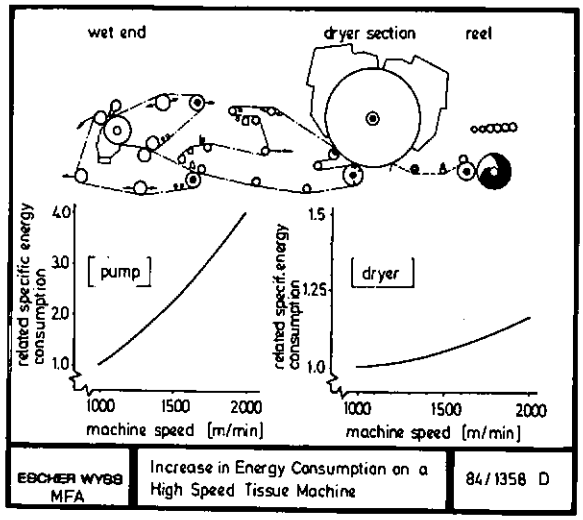

Fig. 1

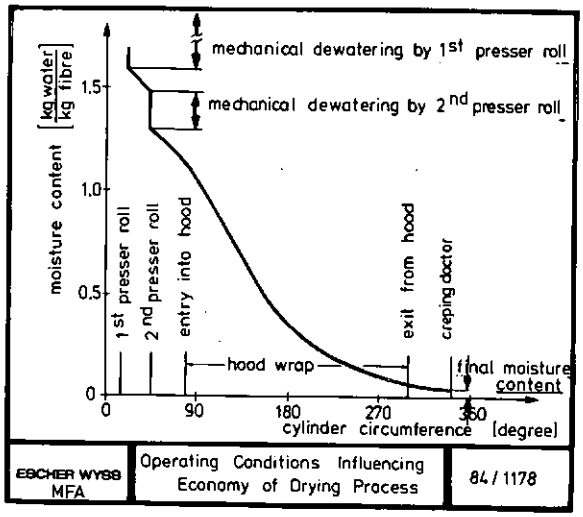

Fig. 2

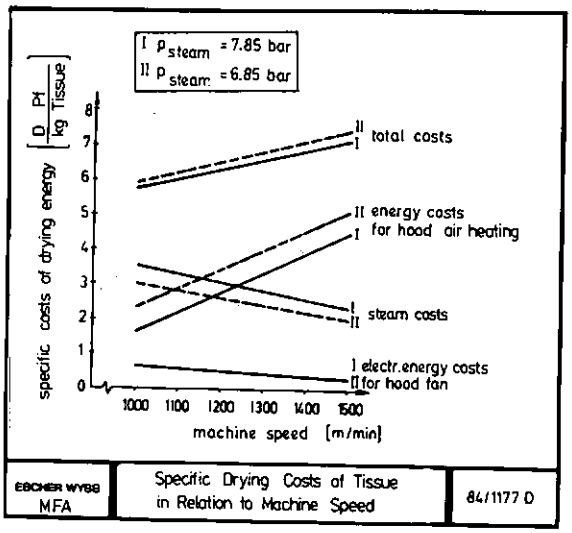

Fig. 3

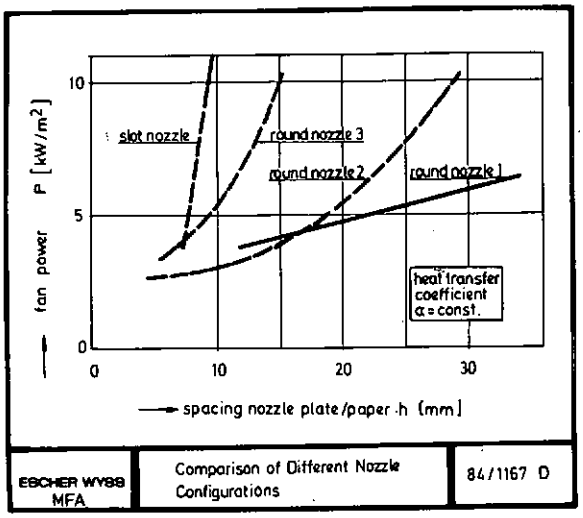

Fig. 4

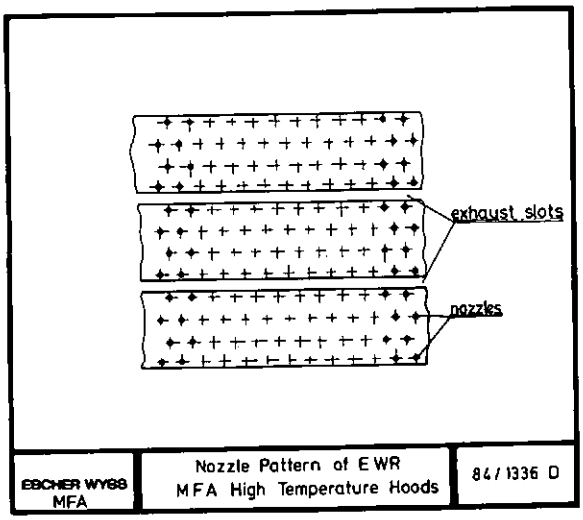

Fig. 5

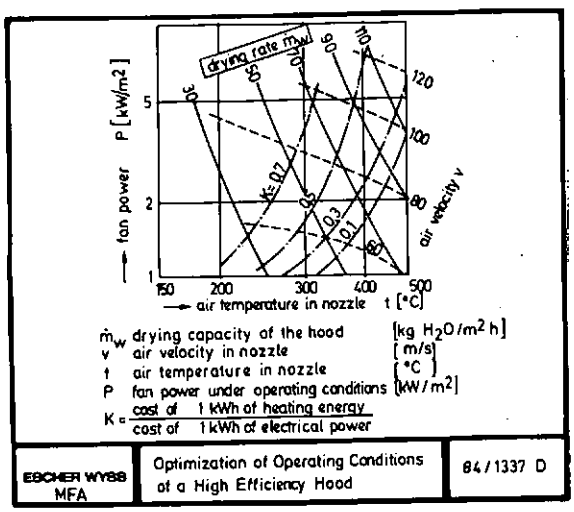

Fig. 6

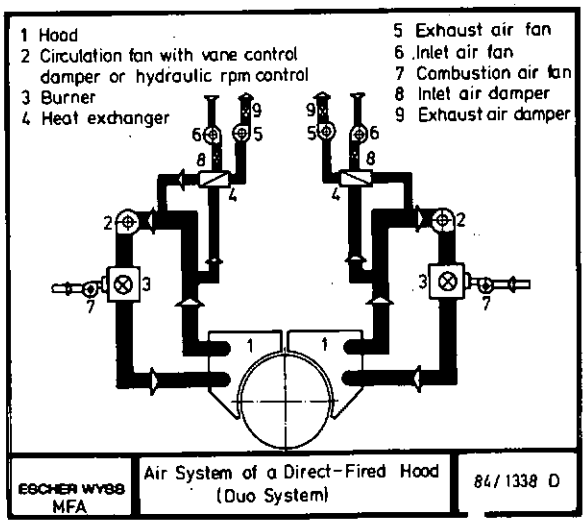

Fig. 7

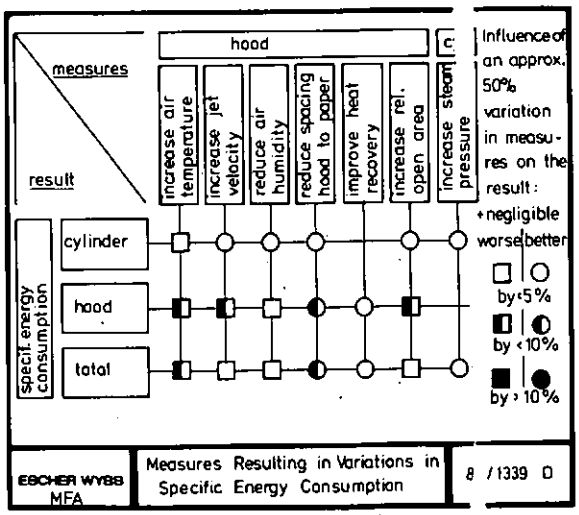

Fig. 8

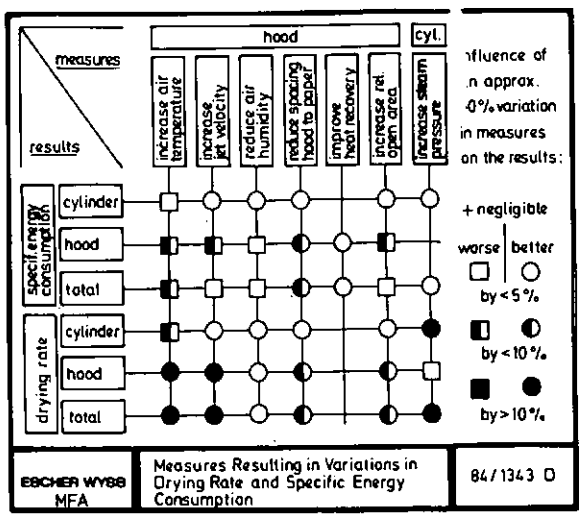

Fig. 9

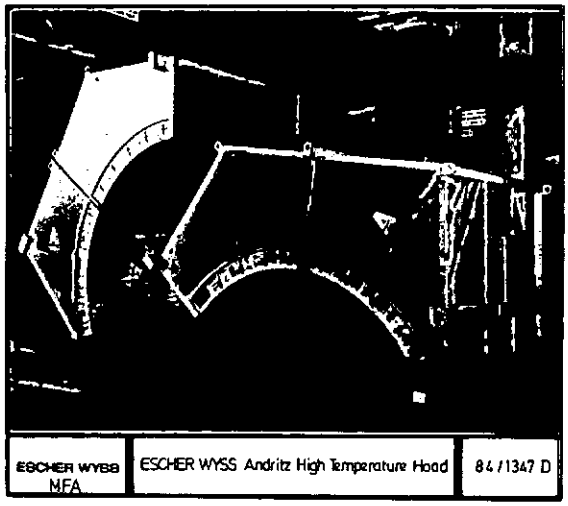

Fig. 10

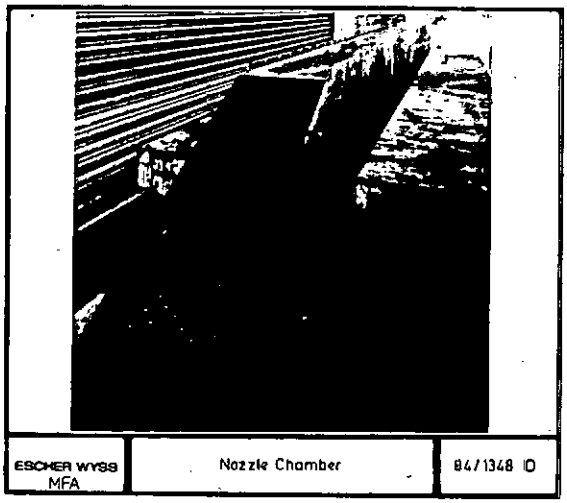

Fig. 11

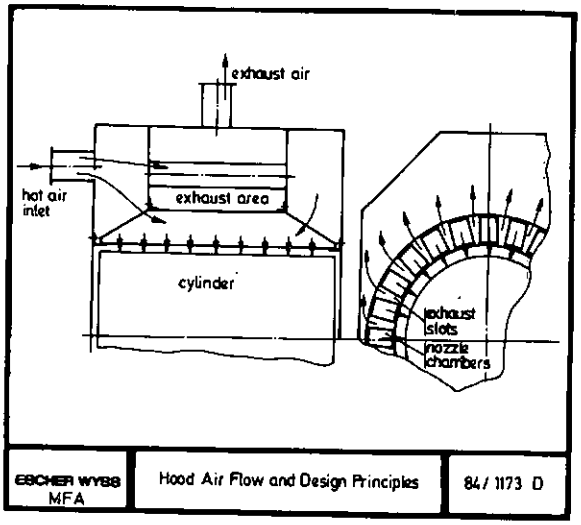

Fig. 12

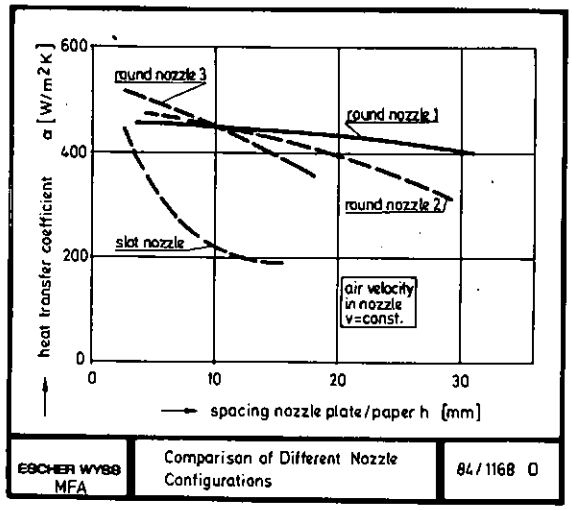

Fig. 13

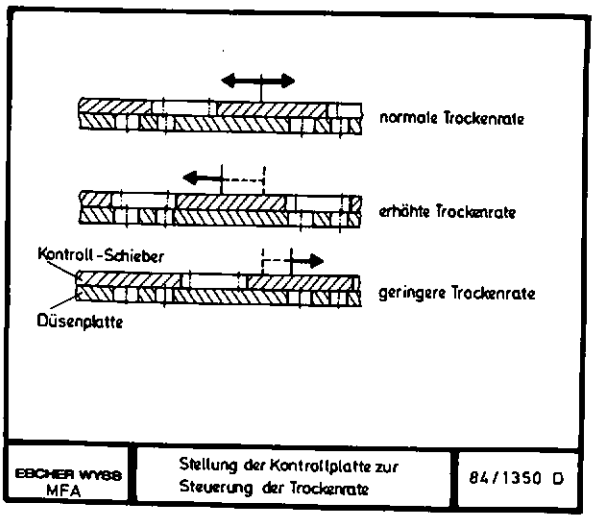

Fig. 14

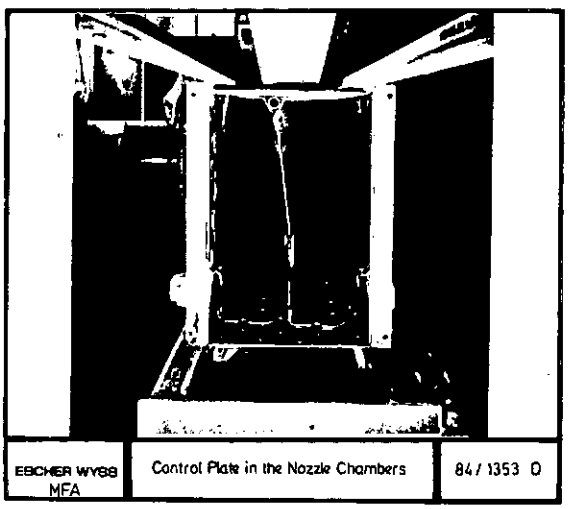

Fig. 15

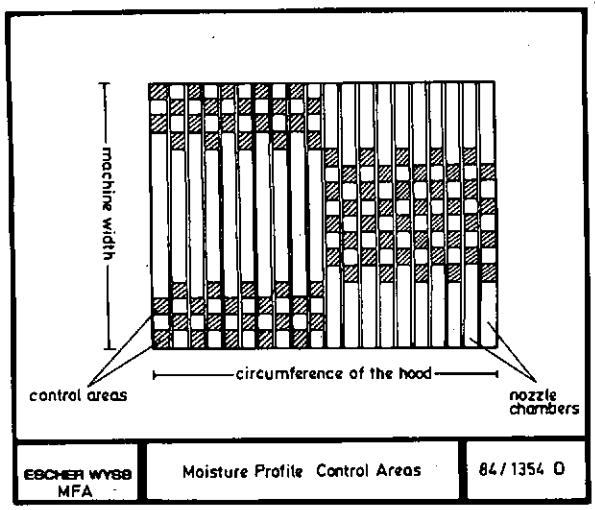

Fig. 16

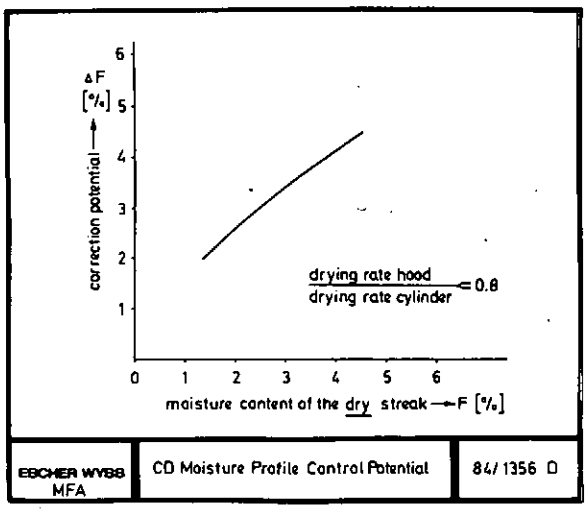

Fig. 18

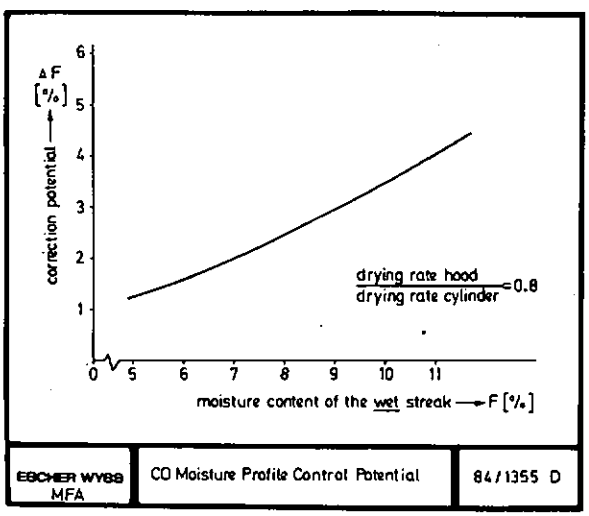

Fig. 17

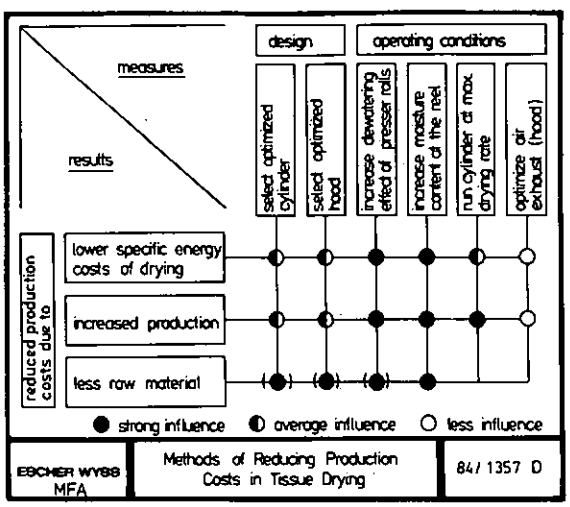

Fig. 19

ENERGY CONSUMPTION AND DRYING COSTS IN HIGH SPEED TISSUE DRYING

Dr. techn. R. Pinter[1]
Dipl.-Ing. H. Holik[2]

1. Maschinenfabrik Andritz, Graz / Austria
2. Escher Wyss GmbH, Ravensburg / F.R.G.

1. INTRODUCTION

Modern tissue machines run at high speeds of up to 1500 m/min and more. This means an extremely short time for drying the web which in turn means high drying intensities. This leads to high energy consumption so that energy costs represent a considerable part of the production costs of tissue.

Fig. 1 shows schematically the design of a modern tissue machine. The fibre suspension jet from the headbox (1) is fed into the gap between the two wires (2 and 3). Here the paper web is formed during contact with the roll (4) and then picked up by a felt (5) and pressed against the Yankee dryer (6) by either one or two presser rolls (7). Drying occurs within less than one revolution of the Yankee dryer, where the sheet is brought from a moisture content of approximately 1.5 kg water/kg fibre at the first press to a final dryness of about 95% at the creping doctor (8). The speed of the reel (9) is about 20-30% slower than the wet end and Yankee dryer, depending on the creping process.

About 2/3 of the steam-heated Yankee dryer are enclosed by a high temperature high velocity hood (10) which contributes up to 60% of the total capacity of the dryer section. The hood also increases the drying efficiency of the cylinder and provides the exhaust for the evaporated water.

Fig. 2 gives a rough idea of the energy consumption of the fan pump, machine drive and the dryer section. The energy consumption is related to the total drying energy required at a machine speed of 1000 m/min. Efficiency factors for steam generation of ηsteam = 0.85 and for electrical power generation of ηelectr = 0.33 are assumed. At a machine speed of 1500 m/min, about 23% of the total energy consumption is spent on the machine drive and about 11% on the fan pump at a stock consistency of 2.5 g fibres/kg water. Against this, 66% of energy consumption is required to remove the last 1.5 kg of water per kg fibre. It is therefore obvious that the greatest potential for reducing energy consumption lies in the dryer section and it is worthwhile analysing in detail the drying process and all the parameters affecting energy consumption in tissue drying.

For this reason, a thorough investigation of the drying process on a Yankee dryer with a high temperature, high velocity hood has been undertaken, including theoretical calculations as well as measurements on several tissue machines.

2. DRYING PROCESS

Continuous drying of a paper web is a complex process of heat and mass transfer which takes place in the structure of the web, on its surface and in the boundery layer within less than one second. Many mathematical models for simulating the drying process have been developed but they cannot take into account all the influences in such a drying system. The necessary information must therefore be elaborated by extensive measurements on tissue machines in operation.

2.1 Drying Curve

The drying curve shows the amount of moisture reduction in the tissue web during one revolution of the tissue cylinder and provides the most important basic information on the drying process. To obtain data for the drying curve, paper samples were taken from the Yankee dryer at the following points (Fig. 3):

1) between the presses

2) after the second press

3) at the 12 o'clock position and

4) at the creping doctor

At each point several samples were taken with a special device for each test run. This procedure was repeated for different operating parameters such as machine speed, steam pressure of the Yankee dryer, temperature, velocity and humidity of the impinging air and for different types of drying systems.

Fig. 4 showing the moisture content of the web plotted against the cylinder circumference is one of the results. The paper web leaves the first press with a moisture content of about 1.6 kg water/kg fibre and is at first heated up and dried by only the Yankee cylinder. It is then dewatered mechanically in the second press. On entering the hood, the drying intensity increases. Later on, the slope of the drying curve decreases distinctly with lower moisture contents.

It can be seen from the drying curve that a significantly higher amount of water has to be exhausted by the first half of the drying hood by comparison with the second one. Furthermore, it is obvious that a larger part of the dryer surface is necessary to evaporate the last few percent of water.

2.2 Drying Intensity

The drying intensity or the drying rate is represented by the gradient of the drying curve. In Fig. 5, the drying intensity is plotted against the water content of the web. It shows the typical curve to be expected when drying hygroscopic materials, i.e. a constant drying rate zone and one or two falling rate zones.
With drying intensity curves, such as given in Fig. 5, theoretical calculation and practical operation of the dryer section can now be coordinated. These types of curves are important for the layout of the dryer section. The drying intensity in the constant drying rate zone can be calculated by simple application of mass and energy balances and the use of equations for heat and mass transfer such as the Lewis relation. In the falling drying rate zones, the mean value of the drying rate is lower than in the first period of constant drying rate. To achieve the required mean drying capacity, the hood layout has to take this falling drying rate at the end of the drying process into account. This is done by the introduction of a so-called drying coefficient k_d.

This factor k_d depends on the operating parameters of the Yankee dryer and the hood, on the raw material input and especially on the moisture content of the web on entry into and exit from the dryer. Fig. 6 shows the related drying coefficient as a function of the final dryness at the creping doctor and of the moisture content on entry into the hood. The related drying coefficient is shown as a ratio of the drying coefficient k_d and the standard coefficient k_d, referring to standard drying conditions. It can be seen that a very low final moisture content causes a high drying coefficient. This results in high installation and energy consumption costs.

2.3 Heat Supply by the Yankee Dryer

In operation, the heat flux from the Yankee dryer to the web during one revolution is not constant whereas inside the dryer, there is a constant transfer of heat from steam to shell.

In Fig. 7, heat flux from cylinder to paper and Yankee surface temperature are plotted against the circumference of the cylinder. At the first presser roll, the cold wet paper web is pressed on to the Yankee dryer, causing an immediate drop in cylinder surface temperature. This results in an extremely high heat flux to the paper at this point. At lower moisture content of the paper, the surface temperature is increased by unsteady heat conduction within a small area near the surface of the cylinder shell. The heat flux decreases. Between the creping doctor and the first press no heat is transferred (except for small losses to the surroundings). This results in a further increase in surface temperature. Thus the Yankee dryer provides only a small contribution to the required drying rate during the last drying period in the falling drying rate zone. During the short duration (approx. 0.7 seconds) of one revolution, variation in cylinder surface temperature occurs within a very thin layer of the cylinder shell whereas a steady temperature distribution is found a few millimetres away from the outer surface.

2.4 Water Removal in the Dryer Section

Taking sheet moisture contents after the first presser roll and at the creping doctor as constant, the total amount of water to be removed in the dryer section

depends only on the machine speed.
In Fig. 8, the amount of water relates to the required water removal at a machine speed of 1000 m/min. Part of the total amount is extracted mechanically by the second presser roll.
The main part is evaporated by the Yankee dryer and the hood. Due to the necessary higher impinging air temperature, the drying capacity of the Yankee dryer decreases for higher machine speeds.
A considerable amount of water is removed mechanically in the second press and need not be evaporated. Besides the dewatering effect, the second presser roll is effective in giving a closer contact between paper web and cylinder surface which leads to higher heat transfer coefficients.

3. ENERGY CONSUMPTION

3.1 Energy Flux in the Dryer Section

The total heat energy necessary for the evaporation of water in the dryer section can easily be calculated. If the different losses of primary energy in the process are taken into account, the required amount of fuel is in practice far larger than the theoretically calculated energy consumption required for evaporation.
Fig. 9 shows a Sankey diagram for the energy flux in the dryer section (excluding electric power consumption).

The fuel energy for hood burner and steam production together is taken as 100%. It is assumed that steam is produced in a power station where about 10% of energy is lost on conversion and transport.
Further heat losses occur from the Yankee dryer and hood system to the surroundings. The greatest amount of energy is contained in the humid exhaust air. It includes the necessary heat for evaporation, for superheating the vapour to the exhaust temperature and the heat content of the dry air. About 5% of the energy is used for heating fresh air in the heat recovery system.

3.2 Cylinder Heat Losses

On the Yankee cylinder the following principal heat losses occur

- by convection and radiation:
  - heat losses from cylinder heads
  - heat losses from those parts of the shell not covered by the paper web
  - heat losses from steam and condensate system
- by contact:
  - heat losses to the felt.

Fig. 10 shows the use of the total heat input resulting from the maximum capacity of the steam fed to the Yankee dryer at different machine speeds. The energy is used for heating up the wet paper web, for evaporation as the actual goal of the process or is partly lost. The losses from cylinder heads to surroundings could be reduced by insulation. A reduction of the heat losses to the moving felt could be achieved by heating felt and paper web, i.e. with exhaust air, before touching the Yankee dryer.

3.3 Heat Recovery

Part of the exhaust energy is used for heating the fresh air in the recovery system of the hood. By installing a larger heat exchanger which results in a lower temperature difference Δt between the inlet and the exhaust air flow at the hot end of the heat exchanger, fuel consumption can be slightly decreased.
Fig. 11 shows the related fuel consumption and the related area of the heat exchanger as a function of Δt, where $\Delta t = 60^{o}C$ is taken as the normal condition. In practice a compromise must be found between energy consumption and capital costs.
A great amount of energy is still contained in the humid exhaust air which usually cannot be used in the dryer section due to the low temperature level.
A further heat recovery e.g. for heating stock and white water or buildings can reduce these losses considerably.

3.4 Operating Parameters

3.4.1 Air Temperature

The blow air temperature is one of the parameters affecting both drying capacity and energy consumption of an existing system. Fig. 12 shows the related primary energy consumption for steam, electricity and gas as a function of air temperature. Since the steam pressure in the Yankee dryer was held constant, the total drying capacity was increased with raising air temperatures. Efficiencies of 33% for electric power generation and of 85% for steam generation are used in the diagram. Knowing the actual costs for the different fuels, an optimum operating air temperature - as far as energy costs are concerned - can be found.

3.4.2 Air Velocity

The impinging air velocity is a further operating parameter. Fig. 13 shows the influence of the air velocity on the drying rate and on the energy consumption. The steam pressure and the blow air temperature were kept constant. The efficiencies for electric power and steam generation are the same as in Fig. 12.

3.4.3 Air Humidity

During operation, the humidity of the blow air can be varied by changing the air recirculation ratio. In Fig. 14, the results of tests on a tissue machine running at a constant speed (constant required total drying rate) and with a constant steam pressure are given. The loss in drying capacity due to variations in heat and mass transfer parameters caused by increased air humidity had to be balanced out by higher air temperatures. Specific steam and fan power consumption decrease with higher air humidity and there is a simultaneous increase in hood fuel consumption. The optimum air humidity for the lowest energy costs in the dry dryer section depends on the costs for the different kinds of fuel as primary energy.

The operating parameters of air temperature, velocity and humidity as shown in the Fig. 12, 13 and 14 are related to the same basic value for reasons of comparability.

3.5 Optimum Ratio of Yankee and Hood Drying Capacity

The total required heat energy for the drying process is delivered by the Yankee dryer and hood. By varying the steam pressure of the cylinder and the blow air temperature, this ratio can be changed as shown in Fig. 15. Depending on the efficiency of Yankee dryer and hood and on the costs of the different fuels, the energy costs will also vary. In Fig. 16, the total costs for a constant drying rate are plotted against the ratio of evaporation produced by the Yankee dryer or the hood. The parameter c_e is the relationship between the fuel energy costs for hood and Yankee dryer. Electrical energy consumption of the fans is not included here.

Since usually the primary fuel for steam is cheaper than that for the burner, the Yankee dryer should be operated at the highest admissible steam pressure. Thus an optimal design of the Yankee dryer having the highest drying capacity is in most cases a further means for reducing energy costs.

4. SUMMARY

The greatest amount of energy in a tissue machine is consumed in the dryer section and energy costs represent a large part of production costs. Different parameters influence the energy consumption and have been studied in detail to show possibilities for cost reduction.

The most valuable information on the drying process is the drying curve. In this curve, the physical process of drying hygroscopic materials and the behaviour of this special kind of dryer system is included. This curve can only be found by undertaking measurements on actual production machines. The knowledge of the drying curve is necessary for the layout of the dryer section and especially for the hood.

In the dryer section, only part of the fuel energy is used for the evaporation of water. Here, various energy losses occur. A detailed study of these losses leads to possibilities for reducing them.

Operating parameters such as air temperature, impinging velocity and air humidity of the hood as well as steam pressure in the Yankee dryer show distinct influences on the consumption of steam, gas and electric power. The optimum operating conditions depend on the costs for different fuels and can be found with the help of the diagrams shown.

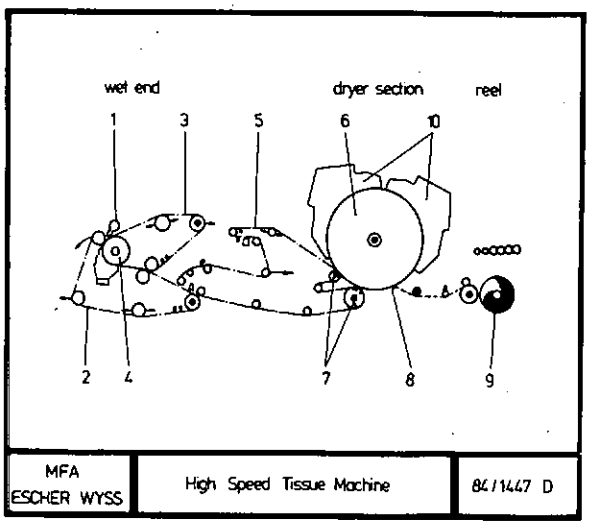

Fig. 1

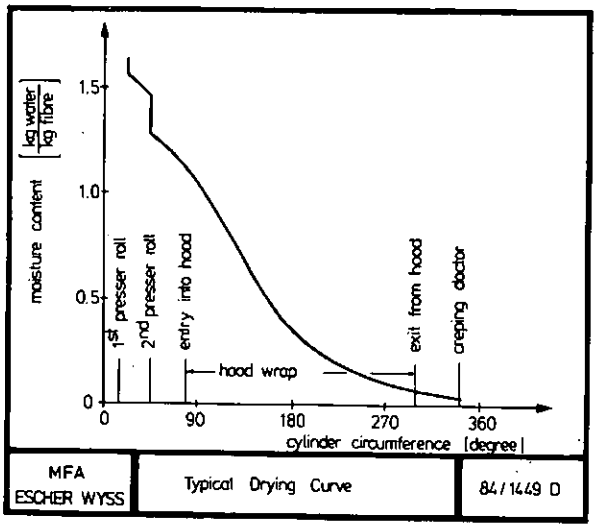

Fig. 4

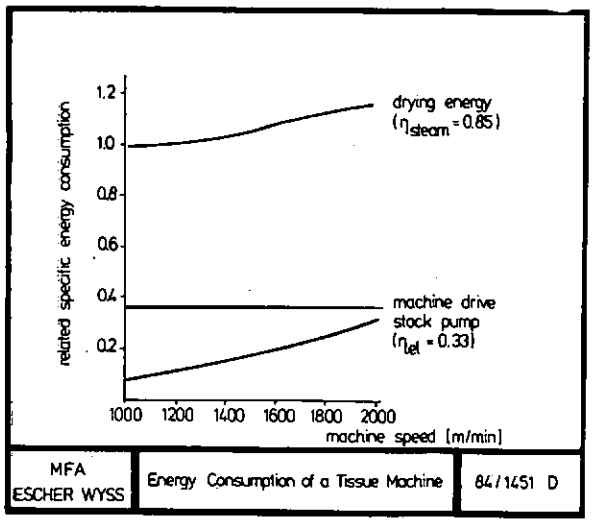

Fig. 2

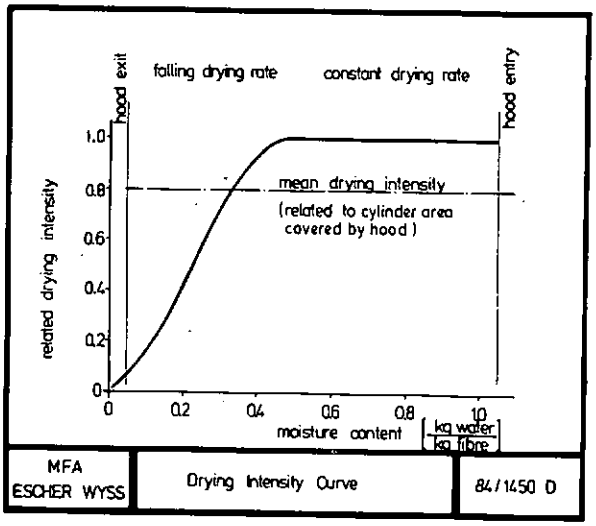

Fig. 5

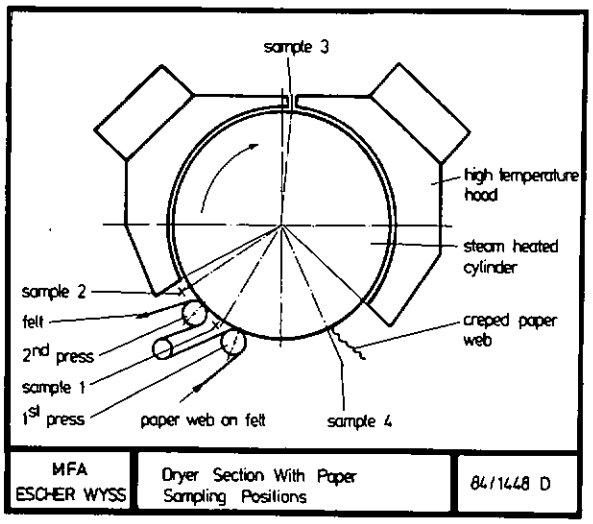

Fig. 3

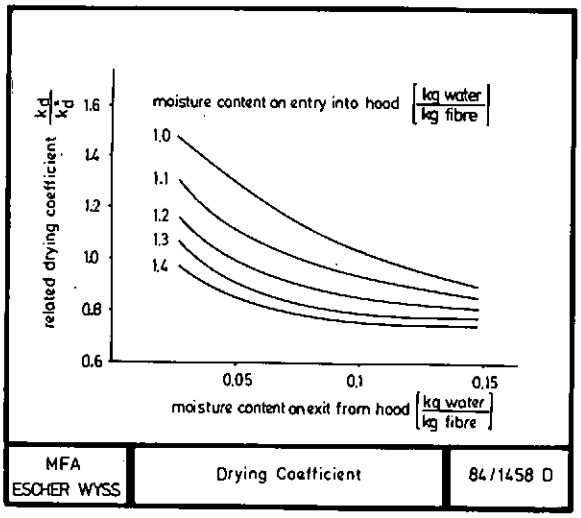

Fig. 6

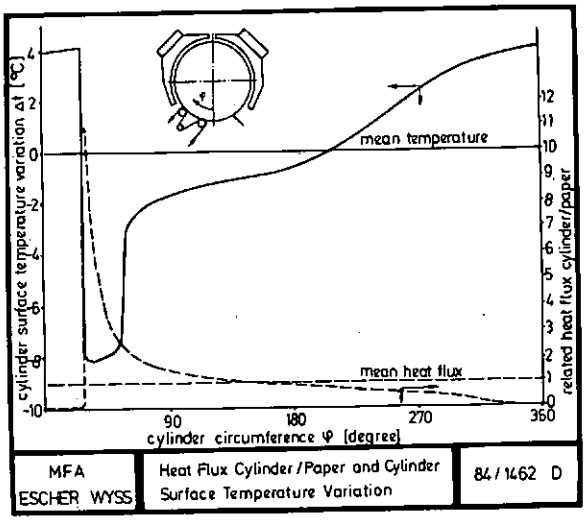

Fig. 7

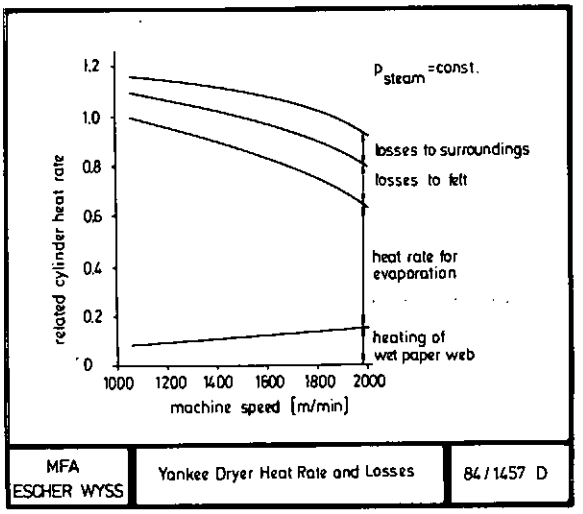

Fig. 10

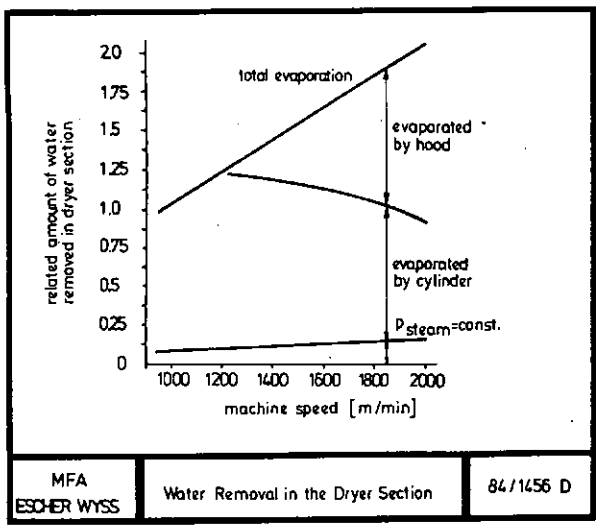

Fig. 8

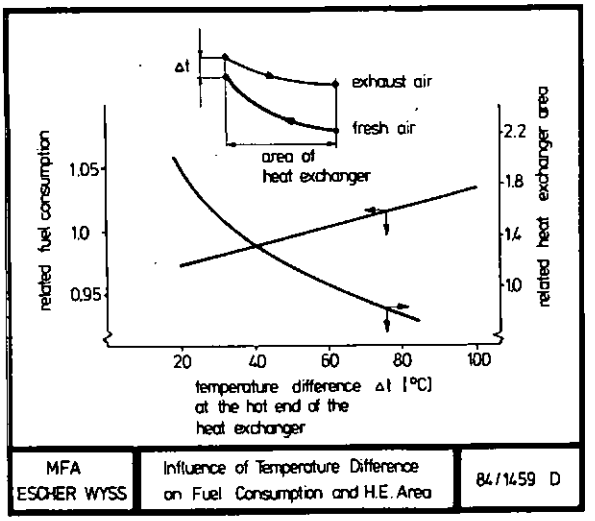

Fig. 11

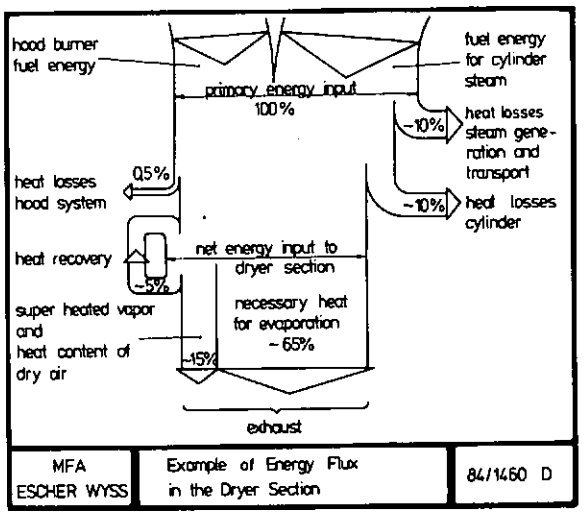

Fig. 9

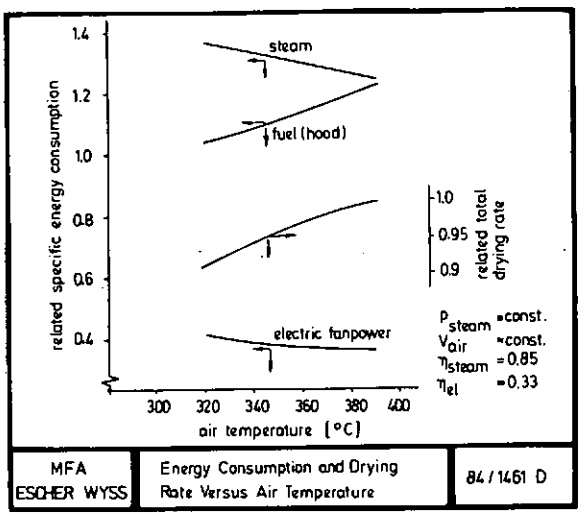

Fig. 12

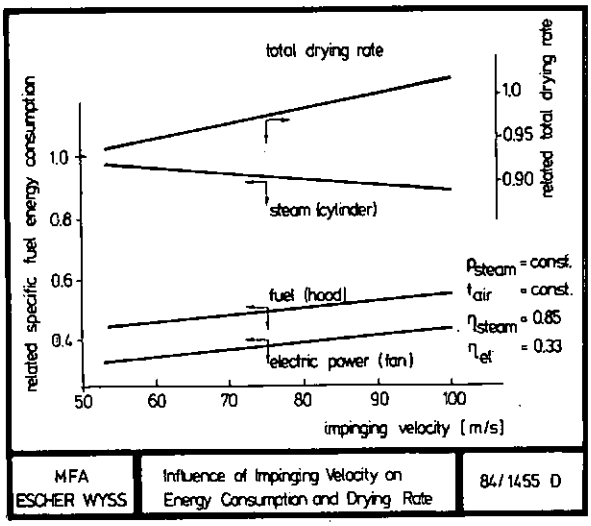

Fig. 13

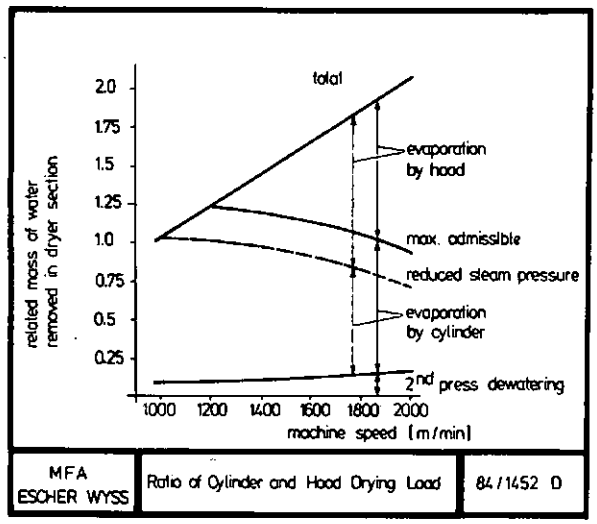

Fig. 15

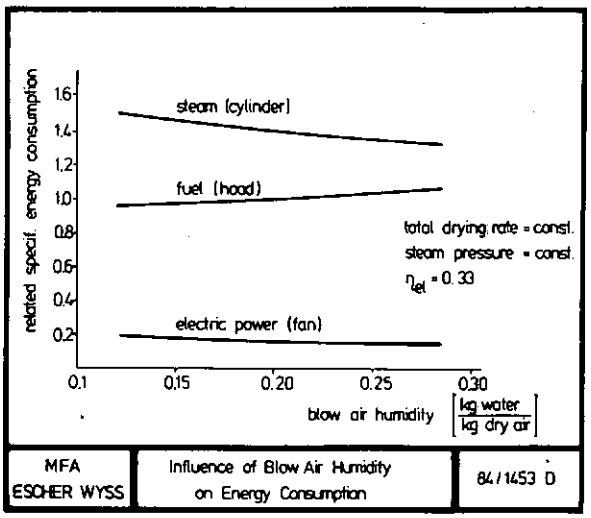

Fig. 14

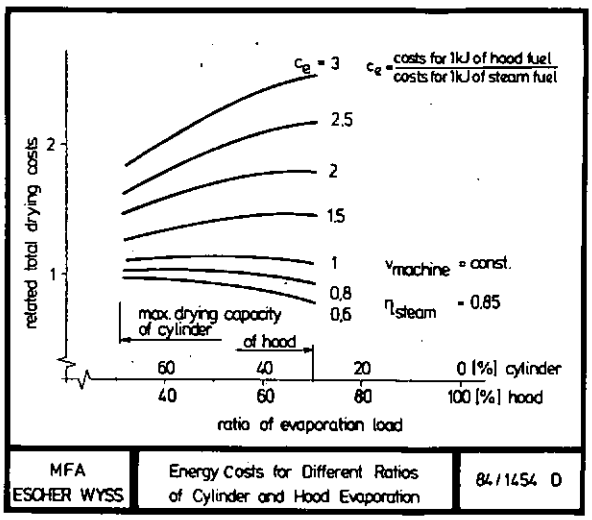

Fig. 16

THE EFFECT OF AIR FLOW ON HEAT CONSUMPTION IN CONTACT DRYER

A. Strawiński

Instytut Celulozowo-Papierniczy, Łódź, Poland
/The Pulp and Paper Research Institute/

ABSTRACT

General heat balance of dryers was analyzed. Attention was paid to specyfic cases of the balance shaping. One of these cases characterizes the drying process in paper contact dryer. Allowable simplifications were already introduced and a simple method to determine heat consumption based on psychrometric measurements was established. The results of 62 tests, carried out for 7 commercial drying sections of paper machines were collected. Basing on this method of meadurements and analysis the dependance of the heat consumption on the amount of air passing through the dryer and on temperature of fresh air comming into dryer was determined. The presented method of the heat consumption measurements and the analysis of results can be applied not only to paper cylinder dryers but also to all convection dryers that comply with the condition that moisture content decrease in the dryed product is higher than 1 kg/kg of dry material.

NOMENCLATURE

q_t = total specific heat consumption, kJ/kg

q_m = part of specific heat consumption for material preheating, kJ/kg

q_a = part of specific heat consumption for air preheating, kJ/kg

q_l = part of specific heat consumption used to cover the losses to the environments, kJ/kg

$q_{net} = q_t - q_l$

Δh_v = specific latent heat of vaporisation, kJ/kg

Δh_a = specific enthalpy difference of air, kJ/kg

c_p = specific heat at constant pressure, kJ/ (kg . K)

x_m = moisture content in dryed material, kg/kg dry material

Δx_m = moisture content decrease in dryer, kg/kg

y_a = humidity of air, kg/kg dry air

Δy_a = humidity increase in dryer, kg/kg dry air

Θ = temperature, ^{o}C

$\Delta\Theta$ = temperature difference, K

Superscripts

' = dryer inlet

" = dryer outlet

Subscripts

m = dryed material

a = air

w = water

s = evaporated water /steam/

INTRODUCTION

Dryers are one of the most common technological heat receivers and, therefore, in view of present situation in energy balance it seems justified to put some more concern on heat consumption. Thermal analysis of a dryer can be put down to heat balance analysis provided it is assumed that electric energy applied to drives will be transformed inside the dryer into heat. The heat balance may be determined in the same way for dryers of different designs, operation principles and different materials to be dried.
Usually heat balance is determined on the basis of detailed measurements: parameters and amount of steam going in and condensate going out, dried material and air at the inlet and outlet of the dryer. Sometimes the measurements may be simplified and used to determine the influence of some components which change in the course of the drying process.

DRYER HEAT BALANCE ANALYSIS

The most useful form of heat balance generally accepted is the balance related to the unit of evaporated water in the dryer. In most simple way it may be presented as:

$$q_t = \Delta h_v + q_a + q_m + q_l \qquad (1)$$

To simplify the reasoning the heat used for preheating of equipment that conveys the dried material throughout the dryer was disregarded in formula (1) for not all dryers are provided with this kind of equipment.
When loss value q_l is deducted from total heat supply q_t the characteristic value for the drying process is obtained and called further q_{net}.

$$q_{net} = q_t - q_l = \Delta h_v + q_m + q_a \qquad (2)$$

As it is shown q_{net} determines heat flux which should be delivered with heating medium to the dryer working without losses to ambient atmosphere. Latent heat of vaporization Δh_v may be regarded as constant provided the values q_m and q_a are adequately described:

$$q_m = \frac{c_{pa} + x''_m \cdot c_{pw}}{\Delta x_m} \cdot \Delta\Theta_m - c_{pw} \cdot \Theta'_m \qquad (3)$$

$$q_a = \left(\frac{c_{pa} + y'_a \cdot c_{ps}}{\Delta y_a} + c_{ps} \right) \cdot \Delta\Theta_a + c_{ps} \cdot \Theta'_a \qquad (4)$$

Some of the values mentioned in formulas (3) and (4) may be assumed as constant for the particular dryer or group of dryers. These are all the values of specific heat, material and air temperatures at the inlet to the dryer, as well as moisture content in the material at the outlet and the humidity of the air at the inlet to the dryer. The assumption being such both of the values q_m and q_a become function of two variables: $q_m = f(\Delta x_m, \Delta\Theta_m)$ and $q_a = f(\Delta y_a, \Delta\Theta_a)$. Such simplifications allow for graphic presentation of value q_{net} (example on Figure 1).

If the values regarded on the diagram Figure 1 as constant c_{pw}, c_{ps}, Θ'_m, Θ'_a change, this causes the change in shift of origins of both families of curves shown on this diagram

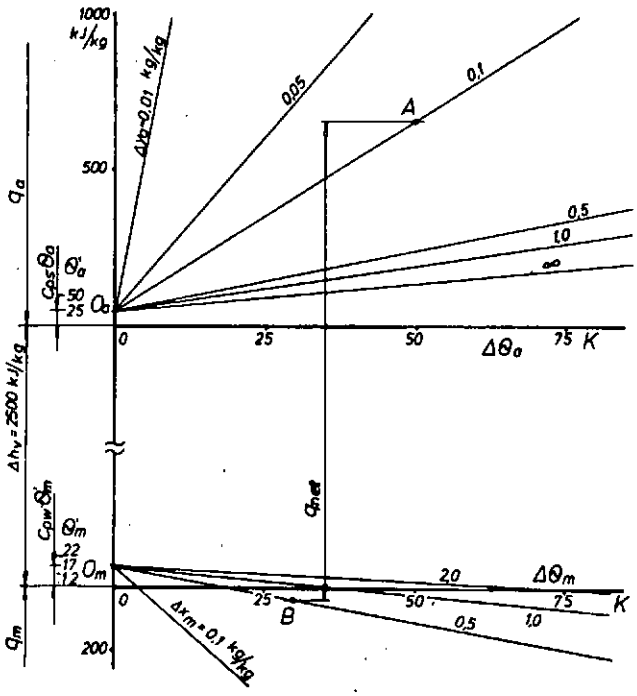

Figure 1 Diagram for q_{net} determination (c_{pm} = 1,34; c_{pa} = 1,005; c_{pw} = 4,19; c_{ps} = 1,92 kJ/(kg.K); x''_m = 0,08 kg/kg; y'_a = 0,012 kg/kg; Θ'_m = 17°C; Θ'_a = 25°C)

(points O_m and O_a). Point A on the diagram indicates the value of part of the specific heat consumption q_a based on known $\Delta\Theta_a$ and Δy_a and point B - the value q_m based on $\Delta\Theta_m$ and Δx_m. The distance between these points shown on the diagram determines value of q_{net}. The consideration of the diagram leads to few conclusions:

a. in some cases when $\Delta x_m \geq 1{,}0$ kg/kg, q_m generally assumes small values and may be regarded as close to 0, and thus may be omitted in the heat balance sheet,

b. there may be cases when q_m or q_a or both at the same time are negative, then, they become items of heat income in the balance, not the loss, and q_{net} is lower then Δh_v (Figure 2 a) or even equal to 0 in some specific cases (Figure 2 b).

Case "a" occurs very often when drying natural organic materials natural fibres, skin, paper after mechanical dewatering (couching or suction). Case "b", on the other hand, refers, for example, to dryers which dry in so called "natural conditions", it means, with air taken from the ambient atmosphere without preheating, neither heating inside or with very small

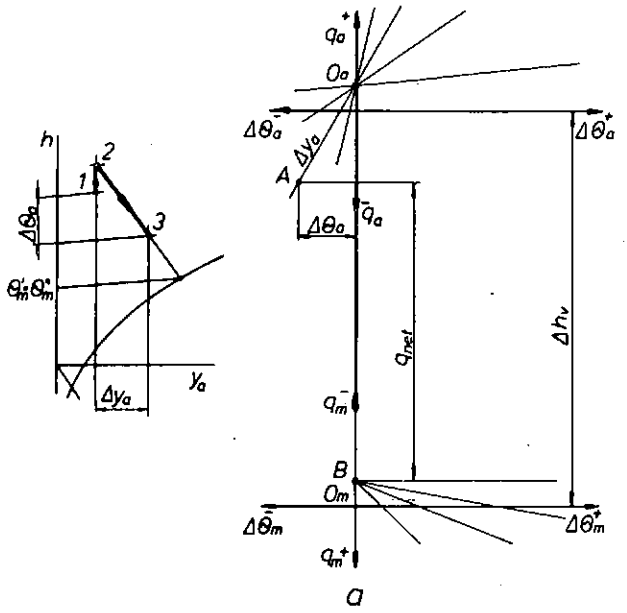

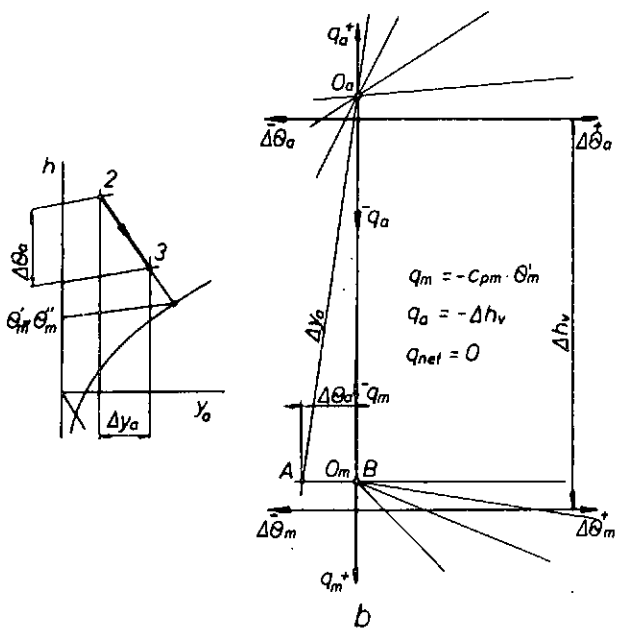

Figure 2 Special cases of q_{net}

preheating without supply of the heating medium or with this supply being insignificant .
For paper dryers which will be the subject of further consideration conclusion "a" becomes essential i.e. $q_m \cong 0$. It leads to the simplification of formula (2), which now may be presented as formula (5).

$$q_{net} \cong \Delta h_v + q_a = \frac{\Delta h_a}{\Delta y_a} \qquad (5)$$

The sum of values $\Delta h_v + q_a$ is the ratio of entalphy increase to the humidity increase in the air flowing through the dryer. Thus, it may be determined on the basis of psychrometric measurements for the air at the inlet and outlet of the dryer. The method of q_{net} measurements becomes very simple then. Sometimes the method of measurement is much more complicated. This occurs when there are several inlets and outlets from the dryer, let us take for instance paper dryers.

INVESTIGATION RESULTS

To estimate the change of q_{net} values in paper dryers (drying parts of paper machines) 62 measurements of 7 full-scale commercial dryers of different capacities, giving different products and provided with open hoods were taken.
The taken measurements were reduced to psychrometric measurements at the inlet of air to the dryer and at air ducts discharging exhausted air (warm and damp) to heat recovery units. In this case paper dryers were provided with very wide air inlet along the dryer and with few air exhaust. Weighted mean values of several individual measurements were, therefore, applied to each dryer. General characteristics of the discussed dryers are given in Table 1. The amount of water evaporated on 1 m^2 of total surface area of drying cylinders (evaporation) varied from 7,2 to 8,7 kg/(m^2 . h). Ratio of the area of cylinder in contact with paper sheet to the total surface area of drying cylinders together with bottoms ranged from 48 to 56 %. Based on measurements function $\Delta h_a = f(\Delta y_a)$ was determined. After first approximation the linear relation was obtained (Figure 3) which is as follows:

$$\Delta h_a = 2880 \cdot \Delta y_a + 7{,}55 \qquad (6)$$

$$\frac{\Delta h_a}{\Delta y_a} = 2880 + 7{,}55 \frac{1}{\Delta y_a} \qquad (7)$$

$\frac{1}{\Delta y_a}$ represents "the specific air consumption of the dryer" as ratio of amount of fresh and dry air introduced to the dryer to the amount of water evaporated in the dryer. Further analysis of results showed additional effect of temperature of the air introduced to the dryer. After approximation of results with multinominal of second degree for two variables

Table 1. General characteristics of the examined dryers

Dryer	A	B	C	D	E	F	G
Output, kg/h	6700	4750	4100	2150	2600	2500	3450
Machine width, mm	5800	4825	3500	2300	3500	4700	4800
Mean sheet speed, m/min	430	240	60	46	280	140	364
Evaporation, kg/ m^2 . h	8,55	8,7	7,65	8,21	8,1	7,22	n.a.
Dryed paper	news-paper	sack paper	multiply board	roofing paper	news paper	printing paper	news-paper

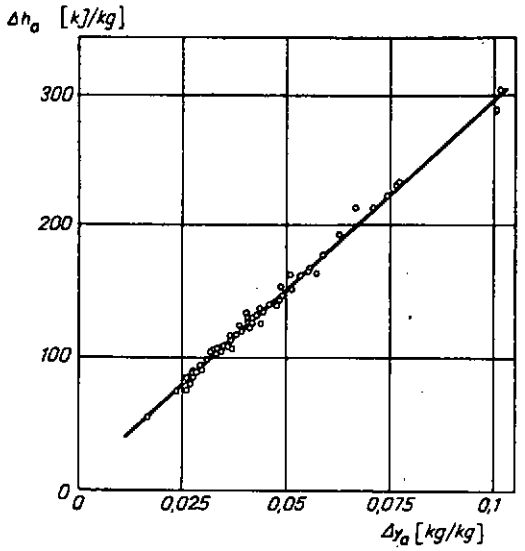

Figure 3 Measurement results

$$\Delta h_a = f\ (\Delta y_a)$$

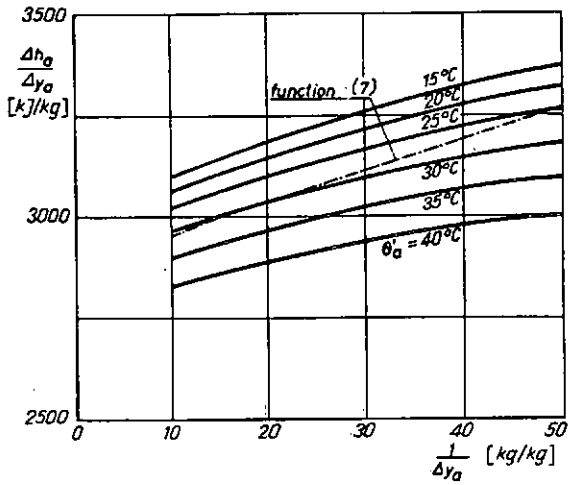

Figure 4 Measurement results

$$q_{net} = \frac{\Delta h_a}{\Delta y_a} = f\left(\frac{1}{\Delta y_a},\ \theta_a'\right)$$

the family of curves (Figure 4 or for other coordinates-illustrated on Figure 1 - Figure 5) was determined. The diagram (Figure 4) presents also the relation (7) which indicates mean values of the results obtained. The shape of this function makes it clear and justifiable that for certain group of dryers when the value $\frac{1}{\Delta y_a}$ increases the temperature of air introduced to the dryer decreases. This results from better ventilation of the paper machine room when the hoods are of an open type.

HEAT CONSUMPTION ANALYSIS

An additional trial to describe these phenomenona with the analytical formula on the basis of mathematical model of the paper dryer was carried out. The formula obtained did not proved to be directly appliable to the determination of q_{net} as it consists of values difficult to determine as, for instance, the heat transfer coefficient from cylinder surfaces to

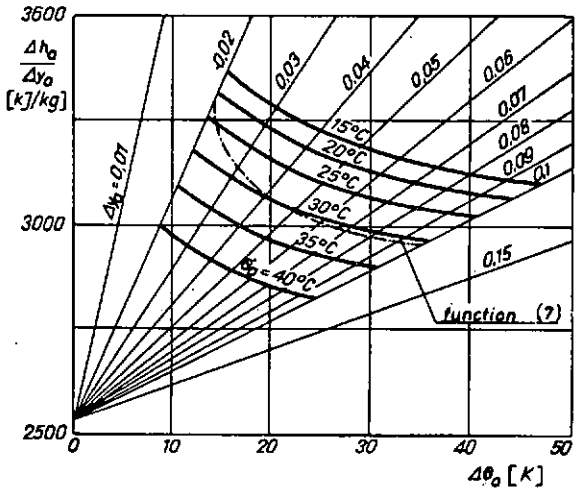

Figure 5 Measurement results

$$q_{net} = \frac{\Delta h_a}{\Delta y_a} = f\ (\Delta y_a,\ \Delta\theta_a)$$

(diagram as on Figure 1)

the flowing air. This formula when somewhat simlified may be used in correction of the value obtained from the said measurements to determine heat consumption for dryers in which evaporation or surface proportions differ significantly from those examined.
Farther analysis and comparision of total heat supplied to the dryer in heating medium q_t with q_{net} value may indicate the method of heating medium (eg. steam) utilization in the dryer. Too high differences $q_t - q_{net}$ indicate excessive steam losses in condensate discharged from the dryer or steam losses resulting from leakages in ducts, valves, etc. It should be noted here, however, that in such case it is necessary to check if there is no error in calculation of the amount of heat leaving the heating system with condensate or in accuracy of steam supply measurements (flow rate).

CONCLUSIONS

The results obtained indicate that reduction in "specific air consumption" in paper dryers from 40 kg/kg to 10 kg/kg decreases heat consumption about 5 to 6 %. Such air reduction is possible only when hoods applied are of the completely closed type. Unnecessery to mention, the hood completely closed gives additional advantages such as better cross direction uniformity of paper and better microclimate in paper machine room.
The presented method of measurements and heat consumption analysis may be successfully applied to all dryers - not only of contact type - in which air or any other medium flowing through the dryer is a humidity carrier.

Basing on these results it is possible to determine the enthalpy of humidified air discharged from paper dryers when, for example, air flow through the dryer changes. This information constitutes an input-data when calculating the size of the heat recovery units.

REFERENCES

1. Strawiński,A., Przegląd Papierniczy, Vol. 33, p. 403-409, 1977. Komunikat ICP No 313 (in Polish),

2. Strawiński,A., Zeszyty Naukowe Politechniki Łódzkiej, No 341, p. 27-36, 1979 (Scientific papers of Technical University in Łódź) (in Polish).

SYSTEM OF DRYING PLASTER BLOCKS USING A HEAT PUMP

R. Gauthier, R. Legoff, and C. Bassac

Electricité de France - Direction des Etudes et Recherches

Moret-sur-Loing 77250

The studies conducted in the laboratories of "Les Renardières"research center of the Electricité de France, have allowed the realisation in 1977 of a prototype installation to dry plaster blocks equiped with a heat pump. This installation of an industrial size, situated in the Paris area, after some difficulties to start it has been working normally since the beginning of 1978. After a trial period, the equipment set up has allowed us to evaluate the performance. The following text describes the main characteristics of the installation and comments on the main measurement reading.

A second installation planned to dry 1000 m^2 of plaster blocks a day is now being set up, this document also gives the main features of this last installation and out lines the main alterations which were done after an operating period of the prototype.

On the level of energy consumption, the consumptions garanteed by the builder of this last drying unit are less than 300 kcal per kg of water, evaporated from plaster, it must be mentioned that for a good traditional drying unit the amount consummed is 900 kcal per kg of water. The analysis of the working operation of these two installations has allowed us to establish a complete work study evaluation.

INTRODUCTION

Drying by hot air is an ideal outlet where you can use a heat pump, in fact almost the complete amount of energy supplied to heat the air at the entrance of the drying unit, is present in the form of steam in the extracted air. Therefore at the outlet we have a cold source of a power almost equal to the calorific needs of the inlet. In France there are over 2000 working installations for drying wood. These installations use a fairly small - sized static drying unit and the refrigeration units used are derived from the ones currently rised for air conditioning therefore the capital investment is low and the overall working operation is favorable.

When the drying operation requires a continuous drying unit, the heat pump, then appears more favorable from the point of view of economy of energy; but this type of drying applies only to a large installation and in that case the capital investment of the installation of a heat pump is rather high. For this operation to be profitable it requires a long operational time (more than 6000 hours per year).

The drying of plaster blocks is very favorable from this point of view and two installations have recently been put into service. The first in 1976 at the PIC Company (Procédés industriels de construction), the second in 1979 at PREMACO Company (Préfabrication des matériaux du Cotentin).

• Principle ofdrying using a heat pump

The heat pump

The heat pump is a unit which conveys energy from a cold source to a hot source; it is comprised of a compressor, two heat exchangers and an expansion valve. It works with a refrigerant; in the condenser this compressed fluid changes from a gas to a liquid and during this changing process supplies heat at the hot source. The expansion valve decreases the pressure of the liquid. This liquid is vaporised in the evaporator at low pressure taking heat from the cold source, the steam is sucked by the compressor and the whole process goes on. It is essentially the change from liquid to steam that allows the calorific fluid to give or absorbs calories.

- Diagram of the principal of a heat pump

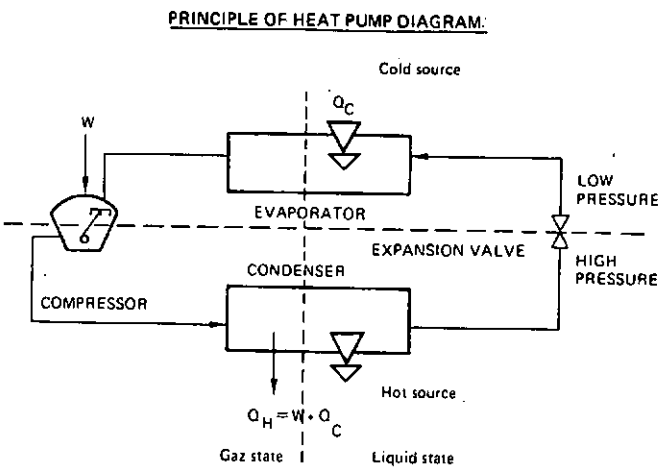

- Thermodynamic cycle of the calorific fluid

The sketch below represents the different changing states of the fluid on an enthalpy pressure diagram and clearly shows the relationship between the thermic energies exchanged with the outside elements (Q_C = quantity of heat at the cold point) (Q_H = quantity of heat at the hot point)

and the mechanical energy (W) necessary to obtain the compression.

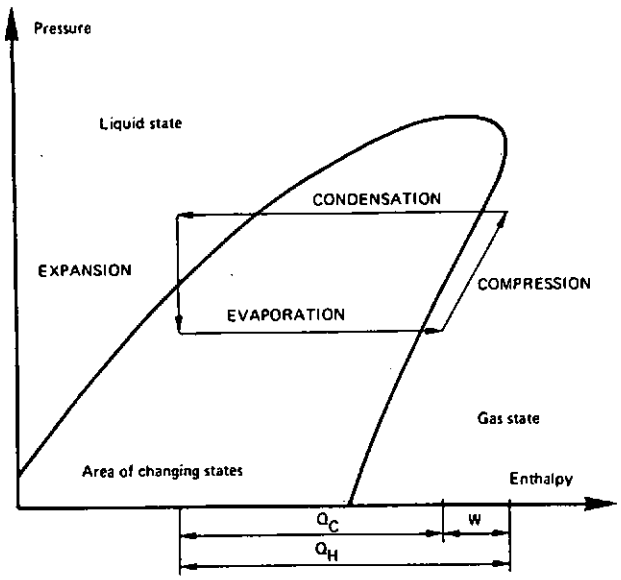

The effeciency of a heat pump is characterized by its coefficient of performance, relationship between the quantity of heat (Q_H) given at the hot source and the quantity of energy (W) necessary for the conveyance. The coefficient of performance $Cop = \frac{QH}{W}$. In the case of an ideal unit following a Carnot cycle, this coefficient is equal to:

$$\frac{T_H}{T_H - T_C}$$

T_H = absolute temperature of the hot source (Kelvin)
T_C = absolute temperature of the cold source(Kelvin)

In the case of an actual working installation, the different irreversibilities of an electric motor and the elements of the thermodynamic circuit balance the coefficient of performance by a factor approaching $\frac{1}{2}$. The smaller the variation of temperature ($T_H - T_C$) between hot and cold source is, the greater is the coefficient of performance.

- Connection of a heat pump to a drying unit

In the case of a static drying unit using hot air, the working principle is as follows:

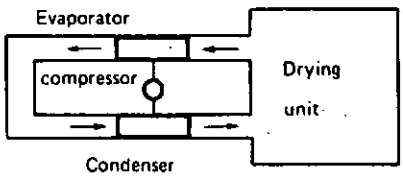

The air extracted from the drying unit is the cold source from which the evaporator takes of its calories. This air cooled and dried, is conveyed to the condenser which at a higher temperature return the calories previously taken. This type of system is used in the majority of drying units with heat pump in France.

In the case of hot air continuous drying unit the connection of a heat pump is equally possible. The positive aspect of such equipment depends on the way the calories are supplied into the drying unit.

In certain classical drying units the drying capacity is supplied at only one point at the inlet of the drying unit, the temperature of the air is over 150°C and the drying capacity and speed are high. For this type of drying unit, the heat pump is not very profitable because the constraint of a small variation of temperature between hot and cold source to get a good coefficient of performance means you have to considerably increase the flow of air and therefore increase your capital investment costs.

In the case of many continuous hot air drying unit the supply of energy is spread inside the tunnel, and the heating is produced by counter flow action. That's the way many thermosensitive products out of which dumpness goes slowly and which need low temperature are treated. The evaporating capacity of the drying unit is not directly linked to be level of temperature obtained but to the succesive reheating of the air; in this case the connection of the heating pump is profitable. The descriptions of the two installations that follow are based on this principle.

THE PIC DRYING UNIT

DESCRIPTION

The PIC Companie manufactures plasters blocks size 0,50 x 0,66 metres in 7, 10 or 14 cm thickness. The drying unit conceived in 1976 is a two way tunnel of about 35 metres long, 3 metres wide and 2 metres high. The lay out by the heating exchangers is represented on the sketch below. The air extracted where the plaster blocks enter is recycled towards the other and where the blocks

come out, by means of a sheeve placed on top of the drying unit which contains 3 evaporators and a condenser, the other two condensers are placed inside the drying unit.

The drying unit has been planned to contain 18 trolleys and on each one 48 blocks can be laid. The production is about 900 blocks, a day. The air cycle is as follows: at the extraction point the air is cooled and dried by passing over the evaporators E_1, E_2, E_3, then it is reheated on the condenser C_3 and enters the drying unit, it goes through it, becomes damp by contact with the blocks. It then goes into the intermediate area and is reheated through the condenser C_2. Coming out of the intermediate area and after reheating through condenser C_1 it goes through the dampest plaster blocks in the drying unit and then starts another cycle again.

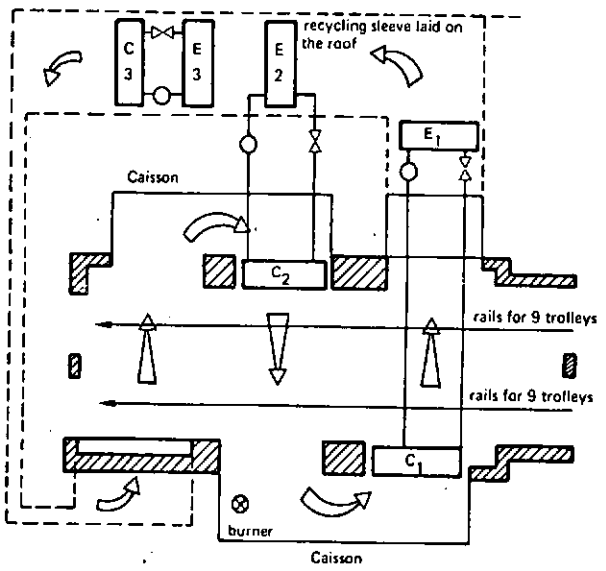

PIC drying unit: sketch of the drying unit seen from above the recycling sleeve which is normally on top of the drying unit is represented here by a dotted line on the same sketch to simplify the drawing.

The three heat pumps are identical. Each compression group is made up of 2 compressors COMEF (1) monted in parallel: a 6 CF 80 driven by a 40 h.p. electrical motor and a 8 CF 80 driven by a 60 h.p. electrical motor.

The refrigerant initially used was R12 B1, a gas burner installed before condenser C_1 was planned for fast temperature rise in the drying unit. The mixing ventilation and the recycling represent a power of about 50 kW.

- Technical problems met during adjustment

The first problem which appeared immediately is the one of spreading the air inside the drying unit, a better spreading of the blocks on the trolleys and the positioning of doors at the ends improve the air circulation in the drying unit.

The setting up of time switches on the starting system very quickly proved to be absolutely necessary to remedy the drawbacks resulting from the numerous micro cuts in the electrical circuit.

After operating for 6 months considerable leaks of refrigerant prevented the drying unit from working, the gasproof joints had deteriorated and the oil showed to contain considerable acidity, it then shows that the stability of the refrigerant R12 B1 is bad for the temperatures that are reached at the backward flow from the compressor i.e. 120°C. After the troubles Group 1 & 2 are loaded with R114, group 3 with R12. Since the beginning of 1978 the drying unit has worked normally for a total of about 6000 hours.

- Main measurement readings

During trial periods, because of the hazards in fabrication it has not been possible to obtain accurate measurements under normal working conditions; the following curve shows the specific consumptions in relation to be daily production. We can estimate a consumption of 370 Wh per kg of evaporated water under nominal working conditions, compared to a classical drying unit running on gaz that exists in that same company the cost saving is about 40 %. That result though it is far from what was hoped is nevertheless satisfactory taking into account the numerous imperfections in the conception of the first prototype.

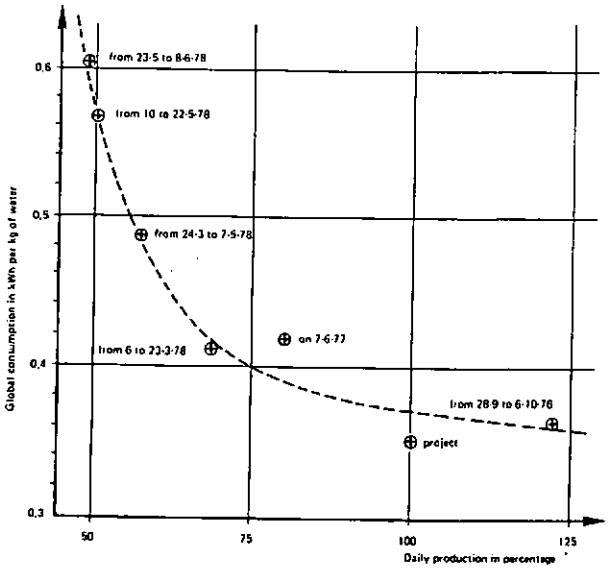

This installation was built by : SAT company (2) and CLIREF (3).

PREMACO drying unit

The first project of drying using a heat pump that allowed an increased production for this company of 300.000 m^2 of blocks per year dates from June 1977, the construction started in 1979. The Ministery of Economy of Energy granted a subsidy and a participation convention has been signed between Electricité de France and PREMACO.

- Description of the installation

The drying unit is a tunnel composed of 3 rails for trolleys. It is about 35 metres long, 8 metres wide and 5 metres high. Each rail holds 14 trolleys and each trolleys is loaded with 126 blocks. The capacity of the drying unit is 5292 blocks, compared to a daily production of 3700 blocks that means a drying period of 34 hours.

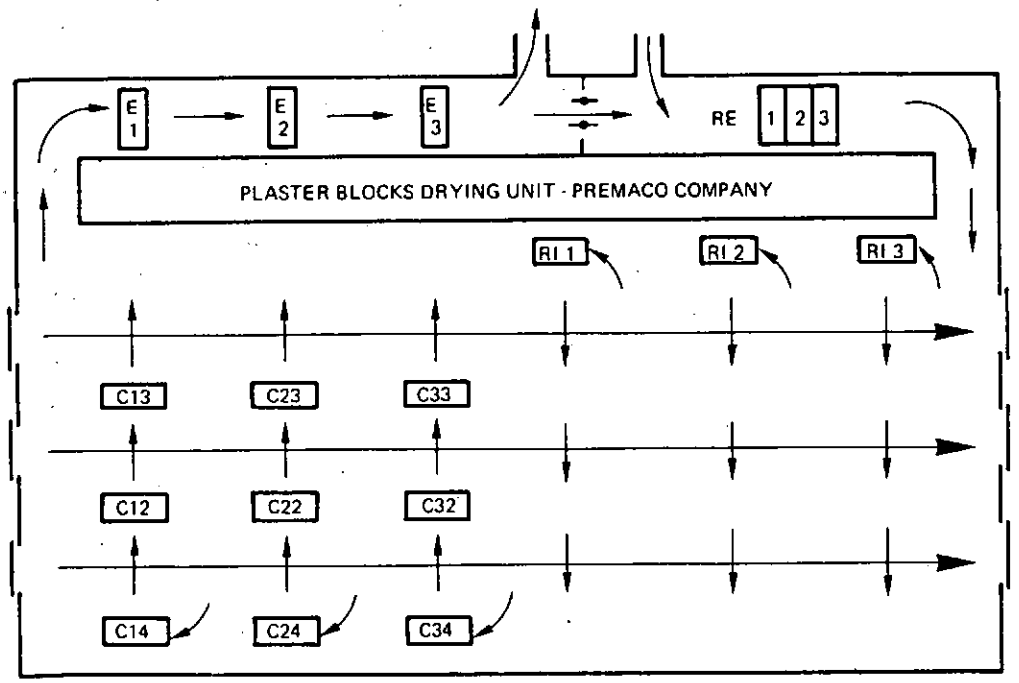

The drying unit is composed of 2 areas. The first one, where the damp blocks enter is equiped with condensers of 3 heat pumps wich garantee the drying process. The second area, wich is near the exit, is heated by the cooling batteries of liquid refrigerant condensed in the first area.

The recycling of the air is garanteed from zone 1 to zone 2 from the top of the drying unit through an exterior caisson containing the evaporators and the cooling units of liquid refrigerant.

A regulation by mixing with outside air allows a thermodynamic balance of the system.

To avoid the troubles we had with the PIC drying unit the temperature level of the PREMACO drying unit is lower. The heat pump condenses at a temperature of 60°C, with allows the groups to fonction with freon R12 (Nevertheless you must take into account that the recent studies concerning the technology of heat pumps, now allows to use materials up to an air temperature of 120°C). The power of the evaporators is estimated at 1300 kW and the one of the condensers and refrigerator unit liquids at 1500 kW. for an electrical power of 270 kW. The overall return of the engines and the compressors is about 0.6 and the overall coefficient of performance of the drying unit is about 4 (taking into account the power of the ventilators which is of about 100 kW).

The builder garantees a specific consumption of 250 Wh per kg of water. The drying unit must allow the evaporation of 1540 kg of water per hour for 3700 blocks per day.

- Financial justification

We have taken measures on the actual drying unit that runs on heavy fuel n° 2.

They have allowed us to determine the specific consumption in primary energy, at its nominal production, as well as the energy cost of the drying process:

1050 primary kcal per kg of water and 6.99 FFC per kg of water (FFC : French Francs Centimes).

On the base of the garantees given by the builder and for an electrical kWh sold 15.7 FFC, we get for the drying unit with a heating pump:

625 primary kcal per kg of water and 3.93 FFC per kg of water.

Therefore there is a primary energy saving of 40 % which represents almost 570 tons of oil a year. On energy cost it's a saving of 44 % which represents almost 400,000 FF per year.

The cost of the drying unit with a heat pump is about double the cost of the classical drying unit and the return on the over capital investment, is estimated from the elements above at 2 years.

This installation was planned by Fläkt industrie (4).

Taking into account the financial Aids of the ministery of Economy of Energy and the Electricity of France, this period is reduced by half for this present company.

ACKNOWLEDGMENT :

Nous remercions la Société PIC et la Société PREMACO qui nous ont autorisé à présenter la description de leurs installations.

REFERENCES

(1) COMEF - rue de Savoie 69800 ST PRIEST FRANCE

(2) SAT - AIX-LES-BAINS FRANCE

(3) CLIREF - Les Meurises 69780 MIONS FRANCE

(4) FLAKT INDUSTRIE - 26 quai Carnot 92212 St CLOUD - FRANCE

PIC : Bray-sur-Seine 77480 - FRANCE

PREMACO : Ste Mère Eglise 50480 MANCHE FRANCE.

ENERGY SAVING IN DRYERS

Kai Richardt

ANHYDRO A/S
Copenhagen, Denmark

ABSTRACT

In recent years there has been a substantial development in reducing the energy consumption in dryers.

This development has been moving in two directions,
1. Development of the actual drying processes to make them consume less energy.
2. Development of heat recovery systems.

A number of different heat recovery systems are discussed and emphasis is put on systems where heat is recovered from the exhaust air on the dryer and transferred to the inlet air of the dryer.

Efficiency and applications of the different heat recovery principles are discussed as well as optimization.

NOMENCLATURE

e_t = thermal efficiency
G'' = rate of outgoing product, kg/min.
t_i = dryer inlet temperature, °C
T_m = residence time, min.
t_o = ambient temperature, °C
t_u = dryer outlet temperature, °C
t_1 = temperature of spent air before recuperator, °C
t_2 = temperature of spent air after recuperator, °C
t_3 = temperature of fresh air before recuperator, °C
t_4 = temperature of fresh air after recuperator, °C
U_s = mean vertical velocity, m/sec.
U_t = terminal falling velocity, m/sec.
Z = active quantity of powder in the chamber, kg

INTRODUCTION

Because drying is a very energy consuming process, the increasing energy prices have forced a rapid development in reducing energy consumption.

In the following some examples are given on development to make the drying processes less energy consuming as well as a variety of heat recovery systems.

The greatest importance is attached to practical solutions, which have been applied on dryers.

DEVELOPMENT OF LESS ENERGY CONSUMING DRYING PROCESSES

Spray Drying

Traditionally, a large number of products were spray dried in one single stage to their final moisture content.

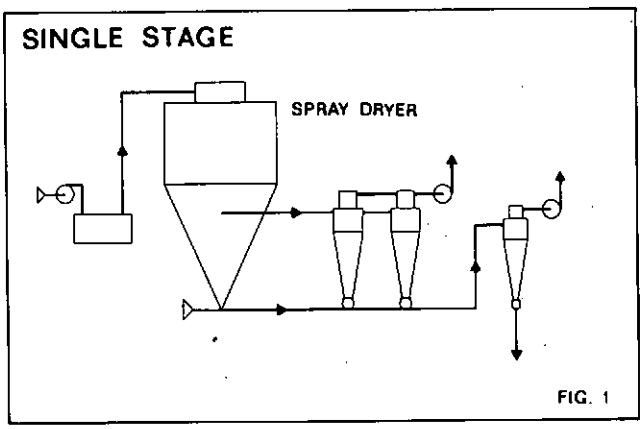

Fig. 1. Single Stage Spray Dryer.

This means that when evaporating the last water from the particles, the drying medium has a high humidity content, and consequently the dryer needs to run at a relatively high outlet temperature. The result is, of course, a poor efficiency or a high energy consumption.

To improve this efficiency, the dryers were developed into two-stage dryers (mainly in the dairy and food industries)

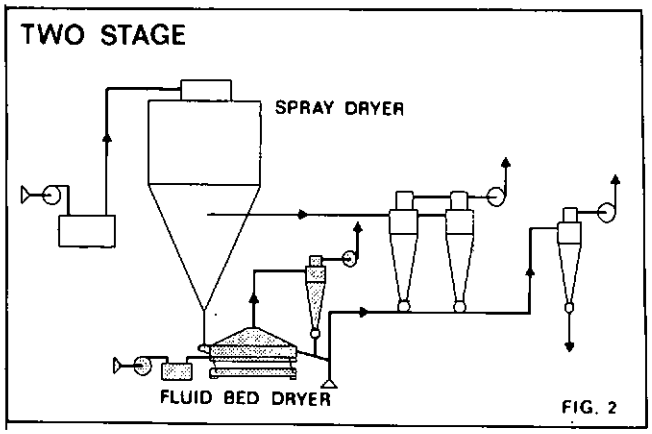

Fig. 2. Two-Stage Drying Plant.

Instead of drying the powder to the final moisture content in the drying chamber, moist powder is discharged from the chamber into an attached fluid bed, where it is secondary dried to the desired moisture content.

The thermal efficiency for the spray dryer

$$e_t = \frac{t_i - t_u}{t_i - t_o}$$

is

Single stage, t_i=200,t_u=93:e_t=.59,index=100
Two-stage , t_i=200,t_u=76:e_t=.69,index=117
Two-stage , t_i=250,t_u=82:e_t=.73,index=124

Of course, the energy costs of the second stage should also be considered and fig. 3 shows the total energy costs as a function of the evaporation in the second stage.

But also the investment costs (depreciation and interest) must be considered in order to get a complete picture of the economy. In fig. 4 the energy-and investment costs are shown as a function of evaporation in the second stage.
(Interest rate 12% p.a., 10 years' depreciation).
Curves for four different spray dryer inlet temperatures are shown.

As for two-stage drying, it can be concluded that for a typical dairy or food industry application, the total energy costs (heat and power) can be reduced by approx. 20%, and when taking investment costs into consideration too, the complete energy and investment costs can be reduced by approx. 17%.

The same development i.e. introducing more drying stages, is also applied to other types of dryers. By way of example two-stage flash drying and multi-stage flash-fluid bed drying may be mentioned.

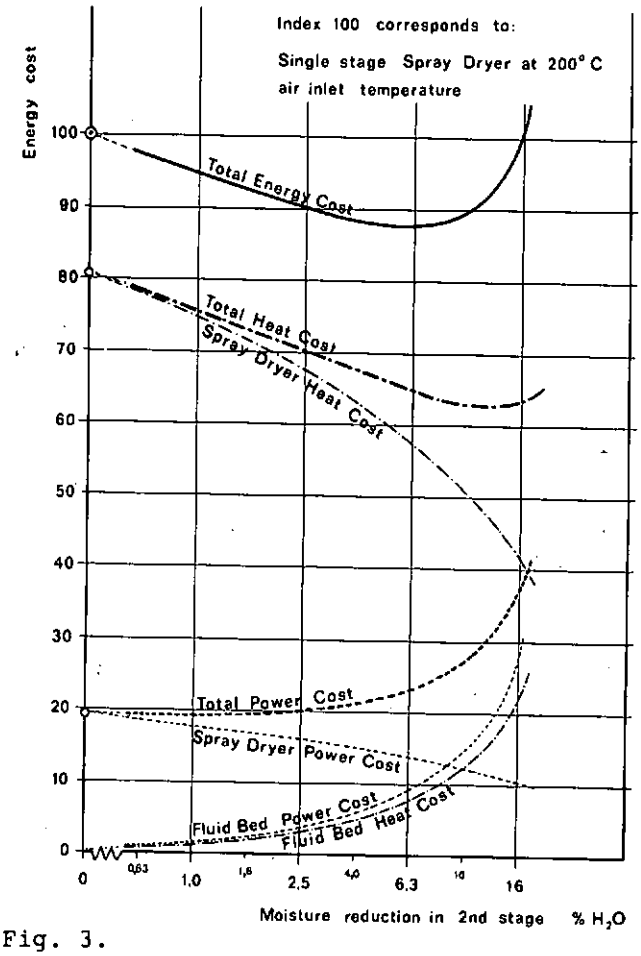

Fig. 3.

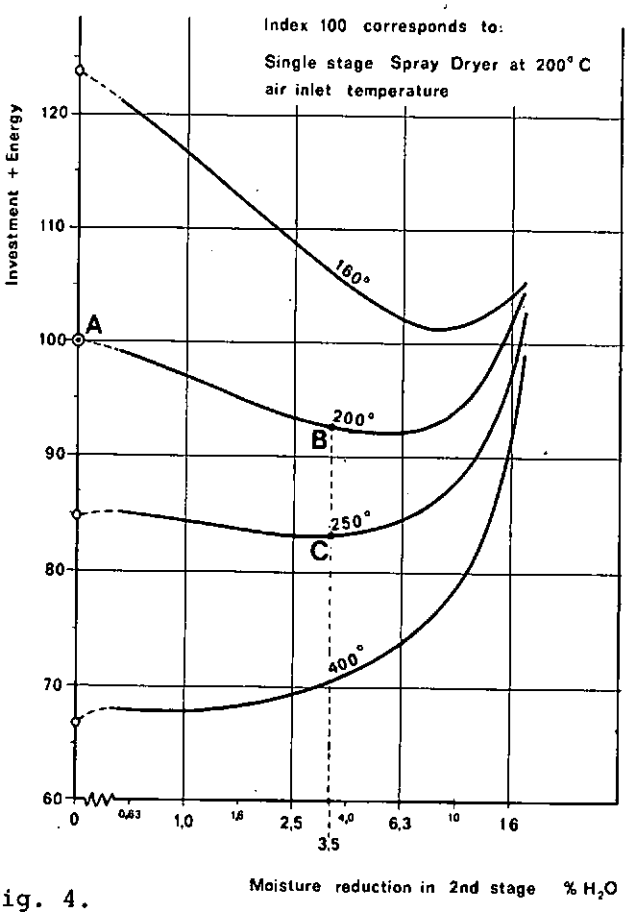

Fig. 4.

However, these principles are based on the same ideas as for reducing energy consumption, and instead of describing them in detail, I should like to go over two examples, where the reduction of energy consumption is based on other ideas.

PASTE AND FILTER CAKE DRYING

A number of products were traditionally dried with a relatively low solid content even if a considerably higher solid content in the feed product could be achieved by using e.g. mechanical dehydration. Often the reason for doing so was that there was no drying equipment available, which could dry the product with a high solid content in a rational, continuous operation.

The increasing energy prices have, of course, called such extravagance to question and have forced the development of new drying equipment able to handle pastes/filter cakes in one continuous operation.

The Spin Flash dryer is a result of this development, and it has proved efficient in an increasing number of industrial installations throughout the past ten years.

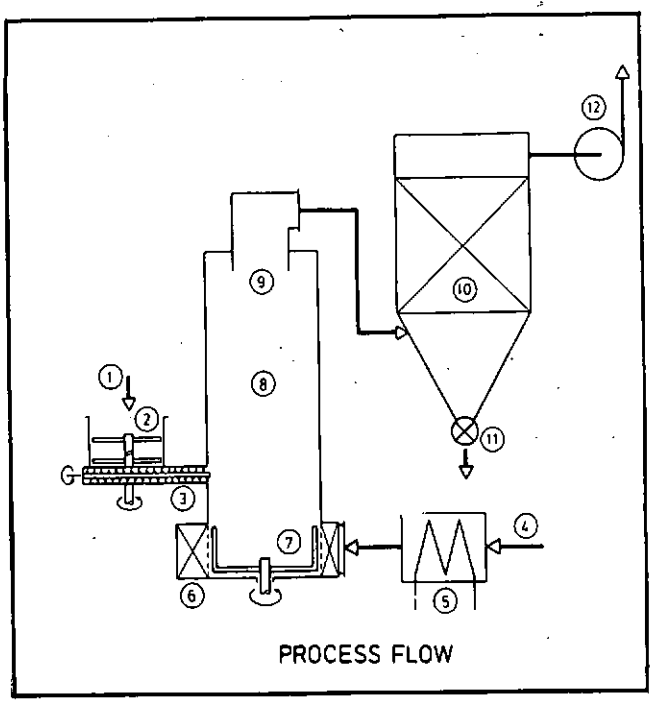

Fig. 5. Principle of the Spin Flash Dryer.

At 1 the wet product is introduced in the form in which it leaves the preceding process, e.g. as filter cakes. In the feed vat 2, equipped with agitator, the product is forced down into the screw feeder 3. The screw has an infinitely variable drive enabling it to introduce the product into the drying chamber 8 at the rate, which gives the required drying out of the product. The agitator 7 in the drying chamber bottom rotates at approx. 100 r.p.m. and has two functions: it supports the fluidization arising from the hot drying air flow from the air distributor 6. Moreover, the agitation has a mechanical effect on the fluidized layer in the drying chamber bottom, i.e. disintegrating the still wet lumps, resulting in an increased rate of evaporation.

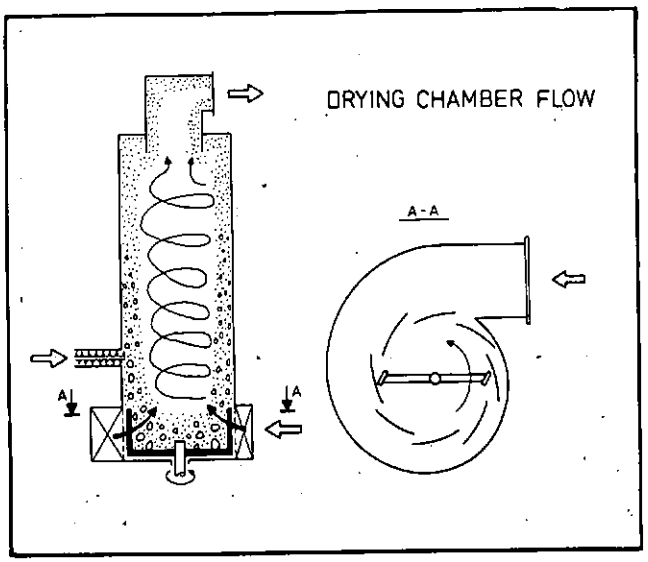

Fig. 6. Spin Flash Flow Principle.

The vertical velocity through the cross section of the chamber has a great influence on the process. The mean vertical velocity U_s is chosen in relation to the terminal falling velocity, U_t of the dried powder.

The ratio

$$U_s/U_t$$

is an important design factor, as it affects the product residence time T_m in the chamber. The residence time is given by the equation:

$$T_m = Z/G"$$

where Z = active quantity of product in the chamber kg
G"= rate of outgoing product kg/min

Very short residence times (<1 min.) will occur for products, which easily disperse and easily dry up.

A long residence time is necessary for products difficult to disperse. Most common residence times are between 1 and 20 min.

Fig. 7 shows the relation between the residence time T_m and the ratio of velocities. The diagram is based on tests with a large number of products.

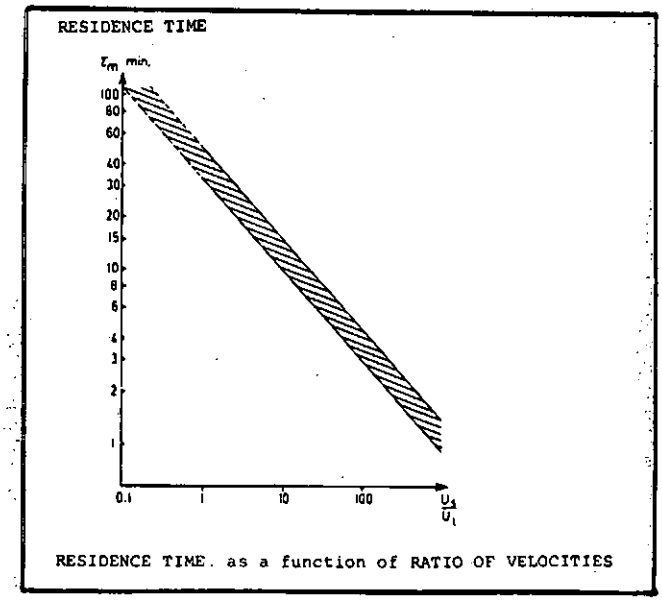

RESIDENCE TIME as a function of RATIO OF VELOCITIES

Fig. 7.

The Spin Flash plant is mainly applied in the chemical, ceramic and pharmaceutical industries, where more than 50 dryers are now in operation.

Especially the pigment and dyestuff industries have found it attractive to utilize the capability of the Spin Flash dryer to dry high viscous pastes/filter cakes direct to a dry powder in a continuous and automatically controlled operation.

The Drying of Green Crops.

Another example of a less energy consuming process has been developed for the treatment of green crops.

Green crops, e.g. alfalfa, were traditionally just dried after harvesting and used for animal feed. The disadvantages of this procedure are,

- The moisture content is removed by using a very energy consuming drying process.
- Because of the high fibre content the dried green crops can be used for ruminants only.

The main principle of the VEPEX process is the mechanical pressing of e.g. alfalfa and thereby getting 2 fractions.

1) A fibre-containing "press cake" with a very low water content, which is dried in a normal way.
2) A protein juice containing the greater part of the plant protein. The juice can be evaporated before drying and protein fraction can be used to feed monogastric animals or for human consumption.

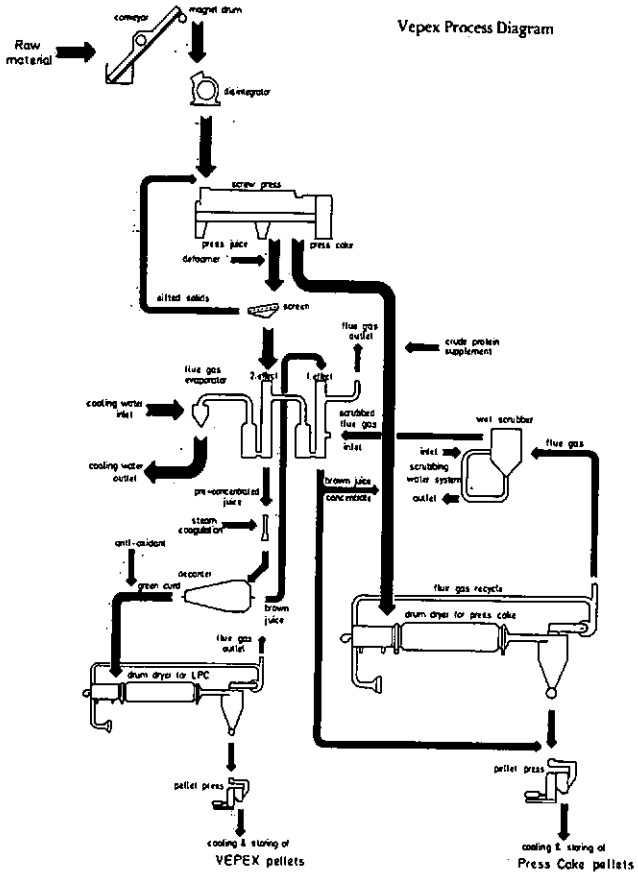

Fig. 8. Vepex Process Diagram.

As can be seen from the process diagram the flue gas from the drum dryer is utilized as heating medium for the evaporator. In fact, you get a three-stage dehydration system with heating medium and product in a counter-current flow.

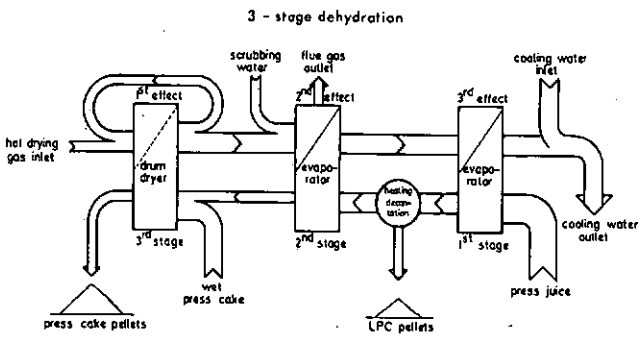

Fig. 9. Three-Stage Dehydration. By this dehydration system the specific fuel cost can normally be reduced by more than 50% compared to traditional drum drying.

HEAT RECOVERY IN DRYERS

Because of the numerous different principles in heat recovery, it might be practical to clarify a few concepts:

Direct Recovery

By direct heat recovery we here understand processes in which the heat exchange takes place through convection from one medium to the other without an inserted heating surface.

Indirect Recovery

Contrary to the direct heat exchange, a heating surface has here been inserted between the two flowing media to avoid them from getting into contact with eachother.

Transitive Recovery

Transitive recovery is characterized by the fact that the heat, recovered in a process, is transferred to and utilized in another process.

Intransitive Recovery

The characteristic of the intransitive heat recovery is that the heat, which is recovered in a process is utilized in the same process.

Fig. 10 gives a schematic survey of the recovery principles and fig. 11 shows the same processes in a flow diagram (in the flow diagrams the dryer is shown as a spray dryer, but in most cases the principle could be used with other types of dryers.

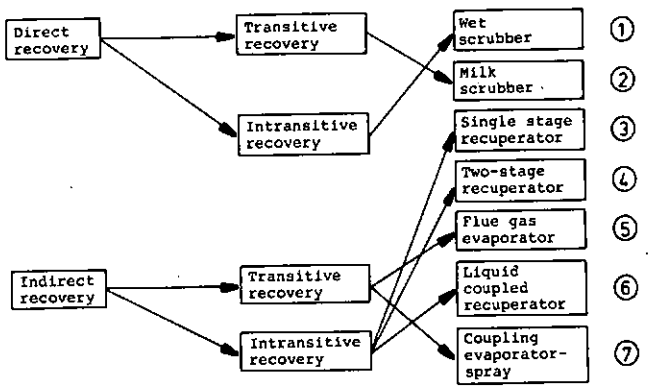

Fig. 10. Schematic survey of recovery principles.

Recovery Principles

The principles in fig. 11 show some typical methods for heat recovery. They will be briefly taken through in the following.

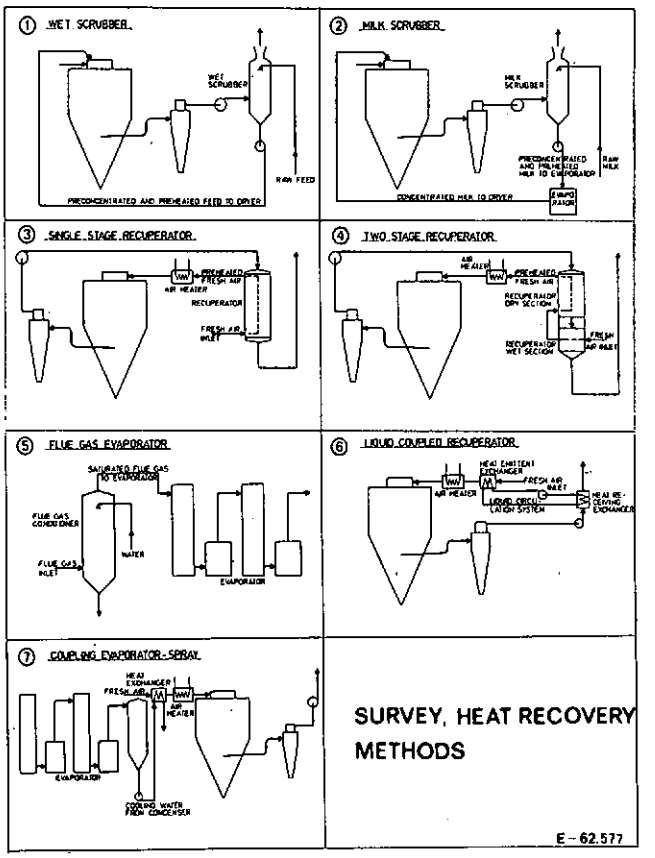

Fig. 11.

Wet Scrubber

In this process, fig. 11,1, the outlet air is washed by leading the feed product through the scrubber before it is led to the drying plant. By doing so the feed product is heated at the same time as enough water is evaporated to saturate the drying air. It goes without saying that this is a favourable solution and furthermore an inexpensive investment.

Unfortunately, the method is not very applicable, because only few products can be further concentrated just before the final drying. Foam formations and deposits in the washer are common problems. Such washers have been supplied mainly for the chemical industry, e.g. for $CaCl_2$

Milk Scrubber

Until now, this principle has, as indicated by the name mainly been connected to milk plants, and the process is very much the same as the one previously mentioned. It is however, transitive, as the energy recovered from the spray dryer is utilized in the evaporator. The method is not very heat economical, as the evaporator has already got a very low energy consumption. (A spray dryer uses approx. 15 times as much heat to evaporate one kg og water).

By way of comparison it may be mentioned that the efficient heat recovery from milk scrubber is only 25% of the heat recovery when using heat transfer from outlet air to inlet air (fig. 11,3 and 11,6) provided the same drying temperatures.

The far most important economic advantage of the milk scrubbers is the recovery of the residual powder in the outlet air from the cyclones. But for milk products this advantage is questionable because of the still unsolved bacteriological problems in the scrubber.

Single Stage Recuperator

When using fig. 11,3 the hot outlet air from the drying plant is heat exchanged with the cold inlet air in a plate or tubular heat exchanger.

This will mean an energy saving of 20-25%.

In order to be able to handle drying air with a certain dust load, the heat exchanger must be designed for and equipped with an automatic wet cleaning system. Typical cleaning procedure is 10 min. every 4 hours of operation. The cleaning takes place during production and does not affect the normal dryer operation. The principle is described in a subsequent paragraph.

Two-Stage Recuperator

When using the single stage recuperator principle, only the sensible heat in the outlet air is utilized, as it does not reach the saturation temperature. When using the two-stage principle,part of the latent heat in the outlet air is utilized for a pre-preheating of the fresh drying air.

This takes place in a separate, constantly sprinkled heat exchanger at the same time acting as a wet scrubber. Patent is pending on this principle, which will be described in a subsequent paragraph.

Flue Gas Evaporator

It is a condition for using a flue gas evaporator that there is a high content of latent heat in the air,which is recuperated, i.e. the air has a high dew point. Therefore, the process is limited to be used in cases, where the drying process takes place at high inlet temperatures.The residual part of the free energy, if any, in the air is converted to latent by humidifying the air in a scrubber, this results in a higher dew point, typically about 80°C.

After humidification and cleaning, the humid drying air is passed to the steam side of the evaporator giving off energy for evaporation of water from the product. An example was explained in detail under "Vepex Process".

Liquid Coupled Recuperator

In reality this principle is identical with the one shown in sketch 11,3, the only difference being that a heat transferring medium e.g. water is placed between the heat receiving surface and the heat emitting surface.

In practice, one heat exchanger is installed in the outlet air and a separate heat exchanger in the fresh air inlet. A circulating pump provides for transport of the hot water from the heat receiving heating surface to the heat emitting one and for recirculation of the cooled water.

It is an advantage to be almost independant of the distance between the outlet duct and the fresh air inlet. The principle will be described in detail in a subsequent paragraph.

Coupling Between Evaporator and Spray Dryer

From an evaporator the cooling water or the waste condensate at a temperature of about 45-50°C is led to a heat exchanger in the fresh air intake to the drying plant. The installation costs are very low, because it is possible to use relalively small heat exchangers.

Of course, the principle is limited to applications, where there is an evaporator working at the same time as the drying plant.

HEAT RECOVERY FROM DRYER OUTLET AIR TO HEAT THE INLET AIR

Among the mentioned principles of heat recovery there are several linked to specific upstream or downstream equipment or to specific products.

The most universal heat recovery principles are the ones recovering the heat from the dryer outlet air to heat the inlet air, i.e. No. 3, 4 and 6 in fig. 11.

Let us leave No. 11,4 - two-stage recuperation for a moment and just look at No. 11,3 - single stage recuperation and No. 11,6 - liquid coupled recuperator. They are both operating without condensation. i.e. the outlet air from the dryer is cooled to just above the saturation temperature.

These two recuperator systems are doing approximately the same duty, and the choice between them is connected to the dust load in the air leaving the dryer. If conventional cyclones are used for powder separation, i.e. the dust load is 50-300 mg/m^3, the single stage recuperator with its automatic cleaning in place system should be chosen.

If the dryer is equipped with a bag collector, i.e. the dust load is below 10 mg/m^3, the liquid medium recuperator (No. 11,6) should be chosen. Technically the single stage recuperator will, of course do the job, but the liquid medium recuperator is less expensive and there is no need for the sophisticated cleaning system.

The typical energy savings from these recuperators can be seen from the following example:

Dryer: $t_i = 180°C$, $t_u = 90°C$

Recuperator: $t_3 = 25°C$, $t_4 = 65°C$

Energy Saving = $\frac{65-25}{180-25}$ = 26% of the energy used to heat the drying air to 180°C.

The energy used because of the pressure loss over the recuperator and recirculation pump for the cleaning system, if any, should, however, be deducted. These two factors will typically be 3-4%, which will then give an energy saving of 22-23%.

The Two-Stage Recuperator

This is a further development of the single stage recuperator in order to improve the heat recovery and also include powder recovery from the dryer outlet air.

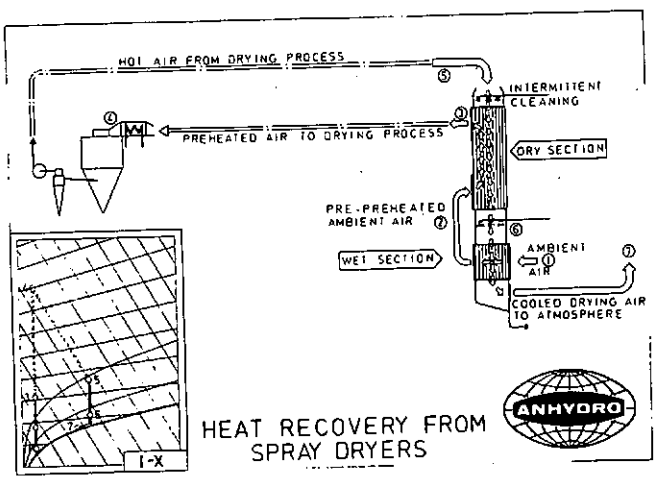

Fig. 12. Two-Stage Heat Recuperator. Principle of Operation.

The upper section is identical with the single stage recuperator and is also dry working, i.e. without condensation. From this section the spent drying air at a temperature just above the saturation point passes down through the wet section where condensation takes place and latent heat is removed from the spent drying air.

The advantages of the two-stage recuperator are:

1) Because also latent heat is recovered the recovery efficiency is higher than for normal dry air to air heat recovery systems.

2) The temperature of the preheated drying air after the recuperator is practically independent of the temperature of the same air before the recuperator (at lower ambient temperature more latent heat is recovered). This also means that temperature variations (e.g. day/night) do not affect the temperature of the fresh air after the recuperator.

3) Powder recovery is automatically included, - approx. 85% of the dust in the spent drying air is collected in the wet section. This, of course, makes two-stage recuperation an obvious solution in cases where scrubbers are required because of environmental protection.

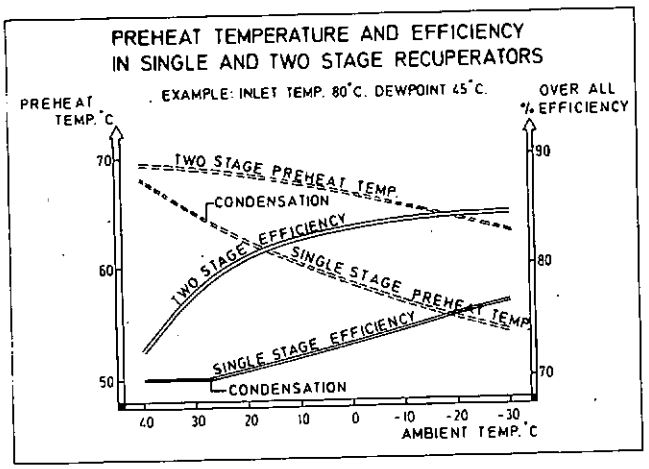

Fig. 13. Comparison of Single Stage and Two-Stage Recuperator Efficiency

Optimization of Heat Recuperators

For a short moment one may think that the more the ingoing air is preheated, the more economic a dryer.

This is, of course, not true, because one must see the energy savings in connection with the investment costs. In order to optimize the recuperator (with regard to savings/investments) a diagram as shown in fig. 14 can be used.

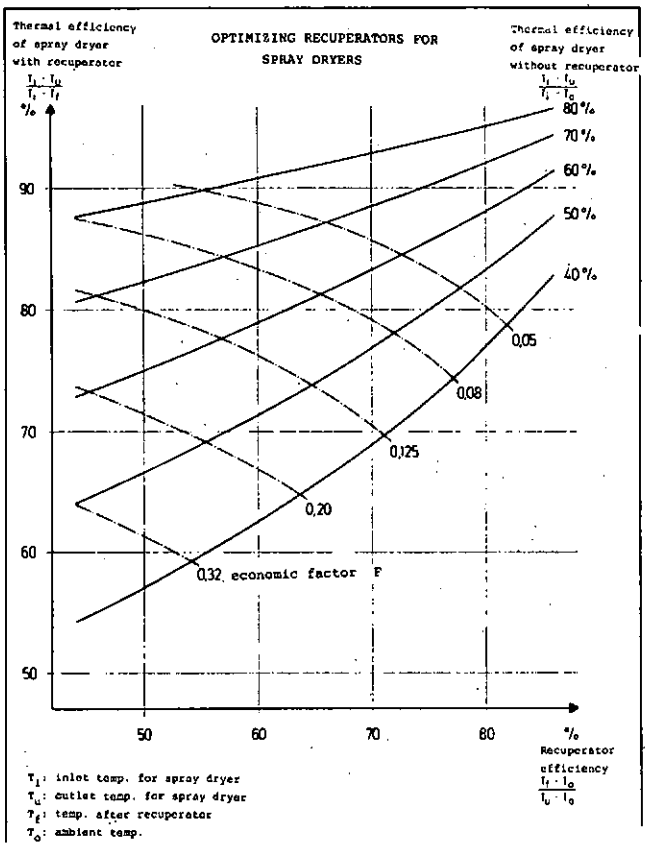

Fig. 14.

The economic factor F =

$$F=10x\frac{(depreciat.+interest\%)x(recu.price/m^2)}{(operat.h/year)x(price/Mcal)x15(t_i-t_u)}$$

Example of how to use the diagram:
If a dryer has a thermal efficiency without recuperator of 60% and the economic factor F is calculated to be 0.05, then the optimum recuperator will be of 72% efficiency giving the dryer with the recuperator a thermal efficiency of approx. 85%

As can be seen from the above, there are a variety of possibilities of saving energy in dryers and with the still unstable energy situation, the development in energy saving will continue in the years to come.

REFERENCES

1. O.T. Kragh: An analysis of the two-stage drying process (English/German) Nordeuropæisk mejeritidsskrift nr. 1-2, 1977.

2. P.S. Antonsen: A new generation of milk drying plants (English/German) Nordeuropæisk mejeritidsskrift nr. 11-12, 1976.

3. Milchwerke Westfalen eG: Inbetriebnahme eines neuen Sprühturmes, Deutsche Milchwirtschaft, Juli 1979.

4. P.S. Antonsen: Low energy milk drying Plant of high Sanitary Standard. World Galaxy No. 7, 1978.

5. The new Toni Dairy Plant, American Dairy Review, November 1977.

6. O.T. Kragh: Spin Flash Trocknung. Keramische Zeitschrift (30. Jahrgang Nr. 7 1978, p. 369).

PRECONCENTRATION OF WHEY: RESULTS FROM USE OF AN EVAPORATOR EQUIPPED WITH MECHANICAL RECOMPRESSION OF STEAM

Messrs DESCHAMPS G. - GAUTHIER A. - LEGOFF R.

E.D.F. ETUDES ET RECHERCHES - Centre des Renardières

BP N°1 - 77250 MORET S/LOING

ABSTRACT

In June 1978, an installation for preconcentration of whey equipped with mechanical recompression of steam started up in a cheese-dairy plant in the Centre of France. This installation conceived in the desire to save energy, was subsidized by the Energy Conservation Agency; it has been implemented and is the subject of a series of measurements in order to establish real consumption during use.

Treating a thermosensitive product in partial vacuum, it forms the first reference work in the French dairy industry.

Results are as follows:

For an evaporating capacity of 10 tons/hour and evaporation at 65°C, consumption measured under normal working conditions is:

- electric energy : 20 Wh/kg of evaporated water (including auxiliaries),
- thermic complement : 22 Wh/kg of evaporated water (19 kcal/kg).

It should be noted that this thermic complement is made starting from hot water.

The overall consumption of primary energy during use is about 7 x 10^{-3} TEP/ton of evaporated water; this consumption is equivalent to that of a "theoretically ideal" evaporator comprising 7 or 8 effects.

For 6000 hours running per year and in comparison with a standard 4 effect evaporator with thermocompressor, primary energy saving achieved thanks to this installation, is about 300 TEP/year.

In the text of the communication, the main characteristics of the installation, the measurement results and a few figures relating to economic data, will be given.

NOMENCLATURE

TEP = ton of equivalent oil (10000 thermies)

EDF = Electicity of France

TC = Absolute temperature of condensation (°K)

TF = Absolute temperature of evaporation (°K)

Δt = Difference between temperature of condensation and evaporation (temperature of satured steam)

TS = Total Solid

F = French Francs

HT = Duty Free

1 cal = 4,18 J = 1,16 Wh = 10^{-6} Thermie.

INTRODUCTION

The dairy industry is a large energy consumer, particularly for concentrating and drying operations.

Faced with the rise in price of energy, manufacturers have very quickly felt the necessity of economizing energy in order to reduce their production costs, by optimizing their existant installations or by making use of techniques different from those normally found in the trade.

In France, the turnover of the dairy industry represents approximately 27% of the turnover of all the agricultural and food industries, and is equivalent to that of metallurgy.

On a total production of 33 x 10^9 litres per year, approximately 2/3 are collected by 2000 factories.

This industry which employs one worker out of thirty, is a sector where investments are very high and where at the present time great technological progress is noted, on the operating process level as well as that of automatization. It therefore lends itself fairly easily to a certain penetration of electricity and this is why EDF have undertaken several research steps in this field (separation on membranes, mechanical recompression of steam) in order to increase the relative part of electricity when it can be economically substrited for other energy sources.

EVAPORATION

We recall here a definition of evaporation. "It is the operation which consists in vaporizing a liquid (a solvent) in order to obtain in more concentrated state or even in pure state, the substance considered as non volatile which was dissolved there".

Vaporization of the solvent requires an energy supply corresponding to the latent heat.

Standard process: multiple effects

In the standard process, energy is supplied by steam generated in a boiler, generally by burning fuel oil or gas.

The steam, condensing on the fire-chamber surface of the evaporator frees the calories necessary for vaporization of the solvent. Nearly all the energy introduced into the system is recovered in the form of latent heat in the steam coming from the solvent and it is possible to re-use this energy in another heating bundle at a temperature and pressure level lower than that of the first bundle; in this way the steam given off in the first effect serves as steam heating for the second, and so on. The consumption of steam is, at a first approximation, in inverse ratio to the number of effects.

Considerations both technical and economic limit in practice the number of effects carried out for a given installation.

Finally, it is indispensable to condense the steam which is emitted in the last effect and generally it is not possible to recuperate these calories for they are at a too low temperature level.

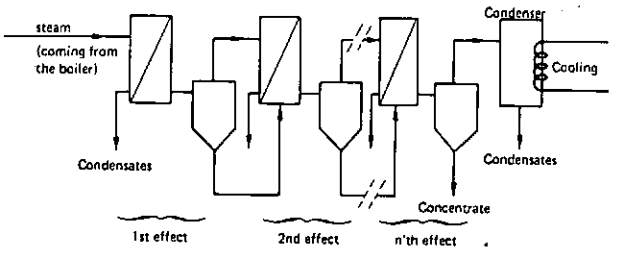

Figure n° 1 : General diagram of a multiple effect evaporator.

The circulation of steam is effected in series. That of the product is also carried out in series but different solutions can be considered; there can also be a recirculation of the product on certain evaporation bundles.

Finally it is also possible to reduce consumption of steam by adding one or several thermo-compressors.

Mechanical vapor recompression (MVR)

In mechanical recompression, steam coming from the solution to be concentrated, instead of being directed towards a second bundle, is drawn off by a compressor which raises its pressure,and consequently the temperature of saturation steam. This steam, the temperature level of which has just been raised, is then used as steam heating for the evaporator.

The rise in temperature at saturation must be sufficient to ensure thermic transfer with the solution to be concentrated, and generally a rise by a few centigrade degrees is sufficient. All the calories contained in the steam coming from the solution can therefore be reused directly (after revalorization by compression) in the process and it will only be necessary to supply mechanical energy for compression; this energy is very low in comparison with energy interchanged in the evaporator.

Practically, a thermic complement is often necessary since the power introduced for mechanical work is not generally sufficient to cover thermic loss in the installation.

Finally, a thermic complement is also indispensable when starting up the installations, but the power to be provided is, however, much less than that which is used in the standard process (multiple effect).

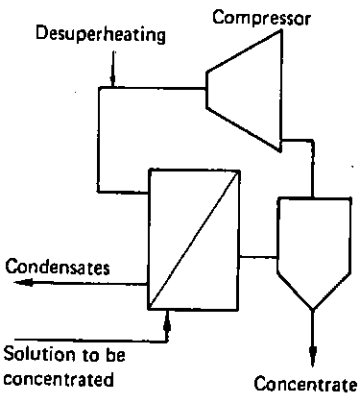

Figure n° 2 : General diagram of an evaporator with mechanical recompression of steam.

The actual carrying out varies depending on the product to be treated and the size of the installations. There can be a central vacuum to ensure regulation when work is done below atmospheric pressure (thermosensitive products).

Equally for technical reasons, the evaporator can be made up of several bundles. They are then connected in parallel for the steam and in series for the product. However for economic reasons and for large installations (> 15 tons evaporation/hour)

.../...

one can envisage a double effect in recompression of steam: the steam in that case is drawn by suction to the second effect then reinjected to the first.

The difference in temperature between evaporation and condensation at each effect will then be very small (about 3 degrees).

Theoretical comparison

A simplified theoretical study makes it possible to compare the various techniques.

For the multiple effect process, it can be supposed that 1 kg of steam evaporates 1 kg of water, wich is not entirely true and that adjunction of a thermocompressor is equivalent to a supplementary effect (one can go up to two in the case of high performance material). Consumption of steam will be inversely proportional to the number of effects increased by 1 (or 2).

In the case of mechanical recompression of steam, mechanical expenditure connected to steam compression will of course depend on the variation in temperature (at saturation) supplied by the compressor.

The following graph compares the theoretical specific consumption of an evaporator with mechanical recompression for two values of Δt.

The values indicated are at utilization, they do not take into account production and distribution outputs of the different forms of energy, the basis of comparison being very variable from one country to another*.

For mechanical recompression, we have supposed that the coefficient of practical performance was half the theoretical coefficient determined for a Carnot cycle.

In reality, experience shows that depending on the efficiency of the motor and above all that of the compressor, ponderation can be set between 0.5 and 0.7.

---

* We make no distinction between energy used in thermic form and that used in mechanical form, as an indication, in France, the Energy Conservation Agency has adopted the equivalence:

1 electric kWh = 2.5 thermal units in production.

FIRST APPLICATION IN A DAIRY IN FRANCE

The installations

It was effected by the ORLAC group at the St. Etienne plant (1).

- Characteristics:

The nominal capacity of the cheese-dairy in which the first installation for concentration by mechanical recompression of steam was set up, has a nominal capacity providing for the daily treatment of:

- 100.000 l of milk for consumption (pasturized milk)
- 150.000 l of milk treated for cheese.

The main characteristics of the concentrator started up in 1978 are as follows:

- Evaporator : tubular type with falling film: constructor LAGUILHARRE SA (2)
- Compressor : centrifugal type bi-stage low speed (3000 tr/mn), construction entirely in stainless steel - constructor Ets NEU (3) (this material was conceived to reduce to a minimum the risks of stoppage for intervention, and maintenance time).

Electric power required is about 210 kW, approximately 40 kW of which for the auxiliaries (circulation pumps, vacuum pump, ...).

The calorific supply comes from hot water at 95°C.

- Nominal capacity : Whey intane : 12.5 T/h
  Evaporation : 10 T/h
  Concentration from 5% to 25% of T.S.
  Evaporation temperature : $\simeq$ 65°C
  Compressor temperature difference (between vapor in and vapor out) $\simeq$ 6°C.

- General diagram and working process

The general diagram of the installation is mentioned in Figure 4.

The apparatus comprises 3 evaporation bundles, working in parallel on the steam, and in series on the product; this disposition has been adopted as being the (most economical) configuration and the most supple one to answer the problem submitted by the client, that of whey preconcentration, intended for transport.

The resulting concentration is voluntarily limited to 25 to 30% rate of total solid.

With the same compressor it is also possible to make an apparatus able to reach directly a concentration of 45 to 50% TS, but this was not the aim in the present case.

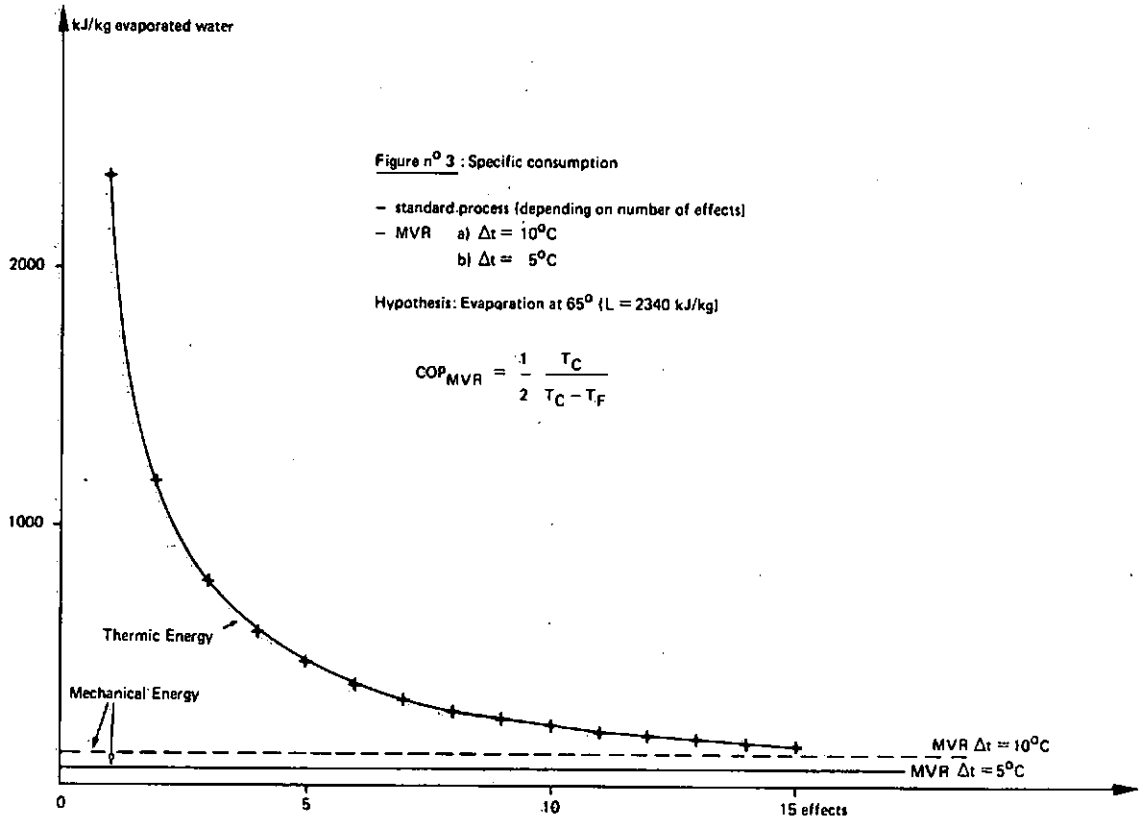

Figure n° 3 : Specific consumption

- standard process (depending on number of effects)
- MVR a) $\Delta t = 10^{\circ}C$
  b) $\Delta t = 5^{\circ}C$

Hypothesis: Evaporation at 65° (L = 2340 kJ/kg)

$$COP_{MVR} = \frac{1}{2}\,\frac{T_C}{T_C - T_F}$$

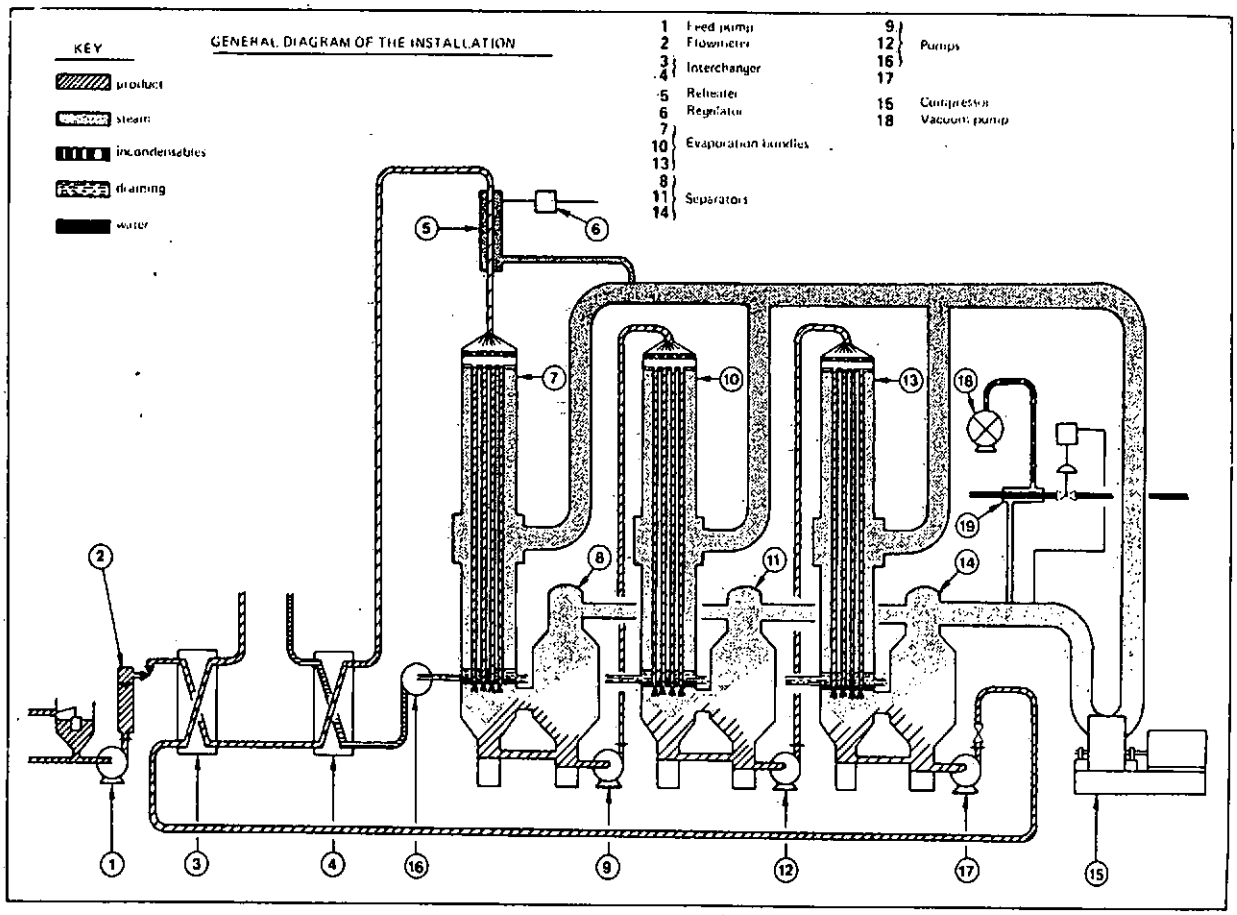

- Circuit of fluids

Whey at 5% TS is aspirated by the pump (1) and driven back through a rotameter (2) into the first interchanger (3).

The calories supplied by this interchanger come from the cooling of the concentrate leaving the evaporator.

The interchanger (4) takes its calories from cooling of condensation water in the evaporation nest of boiler tubes.

A last reheater (5), fed by live steam or hot water brings a slight calorific complement eventually necessary, by means of the regulator (6).

The product to be treated, thus reheated, penetrates into the head of the first nest of boiler tubes (7) to be distributed inside each tube.

The solution evaporates in each tube; the concentrate and the produced steam are separated at the base of the nest (7) and in the separator (8).

The pump (9) returns the preconcentrated product to the head of the nest of tubes (10) where evaporation continues. The preconcentrated product and the produced steam are separated at the base of the nest (10) and in the separator (11).

Equally, a pump (12) returns the preconcentrated product at the head of the last nest (13) where evaporation continues.

The concentrate and the steam produced are separated at the base of the nest (13) and in the separator (14).

The centrifugal compressor (15) aspirates the evaporation steam and returns it at a higher temperature outside the heating tubes of the nests (7), (10), (13).

The steam coming from the compressor is desuperheated before getting in the nest of tubes.

The pump (16) draws the condensation water from the three nests, to return it outside, through the interchanger (4).

The pump (17) extracts the 25 to 30% of TS concentrate to return it through the interchanger (3).

In the present case, the evaporation temperature is 65°C and the vacuum is made by a liquid ring pump (18), equipped with an auxiliary condenser. The vacuum in the auxiliary condenser can be maintained by regulating the water flow.

The initiate temperature of whey is 3 to 5°C, the condensates outflow temperature is 20°C, and the concentrate one is 9°C.

Due to the very low temperature of the entering whey, a small calories complement must be made under normal running conditions (19).

In the same way, upon starting up, a calory complement (hot water or steam) is necessary to reheat the installation.

ACHIEVED TESTS

The first tests were aimed at determining the balance-sheets of the installation during actual use, that is to say:

- Energy necessary to start up the installation
- The working characteristics during concentration
- Energy used during cleaning.

When the outgoing product reaches the required concentration, this is stored and then the concentration phase is started which is taken into account when drawing up the balance sheets.

When there is no more product to be concentrated, a "water pressure" action is effected to evacuate the concentrate retained in the installation. The operation continues by washing out the piping. During this phase the compressor and all the auxiliaries remain in service as well as the hot water calory complement.

For these tests, the whey to be treated has been stored in a tank with a total capacity of 50 cu.m. equipped with a weighing device. However when all the stock as been used, the concentration is continued with whey coming directly from pasturization; the entering product flow information is then lost. Subsequently a device for continuous measuring of whey flow and concentrated whey will make it possible to break away from certain operating imperatives. Furthermore, cheese making in this plant has not yet reached its nominal production capacity, which explains why working periods are so short.

- Development of measures

As we have already stated above, several transitory phases exist during working.

The period taken into account for drawing up the balance-sheet during the concentration period excludes the transitory starting up phases (reheating of the installation and rise in concentration) and the end of the treatment (water pressure).

RESULTS

- Overall results

Tables 1 - 2 summarize the main results obtained during two days of tests.

Energy consumed during starting up and cleaning is independent of the duration of concentration (in the normal limits of the installations working).

Under present working conditions, this energy represents a relatively important part in the overall expenditure.

On the other hand, starting up and washing out are not completely automatic, so there are variable lengths of time for these phases, left to the operator's initiative.

TABLE 1

	Duration h - mn	Energy kJ Electric	Energy kJ Hot water	Serum kg Entering	Serum kg Leaving	Evaporated water kg	Condensates collected kg
– Starting up (setting temperature of installation)	0	0	0	0	0		
– Injection of whey	1 h	241 000 (67 kWh)	972 930 (233×10^3 kcal)				
– Start of storage concentrated whey	10 mn	122 520 (34 kWh)	180 170 (43×10^3 kcal)	2800	0		
CONCENTRATION PERIOD	3 h 20	2 522 400 (700 kWh)	3 135 000 (750×10^3 kcal)	41900	7500	34400	34630
– Stop of whey flow	1 h 20	1 016 170 (282 kWh)	1 117 070 (267×10^3 kcal)	16790*	2900	13890*	13980
– End of storage Start of washing out	15 mn	183 780 (51 kWh)	252 240 (60×10^3 kcal)	0	600		
– Stoppage	2 h 05	1 163 910 (323 kWh)	1 297 240 (310×10^3 kcal)	0	0		
Total	8 h 10	5 250 220 (1457 kWh)	6 954 660 (1664×10^3 kcal	61490	11000		

* Values deducted: The flow of entering was not able to be measured during this period due to storage operating imperatives.

TABLE 2

	Duration h - mn	Energy kJ Electric	Energy kJ Hot water	Serum kg Entering	Serum kg Leaving	Evaporated water kg	Condensates collected kg
– Starting up (setting temperature of installation)	0	0	0	0	0		
– Injection of whey	50 mn	291 880 (81 kWh)	1 008 970 (241×10^3 kcal)	0	0		
– Start of storage concentrated whey	10 mn	133 330 (37 kWh)	180 170 (43×10^3 kcal	2000	0		
CONCENTRATION PERIOD	3 h 30	2 623 310 (728 kWh)	2 846 720 (681×10^3 kcal	44200	8500	35700	36000
– Stop of whey	5 h	3 661 100 (1016 kWh)	3 927 760 (940×10^3 kcal			49335*	39750
End of storage Start of washing out	10 mn	115 310 (32 kWh)	144 140 (35×10^3 kcal	0	400		
Stoppage							
Total							

* Value deducted. The flow of entering was not able to be measured during this period due to storage imperatives. Stoppage of measuring at end of concentrated whey stoppage.

- Concentration period

	TEST N° 1		TEST N° 2	
	Total energy kJ	Average power	Total energy kJ	Average power
Reference period	9 h 40 à 14 h 20		9 h 10 à 17 h 40	
Electricity	3 538 590 (982 kWh)	210 kW	6 284 410 (1744 kWh)	205 kW
Hot water (3)	4 252 070 (1180 kWh) (1017×10^{-3} kcal)	253 kW (218×10^{-3} kcal/h)	6 774 480 (1880 kWh) (1621×10^{-3} kcal)	221 kW (190×10^{-3} kcal/h)
Whey entering	58690 kg	12576 kg	44200 kg	12629 kg (1)
Whey leaving	10400 kg	2229 kg	8500 kg	2429 kg (1)
Evaporated water	48290 kg	10347 kg	36300 kg (1)	10371 kg (1)
Condensates collected	48610 kg	10416 kg	87750 kg (1)	10088 kg (1)
Specif. consumption				
– Electric	73,2 J/kg evaporated water (20,3 Wh/kg evaporated water)		72,1 J/kg evaporated water (20 Wh/kg evaporated water)	
– Thermic	88 J/kg evaporated water (24,4 Wh/kg evaporated water) (21 kcal/kg evaporated water)		78 J/kg evaporated water (21,6 Wh/kg evaporated water) (19 kcal/kg evaporated water)	
– Primary energy (2) (as reminder)	$7,2 \times 10^{-6}$ tep/kg evaporated water (72 kcal/kg evaporated water)		$6,9\ 10^{-6}$ tep/kg evaporated water (69 kcal/kg evaporated water)	

(1) Values corresponding to the period 9 h 10 to 12 h 40.

(2) Primary energy : – 1 electric Wh equivalent to 0.25×10^{-6} TEP.

(3) – The value indicated is that measured during use. It does not take into account combustion and distribution output.

A perceptible difference can be noted on consumption of hot water energy. This is explained by a series of interventions by the constructor who optimized the working balance-sheet starting from measures taken during test n° 1.

The constructor considers that the results obtained during test n° 2 correspond to normal working of the installation and are lower than the values expected by the constructor, i.e.

For evaporation of 10 T/h:

- Electric power consumed: 210 kW
- Thermic complement : 272 kW (235 000 kcal/h)

The different measurements taken were made every 10 minutes: during the reference periods, one does not see significant variations in consumption, flow and temperatures.

The quantity "Evaporated water" is determined by the difference between the weight of the entering and the weight of concentrated whey.

The "collected condensates" are measured and include:

Evaporated water + Desuperheated water - Entrainment of steam by incondensables.

ECONOMIC DATA:

We give here the figures in respect to two installations. The first concern the installation on which the measurements were taken as described above; the values mentioned are those supplied by the constructor. The other case concern an installation which will start up during the first semester of 1980. The values mentioned are given by the client. (It is the same constructor in both of them).

- Comparative balance-sheet between the chosen solution (MVR) and a standard solution, multiple effect:

The comparison is made out of measured values, constructor's figures (investment) and the price of energy in force with the client.

A quadruple effect evaporator with thermo-compressor and having also an evaporating capacity of 10 tons per hour, has been taken as a basis of comparison.

- Compared investments:

	Mechanical recompression (MVR) (kF HT 1979)	Multiple action (kF HT 1979)
Evaporator	1 600 (delivered assembled)	1 400 (delivered assembled)
Cooling-tower		200
Boiler	70	300
Compressor	750	
Transformer (fraction)	100	30
Total investment	2 520	1 930

Surinvestment: 590 kF.

- Hourly consumption of energy

	MVR	Standard (4 effects + TC) C_s = 0,185 kg/kg
Steam	0,315 ton	1,85 ton
Electricity	205 kW	30 kW
Cooling-tower	–	25 kW

Corresponding annual energy expenditure:

- Running: 6000 hours per year.
- Steam: 53 F/ton.
- Electricity: 0,17 F/kWh.

	MVR	Standard
Expenditure (F/year)	310 000 F	645 000 F
Working profit	335 000 F	0

Economy in operating, on the level of expenditure in respect to energy, bring to light a net return time on surinvestment which is UNDER TWO YEARS.

We mention below the figures relating to an installation in course of construction: these figures have been given by the future user during electro-industrial information days organized by the French Electrotherm Committee, and in respect to the actual context of the firm.

Investment (evaporating capacity: 7,5 t/hour) in kF.

	Standard	MVR
Evaporator	890	1 790
Cooling-tower	250	25
Boiler	450	–
Building	120	150
Electric network	–	75
Connection of fluids	200	180
Spare parts	–	80
Total	2 010	2 300
Premiums: Agency*	–43	–293
EDF**	–	–100
Real investment payable by the user	1 967	1 907

* The Energy Conservation Agency grants premium to any user who carries out methods which make it possible to effect energy saving. These premiums vary according to the annual quantity of primary energy which is economized (following criteria in force in France).

** EDF grants an aid to firms which carry out innovative methods which call for electricity.

According to criteria of the firm (steam 50 F/ton, electricity 0.165 F/kWh) and taking into account the characteristics of the installations compared, one reaches the following hourly working costs:

	Standard	MVR
Steam	2,47	11,80
Electricity	90,81	13,52
Total	93,28	33,32

so an operating profit of 59,06 F/hour.

On the basis of 6000 hours per year operating, a gain on energy expenditure in the region of 360,000 F/year.

CONCLUSION

If the advantage of the MVR no longer needs to be shown, generally superheating installations operating in a vacuum are rare. The first application made by ORLAC has proved that it is technically possible at the industrial stage, thus opening up a new market for this technique. Equally, it has been possible to check on this installation that the provisional operating balance-sheets were correct and that this technique not only made substantial energy conservation possible, but also reduced operating costs. Consecutive to this application, the constructor has received orders for 4 other installations with closely related characteristics. One will note however, that in France, all installations in course of construction provide for preconcentrating whey, but so far, no project for total concentration (up to 50 or 55% of TS on whey) is being followed up; it is the same for milk (full cream or skimmed) and we shall direct our efforts in this field.

Finally this technique which is not specifically for the milk industry, might develop in other sectors, in the agro-alimentary industry as well as in the chemical industry; it should also be able to be transposed without major difficulties to other operations, in particular to distillation.

ACKNOWLEDGMENT

Nous remercions la Sté ORLAC qui a autorisé la réalisation des mesures et la publication des résultats, ainsi que le constructeur qui a participé à la campagne de mesures.

REFERENCES :

(1) ORLAC — Siège Social : Chemin des Mines, ESTRESSIN, 38208-VIENNE (France)
Usine : ZI Molina la Chazotte, 42350-La TALAUDIERE (France)

(2) Ets LAGUILHARRE — 18 à 22, rue d'Arras, 92000 NANTERRE (France)

(3) Ets NEU — 47, rue Fourier, 59000 LILLE (France)

APPROACHES TO MORE ECONOMICAL DRYING OF PARTICLES AND LUMPS

O.E. Potter

Monash University, Melbourne, Australia.

ABSTRACT

Approaches to more economical drying of particulate and lump materials will be discussed. In the case of particles, drying occurs in a heated fluidized bed of dry particles, fluidized by steam. This arrangement lends itself to multiple-effect operation or to the fitting of a dryer into a power-station whereby back-pressure steam is used for drying and the vapour produced in the dryer is used partly for feed-water heating and also for further generation of power in low-pressure steam turbines. It is also possible to have two effects at atmospheric pressure - the first effect being heated and steam-fluidized, the vapour produced in drying being used to heat the second effect, which is fluidized by air or other relatively dry inert gas. Lump drying is also possible e.g. black coal may be dried in a bed of sand fluidized by steam. Some pilot-plant results for alumina hydrate and for brown coal are discussed.

INTRODUCTION

Drying is the forgotten unit operation. It is a puzzle why this should be so when the cost of drying operations is so high. In Victoria, brown coal is mined containing 2 kg water per kg dry coal and 30 million tonnes are burnt each year releasing 20 million tonnes of water to the atmosphere, the energy required to vaporise the water being lost completely. Other minerals besides coal are handled in large tonnages and frequently dried by oil or gas. Ways must be found of reducing the energy consumption in drying and this paper is concerned with suitable ways for particulate and lump material. If more economical drying is attainable then it may be possible to reduce transportation costs significantly by pre-drying when moist coal has to be hauled over long distances. The principal factor preventing energy economy has been the difficulty of recovering heat from the mixture of water-vapour and non-condensible gases which flows from the dryer. Energy economy must be sought in a different approach. In his book, "Drying by means of Air and Steam", Hausbrand (1) discusses a dryer in which superheated steam is blown over material to be dried and then some product steam is reheated and utilised for further drying. When steam-drying is allied to the good heat transfer capabilities of fluidized beds a very powerful tool is created and substantial energy economy follows because heat can now be recovered easily, there being little, if any, non-condensible gas present.

MULTIPLE-EFFECT DRYING OR EQUIVALENT

Given a steam-heated, steam-fluidized dryer, multiple-effect operation is possible (2). Figure 1 shows a cross-current multiple-effect dryer. Coal enters a high-pressure, intermediate pressure or low pressure dryer and dry coal, at different temperatures is withdrawn from each dryer. The heating steam enters the heating tubes

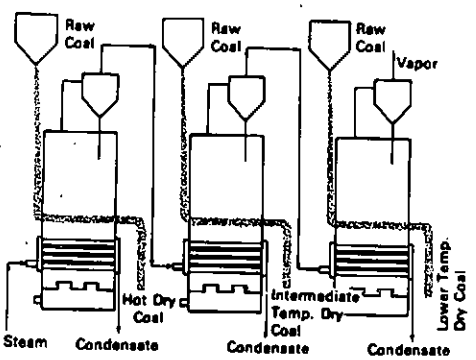

Coal Transfer - diagrammatic only

Figure 1: Cross-current multiple-effect steam dryer. Carrier steam- enough steam to maintain fluidization - is not shown. Each dryer is at a different pressure as in multiple-effect evaporation.

of the first dryer, some of the vapour is recycled to maintain fluidization and the remainder after cleaning by cyclones or bag-filter is fed to the heating tubes of the second dryer, and so on. Thus multiple-effect economy is possible in drying. Co-current or counter-current systems can also be employed. A useful variant is to have two drying stages at one pressure, normally atmospheric pressure, see Figure 2. A steam-drying unit as discussed above is the first effect and the vapour from the first effect passes to the heating tubes of the second effect which is similarly constructed, but somewhat larger, with air or other suitable gas as the

fluidizing medium. This second-stage might be at 50°C with an overall ΔT of 50 Cdeg. Approximately 2 kg water is vaporised per kg steam fed to the heating tubes of the first effect.

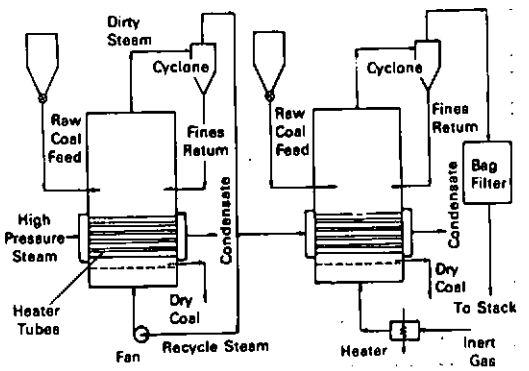

Figure 2: Two-stage atmospheric pressure dryer. First stage is heated by steam and generates steam which is used for heating the second stage which is, e.g. air-fluidized at, say, 50°C.

Furthermore the stages in the system need not be dryers, but any means of utilising effectively the energy in the steam. For example, in brown coal combustion, high pressure steam is used in turbines for power generation, then steam may be withdrawn for drying the coal and the product vapour can be used, indirectly if required, in the low pressure turbines. In an alumina plant where large quantities of steam are used in bauxite digestion and caustic recovery, back-pressure steam may be withdrawn for drying and the product vapour from the dryer may be used for process heating e.g. double-effect evaporation of weak caustic solution.

DRYING OF LUMP MATERIAL

The discussion so far has been applicable primarily to particulate material which is easily fluidizable in the dry state. In the case of lumps, as illustrated in Figures 3 and 4 the lump material e.g. black coal, is carried in a particulate carrier-solids e.g. sand. The heating surface is so arranged as to enable lump material to move through the system supported by the fluidized bed of fine sand. Roughly speaking the density of the carrier solids should be twice that of the coal or other lump material to be dried. Additional complication arises because it is necessary to separate lump material from the sand. Also if the lump material is friable it is necessary to make provision to separate fine particles broken off the lump material from the sand. This separation can be achieved in a quiescent fluidized-bed where the coal floats to the surface and may be 'drained' off. Fines carried overhead can be recovered from the cyclones or bag filters. The carrier particles e.g. sand are returned to the dryer with more lump material feed.

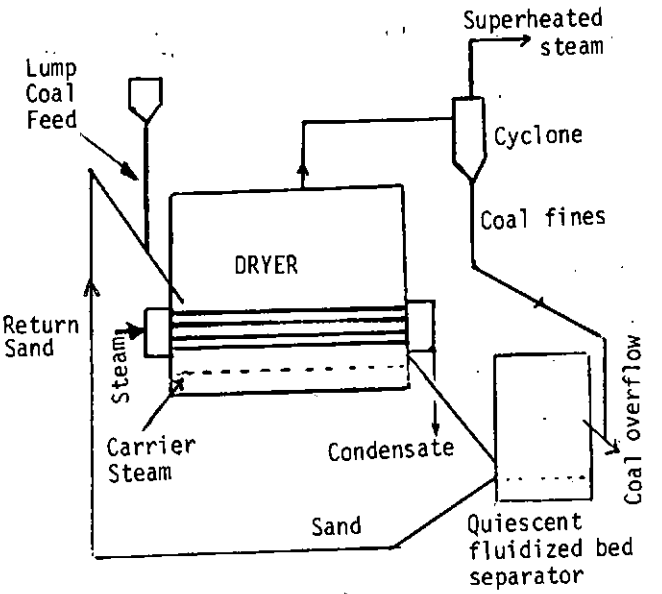

Figure 3: General arrangement of steam-fluidized steam-heated lump coal dryer showing coal-sand separator.

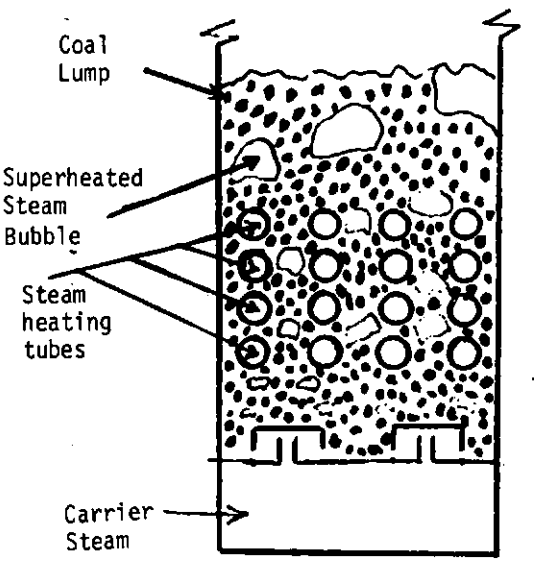

Figure 4: Detail of lump coal dryer showing coal lumps in sand like fruit in a fruit-cake.

STEAM (OR SOLVENT-VAPOUR) DRYING

Because the situations in which superheated steam-drying is practised are rare, there is a dearth of the equilibrium data that will be required for the wide application of the proposed method. One case where superheated steam-drying has been employed is timber-drying and Figure 5 from Kollman (3) shows how the equilibrium moisture content of different timbers varies as the wood attains equilibrium with steam at atmospheric pressure and different degrees of superheat. A timber with an equilibrium moisture content of 25 per cent w/w in

saturated steam at 100°C has its moisture equilibrium content reduced to 5 per cent w/w in superheated steam at 120°C.

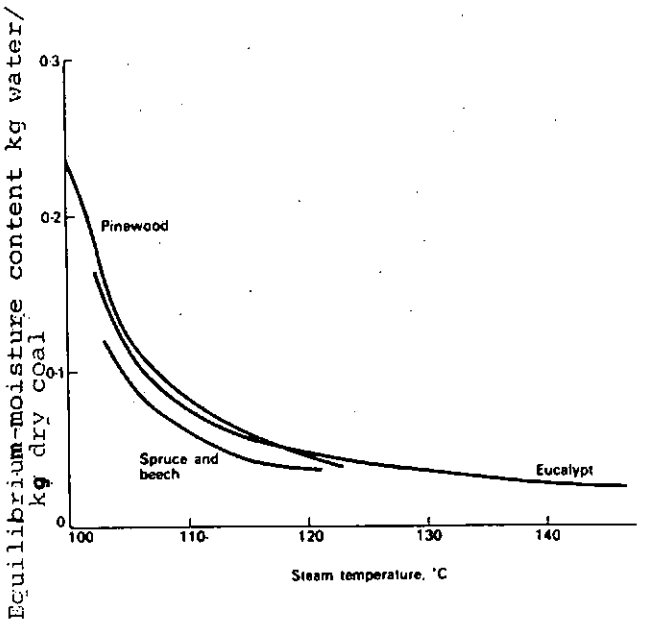

Figure 5: Equilibrium moisture content of different timbers in equilibrium with steam at different degrees of superheat at atmospheric pressure.

Vapour pressure isotherms for Victorian brown coal at temperatures up to 60°C were measured by Allardice & Evans (4) and their data are presented in Figure 6 taken from McIntosh (4). From this figure we may conclude that for Victorian brown coal, initially containing 2 kg water/(kg dry coal), the vapour pressure remains that of water until the moisture has been reduced to 0.8 kg water/(kg dry coal). At lower moisture contents the partial pressure is reduced e.g. at 0.2 kg water/(kg dry coal) the partial pressure is approximately 70 per cent of the vapour pressure of water and a temperature of about 110°C is required for the partial pressure to equal one bar. These conclusions require an extrapolation which is only partially justifiable but serve to indicate that if a bed of Victorian brown coal is maintained in a fluidized state at 1 bar pressure and 110°C by superheated steam then the coal will be dried to a moisture content of approximately 0.2 kg water/(kg dry coal). Most of the data in the literature on equilibrium moisture content has been determined at temperatures less than the boiling point at atmospheric pressure and for the systems envisaged here new data are required. The same comment applies to solvents as well as to water. An investigation is proceeding.

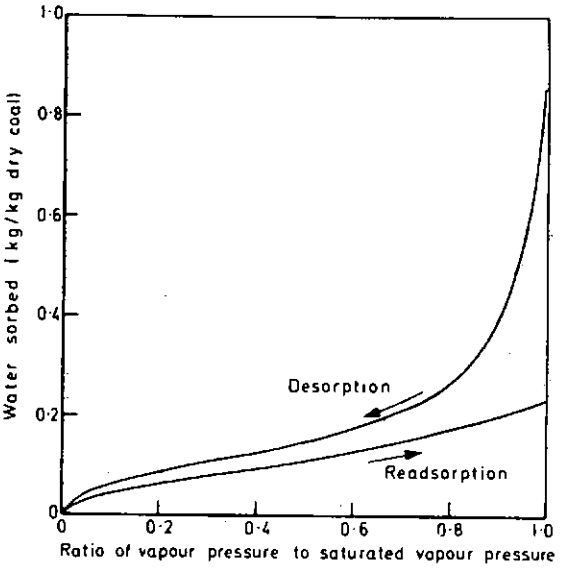

Figure 6: Brown coal. Equilibrium moisture content as a function of relative vapour pressure based on data at temperatures up to 60°C.

RATE OF DRYING OF PARTICLES AND LUMPS

In the fluidized bed fitted with heat exchange surfaces the drying process proceeds as a result of particles adjacent to the surface being heated and then mixed back into the bulk bed of particles. Thus the heat-transfer takes place as a result of particle-tube-superheated steam interactions and not simply by convection. In an engineering sense, the drying time of an individual particle is important only if it approaches the residence-time of the system. Depending on moisture, and tube surface per unit volume of bed and the corresponding heat transfer coefficient the residence time may vary widely. In a dryer design for Victorian brown coal the residence-time is about 20 minutes. For such coal, Stanmore and Boyd (6) measured the temperature rise of coal cylinders exposed to pressurised hot water at temperatures from 220-260°C. Cylinders of radius 8.69 mm adjusted to the temperature change in about 8 minutes. Where lump coal is being dried, intra-particle effects may start at 1-2 cm dia. and data for such cases, under drying conditions, needs to be determined.

FLUIDIZED BED HEAT TRANSFER WITH SUPERHEATED VAPOUR

The process which takes place is that moist material is introduced into the bed and broken up by the bubbles formed in the bed so that the mixing processes of the fluidized bed can distribute the moist material through the bed. At any time there will be a small amount of moist material distributed throughout the fluidized bed of dry material. Thus drying occurs by heat-transfer from the heating surfaces to the dry solids, followed by the inter-mixing of the heated

dry solids, with the bulk solids containing some moist solids. This heat-transfer process is slightly augmented when moist material approaches the hot surface and is more or less dried before being mixed in with bulk material. Baskakov et al. (7) found that the rate of heat-transfer to activated carbon with 13 per cent water w/w was about 25 per cent more than when the activated carbon was dry. In the present case only a small proportion of particles will be moist, hence the effect will not be large.

PILOT-PLANT OPERATION

The pilot-plant is illustrated in Figure 7. The bed is 0.305 m square and has electrically heated tubes, 25.4 mm dia. on 50.8 mm centres, triangular pitch. The tubes are fitted with thermocouples and the surface temperature controlled. Carrier-steam to maintain fluidization near the distributor is introduced through a single bubble cap.

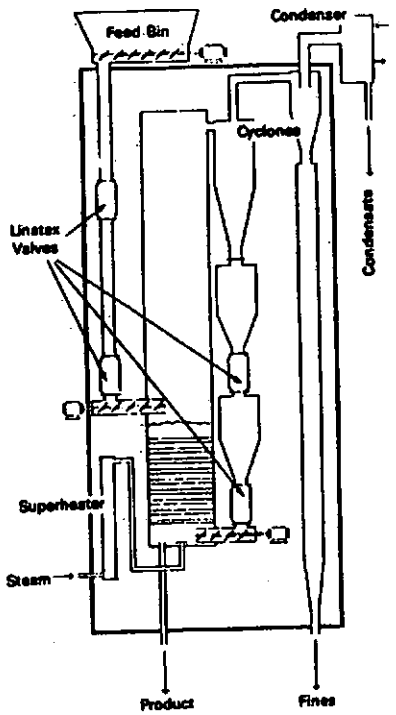

Figure 7: Pilot-plant. Bed is operated just above atmospheric pressure. Particulate material is fed through lock-hopper and screw. Particles removed from first cyclone are returned to bed via lock-hopper and screw. Superheated carrier steam is admitted to the distributor. Steam remaining after gas-cleaning by cyclones is passed to the condenser. Heating tubes are electrically heated and fitted with thermocouples so that tube temperatures may be controlled.

Trials have been completed very successfully with alumina hydrate and have begun with brown coal. Other minerals and coals are under consideration.

Heat-transfer coefficients have been about 340 watts/(m^2)(Kdeg) for sandy alumina hydrate and about half that value for brown coal (0-3 mm). Final moisture content for a bed of alumina hydrate maintained at 110-115°C was negligible. For Victorian brown coal, Yallourn North Extended seam 50 per cent w/w moisture, the product under the same conditions contained about 6 per cent w/w moisture and was a free-flowing solid. It is anticipated that heat-transfer coefficients would be slightly better on plant-scale.

TAPERED BEDS

Among the methods considered to allow for the increase in superheated steam flow from bottom to top of the bed is the use of tapered beds of greater cross-sectional area at the top than at the bottom. Such tapering can lead to a considerable reduction in carrier-steam requirement and facilitate the handling of solids with a wide size distribution. Investigations are proceeding.

APPLICATIONS

(a) Cheaper power from high-moisture brown coals and cheaper drying for coal processing to gaseous and liquid fuels.

Boilers for the combustion of high moisture brown coals are larger and more costly than for dried brown coal or (low-moisture) black coals. Hence substantial capital savings are available from use of the system illustrated in Figure 8. As discussed by Potter and Keogh (8),(9), (10), back-pressure steam may be withdrawn after the high-pressure turbine or from some point in the intermediate pressure turbine and used for heating the dryer. Dirty steam produced is cleaned by cyclones or bag-filters and passes to a steam-generator or evaporator which produces clean steam to pass to the low-pressure turbines.

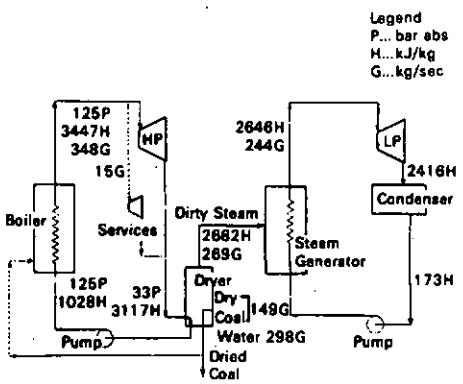

Figure 8: Simplified flow-sheet of a brown coal power station used for producing dried coal and some power. If power only is required only sufficient coal is dried for combustion needs and there is no dried coal output.

(b) Oil savings in alumina calcination

In an alumina plant large quantities of steam are available some of which may be used to dry the moist alumina hydrate from the filters. The removal of this moisture not only reduces the oil demand by about 16 per cent but leads to a reduction in the flue-gas volume and hence the possibility of increased throughput from existing plant. There is a pinch at the cold-end of the kiln or fluid-bed calciner so some additional gas-solid contacting may be required. The dirty steam at atmospheric pressure can be used for process heating e.g. in a two-stage evaporator to concentrate the weak caustic liquor before returning it to the digestion system. The condensate from the first effect can be used to wash the filter-cake.

REFERENCES

1. Hausbrand, E., "Drying by means of Air and Steam", Scott and Greenwood, London, 1901.
2. Potter, O.E., *Chemical Engineering in Australia*, No. 2, June 1979, pp.26-29.
3. Kollman, F.F.P., *Forest Production, J., 11*, 508, 1961.
4. Allardice, D.J. and D.G. Evans, *Fuel*, Lond., *50*, 236, 1971.
5. McIntosh, M.J., *Fuel*, Lond., 55, 47-52, 1976.
6. Stanmore, B.R. and A.R. Boyd, Second Australasian Conference on Heat and Mass Transfer, Sydney, Feb., 1977, pp.115-120.
7. Baskakov, A.P., B.V. Berg, O.K. Vitt, N.F. Phillipovsky, V.A. Kirakosyan, J.M. Goldobin and V.K. Maskaev, *Powder Technology.*, *8*, 273, 1973.
8. Potter, O.E. and A.J. Keogh, "Cheaper Power from High-moisture Brown Coals, Part I System Description and Preliminary Costing", *J. Inst. Energy, Vol. LII*, pp.143-145, Sept. 1979.
9. Potter, O.E. and A.J. Keogh, "Cheaper Power from High-moisture Brown Coals Part II Feasibility and Development", *J. Inst. Energy, Vol. LII*, pp.146-149, Sept. 1979, No. 412.
10. Potter, O.E. and A.J. Keogh, "Drying High-moisture Coals Before Liquefaction", accepted for publication.

SECTION VII: SPRAY DRYING

SPRAY DRYING IN ENVIRONMENTAL CONTROL WITH SPECIAL REFERENCE TO FLUE GAS DESULPHURIZATION

K. Masters

A/S Niro Atomizer, Denmark

ABSTRACT

The spray drying absorbtion technology, which offers an attractive dry processing alternative to the wet scrubbing technology, is discussed with reference to emission control of pollutants to atmosphere. The development of spray dryers as absorbers for flue gas desulpherization and for toxic gas removal is also discussed.

INTRODUCTION

In recent years, spray dryer development has been greatly influenced by the environmental controls now being placed on industry. These controls have necessitated reduction in powder and odour emissions to atmosphere, elimination of organic solvent vapour emissions to atmosphere, and the ability to handle large volumes of flue gas and industrial process off-gases prior to atmospheric discharge. Spray dryer devlopment has also been active in the field of toxic gas emission control, especially in the control of such emissions as sulphur dioxide, hydrogene chloride and hydrogene floride gases.

This paper describes the spray drying systems available to prevent emissions of pollutants to atmosphere. Special reference is given to the development of spray dryers as spray dryer absorbers for both flue gas desulphurization and for toxic gas removal from off-gases leaving incinerators, metallurgical and other industrial processes. This development is of special significance, as spray dryer adsorbers represent an attractive dry processing alternative to the wet scrubbing techniques currently used for example by the utility industry with certain misgivings.

SPRAY DRYER DESIGNS TO MEET ENVIRONMENTAL STANDARDS

a) Designs to Ensure Low Powder Emissions to Atmosphere (Table 1)

Powder emissions in open cycle spray dryers are controlled by the correct selection of the dry collection equipment associated with the spray drying chamber. The expected powder loss from the most common spray dryer dry collector, i.e. cyclone, is 100-300 mg/Nm^3, and if associated with a wet scrubber 10-75 mg/Nm^3. Loss from a bag filter is normally within 5-20 mg/Nm^3. A range of values is given, since actual loss levels depend upon product particle properties, i.e. bulk density, particle size distribution, and particle resistance to attrition.

One of the best ways of reducing powder emission to a minimum level is the use of semi-closed drying systems where only a small proportion of the total powder containing exhaust air is discharged to atmosphere. Hence, quantities of powder discharged are negligible.

As it stands today, the use of the latest designs of dry collectors (e.g. dual vortex separator: expected loss range when operating alone: 30-150 mg/Nm^3, see figure 6) and associated scrubbers can reduce emission levels to acceptable limits, but to reduce powder emissions to the extremely low levels that are expected to come into force as standards in the near future, then semi-closed cycle designs will have to be adopted. Semi-closed cycle system are best used for handling products that create odour during drying.

b) Spray Dryers for Preventing Emissions of Solvent Vapour to Atmosphere (Table 1)

When drying organic solvent based feedstocks, it is impossible to emit solvent vapour to atmosphere, as a serious toxic and odour problem will arise. The cost of expensive solvent loss is also formidable. A fully closed gas-tight spray dryer design is necessary, and hence closed cycle lay-outs are used where vapour and powder emissions to atmosphere must be completely prevented.

Recent years have seen the completion of a development programme which now enables large capacity closed cycle spray dryers to be designed with either rotary or nozzle atomization.

c) Spray Dryers for Handling Large Volumes of High Temperature Exhaust Air Contaminated with Particulates

Another area of environmental pollution that can be combatted by use of spray drying equipment is the conditioning of very large volumes of high temperature exhaust gases emitted to atmosphere from such plants as waste heat incinerators, high

tonnage kilns, etc. Such exhaust gases contain much particulate matter, and this must be removed to prevent excessive air pollution.

An efficient way of handling such large volumes of hot exhaust gases is the use of a spray dryer as a gas cooler and placed prior to an electrostatic precipitator. The contaminated exhaust gases are cooled and conditioned in such a way that electrostatic precipitator performance is significantly improved resulting in optimum separation of particulate matter from the exhaust gases.

d) Spray Dryers for Sulphur Dioxide Removal from Flue Gases

Flue gas desulphurization is accomplished in spray dryers operating as spray dryer absorbers. Effective desulphurization of flue gas is an example where spray drying technology has been recently applied in environmental control. Various desulphurization plants are currently in use based upon wet processing techniques, but as wet processing (wet scrubbing) presents severe problems surrounding plant reliability and ease of operation, alternative dry processes have long been sought. One of the methods considered to have superior characteristics in terms of its concept and potential over any other, is dry scrubbing in spray dryer absorbers (SDA).

Flue gases containing toxic components are thoroughly cleaned during passage through the spray dryer absorber (SDA) and particulate collection equipment (dry collector). This is accomplished by spraying a fluid absorbent, which is preferably slaked lime, into the flue gas. Sprays are produced by an atomizer. The intimate contact required between spray and gas for high absorption efficiency is achieved by optimum location of gas disperser and atomizer. This gives full control of the absorption drying zone. Absorption drying takes place while the absorbent droplets are suspended in the gas flow. Spent absorbent is recovered from the base of the absorption chamber and associated dry fines collector which is a bag filter or an electrostatic precipitator. Utilization of absorbent is further improved by partial recycle of dry product within the process. A simplified flowsheet is shown in figure 1.

The advantages of applying spray drying technology to flue gas desulphurization are many and are listed as follows:

1. Greater than 90% SO_2 removal at low absorbent usage stoichiometric ratios between 1 and 1.5).
2. Dry product handling - no wet sludge.
3. Flexible in operation. High removal efficiency even at varying SO_2 levels.
4. High turn-down capabilities.
5. No wet-dry interface problems (corrosion, scaling).
6. No risk of flue gas obstruction.
7. Low pressure-drop operation.
8. Both capital investment and power consumption significantly lower than for wet scrubber of comparative capacity (see Table 2).
9. High reliability - few moving parts.
10. Gas conditioning improves dry collector efficiency and operation.
11. Reheating gases after process not necessary.

Apart from SDAs achieving very high degrees of sulphur dioxide removal, the placing of the SDA up-stream of the particulate collection system reduces atmospheric emissions through improved spect absorbent/flyash collection. Flow rate, temperature, humidity, SO_2 content of flue gas entering the collector are vitually constant irrespective of the gas conditions leaving the boiler. Furthermore, gas volumes are reduced in the SDA enabling smaller collection systems to be used. Where electrostatic precipitators are selected, the increased gas humidity and reduced temperature in the SDA oulet decrease particulate resistivity and improve precipitator performance.

The first commercial installations involving various designs of SDA will soon be in operation, handling flue gas from low sulphur coal-fired power generating plants. These designs involve both the use of either rotary or two-fluid nozzles for absorbent spraying, and either bag filters or electrostatic precipitators as the spent absorbent dry collectors. Companies involved in the promotion of FGD dry scrubbing systems are reported elsewhere (2) and (5).

A SDA complex designed for flue gas flows leaving very large power stations is shown in figure 2. It is a model of the NIRO/JOY plant currently under construction to handle 2.0 million Nm^3/h flue gas, which consists of five absorber chambers in parallel, each co-current absorber chamber equipped with a single rotary atomizer, compound gas disperser, and two-point product discharge.

Flue gas enters the chamber through the compound gas disperser which directs flue gas around the atomizer both from above and below the atomizer wheel. This atomizer/gas disperser design and location gives ideal spray/gas mixing, and controls gas flow in the chamber to secure optimum absorbing conditions.

The rotary atomizer features an abrasion-resistant atomizer wheel containing conical carbide inserts in pretension steel sleeves. The sleeves enable easier removal and turning for utilization of four possible wear tracks before insert replacement. Experience drawn from the use of this wheel on feedstocks more abrasive than lime/flyash slurries suggests long periods of operation will elapse between necessary insert replacements.

The atomizer wheel is powered by a vertically mounted flange motor and atomizers are available to take motor sizes up to 600 kW.

The compound gas disperser is adopted following experience drawn from operating large spray dryers under similar temperature and air flow conditions. The design overcomes the problems associated when high flows are handled in conventional roof-mounted gas disperser systems, i.e. spray cannot be controlled due to the vast amount of energy present in the single inlet gas stream.

The absorber features two-point product discharge which involves primary discharge from the chamber base and secondary discharge from the dry collector. This approach is advocated to eliminate the chance of blockage of the exhaust gas duct between the absorber chamber and the dry collector. Any such blockage will cause serious problems in the boiler operation. Spent chemicals recovered from the two-point discharge system are disposed of by means of traditional ash conveying systems.

However, a portion of the chemicals and flyash is recycled and mixed with fresh incoming feed. The effect of this partial solids recycle is threefold: Firstly, the recycled material contains some non-reacted chemicals, and this can be utilized for further absorption. Secondly, recirculation provides inert particles on which the fresh lime is dispersed on the surface. This leads to a considerable increase in available surface area of active absorbent, and since the inert interior of the atomized droplet contains some moisture, the overall active time available for SO_2 absorption is also increased. Thirdly, much flyash contains alkaline material which during reslurrying can be made available for SO_2 absorption. The benefits of this partial solids recycle system have been demonstrated where it has been found that up to 30-40% savings in lime consumption is achieveable for the same SO_2 removal.

Further information on the use of spray drying in environmental control through flue gas desulphurization is given in references (2) to (5).

e) Spray Dryers for Toxic Gas Removal from Industrial Off-Gases

Although developed for desulphurization of flue gases in fossil fuel burning utilities, SDA technology has been successfully adapted to scrubbing other toxic gases, for example HCl, HF, and HBr, which exist in exhaust gases from waste incinerators, metallurgical and allied industrial processes.

REFERENCES

1. Masters, K., "Spray Drying Handbook", 3rd edition, 1979, George Godwin Limited, London
2. Chemical Engineering, "Dry Scrubbing Looms Large in SO_2 Cleanup Plans", August 27, 1979 - p. 52
3. Processing, Report: "Spray Dryer Plant Curls SO_2 Emission", November 1979
4. Davis, R.A., Gude, K.E., Meyler, J.A., Power Engineering, "Dry Scrubber Maintains High Efficiency", October 1979 - p. 83
5. Smock, R., Electric Power and Light, "Dry Sulfur Scrubbers Favored for Low Sulfur Coal Plants", December 1979 - p. 28
6. Janssen, K.E., Eriksen, R.L., "Basin Electric's Involvement with Dry Flue Gas Desulphurization", Paper presented at EPA Symposium on Flue Gas Desulphurization, Las Vegas, Nevada, U.S.A., March 1979

TABLE 1

CHOICE OF SPRAY DRYER SYSTEM TO MEET ENVIRONMENTAL SPECIFICATION

	Powder Emission Control	Organic Vapour Emission Control	Toxic Gas Emission Control
Open Cycle with			
- cyclone/high efficiency scrubber	*	-	-
- dual vortex separator	*	-	-
- bag filter	*	-	*
- electrostatic precipitator	*	-	*
Closed Cycle (Inert)	*	*	*
Semi-Closed Cycle	*	-	*

TABLE 2

ECONOMIC EVALUATION OF DRY AND WET SCRUBBING FOR FLUE GAS DESULPHURIZATION

(Basis: 440 MW Station, Inlet SO_2 800 ppm, particulates 5 g/acf)

	Dry Scrubbing (SDA)	Wet Scrubbing
Capital Cost	Base	13% higher
Absorbent Cost	Base	10% higher
Power Cost	Base	75% higher
Manpower Cost	Base	130% higher
Replacement Materials	Base	60% higher

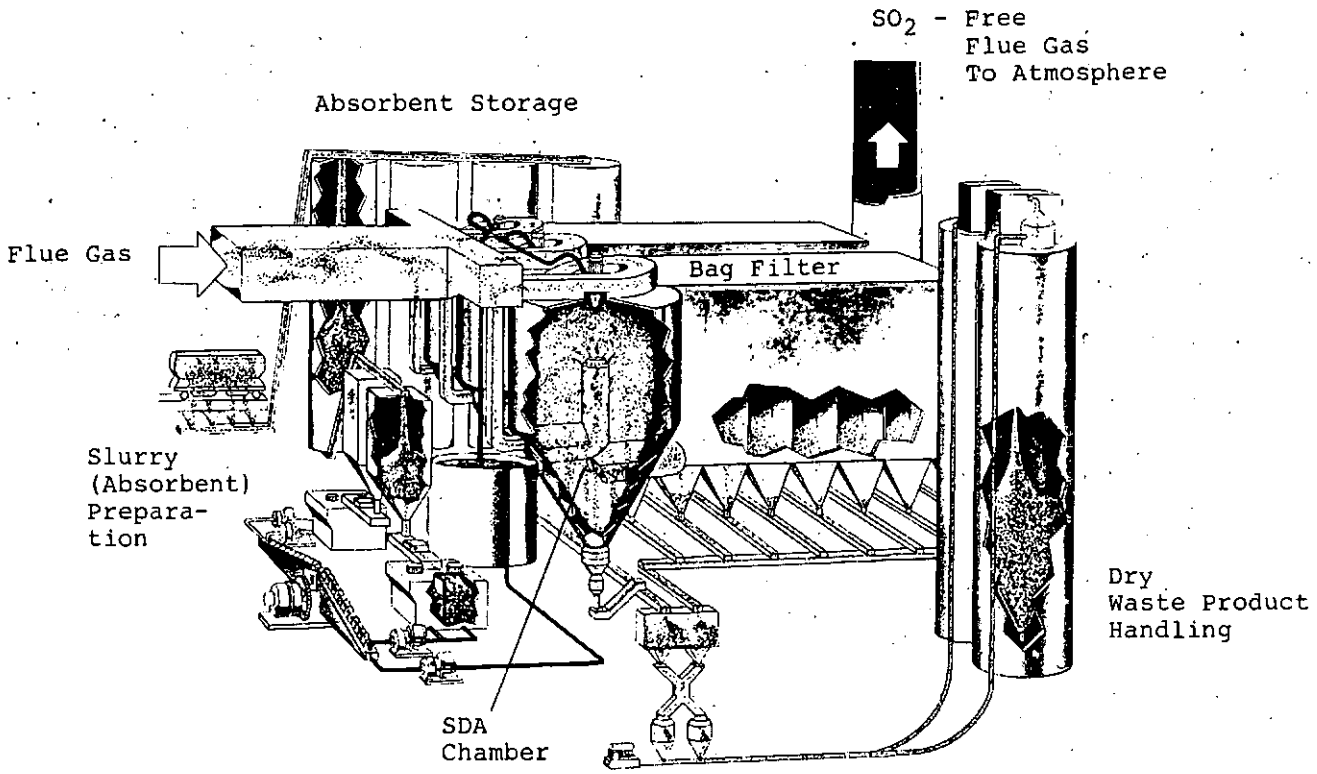

Figure 1 Spray Drying Absorption Layout

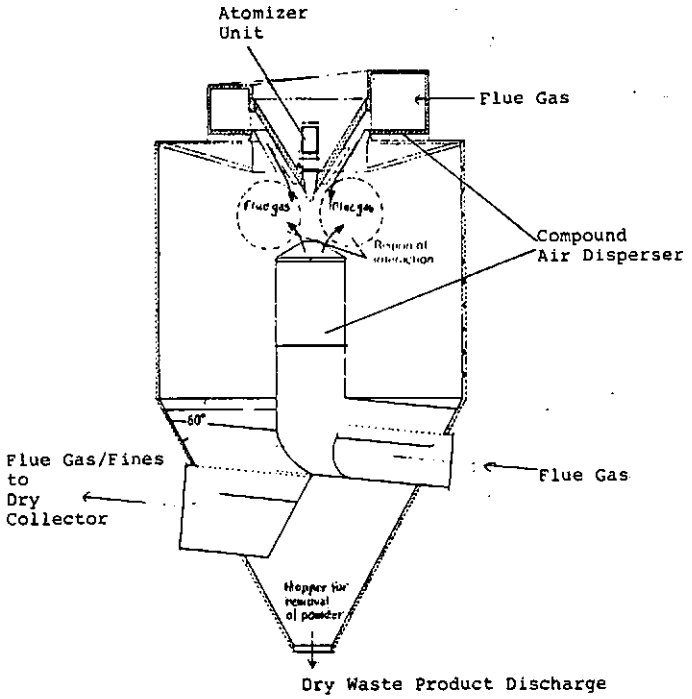

Figure 2 The Niro Atomizer Spray Dryer Absorber Chamber showing centrally located Atomizer, Compound Air Disperser, and Two-Point Product Discharge.

MATHEMATICAL MODEL OF SPRAY DRYING RECKONING WITH DROPLET SIZE DISTRIBUTION

J. Topár

Department of Chemical and Food Engineering, Technical University
Budapest, Hungary

ABSTRACT

Because of the complicated physical process during spray drying the mathematical model of the process and the approximations used when setting up the model are of great importance. These models help in designing equipment and give a possibility to set up the most advantageous parameters in the course of operation.

In our study a mathematical model is presented considering that no droplets of homogenic size originate in spray drying. The model set up contains the balance, kinetic and transport equations.

This mathematical model was simultaneously applied to the droplet size ranges taken up on the basis of the size distribution.

The obtained simultaneous equations were solved with numerical method, by computer.

The results were compared with those given by some more simple models. Using the Sauter average diameter instead of the real size distribution it was found to cause great error in the results and in determination of the main sizes of the equipment as well.

The model applied gives a good possibility to determine the optimal operating parameters of the dryer.

NOMENCLATURE

A	surface area m^2
D	diameter m
c_p	specific heat capacity J/kgK
F	force N
f	drag coefficient
g_n	acceleration of gravity m/s^2
h	entalpy J/kg
Δh_v	specific latent heat of vaporization J/kg
L	air mass flow rate kg/s
M	mass kg
$\dot{m}$	mass flux density kg/m^2s
r,ϕ,z	cylindrical coordinates m
t	time s
u,v,w	velocity m/s
V	volume m^3
x	moisture content
α	heat transfer coefficient W/m^2K
β	evaporation coefficient kg/m^2s
θ	Celsius temperature ^oC
ρ	mass density kg/m^3
ψ	number of droplets

Dimensionless numbers

Le	Lewis number
Nu	Nusselt number
Pr	Prandtl number
Re	Reynolds number

Subscripts

e	equilibrical
F	on droplet surface
i	in the i-th class of droplets
L	air
na	wet droplet
nL	wet air
pWG	wet bulb or for the temperature of the particles
r	radial
t	tangential
w	for moisture
z	longitudinal

INTRODUCTION

Much research work had and has been spent on processes in spray drying, aiming at an ampler knowledge of the phenomena in the dryer, helping a more efficient use of existing equipment or the design of an equipment better coping with the actual task (1, 2, 3, 4).

Hitherto investigations involved mathematical models, ignoring, however, droplets of different sizes to move in the dryer. Droplet size distribution was averaged to enter the model. The described examinations aim at developing a model of processes affecting different size droplets.

1. MATHEMATICAL MODEL

To establish the mathematical model of spray drying, the involved physical processes have to be analyzed and mathematically formulated. Our investigations concerned the development of existing models (5, 6).

The material to be dried is sprayed into the dryer in form of different size droplets. Droplet size distribution for various atomizers had been much investigated both experimentally and theoretically.

Droplet size distribution also affects the drying processes:
- droplet motion being affected by its size;
- transfer coefficients depend both on the relative velocity between drying medium and droplet, and on the droplet size;
- fast drying small droplets saturate air near the atomizer, thereby larger droplets may even be humidified over a short length.

The mathematical model has to contain non-uniformity of droplet sizes, the actual size distribution in the arising spray, described by any distribution function presented for spraying. Actually, the upper-limit distribution suggested by Mugele and Evans will be applied.

Let us partition the arbitrary distribution function: thereby drops in the interval ΔD may be replaced by the number of droplets of size D_i in this interval /Fig.1/. In establishing the mathematical model, an infinitesimal height dz of the dryer will be considered, where droplets of different sizes enter at different velocities.

Thus, time scales for different droplet fractions have to be determined so that the droplet travels by this distance dz along the dryer height:

$$dt_i = \frac{dz}{u_{zi}}$$

This hypothesis provides for an accurate result in steady state. Thereby, however, the infinitesimal dryer section includes droplets of different ages. The model will be written for the diameter D_i of the distribution function.

The mathematical model will involve

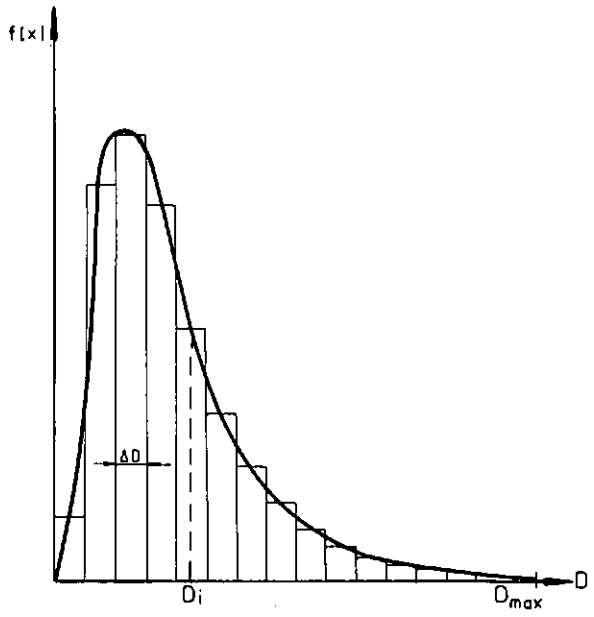

Figure 1

the following simplifying assumptions:
- in the section of constant drying rate, the vapour pressure at the droplet surface depends only on temperature;
- droplets are exempt of temperature or concentration gradient inside;
- in a given dryer cross section, the drying medium is perfectly homogenized, uniform by both temperature and humidity. Thus, radially the drying medium is exempt of temperature and concentration gradients.

Let us write first the droplet motion equations:

relative droplet velocity: $\underline{w} = \underline{u} - \underline{v}$

Droplet motion is determined by force effects, and in our case, forces of resistance and of gravity may be stated to prevail:

$$m\,\underline{a} = \underline{F}$$

The force of resistance:

$$\underline{F} = -\frac{1}{2}\,\rho r L\, A\, \underline{w}/\underline{w}/$$

The gravity force:

$$\underline{F}_G = \frac{D_i^3\,\Pi}{6}\,\rho_{na}\,\underline{g}_n$$

Arranging the equations and decomposing them into components of different directions:

$$\ddot{r} - r\,\dot{\phi} = -\frac{3}{4}\,\frac{\rho_{nL}}{\rho_{na}}\,\frac{1}{D_i}\,f\,|\underline{w}|\,|\underline{w}_r| \qquad (1)$$

$$r\ddot{\phi} + 2\dot{r}\dot{\phi} = -\frac{3}{4}\,\frac{\rho_{nL}}{\rho_{na}}\,\frac{1}{D_i}\,f\,|\underline{w}|\,|\underline{w}_t| \qquad (2)$$

$$\ddot{z} = g\left(1-\frac{\rho_{nL}}{\rho_{na}}\right) - \frac{3}{4}\frac{\rho_{nL}}{\rho_{na}}\frac{1}{D_i} f |\underline{w}| |\underline{w}_z| \qquad (3)$$

In knowledge of a given equipment, the drying medium velocity may be better approximated /mode of air injection, design/.

Axial velocity will be obtained from the volume flow:

$$v_z = \frac{L}{\frac{D_r^2\,\pi}{4}} \qquad (4)$$

Heat and material balances:

Material balance for the drying gas:

$$L\,x_L + \sum_i \psi_i M_{sz} x = L(x_L - dx_L) + \sum_i \psi_i M_{sz}(x - dx)$$

hence:

$$L\frac{dx_L}{dz} = \sum_i \frac{\pi}{6}\frac{\psi_i D_i^3 \rho}{1+x}\frac{dx}{dz} \qquad (5)$$

Material balance for a droplet:

$$M_{sz} x = M_{sz}(x + dx) + \dot{m}\,A\,dt$$

hence:

$$-\frac{\rho_{na}}{1-x}\frac{dx}{dz} = \frac{6\dot{m}}{D_i u_z} \qquad (6)$$

Heat balance for a droplet:

$$c_{na}\,\rho_{na}\,V_{na}\,\theta_F = (V_{na}\,\rho_{na}\,c_{na} + d(V_{na}\,\rho_{na}\,c_{na}))(\theta_F + d\theta_F) + (\dot{m}h_F - q_s)\,A\,dt$$

hence:

$$\frac{d\theta_F}{dz} + \frac{\theta_F}{1-x}\frac{dx}{dz}\left(1 + (1-x)\frac{c_w}{c_{na}}\right) = 6\,\frac{(\theta_L - \theta_F) - \dot{m}(h_v + c_{pw6}\,\theta_L)}{c_{na}\,\rho_{na}\,D_i\,u_{zi}} \qquad (7)$$

Heat balance for the drying gas:

$$Lh_L + \sum_i \dot{m}h_F \psi_i A\,dt = L(h_L + dh_L) + \sum_i \alpha(\theta_L - \theta_F)\psi_i\,A\,dt$$

hence:

$$Lc_{nL}\frac{d\theta_L}{dz} + L(\Delta h_v + c_{pwG}\theta_L)\frac{dx_L}{dz} = \sum_i \frac{\psi_i D_i^3 \pi}{u_{zi}}(\dot{m}(\Delta h_v + c_{pwG}\theta_L) - \alpha(\theta_L - \theta_F)) \qquad (8)$$

In addition to motion and balance equation, also other equations are needed to solve the mathematical model. First, let us examine the behaviour of droplets during drying: in the section of constant drying rate, drying rate will be interpreted as:

$$\dot{m} = \beta(x_F - x_L) \qquad (9/a)$$

Droplet diameters are assumed here to decrease in conformity with the evaporated water quantity. The momentary droplet diameter:

$$D_i = D_{i_o}\sqrt[3]{\frac{\rho_{nao} - \rho_w}{\rho_{na} - \rho_w}} \qquad (10/a)$$

The so-called critical moisture content is followed by the section of slower drying where the variation of drying rate is approximated as:

$$\dot{m} = \beta\frac{x - x_e}{x_{kr} - x_e}(x_F - x_L) \qquad (9/b)$$

At and beyond the critical moisture content, the droplet surface gets a solid coat. Upon further drying the droplet does not shrink any more but its porosity and its density changes:

$$\frac{d\rho_{na}}{dz} = -\frac{6\dot{m}}{\rho_w D_i} \qquad (10\,b)$$

or

$$\frac{d\varepsilon}{dz} = \frac{6\dot{m}}{\rho_w u_z D_i}$$

Transfer coefficients have been determined by means of the Ranz-Marshall equation:

$$Nu = 2 + 0{,}6\,Re^{1/2}\,Pr^{1/3} \qquad (11)$$

The evaporation coefficient has been determined from the heat transfer coefficient by means of the Lewis' relationship:

$$\beta = \frac{\alpha}{c_{nL}Le} \qquad (12)$$

Also the saturation curve equation will be involved:

$$x_F = f_1(\theta_F) \qquad (13)$$

and the equation of the resistance coefficient:

$$f = f_2(Re) \qquad (14)$$

The equilibrium humidity has been calculated from:

$$x_e = f_3(\varphi) \qquad (15)$$

Thus, for solving the model, a set of e-

quations (1) to (15) is available.

Droplet balance euqations have been solved for the infinitesimal dryer length dz proceeding from small diameters towards increasing ones. Drying processes of each droplet fraction continuously alter the air characteristics but the drying medium is assumed to be perfectly homogeneous in an infinitesimal dryer length dz.

The solution procedure started from the dryer top for drying elements of infinitesimal length dz, by the method of finite differences.

This model lends itself to replace droplet size distribution by a given droplet diameter.

2. EXAMPLE

This model has been applied to examine different atomizers with different service ratings. The results to be presented refer to a uniflow drying equipment with a nozzle ϕ 1,5 mm under pressure. The spraying pressure of 490.10^4 Pa produces droplets $D_{max} = 305.10^{-6}$ m leaving the nozzle at axial and tangential velocities u_z = = 81,74 m/s and u_t = 43,85 m/s, resp.

The solution injected at 0,15 kg/sec at a moisture content of 2,33 kg per kg of solids has a density of 1140 kg/m^3. The rate of drying air is 1,5 kg/sec. Dividing the droplet size distribution into eight fractions:

i	D_i(m)	$\psi_i(\frac{\text{droplet}}{\text{sec}})$
1	$32\ 10^{-6}$	$3{,}79\ 10^8$
2	$81\ 10^{-6}$	$7{,}00\ 10^7$
3	$110\ 10^{-6}$	$2{,}80\ 10^7$
4	$133\ 10^{-6}$	$1{,}58\ 10^7$
5	$153\ 10^{-6}$	$1{,}04\ 10^7$
6	$174\ 10^{-6}$	$7{,}07\ 10^6$
7	$206\ 10^{-6}$	$4{,}26\ 10^6$
8	$265\ 10^{-6}$	$6{,}67\ 10^5$

Among the results, variations of droplet moisture content and temperature will be presented in Figs 2 and 3.

Minor droplets are seen to dry out already near the atomizer. Temperature of dried droplets abruptly tends to that of the drying medium. Larger droplets much travel humid even in the dryer.

Fig.3 shows temperature variation of drying medium and drying droplets along the dryer length. Depending on their size, droplets

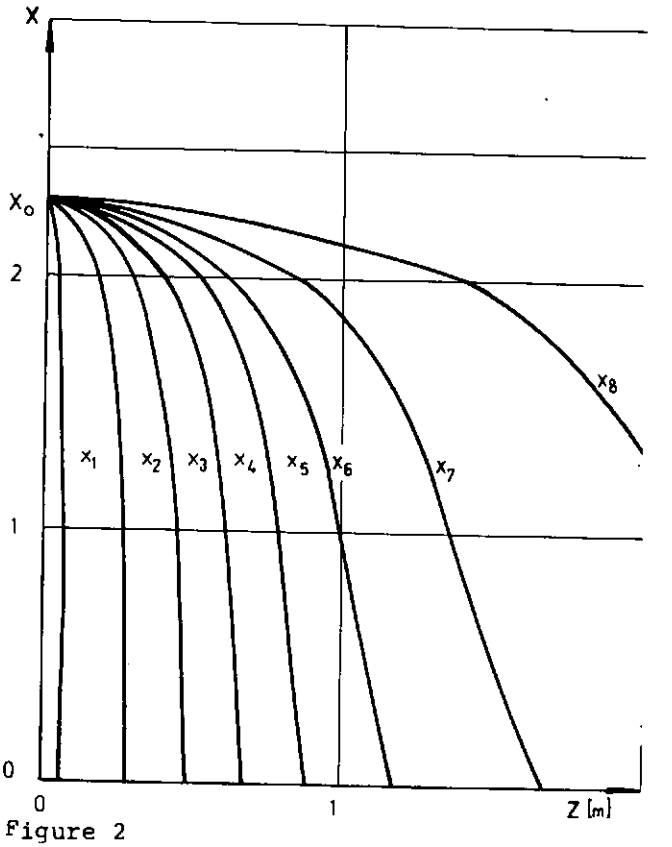

Figure 2

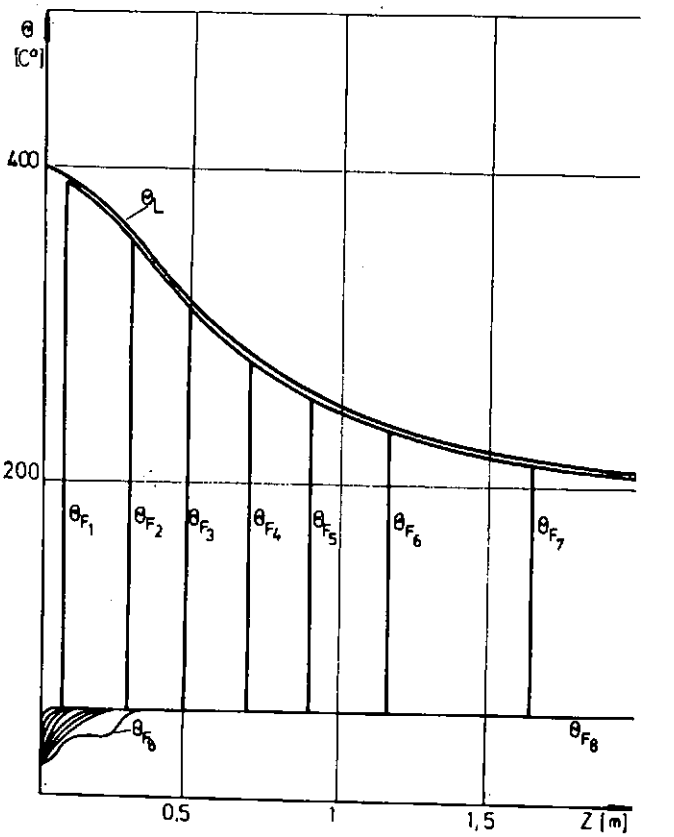

Figure 3

rather soon are heated to the air dry-bulb temperature, then, after drying, they instantaneously are heated near the temperature of the drying medium. Minor drops are

seen in the figure to take the hot air temperature already at the dryer top.

Let us compare this result with that obtained for a droplet size distribution substituted by the Sauter mean diameter. In the actual case, the mean diameter is, from the size distribution:
$D_{32} = 123 \quad 10^{-6}$ m, involving $1{,}33 \quad 10^{8}$ droplets per sec.

The comparison will refer to the droplet moisture content variation:

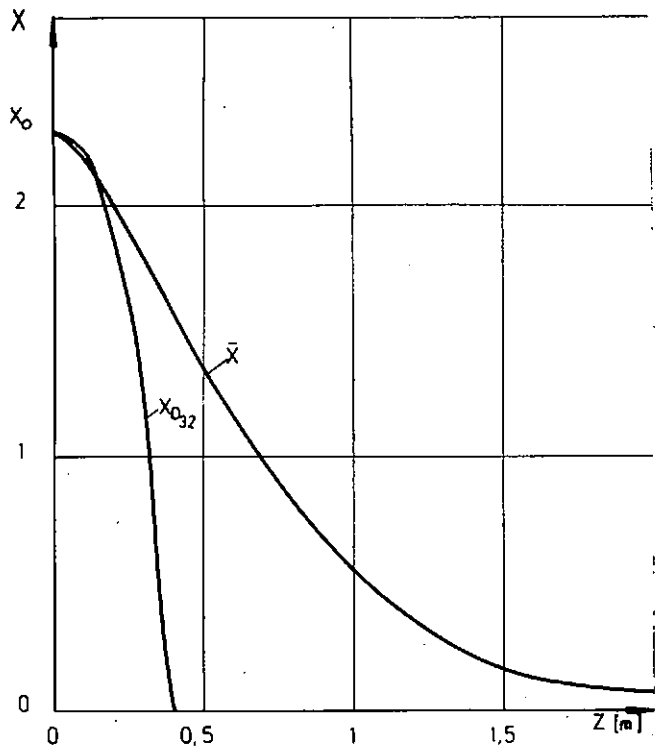

Figure 4

Beside moisture content variation in each droplet size, Fig. 4 will present the average humidity distribution obtained by taking the droplet size distribution into account, as well as the moisture content calculated for D_{32}.

Applying the mean diameter, the droplet is seen to be dried out over a much shorter dryer length than in reality. Though, from productional aspects, respecting the upper limit of humidity even in the largest drop is imperative.

Thus, for the sake of truly modelling the dryer, it is improper to substitute mean diameter for droplet size distribution, absolutely to be involved.

SUMMARY

A mathematical model suiting to describe spray drying have been presented, solved in a unique way, by taking droplet size distribution, rather than a mean diameter, into consideration. A mean diameter involved in the dryer model was found to be a rather important source of error in determining the principal dimensions of the dryer. In spite of the increased running time for solving the model involving droplet size distribution, in order to obtain more accurate results it is suggested for determining drying equipment size, or for analyzing operating conditions.

REFERENCES

1. Marshall,W.R., Atomization and Spray Drying, C.E.P.Monograph Ser.No.2, Vol.50, 1954

2. Gauvin,W.H.-Katta,S., Some Fundamental Aspects of Spray Drying AIChE Journal, Vol.21, pp 143--152, 1975

3. Stein,W.A., Berechnung der Trocknung wasserfeuchter Produkte im Sprühturm, Chemie Ing.Techn., Vol.44, pp 1241-1246, 1972

4. Poliakov,E.V.-Ananikov,S.V.-Ahmetov, T.G., Raschem teplomassobmena v struino-raspulitelnoi sushilke, Chimicheskaia Prolyshennost, pp 49-51, 1979 /in Russian/

5. Parti,M-Paláncz,B., Mathematical Model for Spray Drying, Chem. Eng.Science, Vol.29, pp 355-362, 1974

6. Parti,M-Topár,J., A porlasztásos szárító üzemi viszonyainak vizsgálata matematikai modellel, Energia és Atomtechnika, Vol. 27, pp 301-304, 1974 /in Hungarian/

ASSESSMENT OF NUMERICAL MODELS FOR SPRAY-DRYING

G. Arnason and C. T. Crowe

Washington State University, Pullman, Washington

ABSTRACT

Many models have appeared in the literature for gas-droplet flow in a spray dryer. These models range in complexity from the simple one-dimensional models in which the effect of the droplets on the gas flow field is neglected, to the two dimensional model in which the complete coupling phenomena are accounted for. In this paper, three models representing one dimensional, quasi-one dimensional and axisymmetric (two dimensional) models are used to predict the properties of a water spray in a hot gas flow field. The predictions are compared with experimental results and the relative adequacy of the models is discussed.

NOMENCLATURE

A	duct cross-sectional area
c	concentration of vapor
d	droplet diameter
D_v	diffusion coefficient
k	thermal conductivity
m	mass of droplet
Nu	Nusselt number
Pr	Prandtl number
Q_d	heat transfer rate to droplet
Re	Reynolds number
Sc	Schmidt number
Sh	Sherwood number
SMD	Sauter mean diameter
t	time
T	temperature

Greek Letters

β	empirical coefficient
Δx	spatial increment
ρ	density

Subscripts

s	droplet surface
∞	drying air condition

INTRODUCTION

Spray-drying is a widely used dehydration method. It is ideal for drying materials that are heat sensitive because the process is rapid even though the drying medium is at comparatively low temperatures. Also, the powdered form of the final product is often preferred.

Conceptually the process is divided into three phases: the spraying phase, the drying phase and the residue-collecting phase. The operation of each phase has a significant impact on the overall performance of the spray-dryer. In the spraying phase, an atomizer breaks up the liquid solution into droplets that are discharged into the drying medium. Although considerable study has been devoted to this part of the overall process, the results are presented mainly through empirical correlations for atomizer performance. When the particles are dry they are usually collected from the drying medium by a cyclone separator. This paper is concerned primarily with the drying phase.

Drying occurs due to evaporation of liquid from the droplets, by the drying medium, leaving only dry particles. Considering a typical spray-dryer where the drying medium is air and the liquid removed is water, the following phenomena, shown schematically in Fig. 1, will occur. As the drop-

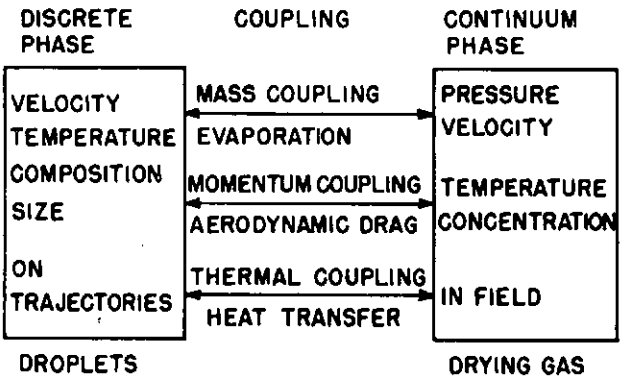

Figure 1

lets enter the gas, evaporation, caused by a vapor concentration gradient, occurs which, in turn, requires a transfer of energy from the drying medium to account for the energy required for a change of phase. Also, the velocity of the droplets relative to the gas, gives rise to a drag force (momentum exchange) which affects the velocity and the convective mass and heat transfer rates. Thus, the three basic transfer mechanisms are operative and interact, making the process very complex.

A typical dryer operates at air temperatures from 100°C - 700°C with droplets less than 1000 μm and droplet Reynolds number less than 1000. The feed rate of water is of the order of 5% of the air flow rate.

The design of a spray dryer is usually accomplished by modifications of previous designs and/or by application of empirical or simplified expressions for droplet trajectories and drying rates. In many instances, such as in the development of radically different designs or the drying of new materials, the empirical approach may not be valid. Thus, the designer desires to use more viable numerical models to supplement the design. In this paper, three different numerical models are evaluated by comparing predictions with experimental results.

The mechanisms governing the transfer processes to an isolated droplet must be known to formulate the behavior of the spray. We will now consider the transfer processes that are dominant for a typical dryer. A more complete discussion can be found in Crowe [1].

Droplet mass transfer

The driving force for evaporation is the gradient in vapor concentration from the droplet surface to the surrounding medium. The following equation has general acceptance as the governing equation for mass transport from a spherical droplet.

$$\frac{dm}{dt} = Sh\pi\rho D_v d\cdot(c_\infty - c_s) \qquad (1)$$

Sh is the Sherwood number which is empirically related to Reynolds number and Schmidt number by

$$Sh = 2 + \beta Sc^{1/3}\cdot Re^{1/2}. \qquad (2)$$

The most widely used value for β is 0.6 as given by Ranz and Marshall [2].

In a droplet containing solids or solutes, there is also an internal mass transfer that establishes the vapor concentration at the surface. The internal transport rate may be hard to quantify in that it involves the complexities of diffusion in a porous medium, because a crust may be formed during the drying process.

Droplet momentum transfer

The dominant force acting on droplets in a typical dryer, is the aerodynamic drag. Other possible forces include "thrust" due to nonuniform evaporation, a Basset force due to transient effects, a buoyancy force if pressure gradients exist in the drying medium, and lift if high velocity gradients exist or if the particle has spin (Magnus effect). Typically, these forces are small compared to the steady state aerodynamic drag. The drag force is represented by a drag coefficient which may be influenced by evaporation, particle spin or turbulence. Once again these effects are not significant in modelling droplet motion in a spray-dryer.

Droplet heat transfer

Analagous to mass transfer, the driving force for the heat transfer is a temperature gradient. Using Fourier's law we obtain

$$\dot{Q}_d = Nuk\cdot\pi\cdot d(T_\infty - T_s) \qquad (3)$$

where Nu is the Nusselt number and empirically related to Reynolds number and Prandtl number by

$$Nu = 2 + \beta Re^{1/c}Pr^{1/3} \qquad (4)$$

The value of β is again 0.6 according to Ranz and Marshall [2]. Nusselt number might change with droplet rotation or due to turbulence, but little information is available on these effects. Radiative heat transfer becomes important at high temperatures, but scattering in the particle cloud makes radiation complicated to model. Atmoderate operating temperatures, radiative effects are negligible. The temperature gradient can be influenced by heat transfer internal to the droplet and also by mass transfer effects if the evaporation is very rapid (blocking effect). For a typical dryer, and pure water droplets, a uniform droplet temperature can be assumed.

Modeling

A spray-dryer designer often needs to predict behavior or performance of dryers before they are built. For that purpose, models are necessary. In the past thirty years many such models have been introduced. It is convenient to categorize such models in terms of their geometry and degree of phase coupling. By coupling we mean the interacting influences of one phase on the other. Coupling involves the three transfer mechanisms, mass, momentum and heat transfer. Models that account only for the effect of the gas on the droplets have one-way coupling. But models that allow the transfer to result in property changes of both phases are two-way coupled. Actually a model with one-way coupling treats the spray as individual droplets uninfluenced by neighboring droplets. Fullycoupled models include the effect of neighboring droplets because each droplet contributes to a change in the local droplet surroundings (the drying medium). These models are more capable of simulating the evaporation of a cloud of droplets.

Geometrically we classify models as being one, quasi-one, or two dimensional (axisymmetric). A one dimensional model accounts only for axial changes in properties and is based on the assumption that properties be uniform over cross-sections. This assumption is clearly inaccurate for a spray-dryer, especially close to the atomizer. A quasi-one dimensional model allows changes in the radial direction, but only in discrete regions, each assumed to have uniform properties. An axisymmetric model allows changes in both radial and axial directions.

Table I, adopted from Crowe [1], shows these models in appropriate categories. In the table, two-way coupling means that at least one of the coupling phenomena is considered both ways.

Table I

Summary of Models Developed for or Applicable to Spray-Air Contact in Spray-Drying Systems

	ONE-WAY COUPLING	TWO-WAY COUPLING
one-dimensional	Marshall and Seltzer (1950) Sjenitzer (1952) Duffie and Marshall (1955) Marshall (1955) Miesse (1957) Kerkhof and Schoeber (1974) Masters (1976)	Dickinson and Marshall (1968) Parti and Palancz (1974)
quasi one-dimensional	Gluckert (1962)	Katta and Gauvin (1975)
axisymmetric	Coulson and Richardson (1968) Bailey, Slater and Eisenklam (1970) Kerkhof and Schoeber (1974) Masters (1976) Boyson and Swithenbank (1978)	Baltas and Gauvin (1969) Crowe, Sharma and Stock (1977) Ellail and Khalil (1978)

Comparison to experimental results

A meaningful assessment of a computer model is its capability to predict actual experimental results. As we wanted to eliminate the need to model the added complexity of transport mechanisms internal to the droplets, we searched the literature for data for the simple case of evaporating sprays of pure liquids. We found that only the data of Manning [3] for the evaporation of pure water droplets in air, had sufficient detail for comparison with numerical models.

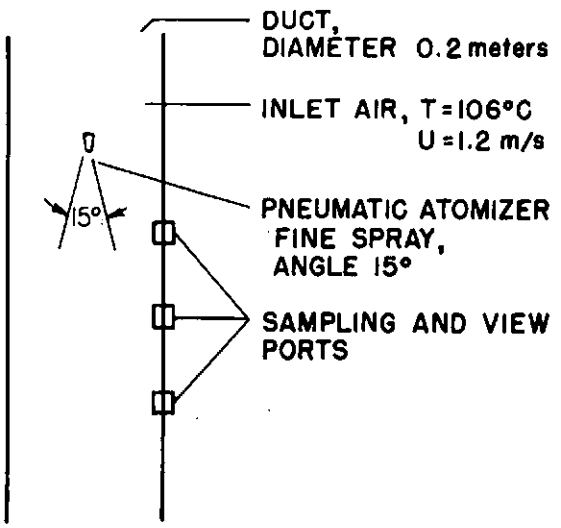

Figure 2

Manning's experimental set-up is shown in Fig. 2. Hot air, which serves as the drying medium, flows vertically downward in a .2 m diameter pipe. A nozzle, positioned on the centerline, sprays a droplet cloud into the drying air. Several access ports downstream of the nozzle enabled Manning to measure droplet and air properties.

The droplet sizes were determined by collecting samples from the spray on a small immersion cell containing Varsol, a liquid immiscible with water. The samples were photographed under a microscope and the droplet diameter measured from the enlarged photographs.

Manning measured droplet velocities using a photographic method. The droplet field was photographed using a high speed camera under illumination from a high intensity flood lamp. Analysis of the high speed motion picture yielded droplet velocity and associated droplet size. Velocities of droplets less than 10 μm could not be measured.

The droplet temperature was measured by a thermocouple located in the droplet field. Droplets accumulated on the thermocouple and, by bending its tip slightly in the flow direction, a steady flow of liquid along the thermocouple was achieved. The temperature read-out represented the droplet temperature.

The fraction of water evaporated was measured using a colorimetric method. The water was mixed with a dye creating a mixture with a very intense color but of very low dye concentration. The dye was assumed to have no effect on the evaporation of the droplets. Droplets collected from the spray were immersed in silicon oil in order to arrest further evaporation. The concentration of dye in the sample was measured by colorimetry to determine the fraction of water evaporated.

Local air velocities in the spray could not be measured directly. The air velocity was assumed to be the velocity of the smallest measureable droplets.

To determine air temperatures, a shielded thermometer was used. An especially designed aluminum shield prevented droplets from impacting the mercury thermometer and thus affect the gas temperature

measurement. Although temperatures were measured at different radial locations across the duct, only an average temperature was reported.

Manning tried various methods to determine the humidity of the drying air but, for most of his measurements, he used a volumetric method. The air sampled from the dryer was exposed to magnesium perchlorate which absorbs only the water vapor from the gas. The volume change of the gas then allowed him to determine the humidity.

Run 29 from Manning's data was used to assess the numerical models. The air flow rate was 0.038 kg/s with an initial temperature 106°C. The air velocity just upstream of the nozzle was 1.22 m/s. The water feed rate was $5.5 \cdot 10^{-4}$kg/s and the flow rate of the atomizing air was $9 \cdot 10^{-4}$kg/s. The atomizer was a pneumatic nozzle, 1/4JN No. 12 from Spraying System Co., Chicago, which produced a solid cone spray with a spray angle of 15°. The initial mean Sauter diameter of the droplets was measured to be 13μm.

The distribution of droplet sizes was discretized into four sizes with corresponding initial velocities as shown in the following table.

Droplet diameter μm	Mass fraction	Velocity m/s
5	0.21	9.5
15	0.33	24.0
25	0.32	44.0
40	0.14	80.0

The same discretized droplet size distribution was utilized for the three computer models.

THE MODELS

The three numerical models considered in this study can be classified as one dimensional, quasi one dimensional and two-dimensional models.

One dimensional model

The one-dimensional model developed in this paper is the simplest of the three models. It utilizes the Lagrangian approach in that it keeps track of a control mass traveling downstream in the duct with the air velocity as shown schematically in Fig. 3. The volume of the control mass is $A \cdot \Delta x$ where A is the cross-sectional area of the duct and Δx is its length along the duct. It is assumed that properties are homogeneous in the control mass. Step by step the control mass is allowed to advance Δx (its own thickness) downstream. After each step the droplet equations are integrated over the same length, to determine the evaporation, heat transfer and deceleration of the droplets traversing the control mass. The Sherwood number, Nusselt number and Reynolds number used in the integration were the average values over the step. These transfer numbers were updated with each iteration and the calculation repeated until droplet diameters at the end of the step fail to change within a prescribed tolerance. The changes in droplet properties together with the droplet number flow rates are used to calculate the mass and heat transfer to the control mass. The control mass properties are updated before advancing the control mass to the next location. Changes in droplet momentum are assumed to have negligible effect on air velocity.

Starting with the droplet and air properties at the nozzle, the control mass is marched downstream until a preset distance is reached or until all droplets have totally evaporated. This method requires very little storage capacity because all information is retained in the control mass and droplet properties at the upstream step.

In that the smallest droplets decelerate very rapidly to their terminal velocity, Δx had to be chosen very small to start the calculations. For this specific application, a Δx of 10^{-3}m was adequate.

This model is one-dimensional, fully coupled in mass and thermal energy transport but one way coupled in momentum. It was run on a Digital PDP11/03 minicomputer. A typical run lasted about three real time minutes.

Quasi-one dimensional model

In 1975, Gauvin et al. [4] presented a model to simulate the drying process. They divide the dryer radially into two regions, a jet or spray region and a free stream region. Each region is assumed to have uniform temperature and humidity. The jet region, however, is assigned a radial velocity gradient. The coupling between the regions is accomplished through an empirically determined entrainment rate; that is, the rate at which the free stream air enters the jet region. The entrainment rate for jets without particles is used. Also, at a specific axial location, the jet region is assumed terminated, and the model becomes one-dimensional.

This method provides a useful way to account for the fact that the droplets enter the duct in a jet, and thus do not encounter the average air velocity.

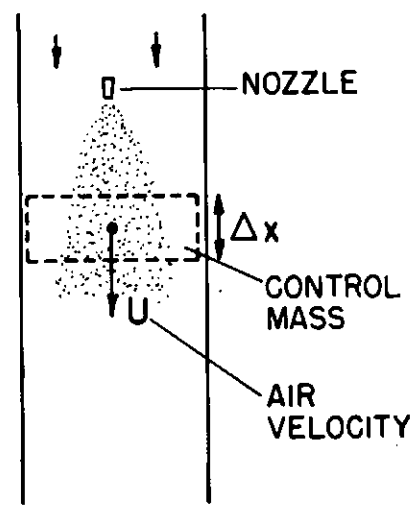

Figure 3

This model simulates the actual spray nozzle region much better than a totally one-dimensional model.

The droplet trajectories are obtained by integrating the droplet equation of motion. The evaporation of the droplet is calculated along the trajectory assuming the droplets are always at the wet-bulb temperature. The model is fully coupled in regards to mass and energy but includes only one-way coupling for momentum. In the region where the model is quasi one-dimensional the changes in temperature and humidity in the jet are determined from evaporation and entrainment, whereas the properties in the outer region remain constant.

Instabilities in the calculations required time-steps to be 10^{-6} sec. initially but could gradually be increased to 10^{-4} sec. CPU-time for the calculations was 15 CPU-sec on an Amdahl 470 computer.

Two dimensional (axisymmetric) model

The axisymmetric model was developed by Crowe et al. [5] and published in 1975. The model is an extension of the TEACH program, developed at Imperial College in London, to include dispersed phase droplets or particles. It is called the PSI-Cell (Particle-In-Cell) model.

The flow field is divided into a network of computational cells and the conservation of mass, momentum and energy for each cell is expressed as an algebraic equation. Solving the set of algebraic equations using the tridiagonal algorithm and appropriate boundary conditions yields the pressure, temperature and velocity in each cell.

The flow field is first solved assuming no droplets are present. The droplets are then assumed to enter at discrete locations with a given initial size, temperature and velocity. The droplet equation of motion is integrated to yield the trajectory through the flow field. The size and temperature are continually updated as the droplet proceeds along its trajectory. As the droplet passes through each computational cell, its change in mass, velocity and temperature are interpreted as a source of mass, momentum and energy to the conveying gaseous phase. The gas flow field is recalculated incorporating these source terms to yield the effect of the droplets on the gas flow field. The droplet trajectories are recalculated using the updated flow field, the source terms are reevaluated and the iteration continues until the gas flow field fails to change with repeated iterations. In this fashion, a fully coupled solution is obtained.

The PSI-Cell model is the most detailed of the three models. It predicts the radial distribution of both the droplet and gaseous phases. It requires a minimum of empiricism, specifically, the Sherwood number, Nusselt number and drag coefficient as functions of Reynolds number based on the relative velocity between phases. The program can handle an arbitrary droplet size distribution and inlet mass flow distribution, the limit being the degree of discretization and associated cost. One feature not incorporated into the numerical scheme is droplet dispersion due to turbulence.

The details of the numerical calculation applying the PSI-Cell model to Manning's experimental conditions are provided in the reference [1]. The CPU time to execute the program was approximately 11 seconds on the Amdahl 470 which is comparable to the execution time for the quasi-one dimensional model.

RESULTS

The most important parameter for spray dryer design is the fraction of liquid evaporated as a function of distance from the nozzle, as plotted in Fig. 4. Manning's experimental results and the models' predictions are shown on this figure along with predictions given by an uncoupled model. Clearly, the uncoupled model is incapable of simulating the process. The one dimensional model is also inadequate and unreliable in that it predicts much too high an evaporation rate. The quasi-one dimensional model is acceptable although its predictions are somewhat low. The two dimensional model is also acceptable and yields results comparable to the quasi-one dimensional model.

The air temperature predictions are plotted in Fig. 5. The predictions corresponding to no coupling is included for comparison. The temperature predicted by the one dimensional model is an average over the total cross-section, whereas the other temperatures result from averaging only over the spray cone. The figure is difficult to interpret as the averaging process used for the experimental results is not known. But it is noted that the temperatures tend to the same value far downstream, as would be expected.

The Sauter mean diameter as measured by Manning and predicted by the numerical models is shown in Fig.6. The one dimensional model is again inaccurate in that it predicts a rapidly increasing SMD near the nozzle. This trend is the result of the one dimensional assumption leading to an unrealistically high evaporation potential and the smallest droplets tend to evaporate very rapidly, thus, the SMD increases. The quasi-one dimensional model is in fair agreement with data. The two dimensional model predicts very little change in SMD and thus, does not follow the data. This discrepancy is interesting as both the quasi-one dimensional and the two dimensional model predict the overall evaporation quite accurately. The source of the discrepancy is clarified by considering the droplet size history for these two models as shown in Fig.7. The two dimensional model gives a more rapid evaporation of the larger droplets than predicted by the quasi-one dimensional model. The opposite trend is observed for the smaller droplets. The net evaporation, however, is similar. The difference in SMD is due to the fact that the larger droplets travel on the edge of the spray cone in the two dimensional model and experience a low free stream humidity, whereas the larger droplets in the quasi-one dimensional model experience the higher average humidity in the spray region. The constant humidity over the spray cone in the quasi-one dimensional model subjects all droplets in the spray to the same evaporation potential, resulting in a slow diameter change of the larger droplets,

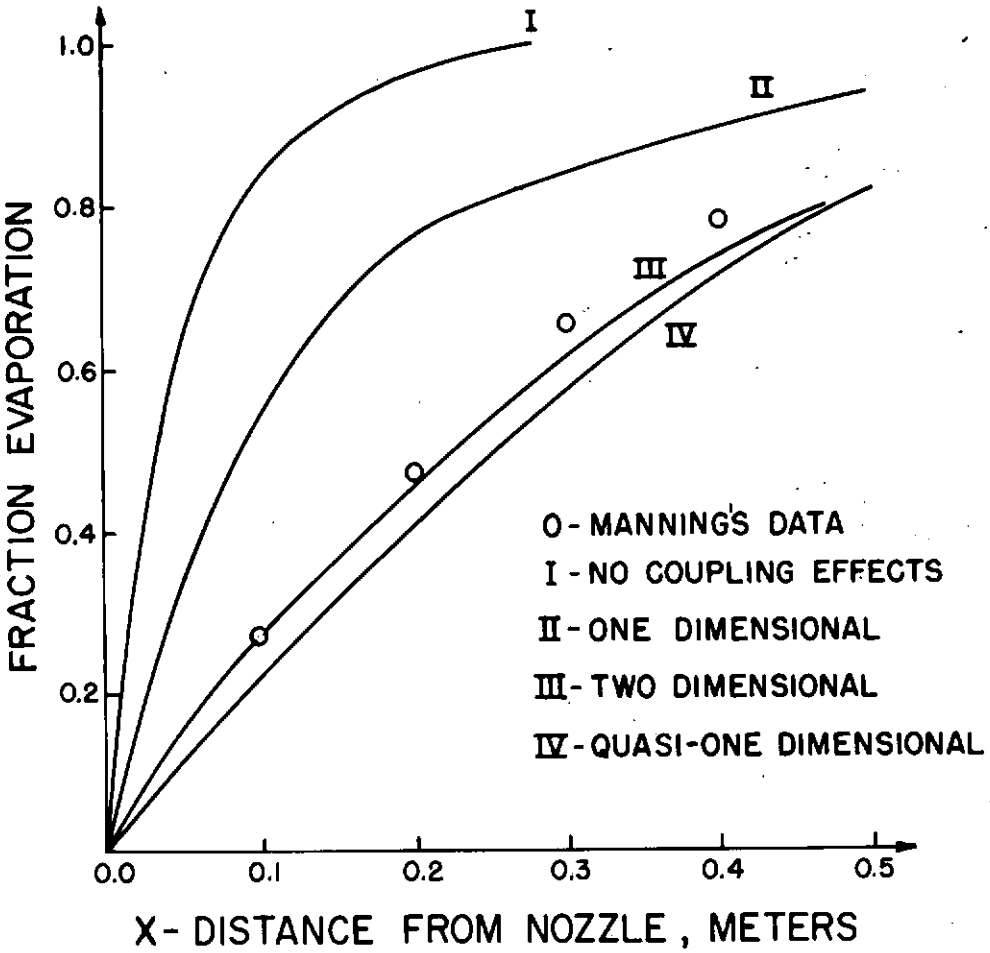

Figure 4

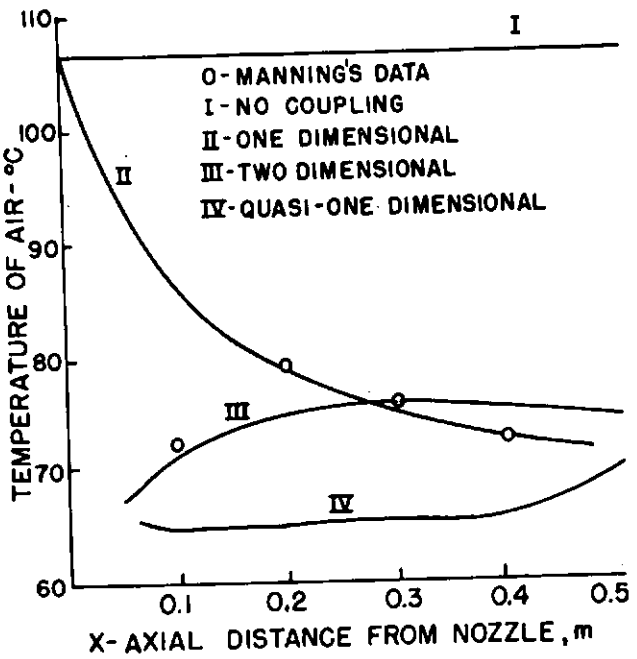

Figure 5

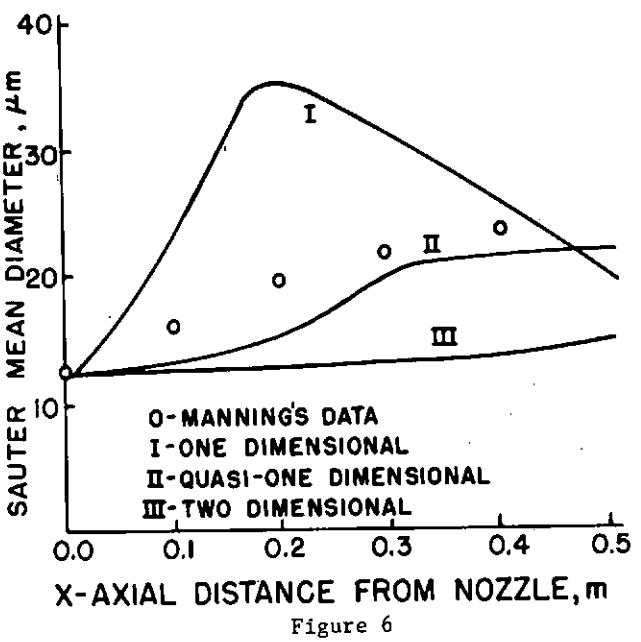

Figure 6

relative to the smaller ones. With the two dimensional model, if the large droplets traveled near the centerline of the spray and the smaller droplets on the spray edge, the latter would evaporate more rapidly resulting in an increasing SMD, but lower overall evaporation. Unfortunately, insufficient information is available to model the actual initial conditions near the atomizer, yet these conditions appear to have a significant effect on the numerical predictions.

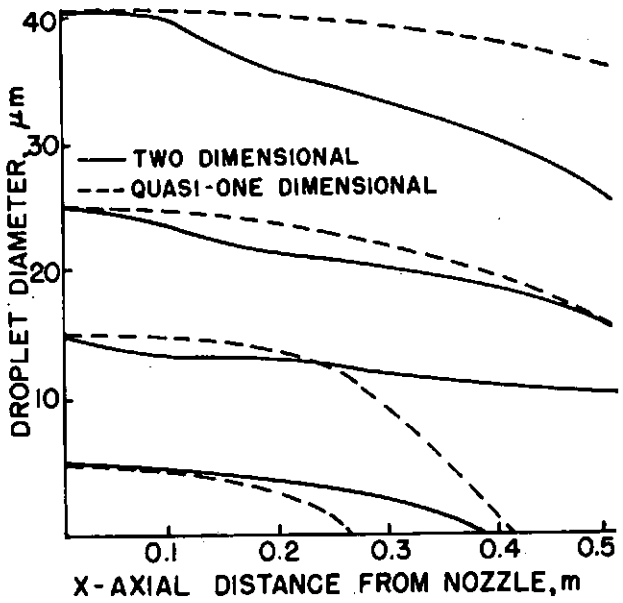

Figure 7

CONCLUSIONS

Simulation of the spray drying process cannot be done adequately with uncoupled or coupled one dimensional models. The fully coupled quasi-one dimensional and the two dimensional models are capable of predicting evaporation in spray dryers with acceptable accuracy provided that information on droplet velocity and size distributions in the immediate nozzle region are available. The development of viable numerical models for the drying process is contingent upon knowing the nature of the droplet field (size, velocity and mass flux distribution) at the atomizer. The numerical predictions suggest that atomizer design can strongly influence spray-dryer performance.

ACKNOWLEDGEMENT

The authors acknowledge the support of the Mechanical Engineering Department and the partial support of NSF Grant ENG-77-09855.

REFERENCES

1. Crowe, C.T., On Modeling Spray-Air Contact in Spray-Drying Systems, Hemisphere Pub. (in press).

2. Ranz, W.E. and Marshall, W.R.,Jr., "Evaporation from Drops," Chem.Engr.Progress, 48, pp.141-146, 173-180, 1952.

3. Manning, W.P., "Heat and Mass Transfer to Decelerating Finely Atomized Sprays," Ph.D. Thesis, McGill Univ. (1958).

4. Gauvin, W.H., Katta, S. and Knelman, F.H.,"Drop Trajectory Predictions and Their Importance in the Design of Spray Dryers," Int.J.of Multiphase Flow, 1, pp. 793-816 (1975).

5. Crowe, C.T., Sharma, M.P., and Stock, D.E.,"The Particle-Source-in-Cell (PSI-Cell) Model for Gas-Droplet Flows," Jnl.Fluids Engr., 99, pp.325-332 (1977).

EFFECT OF VANE GEOMETRY ON DROPLET SIZE AND SIZE DISTRIBUTION IN SPRAY DRYER

I. Filková
J. Weberschinke

ČVUT, Faculty of Mechanical Engineering,
Praha, Czechoslovakia

ABSTRACT

Atomizer wheels for spray drying are usually designed with straight or curved vanes. The vanes can be shaped to form different flow channels. In this paper, attention is paid to the effect of vane geometry on the quality of arising droplets. Three atomizer wheels differing only in the shape of straight vanes were tested. Experiments were carried out in pilot spray dryer by means of wheels with circular, square and rectangular vanes. The equivalent diameters of flow channels of all wheels are the same. Besides distilled water and glycerine, also non-Newtonian solution of CMC was used. Mean droplet diameter and size distribution in the dependence on wheel diameter, vane shape and revolutions were measured. The effect of different vanes on homogenity of spray was also observed.

NOMENCLATURE

D = wheel diameter, m
D_{ev} = equivalent diameter, m
D_v = circular vane diameter, m
K = consistency coefficient, kg/m s^{2-n}
M = mass feed rate, kg/s
M_v = mass feed rate per vane, kg/s, vane
N = revolutions
Qu = quality group, -
R = wheel radius, m
d_s = Sauter volume - surface diameter, m
d_q = dispersion factor, -
g = gravitational constant, m/s^2
h = vane height, m
n = flow index, -
n_v = number of vanes, -
v_r = radial velocity, m/s
v_p = peripheral velocity, m/s
$\dot{\gamma}$ = velocity gradient, 1/s
μ = dynamic viscosity, Pas
μ_a = apparent viscosity, Pas
ϱ = density, kg/m^3
σ = surface tension, N/m
ω = angular velocity, rad/s
τ = shear stress, Pa

1. INTRODUCTION

The final product of spray drying tower is powder. There are lots of different factors that influence the powder quality. Two most important of them are the mean size of particles and the size distribution. Both determine the bulk density of dry powder. Drying process can be generally divided into two stages :

a) atomization of the solution or slurry to form droplets
b) evaporation of liquid from droplets.

This paper concentrates on the first stage, atomization, using vaned rotation wheels at high rotation speeds.

The left side of the diagram in fig. 1

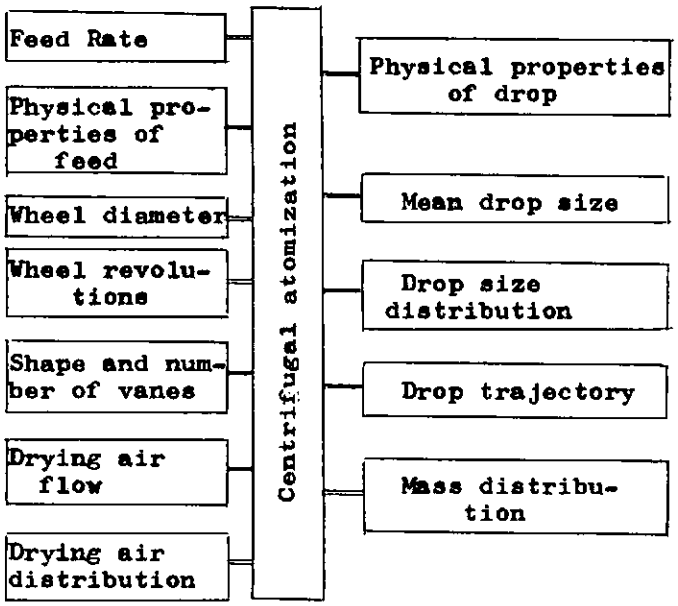

Figure 1

contains all main factors which influence the process of drop formation. Factors determining the properties of spray are mentioned on the right side. The change of each factor on the left side results in a change of one or more factors on the right side. Although considerable attention has been paid to centrifugal atomization, no suitable and general correlation has been developed that would express mutual influence of both sides. This problem is very complicated, as there exists mutual dependence even among operating factors of the left side. Physical properties, for example, represent a complex of properties that vary with temperature and pressure, and viscosity also with velocity gradient. The effect of each factor can be experimentally determined only when maintaining other factors constant. The analytical expression by means of dimensional analysis was also carried out. However the influence of single factors is not evident from the resulting equation, as one factor can be found in two or more dimensionless groups. Hence a lot of analytical and experimental work remains to be done until the process of atomization is satisfactoryly described.

This paper deals with one of the left-side factors that hasn't attracted much attention till now, the one with vanes. The influence of the shape of flow channels on droplet size, size distribution and homogenity of spray has been studied. The aspect of different behaviour of non-Newtonian liquids has been also considered. Some interesting results are presented here. This paper contains mainly experimental results because the theoretical relations are reported comprehensively in (1) or (2) and others.

2. EXPERIMENTAL CONDITIONS

Three experimental liquids were tested : distilled water*) and 4 % aqueous solution CMC as the non-Newtonian pseudoplastic one. Their physical properties were kept constant at 18°C during all experiment and feed rate was $M = 8,3.10^{-3}$ kg/s. Physical properties are listed in table 1.

*) and glycerine as Newtonian fluids

Table 1

	water	glycerine	CMC
ρ kg/m^3	998,2	1160	1032
σ N/m	$72,7.10^{-3}$	$63,5.10^{-3}$	$54,7.10^{-3}$
μ Pas	$1,0.10^{-3}$	$207,2.10^{-3}$	16.10^{-3}
n K	-	-	0,6 2,44

Non-Newtonian characteristic parameters of CMC : flow index n and consistency coefficient K were obtained from corresponding flow curve. However, the existing correlations for atomization have been developed for Newtonian liquids only, using dynamic viscosity. Instead of

Newtonian viscosity so called apparent viscosity μ_a can be applied, the calculation of which is quoted as follows (3). It is necessary to determine the velocity gradient :

$$\dot{\gamma} = \frac{8\, v_r}{D_{ev}} \qquad (1)$$

where D_{ev} ... equivalent diameter for non-circular cross section of flow channel

v_r ... radial velocity of liquid on the wheel edge, eq. (2)

$$v_r = \frac{M_v\, \rho\, \omega^2\, R}{3\, \mu\, h^2}, \qquad (2)$$

then apparent viscosity

$$\mu_a = \frac{\tau}{\dot{\gamma}} \qquad (3)$$

where shear stress τ is obtained from the flow curve for $\dot{\gamma}$ calculated by eg. (1). Hence for determining the apparent viscosity it is necessary to predict viscosity in the eq. (2) and compare both values as long as they are equal. The common iteration method has been used for this purpose. The present research has been carried out at rotation speeds above 20 000 RPM i.e. velocity gradient $\dot{\gamma}$ above 27 000 1/s. Apparent viscosity within this range is approaching some limit value and remains nearly constant, so that CMC under these experimental conditions can be considered as Newtonian fluid with viscosity $\mu_a = 16.10^{-3}$ Pas. It stands to reason that in case of different velocity gradient different apparent viscosity must be calculated.

W h e e l a t o m i z e r s used in this work were the standard type with straight vanes for ANHYDRO Compact Spray Dryer, where all experiments have been carried out. Wheels have been divided into two groups, see table 2.

D, m		0,09	0,1	0,12
group 1	n_v	8	8	8
	shape	◍	◍	◍
	D_v mm	4	4	4
group 2	shape mm		▨ 4x4	
	D_{ev} mm		4	
	shape mm		▮ 8x2,7	
	D_{ev} mm		4	
N, 1/min		17 000 - 25 000		
v_p, m/s		99 - 157		

Table 2

In the first group the wheels have the same circular vanes but 3 different diameters. Wheels in the second group have the same diameter but 3 different shapes of vanes : circular, square and rectangular. The equivalent diameter D_{ev} (=4 × hydraulic radius) for all vanes is the same, so that mutual comparison is possible.

T h e i m p a c t m e t h o d has been used for spray analysis of all described experiments. This method is suitable especially for sampling fine sprays and can be also applied in industrial dryers. Droplets were collected on magnesium oxide coated slides where they left a well-defined craters. Slides were magnified 60 times by microscope and then photographed. Also correction of craters to actual drop size has been made (4). The slides were placed in the impactor and fixed in the horizontal position 10 cm under the wheel. Five slides covered the distance 0,62 m between the chamber axis and the wall (5). To establish the form of the size distribution and to reduce the statistical error

to a reasonable value, it was necessary to count at least 300 droplets. The error was $100/\sqrt{300} = 6$ %.

Experimental sprays were represented by the log-normal distribution with the Sauter volume - surface diameter as the size parameter. All experiments have been carried out in co-current air flow in order to achieve agreement with the industrial conditions. Air velocity 10 m/s, air rate 0,23 kg/s, air temperature 18°C was the same as feed temperature.

3. MASS DISTRIBUTION

Mass distribution offers a simple way how to confirm that a really representative part of spray is sampled. The spray was collected in 10 cells situated along the radius of the drying chamber and weighed. Mass distribution for water and wheel D = 0,1 m with rectangular vanes is shown in fig. 2, where the influence of different revolutions is illustrated.

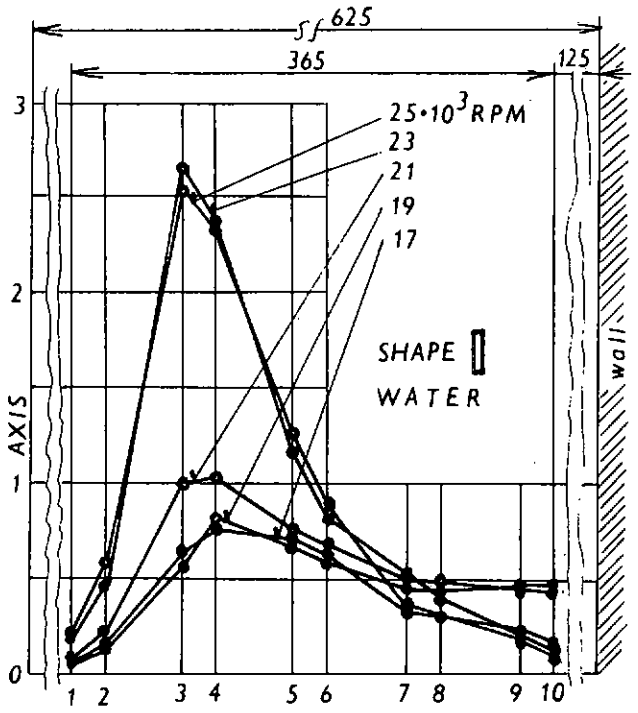

Figure 2

At speeds 17 000 and 19 000 RPM considerable part of spray falls on the wall of the drying chamber, so that the resulting size distribution couldn't be complete. Therefore all experiments have been carried out at higher revolutions, above 20 000 RPM.

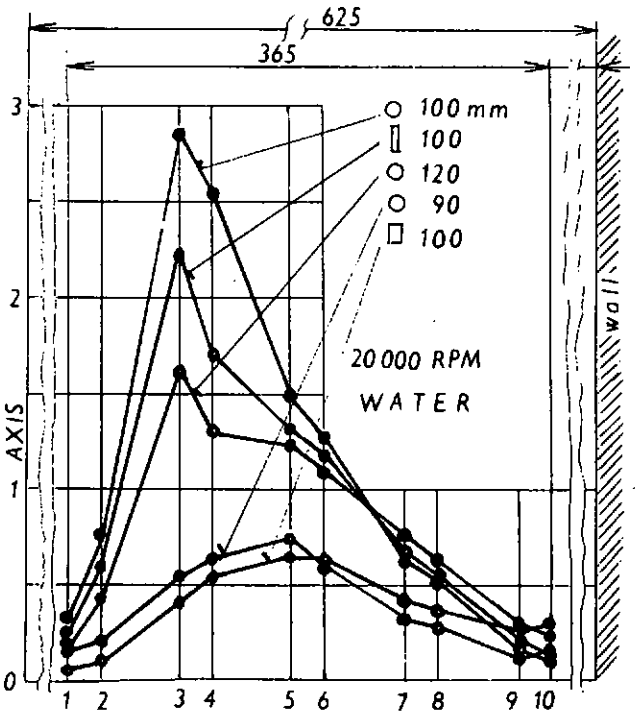

Figure 3

Mass distribution for water at 20 000 RPM when different shapes of vanes are considered is shown in fig. 3. Considerable influence of vanes is evident there and so it is for other fluids. These results confirmed the decision to pay attention to the effect of vane shape on the drop formation.

4. EFFECT OF VANE SHAPE ON DROPLET SIZE

There are many relationships for prediction of drop size by centrifugal atomization. Most of them contain besides number, the vane height as the only vane parameter. It means that the same droplets are predicted for two wheels with the sa-

me number and height of vanes, although the first one has circular vanes ϕ 5 mm and the second one rectangular vanes 5x1 mm. But the results of mass distribution (section 2) don't confirm this prediction.

The most suitable correlation for operating conditions described above was the equation recommended by Herring and Marshall. This equation also enables to respect the form of vanes by their height and wetted periphery, but it has been developed for low viscosity fluids only.

$$d_S = 0,4\ R\left(\frac{M_v}{\rho N R^2}\right)^{0,6}\left(\frac{\mu}{M_v}\right)^{0,2}\left(\frac{\sigma \rho n_v h}{M^2}\right)^{0,1} \qquad (4)$$

We tried to use it for wider viscosity range as well. The predicted and experimental Sauter mean diameter are summarized in table 3 and some of them plotted in fig. 4.

A good agreement of both experimental and predicted values for water, especially for square vanes confirms the applicability of eq. (4). The comparison of experimental drop sizes and those predicted by some other well known relationships, are not mentioned here because the agreement was less satisfactory. Fig. 4 also illustrates a wide dispersion of experimental results for different vanes. Minor dispersion is found for CMC which is considered as Newtonian liquid within the range of revolutions applied (see section 2). On the other hand the discrepancy in predicted values is for CMC considerably higher. Rather surprising fact is that although CMC has higher viscosity than water, the experimentally obtained droplets are smaller. Similar partial results have been obtained for another CMC concentration as well. The most probable cause of such anomaly is the pseudoplastic flow character of CMC.

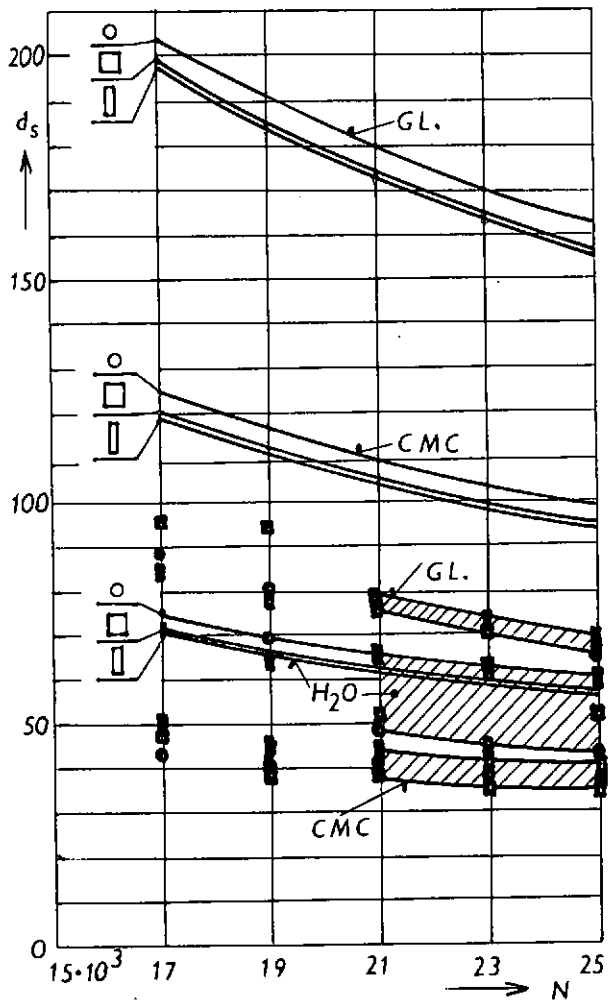

Figure 4

Minimal dispersion and maximal discrepancy demonstrates glycerine. At high speed, between 20 000 and 25 000 RPM (at wheel peripheral speeds 104 - 131 m/s), the effect of vane shape is no more so significant.

The results from fig. 4 can be simply explained in terms of viscosity. The effect of vane shape is important in the atomization of liquids with low viscosity. In this case the square shape produces largest drops, meanwhile the circular and rectangular ones give smaller drops. This phenomenon decreases with increasing viscosity and at certain value practically

Table 3

		d_S, water					d_S, glycerine					d_S, 4% CMC				
N 10^{-3}	D shape	0,1 ▯	0,1 □	0,1 ○	0,12 ○	0,9 ●	0,1 ▯	0,1 □	0,1 ○	0,12 ○	0,9 ○	0,1 ▯	0,1 □	0,1 ○	0,12 ○	0,9 ○
17	exp.	62,1	67,9	78,2	57,7	72,4	86,3	96,6	89,1	68,2	150,5	50,2	48,6	42,9	39,0	76,9
	eq.4	71,8	71,6	75,3	45,8	76,9	196,5	195,9	204,4	124,4	208,7	121,2	119,8	125,7	100,6	143,0
19	exp.	61,7	66,1	55,8	49,4	67,7	77,1	95,6	80,3	52,8	137,1	46,3	37,7	41,6	34,2	72,6
	eq.4	67,2	67,0	70,5	42,9	72,0	183,8	183,2	191,2	116,3	195,3	113,0	114,1	117,3	93,8	133,5
21	exp.	50,8	64,9	48,7	48,2	65,9	76,9	75,0	78,9	52,2	108,4	45,1	39,2	39,2	33,4	48,2
	eq.4	63,2	63,1	66,4	40,4	67,8	173,1	172,6	180,1	109,5	183,9	106,2	111,8	110,2	88,2	125,3
23	exp.	46,1	63,1	46,0	39,9	62,1	72,6	71,0	73,4	47,6	91,9	42,1	35,2	38,2	31,9	47,4
	eq.4	59,9	59,7	62,8	38,2	64,2	163,9	163,4	170,5	103,7	174,1	100,3	105,0	104,1	83,3	118,5
25	exp.	35,0	53,4	43,3	37,1	60,7	69,0	68,8	66,5	38,9	85,4	41,0	34,8	37,5	28,5	40,3
	eq.4	57,0	56,8	59,8	36,4	61,1	155,9	155,4	162,2	98,6	165,6	95,3	94,2	98,9	79,1	112,5

disappears. The dispersion of CMC spray represents about 30 % of mean drop diameter, but glycerine shows only 7,5 %. The discrepancy between experimental values and those predicted by eq.(4) increases with increasing viscosity, so that this relation is not suitable for high viscosity liquids. The survey of demonstrated results shows, that the effect of vane shape on droplet size at high rotation speeds can be neglected for liquids with viscosity $\mu > 150.10^{-3}$ Pas. The max. error is about 10 %.

More suitable and general parameter that characterizes physical properties of fluid instead of viscosity is so called quality group Qu. Besides viscosity it takes into consideration the effect of all important properties for atomization (6).

$$Qu = \frac{g \mu^4}{\rho \sigma^3} \qquad (5)$$

In terms of this more complex parameter, it can be concluded, that the effect of vane shape can be neglected when $Qu > 10^{-3}$.

5. EFFECT OF VANE SHAPE ON SPRAY HOMOGENITY

For estimation of optimal operating conditions of drying process, it is necessary to know the spray distribution. Only perfectly homogeneous spray with uniform droplets enables the optimal drying. In practice we try to approach as ideal homogenity of spray as possible. Therefore it is important to study all factors effecting spray homogenity. Homogenity of spray is here expressed by dispersion factor d_q defined as follows (7):

$$d_q = \frac{d_{95} - d_5}{d_S} \qquad (6)$$

where d_{95} ... droplet diameter at the 95% line

d_5 ... droplet diameter at the 5% line

The suitability of factor d_q for heigh rotation speed was also proved (7). Experimental results were plotted in the log-normal distribution which enables to read all data for evaluation d_q. Fig. 5 shows such distribution for glycerine at revolutions 21 000 and 25 000 RPM.

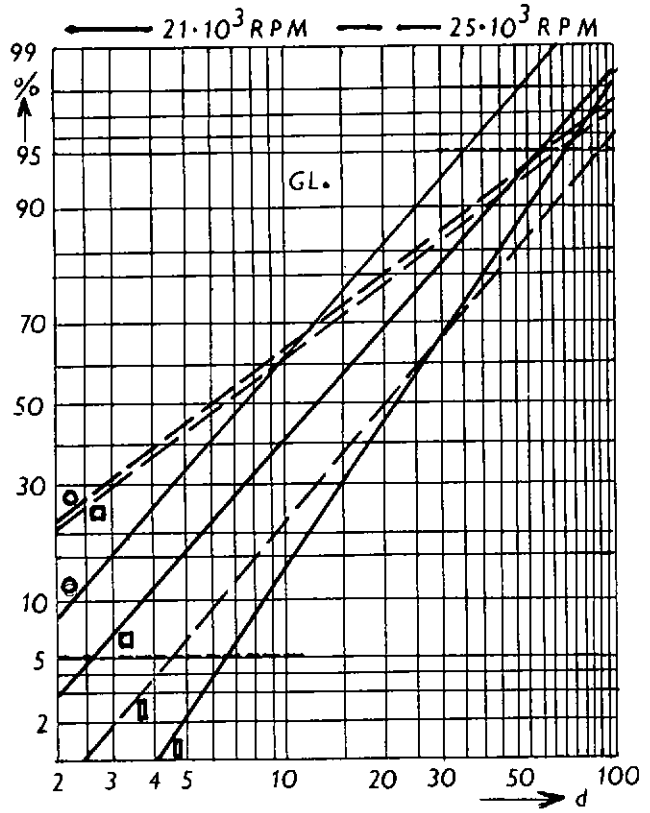

Figure 5

In table 4 are summarized the resulting dispersion factors for different vane shapes. Sauter mean diameter is written in table 3. Homogenity of spray increases with the decreasing value of dispersion factor. The best results for glycerine are shown by the circular flow channel and the worst are given by the rectangular one. Similar conclusion was also drawn for water, while CMC demonstrates different behaviour. Its results are plotted in fig. 6 and values of dispersion factor are shown in table 5.

Table 4

N	shape	d_{95}	d_5	d_q	d_q average
$21 \cdot 10^3$	▯	90	4,5	1,11	▯ 1,03
	□	68	0,3	0,9	
	○	63	0,27	0,79	□ 0,86
$25 \cdot 10^3$	▯	73	7	0,96	
	□	60	2,75	0,83	○ 0,65
	○	36	1,65	0,52	
		glycerine			

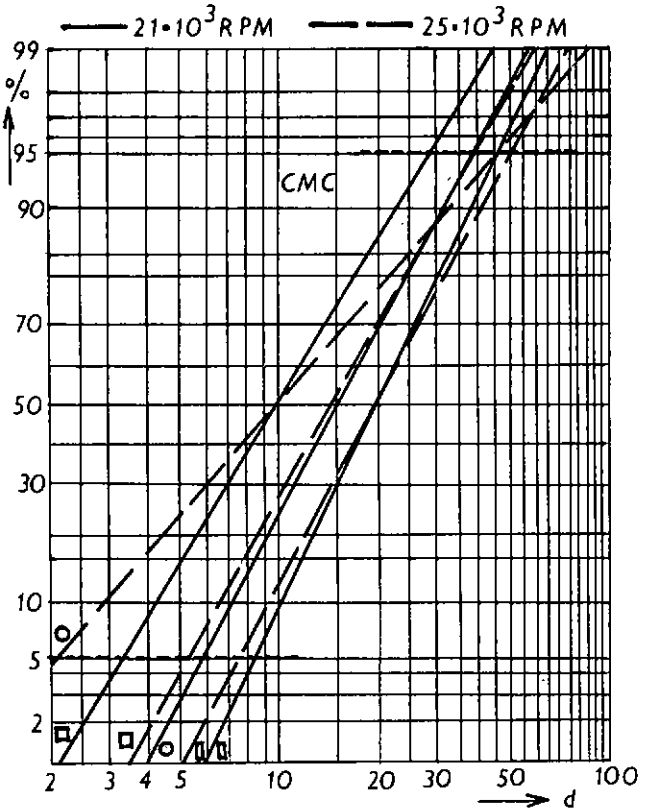

Figure 6

The best homogenity is reached by the square vane and the worst by the circular one. Similar experimental results were obtained for 2 % CMC.

Probable and possible cause of this phenomenon is again the pseudoplastic structure of CMC. Satisfactory answer can be obtained only by further investigation of non-Newtonian fluids flowing through the vanes of wheel atomizer. From the point of view of spray homogenity the shape of vanes is not negligible, more-

over it is possible to improve the homogenity of spray in unchanged operating conditions by more suitable vane geometry.

Table 5

N	shape	d_{95}	d_5	d_q	d_q average
$21 \cdot 10^3$	▯	50	7,2	0,95	▯ 0,92
	□	38	5,2	0,84	
	○	45	2,15	1,1	□ 0,85
$25 \cdot 10^3$	▯	45	8,3	0,9	
	□	29	3,3	0,86	○ 1,1
	○	38	5,6	1,1	
		CMC			

6. CONCLUSION

The presented results can be discussed from various points of view.

a) Rheological behaviour of liquid by atomization.

The apparent viscosity can be used instead of rheological parameter in determined velocity range for aproximate prediction of droplet size. Considering homogenity of spray it is not possible to neglect pseudoplastic character of fluid, because the results for newtonian and non-Newtonian fluids differ.

b) Droplet size prediction for different revolutions.

Herring and Marshall relation seems to be very suitable for low viscosity even in the range of high revolutions. The discrepancy increases with increasing Qu (μ resp.) so that the validity of this equation for high Qu or μ hasn't been proved.

c) Effect of vane shape on droplet size.

The form of vane cross section is important at low Qu or μ and can be neglected for Qu $> 10^{-3}$ ($\mu > 150.10^{-3}$ Pas resp.).

d) Homogenity of spray.

The discrepancy between newtonian and non-Newtonian liquids in different vanes is evident here. It is possible to use this fact and improve homogenity of sprays which have high value of Qu (or μ). For such spray, the effect of vane shape on droplet size is negligible so that the most convenient cross section for homogenity can be used. The influence of vane cross section becomes unimportant for low viscosity fluids. Although these conclusions are valid only within the range of experimental conditions, they give us some information about centrifugal atomization. These conclusions can be proved only by further investigation.

REFERENCES

1. Masters, K., Spray drying, John Willey Sons, N.Y., 1976
2. Marshall, W.R., Chem.Eng.Progress. Mon.Ser. No 2, Vol. 50, 1954
3. Filková,I., Developments in Drying, Science Press, Princeton, 1979
4. May, K.R., J.Sci.Instr. 27, 128,1950
5. Weberschinke,J., Research Report, Czech Technical University, Praha, 1979
6. Timkó,J., Doctorate Dissertation, Budapest, 1974
7. Masters,K., Doctorate Dissertation, University of Birmingham, 1964.

THE KINETIC BEHAVIOR OF SUBBITUMINOUS COAL DRYING; EFFECTS OF CONFINING PRESSURE

Lee F. Brown[1*]
Bryan A. Kashiwa[1]
Nicholas E. Vanderborgh[1]
Richard C. Corlett[2]

1. Basic and Applied Geosciences Division
Los Alamos Scientific Laboratory, Los Alamos, NM 87545

2. Department of Mechanical Engineering
University of Washington, Seattle, WA 98195

ABSTRACT

A model is developed which explains drying behavior of a subbituminous coal. This model, a variation of the moving-boundary approach, has the vapor-liquid interface in the macroprores receding from the exterior surface of the coal as drying progresses. On the liquid side of the interface, liquid water exists in all three pore systems -- macropores, transitional pores, and micropores. On the vapor side of the interface, in the transitional and micropore systems branching off the macropores, the moisture essentially is in equilibrium with the water vapor in the macropore system. Water diffuses from the liquid interface in the macropores through these pores to the exterior surface of the coal.

Experiments with a Washington State subbituminous coal are described which test this model. The predictions of the model match the behavior of experimental drying curves. The effective diffusivities obtained were within the range expected for the constricted pore systems which coal possesses. Higher initial stresses apparently decrease the total porosity and increase the severity of pore constrictions. Disparities between model prediction and experimental behavior, which occurred at a late drying time, result from the assumed water adsorption isotherm.

NOMENCLATURE

A_x	Cross-sectional area across which vapor is diffusing, cm^2
a	Parameter in equilibrium relationship between water in transitional-micropore system and water vapor in macropore system, dimensionless
b	Parameter in equilibrium relationship between water in transitional-micropore system and water vapor in macropore system, $cm^3/gmole$
C	Concentration of water in coal, gmole/(cm^3 of total porous solid)
c	Dimensionless concentration, C/C_o
D	Diffusion coefficient of water vapor in air within a pore, cm^2/s
L	Distance between exterior surface and vapor-liquid interface within porous solid, cm
M	Mass of water within porous solid, g
R	Distance between exterior surface of pore system and centerline of pore system, cm
t	Time, s
y	Distance from exterior surface of transitional-micropore system, cm
z	Distance from exterior surface of macropore system, cm
ε	Void fraction or porosity, dimensionless
ζ	Dimensionless distance in macropore system, z/R_a
ρ	Density, g/cm^3 or $gmole/cm^3$
σ	Compressive stress
τ	Tortuosity factor, dimensionless; also dimensionless time, $D_{ea}t/R_a^2$
ξ	Dimensionless distance in transitional-macropore system, y/R_t

Subscripts

AW	Bulk value in air-water binary system
a	Referring to macropore system
e	Effective value when nonidealities of porous structure are considered
f	Referring to amount filled with water
i	Referring to transitional-micropore system
K	Referring to Knudsen flow or diffusion
M	Denotes a molar quantity
o	Denotes initial value or value at vapor pressure of water
t	Denotes total amount

* Present address: Department of Chemical Engineering, University of CO, Boulder, CO 80309

INTRODUCTION

This work analyzes experimental data on the removal of water from a Washington subbituminous coal (1). Effects of compressive stress on the moisture removal were also investigated in that study, and are analyzed here as well. This investigation was part of the program studying in situ conversion of coal. In underground coal conversion, water motion, phase transformations and water effects on the physical properties of geomaterials create problems which have been previously stressed as important factors in the conversion process (2-6).

Three somewhat arbitrary forms of water in coal will be considered. First water is trapped in the fissures and faults of a coal seam and retained by small capillary forces. This water can be pumped from process wells through extant fracture systems and is termed "excess water." Excess water exhibits normal thermodynamic properties of free water. More strongly held is the second form, "adsorbed water," located at or near the surfaces of the intrinsic porous structure, and held by dispersion forces. Adsorbed water has thermodynamic properties different from those of free water due to the forces exerted by the surfaces in the small pores. It has been suggested that in openings less than 100 nm, water is adsorbed through this mechanism (7). The most tightly bound form of water is the third form, "chemisorbed water," associated with the chemical structure of the coal and bonded through valence forces. Ode (8) describes these forms of water in coal in more detail. Primarily, the present study treats the removal of adsorbed water from coal.

EXPERIMENTAL PROGRAM

Methodology

The basis of the laboratory investigations was the simultaneous measurement of the drying rate and stress level on a cylindrical slab of coal subjected to a sudden change in ambient moisture content, from saturation to zero humidity. By using an instrumented clamp, initial stress was applied radially and computed from strain measurements. Specimens were cylindrical discs of coal about seven centimeters in diameter and one centimeter in thickness. The mating surface between the coal and the clamp was sealed to prevent radial transport of moisture and allow one-dimensional analysis. The drying rate was determined gravimetrically.

The apparatus is shown schematically in Fig. 1. This figure shows a specimen, confined in a clamp equipped with two strain gages, suspended from a balance by the gage lead wires. The specimen was housed in a humidity chamber controlled by an air conditioning system capable of passing saturated air, dry air or any mixture of the two through the thermostated chamber. The volume capacity of the system was such that the atmosphere in the chamber was changed 2.4 times per minute. The balance had a capacity of 160 g

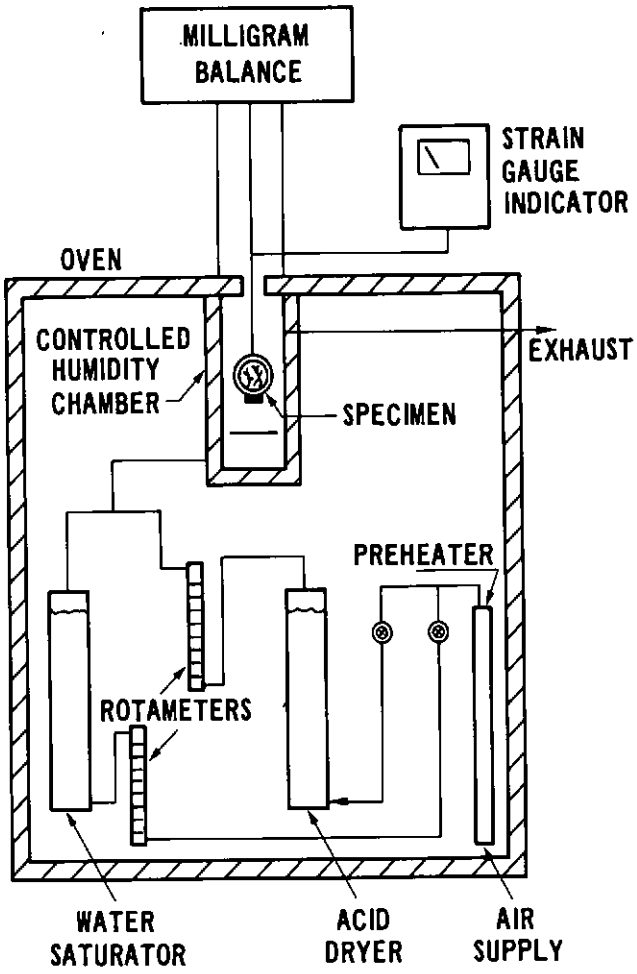

Figure 1. Schematic Diagram of Experimental Apparatus.

and a sensitivity of ± 1 mg. Coal specimens were on the order of 45 g and had a total moisture content of about 5 g. Total time for most runs was more than 8 hours. Time and weight readings gave adequate resolution of the drying rate curve. Inlet and outlet air temperatures were measured.

Sample Preparation Procedure

The coal was removed from the Landsberg seam near Black Diamond, Washington and supplied by the Palmer Coking Company. The proximate analysis for these samples was: As Received Moisture, 10%; Ash, 13%; Fixed Carbon, 41% and Volatile Matter, 36%. Coal was stored immersed in water from mine-mouth until cores were cut. The cores and specimens were then reimmersed in water and kept until testing began.

Specimens were prepared by cutting cores from blocks of coal with a water-cooled, diamond bit core drill. The cores were cut to a rough thickness dimension with a tungsten carbide tipped band saw blade under a water wash. The specimens were then sanded to an accurate thickness dimension on a platen belt sander while continuously wetted for cooling.

Test Procedure and Results

Prepared specimens were stored in a sealed chamber at room temperature over a saturated solution of potassium sulfate until use. They were monitored to insure that they reached an equilibrium weight. For testing, a specimen was placed in the clamp and brought to a given level of stress. This assembly was placed in the humidity chamber and brought to the test temperature with saturated air flowing through the chamber until a constant weight was observed.

At the start of a run, flowing air was changed from saturated to dry and the weight, strain on the clamp and temperature of the air leaving the humidity chamber were monitored. Typical raw data are shown in Fig. 2.

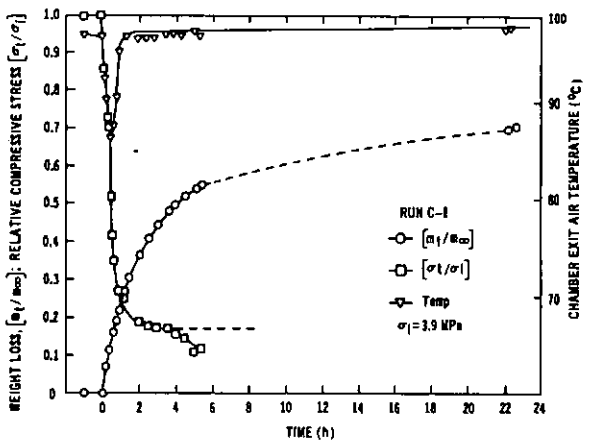

Figure 2. Relative Weight Loss, Relative Compressive Stress, and Temperature During Typical Experimental Run. Run C-1--Temperature, 371K; Initial Stress, 3.9 MPa; Initial Moisture Content, 7.8%.

After scouting experiments with specimens A and B, specimen C was dried to a significant extent four times at different levels of stress and rewetted each time. The specimen was then removed from the system and placed in a vacuum desiccator over concentrated sulfuric acid for complete drying and determination of total moisture in the coal. The data from each of the partial drying runs are presented later, for comparison with the mathematical model presented next.

During one of the scouting runs, the flow rate of dry air past the specimen was increased by a factor of three, and no change in drying rate was observed. As a result, boundary-layer resistance to mass transfer at the external surface of the coal was deemed negligible.

MODELING THE SYSTEM

The Moving-Boundary Model

Kisakurek and Gegizlioglu (9) suggest that three approaches to the development of models for explaining drying behavior have gained credibility. These three are diffusion theory, capillary theory, and the moving-boundary approach. Preliminary results from applying diffusion theory to our data have been reported (6). Significant differences were noted between the behavior of the data and the simple constant-diffusivity solution. This solution did not show any induction period before the constant-drying-rate portion of the curve, although there was such an induction period in the experimental results. Moreover, the concave-downwards break in the slope occurred much later theoretically than found experimentally. Essentially, the data show a short constant-drying-rate period between the induction portion and the concave-downwards break in the drying curve. When a constant-drying-rate period is observed, this rate normally is measured initially and the same rate persists for a significant period of time. For example, van Bakel and Heertjes (10) show a constant-drying-rate period which starts at $t = 0$ and covers 80% of the water removal from a porous material.

Van Bakel and Heertjes implied that if a period of constant-drying-rate is not observed, and if the external boundary layer does not affect the drying, then the moving-boundary approach is the only valid one. Apparently boundary-layer effects were not present in our drying experiments. In addition, the constancy in the rate of drying in our data did not show the usual characteristics of this phenomenon. Thus it appears that the moving-boundary approach was suggested for developing a model to explain these coal drying results.

Coal is thought to have transitional and micropore systems branching off the larger pore, or macropore, system (11). Applying the moving-boundary approach to this pore structure requires that the liquid is in the central regions of all the pore systems, with equal amounts on both sides of the systems' centerlines. The regions on the vapor sides of the pore systems' interfaces contain only water vapor and air, and during drying these interfaces recede from the exterior surface of the particular pore system. This model is illustrated in Fig. 3.

At first sight, it would appear that moving boundaries exist in all three pore systems, and equations are needed for describing the behavior of the water in each pore type. Fortunately, this complexity is not required. Scaling arguments show that, for the coal studied, the water within the transitional and micropore systems is in equilibrium with the water in the macropore system. These arguments are presented in the Appendix. As a result, only the behavior of the water vapor in the macropore system needs to be described, and the amounts of the moisture in the transitional and micropore systems follow. Thus a single equation describing all three pore

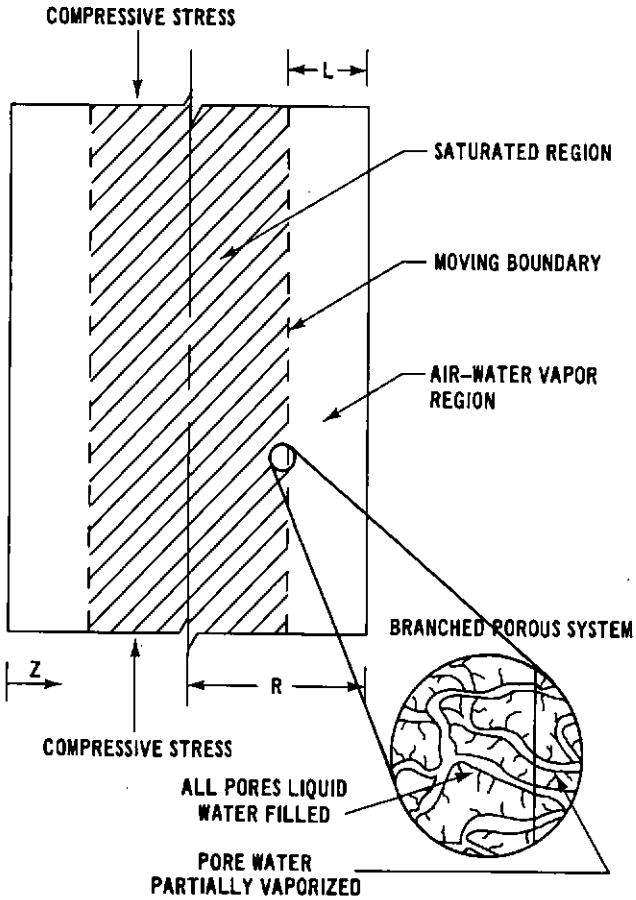

Figure 3. Physical Model of Wet Coal as it is Drying.

systems simultaneously can be derived. This equation, with its associated boundary conditions, is the thrust for the proposed moving-boundary description of dewatering in coal.

Assuming equilibrium between the water in the transitional and micropore systems and the vapor in the macropore system, and assuming diffusion for the transport of water vapor through the macropore system, a material balance within the region $0 > z > L$ yields:

$$\frac{\partial C_a}{\partial t} + \frac{\partial C_i}{\partial t} = D_{ea} \frac{\partial^2 C_a}{\partial z^2} \qquad 0 < z < L \qquad (1)$$

The initial condition for the macropore vapor concentration in our system is:

$$C_a = C_o \quad @ \quad 0 < z < L \quad \text{and} \quad t = 0 \qquad (2)$$

Since dry air was blown across the exterior surface of the coal, the boundary condition at this surface is:

$$C_a = 0 \quad @ \quad z = 0 \quad \text{and} \quad t > 0 \qquad (3)$$

The other boundary is the moving one. As the vapor-liquid interface recedes, L increases. This progresses until $L = R_a$. As a result:

$$C_a = C_o \quad @ \quad z = L \quad \text{if} \quad L < R_a \qquad (4)$$

$$t > 0$$

$$\frac{\partial C_a}{\partial z} = 0 \quad @ \quad z = L \quad \text{if} \quad L = R_a \qquad (5)$$

The rate of change of L is calculated from the rate of evaporation of the liquid at the interface:

$$\frac{dL}{dt} = \frac{D_{ea}}{\epsilon_a \rho_M} \frac{\partial C_a}{\partial z} \Bigg|_{z=L} \qquad (6)$$

For the equilibrium relationship between the water in the transitional and microproes and the water vapor in the macropores, a two-parameter relationship similar to the Langmuir adsoprtion isotherm was followed:

$$C_i = aC_a/(1 + bC_a) \qquad (7)$$

It was assumed that complete filling of the transitional and micropore systems by liquid water occurred at $C_a = C_o$. The form approximates the behavior of water adsorbed and condensed in coal described by Mahajan and Walker (12).

Substituting the equation for the adsorption isotherm into the second term of the LHS of Eq. (1) and carrying out the required differentiation yields:

$$\frac{\partial C_a}{\partial t} = D_{ea} \left[\frac{1}{1 + \frac{1}{(1+bC_a)^2}} \right] \frac{\partial^2 C_a}{\partial z^2} \qquad 0 < z < L \quad (8)$$

Equation (8) and the equations concerning the initial and boundary conditions, (2)-(6), make up the mathematical description of the moving-boundary diffusion model for this experimental system.

In addition to assuming the smaller pores were filled at $C_a = C_o$, two other assumptions were made to estimate values of particular parameters in the model, an average radius of the macropore system was needed. Pore structures of coal presented by Gan et al. (13) indicate that 70 nm is an average pore radius for the macropore system. This value was adopted.

A third assumption concerned the total porosity of the coal at zero percent water saturation. Moisture analysis indicated that the total void fraction was at least 0.14. The accuracy of coal moisture analyses is questionable. Most indications suggest that the amount of moisture measured is under-reported (8). If only 80% of the water was found, then the total void fraction was 0.17. This latter value was used in calculating the effective concentration of vapor and liquid in the coal sample.

Under these experimental conditions, diffusion in the macropores is in the transition region between Knudsen flow and bulk diffusion. The diffusivity of the water vapor in air at these condtitionswas calculated using the relationship

proposed by Pollard and Present (14):

$$\frac{1}{D} = \frac{1}{D_K} + \frac{1}{D_{AW}} \qquad (9)$$

The value of D_K was calculated from the formula for Knudsen flow as given by Present (15). The experimental value of D_{AW} reported by Reid et al. (16) was used, corrected for differences in temperature. [The bulk diffusivity is normally proportional to the absolute temperature raised to the 1.75 power (16).]

Adjustable Parameters and Their Evaluation

As with most models of physical processes, some parameters must be adjusted to give an optimal fit to experimental data. In this analysis, there are three such parameters. The first is the tortuosity factor τ:

$$D_{ea} = D/\tau_a \qquad (10)$$

The second is the fraction of the total porosity which is occupied by the macropores, ϵ_a/ϵ_t. The third is used to calculate the terms a and b in the equilibrium relationship between the water in the transitional and micropores and the vapor in the macropores. The required parameter is the fraction of the transitional and micropores which were filled when the macropore concentration was some arbitrary fraction of saturation. The fraction we selected was one-tenth, and so the parameter was ϵ_{if}/ϵ_i @ 0.1 C_o.

The optimization technique utilized a series of consecutive one-dimensional searches. Values for both the macropore void fraction and the fraction of the smaller pore systems filled at $0.1C_o$ were chosen, the macropore tortuosity factor was varied and the system of equations was solved for every value of the tortuosity factor until an optimum fit was obtained. Using the optimum value of the tortuosity factor, the macropore void fraction was varied until the optimum fit was obtained, then the fraction of the smaller system filled was varied and the optimum value obtained. The entire process was then repeated. Since the three adjustable parameters had essentially independent effects upon the behavior of the data, as pointed out below, relatively few solutions of the system of equations actually were required.

In doing this, Eq. (8) was solved using the simple explicit technique described by Ames (17). The mesh size was deemed sufficiently small for the desired accuracy when decreasing the Δz value by two and the Δt value by four resulted in a maximum change less than 0.005 in the calculated fractional amount desorbed at any point. To check the accuracy of the numerical evaluation procedure, the equation was linearized and the calculated solution compared with the analytical solution presented by one of the authors (1). There was no detectable difference at small mesh sizes.

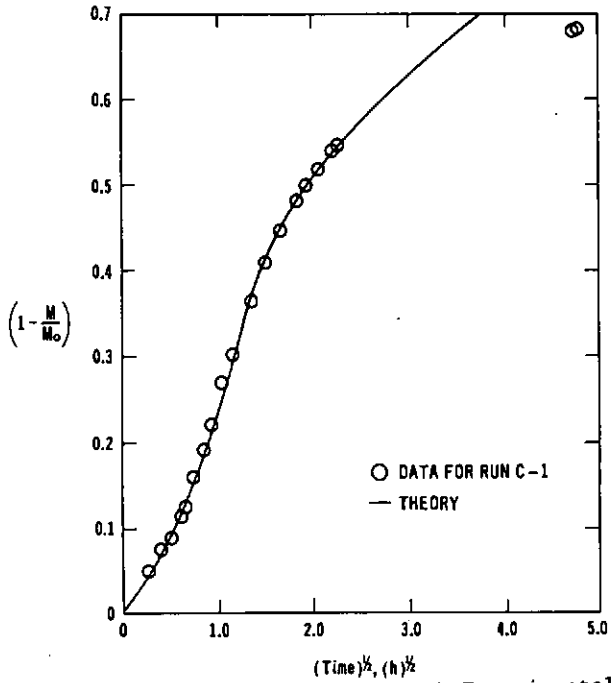

Figure 4. Agreement of Theory with Experimental Behavior for Run C-1. Temperature, 371K; Initial Stress, 3.9 MPa, Initial moisture Content, 7.8%.

In Fig. 4 are plotted the predictions of the model and the behavior of the experimental data for the run carried out at 371 K and at an initial compressive stress of 3.9 MPa. The abscissa is $(\text{time})^{\frac{1}{2}}$ chosen to accentuate the early part of the run where the solution is most sensitive to values of the three adjustable parameters. The amount of water desorbed from the coal are forecast by this model to a high degree of precision over the first six hours of the run.

At the twenty-two hour point, there is considerable disagreement between predictions and data. This may result from the simple form of the adsorption isotherm, as will be discussed below.

Parameter Sensitivity

It was mentioned above that each of the three adjustable parameters had quite different effects upon the solution. Changing the tortuosity factor did not influence the shape of the solution, but varied the time at which a particular level of drying was reached. This result occurred in a linear fashion. A change in the third significant figure of the tortuosity factor caused a difference in the solution which was just detectable graphically.

Changing the macropore fraction, on the other hand, changed both the slope of the straight-line portion of the solution and also the point at which the solution curved in a concave-downwards direction. With this model, it was not possible to change the slope independently from the point at which it curved in the latter part of the run. A change in the third significant figure of the macropore fraction made an easily detectable change in the equation solution.

Changing the fraction of the smaller pore systems filled at one-tenth saturation changed only

the slope of the solution when the slope was decreasing following the constant-rate period. Besides requiring a small change in the tortuosity factor to give a good fit to the data, varying this parameter did not otherwise change the form of the solution. Thus the three parameters had essentially independent effects upon the solution. This immensely simplified the parameter optimization. A change in the second significant figure in this last parameter detectably changed the solution.

Values of the Adjustable Parameters

This simple model assumes more credibility if values of the adjustable rameters suggested by the optimization procedure must lie within sensible (physically-expected) ranges. In the match between the model and the run at 371 K and 3.9 MPa (Run C-1), the values of the adjustable parameters are quite reasonable. The macropore tortuosity factor is 10. Although typical tortuosity factors for porous catalysts seem to lie between 1.5 and 7 (18,19), tortuosity factors as high as 30 have been observed in catalysts with constricted pores (18, 20). Constricted pores are postulated to be present in coals (11), so this tortuosity factor of 10 is expected. The macropore fraction of the total porosity is 0.51, well within the range which would be expected from the descriptions of coal pore structure (13). For the adsorption isotherm, it was assumed that 80% of the transitional and macropores were filled when the vapor in the macropores was one-tenth of saturation.

Comparisons of the experimental performances with those predicted theoretically for three runs at different temperatures and initial compressive stresses are presented in Fig. 5. The agreement is excellent.

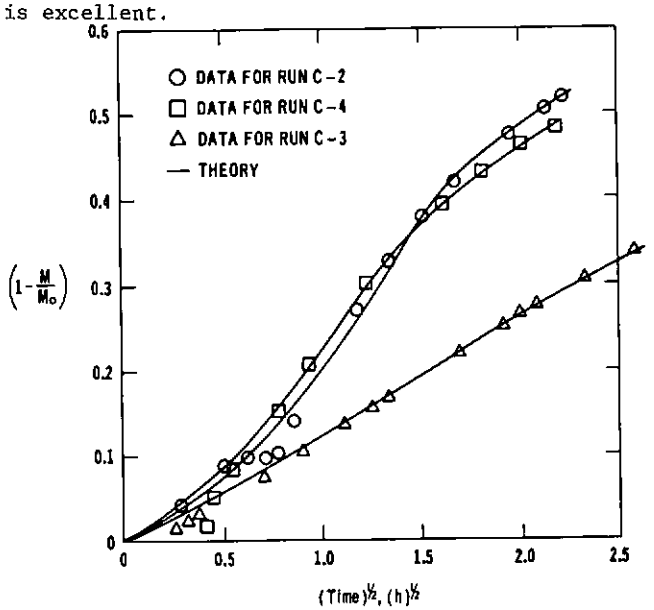

Figure 5. Agreement of Theory with Experimental Behavior for Three Runs. O: Run C-2--Temperature, 369K; Initial Stress, 4.5 MPa; Initial Moisture Content, 8.6% Δ: Run C-3--Temperature 341 K; Initial Stress, 1.4 MPa; Initial Moisture Content, 9.1% □: Run C-4--Temperature, 371K; Initial Stress, 0.12 MPa; Initial Moisture Content, 8.6%.

A second goal of this investigation was to study the effect of confining stress on the dewatering behavior. The effect of initial stress on the values of the adjustable parameters obtained for the last three runs is shown in Table 1. While all three adjustable parameters remain within a reasonable range, they exhibit significant and consistent changes when the confining stress is varied. The tortuosity factor, the macropore fraction of the pore system, and the fraction of the smaller pores filled at one-tenth saturation all increase as the initial confining stress increases.

DISCUSSION

Physical Realism of Model

Several factors attest to the physical realism of the model presented here. The ability to rationalize the model physically is the first of these. This moving boundary does appear to be physically reasonable. The second is the ability of the model to predict quantitatively the behavior of the experimental system. The experimental data are matched well. In addition, the various adjustable parameters have different and independent effects upon the solution. The agreement is not an empirical result with a large number of adjustable parameters. Still a third set of the model results from the sensible values of the adjustable parameters resulting from the optimization procedure were all within physically-expected ranges. The probability of all these happening by chance is regarded as low. Thus, having a physically reasonable model which predicts the behavior of the experimental data well and whose adjustable parameters are within physically expected ranges gives support to the validity of this model.

Values of the Adjustable Parameters

Table 1 shows that an increase in the initial stress within the sample by a factor of three changed the tortuosity factor by about 40%. As might be predicted, the lower the initial stress, the lower the tortuosity factor and, as a result, the higher the effective diffusivity. This can be ascribed to either or both of two causes. An increase in stress might decrease the porosity of the sample, and in our model this would be reflected by an apparent decrease in the effective diffusivity. Or, the shape of the pores within the coal could change with stress, and pore constrictions could become more severe with increasing stress.

Changing the macropore fraction, $\varepsilon_a/\varepsilon_t$, only slightly has a pronounced effect on the solution to the model's equation, as discussed earlier. The reason why the change in a macropore fraction resulted in such larger differences in the solution was that varying this parameter made a marked change in the initial distance between the interface and the exterior surface of the macropore system, L_o. Scouting runs to identify the sensitivity of the solution to various factors in the equations showed that a very small change in L_o made a detectable change in solution behavior. Thus the apparent changes observed in the macropore fractions with initial stress cannot be interpreted literally. Rather, these changes

Table 1
EFFECT OF INITIAL STRESS WITHIN COAL ON PORE STRUCTURE PARAMETERS

Run No.	T, K	σ_o, MPa	τ	$\varepsilon_a/\varepsilon_t$	$\varepsilon_{if}/\varepsilon_i$ @ $0.1C_o$
C-3	341	1.4	7.3	0.37	0.60
C-4	371	3.5	9.6	0.45	0.75
C-2	369	4.5	10.4	0.48	0.80

should be regarded as evidence of changing the value of L_o for a given quantity of water in the coal. Although a change in macropore fraction would cause this, a change in total porosity would have had a similar result.

In Table 1, data show that an increase in initial stress within the coal sample by a factor of three changed the apparent macropore void fraction by about 30%. This is close to the percentage change in tortuosity factor that resulted from the same stress alteration. Perhaps both of these effects were caused by a change in total porosity with increasing stress. Permeability measurements at different levels of internal stress in coal have been interpreted in a similar fashion (6).

This need not be the only answer, however. The changes in the adsorption isotherms show that the water is held more tightly in the smaller pore systems when the internal stress is higher. This suggests that the pores, especially the micropores, are more constricted at the higher internal stresses, creating a tighter molecular-sieve adsorbent. So, while the porosity is almost unquestionably decreasing with an increasing level of stress, some changes in the shapes of the pores also seem to be taking place.

Larger values were needed for the fraction of the smaller pores filled at one-tenth macropore saturation than would be indicated by the adsorption isotherms of Majahan and Walker (12). The work of these authors indicated that values of 30-50% would be reasonable, instead of the observed range of 60-80T. The higher required values compensated for the tightly-held water. At values of C/C_o below 0.05, the Langmuir form predicts significantly less water will be adsorbed than was observed by Mahajan and Walker. A higher value is needed for the amount adsorbed at $0.1C_o$ to give a better match between the observed isotherm and the simple form at low values of the relative pressure.

Early Periods of Runs

The model had two minor deficiencies during the initial periods of an experimental run. The model did not consider the probable presence of liquid separate from the centered bulk liquid within the moving boundaries. Secondly, it did not consider the temperature drop observed initially. These two factors would have opposite effects on the ability of the model to match the data. This may account in part for the successful agreement between the model and the data during the early periods of the runs in spite of these deficiencies, Minor deviations in either direction can easily be accounted for by these factors.

The drops in temperature observed in the early periods of the runs suggest that initially the drying is affected by heat transfer to the evaporation site. Nevertheless, after about 20% of the water is removed from the coal, the situation reverts to a mass-transfer-limited diffusion problem.

Late Period of Run C-1

Only Run C-1 was extended past eight hours. The model predicts higher drying rates at long times than observed. The model predicted that 68% of the water would be removed at 16 hours, and it actually required 22 hours to reach this point. We believe that this difference between prediction and experiment at long times results from the nature of the equilibrium relationship between the liquid and vapor in the transitional and micropores and the vapor in the macropores that was selected. A simple two-parameter relationship was employed, while isotherms of water on coal are complex. For example, it is routinely observed during desorption that a significant amount of water remains in coal until regorous drying conditions, such as heating at 110°C and 10^{-4} Pa (10^{-6}torr) are imposed (12). It is often observed in adsorption measurements using carbonaceous adsorbents that there is initially a rapid uptake of adsorbate, followed by a very slow approach to equilibrium (21). An explanation for both these phenomena is that a significant portion of the adsorbate is very tightly bound. This may be typical of a molecular-sieve structure. This portion of the adsorbate is not described in this adsorption isotherm, nor can it be in any simple one.

Thus it appears that a more complex adsorption isotherm is needed to predict the behavior of Run C-1 at the longer times. Implementation of this concept will have to await further work using measured adsorption isotherms.

The Dewatering of Coal

These results lead to new understandings of coal dewatering that may have significant implications during underground processing or other coal utilization processes where the effective particle size is large enough to preclude rapid heating. Although the extant fissure systems may be pumped dry with subsurface operations or water in such fissure systems may be removed by forced flow from pressurized gases (assuming that the fracture system intersects a well bore), such dewatering will only remove a fraction of the total coal moisture. Following this, water removal is mainly a diffusive process, with diffusion through the macropores the principal limiting process. The water in the transitional and micropores remains in essential equilibrium with the water in the macropores. This suggests that isothermal dewatering may be an extremely slow process.

For drying coal in any reasonable amount of time, heating is essential, or some other technique must be used to increase water activity. At elevated temperatures, coal drying is affected by heat transfer rates during the removal of the first portion of the water, but the majority of the moisture removal process remains a diffusion-limited process. A significant portion of the water, between 5% and 10% of the total moisture content, is strongly bound within the micropore system and will probably not be removed until high temperatures, i.e., combustion, are reached.

Since it has been well demonstrated that appreciable permeability results from coal drying, at least with shrinking (low rank) coals, it is apparent that in situ processing might be facilitated by preheating the target processing area. Such preheating may be the only reliable technique to generate a zone with appropriate reaction parameters.

REFERENCES

1. Kashiwa, B. A., M.S. Thesis, University of Washington, Seattle, WA, 1978.
2. Underground Coal Gasification Program, Department of Energy Report ERDA 77-51, 26, (1977).
3. Vanderborgh, N. E., Elliott, G. R. B., and Cort, G. E., 4th Annual Underground Coal Conversion Symposium, Steamboat Springs, CO, July 17-20, 1978.
4. Westmoreland, P. R., and Forrester, R. C., III, Am. Chem. Soc., Div. Fuel Chem., Prepr., 22 (1) 93 (1977).
5. Dossey, J. L., SAND 76-0380, Sandia Laboratories, Albuquerque, NM 87115, July, 1976.
6. Kashiwa, B. A., Corlett, R. C., Trujillo, P. E., Elliott, G. R. B., and Vanderborgh, N. E., 5th Annual Underground Coal Conversion Symposium, Alexandria, VA, June 18-21, 1979.
7. Luikov, A. V., "Heat and Mass Transfer in Capillary-Porous Bodies," p.220. Pergamen Press, Oxford, 1966.
8. Ode, W. H., Coal Analysis and Mineral Matter, in The Chemistry of Coal Utilization, Supplementary Volume, (H. H. Lowry, ed.), pp 202-7, Wiley, New York 1963.
9. Kisakürek, B., and Gebizlioglu, O., Proc. 1st Int. Symp. Drying, 59 (1978).
10. van Brakel, J., and Heertjes, P. M., Proc. 1st Intl. Symp. Drying, 70 (1978).
11. Mahajan, O. P., and Walker, P. L., Jr., USDOE Report FE-2030-TR-7 (1978).
12. Mahajan, O. P., and Walker, P. L., Jr., Fuel, 50, 308 (1971).
13. Gan, H., Nandi, S. P., and Walker, P. L., Jr., Fuel, 51,272 (1972).
14. Pollard, W. G., and Present, R. D., Phys. Rev., 73, 762 (1948).
15. Present, R. D., "Kinetic Theory of Gases," P. 60. McGraw-Hill, New York, 1958.
16. Reid, R. C., Prausnitz, J. M., and Sherwood, T. K., "Properties of Gases and Liquids," 3rd ed., pp 554, 557. McGraw-Hill, New York, 1976.
17. Ames, W. F., "Numerical Solution of Partial Differential Equations," 2nd ed. Academic Press, New York, 1977.
18. Brown, L. F., Haynes, H. W., Jr., and Manogue, W. H., J. Catal., 14, 220 (1969).
19. Satterfield, C. N., and Cadle, P. J., "Diffusion in Commercially Manufactured Catalyst Pellets," Ind. Eng. Chem. Process Des. Dev., 7, 256 (1967).
20. Haynes, H. W., Jr., and Brown, L. F., AIChE J., 17, 491 (1971).
21. Zogorski, J. S., Faust, S. D., and Haas, J. H., Jr., J. Colloid Interface Sci., 55, 329 (1976).
22. Walker, P. L., Jr., Austin, L. G., and Nandi, S. P., in "Chemistry and Physics of Carbon," vol. 2 (P. L. Walker, Jr., ed.), pp 257-371. Dekker, New York, 1966.

APPENDIX

The following is a demonstration that, for our system, water in the transitional and micropore systems is in equilibrium with the water vapor in the macropore system. Looking at water vapor diffusing through the macropore system, a mass balance on the water over a section of coal δz in length yields:

$$A_x \delta z \frac{\partial C_a}{\partial t} = \frac{\partial}{\partial z}\left(-D_{ea} A_x \frac{\partial C_a}{\partial z}\right) \delta z + \left(-D_{ei} \frac{\partial Ci}{\partial y}\right)_{y=0} \delta z \qquad \text{(A-1)}$$

in which A_x is the surface area of the micropore system per unit length. The following dimensionless parameters are defined:

$$c_a = C_a/C_o \qquad \text{(A-2)}$$

$$c_i = C_i/C_o \qquad \text{(A-3)}$$

$$\tau = D_{ea} t/R_a^2 \qquad \text{(A-4)}$$

$$\zeta = z/R_a \qquad \text{(A-5)}$$

$$\xi = y/R_i \qquad \text{(A-6)}$$

Dividing Eq. (A-1) through by A_x, cancelling ∂z, multiplying through by $R_a^2/D_{ea}C_o$, and expressing the result in terms of the dimensionless parameters defined above gives the following dimensionless equation:

$$\frac{\partial c_a}{\partial \tau} = \frac{\partial^2 c_a}{\partial \xi^2} - \frac{D_{ei}}{D_{ea}} \frac{1}{A_x} \frac{R_a^2}{R_i} \left(\frac{\partial c_i}{\partial \xi}\right)_{\xi=0} \qquad \text{(A-7)}$$

To evaluate the relative weights of the terms on the RHS of the equation, it is necessary to calculate an approximate value for the coefficient of the second term on the RHS. If the macropores have an average radius of about 70 nm, and the transitional pores a radius of about 7 nm, the factor D_{ei}/D_{ea} should approximate 1/5. (A calculation of this ratio for cylindrical pores with these radii, identical tortuosity factors, and 98°C gives a value of 0.233). A rough value for the other factors may be obtained by considering a very simple model of the porous material illustrated in Fig. A-1, in which the substance consists of cubic blocks separated by slit-shaped macropores. The blocks contain the transitional and micropores.

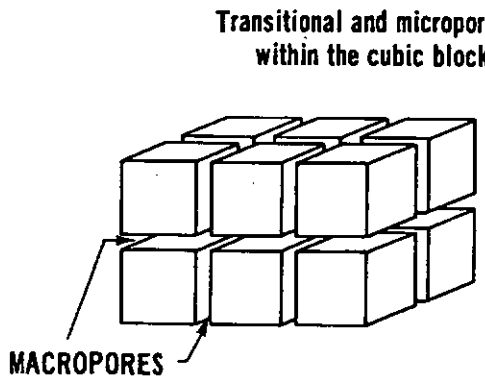

Figure 1-A. Pore-structure Model of the Porous Coal

Using this model, a total porosity of 0.17, a macropore fraction of the total voids equal to 0.51, and a slit width of 70 nm, the length of a side of one of the basic cubic blocks is easily calculated to be 7.4×10^{-5} cm. This means that R_i, which equals approximately V/S for particles of intractable geometry, is about equal to 9×10^{-6} cm. The fraction ∂/A_x is calculated to be 6.2×10^{4} cm^{-1} for this model. The dimensionless combination of parameters which is a premultiplier for the second term on the RHS thus has a value of about 2.5×10^{8}. Equation (A-7) then becomes:

$$\frac{\partial c_a}{\partial \tau} = \frac{\partial^2 c_a}{\partial \zeta} - (2.5 \times 10^{8}) \left.\frac{\partial c_i}{\partial \xi}\right|_{\xi = o} \qquad \text{(A-8)}$$

While the coefficient for the second term on the RHS may not be exactly 2.5×10^{8} for the coal we used, it is almost certainly near this order of magnitude since the porosity and pore dimensions used were those of our coal. This means that at any appreciable value of $(\partial c_i/\partial \xi)_{\xi=0}$ the second term on the RHS dominates the macropore material balance. Only when $(\partial c_i/\partial \xi)_{\xi=0}$ is almost equal to zero does the axial diffusion along the macropores affect the change in concentration at any point. Equilibrium exists when $(\partial c_i/\partial \xi)_{\xi=0}$ and thus approximate equilibrium is present when axial mass transfer affects the internal concentration, that is, when diffusion is effectively occurring within the macropore system.

Another way of looking at the scaled dimensionless equation is that diffusion from the transitional and micropore systems occurs so fast that equilibrium is established by the time any significant macropore diffusion occurs. Thus the assumption of equilibrium existing between the water in the transitional-macropore system and the water vapor in the macropore system is a very good one.

STUDIES ON LIGNITE DRYING

B. Kısakürek[1]
S. Yeşil[2]

1. McGill University, Quebec, Canada
2. Middle East Technical University, Turkey

ABSTRACT

The purpose of this study is to investigate the heat and mass transfer characteristics of the Turkish lignites in drying. The air velocity, humidity, and dry-bulb temperature are considered as the main parameters.

The drying model assumes that the movement of moisture in the solid body is by capillary motion, and that the major resistance to heat and mass transfer lies on the boundary layer at the solid surface.

The drying rate at the constant-rate period increases rapidly as the temperature and velocity of air increases. The rate of this increase slows down at high velocities. The corresponding heat and mass transfer coefficients are mainly affected by air velocity rather than air temperature. Increasing velocity increases the transfer coefficients. On the other hand, they decrease with concentration in the falling-rate period but the heat-to-mass ratio stays nearly as constant. The concentration profiles are represented by a single "generalized drying curve" in Figure 9 as: (C=exp(-E)), where E is dimensionless drying time in the falling-rate period.

NOMENCLATURE

A_H : heat transfer area, cm^2/g
A_M : mass transfer area, cm^2/g
C : moisture concentration, dimensionless
c : heat capacity of moist solid, cal/g.°C
E : drying time, dimensionless
F : drying time, dimensionless
G : heat-to-mass ratio, dimensionless
Gu : Gukhman number
H_R : relative humidity
L : length, cm
Le : Lewis number
m : Coefficient of dimensionless time, E
N_W : vapor flux at solid surface
Nu : Nusselt number
P_o : saturated vapor pressure at T_R, atm
P_R : partial pressure of vapor in dryer, atm
P_s : vapor pressure at the solid surface, atm
P_{BM}: log-mean pressure, atm
Pr : Prandtl number
q : heat transfer rate, $cal/cm^2.min$
Re : Reynolds number
T : temperature, °C
u : air velocity, m/min
w : wet weight of coal, g
W : moisture content of solid, g/g

Subscripts

a : air
c : critical point, convective
CRP: constant-rate period
DS : dry surface
e : experimental
o : initial, air
p : predicted by model
R : dry-bulb temperature
s : solid surface
w : water
WB : wet-bulb temperature

Greek Letters

α : heat transfer coefficient, $cal/cm^2.min.°C$
β : mass transfer coefficient, $g/cm^2.min.atm$
λ : latent heat of vaporization, cal/g
θ : drying time, min
ϕ : psychrometric ratio, dimensionless
ΔT : temperature difference, °C

INTRODUCTION

The drying of solids is an important operation in the field of of chemical engineering. There exists only a few processes which do not include this operation. Drying occurs when a wet solid is subjected to a hot air stream. Two fundamental and simultaneous processes occur during the course of drying; (i) heat is transferred to evaporate the solid moisture, and (ii) mass is transferred as a liquid or/and vapor moisture within the solid structure and as a vapor from the surface.

The relation between the heat and mass transfer mechanism during the course of drying can be expressed as

$$-\frac{dW}{d\theta} = \frac{\alpha_t A_H}{\lambda_s}(T_R - T_S) \quad (1)$$

where $dW/d\theta$ is drying rate, g.water evaporated/min-gdry solid; α_t is heat transfer coefficient, cal/cm^2-min-C and, (T_R-T_S) is the temperature driving force, ^oC.
A similar expression can also be written in terms of mass transfer as

$$-\frac{dW}{d\theta} = \beta_G A_M (P_S - P_R) \quad (2)$$

where β_G is mass transfer coefficient and (P_S-P_R) is the pressure driving force between the vapor pressure at the solid surface and the partial pressure in the dryer.

At the constant-rate period the surface temperature is equal to the wet-bulb temperature but it increases with a 'sigmoidal' profile in the falling-rate period. This shape is generally observed for coal drying experiments (1). The surface of the solid is initially very wet and generally a continuous film of water exists on the surface. This water is entirely unbound and it acts as if the solid were not present. The rate of drying under the given air conditions is independent of the solid and is essentially the same as the rate of evaporation from a free liquid surface. Hence, in the absence of heat transfer by radiation or conduction, the surface temperature is approximately that of the wet-bulb temperature.

In drying rate calculations the use of heat transfer coefficient is generally preferred because it is more reliable than the mass transfer coefficient. Small errors in the temperature measurement may have small negligible effect on heat transfer coefficient but can introduce relatively large errors in partial pressure calculations.

The most important mode of heat transfer for drying is that due to convection as the majority of dryers available in industry rely on convection of heat to and moisture away from the drying surface. The transfer coefficients depend on the geometry of the system, the gas velocity past the evaporating surface and the physical properties of the drying gas. Many correlations are available in the literature but only a few are presented here. Among these the followings are used frequently.

Luikov Correlation (2):

$$Nu = 0.086 Pr^{0.33} Re^{0.8} Gu^{0.2} \quad (3)$$

Lebedev Correlation (3):

$$Nu = c_1 Re^{0.5} (T_R/T_{WB})^2 N_W \quad (4)$$

where c_1 is a dimensional constant. Lebedev correlation is considered as the most useful one because it directly relates the constant drying rate value to Nusselt Number.

Care should always be exercised in using particular correlations to ensure their validity for a given problem. For general speaking, for many cases in drying, the transfer coefficient can be expressed as;

$$\alpha_c = c_2 u^m L^n \quad (5)$$

where c_2,m,n are constants and L is the characteristic dimension of the solid which is also used for determining the Reynolds number, Re.

In the falling-rate period the mass transfer area A_M decreases with moisture content. The rate of this decrease is proportional to drying rate and solid thickness. An experimental measurement of A_M is almost impossible for most cases, therefore, a theoretical approach is preferred for its calculation.

THEORY

General Description of the Model

Many solids can be considered as containing a very large number of capillaries extending in all directions. During the constant rate period these capillaries are full and the entire surface is covered with a film of water. As drying proceeds the water film evaporates and dry surfaces begin to appear. With the appearance of the first dry speck, moisture is drawn from the larger capillaries by the smaller ones and is carried to the surface. As the capillaries are drained out, more and more dry surface appears. If the length of these capillaries is large, which is the possible case for thick solids, it may be assumed that there will be a frictional resistance to the flow of liquid within the capillaries. For thin solids this resistance can be neglected.

The only important assumption made in this model is that the liquid moisture moves in the porous lignite by capillary motion and evaporation takes place at the solid surface. Referring to Figure 1, one may assume that the liquid water and air films coexist on the surface and hence a hypothetical film of thickness L_f offers an effective heat and mass transfer resistances.

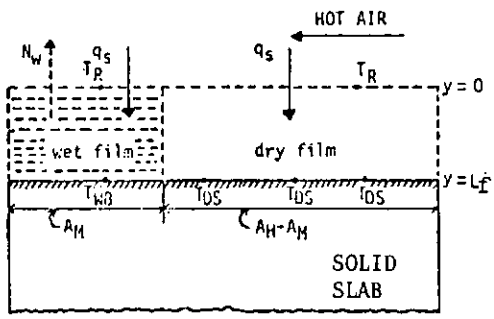

Figure 1. Drying Surface Model.

At any point in the film, an enthalpy balance can be written as,

$$-k_w\frac{dT}{dy}A_M - k_a\frac{dT}{dy}(A_H-A_M) + N_w A_M \lambda_{WB} + N_w A_M c_p (T-T_{WB}) = 0 \quad (6)$$

which states that all the energy required for vaporization is supplied from air through the two films by conduction. The first two terms on the left-hand side of the above equation represent conductive heat transfer, the third term represents the heat required to vaporize the liquid flow the surface and the last term is the heat carried by the diffusing molecules. When Eqn.(6) is integrated numerically a relation for A_M/A_H ratio can be obtained with the help of some simplifying assumptions of which their experimental justification may be questionable. On the other hand, if the wet spots are kept at the wet-bulb temperature, Eqn.(6) can be written as,

$$\bar{q}_s A_H = q^*_s A_M + q_s (A_H - A_M) \quad (7)$$

with,

$$\bar{q}_s = \bar{\alpha}_t (T_R - \bar{T}_s)$$

$$q^*_s = \alpha^*_t (T_R - T_{WB})$$

$$q_s = \alpha_t (T_R - T_{DS}).$$

$\bar{q}_s$, q^*_s, q_s are heat flux to the solid surface, to wet specks, and to dry spots, respectively.

Comparing Eqns.(2) and (7), one can obtain,

$$\beta_G A_M (P_{WB} - P_R) = \bar{q}_s A_H \quad (8)$$

and,

$$\bar{\alpha}_t = \alpha^*_t (A_M/A_H)\left(\frac{T_R - T_{WB}}{T_R - \bar{T}_s}\right) + \alpha_t (1 - A_M/A_H)\left(\frac{T_R - T_{DS}}{T_R - \bar{T}_s}\right). \quad (9)$$

If the total heat input is mainly utilized for evaporation, then Eqn.(9) reduces to

$$A_M/A_H = (T_R - \bar{T}_s)/(T_R - T_{WB}) \quad (10)$$

based on the assumption that $\alpha_t = \alpha^*_t$. The term on the right-hand side of the above equation is defined as 'dimensionless temperature ratio'. On the light of these equations the general drying rate expression takes the following form

$$-\frac{dW}{d\theta} = \frac{(P_{WB}-P_R)(T_R-T_s)}{(T_R-T_{WB})}\beta_G A_H \quad (11)$$

which checks very well with the experimental data of clay and lignite particles (4,5).

Change in Mass Transfer Area

The mass transfer area, A_M, decreases with moisture content in the falling-rate period. The rate of this decrease is proportional to drying rate and solid thickness. Hence, one may write,

$$A_M/A_H = (W_s/W_c)^n \quad (12)$$

where W is moisture content and n is a constant.

Now, consider a solid dried from one face only. Divide it into small imaginary cubes of unit length and consider one of them. At any time in the falling-rate period a certain amount of liquid moisture is kept in the capillaries of that cube. These capillaries are extending in all directions but the ones that extend in the other two directions are being emptied down to a certain level. Hence the system may be confined to those capillaries of size r_{cs}, where r_{cs} is the radius of a capillary which just brings moisture to the surface against gravity. With this simplification we can concentrate all the liquid moisture present in this single capillary into another hypothetical cube of length L and locate it at the corner of the cube of unit length. The volume- and area-ratio of these two cubes would yield,

$$W_s/W_c = L^3/1.0 \quad (13)$$

$$A_M/A_H = L^2/1.0 \quad (14)$$

so that,

$$A_M/A_H = (W_s/W_c)^{2/3} \quad (15)$$

Comparison of Eqns.(12) and (15) indicates n=2/3. No material would exactly fit the above model but it still can be assumed that most solids have regions where the surface area-to-volume ratio inside the solid in one region is greater than in the other region. The liquid moisture will migrate from regions of low ratio to the ones of high ratio.

Dimensionless Quantities

The following dimensionless quantities are used in this study:

$$C = W/W_c \quad (16)$$

$$G = (\beta_G P_o \lambda_{WB})/\alpha_t T_R \quad (17)$$

$$F = (\alpha_t A_H T_R \theta)/W_c \lambda_{WB} \quad (18)$$

$$E = (\alpha_t A_H \theta)(T_R - T_{WB})/W_c \lambda_{WB} \quad (19)$$

When these equations are substituted into the drying rate equations, one can obtain

$$- dC/dF = (T_R-T_S)/T_R \qquad (20)$$

$$- dC/dF = GC^{2/3}(P_S/P_O-H_R) \qquad (21)$$

where C is moisture concentration and F is normalized drying time in the falling-rate period. It can be assumed that the vapor pressure on the solid surface is related to the surface temperature by the following expression,

$$P_S = P_X \exp\left[-(18\lambda/RT_S)\left(\frac{T_X-T_S}{T_X}\right)\right] \qquad (22)$$

where P_X is a dummy variable for the surface vapor pressure. At room temperature, this equation reduces to,

$$\ln(P_S/P_O) = -(18\lambda/RT_S)\left(\frac{T_R-T_S}{T_R}\right) \qquad (23)$$

and then expanding the ln term would give,

$$\ln(P_S/P_O) = \ln b + (P_S/P_O-b)/b \qquad (24)$$

with the second and higher order terms being neglected. Eqn.(24) is exact for $b=P_S/P_O$. The vapor pressure on the surface changes as the moisture content decreses; but a small decrease in moisture content, there is a very small change in P_S. Hence, b may be taken as constant during each integration step. Combining Eqns.(23) and (24), one obtains the following expression which relates the surface vapor pressure to the surface temperature.

$$P_S/P_O = A-b\phi(T_R-T_S)/T_R \qquad (25)$$

where $A=b(1-\ln b)$ and $\phi=18\lambda/RT_S$.

Eliminating the $(T_R-T_S)/T_R$ term from the above equations, and then combining the resulting equation with Eqn.(25), the following differential equation is obtained.

$$(1+G\phi bC^{2/3})\frac{dC}{dF} = -G(A-H_R)C^{2/3} \qquad (26)$$

The integration yields,

$$F_2-F_1 = \frac{3(C_1^{1/3}-C_2^{1/3}) + G\phi b(C_1-C_2)}{G(A-H_R)} \qquad (27)$$

which is used in calculating the drying schedules of porous solids.

EXPERIMENTAL

Apparatus

The drying equipment used in this study consists of a blower, a power-controlled heater and a drying chamber. It is illustrated in Figure 2. The air flow rate is adjusted by a by-pass valve mounted on the steel pipe connecting the blower and the heater. The

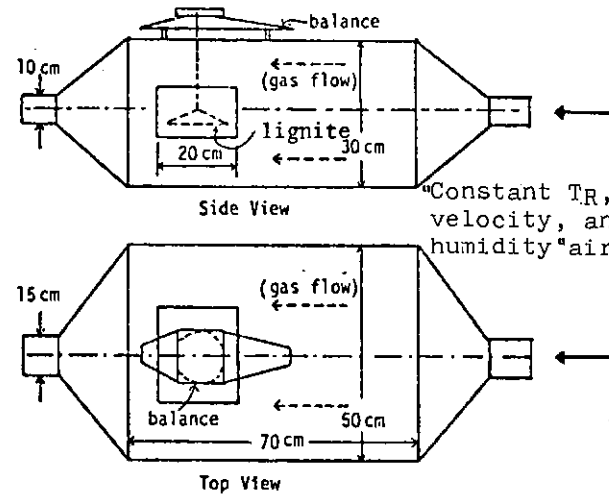

Figure 2. Drying Apparatus.

air heater contains eight resistances each consuming different amount of electric power. The air temperature is adjusted by adjusting the rheostat that controls the power in each individual heater. Hot air passes through the drying chamber. On the top of the chamber a continuous weighing system is mounted. This consists of a balance, an aluminum tray and a connector. The coal samples are placed on the tray and the weight of the coal is continuously recorded. All parts of the apparatus are insulated by asbestos and glass wool. The temperature measurements are made with Cu-constantan thermocouples. In some runs steam is injected to air stream leaving the blower to ensure desired humidity.

Procedure

The experiments are done at six different velocities. The humidity and dry-bulb temperature are varied in each set. The initial parameters are summarized in Table 1.

TABLE 1
EXPERIMENTAL PARAMETERS

Run Number	Air Velocity	Dry-Bulb Temperature	Wet-Bulb Temperature
1	0	40	26
2	"	55	28
3	"	70	29.5
4	"	85	31
5	"	100	33
6	"	115	33.5
7	50	50	26.5
8	"	70	29
9	"	85	31
10	"	110	34

Table 1, Continued.

Run Number	Air Velocity	Dry-Bulb Temperature	Wet-Bulb Temperature
11	"	135	37
12	"	160	40
13	100	40	24
14	"	70	29
15	"	90	31.5
16	"	115	33
17	"	135	34
18	160	40	25
19	"	60	28
20	"	85	31
21	"	115	34.5
22	"	135	37
23	230	45	26
24	"	70	29
25	"	85	31
26	"	115	34.5
27	"	135	37
28	300	40	23
29	"	65	29
30	"	90	31.5

Velocity=m/min.; Temperature=^{o}C.

Approximately 500-600 gram of wet coal with medium size is placed on the tray and hanged in the dryer. The hot air at steady-state conditions of velocity, dry-bulb temperature and humidity is passed over the test sample for several hours. During this time the weight of the coal is measured at two minute intervals. The velocity and temperature of the air are measured at 5 cm. above the surface of the coal sample. After it is observed that the relative change in the weight of the wet coal with respect to its previous value is almost very small the experiment is stopped. The dry coal is then carefully removed from the tray and is placed in a vacuum oven for determining the dry-bone weight.

For each run, the following data is recorded. (i) dry-bulb temperature, (ii) wet-bulb temperature, (iii) air velocity, (iv) wet weight of coal, (v) intermediate point wet weight of coal, (vi) bone-dry weight of coal and heat-transfer area. Then the drying rate is calculated from

$$\text{Rate}_i = (w_{i-1}-w_i)/(t_i-t_{i-1})/\text{g.solid} \quad (28)$$

where i represents point values at time t_i, and w_i is the weight of the wet coal in grams. This rate is called 'differential drying rate'. A similar analysis is also made in order to calculate the 'cumulative drying rate' from

$$\text{Rate}_i = (w_o-w_i)/\text{g.solid} \quad (29)$$

which is primarily used in determining the exact location of the critical point.

The heat transfer area, A_H, is determined by using Aminco Porosimeter. The detailed analysis of coal is given in Appendix. The relative humidity of air is calculated by using relative humidity function HUMID (5). The vapor pressures and partial pressures on the solid surface and in the dryer are calculated from vapor pressure function VAP. The constant-rate period rate and the corresponding critical moisture content are found from the two rate curves obtained. Using the concepts and formulation given before, the variation of the heat and mass transfer coefficients and the mass transfer area in the falling-rate period are examined.

RESULTS AND DISCUSSIONS

The experimental results on the drying rate data of Turkish lignites are given in this section. The moisture concentration versus drying time profiles are shown in Figures. 3-8, each figure representing a set of runs made at different air velocities. The dry-bulb temperature of air is used as a parameter in each figure. The complete list of tabulated data is given elsewhere (5). The detailed analysis of the rate versus moisture concentration curve, for illustrative purposes, Figure 9 is drawn, has shown that the critical point is a narrow zone rather than a distinct point. It does not change much with the external conditions applied in this study, hence a uniqe critical point is preferred in all 30 runs.

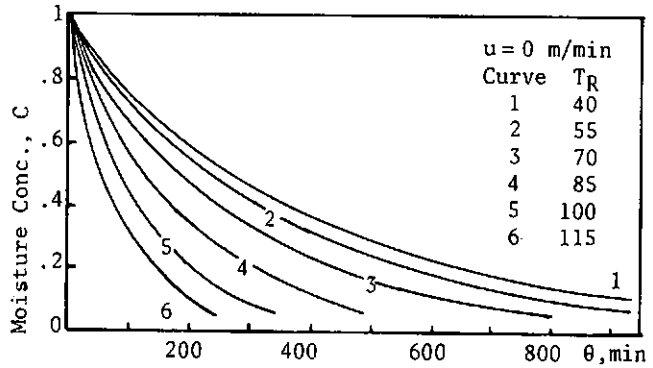

Figure 3. Moisture Concentration Profiles.

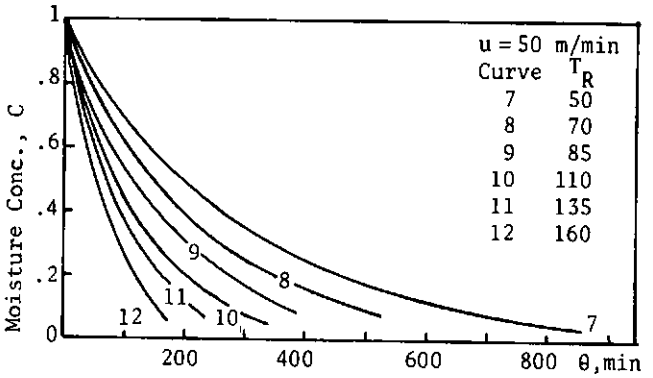

Figure 4. Moisture Concentration Profiles.

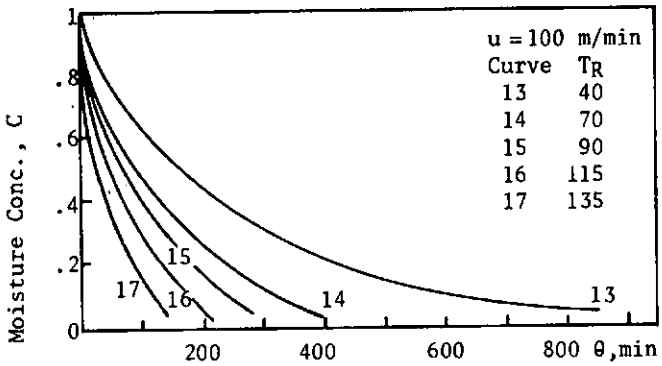

Figure 5. Moisture Concentration Profiles.

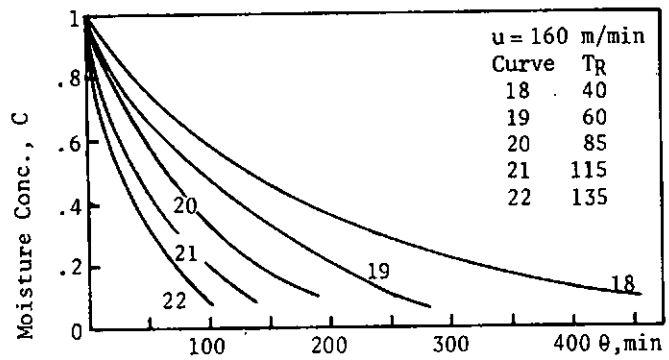

Figure 6. Moisture Concentration Profiles.

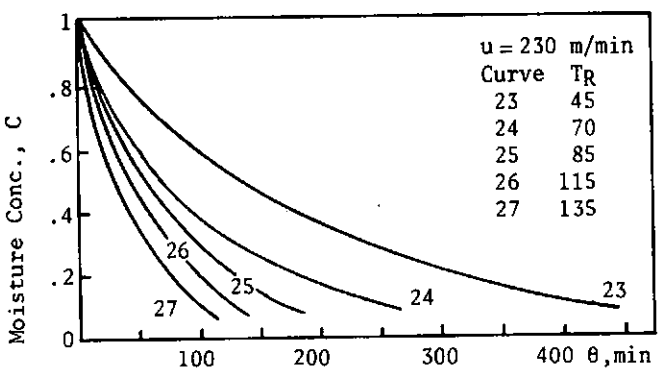

Figure 7. Moisture Concentration Profiles.

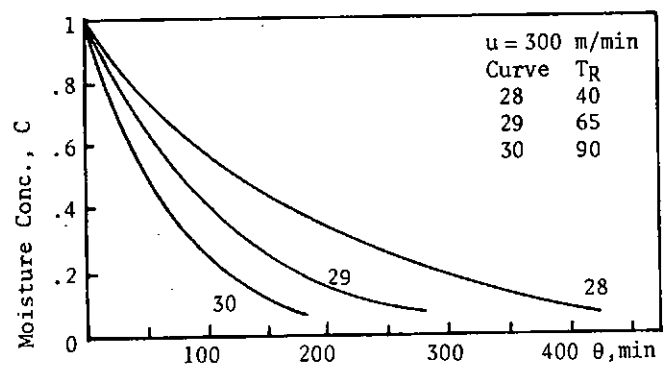

Figure 8. Moisture Concentration Profiles.

The analysis of drying rate diagrams indicate that the drying rate follows almost a linear decrease with moisture concentration. This is expected because it is known that the capillary mechanism controlled drying systems usually yield that linear profile. As a result of this experimental observation, the following model equation for moisture concentration versus time curves is proposed.

$$C = c_3 \exp(-m\theta) \tag{30}$$

where c_3 and m are constants. A statistical nonlinear model fit to all runs are made and the results obtained show that the constant c_3 is approximately equal to one. In addition to that it is found that the coefficient of the time, m, is exactly equal to the coefficient of the time in reduced time expression of Eqn.(19) with $W_c=1.0$. The validity of this model is illustrated for Run.21, as shown below:

C :	.9	.8	.7	.6	.5	.4	.2	.05
θ_e:	6.7	14.0	22.0	31.0	42.0	55.0	95.0	163
θ_p:	6.6	13.7	21.8	31.1	42.1	55.6	97.4	181

Here, θ_e and θ_p are experimental and predicted drying times at given concentration, respectively. The fit is almost perfect at high concentrations and deviation starts at very low concentrations. This may be due to the fact that the diffusion-controlled drying mechanism starts governing the rate of drying instead of capillarity-controlled drying mechanism. Similar results are obtained for other runs (5). Table 2 summarizes them.

The comparison of Eqns.(19) and (30) gives

$$m = (\alpha_t A_H \Delta T_{CRP})/(\lambda_{WB} W_c) \tag{31}$$

upon differentiation of Eqn.(30) with $c_3=1$ and C=1 at the critical point. As a result of this, the following general model equation,

$$C = \exp(-E) \tag{32}$$

is proposed to predict the concentration profiles of lignites in FRP, (Figure 9).

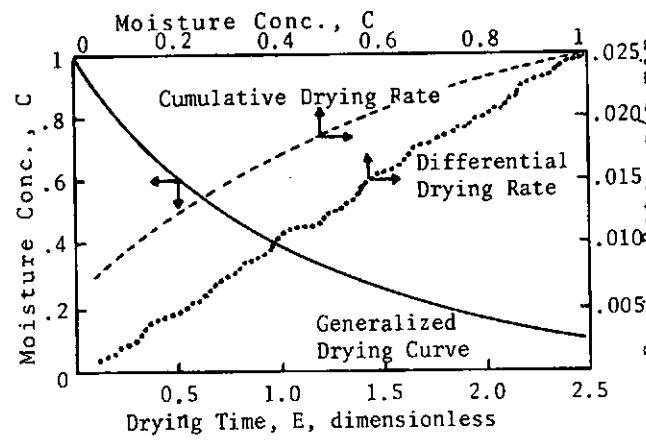

Figure 9. Generalized Drying Curve.

TABLE 2

CONSTANT-RATE PERIOD VALUES

Run	ΔT	Rate	m	α_t	β_G
1	14.0	.0018	.0011	.1258	.111
2	27.0	.0027	.0017	.0972	.108
3	40.5	.0036	.0023	.0862	.103
4	54.0	.0048	.0030	.0902	.109
5	67.0	.0059	.0037	.0848	.106
6	82.0	.0082	.0051	.0868	.121
7	23.5	.0050	.0031	.2070	.556
8	41.0	.0080	.0050	.1893	.533
9	54.0	.0096	.0060	.1721	.481
10	76.0	.0131	.0082	.1663	.475
11	98.0	.0165	.0103	.1625	.474
12	120.0	.0203	.0127	.1600	.477
13	15.0	.0055	.0034	.3352	1.309
14	41.0	.0117	.0073	.2770	.780
15	58.5	.0157	.0097	.2600	.727
16	80.5	.0214	.0134	.2522	.743
17	98.0	.0260	.0163	.2480	.818
18	15.0	.0062	.0038	.4000	1.136
19	32.0	.0113	.0070	.3425	.933
20	54.0	.0179	.0110	.3210	.863
21	80.5	.0254	.0159	.0050	.864
22	98.0	.0300	.0188	.2955	.847
23	19.0	.0083	.0054	.4248	1.200
24	41.0	.0159	.0099	.3770	1.061
25	54.0	.0198	.0125	.3550	.971
26	80.5	.0279	.0177	.3345	.949
27	98.0	.0325	.0222	.3195	.918
28	15.0	.0080	.0050	.4600	2.020
29	46.0	.0152	.0095	.4100	1.150
30	67.0	.0255	.0141	.3723	1.020

The results show that the drying rate at the constant-rate period is affected mainly by the air velocity and dry-bulb temperature. As easily seen from Figure 10, at constant air velocity the drying rate nearly varies linearly with the temperature at low temperatures, however, a slight concave upward profile is observed at very high temperatures. Similar profiles are also observed if the drying rate is plotted against the temperature driving force at the constant-rate period. On the other hand, the effect of air velocity on drying rate at constant air dry-bulb temperature is represented by a series of straight lines, almost parallel to each other, in a log-log plot as in Figure 11. This curve can be used safely if the air velocity is kept less than 200 m/min. This result checks with the general drying correlations given in literature that relates the heat transfer coefficient to air velocity. The slope in Figure 11 is approximately equal to 0.055, which indicates that the power of air velocity at constant dry-bulb temperature does not change much. When the air velocity is increased beyond 200 m/min. level, the rate of increase in the constant drying rate slows down. Hence, the higher the air velocity, the faster the drying rate concept may not be valid above certain air velocity levels. Because of the great danger in extrapolating the rate values beyond 125 °C limit, as can easily be seen from Figure 10, the same conclusion that is reached above can not be stated for dry-bulb temperature values. Figure 10 indicates that higher the dry-bulb temperature, the higher the drying rate in the constant-rate period.

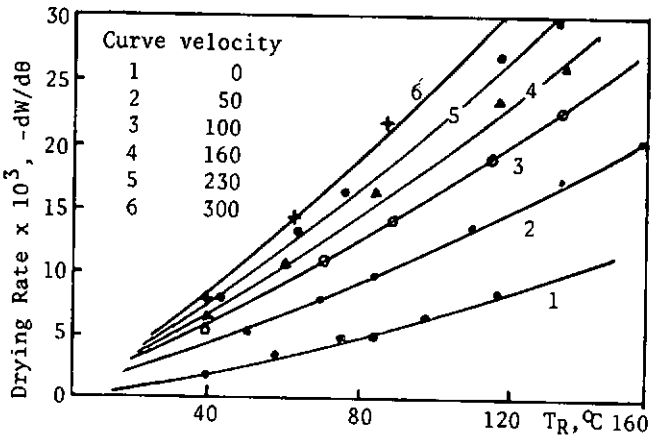

Figure 10. Drying Rate versus Temperature.

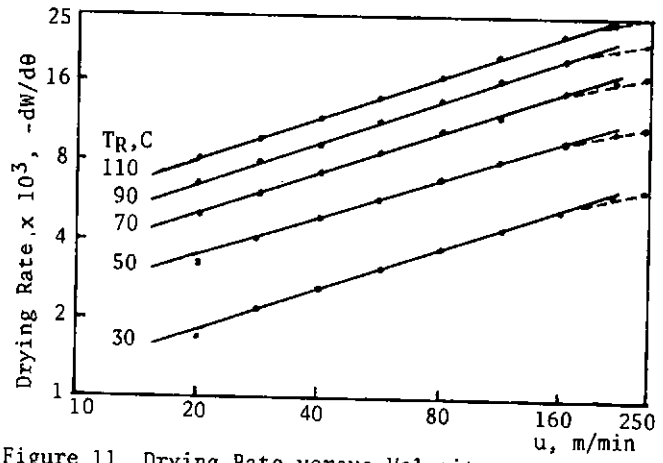

Figure 11. Drying Rate versus Velocity.

Equations (1) and (2) are used for calculating the heat and mass transfer coefficients at the constant-rate period. The results are summarized in Table 2. It is found that air velocity affects the corresponding coefficients relatively more than the dry-bulb temperature. At low air velocities the transfer coefficients remain constant. This behaviour may also hold at high velocity levels even though we obtain high values at low temperature driving forces and nearly constant values at high temperature driving forces. As can easily be seen from Eqns.(1) and (2), the transfer coefficients are functions of the drying rate, temperature driving force, and, area available for heat and mass transfer. At low air velocity and temperature, the experimental determinations of these factors are considered very accurate. However, at

higher external conditions, very high rates occur, hence a considerable amount of scattering in experimental data points is observed. This results in some uncertainties in physical measurement of the exact weight of the wet coal at that specific time, and of the wet-bulb temperature and hence relative humidities. In addition to them, some shrinkage and breakup are also observed. Because of this the transfer areas, A_H and A_M may be variable even in the constant-rate zone. When all these undesired but inevitable effects are taken into consideration, it may be more realistic if we state that the heat and mass transfer coefficients remains constant with the change in air temperature. The corresponding values at low temperatures should be used for this purpose.

In order to analyze the heat and mass transfer coefficients in the falling-rate period, the surface temperature data is required. Previous investigators (1) have shown that the reduced temperature,

$$T_S = (T_R - T_s)/(T_R - T_{WB}) \qquad (33)$$

generally follows a 'sigmoidal' profile with moisture concentration in the falling-rate period. A representative set of curves are shown in Figure 12.

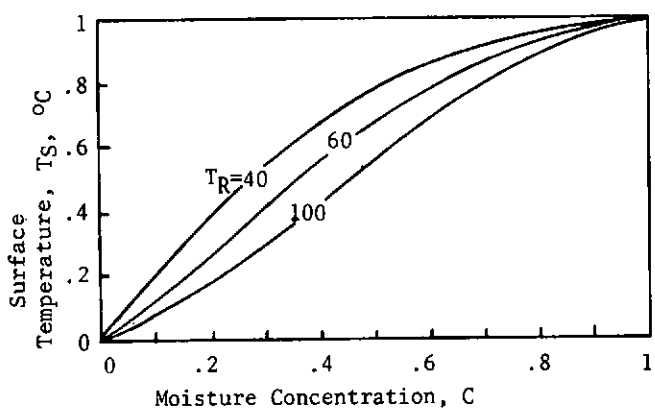

Figure 12. Surface Temperature in FRP.

Rewriting Eqn.(1) for constant-rate period, one may obtain,

$$-\frac{dC}{d\theta} = \frac{(\alpha_t A_H)^* (T_R - T_{WB})}{\lambda_{WB} W_C} = mC \qquad (34)$$

where superscript * denotes constant-rate period. Dividing Eqns.(34) and (1) side by side and using Eqn.(33), it can be shown that,

$$(\alpha_t A_H)/(\alpha_t A_H)^* = (\lambda_S/\lambda_{WB})(C/T_S) \qquad (35)$$

The heat transfer area is deliberately included in the above ratio in order to take the breakup and shrinkage effect into consideration.

Equation (35) is applied to the experimental data and the results obtained are summarized in Figure 13. It is found that the the ratio $\alpha_t A_H/\alpha_t A_H^*$ decreases as the concentration decreases but after a certain concentration, it starts to increase. The concentration at which the minimum occurs is found to be a function of dry-bulb temperature. And in addition to that the minimum is reached at high concentrations for high temperature runs and at low concentrations for low temperatures. This trend may be due to the fact that at low temperatures the breakup starts at the end of the falling-rate period whereas, at high temperatures, there is a great chance for breakup and shrinkage to start near the critical zone. On the basis of this justification, the curvature just before the minimum point is extrapolated. These are represented as dotted lines in Figure 13. Hence the dotted lines may be thought to represent the deviation of heat transfer coefficient from its original value in the falling-rate period. This deviation is maximum at low temperature runs because due to small driving force in temperature, the internal resistances to flow of moisture relatively become larger. A somewhat similar profile is obtained when a linear

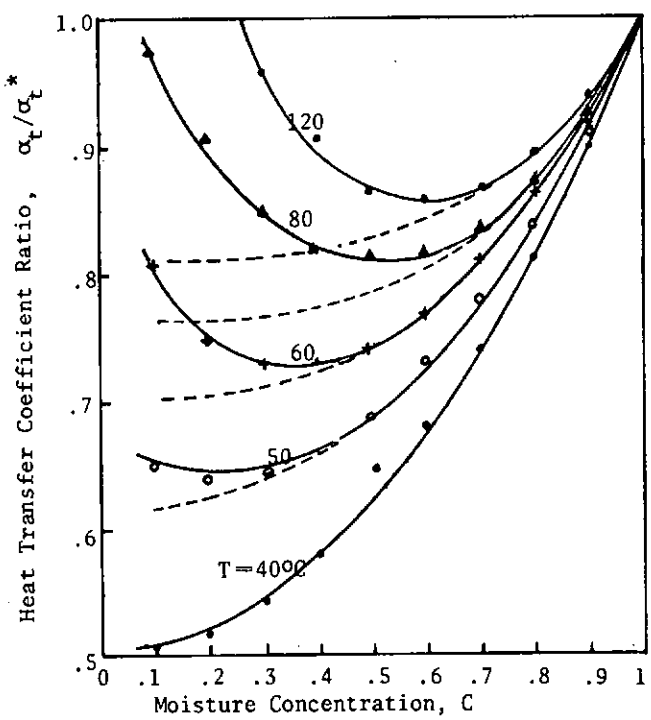

Figure 13. Variation of Heat Transfer Coefficient in Falling-Rate Period.

surface temperature is assumed instead of the sigmoidal profile. Hence, the fast rate of decrease in drying rate mainly controls the heat transfer coefficient in the falling-rate period of drying. The exponential shape of these profiles also indicates the validity of the capillary mechanism.

The effect of air temperature on mass and heat transfer coefficients are almost similar to each other. Even though these coefficients vary at different temperature levels, their ratio stays almost constant. This (7) ratio is defined by Eqn.(17) and is called heat-to-mass ratio. It is analogous to psychrometric ratio, defined as,

$$\phi = (29/18)c_p P_{BM}(P_G/\alpha_t) \qquad (36)$$

where P_{BM} is log-mean pressure between the surface pressure of the solid and the partial pressure in the room, and, c_p is the specific heat content of moist solid.

The use of the term G is preferred in this study because it naturally arises in the integration steps of the model equation. The effect of moisture concentration on the mass transfer coefficient in the falling-rate period gives similar profiles to the ones shown in Figure 13. It is found that G is constant in the falling-rate period, which may indirectly indicates that the complete equilibrium between the heat and the mass transfer mechanisms is still valid in the falling-rate period. However. a small decrease in G is visualized at high temperature runs which may indicate that the dynamic equilibrium between the two mechanisms is somewhat destroyed on the favor of mass transfer (6). The resistance to drying is mainly controlled by the resistance to mass transfer rather than heat transfer.

CONCLUSIONS

The main conclusions reached in this study can be summarized as:

i. For systems where the capillary flow mechanism is governing the moisture migration in the falling-rate period, the "moisture versus drying time" curves can be very well represented by an exponential decay model,

$$C = \exp(-m\theta) \qquad (30)$$

where m is the coefficient of time given in Eqn.(19). It is generally a function of constant-rate drying value.

ii. When Eqn.(30) holds, a "generalized drying equation",

$$(\alpha_t A_H \Delta T_{CRP}/W_c \lambda_{WB})\theta_f = e_1(1-C_f) + e_2(1-C_f)^2 + e_3(1-C_f)^3 \qquad (37)$$

where e_i are constants that should be determined experimentally and subscript f denotes finaltime required to dry the solid from the critical point to any final concentration C_f. If these constants e_i are not available, then Eqn.(30) can be used.

iii. The drying rate at the constant-rate drying period is affected more by increasing the air velocity rather than the air temperature. However, for both cases, the corresponding effects get smaller at higher velocity or temperature. For those cases, the internal resistance to moisture flow becomes predominant.

iv. Even though the heat and mass transfer coefficients slightly decrease as the moisture concentration decreases, the "heat to mass ratio" generally remains constant.

v. A further theoretical study is essential for predicting the change of the mass transfer area in the falling-rate period.

APPENDIX

Lignite Analysis

Calorific Value = 1421 kcal/kg.
Water Content = % 56.7
Ash Content = % 13.9
Volatile Matter = % 17.9
Fixed Carbon = % 11.5

Elementary Analysis:

C	= %19.4	S	= % 2.0
H	= % 1.6	Ash	= % 13.9
O+N	= % 6.4	H_2O	= % 56.7

REFERENCES

1. Gebizlioğlu, O., Capillary Flow Model, M.Sc.Thesis, Middle East Technical University, Turkey, 1976.
2. Luikov, A.V., Int.Chem.Eng., 3: 195 (1963).
3. Lebedev, P.D., Int.J.Heat Mass Tr., 1: 295,302 (1961).
4. Akit, A., Investigation of Heat and Mass Transfer During Drying, M.Sc.Thesis, Middle East Technical University, Turkey 1976.
5. Savaş, Y., Investigation and Determination of Drying Characteristics of Turkish Lignites, M.Sc.Thesis, Middle East Technical University, Turkey, 1979.
6. Kısakürek,B.,R.E.Peck and T.Çakaloz, CJChE., 53: 53 (1975).
7. Henry, H.C. and N.Epstein, CJChE., 48: 595 (1970).

COST-BENEFIT ANALYSIS OF SOLAR GRAIN DRYING AND ITS POLICY IMPLICATIONS

O. Yul Kwon[1]
Peter J. Catania[2]

1. University of Regina, Saskatchewan S4S 0A2
2. University of Regina, Saskatchewan S4S 0A2

ABSTRACT

Cost-benefit analyses were made for a prototype solar grain dryer and a conventional bin batch dryer each having a capacity to dry 15 percent of an average yield of 8,000 bushels per year. The penalty charge to dry high moisture content grain at wheat pools or terminals is equivalent to a benefit for farmers who dry their grain on the farm. The present discounted value for this benefit is $4,156. The discounted present costs for conventional and solar grain drying on the farm are $3,564 and $2,793, respectively. In summary, grain drying on the farm is economically viable with solar drying being "cheaper" than conventional drying.

NOMENCLATURE

BPY = number of bushels produced per year by a typical farmer

c = the investment tax credit rate

CCA_t = capital cost allowance in year t

E = electric power costs in year 1

e = annual rate of increase in E

en = annual rate of increase in energy costs

f = fraction of the annual increase on the penalty changes resulting from energy inputs

G = propane gas costs in year 1

g = annual rate of increase in G

h = fraction of total annual grain to be dried

i = general inflation rate

K = initial capital cost including acquisition, delivery and installation

L_t = remaining balance in year t of the initial loan (L), L being equal to K

M = maintenance costs including insurance, replacement and repair in year 1

m = annual rate of increase in M

n = life of the dryer system

P = penalty charge per bushel in year 1

p = annual rate of increase in P

PVC = present discounted cost

q = effective discount factor defined by Equation (3)

t = number of years

u = marginal tax rate

W = labor costs to operate system in year 1

w = annual rate of increase in W

INTRODUCTION

Despite the importance of solar energy for grain drying in Western Canada, little is done about its economic evaluation, and no specific government policy has been developed in this respect. The objective of the present study is, therefore, to undertake an economic evaluation of solar energy systems for grain drying in Saskatchewan from the private farmers' viewpoint. The benefits of grain drying on the farm arise from not only the obvious reduction in spoilage but also in a timely early harvest. The latter increases the number of harvesting days and allows for a potentially better utilization of farming equipment. Other possible benefits are timely chemical applications and tillage practices (1). Furthermore, in years of poor harvesting conditions the excess tough and damp grain cannot be accepted by the buyers. This problem can be alleviated by drying the grain on the farm.

Farmers in Western Canada have essentially three options to consider in dealing with their high moisture grain: (a) to sell it directly to buyers (wheat pools and terminals) at a certain penalty charge; (b) to dry it at the farm level by conventional energy (propane gas); and (c) to dry

installing and using a bin batch dryer in order to dry 15% of a total crop production of 8,000 bushels of grain. As we compare the estimated present value of the benefits ($4,156) to that of the costs ($3,564), we can draw a conclusion that it is economical to dry grain at farm levels by a conventional drying system.

SOLAR DRYING

The low temperature, high flow rate method (3,4), to dry cereal grains is compatible with a) the low grade energy source - solar energy and b) the batch storage in conventional grain bins. The only difference between solar and conventional drying is that the propane heater is now replaced by a solar collector. The characteristics and quality of the solar collector has a direct bearing on capital costs. Experimental results (5) showed that a collector, having an area of 87.4 m^2, was capable of drying 8,000 bushels of grain per year in Northern Saskatchewan. The capital cost was $1,920. Typical storage bins found in Western Canada have a capacity of 4,000 bushels; therefore, to store a yield of 8,000 bushels requires two storage bins. The capital cost to modify these bins in order to accommodate the solar system is $2,000. The total capital cost is therefore estimated to be equal to $3,920. About one half of this original capital cost may be entitled for the investment tax credit and capital cost allowances for taxable income. The present value of these tax benefits amount to $1,439 at an assumed marginal tax rate of 40%. Therefore, the original cost net of tax benefits is estimated to be $2,481.

Maintenance, labour and annual electric power costs are estimated to be $110, $400 and $80, respectively. Maintaining the assumptions used for conventional drying, i.e., h = 15%; m = 8%; w = 10%; e = 13%; u = 40%; r = 13%; n = 20 years and the capital cost is funded solely by a five year term loan at an interest rate of 13%, we have by Equation (4) the present discounted costs for maintenance, labour and annual power being equal to $137, $585 and $87, respectively. As with conventional drying, we shall assume that the capital cost of $3,920 is fully funded by a five year loan at an interest rate of 13 percent. The present value of tax savings from interest deductions over the same five year period is $497. Therefore, the present discounted value for a solar drying is equal to $2,793. In comparison, the estimated benefits are $4,156 and conventional drying is $3,564. This clearly indicates that solar grain drying is economically viable for on the farm drying.

Even though solar drying is cheaper than conventional drying, there exists a concern over the using of only solar energy to dry cereal grains. The concern is that the solar system may not, due to poor meteorological conditions, be capable of drying the grain and the farmer must therefore rely on a conventional system. This would imply that the solar system should be classified as not purely solar but rather, combination drying. In effect this would indicate that an external dryer (electric, propane or gas) should be incorporated into the overall design to accommodate that particular year wherein solar cannot dry 100 percent of the desired fraction of the crop production. Furthermore, if the solar dryer is appropriately designed it may have multiple use. Hence, the load factor is more evenly distributed and economic competitiveness of the solar drying system would improve significantly.

CONCLUSION

We conclude that solar drying systems are economically viable options for on-the-farm drying of cereal grains in Saskatchewan. To accommodate those years wherein solar drying alone cannot reduce the moisture content to acceptable levels we recommend a combination electrical resistance-solar drying system. Finally, the multiple use of a solar dryer will improve its load factor and economics.

ACKNOWLEDGEMENT

The authors wish to acknowledge the information furnished by Mr. Martin Wrubleski of the Saskatchewan Department of Agriculture.

REFERENCES

1. Saskatchewan Department of Agriculture, "Importance of Grain Drying, Monograph, 1978
2. Kwon, O.Y., Cost-Benefit Analysis of Solar Energy for Grain Drying in Western Canada and Its Policy Implications, presented at Congres Solaire International, Nice, France, November, 1979
3. Catania, P.J., Solar Grain Drying, report for Saskatchewan Department of Agriculture, Engineering Services Branch, April 1977
4. Shove, G.C., editor, Solar Grain Drying Conference, January 11-12, Urbana, Illinois, 1977
5. Wrubleski, E.M., and Catania, P.J., Experience with a Solar Collector for Grain Drying in Saskatchewan, Annual Meeting Canadian Society of Agricultural Engineering, August 14-18, 1977

it at the farm level by solar energy. For farmers who dry their grain at their farms--either by propane gas or solar energy--the penalty charges are equivalent to benefits of grain drying. Benefits (or penalty charges) of grain drying depend on the moisture content and the amount of grain to be dried. Based on available historical data and information from the Saskatchewan Department of Agriculture, the penalty charge was estimated to be 18 cents per bushel in 1978 prices (2).

BENEFIT ANALYSIS

To evaluate conventional versus solar drying on the farm, we must know the effects of inflation and interest rates on the penalty charge which, as previously stated, is equivalent to benefits for grain drying. For this study we have assumed that (a) the general inflation rate will increase 8% per year, (b) energy costs will increase at 15% per year and (c) energy costs account for 50% of the annual increase in the penalty charges. Using these assumptions and Equation (1), the annual rate of increase in the penalty charge, p, is equal to 12%.

$$p = (f)(en) + (1-f)(i) \qquad (1)$$

With Equation (2) and the following assumptions: BPY = 8,000 bushels; h = 15%; P = 18 cents per bushel; p = 12%; r = 13% and n = 20 years, the present value of benefits is equal to $4,156.

$$\text{Benefits} = \sum_{t=1}^{n} (BPY)(h)(P)\left(\frac{1+p}{1+r}\right)^t$$

$$= (BPY)(h)(P)\ \frac{1-q^{n+1}}{1-q} \qquad (2)$$

where

$$q = \frac{1+p}{1+r} \qquad (3)$$

CONVENTIONAL DRYING

It has been argued that a bin batch dryer is the most economical conventional drying system (1,2) and this will be adopted as the base for estimating drying costs. In this system, air, heated by the burning propane gas, is driven by a fan through the perforated floor and into the grain. The moist air exits through a vent in the bin roof. A bin batch dryer having a capacity of drying 8,000 bushels of damp grain would cost approximately $4,500 (2). The life cycle cost of this system, including taxes and tax benefits, can be evaluated by use of Equation (4).

$$PVC = K(1-c) + \left[\sum_{t=1}^{n} \frac{M(1+m)^t}{(1+r)^t} + \sum_{t=1}^{n} \frac{W(1+w)^t}{(1+r)^t} + \right.$$

$$\left. \sum_{t=1}^{n} \frac{G(1+g)^t}{(1+r)^t} + \sum_{t=1}^{n} \frac{E(1+e)^t}{(1+r)^t} \right] h(1-u) -$$

$$\sum_{t=1}^{n} \frac{CCA_t \cdot u}{(1+r)^t} - \sum_{n=1}^{5} \frac{L_t \cdot r \cdot u}{(1+r)^t} .$$

The first term on the right-hand side shows the initial capital cost less investment tax credits. The four terms inside the square brackets comprise operating and maintenance costs. They would be incurred in accordance with the proporation (h) of the total annual grain to be dried, and they are deductable for tax purposes. The third term shows tax savings through capital cost allowances. Finally, the last term shows tax savings from deducting interests on the remaining balance of the initial loan.

Based on the cost estimates provided by the Saskatchewan Department of Agriculture (3), the present discounted cost of a bin batch dryer is estimated as follows: The original capital cost (K) is estimated to be $4,500 in the 1978 price. The major part of the capital cost is entitled for the investment tax credit at about 10% (or $450). The capital cost less investment tax credit (i.e., $4,050) is entitled for capital cost allowances at about 24% under the diminishing balance method. Assuming that the farmer's marginal tax rate is 40%, the present value, discounted at 13%, of tax savings from capital cost allowances amounts to $1,053. As a result, the capital cost net of tax savings is estimated to be $2,997. This is the so-called sunk cost. Once the drying system is installed, it will be incurred regardless of whether it is used or not.

Assuming that the initial moisture level of grain is 18%, annual maintenance costs (M), labor wages (W), costs of propane gas (G) and electric power costs (E) in drying 8,000 bushels of grain are estimated to be, respectively, $56, $400, $213 and $12 in 1978 (2). It is assumed that the annual inflation rates of these costs are, respectively, 8%, 10%, 15%, 13% and the life of the system, n, is 20 years. These costs would be incurred in proportion to the fraction of annual grain to be dried. In accordance with our assumption that 15% of annual grain production will be dried, the actual costs of the four items will be 15% of these estimated costs. Given the marginal tax rate of 40% and the discount rate of 13%, the presence discounted costs of maintenance, wages, propane gas and electric power are estimated to be $70, $585, $482 and $1, respectively, amounting in total to $1,138.

It is assumed that the original capital cost ($4,500) is funded solely by a five-year term loan at an interest rate of 13%. Annual installment payment is then $1,280. Of this installment payment, the interest portions during the five year period are tax deductable. The present value of tax savings over the five year period is then $571. In sum, therefore, the present discounted cost of a bin batch dryer is estimated to be $3,564. This is the cost of

DIGITAL SIMULATION OF A SOLAR HAY-DRYING SYSTEM

Imre,L.
Kiss,L. ; Környey,T. - Molnár, K.

Technical University Budapest
Hungary

ABSTRACT

The valuable internal ingredients /protein, carotin, etc./ of rough fodder /lucerne, hay grass/ start decomposing after being mowed. The decomposition process can be slowened or stopped by drying. At the same time, the circumstances of drying have an influence upon the degradation taking place during drying.

The drying necessary for producing hay is too much expensive with the use of oil or gas heating. It appears therefore desirable to utilize the air in its normal state and the solar energy to the greatest possible extent.

The solar hay-drier under investigation is an industrial building the roof and walls of which serve for accomodating the photo-thermal plane-collectors. With the absorbing surface of the collectors heat-storing masses are connected, which are heated up by the primary radiation. The rough fodder is spread within the building in a loose stack, in layers according to the mowings. Drying the stack takes place by the streaming air heated up in the collectors and/or heat stores. The air can be re-mixed partly or fully.

The system model of the hay-drier is a simultaneous model consisting of part models: the thermal model of the collectors, the mass flow network model of the drying air and the model of the drying space. Each of the part models is a discretized model.

The complete mathematical model of the drier is constituted by the equation systems of the part models and the set of the coupling equations and is solved numerically.

The simulation program supplies the temperature and moisture field of the hay for cases of arbitrary atmospheric variations.

NOMENCLATURE

a	absorption coefficient for the solar spectrum
a_p	mass diffusivity coefficient
A	surface, cross section; constant of the fan characteristic
$\underline{\underline{A}}$	graph incidence matrix
B,C	coefficients of fan characteristic
c_m, c_{pa}, c_{pv}	specific heat /for wet material; for humid air, overheated water vapour, with p = constant, resp./
C, $\underline{\underline{C}}$	heat capacitance, heat capacitance matrix
$\dot{C}$	heat capacity flow /$\dot{C} = \dot{M} c_p$/
d	transmission coefficient of glass, pertaining to the solar spectrum
$\underline{\underline{H}}$	loop matrix
I_o	intensity of total incident radiation
i, j	symbols for nodes
$\underline{\underline{K}}$	heat conductivity matrix
$\dot{m}$	mass flow rate density
$\dot{M}$, $\underline{\dot{M}}$	mass flow rate, mass flow rate column matrix
$\underline{P}_b$; $\underline{P}_s$	difference in branch pressure, column matrix of pressure source
r_o, r_f	evaporation heat /at 0° C and at T_f, resp./
R, $\underline{\underline{R}}$	resistance, diagonal matrix of branch resistances
T, $\underline{T}$	temperature, column matrix of temperature
$\dot{T}$	time derivative of temperature
$\dot{V}$	volume flow rate
W	water content of material, relative to dry mass
Z	variator
X	absolute water content of air
Y	operator
α	heat transfer coefficient
δ	conduction distance
ε_r	relative emission factor pertaining to low temperature radiation

λ heat conductivity coefficient

φ relative moisture content

ϕ, $\underline{\phi}$ heat flow rate, column matrix of heat flow rate source

ρ_s density of dry material

σ evaporation factor; emission factor of absolute black body

ξ_p porosity

τ time

Upper indices

T transposed

/o/ zero-th approximation

/n/ number of part networks /discrete parts/

Lower indices

a air

b number of branches

c node symbol; convective; collector

D drying space

f drying surface

g glass

in inlet

j symbol of loop in graphs

k number of variators

m mass flow

M mixer

out outlet

r recirculation

S, s source; sky

W outside ambiency.

INTRODUCTION

In recent years, the use of solar energy for drying in agriculture [1] has come into the limelight. The photo-thermal collectors of simple design have greatly developed, methods have been elaborated for the dimensioning of collectors, the calculation of their efficiency, the vew-points of economy and also of optimization have been considered [4...11]. The literature dealing with the problem is extending rapidly. Owing to the time-dependent radiation and atmospheric conditions, the application of dynamic models is of great importance [12].

The range of the agricultural products that can be dried by solar energy is determined by the relation of local meteorological conditions and of the harvesting time of the products. In Hungary, the products grown and harvested in the period from June to September may come into consideration in the first place. One of the most important produce is the lucerne.

CONSTRUCTION OF THE HAY DRIER USING SOLAR ENERGY

The hay drier-storer using solar energy is an industrial building constructed to comply with mechanized harvesting, and the surfaces of its roof and walls serve for accomodating the collectors. The scheme of the whole system is shown in Fig.1 [2].

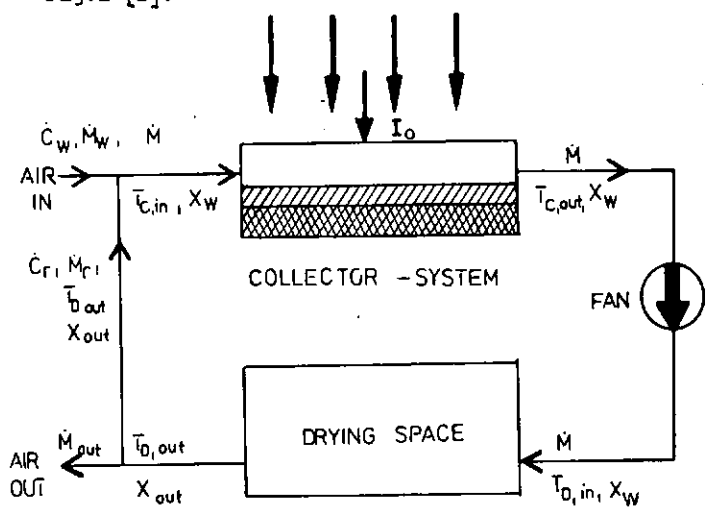

Fig. 1.

To design the elements of the hay-drier system and its control system providing optimum control, it is necessary to know the time functions of the temperature and moisture distribution /$T_m(x,\tau)$/ and $W_m(z,\tau)$, resp./ of the hay stacked in layers /or placed in separate spaces/ in the drying space after each mowing.

A model conception and computer simulation will be presented below, which makes possible to determine the distribution functions wanted, for the cases of arbitrary meteorological conditions and relations of recirculation air.

MODEL OF THE SOLAR HAY DRIER

The model of the hay drier system is a hierarchic simultaneous heat and mass flow network model built from part models.

The model of upper hierarchy level is a non-isothermic mass flow network model /MFN/, the scheme of which is shown in Fig.2. The elements

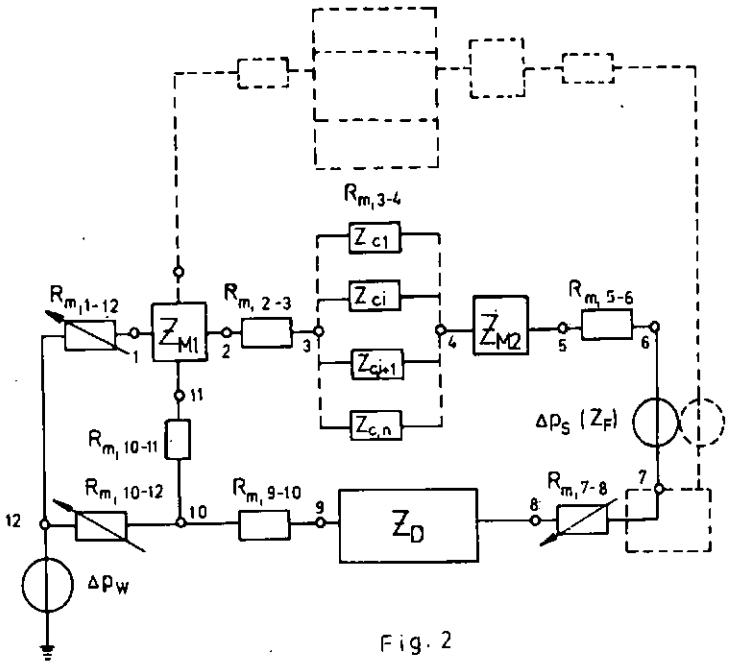

Fig. 2

of the MFN are pressure sources ΔP, flow resistances $R_{m,i-j}$ and variator elements Z_n. In the latter ones, the state conditions of the flowing air change. The variator elements Z_{Ci} of the MFN under consideration correspond to the collectors of the system, Z_{Mk} to the mixing spaces, Z_F to the fan and Z_D to the drying space. $R_{m,1-12}$ and $R_{m,10-12}$ are variable flow resistances.

THE EQUATION SYSTEM DESCRIBING THE MFN

Based on the MFN, the branch mass-flows and, in the flow ducts the local flow velocities have to be determined. Owing to the mass-flow dependence of the flow resistances and of the pressure source ΔP_S the equation system describing the MFN is not linear. The nodal equation system is

$$/\underline{\underline{A}}_M^+ \dot{\underline{M}}_b/_i = \underline{0} \qquad /1/$$

the loop equation system:

$$\underline{\underline{H}}_M^+ \cdot /\Delta \underline{P}_b + \Delta \underline{P}_S/_h \qquad /2/$$

the branch equation system:

$$\Delta \underline{P}_b = \underline{R}_M /\dot{\underline{M}}_b, \; \underline{T}_b/ \cdot \dot{\underline{M}}_b. \qquad /3/$$

State functions of the variators

The variator elements assign to the inlet state vector of the flowing air

$$/\underline{Z}_{be}/_k = [\dot{V}, T, \Delta P, X, \ldots]^T_{be,k} \qquad /4/$$

a determined outlet state vector [13...15]

$$/\underline{Z}_{out}/_k = Y /\underline{Z}_{in}/_k . \qquad /5/$$

The state equation of the fan as a pressure source is determined on the basis of a set of characteristic curves:

$$P_S = A/T/ + B/T/\dot{V} + C/T/\dot{V}^n , \qquad /6/$$

where A/T/, B/T/ and C/T/ are values characteristic of the fan employed. If separate fans are attached to the collector groups of different position, parallel branches will appear in the network and a new mixing space behind the fans /branches drawn in broken line in Fig.2/. The state functions for the mixing spaces /Z_{M1}, Z_{M2}/ are simple equations of heat and moisture mass balance /see below/. The more complicated variator elements, the collectors and the drying space, are themselves subsystems. Part models will be constructed to determine their state functions. The part models appear on the lower hierarchy level of the system model /in the computer procedure: in subroutines/.

DETERMINATION OF THE STATE FUNCTION OF THE COLLECTORS

The collectors change the elements of the state vector $/\underline{Z}_C/_{in}$ of the entering air. For the examination, the change of the temperature and pressure of the air /mainly as a consequence of the flow resistances/ is essential. The latter is calculated from branch equation /3/ on the basis of the flow resistances $R_{m,i-j}$ assigned to the mean temperatures of the air in the collectors. The discretized heat flow network model /HFN/ of the collector can be used for the determination of

$$/T_C/_{out} = Y_T/T_C/_{in} \qquad /7/$$

Figure 3 shows the scheme of the collectors. The HFN model of the collector system is illustrated in Fig.4. The model conditions pertaining

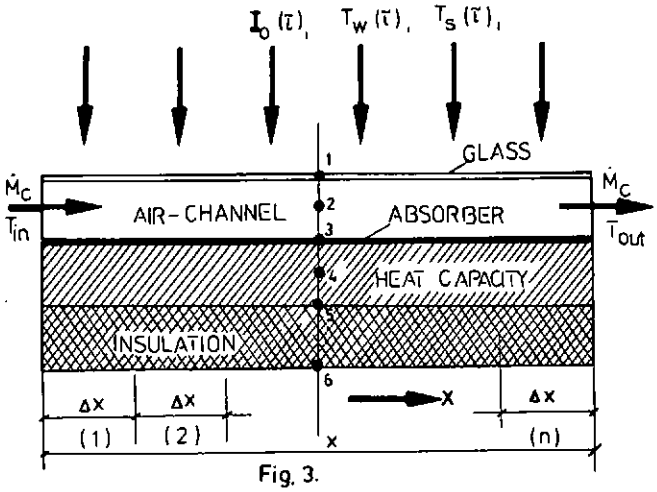

Fig. 3.

to the discretization follow from Figures 3 and 4. The HFN model is built from further part models, in each of which concentrated parameters are used for modeling a portion of length Δx of the collector considered.

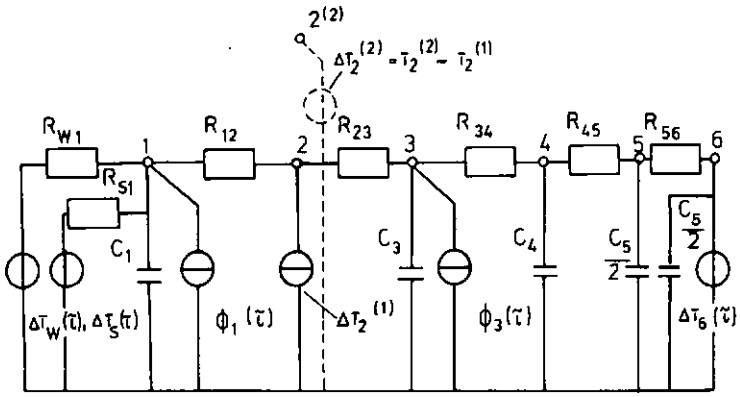

Fig. 4.

The heat flow network part models are coupled by thermal "voltage" sources

$$T_2^{/n/} = \frac{\Phi_{32}^{/n-1/} - \Phi_{12}^{/n-1/}}{\dot{C}_c} \qquad /8/$$

corresponding to the heat capacity flows $\dot{C}_c = \dot{M} c$ of the air flowing through the collector. In nodes 2 of the part models these thermal voltage sources prescribe a temperature corresponding to the warming up of the air flowing through portion Δx of the collector. The notation of the nodes is interpreted according to Fig.3.

For the first part model, $T_2^{/1/}$ is the temperature of the air leaving the mixer according to Fig.2. Using also the notations of Fig.1, the equation

$$T_{C\,in} = T_2^{/1/} = \frac{\dot{C}_w T_w + \dot{C}_r T_{D\,out}}{\dot{C}} . \qquad /9/$$

will be obtained.

The actual temperature of the outside air is prescribed by the thermal voltage source $T_w/\tau/$, the reference temperature of the existing radiation of the sky by $T_s/\tau/$ and the temperature of the drying space by $T_6/\tau/$. The heat flow rate source $\phi_1/\tau/$ is calculated from the total incident radiation $I_o/\tau/$ reduced by the absorption factor a_1 of the glass, relative to the sun spectrum ($\phi_1/\tau/ = I_o/\tau/\ a_1 A$); heat flow rate source $\phi_3/\tau/$ is determined from $I_o/\tau/$ reduced by the transmission factor d_1 of glass relative to the sun spectrum and absorption factor a_3 of the absorbent ($\phi_3/\tau/ = I_o/\tau/\ a_3 d_1 A$). R_{w1} is the heat transfer resistance between the glass and the external air $/R_{W1} = \frac{1}{\alpha_W A}/$, where α_W is the joint heat transfer coefficient of the natural convection and of the forced convection caused by wind. R_{s1} is the linearized heat radiation resistance between the glass and the sky, relative to low temperature radiation ($R_{s1} = \frac{1}{\alpha_{rs} A}$, where $\alpha_{rs} = \frac{\varepsilon_{rs}\sigma/T_1^4 - T_s^4/}{T_1 - T_s}$. The transfer resistance R_{12} is the resultant of the convective heat transfer resistance $/R_{12}/_c$ between the glass and the air, and of the linearized radiation resistance $/R_{12}/_r$ between the glass and the absorber ($R_{12} = /R_{12}/_c x /R_{12}/_r$, where $/R_{12}/_c = \frac{1}{\alpha_2 A}$, $/R_{12}/_r = \frac{1}{\alpha_{r2} A}$, $\alpha_{r2} = \frac{\varepsilon_{r2}\sigma(T_2^4 - T_1^4)}{T_2 - T_1}$.

R_{23} is the convective heat transfer resistance between the air and the absorber ($R_{23} = \frac{1}{\alpha_2 A} = /R_{12}/_c$), and R_{34}, R_{45}, R_{56} are heat conduction resistances $/R_{i,j} = \frac{\delta_{i,j}}{\lambda A_k}/$. The values C_1, C_3 C_4 and C_5 are the heat capacitances of glass, absorbent, heat accumulator and heat insulation layer, respectively.

The state function /7/ of the air flowing in the collectors is produced by the equation system describing the HFN according to Fig.4. Proceeding in direction x, the equation system will be solved for all discrete collector elements. The solution obtained for the last element can be used to calculate $/T_2/_{out}$ on the basis of /8/.

With substitution from the nodal equations into the loop equations /with conductions $K_{i,j} = \frac{1}{R_{i,j}}$/ the nonlinear equation system describing the heat flow network can be written in the form

$$\underline{\underline{C}}\ \dot{\underline{T}}/\tau/ + \underline{\underline{K}}\ /\underline{T},\tau/.\ \underline{T}/\tau/ = \underline{\Phi}/\underline{T},\tau/. \qquad /10/$$

DETERMINATION OF THE STATE FUNCTIONS OF THE DRYING SPACE

The drying space as Z_D variator element of the MFN changes the state vector of the drying air. The - possibly partial - use of the air leaving the drier depends on the outlet temperature and the absolute water content of the air. The design of the control system of the drier requires the knowledge the functions $T_{D,out}/\tau/$ and $X_{out}/\tau/$. In addition it is necessary to know the time-functions of the temperature distribution $T_m/z,\tau/$ and water content $W_m/z,\tau/$ of the hay under drying.

The model used for determining the state function of the drying space is shown in Fig.5. The drying air streams upward from the bottom into the hay stack formed by layers after the mowings, then after having flown through the stack leaves the drying space /in Fig.2: node 9/. The absolute inlet water content X_{in} of the air having a mass flow rate $\dot{M}$ determined on the basis of the MFN model is equal to that of the air leaving the mixer Z_{M1} according to Fig.2:

$$X_{in} = \frac{M_W X_W + M_r X_{out}}{\dot{M}} . \qquad /11/$$

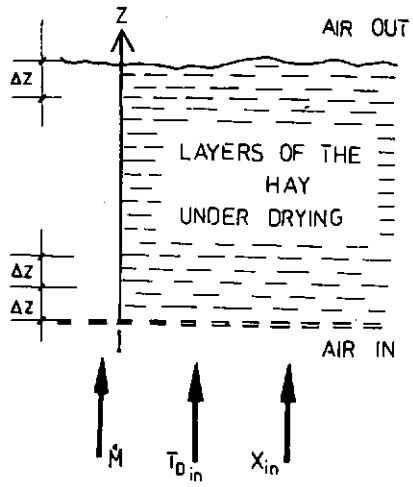

Fig.5.

Assuming that the temperature of the air entering the drying space is equal to that of the air leaving the mixer z_{M2} one has:

$$T_{D\,in} \approx \frac{\sum_{c} \dot{c}_c / T_2^{(n)} /_c}{\dot{c}} \qquad /12/$$

where c is the number of the collectors connected parallel.

Model conditions applied to the drying space:

1. The moisture content of the hay stack in thickness Δz is replaced by its mean value.
2. The local moisture content of the hay is considered equal to the surface moisture.
3. Moisture distribution in direction z is only considered.
4. The moisture transport between the layers is negligible.

The equation system of the drying space /for unit flow cross section/

moisture balance for the drying material [19]:

$$\varrho_s \frac{dW}{d\tau} = -\sigma / X_f - X_a / a_p \,, \qquad /13/$$

moisture balance for the drying air:

$$\dot{m} \frac{\partial X_a}{\partial z} + \varrho_a \xi_p \frac{\partial X_a}{\partial \tau} = \sigma / X_f - X_a / a_p, \qquad /14/$$

enthalpy balance for the drying air:

$$\dot{m}\, c_{pa} \left[\frac{dT_a}{dz} + /r_o + c_{pv} T_a / \frac{\partial X_a}{\partial z} \right] + \alpha_D a_p / T_a - T_f / =$$

$$\sigma / X_f - X_a / . a_p . / r + c_{pv} T_f /, \qquad /15/$$

enthalpy balance for the drying material:

$$c_m \frac{\varrho_s}{a_p} \frac{dT_f}{d\tau} + \sigma / X_f - X_a / r_f = \alpha_D / T_a - T_f /. \qquad /16/$$

SOLUTION OF THE DESCRIPTIVE EQUATION SYSTEMS

The non-linear equation system of the MFN consisting of equations /1/, /2/, /3/ and /6/ can be solved by the Newton-Raphson method. As a result of the solution, the total mass flow rate $\dot{M}$, the mass flow rates $\dot{M}_{on}$ of the air in the collectors and the local flow velocities will be obtained.

The equation system of the collectors including equations /8/, /9/ and /10/ must be solved n times in the case of a division into $n = \frac{x}{\Delta x}$ parts/. Heat capacitances C_1, C_3 and C_5 can in general be neglected as compared with C_4. The values of temperature dependent conductivities in the case of slight temperature variation in direction x / T_2 /n/ $< 3^{\circ}C/m$ can be replaced for the n-th portion on the basis of the temperature value obtained for the /n-1/th portion. If the temperature change in time is considerable, the "mid-point" method can be used: based on the temperatures obtained for the /n-1/th and /n-2/th discrete parts linear extrapolation is performed for the temperatures of the n-th part, the extrapolated temperatures are used to determine the conductivities, then the equation system for to the n-th part will be solved. When there are considerable temperature changes in direction x and a high accuracy is required, iteration is applied with the temperatures obtained.

The transient heat flow network equation system /10/ is not linear, therefore it is practical to use a finite difference time-scheme or a scheme with finite time-elements [16]. It is of advantage to use the difference scheme of Lees with three time levels for determining the time average of the linearized temperature-dependent conduction, by time steps [17, 18] with a starting scheme /e.g. a linear Galerkin finite time-element scheme/.

The equation system of the drying space consisting of equations /11/.../16/ can be solved by the finite difference method. To do this, the hay stack is devided into layers with thickness Δz /Fig.5/. Experience shows that a simple explicite /"forward"/ scheme provides a sufficient accuracy.

In our calculations the Henderson equation of the sorption isotherms of hay

$$\varphi = 1 - e^{k\, T_f\, W^n} \qquad /17/$$

was used with values $k = 6{,}035.10^{-6}$, $n = 1{,}713$, T_f: in Kelvin /see [14], p 977 and 1030/.

SOLUTION STEPS OF THE COMPLETE EQUATION SYSTEM OF THE SIMULTANEOUS MODEL

The complete equation system of the simultaneous model is solved by the solution of the part model equation systems, coupled with proper strategy. Main steps of the solution:

1. Solution of the equation system of MFN with given external and assumed internal parameters $\rightarrow \dot{M}^{/o/}$, $\dot{M}_{cn}^{/o/}$, $X_{in}^{/o/}$.
2. Solution of the HFN equation system of the collectors using $\dot{M}_{cn}^{/o/} \rightarrow T_{D\,in}^{/o/}$
3. Solution of the equation system of the drying space, based on $\dot{M}^{/o/}$, $T_{D,in}^{/o/}$ and $X_{in}^{/o/}$, in the given /initial/ state of the material to be dried $\rightarrow T_{D,out}^{/o/}$, $X_{out}^{/o/}$.
4. Iteration from step 1 with the data obtained.

By the use of a sufficiently small starting time step the iteration may be omitted.

Temperature changes affect the MFN part model to a relatively small extent. A significant influence is exerted by changes in the thickness of the hay stack, in the values $R_{m,7-8}$, $R_{m,1-12}$ and $R_{m,10-12}$ or by a modification of the pressure source due to ΔP_s a change of the revolution number of the fan. Repeated solution of the MFN part model is prescribed only for the case of a temperature change exceeding a pre-determined threshold value or in the case of a change in one of the system characteristics specified.

In the course of the numerical solution of the equation system describing the collectors and the drying space, the "time-stepping" has an influence on the stability and economy of the calculation. The convergence and stability of the solution may require significantly differing /minimum/ time--stepping for the descriptive equation system of the two subsystems. The time-dependent $\Delta T_W/\tau/$, $T_6/\tau/$, $\Phi_1/\tau/$ and the external effects $\Phi_3/\tau/$ affect the collector directly and the drying space with some damping. The primary effects exerted on the drying space are the X_{in} as well as a stepwise change of the moisture distribution in the drying material pile when a newer /freshly mowed/ hay layer has been placed in.

Therefore it is advisable to place before the respective subroutines of the computer program a time-step selection command which takes into consideration the time-variation of the inlet air state.

The simulation of sudden changes /e.g. the storage of a fresh layer of hay/ can practically be performed by dividing /"smoothing"/ the change into one or two time-steps.

RESULTS AND CONCLUSIONS

The presented simulation procedure of a high--capacity solar hay drier-storer is very useful in the stage of the design work, e.g. in choosing favourable system characteristics /M, Ç/ and optimum control methods and parameters /M, $R_{m,7-8}$, $R_{m,1-12}$, $R_{m,11-12}$/ taking also supposed critical weather changes into account. The procedure permits to take into consideration, if necessary, also the effects of the biological heat. It offers the possibility of examining, throughout the drying period, the effects of different condition-combinations. The method may help in deciding the most economical value of M and the most favourable ratio $\dot{M}_r/\dot{M}$, depending in the state of the draying material and on the external conditions.

LITERATURE

1. Auer,W.W.: Solar Energy Systems for Agricultural and Industrial Process Drying, Development in Drying /ed. A.S.Mujumdar/ Sect.V. Science Press, Princeton, 1980.
2. Imre, L.; Kiss, L.; Környey, T.; Pallay, E. -- Szabó, I.: Solar Drying of Agricultural Products, OMFB Report /in Hungarian/, Budapest, 1979.
3. Imre, L.: Recent Results and the Current State of Research and Development of Drying in Hungary, Development in Drying /ed.: A.S.Mujumdar/, Sect.I. Science Press, Princeton, 1980.
4. Dabiri, A.E., Grossmann, G. - Bahar, F.: Experimental and Theoretical Performance Study of Solar Collectors, Proc.Int.Seminar on "Heat and Mass Transfer in Buildings", Dubrovnik, 1977.
5. Dernedde, W. - Peters, H.: Wirkungsgrade von Solar-Luftkollektoren für Trocknungsanlagen, Landtechnik 1. 1978.
6. Marschal, E. - Adams, G.: The Efficiency of Solar Flat Plate Collectors, Solar Energy 20. 413.1978.
7. Macedo, I.C. - Altemani, C.A.C.: Experimental Evaluation of Natural Convection Solar Air Heaters, Solar Energy 20.367.1978.
8. Schlag, J.H.; Ray, D.C.; Sheppard, A.P. -- Wood, J.M.: Inexpensive Solar Collectors for Agricultural Requirements, Solar Energy, 20. 89.1978.
9. Boer, K.W.: Payback of Solar Systems, Solar Energy, 20.225.1978.
10. Duffie, N.A. - Close, D.J.: The Optimisation of a Solar Timber Dryer Using an Adsorbent Energy Sorte, Solar Energy, 20.405.1978.
11. Parrot, J.E.: Theoretical upper limit to the conversion efficiency of solar energy, Solar Energy, 21.227,1978.
12. Savery, C.W. - Hofman, M.: Dynamic Modelling of Water and Air-heating Solar Collectors. Sixth Int. Heat Transfer Conf. EC-24.Toronto, 1978.

13. Imre, L. - Szabó, I.: Static and Dynamic Analysis of Dryers by the Mass and Energy Flow Network Method, Periodica Polytechnica, 18. 145.1974.

14. Imre, L. /ed./: Handbook of Drying, Chapter, 18. /in Hungarian/ Müszaki Könyvkiadó, Budapest, 1974.

15. Imre, L. - Szabó, I.: Role of Relative Transfer Factors in Controlling the Operation of Dryers, Proc. Ist Int.Symp. on Drying, Montreal, Science Press, Princeton,1978.

16. Imre, L.: Heat Transfer in Composite Devices /in Hungarian/, Akadémiai Kiadó, Budapest, /in Press/

17. Comini, G.; Del Guidice, S.; Lewis, R.W.-Zienkiewicz, O.: Finite Element Solution of Non-linear Heat Conduction Problems, Int. Journ. Num.Meth.Eng. 8.613.1974.

18. Barcza, J. - Imre, L.: Model Concept for a Transient Analysis of Non-Linear Thermo-Mechanical Systems, Int.Conf.Num.Methods in Thermal Problems, Swansea, 1979.

19. Szentgyörgyi, S. - Molnár, K.: Calculation of Drying Parameters for the Penetrating Evaporation Front, Proc. Ist Int.Symp. on Drying Montreal, Science Press, Princeton, 1978.

A SIMULATION MODEL FOR CONVECTIVE SOLAR DRYING

C.L. Gupta[1]
T.A. Reddy[2]

Tata Energy Research Institute
Field Research Unit C/o Sri Aurobindo Ashram
Pondicherry - 605002 INDIA

ABSTRACT

The solar convective drying system considered here consists of a solar air heater, a cross flow tunnel dryer, an auxiliary heat source to provide air at constant temperature to the dryer, a blower and a ducting system to allow for air recycle. A simulation model has been developed so as to maximise the solar fraction of energy input for given interface temperatures and product drying cycles spanning constant as well as falling rate regimes. However, for specified environmental conditions, the collector area has an upper bound because at no time the interface temperature can exceed the damage temperature for the product. A procedure has been indicated by which design values of environmental conditions can be specified rationally.

NOMENCLATURE

A_H = Solar collector area, m^2

A_{DI} = Dryer area for constant rate period, m^2

A_{DII} = Dryer area for falling rate period, m^2

a_D = width of dryer, m

a_{ij} = Correlation matrix elements

b_D = mean air passage opening of the dryer, m

C_p = specific heat of air at constant pressure, $KJ.K_g^{-1}°C^{-1}$

F' = Collector efficiency factor, dimensionless

F_R = Heat removal factor

f = friction factor, dimensionless

$\overline{f_D}$ = Daily solar fraction of the total hourly drying load

G = mass velocity of air stream, $K_g\ hr^{-1}\ m^{-2}$

G_s = mass velocity of dry air stream, $K_g\ hr^{-1}\ m^{-2}$

h = enthalpy of moist air per unit dry air, $KJ\ K_g^{-1}$

h_e = convective heat transfer coefficient between air and solid in dryer, $J\ m^{-2}\ °C^{-1}\ hr^{-1}$

I = Hourly Global solar radiation incident on plane of collector, $W.m^{-2}$

$\overline{I}$ = Mean monthly value of hourly global solar radiation intensity on the horizontal plane, Wm^{-2}

L_s = Rate of solid to be dried (dry basis), $K_g\ hr^{-1}$

$\dot{m}$ = mass flow rate, $K_g\ hr^{-1}$

N = Drying rate, $K_{gw}\ hr^{-1}\ m^{-2}$

n = Sun up hours in the drying cycle operation

n_w = Total number of daily hours of dryer operation

P_T = atmospheric pressure

T = air temperature, °C

$\overline{T_d}$ = Mean monthly value of dry bulb temperature, °C

$\overline{T_w}$ = Mean monthly value of wet bulb temperature, °C

V = air stream velocity, $msec^{-1}$

X = moisture content of solid (dry basis), $K_{gw}\ K_g^{-1}$

X^* = Free moisture content of solid (dry basis), $K_{gw}\ K_g^{-1}$

α = absorptance for solar radiation of solar air heater absorber plate, dimensionless

β = Solar altitude

γ = air recycle ratio, dimensionless

θ = time, hr

τ = transmittance of solar air heater glazing, dimensionless

λ = conductivity of air, $W_m\ m^{-1}\ ^\circ C^{-1}$

ν = kinematic viscosity of air, $m^2\ sec^{-1}$

ϕ = Relative humidity of air at state point 5.

Dimensionless Nos.

S_c = Schmidt No.

Nu = Nusselt No.

Pr = Prandtl No.

Re = Reynold's No.

Subscripts

a = dry air

c = Critical

D = Dryer

e = equilibrium

H = Solar heater

i = Initial

o = Final

1 = ambient single point

2 = air outlet from solar heater

3 = air outlet from air heater after recycle

4 = air inlet to dryer after auxiliary heating

5 = air outlet from dryer

INTRODUCTION

In these days of energy crisis, it is particularly advantageous to substitute conventional energy by renewable sources as far as the availability of sunshine at the place, the product drying cycle and reliability requirements of the process permit. In considering retrofitting of solar input to an existing drying system using continous cross flow tunnel dryer, it is necessary to simulate the system so that optimal solar fraction of energy input can be determined without costly trial and error. This paper is an extension of an earlier paper [1] in which economic optimisation model was developed for purely solar systems with drying restricted to constant rate period. Here we consider drying in the falling rate period as well and maximize the solar input fraction. The flow chart for the strategy adopted is shown in Fig.1.

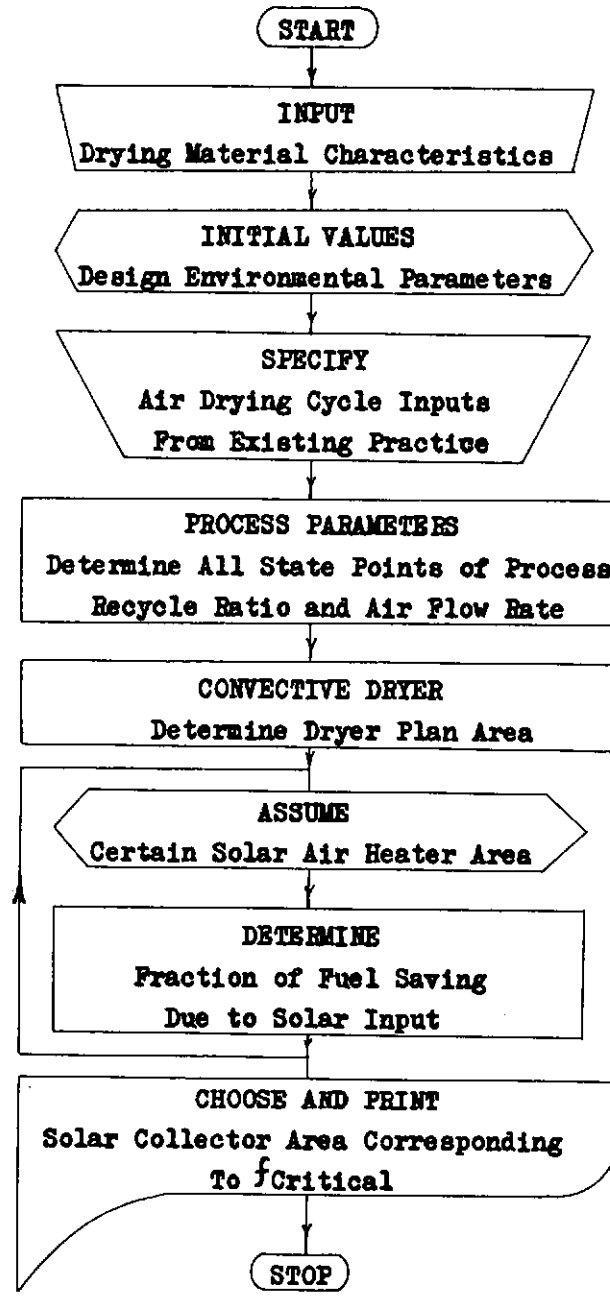

Fig.1 Master Flow Control Chart

SYSTEM CONFIGURATION

The dryer system configuration is shown in Fig.2 and the corresponding process cycle in Fig.3. During the contribution by solar radiation, the path followed is 1-2-3-4-5-2 and during sun down hours, it is 1-6-3-4-5-6 so that solar air heater is bypassed. State points 4 and 5 in Fig.3 characterize the drying system without solar retrofit and are retained. Solar air heater is to be so chosen so that the air temperature T_2,

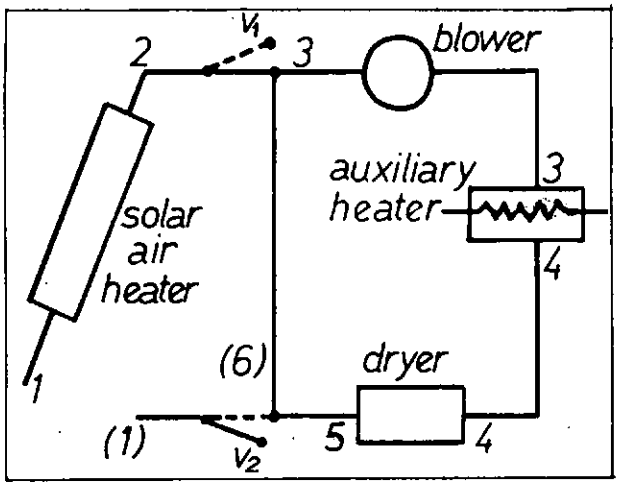

FIG.2. SOLAR DRYER SYSTEM

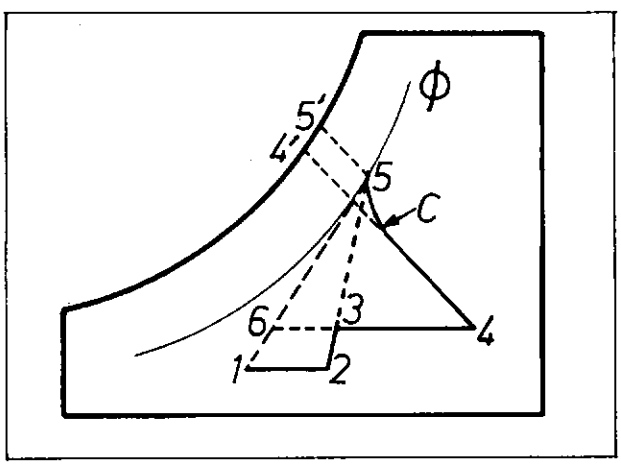

FIG.3. PROCESS CYCLE DIAGRAM

even for maximum solar radiation input, never exceeds T_4 (max), which is the temperature above which the product gets damaged. To avoid the problems of automatically switching on and off the normal fuel system (in many cases only coal/firewood for developing countries), the solar input is so decided that at design ambient conditions, T_2 is usually slightly lesser than T_4 so that fuel system is always in operation to top it up. Solar system capital costs are always additional to the existing system as the boiler/furnance capacity must be sufficient to take the full drying load after sundown hours or during cloudy/rainy days.

SOLAR HEAT FRACTION

Solar heating output temperature T_2 varies over the day and the season whereas absolute humidity is usually constant over the day but may vary from day to day. Temperature of input air to dryer is regulated by the topping up due to fuel fired supply and associated control system whereas the humidity can be controlled by recycle ratio (γ) such that

$$Y_4 = Y_1 + \gamma (Y_5 - Y_1)$$

Also

$$T_6 = T_1 + \gamma (T_5 - T_1) \qquad (1)$$

The solar input fraction on daily basis $\bar{f}_D$, is given by

$$\bar{f}_D = \frac{\sum \dot{m} (1-\gamma) C_{p1} (T_2 - T_1)}{\dot{m}_w C_{p4} (T_4 - T_6)} \qquad (2)$$

where the solar input is taken only over the sun up hours during the drying cycle and the auxiliary fuel is summed over the entire drying cycle. Quasi steady hourly basis is assumed for each of the terms. In case dryer inlet temperature, T_4 is not constant, as is the case for tobacco curing for example, the expression in equation (2) can be modified to yield

$$\bar{f}_D = \frac{\sum \dot{m} (1-\gamma) C_{p1} (T_2 - T_1)}{\sum \dot{m}_w C_{p4} (T_4 - T_6)}$$

The solar input in the numerator is calculated by the Hottel-Whillier equation[3] with the loss term being absent on account of recycle being at the collector outlet. Thus

$$q_{solar} = A_H \cdot F_R [I \overline{\tau\alpha}]$$

$$= \dot{m}_H C_{p1} (T_2 - T_1) \qquad (3)$$

for any hour. We have on combining equations (1), (2) and (3)

$$\bar{f}_D = \frac{A_H F_R I \overline{\tau\alpha}}{\dot{m}_H C_{P4}} \cdot \frac{(1-Y)}{[(T_4 - T_1) - Y(T_5 - T_1)]}$$

$$= X/Y \qquad (4)$$

where

$$X = \frac{A_H F_R I \overline{\tau\alpha}}{\dot{m}_H C_{P4}} \quad ; Y = \frac{(T_4 - T_1) - Y(T_5 - T_1)}{1 - Y}$$

Maximizing $\bar{f}_D$ over a drying season, however, may not yield an economically optimal energy system as the collectors obey the law of diminishing returns. Balancing additional collector costs against incremental savings in conventional fuel over the life of the system by standard economic procedures [3] has not been attempted here even though costing parametere have been defined in an earlier paper [1] for a restricted simulation model. Equation (4) is shown in graphical form in Fig.4.

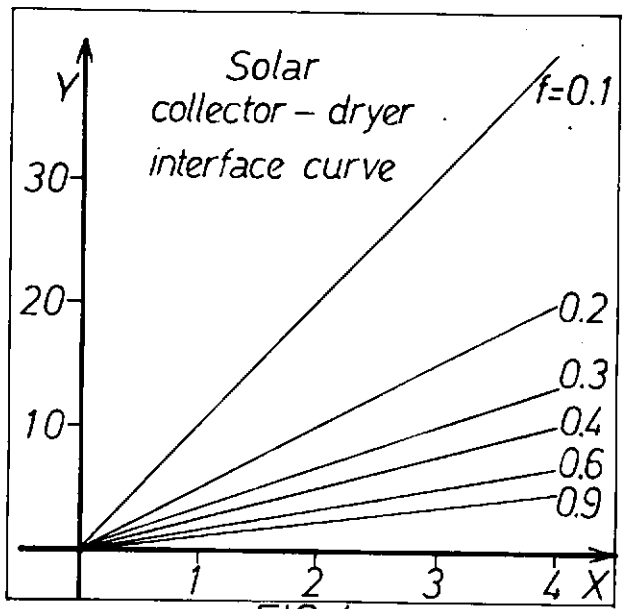

FIG.4

DESIGN ENVIRONMENTAL DATA

To correctly assess the total fuel savings by solar substitution, hour by hour analysis is normally required as mean data for single point design, as in conventional systems, is not sufficient. This is however, costly in computer time. Further, for solar drying systems, not only it is necessary to consider sets of simultaneously occuring values of T_D, T_W and I, but the maximum values must not be underestimated as there is no dissipation and overshooting of product temperature can lead to costly damages. On the other hand under heating can lead to energy wastage.

Following Anand et al. [4], we write the matrix equation

$$\underline{X}(t) = \underline{A}\,\underline{F}(t) \qquad (5)$$

where $\underline{X}(t) = \begin{bmatrix} T_D(t) \\ T_W(t) \\ I(t) \end{bmatrix}$

$$\underline{A} = [a_{ij}]_{3,3}$$

and $\underline{F}(t) = \begin{bmatrix} F_1(t) \\ F_2(t) \\ F_3(t) \end{bmatrix}$

$$F_1(t) = \overline{T_D} \cdot [A_1 \sin \omega t + A_2]$$

$$F_2(t) = \overline{T_W}\,[A_3 \sin(\omega t + \lambda) + A_4]$$

$$F_3(t) = [\bar{I}(A_5 + A_6 \cos\theta) \exp(-K/\cos\beta)]$$

Six Unknown A'S are determined by minimizing the least squared estimates of errors with respect to each of them. Elements a_{ij} of the Correlation matrix [A] have been determined for solar air conditioning systems and are being determined for the solar drying systems.

DRYER AREA DETERMINATION

The process cycle shown in Fig.3 consists of constant rate period between state points 4 and C and of falling rate period between points C and 5. Given the state properties at points 1, 2 and 4 and the material moisture properties as well as the degree of saturation of the air at the dryer exit, the state

properties at all the relevant state points can be easily calculated by standard psychrometric relations. Consequently, mass flow rate of air required can be determined from a moisture mass balance giving

$$\dot{m}_a = \frac{L_s\,(X_i - X_o)}{(Y_4 - Y_3)} \qquad (6)$$

Following the analysis of an earlier paper [1], the dryer plan area required for constant rate period drying between moisture contents X_i and X_c is obtained from a procedure detailed in Ref.[1]

$$A_{DI} = -\frac{C_{pa}}{57.5}\cdot\left(\frac{Sc}{Pr}\right)^{2/3} a_D^{0.8}\cdot b_D^{0.8}\cdot \dot{m}_a^{0.2}\cdot \left(1+\frac{Y_4+Y_c}{2}\right)\cdot \ln\left(\frac{Y_4' - Y_c}{Y_4' - Y_4}\right) \qquad (7)$$

To calculate the dryer plan are required for falling rate period i.e., A_{DII}, we make use of the characteristic drying curve concept [5]. Cross flow batch drying tests were carried out for the available rose petals to test the validity of the concept for loose leafed plant materials such as tobacco. The results, shown in Fig.5 indicate that this concept may not be true for such materials. However, scaling and application of laboratory batch cross flow drying results to full scale continuous tunnel dryer has serious limitations [7, 8]. Further, more materials need to be tested for conclusive results.

Making use of basic assumptions underlying the characteristic curve concept namely the constancy of critical moisture content and similarity of shapes of the falling rate drying curves under varying conditions of ambient drying air, we write

$$N/N_C = \exp\,(P\,X^*/X^*_C) \qquad (8)$$

where P is constant characteristic of the material and by definition

$$N = -\,(L_S / A_{DII})\,\frac{d\,X^*}{d\theta} \qquad (9)$$

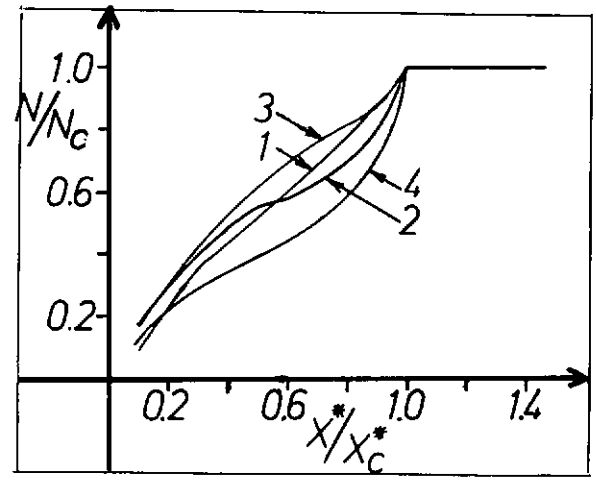

Cross flow dryer — (tray type)

—bed thickness : 20 mm.
—cross sectional area : 3.6×10^3 mm^2
—absolute humidity : 0.02 kg. per kg. of dry air

no.	inlet temperature	outlet air velocity
1	50 °C	1.5 m./sec.
2	40 "	1.5 "
3	50 "	0.7 "
4	40 "	0.7 "

FIG.5. CHARACTERISTIC DRYING RATE CURVES OF ROSE PETALS

The free moisture content X* by definition is

$$X^* = X - X_e$$

However, the equilibrium moisture content X_e, which can be determined by empirical methods [9], varies in the falling rate drying period from point C to point 5 of Fig.3 for a continuous parallel flow tunnel dryer. Representing the driving potential for mass transfer by its log mean value in the falling rate period, we can write from [6],

$$N_C = K_D \cdot LMYD \qquad (10)$$

where

$$LMYD = \frac{(Y_4' - Y_c) - (Y_5 - Y_4)}{\ln(Y_4' - Y_c) - \ln(Y_5 - Y_4)} \qquad (11)$$

and from (10)

$$K_D = \left(\frac{57.5}{C_{pa}}\right)\left(\frac{G_s}{G^{0.2}}\right)\left(\frac{Pr}{Sc}\right)^{2/3} \qquad (12)$$

for $G = \langle 2440 , 29300 \rangle$

and $V = \langle 0.6 , 7.5 \rangle$

using $G = \dot{m}_a/(a_D b_D)$

$$G_S = G/[1 + 0.5(Y_c + Y_5)]$$

and substituting equation (12) in equation (10) we get

$$N_C = \frac{57.5}{C_{pa}}\left(\frac{\dot{m}_a}{a_D b_D}\right)^{0.8}\frac{(LMYD)}{[1+0.5(Y_c+Y_5)]}\left(\frac{Pr}{Sc}\right)^{2/3} \qquad (13)$$

Substituting (9) in (8) integrating, we get

$$A_{DII} = \frac{L_S}{N_C}\cdot\frac{X_c^*}{P}\left[e^{-PX_o^*/X_c^*} - e^{-P}\right] \qquad (14)$$

Substituting equation (13) in equation (14) we get the dryer area required for falling rate period in terms of the dryer geometry and operating characteristics. Total dryer area is thus

$$A_D = A_{DI} + A_{DII}$$

SIMULATION STEPS

To maximise the solar fraction of energy input, the dryer plan area is determined from the product drying rate L_s and the air flow rate through the dryer, $\dot{m}_a$ is given by equation (6). Since the air recycle occurs at the collector exit, the flow rate through the collector $\dot{m}_H$ is given by

$$\dot{m}_H = \dot{m}_a (1-Y) \qquad (15)$$

To determine critical value of f for maximum solar fraction input after which law of diminishing returns starts the upper bound for collector area is first determined by the equation

$$A_H F_R \leq [\dot{m}_a C_{p1} (T_4 - T_1)/I_{peak}\overline{\tau\alpha}] \qquad (16)$$

Since A_H and F_R vary together because of the variation of air velocity for a given drying load and collector configuration, the f versus A_H curve is plotted for various values of A_H subject to the constraint (16) and taking into account the variation of F_R, $f_{critical}$ is then chosen, where the curve starts levelling off.

ACKNOWLEDGEMENTS

Thanks are due to Mr. B. Mohanty for determining the characteristic drying curves for rose petals.

REFERENCES

1. Reddy, T.A., Pushparaj, D. and Gupta, C.L., A design Procedure for Convective Solar Dryer, Presented at Congres Solaire International, Nice, France. 1979
2. Duffie, J.A. and Beckman, W.A., Solar Energy Thermal Processes, Wiley-Interscience, New York. 1977
3. Beckman, W.A., Klein, S.A. and Duffie, J.A., Solar Heating Design by the f-chart Method, Wiley-Interscience, New York. 1977
4. Anand, D.K., Bazkues, E.O. and Allen, R.W., Stochastic Simulation Experiments in Solar Air conditioning System, SUN, pp.1498, Pergammon, Oxford. 1978
5. Keey, R.B., Introduction to Industrial Drying Operations, Pergammon Press, Oxford. 1978
6. Nonhebel, G. and Moss, A.A.H., Drying of Solids in the Chemical Industry, Butterworths & Co., London. 1971

7. Ashworth,J.C., Use of Bench-Scale Tests for Dryer Design, Course Notes in Short Course on Industrial Drying, Montreal., July - August 1978

8. Broughton, D.B. and Mickley, M.S., Design of Full-Scale Continuous Tunnel Driers, Chemical Engineering Progress, Vol.49, n6, pp 319-324 June 1953

9. Hall, C.W., Drying Farm Crops, Lyall Book Depot, Ludhiana, India 1970

10. Treybal, R.E., Mass Transfer Operations, 2nd Edition, McGraw Hill Kogakusha Ltd., 1973

REJECTION OF SUSPENDING LIQUID FROM FINE PARTICLES BY AGGLOMERATION METHODS

C.E. Capes[1]
R.J. Germain[2]

1. National Research Council, Ottawa, Ont., K1A 0R9
2. The Steel Company of Canada, Hamilton, Ont.

ABSTRACT

Fine particles in liquid suspension can readily be agglomerated by agitation with a small amount of a second immiscible liquid which selectively wets the particles. An important application of this technique is in the treatment of aqueous slurries of fine coal. Using hydrocarbon agglomerating liquids, the fine coal particles can be recovered virtually quantitatively while the unwetted ash-forming inorganic impurities are rejected along with the water suspending phase. The technique thus recovers and dries fines by non-thermal means.

This paper presents the results of a detailed study of some of the factors affecting the retention of suspending liquid in the recovered agglomerates. The systems studied experimentally included sand suspended in hydrocarbon and agglomerated with water and coal suspended in water and agglomerated with hydrocarbon. Results for both two dimensional floc-like agglomerates and more compact three dimensional agglomerates are given. Agglomerate size and form are shown to be primary variables in determining the extent of liquid retention and the application of theories which relate bridging liquid quantity to agglomerate size and thus to suspending liquid rejection is considered.

NOMENCLATURE

A = parameter in eqn (1) related to surface component of retained suspending liquid

B = parameter in eqn (1) related to volume component of retained suspending liquid

d = particle diameter, mm

D = agglomerate diameter, mm

f = fraction of agglomerate voids occupied by bridging liquid

k = volume ratio of voids to solid in an infinite agglomerate

t = withdrawal parameter, eqn (2)

V = volume ratio of suspending liquid to solid

y = volume ratio of bridging liquid to solid

INTRODUCTION

The removal of liquid from fine solids by mechanical means is affected by many variables (1). Included are solid properties such as particle size, shape and roughness, liquid properties such as viscosity and density, interfacial properties such as surface tension and solid wettability, and the character of the external field applied, such as gravitational or centrifugal forces. The work reported here is concerned primarily with effects related to solid properties, in particular the size of the particles.

It is well known (1,2) that as particle size becomes smaller, dewatering is more difficult. Assemblies of small particles contain small channels which present greater resistance to fluid flow and inhibit drainage. Small particles have a larger specific surface and a larger number of interparticle contact points which are able to retain greater quantities of liquid at equilibrium. This situation can be improved by using a size enlargement method to increase the average size of particles being treated. One applicable method is "Spherical Agglomeration" (3) in which a small amount of a second immiscible liquid is used to preferentially wet and bridge between the particles directly in the suspending liquid. Multiparticle agglomerates are formed under appropriate agitation conditions.

The results of a detailed study of some of the factors affecting the retention of suspending liquid in agglomerates produced by immiscible liquid wetting are presented here. The systems studied experimentally included sand suspended in hydrocarbon and agglomerated with aqueous bridging liquid and coal suspended in water and agglomerated with hydrocarbon bridging liquid. Results for both two dimensional floc-like agglomerates and more compact three dimensional agglomerates are reported. Agglomerate size and form are shown to be primary variables in determining the extent of liquid retention and the application of theories which relate bridging liquid quantity to agglomerate size and thus to suspending liquid rejection is considered.

EXPERIMENTAL DETAILS

Agglomeration and drainage experiments were carried out using the sand and coal particles whose properties are given in Table 1.

Table 1 Properties of Particles

	Ottawa sand	Western Canadian bituminous coal
Weight average diameter, μm	113	41
Size distribution, μm	-149+63	50% -125+38, 50% -38
Specific gravity, skeletal	2.66	1.3
Tapped % void volume, dry	39.7	46.5
Poured % void volume, dry	48.5	56.3

Agglomeration took place in a laboratory blender for each type of particle. The sand particles were suspended as a 22 wt. % slurry in a light paraffin oil and agglomerated for 5 minutes in a blender with a plastic container using a 20 wt. % $CaCl_2$ solution as bridging agent. The bituminous coal particles were agglomerated from a 7 wt. % aqueous suspension for 5 minutes using a blender with a glass container. The bridging liquid in this case was a mixture of 25 wt. % light paraffin oil in 75% of a heavy white mineral oil and the ash content of 20% in the feed solids was reduced to 11-14% in the recovered agglomerates through the rejection of inorganic impurities (3). The choice of material for the blender container in each system was dictated by the need to prevent the bridging liquids from adhering to the walls during mixing.

The agglomerates were recovered from the suspension on a standard 8-in laboratory sieve and formed a bed less than 0.5 cm thick in all cases. A 250 Tyler mesh screen was used for the sand system while either a 100 or a 400 Tyler mesh screen was used for the coal. The sieve was attached rigidly to a laboratory vibrating feeder so that vibration could be used to drain further the bed of recovered agglomerates. Approximately 100 to 150 g of dry solids were present on the screen in the sand experiments while about 30 to 40 g of solids were on the screen during the coal experiments. The screen was vibrated for 3 minutes in the former case and for 1.5 minutes in the latter. The retained suspending liquid and the bridging liquid contents of the agglomerates were measured immediately by a distillation procedure. With the sand it was found that these analyses could be obtained with equal accuracy from the weight loss of the agglomerates on drying at 110°C with the assumption that all the bridging liquid had been adsorbed on the sand particles during agglomeration. This method of analysis was thus used for the lower bridging liquid levels in the sand experiments. In the case of the coal experiments, the ash contents of the agglomerated solids and of the tailings contained in the suspension which passed through the screen were also measured.

Prior to the screen drainage experiments described above, a portion of the agglomerated suspension was set aside for size analysis of the agglomerates. This was done by hand sieving of the agglomerates after drying from suspension at 110°C. The agglomerates tended to associate during drying and this tendency was reduced by gently shaking the container several times during the drying process. In addition, approximately 0.5 wt. % of "Tween 81" surfactant was added to the suspension as a separating agent during the drying of the sand agglomerates. Aggregates which remained after this treatment and after the hand sieving were assumed to be sufficiently bonded to be considered primary agglomerates. The dried agglomerates derived their strength from $CaCl_2$ salt bridges deposited between the sand particles and from non-volatile (at 110°C) components of the bridging oil mixture which remained in the coal agglomerates.

Fuller details of these procedures and the primary experimental results are available (4) elsewhere.

RESULTS AND DISCUSSION

It is well established (3,4,5) that several different stages of agglomeration occur as progressively larger amounts of bridging liquid are added to a particle suspension. At low levels of bridging liquid, only pendular bridges can form between particles with the result that an unconsolidated two-dimensional floc structure is produced. As larger amounts of bridging liquid are used, the funicular region of pore filling is reached, the flocs consolidate somewhat and eventually, with sufficient bridging liquid, three dimensional compacted micro-agglomerates with their interiors filled by the bridging liquid are produced. Discrete agglomerates of increasing size are encountered until the end of the capillary region of pore filling after which there is an excess of bridging liquid and pasty "lumps" of solids dispersed in the fluid bridging agent result.

The agglomerates produced in the present experiments related to the first two types, that is, two dimensional flocs and three dimensional discrete agglomerates. The results in Figures 1 and 2 show that the drainage characteristics of the low bridging liquid floc regions are quite different from those of the discrete agglomerates at higher bridging liquid levels. With small bridging liquid additions, the unconsolidated floc network structure is able to trap a large amount of the suspending liquid so that the drained agglomerates actually increase in liquid content over that of the unagglomerated feed particles. When discrete and more compact agglomerates are formed at the higher bridging liquid levels, however, the suspending liquid content of the recovered solids decreases in a monotonic fashion. It has been found (6) that with even higher bridging liquid levels beyond the capillary state, the liquid content of the drained solids may increase again when soft, pasty agglomerates are formed, capable of coalescing with each other and trapping larger amounts of suspending fluid.

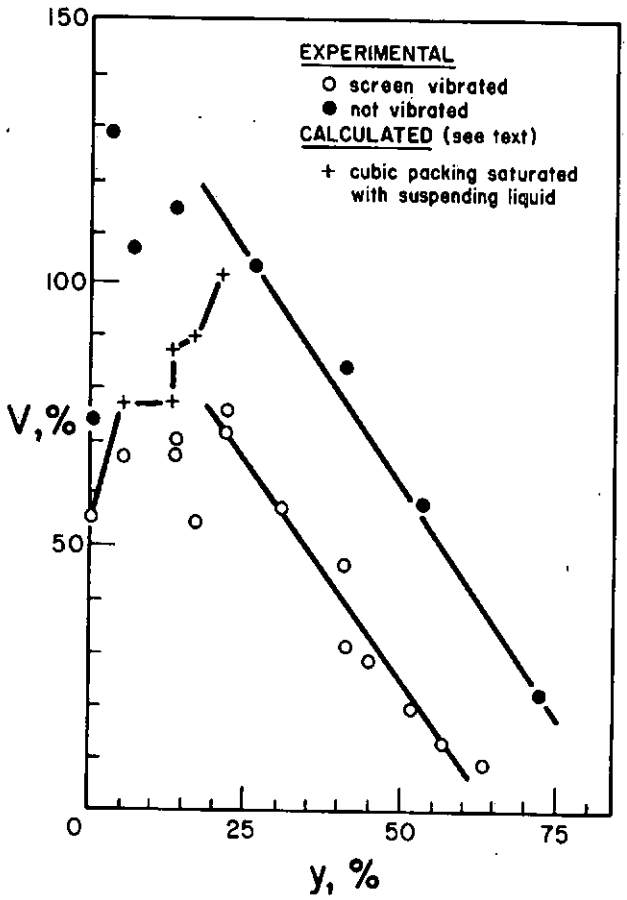

Figure 1 Suspending liquid retention versus bridging liquid concentration for sand agglomerates

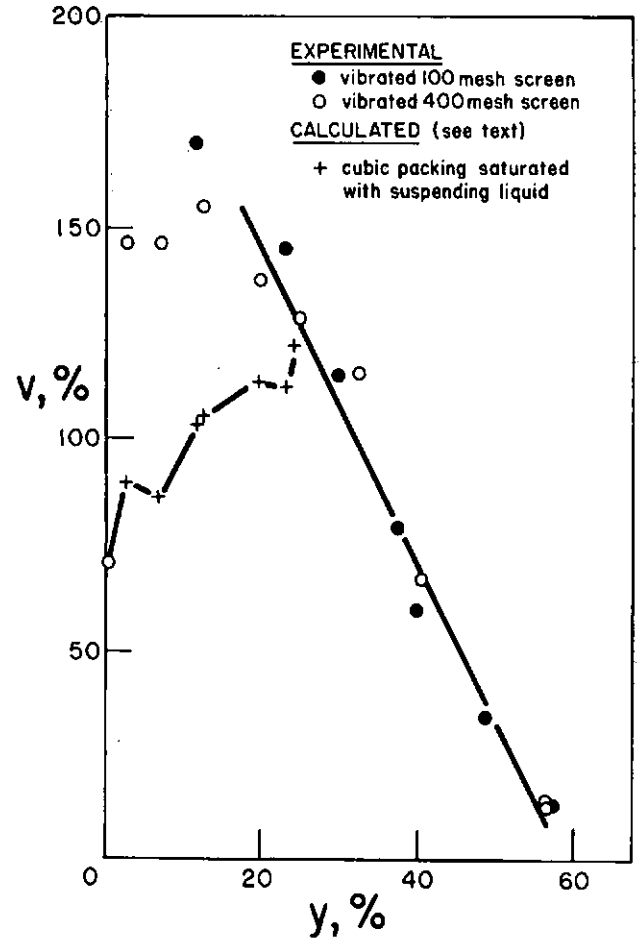

Figure 2 Suspending liquid retention versus bridging liquid concentration for coal agglomerates

If the amount of suspending fluid retained by a bed of particles or agglomerates can be considered to consist of two components, one of which is a constant proportion of the volume of the agglomerate and the other is related to its surface area, eqn (1) results (7,8) to link the amount of retained fluid with the agglomerate size:

$$V = \frac{A}{D} + B \qquad (1)$$

where V is the volume ratio of suspending liquid to solid, D is the agglomerate diameter and A and B are parameters related to the surface and volume components, respectively, of the retained suspending liquid. Equation (1) is tested for the sand and coal data in Figures 3 and 4, respectively. These figures show that V is indeed proportional to the agglomerate surface area (represented by I/D) for discrete agglomerates. With these agglomerates, the bridging liquid occupies the bulk of the interior pore space, displacing the suspending liquid primarily to the agglomerate surface. With the smaller flocculated agglomerates, suspending liquid retained within the aggregate interior plays a greater rôle, as discussed further below.

Figures 3 and 4 emphasize the importance of the size of the entities making up a particle bed in determining the amount of liquid retained by the bed. Agglomerate size is, in turn, determined by the amount of bridging liquid used in their formation. Agglomerate size and bridging liquid concentration can be related by the theoretical models of Sherrington (9) and Butensky and Hyman (10). Both of these models have been shown to apply to small "seed" granules (e.g. up to about 2 mm diameter) produced in a drum agglomerator and are based on similar assumptions. The Sherrington equations are used here because of their greater simplicity. Spherical agglomerates composed of monosized particles of diameter d are assumed to have their interior voids essentially saturated with bridging liquid but the bridging liquid is assumed to be withdrawn by capillarity to a depth, td/2, into the interstices between the surface particles, where t is a "withdrawal parameter". The agglomerates are considered to grow only until they attain this "surface-dry" state for, if this were not the case, it is postulated that the agglomerates could continue to grow by the attachment of particles onto their surfaces through coalescence and wetting by

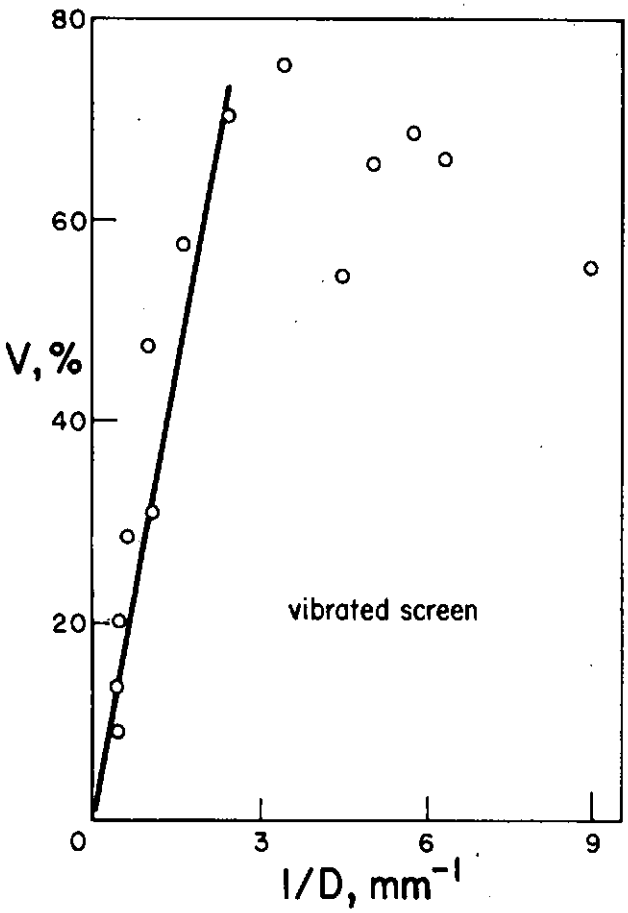

Figure 3 Suspending liquid retention versus reciprocal agglomerate diameter for sand agglomerates

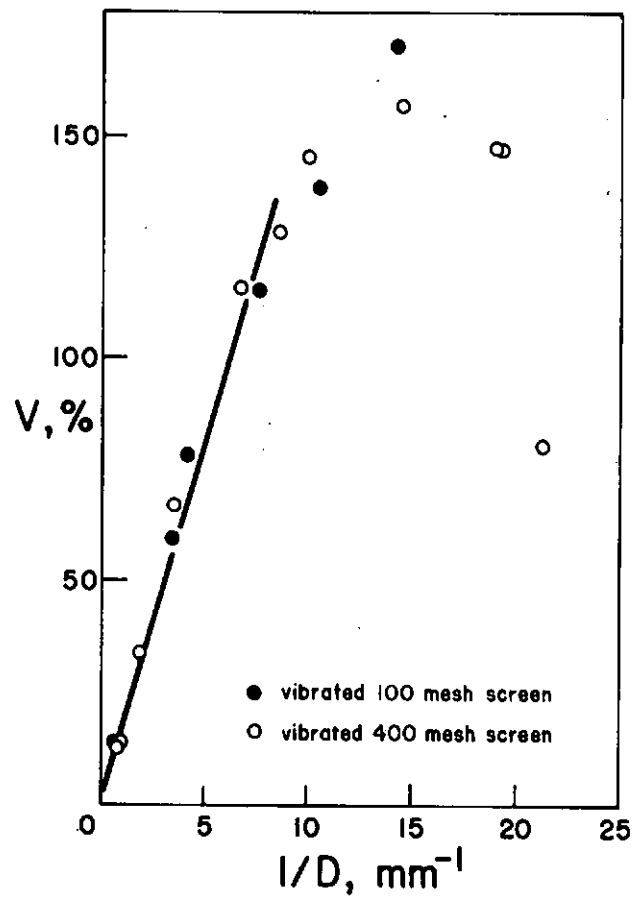

Figure 4 Suspending liquid retention versus reciprocal agglomerate diameter for coal agglomerates

exposed bridging liquid. Geometrical considerations lead to eqn (2) for the bridging liquid requirements of such an agglomerate:

$$y = f\,k\,(1 - \frac{3td}{D}) \qquad (2)$$

where y is the volume ratio of bridging liquid to solid, k is the volume ratio of voids to solid in an infinitely large agglomerate, D is the agglomerate diameter and f is the fraction of voids occupied by bridging liquid (i.e. (1-f) of the voids are occupied by air or suspending liquid).

The sand and coal data are plotted as y versus $(\frac{d}{D})$ in Figures 5 and 6 to test eqn (2). The linear relationship expected between these variables according to eqn (2) is seen to be an adequate representation of the experimental data although the large and small agglomerates form lines of different slopes. The Sherrington model cannot be expected to represent agglomerates of diameter less than 3 or 4 times the particle diameter since the assumption of spherical agglomerates used in deriving the model cannot apply to aggregates containing such a small number of primary particles. Thus a least squares straight line was fitted to the data in each of Figures 5 and 6 only for the points with $(d/D) \leq 0.33$. The fitted parameters for eqn (2) are given in Table 2. By definition, t should be a reasonable fractional

Table 2 Parameters in eqn (2) from fitting of data in Figures 5 and 6 for $d/D \leq 0.33$

	Sand data	Coal data
Withdrawal parameter, t	0.92	0.63
Bridging liquid saturation, f:		
with k based on tapped porosity, Table 1	0.99	0.69
with k based on loose porosity, Table 1	0.68	0.46

number (9) and probably close to 1 (10). The present data fall within these limits. The bridging liquid saturation parameter, f, might be expected to have a value close to 0.9 as has been found (11) for tumbling agglomeration. The low values found here (in Table 2) for coal may be related to the wetting properties of the coal particle surfaces and the fact that inorganic contamination (ash constituents) may tend to retain relatively larger amounts of suspending liquid in the inner voids, leading to reduced

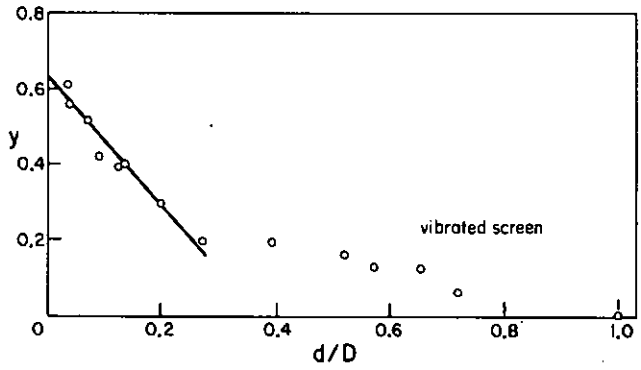

Figure 5 Agglomerate size data for sand plotted according to eqn (2)

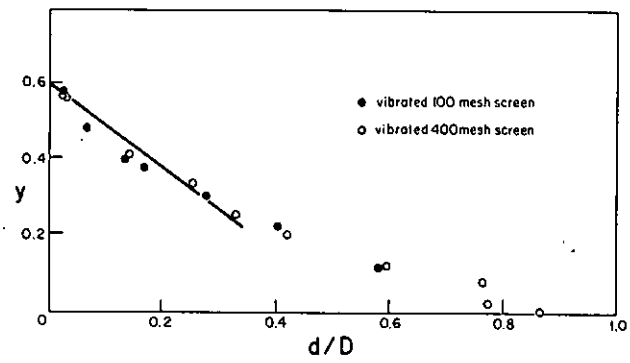

Figure 6 Agglomerate size data for coal plotted according to eqn (2)

f-values.

For the discrete and more compact agglomerates formed at the higher bridging liquid levels used in these experiments, eqn (1) and (2) provide the relationships needed to describe the results noted previously in Figures 1 and 2. If these equations are combined with the elimination of the agglomerate size, D, a linear reduction in the suspending liquid content, V, is predicted as the bridging liquid concentration, y, is increased (8). Figures 1 and 2 show that such a linear reduction is observed experimentally when discrete sand and coal agglomerates are drained by gravity and vibration on a screen.

The experimental results have demonstrated that the small floc-type agglomerates at low bridging liquid levels behave quite differently from the larger discrete agglomerates formed at higher bridging liquid concentrations. The models represented by eqn (1) and (2) do not apply to these smaller agglomerates. In addition, they follow a reverse trend to the drainage relationship for larger entities in Figures 1 and 2 with the amount of retained suspending fluid increasing as the bridging liquid amount is increased and larger agglomerates are formed. The situation is similar to that found when polymeric flocculants are used to treat fine particles in liquids (12). The flocculated particles tend to stick to each other as they settle and form a loose, bulky layer. The pores in the settled layer are relatively large and its filtration and drainage rate is thus enhanced. On the other hand, the high porosity of the settled layer means that a larger proportion of suspending medium is retained by the flocs than is the case with the untreated particles.

Floc-type agglomerates will generally contain only a small number of ultimate particles compared with the larger, more compact three-dimensional agglomerates. It has already been noted that the Sherrington model, assuming a spherical agglomerate, cannot be expected to apply for agglomerates of diameter less than 3 or 4 times the particle diameter. The smaller floc agglomerates are thus expected to contain of the order of two up to 3^3 ultimate particles. In an attempt to model the characteristics of these small aggregates, calculations were performed on assumed regular structures containing various numbers of monosized spherical particles. Two regular packing arrangements were chosen for these structures, cubic packing and hexagonal close packing to represent open and close packing, respectively. For each ideal agglomerate, calculations of bridging liquid volume to solid volume (variable y in eqn (2)) were performed for the four different states of bridging liquid shown for cubic packing in Figure 7. A volume equivalent diameter was also calculated for each agglomerate, defined as the diameter of a sphere having a volume equal to that of an envelope enclosing the extremities of the agglomerate. The results of these calculations (which were done with the aid of macromodels composed of plastic balls) are shown in Figures 8 and 9 for cubic and hexagonal close packing, respectively. Further details of the calculations can be found in reference (4).

It is seen that the calculations using cubic packing in Figure 8 most closely approximate the experimental data. The assumed cubic structures with saturated internal voids is similar to the Sherrington (9) model for "surface dry" agglomerates and, as might be expected, yields a curve in Figure 8 which is quite close to the experimental sand data for the larger agglomerates. For the smaller floc-type agglomerates at low bridging liquid levels, the pendular-bonded structures are an acceptable representation. Although the theoretical calculations fall somewhat below the experimental data in this region, both theory and experiment indicate a significant change in slope as the agglomerates progress from three dimensional compacts to flocs. This change in slope is related, in part, to the fact that the size of an aggregate changes more rapidly for small aggregates than for larger agglomerates as more particles are added to the structure. At the same time, the bridging liquid associated with the solids is increasing more slowly for the small aggregates due to the smaller volume of

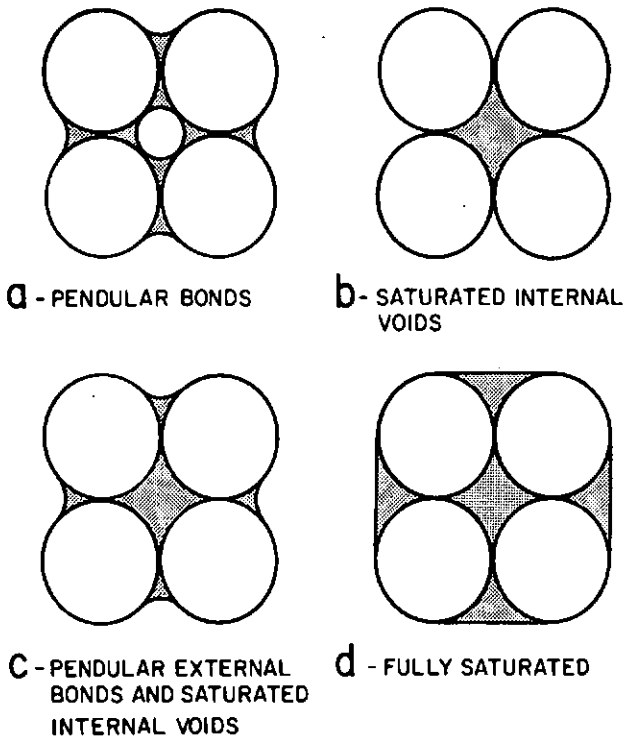

Figure 7 Four states of bridging liquid saturation used in calculations with regular packings

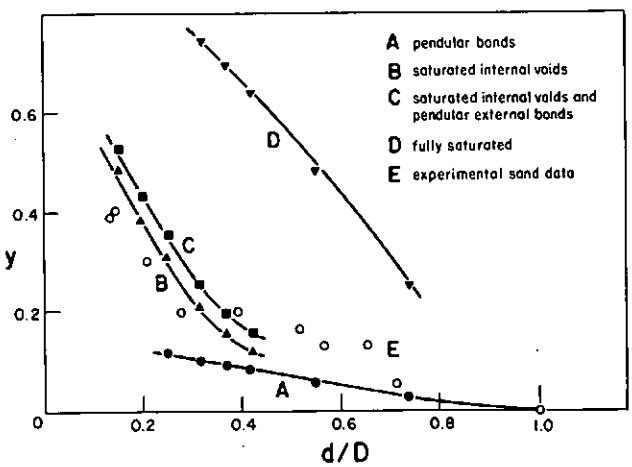

Figure 8 Agglomerate size relationships calculated for cubic packing

pendular bonds compared with saturated capillary bonds. This also contributes to the reduced slope of the curves in the floc region.

The calculations of liquid/solid ratio for aggregates with cubic packing and completely saturated voids (Figure 7d and curve D in Figure 8) also provide a useful indication of the mechanism

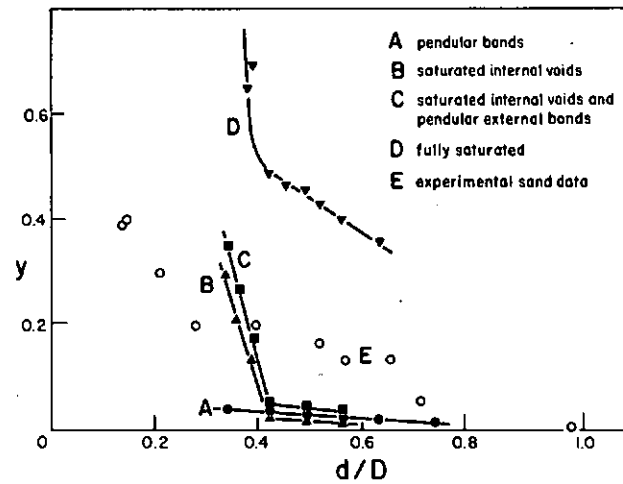

Figure 9 Agglomerate size relationships calculated for hexagonal packing

of suspending liquid retention in the floc region. It may reasonably be assumed that the highly porous structures formed in this region, when drained on a screen, are completely saturated with suspending liquid and pack on the screen with porosity similar to that of the unagglomerated particles. Accordingly, for agglomerates with d/D greater than 0.3, the suspending liquid retained by an agglomerate of a given size was calculated as the saturated liquid/solid ratio from curve D in Figure 8, less the bridging liquid/solid ratio found in the experiments to be needed to produce agglomerates of that size. The resulting value was then added to the experimental liquid retention for the unagglomerated particles to give a measure of the suspending liquid/solid ratio of the drained agglomerates in the floc region. The results of these calculations are included in Figures 1 and 2 for comparison with the experimental data. The calculated curves predict the upward trend in the amount of retained liquid in the floc region and, for the sand experiments, give estimates between the experimental results for the vibrated and non-vibrated beds. For the coal experiments, the result is less satisfactory in that the calculated curve lies well below that found in practice. This means that the finer coal particles, when flocculated with small amounts of bridging liquid, form structures with porosities greater than that of cubic packing. They may also settle with inter-agglomerate voidage greater than that of the untreated particles. Such large porosities are not uncommon in flocculated systems (13). The finer coal particles would be expected to yield flocs of greater porosity than the coarser sand particles since the pendular bonds formed with the bridging liquid would be stronger in the former case and would therefore be more resistant to reorientation and compaction to lower porosities.

CONCLUSION

Two distinct regions exist when considering the amount of suspending liquid retained by agglomerates formed by immiscible liquid wetting. At low bridging liquid levels, increasing amounts of suspending fluid are retained as the size of the floc-like aggregates increases. This trend is predicted by calculations based on cubically packed aggregates saturated with suspending liquid. With higher levels of bridging liquid, three dimensional agglomerates saturated with the bridging liquid are formed. These exhibit a linear decrease in suspending liquid as bridging liquid is increased, a trend which is correlated by existing empirical models of agglomerate growth and drainage characteristics.

ACKNOWLEDGEMENT

This study was carried out at NRCC while R.J.G. was an M.Sc. student at the University of Waterloo. The authors thank Professor P.L. Silveston for his interest and guidance throughout the work.

REFERENCES

1. Ives, K.J. (ed.), The Scientific Basis of Filtration, NATO Advanced Study Institutes Series E, vol. 2, 1975.
2. Wakeman, R.J., Filtration Post-Treatment Processes, Chemical Engineering Monographs, vol. 2, Elsevier, Amsterdam, 1975.
3. Capes, C.E., McIlhinney, A.E. and Sirianni, A.F., Agglomeration from Liquid Suspension - Research and Applications, In K.V.S. Sastry (ed.), Agglomeration 77, A.I.M.E., New York, pp. 910-930, 1977.
4. Germain, R.J.L., Suspending Liquid Rejection from Agglomerates Produced by Spherical Agglomeration, M.A.Sc. Thesis, University of Waterloo, 1977.
5. Capes, C.E., Particle Size Enlargement, Elsevier, Amsterdam, 1980.
6. Capes, C.E., Smith, A.E. and McIlhinney, A.E., Method of Displacing Liquid Suspendant of a Particulate Material Liquid Suspendant Mixture by Micro Agglomeration, Canadian Patent 1020880, Nov. 15, 1977.
7. Capes, C.E., McIlhinney, A.E., Sirianni, A.F. and Puddington, I.E., Agglomeration in Coal Preparation, Proc. Inst. Briquet. Agglom., 12, 53 (1971).
8. Capes, C.E., McIlhinney, A.E., McKeever, R.E. and Messer, L., Application of Spherical Agglomeration to Coal Preparation, Int. Coal Prep. Conf., Proc., 7th, Sydney, Aus., 1976.
9. Sherrington, P.J., The Granulation of Sand as an Aid to Understanding Fertilizer Granulation, Chem. Eng. (London), No. 220, C.E. 201, July/Aug (1968).
10. Butensky, M. and Hyman, D., Rotary Drum Granulation. An Experimental Study of the Factors Affecting Granule Size, Ind. Eng. Chem. Fundam., 10, 212 (1971).
11. Capes, C.E. and Danckwerts, P.V., Granule Formation by the Agglomeration of Damp Powders, Trans. Instn Chem. Engrs, 43, T116 (1965).
12. Yusa, M. and Gaudin, A.M., Formation of Pellet-Like Flocs of Kaolinite by Polymer Chains, Am. Ceram. Soc. Bull., 43, 402-406 (1964).
13. Michaels, A.S. and Bolger, J.C., Settling Rates and Sediment Volumes of Flocculated Kaolin Suspensions, Ind. Eng. Chem. Fundam., 1, 24 (1962).

DISPLACEMENT DRYING WITH FLUOROCARBON SOLVENTS: A STATUS REPORT

T. DEVINE

DU PONT DE NEMOURS INTERNATIONAL S.A., GENEVA, SWITZERLAND

ABSTRACT

Displacement drying by means of fluorocarbon solvents in specially designed systems is widely used in Europe. This paper examines in detail specific applications in the electronic, jewellery, optical and mechanical industries giving cost justifications for the process. Systems under consideration vary from bench models to fully automated systems.
The paper closes with a look to the future and includes potential applications involving spray drying and in line drying systems.

INTRODUCTION

In their paper at the First International Symposium on Drying Brandreth and Johnson Jr. described the mechanism of displacement drying using a fluorocarbon solvent. Competitive advantages of this system and its associated equipment were also discussed. This paper will examine in detail commercial applications already existing in Europe, where displacement drying is proportionately more established than in any other part of the world.

PRINCIPLES OF OPERATION

The "Freon" Solvent Drying System based on FC-113 (trichlotrifluoroetane) simultaneously removes and disposes of water together with its soluble contaminants as water without evaporation or mixing with other materials. "Freon" T-DF is immiscible with water and its density is 50% greater than water. As a result, water is removed by gravity displacement from surfaces immersed in the drying fluid.
The hydrophobic surfactant contained in the drying fluid acts in two ways to detach the water droplets from the surface to be dryed. Firstly, it preferentially wets the substrate with solvent and repels water allowing the heavier immiscible solvent to "get under" the water. Secondly it reduces the interfacial tension of water against the immiscible solvent to the point that water droplets deform and break away from the surface. Freed water rises to the surface where a simple gravity separation disposes of it. Mechanical or boiling agitation is employed to speed the process.

COMMERCIAL SYSTEMS

Simple equipment similar to a familiar two or three stage vapour degreaser forms the basis of the "Freon" solvent drying system illustrated in Figure 1. Water is removed by immersing parts in the "Freon" T-DF drying fluid in the drying sump. There the water film rolls up rapidly into large droplets which float away to the surface of the solvent and over a weir to the water separator. After a short time (30 to 120 seconds) in the drying sump residual drying fluid is removed by immersion of the parts in clean boiling "Freon" TF (pure FC 113) in the sump or sumps depending on the application. Parts are raised to the solvent boiling temperature (48°C) in the vapour zone and residual solvent evaporates as the parts enter the freeboard area above the vapour zone. The parts emerge dry, spot-free and ready for further processing.

Figure. 1

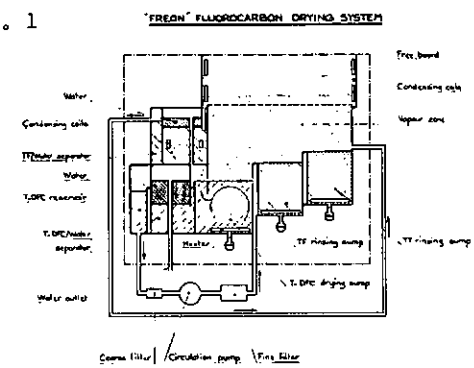

The previous method of drying - Lenses were rinsed in ethyl alcohol, white spirit and trichloroethylene. Drying was done manually with cloths.
Major disadvantages of previous system - Output and quality were irregular.
Major advantages of displacement system - Consistently high standards of finish, together with up to 50% savings in time.
Amortization of displacement drying system - 15 months.

Case History 4. - GOLF BALLS

The displacement drying process - Figure 2 illustrates the use of one property of the drying fluid to conveyorise a standard system. Since the drying fluid at S.G. 1.56 is heavier than the golf balls the latter are fed via a hopper into the machine where their own weight force them under a baffle in the drying sump. On rising to the surface a paddle conveyor carries them into the succeding rinse sumps using the same ducking/flotation principle. The unit has a capacity to dry 7.000 balls per hour.
The drying requirement - Manufacture of golf balls involves a lengthy and complicated process of which the most important sequences are moulding, spue grinding and curing of the rubber and plastic materials, painting, grading and lacquering. Drying takes place after the golf ball has been cured and is ready for painting. To achieve an optimum coating, the balls have to be perfectly clean and dry. The balls are abraded after curing and water rinsed for some minutes before passing to the drying process.
The previous method of drying - Batch drying in acetone.
Major problems with previous system - Hazardous conditions due to flammable nature of the drying fluid. Necessitated a flame proof section in the workshop. In addition a special venting system was necessary to meet occupational health requirements.
Major advantages of the displacement system - Two major hazards eliminated, viz. fire and toxicity. In addition the introduction of the displacement system with its automated process permitted the building of an in line conveyor system eliminating bottlenecks that had occured with the previous system due to balls having to be transported batchwise from one end of the factory to the other.
Amortization of displacement drying system - 9 months.

Figure 2 AUTOMATED GOLF BALL DRYING SYSTEM

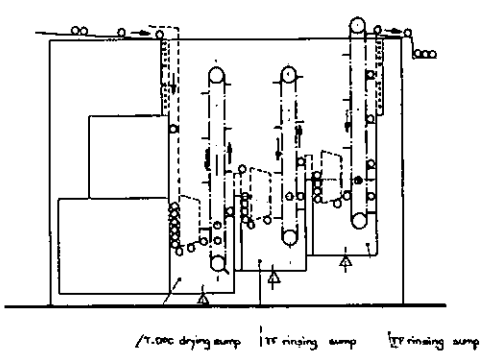

Case History 5. - ELECTROPLATING INDUSTRY - METAL & PLASTIC PARTS

The displacement drying process - Typical parts, including steel umbrella rods and plastic caps for perfume bottles, are automatically processed through either of 2 units of two stages i.e. drying in T-DF with single rinse in "Freon" TF. These are among the largest units in use, one with each sump measuring 600 x 400 x 900 mm and the other with each sump measuring 2000 x 520 x 920 mm. The total drying time required is three minutes. Carried on plating racks of 150 x 480 units at a time or 50 - 160 units at a time, depending on their size, over 1 million steel umbrella rods and 5 million plastic caps are produced annually.
The drying requirement - The drying units are fully integrated into an automated production line with a total cycle time of 2.5 hours for the electroplating process. After electroplating the parts are rinsed with water to remove plating salts and then require spot free drying.
Previous method of drying - Deionised water at 60°C.
Disadvantages of previous drying method - The demineralized water rapidly became contaminated and often caused spotting before being discarded. In addition working at 60°C presented a problem when plastic caps were introduced since these were made mainly from ABS plastic for which the critical temperature, with respect to melting, is around 60°C.
Advantages of displacement drying - Consistent, spot free drying and no harmful effects to the plastic since the boiling point of FC 113 is 48°C. Substantial savings in labour cost were achieved due to the integration of the displacement drying process into the fully automated production line, which was not the case with the previous method.
Amortization of the displacement drying system - 9 months.

DISPLACEMENT DRYING BY MEANS OF SPRAYS

Finally, a look at the latest techniques developed for displacement drying which are intended to further increase its appeal. Figure 3 illustrates the operation of a spray displacement drying system intended for the drying of steel wheel rims. Particular features to note with respect to other displacement systems described above are:

1) The installation is sunk into the ground to reduce head room requirements.
2) The rims are each 45 kgs in weight, of varying diameter and are loaded 6 at a time, in pairs, on 3 telescopic conveyor legs
3) To prevent turbulence in the vapour zone in the condensing area (and so reduce resultant solvent loss) a cover, fixed to the conveyor legs, is positioned just above the spray area. It should be noted that to avoid the solvent loss piston action of this cover it has been

The operation of the dryer provides a continuous supply of freshly distilled drying fluid for rinsing and the hydrophobic surfactant is retained in the drying sump with the "Freon" T-DF. The floating displaced water is skimmed from the surface of the drying sump by circulating drying fluid and collects in the water separator where it drains out by gravity. This effluent water contains essentially no fluorocarbon solvent due to low solubility in water and proper machine design to minimise entrainment. The low boiling point of FC 113 and low water solubility in FC 113 assure very low moisture levels in the rinse sump.

Because "Freon" T-DF contains less surfactant then earlier drying fluids it is more easily rinsed from surfaces. This improvement allows construction of simpler equipment whereby the rinsing step is effected by a spray over the drying sump thus minimising floor space requirements and facilitating automation of the process.

Indeed, in large systems under review for commercial consideration the drying stage, as well as the rinsing, is effected by sprays in a one sump unit. This will be discussed in more detail at the end of the paper.

The low running costs of the system described above essentially derive from the following:

a) Energy requirements are extremely low since FC 113 (B.P. 48 °C) has a latent heat of vaporisation of 146.5 kJ/kg
b) Cooling water requirements (if refrigerated cooling or a heat pump are not used) are also comparatively low (between 8-12 l/minute)
c) Make up losses derive from two sources, diffusion and drag-out, but both of these can be minimised in properly designed machines.

COMMERCIAL APPLICATIONS:

In use in Europe for over a decade, displacement drying using fluorocarbon solvent is finding increasing acceptance in a wide range of end use applications as Table 1 shows:

TABLE 1

ESTIMATED USE OF "FREON" FLUOROCARBON DRYING SYSTEMS BY END USE

a) MECHANICAL INDUSTRY - 46 %

- JEWELLERY
- WATCHES AND CLOCKS
- MINTS AND MEDALS
- METAL PARTS (TOOLS)
- CONSUMER PARTS (LIGHTERS, BALL POINT PENS)
- CUTLERY
- MEDICAL INSTRUMENTS
- HYDRAULIC CIRCUITS AND VALVES
- BEARINGS

b) ELECTRONIC INDUSTRY - 28 %

- PRINTED CIRCUIT BOARDS (AFTER THROUGH HOLE PLATING)
- RELAYS
- THRYSISTORS
- SEMI CONDUCTORS
- ELECTRONIC COMPONENTS
- ELECTRONIC CONTROLS AND INSTRUMENTS
- TV TUBES
- ELECTRONIC ASSEMBLIES

c) OPTICAL INDUSTRY - 17 %

- SPECTACLE FRAMES
- SPECTACLE LENSES
- INSTRUMENTS
- FILMS
- CAMERAS

d) ELECTROMECHANICAL - 3 %

- COUNTERS
- COPIERS
- ELECTRIC MOTORS

e) OTHERS - 6 %

- GOLF BALLS
- NON OPTICAL GLASS

The wide range of end use illustrated above has been made possible by some combination of the following reasons:

FC 113 displacement drying offers these characteristics -

1. High speed system, results in compact, space saving equipment.
2. Capable of handling heavy water loads (over 10% by volume) with no loss of drying efficiency or system capacity.
3. Effectively can handle small parts in bulk to permit conveying in baskets between operations with resultant labour savings.
4. Can be safely used with most metals, plas-

tics, elastomers and composite assemblies due to low temperature, high stability and extreme mild solvency power.
5. Consistent spot-free drying.
6. Low energy consumption.
7. Emerging parts are cool enough to be handled immediately after drying.
8. Drying fluid is low in toxicity (T.V.A.-1000 p.p.m.).
9. Drying fluid is nonflammable.

CASE HISTORIES

A detailed look at 5 case histories will better illustrate the advantages of fluorocarbon displacement drying systems over other potentially hazardous, labour intensive, energy consuming systems in use today:

Case History 1. - ELECTRONIC INDUSTRY - CERAMIC SUBSTRATES

The displacement drying process - The substrates are processed manually in a standard unit placed in a clean-room. Total process time is 6 minutes and baskets contain up to 200 substrates at a time.
The drying requirements - Machined ceramic microstrip substrates are prepared in clean room conditions for vacuum deposition. Imperfect adhesion caused by dirt or moisture in ceramic pores risk costly rejects in subsequent plating operations. The substrates are cleaned in ultrasonically agitated, non alkakine detergent/water emulsion and rinsed in water prior to drying.
Previous method of drying - Dry nitrogen air-gun blow off. Other methods were evaluated including absorbtion, but all were found to have insufficient water removal capabilities.
Disadvantages of previous system - Unreliable, leading to high reject rates.
Advantages of displacement drying system - Consistent spot-free drying leaving no trace of moisture on the substrates. The unit is compact and easy to maintain.
Amortization of the displacement drying system - 6 months.

Case History 2. - JEWELLERY INDUSTRY

Drying of decorative chains, bracelets and watch bands.
The displacement drying process - Racks carrying the jewellery are suspended within the drying sump from an electrically operated pulley. Water removal is achieved through immersion in the drying sump. To aid water removal from minute holes or chain links the boiling action of the drying fluid and the surface sweeping spray are supplemented with a constant vertical movement of the pulley. Residence time in the drying sump averages one minute depending on the articles. The racks are subsequently transported for the equivalent periods of time to two rinse sumps of boiling FC 113.
The drying requirement - Jewellery, following plating in gold, nickel, silver, rhodium and chrome must be rinsed to remove plating salts and subsequently spot free dried before inspection and packing.
The previous method of drying - Manually drying in sawdust sometimes followed by rinsing in petroleum spirit. Subsequent rubbing with cloth to remove water stains or residual sawdust.
Major disadvantages of previous drying method - Incomplete elimination of water between links of a chain or cavity. As a result there is a risk of residue and subsequent corrosion. Surface scratching of the jewellery often occurs when it is taken out of the sawdust. In addition the operation is labour intensive. Physical damage results in about 10% more work in retouching. Explosion danger using petroleum spirit.
Major advantages of the displacement drying system
- Surfaces are completely dry and stain free after only 3 minutes.
No waste, no rework.
Saving of manpower: a) At least two people formerly used for final inspection and removal of stains. b) Several people formerly needed to remove the goods from the sawdust after drying.
Time saving: a) no need to transfer the goods from the electroplating racks to the drying racks. b) through greater flexibility in manufacture. Consequent savings in wages and better use of manpower.
Amortization of displacement drying system - 6 months.

Case History 3. - OPTICAL INDUSTRY - CAMERA LENSES

The displacement drying process - This particular system in practice differs a little from the standard unit shown in Figure 1. The high quality lenses are transported by an overhead conveyor in specially designed baskets which facilitate draining and allow for minimum contact area between the lenses and the baskets.
Firstly the lenses, up to 60 at a time depending on the diameter which varies from 5 to 50 mm, are immersed in the boiling "Freon" T-DF to remove water. In an adjoining ultrasonic vapour degreaser the drying agent residues are removed in three steps all working with "Freon" TF: immersion in boiling solvent, followed by a cold sump with ultrasonic agitation, and a rinse in the vapour zone. The lenses then leave the integreated equipment dry and clean. The "scrubbing" action of the ultrasonics ensures that every last particule of surfactant is removed - essential practice since the lenses are subsequently coated.
The drying requirement - In the course of production optical lenses are subjected to a number of contaminants, such as cement used for fixing on grinding machines and manual handling in general. Thorough cleaning is therefore required prior to quality control and before the lenses are built into the cameras. The two units prior to the displacement drying are boiling solution of trichloroethylene to remove residues of cement and lacquer and then ultrasonic aqueous cleaning and rinsing in water. The lenses now require spot free drying.

designed to descend and rise with open flaps.

4) Once in position in the spraying chamber the wet wheels are dried with a spray of "Freon" T-DF for 20 seconds.
5) The sump stop momentarily, the T-DF valve closes and the "Freon" TF valve opens.
6) The wheels are rinsed in TF for 10 seconds and then spraying stops.
7) The wheels are removed slowly through the vapour blanket to the unload position.
8) The total cycle time from load to unload is 2 minutes.
9) The complete system is automated including the displacement drying process.

CONCLUSION

The above case histories demonstrate the wide applications of displacement drying, supplanting a wide variety of previous methods of drying, showing two and more major advantages with very low amortization periods being realized for the installation.

There are over 600 "Freon" fluorocarbon drying systems in operation in Europe ranging from 40 litres in capacity to several thousands litres. Vapour degreaser based systems will continue to be installed depending on application, but the new generation of spray drying systems will undoubtedly increase the use of fluorocarbon displacement drying particularly for large parts in the metalworking industry.

Figure 3

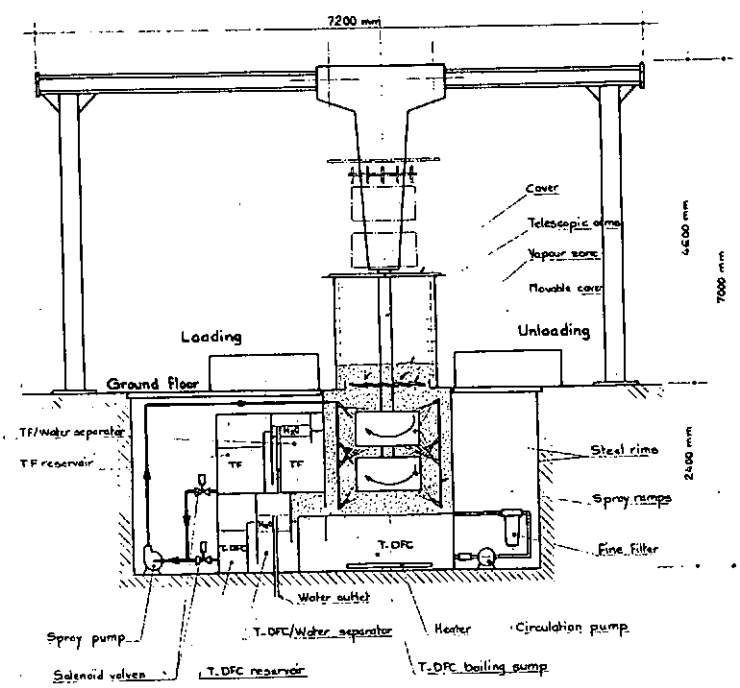

DRYING CYCLE FOR STEEL RIMS

- Loading : 40 s
- Spray T-DFC : 20 s
- Spray TF : 20 s
- Unloading : 40 s

TOTAL CYCLE : 2mn

THE REMOVAL OF SOLVENT FROM NITROCELLULOSE/NITROGLYCERINE MIXTURES

R.P. Ayerst

Propellants, Explosives and Rocket Motor Establishment
Waltham Abbey, Essex, England

ABSTRACT

Propellants for rockets and guns are formulated using nitrocellulose and nitroglycerine mixtures and solvents need to be dried out in the course of manufacture. Little information has been published on the topic. The solvent removal does not follow Fick's law of diffusion but the results of drying trials for a wide range of compositions and solvents may be correlated by an empirical relationship. The effect of temperature is discussed and the concept of increasing the drying rate by removing the solvents under water at higher temperatures is considered.

NOMENCLATURE

a = radius of granule (mm)
C = solvent concentration (kg/m^3)
D = diffusion coefficient
D_o = base value of diffusion coefficient
E_d = energy of diffusion KJ/mol
K = constant
l = diffusion path length (m)
M_o = mass of solvent in propellant at time 0 (kg)
M_r = " " " " " " " t
M_t = " " " " " " " t
n = empirically determined exponent
r = radius of spherical particle
R = gas constant
t = drying time (h)
T = drying temperature (^oC)
TVM = total volatile matter context (%)

1. INTRODUCTION

Double and triple base propellants for guns and rockets are formulated from nitrocellulose, nitroglycerine and several other ingredients including nitroguanidine and a stabiliser. Some propellants in this category are given the name cordites. Their manufacture includes in most cases the incorporation of the principal constituents, nitrocellulose and nitroglycerine, with solvents such as acetone, ether, ethyl alcohol or ethyl acetate to provide a soft extrudable dough suitable for pressure forming. At the end of the processing the solvent has to be removed by a drying operation.

In view of the nature of the product it is not surprising that the drying is accompanied by a considerable degree of hazard so that it is current practice to restrict the upper temperature of the operation to a figure between 45°C and 60°C depending upon a number of processing factors.

There are other complications involved. The solvents exhibit a chemical affinity for the nitrocellulose matrix which impedes their disengagement from the propellant grain. The solvent is held in the body of the particle which are often in the form of right cylinders of length to diameter ratio approximating to unity with diameters varying between 1 mm and 10 mm. The difference between propellant drying and many other drying operations is that it is not a surface phenomenon and, although drying is related to the dimensions, it is not the specific surface which controls the process, instead internal diffusional processes play a dominant role. The initial particle dimensions exert an influence on the drying but owing to shrinkage during solvent removal the size characteristics change and so does the diffusion rate, both of these may affect the mechanism. In addition the final particle dimensions are of critical importance in determining the final ballistic behaviour of the product so that size changes must be carefully forecast and controlled.

Although propellants of this type have been manufactured for over 80 years there is very little published or private information on the topic of solvent removal. Sixty years ago a British chemical engineer K.B. Quinan devised a forced air drying plant for nitrocellulose which still operates but no experimental design data exist for the process. It is surprising that this is the case since the propellant drying operation is dangerous, costly and has

long processing times of up to 14 days. Investigations were commenced by the author at PERME Waltham Abbey, and in recent years studies have been undertaken to elucidate the mechanisms and characteristics of this most important operation. Information has been sought to enable a more efficient chemical engineering design to be achieved. The subject is an extensive one and it will be possible here to consider only limited aspects of the problem.

2. DRYING MECHANISMS

Since the solvent is held within the body of the granules the mass transfer may be considered to act in three modes:

1. Transport of solvent within the solid.
2. Gas film transport at the solid/gas interface.
3. Solvent vapour removal from the surrounding bulk gas phase.

During a typical drying cycle there is a rapid constant rate period lasting for a relatively short time followed by a falling rate period which is the most influential in determining the drying programme. This falling rate period is principally diffusion from the centre of the granule outwards and is analogous to the problem of diffusion of organic vapours through polymeric materials such as nylon and plastics. Extensive studies have been made on such systems (1) (2) and it is possible to describe the falling rate period by a mathematical model of the transport within the solid.

The basic Fickian relationship for spherical diffusion is

$$\frac{dC}{dt} = D\left[\frac{d^2C}{dr^2} + \frac{2}{r}\right]\frac{dC}{dr} \qquad (1)$$

Using boundary conditions of initial uniform solvent, zero surface concentration and assuming an invariant diffusion coefficient (D) the integrated form of the equation is

$$\frac{M_t}{M_o} = 1 - \frac{6}{\pi^2}\cdot\Sigma_{n=1}^{\infty}\ \frac{1}{n^2}\exp\left[-\frac{Dn^2\pi^2 t}{a^2}\right] \qquad (2)$$

If M_r is the mass of solvent retained in the granule after time t, $M_t = M_o - M_r$

$$\therefore M_r = \frac{6M_o}{\pi^2}\ \Sigma_{n=1}^{\infty}\ \frac{1}{n^2}\exp\left[-\frac{Dn^2\pi^2 t}{a^2}\right] \qquad (3)$$

This relationship has been used to model diffusion in other cases. It can be seen that as t the value of M_r is that of the first term of the series viz:

$$\frac{6M_o}{\pi^2}\exp\left[-\frac{D\pi^2 t}{a^2}\right]$$

taking logarithms and differentiating

$$\frac{d(\log_e M_r)}{dt} = -\frac{D\pi^2}{a^2} \qquad (4)$$

The equation predicts that for constant values of the dimension 'a' and the diffusion coefficient 'D' there should be a linear relationship between the logarithm of the remaining solvent content and the elapsed drying time 't'. When drying trials are carried out on actual propellants this relationship fails to hold even over the later stages of drying and it was found that an exponential function of 't' was required to fit the data. It was also found that the exponent varied with the nitrocellulose content of the mixture.

The indications are that the diffusion coefficient varies during the solvent removal and that its value depends upon the composition of the matrix. In correlating the results it would be appropriate to utilise the so-called diffusion parameter $\frac{Dt}{a^2}$ to compare particles of different dimensions. This may be incorporated into an empirical equation of the form

$$\frac{M_r}{M_o} = K\left[\frac{Dt}{a^2}\right]^{-n} \qquad (5)$$

in which a value of n is obtained for the falling rate period of drying from the experimental results.

Temperature affects the rate of diffusion according to the Arrhenius equation

$$D = D_o \exp -\frac{Ed}{RT} \qquad (6)$$

This may be combined with equation 5 to give

$$\frac{M_r}{M_o} = K\left[\frac{D_o \exp -\frac{Ed}{RT}\ t}{a^2}\right]^{-n} \qquad (7)$$

From this relationship experimental drying results may be used to obtain the value of the activation energy (E) for the process.

3. EXPERIMENTAL STUDIES

Compositions Used

Propellant materials and solvent systems have been examined as shown in Table 1 for propellants identified by the letters A to L.

TABLE 1

Composition of Propellants

	Composition				Solvent System
	Nitro-cellulose %	Nitro-glycerine %	Stabi-liser %	Nitro-guanidine %	
A	64	35	1	0	E/Al
B	75	24	1	0	"
C	90	9	1	0	"
D	64	35	1	0	A/Al
E	80	19	1	0	"
F	90	9	1	0	"
G	19	19	7	55	A/W
H	21	21	3	55	"
I	26	26	3	45	"
J	31	31	3	35	"
K	36	36	3	25	"
L	21	21	3	55	EA/W

E/Al = Ether/Ethyl alcohol
A/Al = Acetone/Ethyl alcohol
A/W = Acetone/Water
EA/W = Ethyl acetate/Water

Comparison of Solvent Removal Methods

Conventional techniques are based on tray drying in natural convection warm chambers or stoves which are hot water heated to 45°C to 60°C. Air flow rates are low under these circumstances. A number of experiments were performed on propellants A to F in this type of oven to obtain the data given in Figures 1 and 2 indicating that marked differences occur between propellants with different nitrocellulose contents. The amount of total volatile matter remaining in the sample after various heating periods is plotted against the drying time and it is seen that after a period of between four and ten days the equilibrium solvent level is reached for the conditions applied. The ether/alcohol systems dry more rapidly than the acetone ones. The explanation for the differing rates probably lies in the greater affinity of acetone for nitrocellulose and it has been found that the level of chemical retention for some solvents is surprisingly high.

It might be expected that the removal of the film of vapour from the vicinity of the surface of the particle would be to enhance the solvent removal rate by permitting more rapid evaporation from the surface and hence augmenting the diffusional rate for solvent transfer to the surface by increasing the driving force across the diffusional path. Two methods might achieve the removal of vapour, vacuum drying or forced air drying employing a semi-fluidised bed principle. Experiments were carried out to compare these methods with the conventional process using tray dryers in stoves. Figure 3 shows a typical result obtained for

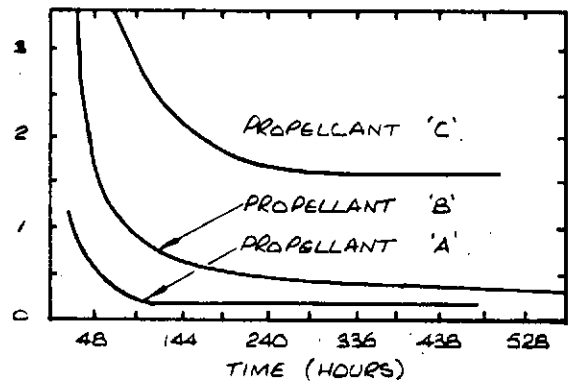

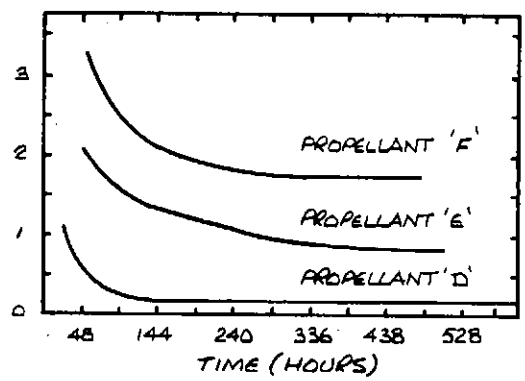

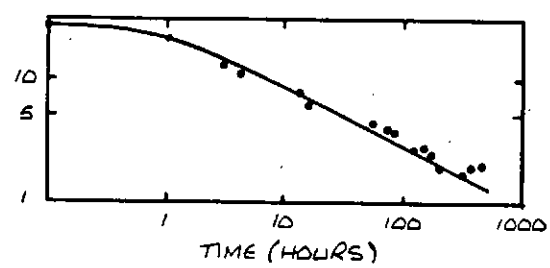

propellant C. The total volatile matter content which includes both solvent and any water present is plotted against the drying time on log/log axes. The curve exhibits for the major part of the drying cycle a linear relationship on the log/log plot with approximately equal slopes for the stove and vacuum drying. Similar results are obtained for forced air drying and Figure 4 shows

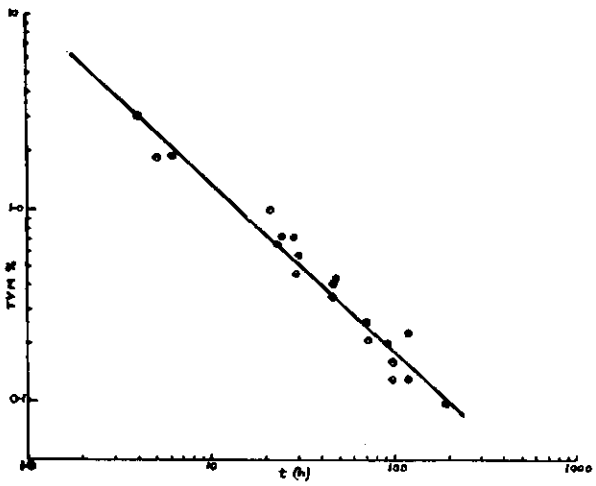

Figure 4 Forced Air Drying Rate 100, 300 and 500 l/min 45°C

the solvent removal process for propellant C under forced air conditions using air rates of 100, 300 and 500 l/min through a 150 mm diameter bed. Within experimental error of the analysis, the results are equivalent for each rate of air flow and the drying times are almost the same as for the stagnant air experiments, thus indicating that the lower rate of 100 l/min is adequate. Evidently the use of forced air flow or vacuum has little effect under laboratory conditions on the rate of solvent removal.

A difference in drying rates arises however when the internal diffusion rate rises for any reason to a level where the external film coefficient exerts an overall control on the removal rate. This occurs during the removal of water from propellants and under these circumstances there is an advantage to be gained from the use of vacuum or forced air drying.

Some caution has to be exercised in scaling up to large scale since the curves shown may not portray the entire mechanism in cases where large propellant masses occur, for example in deep trays and large stacks. Solvent concentrations in the ambient atmosphere may rise significantly and, in addition there may be some hindrance to the transmission of heat to the more remote portions of the bed with a consequential temperature depression. The lower temperature reduces diffusion rates as discussed below and so the early stages of solvent evaporation are extended considerably.

The systems examined are shown in the Table and it was found that for the acetone/water system a value of n of -0.9 was appropriate for composition B whereas for other compositions it varied from -0.5 to 1.3.

It would be satisfactory if the theoretical basis for these variations could be placed on a sounder footing but, although it seems possible that a deeper understanding of the mechanisms of diffusion may ultimately assist in devising more complex equations, it seems that the research effort required to evaluate the necessary parameters is unlikely to be profitable so that the empirical relation of equation (7) is of considerable practical use.

4. THE EFFECT OF TEMPERATURE ON DRYING RATE

It has been shown that the drying rate is related to the drying temperature by the Arrhenius equation both in the case of propellants with high nitroguanidine content and those without. Samples of propellants G were dried at 45°C, 55°C and 65°C under natural convection drying conditions. Log/log plots of M_r against t were made for the three temperatures and the gradient of the straight portions of the curves was measured as 1.14.

M_r may be plotted against $t^{-1.14}$ and the gradient is equal to

$$\frac{KM_o l^{2n}}{D_o^n} \exp - \frac{nE_d}{RT}$$

so that

$$\ln\left[\text{Gradient}\right] = \ln\left[\frac{KM_o l^{2n}}{D_o^n} \exp - \frac{nE_d}{RT}\right]$$

$$= \ln\left[\frac{KM_o l^{2n}}{D_o^n} \exp - \frac{nE_d}{RT}\right]$$

A plot of ln (Gradient) v $\frac{1}{T}$ should give a straight line and in Figure 5 this plot is a line of

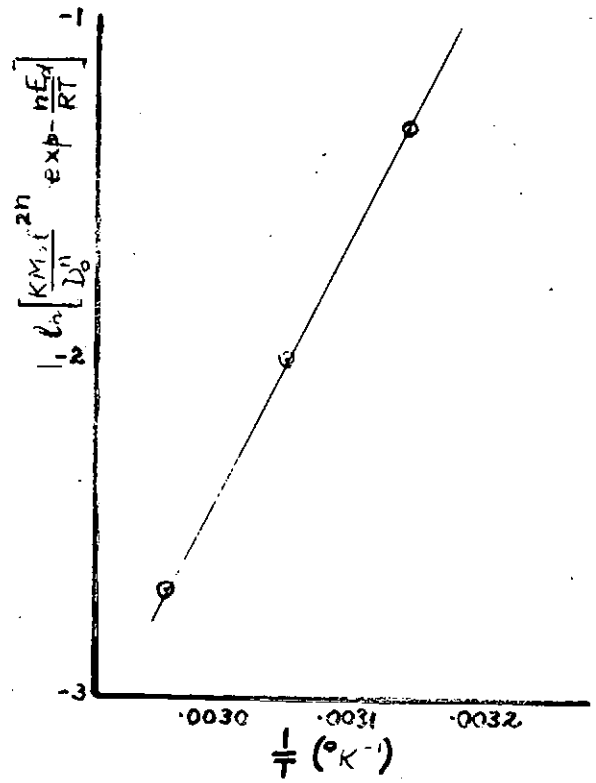

Figure 5 Variation of Diffusional Coefficient with Temperature for Composition H

gradient 7,300 which corresponds to a diffusion energy (E) of 53.5 KJ/mole a value consistent with the diffusion process. The corresponding value determined for a nitrocellulose/ nitroglycerine mix without nitroguanidine using composition B gives a value of 92 KJ/mole.

The results obtained in these experiments indicate that temperature is of prime importance in the drying operation and it was confirmed that no deleterious effects were produced by higher temperature dyring. It would be easy to proceed from this point to recommend even higher temperatures in order to reduce further the time of drying. However the severe results of ignition of these materials means that a restriction must be imposed and the level of 60°C is universally accepted in the safety standards of the industry unless some other methods can be devised to reduce the risk of mass ignition. An alternative drying procedure which reduces the risk of accident is described in American patent literature (3). Initial solvents removal can be achieved at a higher temperature under water without a fire or explosion hazard. The method is not without process limitations but has been successfully extended to the compositions tabulated. A number of problems need to be overcome and, as for other soluble materials in the patent, the solubilities of nitroglycerine and nitroguanidine contained in these compositions have to be suppressed by the use of solutions containing a certain concentration of these materials. The solvent removal process is rapid when the temperature is raised to 75°C and takes only a few hours. After the solvent has been removed the propellant, which has become saturated with water, needs drying at a more normal lower temperature but here the water is more rapidly expelled than the solvent would be at the same temperature.

5. EFFECT OF PARTICLE DIMENSIONS

The use of the diffusion parameter $\frac{Dt}{a^2}$ has been referred to above where a is a linear dimension variable. To test the validity of this expression a series of drying operations were carried out using propellant particles of different sizes and their drying curves were constructed. These were determined for composition E, using an acetone/alcohol solvent system and it was found that the results yield a series of curves for the latter stages of drying (ie after 10 hours when diffusion is the predominant mechanism) which are orderly with respect to size. A curve obtained from all the results is given in Figure 6 showing that

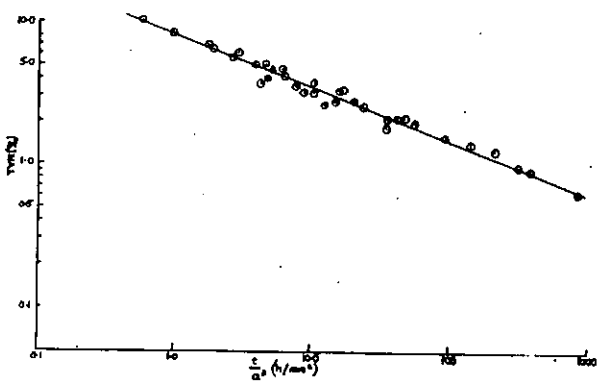

Figure 6 Effect of Particle Dimensions on Drying, Correlation with $\frac{Dt}{a^2}$

the drying is readily correlated using the expression $\frac{Dt}{a^2}$. The scatter observed is accounted for by the problems of sampling and analysis.

6. CONCLUSIONS

It is clear that nitrocellulose compositions are similar to other polymeric materials in their properties of absorbing solvents, but the strong affinity shown by the matrix for certain solvents may be unusual. In drying operations, water is, in general, the commonest solvent encountered and it shows only a limited tendency to behave other than a normal physical surface layer. In the case of nitrocellulose materials water appears to be released more rapidly from the product than solvents so that an advantage may be gained by 'drying' the propellant under water at a temperature higher than that normally permitted by safety considerations. Water may then be removed in a shorter time than is usual by conventional tray drying of solvent wet material.

The drying behaviour has been shown to be correlated by an exponential function of the form

$$\frac{M_y}{M_o} = K\left[\frac{D_o \exp - \frac{Ed}{RT}\, t}{a^2}\right]$$

where the exponent n varies with the nitrocellulose content.

7. REFERENCES

1. Crank, J. — The Mathematics of Diffusion
2. Crank, J, Park, G.S. — Diffusion in Polymers
3. U.S. Patent, 3,622,655 — J.O. Bonyata

Copyright © Controller HMSO, London, 1980

THERMAL DEGRADATION OF PYRETHRINS DURING DRYING OF PYRETHRUM FLOWERS

P. M. Githinji

University of Nairobi, P.O. Box 30197, Nairobi, Kenya.

ABSTRACT

Kenya produces two-thirds of the world crop of pyrethrum flowers, from which a potent but environmentally safe insecticide (pyrethrins) is extracted. Experimental results confirmed that use of high drying air temperatures and overdrying result in pyrethrins loss from the flowers. The experiments were conducted in the temperature range of 60°C to 160°C and drying prolonged by up to four times the nominal drying period at each temperature. The thermal degradation of pyrethrins was found to be a first order reaction whose rate constant is expressable as a function of temperature by the Arrhenius equation, from which the activation energy was found to be 14.7 kcal/mol. It was further concluded that the pyrethrins loss during drying is due to diffusion. A drying air temperature of 80°C is recommended to farmers.

NOMENCLATURE

C = Concentration = $\frac{P}{P_o}$ = pyrethrins ratio

E = activation energy, kcal/mol

K = rate constant, hr^{-1}

n = order of reaction

P = pyrethrins content of test flowers, %

P_o = pyrethrins content of control sample, %

R = universal gas constant

r = coefficient of regression

t = time, hr

T = absolute temperature, K.

1. INTRODUCTION

The pyrethrum plant (chrysanthemum cinerariaefolium) produces daisy-like flowers which contain a very potent but environmentally safe insecticide. Today, Kenya produces two-thirds of the world crop and the commodity ranks fourth in the country's list of exports. Drying of the flowers is done on the farm before delivery to a central processing factory, where they are ground and the insecticide (pyrethrins) extracted by means of a solvent.

Field and literature surveys revealed that there was an urgent need to produce better pyrethrum driers for use by the farmers. For a start, a study on two important aspects of drying was made, as a basis for future design and production of the driers. These aspects are: first, the effect of drying air temperature on the pyrethrins content of the flowers and, secondly, the mechanism of moisture removal from the flower. The desirability of speeding up the drying process dictates that higher drying air temperatures be used but, the use of high temperatures is likely to produce thermal degradation of pyrethrins. The results of research work done on thermal degradation are therefore reported herein and a subsequent paper will present the results on moisture removal.

Previous investigators (1) to (11) but one (5), all working within the air temperature range of 40 C and 175 C, concluded that the use of high drying air temperatures and prolonged drying reduced the pyrethrins content of flowers. None of the authors formulated any equations to correlate the scanty data available, and none of the results obtained by the respective investigators covered an adequate range of temperature and time. The range of temperatures used in the present work was 60 C to 160 C, in 20C increments, and drying periods of up to four times the nominal drying time at each air temperature.

2. EXPERIMENTAL WORK

The initial experiments were done on one clonal material (code-named Clone 4331) grown in Nairobi. Each batch of wet flowers was thoroughly mixed on arrival in the laboratory, and divided into three equal samples. The first sample was used for the determination of the initial moisture content by the Modified Brown-Duvel Method (12) using double refined cotton seed oil at 140 C for 15 minutes. The second sample was dried in a vacuum oven at 35C for 24 hours, and used for pyrethrins control. The final sample was divided into four equal subsamples, all of which were dried concurrently in a ventilated air oven at one of the following temperatures: 60, 80, 100, 120, 140 and 160C. Both ovens were thermostatically controlled. Preliminary experiments had shown that the drying durations for wet flowers at an initial

moisture content of approximately 300% dry basis, to approximately 10% final moisture content, was respectively 5, 3, 1.5, 1.25, 1.0 and 0.75 hours at the above temperatures. At any of these temperatures, therefore, the first sub-sample was removed from the oven after the corresponding nominal drying duration had elapsed. The second, third, and fourth sub-samples remained in the oven for double, triple and quadruple the nominal drying period. In this way, the effects of drying air temperature and overdrying were determined by comparing the pyrethrins content of each sub-sample with that of the control sample for that particular batch of flowers. It is necessary to have a control sample for each batch of flowers due to the variation of pyrethrins content of flowers with climatic conditions, flower maturity, plant agronomy and clonal material. The pyrethrins content, P, varies from approximately 1.5% to 3.0%, dry flower basis. Air flow rate through the air oven was not available from the oven manufacturer, but it was estimated at approximately 0.5 m^3/min by means of a vane anemometer.

To eliminate the effects of flower bed depth such as temperature and moisture gradients, all drying experiments were conducted using a single layer of flowers, which weighed between 20g and 60g, depending upon the initial flower moisture content. The flowers were dried in wire-mesh trays to permit sufficient flow of air and water vapour. All dried sub-samples were regularly despatched to the Pyrethrum Board of Kenya laboratories for spectrophotometric analysis of pyrethrins content, using the method of Beckley (13). The wet and dried flower samples were weighed by means of a balance capable of weighing accurately to 0.01g.

Similar experiments were conducted at the Pyrethrum Research Station at Molo using the same clonal material (Clone 4331) and three others (Clones Ma 62/246, Ma 65/99 and 1708). The four clones have different proportions of the six chemical components of pyrethrins and contain different quantities of pyrethrins. The objective, therefore, was to cover wide spectra of these two characteristics of pyrethrum flowers so as to make the overall results as conclusive as possible. Further details of this work are available in (14).

3. DATA ANALYSIS

It is postulated that thermal degradation of pyrethrins can be explained by the chemical reaction theory. However, to correctly formulate the law of the rate of reaction, it is essential to know the molecular process by which the resultant reaction is actually brought about. In the absence of this knowledge with respect to pyrethrins (which consists of six complex chemicals), it was found necessary to adopt the method of Noyes and Sherrill (15), whereby the experimental data is analysed in order to establish the order of the reaction.

Assuming that pyrethrins behaves as a homogeneous substance, then, the n-th order chemical reaction is represented by the following equation:

$$\frac{dC}{dt} = - KC^n \qquad (1)$$

which, on integration becomes.

$$C^{1-n} = K(n-1)t + \text{const.} \qquad (2)$$

In the case of pyrethrins, $C = \frac{P}{P_o}$ and therefore the constant is equal to unity.

No easy method was found of plotting jointly the experimental data and equation (2) in order to evaluate the order of the reaction and the rate constant. Indeed, Laidler (16) states that the most direct, although not necessarily the most accurate method is to assign different values to n, which makes it possible to evaluate K. This procedure was adopted for its simplicity and n assigned the following values in turn: $\frac{1}{2}$, 1, $1\frac{1}{2}$, 2, $2\frac{1}{2}$, 3, $3\frac{1}{2}$, and 4. An ICL 1900 Statistical Analysis Program, XDS3, was used in the reduction of experimental data at each value of n and the calculation, for each drying air temperature, of the coefficient of regression. The results of that exercise are presented in Table 1, from which it is quite clear that for the range $\frac{1}{2} \leqslant n \leqslant 4$, the best correlation is for n = 1. It was concluded, therefore that unless the order of reaction undergone by pyrethrins is greater than 4, then the correct order of reaction is the first. This implies that pyrethrins loss from flowers during the drying process is most likely by diffusion through the flower head.

The reaction equation therefore becomes

$$\frac{dC}{dt} = - KC \qquad (3)$$

which, upon integration and evaluation of the constant becomes

$$\ell n\, C = - Kt \qquad (4)$$

Figure 1 presents test data on Clone 4331 for the two extreme air temperature used, i.e. 60C and 160C. Regression lines for test data obtained at the intermediate temperatures (80, 100, 120 and 140C) are also shown in the figure, but the corresponding data points have been omitted to avoid overcrowding. It is evident that the use of high temperature and prolonged exposure to drying air result in the

Table 1: Coefficient of regression, r, for different orders of reaction

Temp. C	160	140	120	100	80	60
No. of data points.	46	51	47	45	49	23
Order						
$n = \frac{1}{2}$	-0.192	-0.0765	0.0129	-0.174	-0.315	-0.130
$n = 1$	-0.876	-0.708	-0.656	-0.535	-0.32	-0.180
$n = 1\frac{1}{2}$	0.199	0.0758	-0.0127	0.179	0.336	0.149
$n = 2$	0.200	0.0752	-0.0122	0.179	0.345	0.159
$n = 2\frac{1}{2}$	0.199	0.0743	-0.0116	0.178	0.354	0.168
$n = 3$	0.197	0.0733	-0.0107	0.176	0.361	0.177
$n = 3\frac{1}{2}$	0.192	0.0721	-0.00965	0.172	0.365	0.186
$n = 4$	-0.151	-0.0747	0.0101	-0.151	-0.260	-0.0836

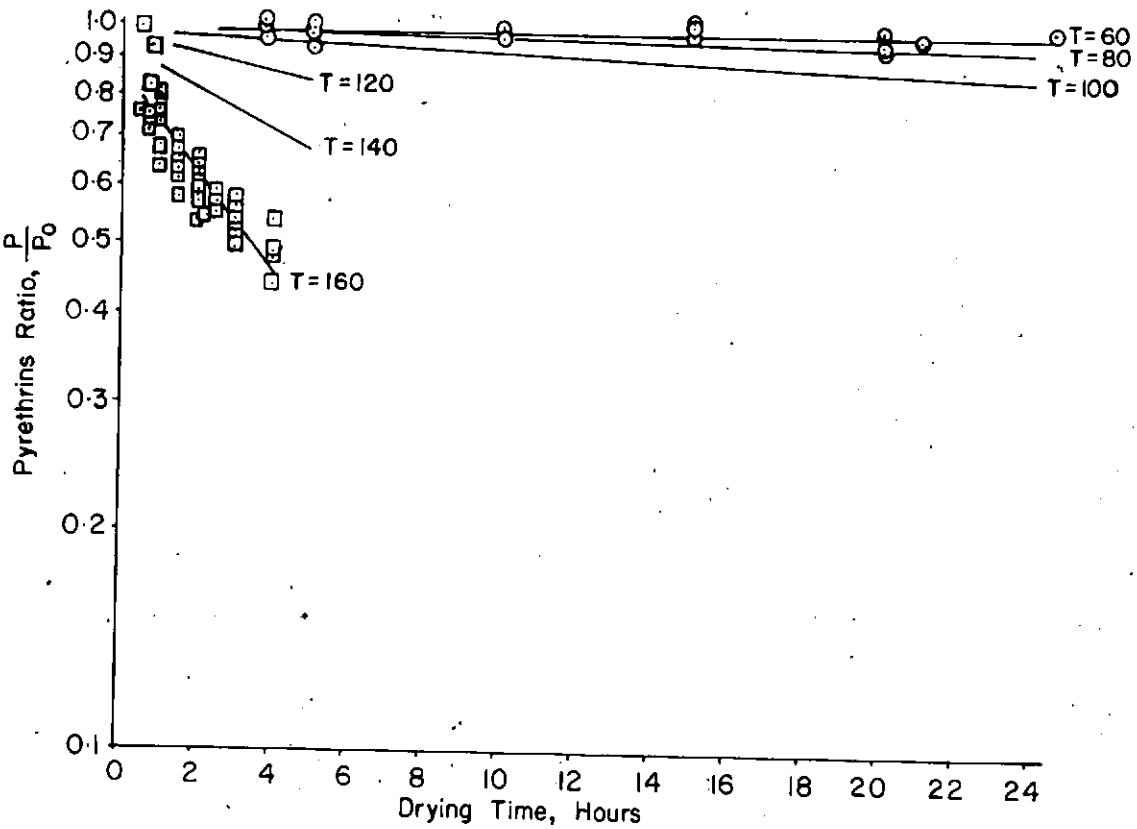

FIGURE 1: EFFECTS OF TEMPERATURE AND OVERDRYING ON PYRETHRINS CONTENT (NAIROBI CLONE 4331).

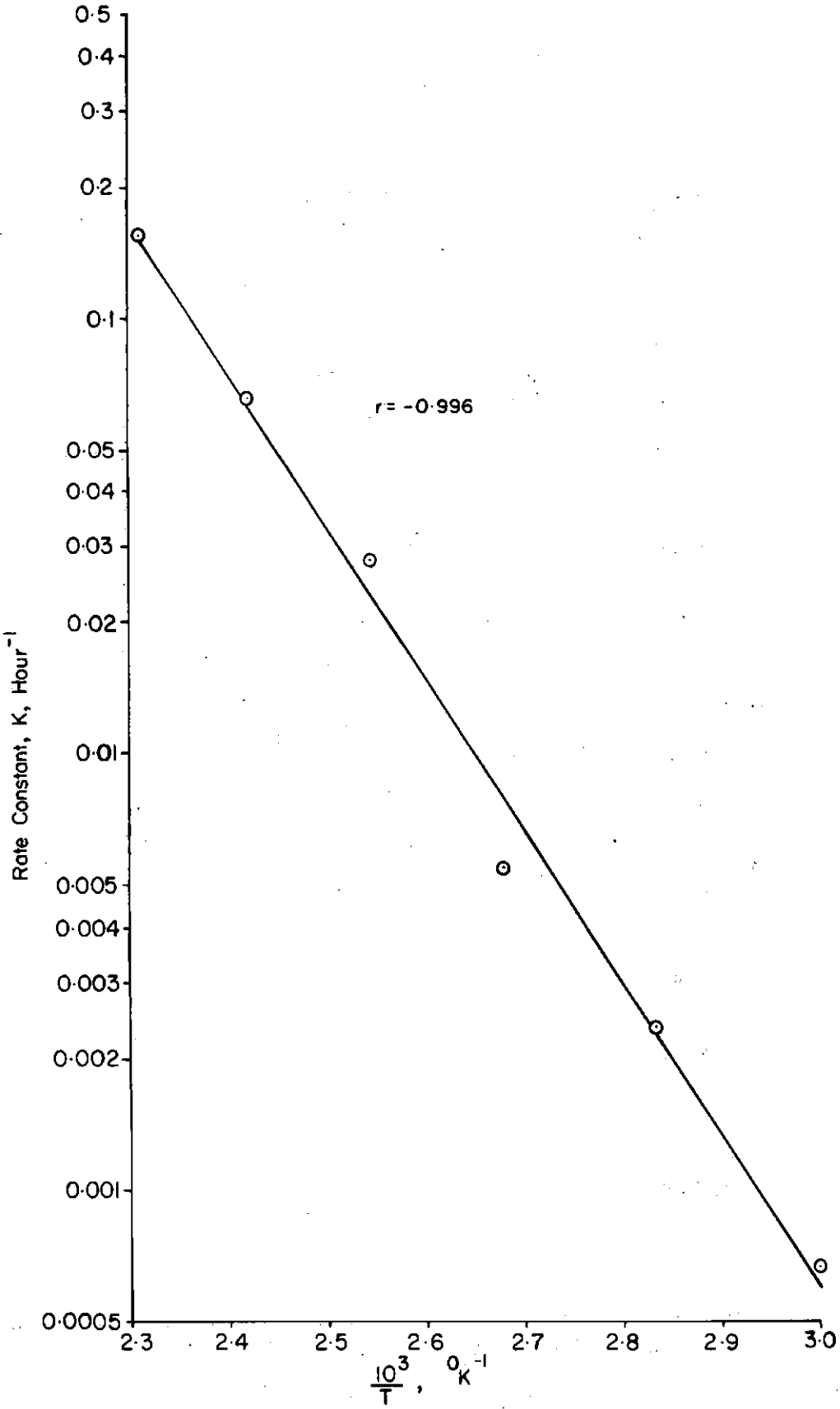

FIGURE 2: EFFECT OF DRYING AIR TEMPERATURE ON THE RATE CONSTANT, K. (NAIROBI CLONE 4331).

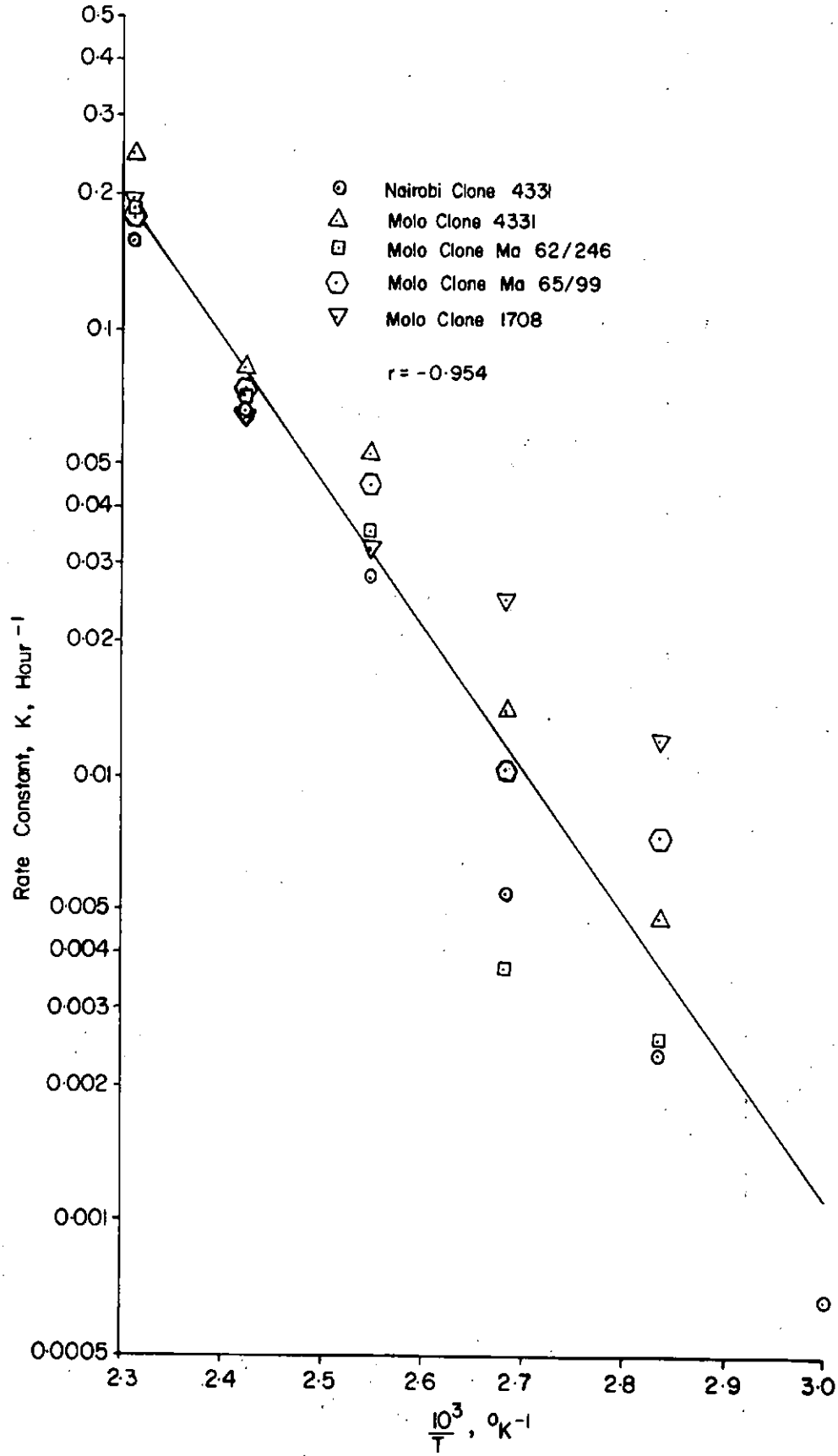

FIGURE 3: EFFECT OF DRYING AIR TEMPERATURE ON RATE CONSTANT, K, FOR DIFFERENT PYRETHRUM CLONES.

Table 2: Rate Constant, K, for different pyrethrum clones

Temp. C	CLONE				
	NAIROBI	MOLO			
	4331	4331	Ma 62/246	Ma 65/99	1708
60	0.000657	-	-	-	-
80	0.00235	0.00476	0.00255	0.00733	0.0121
100	0.00544	0.014	0.00366	0.0103	0.0249
120	0.0278	0.0523	0.0354	0.0452	0.0319
140	0.0654	0.0821	0.0707	0.0713	0.0639
160	0.156	0.244	0.185	0.1812	0.192
Activation Energy, E, kcal/mol	16.0	14.7	17.5	12.6	9.71

Activation Energy, E, based on all clones = 14.7 kcal/mol.

loss of pyrethrins. The rate constant, K, at each drying air temperature is the slope of the respective regression line. The relationship between the rate constant and temperature was obtained by using the Arrhenius equation, and plotting the data as shown in Figure 2. The equation is:

$$\ln K = - \frac{E}{RT} + \text{const.} \qquad (5)$$

The correlation between K and T is seen from Figure 2 to be good, and from the graph, the activation energy for Clone 4331 grown in Nairobi was evaluated as 16.0 kcal/mol. There are no previously published values of activation energy for thermal degradation of pyrethrins, but other investigators have reported 24.6 kcal/mol for isomerization of pyrethrum extract (17) and 64.6 kcal/mol for wheat (18), (19).

Test data for flowers grown and dried at Molo (Clones 4331, 1708, Ma 62/246, and Ma 65/99) were similarly processed and the results were found to be very similar to those already discussed above. The rate constants and activation energy for each clone are shown in Table 2, and are seen to be of the same order of magnitude. The information contained in Table 2 is also presented graphically as Figure 3, from which the overall value of activation energy for all clones tested is found to be 14.7 kcal/mol.

4. CONCLUSIONS

The findings of majority of the earlier investigators on the effects of drying air temperature and prolonged drying on pyrethrins constant are conclusively confirmed. Furthermore, unless the order of reaction of pyrethrins is higher than 4, it has been shown herein that the loss of pyrethrins follows the first order reaction for all clones tested. On this basis, it is concluded that pyrethrins are lost by diffusion through the flower head during drying. A drying air temperature of 80C is recommended to farmers, to allow sufficient drying speed with minimal loss of pyrethrins.

ACKNOWLEDGEMENT

The author wishes to acknowledge, with thanks, the support he received from the University of Nairobi, the Pyrethrum Board of Kenya, and the Pyrethrum Research Station during the research period.

REFERENCES

1. JARY, S.G., MARTIN, J.T., TATTERSFIELD, F., "The artificial drying of pyrethrum flowers". J.S.E. Agric. Coll., Wye, Kent. 1937, No. 40, pp.108-114.

2. BECKLEY, V.A., "Pyrethrum in Kenya" Bulletin of Imperial Institute, London 36, 31, 1938.

3. BECKLEY, V.A., McNAUGHTAN, F., "Pyrethrum drying" E.A. Agric. Jn. 2, pp. 327-338, 1937 and Rhodesia J. of Agric. 41, 313, 1944.

4. GNADINGER, C.B., "Pyrethrum Flowers" - Supplement to 2nd Edn. 1936-45. McLaughlin Gormley King Co. Minneapolis.

5. LOWMAN, M.S., GERSDORFF, W.A., KELLY, J.W., "Effect of drying methods on toxicants in pyrethrum flowers". Soap and Sanitary Chemicals, September/October 1949.

6. BECKLEY, V.A., "Pyrethrum Drying", Pyrethrum Post, 3 (1), p.9, 1952.

7. MUNRO, R.J., "An experiment on the drying of pyrethrum flowers". Pyrethrum Post. 6, (2), 25-29, 1961.

8. NATIONAL INSTITUTE OF AGRICULTURAL ENGINEERING. "Lindeteves 16 in. Drycom Pyrethrum Drier". 11th October 1960.

9. NATIONAL INSTITUTE OF AGRICULTURAL ENGINEERING, "G. & R. Junior MK III Pyrethrum Drier". 22nd August 1960.

10. NATIONAL INSTITUTE OF AGRICULTURAL ENGINEERING, "Schumacher Pyrethrum Drier". 24th July 1961.

11. GODIN, P.J., INGLIS, H.S., STEVENSON, J.H., "Insecticidal activity of fresh and dry pyrethrum flowers". Jn. Sci. Food Agric. 1965. No. 4, pp. 186-191.

12. WARNER, M.G.R., HARRIES, G.O., "The Modified Brown-Duvel moisture test". National Institute of Agricultural Engineering. Report No. 33.

13. BECKLEY, V.A., "The spectrophotometric estimation of pyrethrins". Pyrethrum Post, 2 (1), p.23, 1950.

14. GITHINJI, P.M., "Drying of Pyrethrum Flowers." Ph.D. Thesis, University of Nairobi.

15. NOYES, A.A., SHERRILL, M.A., A Course of Study in Chemical Principles, 2nd Edn. MacMillan Co. 1960. Chapter VI.

16. LAIDLER, K.J., Chemical Kinetics, McGraw Hill, 1950. Chapter 1.

17. GOLDBERG, A.A., HEAD, S.W., JOHNSTON, P., "Action of heat on pyrethrum extract: The isomerization of pyrethrins to isopyrethrins". Jn. Sci. Food & Agric. 1965. Vol. 16, No. 1, pp. 43-51.

18. BECKER, H.A., SALLANS, H.R., "A study of the relation between time, temperature, moisture content and loaf volume by the bromate formula in the heat treatment of wheat and flour". Cereal Chemistry, 1956, 33, pp. 254-265.

19. BECKER, H.A., SALLANS, H.R., "Drying wheat in a spouted bed". Chemical Engineering Science, Vol. 13, No. 3, pp. 97-112, 1960.

DRYING SINCE THE MILLENNIUMS

K. Kröll[1], A.S. Mujumdar[2] and A.S. Menon[2]

1. Bad Hersfeld, F.R. Germany
2. McGill University, Montreal, Canada

ABSTRACT

This paper summarizes the early use and development of drying and dryers, starting from prehistoric times and proceeding upto the machine age. This paper is a condensed version of a detailed German monograph prepared by Dr. Ing K. Kröll to which the interested reader is referred. It may be noted that although most of the drying research and development has taken place during the past three decades the technique of drying is truly an age-old operation. For example, refrigeration dates back to pre-Roman times and was a routine practice under Nero. The stabilization of perishable goods by drying was used by primitive people for millenniums. The combination of the two, however, is the relatively new technology of freeze drying.

INTRODUCTION

The drying technique originated several hundred thousand years ago when man noticed the advantages offered to him by dry leaves and straw for his couch and by dry bushwood to make fire. In the course of millenniums his various desires and necessities caused him to make certain perishables more durable, his tools more useful, his clothing more suitable and his lodging more comfortable. Consequently, things had to be dried. However, his environment, the climate and the change of the world around him required the development of techniques to aid him in drying goods in the momentarily suitable and possible way.

For the sake of brevity, the historical developments in drying which took place from pre-historic to the 19th century A.D. are presented here in a tabular format. The original full text written by Dr. Ing. Kröll is available from the author. This summary was prepared by Mujumdar and Menon on the basis of the original text prepared by Kröll.

Period	Location	Drying Applications
Old Stone Age (Paleolithic) 750,000 years ago	Temperate zones of the world	Firewood (1) Hides of hunted animals
400,000 years ago	All over the world	Wood for tools Meat
250,000 years ago	Foot of the Pyrenees	Hides dried on a framework of branches
100,000 to 40,000 years ago	Neandertal man	Dried hides slowly by the fire (2)
35,000 years ago	Cro-Magnon Man	Sinews and intestines of the reindeer dried for making thread (3,4)
27,000 years ago	Czechoslovakia	People formed figures of animals and human beings from moist clay and bone meal and dried and fired them in ovens (3)
20,000 years ago	Don river, south of Moscow	Meat cut into strips and dried in the sun

Period	Location	Drying Applications
		Dried animal excreta served as inflammable matter for the fire
Mesolithic Age		
17,000 years ago	Central Germany and northern France	Dried guts of the reindeer used to span bows. Tents were made of dried hides.
10,000 years ago	Solvieux (south France)	Nets to catch fish were cleaned and dried. Fish were dried. (3)
12,000 years ago	Iran, Syria, Israel, Jordan and Southern Turkey	Dried clay used for leak-proof roofs Moist grain dried in the sun to prevent sprouting (5).
Neolithic Age		
10,000 years ago	Near East	Peas, beans, lentels and grain dried and stored
10,000 years ago	Jericho in the Jordan Valley	Salt made by drying (evaporating) sea water
9000 years ago	Jarmo in Iraq	Straw and wet clay were mixed and used for walls of houses. The first layer was dried before the next was put on
7500 B.C.	Near East	Drying pads were used for fruit. Brushwood and dried reed used as fuel
7000 years ago	Jericho	Bricks were sun-dried. Walls and floors were plastered with mortar and then dried (6)
6500 B.C.	Catal Hüyük in Turkey	Prismoidal bricks fabricated in wooden frames and dried in the sun
6000 B.C.	Jericho	Works of art made of gypsum which hardened on drying (6)
6000 B.C.	Catal Hüyük in Turkey	Animal hair was washed, dried and spun into thread. This was used to make clothes which could be washed and dried (6,7)
6000 B.C.	Near East and Egypt	Hides were dried to make chamois leather (8,9)
Copper Age		
5000 B.C.	Eridu	People imported dried fish from the Persian gulf (13)
	Egypt (Nile Valley)	Flax that was cultivated was soaked, rinsed and dried (6,11). The fibres which were separated were used in spinning (6, 11)
3500 B.C.	Mesopotamia	Dried bricks were fired and used in building houses (11,12)

Period	Location	Drying Applications
3000 B.C.	Sumerian people	They pressed cuneiform characters into wet plates which were dried and fired to confirm the writing
3000 B.C.	Egyptians	Strips of papyrus marrow were used to make sheets which were hammered, pressed and spread out for drying (16)
Europe: From after the ice age to about 3000 B.C.		
4500 - 4000 B.C.	Central Europe	Walls of houses were plastered with clay on both sides and dried in the wind and sun Harvested grain was kiln-dried (19) Fabrics were dried after dyeing (20)
America Till 3000 B.C.		
9000 B.C.	South-west of the United States	Meat that was not consumed immediately after hunting, was cut into strips and dried in the sun for storage. Dried animal excrements were used as fuel (21)
8000 B.C. - 6000 B.C.	-	Wild plants, their seeds, nuts and berries were dried for later consumption
4000 B.C.	Mexico, tropical coast of Equador	Figures and pottery made from clay were dried and fired
3500 B.C.	Peru	Indians preserved potatoes by alternatively freezing them during the night in the cold mountain air and thawing them in the sun during the day (5,23)
Bronze Age		
2900 B.C.	Sumerian cities on the Euphrates and Tigris rivers	Small houses were built from dried narrow mud bricks. They decorated these buildings with mosaics from coloured stones. These artistic pieces were made of clay, sand and water which had to be dried and fired (6,7,24)
2550 - 2450 B.C.	Egypt	Houses built of dried mud bricks Moist gypsum which was used as a raw material for mortar, plaster, sculpture as well as for paintings had to be dried
2200 B.C.	Egypt	Parchment, which was used for writing, was made from hides which were depilated, soaked in lime solution and dried. Drying of the laundry at the palace of the pharaoh was done by special personnel (11,16,26)

Period	Location	Drying Applications
2500 B.C.	Indus Valley	Fibres of the cotton plant were separated from the capsule, washed and dried for subsequent treatment (11)
2500 B.C.	Harappa in North India	Currents of air were passed through grain stored in the graneries to dry and protect them from deterioration (6,15)
1750 B.C.	Skagerrak (Sweden)	Fish were dried in the wind and sunshine Apples were cut into slices, strung and dried
1750 B.C.	Minos (Crete)	Cereal was left on the field for some days after it was cut and sheaved. It was then threshed, dried and stored in earthern containers
1750 B.C.	Euphrates river valley	Legumes were dried and stored
1750 B.C.	Southern Mesopotamia	Dates and figs dried in the sun
1750 B.C.	India	Grains dried in the sun (11,28,31,32)
2000 B.C.	Denmark	Animals were put in folds and fed dried leaves in winter
1500 B.C.	Crete	Hay was dried and stored in caves (28,32)
1500 B.C.	Egypt, Crete	Furniture made of dried wood. Glue was made by decocting animal bones, gristles, hides and sinews and then boiling and evaporating the water in the broth till it dried (32)
1500 B.C.	Egypt,	Thin sheets of wood were glued cross-wise on top of each other and dried to obtain pieces of wood with very stable dimensions (4,11,15)
1600 - 1400 B.C.	Minos, Crete	Earthern objects were dried (31,32)
1500 B.C.	Crete	Hides were dried in the warm air of rock caves (32) after they were salted, cleaned of meat residues, the hair loosened with lime and were tanned using barks of oak and acacia pods (32)
1500 B.C.	China	The cocoons of silkworm were dried to obtain threads (11)
Iron Age 1000 B.C.	Mesopotamia	Large buildings were made partly from air-dried bricks and partly from fired bricks The Ischtar gate in Babylonia was decorated with magnificient reliefs of dried, lightly fired and colourfully enamelled brick (4,10,11)

Period	Location	Drying Applications
1200 B.C.	Greece	Cloth was dyed and dried
The Age of the Greeks, Romans and Celts		
600 B.C.	Athens	Farmers, tanners, weavers and master builders had a great deal to do with drying. (38) It was also used extensively by potters (11)
320 B.C.	Athens	Felled and barked trees were covered with dung so that they could dry slowly without cracks Washed wood was piled up in the open air in a way which allowed for favourable drying conditions (11,39,40)
500 B.C.	Tiber river basin	Salt was crystallized out in flat basins from sea water. Using this sea salt they produced dry fish (11)
350 B.C.	Rome	Drying was extensively used by pelters, brickmakers, weavers, tanners, fullers, dyers and others (41)
89 B.C.	Naples	Hot air from stoves streamed through earthern pipes or walls of hollow bricks to the living rooms and sometimes other rooms where goods were dried (11)
500 B.C.	Corinthia	Drying used in ceramic production
100 B.C.	Germany, Austria, Switzerland	cereals were dried (36)
Late Antiquity		
50 A.D.	Italy	Hay had to be dried as humid hay could easily catch fire. All grains were kiln-dried (43). Fruit was preserved by drying. Fibres too were dried (41)
79 A.D.	Pompeii Rome	Special drying places were provided for the drying of hides (8) Construction of houses too, involved the use of many drying processes (11,41)
105 A.D.	China	From rags and water Ts'ai Lun prepared a suspension of fibres, shook it on a sieve whereby the water ran off and a thin layer of fibre remained. The layer when dried gave rise to paper (14,16, 40)
630 A.D.	India	Solid sugar was obtained by drying after crystallization from sugar syrup (11,14)

Period	Location	Drying Applications
Around 300-400 A.D.	India	In the preparation of tea leaves, fresh leaves were picked and dried by spreading on grates (11)
590 A.D.	China	In printing with wooden plates, the chinese cut pictures in these plates, coloured the plates with ink and pressed them against paper. This gave copies which had to be dried (14,16,40)
621 A.D.	China	From china clay, feldspar and water the potters formed a homogeneous mass which they used to form the objects, which had to be dried subsequently (11,38,40)
Middle Ages		
After 700 A.D.	Europe	Leather craftsmen, parchment makers and fullers had a lot to do with drying
568 A.D.	Freising	Hop was cultivated for beer. Soon after harvest the umbels were shed on barn floors in order to dry them in air drafts to make them durable (14,48,49,51)
900 A.D.	Norway	Sea-fish were dried in the open air (48,51)
1000 - 1100 A.D.	Middle Europe	Bark-mills were built in which dried bark of young oaks were ground to obtain tanning bark for tanners (14,44,50)
1450 A.D.	Middle Europe	There were 80 different types of trades and at least 15 of them had to do with drying (11,50)
1450 A.D.	Middle Europe	Closed stoves with heat retaining wall tiles were built for the first time. These produced circulating air currents which were used by craftsmen to dry objects. Thus they ran the first circulation air dryers without knowing it (26,52,53)
1390 A.D.	Nuremburg (Germany)	The first paper was produced here. A water driven pounding machine ground textile rags into fibres and produced a pulp which was used to make paper. The paper thus produced was placed between felt and pressed hung over ropes and dried in ventilated rooms (14,16)
1440 A.D.	Strasbourg and Mayence	Gutenberg put together the printing block from single accurately cast metal types. He inked the plate surface and pressed it on book paper. The sheets of paper which were still wet with the ink were dried close to the workshop stove (14,16)

Period	Location	Drying Applications
	Northeast of America	Native Indians cultivated tobacco and dried the leaves (21)
	Mexico	Mexicans dried shelled cocoa seeds on bark pieces (11)
	Peru	Peruans dried the leaves of the cocoa plant and chewed it together with lime as a stimulant (11)
Renaissance to Machine Age		
1300 A.D. - 1500 A.D.	Middle Europe	Forage plants and trade and manufacture plants like flax and hemp were partly dried in the field immediately after harvesting (48)
1700 A.D.	Middle Europe	Hay was dried by spreading it out on the ground under the sun and turning it over a couple of times. However, to prevent the loss of nutrients, mineral substances and vitamins, it was then recommended to use racks for drying (48)
18th century	Livonia (Russia)	For drying, peasants heaped bundles of grain in heated smoke chambers which were usually without a chimney. Some houses burned down due to that (48,55)
	England	Millers used special coke heated drying furnaces These were walled-in chambers with fire vaults, on top of which mezzanines of porous stones, perforated plates or wire meshes were arranged. The grain was shed on these mezzanines. The fumes streamed through the layers of grain and dried them in about 8 hours However these grains were left with a smokey taste (56)
1775 A.D.	Berne	A shaft like grain dryer was built of bricks. It had a roof like installation which staggered one over the other. The grain was poured in from above and it slid down as the discharge was opened. Fumes streamed from a fire chamber through openings in the shaft walls to the grain and dried them. The material had to be cycled through the mill eight times and it required a drying time of 24 hours. The grain from this mill gave somewhat darker flour (57).
	Germany	Drying of flax and hemp in ovens and other furnaces were hazardous as these fibres could easily catch fire, and hence it was forbidden in many towns (53)

Period	Location	Drying Applications
1770 A.D.	Prague	Physicians dried herbs and roots and prepared essences (48)
1770 A.D.	Europe	Corn, tobacco and potatoes were dried for storage
1900 A.D.	Germany	Potatoes were dried mechanically (48)
The Trades		
1524	Augsburg	Printed textiles were dried (27)
1530	Europe	Common salt was gained by evaporation from natural or artifically prepared salt water either from salt pans using suns heat or from pans by means of fire. The basket or moulds into which the pan salt was filled were put in an elevated place so that the salt dried out better in warm air (58)
17th century	England	Lack of wood in the middle of the 16th century forced workshops to use coal. In the 17th century coal was degassed to give coke and heating gas which were used for heating dryers (14,26)
1700 A.D.	Europe	Large woolen cloth mills used various drying appliances The washed wool was dried in shady open air places, also in heated rooms with many story frames. Skeins of dried yarn had to be dried while they were hanging. For stretching, straightening and final drying of cloth, people used frames of wooden beams and slats. In case of fair weather, these frames of wet cloth were stretched out in the open air or unheated rooms where the product could release its humidity (59). Papermakers used the large, many story attics of their homes for the drying of the material. Sheets which had been squeezed out between felts were hung in rows one over the other and exposed either to the outside air or to the warm circulating air of the interior. Outdoor areas close to brick making places as well as roofed seafolds were used for drying bricks (60). Outdoor drying places were also available for pottery (53)
1727	England	First drying furnace for wood for the naval dock yard was constructed. Probably all "closed" dryers of the 18th century worked with so called "natural" air currents. Suitable blowers for "forced circulation" were still not available for dryers. Air heaters for grain dryers were proposed soon after 1800.

Period	Location	Drying Applications
1765	England	Watt invented the steam engine. Sometime later Hargreaves built the first spinning frame and Cartwright the mechanical Jacquard loom. This caused the development of many mechanical dryers in the 19th and 20th century (40,62)
Science		
1577 - 1644 A.D.		Van Helmant was the first one to demonstrate at a university the processes of distilling, drying and calcining (40). However, although the discoveries of Lavoisier, Galilei , Bacon, Boyle, Newton, Black (40,63) gave us a lot of valuable knowledge, they did not contribute noticeably to the progress of the drying techniques. The main laws of thermodynamics were still not known, the knowledge of gas flows still poor, the theory of transfer of energy and matter was still missing and nothing was known about the physical processes and the potential material changes in the goods. Not before the end of the 19th century the natural sciences began to influence the practical drying technique, and only in the twenties of our century did the scientists begin to investigate more thoroughly the processes which play a role in drying (62). It would require a special contribution to point this out in detail and to describe the development of drying techniques and machines in the last two centuries.
1600 - 1800 A.D.		

BIBLIOGRAPHY

1. White, E.; Brown, D.: Die ersten Menschen. Time-Life International (Nederland) B.V. 1973/74. (The First Men).
2. Constable, G.: Die Neandertaler. Time-Life International (Nederland) B.V. 1972/73. (The Nederthals).
3. Frideaux, T.: Der Cro-Magnon Mensch. Time-Life International (Nederland) B.V. 1973. (Cro-Magnon Man).
4. Hawkes, J.: Bildatlas der fruhen Kulturen. Gutersloh 1977.
5. Leonard, J.N.: Die ersten Ackerbauer. Time-Life International (Nederland) B.V. 1973/74. (The First Farmers).
6. Hamblin, D.J.: Die ersten Stadte. Time-Life International (Nederland) B.V. 1973. (The First Cities).
7. Portner, R.: Alte Kulturen ans Licht gebracht. Disseldord, Wien 1975.
8. Bravo, G.A.; Trupke, J.: 100 000 Jahre Leder. Basel und Stuttgart 1970.
9. Fasol, Th.: Was ist Leder? Stuttgart 1954.
10. Knaut, P.: Die Entdeckung des Metalls. Time-Life International (Nederland) B.V. 1973/74. (The Metal Smiths).
11. Vom Ackerbau zum Zahnrad. 7000 Jahre fruhe technische Kultur. Stuttgart 1969.
12. Durant, W.: Der alte Orient und Indien. Bd. 1 der "Kulturgeschichte der Menschheit" von W. u. A. Durant. Munchen 1977.
13. Steinert, H.: Uberseehandel schon im 6. Jahrtausend v. Chr. Frankfurter Allgemeine Zeitung 7.12.1977.
14. Klinckowstroem, von, C.: Knauers Geschichte der Technik. Munchen, Zurich 1959.
15. Sandermann, W.: Das erste Eisen fiel vom Himmel. Die großen Erfindungen der fruhen Kulturen, Munchen 1978.
16. Vom Amulett zur Zeitung, 7000 Jahre fruhe technische Kultur. Stuttgart 1967, 1969.
17. Bibby, G.: Faustkeil und Bronzeschwert. Reinbeck bei Hamburg 1977.
18. Wernick, R.: Steinerne Zeugen fruher Kulturen. Time-Life International (Nederland) B.V. 1973/74. (The Monument Builders).

19. Knorzer, K.-H.: Untersuchungen subfossiler pflanzlicher Großreste im Rheinland. Archaeo-Physika 2. Koln, Graz 1967.
20. Rinne, W.: Revolution im Faserreich. Funf Jahrtausende Textilgeschichte, 1950.
21. Claiborne, R.: Die Besiedelung Amerikas. Time-Life International (Nederland) B.V. 1973. (The First Americans).
22. Fruheste Amerikaner vor 40 000 Jahren? Frankfurter Allgemeine Zeitung 23.3.1977.
23. Behm, H. W.: Korn wachst fur alle. Berlin 1959.
24. Schmokel, H.: Ur, Assur und Babylon, 2. Aufl. Stuttgart 1955.
25. Wolf, W.: Die Welt der Agypter. Stuttgart 1954.
26. Meyers Handbuch uber die Technik. Mannheim 1964.
27. Stein, : Kulturfahrplan. Munchen, Berlin, Wien 1968.
28. Bibby, G.: Als Troja brannte und Babylon fiel. Reinbeck bei Hamburg 1976.
29. Hicks, J.: Die ersten Reiche. Time-Life International (Nederland) B.V. 1974. (The Empire Builders).
30. Francek, Th.: Abenteurer aus dem Norden. Time-Life International (Nederland) B.V. 1974/75. (The Northmen).
31. Edey, M. A.: Die verlorene Welt der Agais. Time-Life International (Nederland) B.V. 1975. (Lost World of the Agean).
32. Faure, P.: Kreta. Das Leben im Reich der Minos. Stuttgart 1976.
33. Die Bucher des alten Testaments.
34. Homer: Ilias. Deutsch von J.H. Voss, 1793.
35. Homer: Odysee. Deutsch von J.H. Voss, 1781.
36. Jankuhn, H.: Vor- und Fruhgeschichte vom Neolithikum bis zur Volkerwanderungszeit. Bd. I von "Deutsche Agrargeschichte", Hrsg. Franz, G. Stuttgart 1969.
37. Hesiod: Samtliche Werke. Deutsch von Thassilo von Scheffer. Wiesbaden 1947.
38. Durant, W.: Der ferne Osten und der Aufstieg Griechenlands. Bd. 2 der "Kulturgeschichte der Menschheit" von W. u. A. Durant. Munchen 1976.
39. Durant, W.: Das klassische Griechenland. Bd. 3 der "Kulturgeschichte der Menschheit" von W.u.A. Durant. Munchen 1976/77.
40. Mason, St.F.: Geschichte der Naturwissenschaft. 2. Aufl., Stuttgart 1974.
41. Durant, W.: Der Aufstieg Roms und das Imperium. Bd. 4 der "Kulturgeschichte der Menschheit" von W.u.A. Durant. Munchen 1977.
42. Norton-Taylor, D.: Die Kelten. Time-Life International (Nederland) B.V. 1974/76. (The Celts).
43. Columella, L.J.M.: De re rustica.
44. Vitruvius Pollio, M.: De architectura.
45. Bauer, P.: Bindemittel und Pigmente in der Literatur des Altertums. Farbe und Lack 77(1971)5-10.
46. Dopsch, A.: Wirtschaftliche und soziale Grundlagen der europaischen Kulturentwicklung aus der Zeit von Casar bis auf Karl den Großen. I. Teil Wien 1918, II. Teil Wien 1920.
47. Durant, W.: Das fruhe Mittelalter. Bd. 6 der "Kulturgeschiohta der Menschheit" von W. und A. Durant. Munchen 1978.
48. Abel, W.: Geschichte der deutschen Landwirtschaft vom fruhen Mittelalter bis zum 19. Jahrhundert. Stuttgart 1962.
49. Mummenhoff, E.: Der Handwerker in der deutschen Vergangenheit. Leipzig 1901.
50. Wernet, W.: Kurzgefasste Geschichte des Handwerks in Deutschland. Dortmund 1953.
51. Dopsch, A.: Die Wirtschaftsentwicklung der Karolingerzeit. Weimar 1913.
52. Volkers, O.: Deutsche Hausfibel. Leipzig 1937.
53. Antz, E.L.: Aus der Geschichte der Keramik in Deutschland. Feldhaus, Enzyklopadie, Poppe 1922. Technikgeschichte 12. Bd.
54. Traunfelder, A.: Die erste deutsche und die erste markgrafliche Papiermuhle. Ansbacher Kulturspiegel 18 (1968), 6 Seiten.
55. Hoffmann, J.F., Mohs, K.: Das Getreidekorn. Berlin 1931.
56. Jones, J.: Beschreibung eines senkrecnten Ofens zum Trocknen des Kornes. Polytechnisches Journal 14(1824)88-97.
57. Fournier de Faye: Auszug aus einer Notiz uber die zur Trocknung des Getreides bestimmte Darre zu Bern. Polytechnisches Journal 14(1824)80-87.
58. Agricola, G.: De re metallica libri XII. Basel 1556. Ubersetzt ins Deutsche von Schiffer, C.: Zwolf Bucher vom Berg-und Huttenwesen, 3. Aufl. Dusseldorf 1961.
59. Schmutzler, M.: Die Tuchmacherkunst um 1700. Textilpraxis 24(1969)528-529; 593-595; 666-668; 25(1970)177-179; 218-219; 735-737.
60. Pinkl. V.: Das Trocknen von Ziegelformlingen. Halle (Saale) 1928.
61. Moll,F.: Kunstliche Holztrocknung, ein Grundriß. Berlin 1930.
62. Kroll, K.: Einige Entwicklungslinien der Trocknungstechnik, Verfahrenstechnik 5(1971) 279-288.
63. Newton, I.: Philosophiae naturalis principia mathematica 1723.
64. Bernouilli, D.: Hydrodynamica. Straßburg 1738.
65. Ginsburg, A.S.: Die Entwicklung von Theorie und Praxis der Trocknung in den Jahren der Sowjetmacht. Die Technik 25(1970) 399-404.
66. Eucken, A.: Physikalische, chemische und technische Thermodynamik. In Muller-Pouillets Lehrbuch der Physik, 11. Aufl. 3. Bd., erste Halfte. Braunschweig 1926.
67. Thompson, B.: Experiments made to determine the positive and relative Quantities of Moisture absorbed from the Atmosphere etc. Phil. Trans. Roy. Soc. 77(1787)240.
68. Tompson, B.: Experiments on Heat. Phil. Trans. Roy. Soc. 82(1792)480.

ENERGY MANAGEMENT FOR DRYING SYSTEMS BY A COMPUTER - BASED DECISION AID

M. H. Waller[1]
S. C. Curtis[2]

1. Miami University, Oxford, Ohio 45056
2. Raytheon Company, Norwood, Massachusetts 02062

ABSTRACT

An analytical calculation routine has been developed which can achieve solutions to minimize overall energy expenditure costs for drying systems in general, and paper drying in particular. The routine can provide operators and first-level managers with a calculation for the most economical use of electricity, fossil fuel and steam for paper drying demands while supplying improved information on how drying tradeoffs affect energy usage.

The method employed is to first model the drying process in traditional block diagram/node fashion, then use a Fletcher-Powell approach to extract the minimum energy usage. The resultant program is small enough to fit on most control mini-computers and the technique can be used for several drying processes other than paper.

NOMENCLATURE

c_p = specific heat at constant pressure, J/kgK
T_{in} = entering temperature, K
T_{out} = leaving temperature, K
T_s = saturation temperature, K
λ = latent heat of vaporization per unit mass, J/kg

Subscripts

l = liquid
v = vapor

INTRODUCTION - GENERAL DRYING PROBLEM

Although the heat and mass transfer mechanisms of conventional drying processes for solids are fairly well understood and documented (1),(2), the energy tradeoffs for various design options and operating strategies are not. One situation in particular for which the merits of various recirculation schemes is being actively discussed is for the drying of paper (3),(4),(5). Not only is paper manufacturing an extremely energy-intensive industry, but the complexity of the several non-linear drying processes, with the subtle effects of process changes on energy consumption, interact with the energy cost structures for gas, oil, steam and electricity to produce a situation which is extremely difficult to analyze.

Depending on the process complexity, production schedule and local cost structures, the energy tradeoffs for many drying processes can also change markedly in a short period of time, and thus present an opportunity to significantly improve the operation from the standpoint of economics. The system described herein can analyze the process and economic implications of energy tradeoffs by solving a set of simultaneous non-linear equations and present to the operator an immediate calculation of the optimum processing centerline for which the energy cost is minimized. As an example, a typical hot air thermal dewatering situation is analyzed.

THE PAPERMAKING DRYING PROBLEM

General Description

Most drying processes can be analyzed for a given situation by breaking them down into discrete processing blocks with enough known information (typically a transfer function, an equilibrium condition and an energy conservation expression) to calculate a resultant condition. For the usual papermaking drying system, energy is typically expended in these areas:

- Steam - Yankee and can dryers; heating of hood air
- Fossil fuels - Furnace hot air for through-dryers or Yankee hoods
- Electricity - Fans for air circulation

The implications of tradeoffs between these energy sources can be determined by modeling their interactions in a General Drying Block, an example of which is presented in Figure 1.

Although extremely complex drying processes can be analyzed by allowing block optional features such as multiple energy sources, partial internal exhaust/recycle, or partial exhaust transfer to another block, two typical configurations for paper drying are shown in Figure 2 and Figure 3. Figure 2 shows the simple recirculation scheme typical of conventional, non through-dryer, paper-machines, where a portion of the exhaust air from

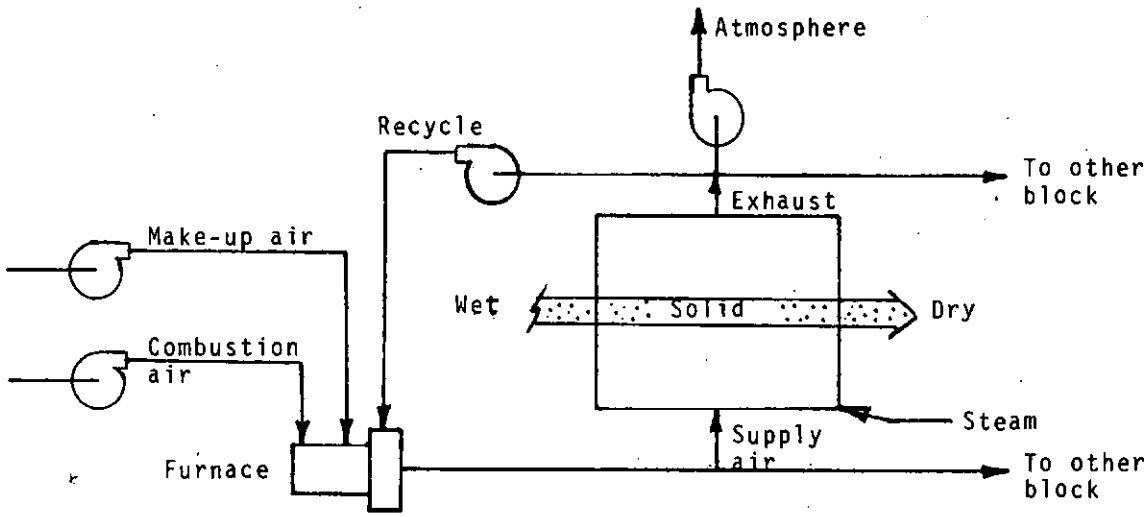

Figure 1 General Drying Block

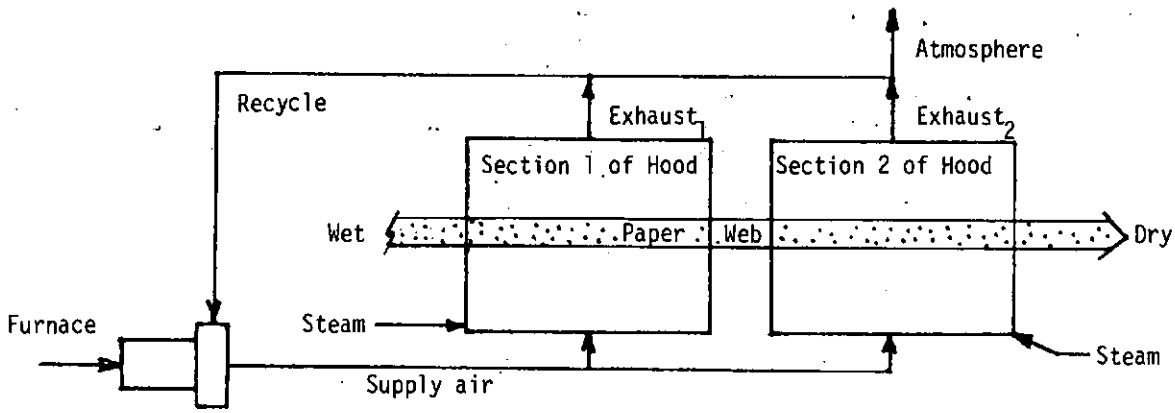

Figure 2 Recycle Drying Process

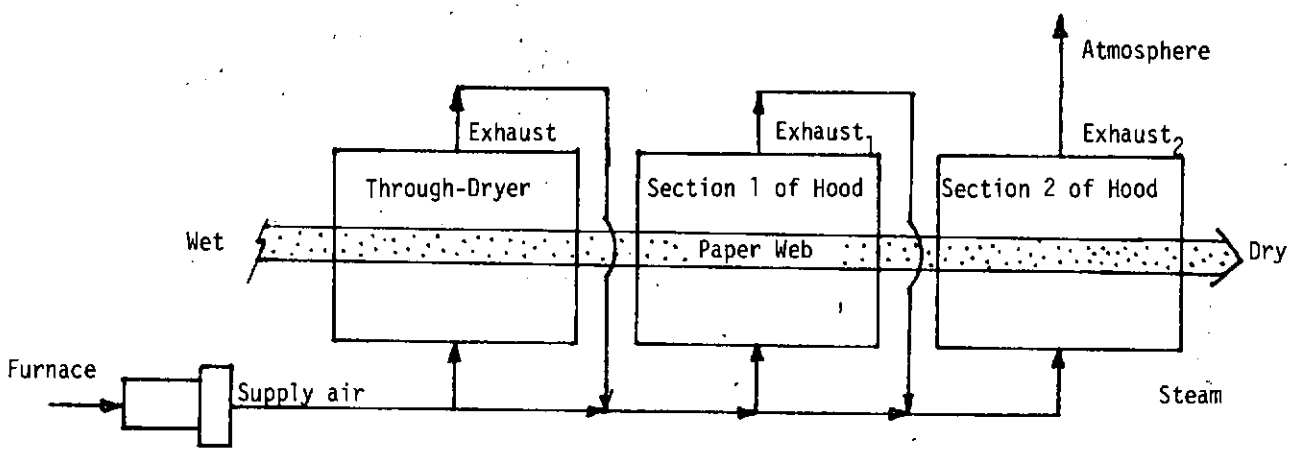

Figure 3 Cascaded Drying Process

both sections of hood is recycled to the furnace for reheating. Figure 3 shows a more complicated cascaded process that includes through-dryers as well as (Yankee) hood blocks.

Optimization Approach

For the purposes of illustrating the energy/drying analysis and optimization technique, let us return to the system depicted in Figure 1. For this simple recirculation scheme, the drying energy issues can be modeled by one General Drying Block. Figure 4 shows a node diagram of the block, for an energy/mass balance around the system. Since there

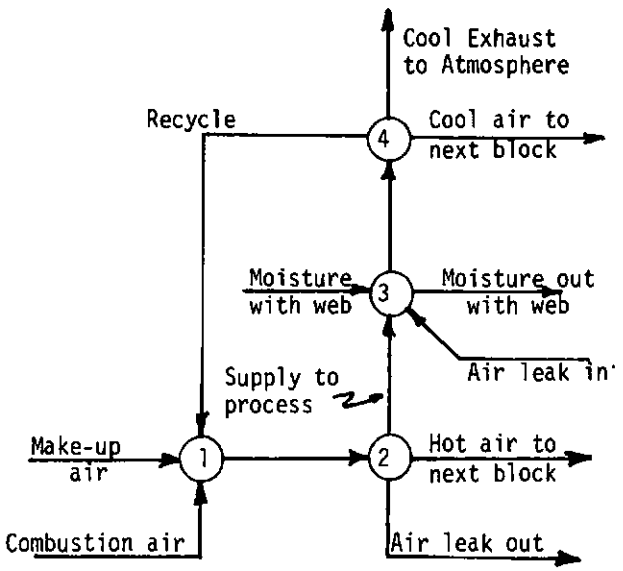

Figure 4 Node Diagram
For Balance Equations

are four nodes with three components (air, water and enthalpy) in each stream or arc, the problem can be formulated as a set of simultaneous non-linear equations, with four linear air balances, four linear water balances, and four non-linear enthalpy balances. The driving function, or demand equation, is the specified drying load (mass of water which must be removed), plus losses and extra demands, which amounts to another non-linear heat/mass transfer balance. Thus for any machine speed, given a sheet basis weight and its incoming and exiting moistures, the drying load can be found by finding a solution to the above system of 13 equations.

Unless the drying demand is pushing the system to its maximum heat transfer capability, there will be several ways to achieve the desired water removal. To select among the family of acceptable and thus feasible solutions for the constraints imposed by the system equations, a criterion must be specified to rank order the options in order to determine the non-linear objective function which minimizes steam, fuel and electricity costs. If the cost for each energy source is known, the optimal energy operating strategy for the simple recirculation scheme can be computed by calculating steam, fuel and electricity consumption as a function of system variables of air, water and enthalpy. Since the energy carried into the system by the air, water, paper and fuel must balance the energy that is leaving, the overall balance can be formulated by constructing a series of balance expressions for each component. For example, the specific energy gain of the water would be:

$$c_{pl}(T_s - T_{in}) + \lambda + c_{pv}(T_{out} - T_s) \qquad (1)$$

For the paper or air, only the sensible heat gain is appropriate, typically:

$$c_p(T_{out} - T_{in}) \qquad (2)$$

These energy equations are structurally rather simple, involving only sensible heat gains and heats of vaporization. For a given machine speed, the needed vaporization load and mass transfer rate are fixed, and the only energy loss which can change significantly is the energy of the water vapor and air in the exhaust stream. Indeed, from a cost standpoint, the energy contained in this stream should be minimized by focusing on ways to approach saturation conditions for this stream.

Ignoring small side flows, the amount of water in the exhaust stream equals the water vaporized from the sheet. Thus, there are only two variables that need to be computed for each energy strategy: exhaust stream temperature and humidity (or air flow). So for the simple one block recycle problem, energy strategy is a function of two variables and 13 system equations. If there is no recycle or no furnace, there is only one variable. Problems of this size are easily handled using standard non-linear optimization techniques. The method employed here was a modification of Powell's algorithm, commonly refered to as the Fletcher-Powell Method (6).

To analyze a multi-block problem, calculations are made for each block as described above, but intermediate air flows and sheet moistures are also computed. Blocks with furnaces are calculated first, blocks with exhaust-to-atmosphere are computed last. Given the option, the program assumes counter-current recycle of exhaust, with a higher temperature and lower air flow on the dry end, and a lower temperature and higher flow at the wet end. Additional process constraints can be entered to keep temperatures, humidities and intermediate moistures within process and material design limits.

Detailed Program Characteristics

The algorithm is implemented in IBM Fortran and requires 40K core. Because the problem is divided into subproblems (blocks), very few variables and subroutines need to reside in memory at any one time. This allows easy implementation in small process-control minicomputers. For a single block problem, the program is very fast, requiring only 10-15 iterations to find the optimal solution. For multi-block problems, the computational difficulty increases quite rapidly

because the number of variables is approximately 2N+1, where N is the number of blocks. A problem similar to the three block cascaded system (Figure 3) requires about 5000 iterations. The overall program logic is outlined in Figure 5.

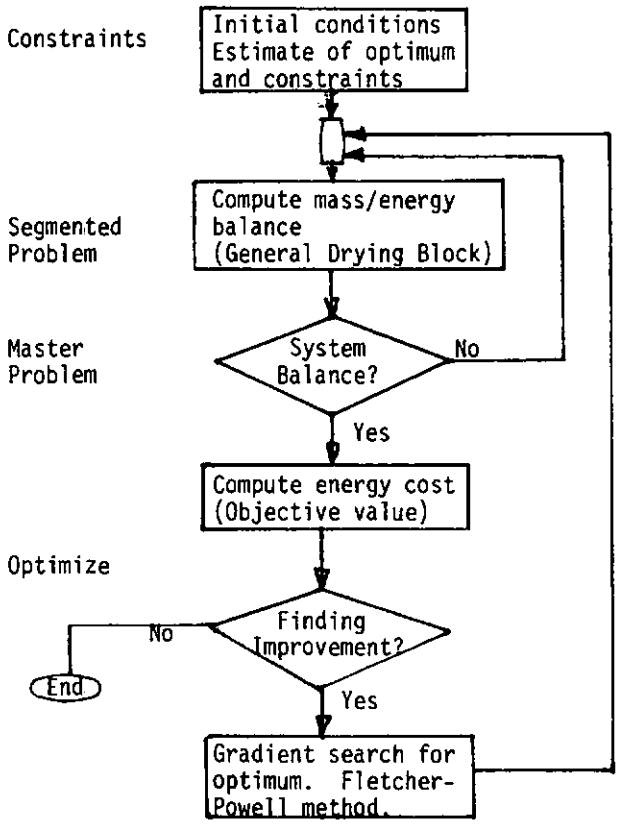

Figure 5 Block Diagram of Program Logic

While trying various optimization algorithms, we found some problems with low humidity high temperature blocks. Several approaches converged incorrectly to a low humidity high temperature local minimum, so the Fletcher-Powell method was used to check global options before settling into any local minimum. This points to potential problems with "blind", purely data-driven models; they may be sensitive to initial process set point. More importantly, a theoretical model allows intuitive interpretation.

Management/Operator Interface

When members of the operator/management team understand the basis for the computer calculation procedure, and thus have confidence in the output, ideas will be generated for energy savings concepts and strategies which ultimately will result in process design improvements. The theoretical model can thus be improved if the program is routinely run for each machine drying system or product change, for which the optimal centerline can be computed. For program startup, initial process parameters must be specified if different from previous default values, otherwise only the cost(s) need be updated. Figure 6 shows a schematic of the inputs and outputs.

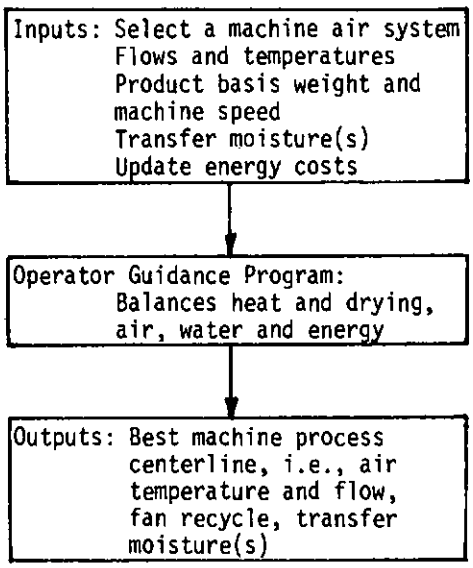

Figure 6 Schematic of Inputs and Outputs

Extending the Approach

Because of the theoretical, as opposed to data driven, basis for this approach the program can also be used to evaluate energy design considerations such as optimum machine size (heat transfer surface area), and the optimum fan/duct sizing for recirculation of exhaust. This can be useful in upgrading the efficiency of existing processes or optimizing the design of new systems. As mentioned earlier, the program could also be implemented in real-time on a fairly small process control computer. For plants with co-generation or ample steam condensate load, the cost structure may be a strong function of other plant capabilities. This may lead to some interesting hierarchial control applications where a supervisory energy control computer would provide set point information to local process control loops. Takamoto and Williams (7), report on a hierarchial structure for production control in the steel industry with energy as a constraint. Energy information could also flow up to an overall plant computer, providing input on production scheduling or order filling to minimize cost. Finally, it should be pointed out that in many cases the optimization strategy could also be data driven, and the theoretical model could then give the best explanation of existing operating data before optimizing. Trends of process parameters could then be used to indicate process problems and the need for subsequent correction.

ACKNOWLEDGEMENT

The support of the Procter & Gamble Co., where both authors were employed during the development of the computer program, is acknowledged. The assistance of both Miami University and Raytheon Company during the preparation of this paper is appreciated.

REFERENCES

1. Perry, J.H.(ed.): "Chemical Engineers' Handbook," 5th ed., McGraw-Hill, New York, 1973.
2. Han, S.T., "Drying of Paper," TAPPI, Vol.53, No.6, pp 1034-1046 (1970).
3. Wedel, G.L., and Chance, J.L., "Analysis of through-drying," TAPPI, Vol.60, No.7, pp 82-85 (1977).
4. Gardiner, F.J., "Design of convective dryers for best efficiency and productivity," TAPPI, Vol.60, No.7, pp 90-93 (1977).
5. Villalobos, J.A., "Engineering considerations in through drying," Paper Tech. and Ind., Vol.16, No.5, pp 290-301 (1975).
6. Fletcher, R., and Powell, M.J.D., "A rapidly convergent descent method for minimization," Computer J., Vol.6 (1963).
7. Takamoto, H., and Williams, T.J., "Production Control in the Steel Industry with Energy Conservation Considerations - A Preliminary Evaluation," Report 114, Purdue Laboratory for Applied Industrial Control, Purdue Univ, West Lafayette, Indiana (June 1979).

PSYCHROMETRICS AS THE THERMODYNAMICS OF MOIST AIR

John A. Goff

Philadelphia, Pennsylvania, U.S.A.

INTRODUCTION

Thermodynamic analysis of, say, a unit operation, real or proposed, usually consists of weight and energy accountings to which should sometimes be added an entropy accounting. For the operation to be real or physically realizable these accountings need show zero weight, zero energy and non-negative entropy balances, overall as in all parts.

It is in the making of the above accountings that P.W. Bridgman's (1) notion of convected (sic) energy, to which is here added that of convected entropy, are especially useful. Both are derivable from the identical relation,

$$T(t)ds = du + P(p)dv, \tag{1}$$

of thermodynamic theory, a relation governing quasi-static changes of a simple substance whose thermodynamic states are delineable as points on, say, its p, v-plane.

In relation (1) the lower case letters s, u, v denote specific entropy, energy and volume, respectively, each per unit weight of substance; the lower case letters t and p, however, denote empirical isotherm (t=const.) and isobar (p=const.) numberings completely arbitrary as to scale. With these empirical are associated canonical numberings T(t) and P(p), each having but one degree of arbitrariness, a multiplicative constant, each being therefore called absolute.

Practical realization of the function T(t) has long been a major problem of experimental thermodynamics; but not so of P(p), it being generally believed that, as its name implies, thermodynamics is but a branch of mechanics, hence that the isobar numbering of thermodynamics and that of mechanics are identical; that is, P(p) = p, here accepted for practical reasons as valid within the accuracy of existing knowledge, relation (1) to be rewritten in familiar form as

$$Tds = du + pdv \ . \tag{2}$$

From relation (2) via definitions,

$$S/s = U/u = V/v = M = G/g \tag{3}$$

are readily derivable the identical relations,

$$(dU/dM)_{V,s} = h \text{ and } (dS/dM)_{v,s} = s, \tag{4}$$

naming enthalpy h as convected energy and entropy s as convected entropy.

To find support for the above namings consider the operation: smooth withdrawal of air of energy,

$$u(p,v) = pv/(k-1) \tag{5}$$

with k>1 a constant characteristic thereof, from an adiabatic enclosure of unvarying volume V. The change inside the enclosure during withdrawal is, by definition, adiabatic and quasi-static, delineable as a continuous curve on, say the p, v-plane; it is, therefore, isentropic (s=const.) and, by identical relation (2) governed by the Pfaff equation in two variables,

$$vdp + kpdv = 0, \tag{6}$$

which, by Pfaff's Theorem, has but the one integral equivalent,

$$pv^k = \text{const.} \tag{7}$$

Thus, by identical relation (2), does relation (5) imply:

$$s = s(pv^k), \text{ hence } s'(pv^k) = R(pv^k)/(pv^k)(k-1) \text{ with} \tag{8}$$

$$R(pv^k) = pv/T; \tag{9}$$

therefore as volume v = V/M of inside air increases isentropically toward infinity during withdrawal its pressure p and temperature T decrease likewise toward zero, a prediction well and easily confirmed experimentally.

The same prediction can be made in another way using the convected energy notion. Thus, withdrawal of weight -dM of air and with it energy -hdM decreases the energy u of inside air; because

$dU = Mdu + udM = hdM$, whence $du = pv(dM/M) < 0$. (10)

And, since the change of u is isentropic (pv^k = const.) and so is pv/T constant by relation (9); therefore do pressure p and temperature T both decrease with increasing volume v.

Confidence in the above interpretation of identical relations (4) is strengthened by consideration of the filling of an adiabatic enclosure of unvarying volume V, initially evacuated, with air from ambient atmosphere at temperature T and pressure p, air of energy $u = pv/(k-1)$ and temperature $T = pv/R$, where R is another constant characteristic thereof. The combined weight and energy accountings is:

$$M_2u_2 = M_1u_1 + (M_2-M_1)h_o \text{ or } u_2-h_o = (M_1/M_2)(u_1-h_o), \quad (11)$$

which, for $M_1/M_2 = 0$, $u = pv/(k-1)$ and $T = pv/R$, reduces to

$$T_2 = kT_o = kT_1. \quad (12)$$

In principle, therefore, the subject filling operation is a form of calorimetry by which experimentally to determine the constant k. H. Oestrich (2) in his 1936 paper, "Erwärmung von Gasen bei gedrosselter Einströmung", has reported a temperature rise of 115.2C from 15C in the temperature of the outer surface of a thick-walled, 78kg oxygen cylinder alternately evacuated and filled with air in quick succession until the outer surface temperature reaches a steady state. From these data he infers the value, k = 1.400, exactly that predicted by the Kinetic Theory of Gases for a diatomic gas.

That the above filling operation is physically realizable is obvious, hence that it is, at least in part, non-static and that a combined weight-entropy analysis of it must show a non-negative balance called the entropy generated by it.

To make such an accounting calls for knowledge of the entropy function $s(pv^k)$ for air of energy $u = pv/(k-1)$ and temperature $T = pv/R$ derivable from the second of relations (8) with $R(pv^k) = R$, a constant. The required knowledge is:

$$s = c_v\ell n(pv^k) = kc_v(\ell nT - a\,\ell np) \text{ with}$$

$$a = (k-1)/k,\ c_v = R/(k-1), \quad (13)$$

from which

$$s_1-s_o = kc_v\left[\ell nT - a\ell n(p_o/p_1)\right] \text{ with } T_o = T_1$$

and $p_1 = 0$; and (14)

$$s_2-s_o = kc_v\ell nk \text{ with } T_2 = kT_o \text{ and } p_2 = p_o. \quad (14)$$

Finally, therefore, like the second of relations (11) the relevant weight and entropy accounting is:

$$M_2s_2 - M_1s_1 - (M_2 - M_1)s_o = M_2(s_2 - s_o) - M(s_1-s_o) > 0, \quad (15)$$

which, with relations (14,15), becomes

$$kc_v\left|M_2\ell nK - M_1a\ell n(p_o/p_1)\right| = p_oV\ell nk/T_o(k-1) > 0$$

... $M_1 = p_1 = 0$. (16)

positive definite. Q.E.D.

2.

MOIST AIR

An essential part of the Goff-Gratch formulation of the thermodynamic properties of moist air adopted 1947 as standard pending further research by the International Meteorological Organization (IMO) as recommended by the International Joint Committee on Psychrometric Data (IJCPD) as being thermodynamically consistent within the accuracy of existing knowledge are its working definitions including the following:

Dry Air as a gas mixture of Oxygen O_2 (.2095), Nitrogen N_2 (.7809), Argon A(.0093) and Carbon Dioxide CO_2 (.0003) ...mol fractions in parentheses;

Moist Air as a binary gas mixture of dry air (28.966) and water vapor (18.016) ... molecular weights in parentheses;

Saturation, a state of, is one in which moist air as vapor phase of the water (H_2O) - dry air system can coexist in equilibrium, not distinguished as to kind in respect of stability, with a condensed phase or phases, liquid and/or solid, of the same chemical components.

Mixing Ratio W as the weight of water vapor per unit weight of dry air;its value at saturation is $W_s(T,p)$.

Relative Saturation as measure of relative proximity to saturation on a line of given temperature and pressure from dry air (0%) to moist air at saturation (100%). For obvious reasons to be advanced later, the measure of relative saturation adopted is the ratio $\mu = W/W_s(T,p)$ defined in the interval $0\% \le \mu \le 100\%$ only.

Associated Condensed Phase as what the physical chemist calls an ideal solution of water substance as solvent and dry air as solute, one of sufficiently high dilution that its thermodynamic properties are arbitrarily little affected by intermolecular forces.

Mol-fractional Pressures $x_i p$ of a mixture of uniform pressure p and of component weights n_i are necessarily.

Partial Pressures $\Sigma p_i = p$ not necessarily mol-fractional pressures.

Coexistence Pressures $p_i(T,p,n_i,n_j)$, where index j counts all components except that of repeated index i .... (i, j = 1,2, ..., α) as the observable pressures of pure-component samples in coexistence with their mixture across NDP_i partitions non-supple (N), diathermic (D), selectively permeable (P_i) to component i only.

A mixture in coexistence across NDP_i partitions with samples of its pure components as alone and apart therefrom is a system in equilibrium iff (if and only if) in the near neighborhood of the given state all states having the same entropy S and same volume V have also the same energy U as has the given state; that is, if each component chemical potential $\mu_i(T,p,n_i,n_j)$ of the mixture is identically equal to its associated pure-component free enthalpy $g_i(T,p_i)$ for NDP_i or $g_i(T_i,p)$ for SAP_i partitions.

Thus are the coexistence pressures p_i or temperatures T_i of a mixture of uniform temperature T and uniform pressure p defined by the identical relations:

$$\mu_i(T,p,n_i,n_j) = g_i(T,p_i) \text{ or } g_i(T_i,p)$$
$$j \neq i = 1,2, \ldots,\alpha \qquad (17)$$

The coexistence pressures p_i of a mixture are subject also to the following conditions of general validity:

$$\text{for } x_i=0,\ p_i=0;\ \text{for } x_j=0,\ p_i=p;\ \text{for } p=0,\ p_i=0. \qquad (18)$$

sometimes useful in checking semi-rational formulations for thermodynamic consistency. Rewritten with interchange of T and p they become applicable to coexistence temperatures T_i.

Identical relation (2) rewritten as du = Tds - pdv proclaims u(s,v) a so-called characteristic function from which are derivable all other thermodynamic properties of the simple substance considered free of any constants or functions of integration not disposed of in formulating the function itself; thus

$$T = \partial u/\partial s,\ p = -\partial u/\partial v;\ h = u+pv,\ g = h-Ts \text{ etc.} \qquad (19)$$

The above rewriting of relation (2) can in turn be rewritten as

$$dg = -sdT + vdp \text{ with } s=-\partial g/\partial T \text{ and } v=\partial g/\partial p \qquad (20)$$

proclaiming g(T,p) another characteristic function.

Identical relation (2) can, with the aid of definitions (3) to which is added G/g = M, be rewritten as

$$dU = TdS - pdV + gdM \text{ with } g=u+pv-Ts \qquad (21)$$

for a simple substance of variable weight M, by obvious extension as

$$dU = TdS - pdV + \Sigma\mu_i dn_i \quad (i=1,2,\ldots,\alpha) \qquad (22)$$

for a mixture of component weights n_i. Rewritten with G = U + pV - TS this becomes (23)

$$dG = -SdT + Vdp + \Sigma\mu_i dn_i \qquad (24)$$

to proclaim the free enthalpy function $G(T,p,n_i)$ of a mixture of components n_i a characteristic function.

The function $G(T,p,n_i)$ is clearly homogeneous of degree one in the n_i, hence satisfies the Euler equation,

$$G = \Sigma n_i \partial G/\partial n_i = \Sigma n_i \mu_i = \Sigma n_i g_i(T,p_i), \qquad (25)$$

the last by virtue of coexistence relations (17); its derivatives μ_i are therefore homogeneous of degree zero therein, hence satisfy the Euler equation

$$0 = \Sigma n_k(\partial\mu_i/\partial n_k) = \Sigma n_k(\partial\mu_k/\partial n_i) = \Sigma n_k v_k(\partial p_k/\partial n_i),$$
$$i,k = 1,2 \ldots,\alpha \qquad (26)$$

the second because by (24) $\partial\mu_i/\partial n_k = \partial\mu_k/\partial n_i$ and because $v_k = \partial g_k(T,p_k)/\partial p_k$.

The last of equations (26) are a system of linear, homogeneous, algebraic equations with the $n_k v_k$ as unknowns, the $p_{ik} = \partial p_i/\partial n_k$ as coefficients and zeros as knowns.

At this point, to simplify the writing without loss of generality, the special case of a binary mixture (α=2) of which Moist Air is one of special interest here will be studied as an example; also will μ_{ik} and p_{ik} be written for $\partial\mu_i/\partial n_k$ and $\partial p_i/\partial n_k$, respectively. Thus do the last of (26) become:

$$0 = n_1\mu_{11} + n_2\mu_{12} = n_1\mu_{21} + n_2\mu_{22}$$
$$= n_1 v_1 p_{12} + n_2 v_2 p_{22}, \text{ the last of} \qquad (27)$$

which since $\mu_{21} = \mu_{12}$.

The determinant $n_1 n_2 \ldots n_\alpha D$, where D is that of coefficients of (27), is

$$\begin{vmatrix} n_1p_{11} & n_2p_{21} \\ n_1p_{21} & n_2p_{22} \end{vmatrix} = \begin{vmatrix} 0 & n_2p_{21} \\ 0 & n_2p_{22} \end{vmatrix} = \begin{vmatrix} p_{11} & p_{21} \\ p_{21} & p_{22} \end{vmatrix} = D = 0. \qquad (28)$$

the second by 'column addition' (4), the sum of row elements being zero since the $\mu_i(T,p,n_i,n_j)$ are homogeneous of degree zero in the n's, $G(T,p,n_i)$ being homogeneous of degree one therein.

The vanishing identically of determinant D of order $\alpha=2$ and rank $\alpha-1$, there being no further identical relations among the p_i, means that any set of solutions of a minor system of one fewer equations automatically satisfies the one omitted. Here the minor system could be the one equation whose coefficients are the top-row elements of the last of determinants (28); thus

$$(n_1v_1 - 1)p_{11} + (n_2v_2 - 1)p_{21}$$

$$= -\partial(p_1 + p_2)/\partial n_1 \qquad (29)$$

the only solution of which for $\Sigma p_i = p$ is $n_iv_i = n_1v_1 = V$, the volume of component 1 and simultaneously of the mixture itself at mixture temperature T, pressure p and pure-component specific volumes $v_i(T,p_i)$; in general

$$\Sigma p_i = p \text{ implies } n_iv_i(T,p_i) = V \qquad (30)$$

And so it is, to paraphrase GIBBS, in this sense that we should understand the law of partial temperatures, that every component of a mixture is as devoid of entropy to every other component; or that

$$\Sigma T_i = T \text{ implies } n_is_i(T_i,p) = S. \qquad (31)$$

Here it is worth noting that (30) becomes (31) while (24) remains as is under interchanges, each in place of other, of: T,p;-s, v; -S,V.

That the converse of deduction (30) is true is easy to prove. From identical relations (24,25) and $v_i = \partial g_i/\partial p_i$ it follows that:

$$V = \partial G/\partial p = \Sigma n_iv_i\partial p_i/\partial p,$$

which for $n_iv_i = V$ becomes $\partial\Sigma p_i/\partial p = 1$; or $\Sigma p_i = p + \phi(T,n_i)$ with $\phi = 0$ by the last of conditions (18).

Also from (24) with the aid of (17) is

$$S = -\partial G/\partial T = -\Sigma n_i\partial g_i/\partial T = \Sigma|n_is_i+n_iv_i\partial p_i/\partial T\ |,$$

which for $n_is_i = S$ becomes $V\partial\Sigma p_i/\partial T = 0$; or $\Sigma p_i = \phi(p,n_i)$ with $\phi=p$ by (18).

4.

In summary to urge the importance of thermodynamic consistency within the accuracy of existing knowledge in the prediction of thermodynamic properties of mixtures, not necessarily gaseous, from those of their pure components as alone and apart therefrom, the following short paragraphs are here added.

a) For a mixture of pressure p, temperature T and component weights n_i there exist well-defined coexistence pressures $p_i(T,p,n_i,n_j)$ and temperatures $T_i(T,p,n_i,n_j)$, all in principle realizable in practice. Supposed known are the pure-component free enthalpies g_i as functions of temperature and pressure.

b) Following is a theory of the practical realization of, say, the coexistence pressures p_i: the mixture within an enclosure much larger than those, initially evacuated, in communication with mixture across NDP_i partitions non-supple (N), diathermic (D) and selectively permeable (P_i) to component i only. In time each small enclosure i will be filled with pure component i at mixture temperature T and coexistence pressure $p_i = p_i(T,p,n_i,n_j)$ without appreciably changing mixture component weight n_i. Temperature T, pressure p and coexistence pressures p_i are then observable.

c) Coexistence temperatures T_i are in principle determinable in like manner but with, in lieu of NDP_i, SAP_i partitions supple (S), adiathermic (A), selectively permeable (P_i).

d) The system, mixture and coexisting pure components i, is in equilibrium if

$$\mu_i(T,p,n_i,n_j) = g_i(T,p_i) \text{ or } g_i(T_i,p)$$

$$j\neq i = 1,2,\ldots,\alpha$$

e) Of the mixture the free enthalpy function $G(T,p,n_i)$ is identically the sum of separate contributions from its several pure components i at mixture temperature T and component coexistence pressures p_i.

f) From a knowledge of $G(T,p,n_i)$ are derivable all other thermodynamic properties of the mixture considered. If its coexistence pressure p_i were partial pressures $\Sigma p_i=p$, all so derived properties except volume V would, like free enthalpy G, be sums of separate contributions from the several coexisting pure components i.

g) For Moist Air the coexistence pressures p_a, p_w are not partial pressures because of pair-wise forces, electrostatic in nature, between unlike (aw) molecules; not, that is, at low pressures and within the accuracy of existing knowledge.

h) Mol-fractional pressures x_ip are partial pressures $\Sigma p_i = p$ identically, but the converse of this statement is not necessarily true. Coexistence pressures are seldom if ever partial, less often mol-fractional pressures.

i) Thermodynamic consistency within the accuracy of existing knowledge calls for abrogation of Dalton's Law of partial pressures; and, more explicitly of Lewis' Fugacity Rule which, in the case of Moist Air, would predict the effect of forces between unlike molecules

(aw) to be the arithmetic mean of those between like molecules (aa,ww).

j) In identical relation (24) interchanges T,p and -S,V, each in place of other, leave G unchanged. It is to be expected, therefore, that by such interchanges including -s,v can statements about coexistence pressures p_i become statements of coexistence temperatures T_i, and vice versa.

k) A tidbit of academic interest only are the relations $p_i = x_i^c p$ with exponent $c(T,p)>0$, relations satisfying conditions of general validity (18) on the p_i as coexistence pressures of perfect-gas mixtures, $(pv)_i = RT$. If, then, $c(T,p) \neq 1$ the mixture is not a perfect gas-mixture $pV = \Sigma n_I RT$.

5.

A chart, on which are delineated isopleths of thermodynamic properties of Moist Air most needed by engineers and meteorologists in graphical solution of practical problems, has somehow come to be called a Psychrometric Chart, usually an isobaric chart of stated chart pressure p. It is agreed among engineers and meteorologists that such a chart should have mixing ratio W as ordinate and enthalpy h, per unit weight of dry air, as convected energy as abscissa.

On the Goff Diagram for Moist Air the abscissa is reduced enthalpy h-eW, the constant e being assigned arbitrarily the exact value 1000 Btu/lbw so to reduce chart format from scroll to page and multiplication to shift of decimal point. Besides e there are ordinate and abscissa scale constants b, c both multiplicative, and enthalpy constants w, a both additive, to be assigned arbitrarily exact values so to assure thermodynamic consistency with the Goff-Gratch formulation referred to earlier.

Identical relation (2) can, with the aid of definition h = u + pv, be re-written as Tds = dh - vdp, in which temperature T, pressure p and specific volume v are absolute, each as having but one degree of arbitrariness, a multiplicative constant. Entropy s and enthalpy h, however, are both relative, determinable only to within an additive constant of integration. These constants have to be disposed of arbitrarily.

For the Goff Chart with mixing ratio W as ordinate and reduced enthalpy h-eW as abscissa there are five constants so to be disposed of: two multiplicative ordinate and abscissa scale constants, the multiplicative constant e in reduced enthalpy and the two additive constants w and a in the specific enthalpies of water (H_2O) and dry air, respectively. The appearance, readability and usefulness of the chart in graphical solution of practical problems derive from the way in which these constants are disposed of.

On the Isogonal Chart referred to earlier a uniform angular spacing of dewpoint (0^θ), dry-bulb (45°), reduced enthalpy (90°) and wet-bulb (135°) isopleths is achieved without adverse effects on chart appearance but with improvement of readability, especially in distinguishing dry-bulb from reduced enthalpy isopleths, rather difficult on the Goff Chart.

There is good reason to accept the Goff-Gratch formulation value of the additive constant a since to change would only shift chart origin to left or right on the dry-air axis; but substantially to increase the too small angular separation of dry-bulb and reduced enthalpy isopleths on the Goff Chart would call for a substantial change in the additive constant w.

On the Goff Chart the reciprocal slope of a line is $(b/ae)(dh/dW - e)$, which suggests e and b/ae as parameters in terms of which to compare the psychrometric charts: Mollier, Goff, ASHVE, Grubenmann, Isogonal, Carrier, Baker and perhaps others.

On the above chart are delineated isopleths of: Relative Saturation μ, reduced enthalpy h-eW with e = 1000 Btu/lbw, dry-bulb temperature tF nearly straight and too little inclined to those of reduced enthalpy for good readability, of thermodynamic wet-bulb temperature t* by definition straight with negative slopes $h'_w(t^*,p)$ the specific enthalpy of pure compressed liquid water at chart pressure p, of thermodynamic dew-point $t_d \geq 32F$ and ice-point $t_i \leq 32F$ temperatures numbered as are the dry-bulb isotherms t = const. at their meetings on the Saturation Curve μ = 100% concave upward and asymptotic to the pure-water saturation $t_s(p)$ = const. at chart pressure p.

The Saturation Curve separates Region I of moist air proper as the vapor phase of the water (H_2O) - dry air system from Region II of said system at saturation. In Region II for practical reasons mixing ratio W is defined as weight of water (H_2O) per unit weight of dry air, an extension of the strict definition applicable to moist air as weight of water vapor per unit weight of dry air. Relative Saturation μ is undefined in Region II.

6.

An earlier statement that thermodynamic wet-bulb isotherms t* = const. are by definition straight lines on the Goff Chart with negative slopes $h'_w(t^*,p)$ calls for documentation. A psychrometer is an instrument consisting of two similar thermometers, the bulb of one covered with a thin film of liquid water, that of the other kept dry. The temperature reading t* of the one thermometer is lower than that of the other because of continuous evaporation of liquid from the film into ambient air across a water-air interface at which, in the steady

state, water and air would have the same temperature t* if the mixing operation were strictly adiabatic. A combined weight and energy accounting for the operation would then be:

$$h_s(t^*,p) = h(t,\mu,p) + [W_s(t^*,p) - \mu W_s(t,p)]h'_w(t^*,p) \quad (32)$$

in which h_s is the enthalpy of moist air at saturation per unit weight of dry air. This relation defines what is called thermodynamic wet-bulb temperature $t^*=t^*(t,\mu,p)$.

7.

To the air conditioning engineer and meteorologist Relative Saturation μ is the obvious measure of relative proximity of moist air to saturation on a line of given temperature t and pressure p from exactly 0% for dry air to exactly 100% for moist air at saturation - undefined outside the interval $0 \leq \mu \leq 1$. By definition it is precise, unambiguous and useful as interpolant for linear interpolation of volume v, enthalpy h and entropy s of moist air per unit weight of dry air, at given temperature and pressure, of course.

Relative Humidity, variously defined as the ratio of vapor pressures or vapor densities is a more familiar parameter generally supposed, in some cases wrongly, to be a measure of relative proximity to saturation. In 1947 the International Meteorological Organization (IMO) recommended appropriation of the designation Relative Humidity to the ratio of mixing ratios here called Relative Saturation. In May 1949 the International Joint Committee on Psychrometric Data (IJCPD) endorsed the IMO recommendation, inviting interested parties to submit comments and suggestions for later consideration by the Committee. Practically all responses submitted were unfavorable, some with righteous indignation against. All admitted that the notion of relative humidity stands in much need of precise and unambiguous definition to make it thermodynamically consistent, meaningful and useful especially to the engineer and meteorologist. All contended, however, that as the ratio of vapor pressures the notion is altogether too firmly established in hygrometric formulae of the type usually attributed to Regnault (1845), on which hygrometric tables used world wide are based, to warrant appropriation of the name relative humidity for designation to some essentially different notion.

Relative Humidity $\lambda(\mu)$ as the ratio of vapor molfractional pressures $x_w p$ is delineable as a curve concave downward on the λ,μ-plane with maximum upward displacement from the straight line $\lambda=\mu$ of amount $\underline{\lambda-\mu} = \underline{\mu}(1+a)/r$ at $\underline{\mu}=(r-1)/a$, where $a(t,p) = (28.966/18.016)W_s(t,p)$ and $r(t,p)=+\sqrt{(1+a)}$. Being exactly 0% for dry air and exactly 100% for moist air at saturation, it is indeed a measure of relative proximity to saturation. At (0,0) on the λ,μ-plane the relative humidity curve has slope (1+a), at (1,1) the slope 1/(1+a). On the curve 70F, 1 atm. at μ = .49686 its maximum upward displacement from the straight line $\lambda=\mu$ .00628 to λ = .50313. Thus is Relative Humidity not an obvious measure of relative proximity to saturation.

Again on the λ,μ-plane Relative Humidity $\lambda(\mu)$ as the ratio of vapor densities W/v, v being assumed linear in Relative Saturation μ, is delineable as a curve concave downward with slope a(t,p) at (0,0) and 1/a(t,p) at (1,1); also with maximum upward displacement from the ray $\lambda=\mu$ of amount $(r-1)\underline{\mu}$ at $\underline{\mu} = (r-1)/(a-1)$, where $a(t,p) = v_s/v_a$ - see Thermodynamic Properties of Moist Air at Standard Atmospheric Pressure, ASHVE GUIDE 1960 - and $r = \sqrt{a}$. On the curve 70F, 1 atm. a(t,p) = 13.687/13.348 = 1.0254 hence r = 1.0126, $\underline{\mu}$ = .4968 and $\underline{\lambda-\mu}$ = .0063 to make the density ratio curve much like the pressure ratio one, neither as obvious, precise, unambiguous and useful, at any rate to the engineer and meteorologist, a measure of relative proximity to saturation as is Relative Saturation μ.

Besides the above two meanings of Relative Humidity are two hybrids: $\lambda = x_w p/p_s$ and $\lambda = Wv_g/v$, where $p_s(t)$ is the saturation pressure of pure water and $v_g(t)$ is the volume of saturated water vapor, as if in each to say that moist air is saturated when so is its vapor component as existing alone and apart from the mixture. Unlike Relative Saturation μ exactly 0% for dry air and exactly 100% for moist air at saturation, these hybrids are significantly different from unity at saturation, but well-defined at temperatures above the saturation temperature of pure water if only up to its critical temperature. This is regarded by some as an essential feature of relative humidity, by others as a source of confusion. Both should be dispatched as being thermodynamically inconsistent.

8.

For practical reasons the experimental part of our moist air investigation avoided direct determination of its coexistence pressures p_a and p_w; it did, however, depend on the practical realization of phase coexistence (saturation) of moist air with its associated liquid phase as a so-called ideal solution of dry air in liquid water, a solution of sufficiently high dilution that its thermodynamic properties are arbitrarily little affected by intermolecular forces.

A steady stream of dry, carbon-dioxide free air was saturated (presumably) at set temperature $T \pm \delta$, then at set temperature T and pressure p_1. It was then throttled to reduced pressure p_2, presumably reduced to dry air by removal of measured weight m_1 of water, then presumably resaturated at temperature T and pressure p_2, again throttled and dried thereat with removal of measured weight m_2 of water before being discharged to atmosphere.

From the five observed data: T, p_1, p_2, m_1, m_2 was derived the ratio $\lambda = 2A_{aw}/(A_{aa} + A_{ww})$ and the weight m_a of dry air from which the weights m_1, m_2 of water were removed in the chemical driers. Here are $A_{aa}(T)$ and $A_{ww}(T)$ the dry air and water vapor Second Virial Coefficients, both well known in advance as bits of existing knowledge.

Experimentally to test the several presumptions noted above, arrangement was made accurately to weigh the dry air passing at low velocity through the driers during removal of weights m_1, m_2 of water from the stream; preliminarily to saturate the stream, so to approach saturation in the first main saturator by condensation or evaporation; from run to run to change pressure settings and flow rate. The fact that no appreciable effect of these changes on the inferred value of A_{aw} at set temperature T was observed was considered convincing evidence that saturation was indeed realized, very closely if not precisely.

Analytically, encouraged by Professors Debye of Cornell and Margenau of Yale, we looked further support from the theory of van der Waals forces, electrostatic in nature, to find, much to our satisfaction, suprisingly close agreement over the whole range of our experiment with only a small adjustment of a single constant in the relevant force potential. This excellent agreement between well-tested theory and experimental findings we think warrant the reasonable extrapolation used in formulating the thermodynamic properties referred to earlier and at higher pressures of moist air.

9.

By Gas Thermometry to determine the canonical isotherm numbering function T(t) of identical relation (2) is formed a succession of non-static, restored-temperature expansions of a well-chosen thermometric gas. This non-static change is delineable at best as a countable set of discrete state-points p_i, v_i $(i=1,2,\ldots)$ on the pv, p-plane. By suitable interpolation and extrapolation to zero-pressure (p=0) is then determined a smooth-curve locus of the point set, all points of the same temperature t.

The above smooth-curve locus is found to show a finite, non-zero intercept $(pv)^o$ reached on a finite, non-zero slope A(t); thus

$$pv = (pv)^o + A(t)p + \ldots, \qquad (33)$$

where $(pv)^o$ like A(t) is a pure temperature function.

"The increasingly precise measurements made over more than a century [on a number of <u>different</u> well-chosen so-called thermometric gases] have only served to deepen the conviction that the entire structure of ideas and concepts [on which the belief that close agreement among different gases implies $(pv)^o = RT$] is sound", say Keenan and Keyes (6). In this connection, however, note that C. Caratheodory (7) in his 1908 elegant and perceptive re-formulation of thermodynamic theory, its stated purpose being to show that the whole theory can be derived without the notion of heat, shows that T(t) can be determined only to within an additive constant of integration from measurements on quasi-static changes; that its determination requires appeal to at least one non-static change, say one in which energy is restored to its initial value but entropy is not; but that it can be uniquely determined once and for all from measurements on <u>any one</u> simple substance not necessarily gaseous.

10.

From relation (33) with the aid of identical relation $v = \partial g(T,p)/\partial p$ and of the generally accepted relation $(pv)^o = RT$ is derivable

$$g(T,p) = gr(T,0) + RT\ell np + A(T)p + \ldots \qquad (34)$$

where $gr(T,p) = g(T,p) - RT\ell np$ is reduced free enthalpy, its finite, non-zero zero-pressure value at temperature T being $\overset{o}{gr}(T) = gr(T,0)$.

From relations (34 & 25) it follows that for moist air as a binary gas mixture

$$G(T,p,n_i) + \Sigma n_i \overset{o}{gr}_i(T) + \Sigma n_i RT\ell np_i + A(T,n_i)p_i + \ldots \qquad (35)$$

of which Statistical Mechanics predicts

$$A(T,n_i) = A_{aa}(T)n_a n_a - 2A_{aw}(T)n_a n_w + A_{ww}(T)n_w n_w, \qquad (36)$$

from which are derivable the coexistence pressures p_i of moist air;namely

$$\begin{aligned} p_a &= (x_a p)[1 + (a_{aa} - ax_w)(x_w p) + \ldots] \\ p_w &= (x_w p)[1 + (a_{ww} - ax_a)(x_a p) + \ldots] \qquad (37) \\ p_a + p_w &= (p)\ [1 + 2a_{aw}x_a x_w p + \ldots] \end{aligned}$$

$$A_{ik} = a_{ik}RT;\ a = a_{aa} - 2a_{aw} + a_{ww}$$

to show that the p_i of moist air are not mol-fractional pressures because of pair-wise forces between unlike molecules only.

It is on relations (35) and (36) that the Goff-Gratch formulation is firmly based.

REFERENCES

1. Bridgman, P.W., "The Thermodynamics of Electrical Phenomena in Metals", New York p. 66, 1934.

2. Oestrich, H., "Ermarmung von Gasen bei gedrosselter Einstromung", Forschung 7. Bd./ Heft 6, s. 287, Berlin.

3. Gibbs, J.W., "The Scientific Papers of J.W. Gibbs", Vol. I, New York, p. 157, 1906.

4. Goff, J.A. and Gratch, S., "Thermodynamic Properties of Moist Air," ASHVE Journal Section, Heating, Piping & Air Conditioning, New York, 1945.

5. Guggenheim, E.A., "Modern Thermodynamics by the Method of Willard Gibbs,", London, p. 73, 1933.

6. Keenan, J.H. and Keyes, F.G., "Thermodynamic Properties of Steam," New York, p. 11, 1936.

7. Caratheodory, C., "Untersuchungen uber die Grundlagen der Thermodynamik", Leipsig. Mathematische Annalen, s. 381, 1909.

USE OF SIMULATION TECHNIQUES TO EVALUATE STRATEGIES FOR IMPROVEMENT OF INDUSTRIAL MULTIZONE THROUGH-CIRCULATION TROLLEY DRYER

J.C. Ashworth[1]
M.C. Hill[2]

1. Dept. of Chem. Eng., University of Birmingham, Birmingham B15 2TT.
2. Foseco International Ltd., 285 Longacre, Nechells, Birmingham B7 5JR

ABSTRACT

The performance of a direct gas-fired four-stage through-circulation trolley dryer used to process insulation tiles was investigated in order to improve its production rate and energy efficiency. Performance data from the dryer and the measured drying characteristics of the material were used to develop a lumped parameter model for the dryer based upon the characteristic drying curve. Various methods for the improvement of the dryer were evaluated with the aid of this simulation model to find the optimum strategy. These included replacement of atmospheric gas burners with packaged burners, improved loading of trolleys, linking together of zonal airflows, and possible incorporation of an exhaust heat recovery exchanger. Although some improvement strategies were not financially viable because of the nature of the existing installation, the most valuable single factor was improved trolley loading as both the production rate and energy efficiency can be simultaneously improved.

NOMENCLATURE

a	surface area per unit volume of solids	m^{-1}
A	cross-sectional area of dryer	m^2
$\bar{C}_p$	specific heat capacity at constant pressure	J $kg^{-1}K^{-1}$
$\bar{C}_{pY}$	humid specific heat capacity $(\bar{C}_{pG} + Y_G \bar{C}_{pV})$	J $kg^{-1}K^{-1}$
f	characteristic drying rate function	-
G	dry gas mass flowrate through empty dryer	kg $m^{-2}s^{-1}$
h_c	convective heat transfer coefficient	W $m^{-2}K^{-1}$
NTU	number of transfer units $(h_c a(1-\varepsilon)Z/G\bar{C}_{pY})$	-
Q	energy flowrate	W
t	time	s
T	temperature	K
V	dryer volume	m^3
W	velocity	ms^{-1}
X	moisture content (dry-basis)	-
Y	humidity (dry-basis)	-
z	distance along dryer in airflow direction	m
Z	dryer length in airflow direction	m
η	evaporative energy efficiency	-
ε	dryer void ratio	-
$1-\varepsilon$	fraction of dryer volume occupied by solids	-
ρ	dry substance density	kg m^{-3}
Φ	characteristic moisture content	-
π	transfer potential	-
τ	dimensionless drying time	-
ζ	dimensionless distance in airflow direction	-
ΔH_V	latent heat of vaporisation	J kg^{-1}

Subscripts

as	adiabatic-saturation
cr	critical point
eq	equilibrium
G	gas
o	initial
S	solid
V	vapour
w	wet-bulb
Y	humid dry-basis

Superscripts

F	fresh-air
I	inlet-air
O	outlet-air
$\bar{}$	average
$\wedge$	overall

INTRODUCTION

Of all the unit operations used by the process industries, solids-drying is one of the most energy intensive operations. For example, a recent study (1) notes that approximately 2½% of the total U.K. energy demand is used for drying compared to 2% for distillation operations. Although the general principles of energy conservation have been outlined in depth in several monographs (2,3,4), their application to the operation of industrial drying equipment has only been briefly considered. Similarly this problem has received little attention in other research publications except for recent research work carried at the University of Birmingham (5,6,7). This work has led to a detailed understanding of the factors that influence the thermal efficiency of dryers which are briefly summarised below.

The energy demand of an industrial dryer may be represented by a summation of several components. These include the energy required for evaporation of moisture, energy lost in exit airstream, energy lost through walls of dryer, energy associated with hot solids when removed from dryer, energy required for air-circulation, energy required to heat dryer structure, energy required to rotate or vibrate dryer, and energy required for operation and sensible heating of mechanical handling equipment. Clearly the relative significance of these terms depends upon the difficulty of the drying process, the type of equipment used, the scale of the operation, and the nature of the energy supplied. For example, for a continuous-through-circulation trolley dryer the most significant source of inefficiency is the energy lost in the exit airstream. Therefore an ideal energy efficiency η can be defined as the ratio of the evaporative energy demand to the sum of the energy lost in the exhaust air and that supplied for evaporation. The following approximate formula is obtained (6) if the efficiency is defined relative to the energy required for evaporation of moisture at the solids feed temperature, T_S^I,

$$\eta \simeq \frac{1}{\left\{1 + \frac{\bar{C}_{PY}^{F}(T_G^o - T_G^F)}{\Delta H_{vas}(Y_G^o - Y_G^F)}\right\}} \cdot \frac{\Delta H_{vs}}{\left\{\Delta H_{vs} + \bar{C}_{Pv}(T_G^o - T_S^I)\right\}} \quad \ldots\ldots(1)$$

That is, the efficiency is maximised at low exhaust air temperatures, high humidities, and high wet-bulb temperatures when the moisture carrying capacity of the airstream is highest. Similar expressions have also been derived for various operational configurations of straight-through or recycle flow, indirect and/or direct heating, and incorporation of exhaust heat recovery exchangers. For most drying operations an ideal efficiency of 80% and actual efficiency of at least 60% should be attained if the dryer is properly configured (6).

These efficiency relationships provide useful guidance for the improvement of thermal performance of dryers already installed. However for any such work it is essential to understand the interactions that arise between energy performance and solids production rate as these two requirements often conflict. The nature of these interactions depends on whether the dryer is sized on a volume or area basis and can only be satisfactorily understood with the aid of dryer models (7,8). For a given drying problem the variables $\bar{P}_s$, q, $(\bar{X}_{cr} - \bar{X}_{eq})$ are fixed and $\bar{C}_{PY}$ and ΔH_{vw} vary little over a wide range of operating conditions. The significance of the remaining parameters is examined in Table 1 where the positive sign indicates an increasing function and a negative sign a decreasing function. Note that increasing the parameter $(T_G^I - T_W)$ can affect the efficiency both ways (5). If its magnitude is increased by raising T_G^I and keeping T_W constant the efficiency will also improve. But if it is increased by lowering T_W and maintaining T_G^I constant then the efficiency will decrease.

Table 1
Significance of Dryer Design Parameters Upon Size, Time and Energy Efficiency

Parameter	V/m^3	A/m^2	t/s	η
increasing Z	+	−	+	+
increasing G	−	−	−	−
increasing h_c	−	−	−	+
increasing $(1-\varepsilon)$	−	−	+	+
increasing $(T_G^I - T_W)$	−	−	−	− / +

The most interesting results summarised by Table 1 concern the variables $(1-\varepsilon)$ and $(T_G^I - T_W)$ as these are the only parameters that can be altered to improve simultaneously the production rate and thermal efficiency of a dryer.

Because of the continuing rapid escalation of energy costs many industrial drying operations are the subject of careful scrutiny at present because in the past the main criteria for dryer design were to specify a machine of low capital cost which dried the solids as quickly as possible. The consequences of this design policy are that many existing direct contact drying installations have poor thermal performance such that their efficiency is often less than 30% as noted by Pratt (9). This last statement is well illustrated by the ten continuous multistage through circulation trolley dryers used by Foseco Ltd. in the main processing area of their Tamworth plant for the manufacture of insulation tiles. In 1978 the total annual charges for energy used by these dryers was £250,000. After the installation of gas meters on each oven, a preliminary investigation revealed that the energy performance varied markedly between ovens and from week to week. This is illustrated by the energy consumption statistics for oven no.3 presented in Table 2 whose performance was average of all those in the plant. The minimum evaporative energy requirement for drying this product is 14.5 therms per tonne dry product based on the gross calorific value of the fuel. The average thermal efficiency of the dryer for this 12 week period was 18.1%.

As a result of this preliminary study a collaborative project between the University of Birmingham and Foseco International Ltd. was initiated to investigate the performance of this dryer more closely in order to provide guidance for the most cost-effective modifications to upgrade its thermal efficiency. The remainder of this paper summarises the results of the monitoring programme and the interpretation of these data with the aid of simulation techniques.

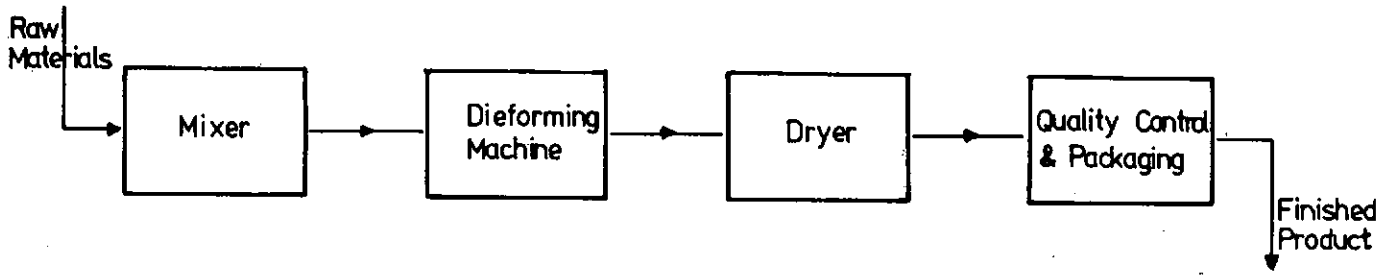

Fig. 1 Insulation tile manufacturing process

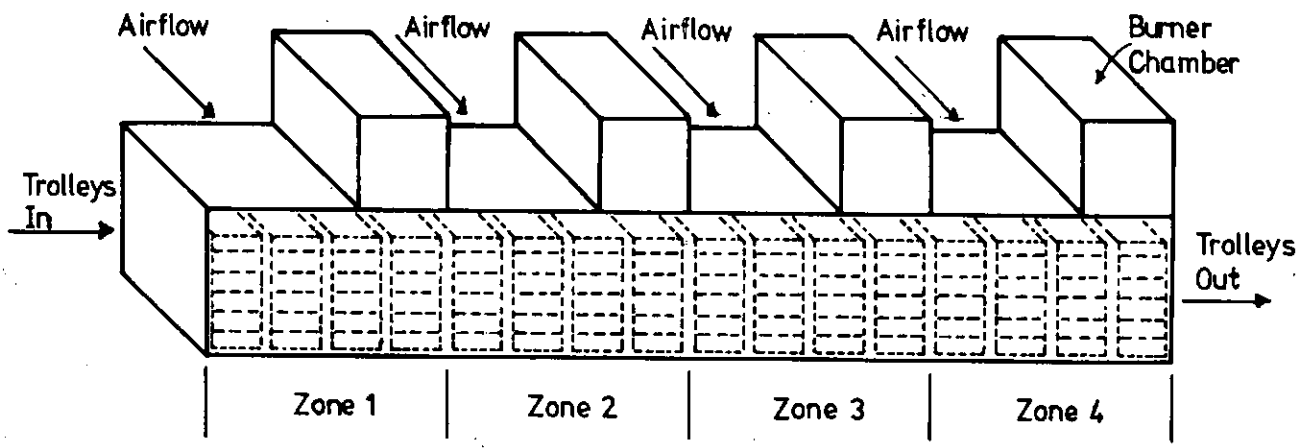

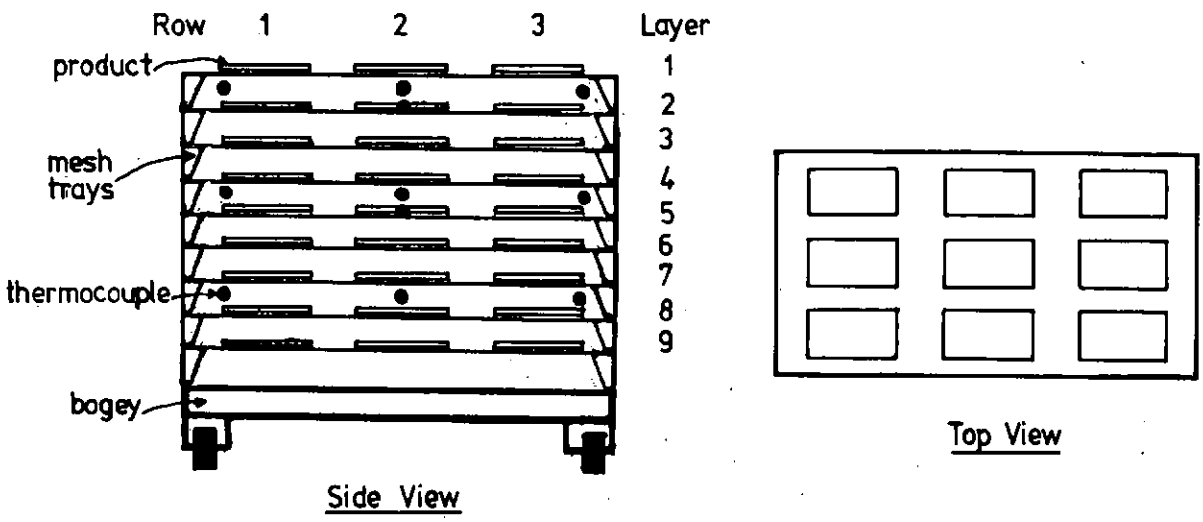

Fig. 2 Detail of multistage through-circulation trolley dryer and tray loading pattern of tiles on trolley

Table 2
Performance Data of Dryer

Week	Operating hours	Gas Consumption /therms	Production /tonnes	Production rate /tonnes hr^{-1}	Energy Consumption /therms $tonne^{-1}$	Thermal Efficiency /%
1	70	2334	17.8	0.25	131	11.0
2	120	3780	44.3	0.37	85	17.0
3	115	2930	30.4	0.26	96	15.0
4	118	3152	35.6	0.30	89	16.4
5	120	3626	61.9	0.52	59	24.6
6	120	3370	46.1	0.38	73	19.8
7	120	3193	40.9	0.34	78	18.6
8	120	3015	33.8	0.28	89	16.2
9	120	3155	39.0	0.33	81	17.9
10	119	3239	40.7	0.34	80	18.2
11	120	3311	46.4	0.39	71	20.3
12	120	3293	43.3	0.36	76	19.1

MONITORING OF DRYER PERFORMANCE

Description of Insulation Tile Manufacturing Process

As the dryer is only one stage of a sequence of operations for this manufacturing process it is important to examine briefly the overall process which is outlined in block diagram form in Fig.1. Initially a number of fibrous materials are blended together with water and a thermosetting resin compound to produce a mix which has the consistency of a thick sludge. The mix is pumped to a dieforming machine which produces the required shape of tile under pressure while excess water is squeezed out. This machine casts the green tiles directly onto wire-mesh trays for drying. Several layers of tiles make up a complete trolley load, and two trolleys are fed into the dryer every 40 minutes.

The dryer itself is a four-stage through-circulation trolley type such that each zone can be controlled independently. This can be achieved because each zone is equipped with its own circulation fan, exhaust fan, and atmospheric gas burner. The airflow direction is the same for all zones and it is perpendicular to the direction of the trolley's movement along the oven. In an attempt to improve the thermal performance of the dryer the exhaust gases from zones 3 and 4 are recycled to the inlet of zones 1 and 2 respectively. The exhaust gases from zones 1 and 2 are exhausted to atmosphere. After approximately 5 hours residence time, the trolley load is pushed out the other end of the dryer and then left to cool before quality control checks and packaging.

Dryer Monitoring Trials

In order to monitor the dryer performance in detail, sensors were installed in strategic positions to measure air temperature, humidities, air flowrates and solids temperatures. The air temperatures were measured by chromel-alumel thermocouples at the inlet, outlet and exhaust points for all four zones. The exhaust humidities were monitored by a Mahlo AML humidity meter which utilises the speed of sound technique and velocities in the exhaust air ducts were determined by pitot-tube traverses. A wet- and dry-bulb psychrometer was used for atmospheric temperature and humidity measurements. In addition one trolley load of tiles was fitted with thermocouples to monitor its progress as it travelled through the oven. Air temperatures at the inlet, middle and outlet were monitored at three different levels and solid temperatures at two positions by inserting thermocouples into the tiles as shown in Fig.2. Attempts to measure air-velocities within the oven by a pitot-tube and micromanometer system proved unsuccessful because snagging of the pressure tapping lines could not be avoided. For the trolley monitoring experiment the complete set of signals were scanned automatically every 60 seconds with a data-logging system and punched out onto paper-tape. In addition the surface losses from the outside shell of the dryer were estimated from surface thermocouple measurements and fuel usage of the burners from daily readings of a gas meter installed in the main supply line to the dryer.

These monitoring trials were carried out over a period of three weeks but even though the results presented here were obtained during one trolley monitoring experiment of four hours duration they are representative of the trends

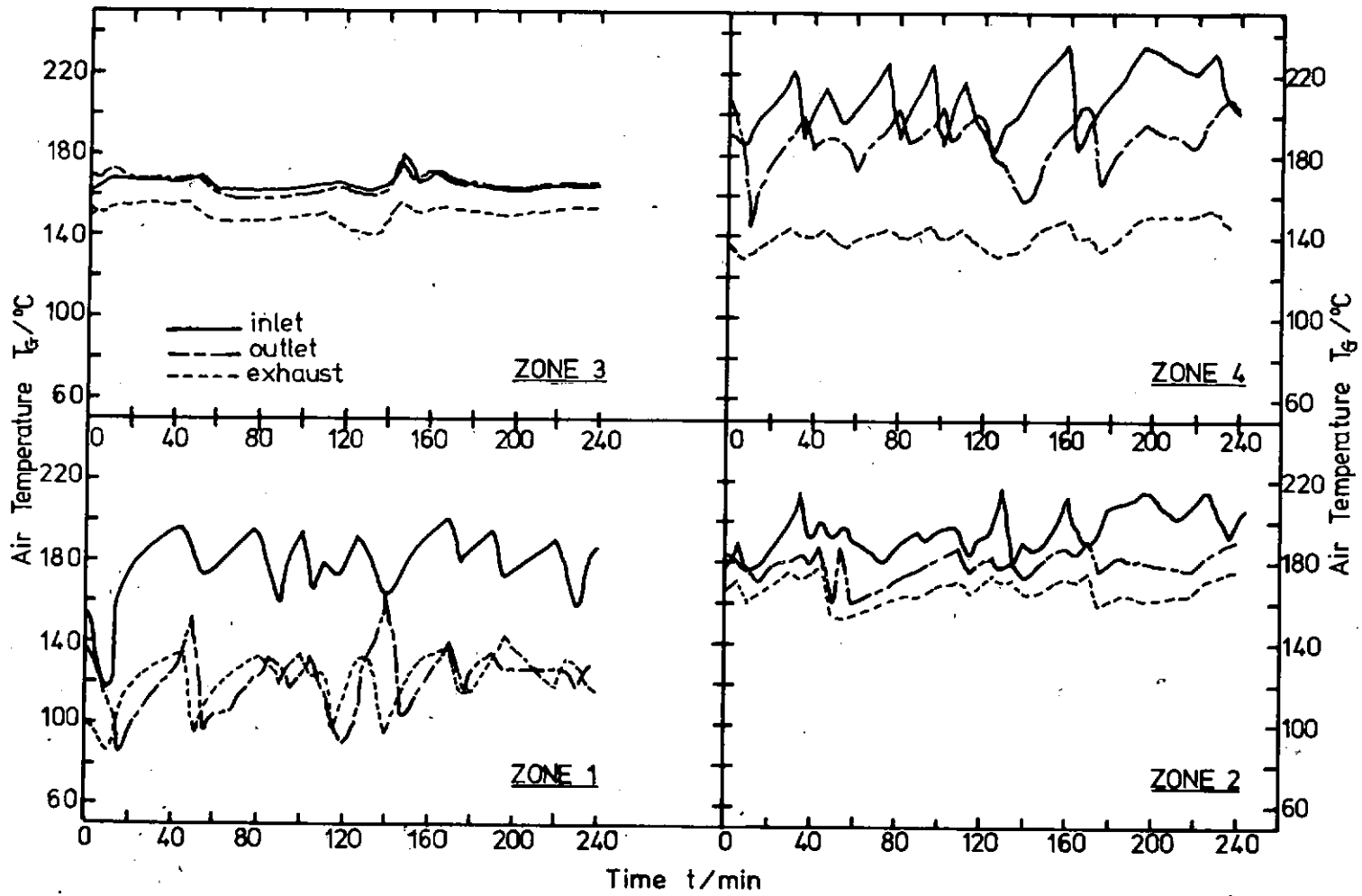

Fig. 3 Airstream temperatures at inlet, outlet and exhaust positions of each zone of trolley dryer

observed throughout the trials. The variation of the zone inlet, outlet and exhaust temperatures are presented in Fig.3. Clearly the temperature control obtained is rather poor which is due to the fact that there is no automatic control on the gas feed to the burners. The cycling in temperature in the end zones 1 and 4 is a natural consequence of the doors opening at regular intervals so that fresh stock can be admitted and dry stock removed at the other end. Nevertheless the energy lost during this phase of operation is clearly a significant proportion of the overall heat load, particularly if the plant operator leaves them open longer than necessary. This effect is shown most dramatically by the crossover of the exhaust and outlet temperature profiles plotted for zone 1 whenever the door is opened and closed. This phenomenon probably arises due to unbalanced pressures around the flow circuit when the door is opened so that there is some short-circuiting of the hot gases from the burner chamber into the exhaust system while cold air is sucked into the dryer through the doorway.

and air-velocity about the load. As the temperature drops across the trolley are reduced for the top and bottom layers compared to the middle it follows that a considerable proportion of the airflow must short-circuit around the top and bottom of the trolley. This observation was also confirmed by examination of the moisture loss of individual tiles from another similar loaded trolley. These results are summarised in Table 3.

The slowing of the drying from row to row due to humidification effects is shown and the average values for each layer suggest significant air-velocity variations as the amount of moisture evaporated will increase with airspeed.

Heat and Mass Balances About Dryer

The data collected on the dryer performance enabled heat and mass balances to be undertaken. Most of the information summarised below is based on the period of 24 hours, starting at 6 a.m., which encompassed the trolley monitoring experiment. The measurements for the exhaust air flowrates and humidities were obtained

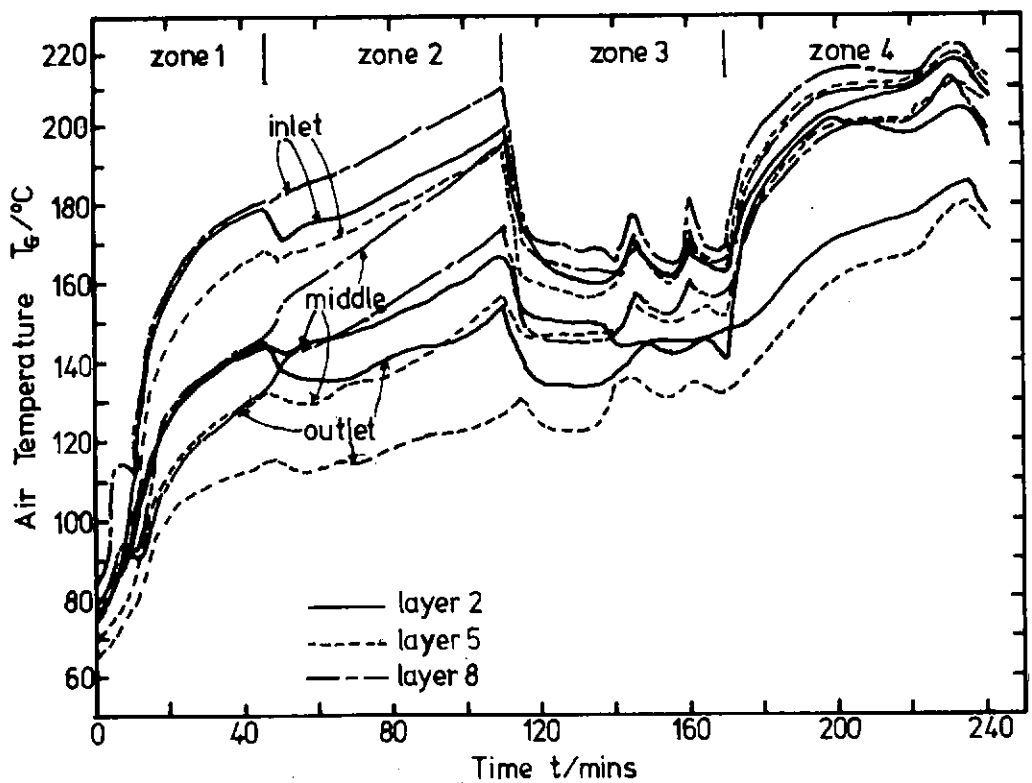

Fig. 4 Variation of airstream temperatures at several positions within loaded trolley of tiles as it travels along dryer

The air temperatures measured at several positions within the trolley load are plotted in Fig.4. For a given layer of tiles the drop in temperature due to humidification of the air as it passes across the tiles is clearly apparent. Another conclusion that can be drawn from these plots is the marked stratification of temperature

by averaging results collected over the three week timespan of the monitoring period.

Table 4 illustrates some of the problems of metering gas flows around dryers. It is impossible to measure the secondary air flow because of the atmospheric type burner

Table 3
Variation of Moisture Evaporation of Tiles with Loading Position on Trolley

Layer Number	mass moisture evaporated per unit mass of dry tile			
	Row 1	Row 2	Row 3	Average
1	.581	.585	.579	.582
2	.575	.570	.563	.569
3	.562	.559	.557	.559
4	.582	.570	.559	.570
5	.555	.552	.550	.552
6	.558	.536	.534	.543
7	.589	.553	.525	.556
8	.566	.556	.540	.554
9	.565	.569	.574	.569
Average	.570	.560	.553	.561

$Wm^{-2}K^{-1}$ (2 BTU $hr^{-1}ft^{-2}F^{-1}$) was assumed at a surroundings temperature of 23°C for the construction of Table 5. The heat lost through the floor was assumed equal to that lost through the top of the dryer.

Table 5
Surface Heat Losses from Trolley Dryer

Part of Dryer	Surface area/m^2	T_{surf}/°C	Q/kW	Percentage heat loss
fan casings	5.8	128	7.0	9.8
burner chambers	57.6	53	19.7	27.8
top	31.6	52	10.4	14.7
floor	44.6	52	14.7	20.8
inlet door	6.5	31	0.6	0.8
outlet door	6.5	62	2.9	4.1
air inlet wall	31.2	51	10.0	14.0
air outlet wall	31.2	39	5.7	8.0
		Total	71.0	100.0

Table 4
Mass Flows for Trolley Dryer

Stream	Temperature /°C	Dry-gas flowrate /kg s^{-1}	Water flowrate /kg s^{-1}	Humidity or moisture content/kg kg^{-1}	Solids flowrate /kg s^{-1}
INPUTS					
combustion gases (stoichiometric mixture)	30°C	.172	.026	.151	-
secondary air*	30°C	1.575	.016	.010	-
green insulation tiles	15°C	-	.053	.564	.093
trolleys	15°C	-	-	-	.292
	Totals	1.747	.095		.385
OUTPUTS					
exhaust gases from zones 1 and 3	120°C	.874	.073	.083	-
exhaust gases from zones 2 and 4	175°C	.841	.054	.064	-
dry insulation tiles	200°C	-	.000	.003	.093
trolleys	200°C	-	-	-	.292
	Totals	1.715	1.127	-	.385

* estimated from overall mass balance

design. The exhaust flows are also subject to much uncertainty as there are no suitable lengths of straight duct to enable measurements to be taken at a position where the flow is steady and well-developed.

The surface heat losses from the dryer shell were estimated from surface temperature measurements. A convective heat transfer coefficient of 11.4

Perhaps the most significant result expressed by Table 5 is that 52% of this heat is lost from the top of the dryer. Clearly there is considerable scope for improvement of the insulation of the dryer as the area weighted average surface temperature is 52°C.

The energy flows for the trolley dryer are itemised below. All enthapies are defined

relative to a datum of 0°C and all the flowrates, specific heat capacities and enthalpies are expressed in dry basis units.

of the dryer. Based on these results the ideal efficiency is 44% and the actual efficiency is 22%.

Table 6
Energy Flows for Trolley Dryer

Stream	Specific heat capacity /J $kg^{-1}K^{-1}$	Flowrate /kg s^{-1}	Specific enthalpy /kJ kg^{-1}	Energy flow /kW
INPUTS				
Heat of combustion of fuel gas	-	.0112	53420	598
Fuel gas	1490	.0112	45	1
Combustion air (primary and secondary)	1024	1.760	55	97
Green insulation tiles	3273	.093	49	4
Trolleys	490	.292	7.4	2
Heat of reaction of curing resin*	-	-	-	14
			Total	716
OUTPUTS				
Exhaust air from zones 1 and 3	1161	.874	346	302
Exhaust air from zones 2 and 4	1130	.841	354	298
Dry insulation tiles	921	.093	184	17
Trolleys	490	.292	98	28
Surface losses	-	-	-	71
			Total	716

*estimated from overall energy balance

One interesting aspect of this drying problem, which is referred to in Table 6, is that there is some internal heat generation within the material due to the exothermic curing reaction of the resin binder. The heat of reaction or extent of resin cure is not known but in some instances when processing thick tiles the product has caught fire. The data presented in Fig.3 shows some evidence of this phenomenon from the temperature profiles obtained in zone 3, where the outlet and inlet temperatures are closely similar despite significant moisture uptake by the airstream. Despite the uncertainty of this effect an overall heat balance was obtained within 2%.

The results presented in Table 6 can be rearranged to estimate the significance of various terms upon the thermal efficiency of the dryer as shown below. The heat lost via the doors is estimated from the difference between the total exhaust energy loss and that predicted from the ideal energy efficiency relationship.

The dominant term for the dryer inefficiency is the energy lost in the exhaust gases so this is the term which should be examined most closely with a view to improving the energy performance

Table 7
Thermal Inefficiency Factors for Trolley Dryer

No.	Stream	Energy Flow /kW	Percentage Inefficiency
1	moisture evaporation	129	-
2	sensible heating of solids	16	12
3	sensible heating of trolleys	26	20
4	surface heat losses	71	55
5	water of combustion	59	46
6	heat lost via doors	133	103
7	energy lost in exhaust gases	164	127
	Total	598	363%

MODELLING OF DRYER

Dryer Equations

From the point view of modelling, the through-circulation trolley dryer is mathematically equivalent to the simple batch dryer chamber. For a batch-dryer the load is stationary but the drying-rates vary with time and distance across the load in the airflow direction due to progressive humidification of the airstream. Normally the inlet air conditions are varied throughout the drying cycle. Exactly the same results apply to the trolley-dryer. As the trolleys move along the dryer in a direction perpendicular to the airflow direction, their movement is irrelevant to the modelling of the drying process. Nevertheless in this case the time variable is directly related to the position of the trolley along the dryer and although the inlet air conditions are fixed at a given position, the load will encounter a varying set of inlet conditions as it is moved from zone to zone.

The dimensionless equations based upon the characteristic drying curve concept that are appropriate to this type of dryer are as follows (10,11):

$$\frac{\partial \Phi}{\partial \tau} = \frac{\partial \Pi}{\partial Y} = -\Pi f(\Phi) \quad \ldots\ldots(2)$$

$$\text{I.C.} \quad \Phi = \Phi_o \quad \text{for } Y \geq 0, \tau = 0 \quad \ldots\ldots(3)$$

$$\text{B.C.} \quad \Pi = 1 \quad \text{at } Y = 0, \tau > 0 \quad \ldots\ldots(4)$$

where

$$\tau = \frac{h_c a \int_o^t (T_G^I - T_w)dt}{\rho_s \Delta H_{vw} (\bar{X}_{cr} - \bar{X}_{eq})} = \frac{k_y a \int_o^t (Y_w - Y_G^I)dt}{\rho_s (\bar{X}_{cr} - \bar{X}_{eq})} \quad \ldots\ldots(5)$$

$$Y = \frac{h_c a (1-\varepsilon) z}{G \bar{C}_{PY}} = \frac{k_y a (1-\varepsilon) z}{G} \quad \ldots\ldots(6)$$

$$\Pi = \frac{T_G - T_w}{T_G^I - T_w} = \frac{Y_G - Y_w}{Y_G^I - Y_w} \quad \ldots\ldots(7) \qquad \Phi = \frac{\bar{X} - \bar{X}_{eq}}{\bar{X}_{cr} - \bar{X}_{eq}} \quad \ldots\ldots(8)$$

The variable Φ is the characteristic moisture content, τ is the dimensionless drying time, Y the dimensionless distance along the dryer in the airflow direction, and Π is the dimensionless transfer potential or driving-force. The dimensionless length of the dryer in the airflow direction ($z = Z$) is often termed the number of transfer units, NTU. The equivalence between the mass and heat transfer equations expressed by equations (5) to (7) will only hold for the air/water-vapour system when the psychrometric ratio is approximately equal to one.

The solution of the dryer equations depends upon the nature of the characteristic drying curve function $f(\Phi)$. This function is the ratio of the drying-rate from an unsaturated surface to that of a saturated surface. For a few special cases of $f(\Phi)$, analytical solutions can be obtained but normally finite-difference methods are required. Alternatively if the airflow direction is unchanged along the dryer an approximate method of solution can be adopted where the characteristic curve function is represented by a number of straight-line segments (11). This latter method was used to simulate the trolley-dryer.

Drying Characteristics of Material

The drying characteristics of the insulation tile were determined with the wind-tunnel/balance system at the University of Birmingham (12), which is capable of high accuracy kinetics determinations by continuous weighing in an airstream. In order to simulate closely the trolley-drying of the insulation tiles a small specimen was placed in a special tray so that all the sides and bottom face were sealed off with aluminium foil. Throughout the experiment the sample weight, solid temperature (by infrared radiation thermometer), air velocity, air temperature and humidity were continuously monitored. The main experimental parameters were as follows:

Sample dimensions = 38.6mm x 50.0mm x 15.10mm thick

Sample dry weight/gm = 28.6215

Dry solid density/g cm^{-3} = 0.99

Dry-bulb temperature/°C = 146.0

Wet-bulb temperature/°C = 39.5

Airstream humidity (dry-basis) = 0.0107

Air velocity/ms^{-1} = 1.63

Atmospheric pressure/mm Hg = 749

Initial moisture content (dry-basis) = 52.26%

Equilibrium moisture content (dry-basis) = 0.15%

Equilibrium relative humidity/% = 0.49

Maximum drying rate/g $m^{-2}s^{-1}$ = 1.81

Drying time to 0.5% moisture content/s = 6150

The experimentally determined drying-rate curve and the rate and surface temperature histories are presented in Figs. 5a and 5b. The dotted line on Fig.5a is the limiting rate curve when the drying is completely boundary-layer controlled. This curve was calculated with the aid of the equilibrium moisture content isotherm according to the concepts of the hygroscopic wet-bulb temperature and reduced surface driving-force function (12). By comparing the areas under both curves the apparent degree of internal mass transfer control is 37% and Kirpichev number is equal to 0.59. The Kirpichev number is the ratio of the external and internal mass transfer intensities. The

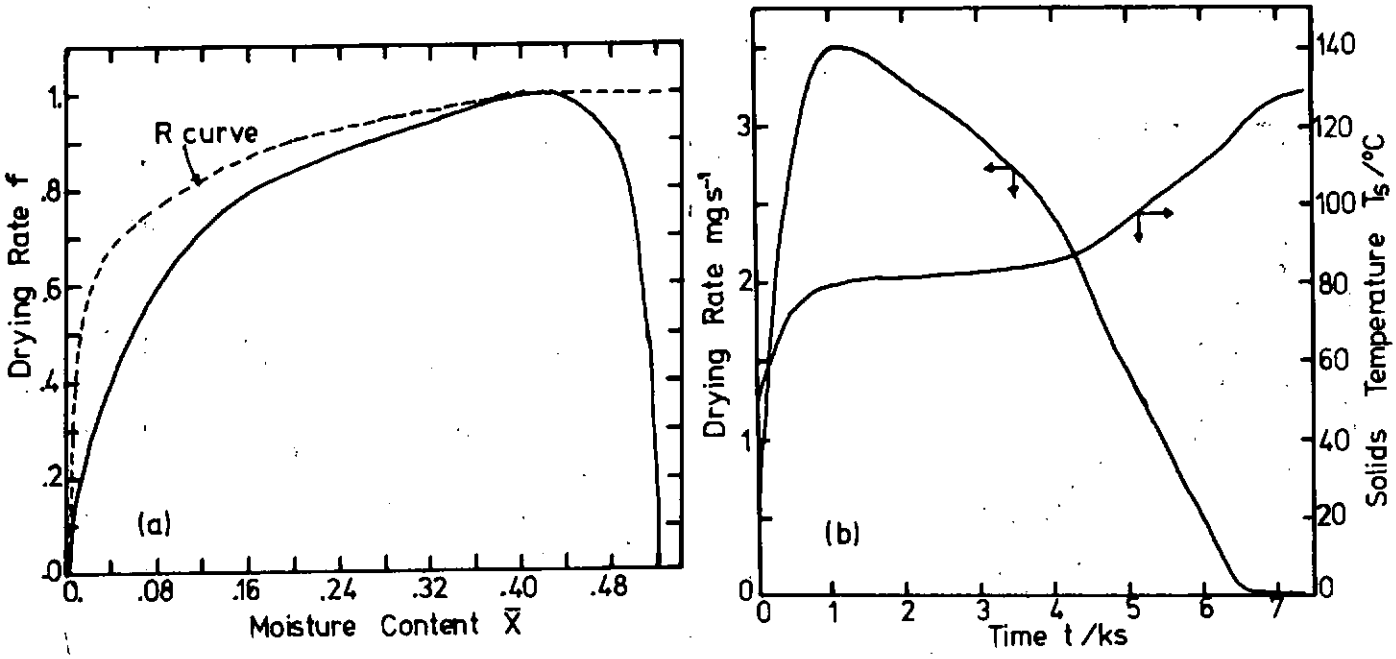

Fig. 5 Experimental drying-rate and surface temperature characteristics of insulation tile as determined by wind-tunnel/balance system.

calculation of the apparent Kirpichev number verifies that the characteristic drying curve concept should hold well for the drying of the insulation tiles as theoretical studies have shown that the concept is valid when $Ki \leq 2$ (10,13). The critical moisture content was assumed to correspond to the value of the average moisture content at the instant the maximum rate was attained (Fig.5a).

Fitting of Model to Trolley Dryer

In order to model the performance of the trolley dryer a number of parameters must be determined. Most of these can be calculated from the geometrical arrangement of the solids in the dryer and the known operating conditions. However certain parameters such as the heat transfer coefficient and dry gas flowrate are best deduced by fitting the model to available performance data. The simplest fitting procedure is to firstly estimate the dryer NTU from the temperature drop across the first zone which corresponds to the constant rate period (during this phase, $\Pi^\circ = \exp(-NTU)$). The dimensionless drying time τ can then be calculated according to the model for the experimental $f(\Phi)$ curve and value of NTU. Then the heat transfer coefficient can be calculated from τ according to eqn. (5) and similarly the gas-flowrate can be estimated from the definition of NTU. The following parameters were appropriate:

Tile dimensions = 457mm x 81mm x 28mm

Loading of trolley = 9 layers of 9 tiles

Trolley volume = 1.51m x .86m x 1.52m

Trolley tray area = $1.35 m^2$

$\therefore$ $a = 85\ m^{-1}$ and $(1-\varepsilon) = .088$

$\bar{X}_o = .560$ kg kg^{-1} $\quad \bar{X}_{cr} = .427$ kg kg^{-1}

$\bar{X}_{end} = .005$ kg kg^{-1} $\quad \bar{X}_{eq} = .001$ kg kg^{-1}

$\therefore \Phi_o = 1.311$ $\quad \Phi_{end} = .012$

$\rho_s = 1066\ kg\ m^{-3}$, $\quad \Delta H_{vw} = 2375\ kJ\ kg^{-1}$

$Z = 1.70\ m$, $\quad \bar{C}_{py} = 1096\ J\ kg^{-1}\ K^{-1}$

From Fig.4, $\Pi^\circ = .53$, NTU = 0.63

for $\frac{Y}{\tau} = .315$, $\Phi_o = 1.311$, $\Phi_{end} = .012$, $\tau = 2.29$

Drying time at $Y = .315$, $t = 240$ mins (Fig.6)

From Fig.4, $\int_0^{240} (T_G^I - T_w)\, dt = 1.797 \times 10^6$ Ks

$\therefore h_c = 16.2\ W m^{-2} K^{-1}$, $G = .298\ kg\ m^{-2} s^{-1}$

The effectiveness of the modelling technique is assessed in Fig.6 where the results of the trolley monitoring experiment are compared with theoretical predictions. These predictions are based upon the parameters obtained from the fitting procedure and the experimentally determined inlet temperature profile for layer 5 as presented in Fig.4. Generally close agreement is obtained between the two sets of curves, particularly for the air temperature variations. The most stringent test is the comparison of the drying-rate curves as expressed by the difference between the air temperature and solids temperature. Although the experimental profiles (which both refer to the middle of the trolley load) exhibit complex trends, these are closely reproduced by the theoretical profile particularly over the last two hours. The solid temperature curves suggest an explanation for the less satisfactory rate predictions that are obtained for the early stages of the drying cycle. During this phase the solids temperatures are significantly enhanced compared to theory. This enhancement is probably

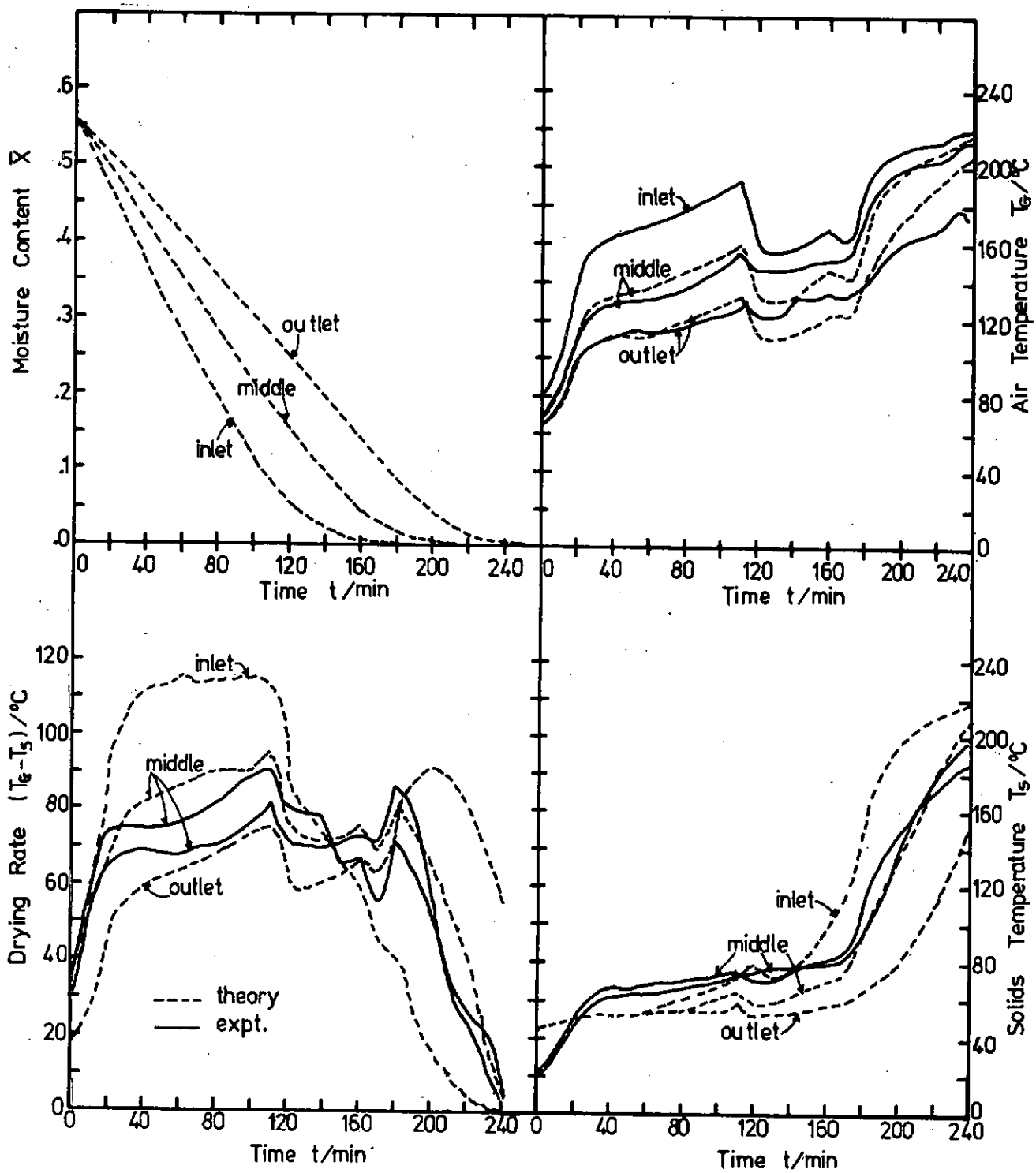

Fig. 6 Comparison of dryer model predictions for air-temperature, drying-rate and solids temperature histories with data obtained from trolley monitoring experiment

due to conduction of heat from the trolley framework and trays to the load. This effect is not taken into account in the dryer modelling equations but should be included if more accurate predictions are required.

EVALUATION OF STRATEGIES FOR IMPROVEMENT OF DRYER PERFORMANCE

The energy audit of this trolley dryer as summarised by Table 7 shows that there is much scope for improvement of the thermal performance. The target set by the operating company was to obtain an overall energy efficiency of at least 50% without loss of production rate. Clearly this target can only be achieved if all the sources of inefficiency are examined closely to reduce each of them as far as practicable. The various factors are evaluated below with the aid of the simulation techniques developed in the previous section.

(a) Replacement of Gas Burners

One essential requirement for improvement of the trolley dryer is the replacement of the existing atmospheric burners with packaged type gas burners with fuel/air ratio control for both the primary and secondary combustion airstreams. Such a system is necessary to ensure close temperature control despite the cyclic nature of the operation and maintain efficient operation. Better control would mean that a constant inlet temperature could be maintained along the dryer instead of the irregular profile obtained at present. For safety reasons this temperature should be limited to the maximum allowable material temperature of 200°C. This change would mean that the temperature driving force for drying is increased from 125°C to 145°C and the required residence time decreased in proportion by 14%. As this improvement also infers a similar increase in production rate, savings will accrue because of reduced investment for new plant. Typically a new dryer costs £100,000 which if written off over a period of five years mean capital charges of approximately £30000 per annum at current interest rates. Hence savings of the order of £4200 per year would accrue from the improved production rate. The savings in energy usage are difficult to quantify in this case particularly as they depend on other improvements which should accompany this change. Because of the strict control that is exerted on the primary and secondary airstreams for combustion this improvement should reduce significantly the energy lost by illicit leaks.

(b) Insulation of Dryer

Table 5 shows that the surface heat losses represent a significant portion of the dryer thermal inefficiency. The replacement of the existing insulation with improved materials that are now available should reduce the average surface temperature from 52°C to at least 35°C. Hence this energy flow could be reduced from 71kW to 29kW. For an operating duty of 6000 hours per year and gas charges at 0.01 £/kWh (30p/therm), cost savings of £2520 per year would result.

(c) Operation of Doors

A large proportion of the wasted energy is lost through the doors when opened for loading and unloading. The cycle of door opening, loading, door closing is semiautomated on the existing dryer but each step of the sequence must be manually initiated by the operator. It is not unusual for the doors to be left open for five to ten minutes each forty minute cycle. It is recommended that the door operation be completely automated so that the time the doors are required to be open should not exceed one minute. The operation could be further improved by installing intermediate doors to isolate the end zones from the remainder of the dryer during loading. Because each zone is four trolleys long, it follows that the most effective mode of operation would be to load the trolleys in batches of four. If the dryer was modified as suggested here, then the energy lost by this means should be reduced by 80% from 133 kW to 27 kW, and the charges for gas reduced by £6400 per year.

(d) Loading of Trolleys

One of the most effective means of improving the dryer performance is to increase the loading density of the trolleys because as Table 1 shows it is possible to simultaneously enhance both the energy efficiency and production rate. There are a number of ways this improvement can be instigated to make better use of the available dryer volume. The existing loading pattern for the tiles, which were the subject of this study, was 9 layers spaced vertically on 12.5cm centres with 9 tiles to each layer. This loading means that only 112.5cm of the available headroom of 150cm is used. Consequently the airflow can short circuit both over and under the load so that the various layers dry at different rates as shown by Table 3. Obviously the first aspect of loading that should be improved is to make full use of the available headroom, i.e. 12 layers of tiles at 12.5cm centres. The loading can be further improved in two other ways. The first method is to stack the layers more closely together and secondly the percentage area coverage of the trays could be significantly increased from the 55% basis used at present. The overall significance of these geometrical parameters upon the annual operating costs is summarised in Table 8. These calculations are based upon the same operating conditions as used for the existing dryer where the capital and energy costs are estimated on the same basis as proposed earlier.

Despite the spectacular advantages that can be gained from improved trolley loading this method will be constrained in practice because of the dieforming operation upstream of the dryer. As the design of the dies dictates the tray area loading ratio that is obtained, this can only be altered at great expense by replacing them. Another complication is that the dryer is required

Table 8
Effect of Trolley Loading Configuration Upon Dryer Operating Costs

Tile spacing /cm	Tray area loading /%	$1-\varepsilon$	NTU	τ	Relative Product Rate	Ideal Energy Efficiency	Exhaust energy saving /kW	Energy saving /£yr^{-1}	Capital Cost Saving /£yr^{-1}	Total Saving /£yr^{-1}
12.5	55	.118	.85	2.92	1.25	.578	87	5200	7500	12700
12.5	65	.139	1.00	3.19	1.34	.612	110	6600	10200	16800
12.5	75	.161	1.15	3.38	1.46	.642	124	8000	13800	21800
12.5	85	.182	1.30	3.58	1.56	.669	157	9400	16800	26200
10.0	55	.148	1.06	3.27	1.39	.615	116	7000	11700	18700
10.0	65	.174	1.25	3.51	1.53	.659	149	8900	15900	24800
10.0	75	.201	1.44	3.75	1.65	.690	175	10500	19500	30000
10.0	85	.228	1.63	4.01	1.74	.715	196	11800	22200	34000
7.5	55	.189	1.35	3.65	1.59	.676	163	9800	17700	27500
7.5	65	.222	1.59	3.95	1.73	.710	193	11600	21900	33500
7.5	75	.258	1.85	4.30	1.84	.739	218	13100	25200	38300
7.5	85	.291	2.08	4.60	1.97	.760	243	15800	29100	44900
5.0	55	.295	2.11	4.64	1.95	.762	241	14500	28500	43000
5.0	65	.348	2.49	5.14	2.08	.788	269	16100	32400	48500
5.0	75	.403	2.89	5.66	2.19	.808	292	17500	35700	53200
5.0	85	.455	3.26	6.15	2.27	.822	309	18500	38100	56600

to process a range of tile shapes, sizes and thicknesses. Nevertheless there are considerable cost incentives to produce a trolley design that offers high loadings for a range of products.

(e) Linking of zonal airflows

Another strategy that can be used to improve the dryer energy performance is based upon the simple idea of making the best possible use of the airstream. For example, this can be achieved by linking the zones together so that the airflow is semi-countercurrent through the dryer. That is, the exhaust air from zone 4 is heated and then admitted to the inlet of zone 3 and so on until the humid air is finally exhausted to atmosphere from zone 1. The dryer model is also equally relevant for this configuration provided the airflow direction is the same for all zones. Therefore the production rate and energy efficiency can be calculated as before for various trolley loadings. If all the improvements suggested above are carried out then substantial cost savings will accrue as shown by Table 9. An inlet temperature of 200°C is assumed for all zones.

Table 9 suggests that the optimum policy to minimise the dryer operating costs is to set the NTU as high as possible. However there are practical constraints that limit this value, such as the energy requirements for pumping air and problems of condensation. An economic balance must be reached between the extra energy required for air circulation as NTU is increased compared to the energy savings due to reduced exhaust losses. In order to avoid condensation it is recommended that the final exhaust temperature exceed the dewpoint by at least 20°C. Therefore the maximum cost savings that can be achieved in practice are £88000 for a dryer of NTU = 2, overall energy efficiency of 57% and specific energy consumption of 23 therms per tonne of dry product.

(f) Other Improvement Strategies

Some other strategies that may prove useful for improving the trolley dryer include exhaust recycle, exhaust heat recovery or heat recovery from the hot solids and trolleys. The viability of recycle or heat recovery largely depends upon the dryer configuration and degree of trolley loading. The use of recycle in a properly configured machine will exacerbate condensation problems and reduce the production rate because of the decreased driving force when the inlet temperature is restricted. However if there is some practical reason why the trolleys cannot be heavily loaded then recycle should be introduced until the condensation limit is attained at the exhaust. Similar arguments apply to the use of heat recovery exchangers. Table 9 shows that low exhaust temperatures will result if the dryer is operated to capacity so that only a small amount of sensible heat recovery can be achieved without condensation occurring on the exhaust side of the exchanger. If condensation does not cause fouling problems then the financial incentive for installing such a device is much improved. The final strategy concerns heat recovery from the hot solids and trolleys once the drying is completed. Normally

Table 9
Operating Costs Savings for Fully Improved Trolley Dryer with Interzone Linking of Air-Flows

Parameter	Dryer NTU					
	0.5	1.0	1.5	2.0	2.5	3.0
Operating Variables						
Dimensionless time τ	2.53	3.19	3.84	4.50	5.15	5.81
Residence time/min	220	280	340	400	460	521
Exhaust temperature T_G°/°C	143	111	93	81	75	72
Exhaust humidity Y_G°	.075	.113	.141	.162	.178	.194
$(T_G^\circ - T_{dp})$/°C	96	56	35	20	12	8
Ideal energy efficiency η	.460	.663	.761	.817	.846	.863
Relative production rate	1.02	1.60	1.98	2.25	2.44	2.59
Energy Audit						
Evaporative energy demand/kW	132	206	255	290	315	334
Exhaust energy loss/kW	155	105	80	61	57	53
Sensible heating solids/kW	16	26	32	36	39	41
Sensible heating trolleys/kW	38	30	24	21	18	16
Surface heat losses/kW	29	29	29	29	29	29
Energy lost via doors/kW	38	30	24	21	18	16
Water of combustion loss/kW	44	46	48	50	52	53
Total energy demand/kW	452	472	492	508	528	542
Actual energy efficiency $\hat{\eta}$	.292	.436	.518	.571	.597	.616
Specific energy required/therms tonne^{-1}	45.2	30.3	25.2	23.1	22.1	21.4
Cost Savings						
Existing dryer energy demand/kW	612	955	1182	1344	1460	1548
Total energy saving/kW	160	483	690	836	932	1006
Energy cost saving/£yr^{-1}	9600	29000	41500	50200	55900	60400
Capital cost saving/£yr^{-1}	600	18000	29400	37500	43200	47700
Total cost saving/£yr^{-1}	10200	47000	70900	87700	99100	108100

the trolley load is circulated with cold air to promote the cooling prior to packaging. Therefore it is worth considering the installation of a proper cooling zone at the end of the dryer so that this available energy can be used to preheat the combustion air for zone 4 of the dryer. Approximately 50 kW of energy could be saved in this manner giving reduced costs of £3000 per year.

CONCLUSIONS

The investigation of the performance of this industrial multizone through-circulation trolley dryer has revealed that there is considerable scope for its improvement. This study has shown that there are a number of alternative strategies for upgrading the dryer performance. The most important of these are replacement of gas burners, improved trolley loading and interzone linking of airflows. Interpretation of these various strategies with the aid of simulation techniques suggests that spectacular cost savings of £88000 per year could be achieved together with a simultaneous increase of at least 100% in production rate and decrease of 250% for energy charges with respect to the existing operation. In fact the cost savings are such that the replacement of the present machines with new dryers would be justified by the short payback period of less than two years.

ACKNOWLEDGEMENTS

The authors wish to thank the management of Foseco Ltd., Tamworth, and Foseco International Ltd., Birmingham for their enthusiastic co-operation throughout this investigation and for their permission to publish the results. One of us (JCA) is also grateful for the financial support received from the Electricity Council Research Council, Capenhurst, during the period of this investigation.

REFERENCES

1. J. Lawton, J.E.T. MacLaren and D.C. Freshwater - "Heat pumps in industrial processes", Report 3, Watt Committee on Energy, London, 1978, pp.47-56.

2. D.A. Reay - "Industrial Energy Conservation", Pergamon Press, Oxford, 1977, 357 pp.

3. I.G.C. Dryden (ed.) - "The Efficient Use of Energy", I.P.C. Science and Tech. Press, Guildford, England, pp.167-185.

4. National Industrial Fuel Efficiency Service - "Fuel Economy Handbook", Graham Trotman Dudley Publishers Ltd., London, 1974.

5. J.C. Ashworth - "Energy efficiency of convective solids dryers", Published in 'Energy for Industry' (ed. O'Callaghan), Pergamon Press, Oxford, 1979, pp.349-360.

6. J.C. Ashworth - "Energy efficiency of dryers", Solids Drying Handbook, I.Chem.E. Continuing Education Course, University of Birmingham, 1979, pp. 93-124.

7. J.C. Ashworth and J.W. Carter - "The performance of convective dryers as a function of energy efficiency, capital cost and solids residence time", published in 'Developments for Drying' (ed. Mujumdar), Hemisphere, 1980.

8. J.C. Ashworth - "Interpretation of small-scale drying tests", 'Solids-Drying Handbook', I.Chem.E. Continuing Education Course, University of Birmingham, 1979.

9. H.R.C. Pratt - "Priorities of Research and Development Needs in Separation Processes", Science Research Council, 1976, London.

10. J.C. Ashworth - "Mathematical Simulation of Batch-Drying of Softwood Timber", Ph.D. thesis, University of Canterbury (N.Z.), 1977.

11. J.C. Ashworth and J.W. Carter - "Examination of drying behaviour of silica-gel granules by continuous weighing in an airstream" Published in 'Developments in Drying' (ed. Mujumdar), Hemisphere, 1980.

12. J.C. Ashworth and J.W. Carter - "Drying of hygroscopic solids", Paper presented at I.Chem.E. Symposium 'Drying of Particulate Solids', Sheffield, 1979.

13. M. Suzuki and R.B. Keey - "On the characteristic drying curve", Int. J. Heat and Mass Transfer, 17, 1974, pp.1455-1464.

MEASUREMENTS OF HEAT AND MASS TRANSPORT WITHIN A SHEET OF PAPERMAKING FIBERS DURING DRYING

Peter Lee
Jeffrey Hinds

Weyerhaeuser Technology Center, Tacoma, Washington, U.S.A.

ABSTRACT

Drying is a capital and energy intensive process in the conventional production of paper. During the production of heavy paper and paperboard grades the thermal resistance of the sheet itself limits the rate of production. Under these conditions there is the potential for large economic returns to be derived from a better understanding of the internal mechanisms of heat and mass transfer within a sheet.

A technique for measuring the local and instantaneous flux of liquid water within a porous medium during drying is described.

A consistent set of data is presented for the overall drying rate, local and instantaneous moisture contents, temperatures and liquid fluxes throughout a 600 g/m^2 sheet of bleached kraft fibers during prolonged contact with a hot surface.

It is shown that under the drying conditions of these tests the overall evaporation rate is limited primarily by the rate of liquid flux within the fiber matrix.

INTRODUCTION

The evaporation of process water entrained within porous materials during their manufacture is generally an essential unit operation in their production. For example, in the conventional production of paper and paperboard, a continuous moist web of fibers is formed by filtration from a dilute suspension in water. Some of the residual water can be expressed mechanically, but the remainder must be evaporated. In most cases evaporation is induced by threading the web around each of a series of rotating, steam-heated cylinders.

The hot-surface drying of paper and paperboard is both capital and energy intensive. A typical dryer comprised of a series of steam heated cylinders may cost on the order of 10 million dollars and consume energy at a rate on the order of 50,000 MJ/hr. In many cases the rate of evaporation during drying limits the production rate from a pulp and paper mill complex, which may cost on the order of 750 million dollars. There is the potential for large economic returns to be derived from increased capital utilization as a result of increased evaporation rate and from lower operating costs as a result of decreased energy consumption.

The mechanisms controlling heat and mass transfer external to a moist web of fibers during drying are relatively well understood and quantified. However, it has been shown (1) that for all but the lightest grades of paper the rate of drying is limited primarily by the resistances to heat and mass transfer within the sheet.

Drying of moist paper is a complex process involving the interactive flows of both heat and mass through a structure which is itself responding to local changes in moisture and moisture gradients. Knowledge of the mechanisms controlling the heat and mass transfer within a moist sheet of paper during drying is largely conjectural and is based upon scanty information.

Experimental evidence for the internal mechanisms of heat and mass transfer during the hot-surface drying of any porous material is generally limited to measurements of the overall drying rate, and local and instantaneous measurements of temperature and moisture profiles. Unfortunately, local temperatures and moisture contents do not provide enough information to completely define the internal transport of either heat or mass during drying. In particular, the local and instantaneous movements of water as both liquid and vapor remain indeterminant.

EXPERIMENTAL

An apparatus and technique have been developed for accurately and continuously measuring the instantaneous rate of evaporation from a moist sheet of paper during prolonged contact with a hot surface. The apparatus consists of an electrically heated aluminum plate supported solely by means of a load sensor. During a test, a moist sheet of paper was held firmly against the hot plate and the load sensor continually measured the combined weight of the hot plate and paper during drying. In the experiments reported here, the hot plate was operated at 105±0.1°C and evaporated water was convected away in an air stream with wet and dry bulb temperatures of 23°C and 45°C, respectively. A more detailed description of this apparatus has been presented in a previous publication (2).

In addition to information on the overall drying characteristics of moist paper, the apparatus provided a convenient test bed for measurements of instantaneous and local temperatures, moisture contents and liquid fluxes within the paper during drying.

In this report, results for all of the above measurements will be presented for identical and uniform fiber pads of never dried, bleached Douglas fir kraft wood pulp. Each pad was formed with basis weight of 600 g/m^2 by laminating six equal plies formed separately by filtration and brought into intimate contact with each other under pressure.

Drying Rate

The instantaneous weight of a fiber pad was measured continuously during prolonged contact with the hot plate. The data were re-expressed as instantaneous drying rate, defined herein as the weight of water evaporated per unit weight of dried fiber per unit time, versus time and are presented graphically in Figure 1. Four distinct regimes of drying can be distinguished. Each regime is delineated by rapid changes in the drying rate. The drying curve in Figure 1 is similar in form to those observed for many other porous materials (3).

Immediately following contact between the moist sheet and the hot surface, there is an initial, short warm up period, regime AB, during which the drying rate increased and approached a constant value. Under the drying conditions used in these experiments, there was a well-defined regime of constant drying rate, regime BC. Following the constant rate period, and for most of the overall drying time, the drying rate decreased continuously as the solids content increased. Two distinct falling-rate periods, CD and DE, are apparent in Figure 1.

Local Temperatures

Local temperatures within the sheet during drying were measured using miniature thermocouples which were inserted between each ply during the preparation of the moist composite sheet. Local temperatures within the sheet and the temperatures of the hot plate and hot air were measured continuously during drying. The results are presented in Figure 2 as a graph of local instantaneous temperature versus time. There are seven curves in Figure 2 corresponding to the temperatures at the surface of the hot plate, at the interface between the layers of the laminated sheet and in the bulk of the stream of hot air. In Figure 2 the circled numbers 1 through 6 represent the ply nearest to the hot plate through to the ply nearest to the open surface, respectively. Periods corresponding to the drying regimes in Figure 1 are delineated by dashed vertical lines in Figure 2. The lines are marked A through to E, according to the convention used in Figure 1.

It can be seen that, during the warm up period AB, local temperatures increased from the hot surface outwardly until at the onset of the constant rate period, Point B, the local temperatures throughout the sheet had become constant with respect to time. During the period of constant drying rate, BC, the local temperatures remained constant. The temperature gradients within the sheet were relatively small compared to the temperature difference between the outer region of the sheet and the air stream.

At the onset of the first falling rate period, Point C, temperatures throughout the sheet began to fall. As drying continued beyond C, local temperatures between each layer continued to fall rapidly until the trend reversed sharply when a distinct front of higher temperatures passed through each layer progressively from the hot surface towards the open surface. This front is represented by the heavy dotted line in Figure 2. Local temperature gradients in the sheet were much higher in regions between the front and the hot surface than in the regions between the front and the open surface.

At the onset of the second falling rate period, Point D, the front of higher temperatures had passed completely through the sheet. At this point the rate of increase in temperature throughout the sheet increased markedly, corresponding to a distinct inflection point on all of the curves of internal sheet temperature versus time.

During the second falling rate period DE, all internal temperatures increased asymptotically to steady state values corresponding to the constant thermal conductivity of a completely dried sheet.

Local Moisture Contents

Local moisture contents within a sheet during drying were measured by interrupting the drying process, quickly delaminating the sheet and gravimetrically measuring the average instantaneous moisture content of each ply. Moisture content is herein defined as the weight of water relative to the sum total of the weight of water and oven dried fiber and is expressed as a percentage. In these experiments the variation of the average moisture content of each ply with time was determined at approximately equal intervals thoughout the drying sequence.

Data for the instantaneous average moisture content of each ply are presented in Figure 3 as a graph of moisture content versus time. The curves are numbered 1 through 6 and are superimposed on a grid of vertical, dashed lines marked A though to E according to the same conventions introduced in Figures 1 and 2.

It can be seen from Figure 3 that during both the warm up period, AB, and the constant rate period, BC, the local moisture contents decreased more or less uniformly, with the greatest rate of decline occurring in the region closest to the hot surface. The onset of the first falling rate period, CD, was characterized by a sudden drop in the local moisture content in the ply nearest to the hot surface, ply 1, and a rapid approach to an equilibrium moisture content of approximately 5%. During the first falling rate period, plies

progressively further from the hot surface exhibited similar decreases in their local moisture contents. By comparing Figures 2 and 3, it can be seen that the passage through the sheet of the front of high local temperatures corresponded to the growth of a layer of dried fibers which formed adjacent to the hot surface and spread through the whole sheet over the first falling rate period.

During the second falling rate period, DE, the rate of loss of local moisture decreased markedly and occurred uniformly throughout the sheet.

Local Liquid Flux

In order to determine the relationship between the overall drying characteristics of moist paper and mass transfer within a sheet of paper, a technique was developed for measuring the local and instantaneous flux of liquid water during drying.

The technique involves monitoring the movement of small quantities of a water soluble, non-volatile, non-substantive, low molecular weight tracer through the paper as it dries.

Consider a thin ply somewhere in the sheet parallel with and separated from the hot plate by a layer with basis weight b. Let the basis weight of the ply equal db and the moisture content equal M. Water can move into and out of this thin ply as either vapor or liquid. If the vapor flux into the ply from the direction of the hot surface is V, the vapor flux leaving the ply in the direction of the open surface will be $(V + (\partial V/\partial b) \cdot db)$. Similarly, if the liquid flux into the ply from the direction of the hot surface is L, the liquid flux leaving the ply in the direction of the open surface will be $(L + (\partial L/\partial b) \cdot db)$. Let the concentration of tracer at the surface of the ply nearest to the hot plate be R and at the surface nearest to the open surface be $(R + (\partial R/\partial b) \cdot db)$. Under these conditions, an elemental mass balance for the tracer around the ply for a short time interval dt yields:

$$R \frac{\partial L}{\partial b} \cdot db + L \frac{\partial R}{\partial b} \cdot db + \left[\frac{\partial M}{\partial t} \cdot R + M \frac{\partial R}{\partial t}\right] = 0 \quad (1)$$

The first two terms in equation (1) represent the net rate of flux of tracer into the ply. The term in square brackets represents the rate of accumulation of tracer in the ply.

By monitoring the distribution of an initially uniformly dispersed tracer during drying, all of the terms in equation (1) except L and $\frac{\partial L}{\partial b}$ can be determined empirically. The liquid flux L at both the open and closed surfaces must be zero throughout the drying period. With these boundary conditions and the relationship between L and $\frac{\partial L}{\partial b}$ given by equation (1) the local liquid flux can be determined at any instance and any position within the sheet during drying.

In this investigation the tracer used was sodium fluorescein. The test sheets were made in an aqueous solution of sodium fluorescein at 100 ppm. The local tracer content in each ply at any time during the drying period was determined by interrupting the drying at that time, quickly delaminating the sheet, reslurrying each ply in a known quantity of water and measuring the final concentration of tracer in the water using spectrophotometry. The test sheets were divided into the same number of plies and the drying period interrupted at the same instances as were used for the determination of local moisture contents.

The diffusivity of sodium fluorescein in a fiber pad with a uniform moisture content of 75% and at a temperature of 105°C was determined experimentally to be 8.0×10^{-8} cm^2/s. It can be shown that, for this value of diffusivity, the mass transfer of sodium fluorescein by diffusion within the test sheet during drying is negligible compared to the mass transfer which occurs by convection as a result of the internal liquid flux.

The results for the measurements of local and instantaneous liquid flux are presented in Figure 4 as a graph of liquid flux versus time. A positive flux means net flow to the open surface and a negative flux means net flow to the closed surface. There are six curves in Figure 4 representing each of the six plies of the laminated test sheet. The same convention for numbering and lettering is used in Figure 4 as in all previous figures.

It can be seen from Figure 4 that for all except the final stages of drying there was a measureable movement of water within the sheet. By comparing Figures 3 and 4, it can be seen that liquid flux could be detected at any location where the moisture content was above approximately 10%.

There were two distinct zones in the sheet with respect to the behavior of the local liquid flux through them. In the four plies nearest to the hot plate the local liquid flux was always towards the hot plate. As drying progressed in these regions, the liquid movement increased to a maximum and then decreased asymptotically to zero. In the two plies nearest to the open surface, the initial movement was towards the open surface. The local liquid movement increased to a maximum, decreased and then changed direction before it asymptotically approached zero.

It can be seen that the onset of the first falling rate regime, Point C, corresponds to the instant at which the liquid flux in the ply nearest to the hot plate became zero. Throughout the falling rate period CD, the position in the sheet at which the liquid flux towards the hot surface became zero progressively receded into the sheet. By comparing Figures 3 and 4, it can be seen that the growth of a zone of zero liquid flux corresponded to the growth of the layer of dried fibers adjacent to the hot surface. The end of the first falling rate period, Point D, corresponded to the point at which there is no longer a measureable flux of liquid water anywhere within the sheet.

THE MECHANISM OF HOT-SURFACE DRYING

The data presented in this report provides a basis for describing the phenomenon which occur within a sheet of paper during prolonged contact with a hot surface. The following mechanisms proposed for drying are based upon and are consistent with the experimental observations presented above.

Warm-Up Period

After initial contact of the moist sheet with the hot surface, local temperatures within the sheet increased to a steady value. The rate of increase was most rapid in the plies nearest to the hot plate. As the internal temperatures increased, the overall rate of evaporation increased and approached a constant value.

Constant Rate Drying Period

In the constant rate period the overall rate of heat absorbed by the sheet was balanced by the overall rate lost as latent heat in the evaporated water. The rate of evaporation was relatively high and the overall moisture content of the sheet in this regime decreased rapidly. Despite the rapid loss of moisture during the constant rate drying period, the sheet was able to support a high rate of internal heat transfer.

It has been proposed (4) that heat transfer in a moist porous material occurs by a process of vaporization at/or near the source of heat, transport by convection of latent heat and release by condensation in cooler regions of the sheet. The condensed water returns to the source of heat as a result of the local gradients in moisture content. If this occurs within a sheet of paper, each layer in the sheet would remain an extremely good conductor of heat while moist.

During the constant rate drying period, the limiting resistance to drying was the boundary layer of air between the open surface of the sheet and the bulk air flow. The temperature drop across this layer was almost twice the temperature drop across the sheet itself. Under these conditions the rate of evaporation at the open surface was appreciable and there was a local flux of liquid toward this surface during the constant rate drying period.

First Falling Rate Drying Period

The rate of the internal transport of water decreased as the concentration gradients of moisture decreased. At the onset of the first falling rate period the internal flux of water towards the hot surface was insufficient to keep up with the local rate of evaporation at the hot surface and a layer of fibers dried to their equilibrium moisture content formed in this region. This layer of dry fibers was a poor conductor of heat and served as an insulating layer between the source of heat and the residual moisture. Local temperatures within the dry layer increased and local temperatures in the moist regions of the sheet insulated from the hot surface decreased. The overall drying rate decreased sharply as the limiting thermal resistance quickly shifted from the boundary layer of air at the open surface to the layer of dried fibers adjacent to the closed surface. As the temperature of the open surface decreased and approached that of the bulk air stream, evaporation from regions close to the open surface and liquid flux to this surface decreased and became negligible.

The end of the first falling rate region corresponded to the time at which the dry layer had grown to occupy all of the sheet. At this time the drying rate was only approximately one-tenth of that in the constant rate period.

Second Falling Rate Drying Period

In this region the rate of evaporation decreased quickly to zero. The local internal temperatures of the sheet increased to equilibrum values corresponding to those of a completely dried sheet. As the temperature increased the equilibrium moisture content of the fibers decreased and they released moisture directly as vapor as a result of heat transferred from the hot surface by conduction.

CONCLUSIONS

A technique has been developed for measuring the local and instantaneous flux of liquid water within a porous medium during drying. The technique was used to monitor the movement of liquid within a moist sheet of paper during prolonged contact with a hot surface.

It has been shown that under the conditions of these experiments, inadequate liquid flux towards the hot surface resulted in the formation and growth of a dry layer of insulating fibers adjacent to this surface. The dry layer severely restricted heat transfer from the hot surface to the residual moisture in the sheet and resulted in a rapid decrease in the overall drying rate. Under these conditions, the internal flux of liquid water largely controls the overall evaporation rate from a sheet of paper.

ACKNOWLEDGMENTS

The authors wish to acknowledge the valuable assistance of David W. Kitts during the acquisition and analysis of the data presented in this report.

REFERENCES

1) Han, S. T., Tappi 53 (6):1034 (1970).
2) Lee, P. F., and Hinds, J. A., Tappi 62 (4):45 (1979).
3) Perry, J. H., and Chilton, C. H., 'Chemical Engineers Handbook, Edition 5', McGraw-Hill, New York, 1973.
4) Eastman, G. Y., Scientific American 218 (5):38 (1968).

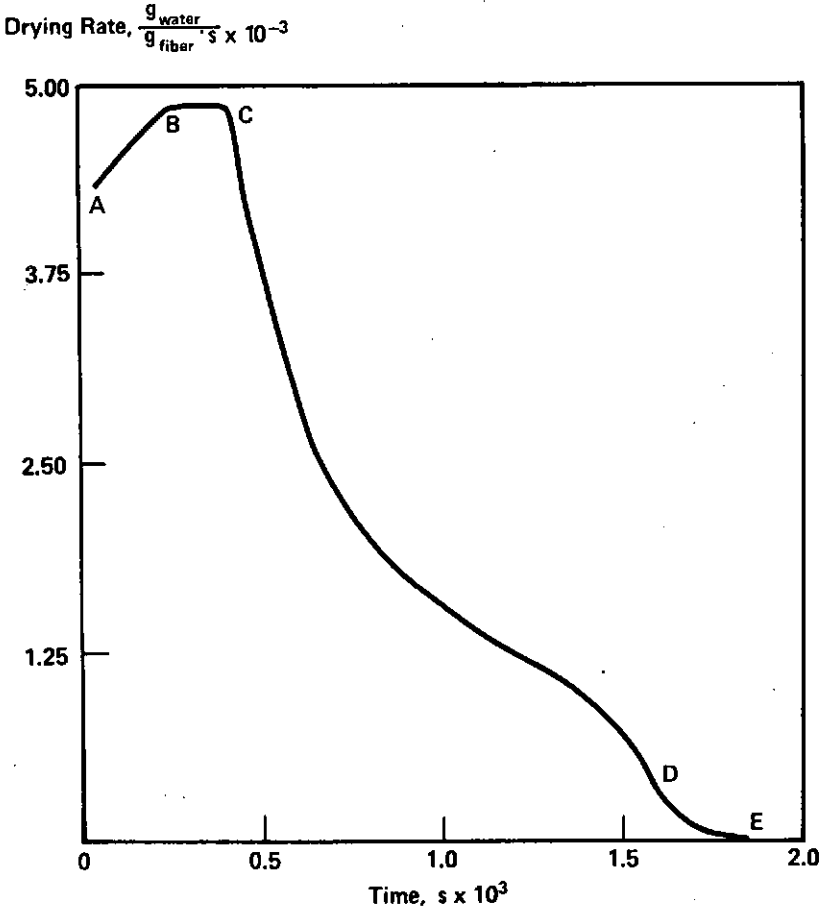

Figure 1
INSTANTANEOUS DRYING RATE vs. TIME

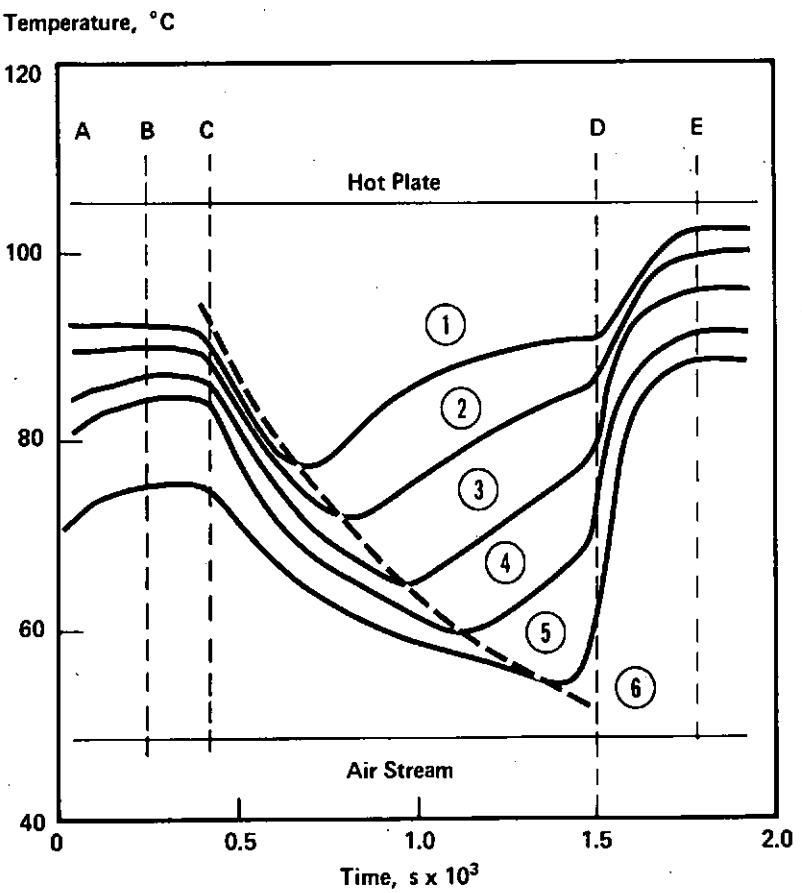

Figure 2
LOCAL TEMPERATURES vs. TIME

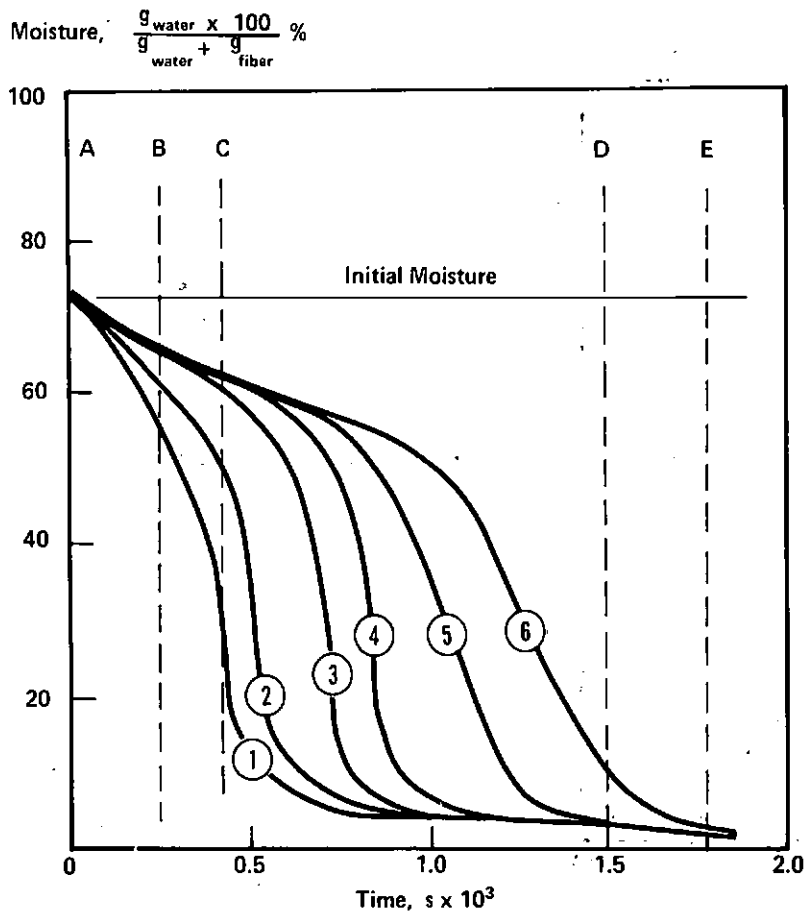

Figure 3
LOCAL MOISTURE CONTENTS vs. TIME

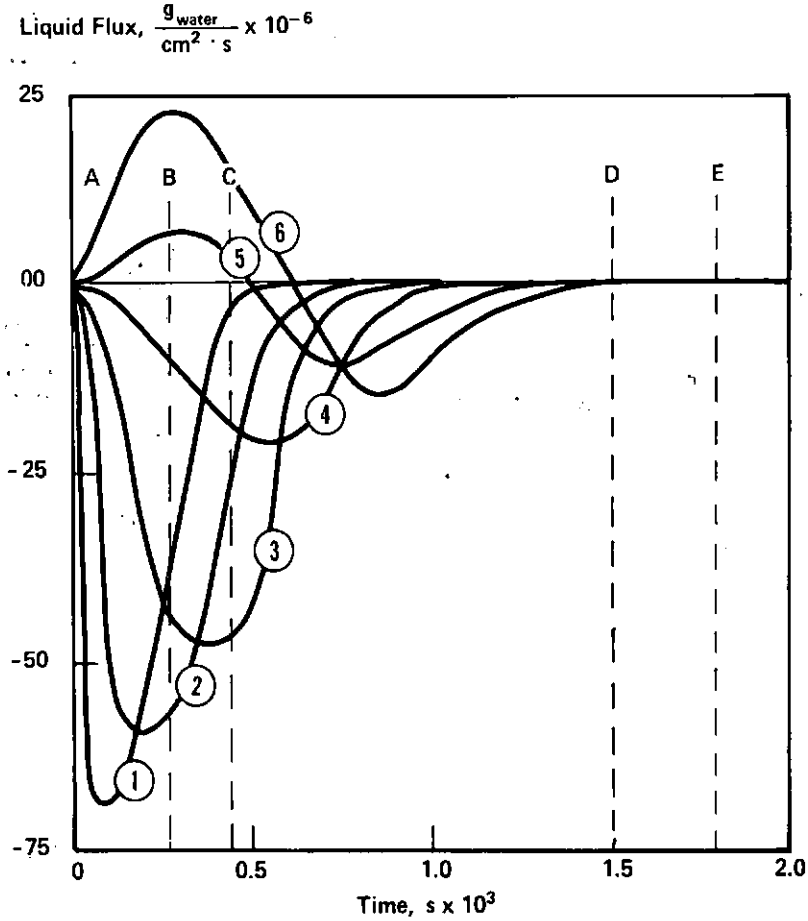

Figure 4
LOCAL LIQUID FLUX vs. TIME

AUTHOR INDEX

Arnason, G. 410
Ayerst, R.P. 472
Bakker-Arkema, F.W. 26
Bakshi, A.S. 282
Bassac, C. 374
Bennett, R.A. 308
Bertin, R. 101, 107
Blazquez, M. 107
Bories, S. 186
Brook, R.C. 263
Brown, L.F. 425
Bruin, S. 233
Capes, C.E. 460
Catania, P.J. 443
Cazaubon, C. 107
Cermak, B. 61
Chen, P.Y.S. 21
Chirife, J. 251
Christian, Gh. 43
Cook, E.M. 158
Corlett, R.C. 425
Cornish, A.R.H. 36
Crowe, C.T. 410
Curtis, S.C. 495
Deschamps, G. 387
Devine, T. 467
Dziubinski, I. 120
Elred, N.R. 343
Endrenyi, S. 80
Fadner, T.A. 343
Filkova, I. 417
Gauthier, A. 387
Gauthier, R. 374
Germain, R.J. 460
Githinji, P.M. 478
Goyel, S.K. 176
Grassmann, H.C. 338
Gupta, R. 201
Gupta, C.L. 453
Gustafson, R.J. 229
Hasatani, M. 163
Havens, J.A. 1
Hayashi, H. 244, 294
Helmer, W.A. 21
Holik, H. 355, 362
Imré, L. 446
Ishioka, Y. 244
Kawamura, Y. 170
Karlsson, M. 322
Kashiwa, B.A. 425
Kisakürek, B. 434
Kiss, L. 446
Kmiec, A. 213
Kornyey, T. 446
Kröll, K. 485
Kumazawa, E. 244
Kuramae, M. 195
Kuts, P.S. 65
Kwon, O.Y. 443
Lampinen, M.J. 11
Legoff, R. 374, 387
Lehtinen, J.A. 347
Lenczyk, J.P. 152
Le Pourheit, A. 186
Leung, P. 201
Levdansky, V.V. 17
Liapis, A.I. 224
Lin, S. 6
Lin, Y.Y. 6
Luyben, K.Ch.A.M. 233
Martynenko, O.G. 17
Masters, K. 401
McConnell, R.R. 330
Menon, A.S. 485
Mielczarski, S. 213
Molnar, K. 29, 446
Mujumdar, A.S. 201, 485
Nastaj, J. 126, 135
Olieman, J.J. 233
Orvos, M. 29
Pakowski, Z. 208
Parikh, R.J. 1
Parti, M. 219
Pavlyukevich, N.V. 17

Pikus, I.F. 65
Pinter, R. 255, 362
Plumb, O.A. 84
Poehlein, G.W. 93
Potter, O.E. 396
Pramojaney, N. 93
Raghavan, G.S.V. 272
Reddy, T.A. 453
Richard, P. 272
Richardt, K. 379
Ringer, D.U. 144
Root, W.L. 158
Roques, M.A. 36
Rosien, H.N. 21
Saiki, Y. 244
Sarkar, C.R. 152
Shah, R.M. 176
Singh, R.P. 256, 282
Soininen, M. 315
Sokhansanj, S. 229
Spirnek, J. 122, 120
Spolek, G.A. 84
Srour, Z. 101
Steffe, J.F. 256
Strawinski, A. 269
Strek, F. 126, 135
Strommen, I. 289
Strumillo, C. 208
Suarez, C. 251
Svensson, C. 301
Szentgyörgyi, S. 29
Taneya, S. 244
Tudose, R.Z. 43
Topar, J. 405
Vadja, T. 182
Valchar, J. 53
Valcharova, J. 53
Vanderborgh, N.E. 425
Vanderhoff, J.W. 93
Viollaz, P. 251
Wada, T. 294
Waller, M.H. 495
Wang, C.L. 6
Wang, S.W. 21
Weberschinke, J. 417
Yamamoto, K. 170

SUBJECT INDEX

Agglomeration Methods 460

Airfoil Dryer 308

Automatic Control 107

Clausius-Clapeyron Equation 13

Coal Drying
  kinetics of 425
  lignite 434
  sub-bituminous coal 425

Codfish Drying 289

Computer Model
  solar-dehumidification of wood 21

Contact Drying 126

Constitutive Equations 37-40

Continuous Vacuum Drying 244

Contact Drying of Paper 322

Cost Benefit Analysis 443

Diffusion Coefficients 233

Displacement Drying 467

Droplet Heat and Mass Transfer 411

Droplet Size Distribution 405, 417

Drying
  capillarity 17, 29
  latex films 93
  mathematical models for 17
  mechanics and thermodynamics of 11

Drying of Explosives 472

Drying of Grains
  cocurrent drying 263
  effect of tempering 266
  model for 229
  parboiled rice 282
  rough rice drying 256
  shelled corn drying 265
  solar drying 443
  soyabean drying 251

Drying of Hay 446

Drying Kinetics 43, 53, 66, 73

Drying of Nitrocellulose 472

Drying of Paper
  airfoil concept 308
  contact drying model 315
  effect of air flow on contact drying 369
  energy management 495
  experimental results 322
  improvement in moisture profile 338
  printed web 343
  review of 330

Drying of Particles and Lumps 396

Drying of Plaster Blocks 374

Drying of Printed Web 343

Economic Factor for Dryers 386

Energy Aspects
  paddle dryers 158

Energy Consumption in Tissue Drying 362

Energy Management 495

Energy Savings in Dryers 379

Entropy Balance 13

Finite Element Model 229

Flash Drying 213

Fluorocarbon Solvents 467

Flue Gas Desulphurization 401

Fluidized Bed
  drying of milk powder 294

Fluid Bed Drying
  effect of reduced pressure 170
  effect of vibration 201, 208
  granulation 182
  of nitrile rubber 152
  of tea 176

Freeze Drying
  model for 6
  rates of 224

Heat and Mass Transfer
  in wood 84
  wet porous media 36, 53, 65

Heat Pump 374

Heat Recovery 383

Heat Sensitive Food Drying 244

Immersion Drying 272

Irreversible Thermodynamics 1, 37

Latex Film Drying 93

Lumber Drying 22, 84

Mechanistic Model for Wood 87

Mechanical Recompression of Steam 387

Mechanical Vapor Recompression 388

Microprocessors 107

Microwave Drying 186

Milk Powder
  cooling 294
  drying 294

Moisture Bonds 61

Moisture Profile Correction 355

Multiple Effect Evaporation 388

Nitroglycerine/Nitrocellulose Drying 472

Nonthermal Water Removal 460, 467

Numerical Model
for contact drying 315
for latex film drying 93
for optimization 101
for wood drying 84
of convective solar drying 453
of textile dryer 112
of tunnel dryer 107
of solar hay-drying 446

Optimum Temperature Distribution 120

Packed Bed Heat and Mass Transfer 163, 219

Paddle Dryers 158

Parameter Optimization 101

Pneumatic Drying 213

Porous Media
analysis of moisture movement in 1
coupled heat and mass transfer 1
diffusivity of 3
model for 1
moisture transfer in 53
sublimation limit 6
thermal conductivity of 3

Preconcentration of Whey 387

Printed Web Drying 343

PSI-Cell Model 414

Pulp Drying 301

Pyrethrins Drying 478

Rebinder Number 67

RF Drying 338

Rice Drying 256

Rubber Drying 152

Selective Wetting 460

Spray Drying
in environmental control 401
model for droplet size distribution 405
numerical models 410

Solar Drying
model for 21, 453
of hay 446
wood dehydration 21

Solar Grain Drying 443

Solar Kiln 22

Soyabean Drying 251

State Function Diagram 61

Steam Drying of Pulp 301

Sublimation Limit 6

Surface Evaporation 80

Taylor and Cary Theory 2

Textile Drying 112

Tissue Drying 355

Tunnel Dryer Control 107

Unsaturated Porous Media 1, 53

Vacuum Contact Drying
falling rate 135
constant rate 126

Vapor Transfer in Granular Beds 195

Vepex Process 382

Vibrating Conveyor Heat Transfer 144

Vibrofluid Bed Drying 176, 201, 208

Wood Drying 22, 84